EXPERIMENTAL, THEORETICAL AND FINITE ELEMENT ANALYSIS OF A REINFORCED EARTH RETAINING WALL INCLUDING COMPACTION AND CONSTRUCTION PROCEDURES

by

Emad Abd El-Moniem Mohamed Osman

B.Sc., M.Sc.

A Thesis Submitted for the degree of Doctor of Philosophy

University of Glasgow

Department of Civil Engineering

October, 1990

TO MY FAMILY

TO FRIENDS IN U.K. MORE THAN BROTHERS

THIS WORK IS GRATEFULLY DEDICATED

TABLE OF CONTENTS

ACKNOWLEDGEMENTS

Although, I believe it is impossible to adequately thank every one who has assisted with my project, I would like to express my sincere thanks to the Head of Department, Dr. D. Green, Professor H. B. Sutherland and Professor D. Muir Wood for the provision of facilities to enable the research completion and for their continued interest in the progress of this research.

In particular, I feel deeply indebted to my supervisor Mr. T. W. Finlay for his appreciated guidance and criticism. His continuous encouragement and help throughout this work are greatly esteemed.

My special thanks to Dr. W. Sharp from the computer centre of Glasgow University for his assistance in running the finite element computer program.

I am grateful to Mr. W. Henderson, Mr. T. Montgomery from the Soil Laboratory and Mr. A. Burnett, Mr. R. Thornton, Mr. A. Gray from the Workshop for the considerable effort and their technical assistance on the manufacture and in setting up the test rig. Thanks also due to Mr. I. Todd and Mr. A. Yuill for helping with the electronic equipment.

Many thanks to all my fellow research students whose friendship made my stay so memorable.

At last but not least, I would like to express my sincerest thanks to my parents, my wife and my sons for their understanding, support, encouragement and boundless patience over all these years.

SUMMARY

This thesis is concerned with an experimental and theoretical study of the behaviour of a reinforced earth retaining wall built on a rigid foundation, during and after construction with special attention paid to the effect of the compaction process.

The theory and development of reinforced earth, four case histories, and tests on full scale models and small scale models related to the effects of compaction and current design methods have been reviewed with comments.

The research work is tackled on two fronts:

– Experimental model study.

– Theoretical studies.

(1) Experimental model study

The model study, a three dimensional model, simulates a vertical reinforced earth retaining wall of height 6.0 m with a model scale "10". The model comprises an open fronted wooden box 1300 mm long, 900 mm wide and 700 mm high, and the box contains the wall retaining 1200 Kg of sand reinforced with aluminium foil strips 0.1 mm thick attached to perspex facing panels of 150 X 150 X 18 mm each. The sand bed in the model was formed using a sand spreader, dust extractor machine and a vibratory compaction device simulating the compaction plant in the field. Sixty six strain gauges, sixteen miniature pressure cells, which were developed and calibrated completely in the laboratory, and eight LVDTs were used to monitor the behaviour of the wall before, during and after

compaction, under various uniform and variable compaction lengths and different methods of construction. Two methods of calibrating the density in the models were established, viz. temporary metal cylinders and permanent perspex cylinders.

(2) Theoretical studies

These were divided into two sections as follows

a– Theoretical study of compaction

The existing theories of compaction with comment and factors affecting modelling of compaction are reviewed. Three proposed models were developed to simulate the compaction plant as well as a computer program (BCOMPP) to calculate the horizontal stresses in the free field or on the vertical wall taking into account the nature of the compaction plant as a three dimensional problem.

b– Finite element method

The computer program (BCOMPP) with another finite element program were used to predict the behaviour of the same model tests used in the experimental work. The program employed plane strain, static and two dimensional finite element procedures. The program contained a model of the construction procedures as used in the field, non linear stress–strain characteristic model of the soil, model of the compaction process and the soil structure interface. The behaviour was predicted before and after compaction.

Results and comparison showed that compaction of the backfill in a reinforced earth retaining wall results in stresses being locked into the fill. This as well as compaction length and construction methods has a great effect on the wall behaviour. For this reason the designer should be wary of placing too much faith on "active" design.

NOTATION

The symbols in general use throughout the thesis are listed below. Symbols peculiar to a particular theory or part of the thesis are defined in the text when they occur.

cat. – category

comp. – compaction

cont. – continuous

horiz. – horizontal

leng. – leng.

max. – maximum

min. – minimum

No. – number

vert. – vertical

SIG1 – major principal effective stress

SIG3 – minor principal effective stress

SIM1 – horizontal effective stress behind the wall face

SIM2 – horizontal effective stress on vertical plane at the middle of the reinforced mass

SIM3 – horizontal effective stress behind the reinforced mass

CHAPTER 1

INTRODUCTION

1.1 GENERAL

Soil is one of the mankind's oldest construction materials. Recently, the combination of the limited supply of land and man's economic growth, has forced engineers to build structures where they are required, almost irrespective of soil conditions. There are two alternatives which may be used to deal with the circumstances. The first is to avoid the trouble, while the second is to make use of and improve the available soil conditions. One method of soil improvement is soil reinforcement.

The general concept of reinforced earth is not new. Recently, in the 1960's the French engineer, Henri Vidal developed a modern form of soil reinforcement, which is termed "Reinforced Earth". Vidal's concept of reinforced earth is more comprehensive than the previous man–made methods of soil reinforcement.

Reinforced earth is a composite construction material composed of soil fill strengthened by the inclusion of rods, bars, strips, fibres or nets. The strength of the composite material is due to the apparent cohesion between soil and reinforcement. This can be achieved by the densification of the composite material.

Reinforced earth is a topic which has attracted the attention of Civil Engineers throughout the world for the last three decades. The widely expanding interest in the subject is due to its advantages such as, economic costs and ease of erection and construction coupled with basic simplicity. Reinforced earth has been used successfully to build roads and railway embankments, retaining walls, bridge abutments, dams and coastal defences in many sites through out the world.

The major application of the reinforcing technique is in reinforced earth retaining walls. The main components are:

- Wall face
- Reinforcement
- Backfill

Reinforced earth retaining walls can be constructed in a variety of ways and configurations. The common factor between different methods of construction is compaction of the backfill in horizontal layers behind the wall face. This is done by using compaction plant which suits the soil and the type of project.

The importance of compaction of the backfill behind a reinforced earth retaining wall can be summarized as follows:

a– To avoid any future settlement after the construction is completed and the wall is ready for use.

b– The composite material (reinforced earth) gains its strength from the apparent cohesion between soil and reinforcement by densification of the composite material to a certain degree. This densification is achieved by compaction of the reinforced earth, so compaction of the fill behind a reinforced

earth retaining wall is essential during construction and no wall is built without using compaction.

Much intensive research work has been done on reinforced earth retaining walls in the last decades in both experimental and theoretical fields. Significant developments have been achieved by finding new materials for the backfill and reinforcement and by the introduction of new design theories. The research however has not covered all the areas which affect the behaviour of reinforced earth retaining walls and these areas still need more investigation. One of these areas is the compaction induced stresses and their effect on the reinforced earth retaining wall.

Several researchers pointed out this need as follows:

" Although conceptually simple, the behaviour of reinforced earth is actually very complex and I imagine many more years will elapse before the basic mechanisms are clearly established to every one's satisfaction"

Lee (1978)

" The main conclusion is that there is still very little known, in quantitative terms, about the effect of compaction. It is evident that considerable research effort is needed to illuminate this darkness".

Ingold (1980)

" There is little reliable field data available regarding compaction induced lateral earth pressures upon which to base development and/or theories and analytical procedures".

Seed and Duncan (1983)

" In general the monitoring — of existing retaining walls— showed that development of earth pressures was influenced by construction methods and that the magnitude of pressures was very much greater than the active condition"

Carder (1988)

It is still an attractive subject for investigation. On the other hand, new applications are continuously being conceived. The present research work was carried out in the soil mechanics laboratory in the Civil Engineering Department, Glasgow University.

1.2 SCOPE OF THESIS

The general object of the present research work is to study the behaviour of a reinforced earth wall under compaction effect and different methods of construction. The study includes both model reinforced earth retaining wall tests and computer analysis employing a plane strain finite element analysis as well as a compaction model.

The thesis consists of the following:

– **Chapter 1:** presents the general introduction and the scope of the present research.

– **Chapter 2:** gives a brief history of reinforced earth, explaining the concepts of reinforced earth and fields of application. It shows the methods of construction of a reinforced earth retaining wall and reviews the previous experimental work done by investigators. Case histories are presented to explain

the effect of compaction on the wall. It shows current design methods with comment.

– **Chapter 3:** contains the objectives of the laboratory investigation, detailed descriptions of the model tests of the reinforced earth wall, instrumentation devices and their calibration. It presents the method of setting up the model as well as the test programme.

– **Chapter 4:** includes the previous work by researchers and the factors affecting the control of density of sand in the model tests. It shows the methods used to control the density in the model tests in this research and gives a description of the devices used and their calibrations.

– **Chapter 5:** presents the experimental results of the model tests and discussion.

– **Chapter 6:** reviews existing theories of compaction with comment. It presents four new proposed models of compaction plant suggested by the author and gives a comparison with other research and field work.

– **Chapter 7:** demonstrates the use of the finite element method in soil problems, emphasizing the reinforced earth retaining wall. It shows the different ways of modelling the compaction effect in the finite element method used by previous researchers.

– **Chapter 8:** presents the objective of the study, describes the computer program employing the static plane strain finite element method, its features and a flow chart. It contains a detailed example of an idealization of one of the

laboratory tests, testing programme and data used.

– **Chapter 9:** presents the results obtained from the finite element analysis and discussion.

– **Chapter 10:** shows the comparison between the experimental work and the computer prediction of the behaviour of the model tests carried out in the laboratory.

– **Chapter 11:** includes the conclusions of the present research and the recommendations for further studies.

The thesis also contains the References and three Appendices **A, B & C.**

CHAPTER 2

LITERATURE REVIEW

2.1 INTRODUCTION

In this chapter a brief history of reinforced earth is reviewed. The mechanism of reinforced earth and different concepts are explained. Different fields of application are presented such as foundation mats, dams, embankments, and reinforced earth walls. The main concepts of reinforced earth walls and methods of construction as well as construction processes are shown. An attempt to explain the influence of compaction plant during the construction process and post construction is made. In order to see this effect, many case histories and small scale tests are illustrated. A review of current design methods and comments on them as well as conclusions are given.

2.2 BRIEF HISTORICAL REVIEW AND DEVELOPMENT OF REINFORCED EARTH

Fukuoka (1988) declared that, the general concept of soil strengthening by adding rods or fibres, as in reinforced earth, is not new. The beneficial effect of plant roots in stabilizing soil has been recognized for a long time. Osman (1980) mentioned that the earliest application was made by villagers in Ancient Egypt who used straw mixed with clay to improve the quality of building material in the construction of dwellings, and such procedures have recently received

careful analytical as well as experimental study.

Temporary roads through swampy areas are often constructed on a foundation of small trunks and branches. During the 17th & 18th centuries, the early French settlers in Canada built many miles of low dikes made of mud and sticks to protect farmland. The use of fibres or branches to stabilize soil along river banks has also been reported (Lee et al., 1973).

The first reinforced soil system was patented by F.H.Reed, as early as 1904, in the United States. Parkin et al. (1966) described a system for reinforcing the downstream slope of a composite earth and rock fill dam in California, the rock fill in the downstream slope being reinforced with horizontal metal railway lines and the facing units consisting of rails in the form of a diamond shaped grid with horizontal reinforcing rails connected to the points of intersection of the grid. This concept was applied in several dams in Mexico (Weiss, 1951); South Africa (Pells, 1969); Australia (Anon, 1967); and New Guinea (Fraser, 1962). Recently the construction of reinforced earth dams has been found to be economical, (Jones, 1985).

Munster (1925) in the United States constructed the wall shown in Fig. (2.1). It consisted of a light facing unit to which was attached the wooden reinforcing members. The reinforcement was attached to the back of the wall by using sliding attachments to allow relative movement to take place, (New Civil Engineer, 1975).

Coyne (1927) a French engineer introduced the quay wall. The wall is 2.5 m height and 0.5 m thick as shown in Fig. (2.2). It was constructed using two horizontal layers of reinforcement in the form of reinforced concrete straps each

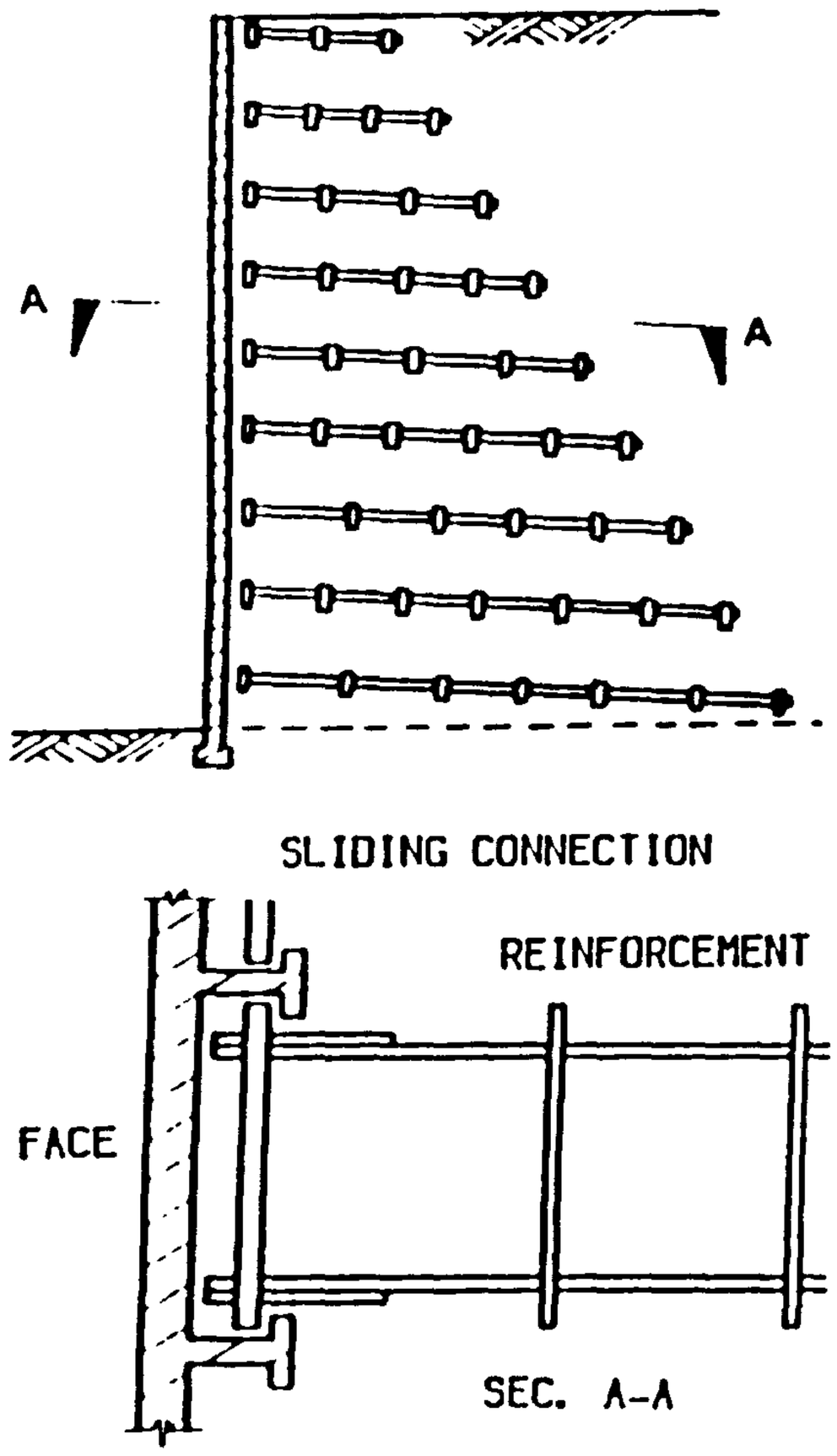

FIG. (2.1) RETAINING WALL WITH SLIDING MEMBERS AT THE BACK (AFTER MUNSTER, 1925).

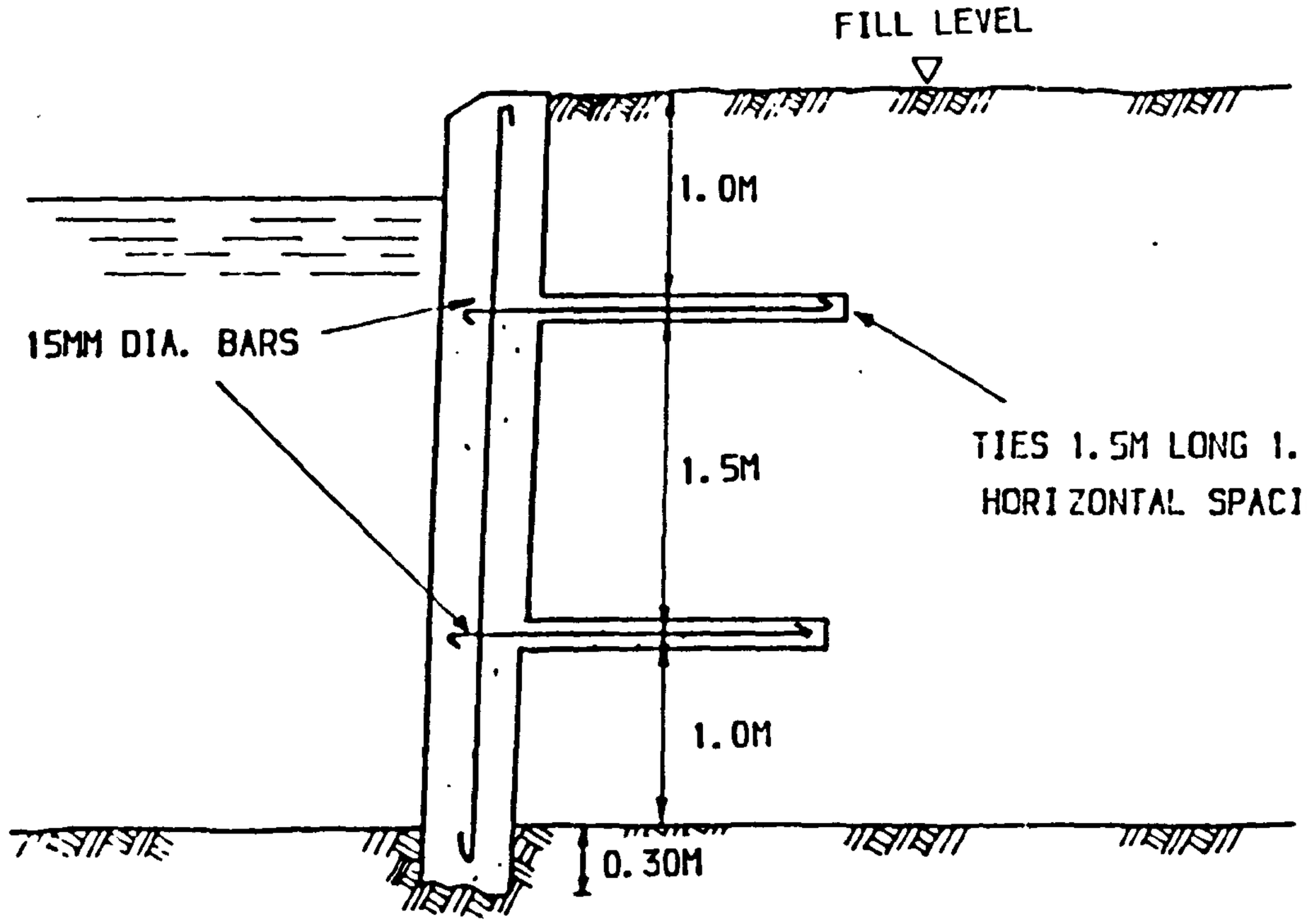

FIG. (2.2) RETAINING WALL AT BREST (AFTER COYNE, 1927).

1.5 m long. Jones(1985) reported that, in 1928 Coyne advocated the "Ladder Wall" which comprised a mass of granular filling unified by a row of tie members each having a small end anchor as shown in Fig. (2.3).

A British patent for a further version of a reinforced soil structure was filed by Schroeter (1933). He constructed a wall as shown in Fig.(2.4) consisting of thin facing units and horizontal reinforcing plates hinged at their connections to the back of the wall to allow rotation of the plates in the case of settlement of the fill.

Lallemand (1959) developed a reinforced element in which a number of rigid claws were arranged along the length of the reinforcement to increase adhesion with the soil.

In the 1960's the French engineer, Henri Vidal developed a modern form of reinforced earth wall as shown in Fig. (2.5). Vidal's concept of reinforced earth "Terre Armée" is more comprehensive than the previous man–made methods of soil reinforcement. The Vidal system enables retaining walls to be constructed in which the soil mass behind the vertical wall face is reinforced by the addition of regularly spaced flat horizontal strips of metal. This system differs from an anchored wall system, as it is the frictional interaction between the fill and the reinforced element which maintains the equilibrium of the structure rather than the tie back force.

Popescu (1979) reported that in 1963 Vidal first published his results, but it was not until 1965, that Vidal was able to design and construct a small reinforced earth wall at Progers in the French Pyrenees. In 1968, the first large scale reinforced wall was built on the Nice–Menton highway in southern France and

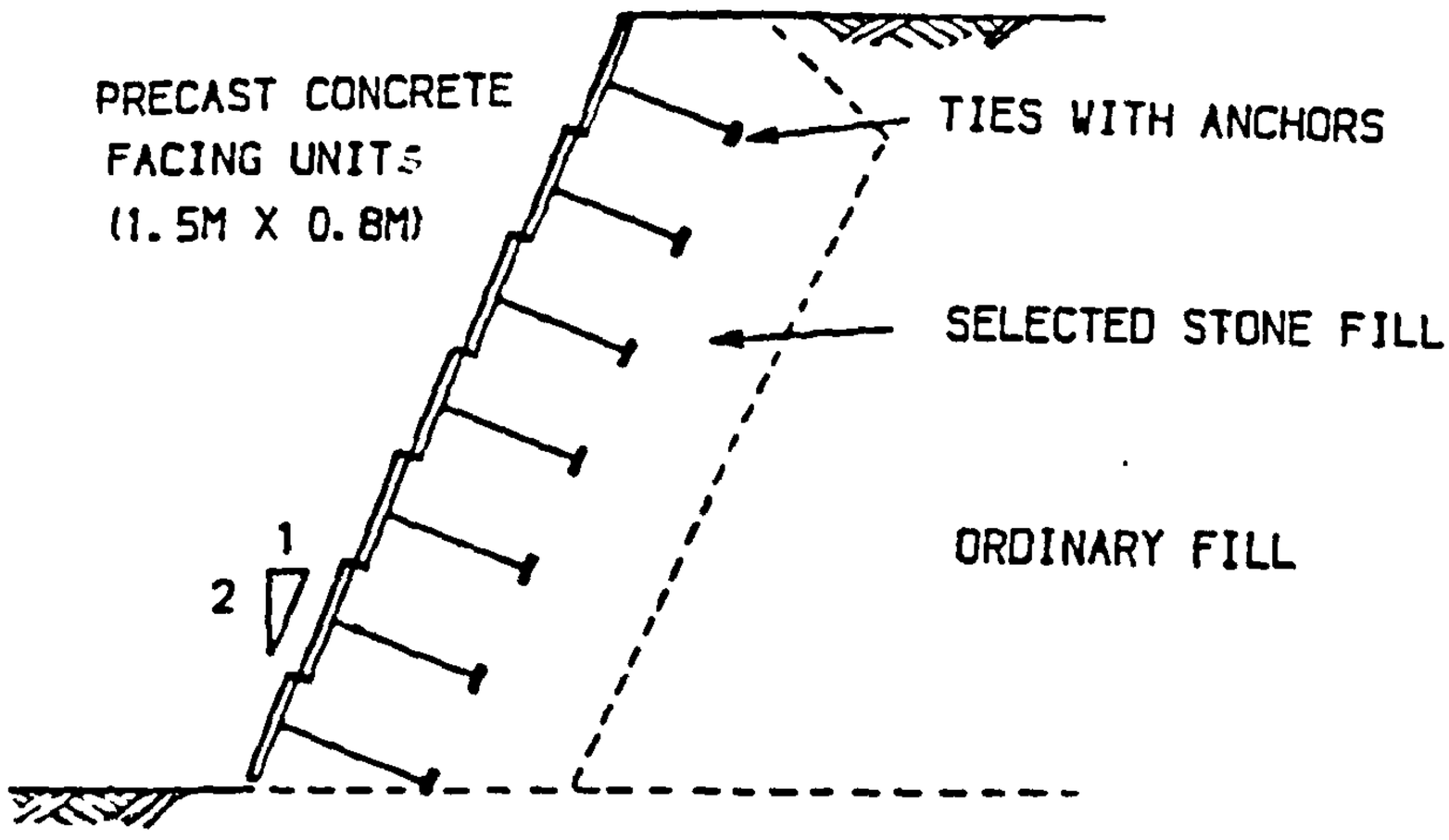

FIG. (2.3) LADDER WALL (AFTER COYNE, 1928).

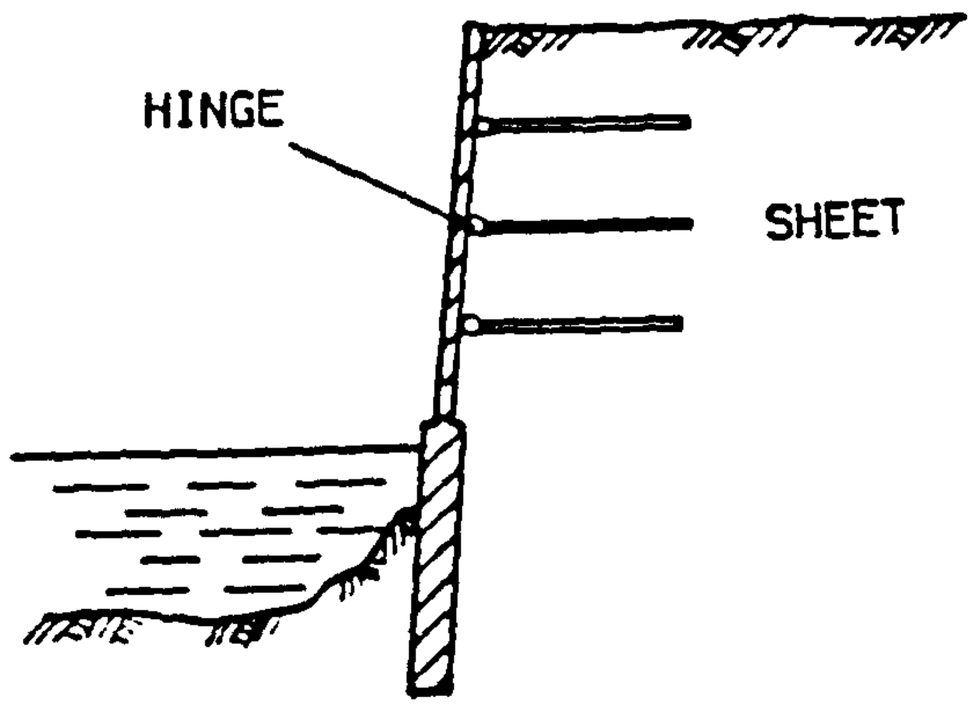

FIG. (2.4) RETAINING WALL WITH SHEETS HINGED AT THE BACK
(AFTER SCHROETER, 1933).

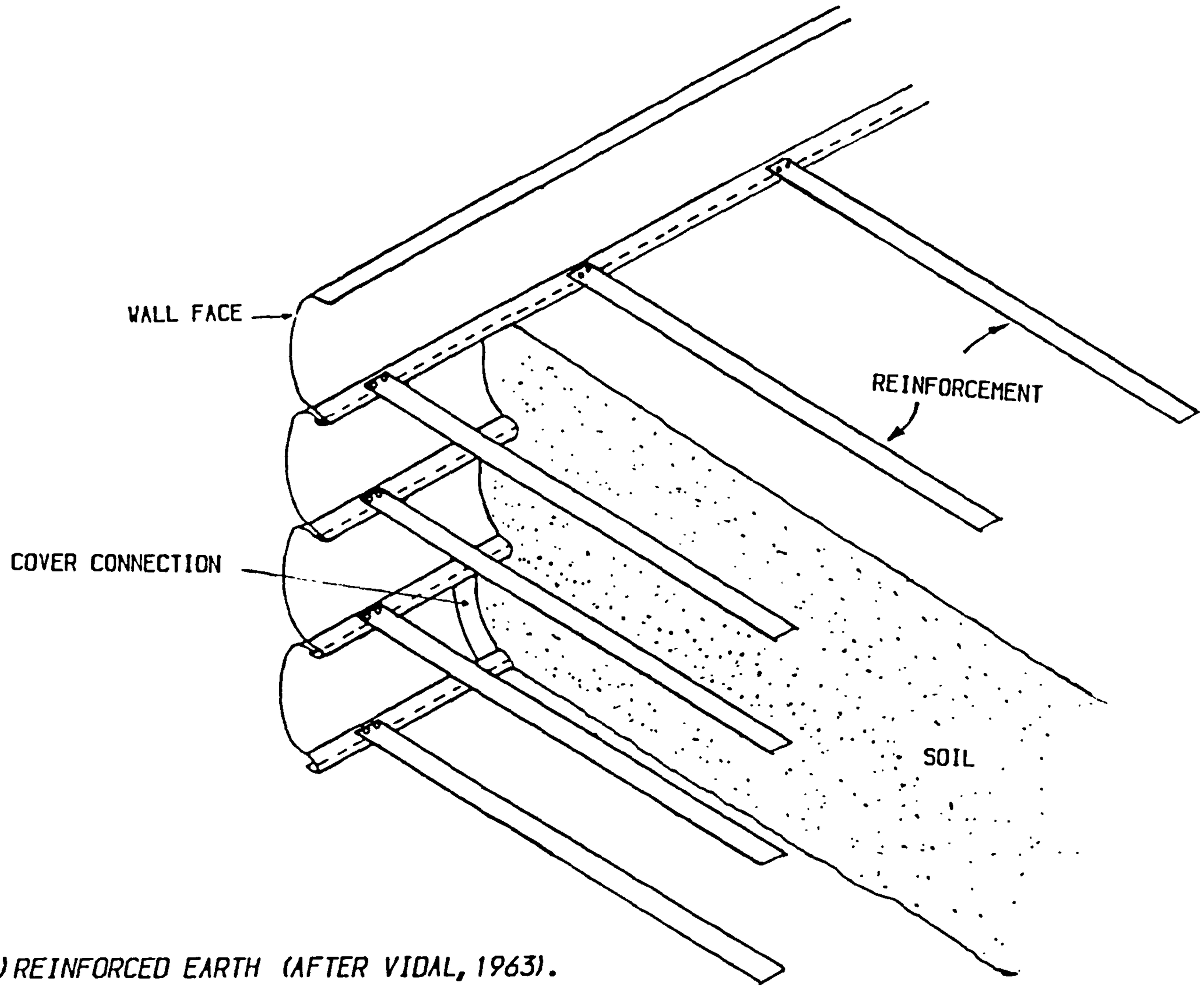

FIG. (2.5) REINFORCED EARTH (AFTER VIDAL, 1963).

was closely monitored by Laboratoire Central des Ponts et Chaussees (L.C.P.C).

Studies were initially carried out on reduced scale models, (Schlosser and Long, 1974). In the same year a full scale instrumented wall was constructed at Incarville, France. The successful completion of this test inspired the erection of numerous reinforced earth walls in Europe, the United States and Japan. In 1969 the precast concrete facing unit Fig. (2.6) was introduced by Vidal, and Table (2.1) gives details of the patents filed by Vidal 1963–1969, Ingold (1980).

The first reinforced earth wall in the United Kingdom was built on the Leith–Granton road near Edinburgh in 1972 by Tarmac Construction Ltd.. The wall which was 106 m long and up to 7 m high was completed in five weeks. The construction and performance of this wall was reported on by Finlay and Sutherland (1977). A British patent for a reinforced earth system (D.O.E) system was introduced in 1973, Jones (1977). It is shown in Fig. (2.7).

2.3 HOW DOES REINFORCED EARTH WORK ?

Vidal (1969) defined reinforced earth as a composite material formed by combining earth and reinforcement. The term earth covers granular soils and soils which exhibit some slight cohesion. The term reinforcement is used to define all linear or planar components which can withstand tensile stress. The reinforced soil was named "reinforced earth" by Vidal to be analogous with the term "reinforced concrete" (Vidal, 1978).

The essential phenomenon in the mechanism of reinforced earth is the friction mobilized at the soil–reinforcements interfaces. There are two concepts

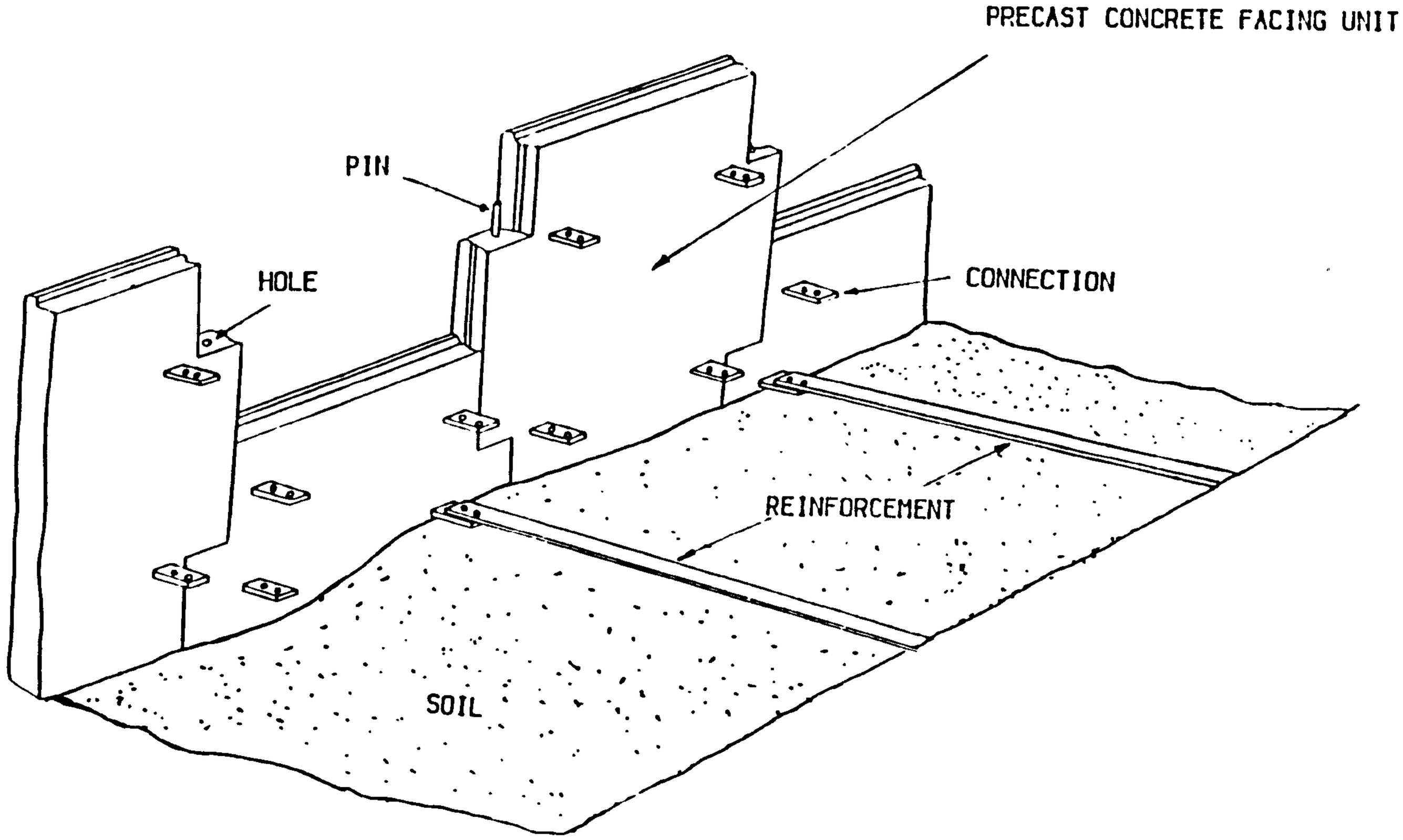

FIG. (2.6) PRECAST FACING UNITS OF REINFORCED EARTH WALL (AFTER VIDAL , 1969).

TABLE (2.1) PATENTS FILED BY H. VIDAL 1963-1969 (AFTER INGOLD, 1980)

FRENCH PATENT SPECIFICATION No.	DATE FILED	DATE PUBLISHED	BRITISH PATENT SPECIFICATION NO.	DATE FILED	DATE PUBLISHED	DETAILS OF INVENTION
1,381,245	27.3.63	2.11.64	1065538	24.3.64	19.3.67	CONCRETE 'NECKLACE'
1,393,988	27.3.63	2.2.65	1069361	25.3.64	17.5.67	STEEL FACING UNIT
1,594,550	22.1.68	17.7.70	1259301	21.1.69	5.1.72	CONCRETE 'NECKLACE'
2,055983	14.8.69	14.5.71	1324686	4.8.70	25.7.73	CONCRETE FACING UNITS

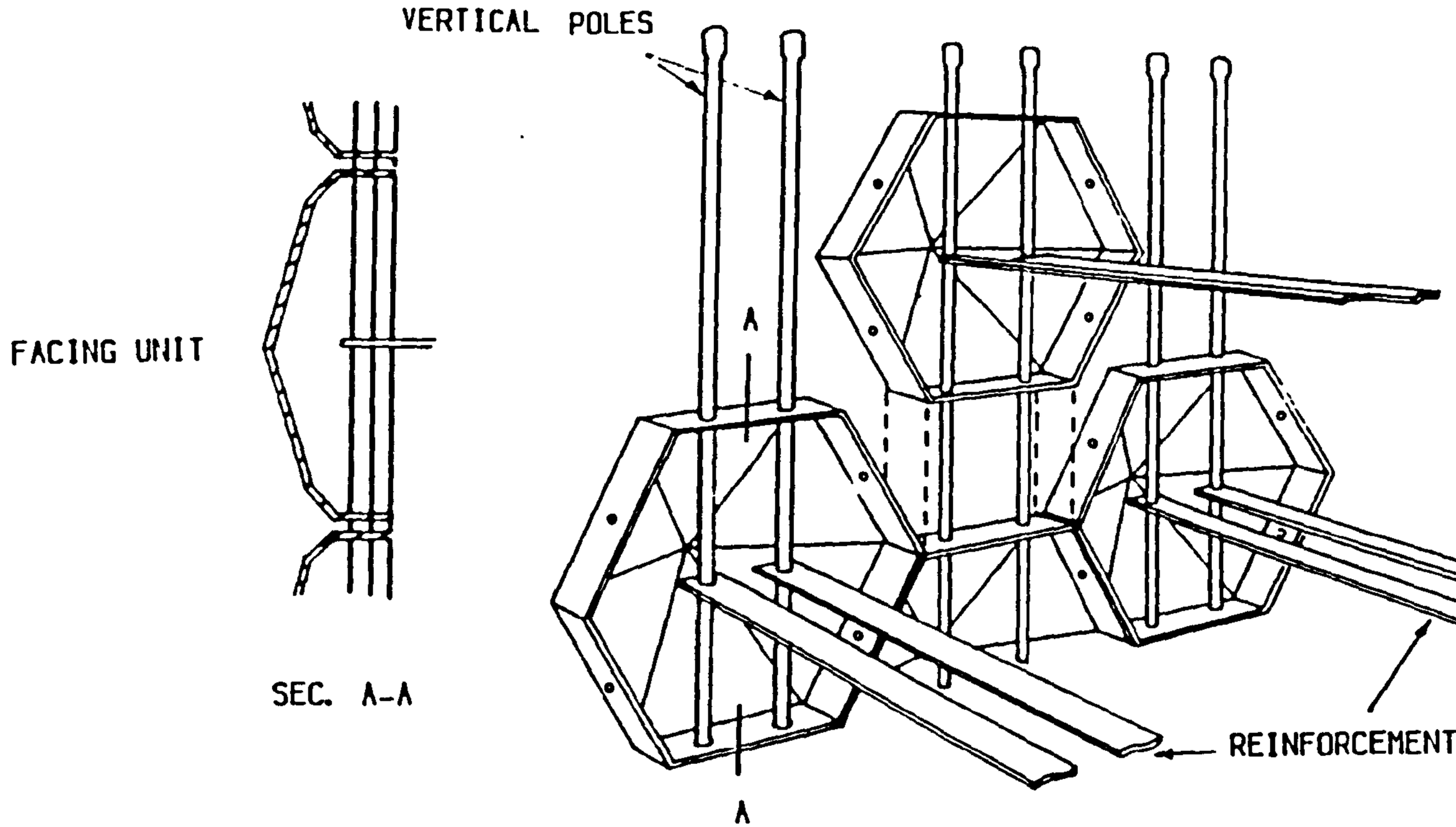

FIG. (2.7) O.O.E. SYSTEM OF REINFORCED EARTH RETAINING WALL (AFTER JONES, 1977).

for the basic mechanism of reinforced earth. Each concept answers the above question.

2.3.1 Stress Concept

Vidal (1969 & 1978) explained or answered as follows:

Consider a sand grain in contact with the surface of the reinforcement as shown in Fig. (2.8.A). If the contact force (F) makes an angle with the normal line smaller than the sliding angle between the grain and the reinforcement, every thing occurs as if the grain was tied by the reinforcement, Fig. (2.8.B). In that case he considered that all the grains along the reinforcement were tied, Fig. (2.8.C).

Mitchell and Schlosser (1979) stated that Vidal's concept is related to the apparent cohesion i.e. the difference between the tensile forces T_1 & T_2 generated at the ends of the reinforcement in an element of reinforced soil of length (dl) as shown in Fig. (2.8.D) will induce compressive lateral stress generated in the soil analogous to a confining pressure. This would of course, impart some finite compressive strength to the soil mass and at the same time the friction mobilized at the soil– reinforcement interfaces would cause a rotation of principal stresses in the soil and modify the initial state of stress. This fundamental principal was examined experimentally and confirmed by Schlosser and Long (1972), Hausmann and Lee (1976) and others.

Swiger (1978) and McKittrick (1979) demonstrated a simplification of these basic mechanisms. As illustrated in Fig. (2.9), an axial load is applied to a sample of granular material. Because of dilation, the lateral strain is more than half the axial strain Fig. (2.9.A). If reinforcing elements are placed within the

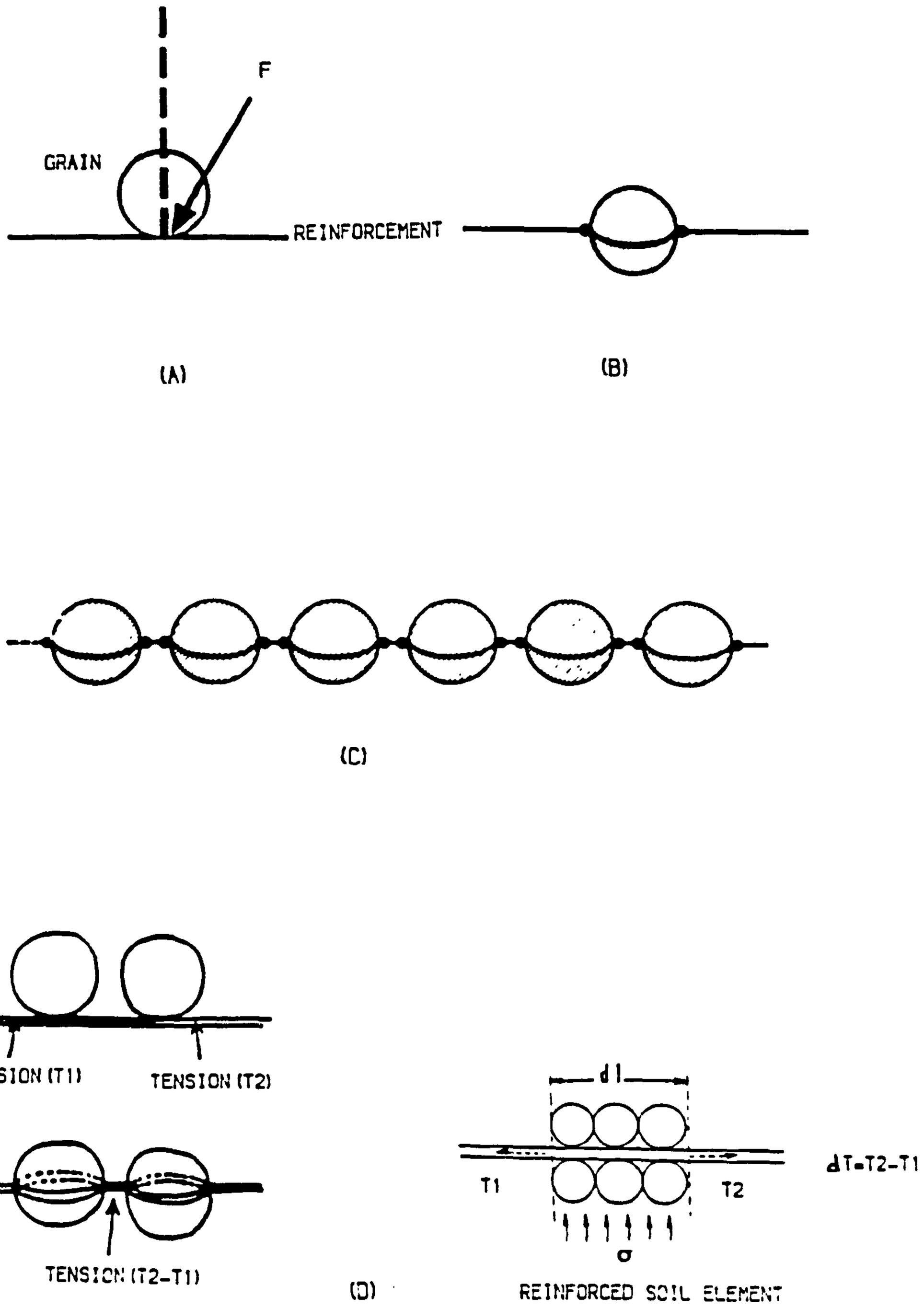

FIG. (2.8) STRESS CONCEPT (AFTER VIDAL, 1969&1978).

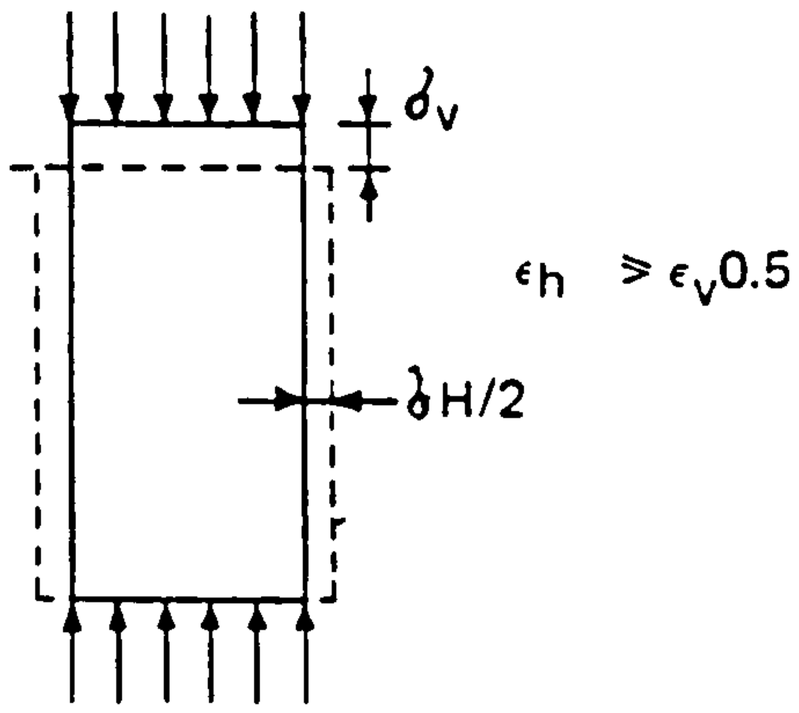

(A) DENSE SAND AND NO REINFORCEMENT.

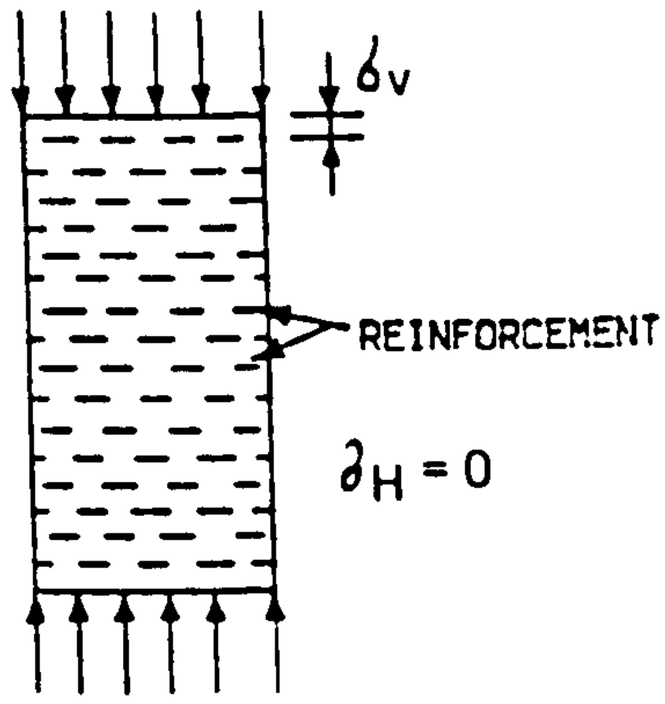

(B) WITH REINFORCEMENT

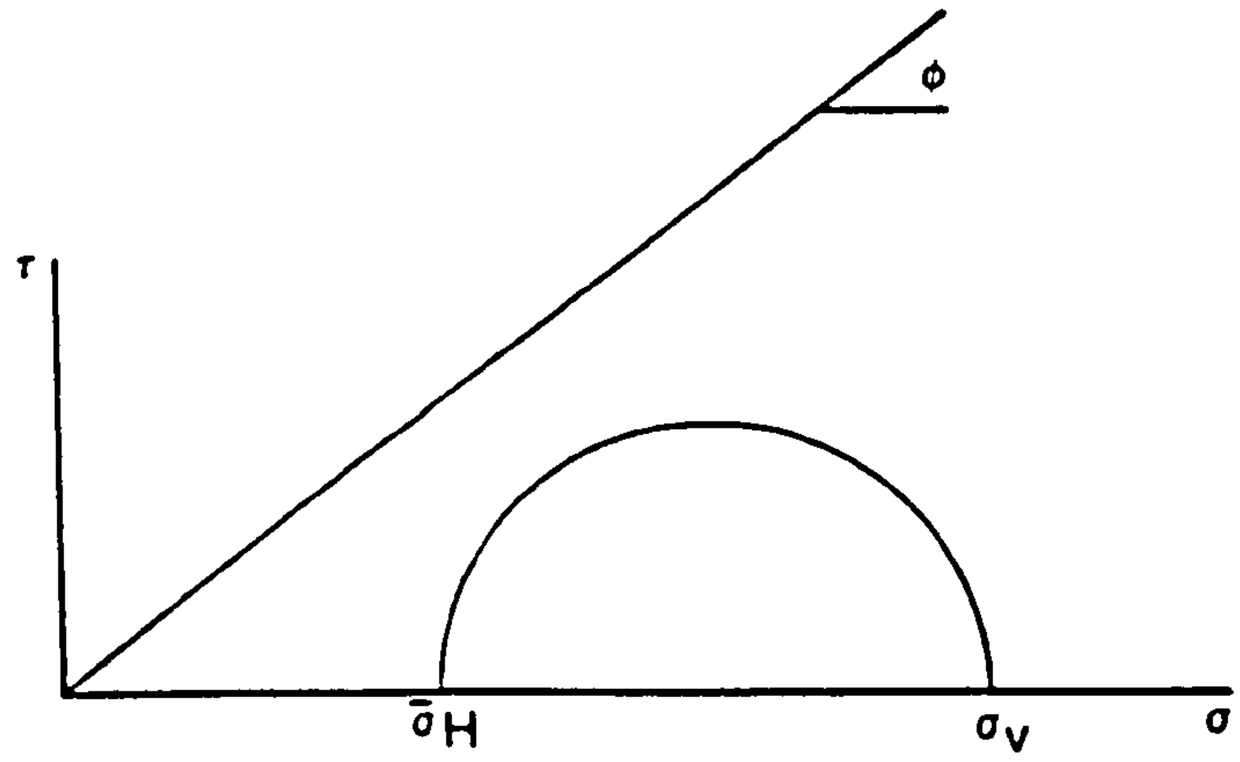

(C) MOHR'S CIRCLE

FIG. (2.9) STATE OF STRESS IN REINFORCED EARTH (AFTER McKITTRICK, 1979).

soil mass as shown in Fig. (2.9.B) these reinforcements will prevent lateral strain because of friction between the reinforcing elements and the soil, and the behaviour will be as if a lateral restraining force had been imposed on the element.

This equivalent lateral load on the soil element is equal to the earth pressure at rest ($K_o.\sigma_v$). Each element of the soil mass is acted upon by a lateral stress equal to ($K_o.\sigma_v$). Therefore, as the vertical stresses increase the horizontal restraining stresses or lateral forces also increase in direct proportion.

Thus for any value of the angle of internal friction, φ, normally associated with granular soil, Mohr's circle of stress lies well below the rupture curve at all points. Failure can occur only by loss of friction between the soil and reinforcements, or by tensile failure of the reinforcements.

2.3.2 Strain Concept

Bassett and Last (1978), have considered the modification of the strain field of a soil caused by the addition of reinforcement, which involves anisotropic restraint of the soil deformation in the direction of the reinforcement. The Mohr's circles of stress and strain are shown in Fig. (2.10.A&B) respectively and α and β are planes at A & B across which the strain $\dot{\epsilon}$ equals zero. The physical conditions delineated by the α & β directions are important, as within the arc segment containing the minor principal strain direction $\dot{\epsilon}_3$ all normal strain will be tensile and hence any reinforcement would be effective, Fig. (2.10.C).

The α & β directions for various points in a strain field can be joined to form zero extension characteristics and represent the potential slip or rupture

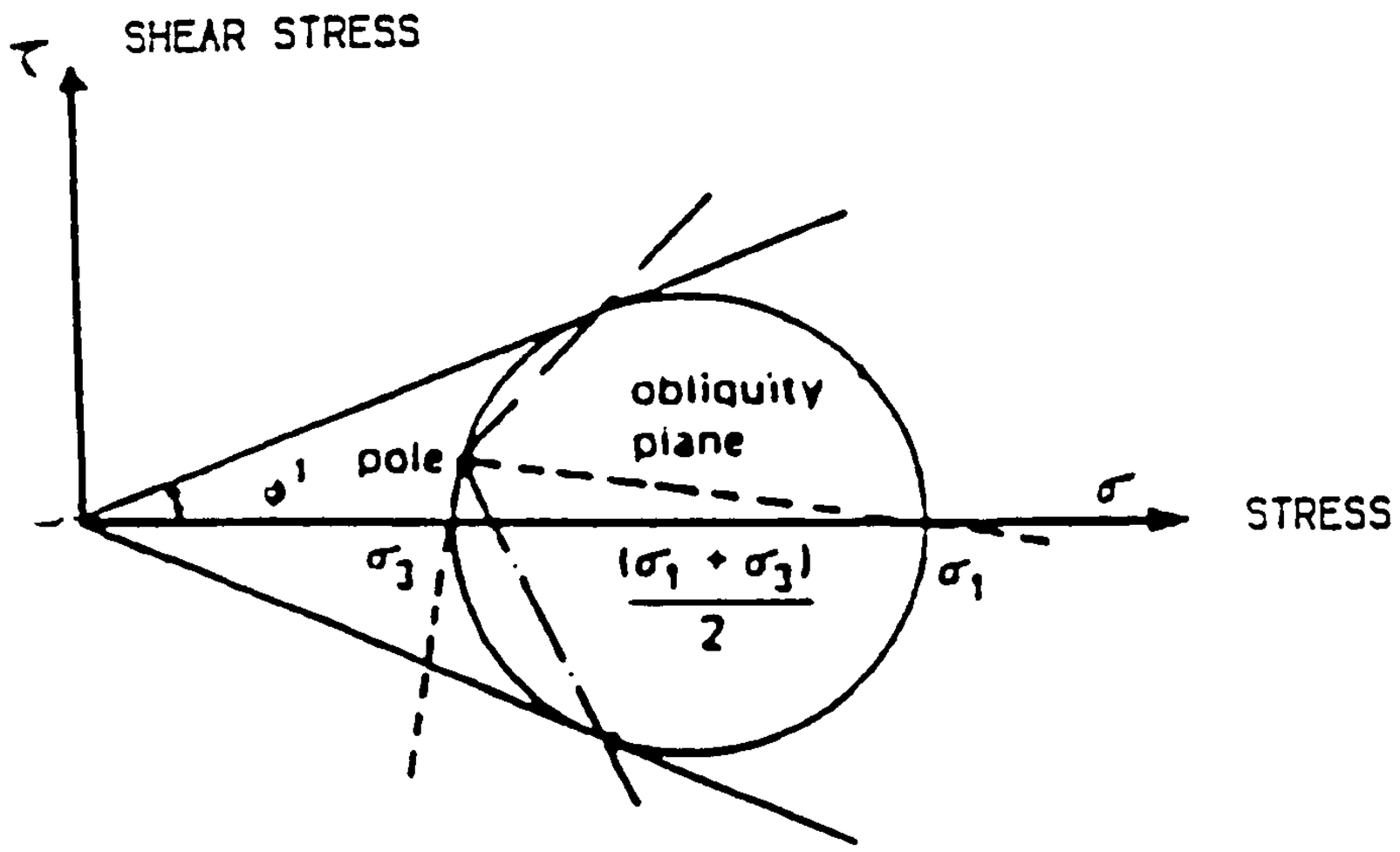

FIG. (2.10.A) MOHR'S CIRCLE OF STRESSES (AFTER BASSET AND LAST, 1978).

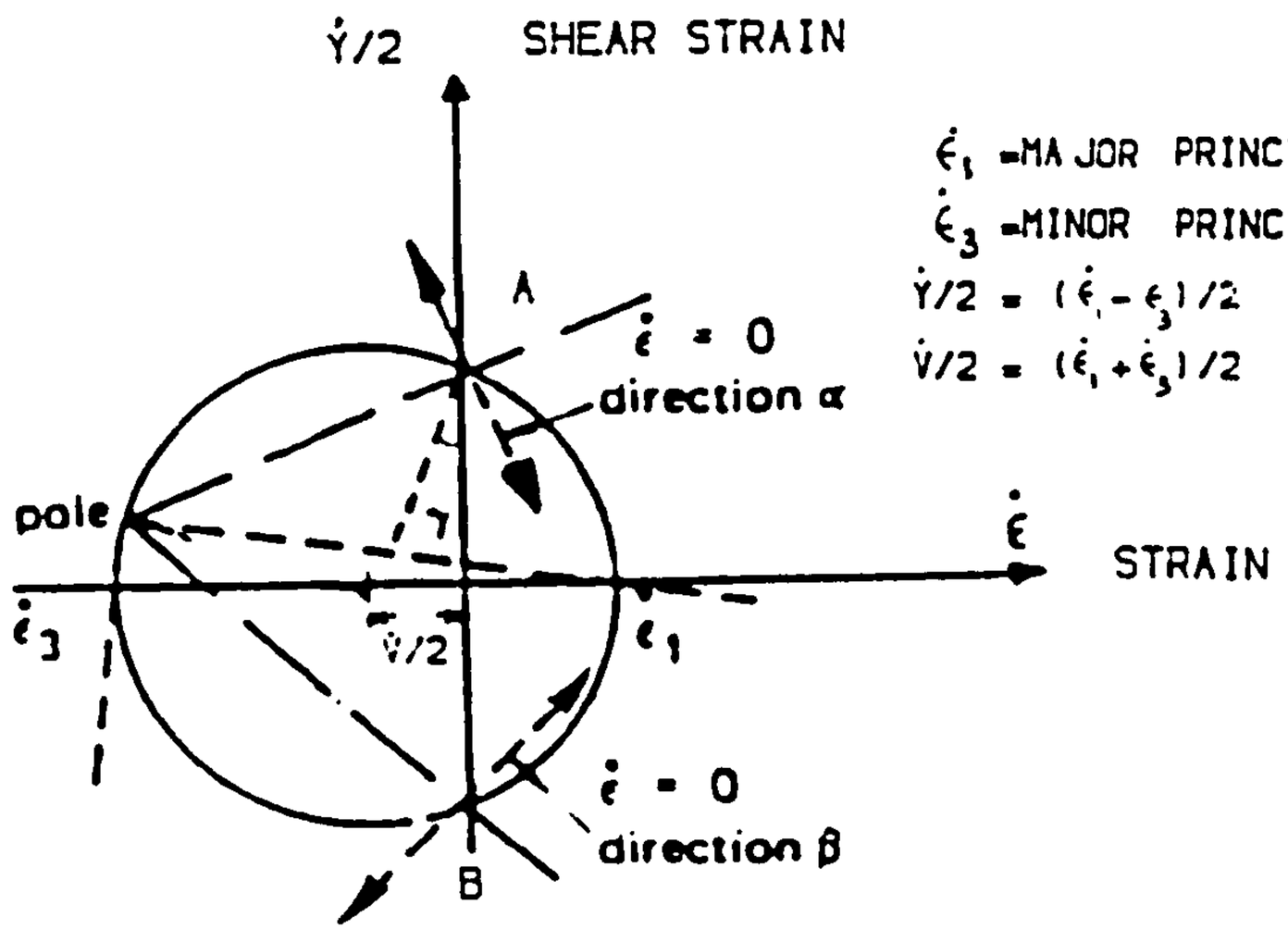

FIG. (2.10.B) MOHR'S CIRCLE OF STRAINS (AFTER BASSET AND LAST, 1978).

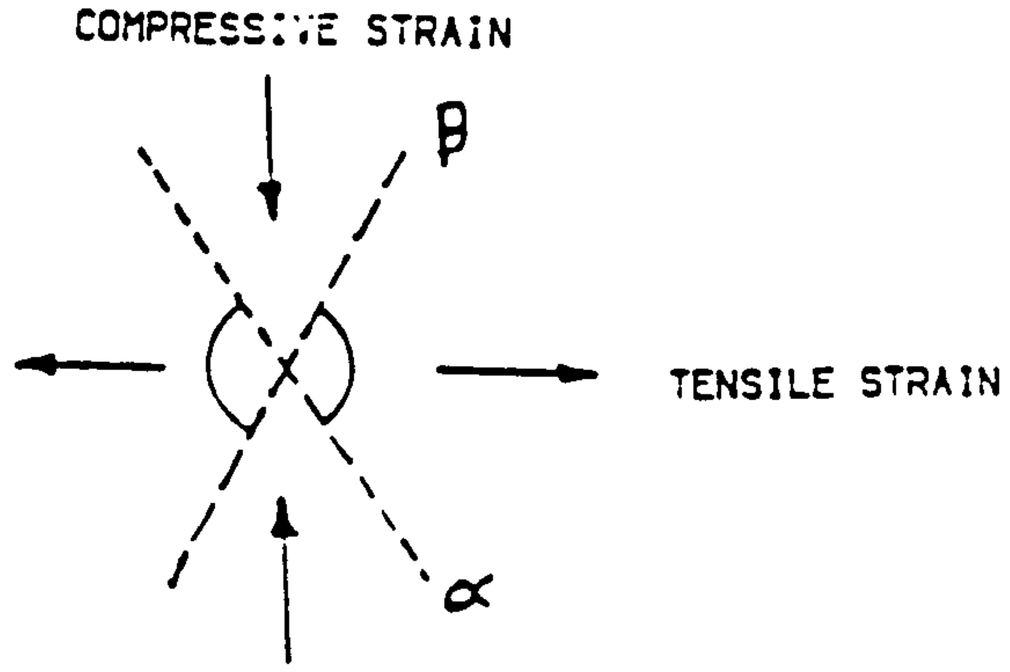

FIG. (2.10.C) PHYSICAL CONDITION FROM α AND β CHARACTERISTICS (AFTER BASSET AND LAST, 1978).

planes as shown in a cantilever wall with sand backfill, Fig. (2.11.A).

The presence of reinforcement has the effect of substantially realigning the potential failure plane as shown in Fig. (2.11.B). Such realignment is in substantial conformity to the locus of maximum tensile strains measured in several full scale structures as shown in Fig. (2.12.A).

Schlosser and Long (1974), Mitchell and Schlosser (1979), and Ingold (1980, 1981 & 1982) arrived at the following conclusion:

There are two well defined zones within the reinforced earth mass, the active zone, adjacent to the facing units, and the restraining zone. The dividing line between these two zones is the locus of the points of maximum reinforcement tension, where the shear stress on the reinforcement is zero. Many researchers in the field of reinforced earth confirm that the tensile force in the reinforcement is not uniform and reaches its maximum value at some distance behind the wall facing. The shear stress distribution is not uniform, its direction is towards the wall face in the active zone, and towards the free end of reinforcement in the restrained zone as shown in Fig. (2.12.B).

2.4 FIELDS OF APPLICATION

At present, reinforced earth is an effective and reliable technique for increasing the strength and stability of soil and has found increasing popularity in a variety of engineering applications including retaining structures, embankments, stabilization of subgrades beneath footings and pavements and stabilization of fill slopes (Benltayef and Subrahmanyam, 1989).

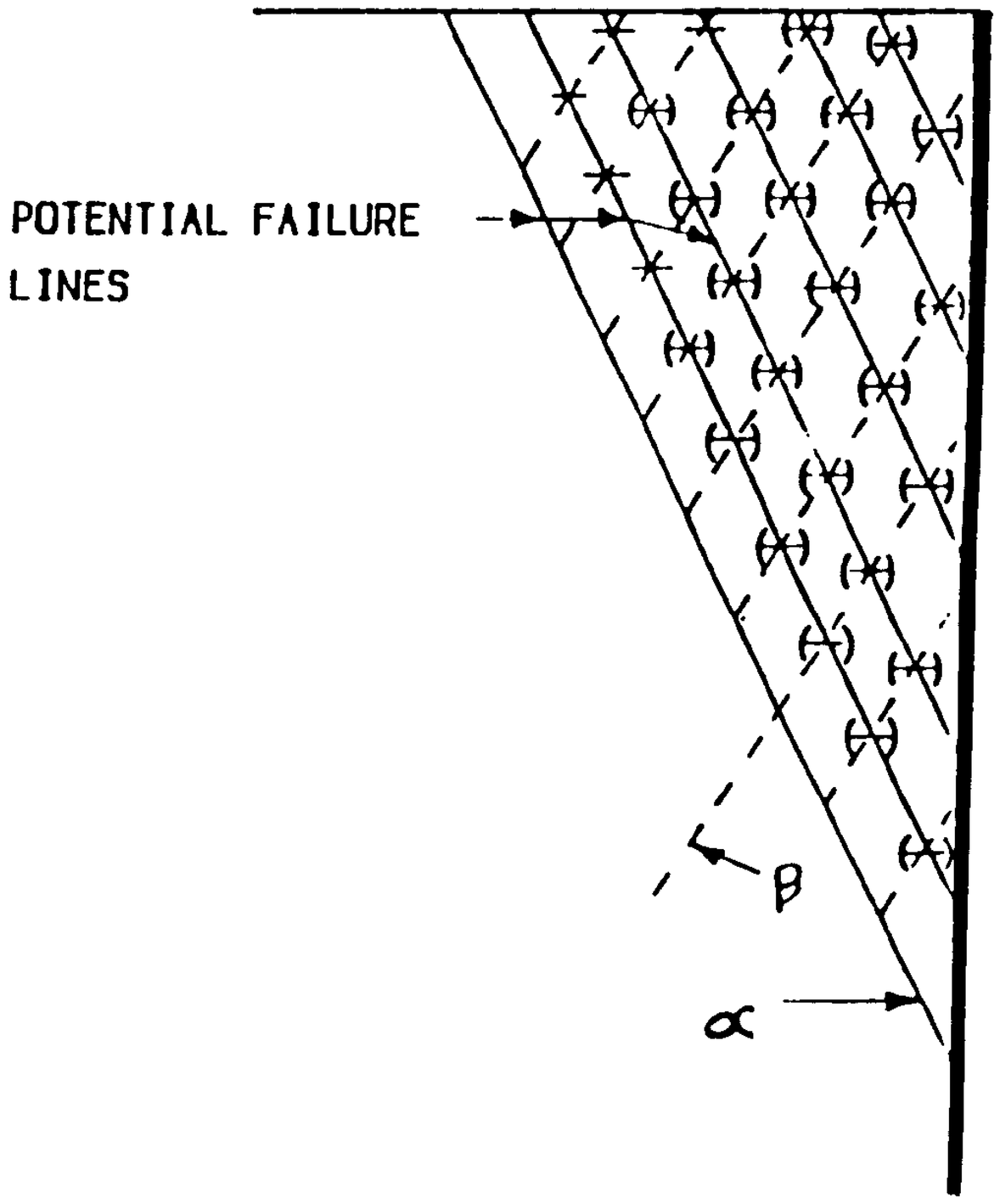

(A) CLASSICAL RETAINING WALL (AFTER MILLIGAN, 1974).

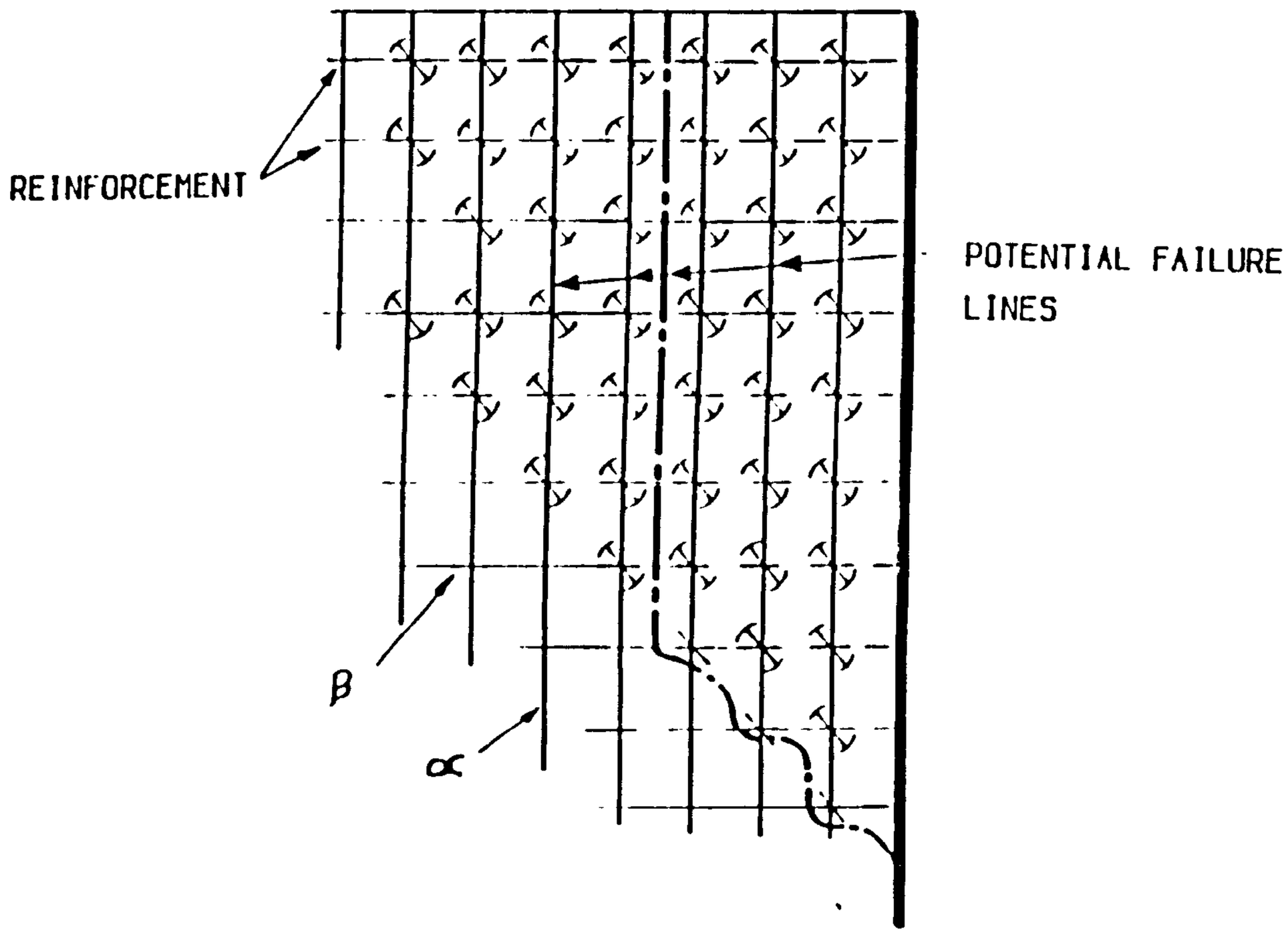

(B) REINFORCED EARTH WALL (AFTER BASSET AND LAST, 1978).

FIG. (2.11) ZERO EXTENSION CHARACTERISTICS (α & β) AND POTENTIAL FAILURE LINES FOR SAND AND REINFORCED SAND STRUCTURES.

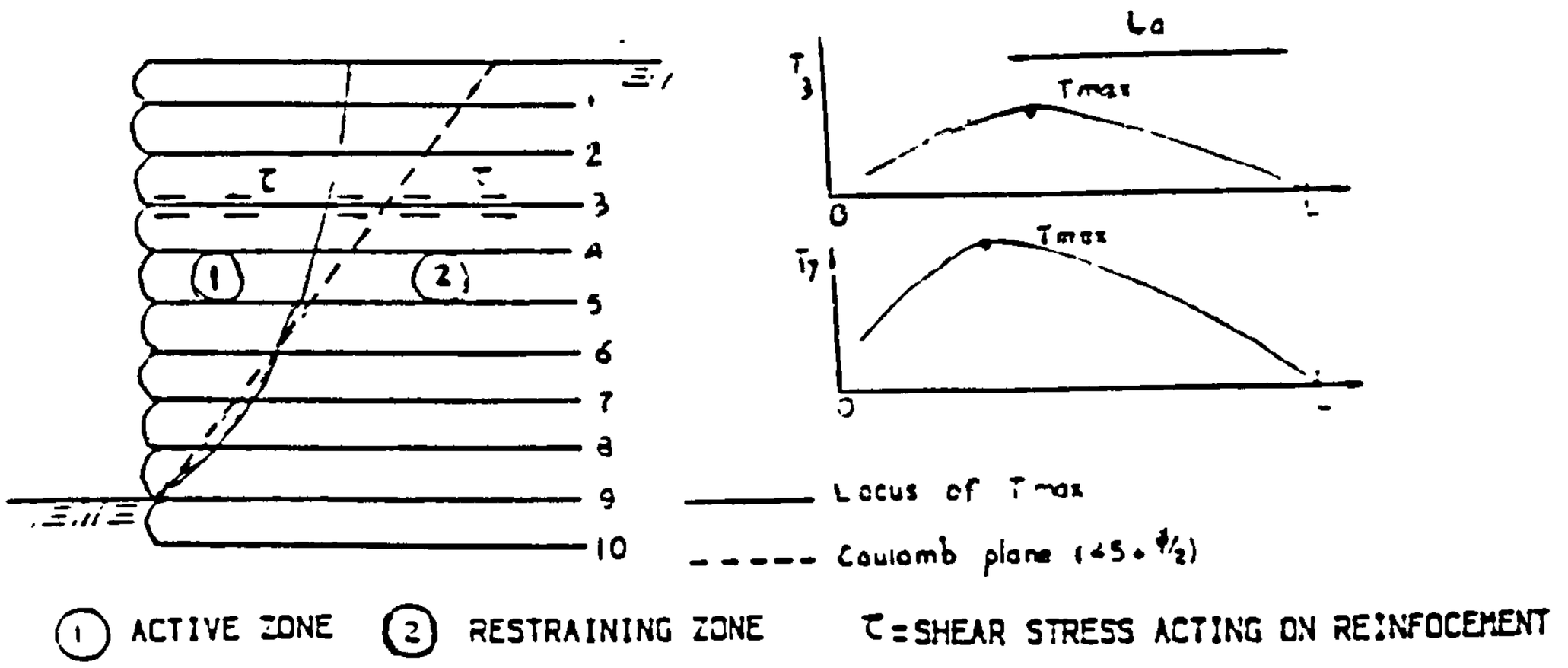

FIG. (2.12.A) ACTIVE AND RESTRAINING ZONES IN A REINFORCED MASS AND TENSILE FORCE DISTRIBUTIONS IN REINFORCEMENT (AFTER SCHLOSSER&LONG, 1974).

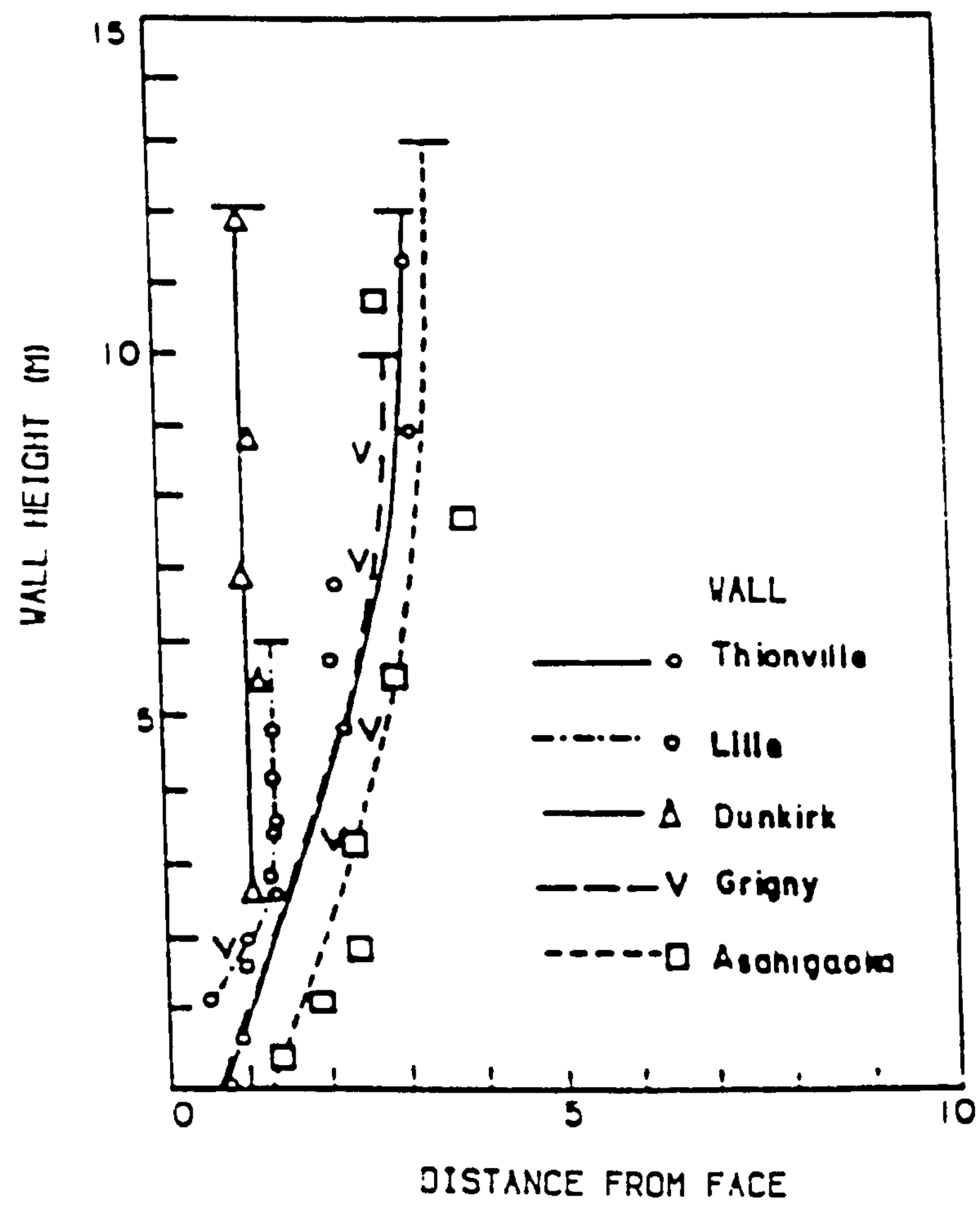

FIG. (2.12.B) LOCUS OF POINTS OF MAXIMUM TENSION IN SOME FULL SCALE REINFORCED EARTH WALLS IN FRANCE (AFTER SCHLOSSER, 1977).

Reinforced earth has been applied in a wide range of civil engineering works, and is an extremely versatile system. The simplicity and the advantages of reinforced earth has led to the widespread use of earth reinforcement for a wide range of earthwork construction and soil improvement applications. Over 2200 reinforced earth structures have been completed all over the world within the period 1968–1979, McKittrick and Darbin (1979), and up to 4000 structure up to 1982 (Ingold, 1982). The growth of the use of reinforced earth world wide has been phenomenal. Recently in a brief history of reinforced earth, Vidal reported that more than ten thousand reinforced earth structures have been built and three structures are completed and placed in service every day somewhere in the world (Vidal, 1986). Examples of fields of application are shown in the following sections.

2.4.1 Foundation Mats And Slabs

A foundation mat was constructed to support a canal that had to pass over a section of ground containing gypsum beds where cavities could be expected due to flowing. A roof was formed over a uranium mine in Gabon. Both structures were made with wire mesh as reinforcement inside a mass of granular soil, Vidal (1969).

An example is shown in Fig. (2.13.A) of a foundation mat to stabilize the soil under a highway in the U.S.A, (Steiner, 1975). The slab is 1 m high with semi–elliptical steel facing units forming the perimeter of the slab. Reinforcing strips were spaced at 127 mm horizontal centres in various lengths and were bolted end to end. A selected granular backfill was placed (300 mm thick for each layer).

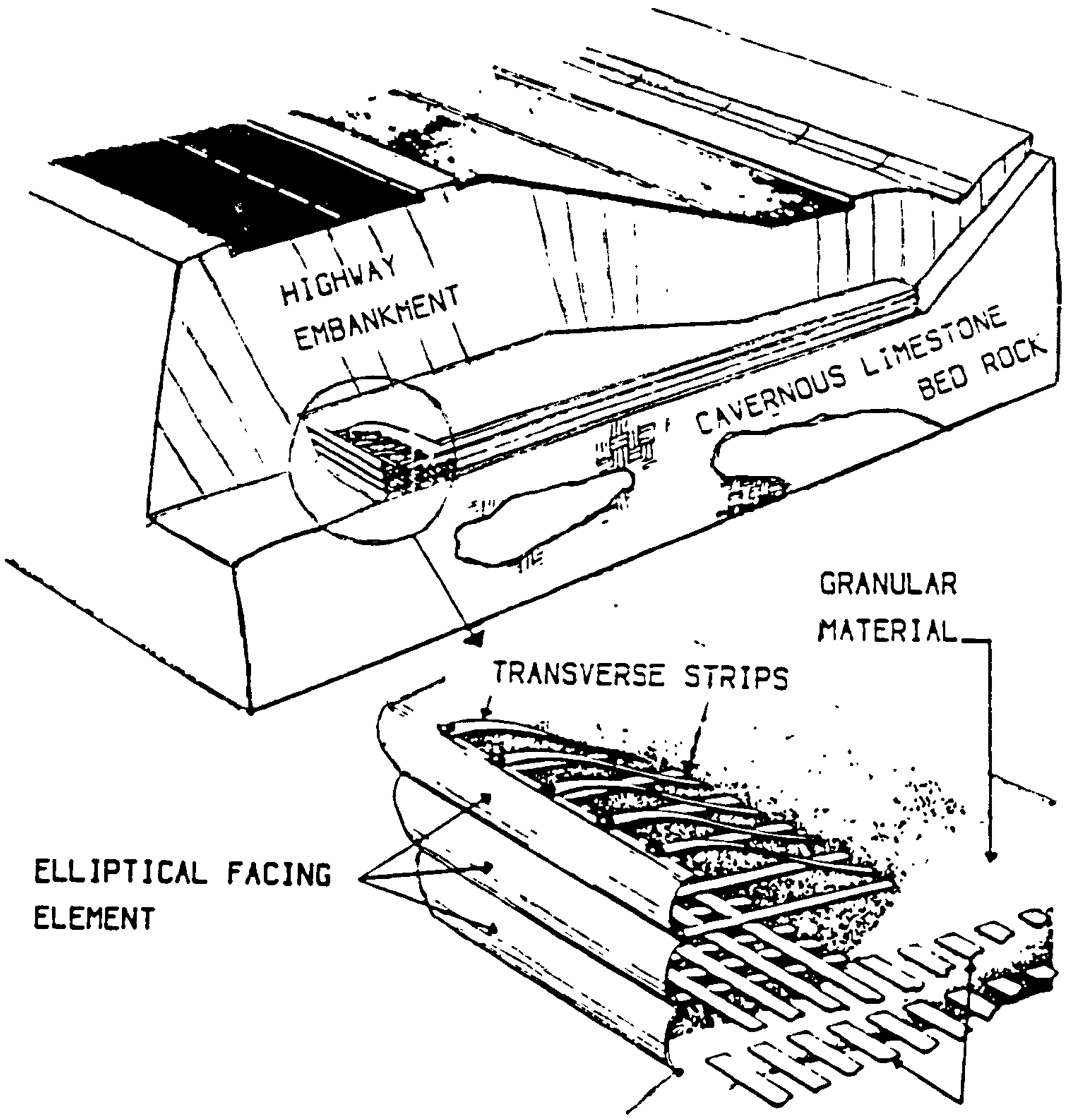

FIG. (2.13.A) REINFORCED EARTH FOUNDATION MATS (AFTER STEINER, 1975).

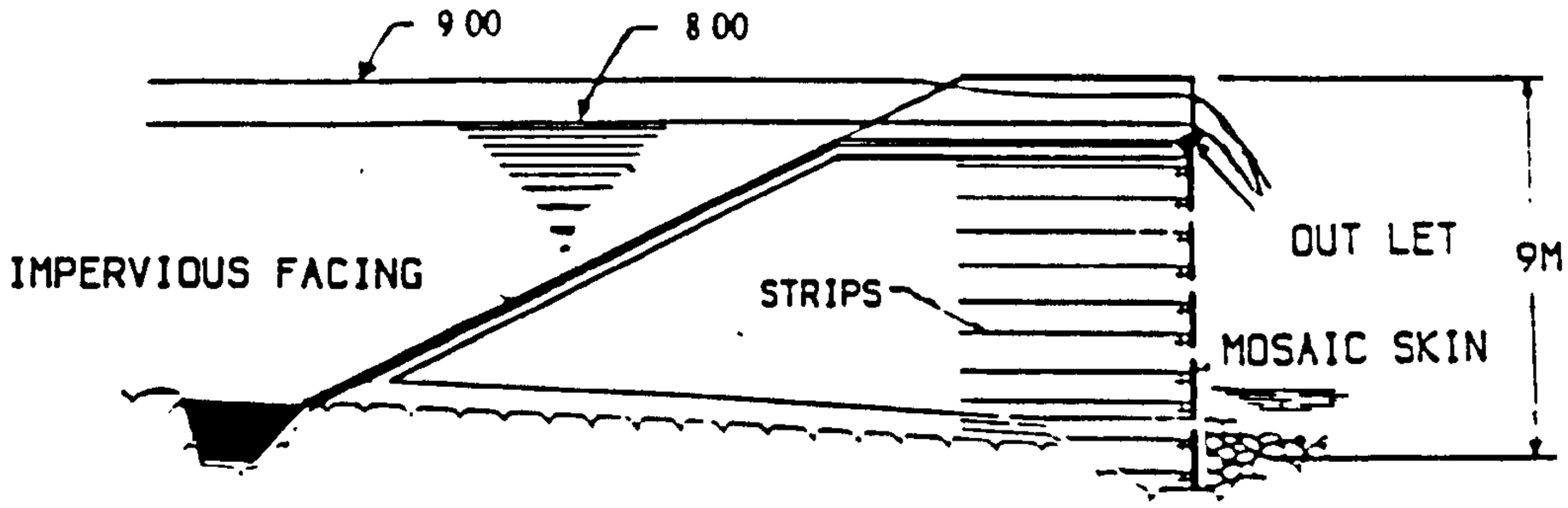

FIG. (2.13.B) BIMES VALLEY DAM IN FRANCE (AFTER CASSARD ET AL., 1979).

2.4.2 Dams

Cassard et al. (1979) reported that the first reinforced earth dam constructed was one 9 m high in the Bimes valley in the south of France. A typical cross section can be seen in Fig. (2.13.B). The dam was constructed with a vertical downstream face formed with interlocking precast concrete facing units. Reinforcing strips with a length equal to 80% of the height of the dam were connected to the facing units. The earth fill has a slope of 1:2 at the upstream face, and was sealed with a bitumen impregnated, nonwoven fabric. The crest of the dam has a width equal to 20% of the dam height.

2.4.3 Embankments

The reinforcing of embankments may be undertaken in three main ways as shown in Fig. (2.14.A). An example of a railway embankment constructed in Japan is shown in Fig. (2.14.B). The use of superficial slope reinforcement was pioneered by the Japanese, particularly in railway embankments (Ingold, 1982). Another example is a snow avalanche barrier at Analsnes in Norway of height 6 m and slope 2:1 and another embankment with a steep slope has been constructed in Oslo (Fannin and Hermann, 1988).

2.4.4 Reinforced Earth Walls

Most reinforced earth structures built world–wide are retaining walls. DuBois (1981) reported that approximately 80% of 2000 reinforced earth structures were retaining walls. Juran and Christopher (1989) stated that reinforced soil has been extensively used during the last decade in the construction of embankments and retaining walls. The application to walls has

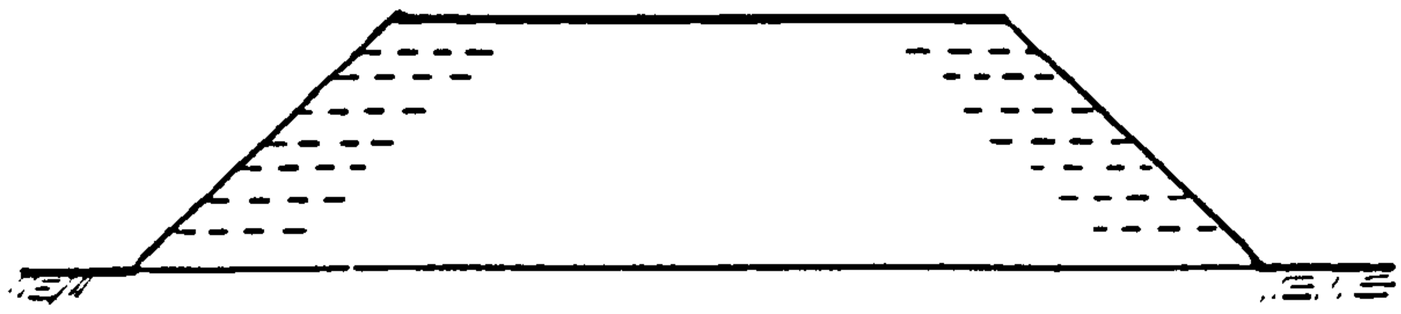

(A) SURFICIAL EMBANKMENT REINFORCEMENT

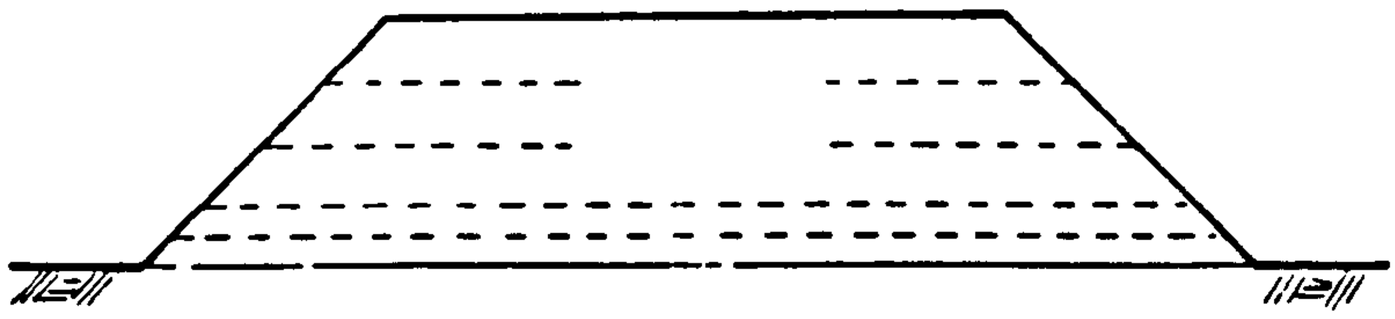

(B) MAJOR EMBANKMENT REINFORCEMENT

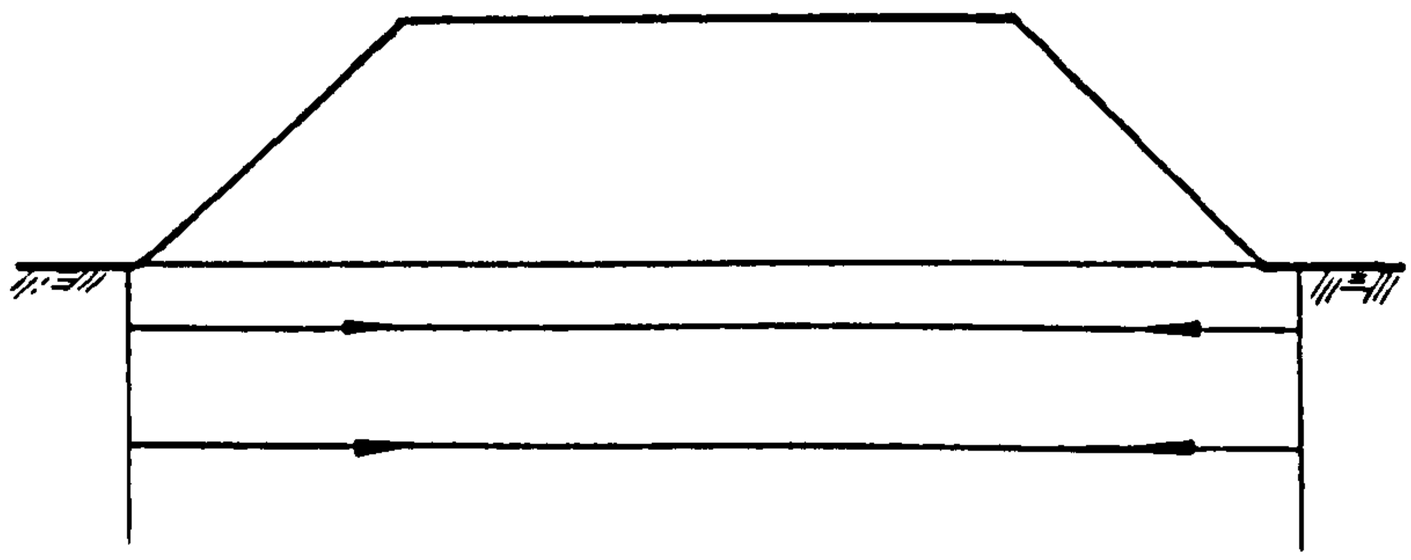

(D) EMBANKMENT FOUNDATION REINFORCEMENT

FIG. (2.14.A) MODES OF EMBANKMENT REINFORCEMENT (AFTER INGOLD, 1982).

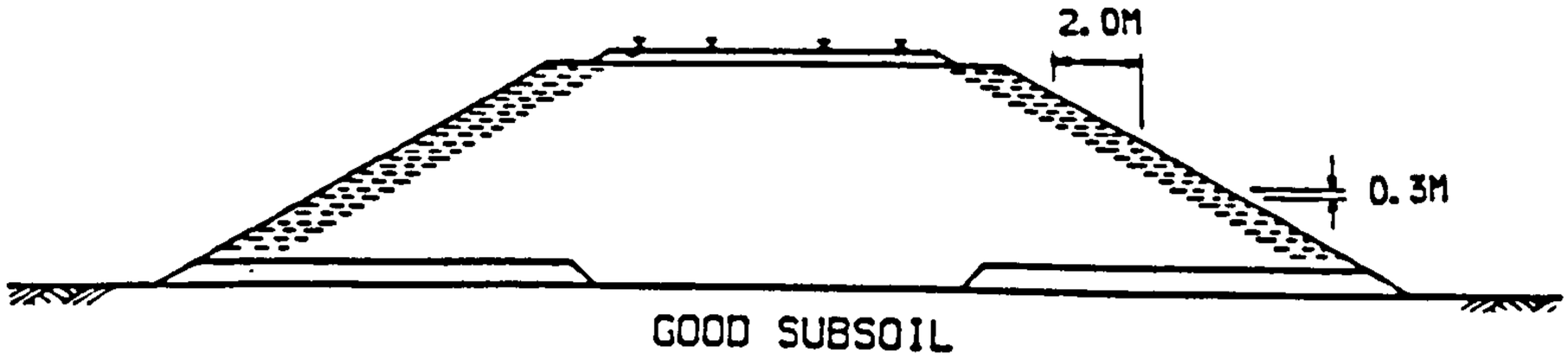

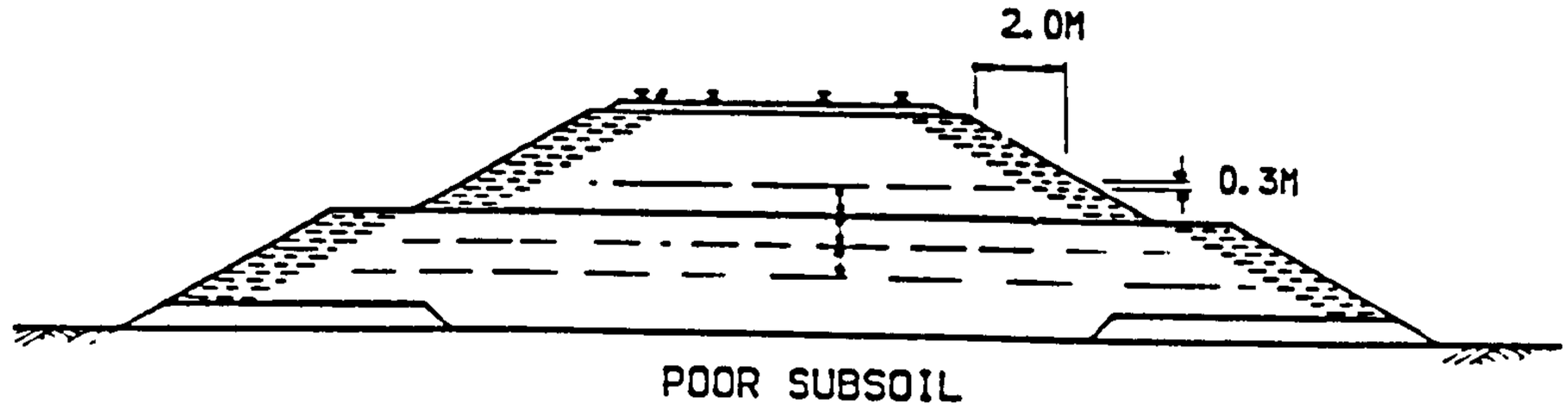

FIG. (2.14.B) RAILWAY REINFORCED EMBANKMENT IN JAPAN (AFTER UEZAWA ET AL., 1975).

ranged from earthquake–resistant walls (McKittrick and Wojciechowski, 1979) to blast–proof nuclear reactor containments (Reddy et al., 1979). Examples are shown in Fig. (2.15.A) for bulk storage and handling units in France using reinforced earth walls. McKittrick and Darbin (1979) reported one of the applications of reinforced earth walls, the slot storage system shown in Fig. (2.15.B). A reinforced earth wall 26.0 m high built for the rock crushing plant at Tarbela dam, Price (1975), is shown in Fig. (2.16.A).

The first reinforced earth structure in a marine environment was in Brunswick in the U.S.A (Al–Hussaini and Perry, 1976). The wall , 336.00 m long and 11.00 m high, was constructed in the dry behind a temporary earth dike. It consisted of interlocking precast concrete panels and aluminium–magnesium alloy reinforcing ties.

The largest application of reinforced earth walls has been in the construction of highways and bridges. Examples are shown for the French Italian highway in Figs. (2.16.B&C) respectively, Vidal (1969 & 1970). The first is the Peyronnet structure which was built to retain a large slope 61.00 m high, and the second at Vigna, was built on a high slope at an angle of 35 degrees.

Other examples of the application of reinforced earth walls in the highways field are walls constructed in the U.K..

The first example is the wall built at Granton just north of Edinburgh as a part of the A901 road improvement. The wall, 106 m long, varied in height between 1.8 m and 7.2 m and was partly curved in plan as shown in Fig. (2.17). The facing panels were concrete panels 180 mm thick of interlocking shape 1.5 m square. Four stainless steel strips 80 mm wide and 1.5 mm thick

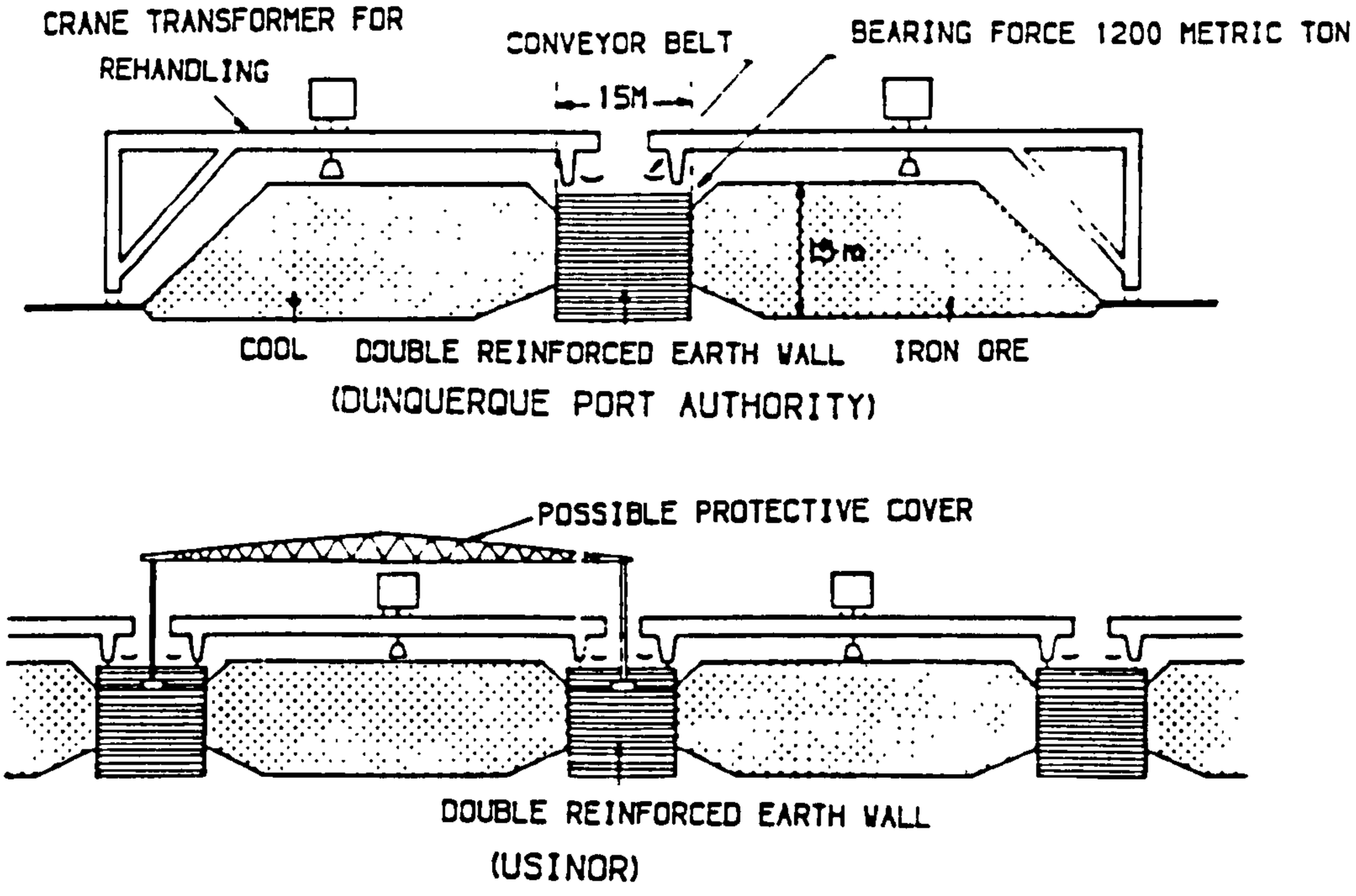

FIG. (2. 15. A) BULK STORAGE AND HANDLING IN FRANCE (AFTER INGOLD, 1982).

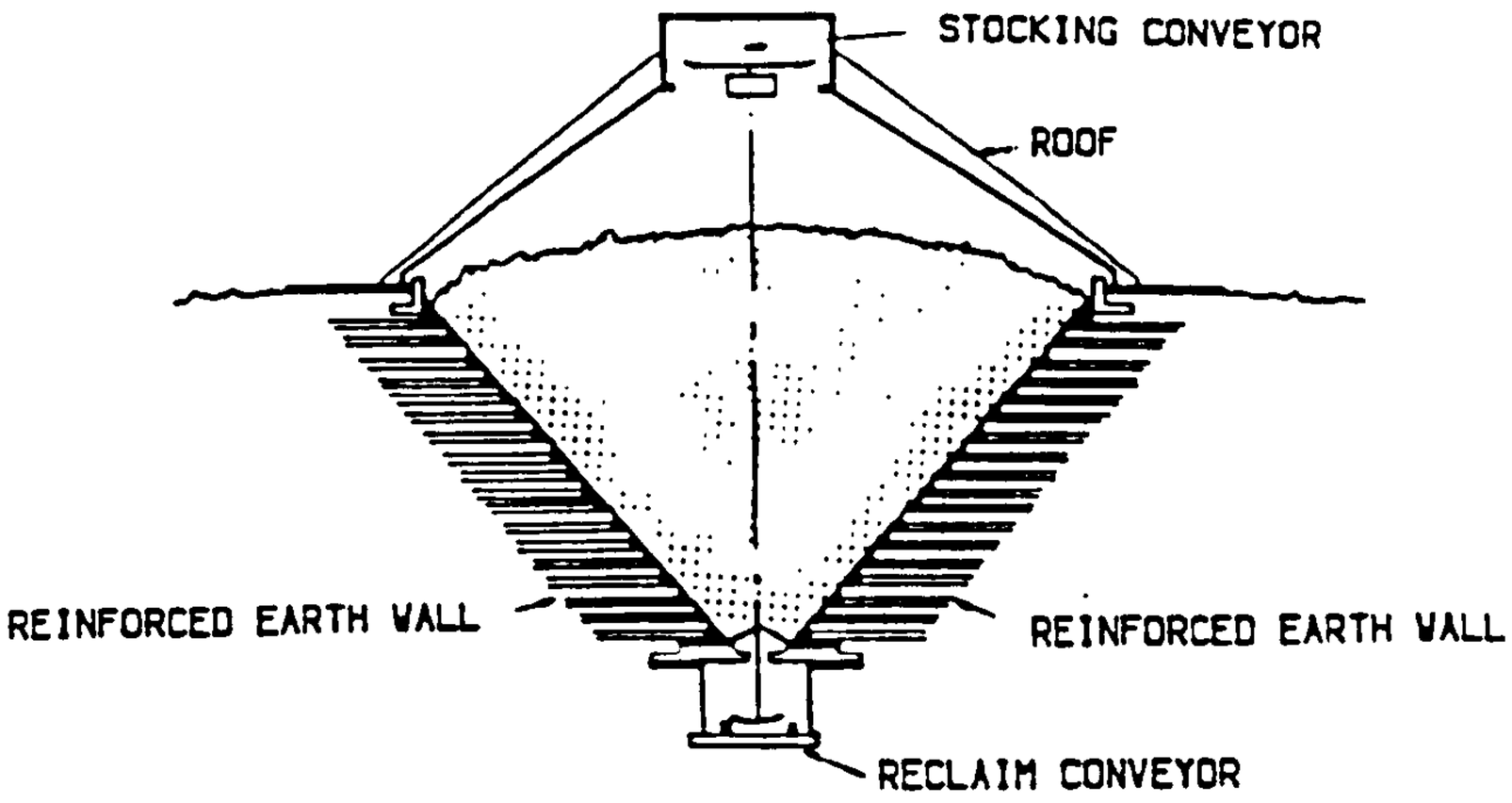

FIG. (2. 15. B) SLOT STRUCTURE FOR COAL STORAGE (AFTER McKITTRICK AND DARBIN , 1979).

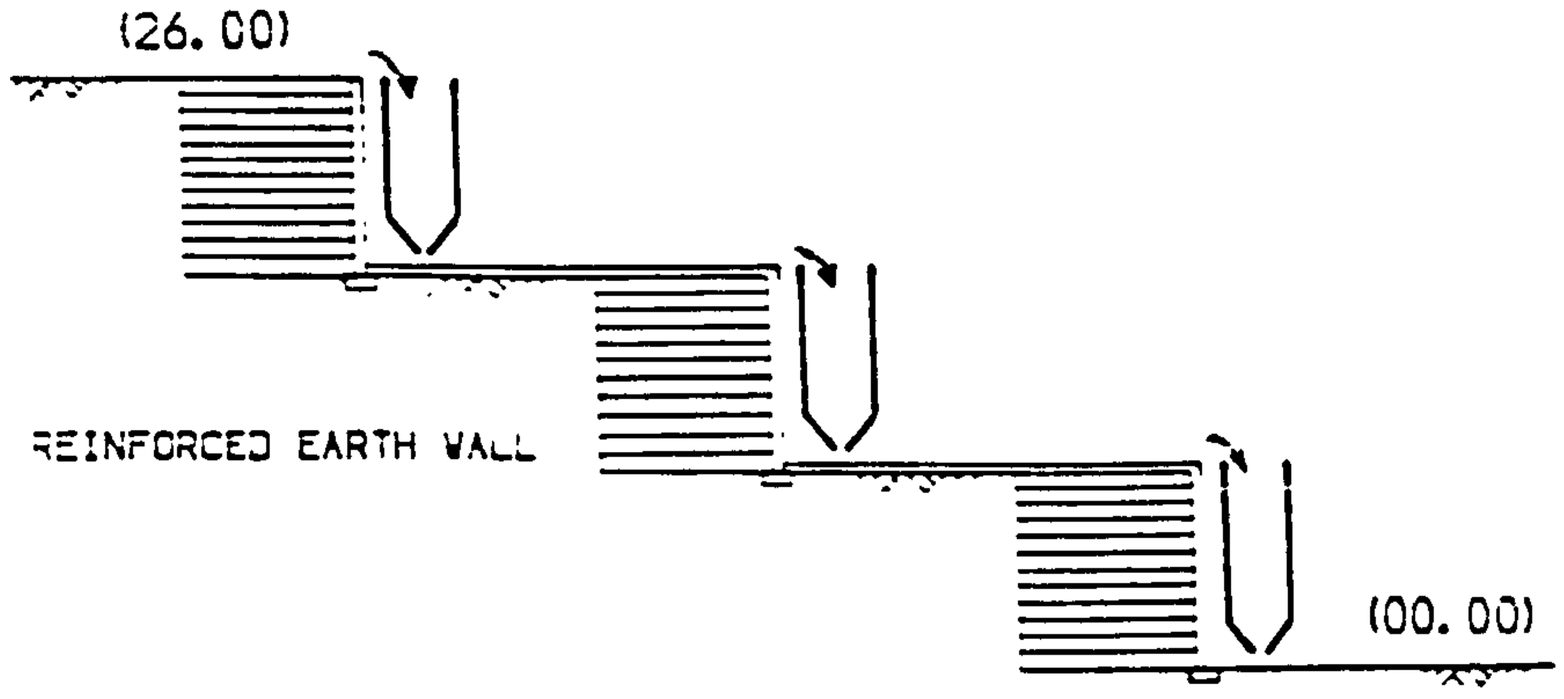

(A) ROCK CRUSHING PLANT WALLS (AFTER PRICE, 1975).

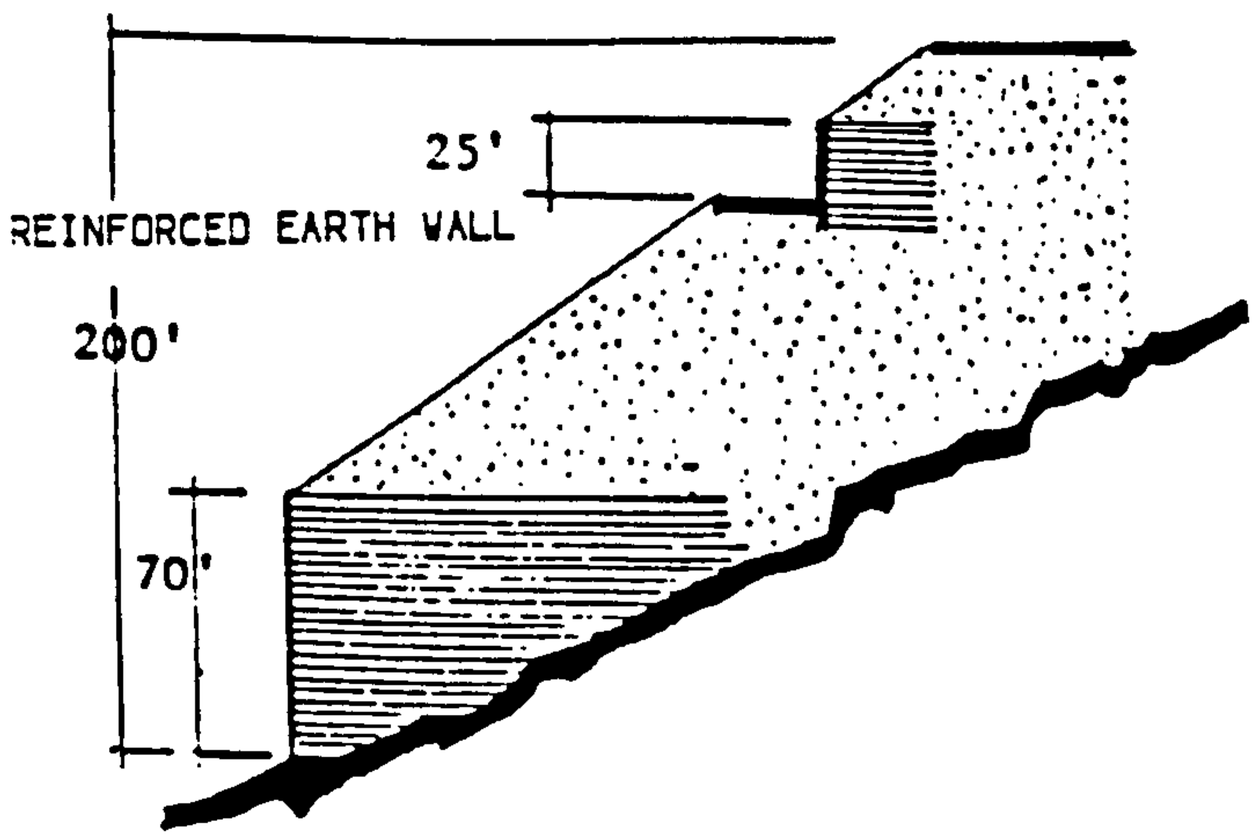

(B) PEYRONNET WALL IN FRANCE (AFTER VIDAL, 1969).

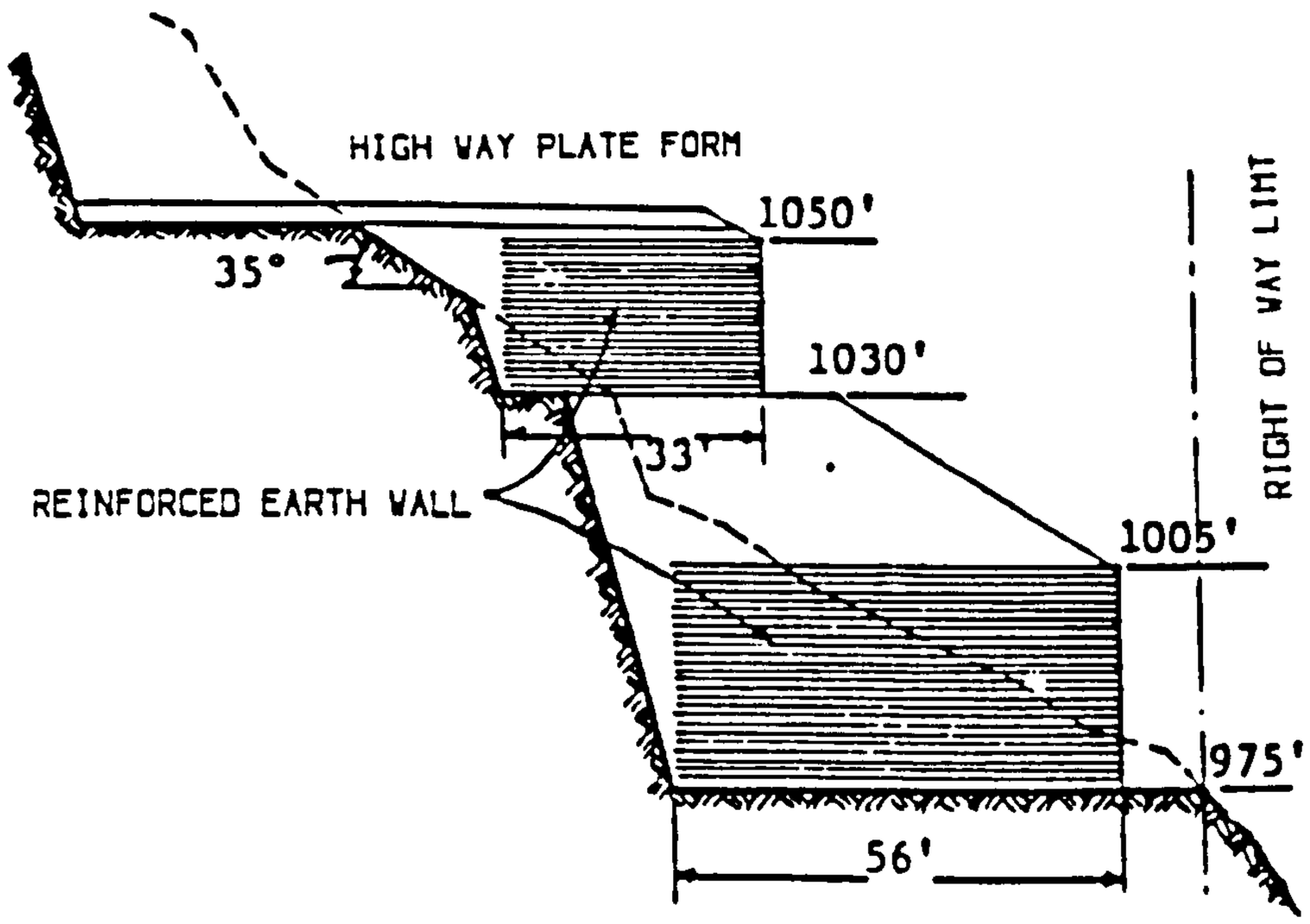

(C) VIGNA WALL IN FRANCE (AFTER VIDAL, 1969).

FIG. (2.16) REINFORCED EARTH RETAINING WALLS SUPPORTING HIGH LEVELS.

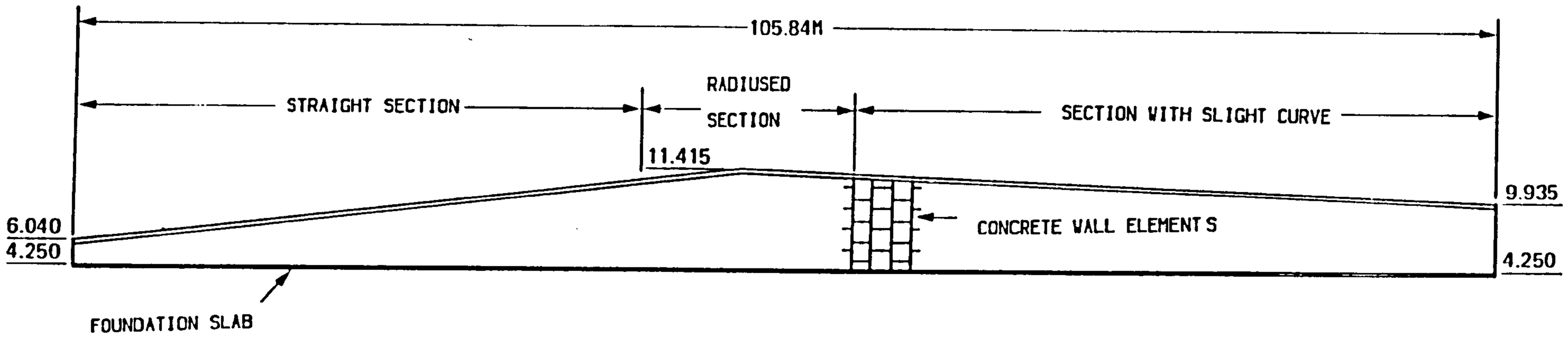

FIG. (2.17) REINFORCED EARTH WALL AT GRANTON IN U.K. (AFTER FINLAY, 1977).

were attached to the back of each panel the strips being up to 6.5 m long. The backfill was burnt oil shale, known as "blaes", Finlay (1977).

The second example is a reinforced earth wall on the A3/A322 interchange road on the Guildford Bypass. The total length of wall was 100 m up to a maximum height of 6 m, as shown in Fig. (2.18.A&B). Light weight facing units of a hexagonal form of precast reinforced concrete were used of dimensions 0.6 m diametrically with a maximum thickness of 0.1 m. The reinforcements were galvanized mild steel strips 5 m long, 75 mm wide and 5 mm thick. The backfill material was a well graded sand gravel mixture, Murray and Hollinghurst (1986).

An example of one of the highest reinforced earth walls is shown in Fig. (2.19). The wall was built in Chogqing in China and was 26 m high, Quyang (1988).

Another important application of reinforced earth walls is in carrying heavy loads as in the case of abutments. The first major abutment structure was built at Thionville over the Moselle River in 1972 in France to support the 38 m end span of a continuous concrete bridge, Boyd (1988). An example of a reinforced earth abutment is shown in Fig. (2.20).

2.5 CONSTRUCTION METHODS FOR REINFORCED EARTH WALLS

The main components of a reinforced earth wall are facing units, reinforcing elements and selected backfill as shown in Fig. (2.21).

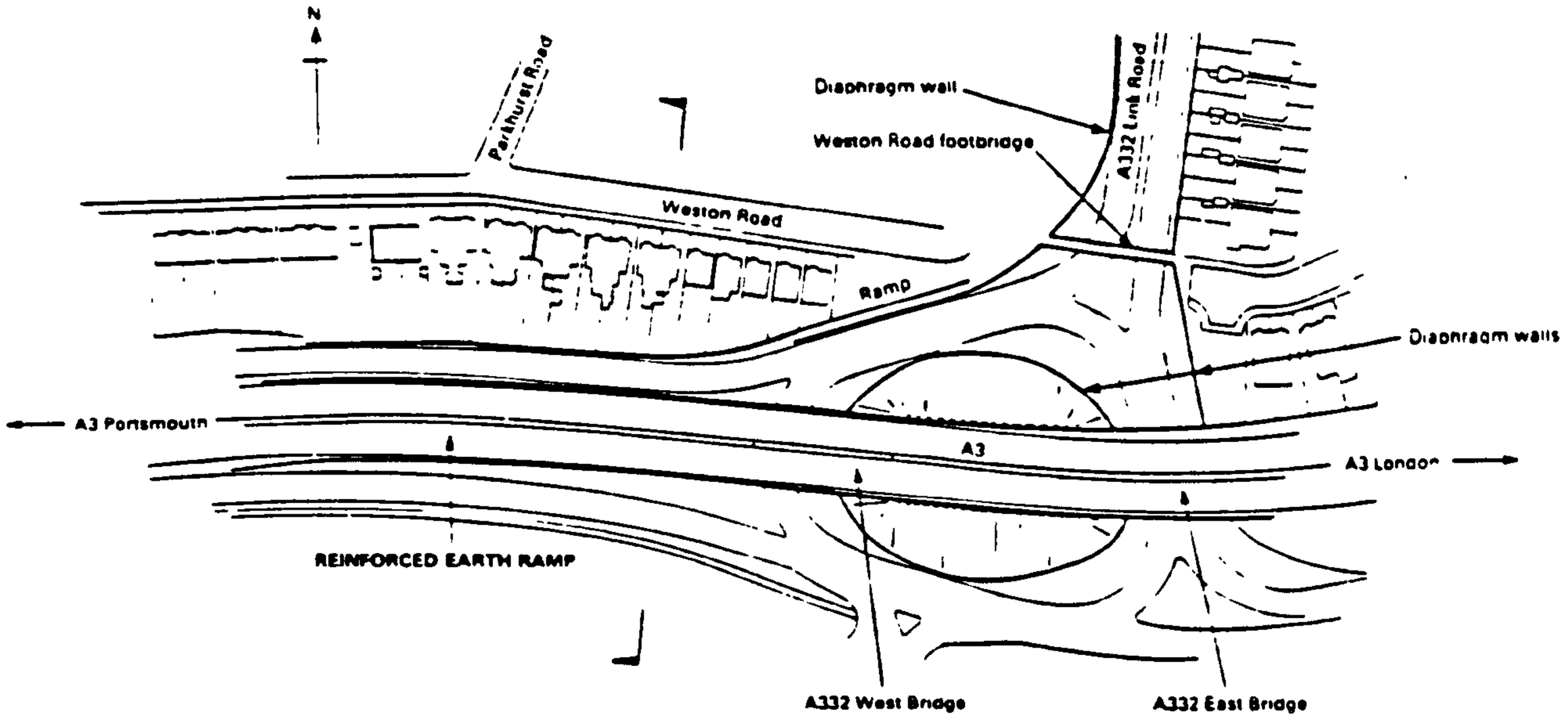

(A) PLAN OF A3/A322 INTERCHANGE AND LOCATION OF REINFORCED EARTH WALL.

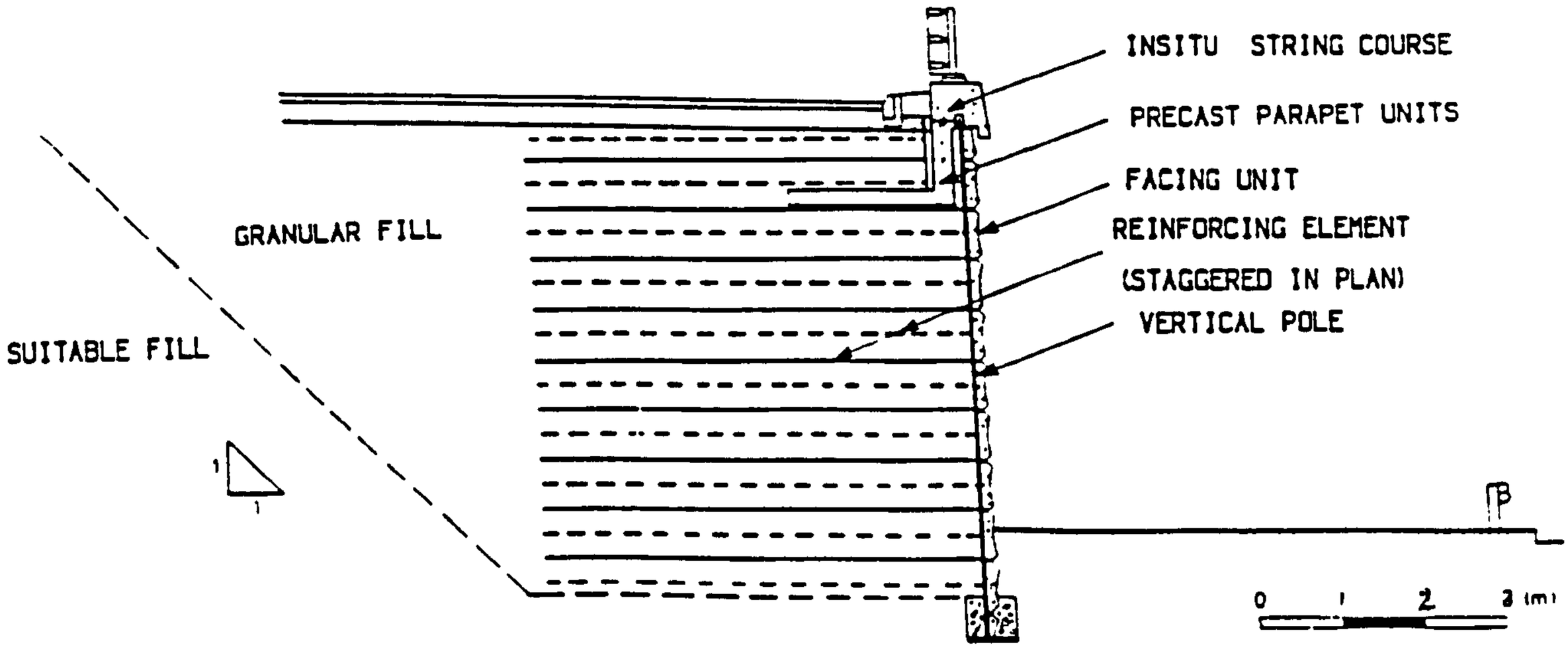

(B) CROSS SECTION OF REINFORCED EARTH WALL AT A3/A332 INTERCHANGE.

FIG. (2.18) REINFORCED EARTH WALL AT A3/A322 INTERCHANGE AT GUILDFORD BYPASS IN U.K. (AFTER MURRAY AND HOLLINGHURST, 1986).

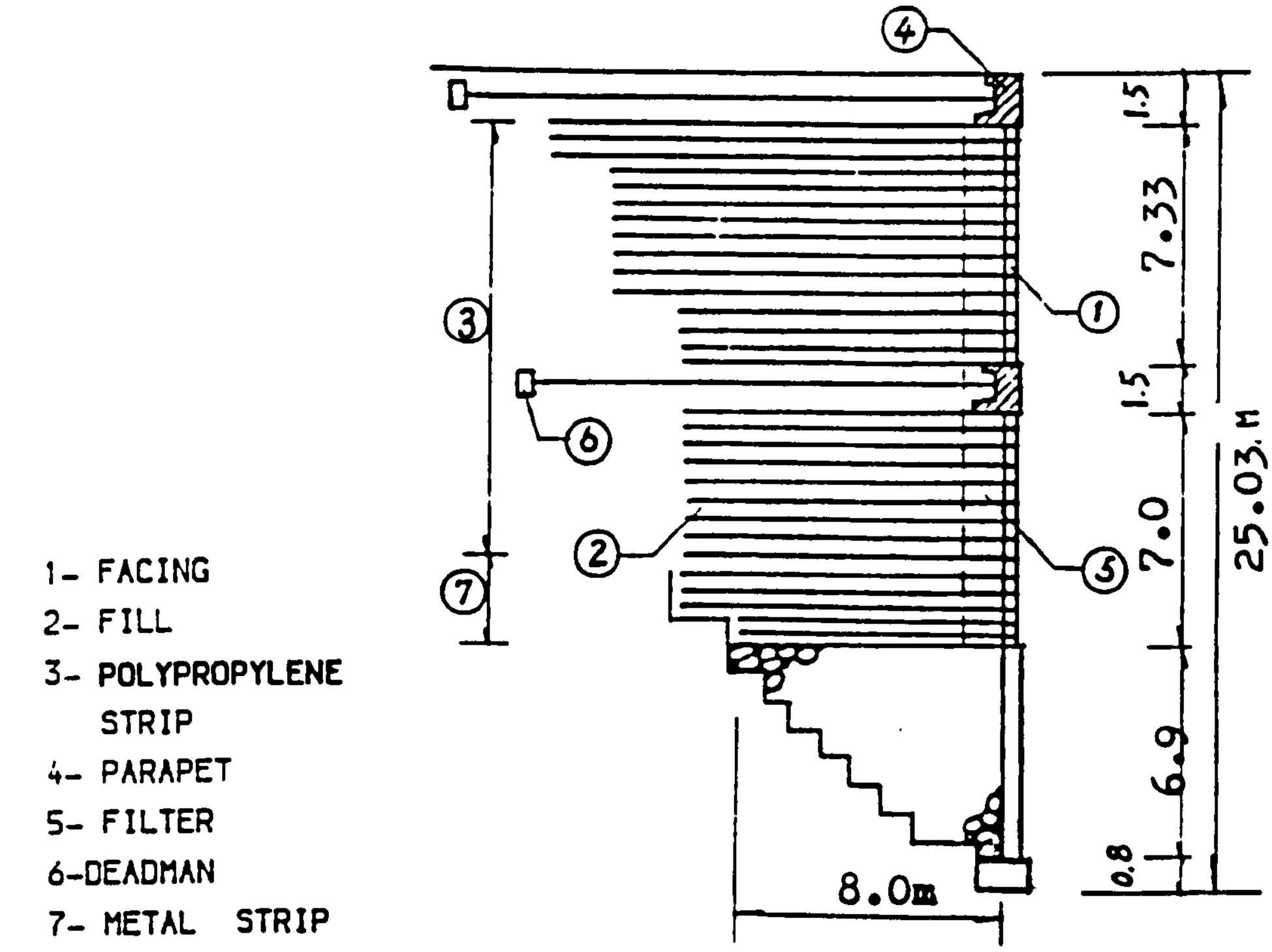

FIG. (2.19) SECTION OF REINFOCED EARTH WALL (AFTER OUYANG, 1988).

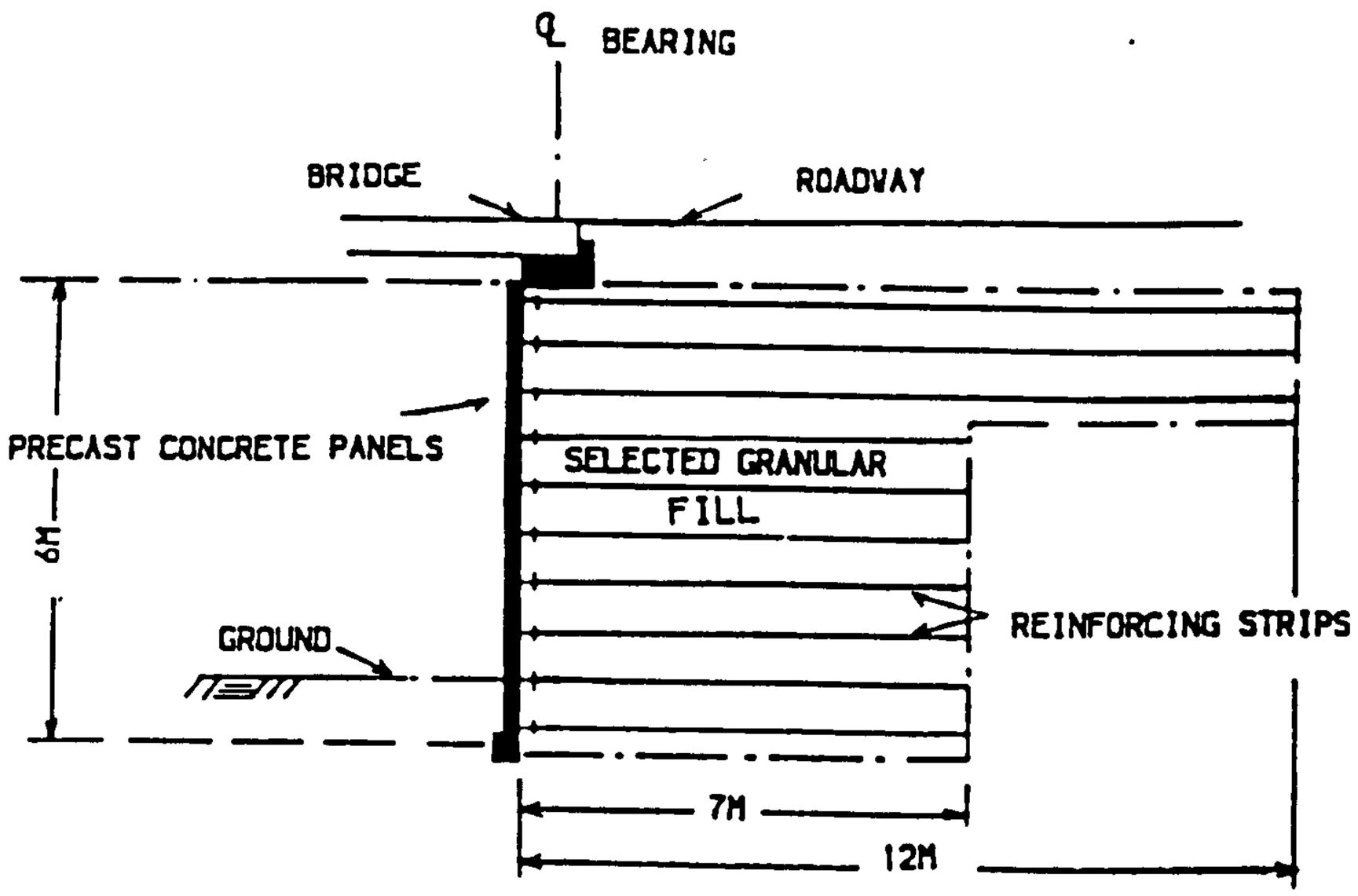

FIG. (2.20) AN EXAMPLE OF REINFORCED EARTH ABUTMENT (AFTER GEDNEY, 1975).

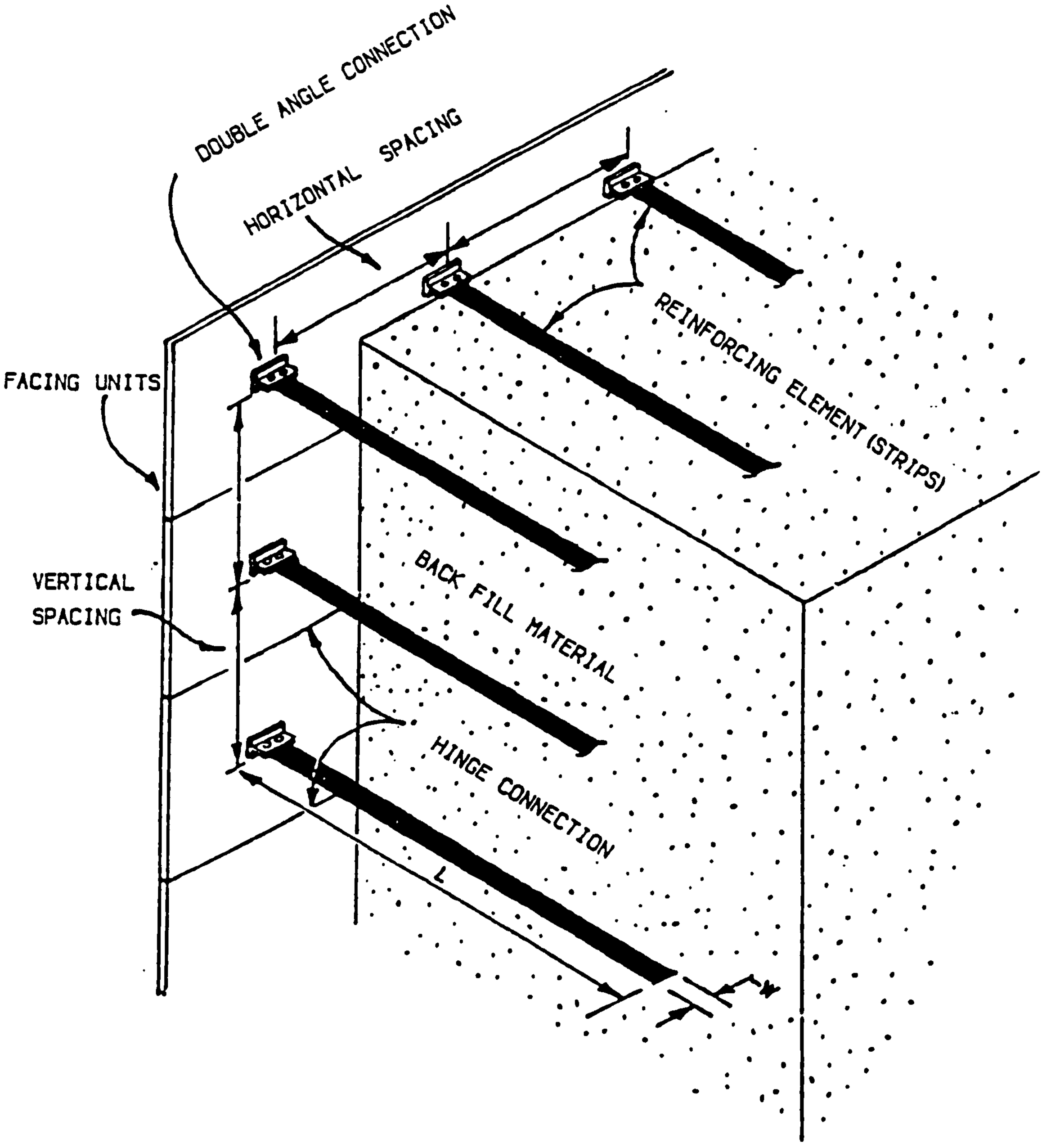

FIG. (2.21) MAJOR COMPONENTS OF REINFORCED EARTH WALL (AFTER AL HUSSAINI AND PERRY, 1976).

(a) Facing units

The function of the facing is to prevent spillage of the fill and provide a suitable architectural treatment to the structure, Vidal (1978) and Jones (1985). Different materials and shapes have been used in facing units such as: semi– elliptical channels made from galvanized steel, Fig. (2.5), interlocking concrete facing panels, Fig. (2.6), and hexagonal fibreglass facing units which are positioned by means of vertical poles, Fig. (2.7).

(b) Reinforcing elements

The reinforcing elements contribute strength to the backfill. They are usually placed at a regular spacing in both the vertical and horizontal directions, connected to the skin elements and extended within the backfill. They may have different shapes and materials such as metal strips with a flat or ribbed surface Fig. (2.22.A) or bars with end anchors Fig. (2.22.B). New materials are being used to overcome the problem of corrosion of metals, basically petrochemical materials, such as: geotextiles, geogrids, geosynthetics, textiles, ... etc., in the shapes of sheets, strips or grids.

(c) Backfill

Vidal (1978) stated that backfill material should be selected which does not contain too much clay and has a sufficient angle of internal friction. According to the Department of Transport in the U.K., Technical Memorandum (BE3/78) which was revised in 1987, both frictional and cohesive frictional fill are limited to a maximum particle size of 125 mm and frictional fill shall not contain more than 10% passing the 63 μm. sieve. Conversely cohesive frictional fill may

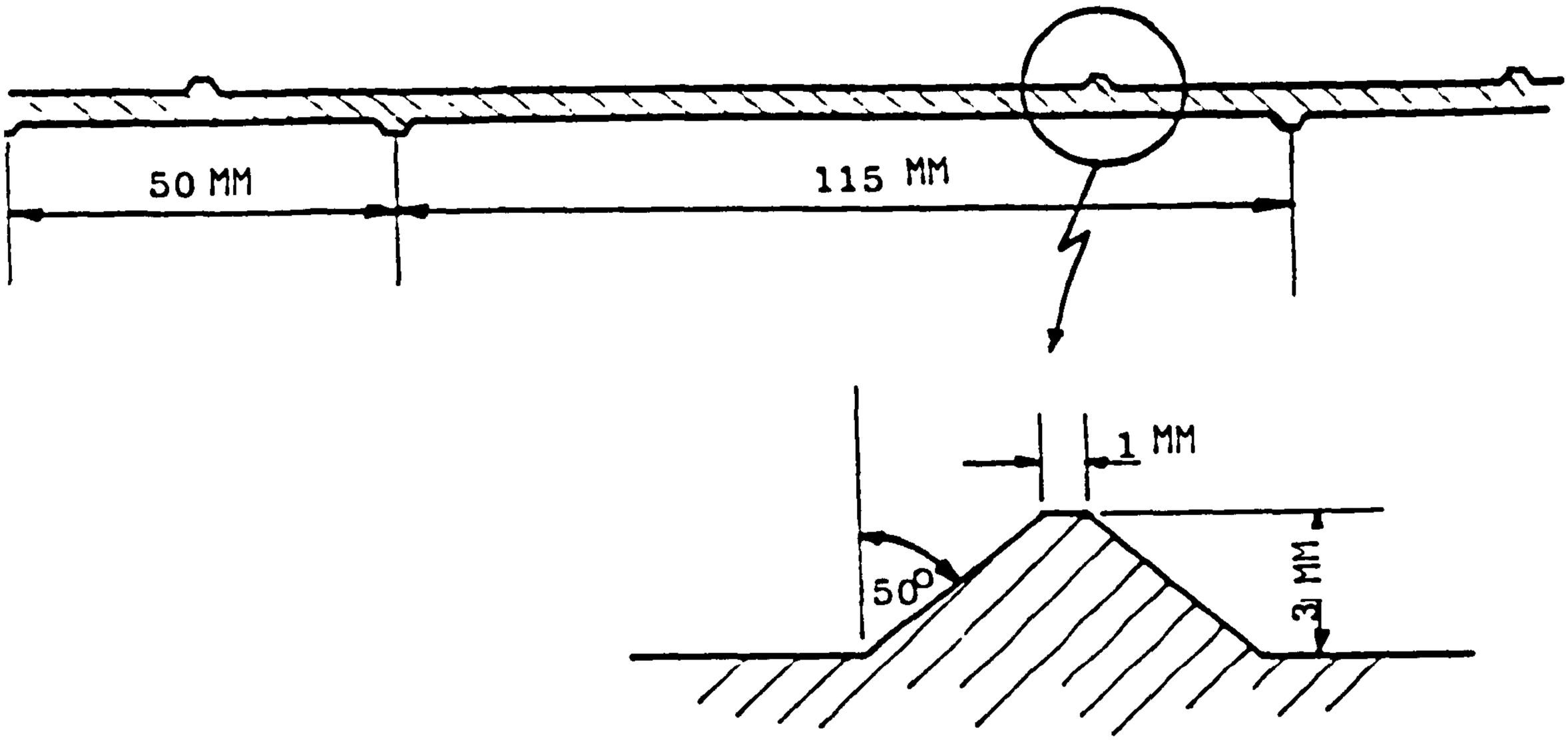

(A) RIBBED STRIP (AFTER SCHLOSSER, 1977)

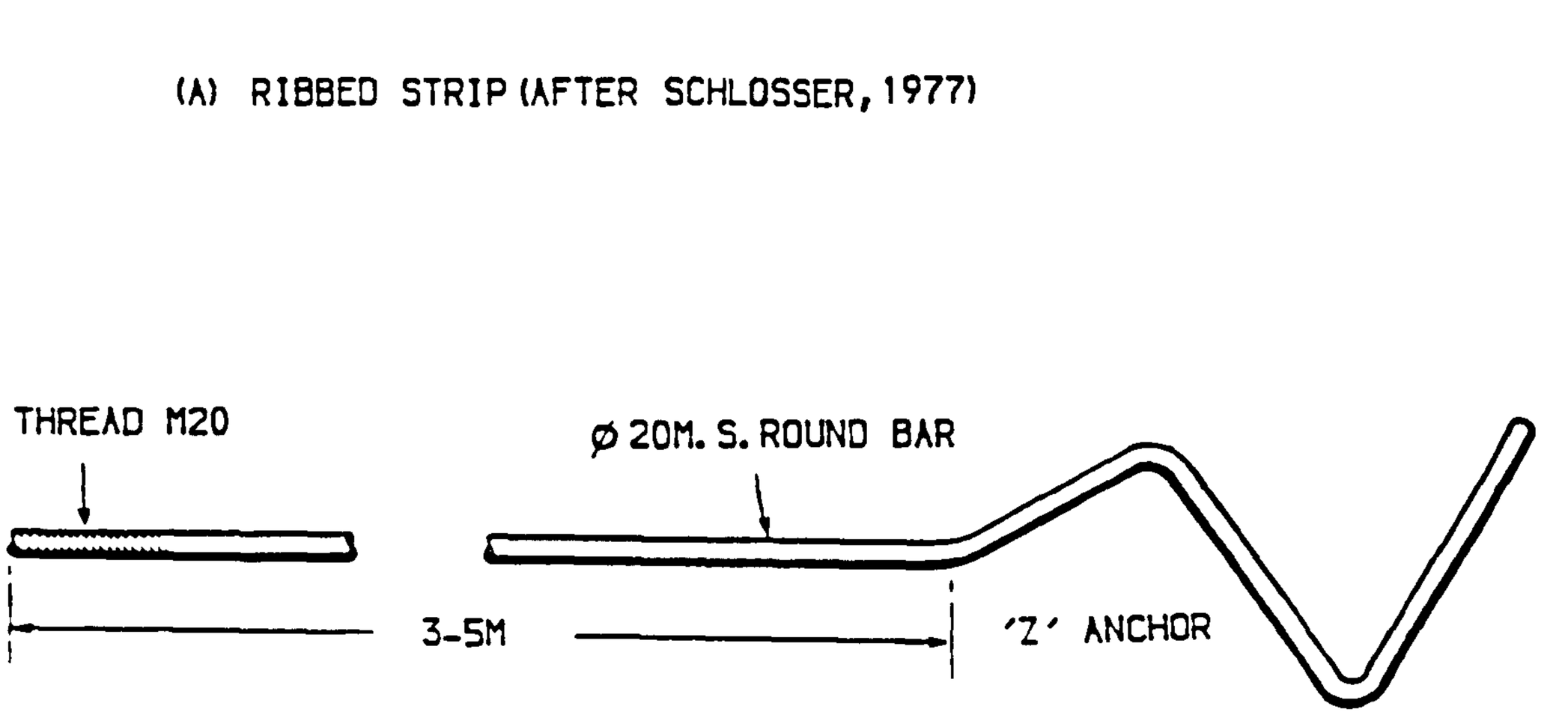

(B) BARS WITH END ANCHORS (AFTER MURRAY AND IRWIN, 1981)

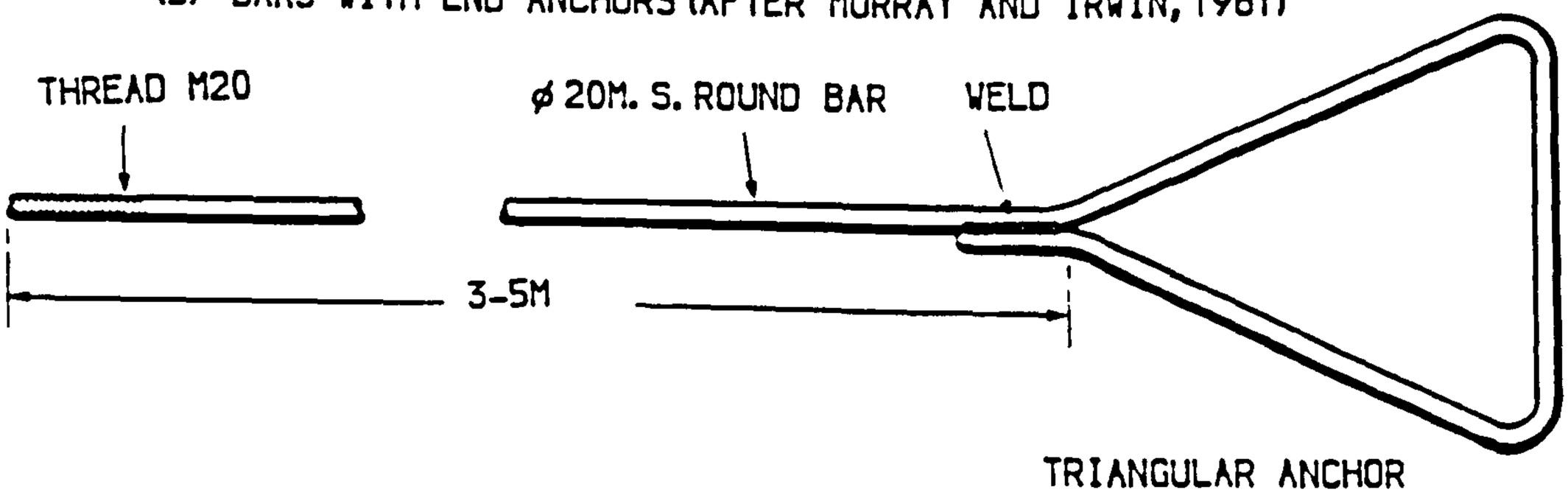

FIG. (2. 22) REINFORCEMENT

contain more than 10% finer than this size provided that the liquid limit and plasticity index do not exceed 45% & 20% respectively. The clay fraction, i.e. 2 μm. finer, is limited to a maximum of 10%. The angle of internal friction of frictional fill and of cohesive frictional fill should be not less than 25 & 20 degrees respectively.

The Memorandum (revised 1987) mentioned that a new backfill material called pulverised fuel ash (PFA) can be used as fill but requires special provisions, particularly in the drainage of water. Details of these provisions can be seen in the Memorandum.

2.5.1 Construction

As seen in the previous section the main components of a reinforced earth retaining wall are facing units, reinforcement with different shapes and materials, and backfill. Reinforced earth retaining walls can thus be constructed in a variety of ways and configurations. Jones (1978 & 1985) divided the method of erection of reinforced walls into 3 categories: concertina method, telescope method, and York or slide method.

The concertina and telescope methods were developed by Vidal in the 1960's. The facing unit in the first is semi–elliptical in cross section made from steel of height 250 mm and has slots along the bottom edge to connect steel strips as shown in Fig. (2.5). In the second system Vidal used precast concrete for facing units which are cruciform shaped in front elevation, weigh 1 tonne and are 1.5 x 1.5 m with a total thickness of 180 mm Fig. (2.6). Each unit has four lugs, cast in situ during manufacture. These lugs are usually at spacings of 1 m horizontally and 0.75 m vertically to connect reinforcing steel strip by means

of bolts. Temporary wedges are used form an open joint and aid vertical alignment. Suitable granular fill material is used according to specifications mentioned by Long (1977).

The York or slide method was developed by Jones (1978). The facing unit is a light–weight glass reinforced cement facing unit weighing 16 kg. in the shape of a hexagon–based pyramid 255 mm deep and 600 mm across the flats as shown in Fig. (2.7). Vertical guide poles of pvc reinforced by mild steel bars are used, and the strips are connected to these poles.

All aspects of design and specification for component parts are clearly set out in Department of Transport, Technical Memorandum (Bridges) BE3/78 (revised, 1987).

2.5.2 Sequence Of Construction

Although there are three different methods of construction which differ according to the shape of the facing units, the method of erection or the sequence of construction is exactly the same. These sequences are shown below. According to Price (1977); BE3/78 (revised, 1987); DuBois (1981); and Jones (1985), the following steps are considered during construction:

(a) Cast a concrete foundation just under the foundation soil level as shown in Fig. (2.23.A). The purpose of this is to get good alignment.

(b) Erect the first level of facing units (half panels first and then full panels) and clamp adjacent units together, Fig. (2.23.B).

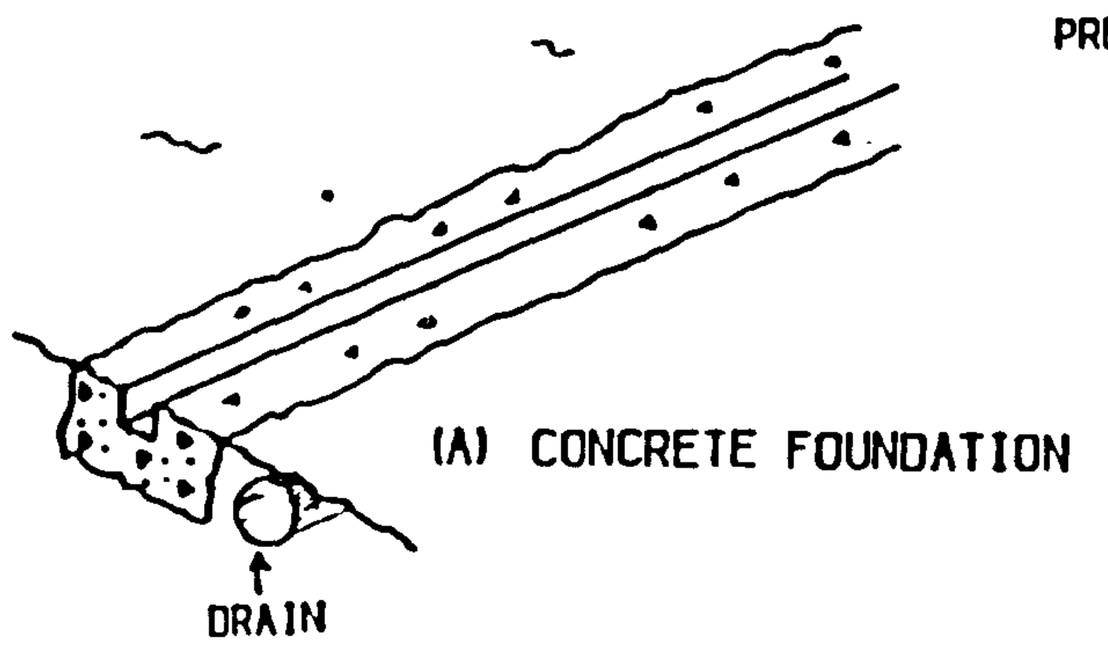

(A) CONCRETE FOUNDATION

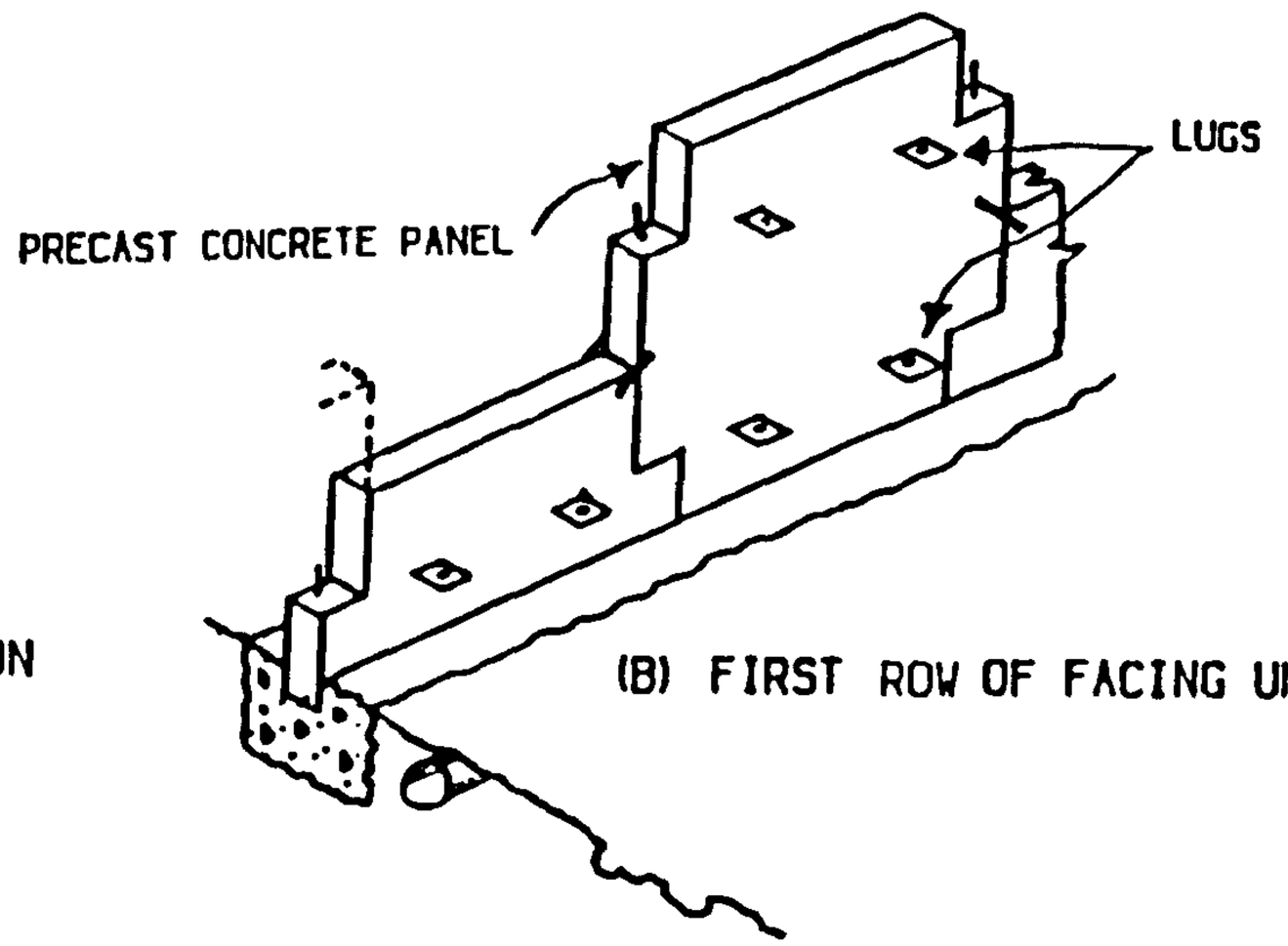

(B) FIRST ROW OF FACING UNITS

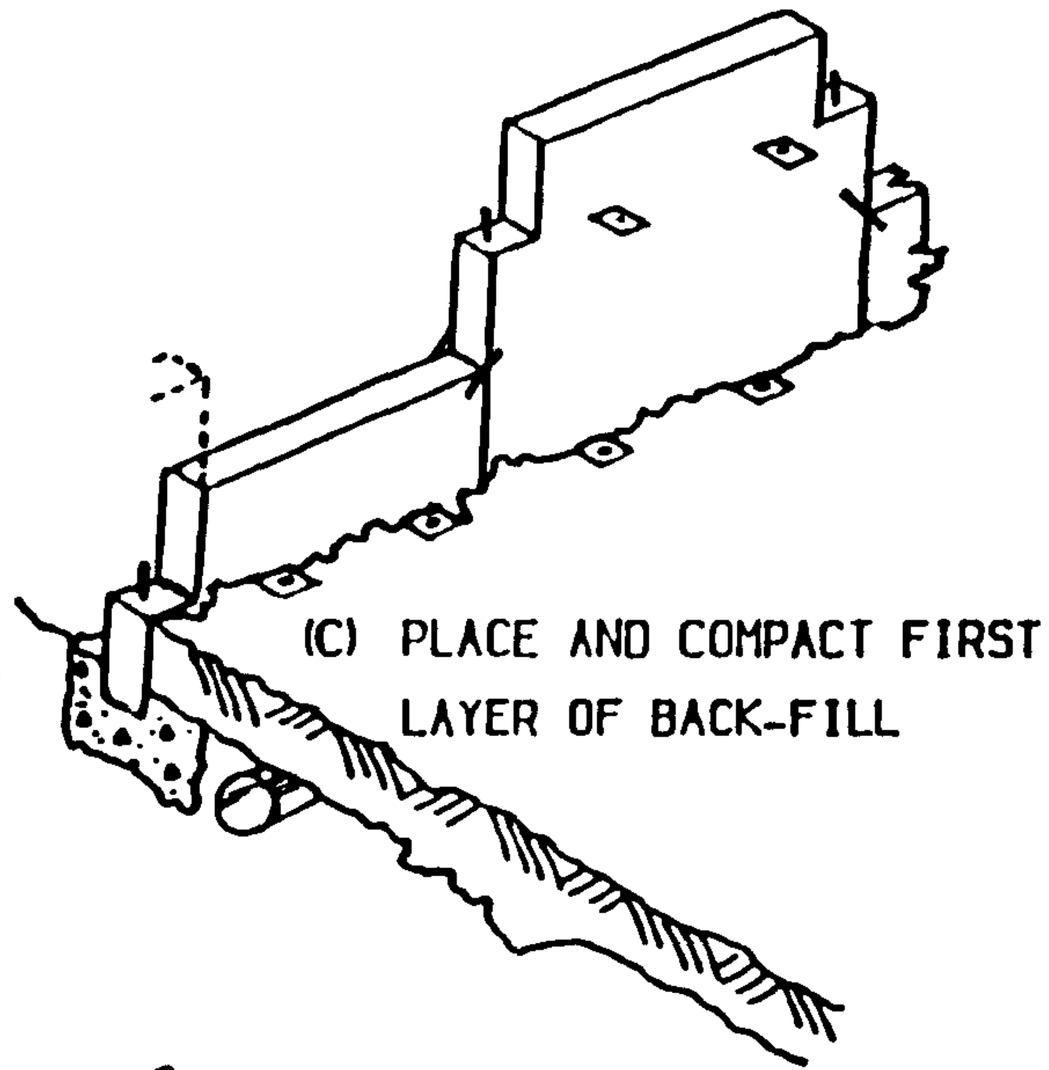

(C) PLACE AND COMPACT FIRST LAYER OF BACK-FILL

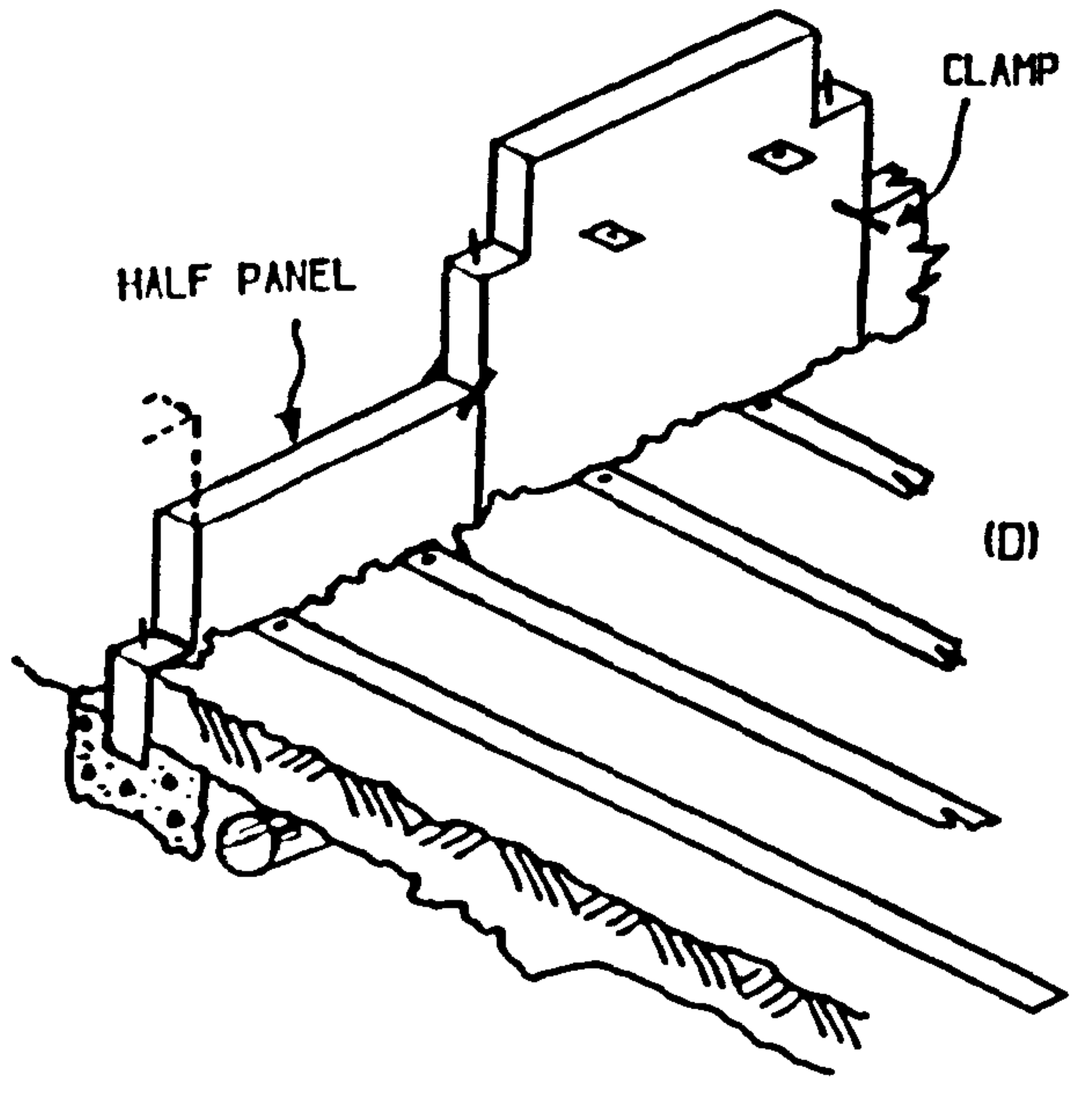

(D) PLACE REINFORCEMENT

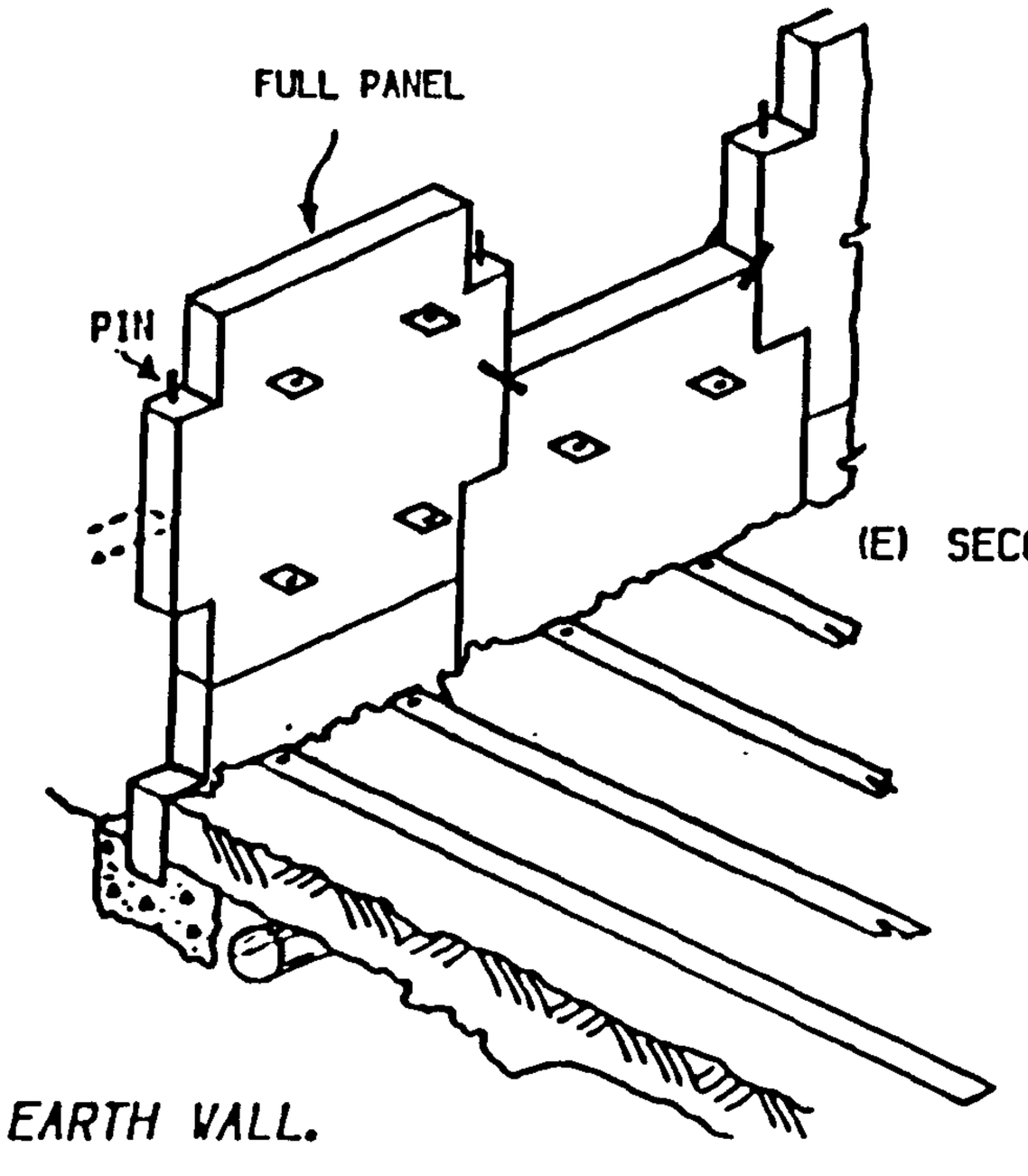

(E) SECOND ROW OF FACING UNITS

FIG. (2.23) SEQUENCE OF CONSTRUCTION OF REINFORCED EARTH WALL.

(c) Place backfill material and compact up to the first level of reinforcing elements, Fig. (2.23.C).

(d) Place reinforcements (any form such as strips, grids, ... etc.) and attach to facing Fig. (2.23.D).

(e) The next level of the panels is erected as before, clamps are removed from the first row of panels and placed at a higher level. The whole process is repeated until the required height is achieved, Fig. (2.23.E).

(f) External loading can be applied.

It is recommended that heavy compaction be avoided within 2 m of the facing panels as this may displace the facing panels. Light compaction is used in this part. It is recommended that the fill be spread, levelled and compacted in horizontal layers of thickness appropriate to the compaction plant to achieve the required degree of compaction, with the compaction plant moving parallel to the facing or edge of the structure.

As seen in the above section, compaction of the fill in the reinforced earth wall is essential during the construction process.

2.6 EFFECT OF COMPACTION ON RETAINING WALLS

2.6.1 General

Compaction is the process by which a mass of soil consisting of solid soil

particles, air, and water is reduced in volume by momentary application of loads, (Winterkorn and Fang, 1972). Compaction is the increase in the dry density of a soil by a dynamic or static load, it is a process by which the soil particles are artificially rearranged, and packed together into a closer state of contact by mechanical means in order to decrease the porosity of the soil and thus increase the dry density and shear strength, and decrease the compressibility, Osman (1980). Biarez (1980) stated that compaction is not only a variation in density but can also be considered to be an irreversible deformation modifying the mechanical properties of the soil.

Terzaghi and Peck (1948) stated that, in ancient times it was customary to compact fills to be used as dams or levees, the method of compaction differing from one soil to another depending mainly on the soil type, moisture content and soil density.

2.6.2 Influence Of Compaction On Lateral Pressures On Earth Retaining Walls

The influence of compaction on lateral pressures has been known for many years. Terzaghi (1934), carried out a series of tests on a large retaining wall Fig. (2.24), 14 ft. long and 7 ft. high, behind which dry sand had been compacted in layers of 6 inches depth. The main purpose of these tests was to determine how any yielding of the retaining wall affected the distribution and intensity of the sand pressure. It was noted that compaction of the soil behind the retaining wall significantly affected lateral earth pressures and resulting structural deflections. Some of the results are shown in Fig. (2.25).

Sowers et al. (1957) compacted sand in 1.5 m deep pit, and clay behind a 1.8 m high wall, and measured the earth pressure. They demonstrated quite

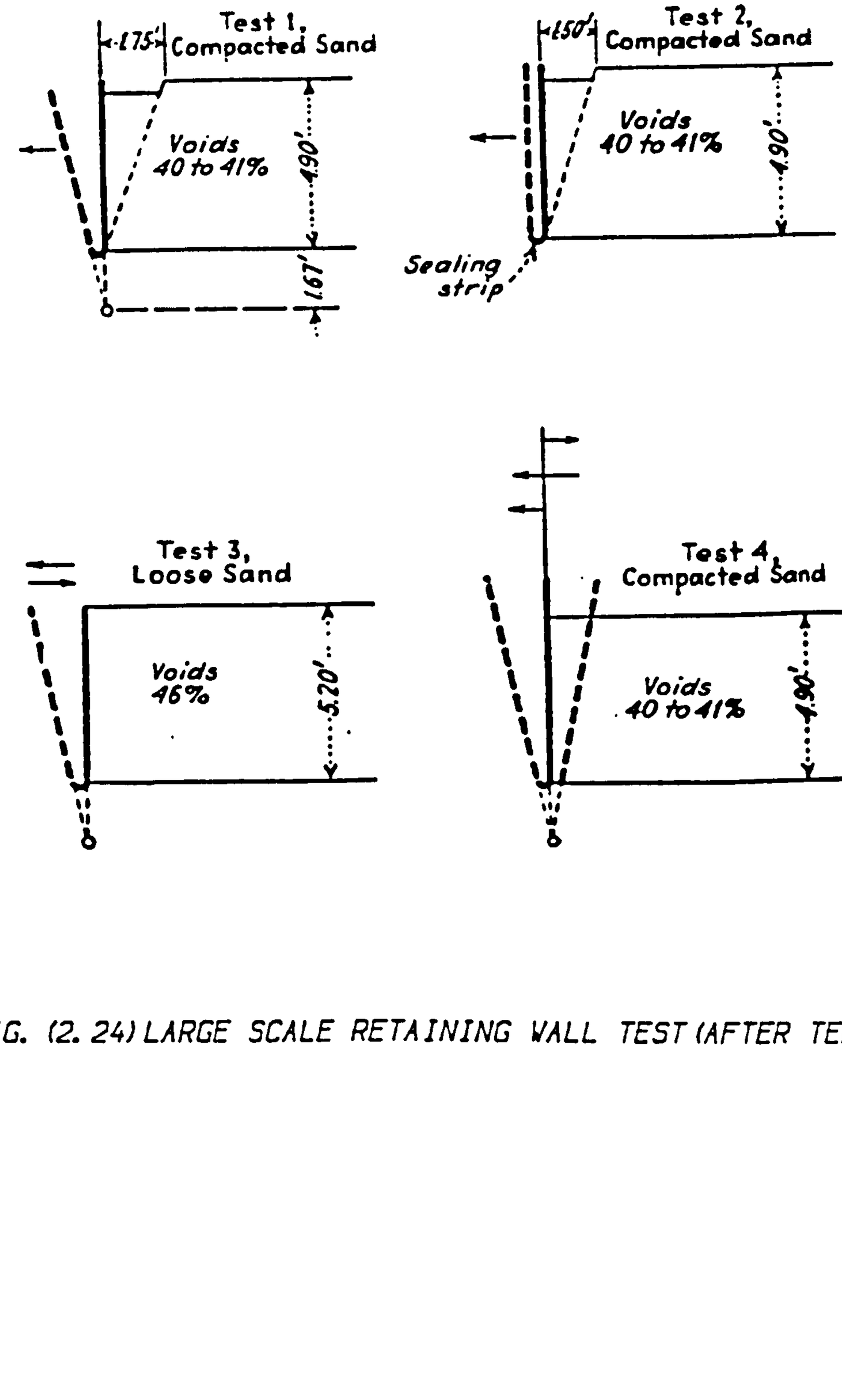

FIG. (2.24) LARGE SCALE RETAINING WALL TEST (AFTER TERZAGHI, 1934).

H/W=HYDRAULIC RATIO

H =HORIZONTAL COMPONENT OF EARTH PRESSURE.

W =HORIZONTAL PRESSURE EXERTED BY A LIQUID WHOSE UNIT WEIGHT IS EQUAL TO THE UNIT WEIGHT OF THE BACK FILL.

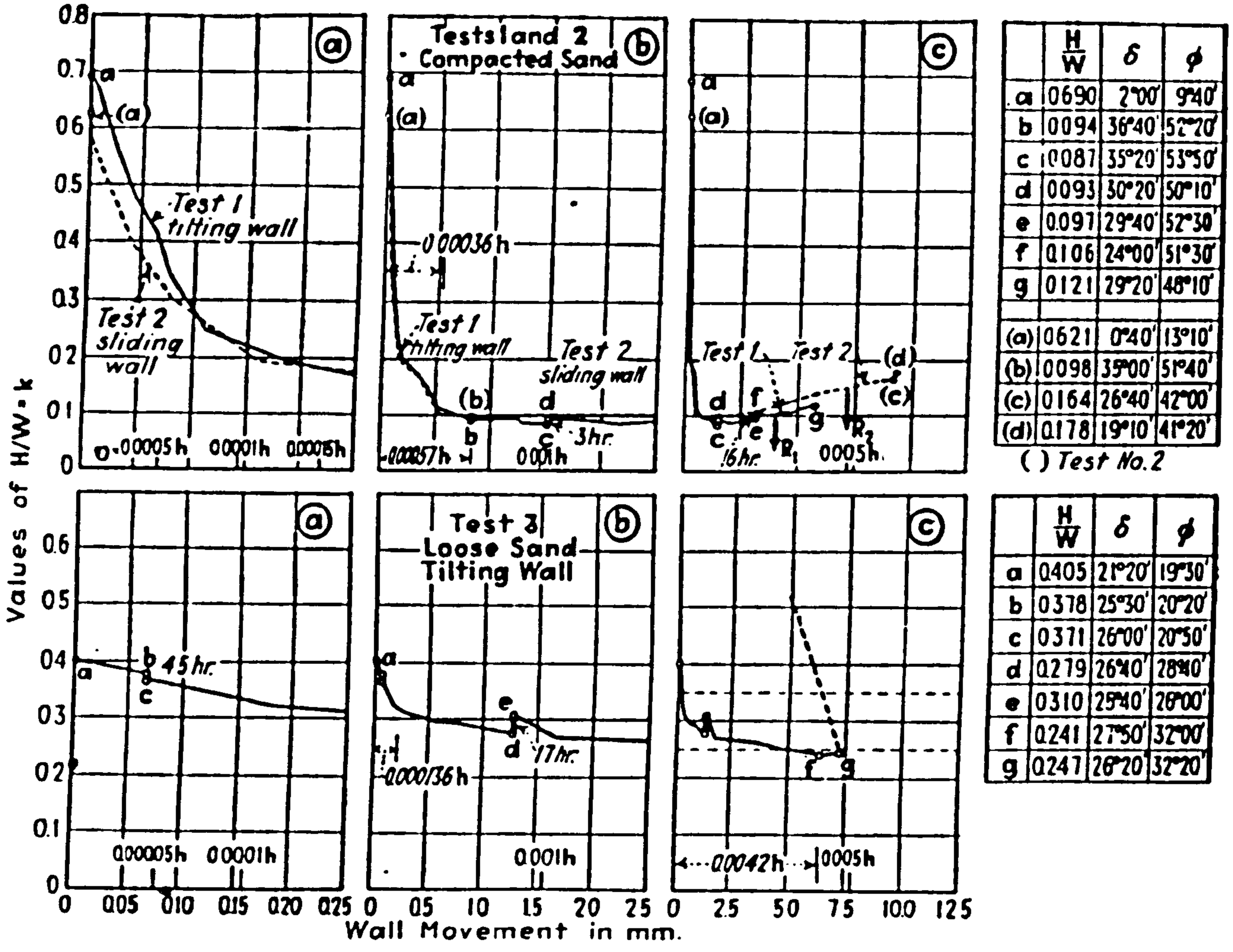

Tests 1 and 2 · Compacted Sand

	H/W	δ	φ
a	0690	2°00'	9°40'
b	0094	36°40'	52°20'
c	0087	35°20'	53°50'
d	0093	30°20'	50°10'
e	0091	29°40'	52°30'
f	0106	24°00'	51°30'
g	0121	29°20'	48°10'
(a)	0621	0°40'	13°10'
(b)	0098	35°00'	51°40'
(c)	0164	26°40'	42°00'
(d)	0178	19°10'	41°20'

( ) Test No. 2

Test 3 Loose Sand Tilting Wall

	H/W	δ	φ
a	0405	21°20'	19°30'
b	0378	25°30'	20°20'
c	0371	26°00'	20°50'
d	0279	26°40'	28°40'
e	0310	25°40'	28°00'
f	0241	27°50'	32°00'
g	0247	28°20'	32°20'

FIG. (2.25) LATERAL EARTH PRESSURE AS A HYDROSTATIC RATIO OF DRY SAND AS AFFECTED BY YIELD OF WALL AND COMPACTION OF FILL (AFTER TERZAGHI, 1934).

clearly that residual lateral pressures for compacted soils greatly exceed those predicted by classical theories.

There are a wide range of compaction plants which suit the soil and the type of project. In general, compaction equipment falls into two categories, i.e. equipment convenient for light compaction and for heavy compaction. Examples of light compaction equipment are: vibratory plate compactors, vibratory tampers, static or vibratory rollers. For heavy compaction– static or vibratory rollers and pneumatic tired rollers and combination rollers are used.

The advantages of soil compaction have led to its use in all earthworks connected with roads, earth dams, embankments, and earth retaining structures. Sometimes it is used as a method of soil improvement.

High lateral earth pressures can develop behind a retaining wall. These pressures are often much larger than those used in the design if the backfill material is compacted according to specifications, Broms (1971).

Sims and Jones (1974) stated that the factors which affect the lateral earth pressure on the retaining wall are:

(a) The form and type of wall retaining the earth including its deflection characteristics.

(b) The nature and type of the backfill materials including their elastic/plastic properties.

(c) The methods adopted in backfilling the wall.

(d) The foundation conditions under the wall.

(e) The type, nature and frequency of any superimposed loading applied on the retaining material.

(f) The drainage details behind the wall and porosity of backfill.

(g) Ground strains caused by external forces.

They concluded that behaviour of earth walls depends mainly upon soil pressure acting on the wall, passive resistance of the ground supporting the wall and rigidity of the wall itself.

The most intractable factor which affects the lateral earth pressure and hence influences the behaviour of a retaining wall is the compaction caused by the superimposed load of the compaction plant which is used in the method adopted in backfilling.

In a review by the Building Research Establishment in 1977, it was found that the classical earth pressure theories of Coulomb (1776) and Rankine (1857) are still widely used by practicing engineers. It was pointed out that although new theories are being developed, the unpredictable behaviour of fill makes it unreasonable to apply more complicated theories. Two important points can be raised from the study. These two points are the futility of incorporating refinements to calculations of much greater apparent accuracy than the assumptions warrant and the need to make some assessment of the effects of compaction plant on lateral earth pressures, Ingold (1979).

Rehnman and Broms (1972) reported that several fatal accidents occurred in Sweden in the late 1960's during the placing of backfill behind basement walls or when heavy machines or trucks came too close to such walls. They indicated from the test results of compacting granular sand and silty fine sand backfill behind a reinforced concrete wall 2.5 m high using vibratory plate compactors, that high lateral earth pressures can develop during and after compaction.

The previous conclusion has been verified by several researchers such as: Aggour and Brown (1974); Coyle and Bartoskewitz (1976); Ingold (1979); Duncan and Seed (1986); and Seed and Duncan (1986).

Recently Carder (1988) reported that an informal discussion by the British Geotechnical Society had been held at the Institution of Civil Engineers on Jan., 13, 1988 to present the results from pilot scale and full scale studies by TRRL, and to discuss the development of a new design code for earth retaining structures. In both pilot scale and full scale studies of earth retaining walls, where vertical and horizontal pressures were measured under the backfill mass and behind the wall face respectively, all the results indicated a significant increase in earth pressure and wall deformation after compaction. These pressures were greater than predicted by classical theories. Examples of this conclusion are shown in Figs. (2.26&27) for rigid reinforced concrete retaining walls.

The effect of compaction on lateral earth pressure on earth retaining walls includes not only rigid walls but also flexible walls such as reinforced earth retaining walls.

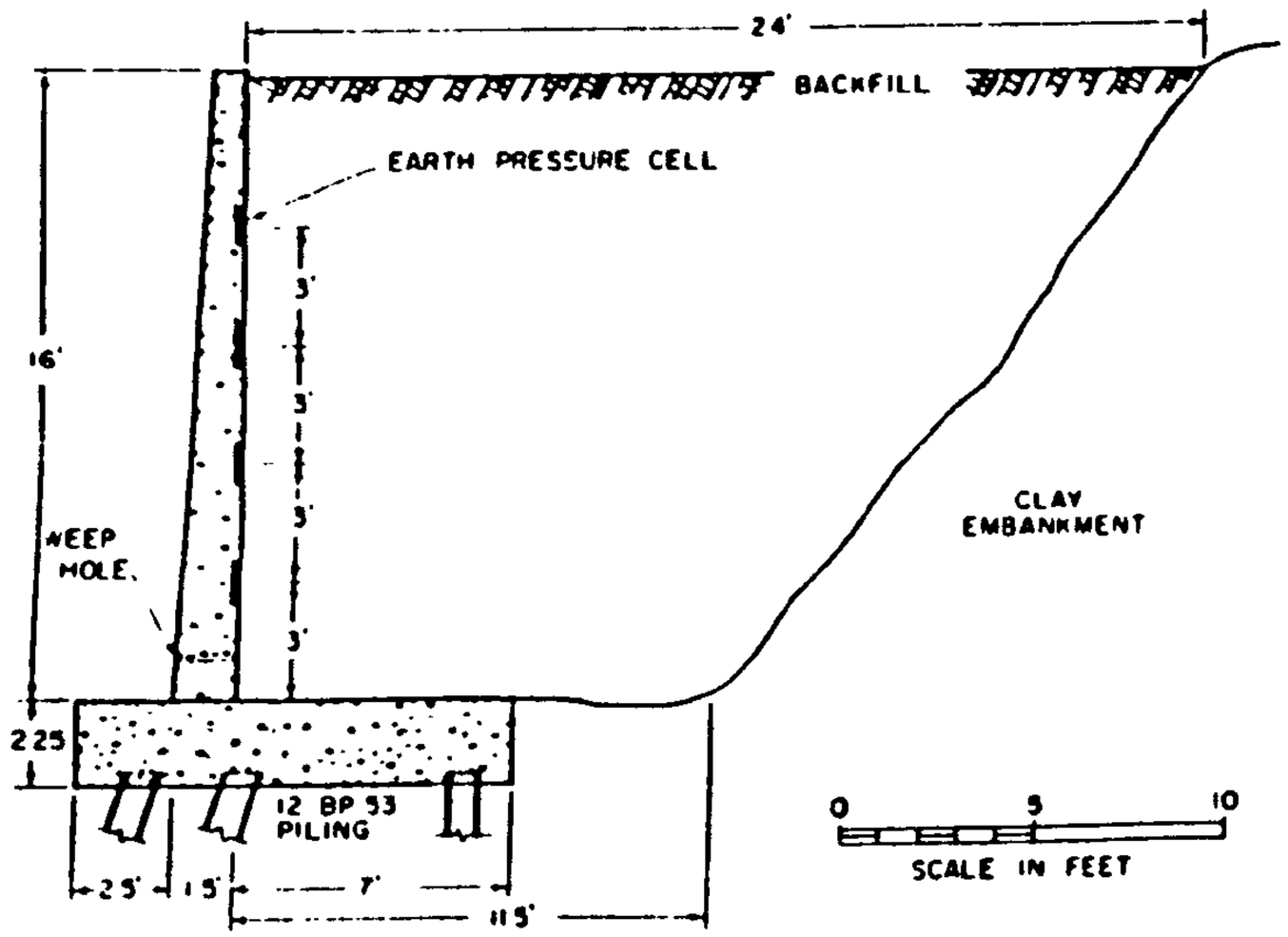

(A) TEST WALL

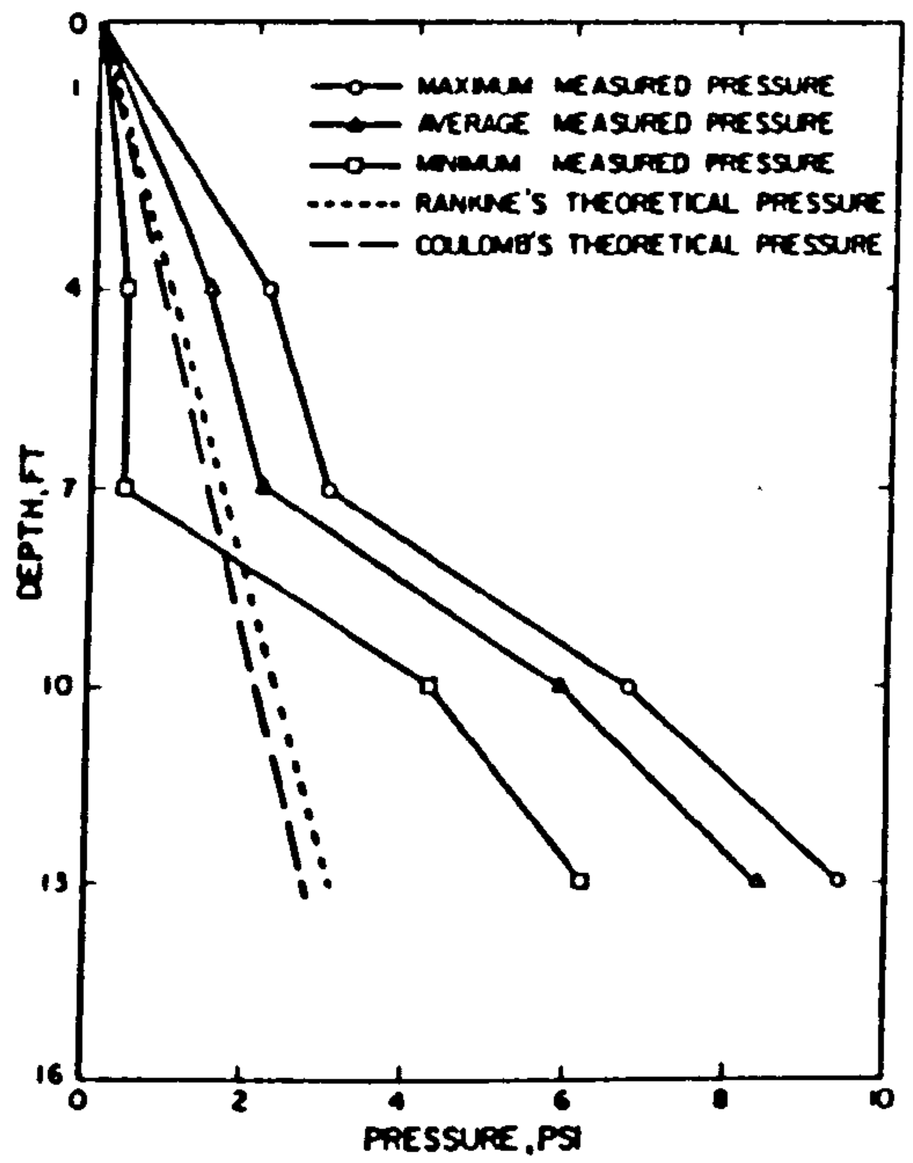

(B) THEORETICAL VERSUS MEASURED PRESSURE

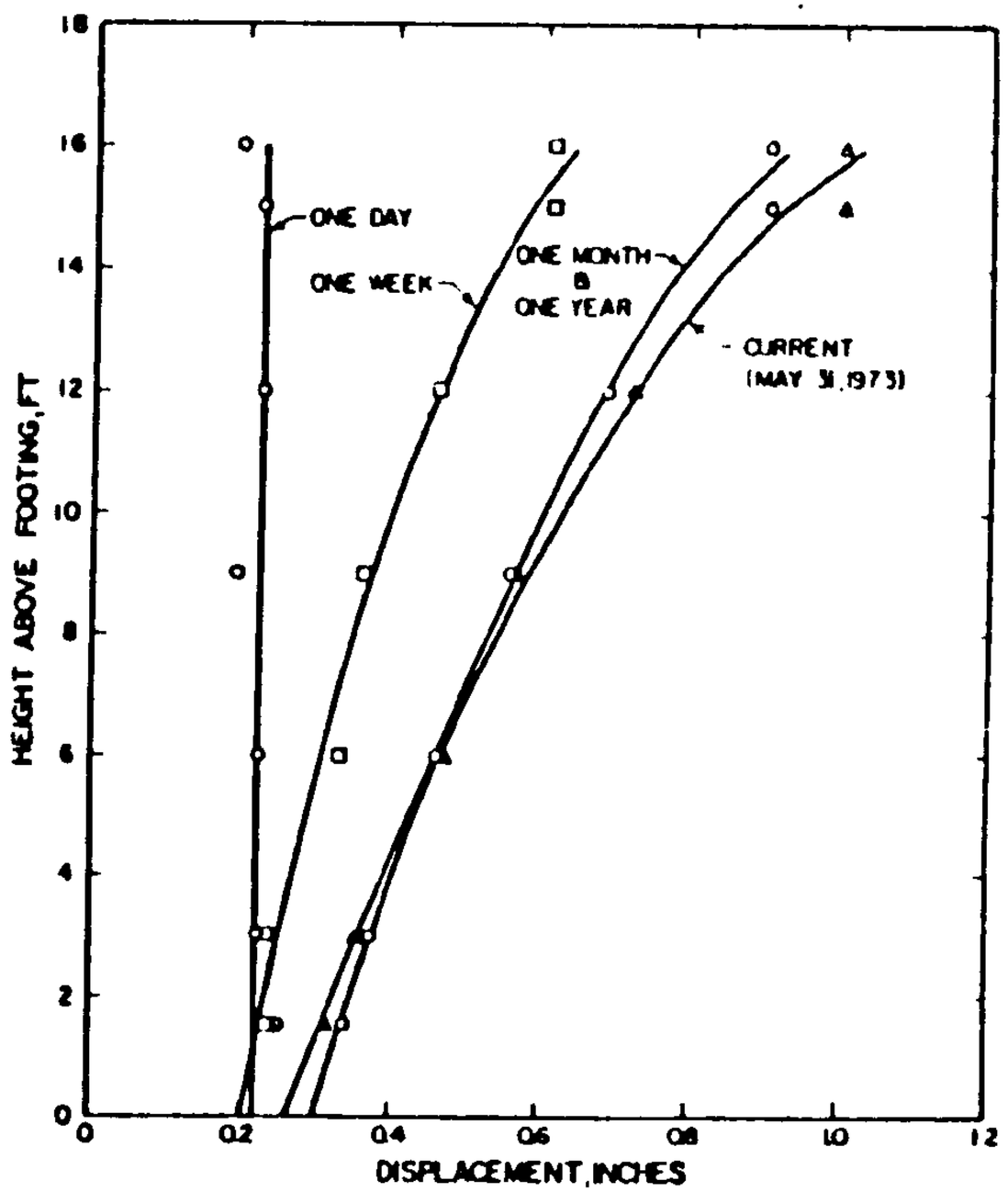

(C) DISPLACEMENT OF THE WALL

FIG. (2.26) FIELD TEST OF A CANTILEVER RETAINING WALL (AFTER COYLE ET AL, 1974).

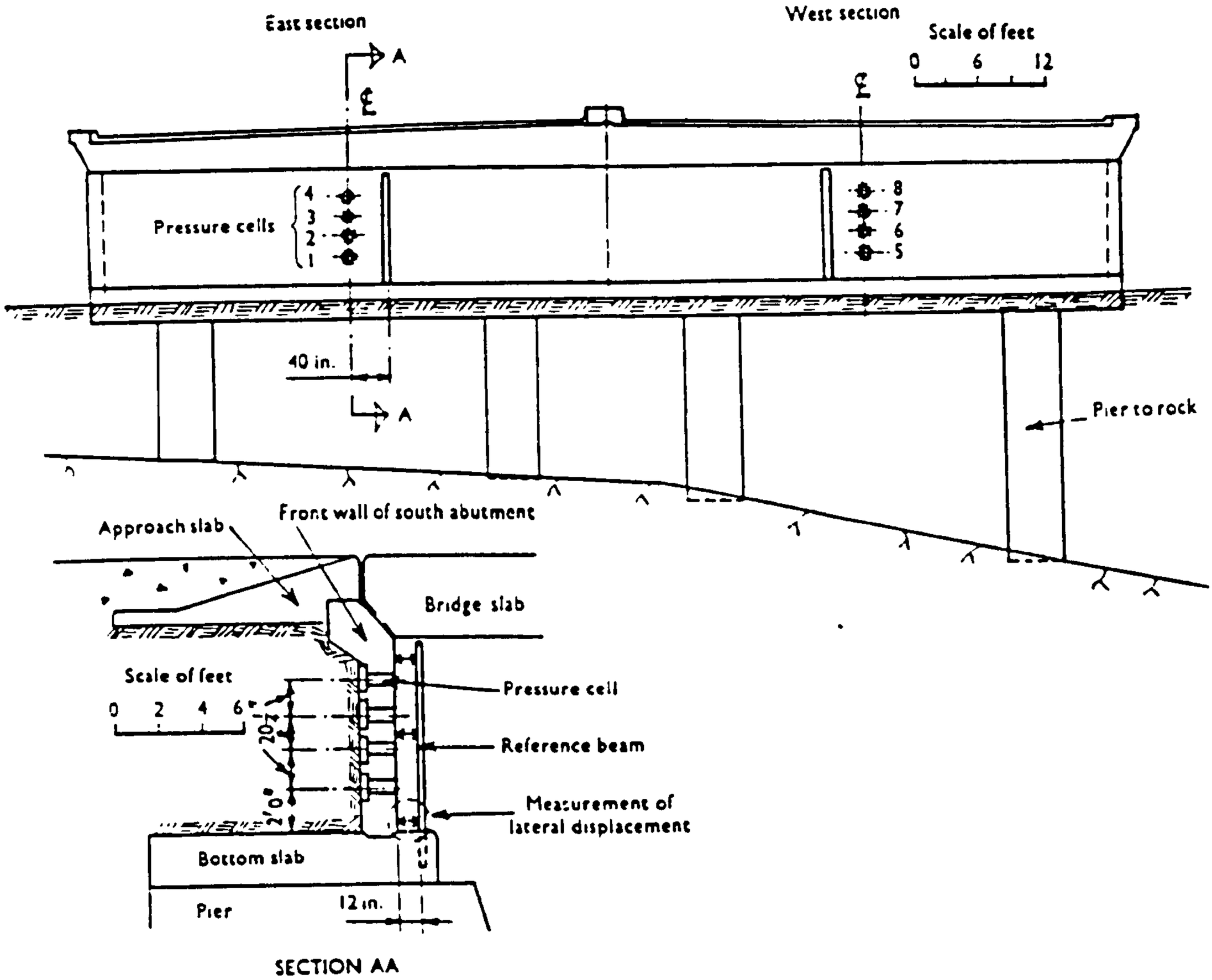

SECTION AA

(A) LOCATION OF PRESSURE CELLS AND CROSS SECTION OF THE WALL.

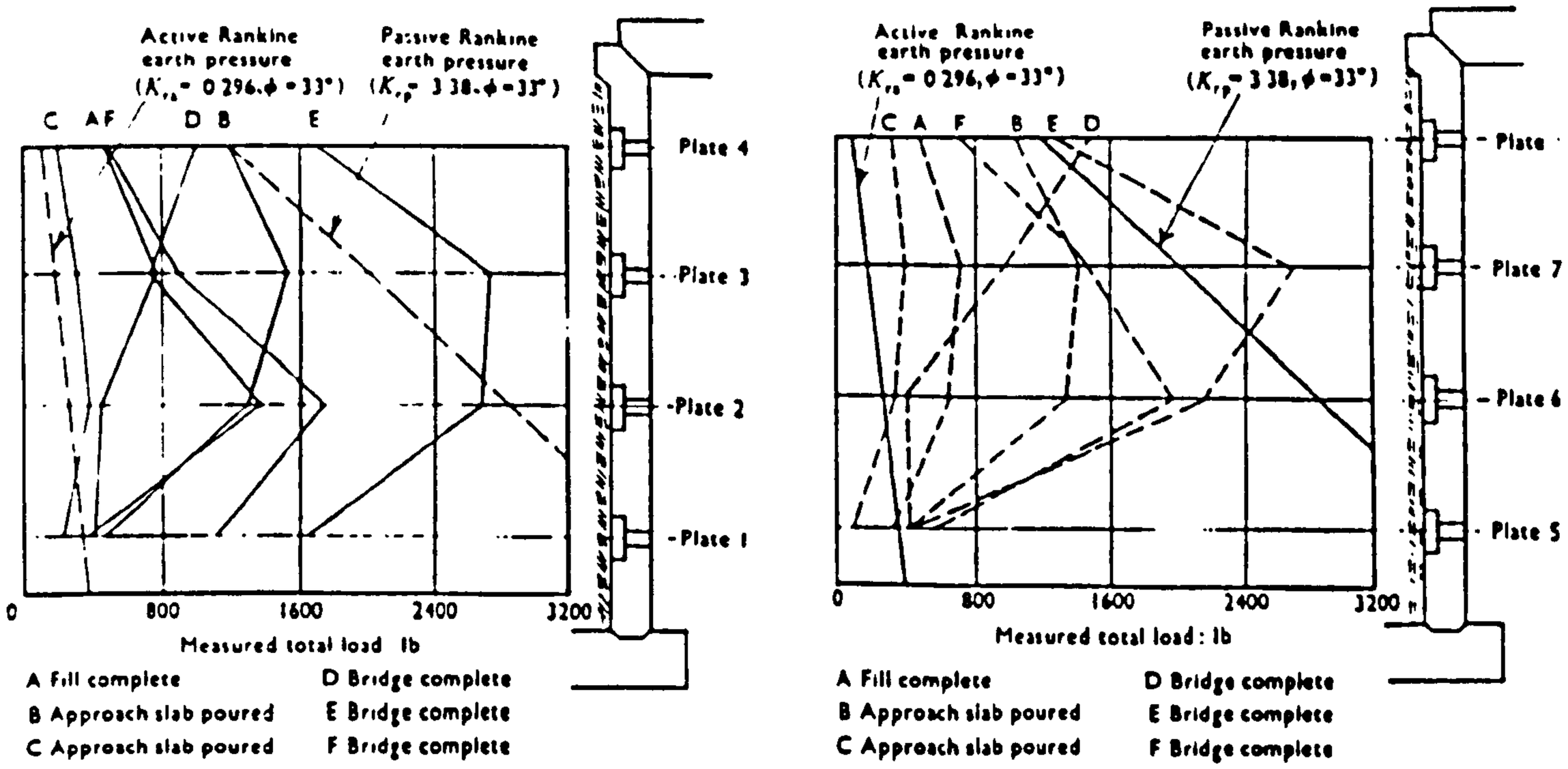

(B) LOAD DISTRIBUTION AT EAST AND WEST SECTION.

FIG. (2.27) ABUTMENTS OF RIGID FRAME BRIDGE-CASE HISTORY (AFTER BROMS AND INGELSON, 1971).

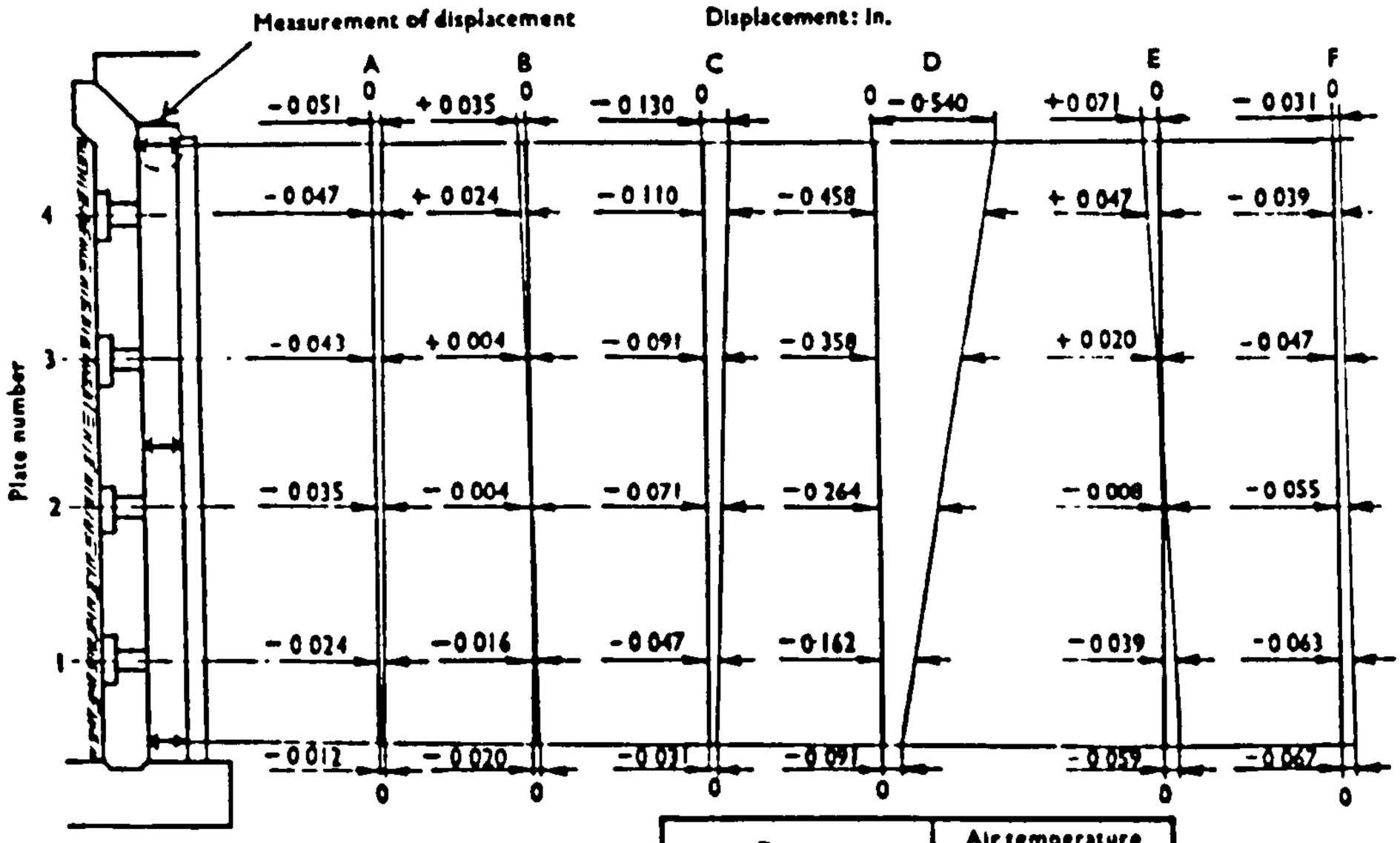

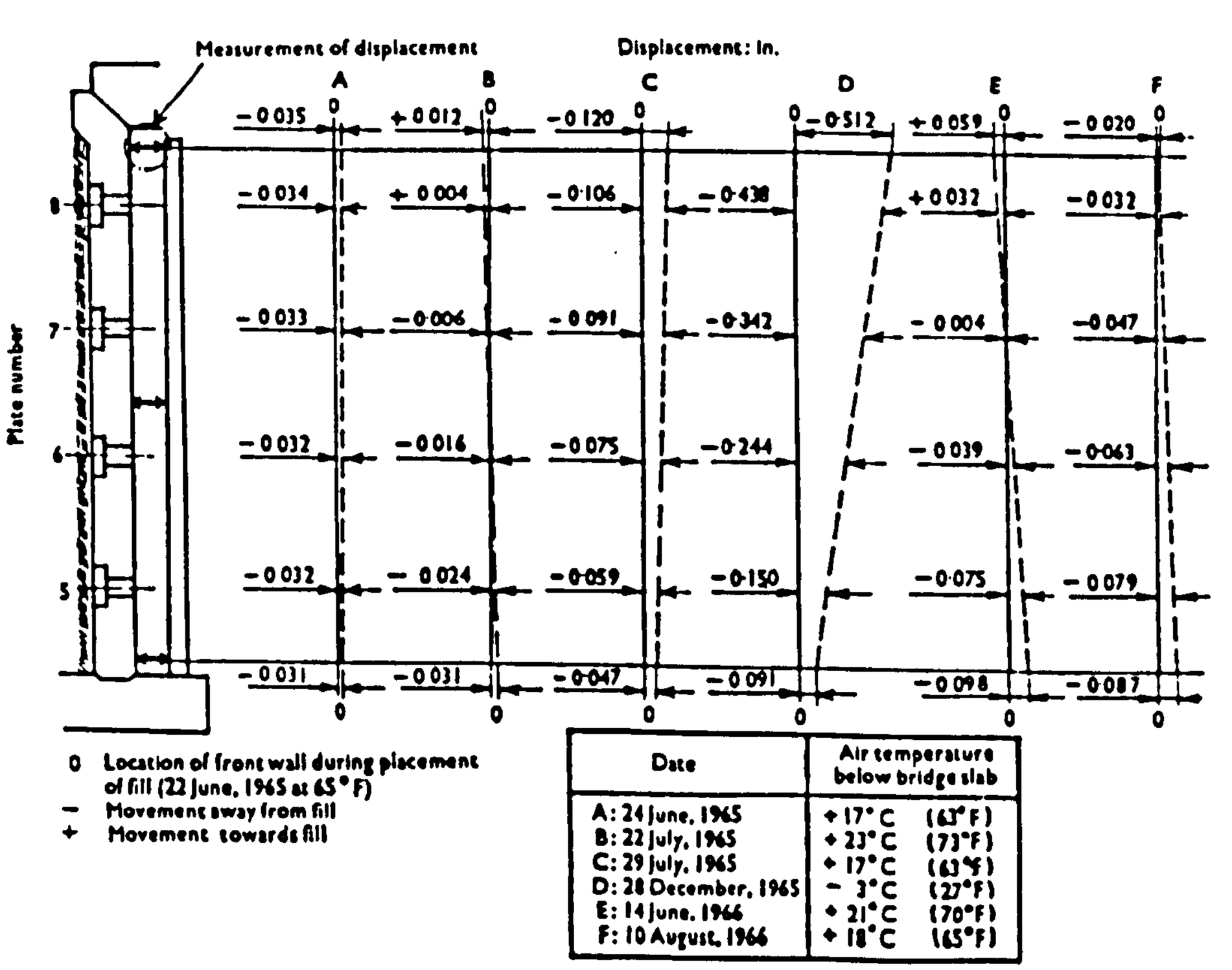

(C) DISPLACEMENT OF THE WALL AT EAST AND WEST SECTION.

FIG. (2. 27) CONT.

2.7 EFFECT OF COMPACTION ON REINFORCED EARTH WALLS

The method of erection of reinforced earth walls is such that internal movements after construction is complete are not normally possible. During construction each layer must be compacted to a certain degree of compaction, which depends on the weight of the compaction plant and the number of passes applied.

The degree and method of compaction during construction is one of the most important factors in determining not only the stresses in the reinforcing members but also the lateral pressures acting on the face of wall, Jones (1973), Finlay and Sutherland (1977).

An increase in lateral earth pressure due to compaction occurs in any compacted backfill of a retaining wall. If stress relief does not occur then the phenomenon of residual compaction stresses leads to values of lateral pressure greater than those calculated, Smith (1977).

Ingold (1980), stated that compaction of backfill behind a reinforced earth retaining wall can result in unacceptably large wall deflections during construction, and if it is necessary to compact backfill, the structure must be isolated from the potentially injurious effects of compaction induced stresses.

Ingold (1983) concluded that field studies of reinforced earth wall movement clearly show an outward rotation about the toe. This is related to the load intensity imposed by compaction plant which induces lateral earth pressure and deformation.

Compaction induced earth pressures and resulting structural stresses and deformations can be of serious concern in the design and analysis of many types of soil–structure such as retaining walls, buried structures and pipes, flexible culverts and reinforced earth walls, ... etc., Duncan and Seed (1986).

As seen in previous sections, compaction has a dominant effect on the behaviour and performance of earth retaining structures especially in reinforced earth walls. The effect of compaction can be seen in the behaviour of documented reinforced earth retaining walls constructed in the field.

Four field reinforced earth retaining walls, covering full scale tests and small scale tests will be used to illustrate this effect in the next section.

2.7.1 Case Histories

(1) Field structure

(a) Granton reinforced earth wall: (U.K.)

Price (1975) reported the Granton wall as being the first reinforced earth wall in the United Kingdom. The wall was built as part of the A901 road improvement at Granton, just north of Edinburgh, between December 1972 and May 1973. The wall, 106 m long, varied in height between 1.8 m and 7.2 m, and was partly curved in plan as shown in Fig. (2.17). It was constructed using standard reinforced concrete cruciform facing units 180 mm thick and of interlocking shape about 1.50 m 'square'. The reinforcement comprised stainless steel strips 80 mm wide by 1.5 mm thick and up to 6.5 m long, at vertical spacings of 750 mm, and horizontal spacing 500 mm and 1000 mm. Burnt oil

shale, known as "blaes" (a local waste product) was placed at a bulk density of 16.65 kN/m³. The angle of internal friction was 46 degrees, and the angle of soil/ structure interaction was 17.7 degrees.

Compaction was achieved using a 10 tonne smooth wheel three point roller (Aveling Barford GNQ roller) generating line loadings of 34.9 kN/m and 54.7 kN/m under the front and rear rollers respectively. The measurements indicated vertical and horizontal movements of the wall and the stresses set up within the reinforcing strips. Measurements were taken on the wall during and after construction, at a section of the wall as shown in Fig. (2.28). During construction of the wall the stresses were measured in one reinforcing strip after it had been initially covered with 0.4 m of fill, after trafficking by a bulldozer and after final rolling, and are shown in Fig. (2.29.A). Stresses in some other strips are shown in Fig. (2.29.B), and vertical and horizontal movements of the wall are shown in Fig. (2.30.A&B) respectively, with distribution of earth pressure shown in Fig. (2.31).

The main conclusion reached from these measurements was the important role played by the construction operations on the performance of a reinforced earth wall, and particularly the effect of compaction carried out close to the wall, Finlay (1977), Finlay and Sutherland (1977), Finlay (1978) and Finlay (special communication).

(b) Reinforced earth wall on Guildford bypass: (U.K.)

The wall was constructed at the A3/A322 interchange (1981) at the Guildford bypass in the U.K. as an extension to improve the A3 trunk route connecting the south coast at Portsmouth with London. It was the subject of a full–scale

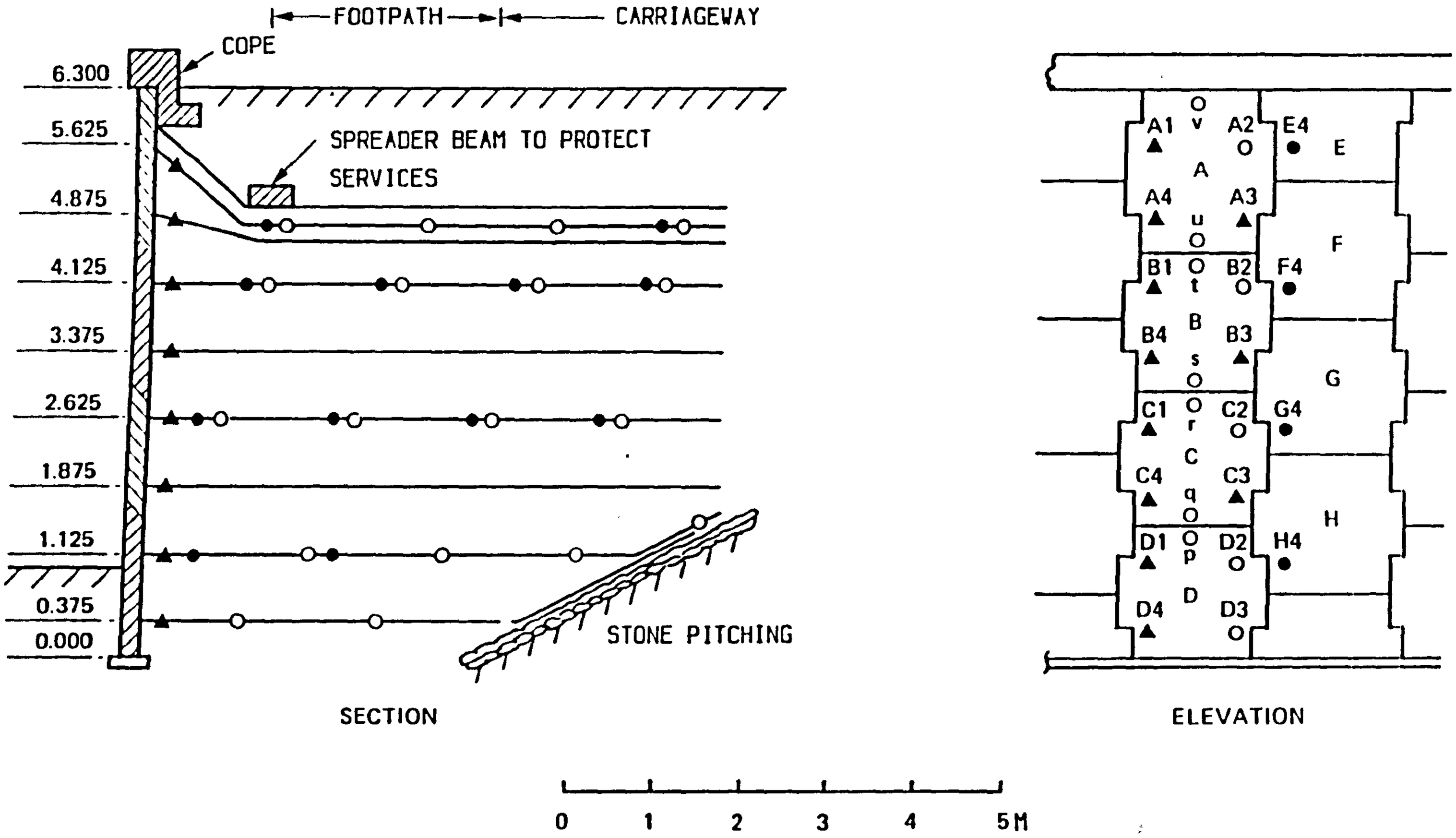

FIG. (2.28) LAYOUT OF GAUGED STRIPS (AFTER FINLAY, 1977).

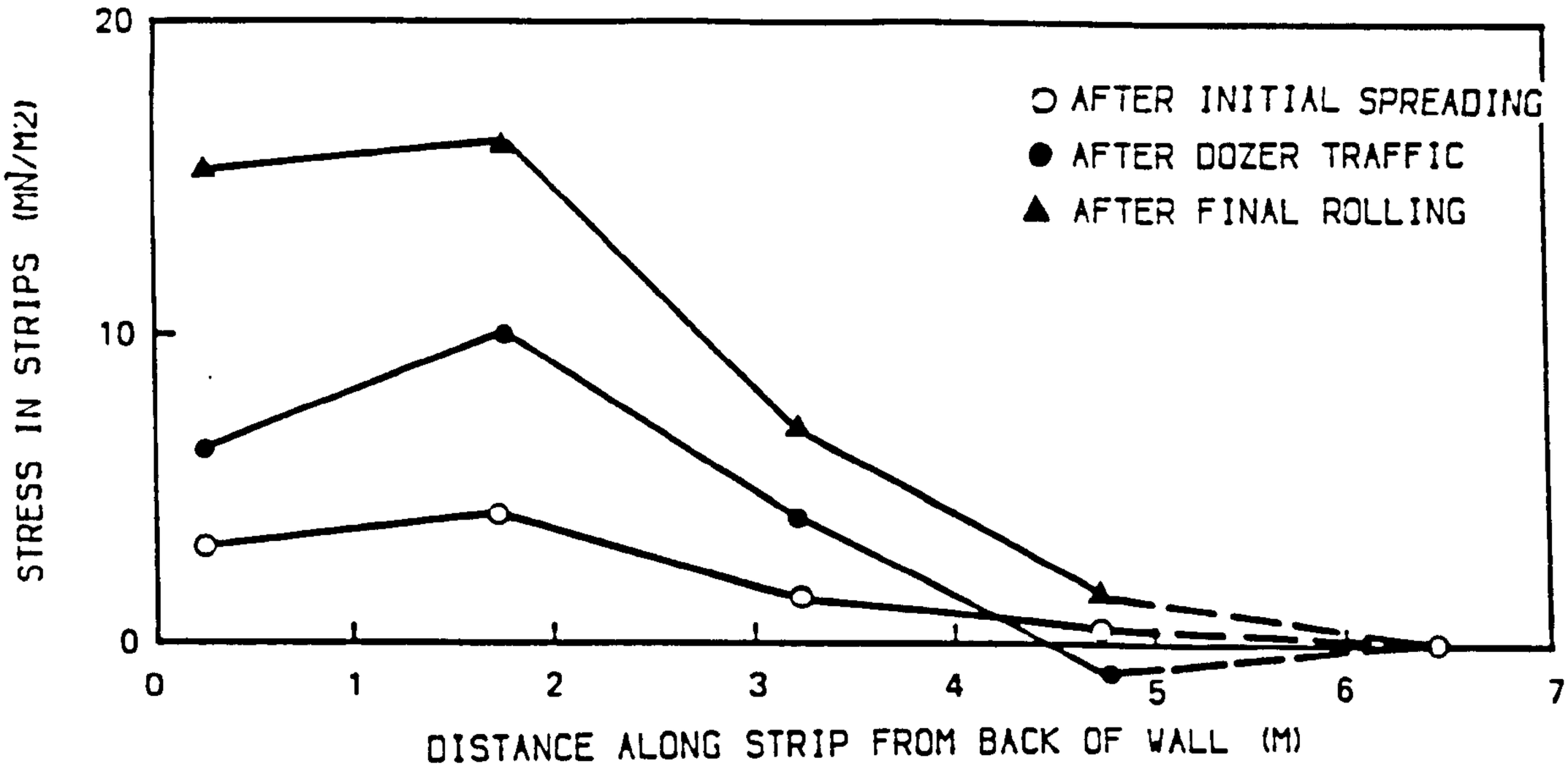

FIG. (2.29.A) EFFECT OF COMPACTION OPERATION ON STRIP D2 (AFTER FINLAY AND SUTHERLAND, 1977).

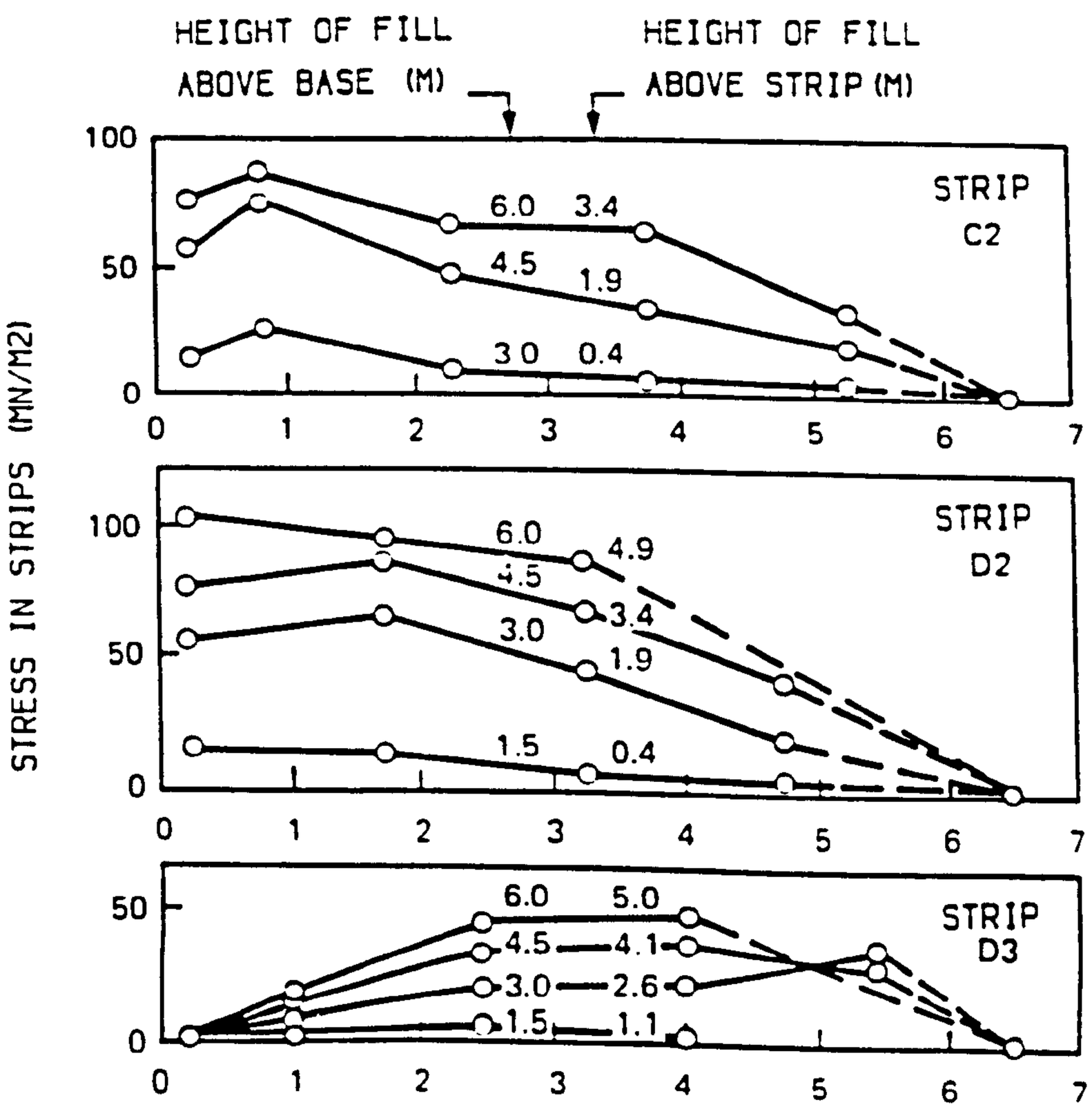

FIG. (2.29.B) VARIATION IN TENSILE STRESS ALONG STRIPS C2, D2, D3 (AFTER FINLAY, 1977).

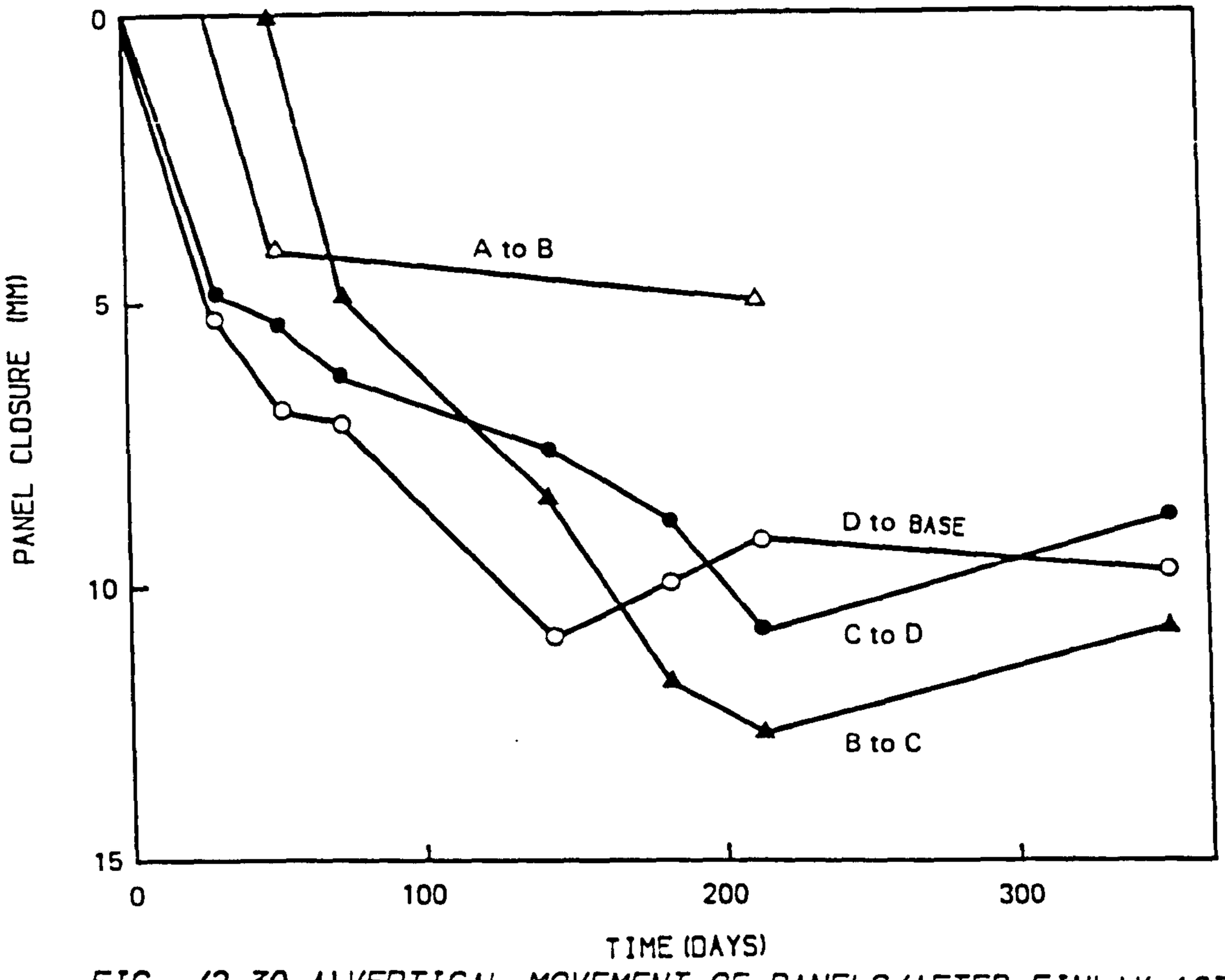

FIG. (2.30.A) VERTICAL MOVEMENT OF PANELS (AFTER FINLAY, 1977).

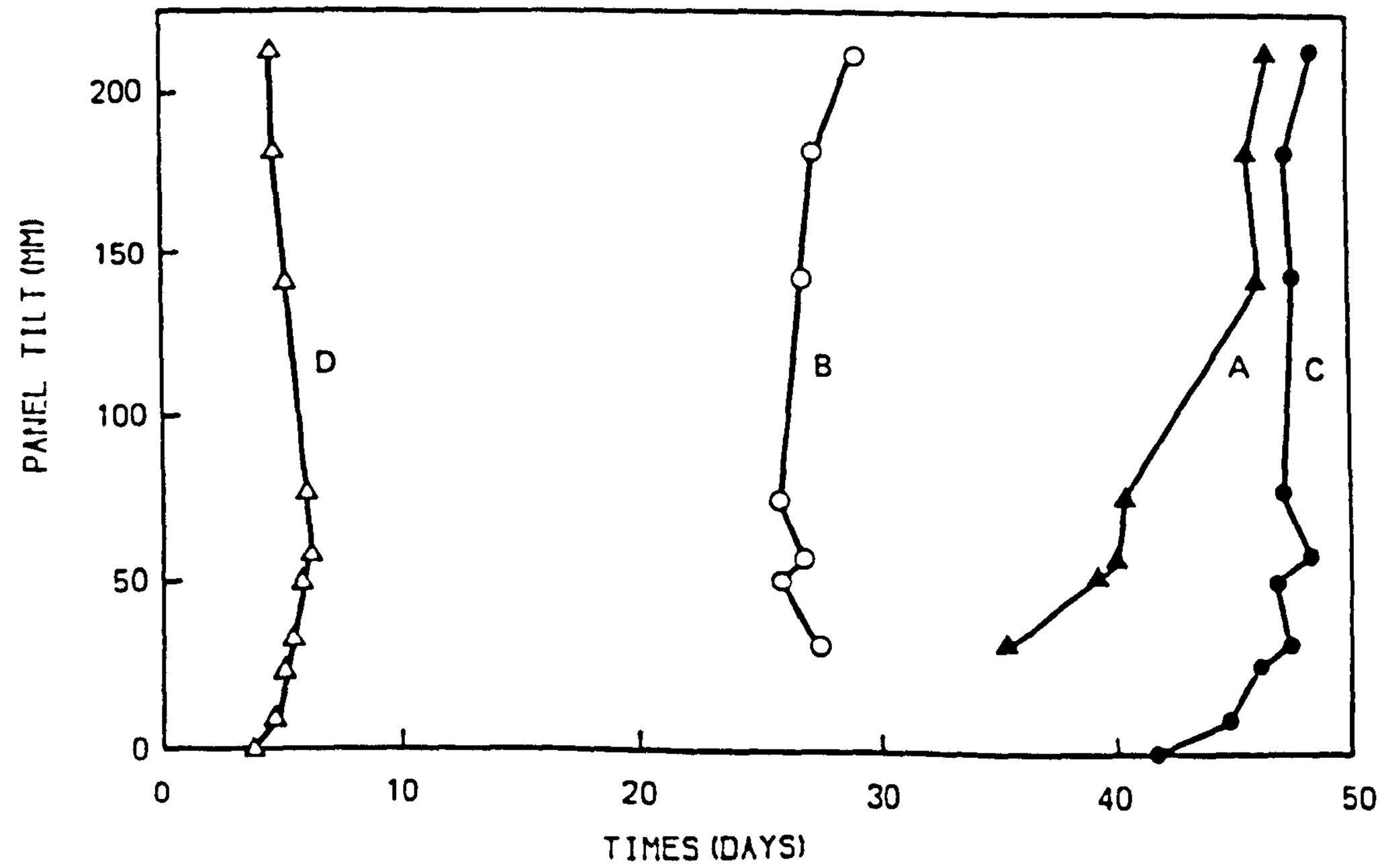

FIG. (2.30.B) VARIATION IN PANEL TILT (AFTER FINLAY, 1977).

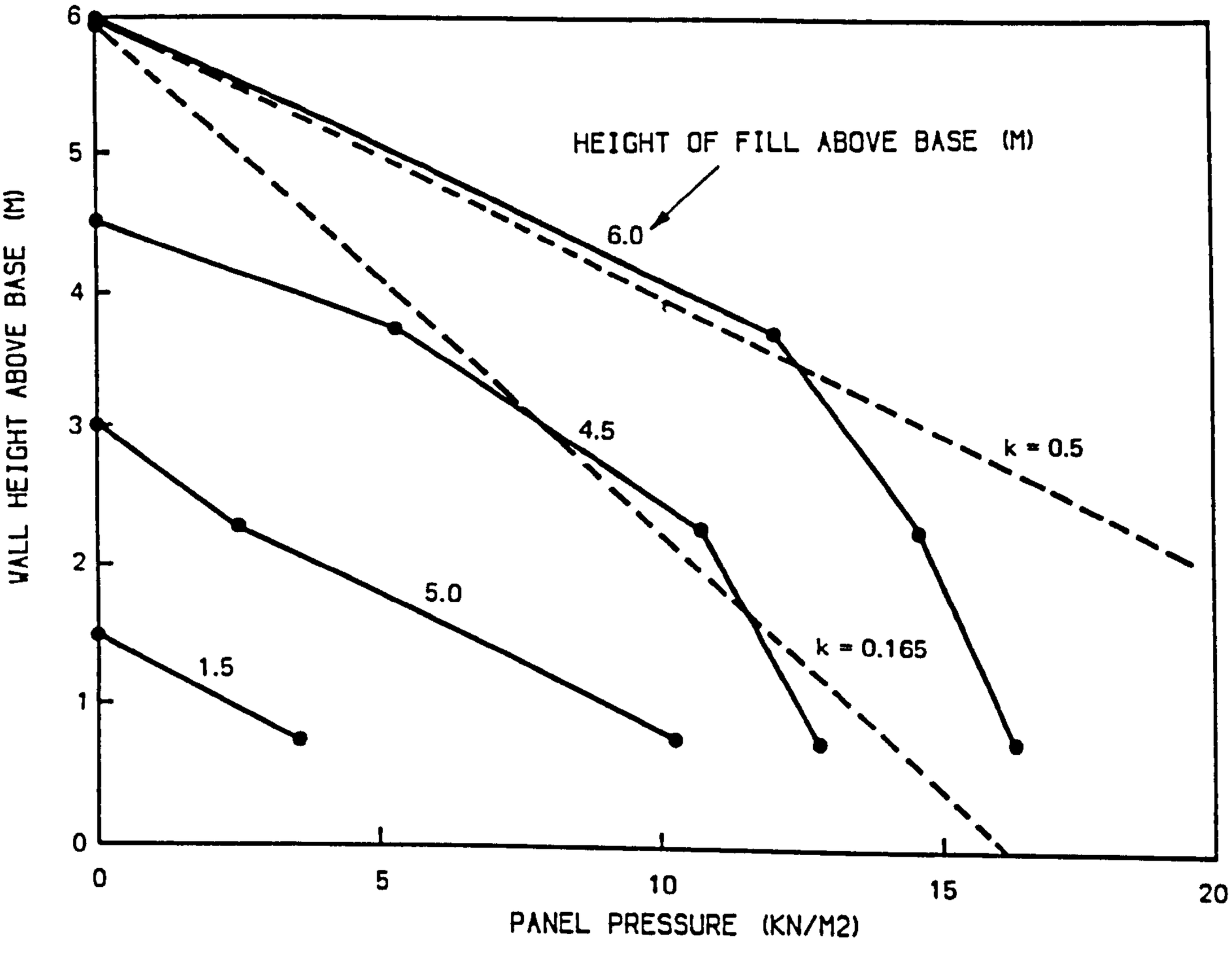

FIG. (2.31) DISTRIBUTION OF PRESSURE ON WALL FACE (AFTER FINLAY, 1977)

investigation by the Transport and Road Research Laboratory (TRRL) for four years. The total length of wall was about 100 m up to a maximum height of 6 m. A layout and cross section of the wall are shown in Fig. (2.18).

The facing units employed were reinforced concrete of spherically dished hexagonal shape, having dimensions 600 mm diametrically across the flats with a maximum thickness of about 100 mm and a weight of approximately 60 Kg. The reinforcing elements were galvanized mild steel strips, each of width 75 mm, thickness 5 mm and 5 m length. The horizontal and vertical spacing was governed by the size of the facing units (one strip for each unit).

The backfill was a well–graded sand–gravel mixture of dry density 1.98 Mg/m^3. The angle of internal friction was 48 degrees, the angle due to soil/reinforcement interaction was 29 degrees.

The method of construction of the wall was the York method, as discussed in Sec. 2.2 and shown in Fig. (2.7). In the York method, sliding was permitted between the facing and reinforcement by interconnecting the reinforcing elements through the vertical mild steel poles which were encased in grout–filled PVC tubes, as shown in Fig. (2.32.A). A construction procedure was established which limited movements due to compaction plant. In the method the front half metre of each layer was left until the next layer had been placed and compacted using heavy compaction. The strip adjacent to the face was then compacted using light compaction with a Wacker plate.

Instrumentation was carried out at two cross sections A & B, where the height of the wall was 6 m. Electrical resistance strain gauges bonded in pairs to the top and bottom of the reinforcing elements and pneumatic earth pressure

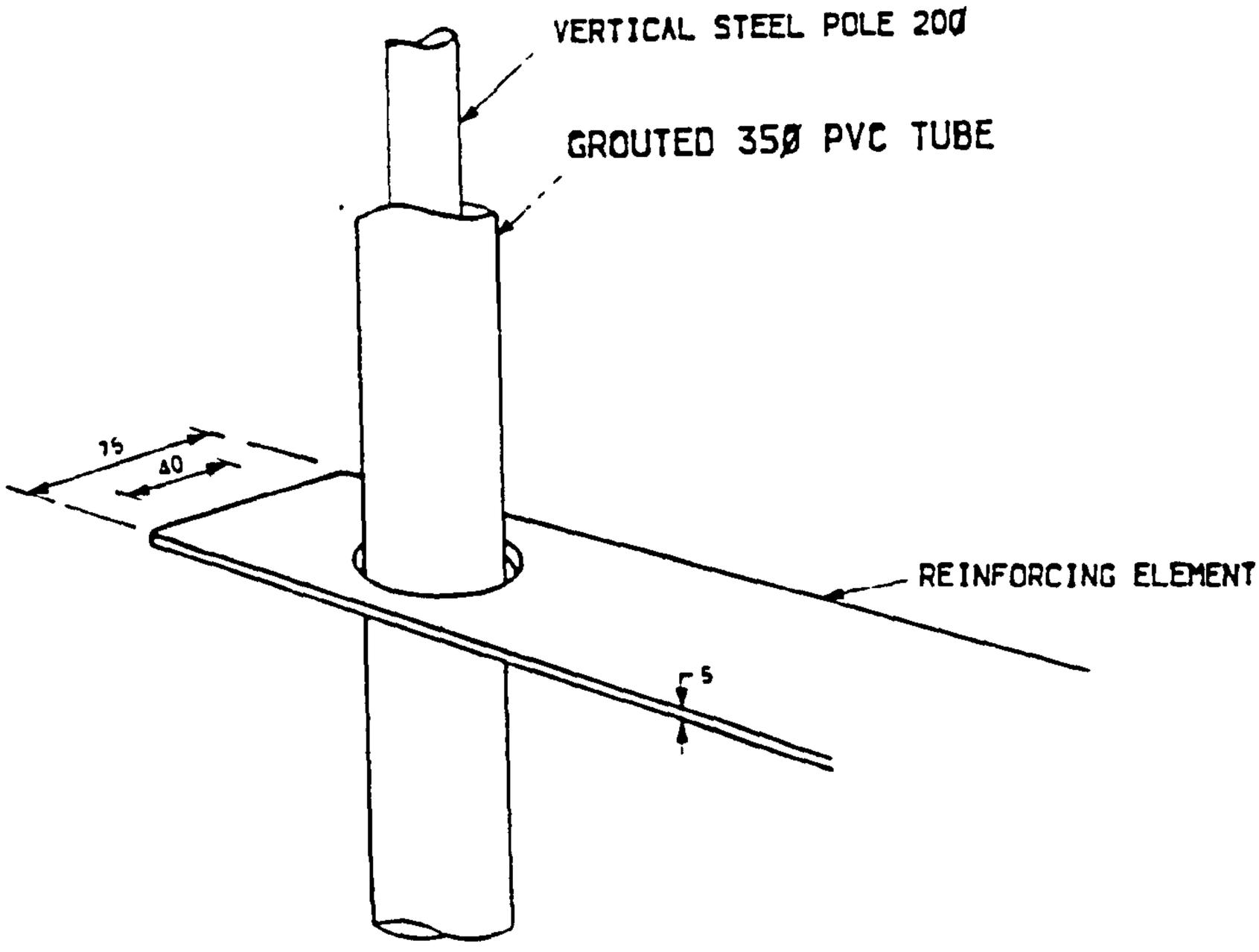

FIG. (2.32.A) CONNECTION BETWEEN THE REINFORCING ELEMENT AND THE WALL FACE (AFTER HOLLINGHURST AND MURRAY, 1988).

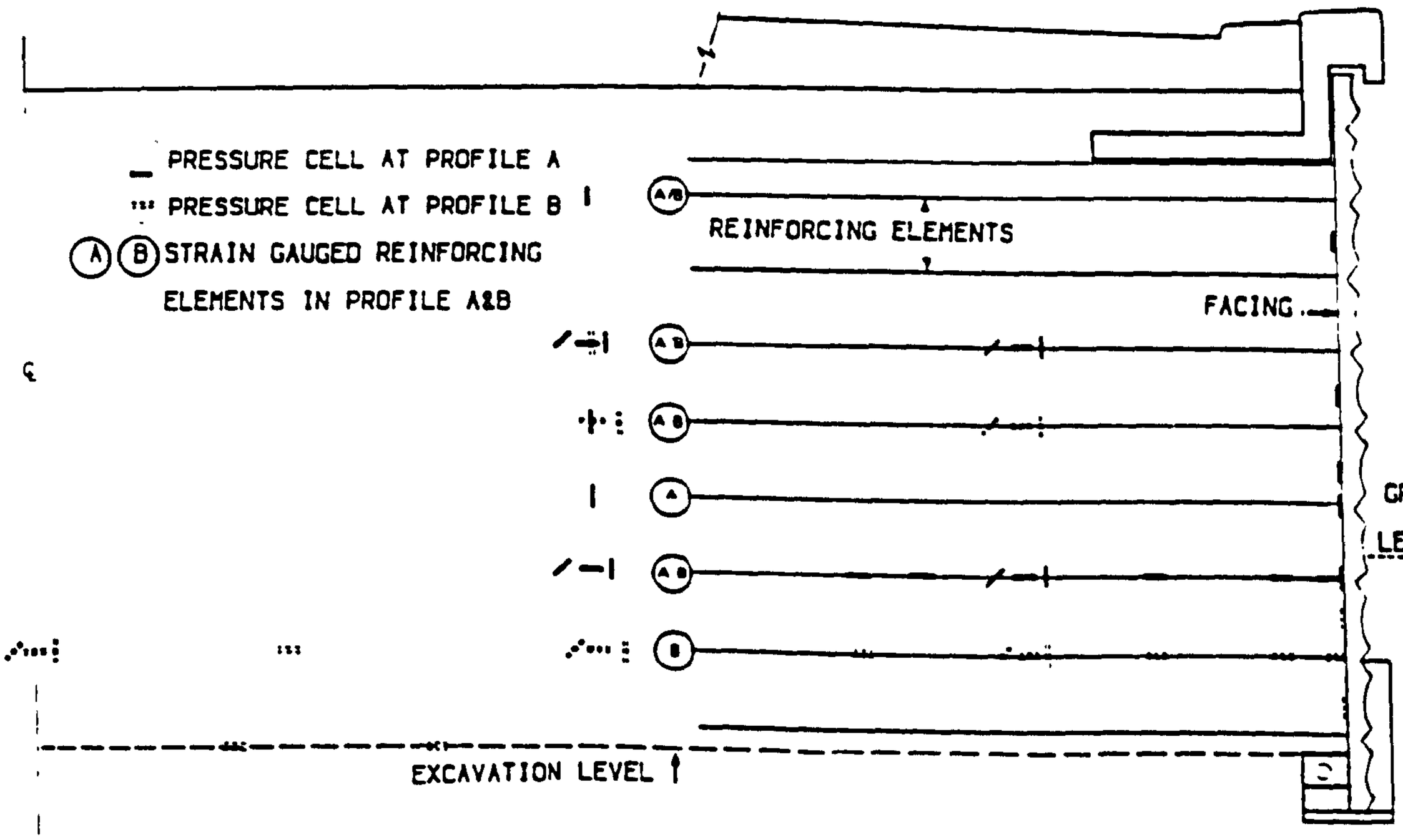

FIG. (2.32.B) INSTRUMENTATION OF GUILDFORD BYPASS WALL (AFTER MURRAY AND HOLLINGHURST, 1988).

cells were employed. The locations of strain gauges and pressure cells are shown in Fig. (2.32.B). The movement of the facing was monitored by means of a theodolite reading on to coned studs in selected facing units. Strain coils were used to measure the soil strain.

The measured tensile forces in the strips are shown in Fig. (2.33). The observed horizontal pressures at different sections are shown in Fig. (2.34), and the horizontal movement of the wall is shown in Fig. (2.35).

The main conclusion which can be drawn from these Figs. is the effect of construction and compaction plant on the forces in the strips, horizontal pressure and horizontal movement of wall, the values measured being greater than those obtained from the design using the classical theories. The small facing pressures are due to the method of interconnecting the reinforcing elements through the vertical rods. Thus the large tensions observed could be redistributed by passive resistance through these rods without greatly influencing the horizontal pressures acting on the facing, Hollinghurst and Murray (1986), and Murray and Hollinghurst (1986).

(C) Reinforced earth wall bridge abutment Lille: (France)

The reinforced earth wall was a highway bridge abutment 5.60 m high and 15 m long constructed at Lille in France in 1973–1974. The facing units were reinforced concrete panels 1.5 m x 1.5 m (cruciform shape), each panel being attached to six stainless steel reinforcing strips, each 80 mm wide, 1.5 mm thick, and 7 m or 10 m long. The horizontal and vertical spacings between strips were 0.75 m and 0.5 m respectively. The backfill material was a red schist compacted to an average density of 1.85 t/m^3. The internal friction angle of the

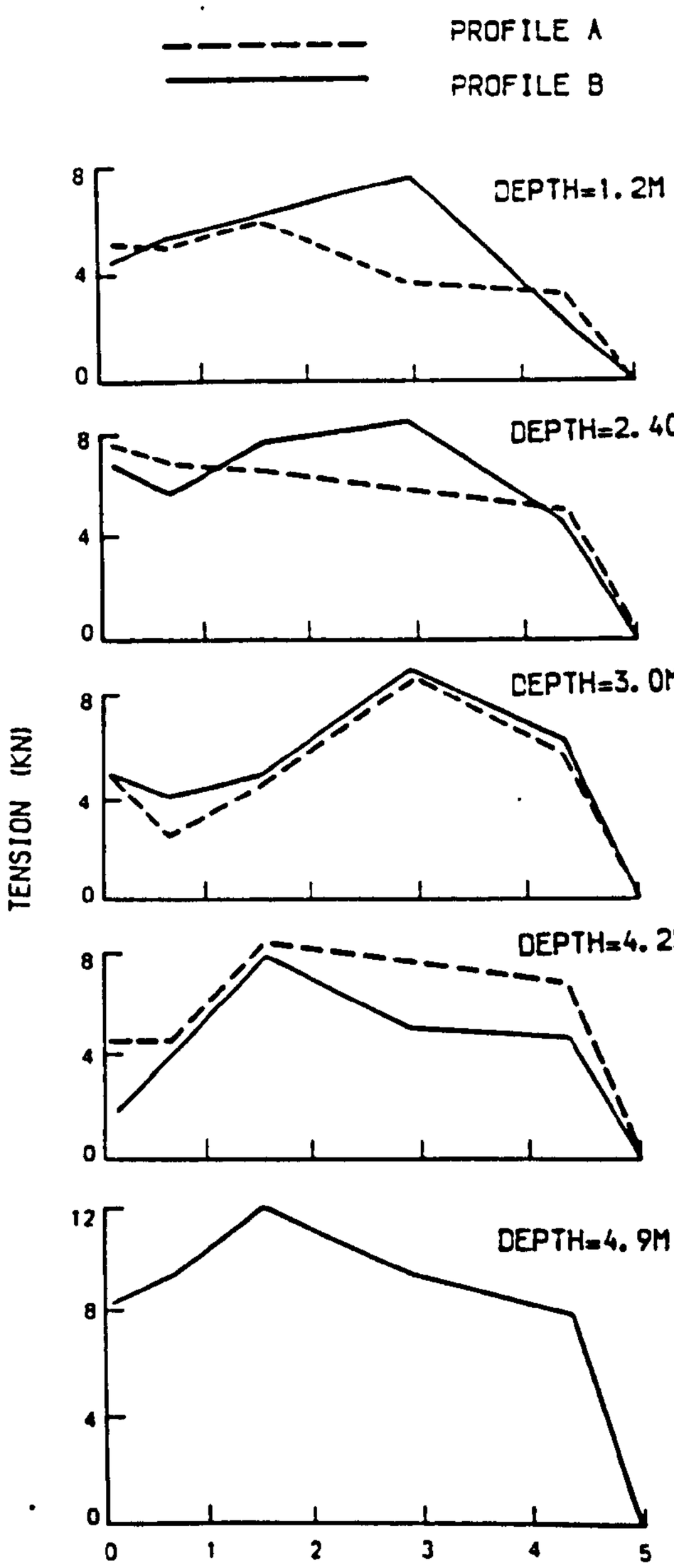

FIG. (2.33) MEASURED TENSILE FORCES IN THE STRIPS (AFTER MURRAY AND HOLLINGHURST, 1988).

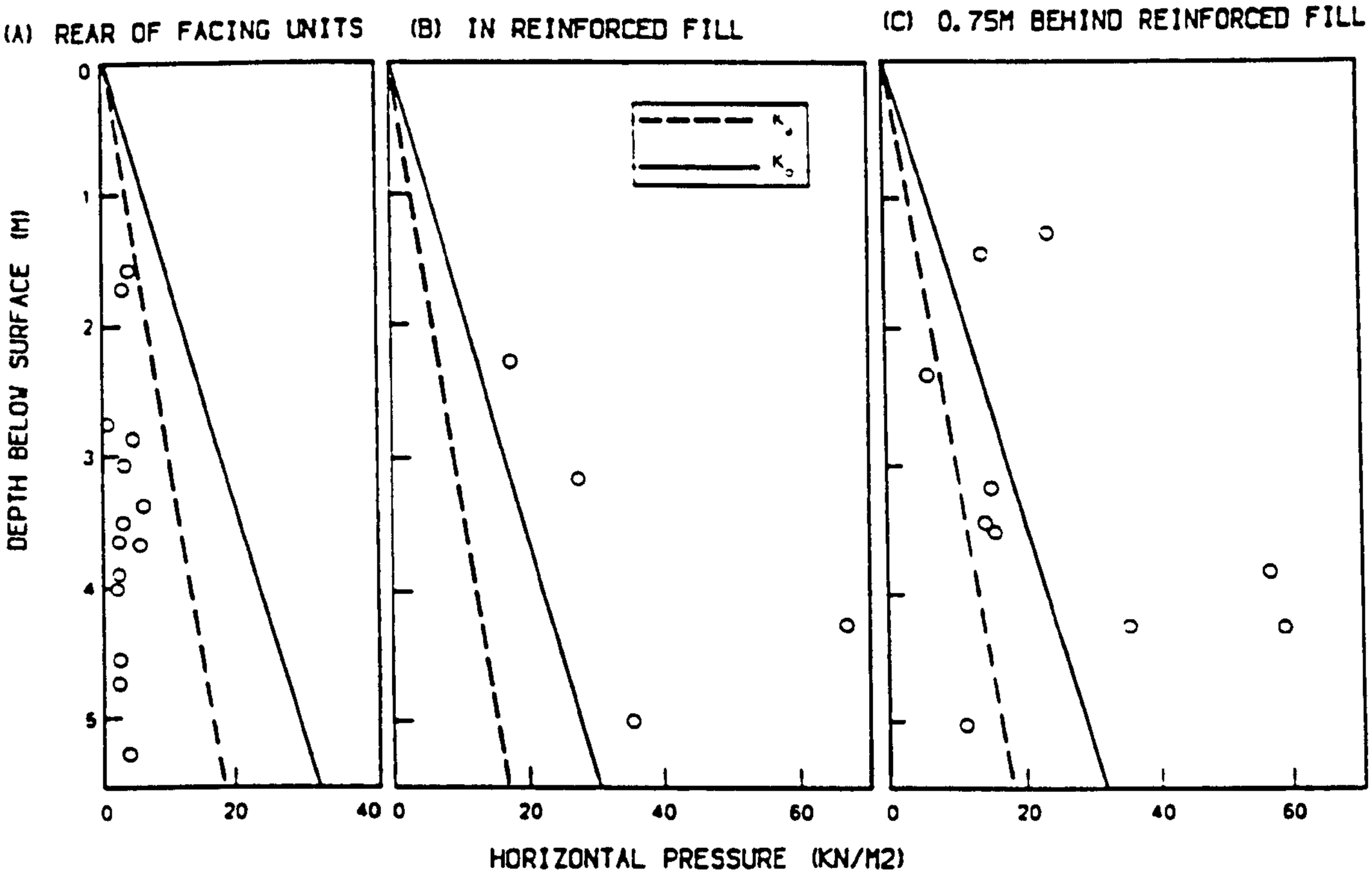

FIG. (2.34) CALCULATED AND MEASURED HORIZONTAL PRESSURES (AFTER MURRAY AND HOLLINGHURST, 1988).

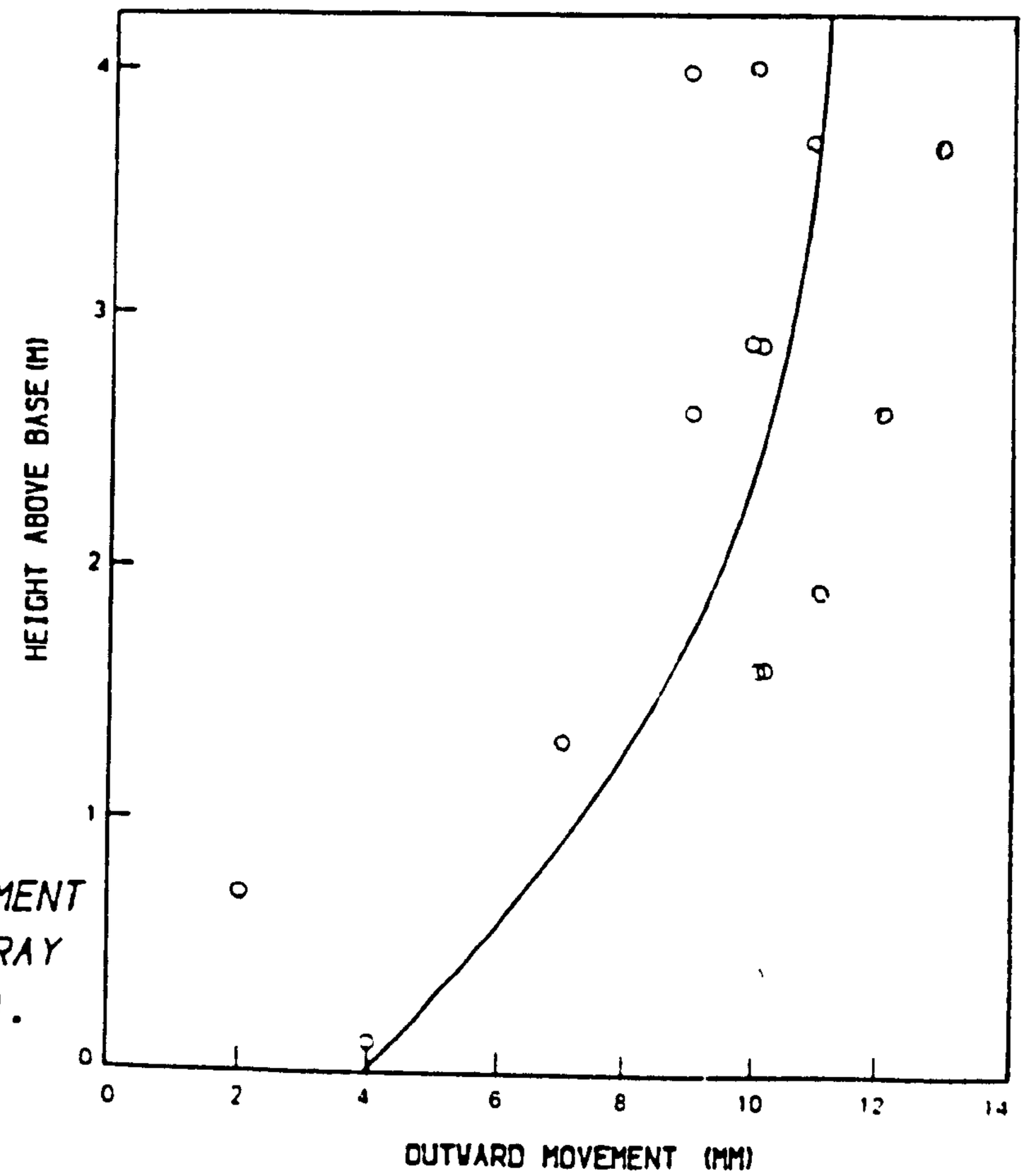

FIG. (2.35) HORIZONTAL MOVEMENT OF THE WALL (AFTER MURRAY AND HOLLINGHURST, 1988).

uncompacted material at a measured dry density of 1.46 t/m^3 was 44 degrees and increased with density up to 48 degrees after compaction.

Strain gauges and pressure cells (Glotzl cells) were used to measure forces in strips, state of stress within the reinforced mass and lateral pressure distribution. Locations and profiles of these measurements are shown in Fig. (2.36). Distribution of tensile forces in the strips and lateral earth pressures are shown in Figs. (2.37&38) respectively. The state of stress not only for the Lille abutment but also for several walls throughout the world is shown in Fig. (2.39).

It was concluded that the actual behaviour of reinforced earth walls depends essentially upon many factors including the construction procedure and compaction conditions. The effect of compaction raises the horizontal pressure in the backfill and the tensile forces in the strips, Juran et al. (1978), and Baguelin (1978).

(d) Reinforced earth wall in Bai Shawan: (China)

Quyang (1988) reported that a reinforced earth quay wall was constructed in 1985 in Chongqing in China. The wall length was 137 m and it varied from 18 to 26 m in height as shown in Fig. (2.19). The facing units were reinforced concrete panels 1.5 x 1.5 x 0.25 m and the backfill was sand and gravel of unit weight 19.6 kN/m^3 with an angle of internal friction of 36 degrees.

The reinforcements were polypropylene (geosynthetic fibre) strips, 20 mm in width and 1.2 mm in thickness. Measurements of earth pressure on the wall face as well as the forces in the strips are shown in Figs. (2.40.A&B) respectively. It is obvious from the Figs. that the measured earth pressures differ

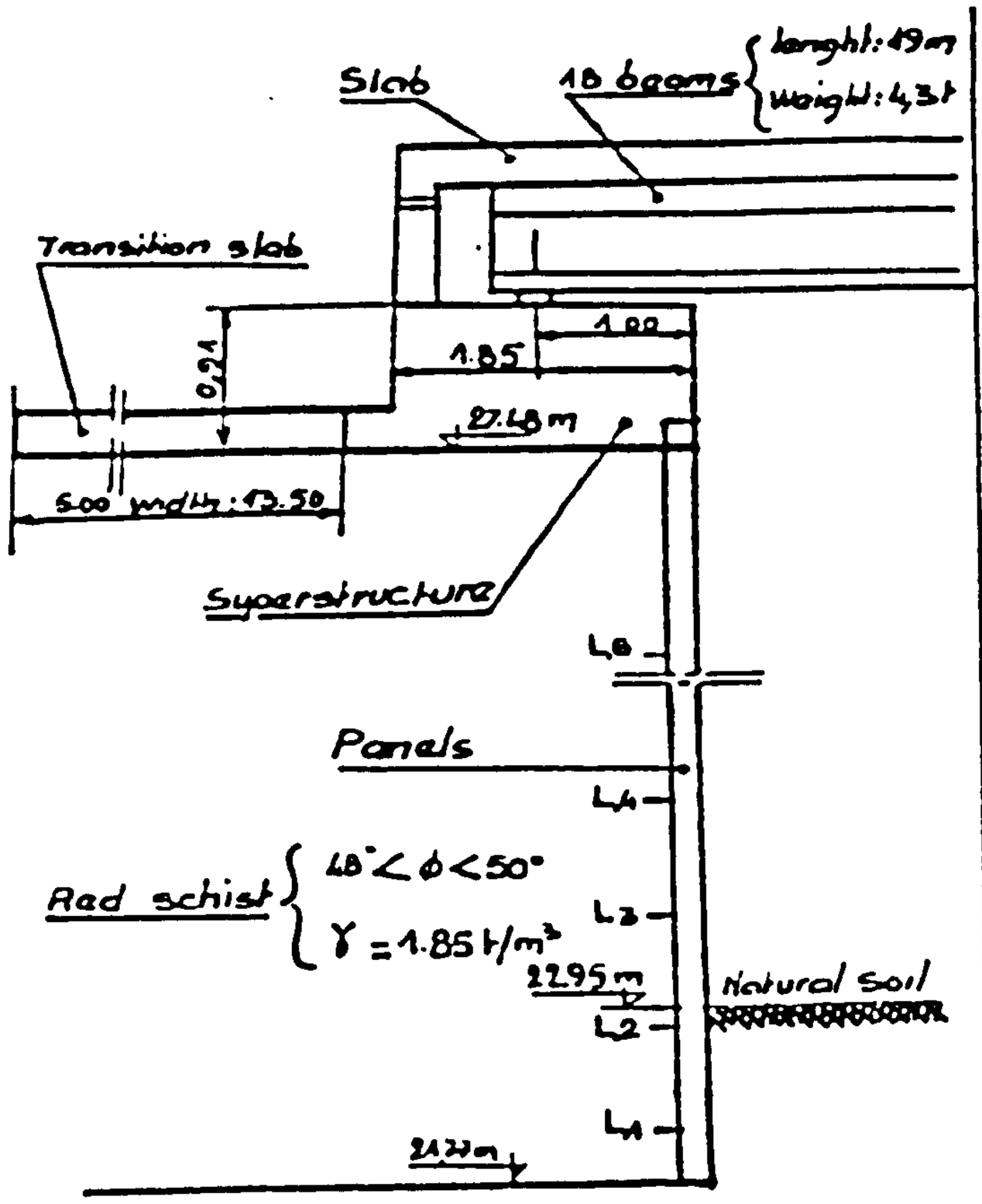

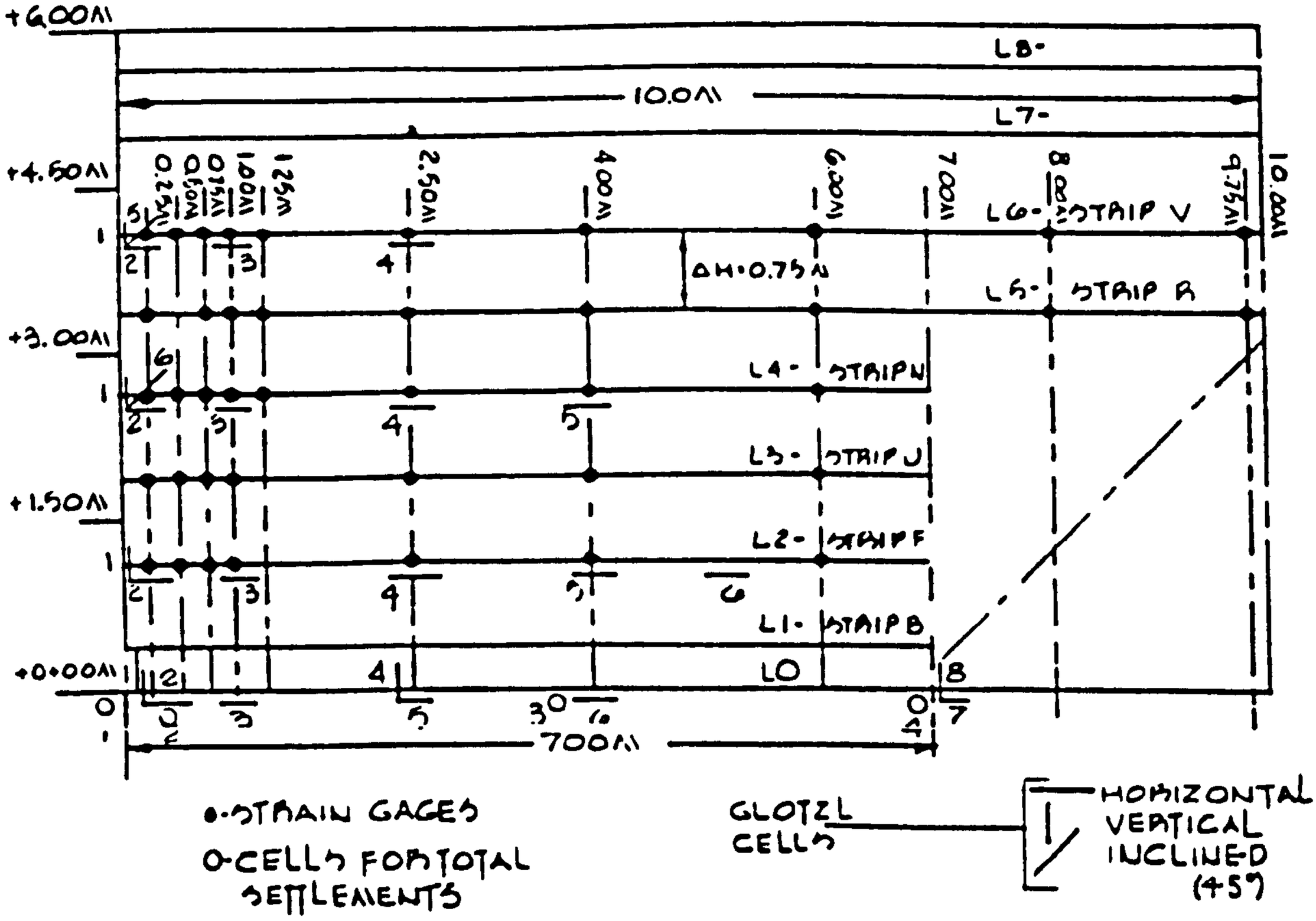

MAIN MEASUREMENT PROFILE

FIG. (2.36) LOCATION AND PROFILE OF MEASUREMENTS (AFTER JURAN ET AL., 1978).

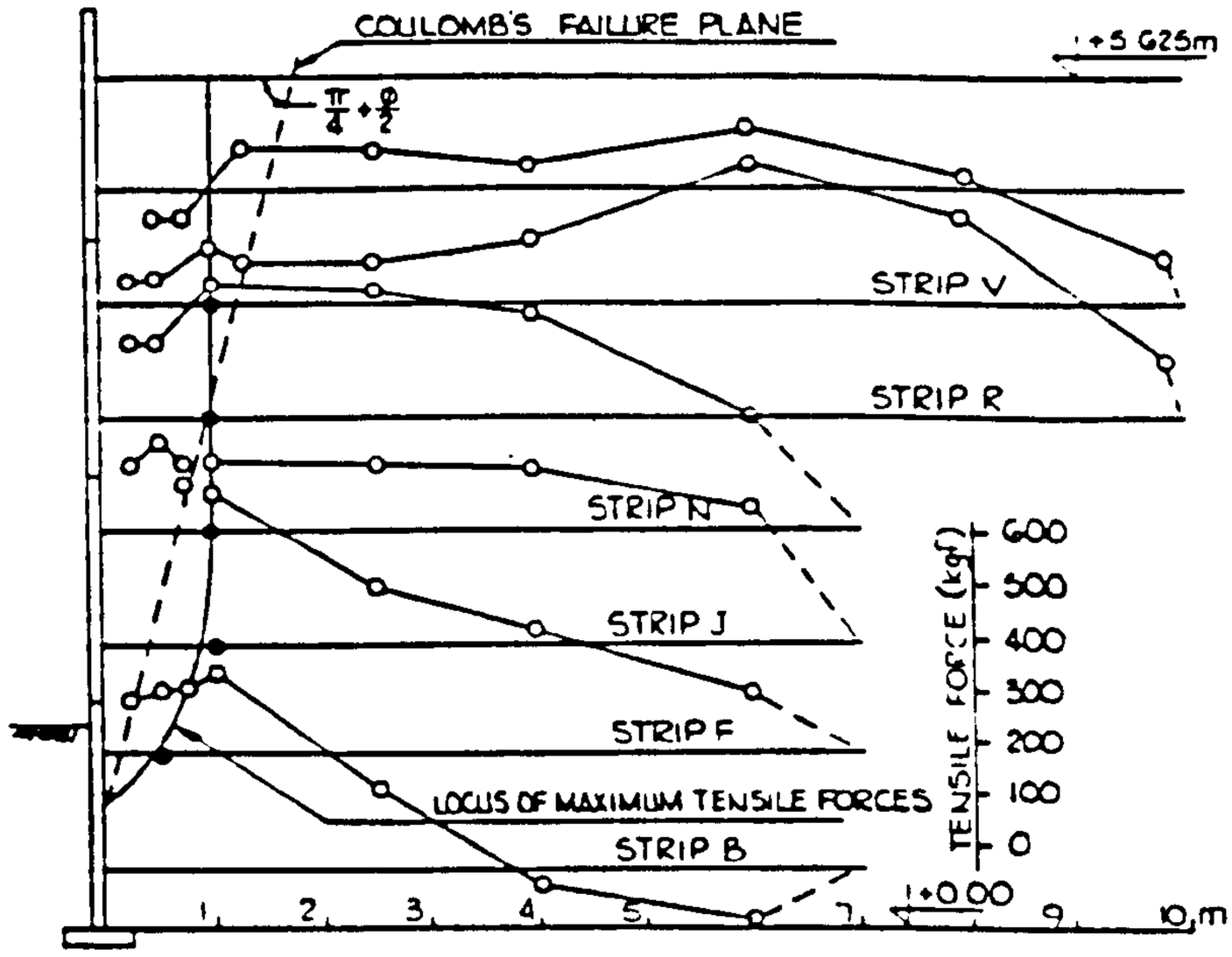

FIG. (2.37) DISTRIBUTION OF TENSILE FORCES IN THE STRIPS (AFTER JURAN ET AL., 1978).

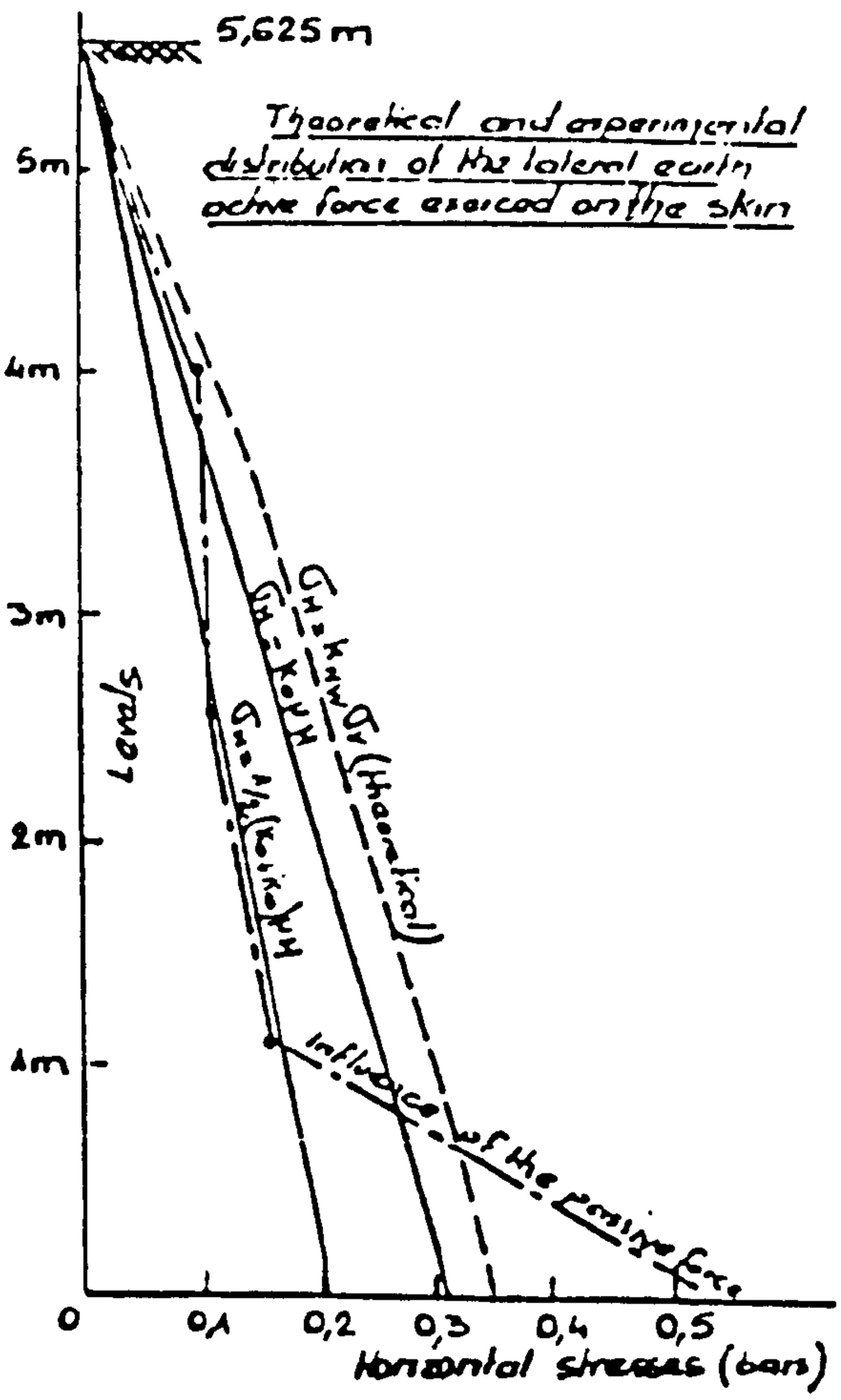

FIG. (2.38) DISTRIBUTION OF HORIZONTAL EARTH PRESSURE (AFTER JURAN ET AL., 1978).

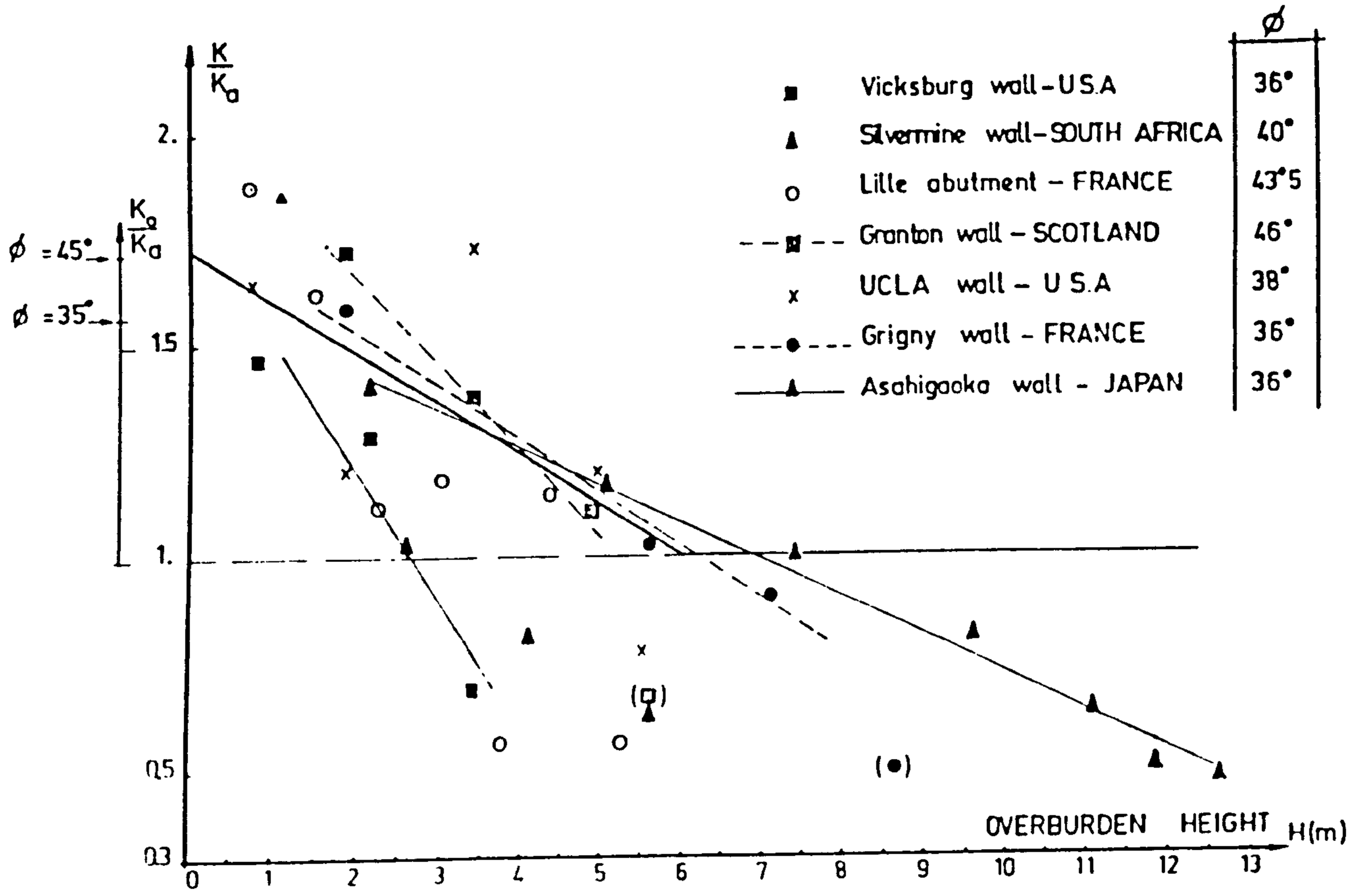

FIG. (2.39) STATE OF STRESS IN SEVERAL INSTRUMENTED WALLS (AFTER BAGUELIN, 1978)

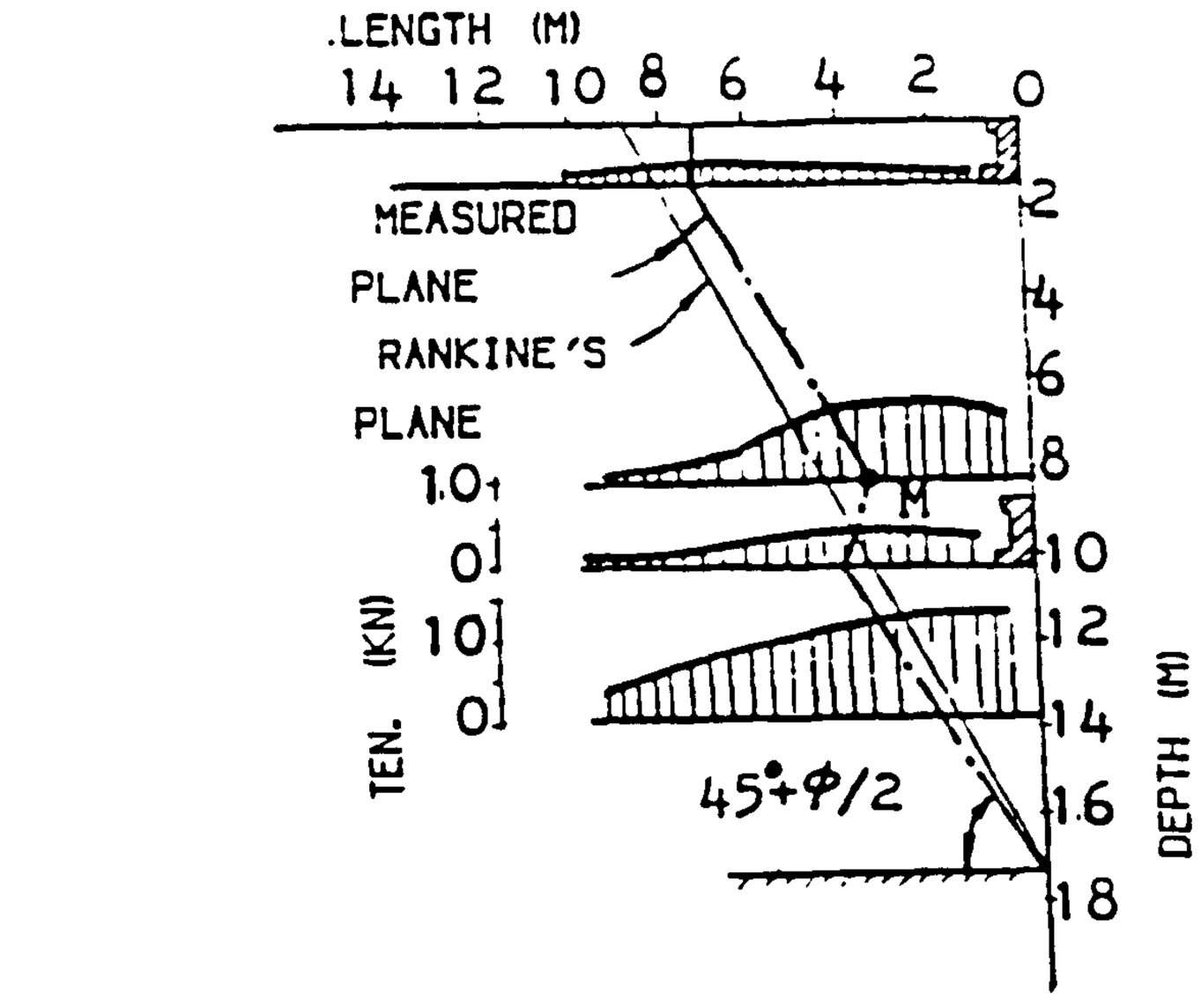

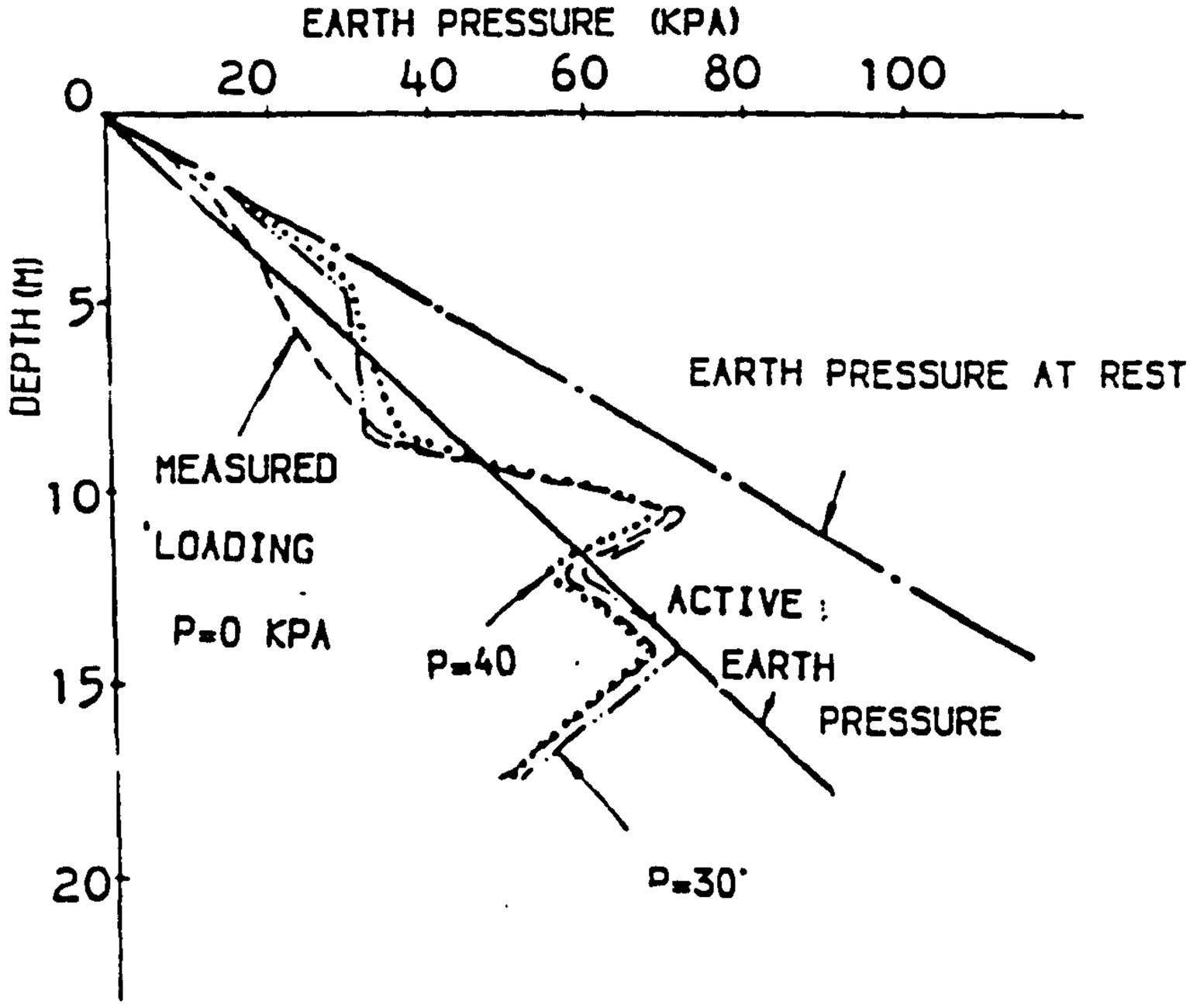

FIG. (2.40) INSTRUMENTED WALL IN CHINA (AFTER QUYANG, 1988).

from those calculated from classical theories. Again the compaction plays an important factor in this difference.

(2) Full Scale Model

Full scale tests can assist greatly in understanding the behaviour of reinforced earth retaining walls. Since the 1960's many full scale tests on reinforced earth retaining walls have been carried out.

A reported and documented reinforced earth wall was constructed by TRRL. Boden et al. (1977 & 1978), and Murray and Boden (1979) carried out full scale trials of reinforced earth walls under the TRRL programme to provide guidance for design, construction, and maintenance. The structure consisted of a 6 m high embankment retained on three sides by facing units. The dimensions of the embankment were 45 m long, 14 m wide and the free side was a 20 m long ramp. Different types of reinforcing elements of constant length 4 m, and the facing units and three different type of backfill are shown in Fig. (2.41). These types were sandy clay at the bottom, gravelly sand at the middle and silty clay at the top.

The fill materials were spread in 255 mm thick layers and compacted to approximately 150 mm thickness using a 5 Mg. towed vibratory roller to within 2 m of the face of the wall and a 1 Mg. pedestrian operated vibratory roller for the remaining area. The average dry density of each soil type from the bottom to top was 1.8, 2.1, and 1.63 Mg/m^3 respectively.

Instruments were installed to measure tension in the reinforcing elements, vertical and horizontal earth pressure, porewater pressure, soil temperature and

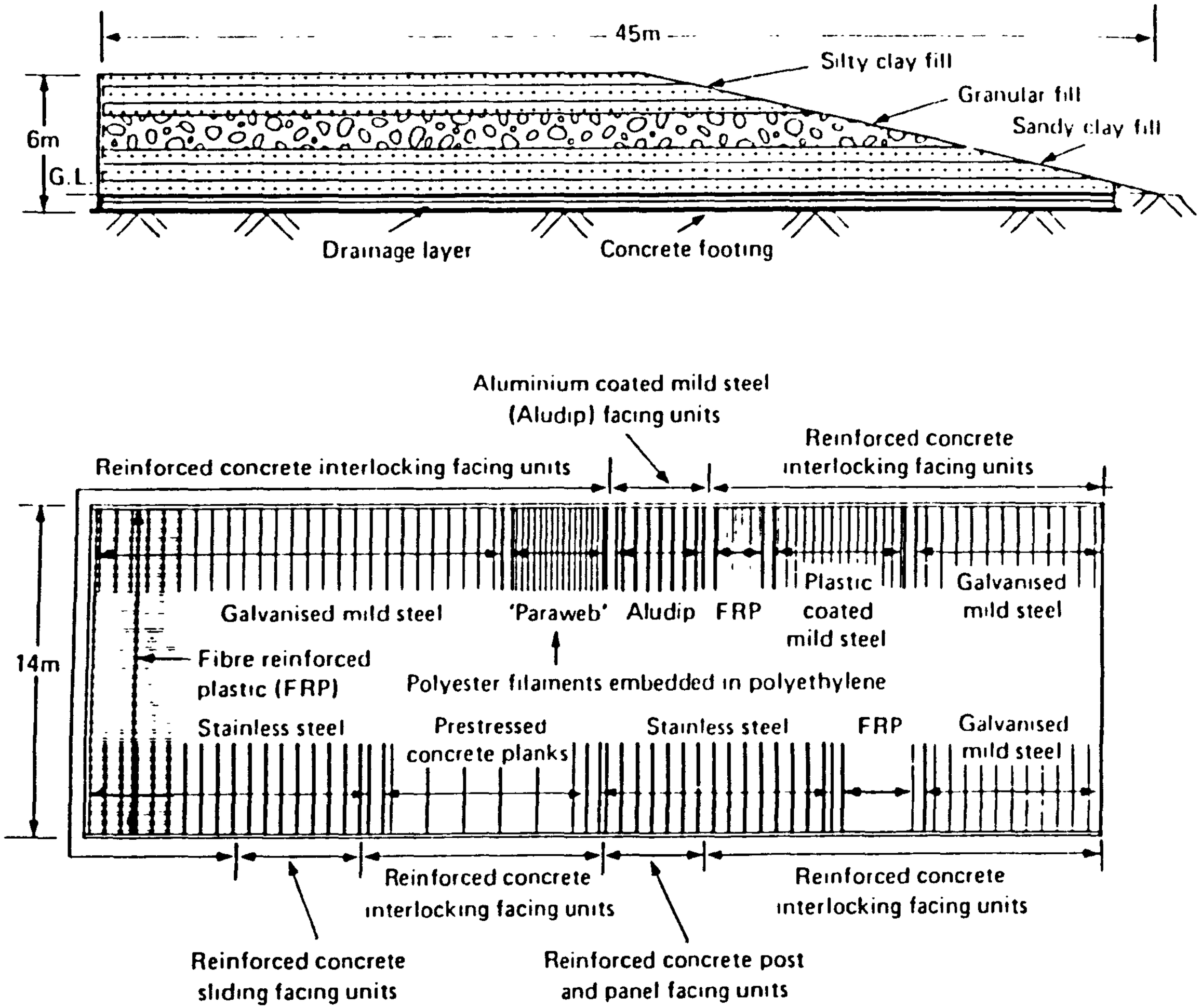

FIG. (2.41) PLAN AND ELEVATION OF FULL SCALE TEST OF REINFORCED EARTH WALL (AFTER BODEN ET AL., 1978).

settlement within the fill mass. Additionally locating studs were inserted in selected columns of the facing units to enable measurements to be made of their horizontal and vertical displacement using a theodolite and optical level respectively. The location of instruments installed in the structure is shown in Figs. (2.42.A,B&C). Distribution of variation of pressure with height of fill above the pressure cell installed 1.125 m above the footing of the wall, is shown in Fig. (2.43). The distribution of vertical stress under the reinforced mass is shown in Fig. (2.44), and the distribution of tensile forces in the strips is shown in Fig. (2.45).

The conclusion presented by Murray and Boden (1979) was that, during construction the compaction plant induced relatively high horizontal pressures near to the wall facing units which remained until the pressures were exceeded as a result of the increasing fill load. Heavy compaction plant can cause excessive deformation and should be kept at least 2 m distant from the facing. These effects should be considered during design.

2.7.2 Small Scale Tests

Since Vidal's patent in the 1960's a large number of experimental studies of model reinforced earth retaining walls have been carried out in different parts of the world such as France, U.S.A., U.K., and Japan. These models have been constructed in order to improve the understanding of the behaviour of reinforced earth structures up to failure, study the internal and external stability under different conditions of load such as static, dynamic, earthquake, ... etc., improve the material of facing units and reinforcement, and choose cheaper backfill material, improve the current design methods, and study the interaction between soil and reinforcement.

(A) PLASTIC STRIPS

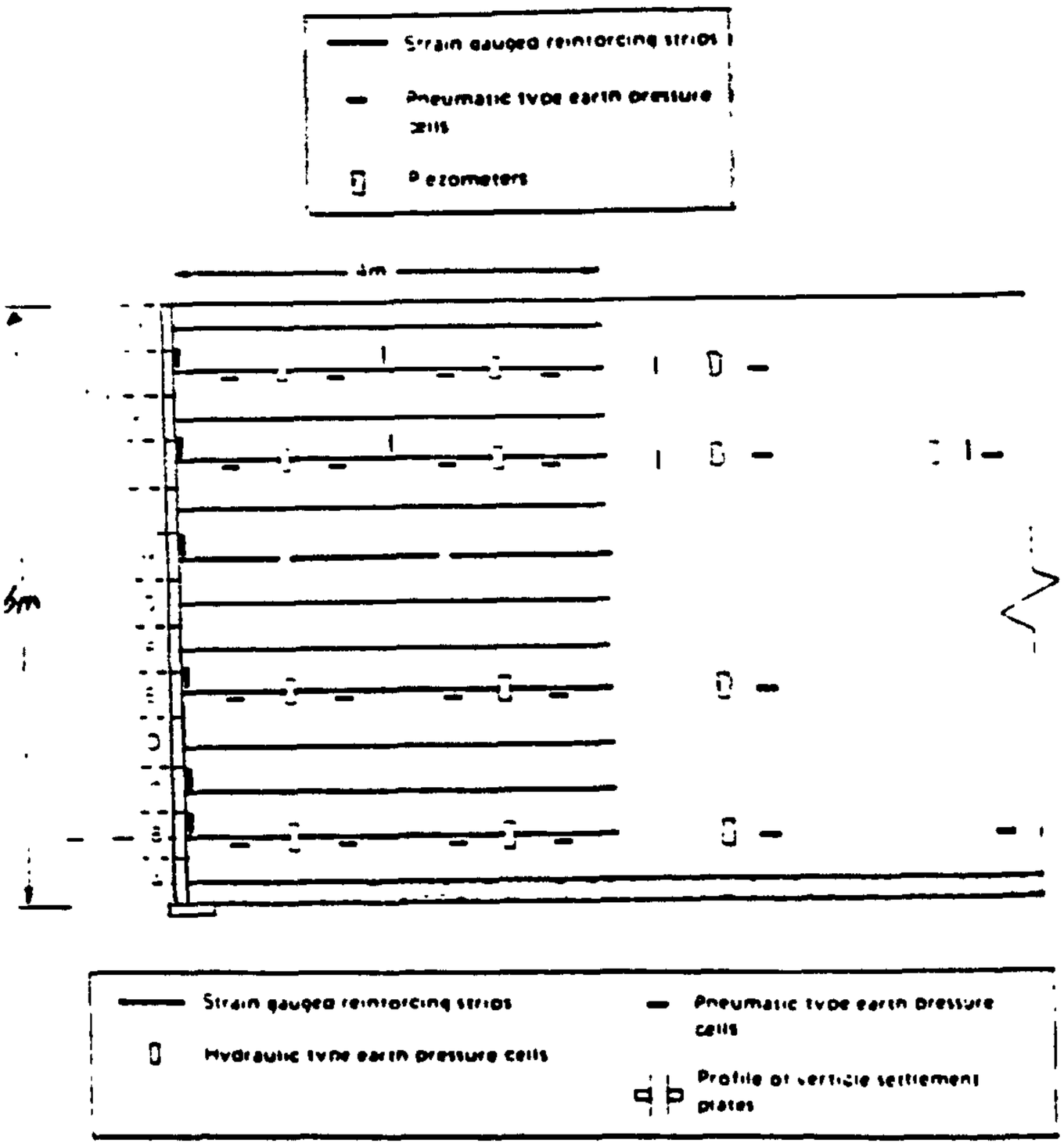

(B) GALVANIZED MILD STRIPS

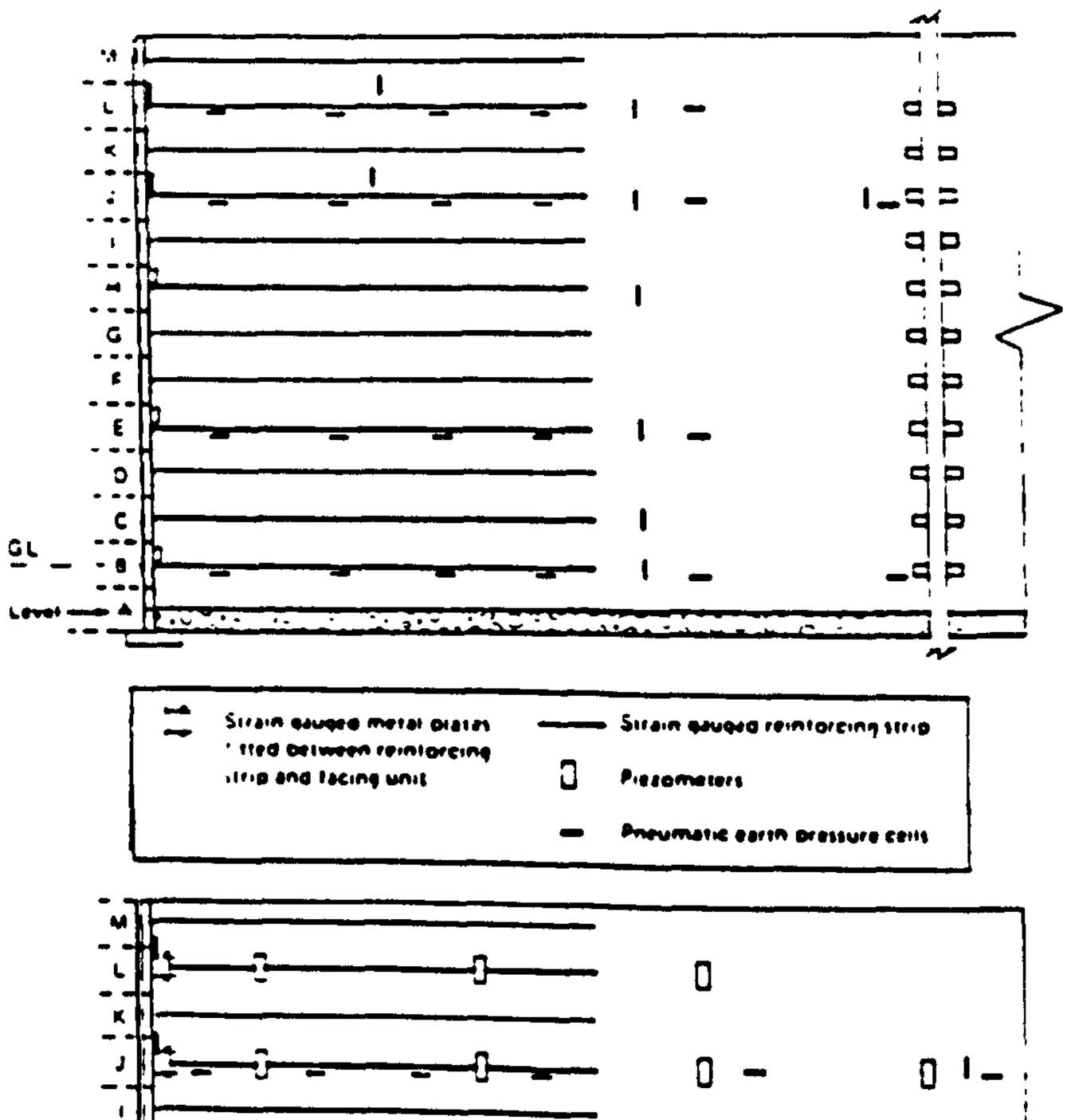

(C) PARAWEB STRIPS

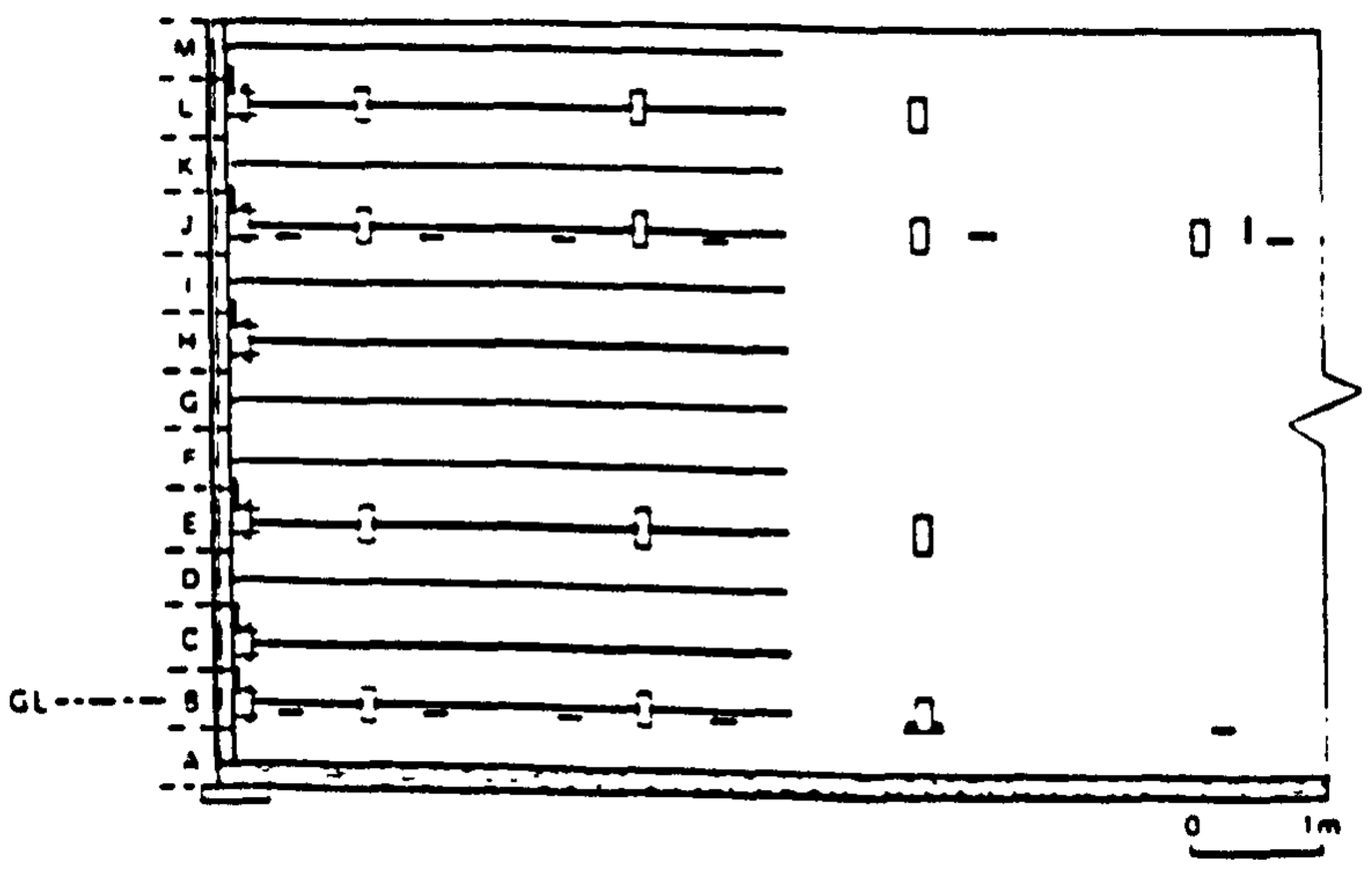

FIG. (2.42) LOCATION OF INSTRUMENTATION (AFTER BODEN AND ET AL., 1978.

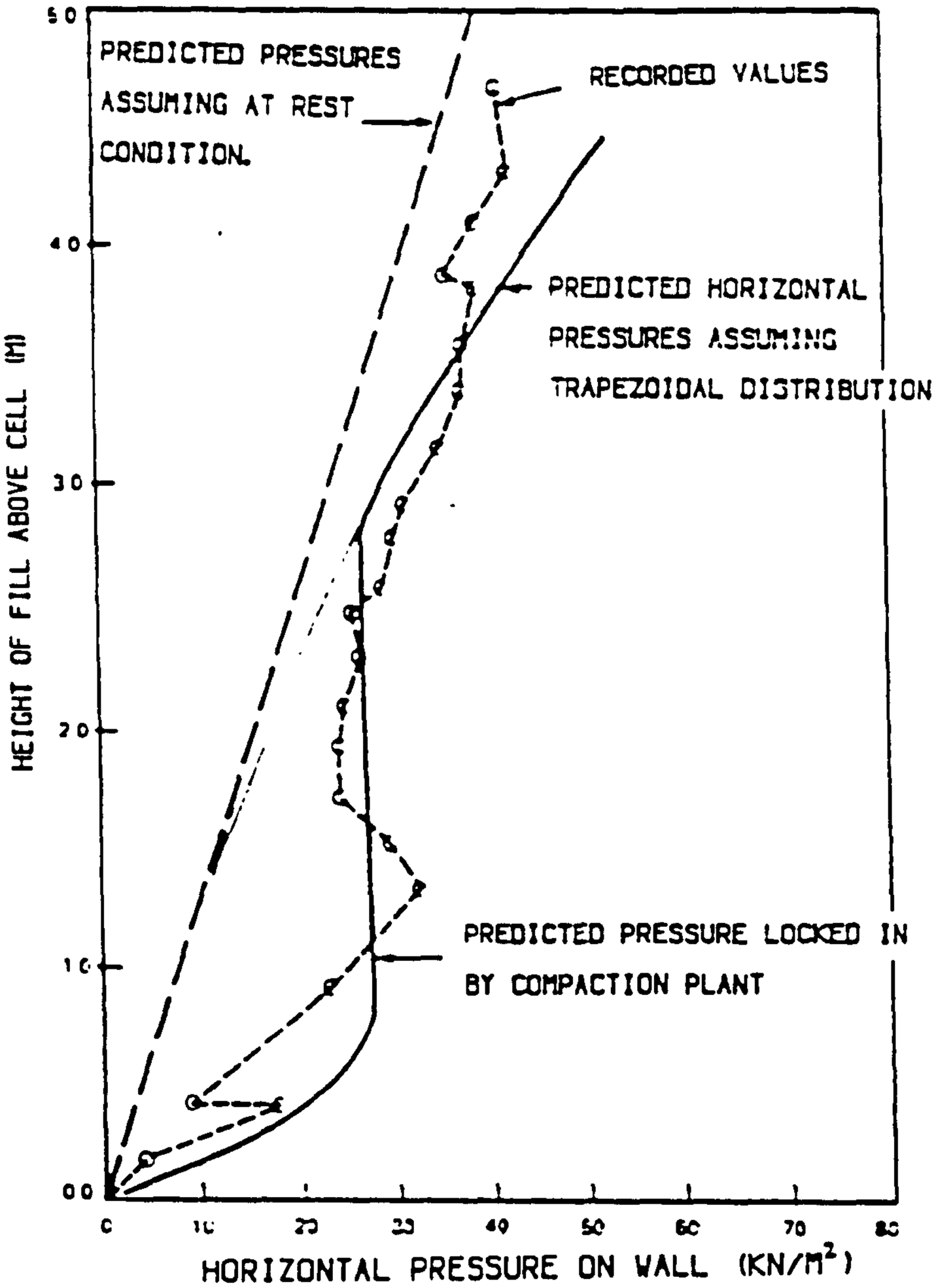

FIG. (2.43) VARIATION OF PRESSURE WITH THE HEIGHT OF FILL (AFTER MURRAY AND BODEN, 1979).

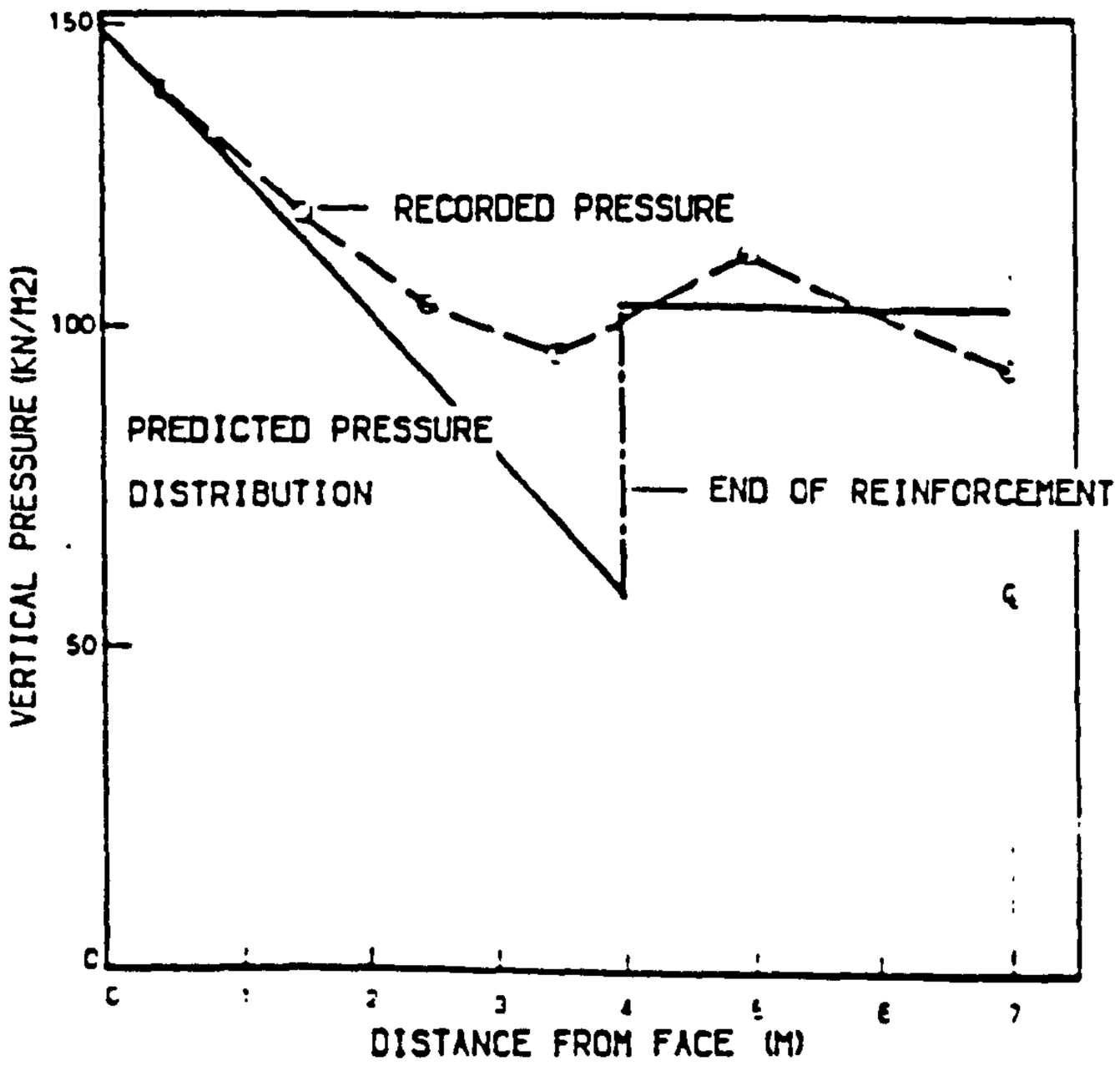

FIG. (2.44) DISTRIBUTION OF VERTICAL STRESS UNDER THE WALL (AFTER MURRAY AND BODEN, 1979).

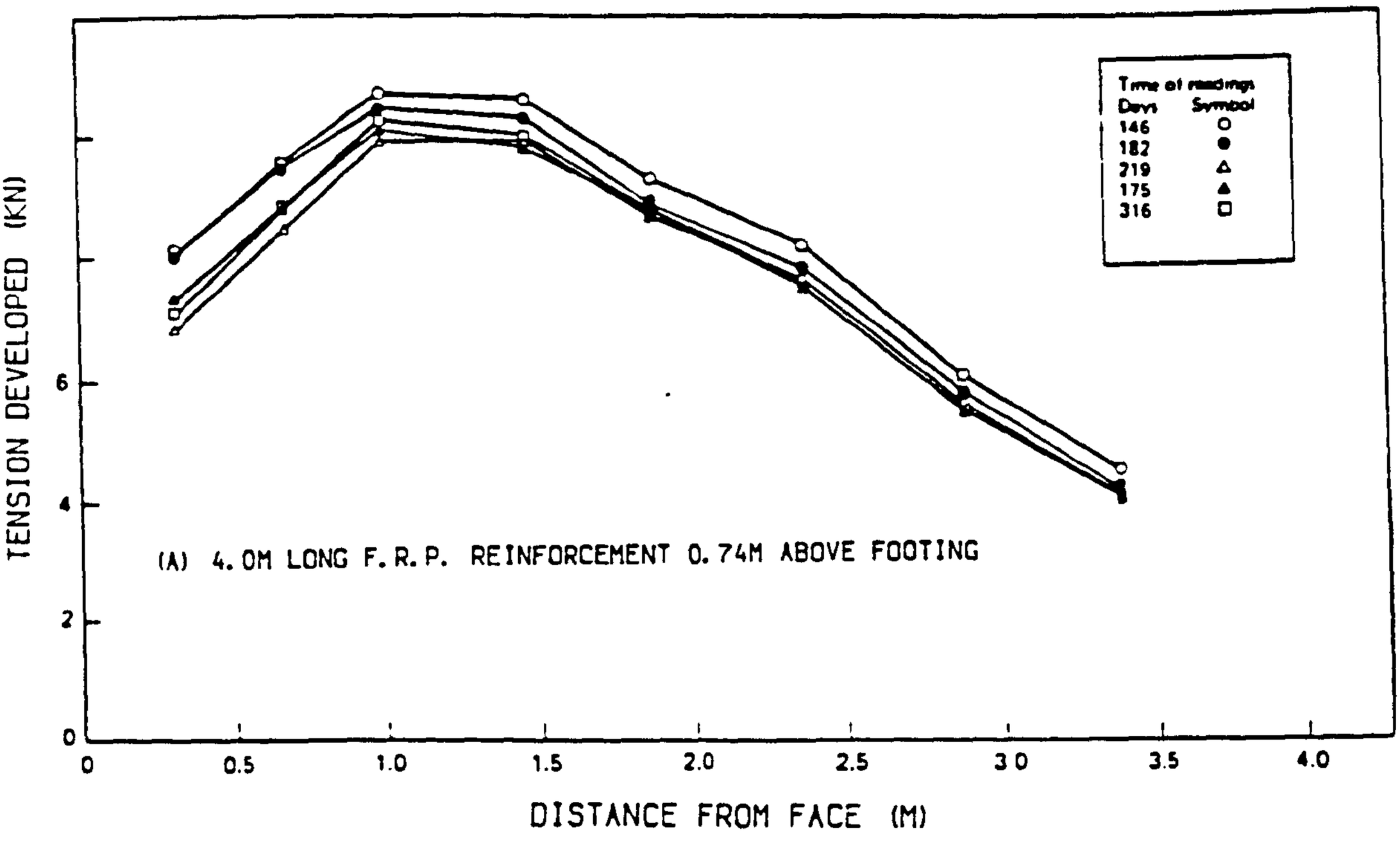

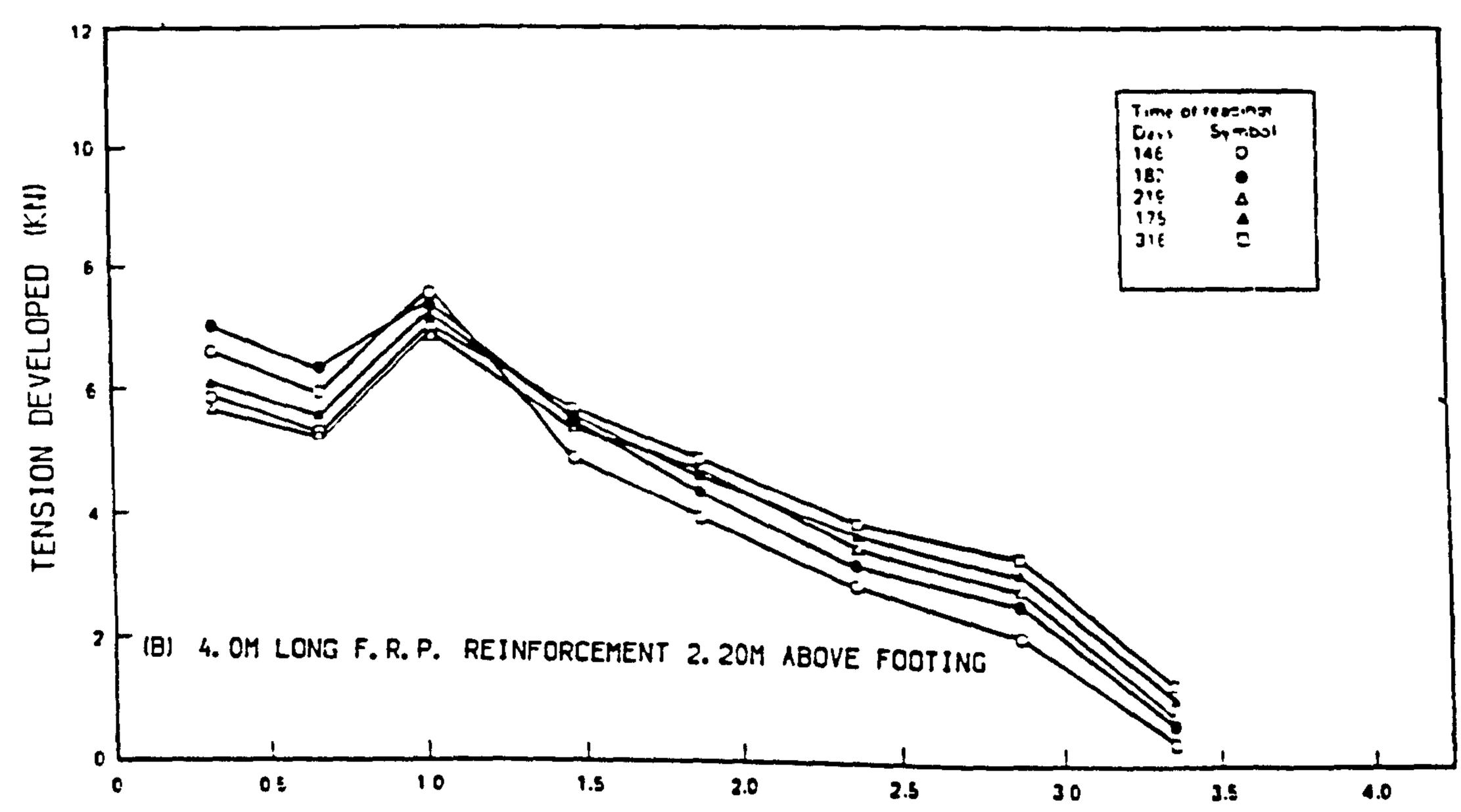

FIG. (2.45) DISTRIBUTION IN F.R.P. REINFORCEMENT IN LOVER COHESIVE FILL (AFTER MURRAY AND BODEN, 1979).

Juran and Christopher (1989) stated that the similitude requirements between the reduced scale model and the actual prototype were found to be difficult to formulate. However, these reduced scale models provide a very efficient, rapid, and economical research tool to investigate mechanisms of reinforced earth walls and can be used in a parametric study to evaluate available design approaches.

The vast majority of backfill material used is cohesionless material particularly sand because of its ease of handling. Most of the models are not compacted at all, the sand being gently placed by means of a free flowing hopper, Smith (1977).

Compaction has been used in only a very small number of reduced model reinforced earth walls and does not simulate what occurs in the field i.e. the compaction plant effect. The compaction device used has been either a bearing plate with a certain weight falling through a certain height as in the model used by Hoshiya (1978), or the method of compaction has not been mentioned because it was not the point of concern as in the model of the reinforced earth wall by Juran and Christopher (1989). The difficulty of simulating the compaction plant has led to this lack of realism in reduced model reinforced earth walls.

2.8 DESIGN OF REINFORCED EARTH WALLS

Failure of reinforced earth walls can be classified as either internal or external. The methods of design are divided into two categories to correspond to the two types of failure.

In the first category the wall can fail internally in two different modes:

(a) The reinforcement has insufficient bond with the soil and slides out i.e. the maximum frictional force mobilized by the soil/reinforcement interaction is exceeded. Sometimes this is called adherence failure as shown in Fig. (2.46.B).

(b) The reinforcement has insufficient strength to resist the bearing stress, the reinforcement breaks, and the resulting almost instantaneous redistribution of stresses fails the structure catastrophically. This is called tension failure as shown in Fig. (2.46.C).

The second category deals with the overall external stability of the structure by considering the effect of the reinforced earth mass on the surrounding region of the soil. These types of failure include slip, bearing and sliding failure, as shown in Fig. (2.46.D,E&F) respectively.

2.8.1 Internal Stability

Internal stability is concerned with estimating the number, size, strength, spacing and length of the reinforcing elements needed to ensure stability of the whole structure, together with the pressure exerted on the facing. The analyses to check internal stability can be divided into two groups depending on the assumptions which are made to calculate the maximum tensile force within any of the reinforcing elements.

These two groups are:

(a) Methods which consider the local equilibrium of individual reinforcing elements and are based on Rankine theory. They considered the transfer of stress from the soil to a single strip. These methods have been developed by

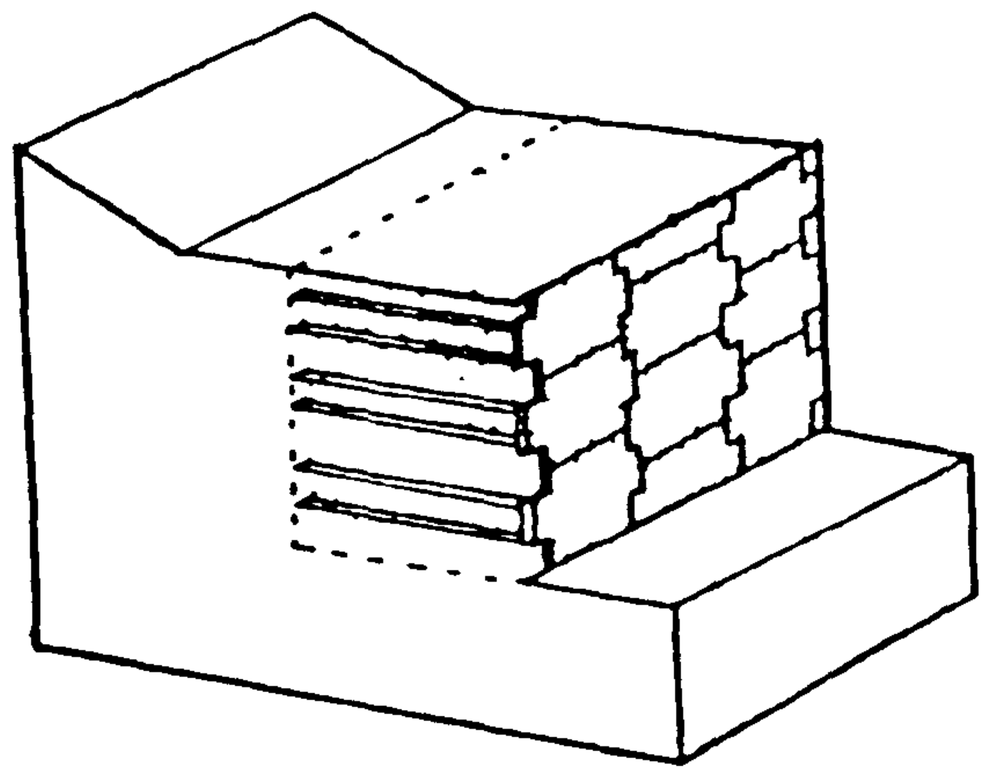

(A) REINFORCED EARTH WALL

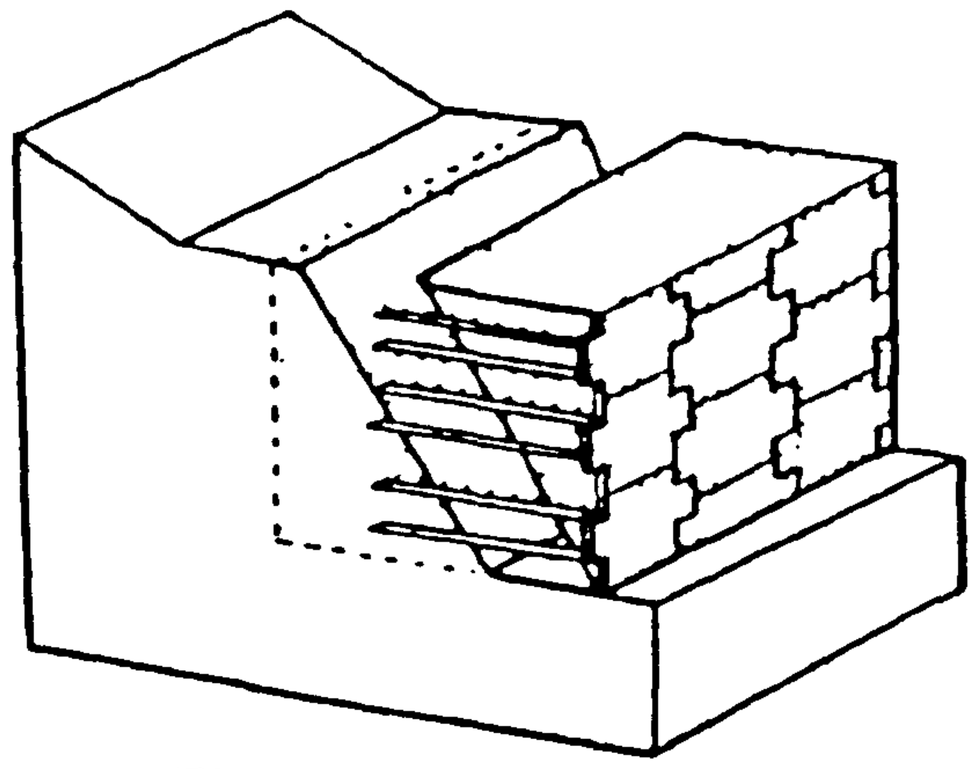

(B) ADHERENCE

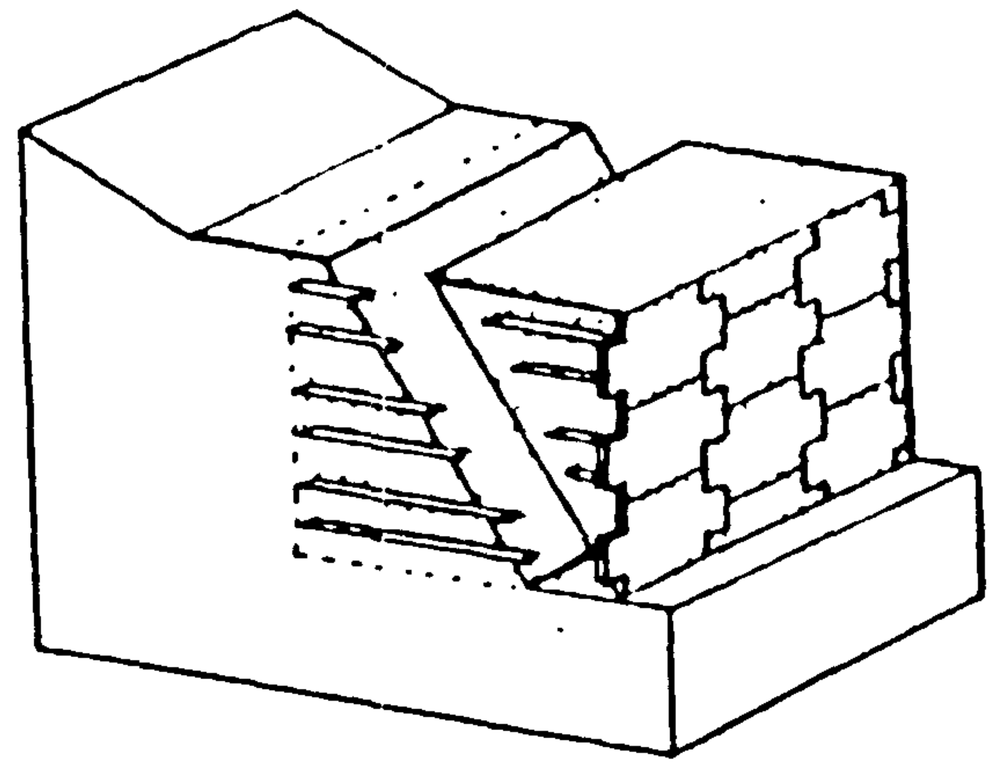

(C) TENSION

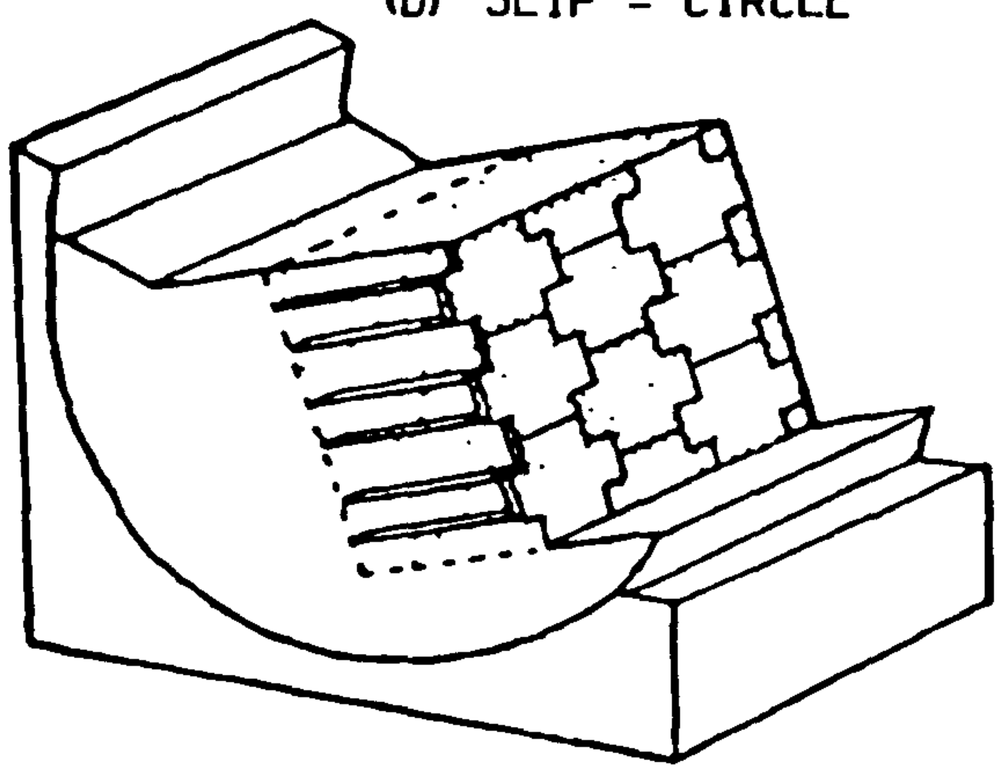

(D) SLIP - CIRCLE

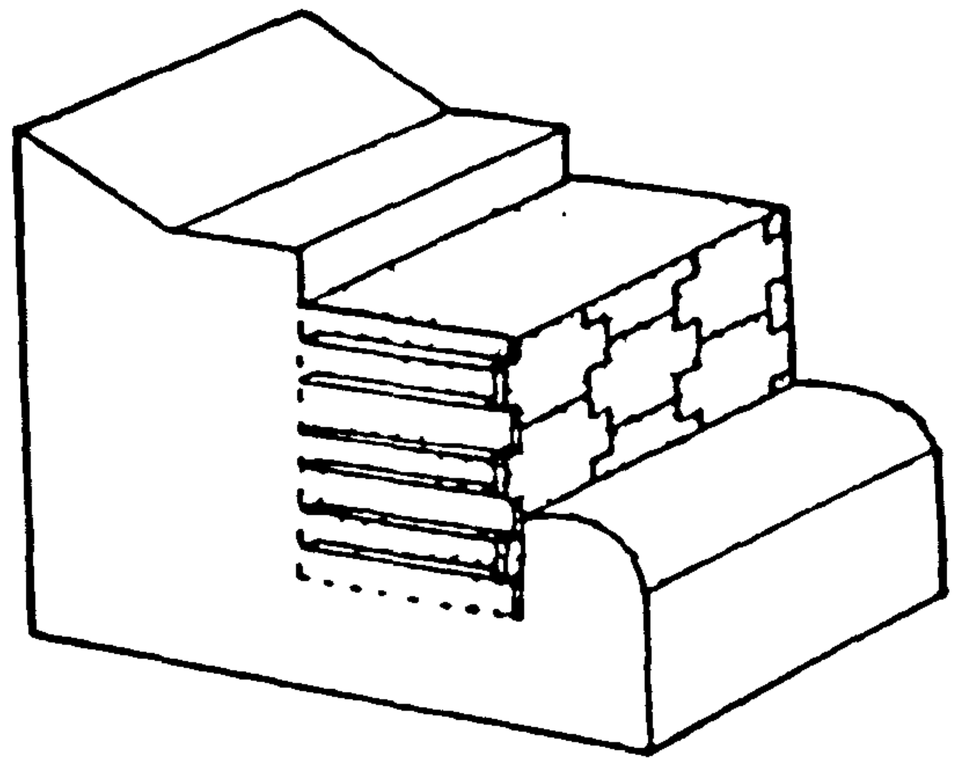

(E) BEARING

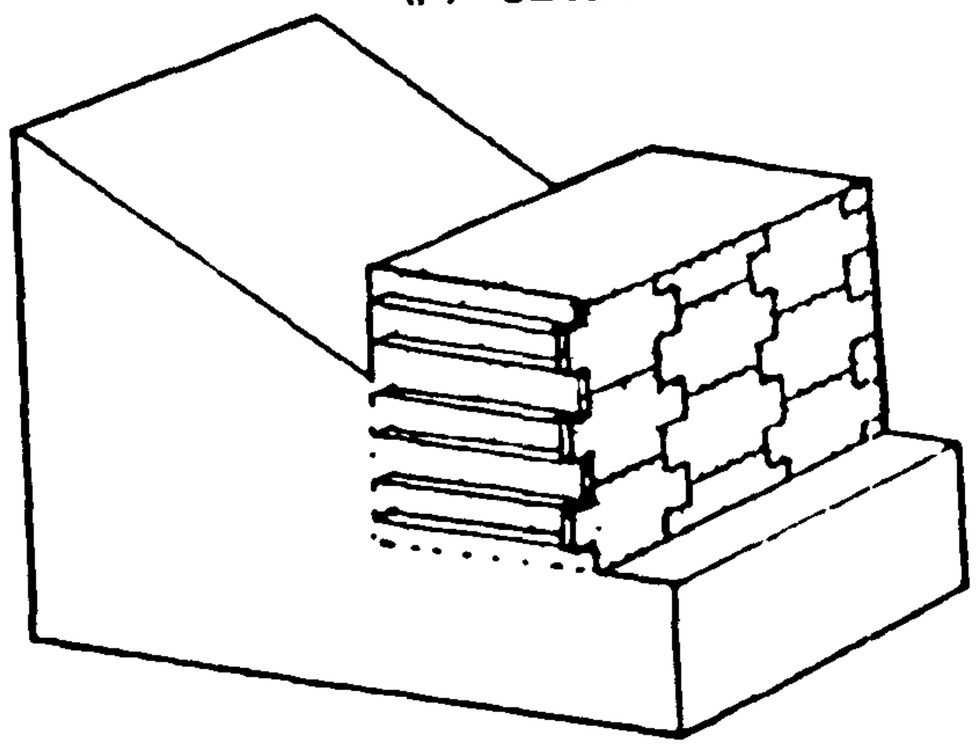

(F) SLIDING

FIG. (2.46) TYPES OF FAILURE IN REINFORCED EARTH WALL

many researchers such as: Vidal (1967 & 1969); Lee et al. (1973); Price (1975); Bolton and Choudhury (1976); Smith (1977); and the Department of Transport (1978 & 1987). They have different assumptions, but they lead to the same force in the strip (T) viz.

$$T = K_a . \sigma_v . S_v . S_h \qquad (2.1)$$

Where S_v & S_h are the vertical and horizontal spacings of the reinforcing elements respectively, K_a is the coefficient of active earth pressure and σ_v is the vertical stress.

(b) Methods which consider the equilibrium of wedges of soil and are based on Coulomb theory, such as methods by Vidal (1969); Lee et al. (1973); Price (1975); Bannerjee (1975); Bacot et al. (1978); and Department and Transport (1978 & 1987). In these methods tensile forces (T) in the reinforcing elements are computed by considering that the equilibrium of a block or wedge within the reinforced earth mass is maintained by the tensile forces in all the reinforcing elements. Either force or moment equilibrium is considered for the wedge and the tensile force can be determined. In applying this method Lee et al. (1973) assumed that the maximum tension within the reinforcing elements increased linearly with depth.

Once the maximum tensile force in the reinforcing element is established, the design criteria for the two modes of failure, tension or adhesion failure can be considered. Factors of safety for both types of internal failure are estimated on a stress developed versus stress capacity basis. The adhesive resistance is

calculated using the normal stress, the coefficient of friction developed between the soil and the reinforcement, the total surface area of reinforcement or the part beyond the failure plane into the restraining zone of soil. The total adhesive resistance is then compared with the maximum tensile force developed in a reinforcing element. For tension failure the maximum lateral force due to earth pressure is compared with the maximum tensile capacity of the reinforcing element.

The equations of tensile forces ($T_{max.}$) based on Rankine or Coulomb and equations of adhesion factor of safety are shown in Table (2.2). Key factors for the different methods are shown in Fig. (2.47). A comparison between these different methods for a real wall is shown in Fig. (2.48).

2.8.2 External Stability

In the external stability analysis of a reinforced earth wall the reinforced earth mass is considered as a unit block, and failure occurs due to slip–circle, bearing or sliding. Jones (1977) suggested that methods which can be applied to design conventional concrete retaining walls can be used to design against bearing and sliding failure. Jone (1979) stated that bearing capacity failure is less likely in reinforced soil since there is not the same concentration of load as in a reinforced concrete wall. Also, he stated that sliding failure is less likely since the base of a reinforced earth wall is wider and the surface friction of selected fill exceeds that of concrete. Smith (1977) suggested that established slope stability analysis should be used to consider slip–circle failure.

TABLE (2.2) FORMULAE FORM DIFFERENT DESIGN METHODS.

DESIGN METHOD	FORMULAE	
	Tension Failure	Adhesive Failure
1- Coulomb force balance Fig. (2.52.c)	$T_{max} = \frac{n}{n+1} K_a \gamma H S_v$	$F = \frac{4bfS_v}{K_a H^2} \sum_{i=N}^{n} i\left[L-(n-i)S_v \tan(45-\frac{\varphi}{2}\right]$
2- Coulomb moment balance Fig. (2.52.c)	$T_{max} = \frac{n^2}{n^2-1} K_a \gamma H S_v$	$F = \frac{12bfS_v}{K_a H} \sum_{i=N}^{n}(n-i) i \left[L-(n-i)S_v \tan(45-\frac{\varphi}{2}\right]$
3- Coulomb wedge Fig. (2.52.c)	$\sum T = \frac{F- \tan\delta \tan\varphi}{\cot\beta \tan\varphi + 1} (\frac{1}{2} \gamma H^2)$ F is factor of safety = 3 $\tan\beta = \sqrt{\tan^2\varphi + F - \tan\varphi}$	$F = \frac{2bf\gamma \left[\frac{L}{2}(n+1)+H(\tan\beta \frac{(1-N^2)}{6N}\right]}{0.5 \gamma H[\frac{F- \tan\beta \tan\varphi}{\cot\beta \tan\varphi + 1}]}$ N is the number of the first layer of the reinforcement to cross failure plane.
4- Rankine Theory Fig. (2.52.a)	$T_{max} = K_a \gamma H S_v$	(i) $F = \frac{2bfL}{K_a}$ (ii) $F = \frac{2bf(L-H \tan 45-\frac{\varphi}{2})}{K_a S_v}$

TABLE (2.2) CONT.

5- Trapezoidal distribution Fig. (2.52.b)	$T_{max} = K_a \gamma H S_v \left[1 + K_a \left(\frac{H}{L}\right)^2 \right]$	
6- Meyerhof distribution Fig. (2.52.b)	$T_{max} = K_a \gamma H \frac{S_v}{1 - \frac{1}{3} K_a \left(\frac{H}{L}\right)^2}$	$F = \frac{L}{\frac{H^2 K_a}{3L} + \left\{1/\left[1 - \frac{1}{3}\left(\frac{H}{L}\right)^2\right]\right\}\frac{K_a S_v}{2bf}}$
7- Elastic analysis Fig. (2.52.d)	$T_{max} = 0.35 \gamma H S_v$	$L_a = \frac{H_f^2 \chi}{\alpha b S_v (n^2+n) \tan\varphi} + H_f \tan\beta - 0.33 S_v (2n+n) \tan\varphi$ H_a is height of wall at failure H_f is height of wall at failure $\chi = \frac{\sum T}{0.5 \gamma H_f^2}$ $\tan\beta = \sqrt{K_a}$ α = 0.4 to 0.6
8- D.O.E method Fig. (2.53)	$T \leq \sum_{i=1}^{n} P_{at} a_{si}$ T is the sum of the forces due to: Overbueden, surcharge, vertical, horiz. loads and due to bending moment.	$T \leq \sum_{i=1}^{n} \frac{P_i L_{ip}}{2} (f \gamma h_i + fq + C_r)$ P_{at} is permissible tensile stresses. a_{si} is cross sectional area of reinf. /m P_i is perimeter of reinf. /m & C_r is the cohesion.

TABLE (2.2) CONT.

9- Reinforced earth company Fig. (2.48)	$T = K \sigma_v S_h S_v$ $\sigma_v = \gamma h$ For $h \leq 6$ m $K = K_o + h(Ka + K_o)$ For $h > 6$ m $K = K_a$	$T = \frac{2bf^* L_a \gamma h}{F}$ $F = 1.5$ f^* is assumed to reduce linearity from unity at the surface to tan φ at depth 6m
10- Energy method	$T_{max} = (D_2 \frac{K_a^{2.5}}{L})^{0.5} \gamma S_v S_h H^{3.5}$ $D_2 = \frac{8}{9}$ for linear distribution of tensile force.	$F = \frac{2 b f L^{3.5}}{Sv\ S_h} \frac{1}{\sqrt{D_4 K_a^{2.5}(H-h)}}$ $D_4 > 6$ for linear distribution of tensile forces.

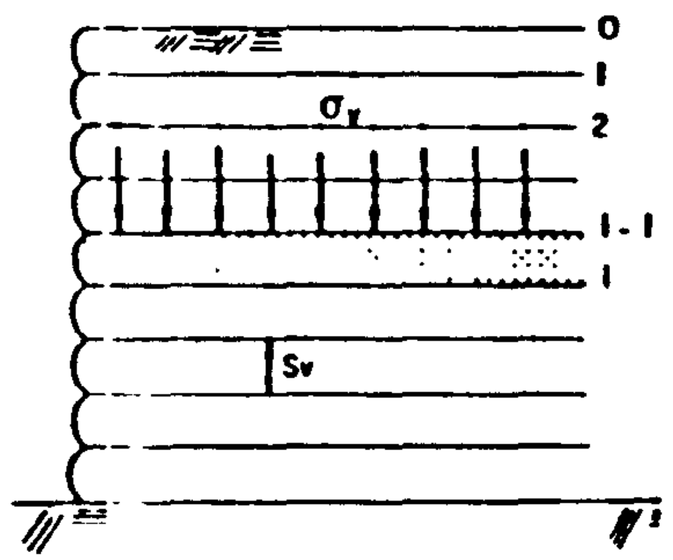

(A) RANKINE METHOD

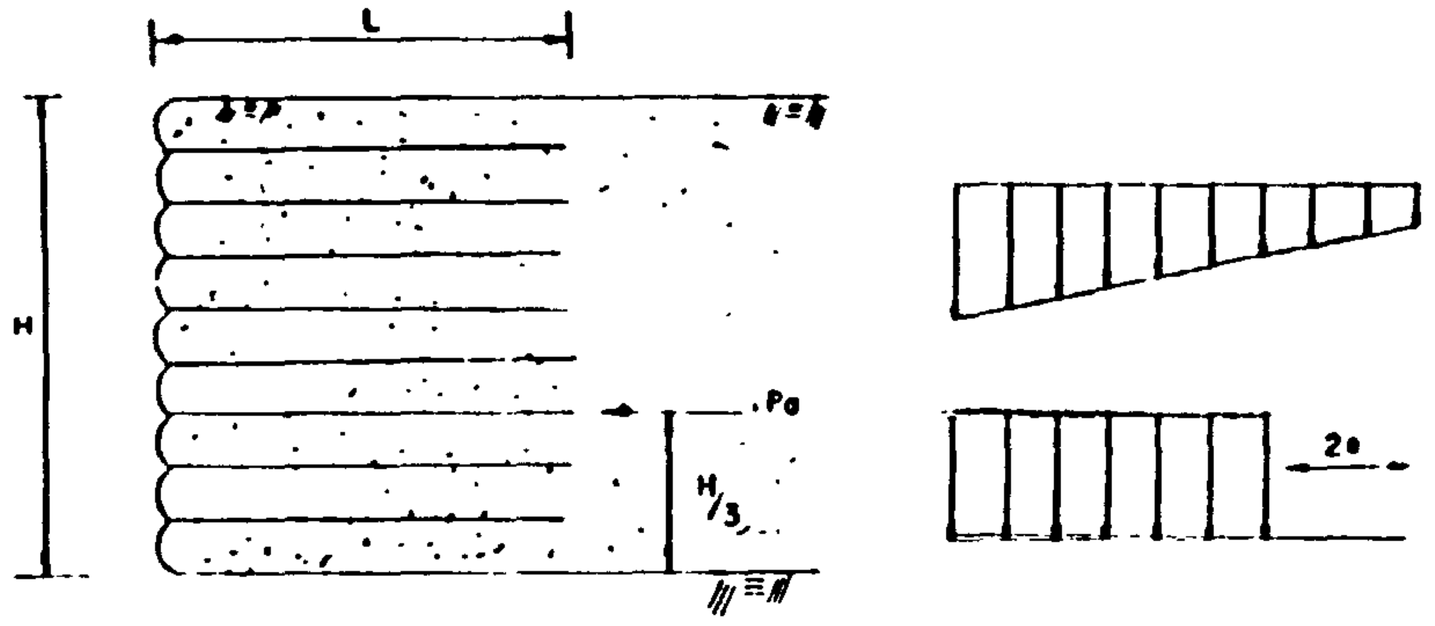

(B) THE TRAPEZOIDAL AND MEYERHOF DISTRIBUTION

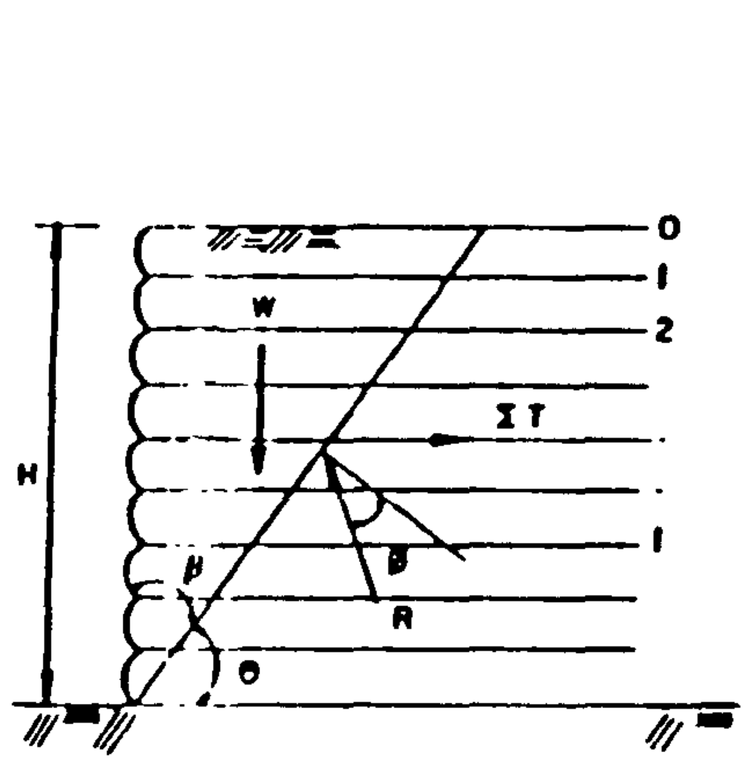

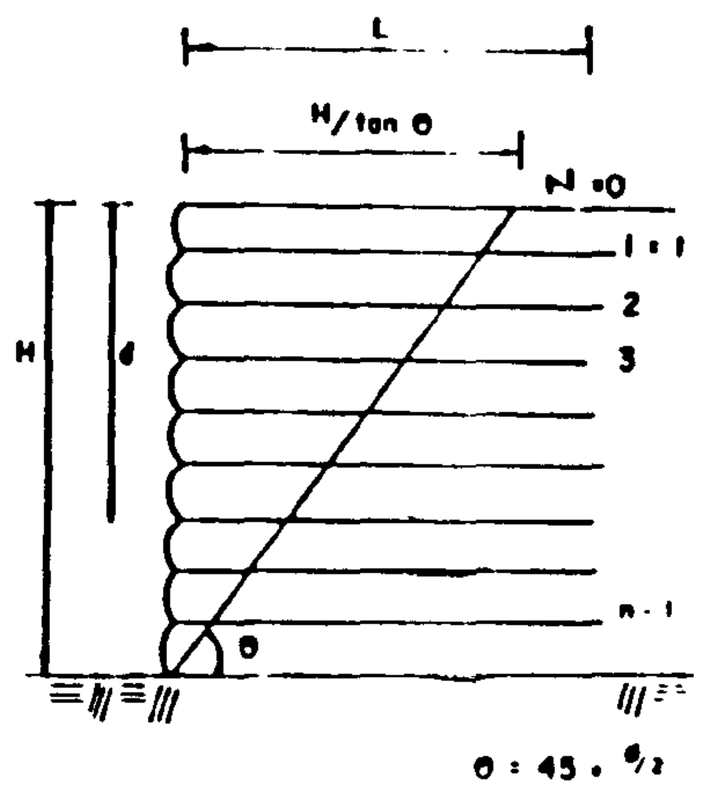

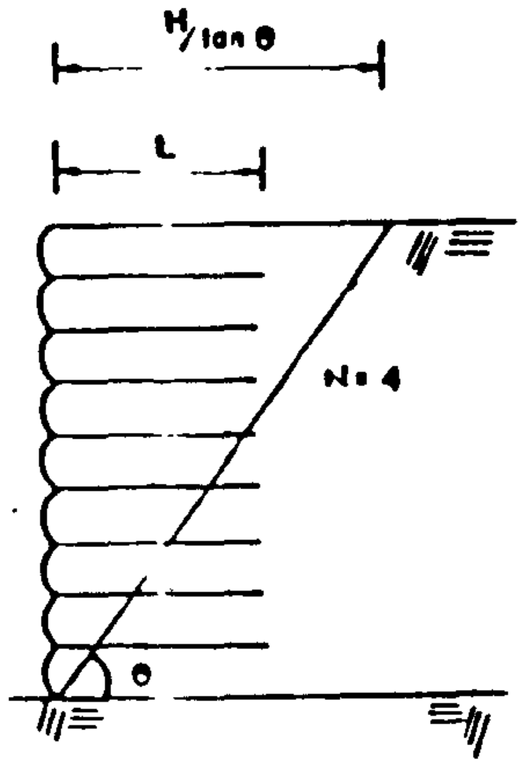

θ = 45 - Ø/2

(C) COULOMB METHOD

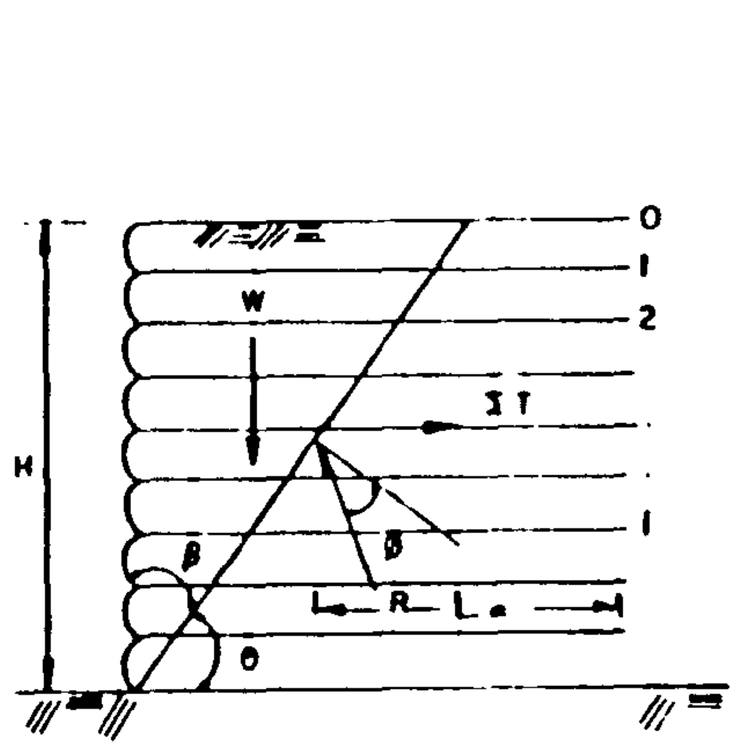

(D) ELASTIC METHOD

FIG. (2.47) KEY FACTORS IN DESIGN FORMULAE (1) TO (6) IN TABLE 2.2 .

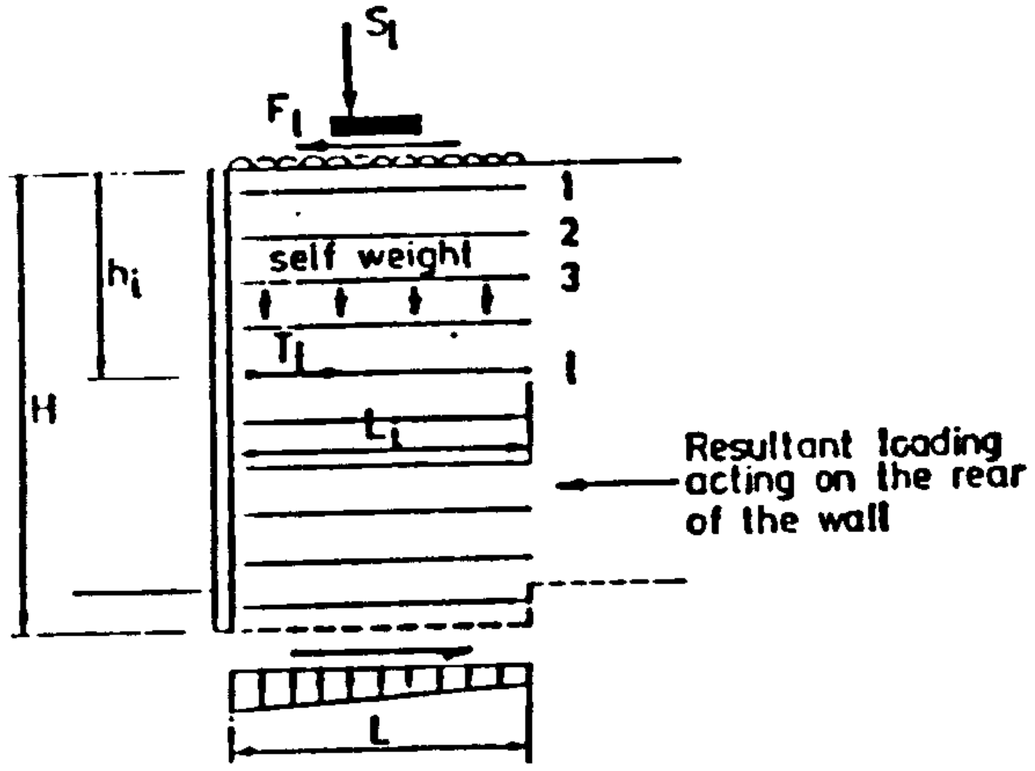

(A) LOCAL STABILITY

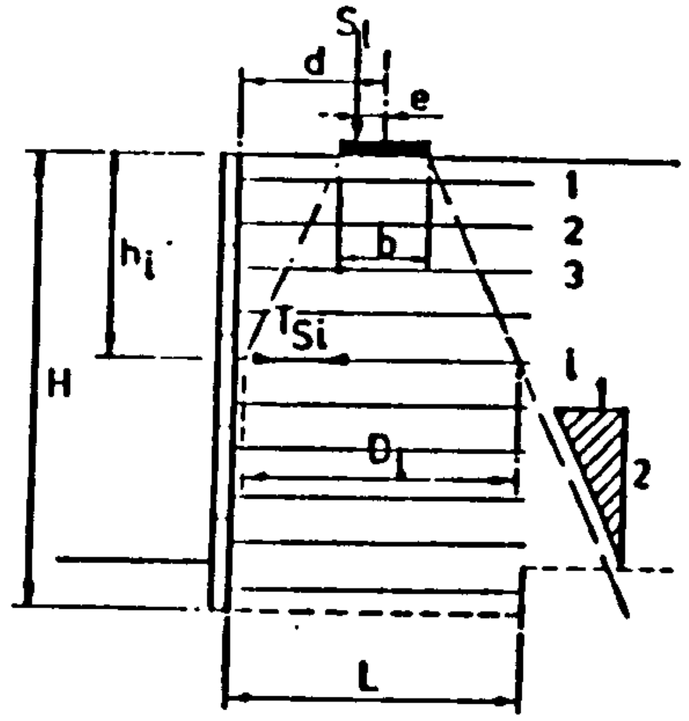

(B) VERTICAL LOAD

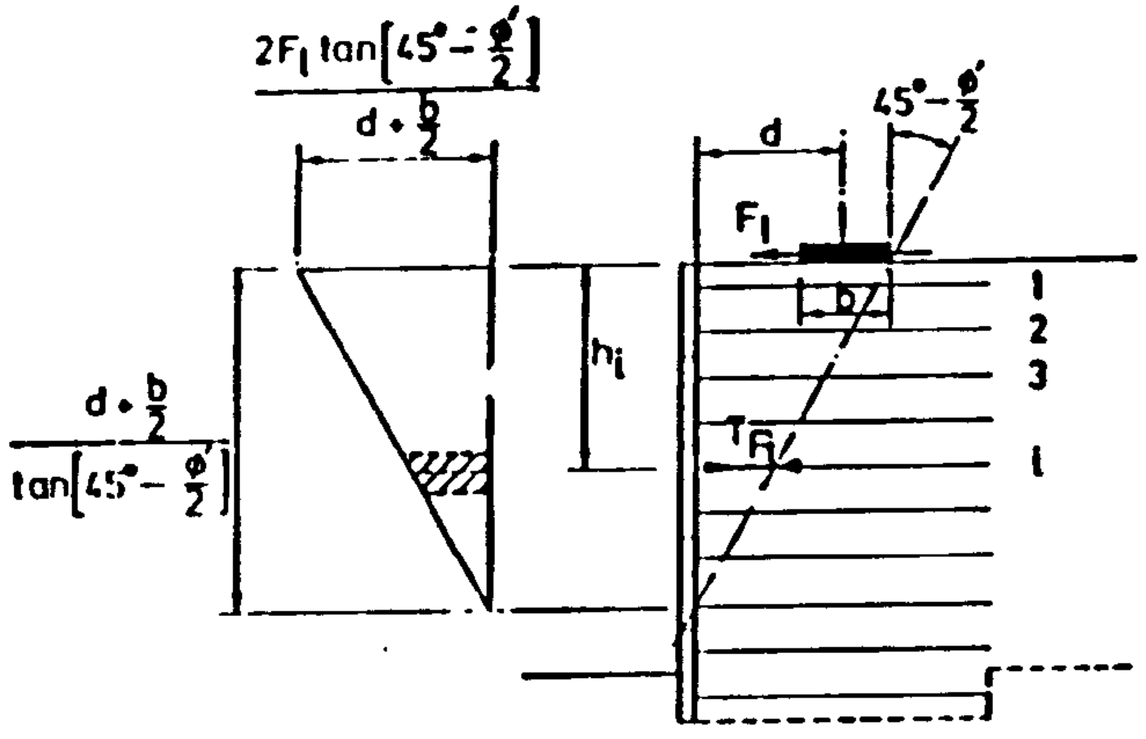

(C) HORIZONTAL LOAD

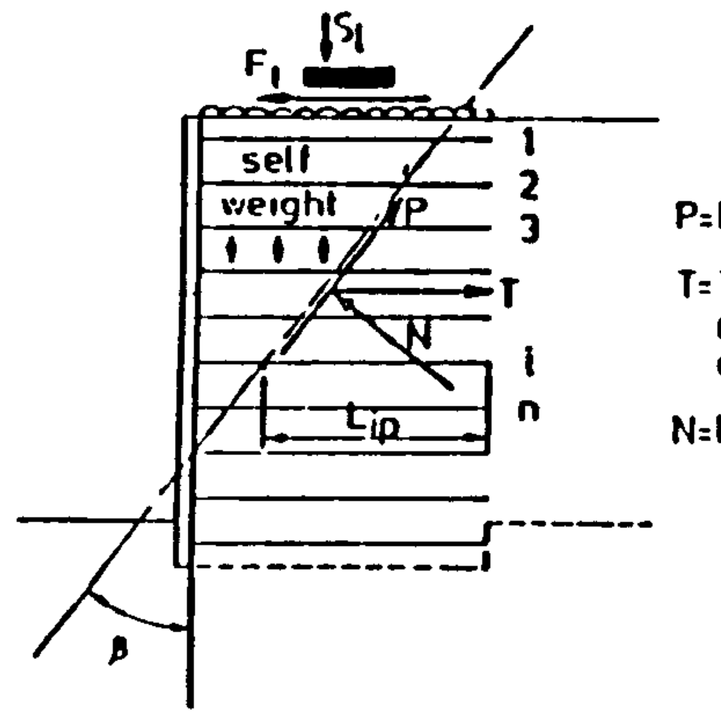

P=Frictional & cohesive forces.

T=Total tensile force to be resisted by the reinforcing elements.

N=Normal reaction.

(D) WEDGE STABILITY

FIG. (2.47) CONT. , KEY FACTORS OF D.O.E. DESIGN FORMULAE IN TABLE 2.2 .

DATA:

H = 5 M

L = 5 M

Y = 2000 KG/M3

K_a = 0.30

0 = 32 DEGREE

f = 0.40

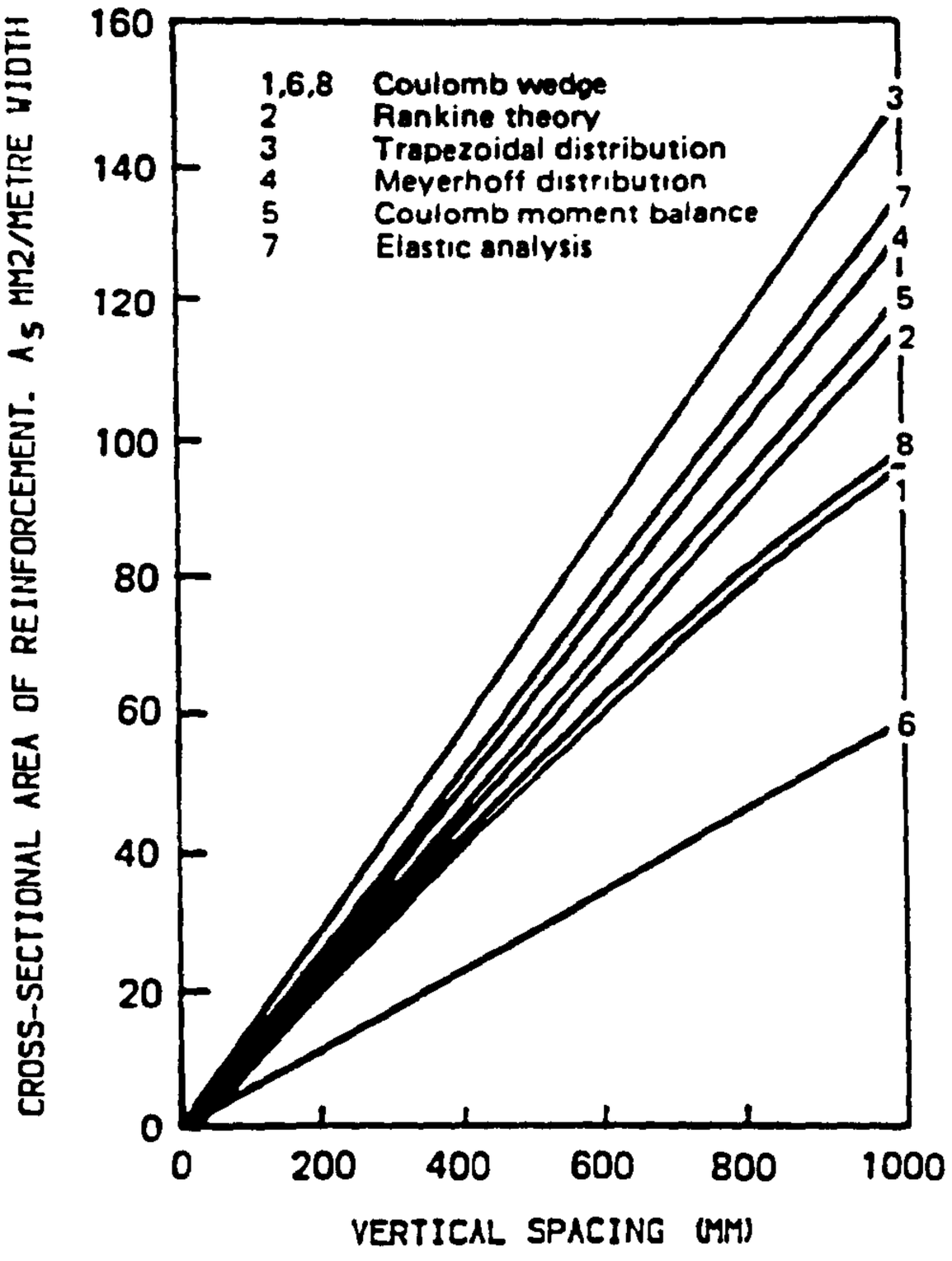

(A) MINIMUM AREA OF REINFORCEMENT - TENSION CASE.

GALVANIZED STEEL REINFORCEMENT-

SIZE = 75X3 MM

,ULTIMATE STRENGTH = 250 N/MM2

&HORIZONTAL SPACING = 1M

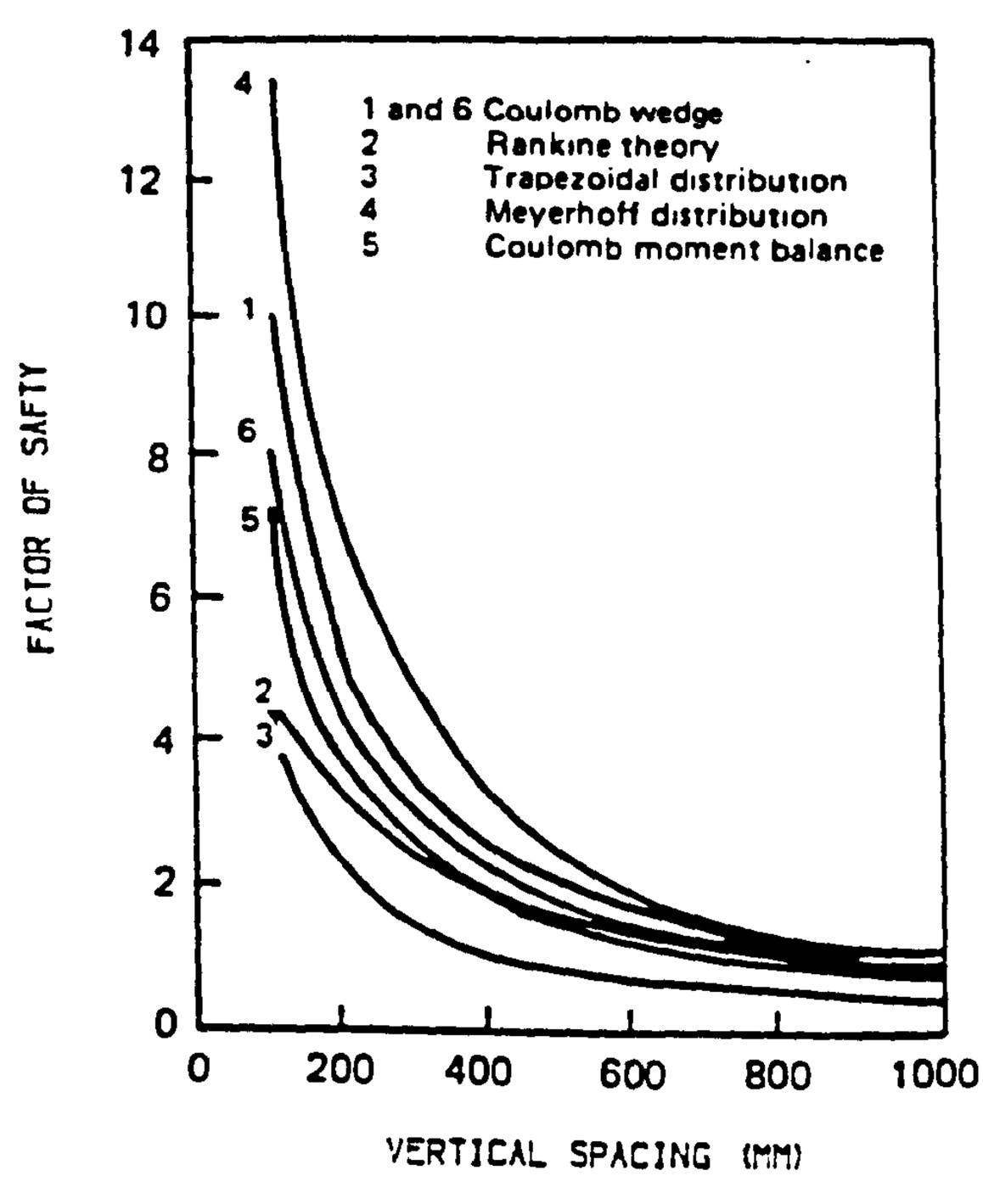

(B) FACTOR OF SAFETY AGAINST BOND FAILURE.

FIG. (2.48) COMPARISON BETWEEN CURRENT DESIGN METHODS (AFTER JONES, 1979).

2.8.3 D.O.E. Design Method

The design method for checking internal stability developed by Department of Environment (D.O.E) is published in, Department of Transport– Technical Memorandum BE (3/78) and revised (1987). It is very conservative, involving both the Rankine and Coulomb methods. First, a check is made on the stability of each layer by calculating the maximum tensile force per meter run of wall, to be resisted in the layer due to

- Overburden.
- Uniform surcharge loading at the top of the wall.
- Strip loading at the top of the wall.
- Horizontal loading at the top of the wall.
- Bending moment caused by external loading acting on the wall.

The total tensile force is checked for tensile and adherence failure. Once the stability of each layer of reinforcement has been checked, the overall stability of several trial wedges is checked using a graphical method, illustrated in Fig. (2.49). Once the maximum value of tensile force is obtained, it is compared with both the allowable tensile and adherence resistance of reinforcing strips within the required depth. A further family of potential failure planes is investigated for another required depth. Recommendations about the backfill material and reinforcing units as well as facing units are given in detail in the Memorandum.

2.8.4 Reinforced Earth Company Method

In the design of reinforced earth walls and from observations on full scale

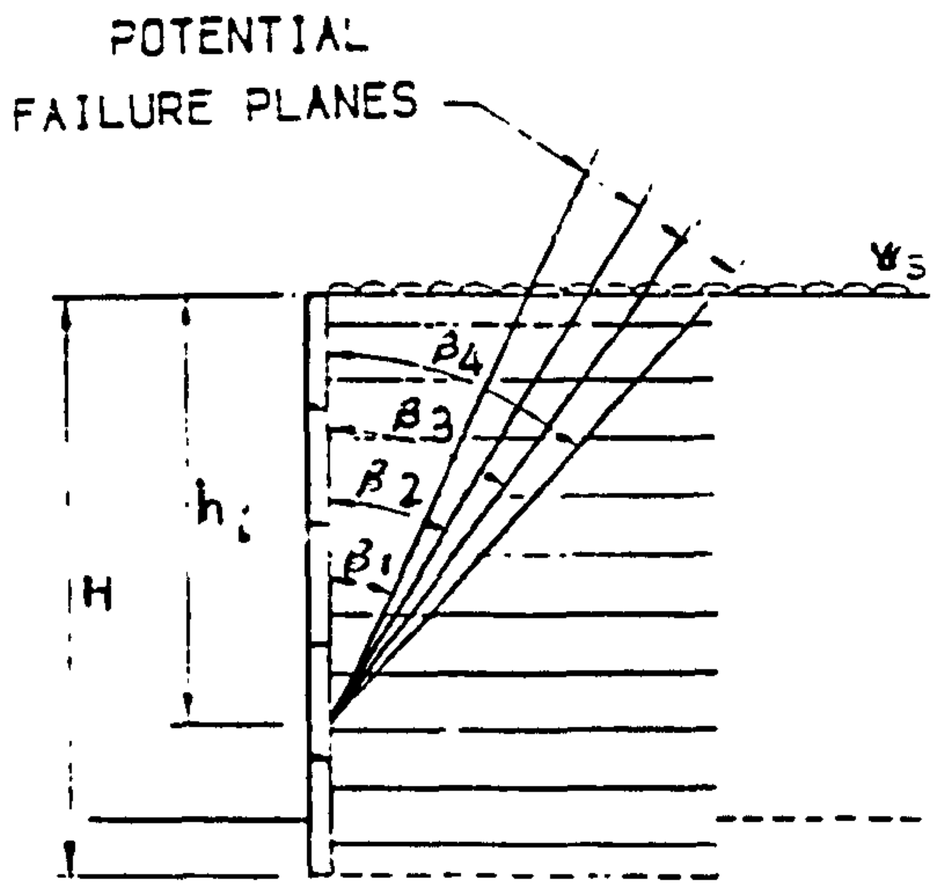

WALL WITH LEVEL TOP
FRICTION FILL
UNIFORM SURCHARGE

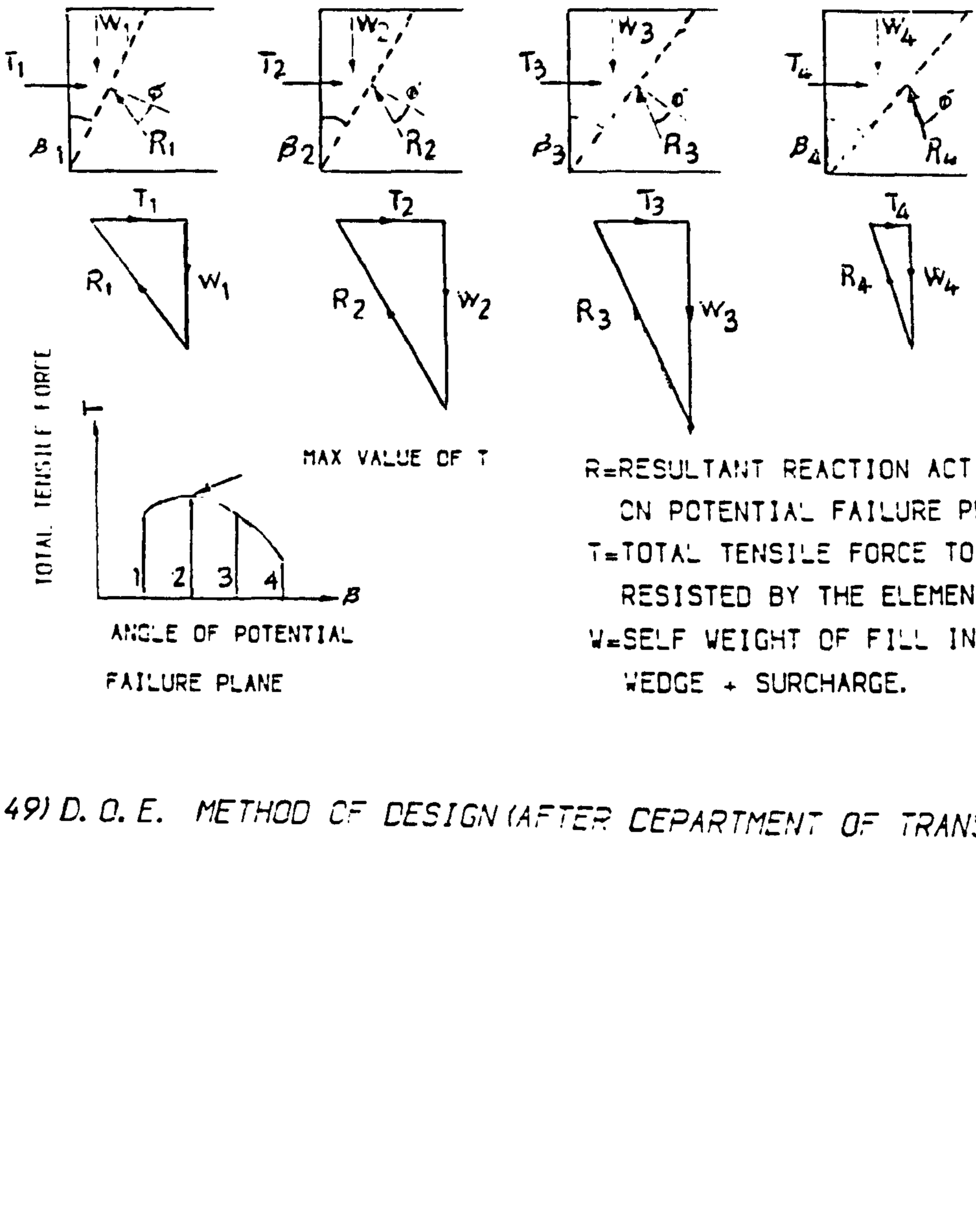

R=RESULTANT REACTION ACTING
ON POTENTIAL FAILURE PLANE.
T=TOTAL TENSILE FORCE TO BE
RESISTED BY THE ELEMENTS.
W=SELF WEIGHT OF FILL IN THE
WEDGE + SURCHARGE.

FIG. (2.49) D. O. E. METHOD OF DESIGN (AFTER DEPARTMENT OF TRANSPORT, 1978).

walls the state of stress varies with depth as shown in Fig. (2.39), and consequently the coefficient of earth pressure (K) varies, from the at-rest condition near the top to the active condition near the bottom, Baguelin (1978).

In view of this, McKittrick (1978) developed the method of design used by the Reinforced Earth Company, in which the variation of (K) is taken into account in calculating the maximum tensile force ($T_{max.}$) in the strips.

Assuming planes of failure as shown in Fig. (2.50),

for $h < 6$ m

$$K = K_o + h\,(K_a - K_o)/6 \qquad (2.2)$$

For $h > 6$ m

$$K = K_a \qquad (2.3)$$

$$T_{max} = K.\sigma_v.S_h.S_v \qquad (2.4)$$

Once T_{max} is obtained checks against tensile failure can be done.
In designing against adherence failure the effective length is taken beyond the failure surface shown in Fig. (2.50). The coefficient of friction is taken to be 0.4 for plain strips and (tan ϕ) for ribbed strips, and the factor of safety against adherence failure is taken as 1.5 . The required length (L_a) is calculated as shown in Table (2.2). Schlosser and Elias (1978); and Darbin et al. (1978) stated that for normal conditions a loss by corrosion of 1.17 mm per side might be associated with a design life of 100 years.

2.8.5 Energy Method

The energy method for designing reinforced earth retaining walls has been proposed by Osman (1977) and is based on a consideration of the equilibrium of the external work due to earth pressure and the internal work due to earth pressure and the internal strain energy stored in the reinforcement. The following variables are considered:

(i) The effect of reinforcement length on the magnitude of tension.

(ii) The variation in tension along a particular reinforcement and the distribution of tension with depth.

(iii) The deflected shape of the facing.

The total external work done by the earth pressure ($U_{ext.}$) per unit width is given by the expression:

$$U_{ext.} = \int_0^H P(h) \quad Y(h) \quad dh \qquad (2.5)$$

Where, P(h) is an earth pressure function; Y(h) is a wall deflection function. Energy theory parameters are shown in Fig. (2.51).

The energy method assumes that the external work done is stored in the reinforcement as elastic strain energy which may be calculated if the distribution

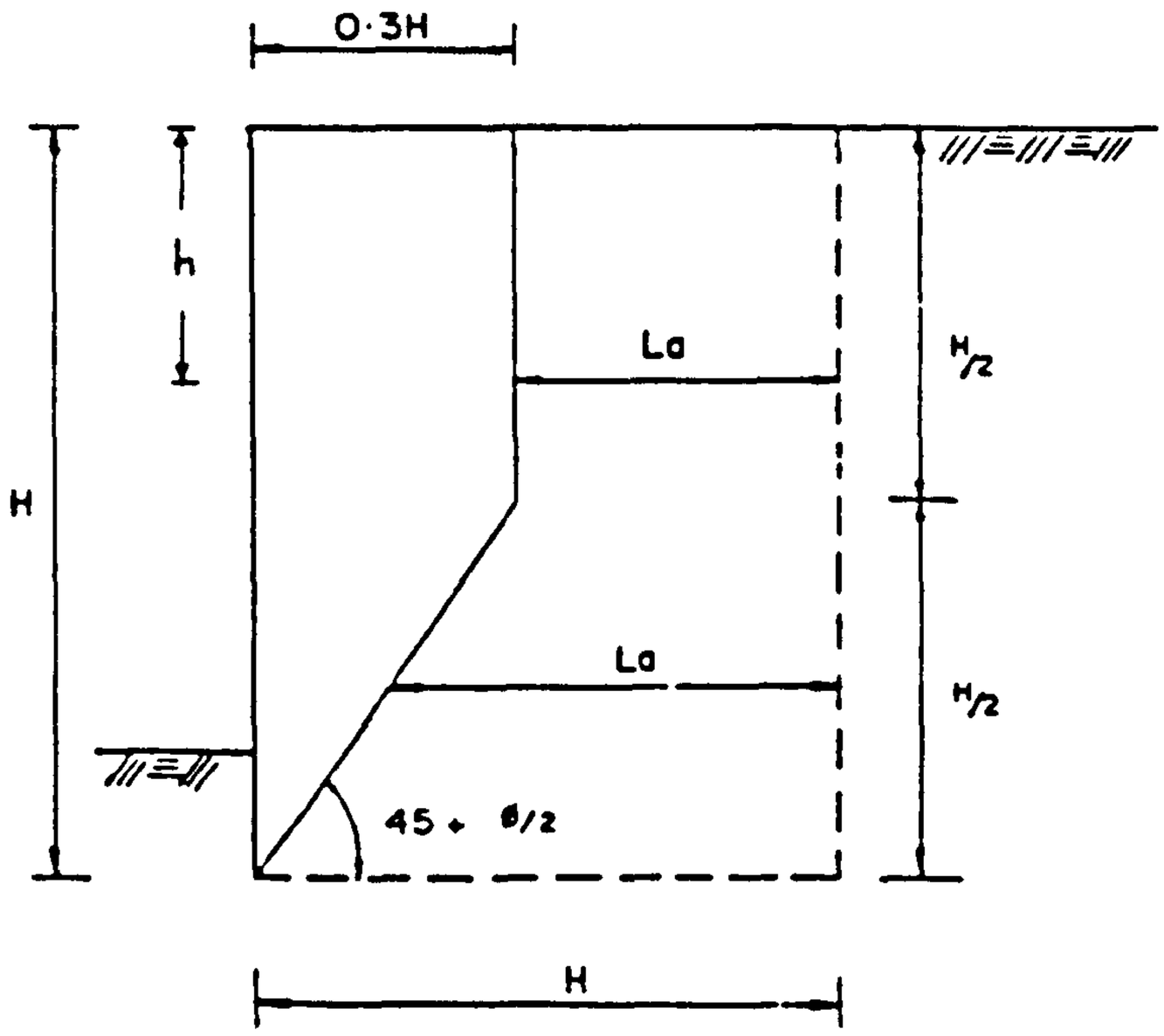

FIG. (2.50) PLANES OF FAILURE IN EARTH MASS (AFTER SCHLOSSER AND McKITTRICK, 1978).

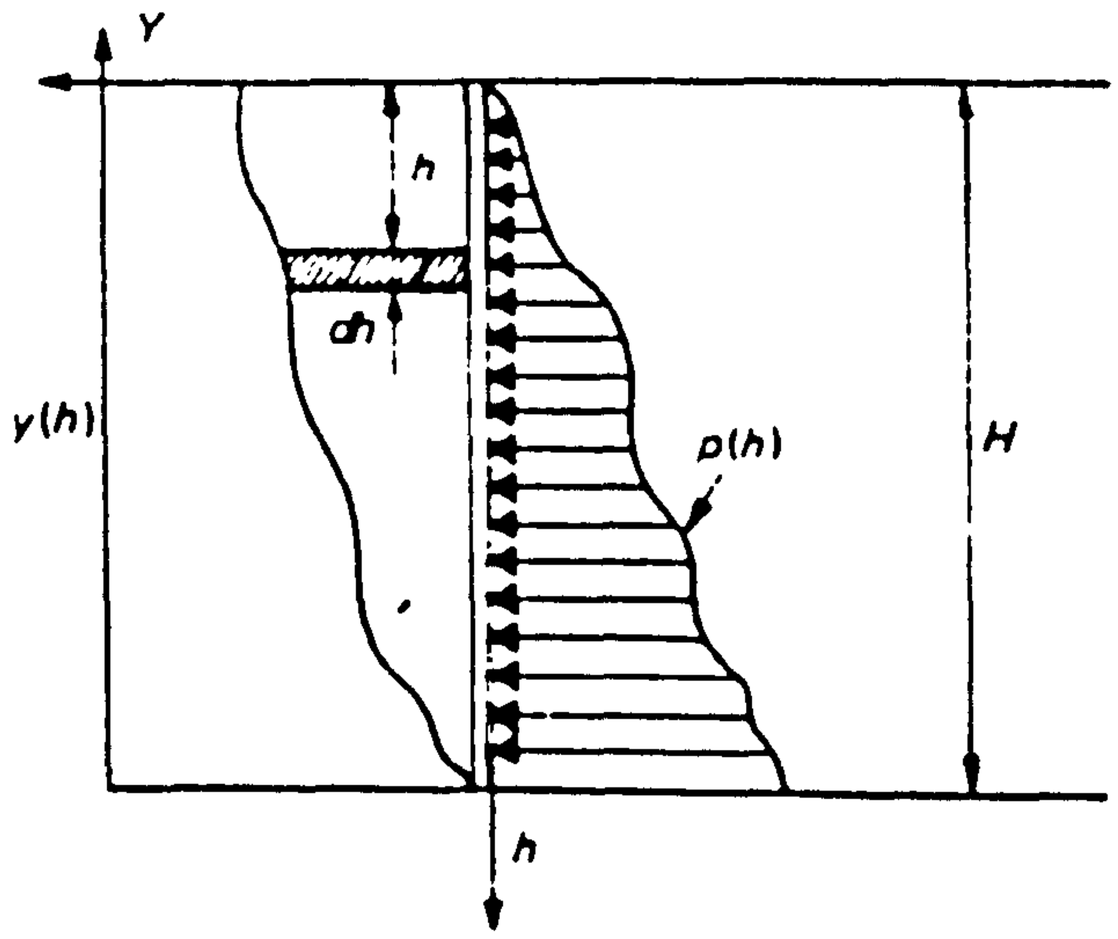

FIG. (2.51) ENERGY THEORY PARAMETERS (AFTER OSMAN, 1978).

of tension in the reinforcement is known. Expressions for maximum tensile force in the reinforcement ($T_{max.}$) and factor of safety against adherence failure are given in Table (2.2).

The main assumptions used to develop these expression were:

(i) The distribution of tension along the reinforcement is linear or parabolic.

(ii) The face deflection is parabolic and a function of the state of stress and the composite action of the soil and reinforcement.

(iii) The earth pressure distribution is hydrostatic.

2.8.6 Finite Element Method

The internal analysis of reinforced earth retaining walls using the finite element method is now widespread. Finite element techniques may be used to consider the overall displacement of the reinforced earth wall on the subsoil. The finite element method is a system capable of providing a wide range of information sought by a designer such as: strains, stresses, deformations in both soil and reinforcement, during and post construction. Also tension along the reinforcement, bearing pressure distribution and the global stability criteria and the effect of surcharge load can be obtained, Jones (1988). The details of the method and its application to reinforced earth wall is given in detail in Chapter 7.

2.8.7 Development Of Design Methods

Recently, a wide range of fabrics has been used for reinforced soil structures (Koerner and Welsh, 1980). As the in-soil properties of fabrics are very different from the in-air properties, care must be exercised to ensure that appropriate material properties are used (McGown et al., 1978).

The normal design methods for reinforced earth structures take no account of the magnitude of the strains induced in tensile members as these are invariably manufactured from high modulus materials such as steel where strains are unlikely to be significant. With fabric, however, large strains may frequently be induced and it is important to determine these to enable suitability of the structure to be assessed (Murray, 1981).

The U.K. Department of Transport issued a Technical Memorandum BE/78 which is considered to be the principal document dealing with requirements for reinforced earth walls and abutments. It was revised in 1987. Among other things this revision sets out the principles for the assessment of the tensile strength of materials which exhibit significant long term creep behaviour.

Ingold (1988) noted that the Memorandum gives no advice on how design strengths are to be determined but presents a check list of factors which should be considered in assessing the mechanical properties and durability of reinforcement. In assessing mechanical properties the Memorandum makes reference to short and long term data relating to load -strain characteristics, creep, ductility and fatigue. Similarly in assessing durability, consideration must be given to agencies, such as site-induced damage and environmental attack from water, chemicals and bacteria in the fill.

A few other analytical approaches, essentially extended from simplified limit–equilibrium methods (classical theories) have been proposed by Christic and El–Hadi(1977); Murray (1981 & 1982); Ruegger (1986); Schneider and Holtz (1986); and Schmertmann et al. (1987).

Gourc et al. (1986); Delmas et al. (1986); and Gourc et al. (1988) developed a method for designing geosynthetics which is called the " displacement method". A number of factors can be taken into consideration such as the stiffness of the geosynthetics, and the connection between the reinforcement and the wall face. Local equilibrium of each layer as well as the overall equilibrium are considered.

Gourc et al. (1987); Gourc et al. (1988) stated that the most widely used method of dimensioning geosynthetic–reinforced walls is the "two blocks method" for internal stability of the wall. The general principle is that internal rupture of the reinforced retaining wall is assumed to consist of two failure planes or two slip lines which intersect the layer of geosynthetic at the maximum tension point. The active sliding zone consists of two blocks with vertical interfaces. The forces produced due to the slip of the two blocks are shown in Fig. (2.52).

By analogy with the behaviour of a conventional retaining wall which must stabilize the soil behind the wall by balancing the soil thrust, the reinforced block must internally balance the thrust of the soil (P) resulting from the slip of the active double block , which must be balanced by the geosynthetic. The method includes also the local equilibrium design for each layer of geosynthetic. It is noticed that the distribution of the tensile forces obtained is independent of the type of geosynthetic used.

Buhan et al. (1989) proposed a new design method for reinforced earth structures which relies on the yield design theory as generally stated by Salencon (1984) and applied to reinforced soils (Buhan, 1986). It proceeds from the basic concept that, on the macroscopic scale, reinforced earth may be treated as a homogeneous but anisotropic material, the strength criterion of which can be explicitly constructed given the strength characteristics of its components (soil and reinforcement). The yield design homogenization procedure derived from this concept is applied to the reinforced wall. Two conditions must be satisfied:

(i) The reinforcing must be placed in the soil in a regular pattern.

(ii) The vertical spacing between reinforcement must be small when compared to the total height of the wall.

Under these conditions and provided the appropriate definition of the macroscopic strength criterion is adopted, the stability analysis of the reinforced earth wall can be performed, by applying yield design approaches to the associated homogeneous structure. An example of an associated homogeneous retaining wall is shown in Fig. (2.53).

2.9 COMMENT ON CURRENT DESIGN METHODS

In the foregoing sections the methods of analysis of reinforced earth walls have been presented. Basically these methods are derived from the Rankine and Coulomb earth pressure theories, which assume that the backfill of a retaining wall is homogeneous and isotropic. Reinforced earth material is essentially a composite material, consisting of backfill and reinforcement, which deviates from

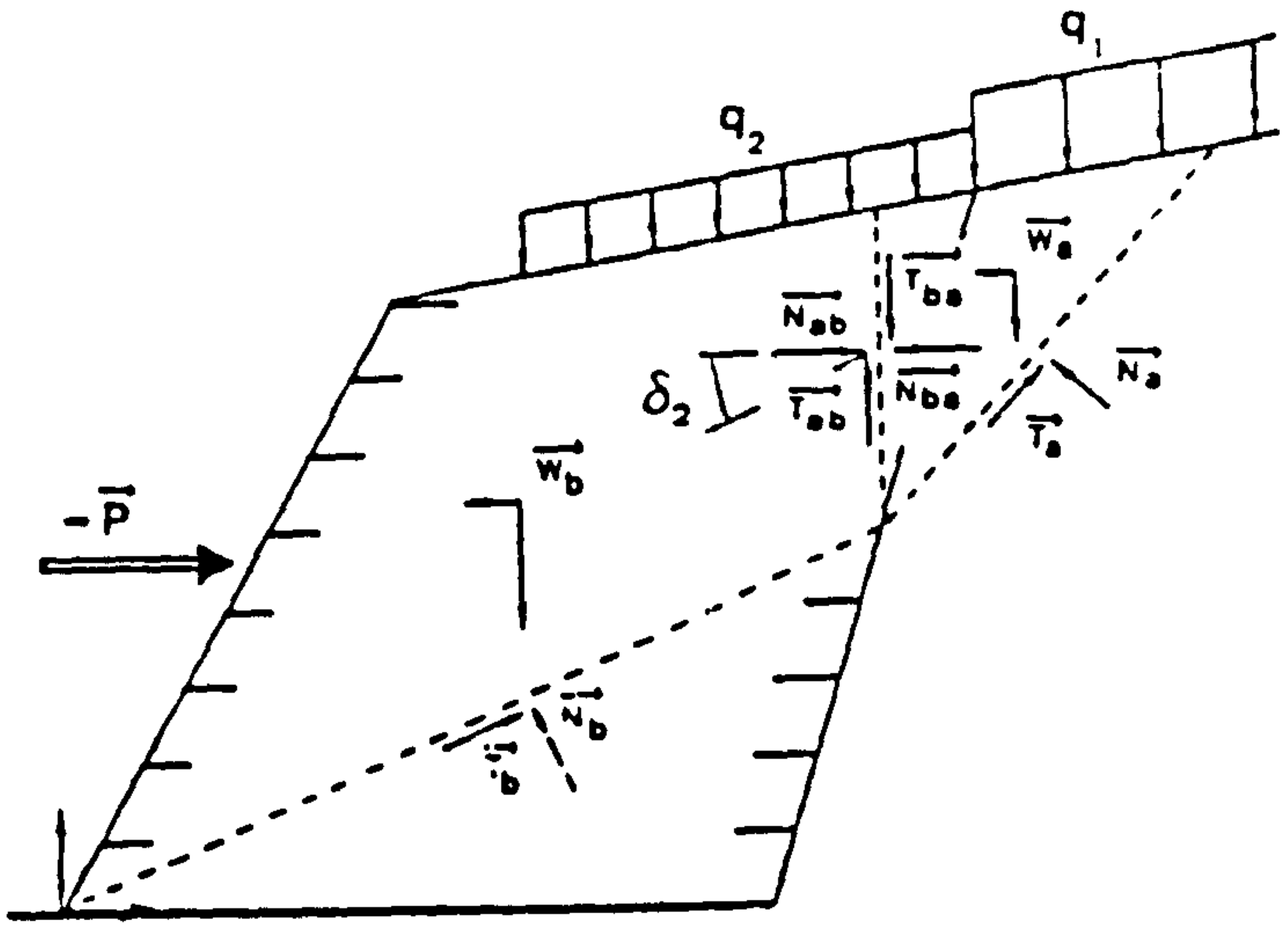

FIG. (2.52) INTERNAL EQUILIBRIUM BY "THE TWO BLOCKS METHOD" (AFTER GOURC ET AL., 1988).

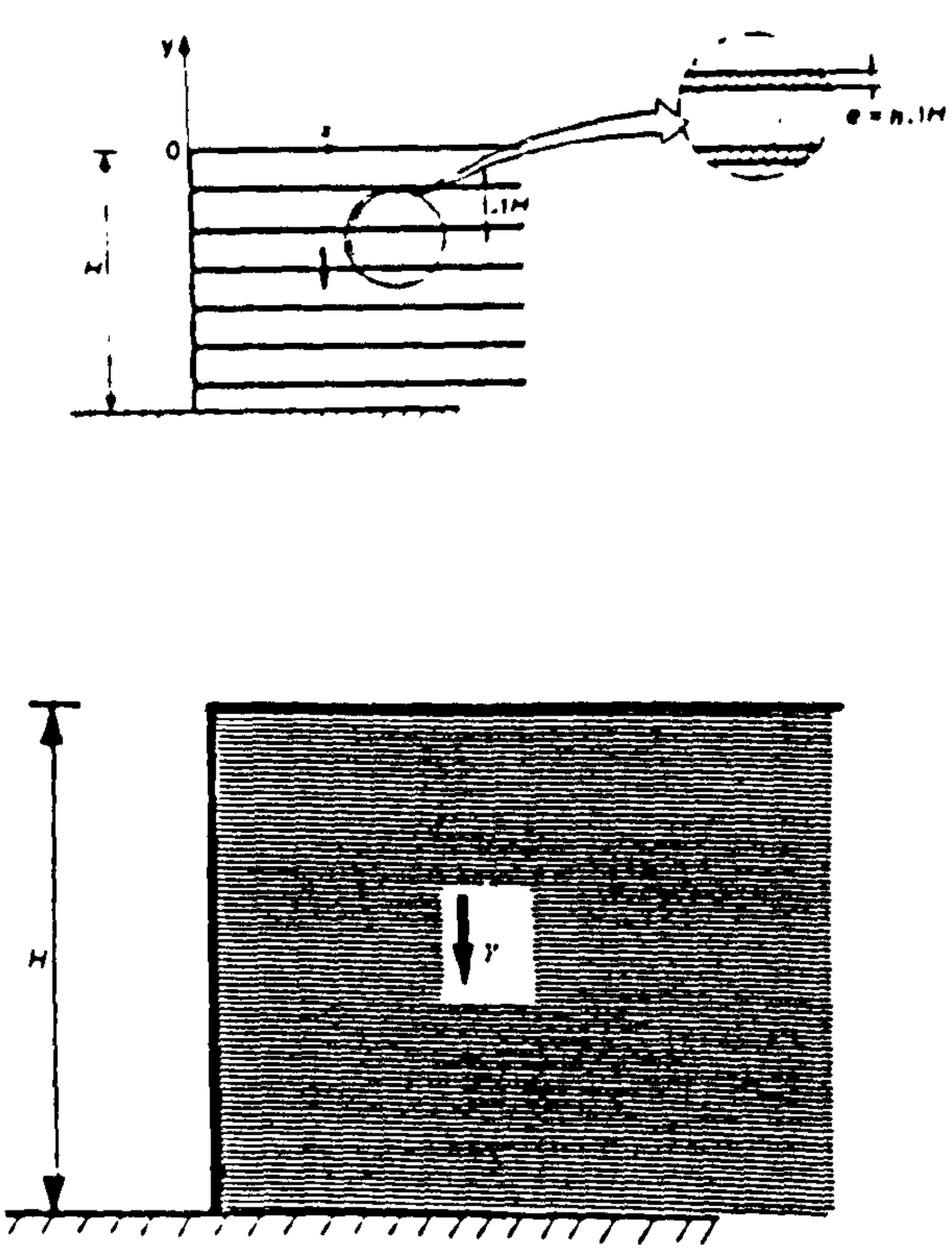

FIG. (2.53) HOMOGENEOUS DESIGN METHOD (AFTER BUHAN ET AL., 1989)

these assumptions.

Also classical theories assume that the plane of failure is inclined at $45+\phi/2$ to the horizontal and there is a linear tension distribution with wall height, which is at variance with observed full scale walls as shown previously in Fig. (2.12.B). In classical theories or the methods based on classical theories, the earth pressure distribution is assumed to be hydrostatic, with a magnitude which is related to overburden pressure by a constant, usually K_a or K_o. Many field test measurements of lateral earth pressures indicate as previously shown – in case histories– a distribution that is far from hydrostatic, and this deviation has been attributed to the effects of compaction induced lateral earth pressure and deformations. The increase of lateral earth pressure is due to reinstatement of stresses during subsequent passes of the compaction plant.

It is clear that the classical theories or methods based on them or even the new approaches for design of reinforced earth retaining walls do not take into account the effect of compaction on the behaviour of the wall, particularly the effect of compaction plant and construction process on the lateral earth pressure.

This shortcoming in the current theories is due to the difficulty of taking the direct effect of compaction plant into consideration. The reason for this, is the cumbersome method of mathematical simulation of the compaction plant and its effect. The current theories consider the increasing density of the back fill as an indirect effect of compaction, and the field studies are good witnesses. For this reason designers should be wary at placing too much faith in an "active" design. A need exists for the development of a formula taking into consideration the compaction plant effect on lateral earth pressure as a part of a design method.

2.10 CONCLUSION

Although a large number of reinforced earth retaining walls have been constructed in different parts of the world some aspects of the behaviour of reinforced earth are still not fully understood. Moreover, much of the available information is ambiguous and conflicting. One of the aspects of the behaviour of reinforced earth which is not fully understood, is the behaviour of reinforced earth walls during and after construction, and the effect of the compaction process on the behaviour.

As discussed before one of the main ccnstruction processes is compaction of the backfill behind the wall and no reinforced earth wall– so far– has been constructed without compaction. To compact backfill behind the wall, a convenient compaction plant for the soil ar.d the project must be used. The compaction plant causes locked in stresses in the soil and sometimes unacceptable deformation of the wall. All the field and full scale tests indicate that the measured pressure and deformations are greater than calculated. Current design methods take no account of the magnitude of effect of compaction plant on the stresses, because of a lack of theoretical simulation of the actual compaction plant. The result is unsafe design which sometimes causes failure, or uneconomic design.

Small scale tests are economic and give good ideas on different aspects of reinforced earth which help in developing safe and economic design. The problem in small scale tests carried out to investigate the effects of compaction on a reinforced earth wall, is the difficulty of simulating compaction plant experimentally.

The conclusion from this chapter can be summarized by asking four questions:

(1) Can we add compaction effect as one of the main components of reinforced earth retaining wall ?

Yes, since we cannot construct a reinforced earth wall without compaction.

(2) Do we need a better understanding of the compaction effect on reinforced earth wall using cheap tools like small scale tests ?

Yes, but how can the compaction plant and its effect be simulated in the laboratory ?

(3) Do we need to improve the design of reinforced earth walls to be safe and economic ?

Yes, but how can the compaction plant and its effect be simulated theoretically ?

(4) Do we need the finite element method as a power tool to complete the laboratory work and answer the questions which are cumbersome to get replies to from the laboratory ?

Yes, but how can be the construction process be represented in a finite element program ?

The author has tried in the next chapters to get answers to the above questions.

CHAPTER 3

A LABORATORY INVESTIGATION

3.1 INTRODUCTION

The use of small scale tests in soil mechanics is quite well–known and generally accepted. Normally small scale tests in geotechnical problems use two or three dimensional models.

The present research work was carried out using a three dimensional model of a reinforced earth retaining wall, constructed to simulate the plane strain condition (i.e. the strain in the soil in a direction parallel to the wall is prevented). This form of model was used to get a satisfactory analysis and also to verify the semi infinite medium of the soil. It was thought to be more convenient in simulation of the prototype wall behaviour during construction and post construction under the effect of compaction plant, using different construction methods.

The dimensions of the wall were chosen to simulate a vertical reinforced retaining wall of height 6.0 m. The model scale of "10" was suitable to provide measurable stresses, and deformations of the wall and provide quantitative information.

All the components of the model e.g. backfill material, reinforcement,facing

units and compaction plant were chosen to simulate the prototype as closely as possible.

In this chapter the objectives of the experimental work are illustrated. The wall model, measurement devices, calibration tests and instrumentation as well as the sequence of construction of the model are described. The conclusions are given at the end.

3.2 OBJECTIVES OF THIS STUDY

In the review of literature, Chapter 2, most of the investigators did not compact the backfill material– as in the field– in their small scale model tests. Moreover, there are no direct studies of compaction effects on reinforced earth walls using small scale models, in spite of the fact that small scale models are cheap and acceptable.

The lack of such tests is due to the difficulty of simulating the construction sequences and compaction plant as in the field. The effect of compaction is not fully understood and hence it has not been taken into account in current theories of design as seen in Chapter 2.

The objectives of this study are to investigate:

(1) The effect of compaction on the behaviour of a reinforced earth retaining wall during and post construction.

(3) The effect of change in the compacted length.

(3) The effect of methods of construction on wall behaviour.

(4) The effect of changing some aspects of a reinforced earth retaining wall such as length of reinforcing strips, and vertical and horizontal spacing between them.

(5) A theoretical approach, taking into account the compaction effect, to help in optimum design of a reinforced earth retaining wall.

These investigations can only be done by measuring stresses in the strips, stresses in the soil, and wall deflection, before, during and after compaction, and will contribute to the understanding of reinforced earth retaining wall behaviour, and allow the various assumptions on which different theories are based to be checked.

3.3 THE COMPONENT PARTS OF THE MODEL

The component parts of the model are:

3.3.1 Wooden Box

The plane strain condition and the semi–infinite medium of the backfill were simulated by using an open–fronted plywood box with rigid sides and rear. The inside dimensions of the box, Fig. (3.1), were:

Length = 1300 mm

Width = 900 mm

Depth = 700 mm

The dimensions of the box are based on the wall height and previous models

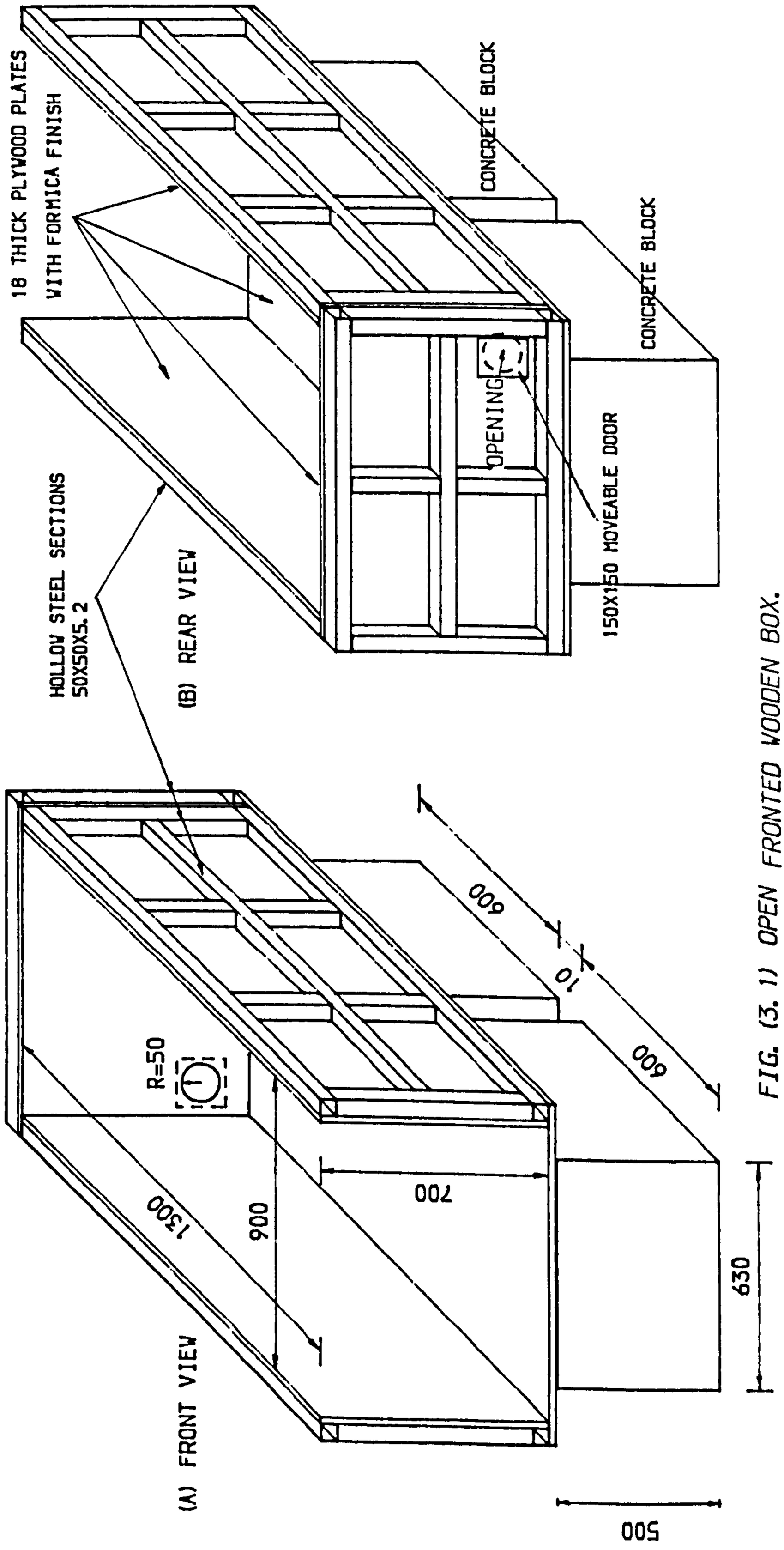

FIG. (3. 1) OPEN FRONTED WOODEN BOX.

which have been constructed by various researchers. The depth was chosen as 600 mm wall height with 100 mm thickness of foundation soil as in the field, giving a total depth of 700 mm. The width of the box was chosen to minimize the effect of side wall shear stresses in reducing the earth pressure on the wall. It has been suggested by Lazebnik and Chernysheva (1968),and Rowe (1971) that the ratio width/depth should be greater than 1.3. The width chosen was therefore 900 mm to give this width/depth ratio.

The length of the box was made equal to the length of reinforcement (600 mm maximum) plus the distance between the back of the reinforced mass and the rear of the box (400 mm), which is sufficient to avoid any effect on the internal stability, because it extends beyond the plane of failure within the reinforced mass. An additional 300 mm was added in front of the wall face to allow for measurements at the wall face. The total length was therefore 1300 mm.

The box was made of four plywood panels 18 mm thick covered with Formica on both sides of each panel assembled together to form the base, two sides and the rear. The surface of the panels is smooth to minimize the friction effect between backfill soil and panels, which reduces the earth pressure on the wall face.

In order to avoid arching caused by deformation of the sides of the box, a set of hollow steel sections of cross–section 50 x 50 x 5.2 mm were welded and fixed at each side of the box and the rear as shown in Fig. (3.1). The box was elevated 500 mm above the laboratory floor and rested on concrete blocks 630 x 600 x 500 mm as shown in Fig. (3.1).

To facilitate the removal of backfill from the box, a circular opening 100 mm diameter was made at the rear of the box. This opening was opened or closed by means of a square metal plate 150 X 150 mm, Fig. (3.1). The three internal surfaces were divided by marked horizontal lines every 25 mm in order to control the level of each layer of backfill.

3.3.2 Reinforced Earth Wall

The reinforced earth wall consisted of:

(a) Facing units.

(b) Reinforcing elements.

(c) Backfill material.

(a) Facing units (panels)

Most facing units in actual reinforced earth retaining walls are rigid reinforced concrete slabs of cruciform shape of dimensions 1.5 x 1.5 x 0.18 m as previously mentioned in Chapter (2). Since the scale model is "10" and in order to simulate the dimensions and rigidity of actual units, the facing units in the model were square plates of perspex material of total dimensions 150 X 150 X 18 mm. The edges of each facing unit were tongued & grooved, with two locating pins and two holes.

Nine slots were provided in each unit to fix the reinforcing elements and to allow a change in vertical and horizontal spacing between the elements, Fig. (3.2). The facing units could rotate on each other by rounding the edges of each unit and increasing the diameters of the two holes. This is to simulate the behaviour of a full scale facing unit.

ALL DIMENSIONS IN MM.

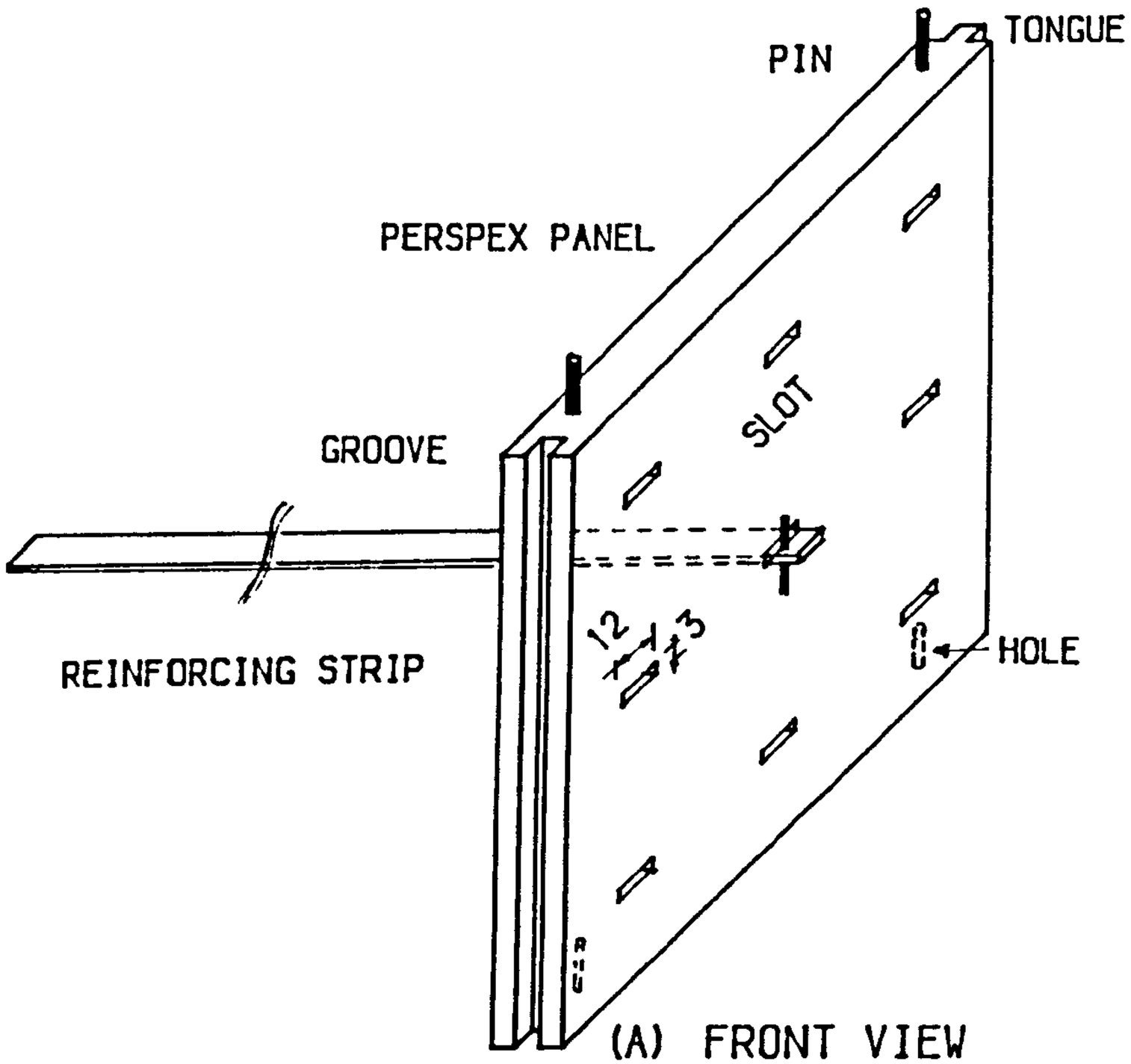

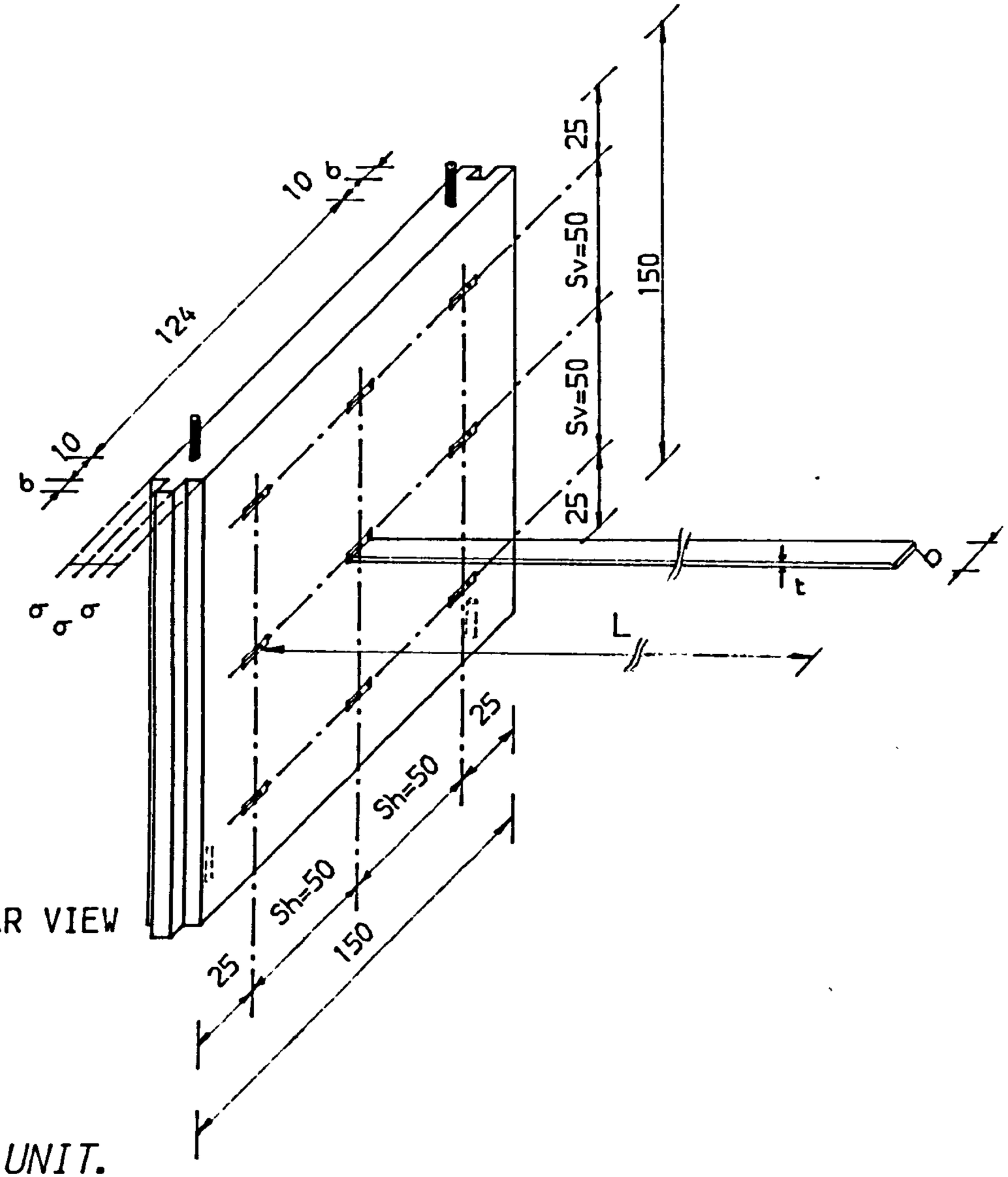

FIG. (3.2) FACING UNIT.

The wall face consisted of 4 rows of panels (facing units), each row having 6 panels. The elastic modulus of 2896 N/mm^2 for the perspex was taken from the Technical Service Note, published by I.C.I. (1973) Plastic Division, at a temperature of 20° C equal to the mean laboratory temperature.

(b) Reinforcing elements

The reinforcing elements used in the test were made from aluminium foil according to British Standard specification (BS 4300/8 : NS 51−H4). This material is one of several kinds of material used in the field and has been approved by British Standard. Also it can be found in small thicknesses to suit small− scale models. The reinforcements were strips, Fig. (3.2), of maximum length 600 mm and constant cross section 12 x 0.1 mm.

These dimensions were based on adherence failure, and methods of design in Table (2.2)−Chapter (2), were applied. The reason for designing the model according to adherence failure was that most failures or excessive movements of reinforced earth retaining walls is due to lack of adherence between soil and reinforcement, and the vast majority of materials are strong enough to resist the catastrophic failure caused by breaking the reinforcement.

The research therefore concentrated on slippage failure only, and to avoid any failure at the connection between wall face and strips, the arrangement shown in Fig. (3.3) was used in the tests.

The strength characteristics of the aluminium foil strips according to BS 4300/8 : NS 51−H4 are,

Permissible stresses:

ALL DIMENSIONS IN MM.

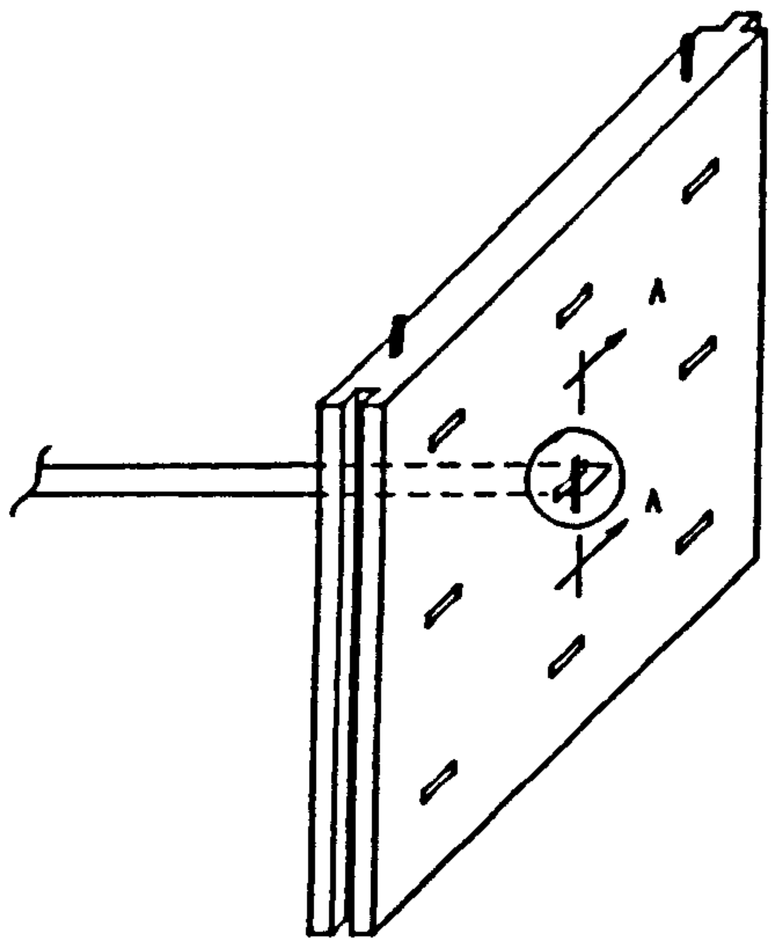

(A) PERSPEX FACING UNIT

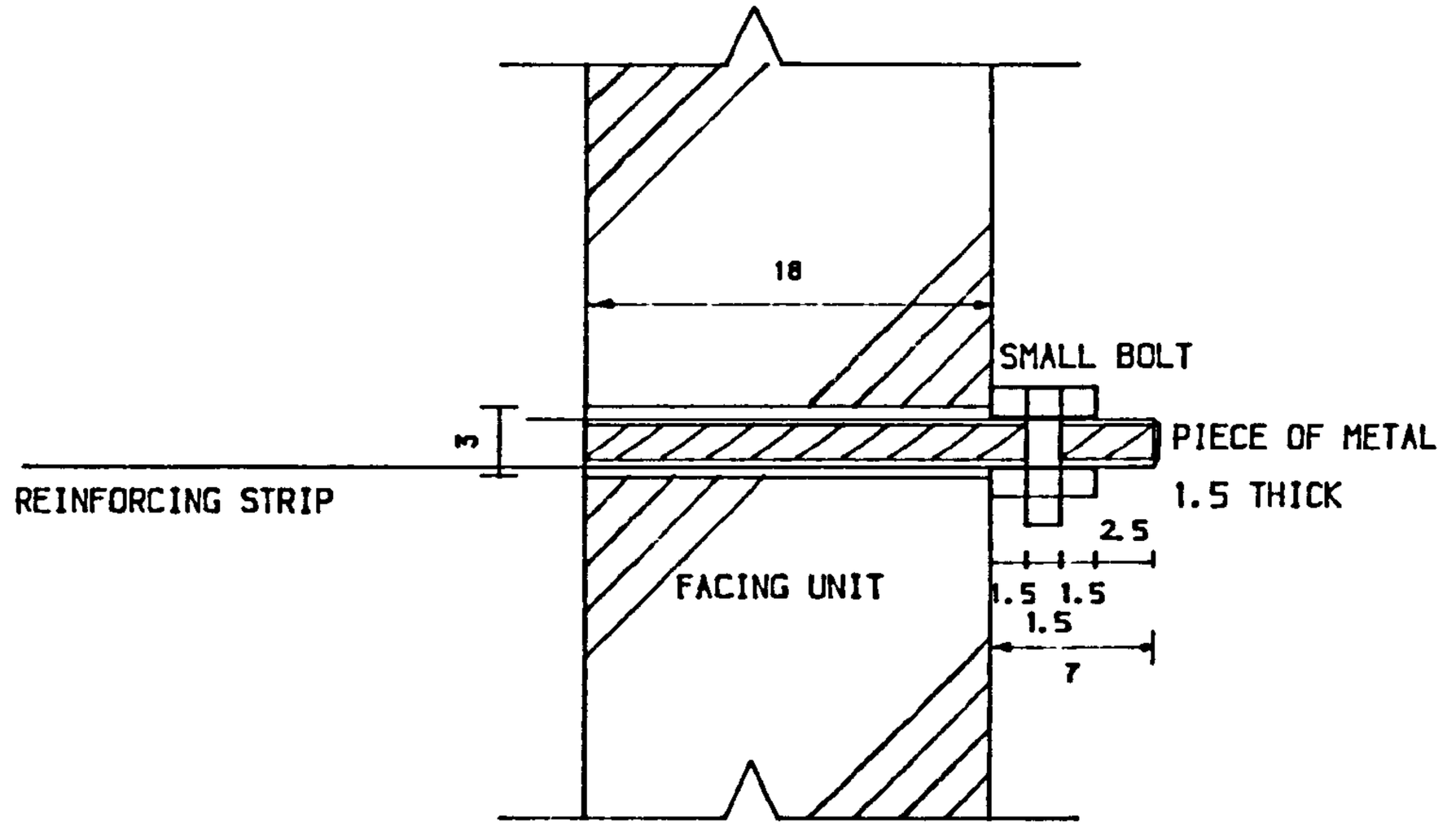

(B) DETAILS A-A

FIG. (3.3) DETAILS OF CONNECTION BETWEEN REINFORCING STRIP AND FACING UNIT.

Axial tension stress	= 120	N/mm^2
Shear stress	= 72	"
Bearing stress	= 180	"
Young's Modulus	= 70000	"
Maximum tensile stress	= 270	"

(c) Backfill material

The backfill material in all the model tests was dry sand from Douglasmuir quarry. The grain size distribution of Douglasmuir sand for three different samples was obtained from sieve analyses, the average values of these result are shown in Fig. (3.4).

A series of laboratory tests was carried out to determine the properties of the sand. The density control, maximum, minimum densities and methods of determination will be discussed in Chapter (4), the values obtained were 14.11 & 18.98 kN/m^3 for minimum and maximum density respectively. The value of specific gravity obtained from five specific gravity tests was 2.66. Hence the maximum and minimum void ratios were 0.89 and 0.40 respectively.

The angle of internal friction ($\dot{\varphi}$) was determined for eleven values of density ranging between maximum and minimum densities using 100 mm diameter, and 200 mm high triaxial samples tested in a dry condition. A typical result of one of the triaxial tests to determine ($\dot{\varphi}$) is shown in Fig. (3.5).

The relation between angle of internal friction and relative density is shown in Fig. (3.6), from which $\dot{\varphi}$ can be determined for any particular value of relative density used in the test.

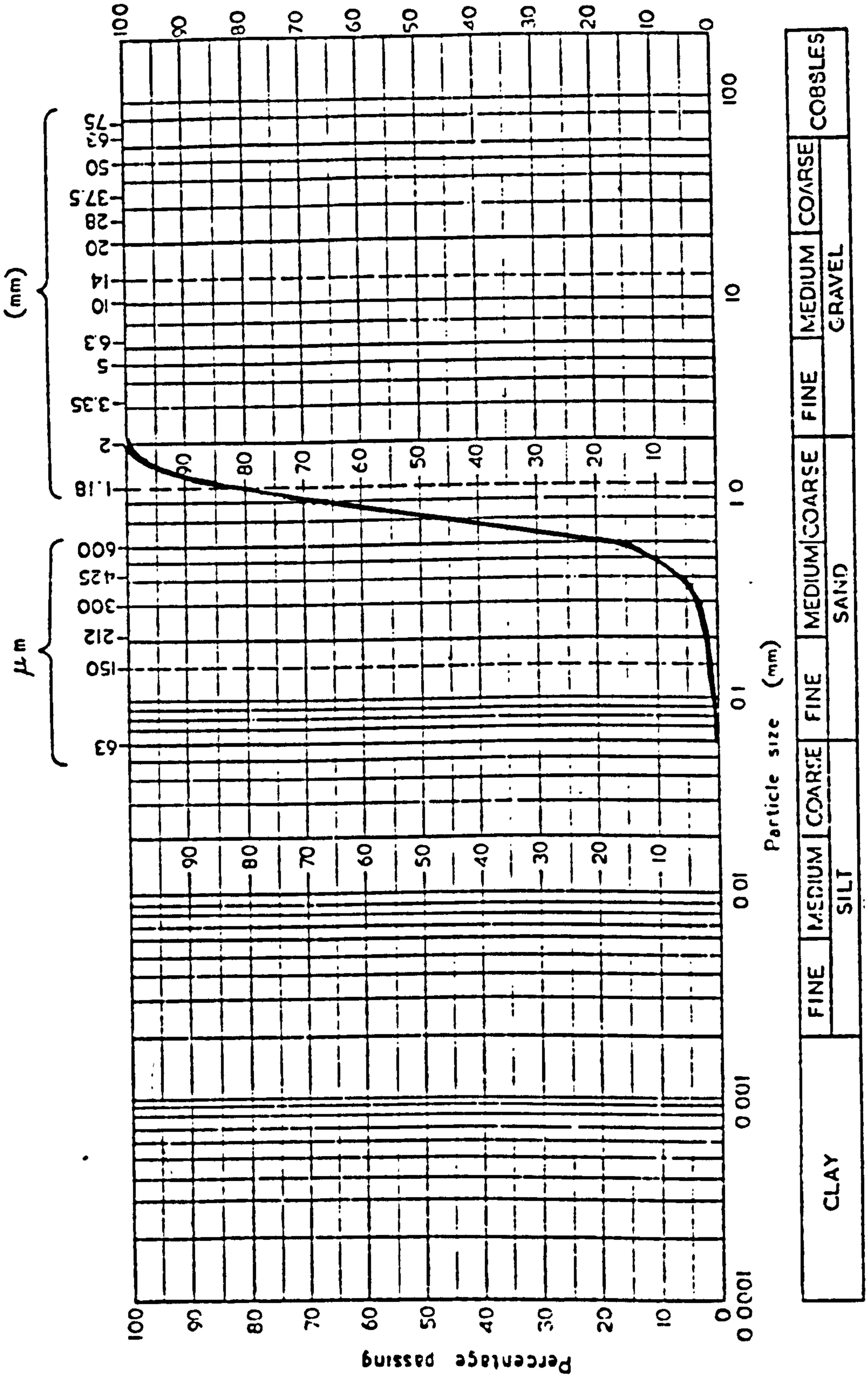

FIG. (3.4) PARTICLE SIZE DISTRIBUTION OF DOUGLASMUIR SAND.

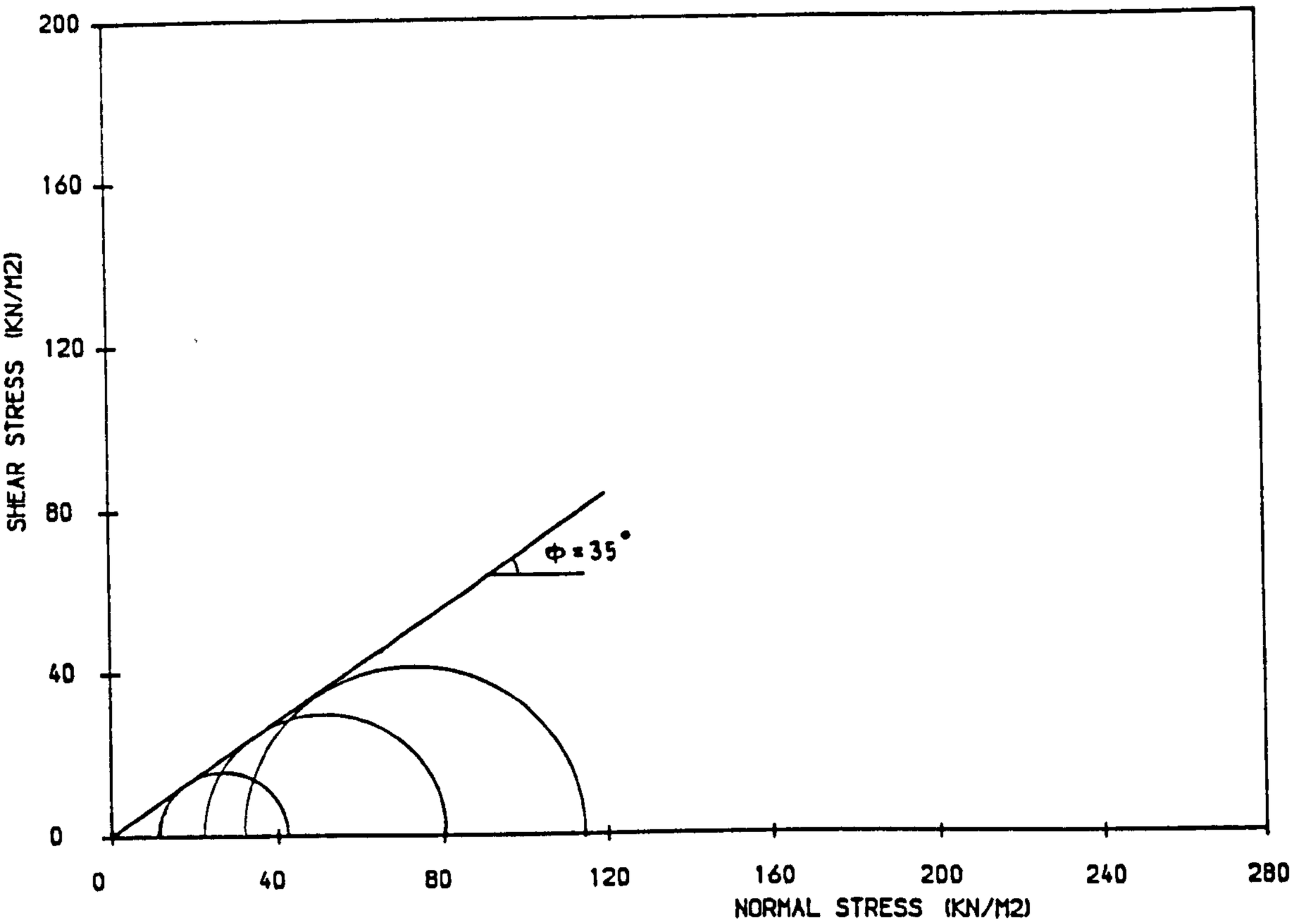

FIG. (3.5) MOHR ENVELOPE FOR DOUGLASMUIR SAND (DRY TEST).

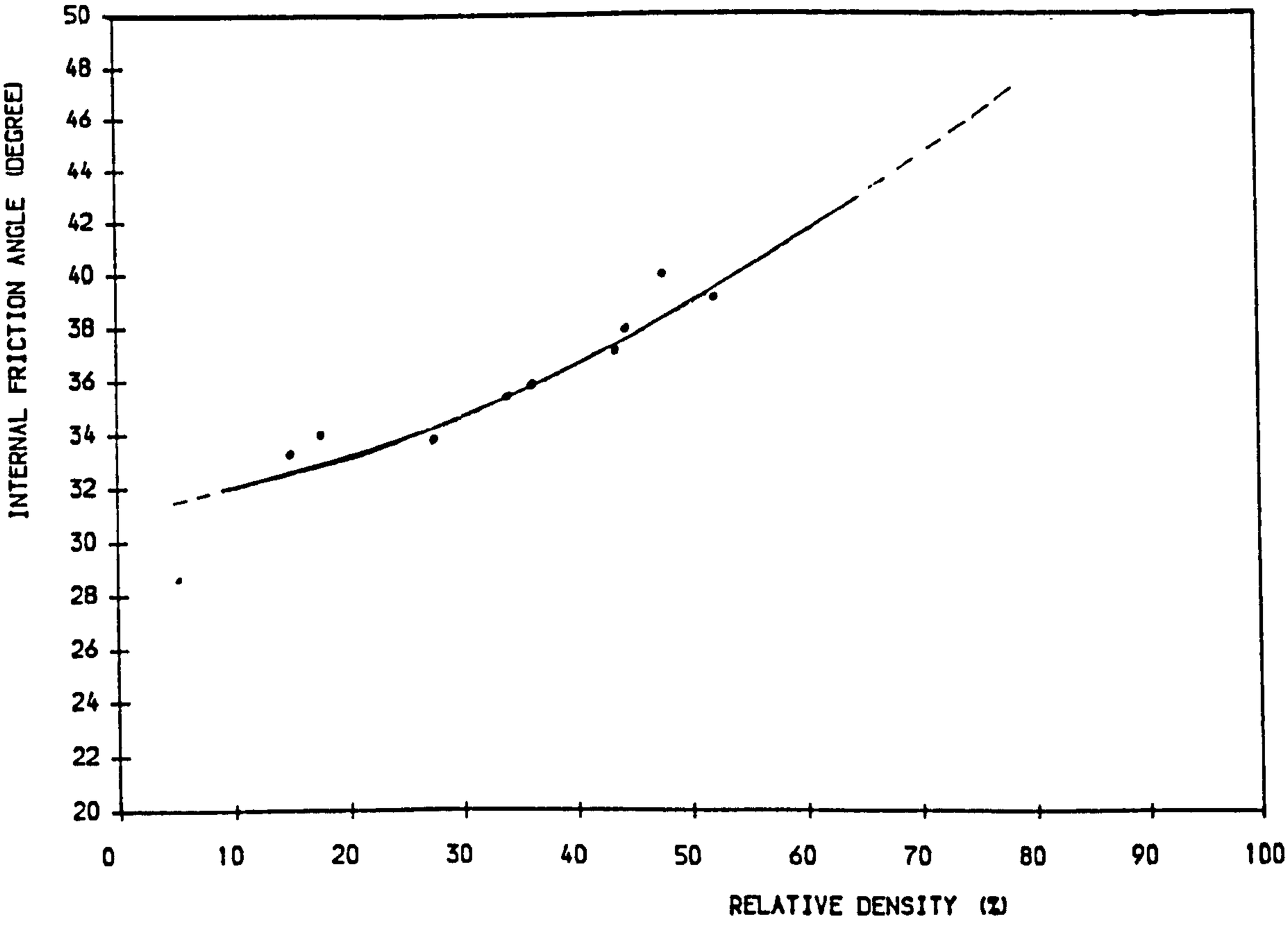

FIG. (3.6) INTERNAL FRICTION ANGLE VS. RELATIVE DENSITY.

3.4 ADDITIONAL ARRANGEMENTS

Arrangements were made to improve the capability of the model test in simulating the studied construction. These arrangements were as follows:

3.4.1 Wall Face Edges

In order to minimize friction between the two edges of the wall face and the sides of box, a gap of 0.5 mm was provided at each side between the wall face edges and the sides of the wooden box.

To prevent sand from flowing through these gaps two polyethylene strips of dimensions 600 x 50 x 0.3 mm, each were placed at the two sides, as a continuous vertical strip and overlapped 20 mm over the facing units and 30 mm over the box side, and pieces of cotton were put at the corner of each strip as shown in Fig. (3.7). The Fig. also illustrates the assembling of the main components of the reinforced earth wall after it had been constructed in the wooden box.

3.4.2 Sand Spreader Device

To form sand layers for the reinforced earth retaining wall of a certain thickness and density in the box, a sand raining device was used consisting mainly of a frame acting as a support to a travelling hopper to discharge sand through a perforated plate fixed to the bottom of the hopper. The details and calibration of the sand raining device will be discussed in Chapter (4).

ALL DIMENSIONS IN MM.

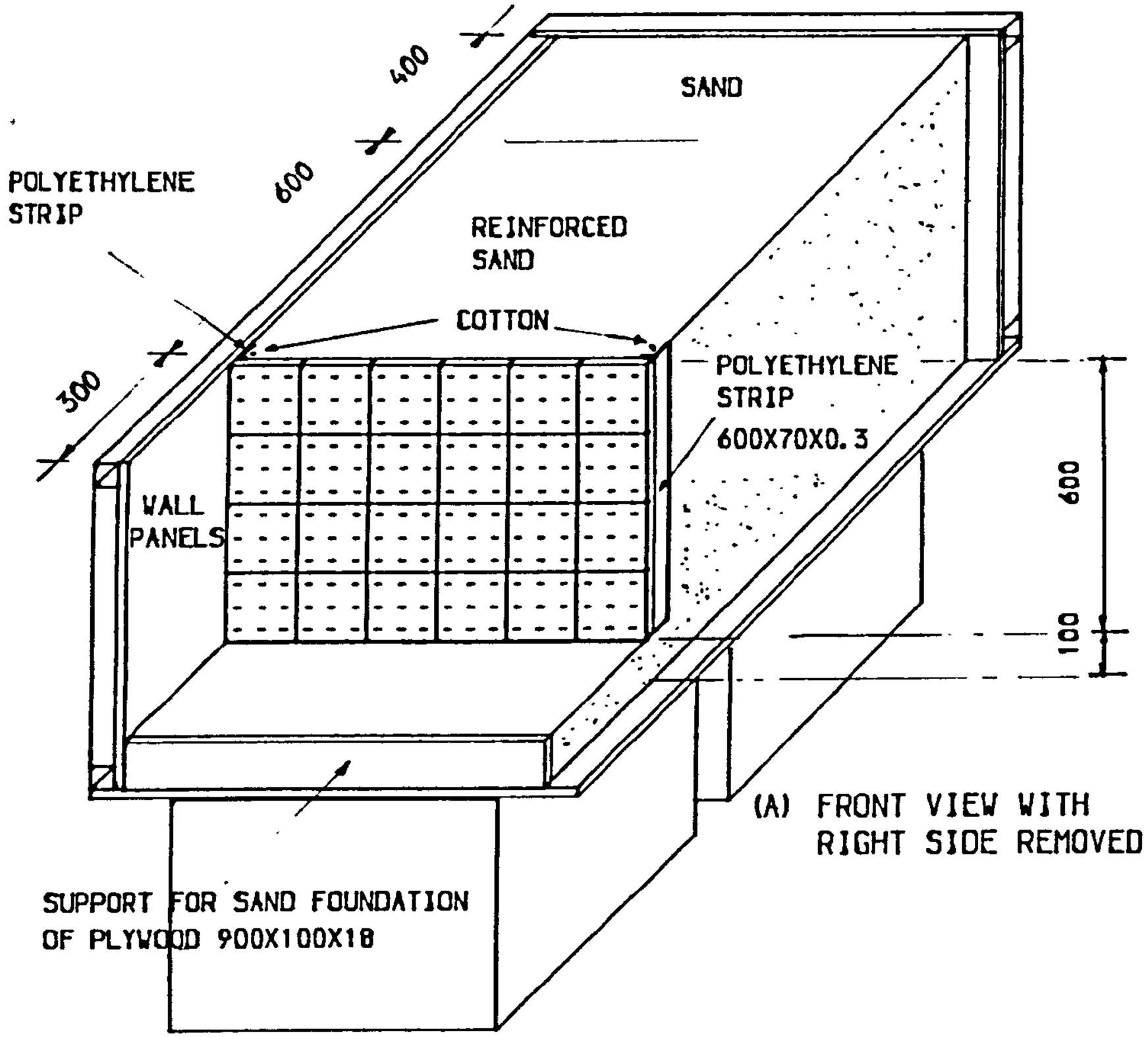

(A) FRONT VIEW WITH RIGHT SIDE REMOVED

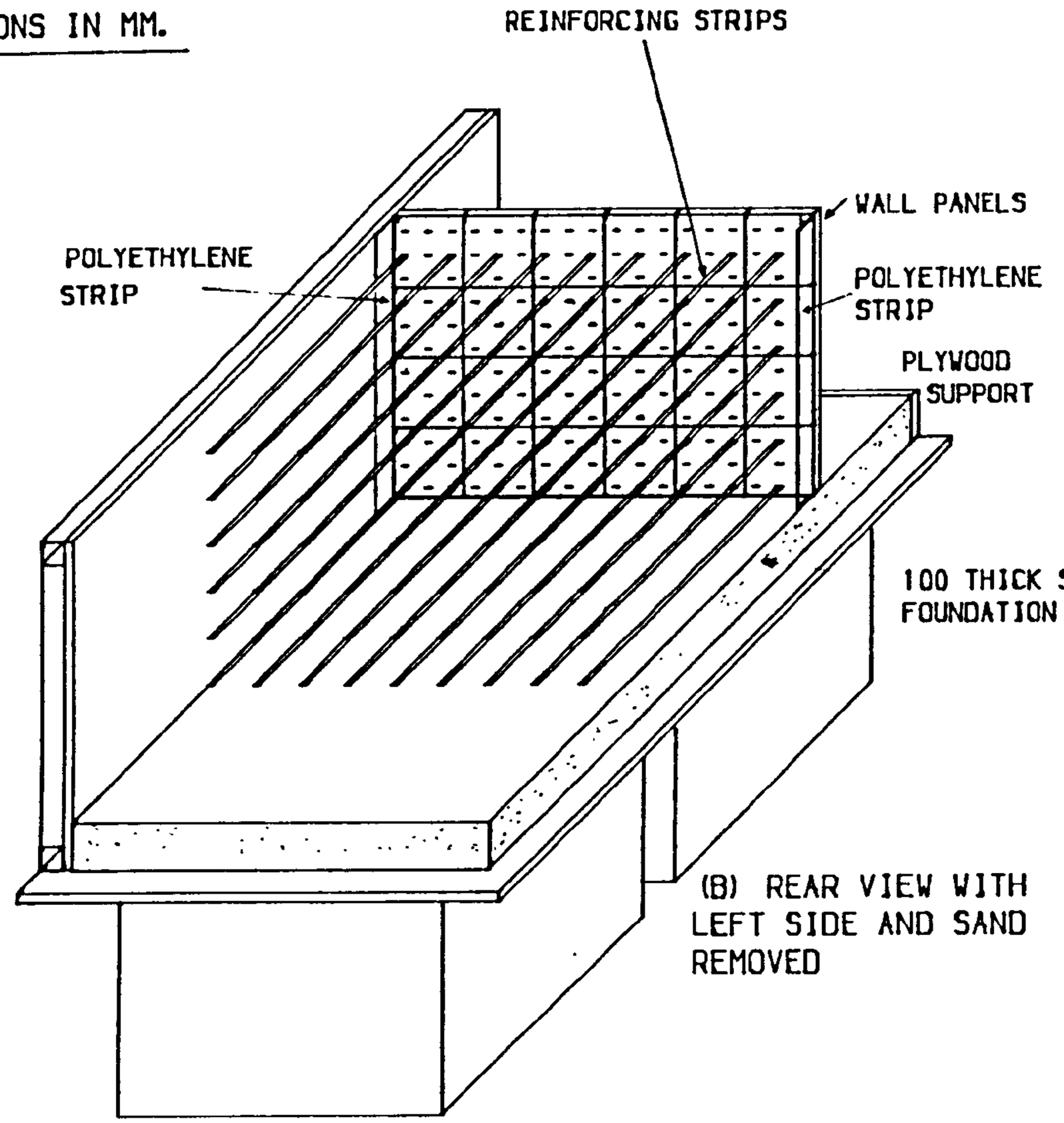

(B) REAR VIEW WITH LEFT SIDE AND SAND REMOVED

FIG. (3. 7) WALL FACE EDGES AND ASSEMBLING OF REINFORCED EARTH WALL.

3.4.3 Compaction Plant Simulation

Cohesionless soil is commonly compacted using vibratory plant (roller, compactor ... etc.) to reach high densities. To simulate this in the model test, two vibrators were used, fixed rigidly to metal and wooden plates to give vertical vibrations. Detail and calibrations are given in Chapter (4).

3.4.4 Dust Extractor Machine

To overcome the problem of dust produced by raining the sand from the raining device, which may affect the velocity of the sand grains and hence the deposition, a special arrangement was used to suck the dust from the box. The details are shown in Chapter (4).

3.4.5 Temporary Support

To provide a temporary support to the facing units while the wall was under construction, five slots were cut in each side of the box. The slots were located close to facing panels. Five removeable metal rods 1050 mm long could be installed through the slots to be tangential to the panels and act as a temporary support for any row of panels. They were also used as a permanent support until the end of construction in one of the construction methods. Some of the supports are shown in Fig. (3.8).

3.4.6 Surcharge Load

Many model tests in the past have relied on surcharge loading of the top surface of the reinforced earth mass to bring about failure. This was felt to be

ALL DIMENSIONS IN MM.

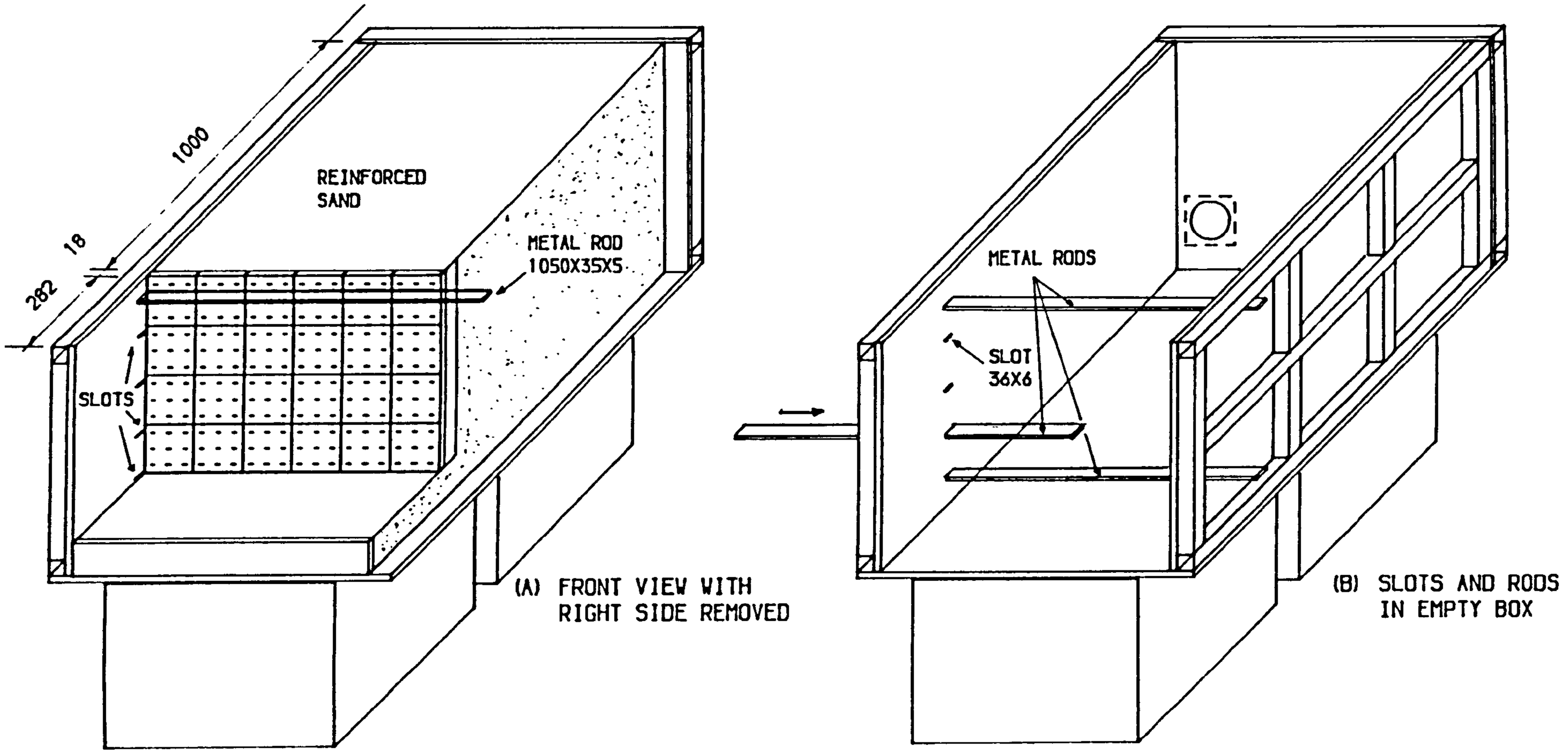

(A) FRONT VIEW WITH RIGHT SIDE REMOVED

(B) SLOTS AND RODS IN EMPTY BOX

FIG. (3.8) TEMPORARY SUPPORTS FOR WALL FACE.

an artificial situation, and the present tests were done without surcharge loading, to simulate a real structure.

3.5 INSTRUMENTATION, MEASUREMENT DEVICES AND CALIBRATION TESTS

To investigate the behaviour of the model walls, measurements were taken to determine the tensile strain developed in the reinforcing strips and hence find the tensile forces and stresses in the strips. Stresses in the backfill sand were measured at different locations, as was the lateral movement of the wall face. Interaction between the strips and the sand was determined. The devices, methods of measurements and calibration used in the model will be illustrated in the following sections:

3.5.1 Tensile Forces And Stresses In Reinforcing Strips

In order to measure the stresses developed in the reinforcing strips before, during and after compaction, while the wall was under construction and post construction, strain gauges were mounted in pairs on selected strips and at selected locations on the two faces of the selected strips. The selected strips were located near to the centre line of the wall and in one vertical plane, to minimize any side effects of the box on the measurements. Three or four locations (depending on the length of the strip) were chosen at critical positions along the strip, and the locations of the strips and the strain gauges for different experimental categories are shown in Fig. (3.9).

The type of strain gauge used was CEA−13−125 UN−120 manufactured by

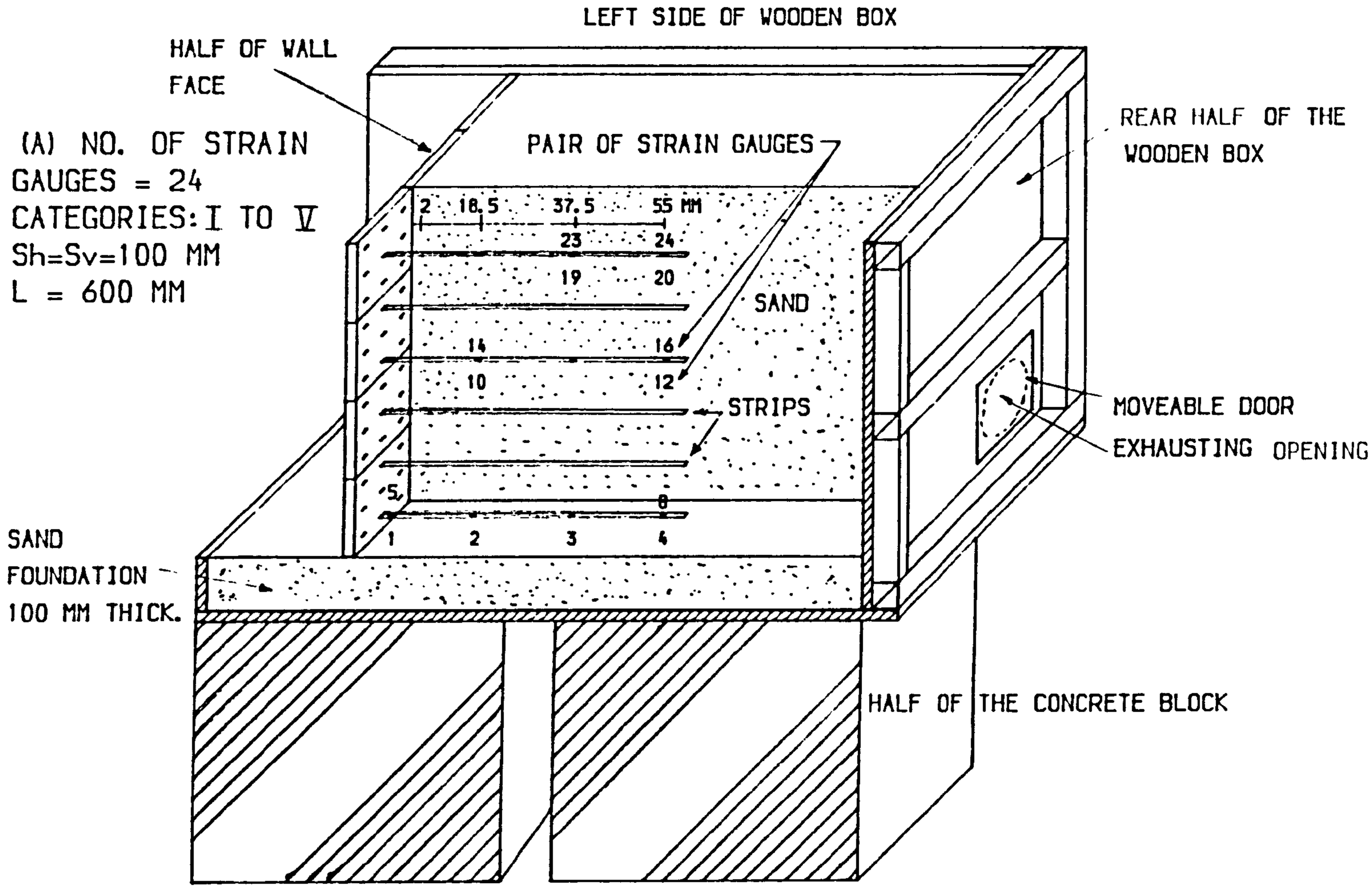

FIG. (3.9) STRAIN GAUGE LOCATIONS

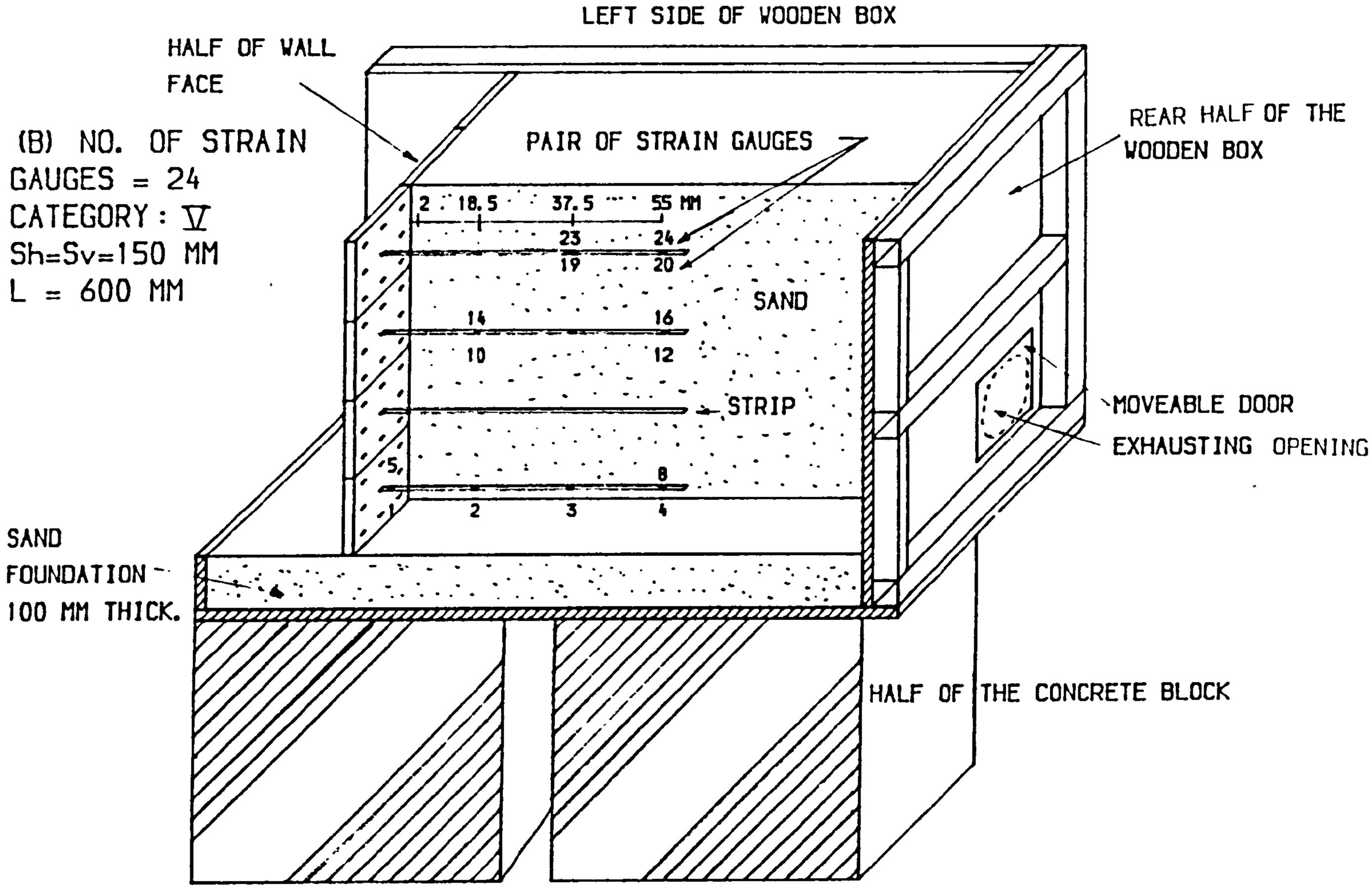
LEFT SIDE OF WOODEN BOX
HALF OF WALL FACE
(B) NO. OF STRAIN GAUGES = 24
CATEGORY : V
Sh=Sv=150 MM
L = 600 MM
PAIR OF STRAIN GAUGES
REAR HALF OF THE WOODEN BOX
2
18.5
37.5
55 MM
23
24
19
20
SAND
14
16
10
12
STRIP
5
8
1
2
3
4
MOVEABLE DOOR
EXHAUSTING OPENING
SAND FOUNDATION 100 MM THICK.
HALF OF THE CONCRETE BLOCK

FIG. (3.9) CONT.

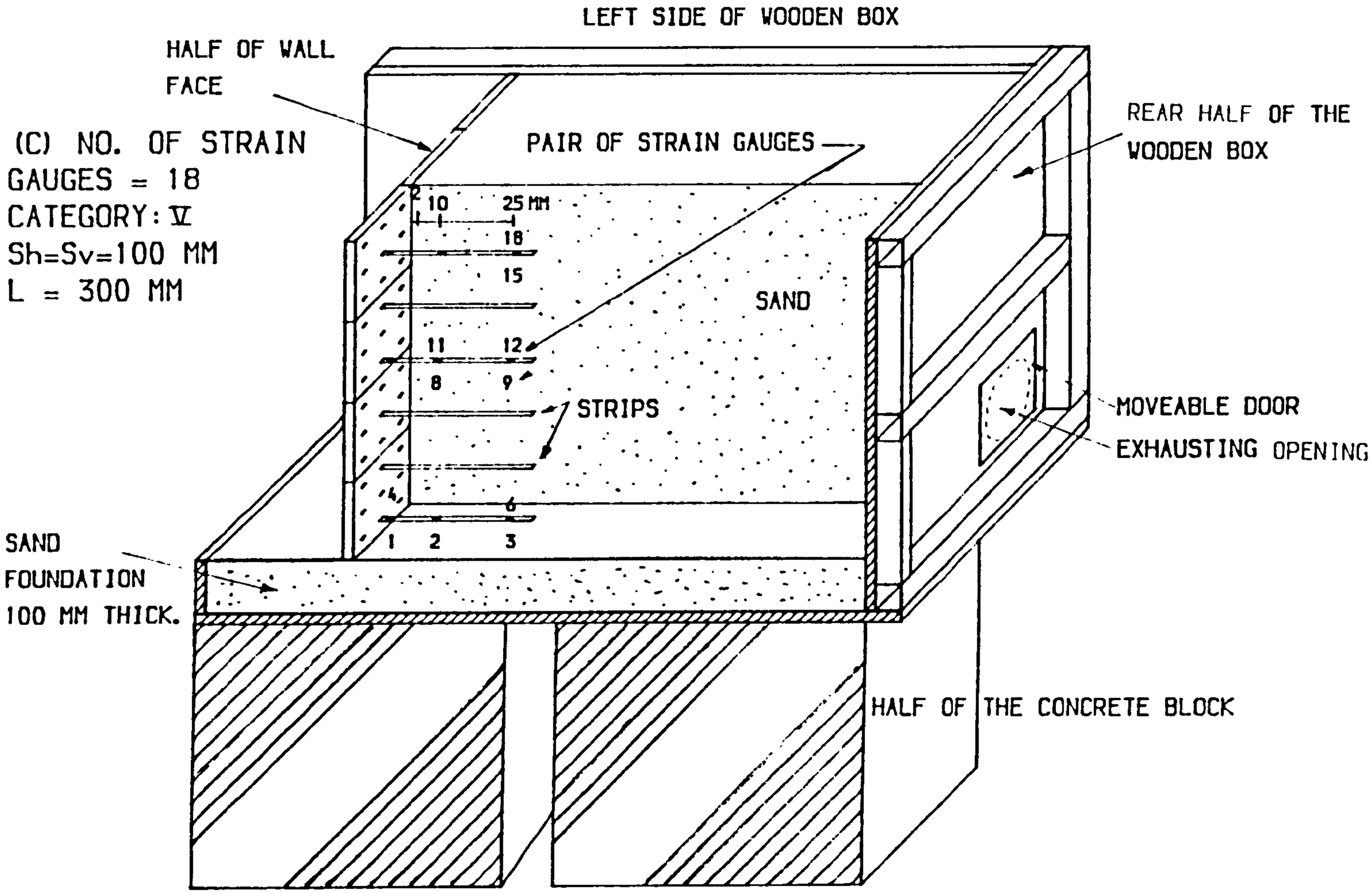
LEFT SIDE OF WOODEN BOX
HALF OF WALL FACE
(C) NO. OF STRAIN GAUGES = 18
CATEGORY: V
Sh=Sv=100 MM
L = 300 MM
PAIR OF STRAIN GAUGES
REAR HALF OF THE WOODEN BOX
10
25 MM
18
15
SAND
11
12
8
9
STRIPS
MOVEABLE DOOR
EXHAUSTING OPENING
6
1
2
3
SAND FOUNDATION 100 MM THICK.
HALF OF THE CONCRETE BLOCK

FIG. (3.9) CONT.

Micro– Measurements division, Measurements Group, INC., Releih, North Carolina, U.S.A. . CEA strain gauges are polyimide– encapsulated A– alloy (constantan 40% Nickel and 55% Copper in self temperature compensation form), featuring large, integral copper– coated terminals for ease in soldering lead wires directly to the gauges, Fig. (3.10). These gauges are very thin, flexible and are resistant to damage in handling.

Strain gauges will perform satisfactorily and produce useful results only if they meet the following criteria:

(a) Correct selection of strain gauges for the problem under investigation.

(b) Use of the correct technique of mounting or installing.

(a) Selection of strain gauges

Pople (1980), Window and Holister (1982) stated that the specification for the ideal strain gauge would list a considerable number of desireable features, the most important of which would be the following:

(i) Small size and mass and low stiffness to avoid reinforcing the item tested.

(ii) Suitability for static and dynamic measurements and for remote recording.

(iii) Freedom from effects of temperature and other environmental conditions.

(iv) Good stability, repeatability and linearity over a wide strain range.

(v) Robustness with ease of handling and application and low cost.

Also they reported some factors to be considered when choosing a strain gauge for a particular purpose. The questions asked come under a general

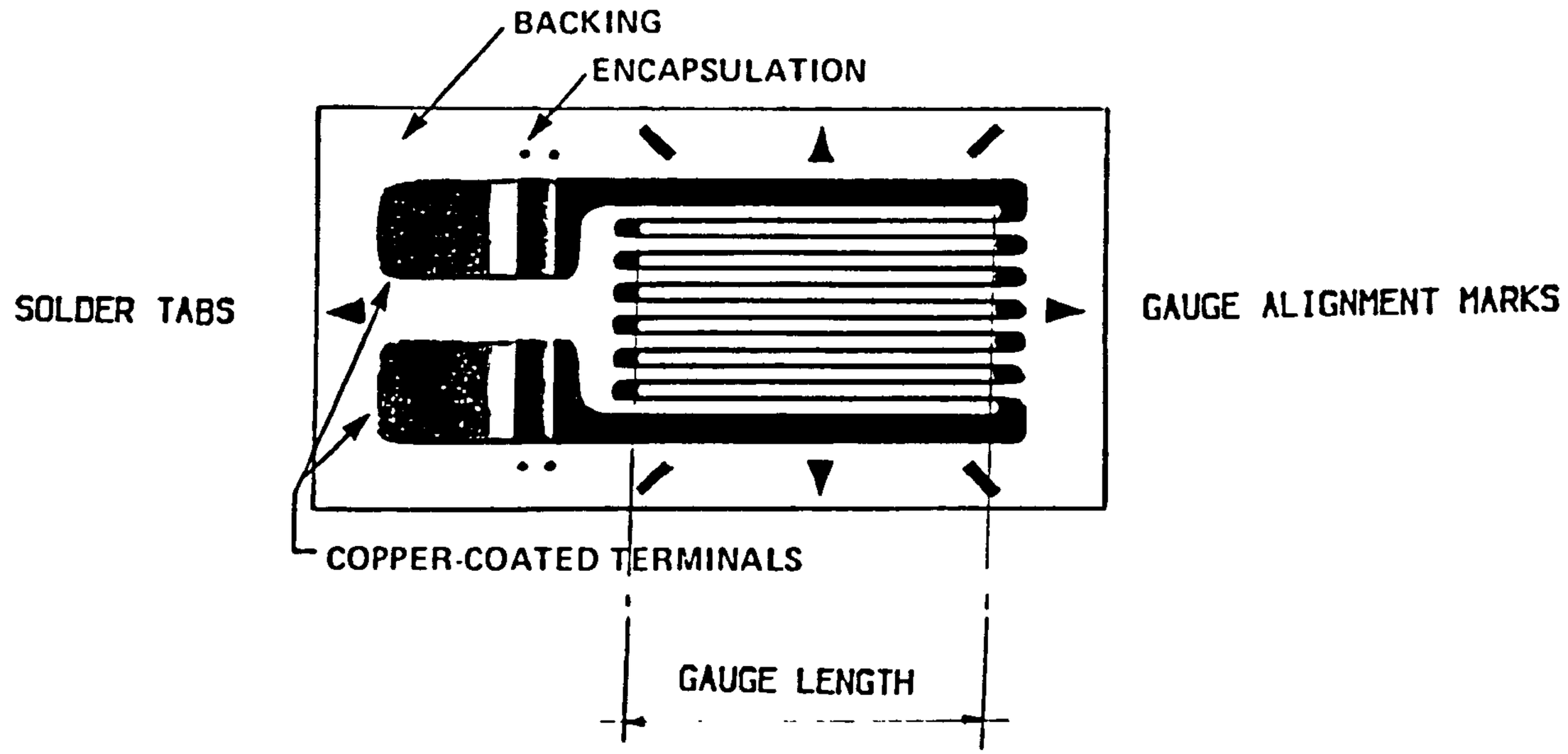

FIG. (3.10) TYPICAL LINEAR STRAIN GAUGE BONDED ON THE STRIPS.

heading of what is to be measured and under what conditions?.

For example:

- Strain, calibrated loads or fluid pressure?
- Tensile, shear or torsional strains?
- Are the directions of principal strains known?
- will the strain distribution be uniform or not?
- Is the specimen large or small?
- Are the expected strain levels high or low?
- What will be the duration of the test and what order of stability is required?
- Will the loads be static or dynamic?
- What will the operating temperature of the specimen be?
- What variation in temperature will occur during the test?
- What material is the specimen?
- What are the environmental conditions?

By replying to the above questions the proper and convenient strain gauges can be determined. In this research the answers to the above questions are:

The basic measurements are axial tensile strains, the strains are not uniform and the specimen is reinforcing strip (aluminium foil) which is thin. The expected strain is not high because it is a small model. Strains will be produced from both static and dynamic loads at laboratory temperature (around 20° C) and the environmental condition is almost constant because it is dry sand. These measurements need small linear strain gauges where the leader wires are soldered directly to the gauge to minimize any disturbance in measurement. The gauges should have self temperature compensation to cancel any effect of temperature

change. Obviously the strain gauges should be flexible, easy to handle and cheap.

From the feature of strain gauges (50,000 type) produced by the Measurement Group Company catalogue 400, strain gauge listings 8/1/84, it was found that strain gauges of type CEA–13–125 UN–120 met the requirements.

(b) Bonding the strain gauges to the reinforcing strips

The strain gauge will work only as well as the installation will allow it, and even the finest gauges will not produce satisfactory results if the application techniques are wrong. Techniques for installing strain gauges are therefore of paramount importance. The technique used to bond the strain gauges to the strips followed the instruction in the Technical Notes, reported by the Measurements Group Company (1982).

In order to eliminate the effect of bending, two gauges were bonded on both faces of the strip at the same location. An epoxy covering was applied to the gauges to protect them and to increase the bending stiffness of the strip at the strain gauge position to make them relatively insensitive to bending as mentioned by several reseachers such as Lee et al. (1973) and Osman (1977).

3.5.2 Calibration Of Strain Gauges

The steps to mount the strain gauges on the reinforcing strips were repeated every time a gauge was mounted on the strip surface. 66 strain gauges were used in the different test categories. There are two methods of converting the measured strains in the strips to stresses:

(a) By using the appropriate value of Young's modulus for the aluminium foil strip which relates stress to strain. Forces can also be obtained where the strip cross section is known.

(b) By individual calibration of the strips.

In this work the second method of finding forces and stresses by individual calibration of the strip was used, as this represents the actual circumstances of the model test and avoids any errors which may have happened during cutting the strips.

All the strain gauges used in the model tests were calibrated using the loading rig shown in Fig. (3.11), to provide a direct reading of tensile force and hence stress against electrical output. Precautions were taken regarding loading and unloading, repetition of loading cycles and the test temperature. A typical calibration curve is shown in Fig. (3.12). Fig. (3.13) shows a typical calibration curve for the same strain gauge – as in Fig. (3.12)– but calculated using method (a) above. The difference between the two calibration factors may be due to some inequality in the width along the strip.

The ranges of calibration factors of all the strain gauges are shown in Appendix (A).

3.5.3 Stress In Backfill

Horizontal stresses on the wall face, the vertical pressure just behind the wall face, the pressure distribution under the reinforced mass, and the horizontal pressure behind the reinforced mass were measured by means of 16 miniature

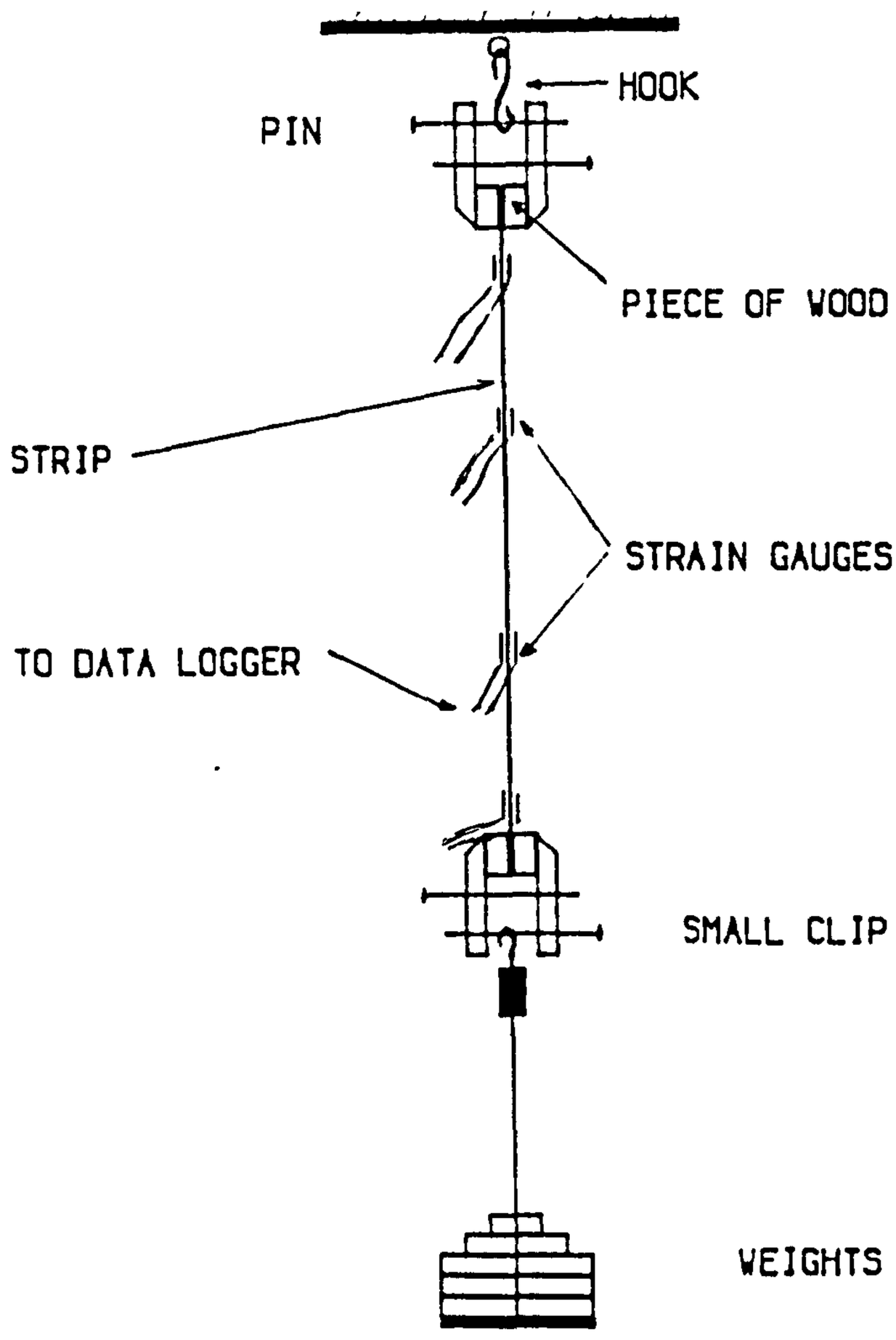

FIG. (3. 11) SET UP FOR THE CALIBRATION OF STRAIN GAUGES.

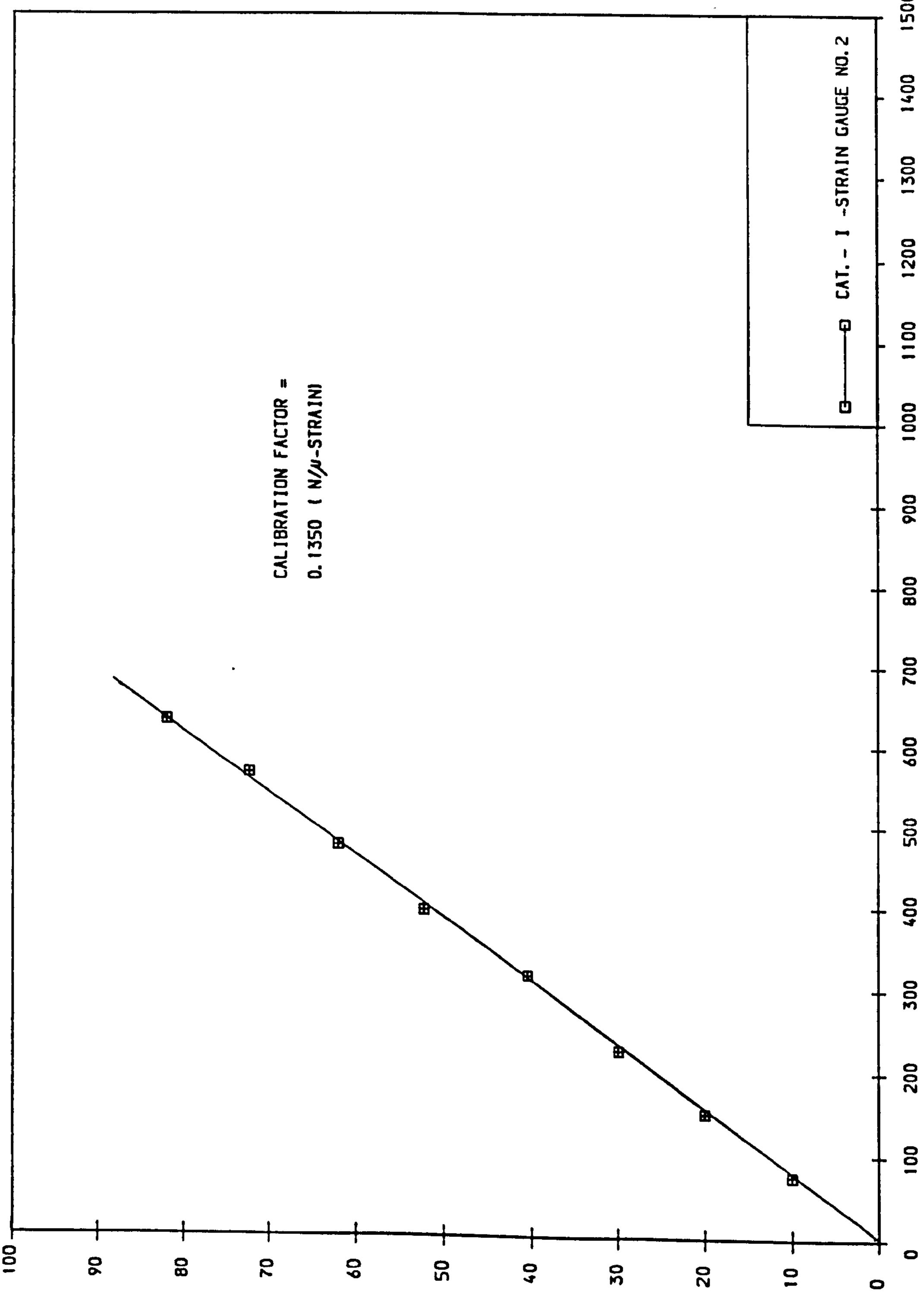

FIG. (3.12) CALIBRATION CURVE OF ONE OF 66 STRAIN GAUGES USED IN THE MODEL TESTS, BY DIRECT CALIBRATION.

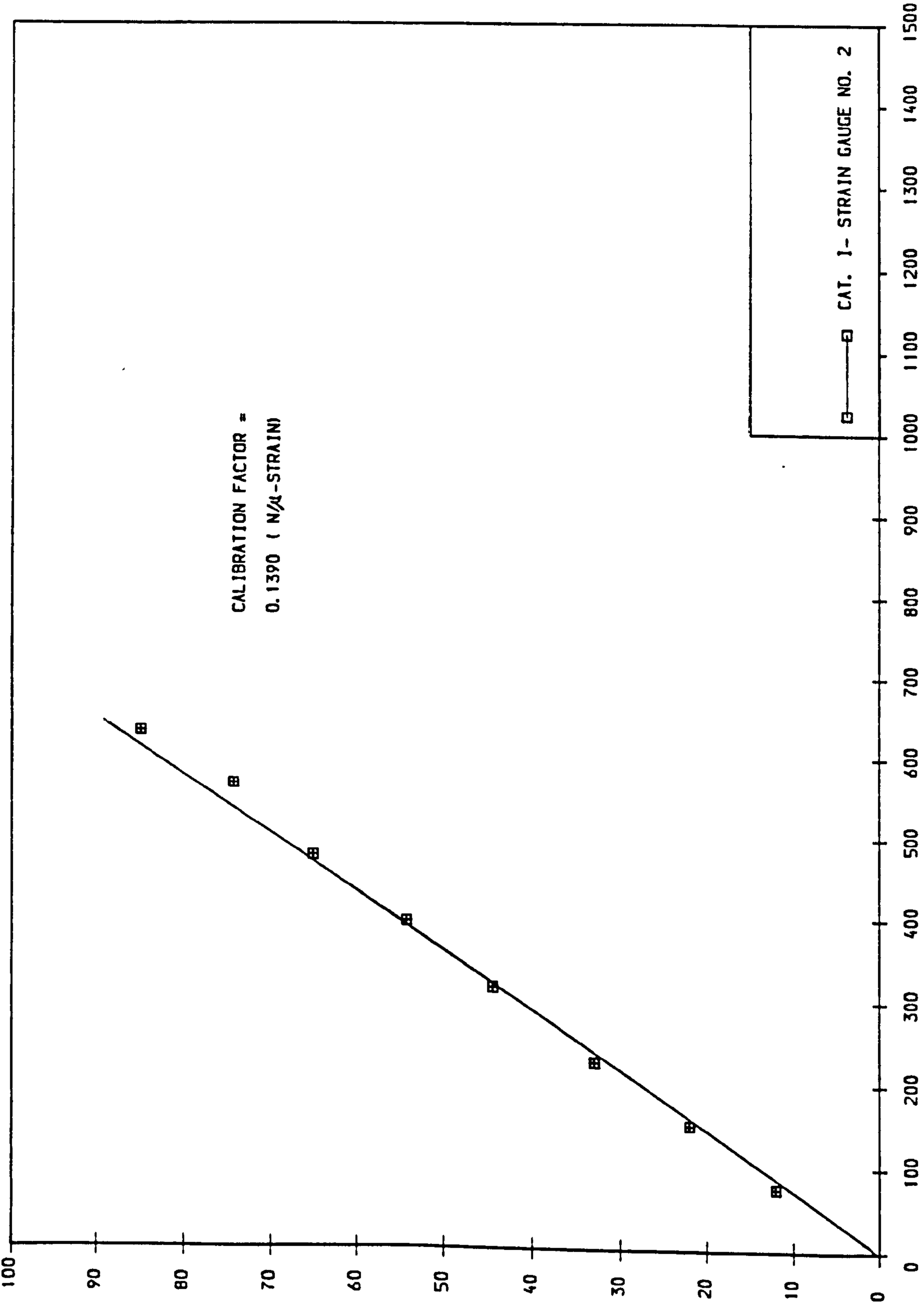

FIG. (3.13) CALIBRATION CURVE OF ONE OF 66 STRAIN GAUGES USED IN THE MODEL TESTS, CALCULATED FROM YOUNG'S MODULUS.

strain gauge cells, which were designed, manufactured and calibrated in the Soil Mechanics Laboratory of the Civil Engineering Dept., University of Glasgow. Details of the pressure cells are given in the next section. The locations of the pressure cells were constant in all tests, as shown in Fig. (3.14.A&B).

It is seen from this Fig. that pressure cells No. 1, 7, 11 and 15 were mounted flush with the back of the wall face in a special arrangement in order to measure horizontal pressure as shown in Fig. (3.14.C). Pressure cells No. 2, 3, 4 and 6 were placed in a horizontal position to measure pressure under the reinforced mass. Pressure cells 2, 8, 12 and 16 measured the vertical pressure just behind the wall face. Pressure cells 5, 9, 13 and 6, 10, 14 measured the horizontal and vertical pressure respectively behind the reinforced mass.

(a) Theoretical background

Kögler and Scheiding (1927) first called attention to the inherent difficulties in measuring earth pressures accurately with a pressure cell. They pointed out that the different rigidity of the cell and the surrounding soil would cause differences between the cell readings and the actual pressure. They indicated that only if the cell has the same deformation characteristics under pressure as the surrounding soil would its use be free from error.

Peattie and Sparrow (1954) criticized the above solution and reported that, unless the pressure cell is to be used in a material of constant known modulus , it is highly undesirable to construct it so that it has nearly the same modulus as the material, and these conditions are unlikely to be found in soils.

The above authors showed that the pressure recorded by the cell may be

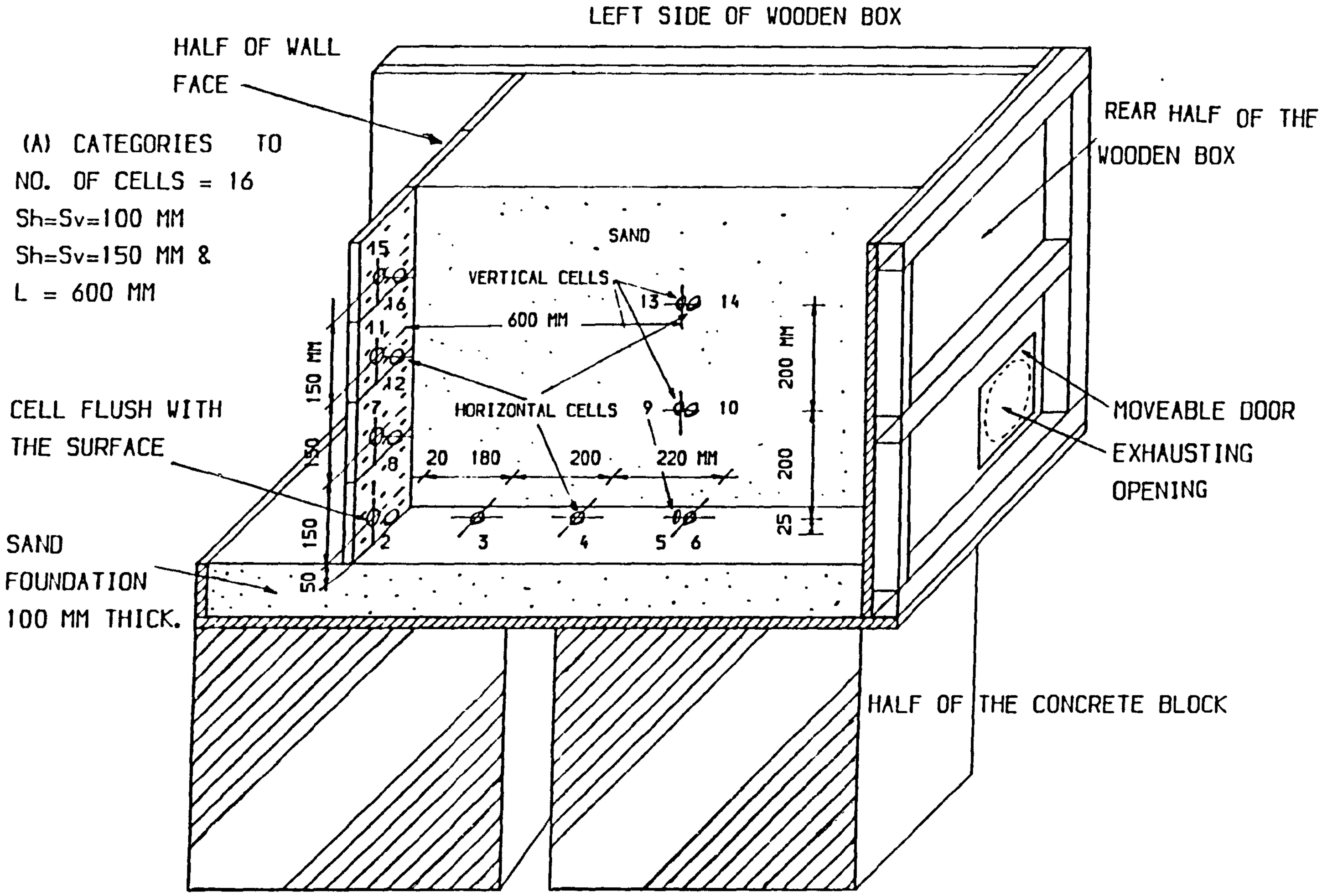

FIG. (3.14) POSITION OF PRESSURE CELLS.

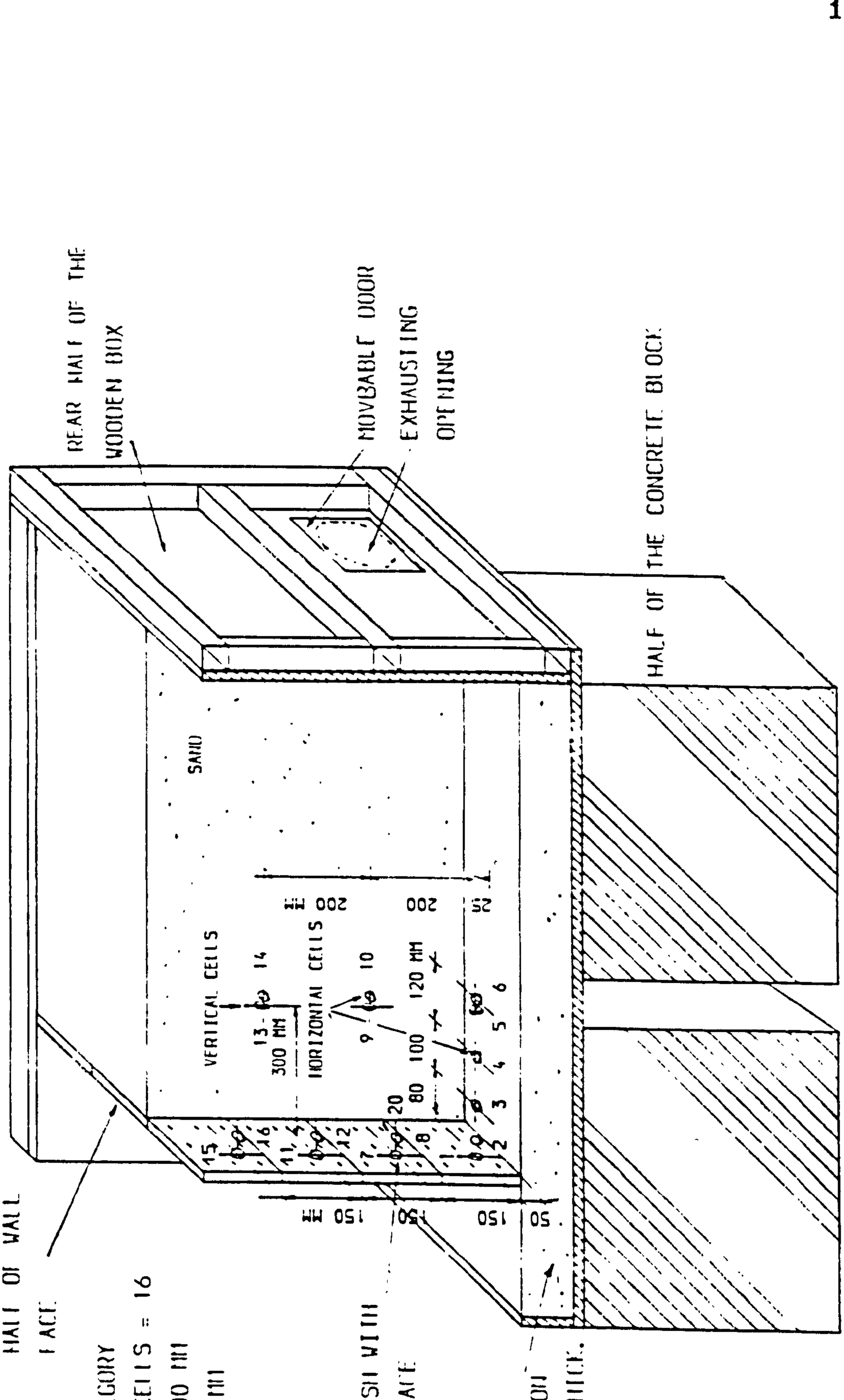
REAR HALF OF THE
WOODEN BOX
MOVABLE DOOR
EXHAUSTING
OPENING
HALF OF THE CONCRETE BLOCK
LEFT SIDE OF WOODEN BOX
SAND
VERTICAL CELLS
13-
300 MM
HORIZONTAL CELLS
14
10
9
120 MM
100
80
20
6
5
4
3
2
1
200
150
50
HALF OF WALL
FACE
(B) CATEGORY
NO. OF CELLS = 16
Sh-Sv-100 MM
1 300 MM
CELL FLUSH WITH
THE SURFACE
SAND
FOUNDATION
100 MM THICK

FIG. (5.14) CONT.

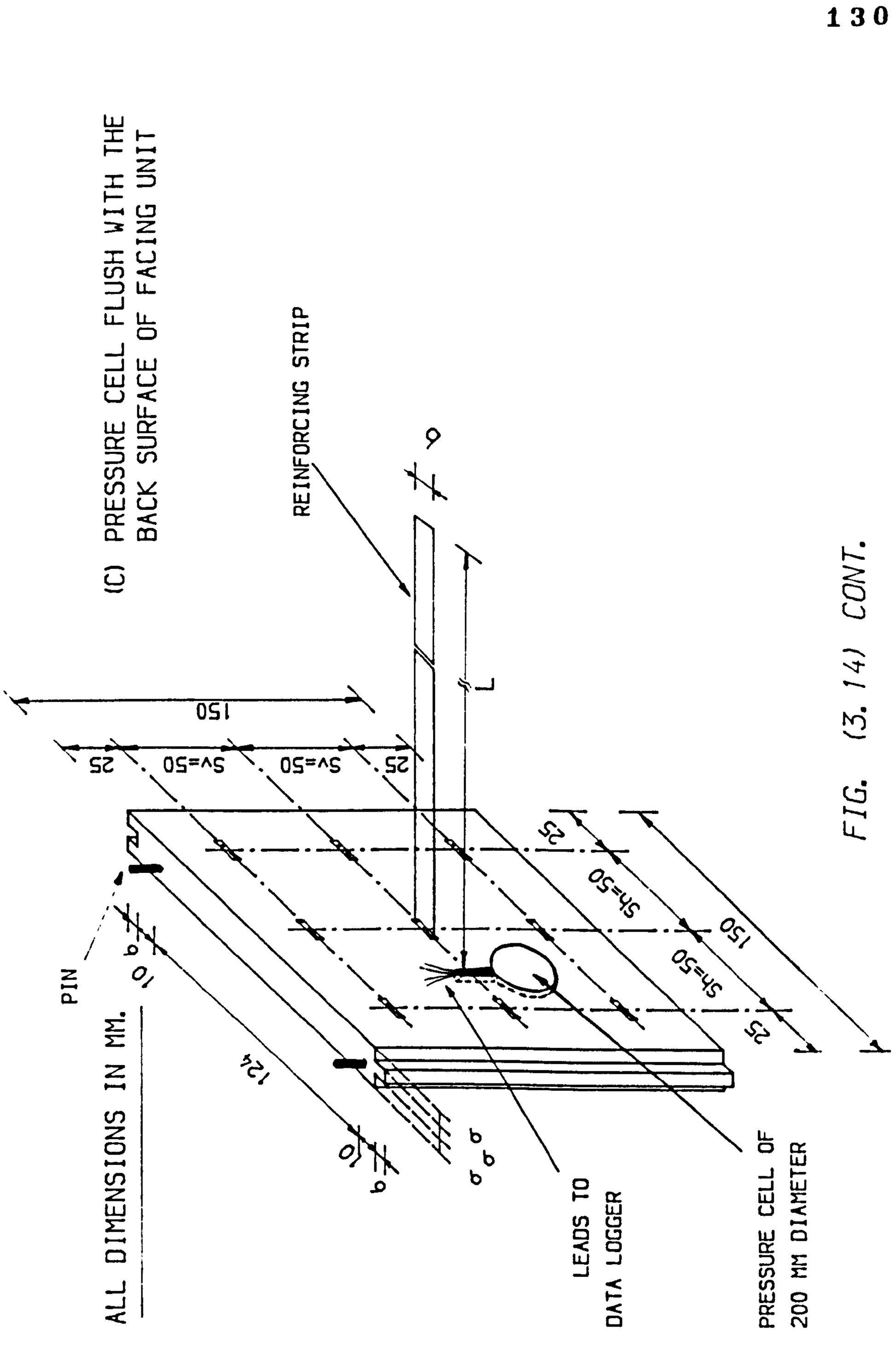
(C) PRESSURE CELL FLUSH WITH THE BACK SURFACE OF FACING UNIT
REINFORCING STRIP
150
25
Sv=50
Sv=50
25
L
52
Sh=45
Sh=45
52
150
PIN
10
12
10
LEADS TO DATA LOGGER
PRESSURE CELL OF 200 MM DIAMETER
ALL DIMENSIONS IN MM.

FIG. (3.14) CONT.

greater or less than the field pressure (pressure before embedding the cell) depending on several factors, which affect the relative deformation characteristics of the cell and the surrounding medium. These factors must be taken into account during the design and calibration of pressure cells in general and particularly the strain gauge cells type embedded in sand. These factors are:

(i) Compressibility effect

If the cell is first considered as a disc, then the total pressure carried by the cell may be greater or less than the field pressure according to whether the rigidity of the body of the cell is more or less than the surrounding medium.

Taylor (1947) and Monfore (1950) have considered the compressibility effect as the problem of an elastic disc embedded in an elastic medium and have expressed the influence of the cell in terms of the physical properties of the disc and the surrounding medium. Peattie and Sparrow (1954) combined these approaches and expressed the pressure variation in terms of "cell action". The "cell action" may be defined in terms of the cell factor as in Eq. (3.1):

$$\frac{P_c}{P} = C_A \frac{B}{D} + 1 \qquad (3.1)$$

Where:

P_c is the recorded cell pressure.

P is the field pressure.

2B is the thickness of the cell.

D is the diameter of the cell.

C_A is the cell factor which can be obtained experimentally.

From the above equation, it will be noted that the physical dimensions of the cell (B,D) as well as the cell factor influence the recorded pressure.

(ii) Diaphragm effect

If the cell is of the type in which the pressure is recorded through the deflection of a diaphragm, then the distribution of the total pressure on the diaphragm, and hence the recorded pressure, may be further affected by the deformation of the diaphragm with respect to the adjacent medium and this has been termed the "diaphragm effect", Trollope and Currie, 1960.

Experimental results obtained at the U.S. Waterways Experimental Station by U.S. Corps of Engineers (1944) pointed out the diaphragm effect and recommended that the diameter:thickness ratio should be not less than 5:1, and diameter:deflection ratio should be not less than 2000:1.

Trollope and Currie (1960) recommended that the ratio of 5:1 may be too severe and that this could be reduced to 2.5:1 without loss of accuracy, but they suggested that the diameter:deflection ratio be not less than 2000:1.
They also suggested that the active area of the diaphragm should be as high a proportion of the total face area as possible. Their conclusions from experimental investigations were:

The major influence on the calibration performance of cells was associated with the diaphragm effect. For small laboratory type cells intended to measure pressures in granular materials the use of a stiff diaphragm supported by a stiff ring is recommended so that the effect of compressibility causing over—registration (recorded pressure less than field pressure), will then tend to be mutually

compensating and the calibration should approach closely the fluid condition.

(iii) Cell placement

Hadala (1967) examined three different types of placement for cell calibration in sand. He pointed out that much of the erratic variation observed in the past is believed to have been the result of the condition of placement rather than variation in the gauge itself. Hadala recommended that the simpler procedures resulted in less data scatter, and suggested a method of setting the cells on the surface of the half–completed sand specimen using normal construction procedures (Sprinkling sand layers) to build up the remainder of the specimen, which showed best overall linearity and least scatter for first loading cycles. Morgan and Gerrard (1968) stated that, in addition, this previous placement method showed least change in the calibration factor for repeated load cycles.

(iv) Linearity

Redshaw (1954) postulated that the structural element of the cell would exhibit zones of positive and negative strain under the loading condition. The circular plate clamped around its circumference (diaphragm) and subjected to a uniformly distributed load normal to its surface will exhibit this characteristic, providing the deflection everywhere does not exceed a small fraction of the diaphragm thickness. If the central deflection is limited to about one fifth or one fourth (as recommended by Measurement Group, 1982), the small deflection theory by Poisson–Kirchhoff is valid and the following equations can be applied:

$$Y_c = \frac{3.q.R_o^4.\ (1-\nu^2)}{16.t^3.E} \qquad (3.2)$$

$$\epsilon_r = \frac{3.q.R_o^2}{8.t^2.E.(1-\nu^2)}\ (1 - \frac{3.r^2}{R_o^2}) \qquad (3.3)$$

$$\epsilon_T = \frac{3.q.R_o^2}{8.t^2.E.(1-\nu^2)}\ (1 - \frac{r^2}{R_o^2}) \qquad (3.4)$$

Where:

Y_c is normal deflection at diaphragm centre.

ϵ_r is radial strain at distance (r) from the centre.

ϵ_T is tangential strain at distance (r) from the centre.

r is distance from the centre to any point.

R_o is diaphragm radius.

q is normal pressure.

t is diaphragm thickness.

ν is Poisson's ratio.

E is modulus of elasticity.

From the above equations, the distribution of strains is shown in Fig. (3.15).

(v) Strain gauges and sensitivity

As shown in Fig. (3.15), the radial strain decreases rapidly as the radius increases, changing from positive to negative values at $r/R_o = \sqrt{1/3}$, becoming negative, and equal to twice the centre strain value at the edges. The values of strain at the centre and edges are:

At the centre

$$\epsilon_{Rc} = \epsilon_{Tc} = \frac{3.q.R_o^2.(1-\nu^2)}{8.t^2.E} \qquad (3.5)$$

At the edges

$$\epsilon_{Ro} = - \frac{3.q.R_o^2.(1-\nu^2)}{4.t^2.E} \qquad (3.6)$$

$$\epsilon_{To} = 0.0 \qquad (3.7)$$

The strain gauge pattern should be designed to take maximum advantage of the diaphragm strain distribution described above, e.g. the strain gauge can be attached to measure the tangential strain in the zone defined by $r/R = 0.0$ to 0.775 and radial strains defined by $r/R_o = 0.577$ to 1.0, also the central sensing elements of the gauge should be oriented tangentially. Similarly, the radial sensing elements should be located near the edge of the diaphragm because of the high radial strain in the region.

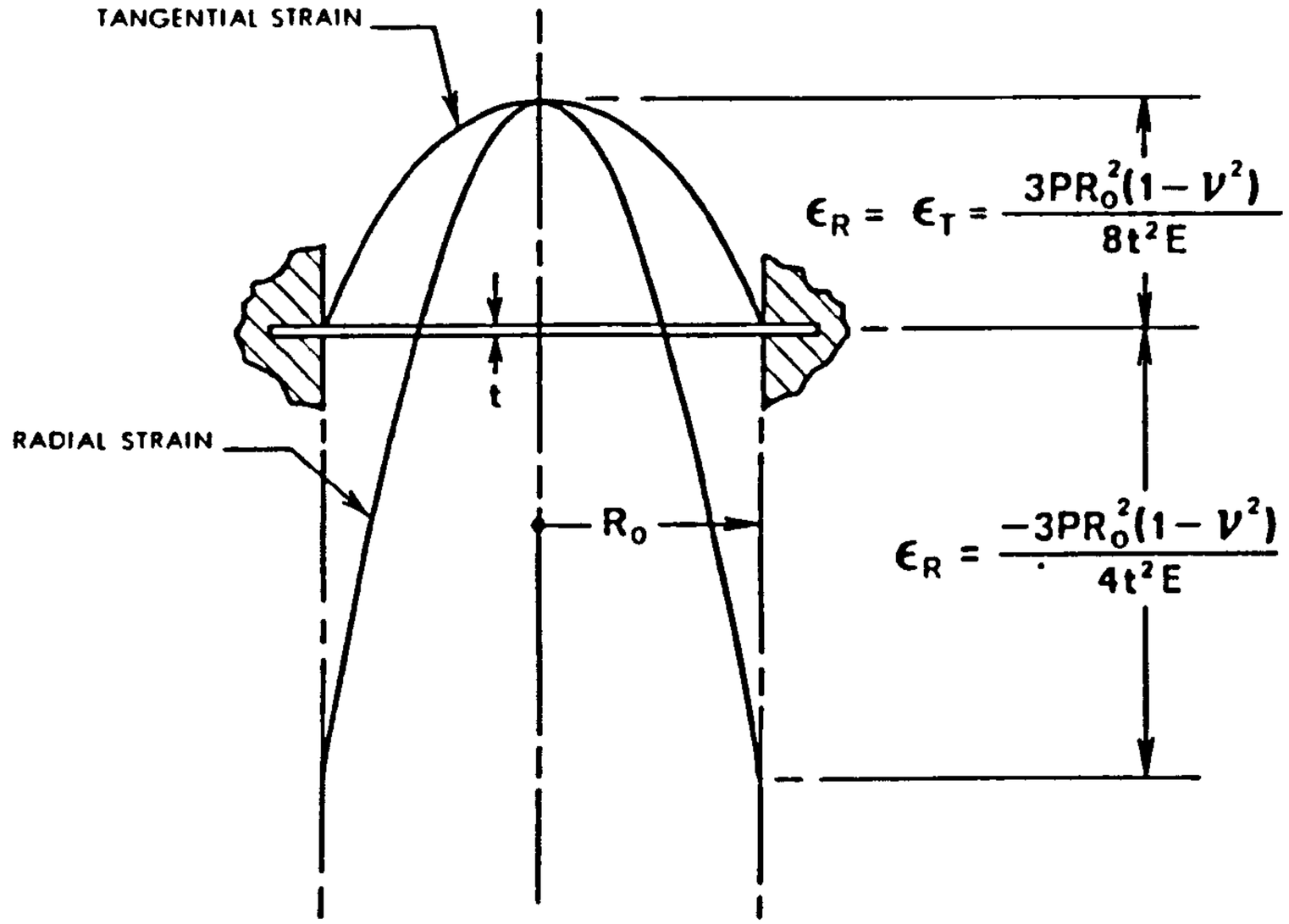

FIG. (3.15) RADIAL AND TANGENTIAL DISTRIBUTIONS OF STRAIN IN THE CELL DIAPHRAGM (TECH NOTE , 1982).

The sensitivity of the gauge can be determined according to Measurement Group (1982), by averaging the strain over the region covered by each sensing element (assuming a gauge factor of 2.0), and averaging the outputs of all sensing elements, the total gauge outputs (e_o) in millivolts per volt can be expressed approximately by the following equation:

$$e_o = 0.82 \frac{q.R_o^2.(1-\nu^2)}{t^2.E} \times 10^3 \quad mv/v \qquad (3.8)$$

(vi) Compaction effect

Hadala (1967); Morgan and Gerrard (1968); and Carder and Krawczyk (1975) mentioned the effect of compaction on the calibration of pressure cells. Since compaction can be done by repeated or dynamic load, so attention must be drawn to the resonant frequency of the diaphragm. The resonant frequency should be at least three to five times as high as the highest applied frequency. Measurement Group (1982) in their Technical Note also suggested an approximate equation for resonant frequency of a rigidly clamped diaphragm as follows:

$$f_n = \frac{0.469\ (t)}{R_o^2} \sqrt{\frac{g.E}{\rho.(1-\nu^2)}} \quad HZ \qquad (3.9)$$

Where:

g is gravity constant.

ρ is unit weight of the material (Kg/cm^3).

(b) Design of the pressure cells

From the previous background regarding the factors which affect the design and calibration of pressure cells, the following assumptions may be made to match these factors:

(i) The diaphragm should have uniform thickness, small deflection, rigid clamping around the periphery, elastic behaviour , maximum effective area with respect to the total area of the cell, and the effects due to the presence of the strain gauge such as its mass and stiffness are neglected.

(ii) The strain gauge should be sensitive and permit a full bridge to be built into a single strain gauge.

(iii) An essential requirement is that the cell should be small and reliable to suit the model tests.

According to the above criteria two types of pressure cell were designed. The two types have the same material, and diameter but different thicknesses. The material used was aluminium alloy NS 51−H8 with the following characterstics:

Tensile strength	= 400	N/mm^2
Specific gravity	= 2.68	
Young's modulus	= 70000	N/mm^2
Permissible tensile stress	= 170	N/mm^2

The dimensions of the diaphragms were chosen according to the previous equations, and the limitations of deflection at the centre:diaphragm thickness ratio

and the cell diameter:thickness ratio, and the guidance of previous background. The two types of cell are shown in Fig. (3.16.A&B). Each cell consists of two identical diaphragms one of them acting as an active diaphragm with the strain gauge attached , the other to increase the edge stiffness and to protect the strain gauge from damage.

The type of strain gauge used in the pressure cells, was a 4 element Redshaw diaphragm gauge type RED/20/240 EC with a full bridge. It was chosen to comply with the previous assumptions such as self temperature compensation, elimination of the effect of resistance in the lead wires and to take the maximum advantage of diaphragm strain distribution as previously described in Fig. (3.15).

The gauge characteristics were as follows:

- Nominal active gauge length = 20 mm
- Nominal gauge resistance = 240 Ohm
- Gauge backing material = Araldite
- Wire alloy = Copper nickel alloy

One of the gauges is shown in Fig. (3.17).

(c) Bonding the strain gauge on pressure cell

Every gauge was bonded to the inner surface of the active diaphragm. The procedure used in mounting the gauge on the diaphragm was:

(i) The gauge on the active diaphragm was cleaned using solvent (Chlorothene SM).

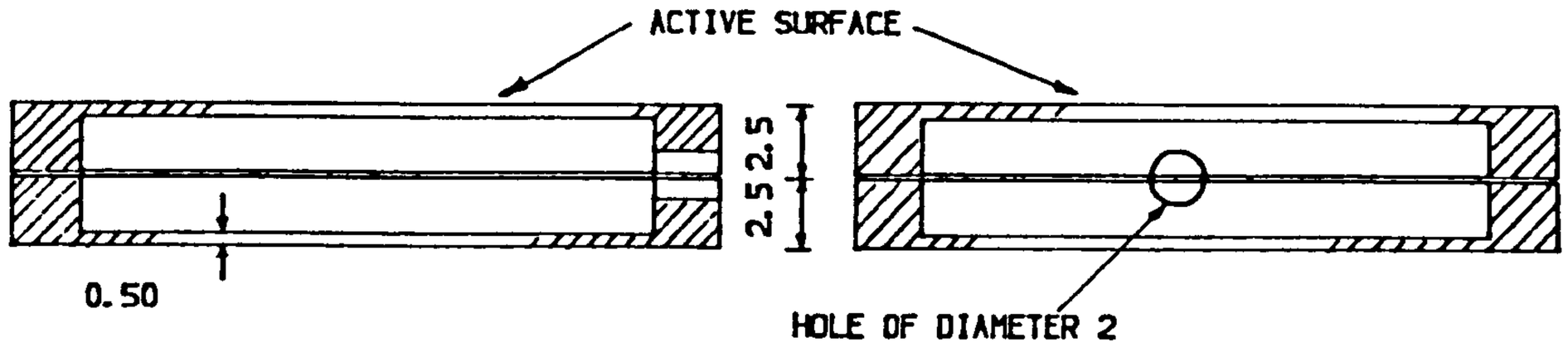

ELEV.

SIDE VIEW

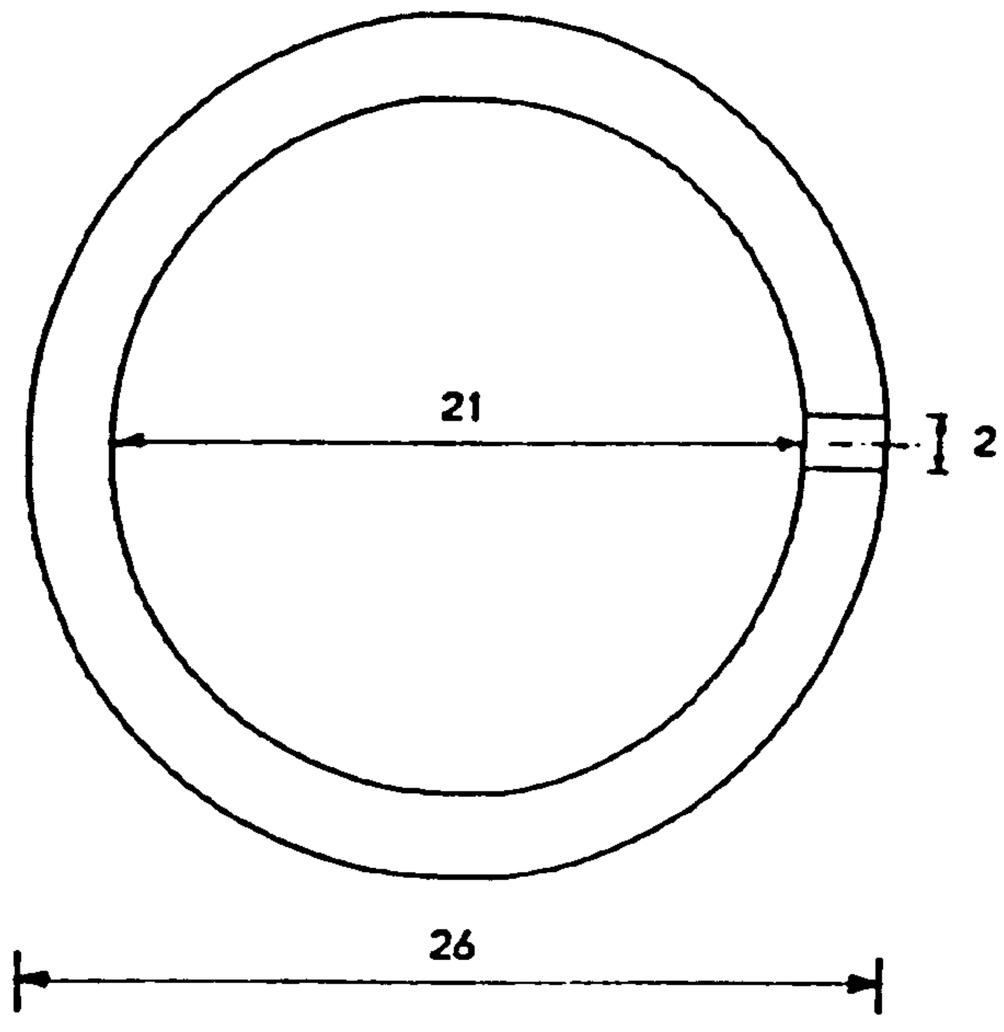

PLAN

ALL DIMENSIONS IN MM.

(A) THE FIRST TYPE

FIG. (3.16) TYPES OF PRESSURE CELLS DIAPHRAGM.

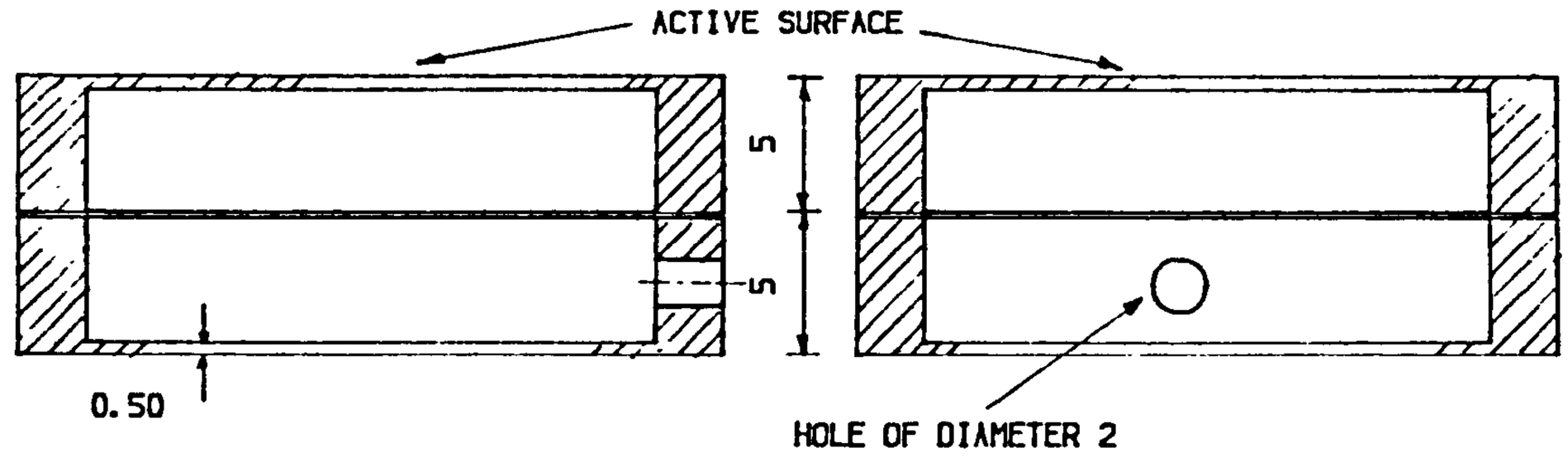

ELEV.

SIDE VIEW

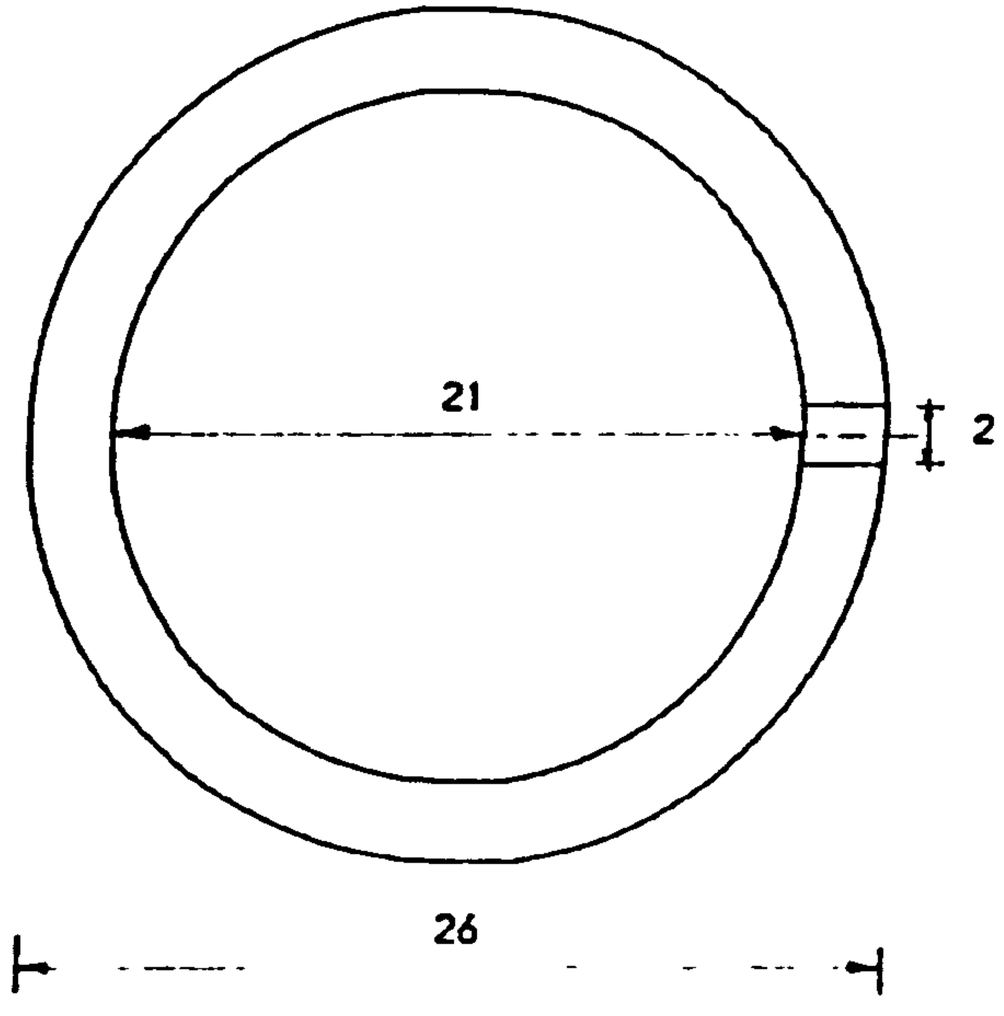

PLAN

ALL DIMENSIONS IN MM.

(B) THE SECOND TYPE

FIG. (3.16) CONTIN.

(ii) Abrading was done by using 400 grit silicon–carbide paper on the surface thoroughly wetted with M–Prep conditioner A. This was followed by wiping dry with a gauze sponge.

(iii) A small amount of M–Prep Neutralizer 5 was applied and scrubbed with a cotton–tip and then wiped by a gauze sponge.

(iv) The backing of the gauge was cut to fit the diaphragm.

(v) The bond side of the gauge was cleaned with M–Prep Neutralizer 5.

(vi) The gauge was bonded using adhesive material consisting of a mixture of Araldite My 753 and hardener Hy 951 (Ciba–Geigy product) of 10:1 by weight respectively.

(vii) In order to obtain an effective bond between the gauge and the surface, curing was done by subjecting the system shown in Fig. (3.18) to a temperature of 60° C for 3 hours.

(viii) 4 lead wires were soldered in accordance with the diagram shown in Fig. (3.19), and the resistances of the elements were checked.

(ix) The four wires were passed through a 2 mm rubber sleeve and the other diaphragm was glued on to form the cell.

(d) Calibration of pressure cells

Preliminary calibration was done on both types of pressure cell as follows:

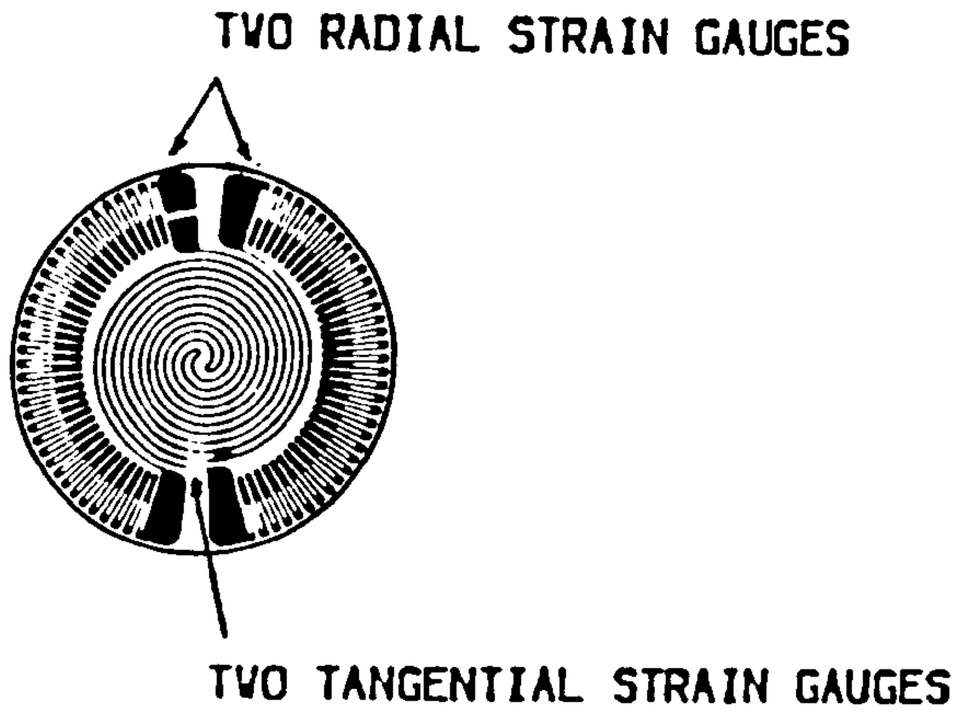

FIG. (3.17) TYPICAL TYPE OF FULL BRIDGE STRAIN GAUGE USED IN PRESSURE CELLS.

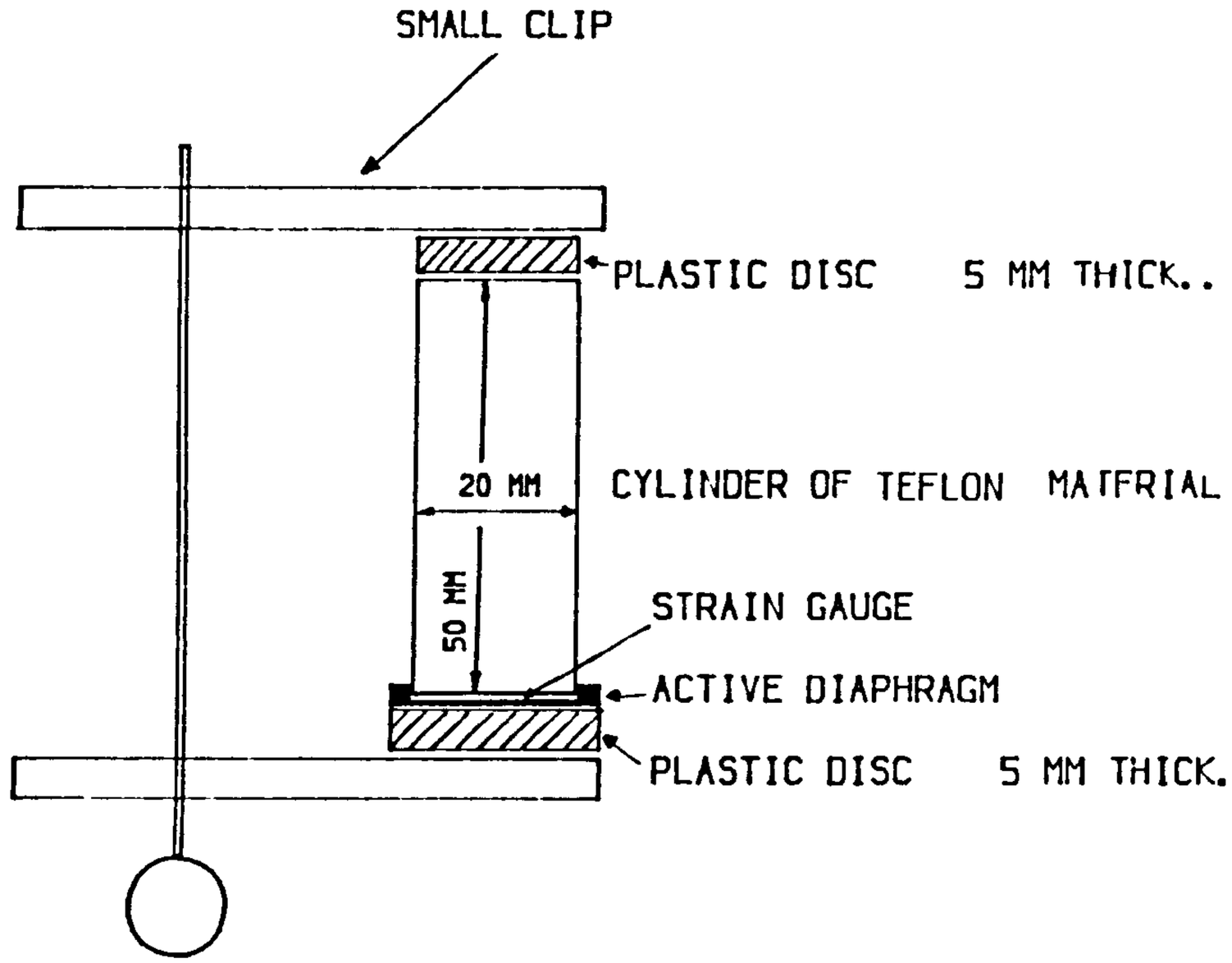

FIG. (3.18) SPECIAL ARRANGEMENT FOR BONDING THE STRAIN GAUGE TO THE ACTIVE DIAPHRAGM OF THE PRESSURE CELL.

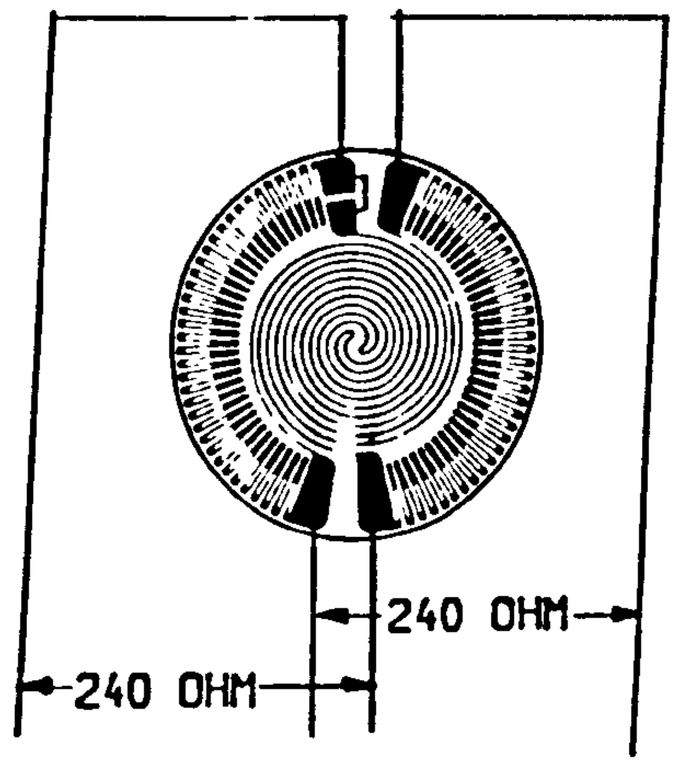

TO DATA LOGGER

FIG. (3.19) FOUR LEAD WIRES SOLDERED TO THE FULL BRIDGE STRAIN GAUGE.

(i) By column of sand overlying the cell. This method produce erratic results and was not pursued.

(ii) Cell buried just below the surface of sand, and sand subjected to an overburden pressure applied by means of a rubber membrane with air pressure on it, in a perspex cylinder as shown in Fig. (3.20). The advantage of ensuring a uniform pressure by air pressure calibration led to its use in calibrating all the cells.

The 5 mm thick pressure cells with a thickness diameter ratio of 1:5 showed better results than the 1:2.5 type, so it was decided to use sixteen 5 mm pressure cells with air pressure calibration.

The sixteen cells were calibrated simultaneously using a set up which closely simulated the situation in which the instruments were to be employed and using air pressure calibration.

A metal box of clear dimensions 2.0 x 0.42 x 0.26 m was filled with the sand to be used in the model tests at a density of 14.39 kN/m^3 (the preliminary density used in all model tests). Two rows of cells, 8 in each row, were set 50 mm. from the top surface of the sand in the box in staggered positions as shown in Fig. (3.21). The box was covered with a rubber membrane 0.5 mm. thick and a metal cover, then connected to a system of controlled air pressure.

A typical calibration curve for one of the pressure cells is shown in Fig. (3.22). The test was repeated three times (loaded/unloaded each time) to examine the degree of hysteresis. A typical calibration curve is shown in Fig. (3.23) and the range of calibration factors is shown in Appendix (A).

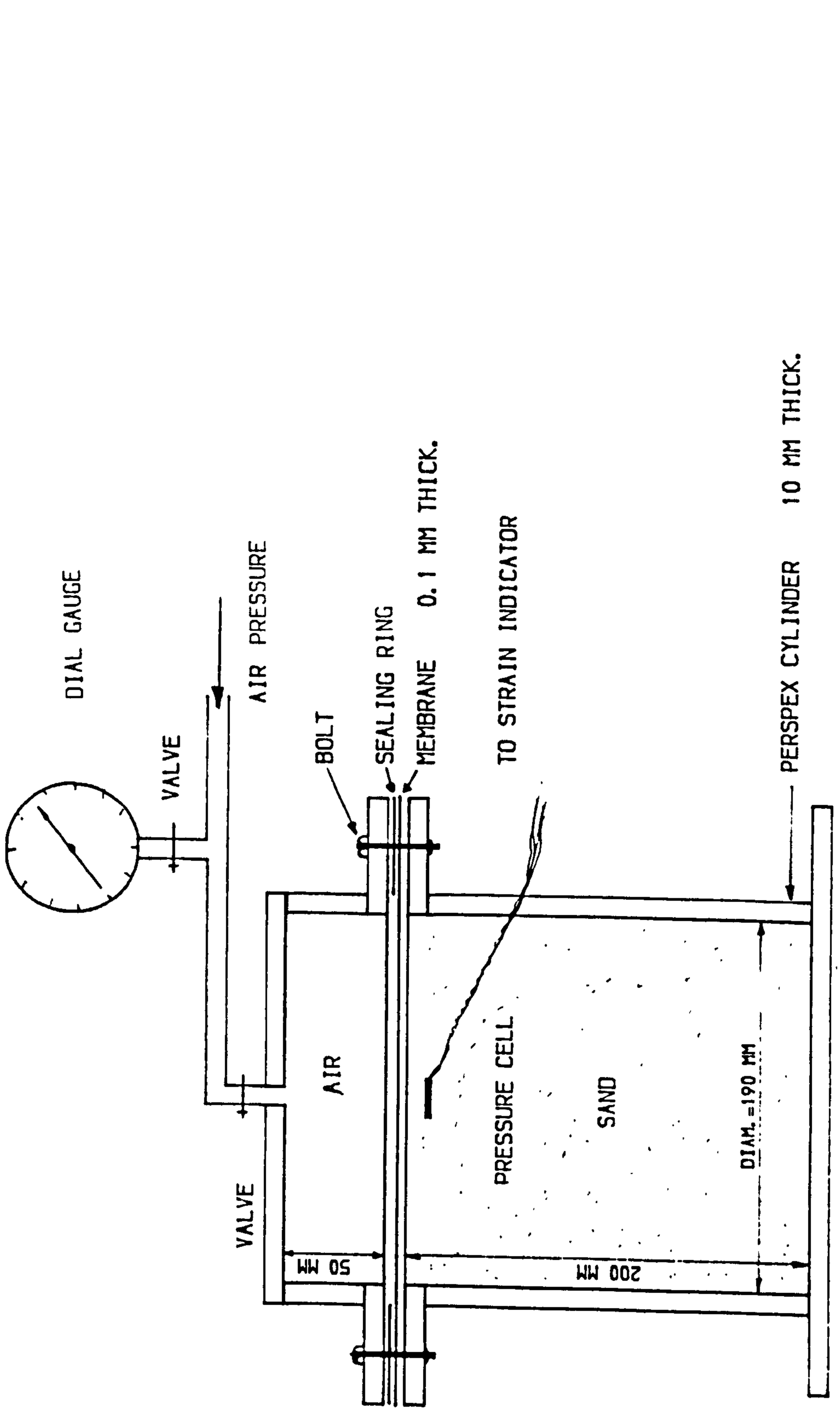

FIG. (3.20) SET UP FOR CALIBRATION OF PRESSURE CELL.

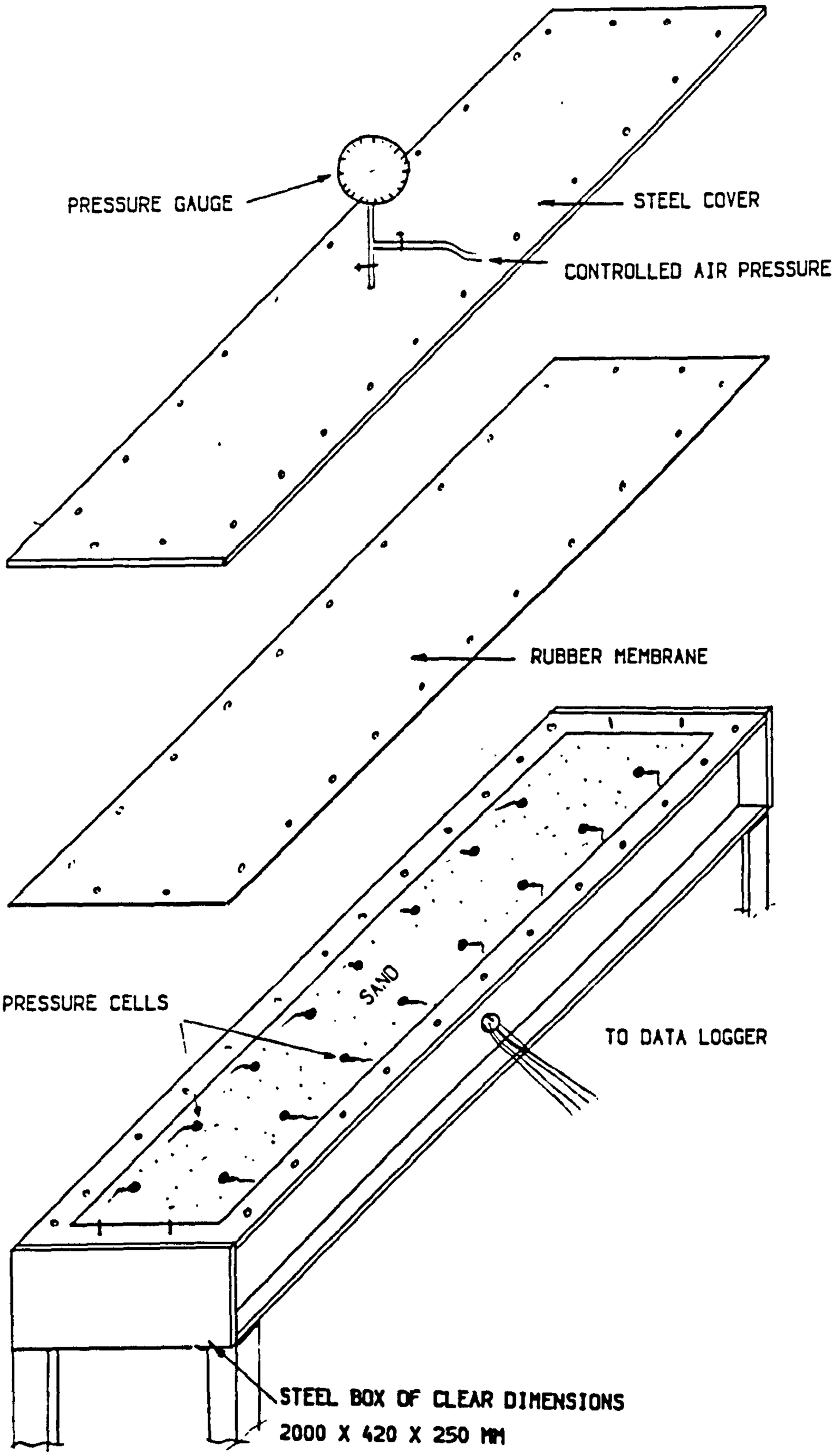

FIG. (3.21) CALIBRATION OF PRESSURE CELLS.

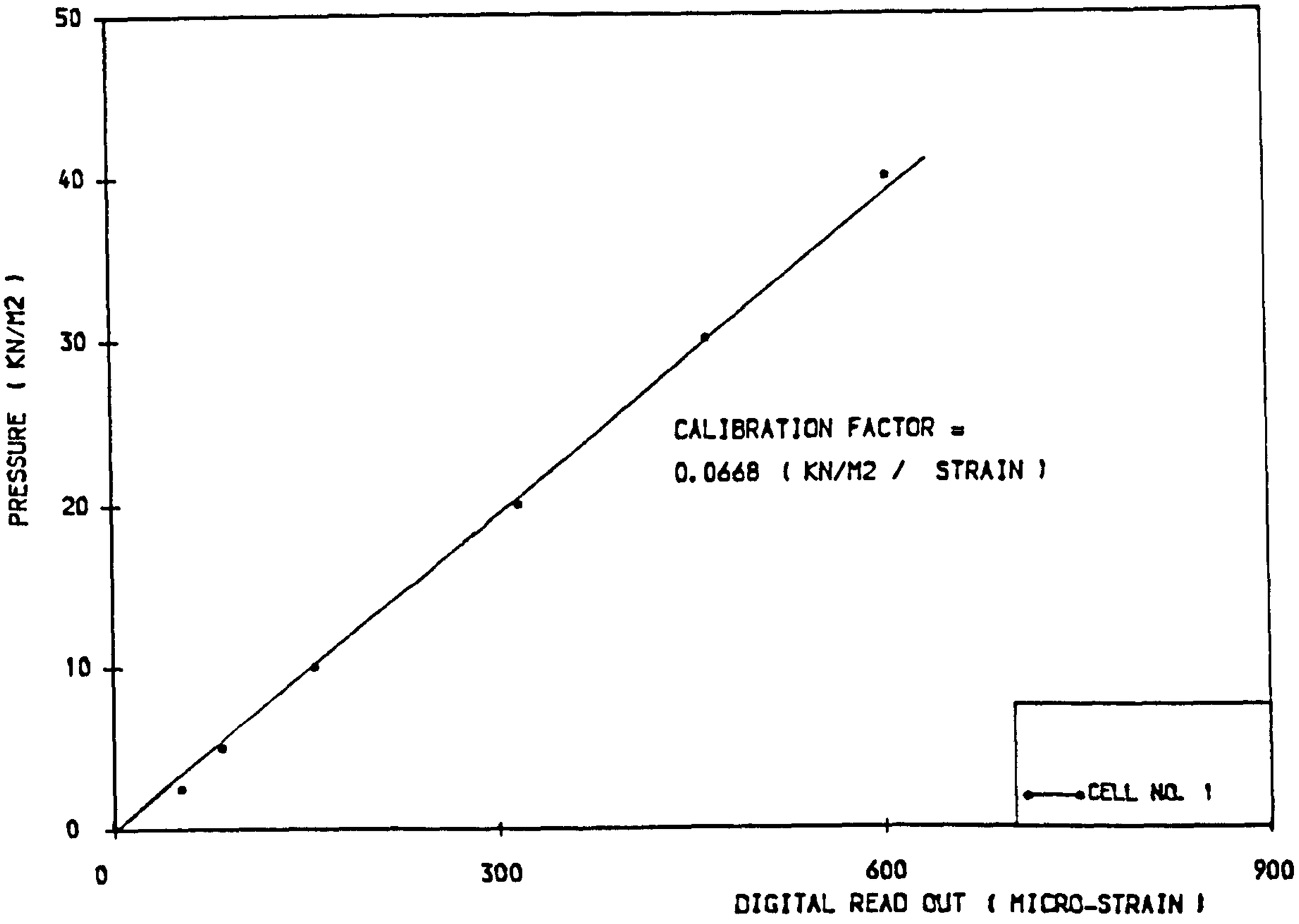

FIG. (3.22) CALIBRATION CURVE OF ONE OF 16 PRESSURE CELLS USED IN THE MODEL TESTS.

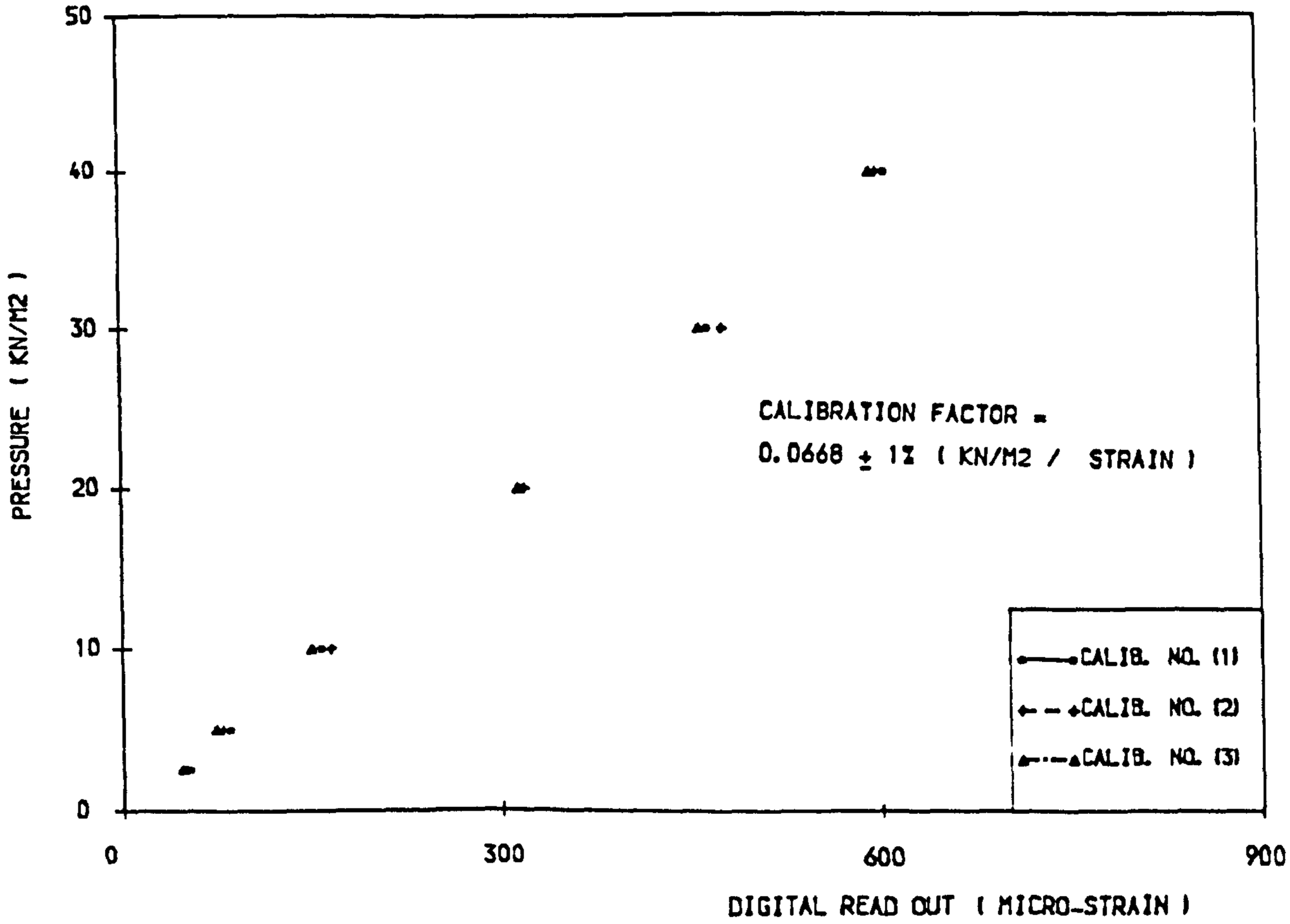

FIG. (3.23) CALIBRATION CURVES OF CELL NO. 1, REPEATED 3 TIMES.

The maximum pressure used in the calibration test was three times the maximum expected pressure in the model tests to minimize any nonlinearity in cell calibration and overcome any problems of hysteresis during model tests.

3.5.4 Lateral Movement Of The Wall Face

The lateral movement of the wall face was measured using 8 LVDTs (linear variable differential transformer). The locations of the 8 LVDTs are shown in Fig. (3.24). An LVDT is an electronic device that produces an electronic signal whose amplitude is proportional to the displacement of a transducer core. The main parts of the LVDT and the linear range of the stroke of the transducer are shown in Fig. (3.25.A&B) respectively, and its specification was:

- Type D5/100 AG (RDP Group, U.K.),
- Dc. to Dc. ± 2.5 mm working range, and
- Sensitivity 2 mv/v/0.025 mm.

The advantages of this type which led to its being chosen were:
It had low friction and non rotating ball ended probes, and its sensitivity matched the requirements for the model test.

In order to obtain a calibration factor as input for the data logger (the device which reads the output and which will be explained later) to give direct readings in mm, 8 tests were made using a micrometer and a set of plates of accurate known thickness, Fig. (3.26), Calibration factors are shown in Appendix (A).

A special arrangement was made to hold the 8 LVDTs in position and

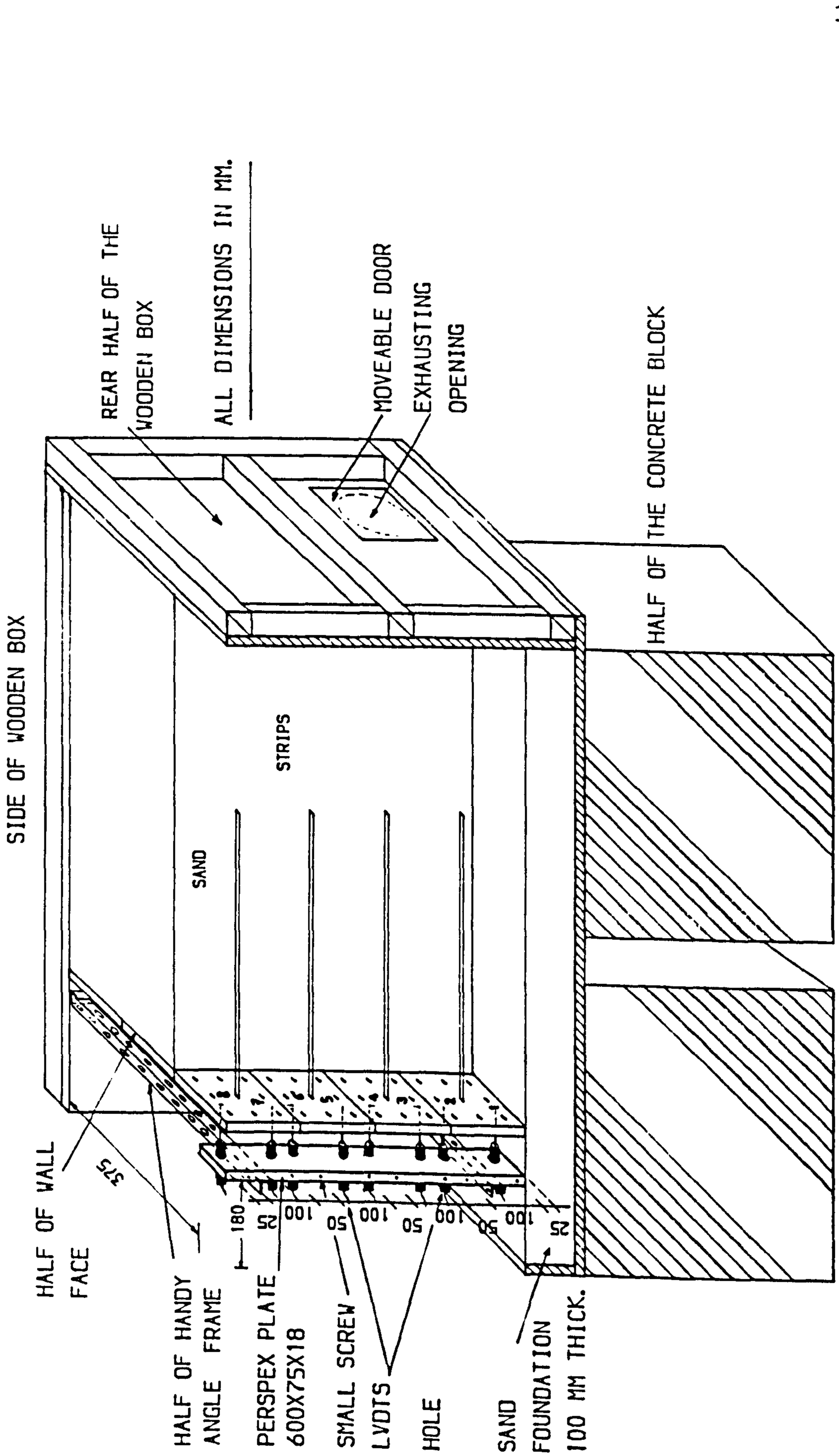

FIG. (3.24) POSITIONS OF LVDTS.

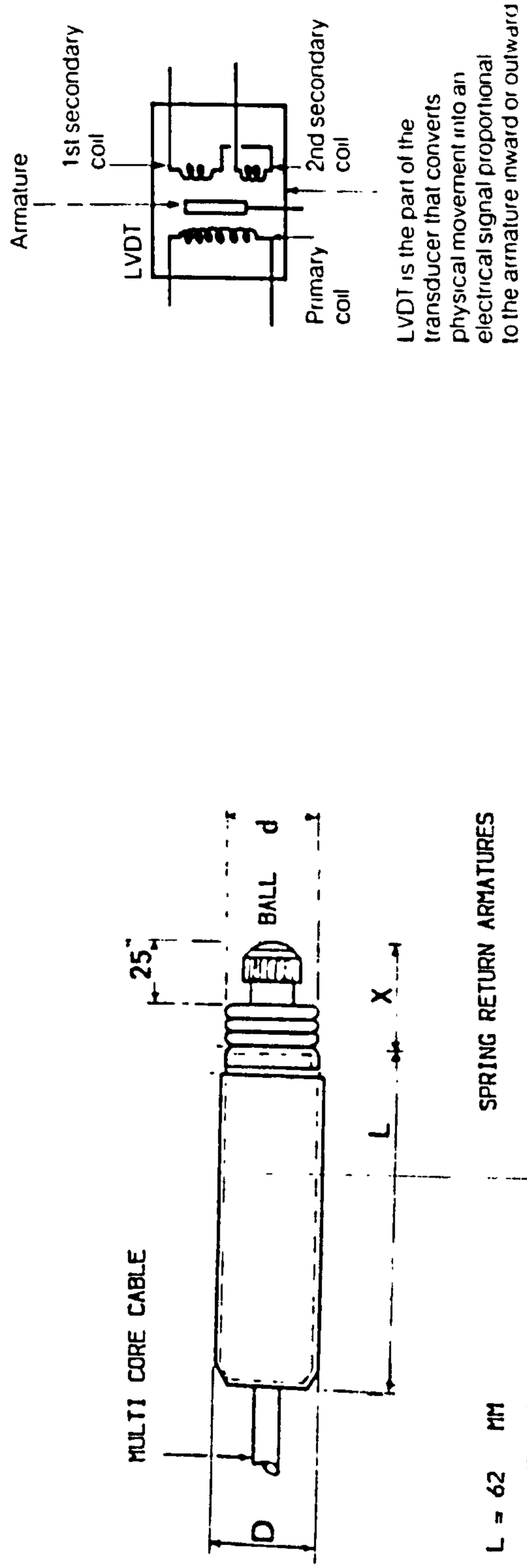

FIG. (3.25) LINEAR VARIABLE DIFFERENTIAL TRANSFORMER (LVDT).

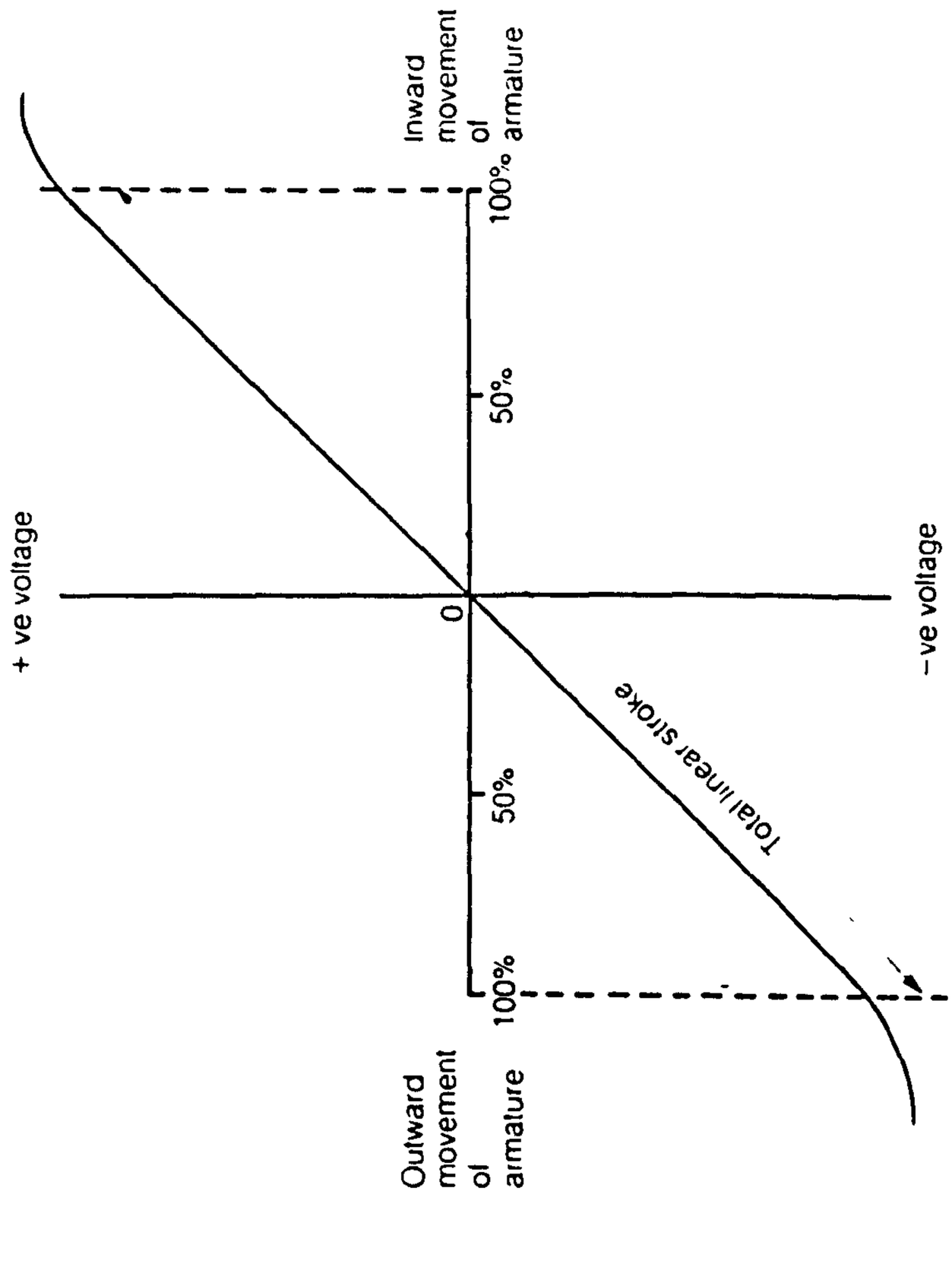

(B) LINEAR STROKE OF LVDT

FIG. (3.25) CONT.

CALIBRATION FACTOR = $\frac{\text{THICKNESS OF THE PLATE}}{\text{DIFFERENCE OF OUTPUT READINGS}}$

(CASE 2 - CASE 1)

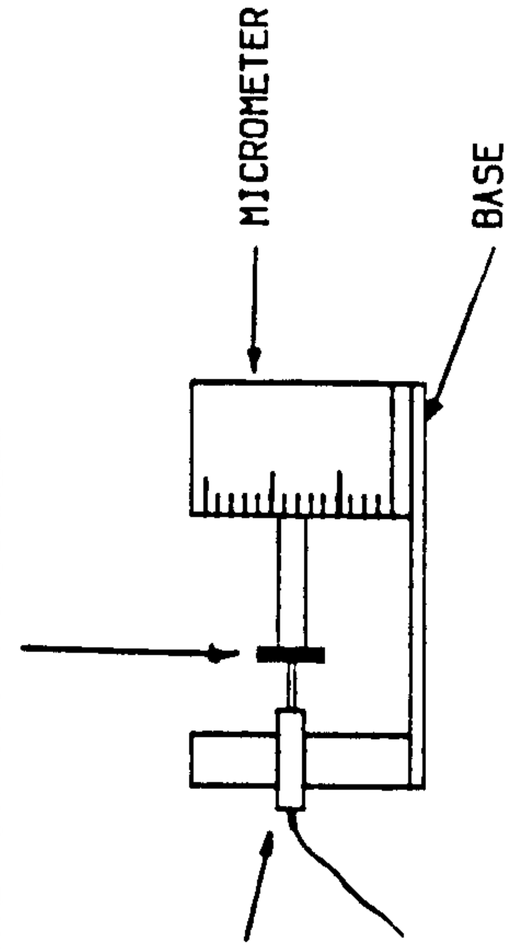

CASE (2) WITH PLATE

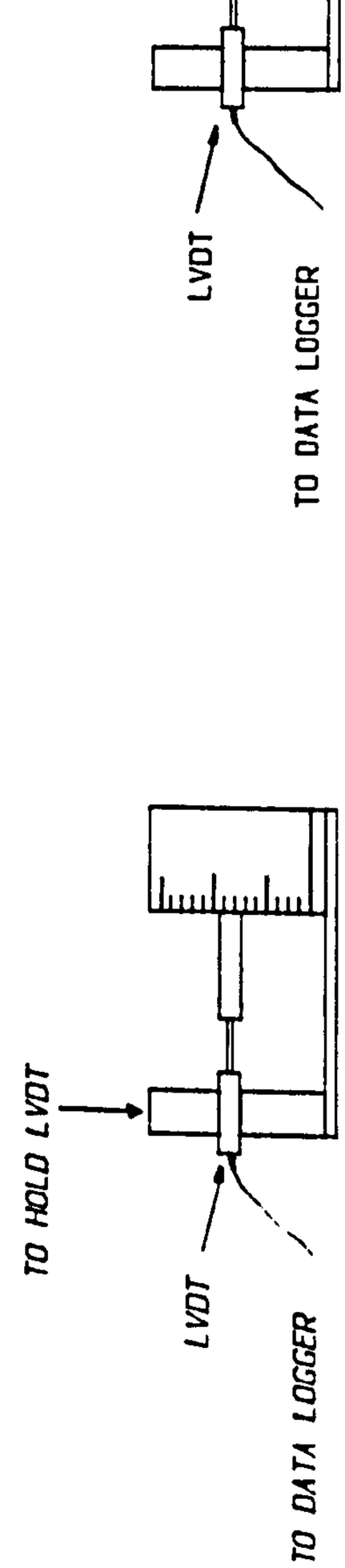

CASE (1) WITHOUT PLATE

FIG. (3.26) CALIBRATION OF LVDTS.

minimize any disturbance caused by positioning which might affect the readings. The arrangement comprised a diaphragm fixed at 100 mm from the wall face. The diaphragm held a perspex post of rectangular cross section in front of the middle of the wall face. The perspex post contained 8 holes where the LVDTs were fixed by means of plastic screws. The diaphragm consisted of 4 angles, two verticals fixed on the inside surface of the box sides and two horizontals near the top and bottom of the wall face and fixed to the two vertical angles as shown in Fig. (3.27).

3.5.5 Data Logger

In order to record and print the output reading of the 24 strain gauges, 16 pressure cells and 8 LVDTs at the same time, before, during, and after compaction, all the measurement devices were connected to an Orion 3530 data logger system with a line printer.

The advantages of using this system were:

(a) All the output could be read at the same time.

(b) Thermal compensation was provided.

(c) The system was convenient for strain gauges of quarter or full bridge.

The data logger is shown in Fig. (3.28).

3.5.6 Interaction Between Sand/Wall Face, Reinforcement

The coefficients of friction between the backfill material (sand) and the aluminium foil strips/perspex of wall face were determine using a displacement controlled small shear box, filled with compacted sand of average density 17.39 kN/m^3.

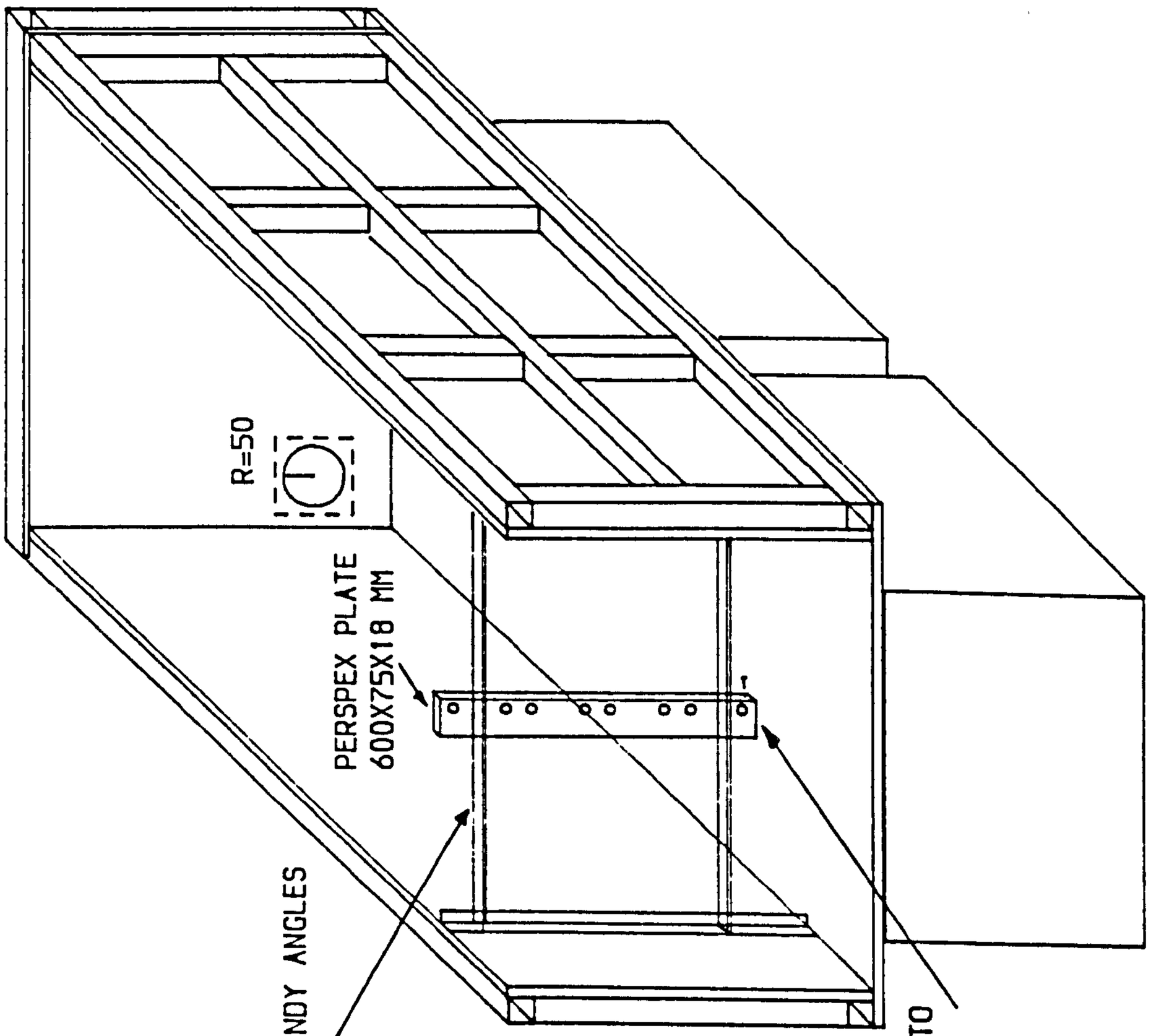

FIG. (3.27) ARRANGEMENT TO HOLD LVDTS IN POSITION

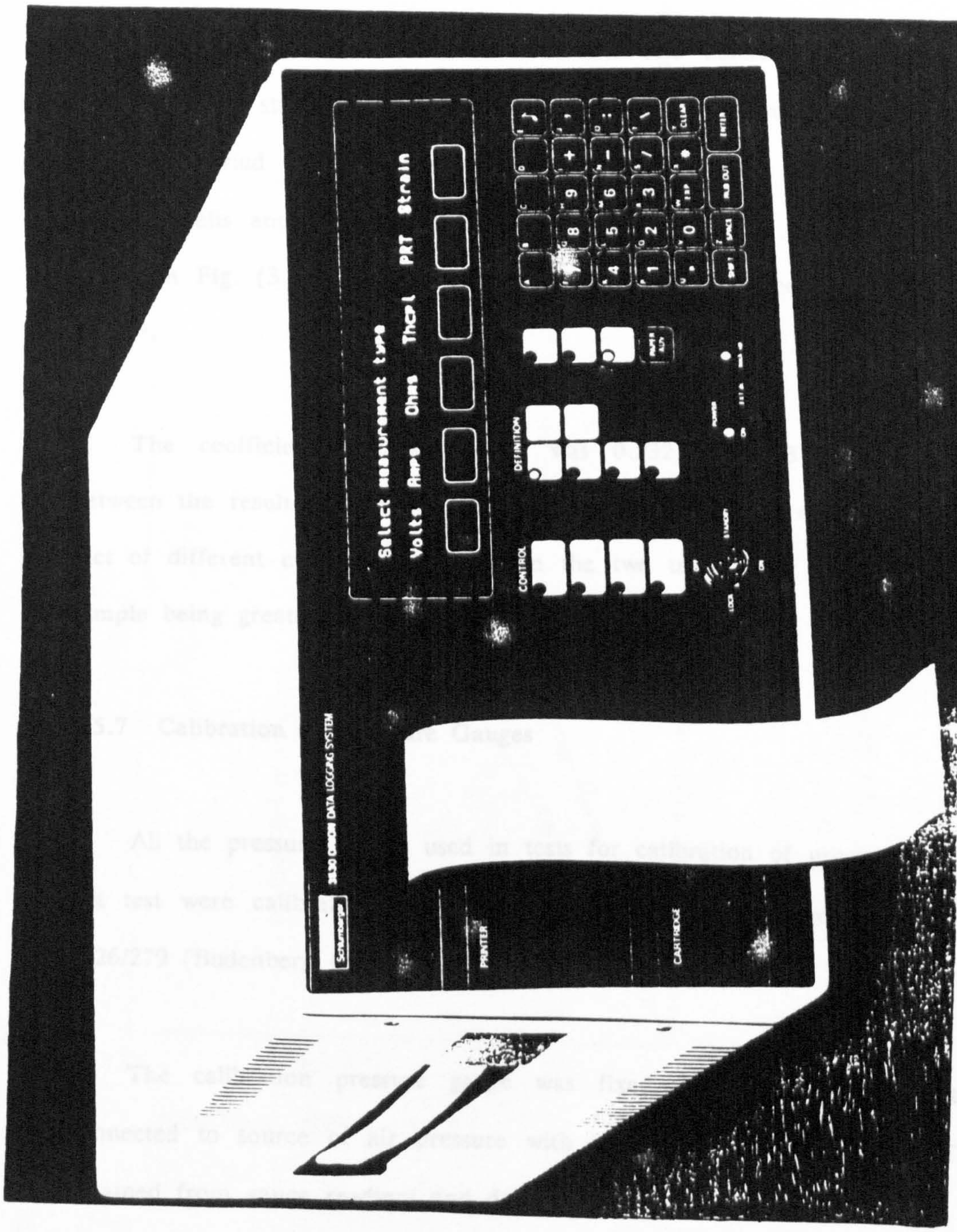

FIG. (3.28) DATA LOGGER.

The coefficients of friction were found to be:

Aluminium foil/sand coefficient (μ) = 0.577, i.e. δ=30°.

Perspex/sand coefficient (μ_1) = 0.367, i.e. δ=20°.

As shown in Fig. (3.29).

The aluminium foil/sand coefficient was also determined using a direct pull out test under stress control and using air pressure as overburden. The pull out test was carried out using the same box as had been used for calibrating the pressure cells and with aluminium strip 1.22 x .041 X .0001 m. The box is shown in Fig. (3.30). The box was filled with compacted sand of density 17.39 kN/m^3.

The coefficient of friction (μ) was 0.532, Fig. (3.31). The difference between the results obtained from the shear box and pull out tests is due to the fact of different circumstances between the two tests, such as the stiffness of the sample being greater in the case of the shear box.

3.5.7 Calibration Of Pressure Gauges

All the pressure gauges used in tests for calibration of pressure cells and pull out test were calibrated using a dead weight pressure gauge tester, type S/NO. 7526/279 (Budenberg Gauge Co. Limited).

The calibration pressure gauge was fixed in the dead weight tester and connected to source of air pressure with an air pressure regulator. The results obtained from gauge readings and dead weight tester were identical.

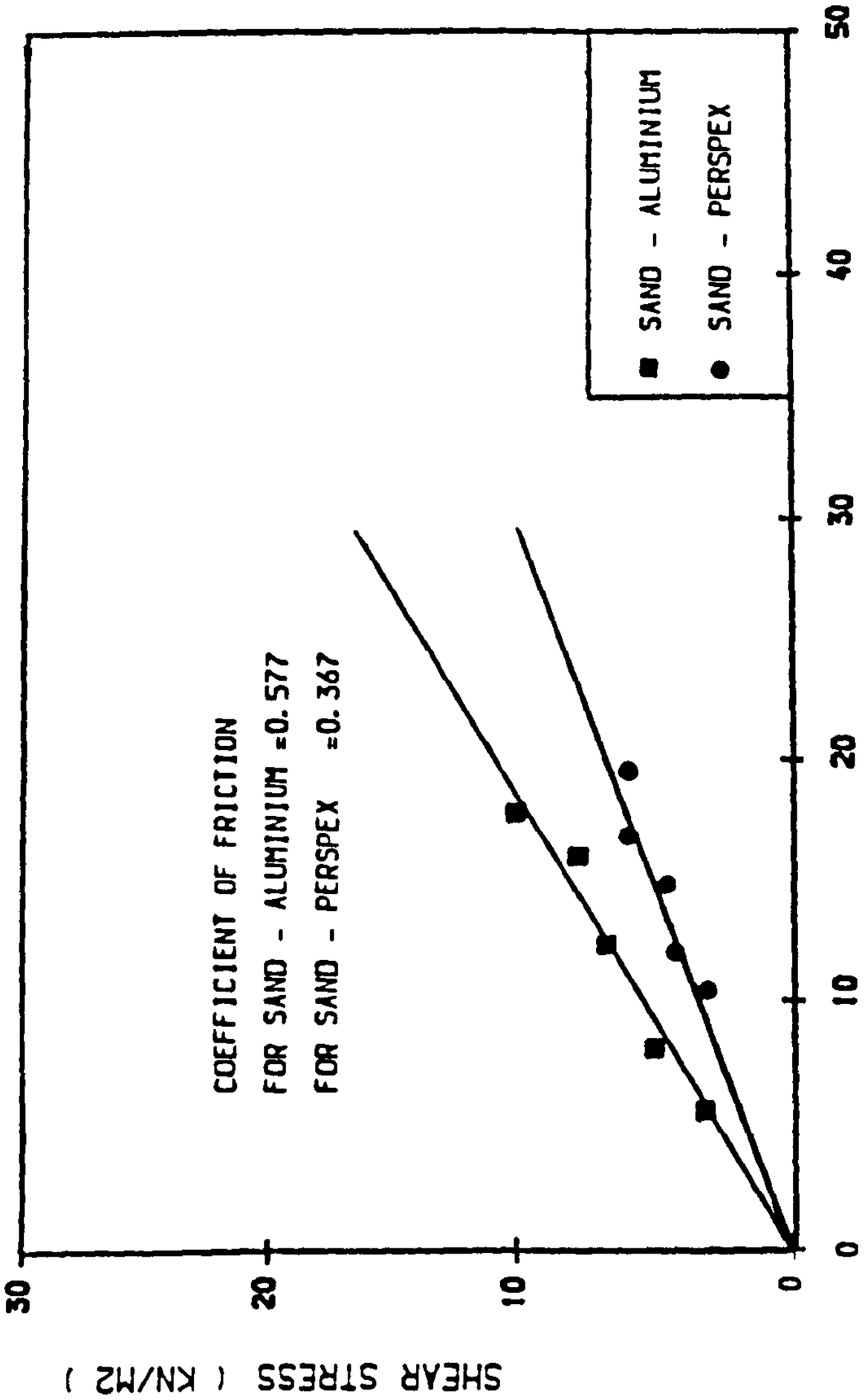

FIG. (3.29) COEFFICIENT OF FRICTION BETWEEN ALUMINIUM, PERSPEX AND SAND (SHEAR BOX TEST).

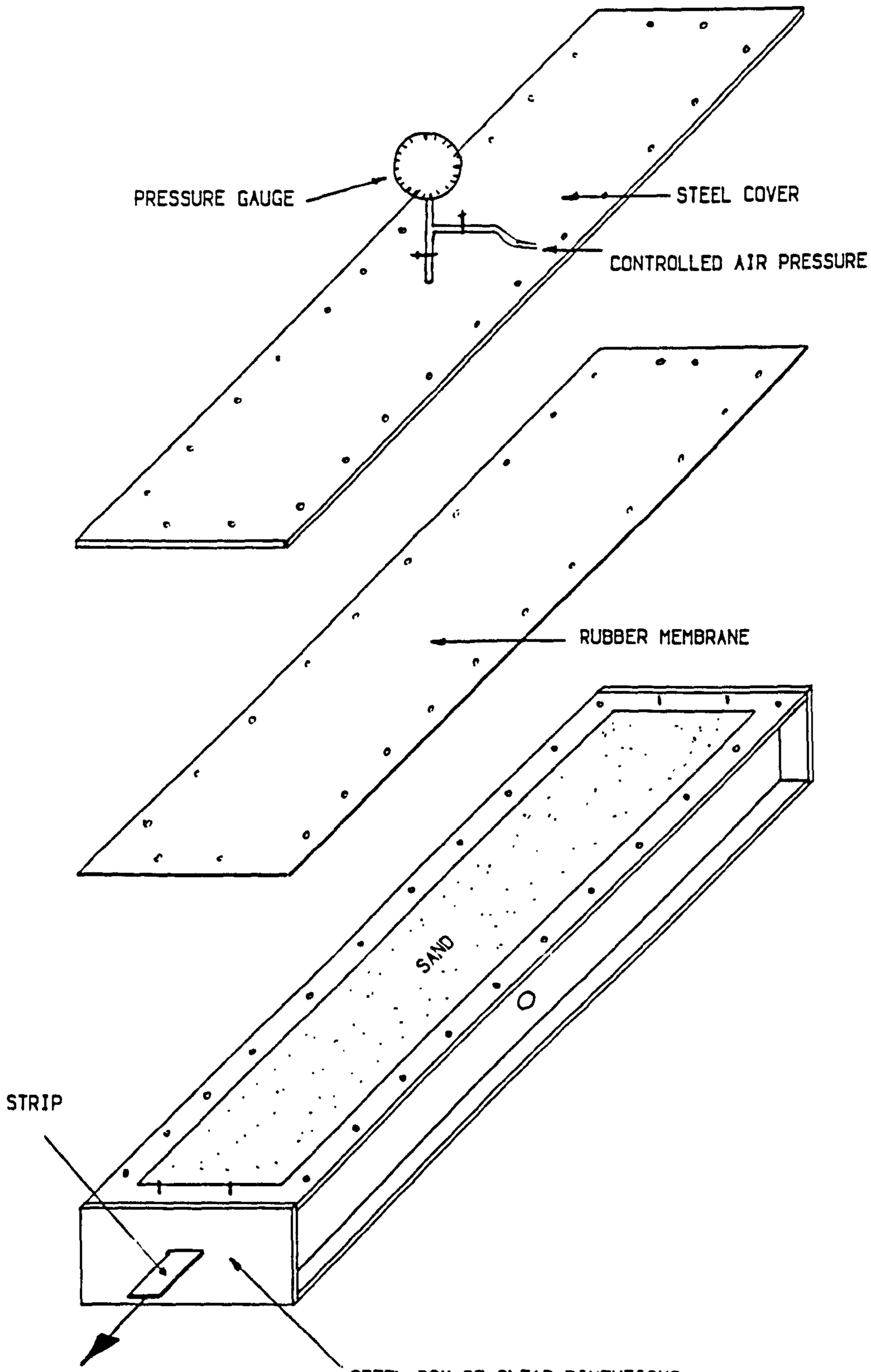

FIG. (3.30) PULL OUT BOX.

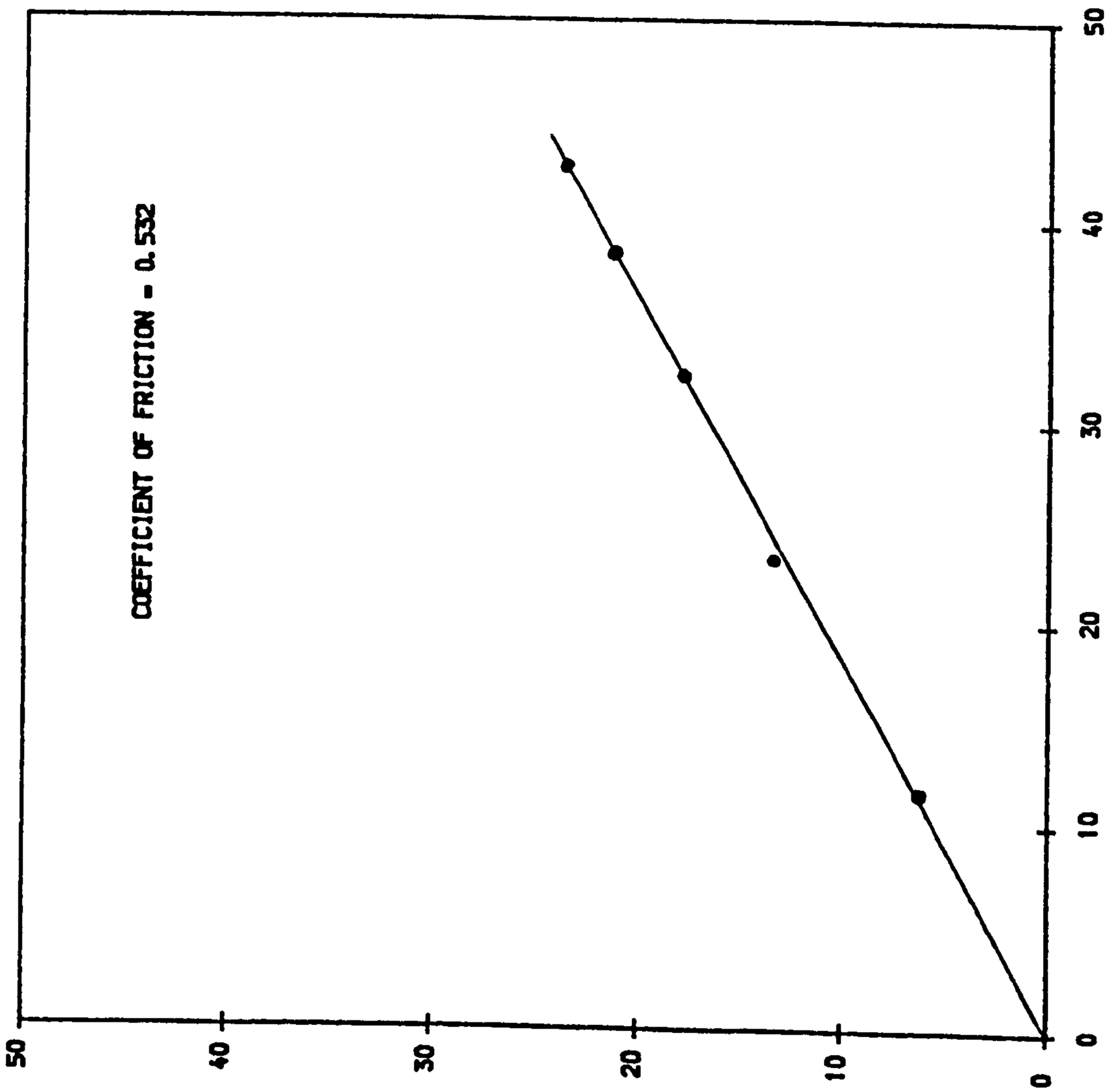

FIG. (3.31) COEFFICIENT OF FRICTION BETWEEN ALUMINIUM, AND SAND (PULL OUT TEST).

3.6 THE MODEL TEST PROGRAMME

The main testing programme consisted of 24 tests divided into 4 categories. In all model tests the plywood box described in Sec. 3.3.1, was used. The backfill material used was Douglasmuir sand, the reinforcing elements were aluminium foil strips of cross section 12 x 0.1 mm and the facing elements were perspex panels, each 150 x 150 x 18 mm. The properties of these materials have been previously described in Sec. 3.3.2. In all the model tests the sand layers were formed using the sand spreader device, Sec. 3.4.2. In the case of tests where compaction was required, this was done using the compaction plant. A key diagram of the test layout is shown in Fig. (3.32).

A summary of the four test categories is outlined in Table (3.1). Details of the programme are shown below.

(1) Category I Tests: Fig. (3.33)

The tests in this category were carried out for several reasons:

(i) To overcome problems during and after construction of the box such as, escape of sand from the gap between the wall face edges and the box sides. In this test the wall was built up without any compaction load, but using the sand spreader, Sec. 3.4.2, only, and no instrument readings were taken. The test was repeated after the problems were solved, to ensure self equilibrium with the model size. The sand was in a loose state (14.39 kN/m^3) and the dimensions of wall, Fig. (3.33.A), were:

CAT. I–1 & I–2

$S_h = S_v = 50$ mm

$H = 600$ mm $\qquad$ $L = 600$ mm

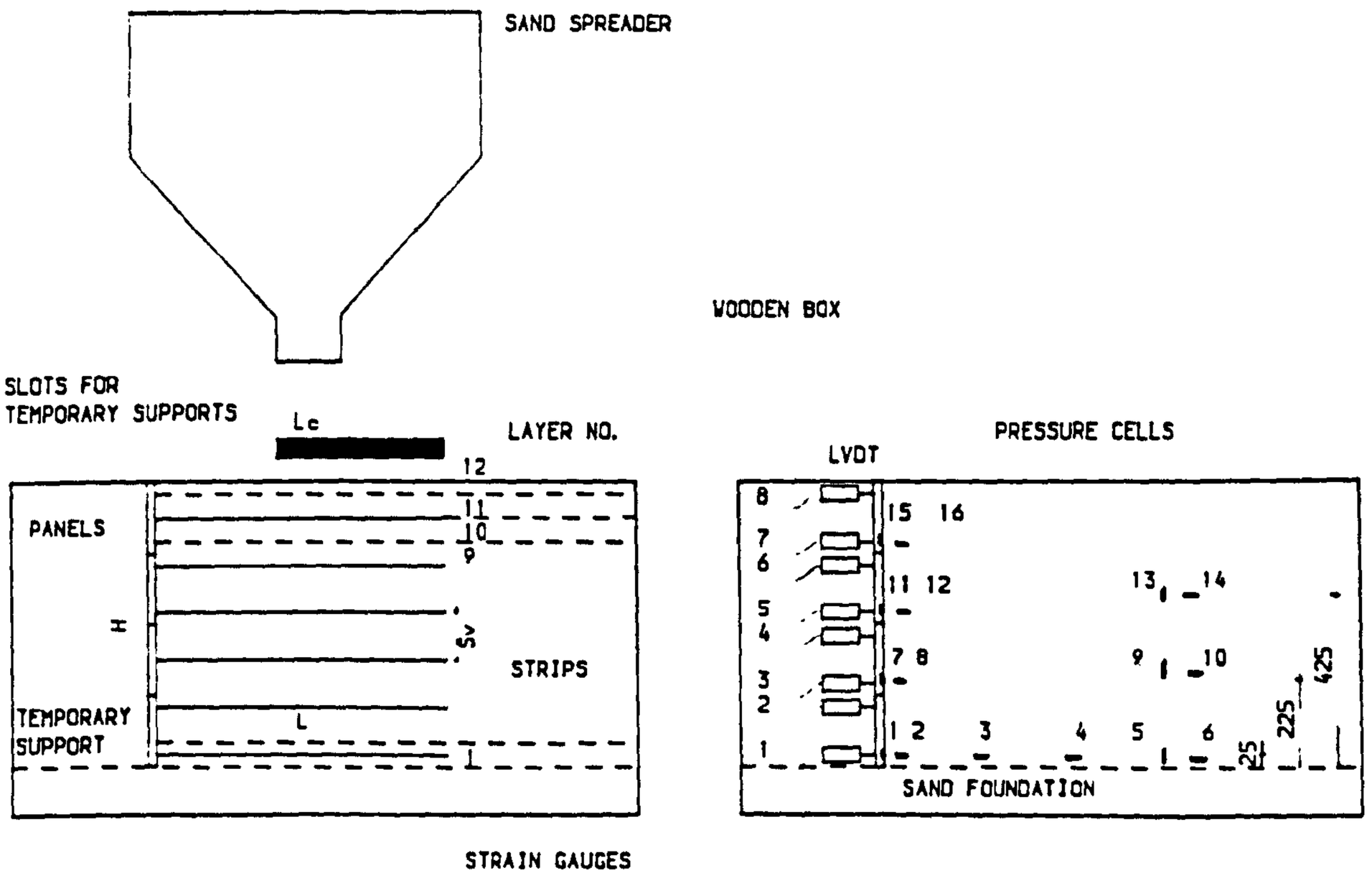

H = 600 MM

Sh &
Sv= HORIZONTAL AND VERTICAL
SPACING BETWEEN THE STRIPS
L = LENGTH OF THE STRIP
Lc= COMPACTION LENGTH
NO. OF SAND LAYERS
= 12
NO. OF PANELS
= 4 ROWS OF 6

NO. OF LVDTS = 8
NO. OF PRESSURE CELLS = 16
— HORIZONTAL CELLS (2,3,4,6,8,10,
12,14&16)
▌ VERTICAL CELLS (NO. 5,9&13)
CELLS (NO. 1,7,11&15) FLUSH WITH
BACK OF PANELS

FIG. (3.32) KEY FIGURE OF THE MODEL TEST.

TABLE (3.1) SUMMARY OF TEST CATEGORIES.

TEST CAT.	NO. OF TESTS	THE PURPOSE OF THE CAT.
I	14	To overcome problems during and after construction, ensure the stability of the wall and reproducibility and repeatability of the results.
II	2	To investigate the behaviour of the wall under minimum and maximum densities without using the compaction.
III	3	To study the effect of compaction in general and the compaction length in particular on the behaviour of the wall.
IV	5	To study the effect of methods of construction, variable compaction length for each layer behind two planes inclined at 65° & 75° to the horizontal from the toe of the wall, length of the strips and horizontal and vertical spacings between the strips on the behaviour of the wall, using compaction in all the cases.

(A)

TEST NO. CAT.-I-1 (2 TIMES)

H = 600 MM
Sh = Sv = 50 MM
= 0.083 H
L = H
NO MEASUREMENTS WERE TAKEN

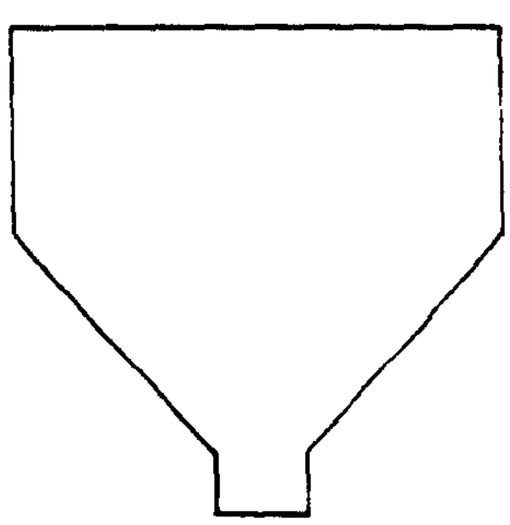

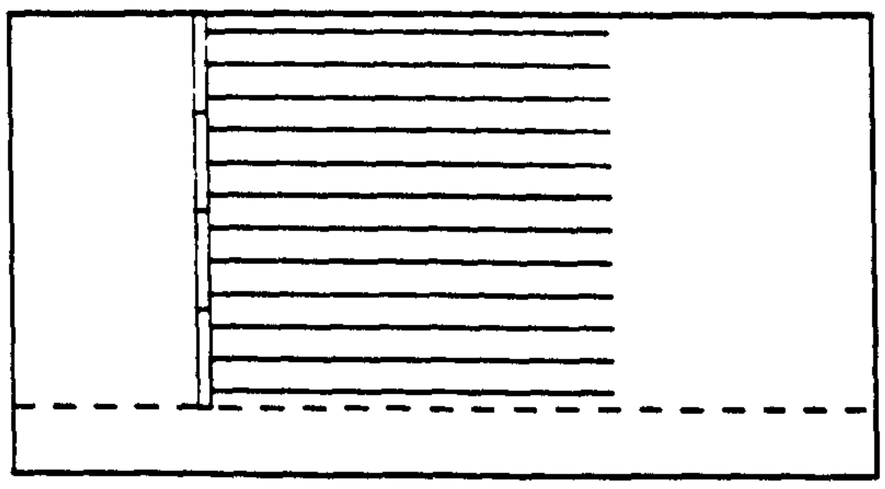

FIG. (3.33) TESTS OF CATEGORY I.

(B)

TEST NO. CAT.-I-3

H = 600 MM
Sh = Sv = 200 MM
= 0.333 H
L = H
NO MEASUREMENTS WERE TAKEN

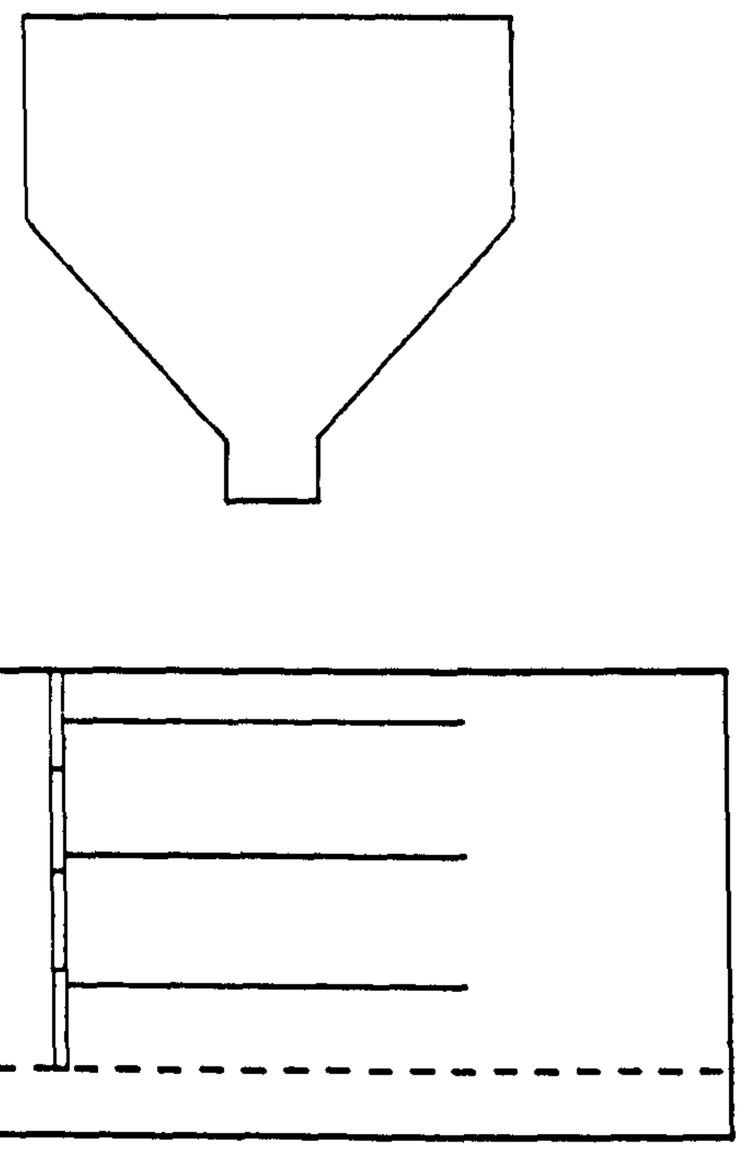

TEST NO. CAT.-I-4

H = 600 MM
Sh = Sv = 150 MM
= 0.25 H
L = H
NO MEASUREMENTS WERE TAKEN

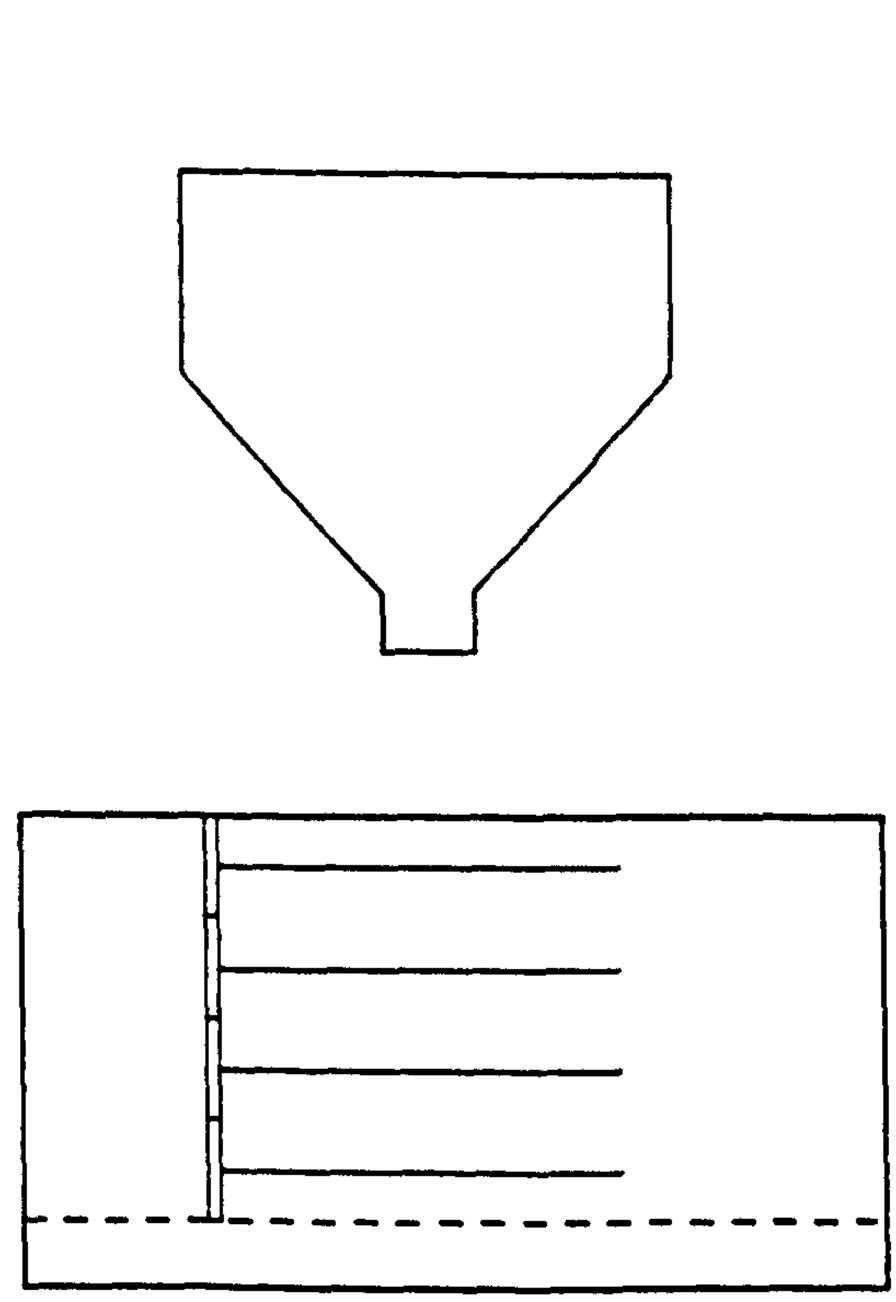

FIG. (3.33) CONT.

(C)

TEST NO. CAT.-I-5&6

H = 600 MM
Sh = Sv = 50 MM
= 0.083 H
L = H
Lc = H
NO MEASUREMENTS WERE TAKEN

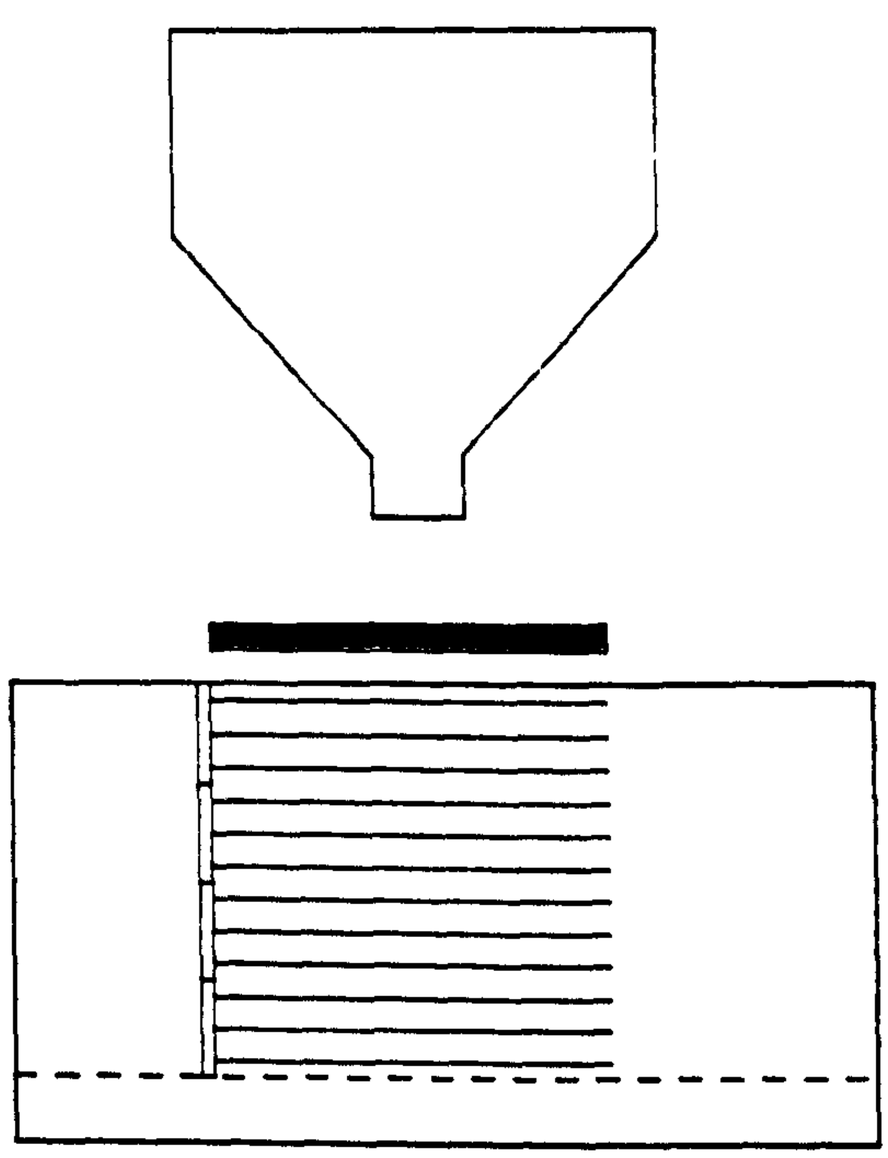

FIG. (3.33) CONT.

(D)

TEST NO. CAT.-I-7

H = 600 MM
Sh = Sv = 50 MM
= 0.083 H
L = H

MEASUREMENTS WERE TAKEN

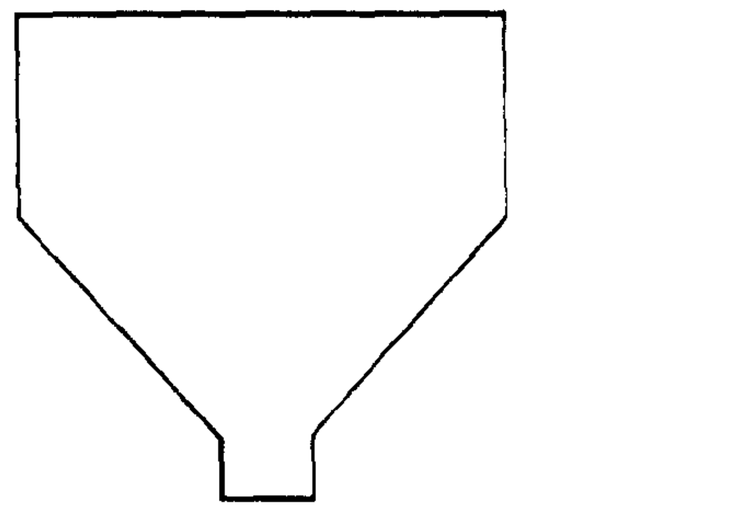

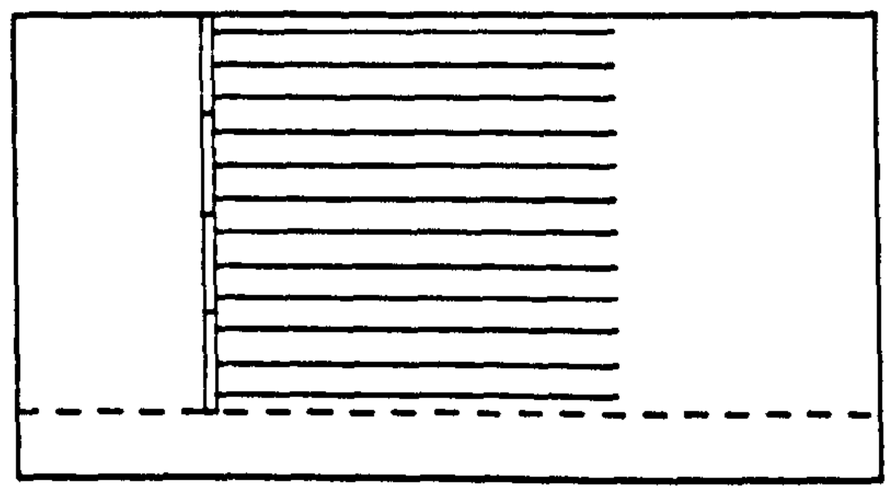

TEST NO. CAT.-I-8

H = 600 MM
Sh = Sv = 150 MM
= 0.25 H
L = H

MEASUREMENTS WERE TAKEN

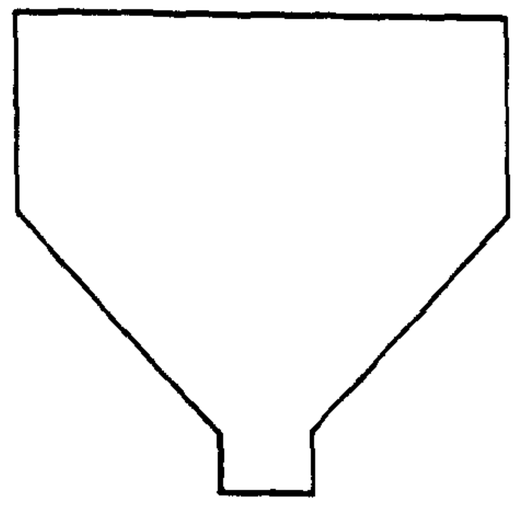

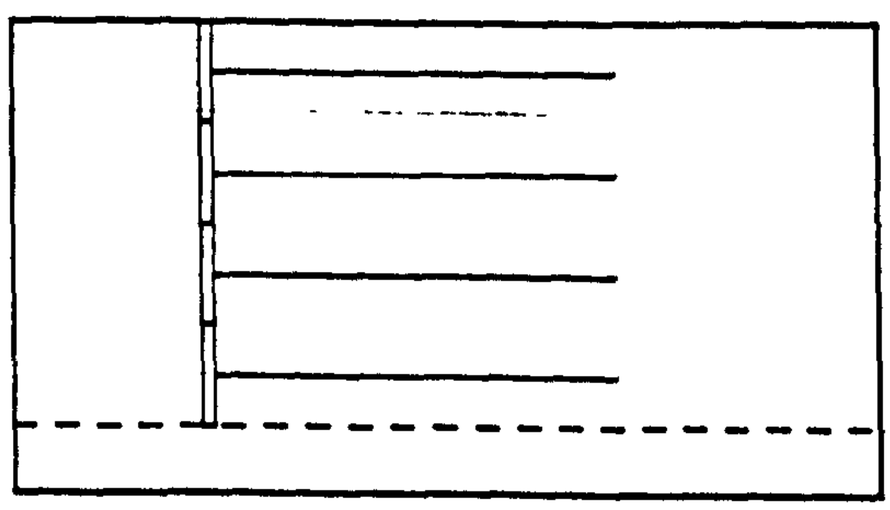

FIG. (3.33) CONT.

(E)

TEST NO. CAT.-I-9 (3 TIMES)

H = 600 MM
Sh = Sv = 100 MM
= 0.167 H
L = H

MEASUREMENTS WERE TAKEN

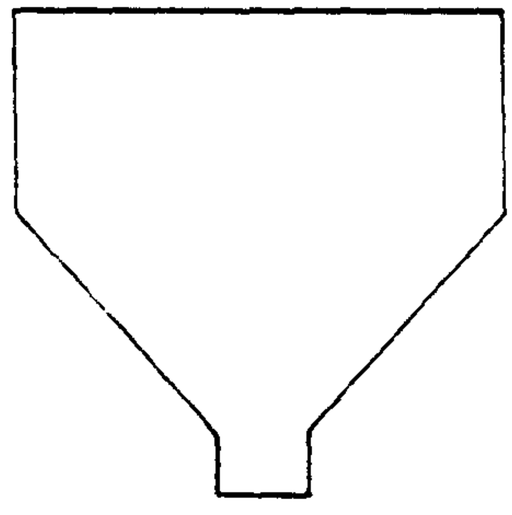

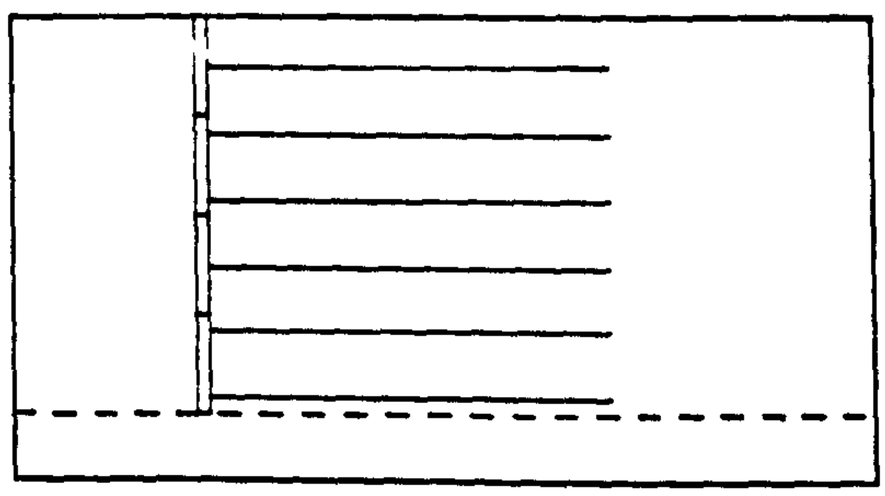

TEST NO. CAT.-I-10 (3 TIMES)

H = 600 MM
Sh = Sv = 100 MM
= 0.167 H
L = H
Lc = H

MEASUREMENTS WERE TAKEN

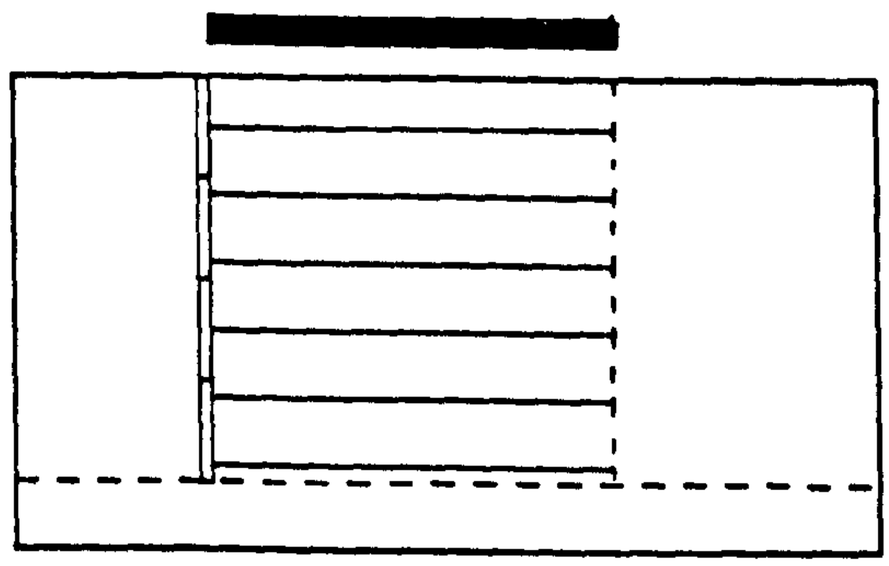

FIG. (3.33) CONT.

(ii) To ensure stability of the wall under the self weight of the backfill. Two tests were carried out with loose sand (14.39 kN/m^3) without compaction load, using the sand spreader only and no measurements were taken. The dimensions of the wall, Fig. (3.33.B), were:

CAT. I–3

$S_h = S_v = 200$ mm

H = 600 mm

L = 600 mm

CAT. I–4

$S_h = S_v = 150$ mm

H = 600 mm

L = 600 mm

The wall was unstable using the first test, but was stable in the second test, therefore tests with $S_h = S_v = 200$ mm were excluded.

(iii) To solve any problems when the full compaction length was used. Two tests were carried out using the sand spreader to form sand layers with a preliminary density of 14.39 kN/m^3 and compaction was done on the whole reinforced mass using the compaction device, Sec. 3.4.3 . The first test done was to find any problems and the second to ensure the success of the solutions applied. The dimensions of the walls, Fig. (3.33.C), were:

CAT. I–5

$S_h = S_v = 50$ mm

H = 600 mm

L = 600 mm

$L_c = 600$ mm

CAT. I–6

$S_h = S_v = 50$ mm

H = 600 mm

L = 600 mm

$L_c = 600$ mm

(iv) To ensure that reasonable output readings of stresses, strains and displacements could be obtained and were within the sensitivity of the measuring

devices. Two tests were carried out without compaction, using the sand spreader only with instrumentation for stresses in the backfill soil, strains in the strips and displacements of the wall face. The sand density was 14.39 kN/m^3. The dimensions of the walls, Fig. (3.33.D), were:

CAT. I–7

$S_h = S_v = 50$ mm

$H = 600$ mm

$L = 600$ mm

CAT. I–8

$S_h = S_v = 150$ mm

$H = 600$ mm

$L = 600$ mm

Readings were taken as each layer of sand (50 mm thickness) was placed. The results of the first tests showed very low values of output readings, almost the same during forming of all twelve sand layers. Tests of these dimensions were excluded from the testing programme.

(v) To ensure and determine reproducibility and repeatability of the results. Two tests were carried out, each one being repeated three times. The first one was carried out with no compaction and the second with. In both tests the sand spreader was used to form sand layers with an average preliminary density of 14.39 kN/m^3 and instrument readings were fully recorded.

In the second test, all the reinforced mass was compacted. The dimensions of the walls in the tests, Fig. (3.33.E), were:

CAT. I–9 (3 times)

$S_h = S_v = 100$ mm

$H = 600$ mm

$L = 600$ mm

CAT. I–10 (3 times)

$S_h = S_v = 100$ mm

$H = 600$ mm

$L = 600$ mm & $L_c = 600$ mm

The results obtained from this test series will be shown in Chapter 5.

(b) Category II tests: Fig. (3.34)

The objective of the category II– tests was to investigate the wall behaviour under minimum and maximum densities without using compaction. Two instrumented tests were carried out in this category, the sand spreader being used to form sand layers 50 mm thick. The minimum density was 14.39 kN/m^3 and the maximum density of 15.96 kN/m^3 was attained using the sand spreader with a special arrangement, which will be explained in Chapter 4. The dimensions of the walls, Fig. (3.34.A&B) were:

CAT. II–1 & II–2

S_h = Sv = 100 mm

H = 600 mm

L = 600 mm

The results will be discussed in Chapter 5.

(c) Category III tests: Fig. (3.35)

Tests in this category were intended to study the effect of compaction in general, and the compaction length in particular, on the behaviour of a reinforced earth wall. In these tests the compaction length was related to the wall height and changed three times (0.33 H), (0.67 H), and (H) measured from the end of the reinforced mass towards the wall.

The sand spreader was used to form the sand layers (50 mm each) at an average preliminary density of 14.39 kN/m^3. The compaction device was used to

(A)

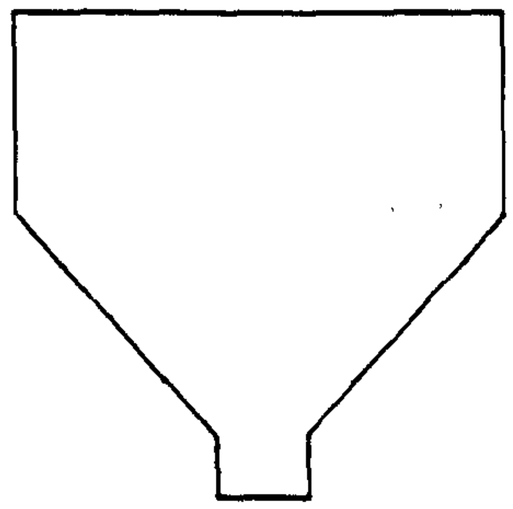

TEST NO. CAT.-II-1

H = 600 MM
Sh = Sv = 100 MM
= 0.167 H
L = H

MINIMUM DENSITY AND
WITHOUT COMPACTION
MEASUREMENTS WERE TAKEN

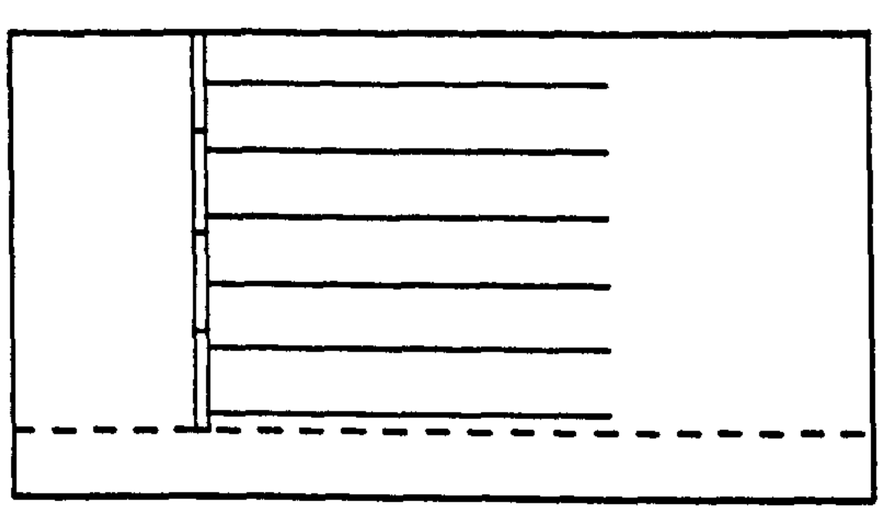

(B)

TEST NO. CAT.-II-2

H = 600 MM
Sh = Sv = 100 MM
= 0.167 H
L = H

MAXIMUM DENSITY AND
WITHOUT COMPACTION
MEASUREMENTS WERE TAKEN

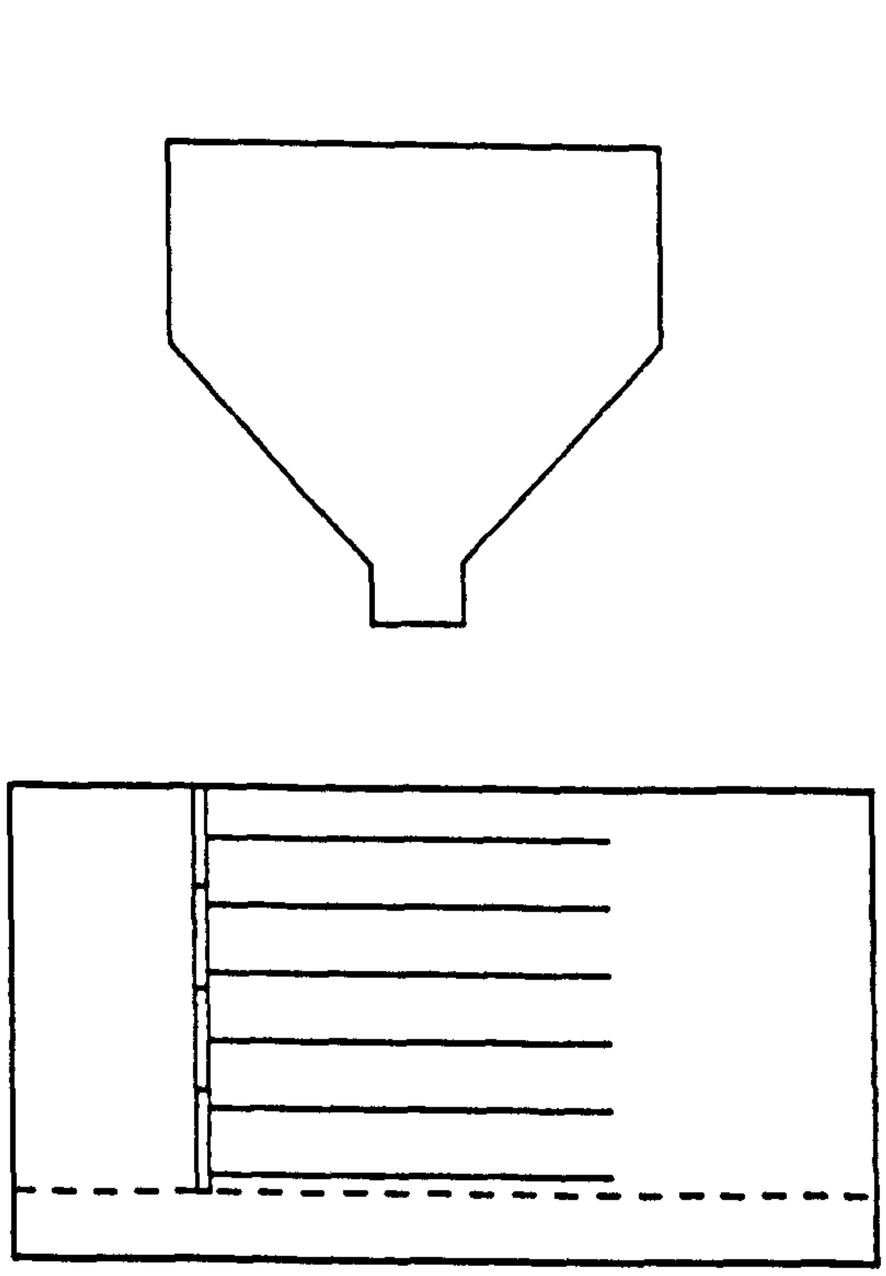

FIG. (3.34) TESTS OF CATEGORY II.

(A)

TEST NO. CAT.-III-1

H = 600 MM
Sh = Sv = 100 MM
= 0.167 H
L = H
Lc = 0.33H
MEASUREMENTS WERE TAKEN

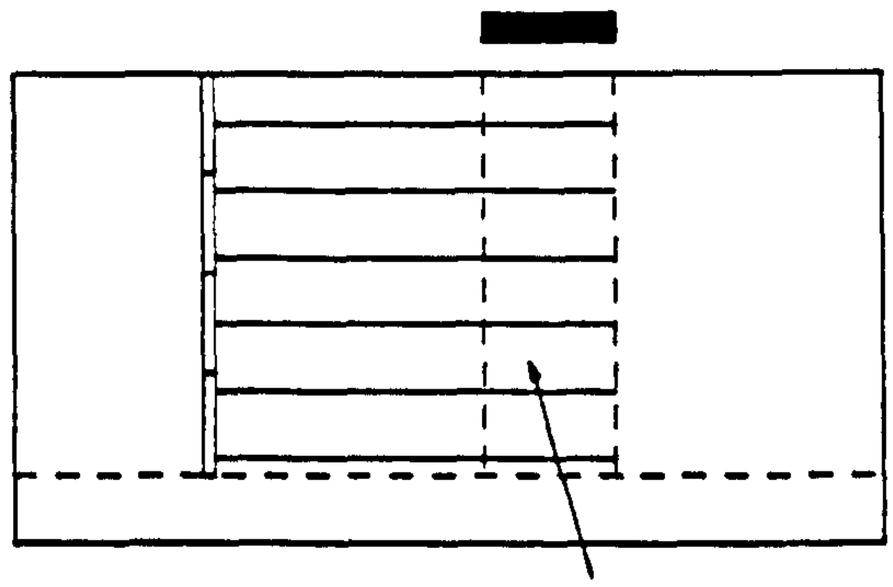

(B)

TEST NO. CAT.-III-2

H = 600 MM
Sh = Sv = 100 MM
= 0.167 H
L = H
Lc = 0.67H
MEASUREMENTS WERE TAKEN

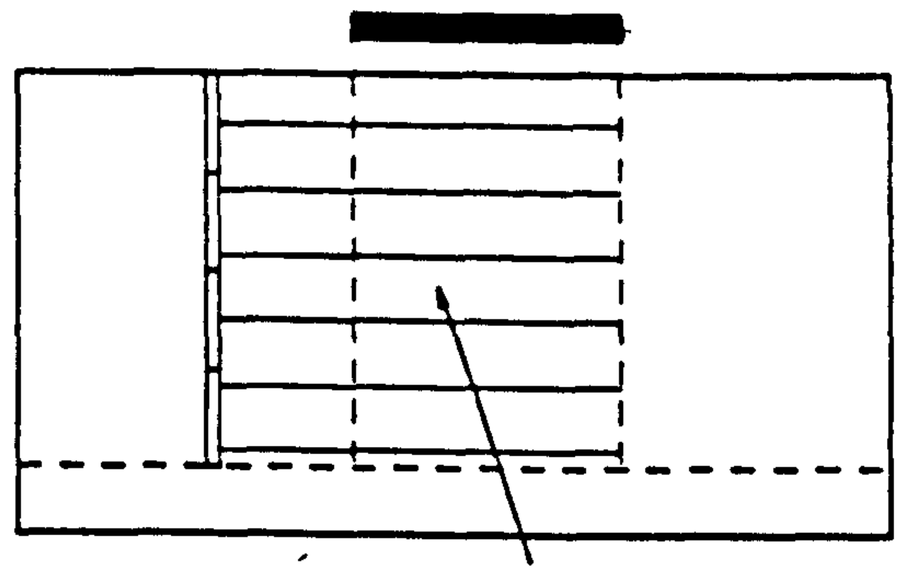

(C)

TEST NO. CAT.-III-3

H = 600 MM
Sh = Sv = 100 MM
= 0.167 H
L = H
Lc = H
MEASUREMENTS WERE TAKEN

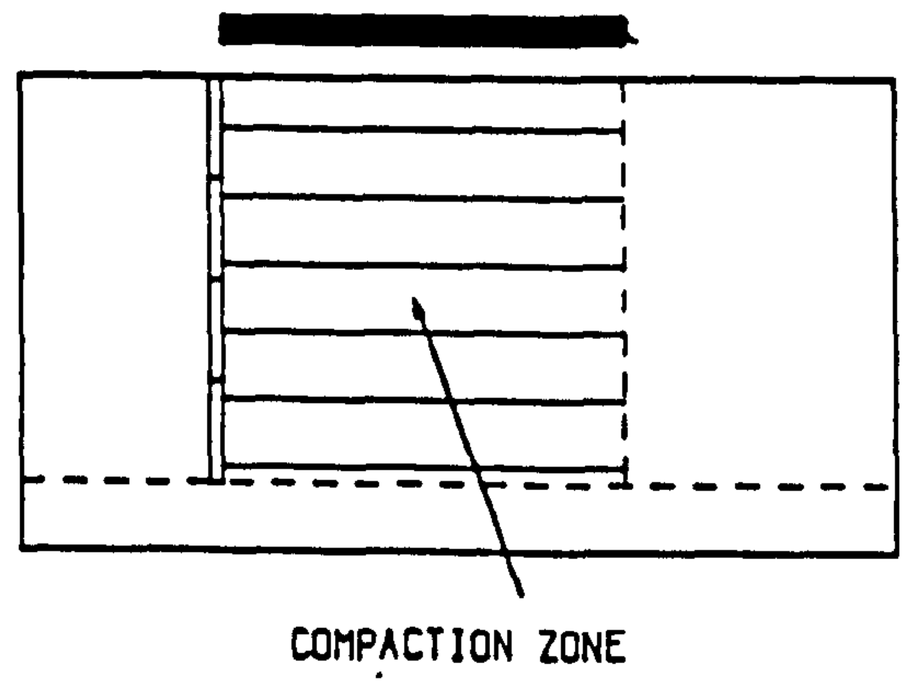

FIG. (3.35) TESTS OF CATEGORY III.

compact each layer as in the field. The average densities according to the different compaction lengths were 14.71, 16.23 & 17.51 kN/m^3 respectively. The dimensions of the walls, Fig. (3.35.A,B&C), were:

For the three tests,

Sh = S_v = 100 mm

H = 600 mm

L = 600 mm

and

L_c = 200 mm CAT. III–1

L_c = 400 mm CAT. III–2

L_c = 600 mm CAT. III–3

The results will be shown in Chapter 5.

(d) Category IV tests: Fig. (3.36)

This category consisted of five tests. The objective was to investigate the effect of compaction on the behaviour of the wall when:

(i) The method of construction was changed and the whole reinforced mass was compacted. The dimensions of the wall, Fig. (3.36.A), were:

CAT. IV–1

S_h = S_v = 100 mm

H = 600 mm

L = 600 mm

L_c = 600 mm

(A)

TEST NO. CAT.-IV -1

H = 600 MM
Sh = Sv = 100 MM
= 0.167 H
L = H
Lc = H
WALL MOVEMENT WAS PREVENTED
DURING CONSTRUCTION
MEASUREMENTS WERE TAKEN

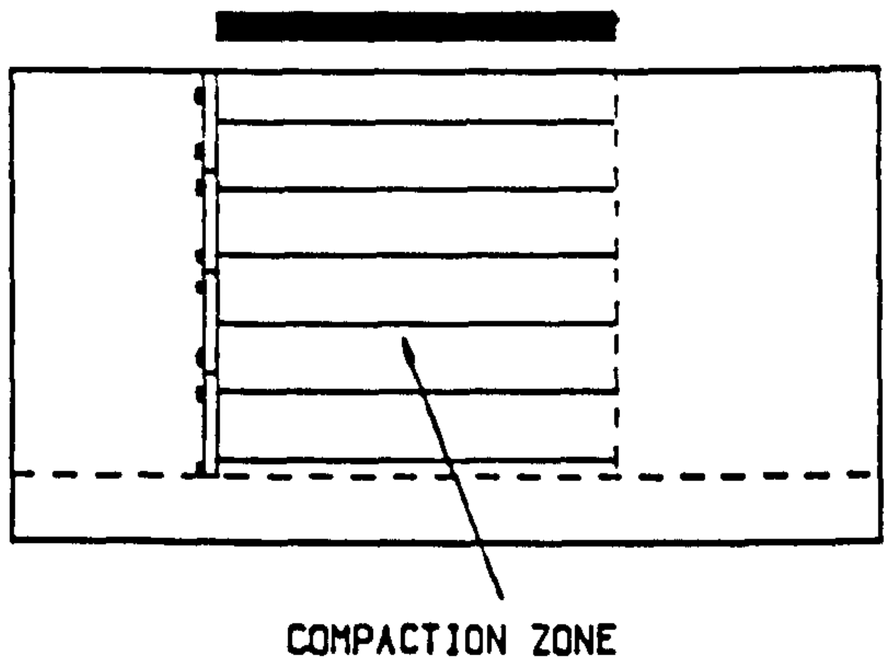

(B)

TEST NO. CAT.-IV -2

H = 600 MM
Sh = Sv = 100 MM
= 0.167 H
L = H
Lc = VARIABLE FROM LAYER
TO ANOTHER
θ = 60.0 DEGREE
MEASUREMENTS WERE TAKEN

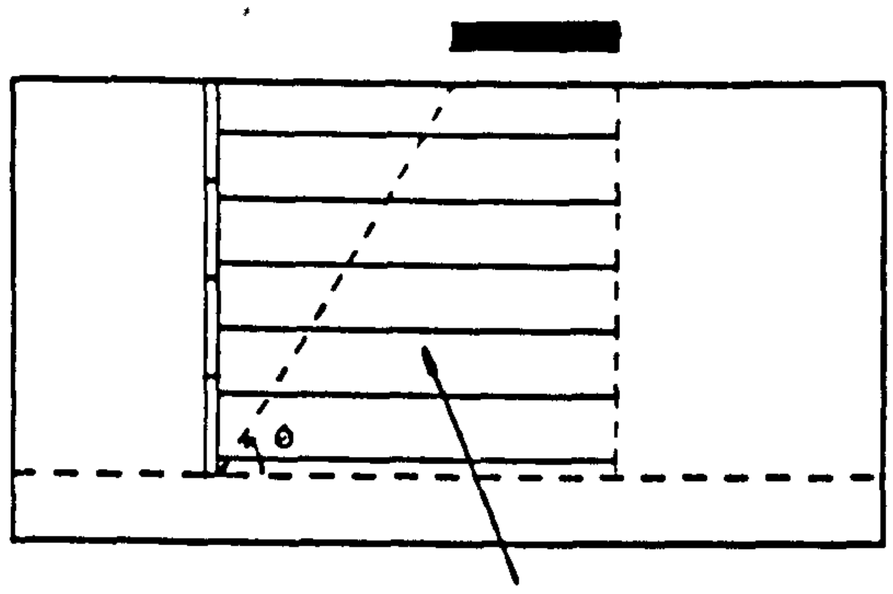

(C)

TEST NO. CAT.-IV -3

H = 600 MM
Sh = Sv = 100 MM
= 0.167 H
L = H
Lc = VARIABLE FROM LAYER
TO ANOTHER
θ = 75.0 DEGREE
MEASUREMENTS WERE TAKEN

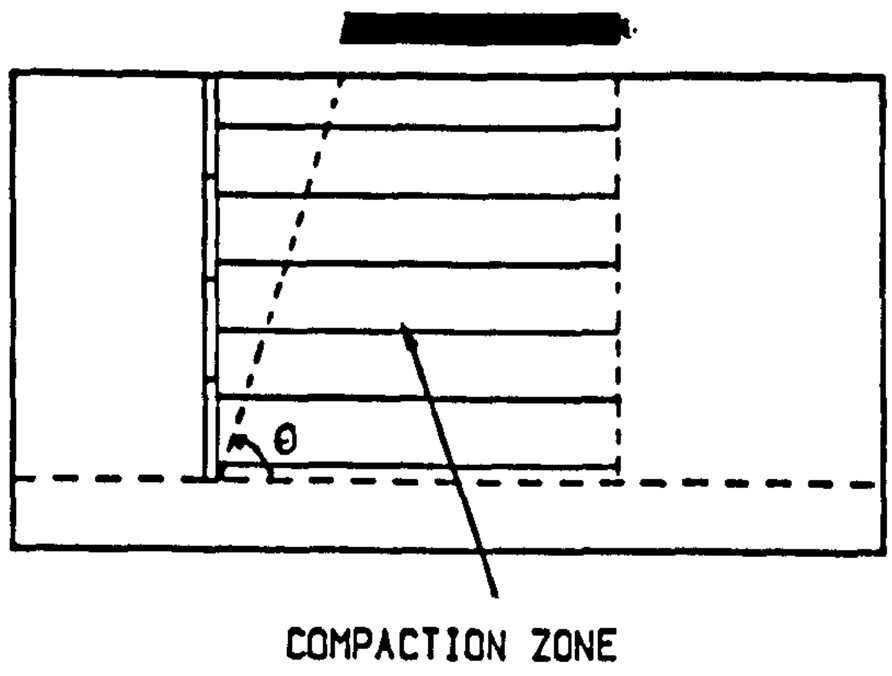

FIG. (3.36) TESTS OF CATEGORY IV .

(D)

TEST NO. CAT.- IV -4

H = 600 MM
Sh = Sv = 150 MM
= 0.25 H
L = H
Lc = H
MEASUREMENTS WERE TAKEN

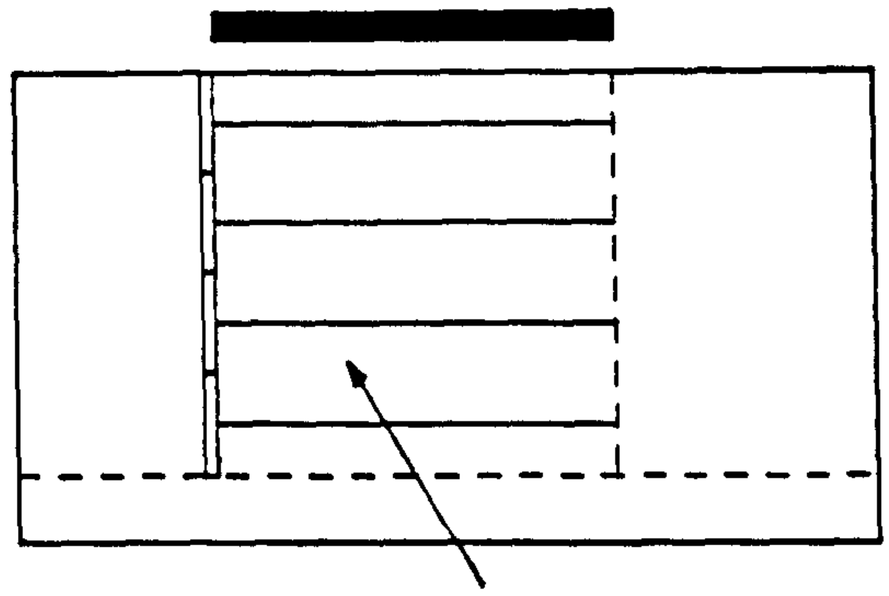

(E)

TEST NO. CAT.- IV -5

H = 600 MM
Sh = Sv = 100 MM
= 0.167 H
L = 0.50 H
Lc = 0.50 H
MEASUREMENTS WERE TAKEN

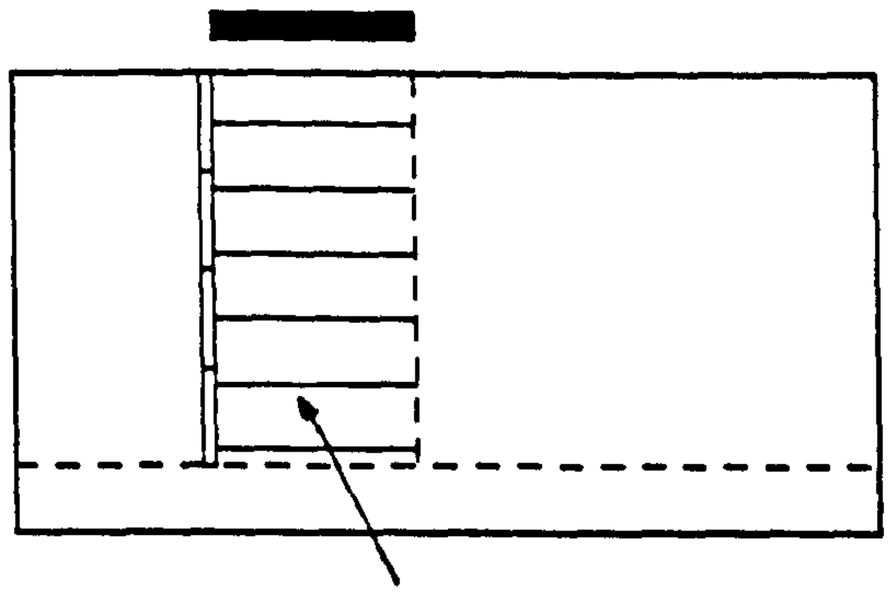

FIG. (3.36) CONT.

Movement during construction was prevented by means of support at the face of the wall using the support system described in Sec. 3.4.5 . At the end of construction the support was removed.

(ii) Using a different compaction length for each layer behind two planes inclined at 60° & 75° to the horizontal from the toe of the wall. The dimensions of the walls, Fig. (3.36.B&C), were:

CAT. IV–2

$S_h = S_v = 100$ mm

$H = 600$ mm

$L = 600$ mm

L_c = variable from one layer to another

$\theta = 60°$

CAT. IV–3

$S_h = S_v = 100$ mm

$H = 600$ mm

$L = 600$ mm

L_c = variable from one layer to another

$\theta = 75°$

(iii) The vertical and horizontal spacings between strips were changed and the whole reinforced mass was compacted. The dimensions of the wall, Fig. (3.36.D), were:

CAT. IV–4

$S_h = S_v = 150$ mm

$H = 600$ mm

$L = 600$ mm

$L_c = 600$ mm

(iv) The length of the strips was changed and the whole reinforced mass was compacted. The dimensions of the wall, Fig. (3.36.E), were:

CAT. IV–5

$S_h = S_v = 100$ mm

$H = 600$ mm

$L = 300$ mm

$L_c = 300$ mm

In all the above tests the sand spreader was used to form sand layers at an average preliminary density of 14.39 kN/m^3. The compaction device was used to compact each layer to average densities of 17.61, 16.32, 16.81, 17.49, and 16.50 kN/m^3 respectively for the five tests. Readings from instrumentation devices were taken and the results will be discussed in Chapter 5 .

3.7 SET–UP AND PROCEDURE FOR MODEL WALL

The general test procedure will be described. Special arrangements adopted for some of the previous categories will be discussed when necessary. Before setting up the model for testing, the following items were prepared:

(1) The internal side surfaces (2 sides & rear) of the wooden box were marked with continuous horizontal lines every 25 mm.

(2) Aluminium strips were cut to the required number and length for all categories of test.

(3) Strain gauges were mounted on the strips in the locations previously selected, as shown in Fig. (3.9), using the procedures previously explained in Sec. 3.5.1 . Calibrations were made according to Sec. 3.5.1 .

(4) The 16 pressure cells were prepared, numbered and calibrated according to Sec. 3.5.2, and four of the cells (No. 1,7, 11 & 15) were fixed flush with the back of the wall face in perspex panels No. 3, 9, 15 & 21.

(5) The eight LVDTs were numbered and calibrated as discussed before in Sec. 3.5.4 .

(6) The required programme and data for data logger was installed.

(7) The sand spreader was set up to form the required density of sand layers. Details of the sand spreader and the arrangement necessary to obtain the sand layers with a predetermined thickness and density will be explained in detail in Chapter 4 .

(8) The compaction device which simulated the compaction plant was calibrated against time of vibration, thickness and number of layers, to reach certain density in the sand layers. Details of the apparatus, methods of calibrations and calibration curves will be given in Chapter 4.

Having done the necessary preparations, the setting up of the model was carried out in several sets to match the field construction sequence for a

reinforced earth retaining wall as closely as possible. The construction sequence in the field has been illustrated in Chapter 2.

The tractor used in the field to spread the sand layers in lifts before compaction plant in the field (usually a vibrating roller for cohesionless soil) was simulated by the sand spreader.

The construction sequence for setting the model tests for $S_h = S_v = 100$ mm, for example, was as follows:

(1) The plywood box was cleaned and the movable door at the rear of box was fixed in the closed position.

(2) An equivalent texture of soil foundation was laid, comprising two 50 mm layers of compacted sand. The sand spreader formed the first layer and it was compacted with the compaction device, a similar procedure being used for the second layer. The average density reached after compaction was 17.51 kN/m^3. The method used to obtained this density will be discussed in Chapter 4. The sand foundation covered the whole area of the box as shown in Fig. (3.37.A). The hopper of the sand spreader was raised 50 mm after each layer to maintain a constant height to get the same density for each layer, up to the end of construction.

(3) The two rubber membrane strips were held in position at the sides of the box to prevent sand spilling from the gap between the edges of wall face and the box sides as previously explained in Sec. 3.4.1 and shown in Fig. (3.7). The half thickness of the first layer of sand (25 mm thick) was formed by sand spreader to cover 1.0 x 0.9 m of the box i.e. the reinforced mass area and 0.40

m behind it, as far as the rear of the box, and compacted, Fig. (3.37.B).

(4) The first row of panels was placed including pressure cell No. 1 flush with the surface of the middle panel. Two temporary supports were put in touching the panels to prevent any movement during construction. The first row of strips including the instrumented strip and the first group of pressure cells (1 to 6) were installed. The first sand layer (50 mm thick) was formed by sand spreader and compacted to an average density of 17.51 kN/m^3 for a compaction length equal to H i.e. all the reinforced mass was compacted.

Two additional points to note were , first that a perspex sand pot was placed on top of the foundation layers before forming the first sand layer in position near the rear of the reinforced mass and far from the instrumented parts. This procedure was repeated in each layer, in order to check the average density at the end of every test, by a method which will be illustrated in Chapter 4. Second, compaction was made from the rear of the reinforced mass towards the wall face as is done in the field.

The second row of reinforcement strips was placed and fixed to the panels. Layers No. 1 & 2 (50 mm each) were formed and compacted and the strips were laid on the top of layer 2. Panels, reinforcement, temporary supports and pressure cells are shown in Fig. (3.37.C&D).

(5) The second row of panels was placed which included pressure cell No. 7 flush with the middle panel. The temporary supports were removed from the first row of panels and support was installed at the top of the second row of panels. Sand layer No. 3 was formed by sand spreader and compacted by the compaction device. Pressure cells No. 7, 6, 9 & 10 were installed. Sand layer

No. 4 was formed and compacted. The third row of reinforcing strips including an instrumented strip was installed. The fifth sand layer was formed and compacted. Two LVDTs N0. 1 & 2 were fixed in position touching the first row of panels at panel No. 3. The temporary support was removed, Fig. (3.37.E&F).

It should be noted that instrument readings were taken just after forming a sand layer, during the time of compaction (i.e. while the compaction apparatus was operating), and after the end of compaction. This was done for each layer of sand. The origin of the lateral movement of the wall at any level is taken from the stage when the sand was first placed at that level.

(6) The third row of panels (including pressure cell No. 11 flush with the middle panel was placed with a temporary support at the top. Sand layer No. 6 was formed and compacted. The fourth row of reinforcing strips was laid and pressure cells Nos. 11 & 12 were installed. Sand layers Nos. 7 & 8 were formed and compacted. Pressure cells Nos. 13 & 14 as well as LVDTs Nos. 3 &4 were installed. The fifth row of strips including the last instrumented strip was laid on the surface of layer 8. The temporary support was removed, Fig. (3.37.G&H).

(7) The fourth (last) row was placed including pressure cell Nos. 15 flush with the surface of middle panel. Sand layer No. 9 was formed and compacted. Pressure cells Nos. 15 & 16 and LVDTs Nos. 5 & 6 were installed. Sand layer No. 10 was formed and compacted and the sixth row of reinforcing strips laid. Sand layers Nos. 11 & 12 were formed and compacted, sand layer No. 12 being 25 mm in this type of test. LVDTs Nos. 7 & 8 were installed and the temporary support was removed, Fig. (3.37.G&H).

The final location of pressure cells, LVDTs and strain gauges on the strips is shown in Fig. (3.37.I&J) respectively. The following should be noted:

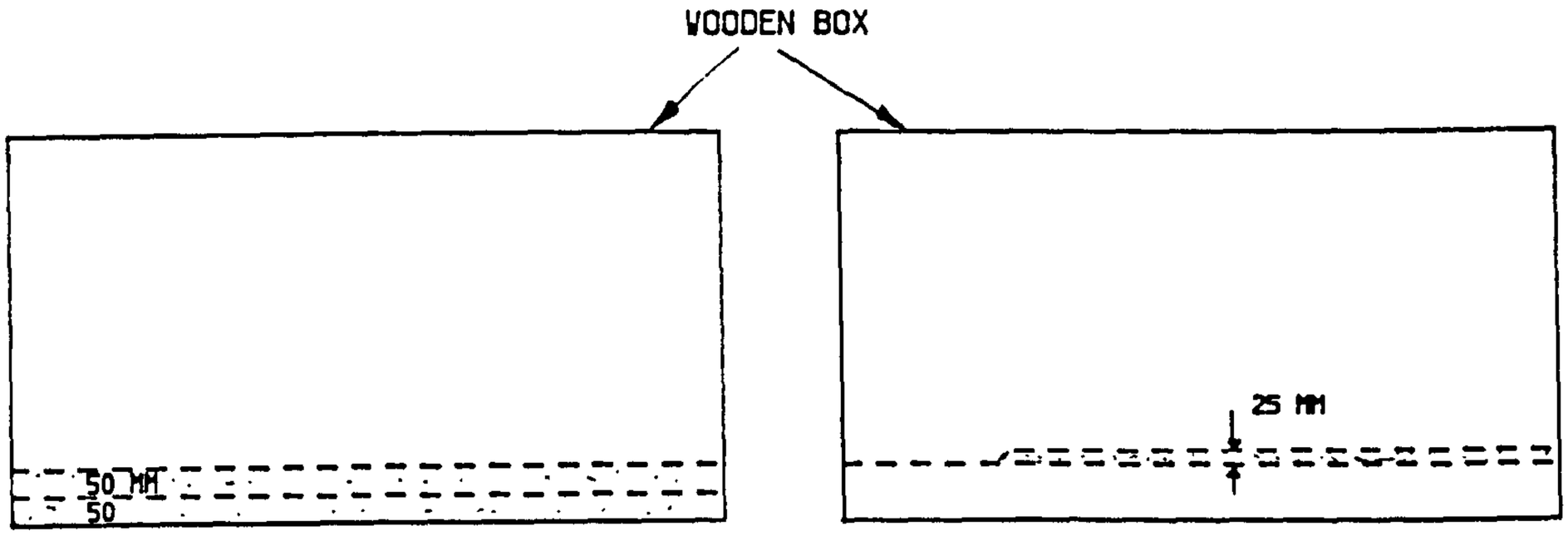

(A) TWO COMPACTED LAYERS OF SAND FOUNDATION

(B) A SAND LAYER OF 25 MM. THICK AS PART OF REINFORCED SAND

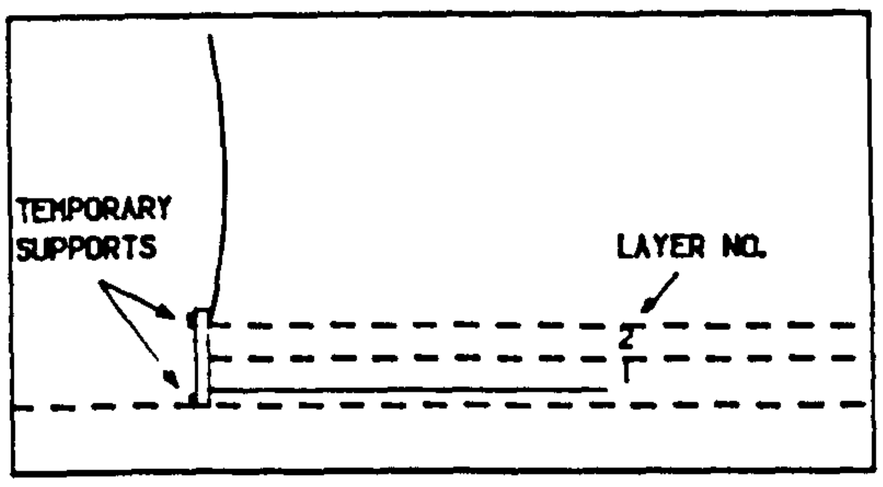

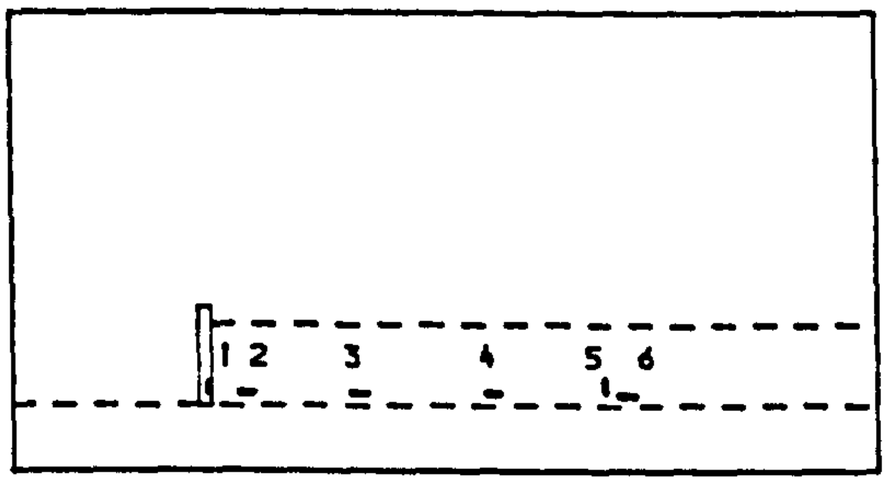

(C) THE FIRST ROW OF PANELS AND LAYERS NO. 1&2

(D) PRESSURE CELLS 1 TO 6

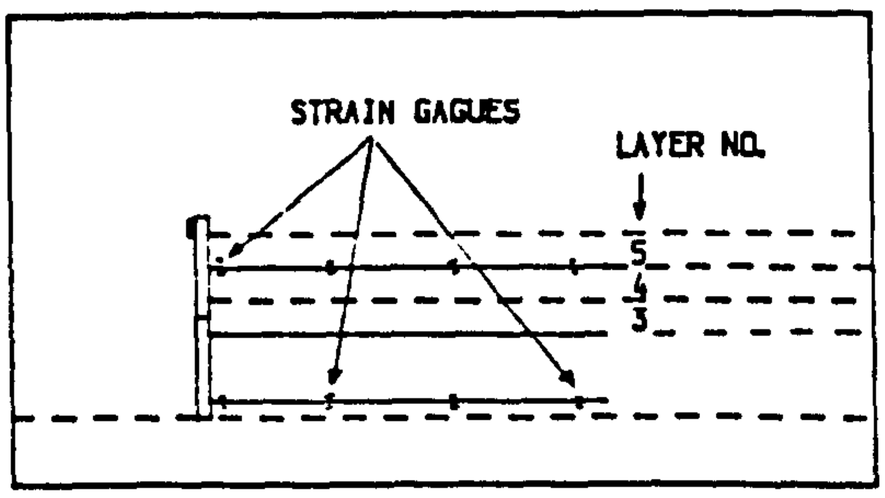

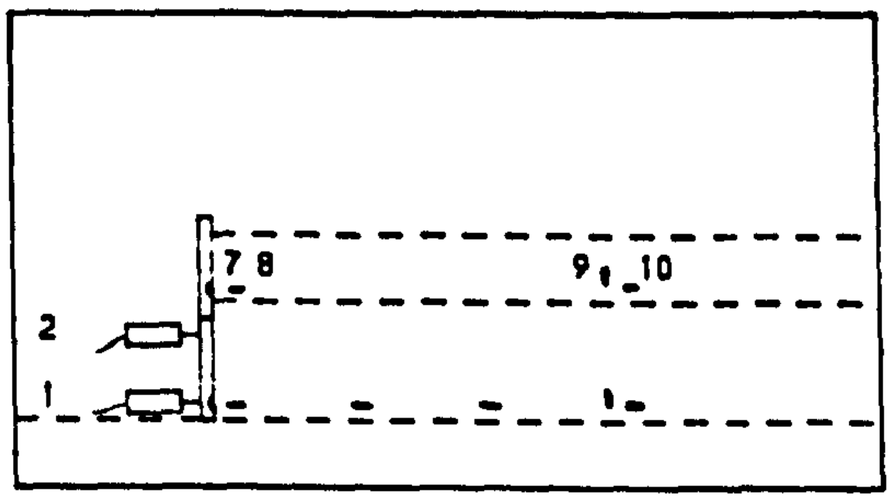

(E) THE SECOND ROW OF PANELS AND LAYERS NO. 3,4&5

(F) PRESSURE CELLS 7,8,9&10 AND LVDTS 1&2

FIG. (3.37) THE PROCEDURES OF THE TEST.

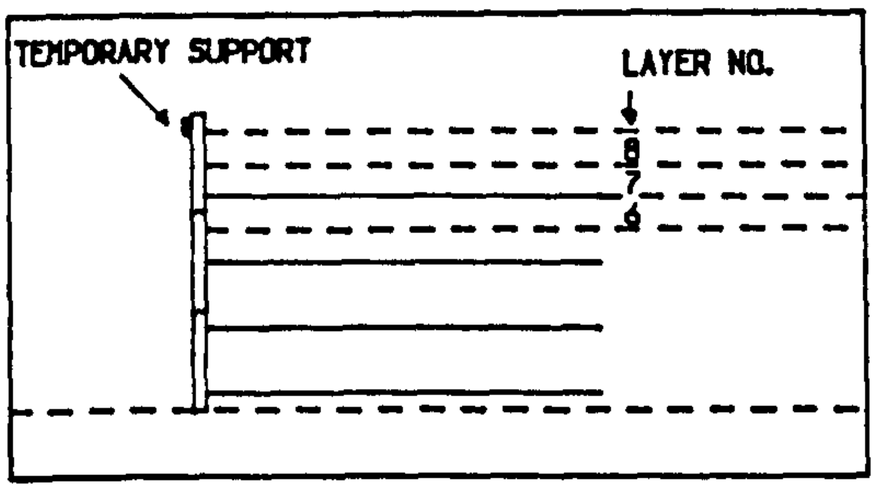

(G) THE THIRD ROW OF PANELS AND LAYERS NO. 6,7&8

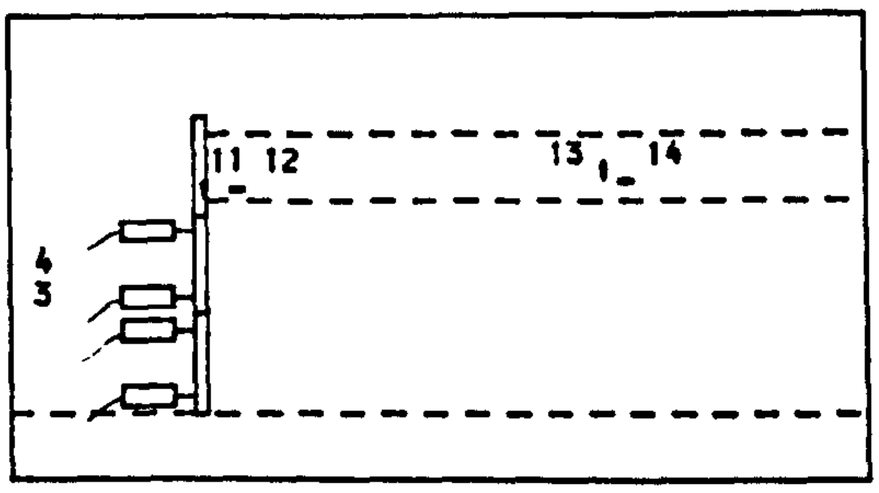

(H) PRESSURE CELLS 11 TO 14 AND LVDTS 3&4

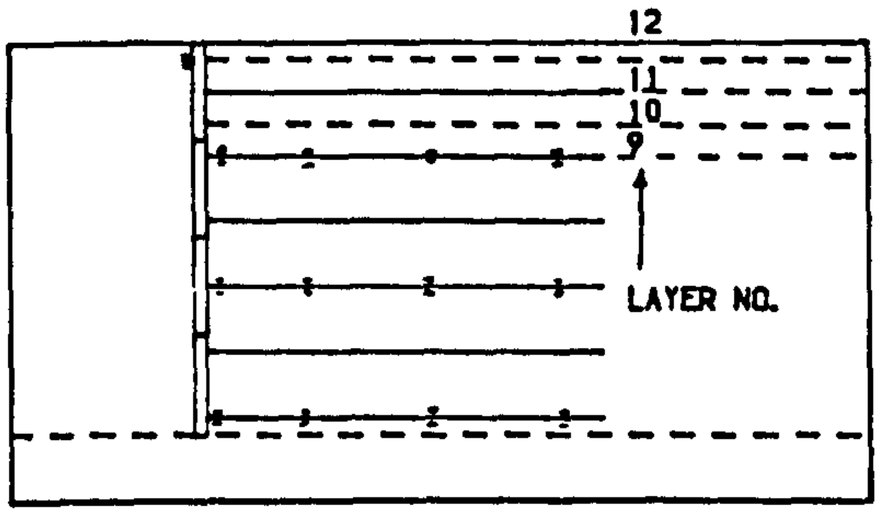

(I) THE FOURTH ROW OF PANELS AND LAYERS NO. 9 TO 12

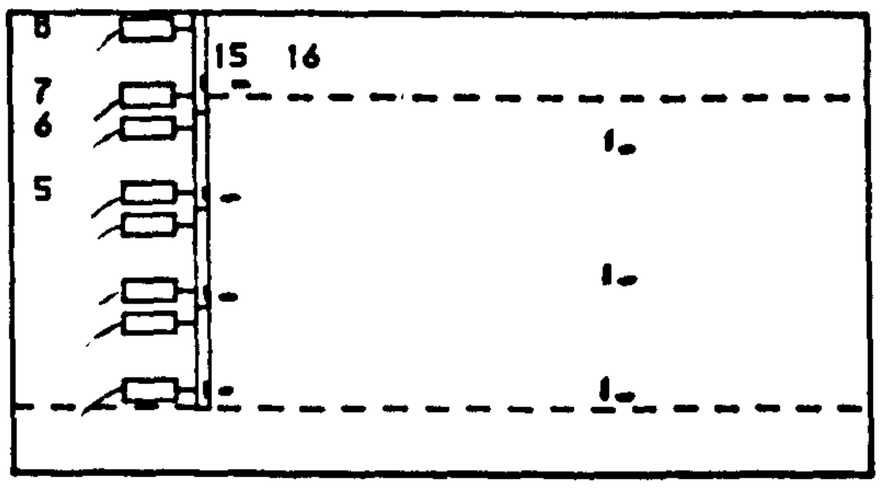

(J) PRESSURE CELLS 15&16 AND LVDTS 5 TO 8

FIG. (3.37) CONT.

- The locations of instrumented strips were different in tests IV–4 & IV–5 as previously shown in Fig. (3.9).
- In test IV–1 permanent supports were used during construction and up to the end of wall construction, and were then removed.
- In tests where no compaction was used as in tests Nos. II–1 & II–2, after forming each layer using the sand spreader no compaction device was used. In test II–2 in order to reach the required density (15.96 kN/m^3) another perforated metal plate with staggered holes fixed at the bottom of the sand spreader was used. Details of this arrangement will be explained in Chapter 4.
- Some of the categories of test were repeated to ensure adequate repeatability.

3.8 CONCLUSION

A model of a reinforced earth retaining wall (6.0 m height) has been designed and constructed. Different accessories which simulate the same construction sequence used in a full–scale wall were designed such as sand layer spreading, vibratory compaction and temporary supports. Preliminary tests as well as a complete series of tests designed to cover different aspects of construction were carried out to study the wall behaviour, during and after construction.

Instrumentation consisted of strain gauges, pressure cells, and LVDTs, which were developed and calibrated to monitor the model wall behaviour.

CHAPTER 4

DENSITY CONTROL IN THE MODEL

4.1 INTRODUCTION

An essential problem associated with all laboratory scale experiments involving granular material is the provision of a sand bed of uniform density. The different methods used by previous researchers to control the density of granular material are reviewed in this chapter as well as the factors which influence the uniformity of sand beds. The apparatus and methods of forming and calibrating sand beds for the present research will be explained in detail. Results from the calibration tests are shown and the conclusion is given at the end.

4.2 Methods Used to Form Sand Beds

The control of soil density is important in laboratory experimental models, since most theories depend on ideal conditions which include uniform density, expressed quantitatively by the porosity or relative density. Because of this the formation of sand beds in model tests has attracted many investigators. Different methods have been used to obtain uniform sand beds that are homogeneous and reproducible over a wide range of porosities or relative densities.

The methods can be divided into two categories:

(a) Methods which aim to obtain the required porosity or relative density by deposition. As an example of this method, **Kolbuszewski and Jones (1961)** used a rectangular hopper 29x17x7 inch, with a duralumin base plate, perforated with a regular pattern of holes. Two other plates were provided with the same pattern of holes. One of these (the control plate) rested on the base plate, and the other (the shutter) was placed immediately beneath the base plate. By displacing the base control plate relative to the base plate the effective aperture and hence the flow of sand out of the hopper could be varied, and the vertical jets of sand issuing from the hopper could then be dispersed into a uniform rain by a sieve mesh placed below the hopper above a receiver. It was noted that controlled intensity of deposition was achieved by raining the sand over the whole area.

Walker and Whitaker (1967) employed a different method to control the intensity of deposition. Sand beds were formed in a series of thin layers by a rain of the sand falling from a hopper which passed forwards and backwards across the container. A steel tube roller was used to control the flow of dry sand from an opening between the two sloping plates forming the base of a 7 cu. ft. hopper, Fig. (4.1).

Butterfield and Andrawes (1970) used the sand curtain technique to get uniform sand beds. The sand spreader comprised a box divided into two portions, the upper portion used for sand and the lower being a pressurized air reservoir discharging air through a wire mesh screen across the full width of the spreader, the discharge of sand from a slot in the travelling spreader being controlled by variation of the air flow through the slot, Fig. (4.2).

Hutchison (1982); Whiteford (1983); Wang (1986); and Zakaria (1986) used a sand raining device to form the sand beds of their models. The device has been

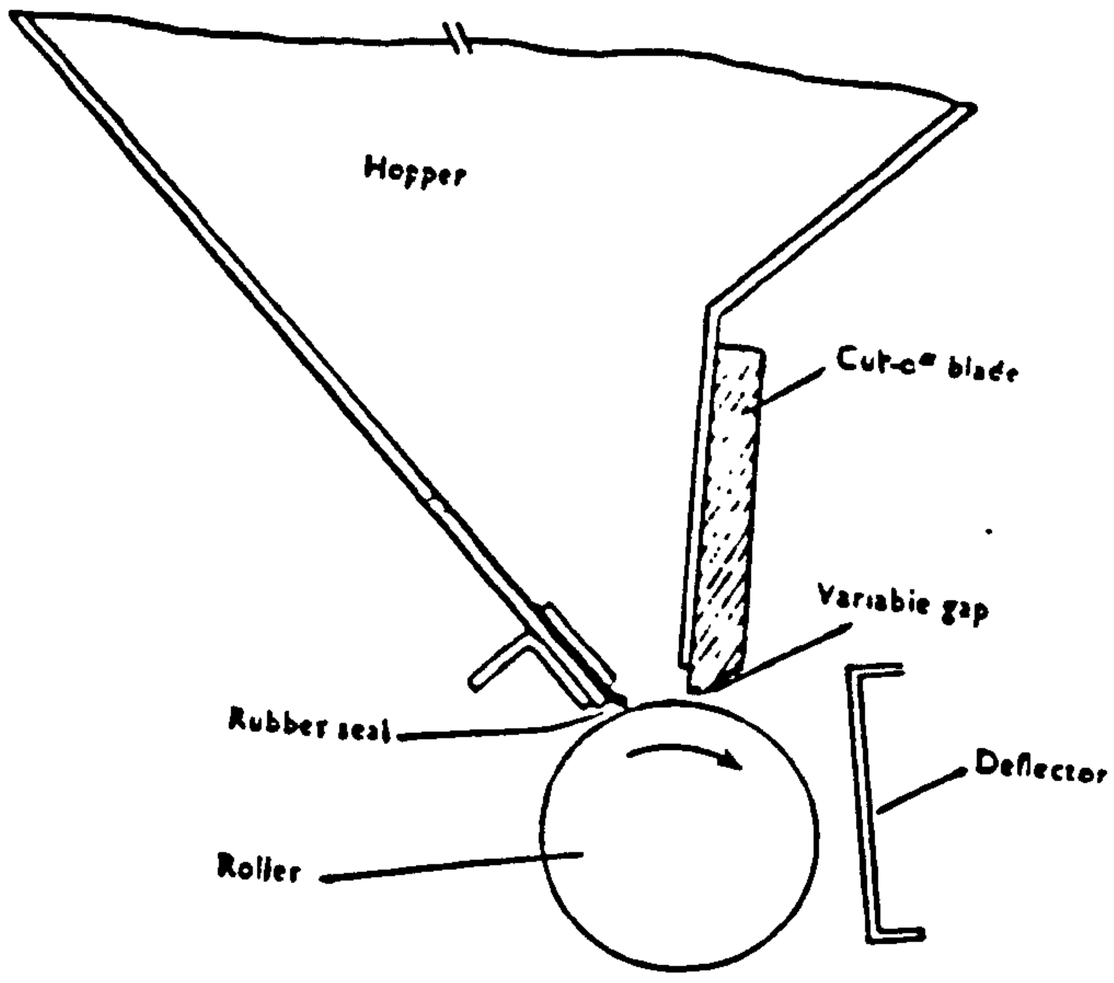

FIG. (4. 1) ROLLER FOR CONTROLLING THE FLOW OF DRY SAND FROM THE BOTTOM OF THE HOPPER (AFTER WALKER & WHITAKER , 1967).

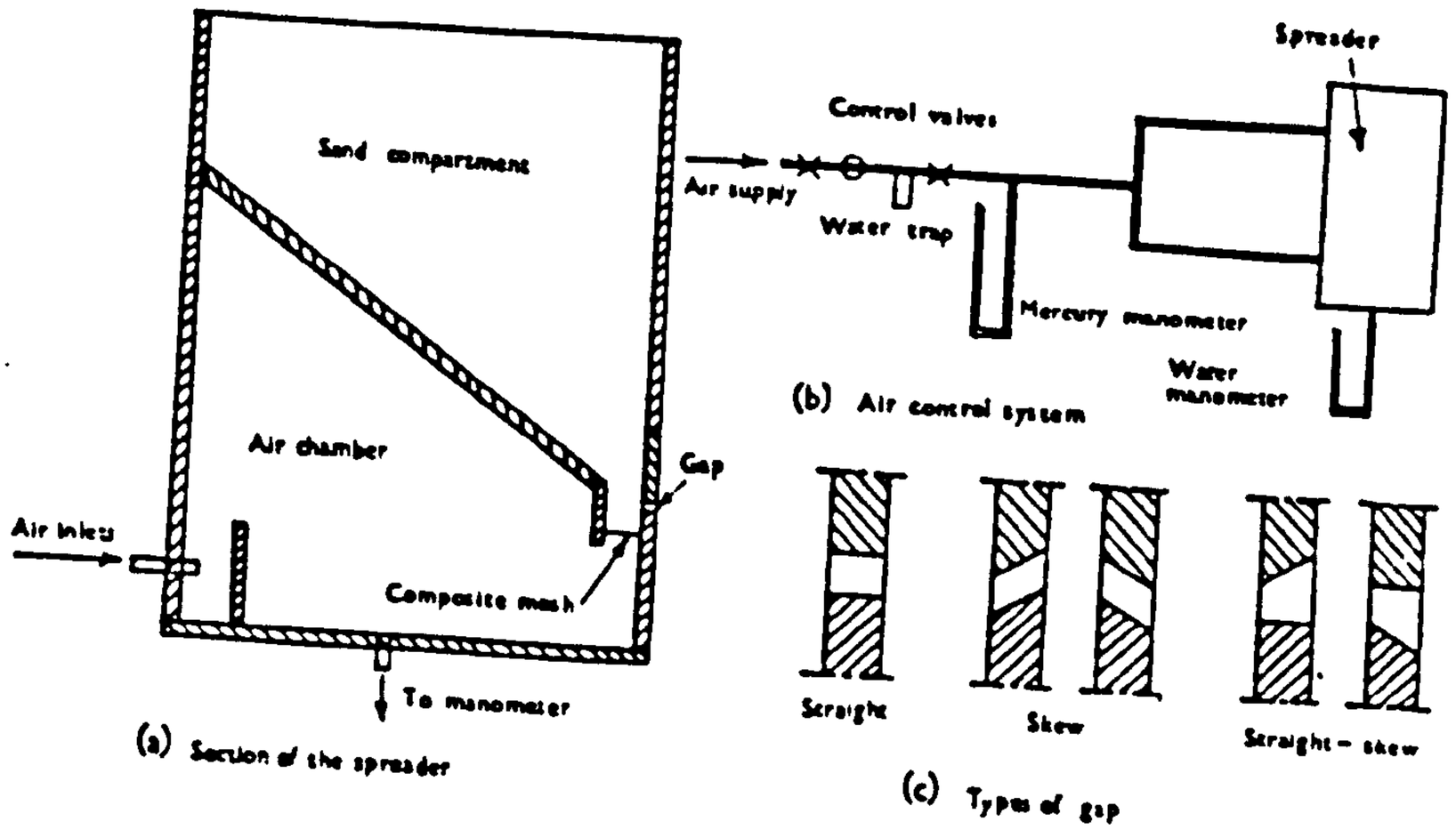

FIG. (4. 2) SYSTEM OF AN AIR PRESSURE FOR CONTROLLING THE FLOW OF DRY SAND (AFTER BUTTERFIELD & ANDRAWES , 1970).

modified by the author and will be described later.

(b) Methods which achieve the required porosity or relative density after deposition and which are suitable for dense sand beds. Shovelling, tamping or vibrating the sand in layers have been used in the technique (Feda, 1961; and Hansen, 1961).

4.3 FACTORS AFFECTING THE UNIFORMITY OF SAND BEDS

Kolbuszewski (1948 a and 1948 b) showed experimentally that a wide range of porosity in dry sand could be produced by allowing the sand to fall as a rain to build up the required bed.

Many factors affect the uniformity of a sand bed when using the technique of controlling the porosity or relative density by deposition as discussed in Sec.4.2. These factors can be summarised as follows:

(a) Intensity of sand raining i.e the weight of sand deposited per unit area in unit time, Kolbusewski and Jones (1961).

(b) The height of fall of the sand particles from the hopper containing the sand to the sand surface in a receiver box, Kolbusewski and Jones (1961).

(c) Particle elasticity (Macrae and Gray, 1961) and sphericity (Mackey, 1963) are also significant, especially when comparisons are made between different sands.

(d) There is evidence by Walker and Whitaker (1967) that during deposition

some dust is created which has some effect on deposition and the equipment used.

4.4 SAND PLACING TECHNIQUES IN THE MODEL

Sand beds in the present investigation were formed using two different techniques in order to get homogeneous beds and to obtain the required relative densities, which had been predetermined as being suitable for various tests. The two techniques were sand raining and vibratory compaction. Sometimes a combination of the two methods was used.

4.4.1 Sand Deposition device (Sand Spreader)

The apparatus used in raining sand had previously been used by Hutchison (1982); Whiteford (1983); Wang (1986); and Zakaria (1986). The sand spreader consisted mainly of a travelling hopper and supporting frame. The author modified the device to match the factors affecting depositions and the requirements of the reinforced earth retaining wall model.

Four main modifications were made and will be discussed in detail later. These modifications were:

(a) Increasing the travelling length of the sand hopper to 1.0 m to cover the whole area of backfill of the reinforced earth model.

(b) Some parts of the frame were removed and the others were altered to increase the workability of the frame.

(c) A perspex chamber was constructed around the frame.

(d) A system of dust extraction was installed.

(1) Sand spreader: Plate (4.1)

The sand spreader as shown in Plate (4.1) consists of the following:

(a) Hopper to discharge sand

(i) The hopper was made from plywood, to the dimensions and shape shown in Plate (4.1), all dimensions being in mm.

(ii) The rectangular perforated base of the hopper, consisted of steel plates 820 mm long, 138 mm, wide and 4 mm thick. The plates were drilled on 20 mm grids (staggered holes), as recommended by researchers such as Kolbusewski and Jones (1961), fixed to the bottom of the hopper to produce the sand rain. It was noted that the larger the holes in the perforated plate, the higher the intensity of sand and vice versa. Also the minimum diameter of the holes was chosen to prevent any blockage of the sand and permit the maximum size to pass through. Two discharge plates were used each having 7 mm and 10 mm diameter holes and giving two rates of deposition to produce medium and loose sand beds according to the densities required in the model.

(iii) A shutter plate which could fully open or close the perforated base of the hopper to retain the sand while the hopper was being filled.

(iv) The sand hopper had four wheels attached which allowed it to run on two horizontal rails fixed on the top of the upper frame. The hopper could pass forward and backward at a speed of about 0.1 m / sec. over the whole area of

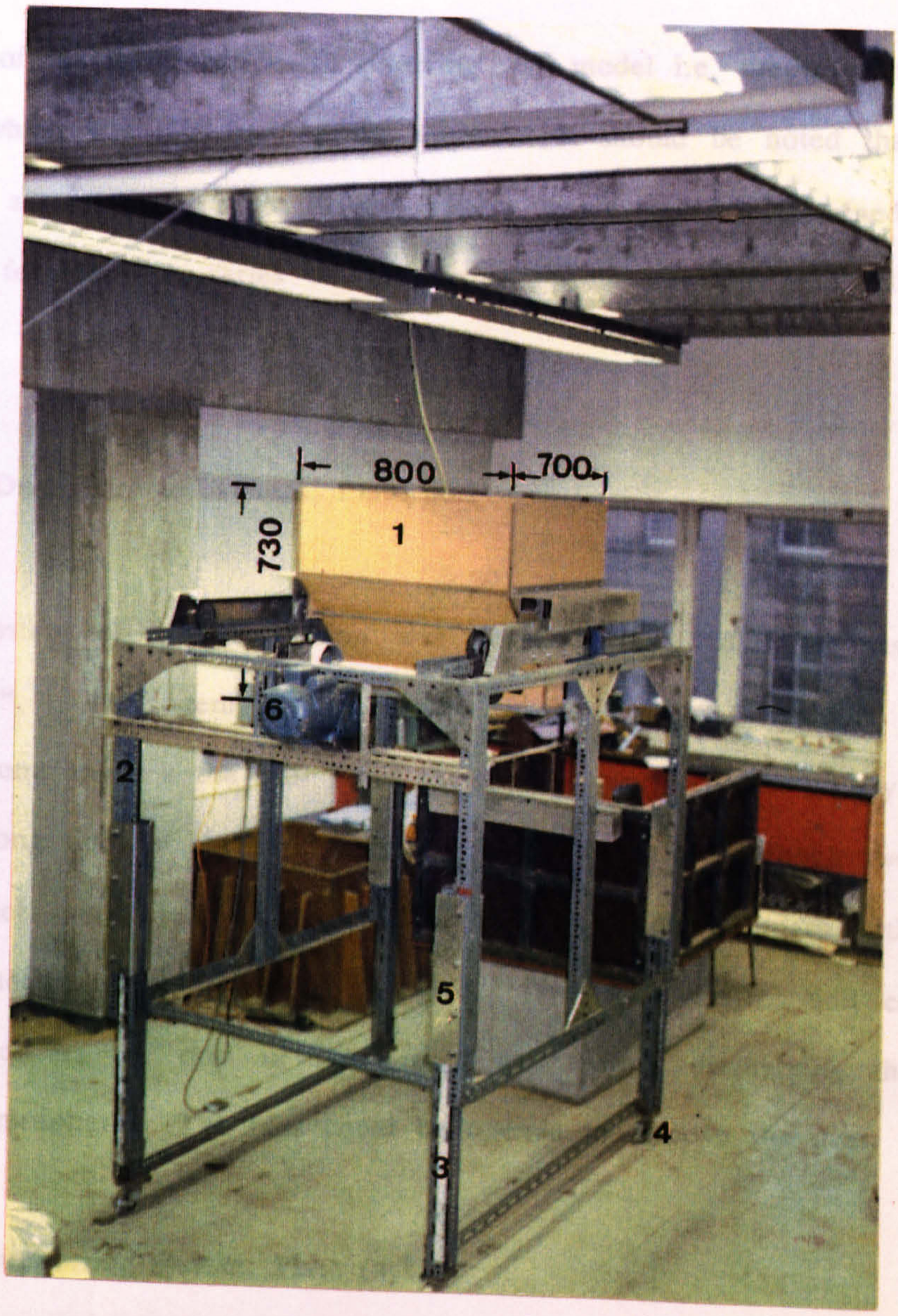

(1) SAND HOPPER.
(2) UPPER FRAME.
(3) LOWER FRAME.
(4) WHEEL WITH SWIVEL JOINTS.
(5) LONG CLAMP.
(6) ELECTRIC MOTOR

PLATE (4. 1) SAND SPREADER WITHOUT DUST EXTRACTOR AND PERSPEX CHAMBER.

back fill of the reinforced earth retaining wall model i.e. the travelling length was 1.0 m, which was modified by the author. It should be noted that the hopper traversed automatically by a driving system which will be explained later. The bed was formed in a series of thin layers by the rain of sand falling from the hopper.

(b) Dust extractor system: Plate (4.2)

A system of dust extraction was installed, the "DCE Unimaster controller type EC9". The system comprised two similar inverted aluminium hoppers with open bottoms to suck the dust from the sand raining process. They connected to the two long sides of the sand hopper. The dust passed through two long rubber hoses which were fixed at the top of the aluminium hoppers with their other ends connected to the dust control unit. The dust control unit consisted of a filter to collect the dust in two closed bins before discharging the air to the outside atmosphere. The bins could be opened to remove the dust.

(c) Supporting system: Plate (4.1)

The supporting system consisted of two main parts made of vertical and horizontal prefabricated angles and channels. The upper part was the frame which supported the sand hopper with the two connected aluminium hoppers. The lower part was the frame which supported the whole system. It was mounted on four wheels with swivel joints so that it could be moved easily. There were no obstructions such as diagonal members in the front side of the system.

The upper frame could be adjusted to maintain a constant height of fall of

(1) INVERTED ALUMINIUM HOPPER TO SUCK DUST.
(2) RUBBER HOSE CONNECTED TO CONTROL UNIT.
(3) CONTROL UNIT.
(4) PERSPEX CHAMBER.

PLATE (4.2) SAND SPREADER WITH DUST EXTRACTOR AND PERSPEX CHAMBER.

sand by means of four jacks, fixed at the upper parts of the four support pillars of the lower frame and connected to the lower part of the four vertical supporting members of the upper frame. By turning 4 nuts in the jacking systems inside the pillars of the lower frame, the upper frame could be adjusted to any required height. The upper frame was mounted to the lower frame by means of four long clamps fixed to the four vertical supporting members of the upper frame only.

(d) Perspex chamber: Plate (4.2)

Perspex sheets covered three sides of the supporting system and were connected to the upper frame. The front side was uncovered to give access to the model wall inside the chamber and install instrumentation devices. The reason for having this chamber was to avoid any air currents affecting the sand falling, as previously mentioned, and to increase the efficiency of the dust extractor system.

(e) Driven system: Plate (4.1)

As mentioned before the bed was formed in a series of thin layers by a rain of sand falling from a hopper which passed forwards and backwards for a travelling distance of 1.0 m over the reinforced earth retaining wall model. This was done using a driving system, which consisted of an electrical motor operating a driving gear. This driving gear rotated a shaft which extended the full width of the frame. A system of gears at both ends of the shaft was driven by the shaft and transmitted the motion to an endless chain connected to the hopper. During the movement of the endless chain it drove the hopper forward and backwards.

4.4.2 Calibration Of Sand Raining Device

In order to assess the reproducibility and repeatability of the density of the sand bed formed by the sand spreader in the model wall tests, it was necessary to calibrate it. As has been mentioned, the density of the bed depended on many factors and some of these factors were matched by modifying the sand spreader, and others such as intensity of deposition and height of sand falling were controlled. The intensity of fall of the sand was controlled by the aperture size of the perforated base plate of the sand hopper and the device had the facility to adjust the height of fall of the sand.

The total height of the sand bed in the model was 700 mm including 100 mm thickness of two sand layers acting as a soil foundation. According to the dimensions of the model and to ease the procedure during the test, the minimum height of drop of sand available was 600 mm.

Two different perforated base plates were used to form the bed in the wooden box as given in Sec. 4.4.1. The perforations were drilled on a 20 mm grid so that the sand would discharge uniformly in the box. After preliminary tests the size of perforations was chosen and the height of drop was set at 600 mm and each layer of sand bed had a thickness of 50 mm.

Two techniques have been used to measure the density of the deposit:

(a) Temporary metal cylinders (single cylinder).

(b) Permanent perspex cylinders (column of cylinders).

(a) Temporary metal cylinders (single cylinder)

In this method four hollow metal cylinders 100 mm diameter and 50 mm height were used with a knife edged upper rim to prevent bouncing of sand grains into them. Most previous researchers have used pots with a solid bottom such as Kolbusewski and Jones (1961); Walker and Whitaker (1967); and Butterfield and Andrawes (1970).

In the present research cling film was used as a base for the cylinders to decrease the effect of the solid bottom and take the same shape as the sand surface . The four cylinders were placed at four chosen locations within the reinforced earth layer. Two locations were near the wall face and the others near the rear of the reinforced mass. All four locations were far from the sides of the box to avoid their effect. The cylinders on a reinforced earth layer are shown in Plate (4.3).

After raining the sand, the excess sand was removed and the cylinders were carefully removed from the wooden box. The density of the sand was obtained by knowing the mass of the sand in the cylinders. The sand in each cylinder was put in its original position again. The same cylinders were replaced on the current surface.

The sand hopper was raised 50 mm to form a new sand layer in the wooden box, so that a constant height of drop could be maintained. The height of drop was taken as the vertical distance between the discharge plate to the mid–height of every layer produced. The procedure was repeated until the required depth of bed was achieved. Another perforated base plate was put on and the test procedures were repeated.

(b) Permanent perspex cylinders (column of cylinders)

(1) REINFORCED STRIP.
(2) SAND.
(3) METAL CYLINDER.
(4) PERMANENT PERSPEX CYLINDER.
(5) WOODEN BOX.

PLATE (4.3) TEMPORARY METAL CYLINDER.

These consisted of hollow perspex cylinders of dimensions 110 mm in diameter and 55 mm high, each one having two knife edges on the outer rims. The first cylinder was put on the surface of the bottom of wooden box. After raining the first layer of sand, an aluminium foil disc was placed on the top of the sand in the cylinder to separate the first and second layer. The second cylinder was fitted on top of the first by means of the interlocking lip. The sand hopper was raised 50 mm to correspond to the increase of depth of sand to maintain a constant height of fall of sand during formation of the bed. The steps were repeated up to the top layer of sand.

Finally the box was emptied very carefully until the column of cylinders was exposed. The sand was removed from the topmost cylinder of the column of cylinders – using a spoon– until the first aluminium foil appeared, thus allowing the density to be determined for the top layer. This procedure was then repeated to obtain the density of each layer of sand. The test was repeated using different perforated base plates for the sand hopper, Plate (4.4).

A comparison of the density measuring methods is shown in Fig. (4.3). For the same sand bed placement technique, the results show that in both loose and medium states, there is a difference between the two methods. Since the metal cylinders measure the density of each layer as it is placed, the results do not deviate appreciably from the average as placed value.

On the other hand, the column of perspex cylinders method measures the density of each layer after the whole bed has been formed and one would expect that a higher density would be measured due to the effect of laying down layers above a particular level.

(1) COLUMN OF PERSPEX CYLINDERS.
(2) SAND.

PLATE (4.4) PERMANENT PERSPEX CYLINDER.

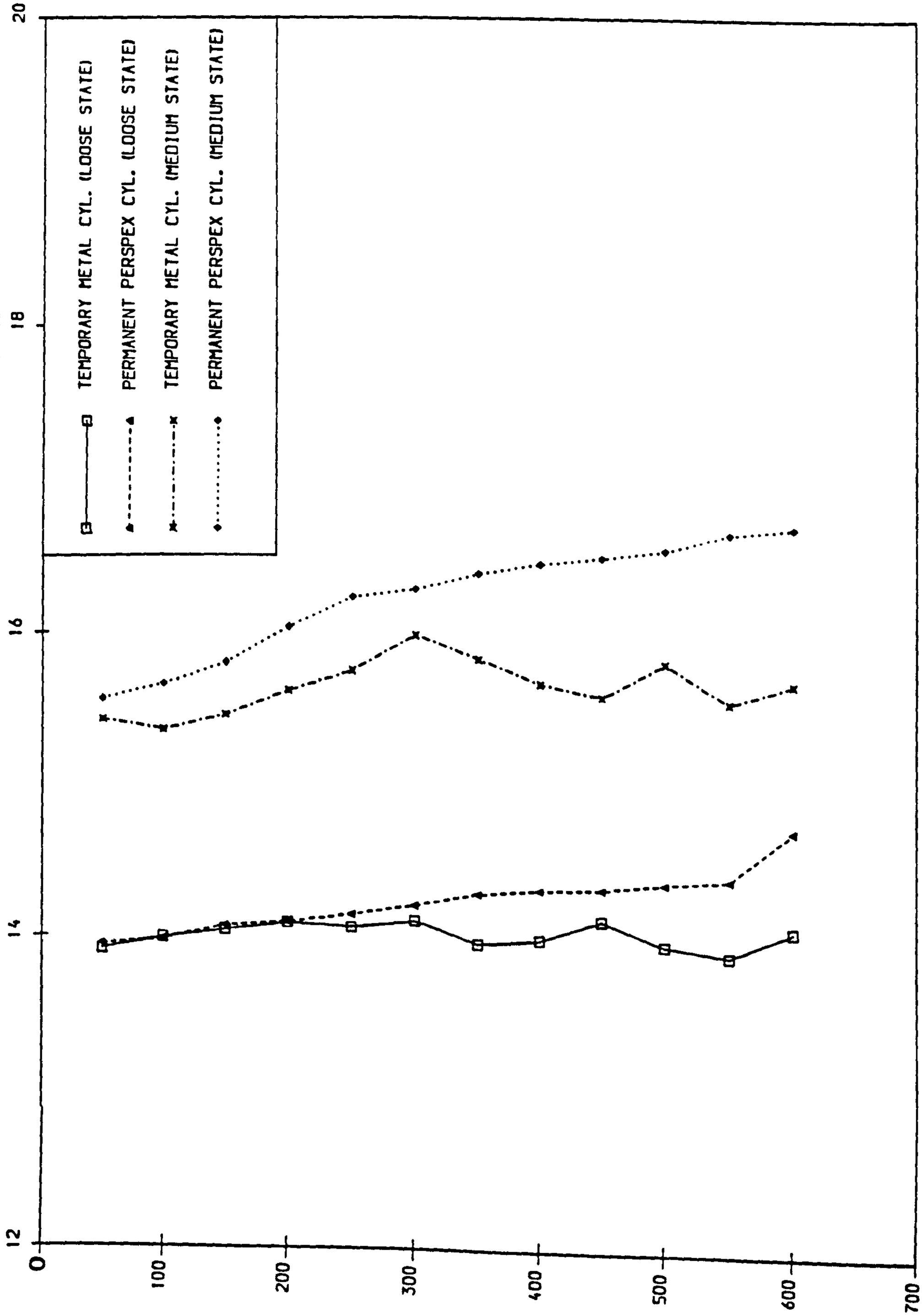

FIG. (4.3) MAX. AND MIN. DENSITY FROM SAND SPREADER.

This is seen to occur, and it is also obvious that the density is higher in the lower layers. In the other words the uniform sand bed is not really uniform but increases slightly in density from top to bottom.

In the column of cylinders method, perspex cylinders were used for ease of identifying the position of the aluminium foil discs, so that removal of sand was made easier. They required a reasonable wall thickness because the cylinders were to be stacked to the thickness of the complete bed and had to be stable. The column of cylinders method is thought to be more accurate than the single cylinders method.

4.4.3 Vibratory compaction

Winterkorn and Fang (1975) stated that cohesionless soils are relatively pervious even when compacted. They are not affected significantly by their water content during the compaction process. The dry density is high when the soil is completely dry or completely saturated, on the other hand lower densities occur when the soil has an intermediate amount of water. The explanation for this involves the phenomenon of bulking in sands where small capillary stresses in the partly saturated soil tend to resist the compactive effort. This bulking phenomenon is not present in completely dry sand and disappears when moist sand is saturated. For this reason the method of achieving maximum density employed in this research used vibratory compaction in dry sand as will be seen later.

In the field a vibratory roller or a plate compactor is often used to compact granular soil. An apparatus was developed for the present research in order to compact the sand beds after deposition to a high relative density. The

compaction was done from the rear of the reinforced mass towards the wall face as happens in the field.

(a) Vibratory compaction apparatus

The apparatus used in the reinforced earth retaining wall model to compact the sand backfill simulated the compaction plant in the field. As previously mentioned, cohesionless soil like sand is compacted by plant which produces vertical vibrations such as vibratory roller or vibratory compactor. D'Appolonia et al. (1969) mentioned that sand compaction by vibration is more efficient than compaction by static rolling.

(b) Plant simulation

The idea was to develop an apparatus which could produce vertical vibration continuously, was suitable for the dimensions of the model and would take into consideration the factors which influence the results of vibratory compaction.

The apparatus consisted of two identical vibrators wired so that they could contra–rotate, as shown in Fig. (4.4). The basic idea was that during the rotation, the horizontal components (F_H) of the centrifugal forces developed by the contra–rotating eccentric weights would be equal and opposite, and therefore cancel each other, whilst the vertical components (F_V) combine, thus setting up an alternating linear vibration in the vertical plane with a value of $2F_V$, which reaches a maximum value of $2F_C$.

Linear vibration could therefore be obtained continuously during the rotation of the two vibrators. The two vibrators were identical and were fixed to a stiff

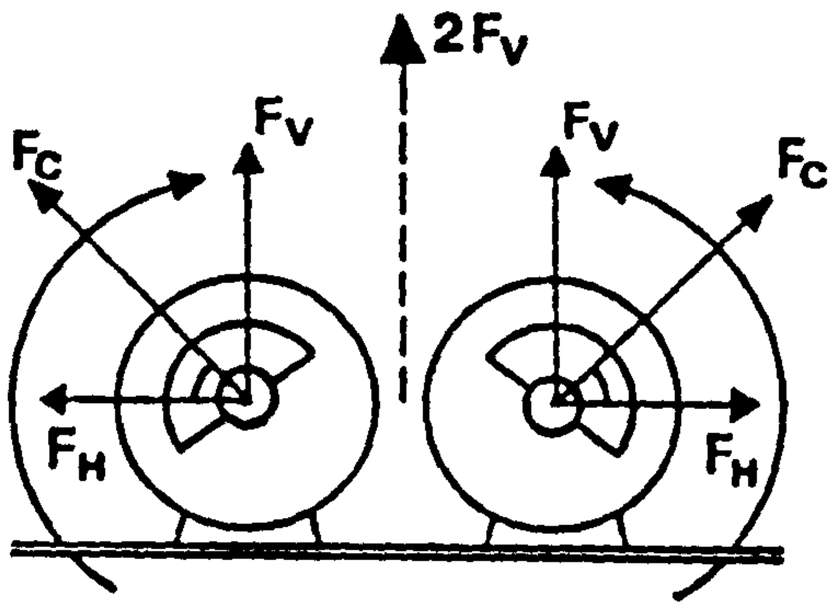

FC = CENTRIFUGAL FORCE
FV = VERTICAL COMPONENT OF FC
FH = HORIZONTAL COMPONENT OF FC
W = ECCENTRIC WEIGHT

FIG. (4.4) BASIC IDEA OF COMPACTION APPARATUS USED IN THE MODEL.

base plate to make sure that they worked properly as required.

(c) Factors affect the vibratory compaction

Terzaghi and Peck (1948); Bernhard (1952); and Converse (1953) generally recommended that a vibratory roller should be operated at the resonant frequency, that is the frequency which produces the maximum vertical displacement of the drum. More recent research by Lewis (1961); Forssblad (1965); and D'Appolonia et al. (1969) recommended that the roller operating frequency should be at least as large as the resonant frequency to obtain the most efficient use of the roller.

Subbarao (1977) carried out tests on vibratory densification of sand and his results implied that frequency has a great influence in the range (25−30) HZ.. Michalski et al. (1986) mentioned the importance of frequency on the efficiency of compaction and density.

Earlier, Terzaghi (1942) stated that the natural frequency of a vibrator with a given weight and a given base area is directly related to the elastic properties of the subgrade between (24.1–26.7) HZ..

Lamb and Whitman (1979) illustrated that a peak density was attained when the acceleration reached 2g when densification of sand was made by vibration, where g is gravity acceleration.

Subbarao (1977) suggested that the maximum density of sand by vibration reaches a high value for acceleration between 1.2g and 2g. Further increase in the acceleration results in insignificant change in maximum density.

The properties of the sand material and thickness of layer being compacted have an influence upon the compaction of sand. D'Appolonia et al. (1969) concluded that the lift height selected should be small enough so that a loose layer is not trapped near the interface between lifts.

Michalski et al. (1986) mentioned that the mass of the roller is of less importance but it is more economical to apply lighter rollers producing higher accelerations and frequencies and to compact thinner layers.

All of the above factors have an influence, to some degree, upon the compaction of sand. The conclusions from these are summarized as follow:

(i) The technical characteristics of the compactor i.e.

- Frequency of the vibration (25– 30) HZ
- Acceleration (1.2– 2) g
- Weight (light)

(ii) Properties of the sand

- Grain size distribution
- Moisture content (dry)
- Thickness of layer being compacted (the thinner the better)

The above factors had been taken into consideration, particularly the technical characteristics of the compactor.

(d) Components of vibratory compaction apparatus

The apparatus employed in the research , Plate (4.5), consisted of:

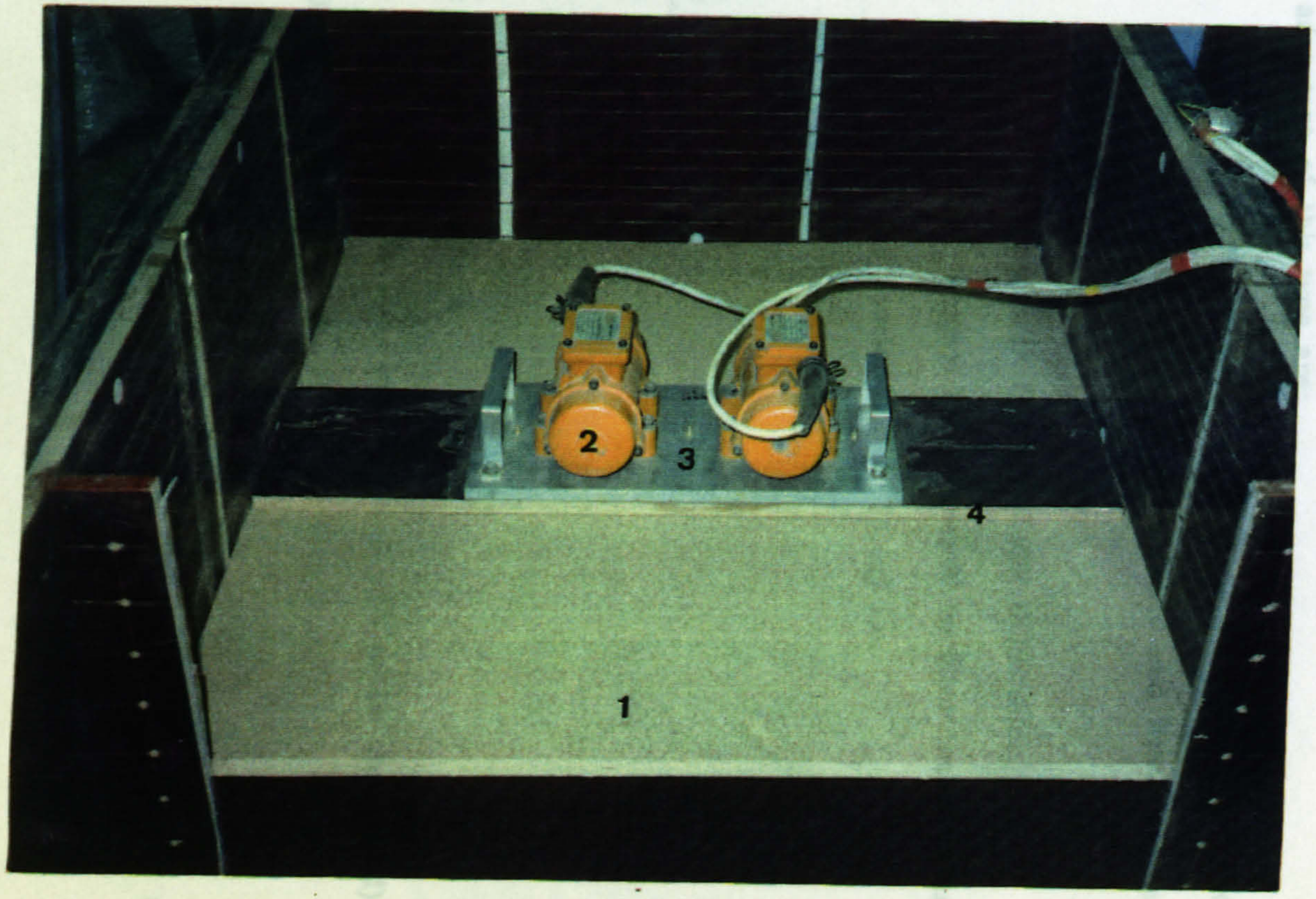

(1) SAND.
(2) VIBRATOR.
(3) METAL BASE.
(4) WOODEN BASE.

PLATE (4.5) VIBRATORY COMPACTION APPARATUS USED IN MODEL TESTS.

(i) Two electrical vibrators.

(ii) Base plates.

(iii) Electrical connection.

(i) Vibrators

Two electrical identical base mounted vibrators of type MVSI 15/35 −1500 r.p.m, Vibtec, U.K., were used in the apparatus, the motor being an asynchronous type with short circuit die−cast aluminium rotor. The natural frequency of each one was 25 HZ., and the parts of one of the vibrators are shown in Fig. (4.5).

The advantage of this type are:

- It has the same natural frequency as the sand in the model tests.
- It has both ends of the shaft extended and fitted with eccentric weights.
- Its size is convenient for the model dimensions.
- The eccentric weights are adjustable to alter the centrifugal force to control the acceleration to (1.5g) i.e.

$$\frac{F_c}{W} = 1.5 \qquad (4.1)$$

Where,

F_c is the centrifugal force

W is total weight (vibrators, base plates & soil to be compacted)

(ii) Base plates

The base plates consisted of two stiff plates. The first was aluminium of

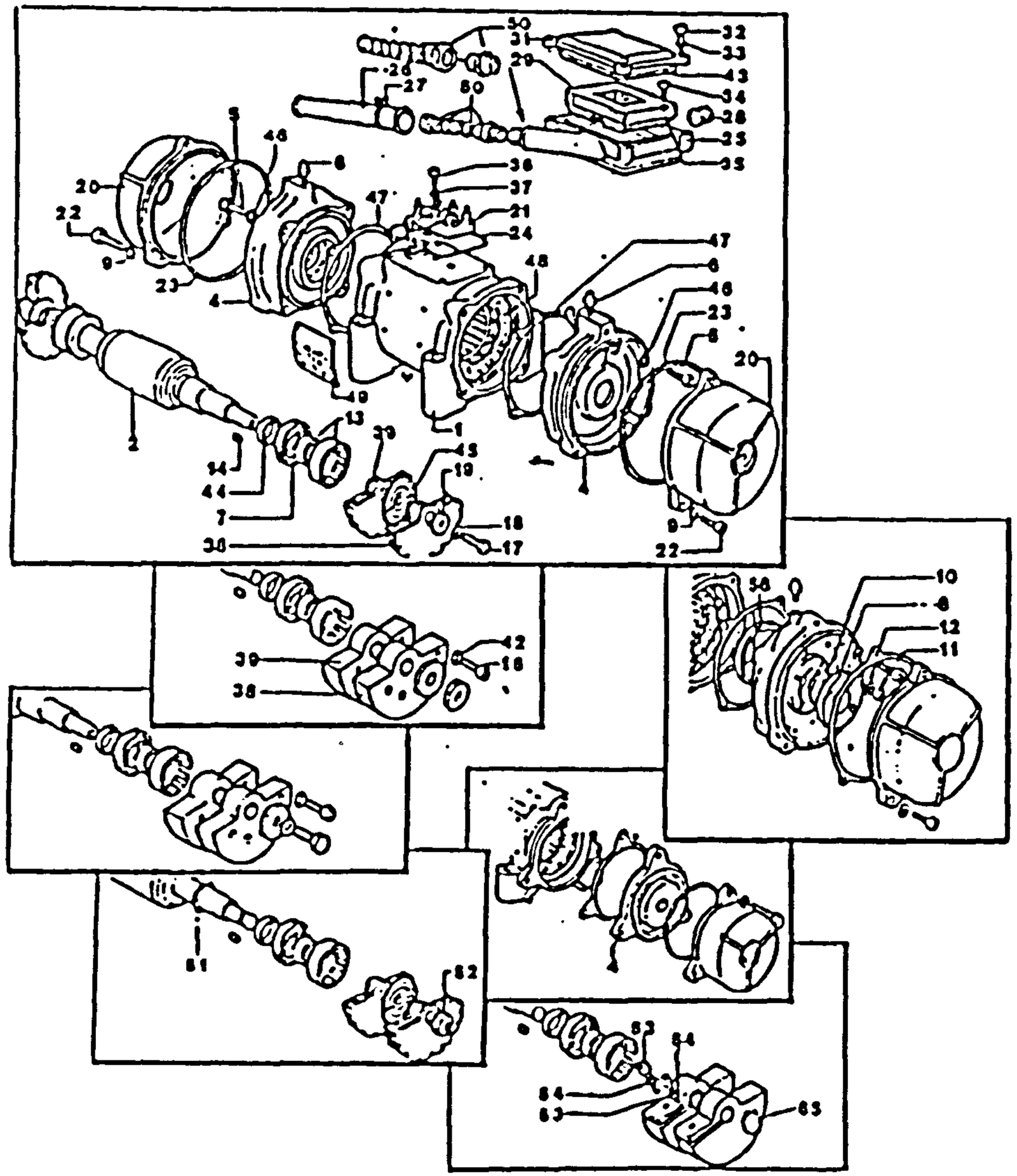

FIG. (4.5) COMPONENT PARTS OF THE VIBRATOR.

REF	DESCRIPTION	•
1	CASING	1
2	COMPLETE SHAFT	
4	FLANGE	
5	SCREW	
6	GREASE NIPPLE	
7	CUP-SHAPED SEAL RING	
8	BEARING CAP	
9	WASHER SPRING	
10	INTERNAL STOP RING	
11	SCREW	
12	WASHER SPRING	
13	ROLLER BEARING	2
14	KEY	
16	SCREW	
17	SCREW.	
18	WASHER SPRING	
19	SPECIAL WASHER	
20	END COVER	
21	TERMINAL BOARD	1
22	SCREW	
23	GASKET	2
24	GASKET	
25	TERMINAL BOX	1
26	VIBRATION DAMPING SPIRAL	
27	CLIP	
28	SCREW PLUG	
29	SMALL RUBBER BLOCK	2
31	COVER FOR TERMINAL BOX	1
32	SCREW	4
33	WASHER SPRING	
34	SCREW	
35	WASHER SPRING	
36	SCREW	
37	WASHER SPRING	
38	ADJUSTABLE WEIGHT	
39	FIXED WEIGHT	
42	WASHER SPRING	
43	GASKET	1
44	RING	
45	WEIGHTS ADJUSTING DISC	
46	WASHER SPRING	
47	GASKET	
48	WOUND STATOR	1
49	NAME PLATE	
50	CABLE GRIP	1
51	OUTER STOP RING	
52	SELF-LOCKING RING NUT	
53	SCREW	
54	WASHER SCHNORR	
55	OUTER STOP RING	
56	RING FOR CUP-SHAPED SEAL RING	

dimensions 450 x 200 x 5 mm to which the two vibrators were rigidly fastened according to the instruction of the manufacturer. It had two handles for ease of carrying. A wooden plate of dimensions 898 x 200 x 18 mm was fixed firmly to the metal plate. The system with this construction allowed the possibility of compacting a layer of sand of area 450 x 200 for preliminary studies and also a layer of 900 x 200 mm in the model test. On the other hand vibration could be spread over a greater area than provided by their bases, Plate (4.5).

The total weight of the system is 11.7 kg.

The total weight less the wooden plate is 11.0 kg.

(iii) Electrical connection

A special arrangement was made to connect the two vibrators to a 3 phase, 400 V, 50 HZ supply.

(e) Adjusting the eccentric weights

As mentioned before, the vibrators had the facility to adjust the eccentric weights to obtain the required centrifugal force (F_c) and hence obtain peak vibration amplitude and the required acceleration.

Each vibrator was capable of producing a wide range of centrifugal force. The method of design of the vibratory compaction apparatus is illustrated in Appendix (A).

4.4.4 Calibration Of Compaction Device

The compaction device was used since the sand spreader gave a limited

range of densities and the research required higher densities, which could be achieved by vibratory compaction to simulate also what occurs in the field. Calibration was done to assess the reproducibility and repeatability of the density of sand bed using vibratory compaction, and to ensure that the maximum density required could be achieved. Four factors have to be considered:

(a) To ensure the identicality of the two vibrators.

(b) Time factor.

(c) Number of lifts.

(d) Thickness of lift.

The first point was to make sure that the two vibrators were identical. This is very important to give equal centrifugal force with vertical vibration only without any disturbances. This can be guaranteed by ensuring that the two vibrators are in phase, and for this vibrator monitoring equipment was used. The two vibrators with the aluminium base plate were connected to the monitoring equipment through three accelerometers fixed at the middle and two edges of the base plate on one line at the center and parallel to a long side. The connection and layout of the equipment is shown in Fig. (4.6). From the vibrations recorded by the equipment at the three points, as shown in Fig. (4.7), it is obvious that the two vibrators are in phase.

For the other three factors, calibration was made using a small wooden box 455 x 205 x 150 mm as well as the actual box used in the model tests.

In the small box the sand was spread by hand and compacted by the compaction device with the aluminium base plate only. The density was obtained after compacting each layer by determining the thickness of the compacted sand

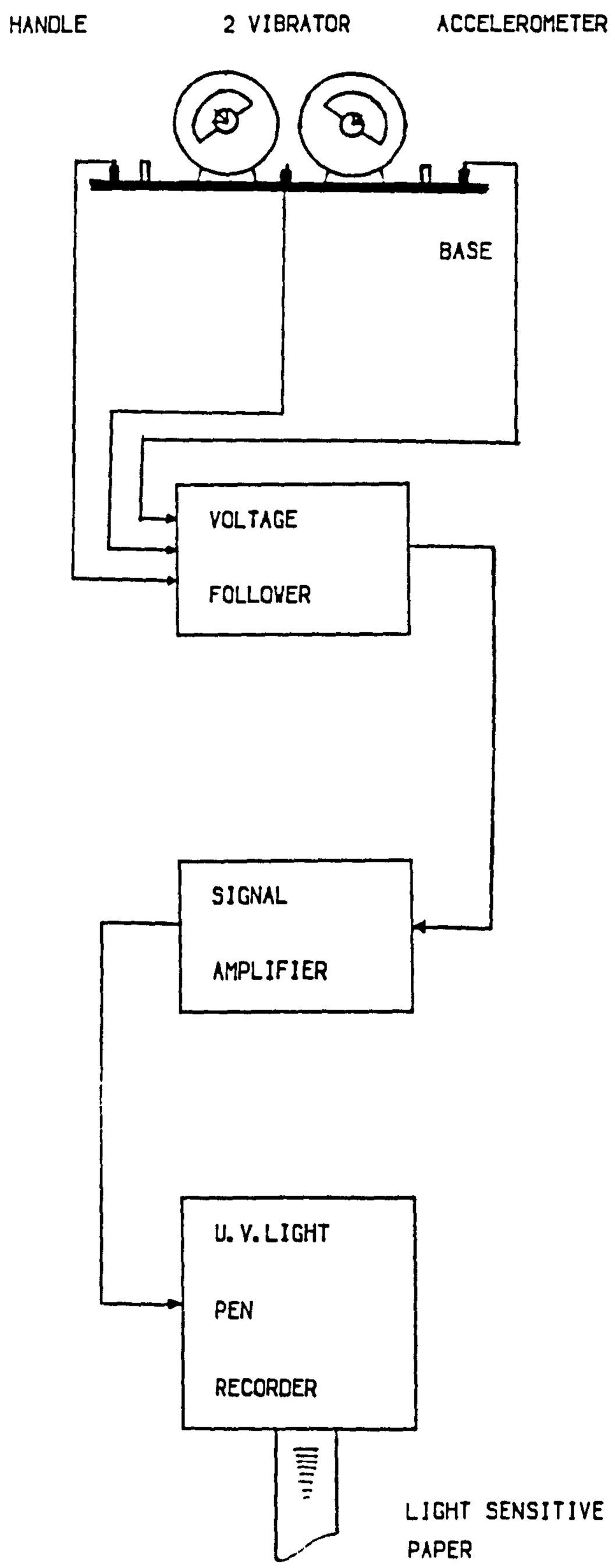

FIG. (4.6) VIBRATOR MONITORING EQUIPMENT.

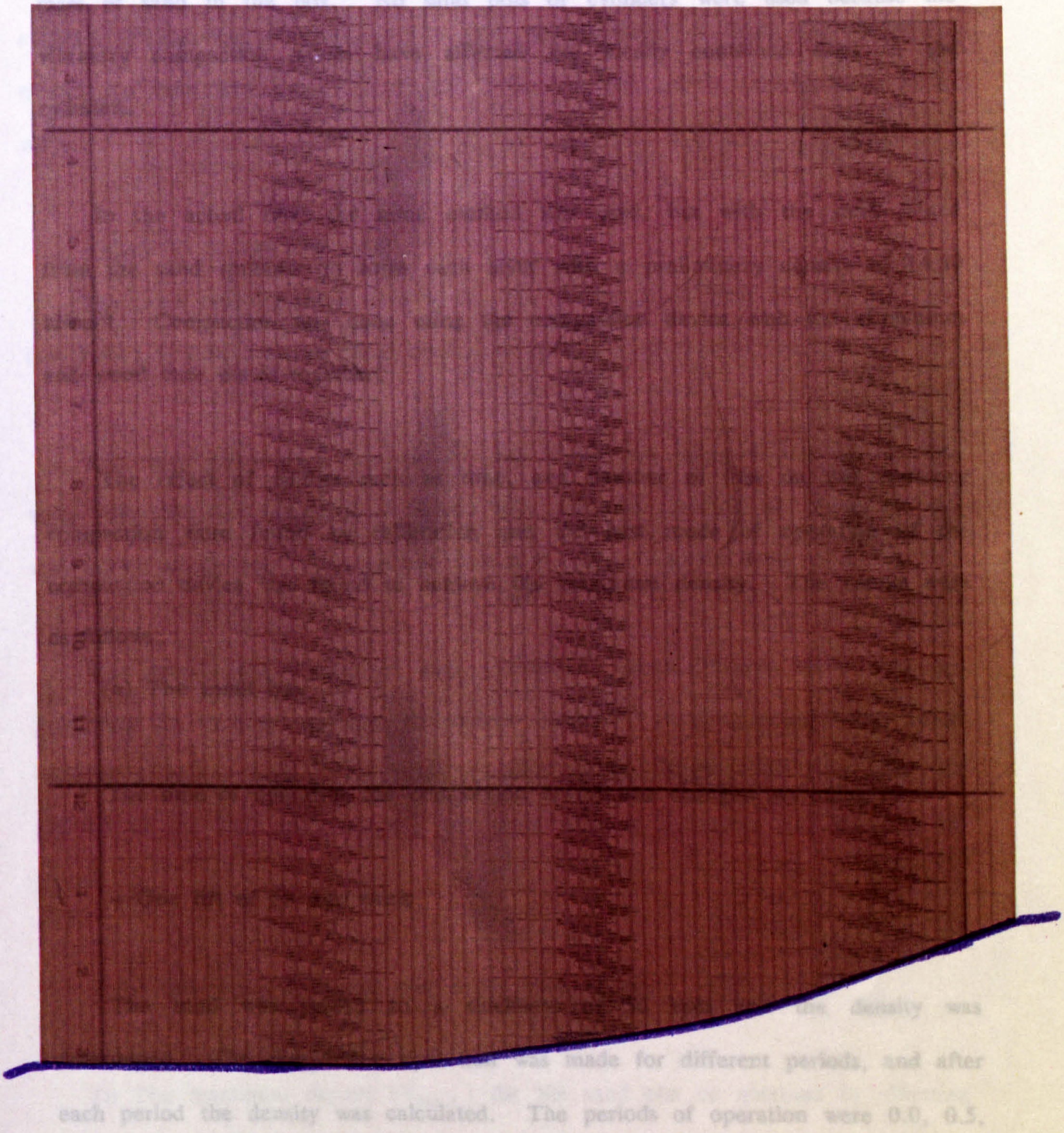

FIG. (4.7) OUTPUT READINGS OF THE VIBRATIONS FOR THE TWO VIBRATORS.

in the box, taking measurements from a datum surface on the top plane of the box to the sand surface at several points, and equating the volume to the total mass of sand in the box. No sand pots or cylinders were used because the vibratory compaction would have affected the locally contained sand in the cylinders.

In the actual box, the same method was used, but with the sand rained from the sand spreader to form each layer with a preliminary density of 14.39 kN/m^3. Compaction was done using the compaction device with the aluminium and wood base plates together.

The effect of factors such as time, and number of lifts on the vibratory compaction were found by calibration and the best mode of operation of the compaction device was found to achieve the maximum density. The results were as follows:

(a) The small box

The time of operating the compaction device was changed according to:

– One lift of 50 mm thick

The sand was spread to a thickness of 50 mm and the density was determined. The compaction operation was made for different periods, and after each period the density was calculated. The periods of operation were 0.0, 0.5, 1.0, 2.0, 3.0, 4.0, 5.0, 10.0 & 15.0 mins..

– Three lifts of 50 mm each

The sand was spread to a thickness of 50 mm and the density was

determined. The first layer was compacted to time (t_1) and the density was calculated. The second layer was spread on the first layer and compacted for the same time (t_1). The same procedure was used for the third layer and the average density was obtained. The test was repeated 8 times for different compaction operation times (t) of 2.0, 4.0, 6.0, 8.0, 10.0, 12,0,14.0, & 16.0 mins..

– One lift of 100 mm thick

The same procedure was used as for the 50 mm thick layer but for times of 0.5, 1.0, 1.5, 2.0, 2.5, 4.0, 10.0 mins..

The same steps were repeated for the actual box using 4 lifts of 50 mm each with the test repeated 4 times with different periods of operating the compaction equipment. The periods were 1.0, 2.0, 4.0 & 8.0 mins..

The results are shown in Fig. (4.8&9). These Figures show that by increasing the time of vibration the density increases, reaching a maximum value between 4 and 5 mins.. A higher density can be obtained by decreasing the number of the lifts while keeping the same time of operation and thickness of layer.

From the above discussion two points were raised:

(i) The maximum density ($\Upsilon_{max.}$) for the sand can be obtained by vibrating the sand in the small container. In this research $\Upsilon_{max.}$ was 18.98 kN/m^3 using this method.

(ii) It was decided to fix the time of compaction to 4.5 mins and the

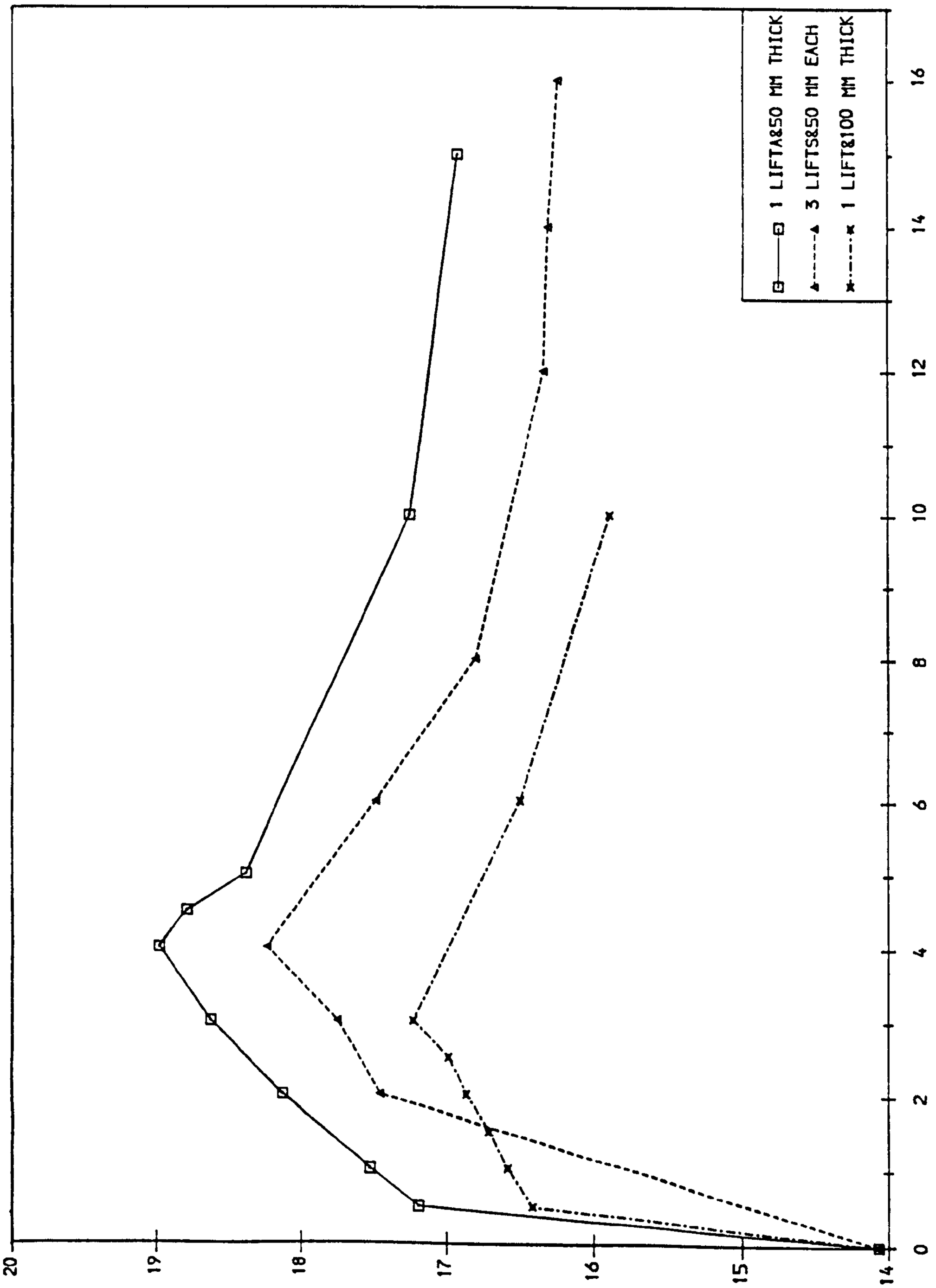

FIG. (4.8) TIME-DENSITY CONTROL BY COMPACTION (BOX 455X210X150 MM).

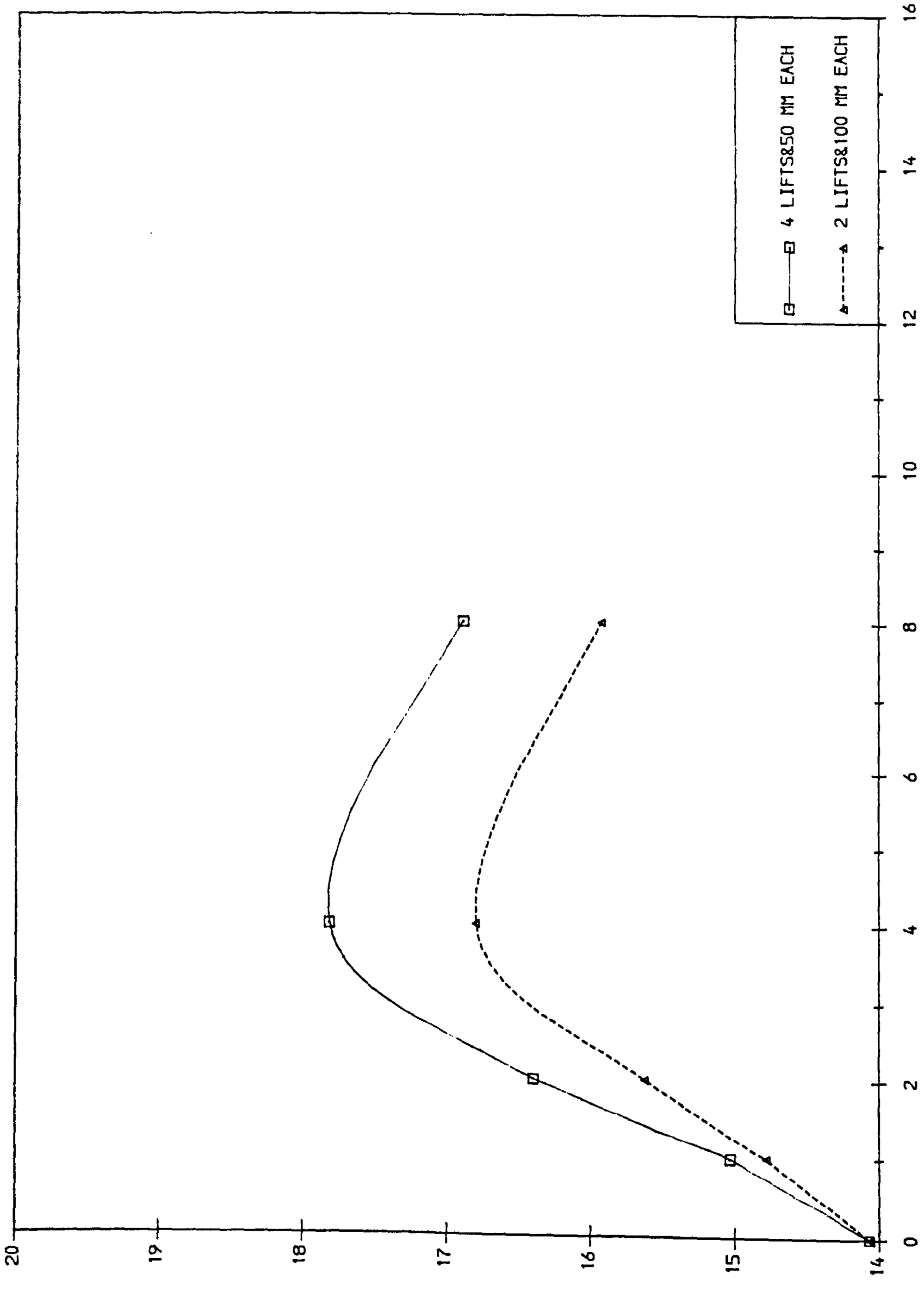

FIG. (4. 9) TIME-DENSITY CONTROL BY COMPACTION (ACTUAL MODEL).

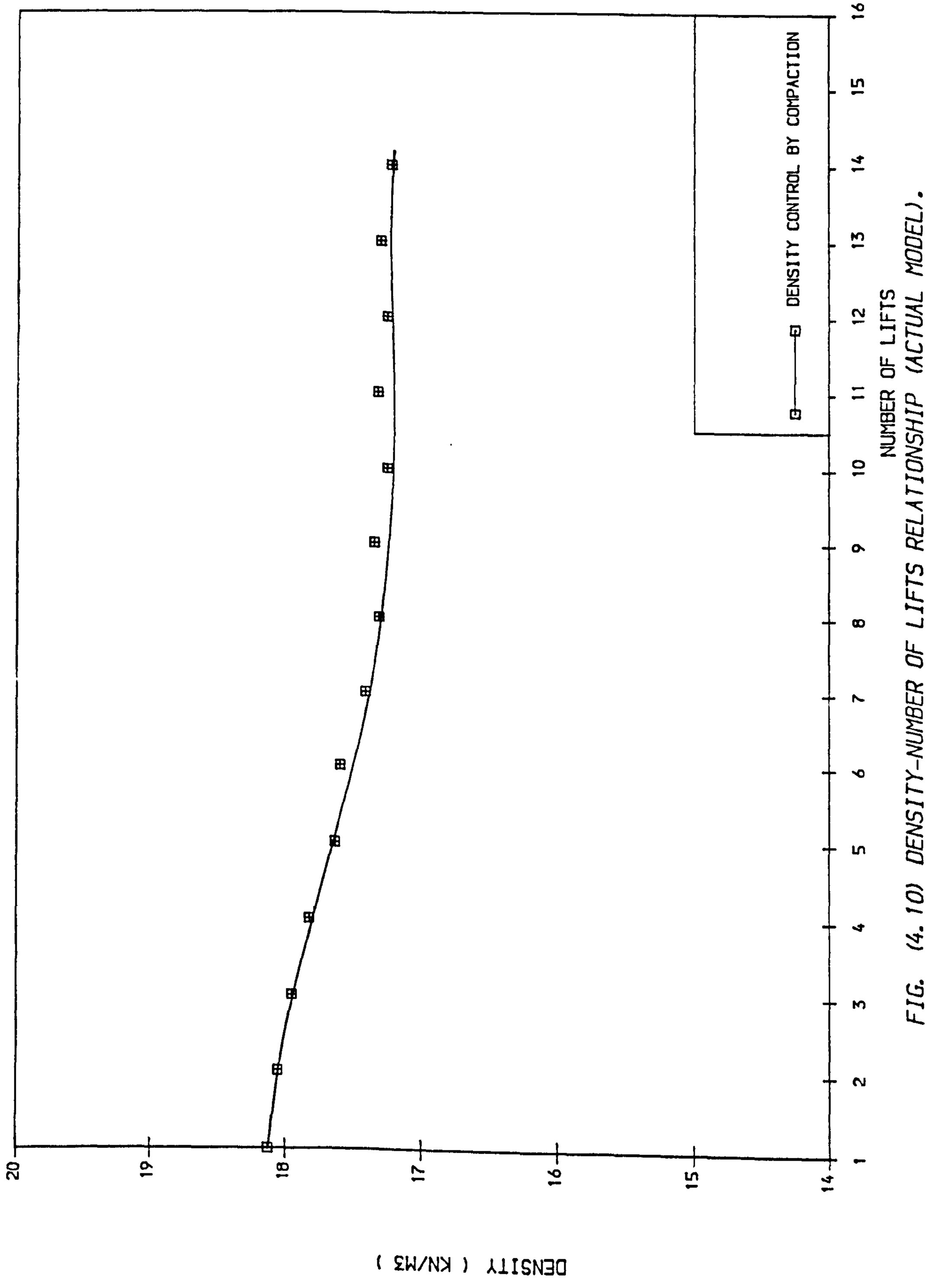

FIG. (4. 10) DENSITY-NUMBER OF LIFTS RELATIONSHIP (ACTUAL MODEL).

sandy soil in the field.

When the density of individual layers in a sand bed, produced by the raining technique, was measured by means of the single cylinders method, the measured densities of each layer were reasonably constant with depth and lay close to an average value for loose of 14.11 and for medium of 15.68 kN/m^3.

When the composite cylinder was used, the density of the layers increased approximately linearly with depth, the increase being from 13.95 to 14.45 kN/m^3 for loose sand, and from 15.55 to 16.75 kN/m^3 for medium sand bed, and the average values were 14.39 & 15.96 kN/m^3 respectively. The composite cylinders were thought to provide a more realistic answer than the single cylinders method.

Vibratory compaction is recommended when maximum dry density is required. The density is influenced by the time of vibration, thickness of lift, and number of lifts.

CHAPTER 5

RESULTS AND DISCUSSION OF MODEL TESTS

5.1 INTRODUCTION

This chapter shows the results obtained from the various models of reinforced earth wall carried out in the laboratory, as discussed in Chapter 3. The results are presented in four sections as follows:

(1) Determination of reproducibility and repeatability of the results.

(2) The effect of compaction on the behaviour of the reinforced earth wall.

(3) The effect of compaction length on the behaviour of the reinforced earth wall.

(4) The effect of methods of construction on the behaviour of the reinforced earth wall.

The conclusion of this study is presented at the end of the chapter. The key figure of the different components of the model reinforced earth wall is shown in Fig. (5.1)

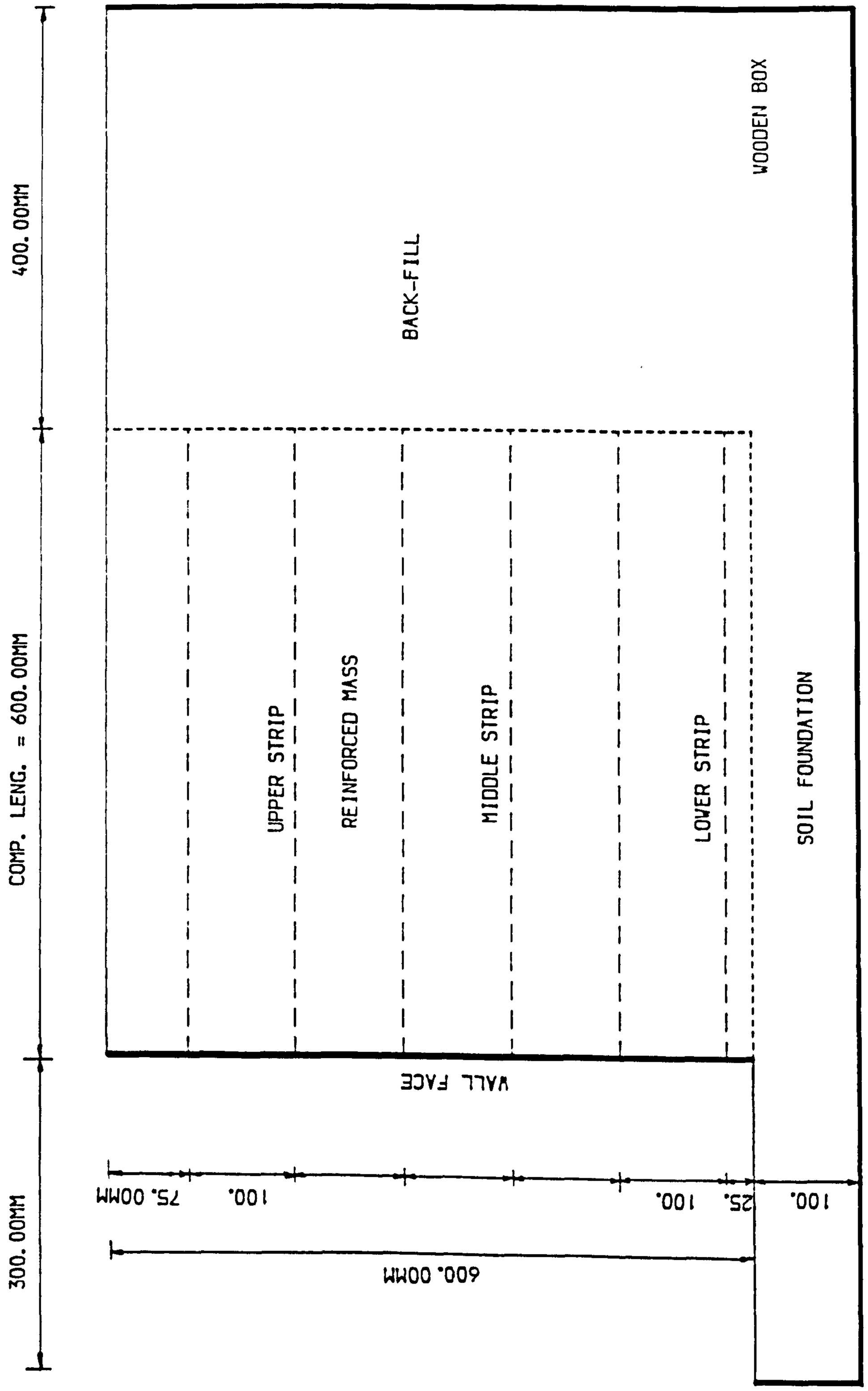

FIG.(5.1) THE MODEL REINFORCED EARTH WALL

5.2 DETERMINATION OF REPRODUCIBILITY AND REPEATABILITY OF THE RESULTS

The reproducibility and repeatability of the readings from the different instruments were obtained from tests CAT. I–9 & 10.

5.2.1 Pressure Cell Readings

(a) Vertical cells

These cells measured the horizontal pressure on the wall face and behind the reinforced mass. Tables (5.1&2) show the readings from the vertical cells in the case of no compaction and compaction respectively. The tests were repeated three times.

It is seen from the tables, that the readings in the upper and lower portions are quite close to each other, although in the middle of the wall they are not very near but are still reasonable.

(b) Horizontal cells

Horizontal cells were installed to measure the vertical pressure under the reinforced mass or at different locations in the backfill. The readings from the horizontal cells under the reinforced mass to get the vertical stress distribution are shown in Tables (5.3&4) for no compaction and compaction cases respectively. It is seen from the tables that the difference in readings is reasonable.

TABLE (5.1) VERTICAL CELLS OUTPUT READINGS,NO COMP., CAT. I-9.

VERTICAL CELL No.	OUTPUT READINGS (N/cm²)		
	FIRST TIME	SECOND TIME	THIRD TIME
1	00.2095	00.2179	00.2011
7	00.1426	00.1369	00.1483
11	00.0720	00.0691	00.0788
15	00.0479	00.0498	00.0460

TABLE (5.2) VERTICAL CELLS OUTPUT READINGS, WITH COMP., CAT. I-10.

VERTICAL CELL No.	OUTPUT READINGS (N/cm²)		
	FIRST TIME	SECOND TIME	THIRD TIME
1	00.3019	00.2944	00.3125
7	00.1823	00.1887	00.1759
11	00.1725	00.1785	00.1673
15	00.2203	00.2148	00.2280

TABLE (5.3) HORIZONTAL CELLS OUTPUT READINGS,NO COMP., CAT. I-9.

HORIZONTAL CELL No.	OUTPUT READINGS (kN/m²)		
	FIRST TIME	SECOND TIME	THIRD TIME
2	9.1042	8.8766	9.3318
3	8.3350	8.5434	8.1266
4	7.9650	7.7659	8.1641
5	7.5400	7.7659	7.3515

TABLE (5.4) HORIZONTAL CELLS OUTPOUT READINGS, WITH COMP., CAT. I-10

HORIZONTAL CELL No.	OUTPUT READINGS (kN/m²)		
	FIRST TIME	SECOND TIME	THIRD TIME
2	17.7250	18.4340	17.0161
3	14.9340	15.5314	14.3366
4	13.0050	12.4848	13.5252
5	12.2270	11.7379	12.7161

5.2.2 Strain Gauge Readings

The strain gauges were bonded on the reinforcing strips to find the strains in the strips and hence the distribution of forces in the reinforcement, and the readings from the strain gauges are shown in Figs. (5.2&3) for the cases of no compaction and compaction respectively. The difference in readings was quite reasonable.

5.2.3 LVDT Readings

The readings from LVDTs to measure the lateral movement of the wall are shown in Tables (5.5&6) for the cases of no compaction and compaction respectively. The difference in the readings was reasonable.

From the above tests in CAT. I, the difference in the readings from the different instruments were within an acceptable range.

5.3 EFFECT OF COMPACTION ON THE BEHAVIOUR OF THE WALL

The effect of compaction on the behaviour of the reinforced earth wall can be seen in the individual components of the wall as well as the wall as one unit. The influence of compaction will be shown on the density of backfill, forces in the strips, and wall face as well as the deformation of the wall, and vertical and horizontal stresses behind and under the reinforced mass.

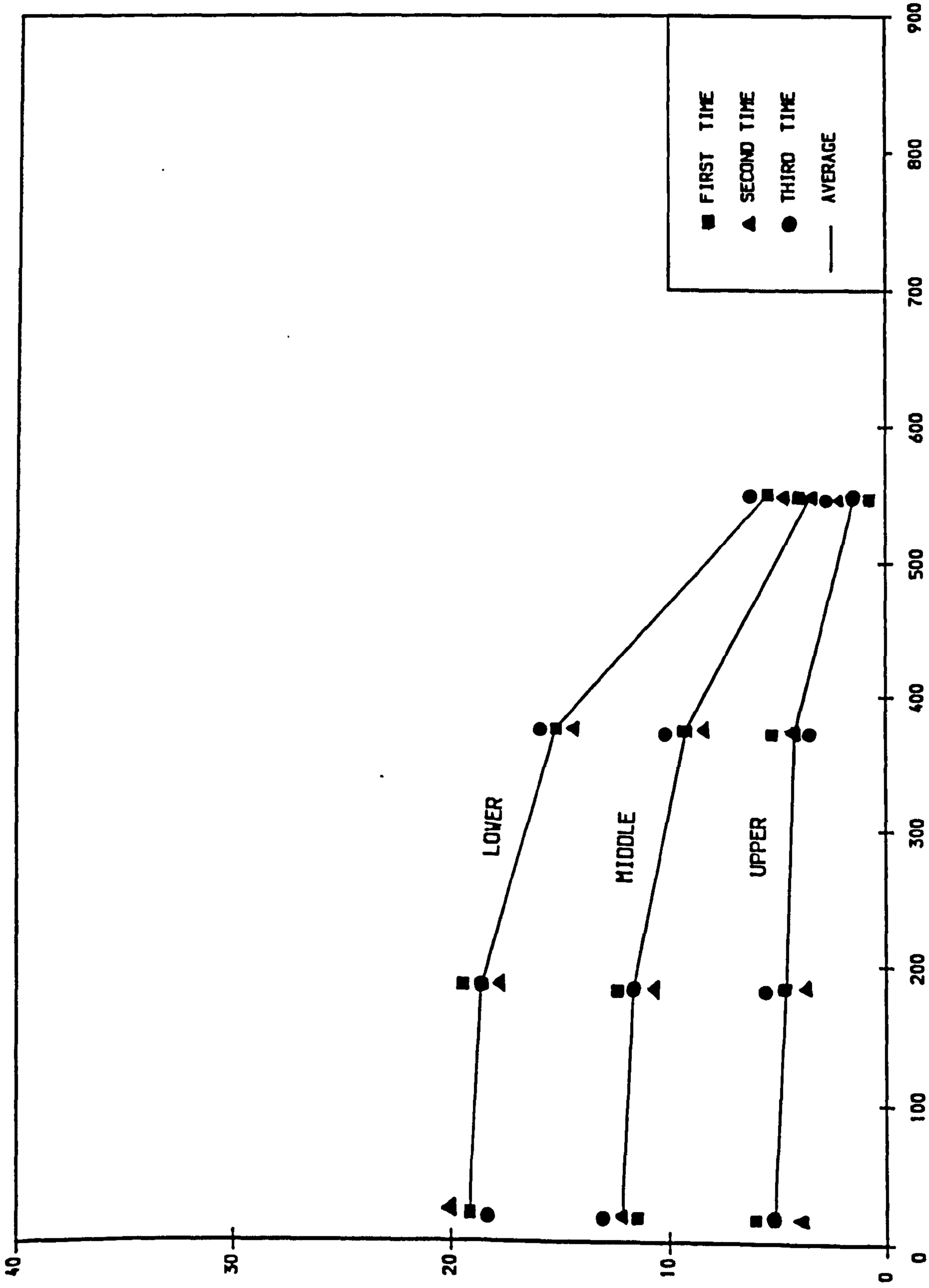

FIG. (5.2) DISTRIBUTION OF TENSILE FORCE IN LOWER, MIDDLE & UPPER STRIP, WITHOUT COMPACTION, CAT. I-9 (REPEATED 3 TIMES).

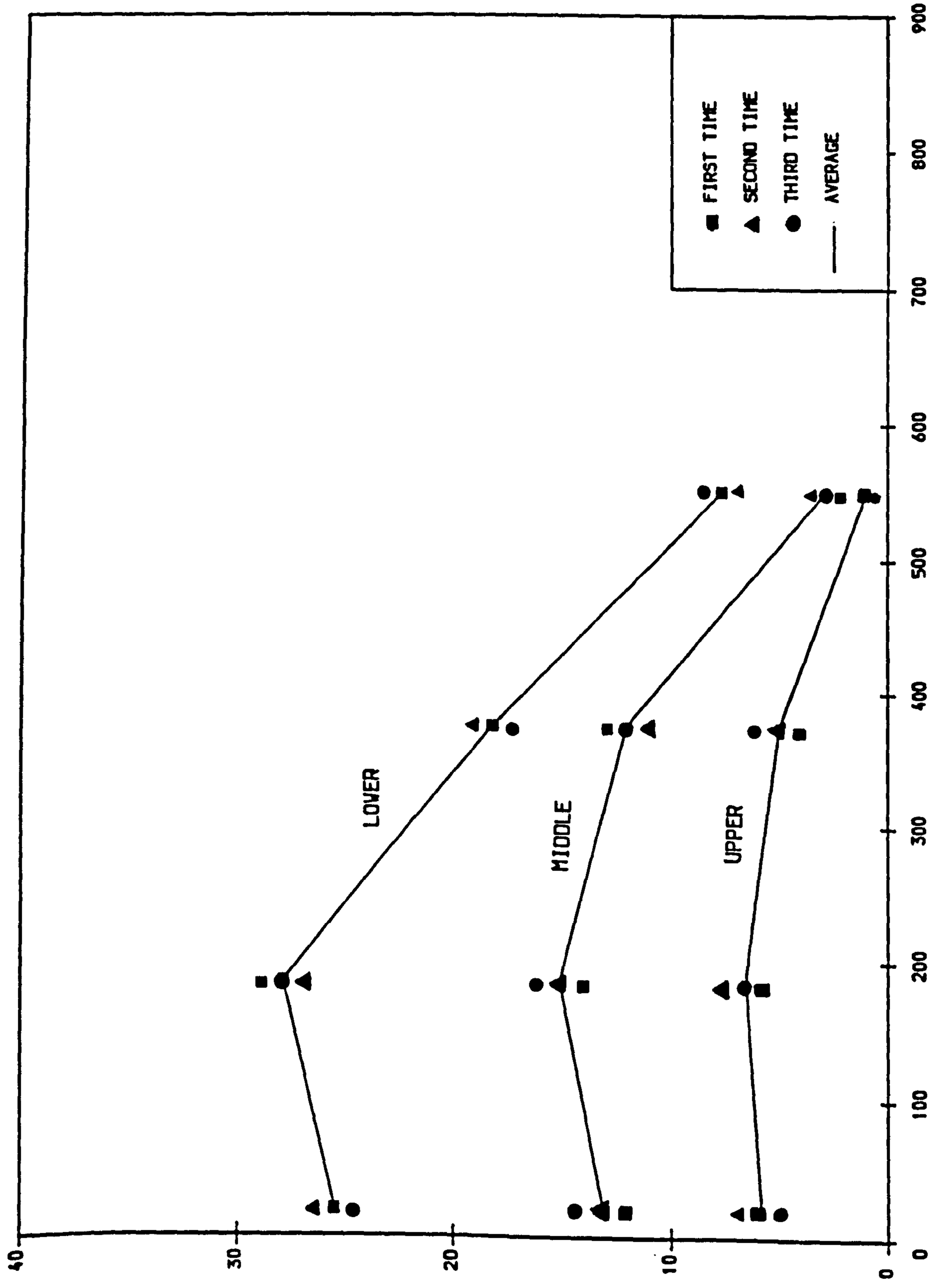

FIG. (5.3) DISTRIBUTION OF TENSILE FORCE IN LOWER, MIDDLE & UPPER STRIP, WITH COMP. LENG. = 600.0 MM, CAT. I-10 (REPEATED 3 TIMES).

TABLE (5.5) LVDTs OUTPUT READINGS,NO COMP., CAT. I-9.

LVDTs No.	OUTPUT READINGS (mm)		
	FIRST TIME	SECOND TIME	THIRD TIME
1	00.4253	00.4125	00.4381
2	00.6854	00.6648	00.7060
3	00.8055	00.8297	00.7813
4	00.9056	00.8784	00.9328
5	00.9473	00.9189	00.9757
6	00.9626	00.9915	00.9337
7	00.9442	00.9159	00.9725
8	00.9314	00.9593	00.9035

TABLE (5.6) LVDTs OUTPUT READINGS, WITH COMP., CAT. I-10.

LVDTs No.	OUTPUT READINGS (mm)		
	FIRST TIME	SECOND TIME	THIRD TIME
1	00.3253	00.3416	00.3090
2	00.5254	00.4991	00.5517
3	00.5755	00.6043	00.5867
4	00.7256	00.6893	00.7619
5	00.7543	00.7920	00.7166
6	00.7666	00.7283	00.8049
7	00.6752	00.7090	00.6414
8	00.4254	00.4041	00.4467

5.3.1 Density of backfill

One of the aims of compaction is to prevent settlement of the backfill. Since the backfill behind the wall face is formed from loose sand layers, these layers should be compacted to reach their maximum density. The effect of density of backfill on the distribution of tensile forces in the strips, horizontal pressure on the wall face, vertical stresses under the reinforced mass and the lateral movement of the wall are shown in Figs. (5.4 to 7) respectively. These figures were obtained from model tests CAT. II−1&2 and CAT. III−3, i.e. for the cases of no compaction and compaction.

The distribution of tensile forces in the lower strip is shown in Fig. (5.4) and in all cases the distribution is non uniform and all the forces are tensile. In the loose state the maximum tensile force in the strip is close to the wall face and in the medium and dense states the location is between 0.2 to 0.3 the strip length.

Fig. (5.5) shows that the distribution of the horizontal pressure was not affected too much by increasing the density from loose to medium, but a significant difference was noticed in the case of dense sand, especially in the upper third of the wall height. This was probably because in increasing the density from loose to medium, no compaction was used, whereas compaction was used to get the dense state.

Fig. (5.6) illustrates the distribution of vertical stress under the reinforced mass. In the case of loose and medium density the magnitudes increased slightly towards the wall face and were near each other. A noticeable difference in both distribution and values of vertical stresses in the dense case can be seen. The

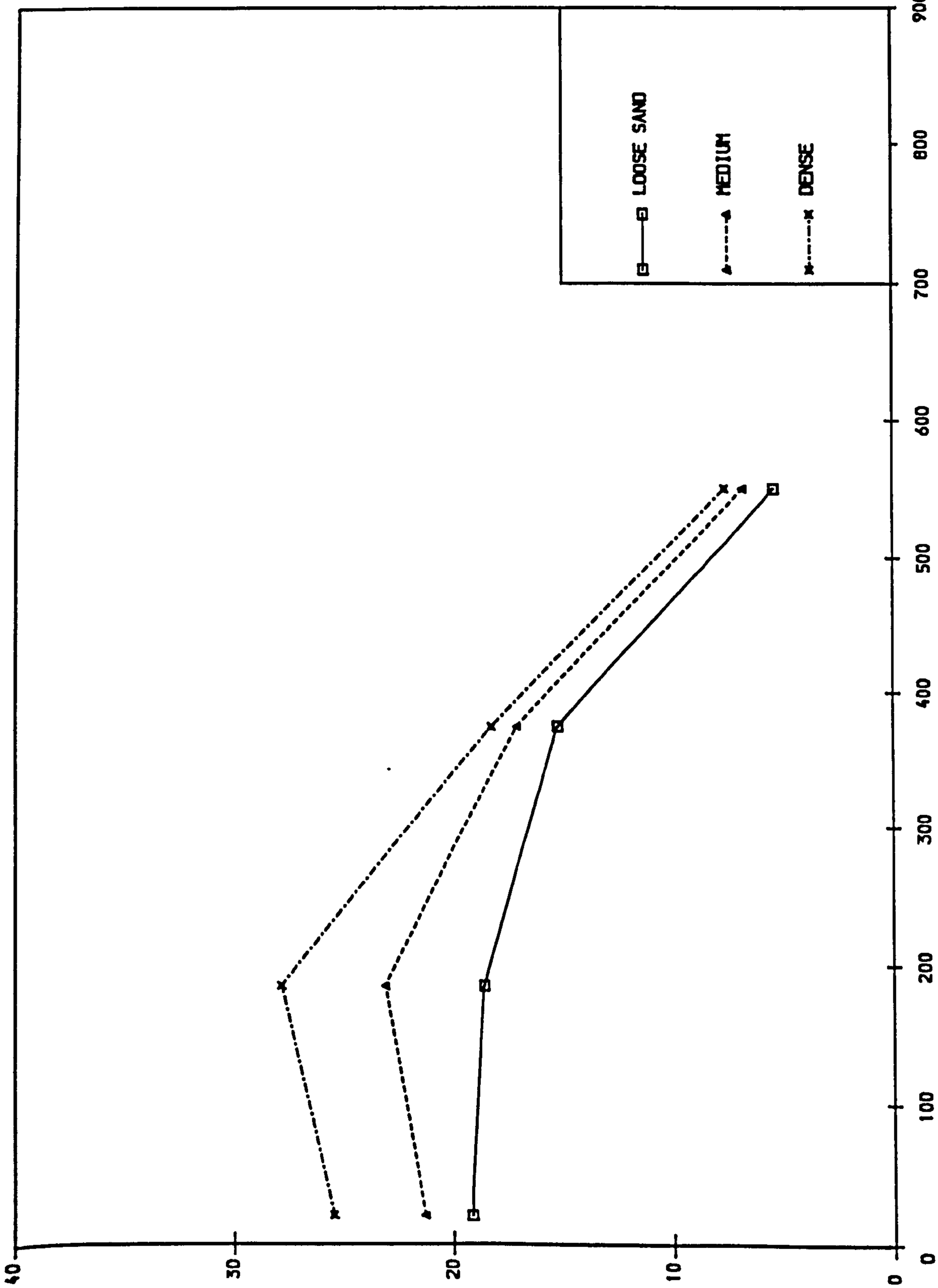

FIG. (5.4) THE EFFECT OF BACKFILL DENSITY ON THE DISTRIBUTION OF TENSILE FORCE IN THE LOWER STRIP, CAT. II-1&2 AND CAT. III-3.

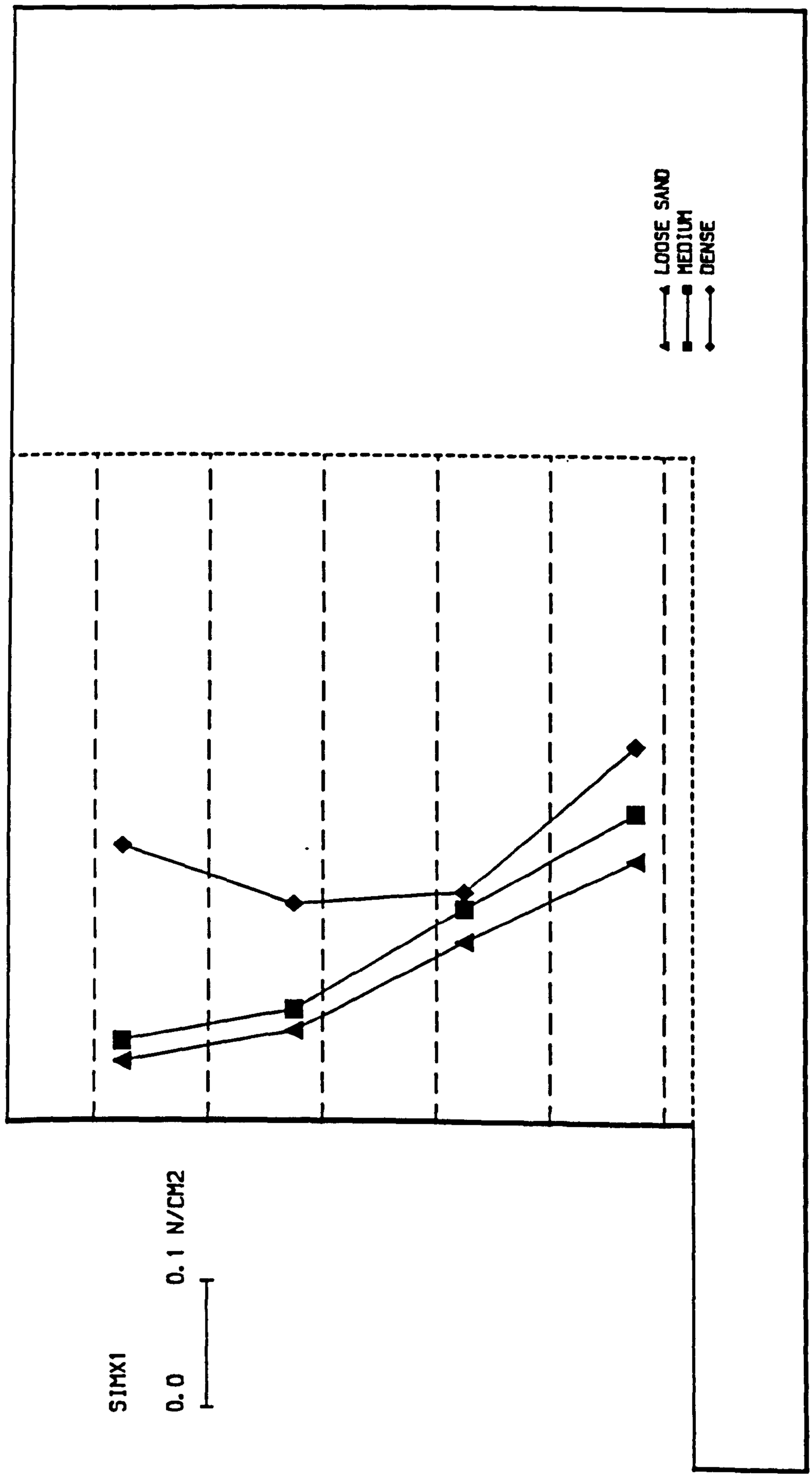

FIG. (5.5) THE EFFECT OF BACKFILL DENSITY ON THE HORIZ. PRESSURE DISTRIBUTION, CAT. II-1&2 AND CAT. III-3.

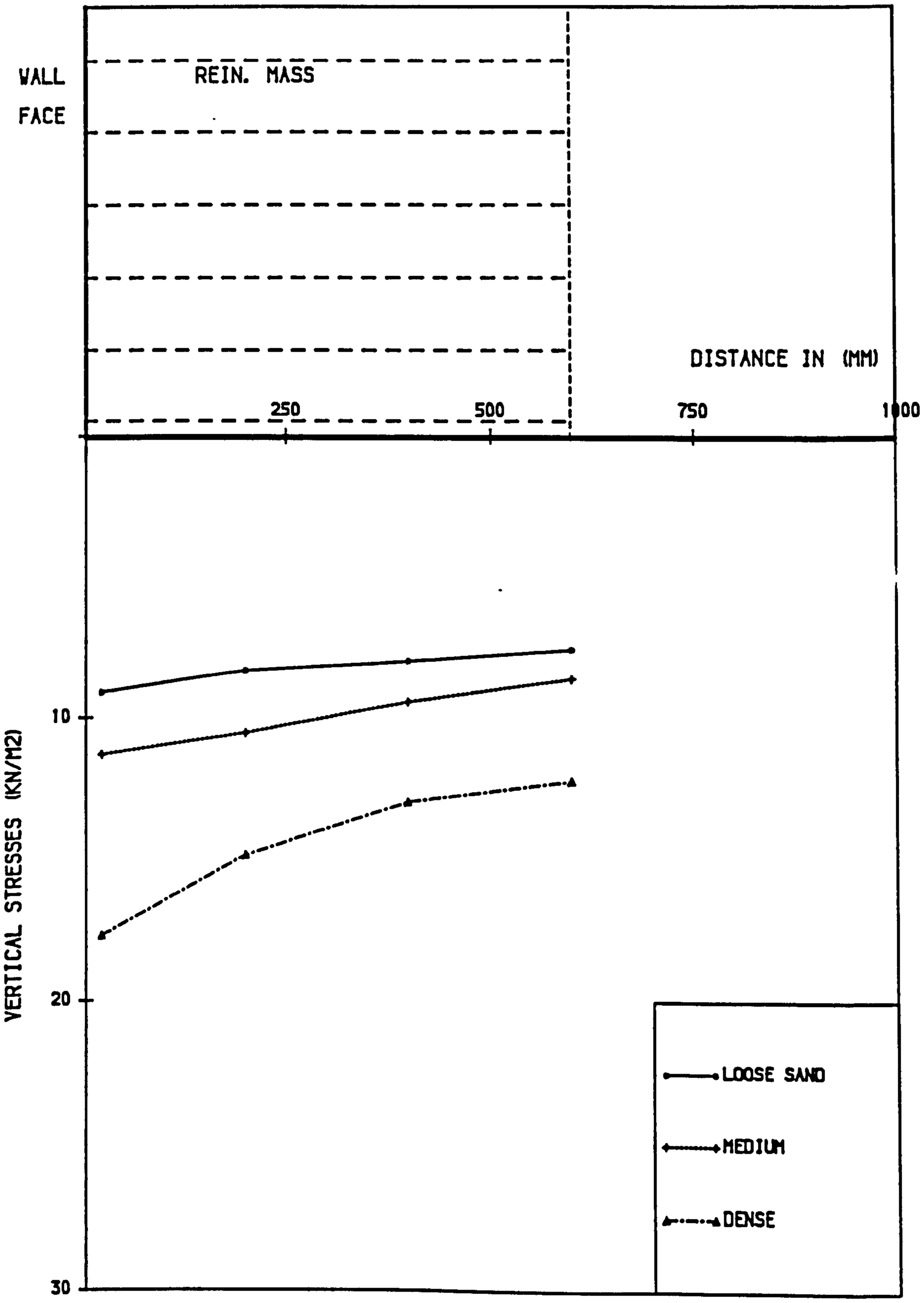

FIG. (5.6) THE EFFECT OF BACKFILL DENSITY ON THE DISTRIBUTION OF VERTICAL STRESSES, CAT. II-1&2 AND CAT. III-3

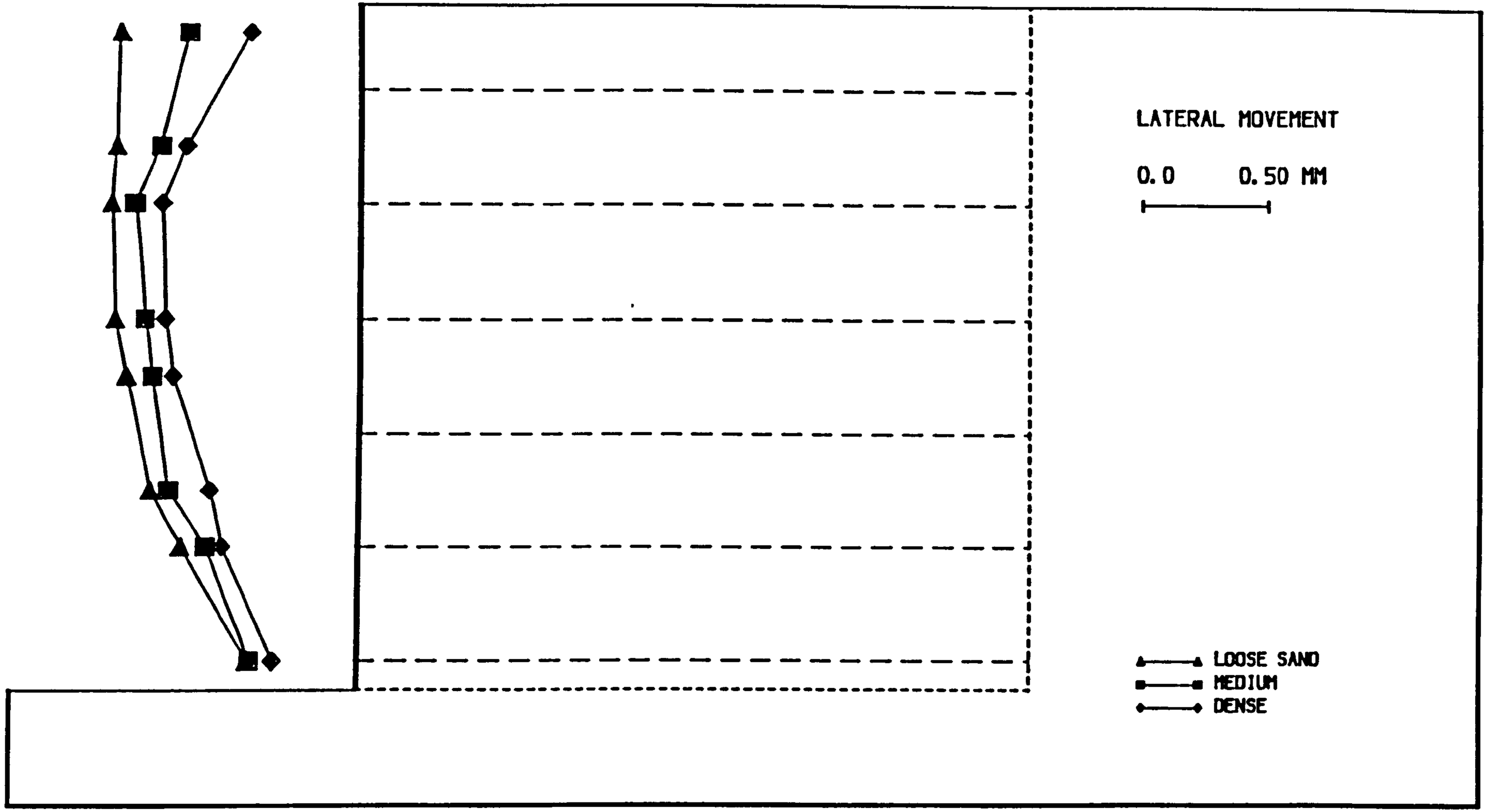

FIG. (5.7) THE EFFECT OF BACKFILL DENSITY ON THE LATERAL MOVEMENT OF THE VALL, CAT. II-1&2 AND CAT. III-3.

values increased sharply from the rear of the reinforced mass towards the wall face. The reason for this significant difference is the method of increasing the backfill density to the dense state by compaction.

The effect of backfill density on lateral movement of the wall is shown in Fig. (5.7). In general, increasing the backfill density decreases the lateral movement of the wall, because the reinforced wall is a flexible system as a whole and greater density decreases this flexibility.

It is seen from the above discussion that the reinforced earth wall was greatly affected by the method of increasing the density especially by compaction.

5.3.2 The Behaviour Of The Wall Before, During And After Compaction.

The effect of compaction on the behaviour of the reinforced earth wall can be seen from the results from the model tests before, during and after compaction. The results of one of the model tests (CAT. III−3), where all the reinforced mass was compacted, will be discussed in detail.

(a) Distribution of forces in strips

The distribution of tensile forces in the three instrumented strips − upper, middle and lower as previously shown in Fig. (5.1)− are given in Figs. (5.8 to 16). It should be noted that the distribution of forces for each strip was obtained before, during and after compaction for each layer of sand. Also, in all the figures the overburden indicates the height of the fill from the base of reinforced mass. The distribution of forces in the three strips are shown to be non uniform and all the forces are tensile.

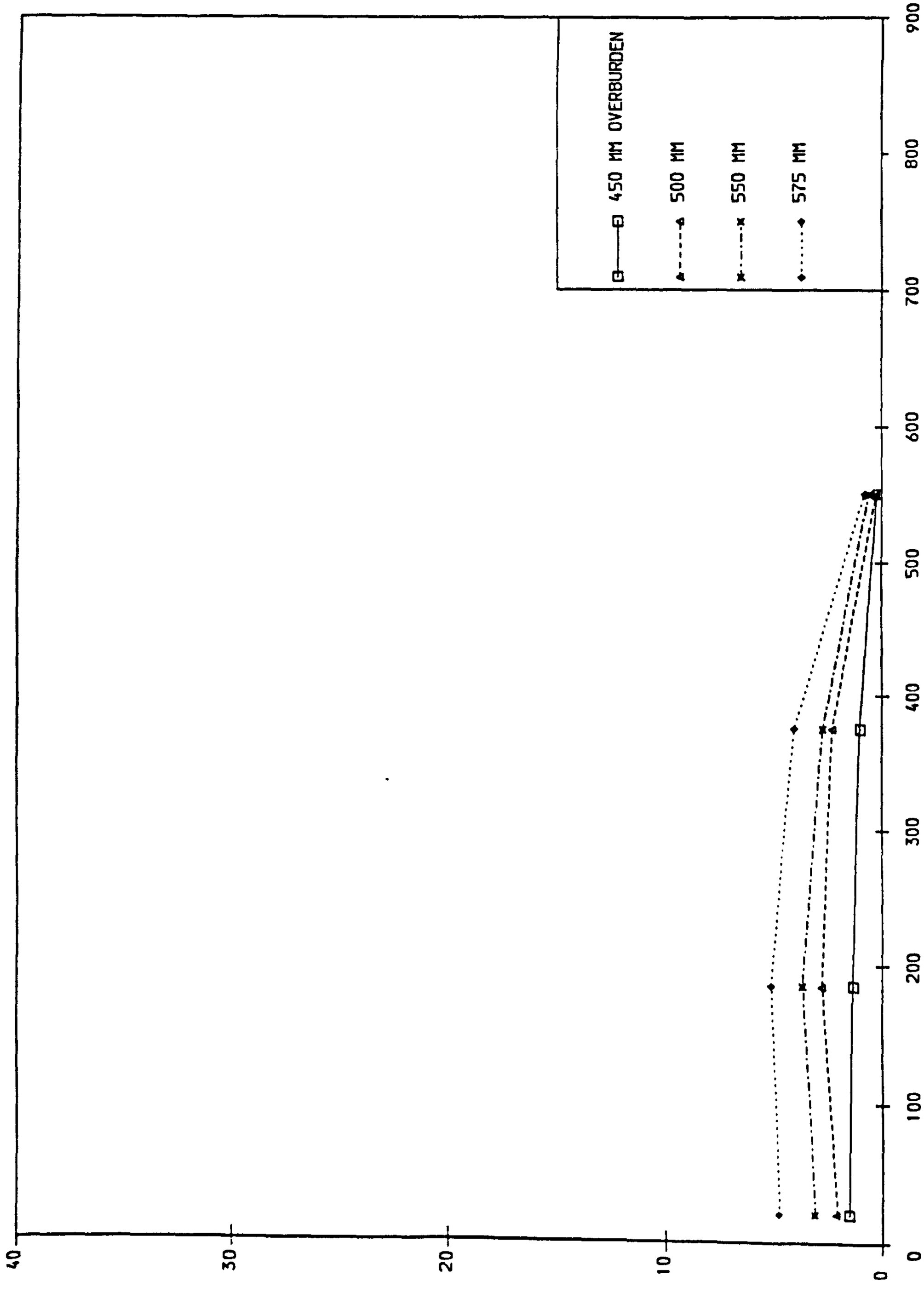

FIG. 15.8) DISTRIBUTION OF TENSILE FORCE IN UPPER STRIP, 600.00 MM, BEFORE COMP. , CAT. III-3.

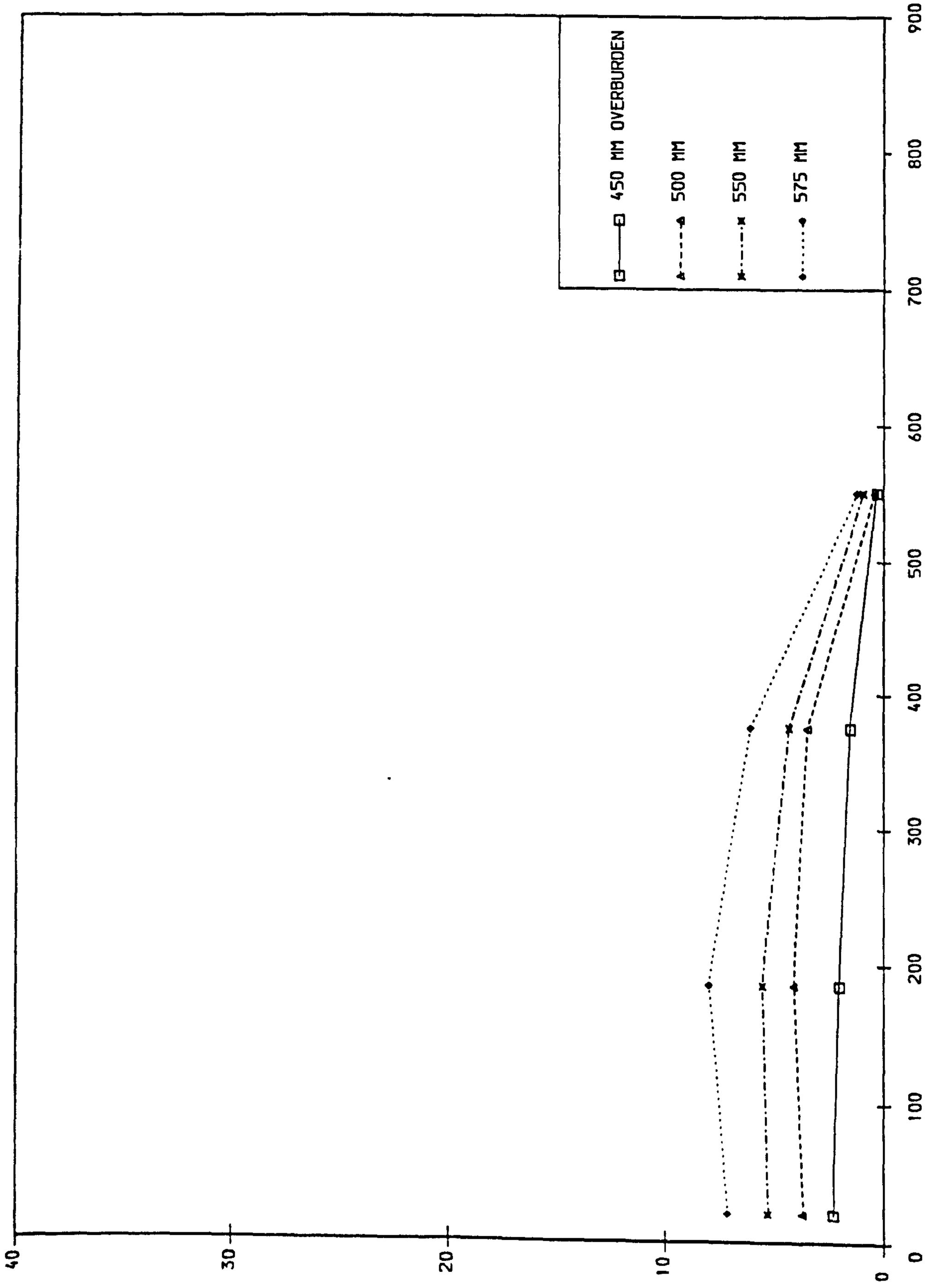

FIG. (5.9) DISTRIBUTION OF TENSILE FORCE IN UPPER STRIP, COMP. LENG. = 600.00 MM, DURING COMP. , CAT. III-3.

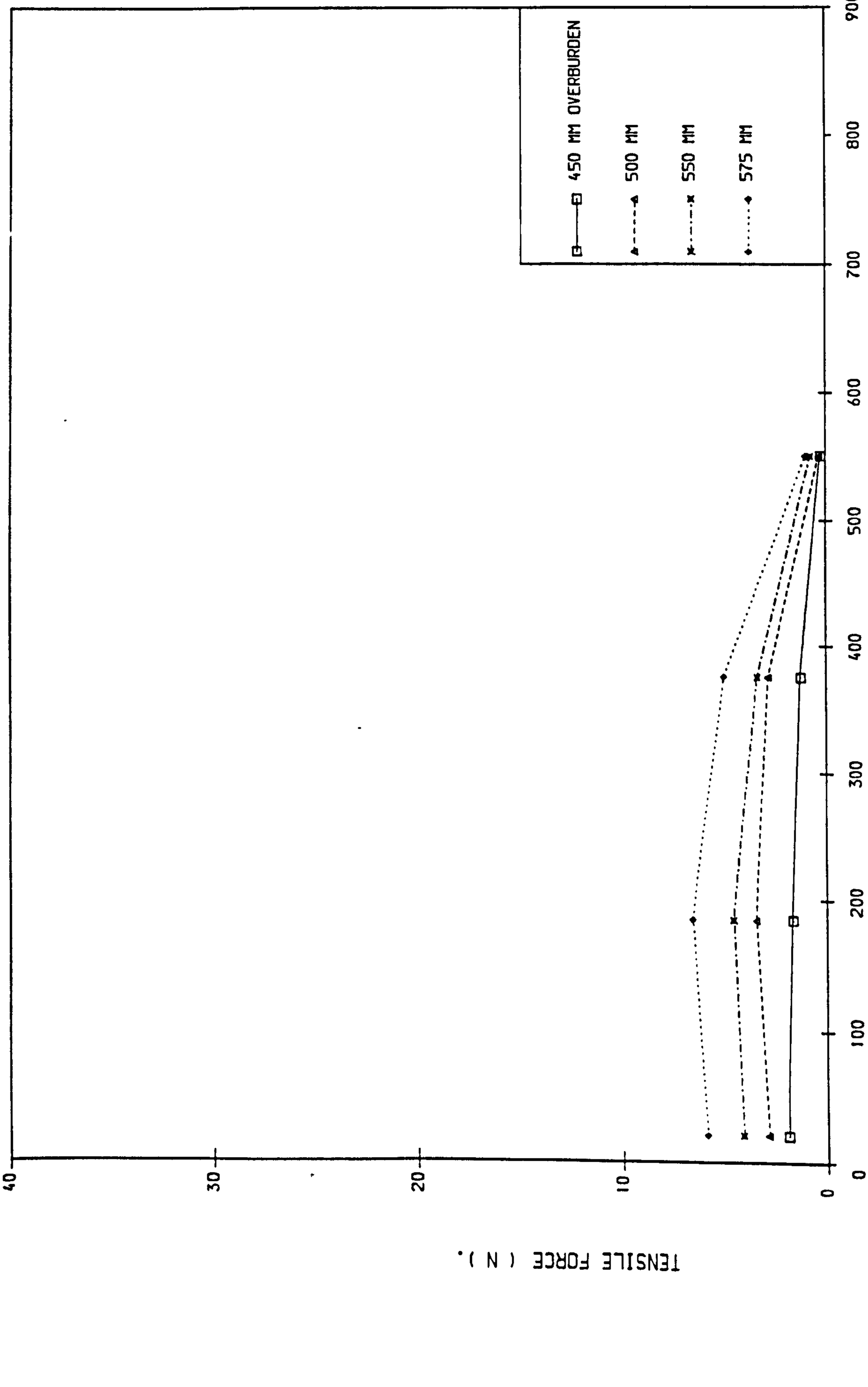

FIG. (5.10) DISTRIBUTION OF TENSILE FORCE IN UPPER STRIP, 600.00 MM, AFTER COMP. , CAT. III-3.

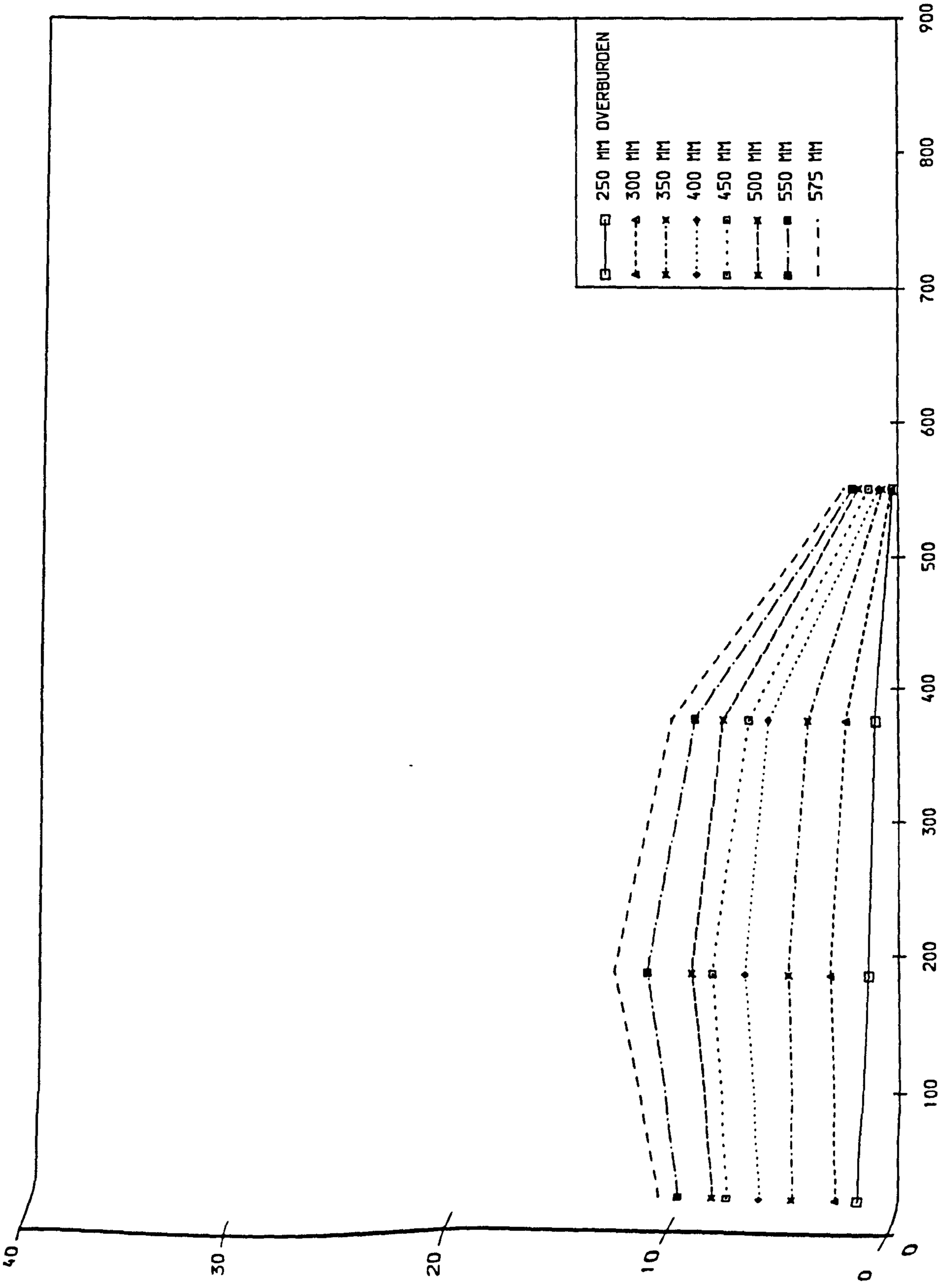

FIG. (5.11) DISTRIBUTION OF TENSILE FORCE IN MIDDLE STRIP, 600.00 MM, BEFORE COMP. , CAT. III-3.

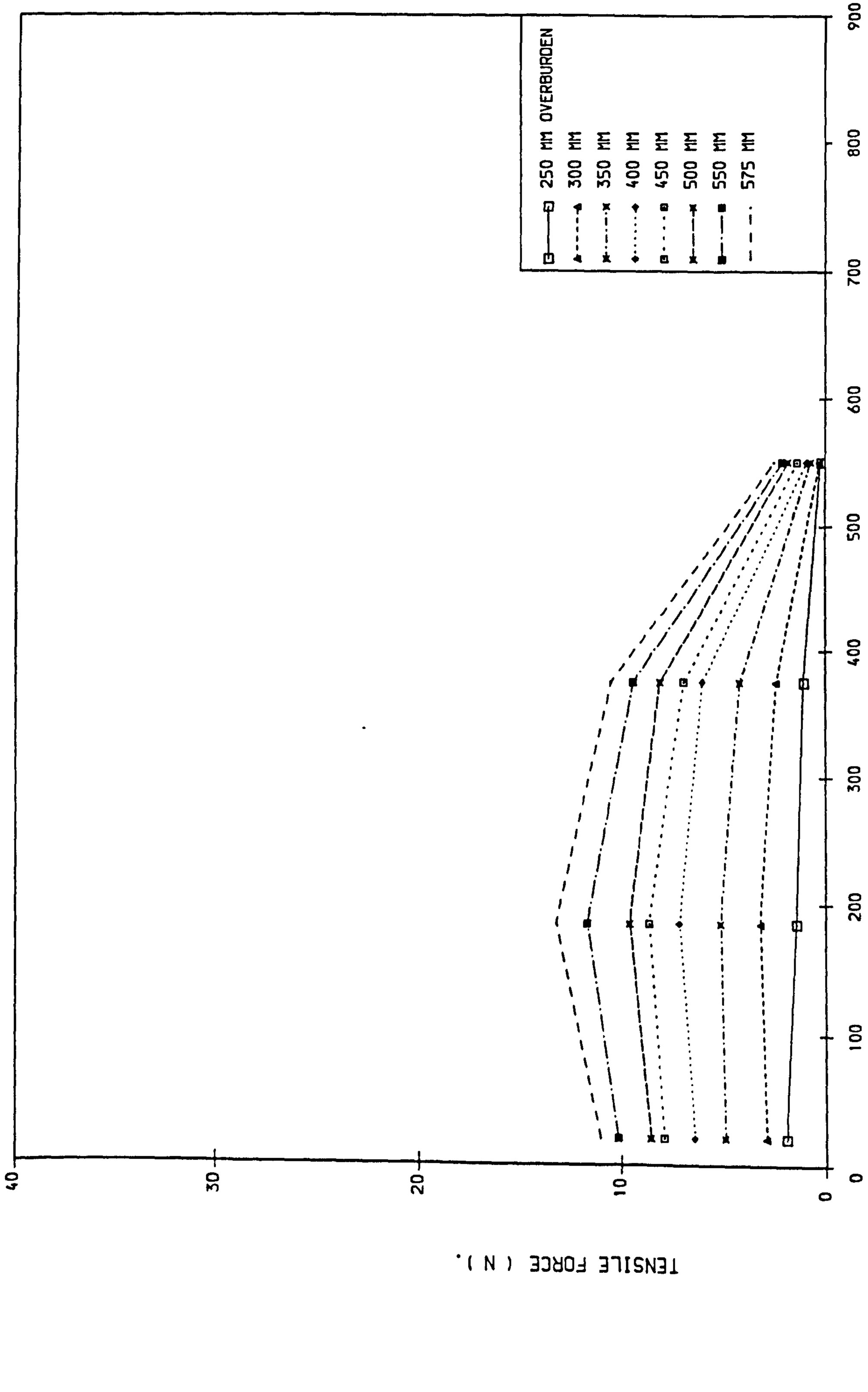

FIG. (5.11) DISTRIBUTION OF TENSILE FORCE IN MIDDLE STRIP, COMP. LENG. = 600.00 MM, BEFORE COMP. , CAT. III-3.

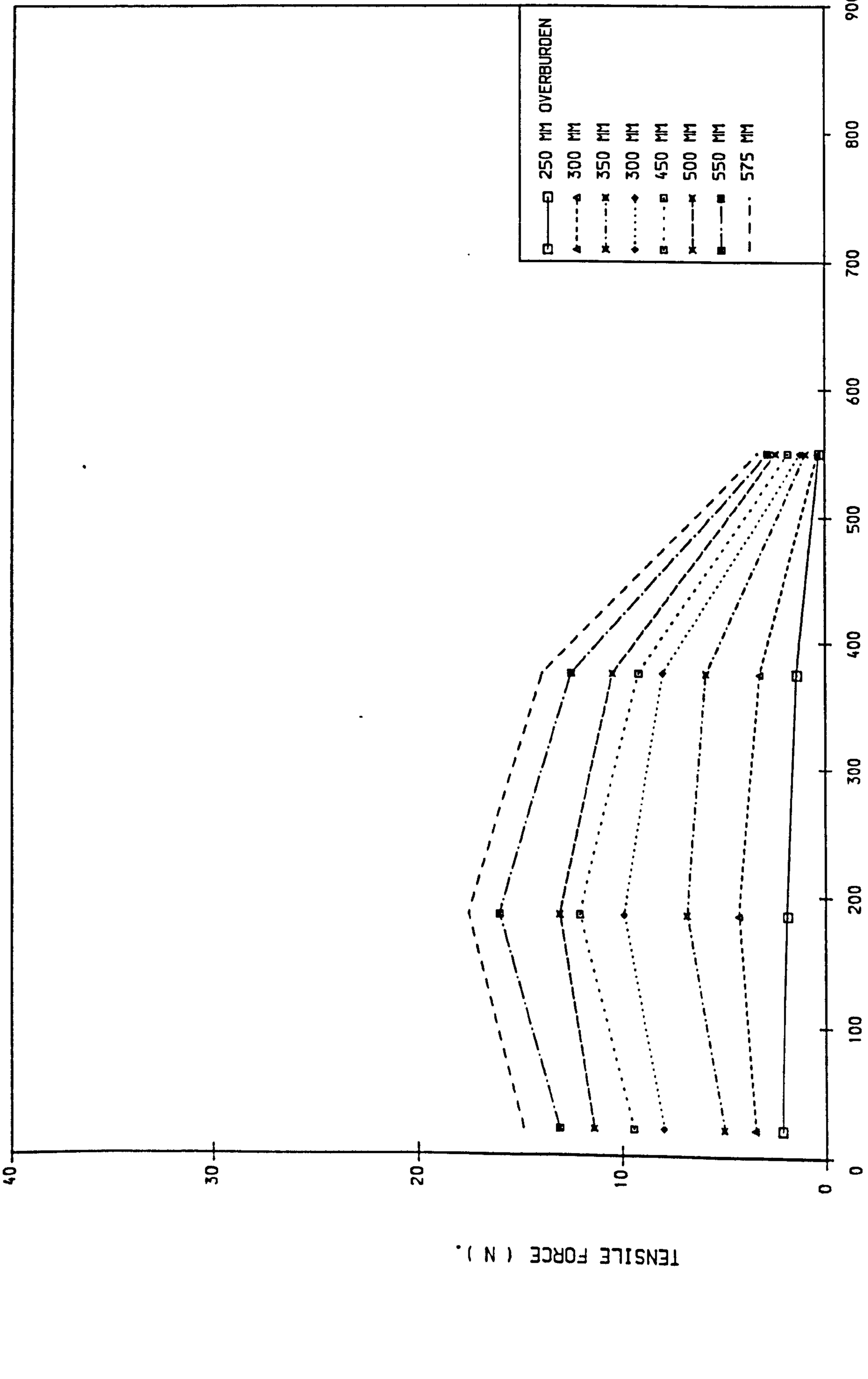

FIG. (5.12) DISTRIBUTION OF TENSILE FORCE IN MIDDLE STRIP, COMP. LENG. = 600.00 MM, DURING COMP. , CAT. III-3.

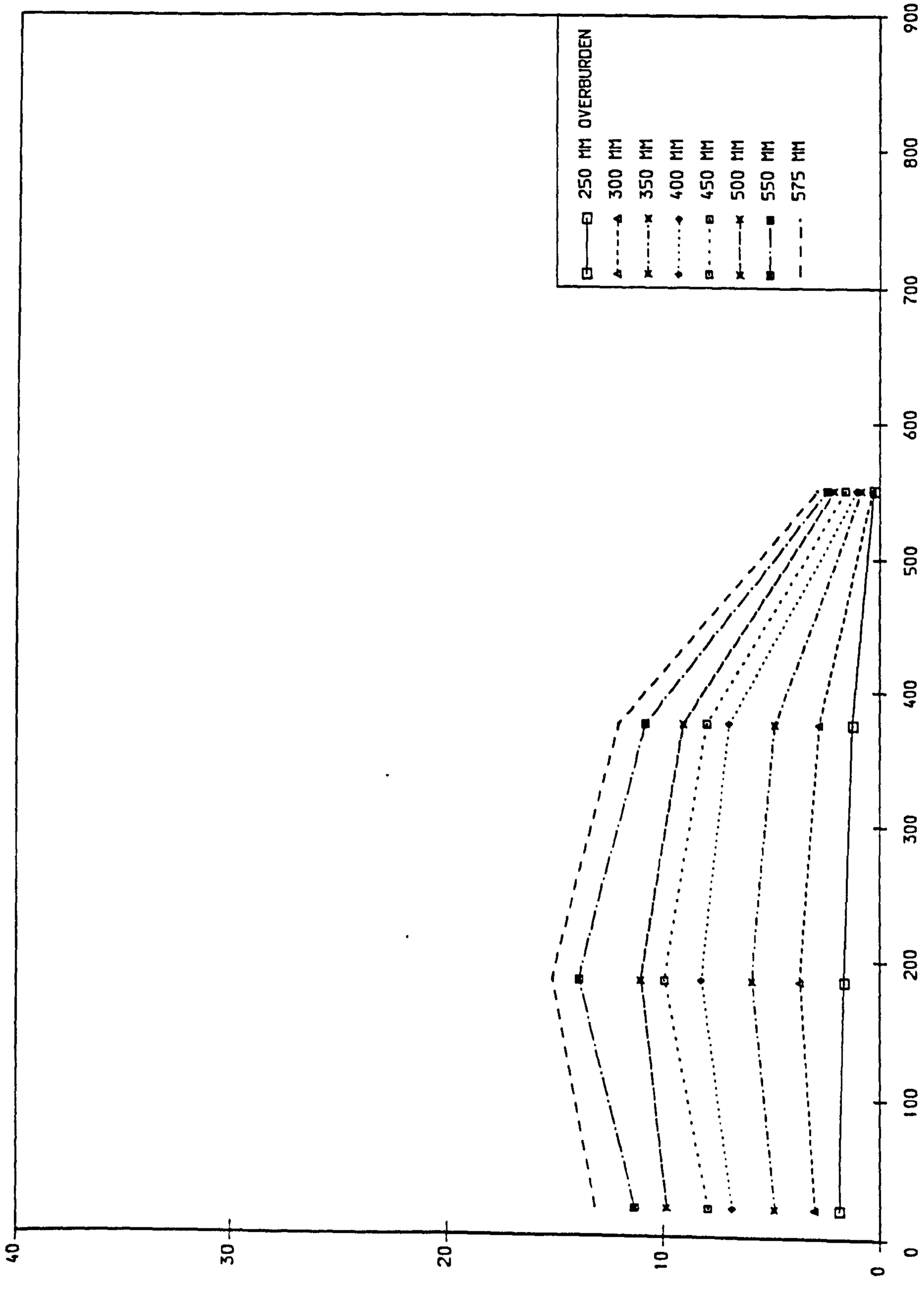

FIG. (5.13) DISTRIBUTION OF TENSILE FORCE IN MIDDLE STRIP, 600.00 MM, AFTER COMP. , CAT. III-3.

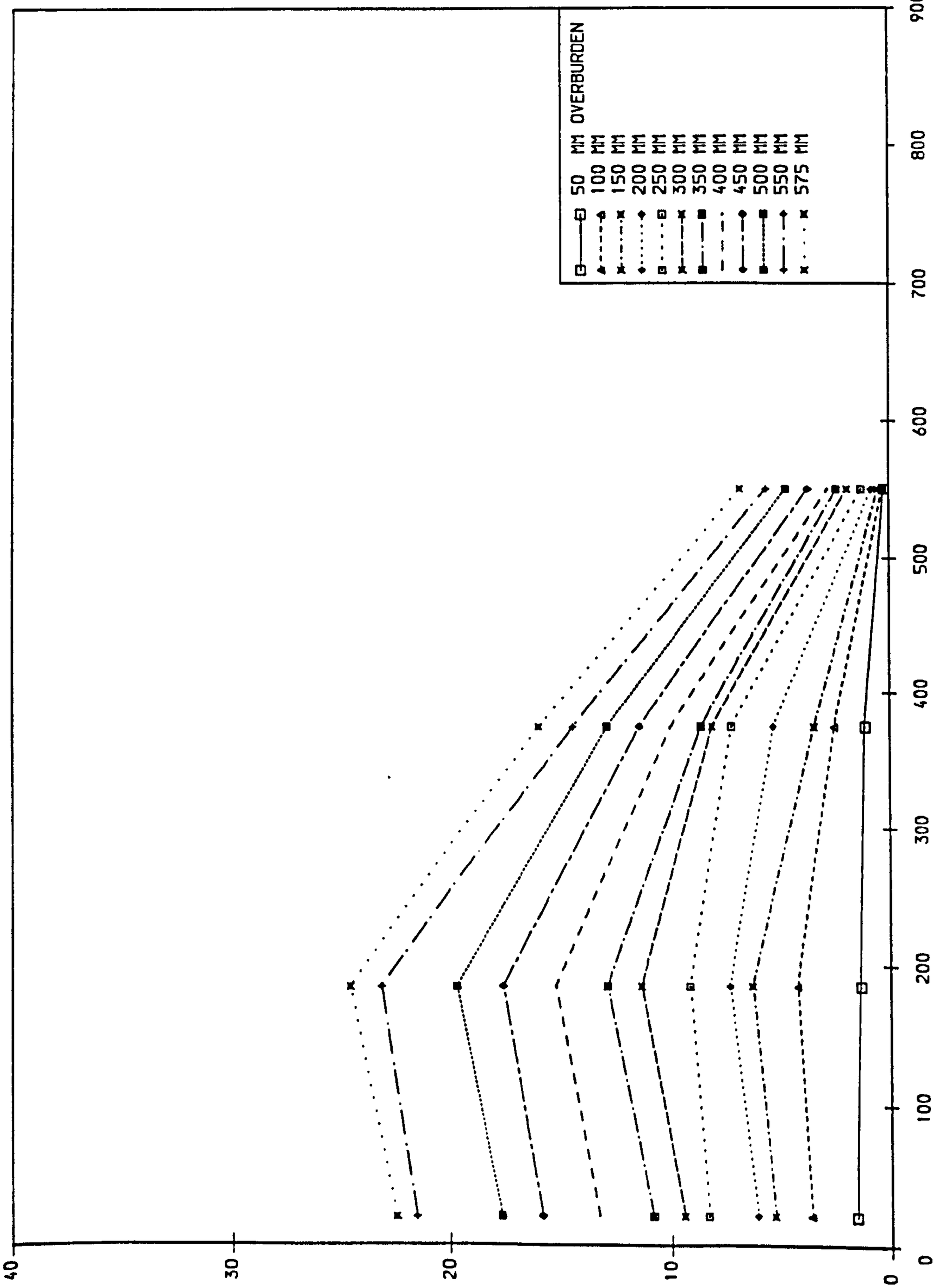

FIG. (5.14) DISTRIBUTION OF TENSILE FORCE IN LOWER STRIP, COMP. LENG. = 600.00 MM, BEFORE COMP. , CAT. III-3.

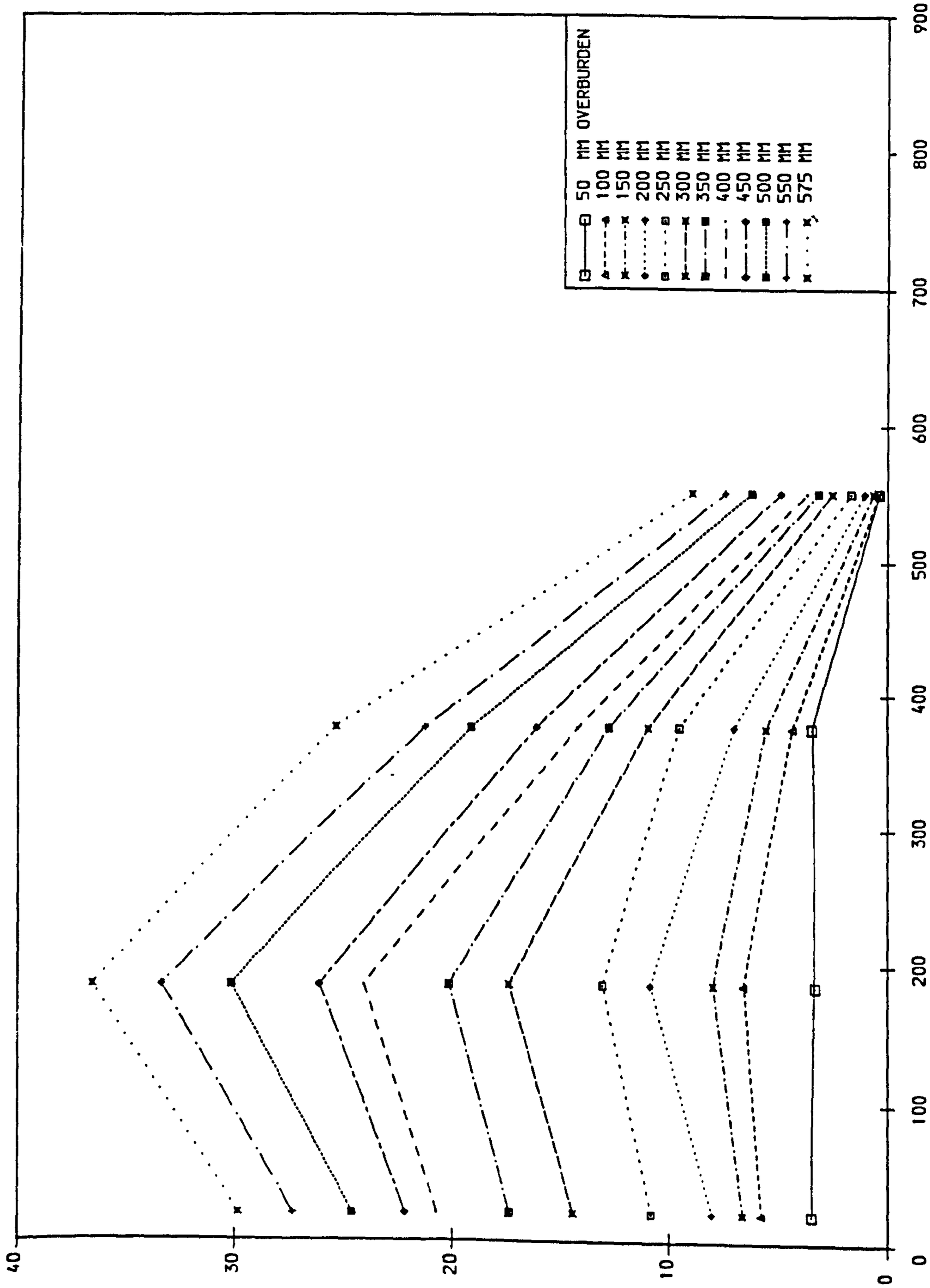

FIG. (5.15) DISTRIBUTION OF TENSILE FORCE IN LOWER STRIP, COMP. LENG. = 600.00 MM, DURING COMP., CAT. III-3.

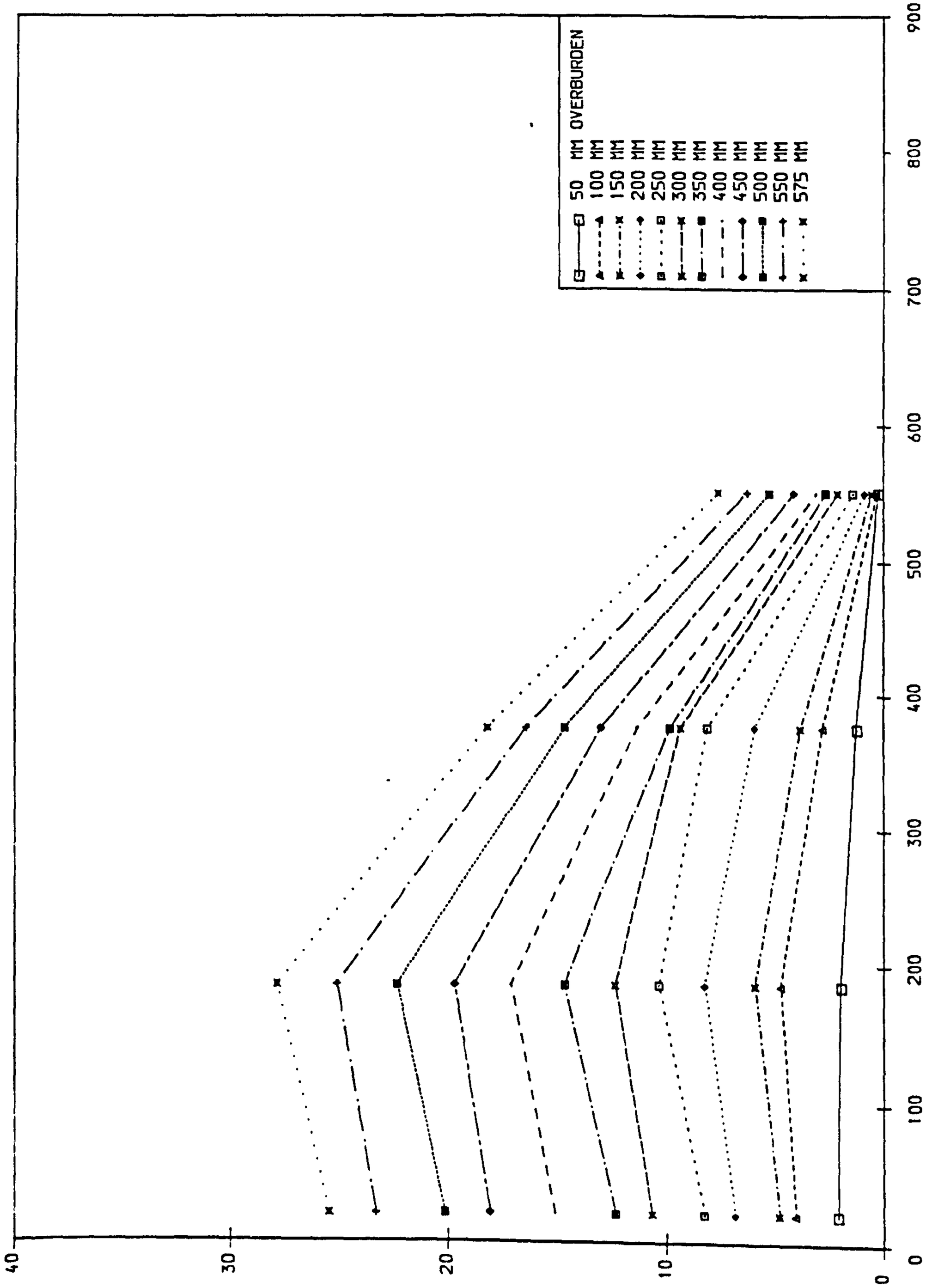

FIG. (5.16) DISTRIBUTION OF TENSILE FORCE IN LOWER STRIP, COMP. LENG. = 600.00 MM, AFTER COMP. , CAT. III-3.

The largest tensile forces occur within the front half of the strips, and this may be due to the rigidity of the wall face material. The forces decrease towards the free end of the strip and reach zero, and the forces decrease towards the wall face but do not reach zero.

The maximum values of tensile forces obtained before,during and after compaction are shown in Fig. (5.17). On average, the increase of the maximum value during compaction was 38% more than the value before compaction, and in the after compaction case the maximum value of tensile force was 16% greater than before compaction. The reason for this is that during compaction the apparent cohesion between soil and strips increases due to densification of soil as a result of the compaction load, but after compaction the soil starts to rebound and lose some of this apparent cohesion, which causes a decrease in the tensile force.

The position of maximum forces lies between 0.1 to 0.3 the length of the strips from the wall face. During compaction it tends to be near the wall face and farther away after compaction.

(b) Distribution of horizontal stresses

Fig. (5.18) illustrates the distribution of horizontal stresses at two sections, behind the wall face and behind the reinforced mass, for cases before, during and after compaction respectively.

It should be noted that the density in the reinforced mass is different to that behind, because only the reinforced earth mass was compacted.

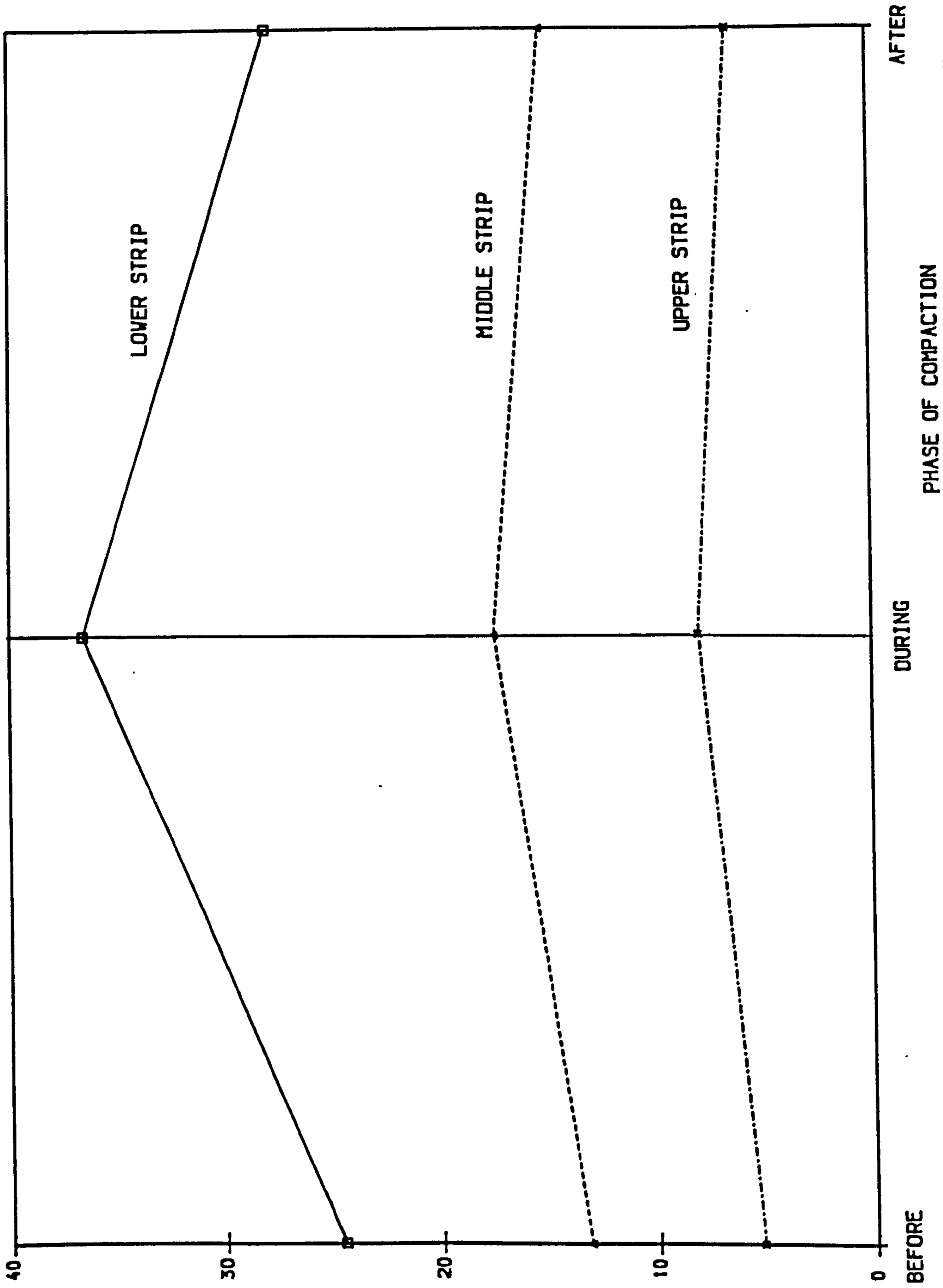

FIG. (5.17) MAX. TENSILE FORCES UNDER MAX. HEIGHT OF FILL BEFOR, AFTER AND DURING COMP., COMP. LENG. = 600.00 MM, CAT. III-3.

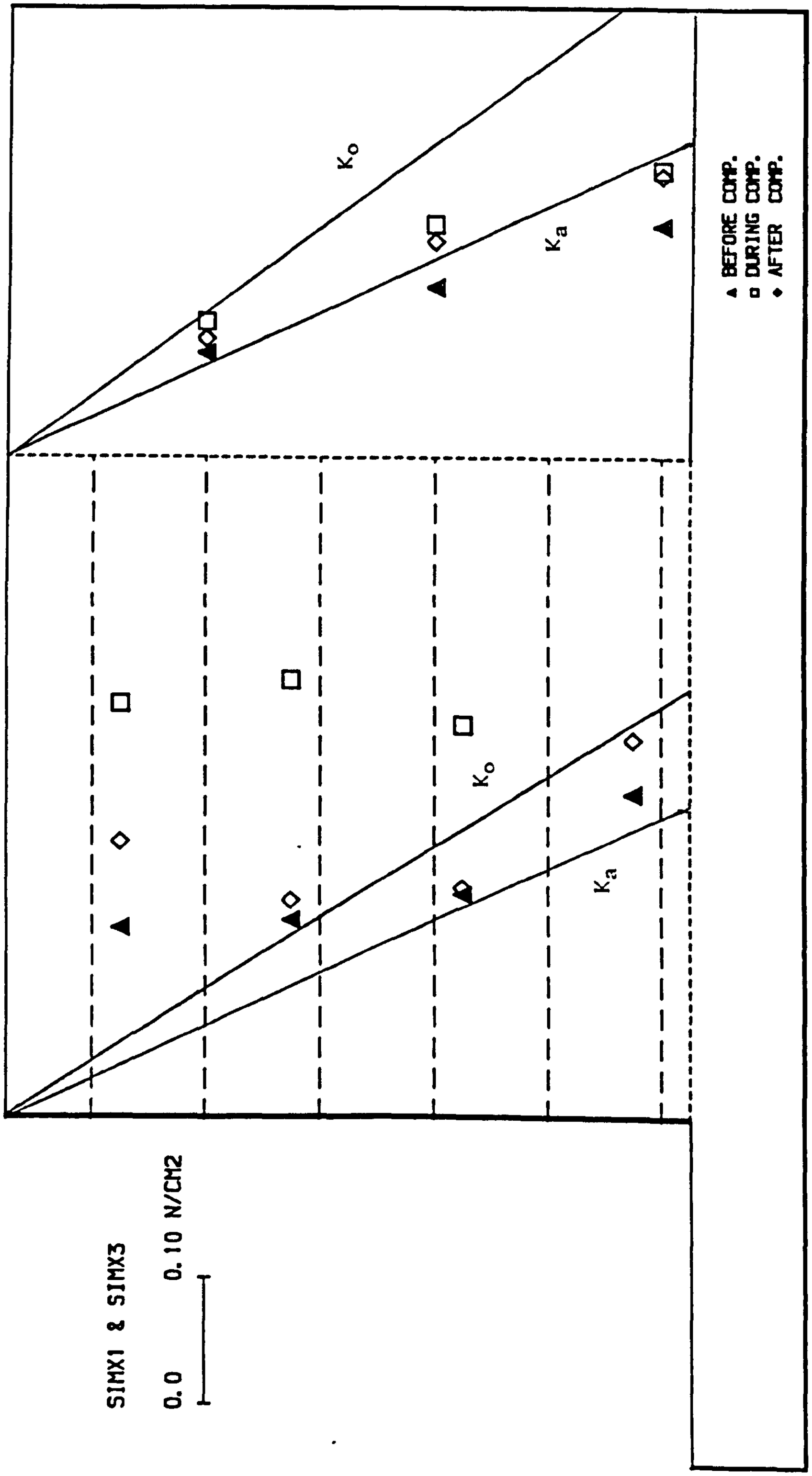

FIG. (5.18) MAX. HORIZ. STRESSES AT THE FACE OF WALL & BEHIND REINF. MASS, LENG. = 600.0 MM & BEFORE, DURING AND AFTER COMP., CAT. III-3.

The distribution of earth pressure behind the reinforced mass is very near to the active state before and after compaction. During compaction it increases slightly especially in the top third of the wall height to reach close to the at rest state. This may be due to the density of the reinforced mass increasing due to compaction, and increasing the rigidity of the reinforced mass as a whole and affecting slightly the density just behind it.

The distribution of earth pressure behind the wall face in the before compaction case exceeds the at rest condition in the upper third of the wall, and decreases with depth to be close to the active state. During compaction, there is a significant increase in the earth pressure, to a value greater than the at rest condition. Generally it reaches 1.2 to 2.3 times the values before compaction especially in the upper third of the wall height. After compaction it decreases and becomes less than during compaction, but is still about 1.1 to 1.3 times the values before compaction. The values are larger than the at rest condition near the top and decrease with the depth to be between the active and the at rest condition. The values become very close to at the rest condition near the bottom.

The explanation of the above is that the earth pressure during compaction increases due to horizontal pressure coming from the compaction plant and increasing the soil density. The soil retains some stresses which are locked in during compaction, and this causes the horizontal pressure after compaction to be greater than before.

(c) Distribution of vertical stresses under reinforced mass

The distribution of vertical stresses under the reinforced mass is shown in

Figs. (5.19,20&21) before, during and after compaction respectively.

AS discussed in Chapter 3, the measurements were taken for each sand layer (12 layers), before, during and after compaction. The figures show the vertical stresses distribution due to the 12 layers. In the cases before and after compaction, and in the first four layers the distribution is almost uniform and the values increase gradually but unequally. At the upper layer the value near the toe is a maximum and decreases towards the rear of the reinforced mass. But during compaction the distribution is not uniform.

Fig. (5.22) is a summary of the effect of before, during and after compaction for the case of maximum overburden pressure. In general, the values of vertical stresses are bigger than in the case before compaction, and particularly near the toe of the wall are about 30% more. In the case after compaction , the value near the toe is the maximum and larger than the case of before compaction being about 15% more. The distribution almost takes a trapezoidal shape, the biggest value is near the toe and decreases towards the rear of the reinforced mass.

The reason for the variation of values and shapes in the above three cases, is that during compaction the vertical stresses increase due to the load caused by the compaction plant. After compaction the soil releases and loses some of its densification, which causes some release of vertical stress to take place. Also the shape after compaction is very near to a trapezoidal shape, due to tilting at the toe of the flexible system caused by the compaction load.

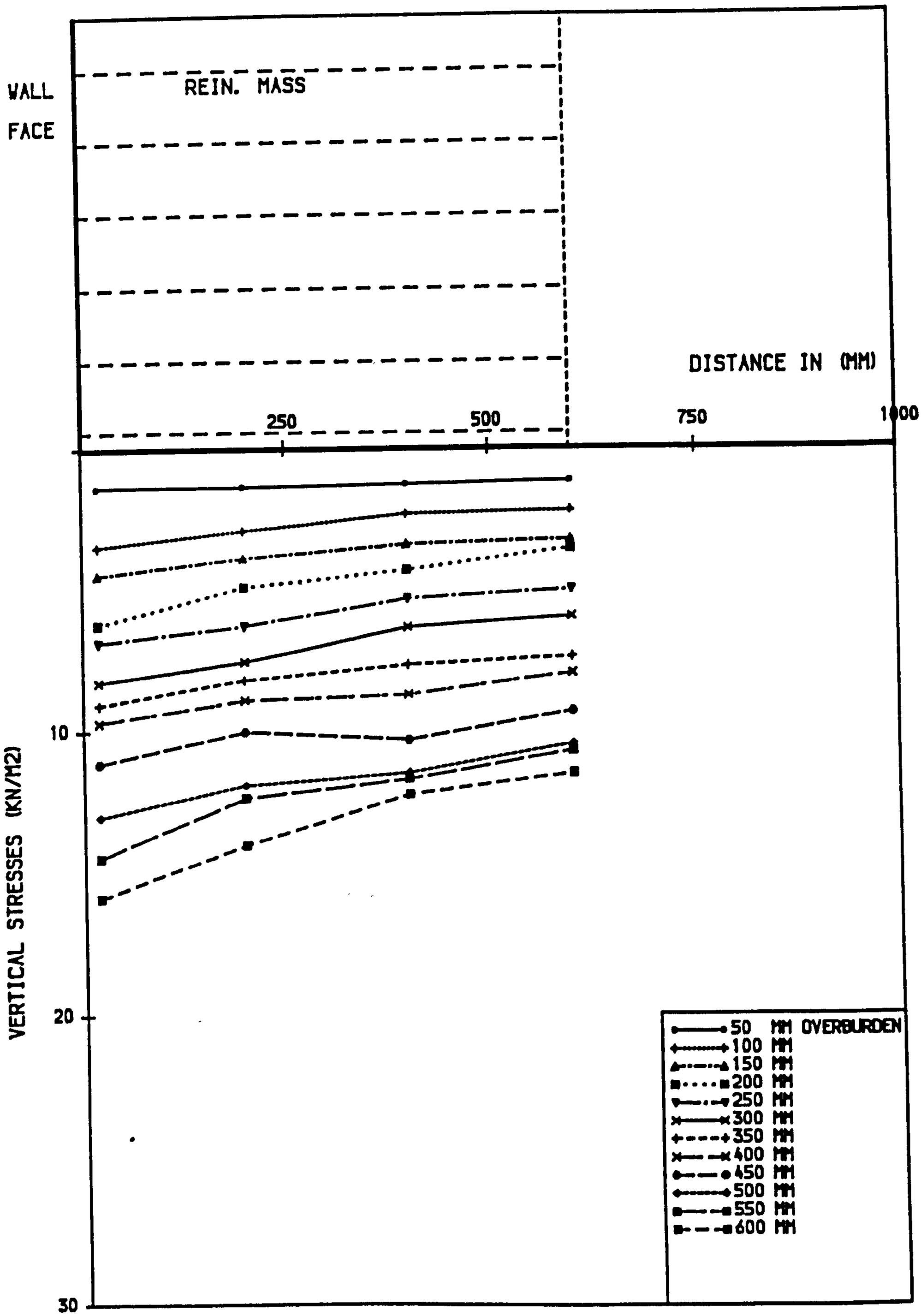

FIG. (5.19) DISTRIBUTION OF VERTICAL STRESSES UNDER THE REINF. MASS, COMP. LENG. = 600.00 MM & BEFORE COMP., CAT. III-3.

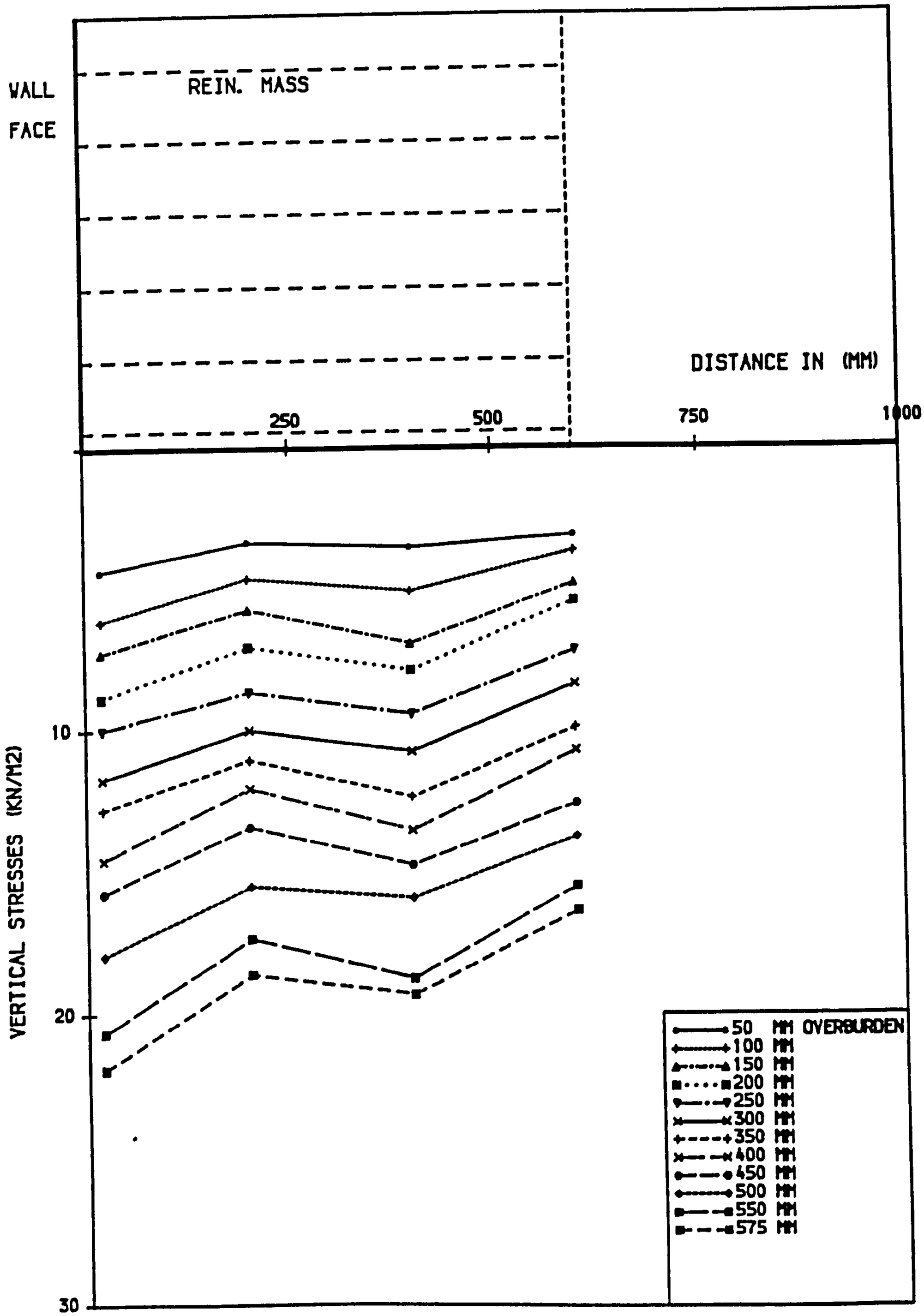

FIG. (5.20) DISTRIBUTION OF VERTICAL STRESSES UNDER THE REINF. MASS, COMP. LENG. = 600.00 MM & DURING COMP., CAT. III-3.

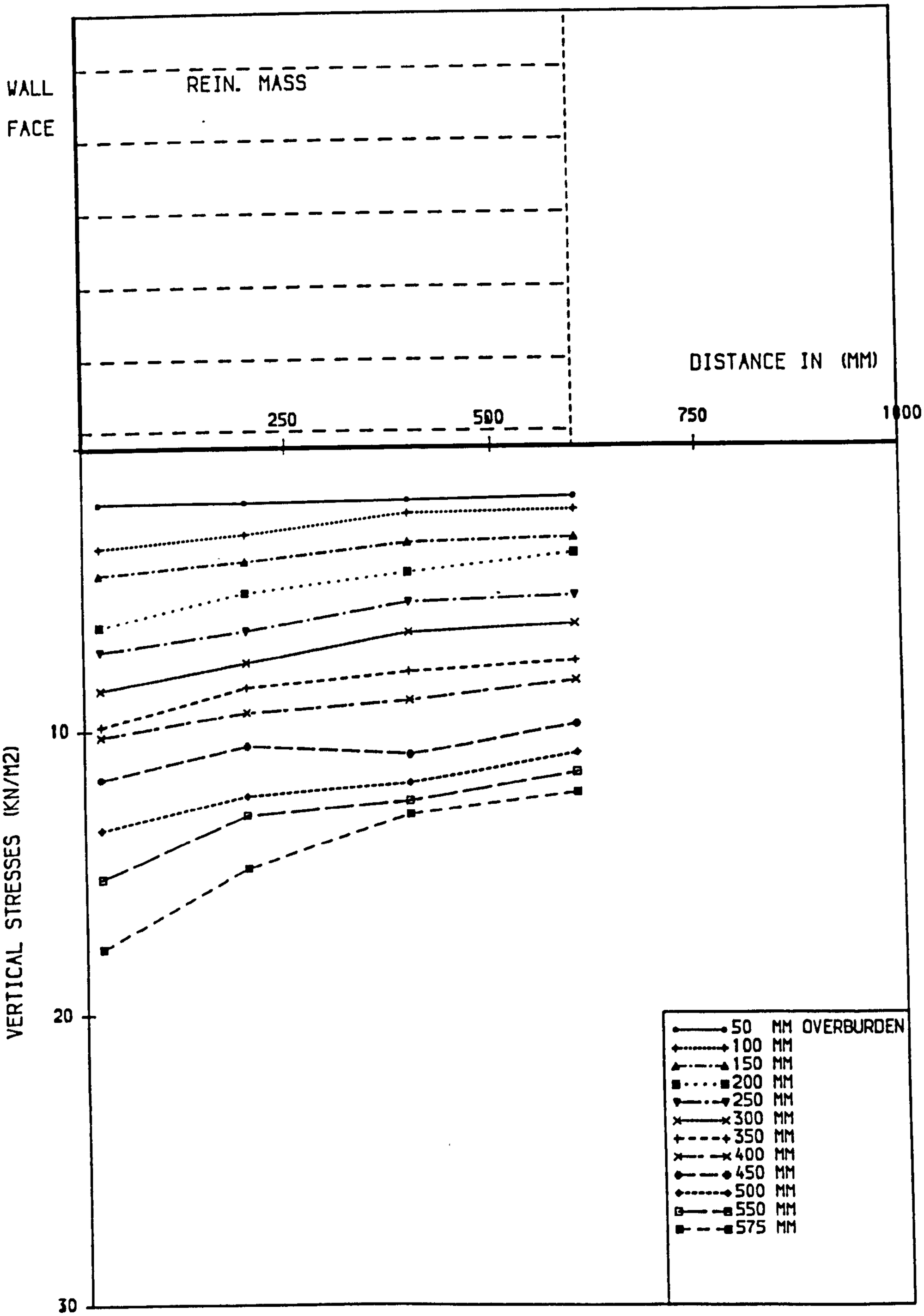

FIG. (5.21) DISTRIBUTION OF VERTICAL STRESSES UNDER THE REINF. MASS, COMP. LENG. = 600.00 MM & AFTER COMP., CAT. III-3.

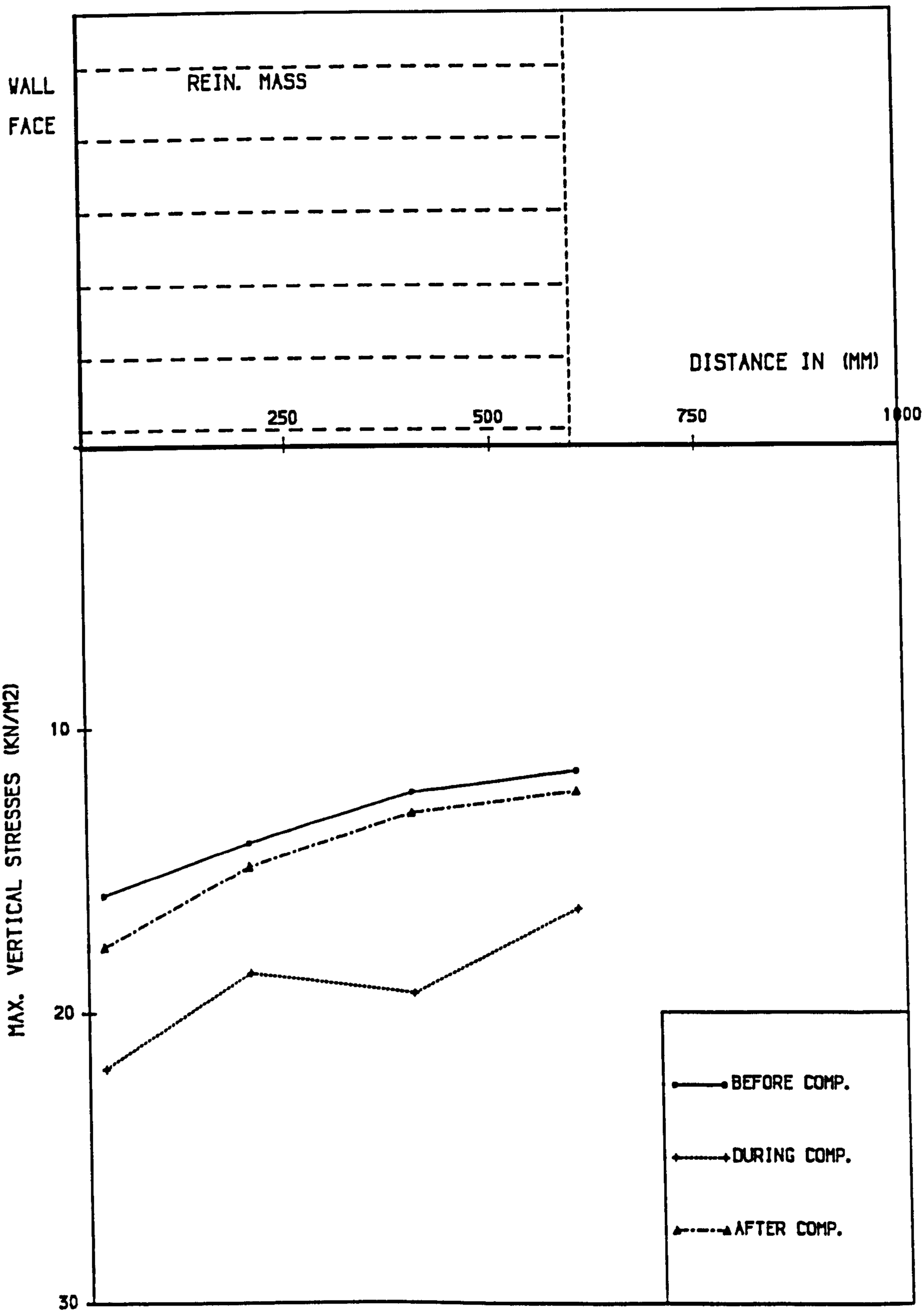

FIG. (5.22) MAX. VERTICAL STRESSES UNDER THE REINF. MASS, BEFORE, DURING AND AFTER COMP., CAT. III-3.

(d) Lateral movement of the wall face

Lateral movement of the wall face of the reinforced earth wall is shown in Fig. (5.23) for cases before, during and after compaction respectively. Generally, in the three shapes there is an indication of sliding and rotational movement around the toe of the wall. The movement in the upper half of the wall is bigger than the lower half.

The values of lateral movement during compaction, are greater than for the case before compaction, and this is due to the compaction load which increases the pressure on the wall face and hence the lateral movement. The lateral movement after compaction is larger than in the other cases, because some densification which take place during compaction is released after compaction and causes movement of the wall.

5.4 EFFECT OF COMPACTION LENGTH ON THE BEHAVIOUR OF THE WALL

The effect of various compaction lengths on the behaviour of reinforced earth retaining walls with sand backfill can be determined from the results of five model tests with different compaction lengths as follows:

For compaction length,

$L_c = 0.33H$ CAT. III–1

$L_c = 0.67H$ CAT. III–2

$Lc = H$ CAT. III–3

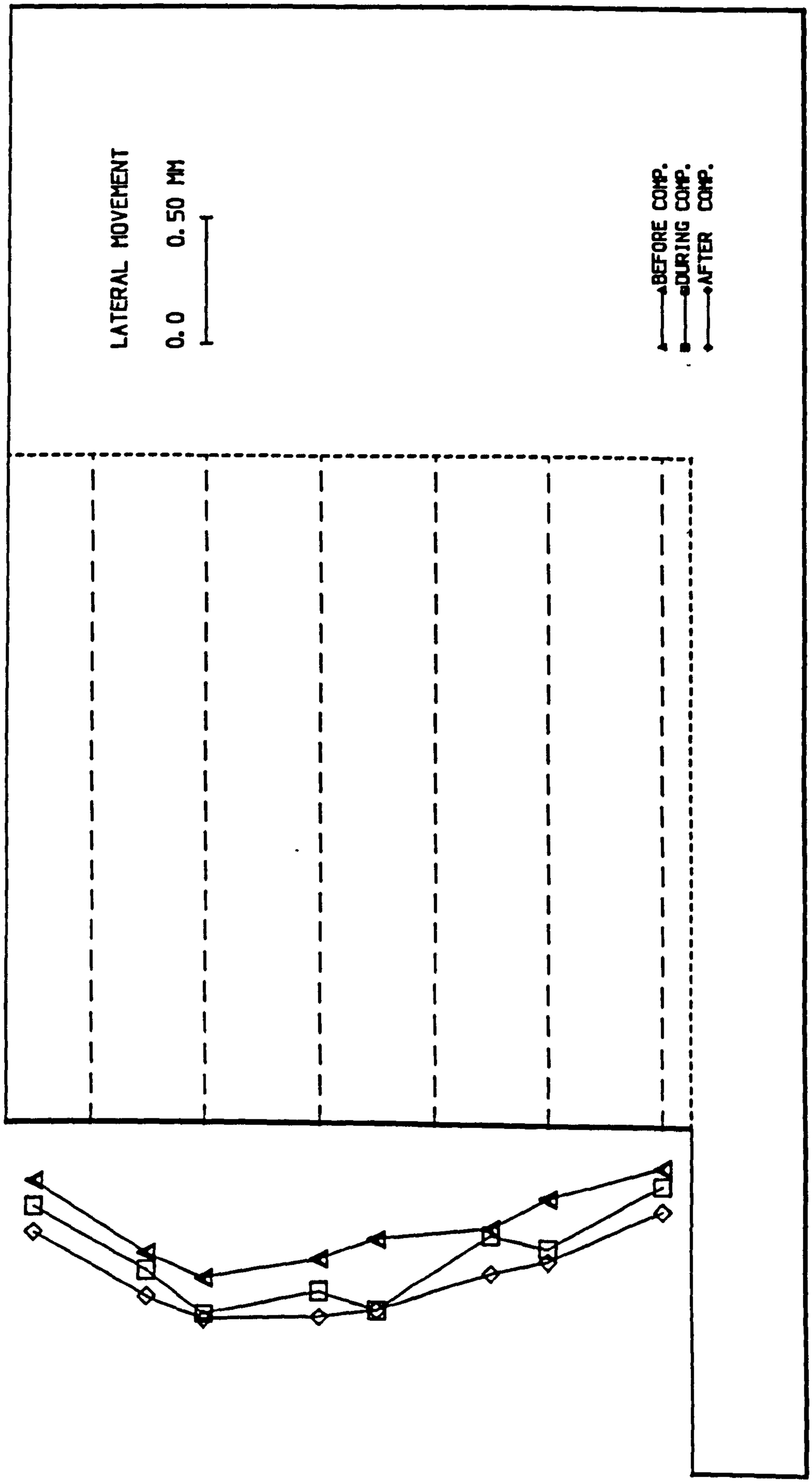

FIG. (5.23) LATERAL MOVEMENT OF THE VALL FACE, COMP. LENG. = 600.00 MM & BEFORE, DURING & AFTER COMP., CAT. III-3.

For variable compaction length,where

θ = 60° CAT. IV–2

θ = 75° CAT. IV–3

5.4.1 The Distribution Of Forces In The Strip

Fig. (5.24) shows the distribution of tensile forces in the lower strip as the results from five model tests. It can be seen from the figure that increasing the compaction length increases the forces in the strips particularly in the front half.

In the case of compaction length = H, which covers all the reinforced mass, the maximum tensile force has been obtained, because a large portion of the horizontal stresses transmitted to the wall are resisted by the strips. In the case of variable compaction length where θ has different values, it is shown that by increasing θ the tensile force increases. This is because a larger part of the reinforced mass has been compacted.

In the case of variable compaction length where θ = 60°, i.e near the value of inclination of theoretical plane (45+ φ/2), the force in the rear half of the strip is bigger than the other cases. This might be because most of the compaction has been concentrated on the rear half. It is interesting to note that in the case of θ = 75° i.e > (45+ φ/2), the values of tensile forces in the strip are very near the values for compaction length = H.

5.4.2 The Distribution Of Vertical Stresses Under Reinforced Mass

This is shown in Fig. (5.25). The distributions in all cases of different

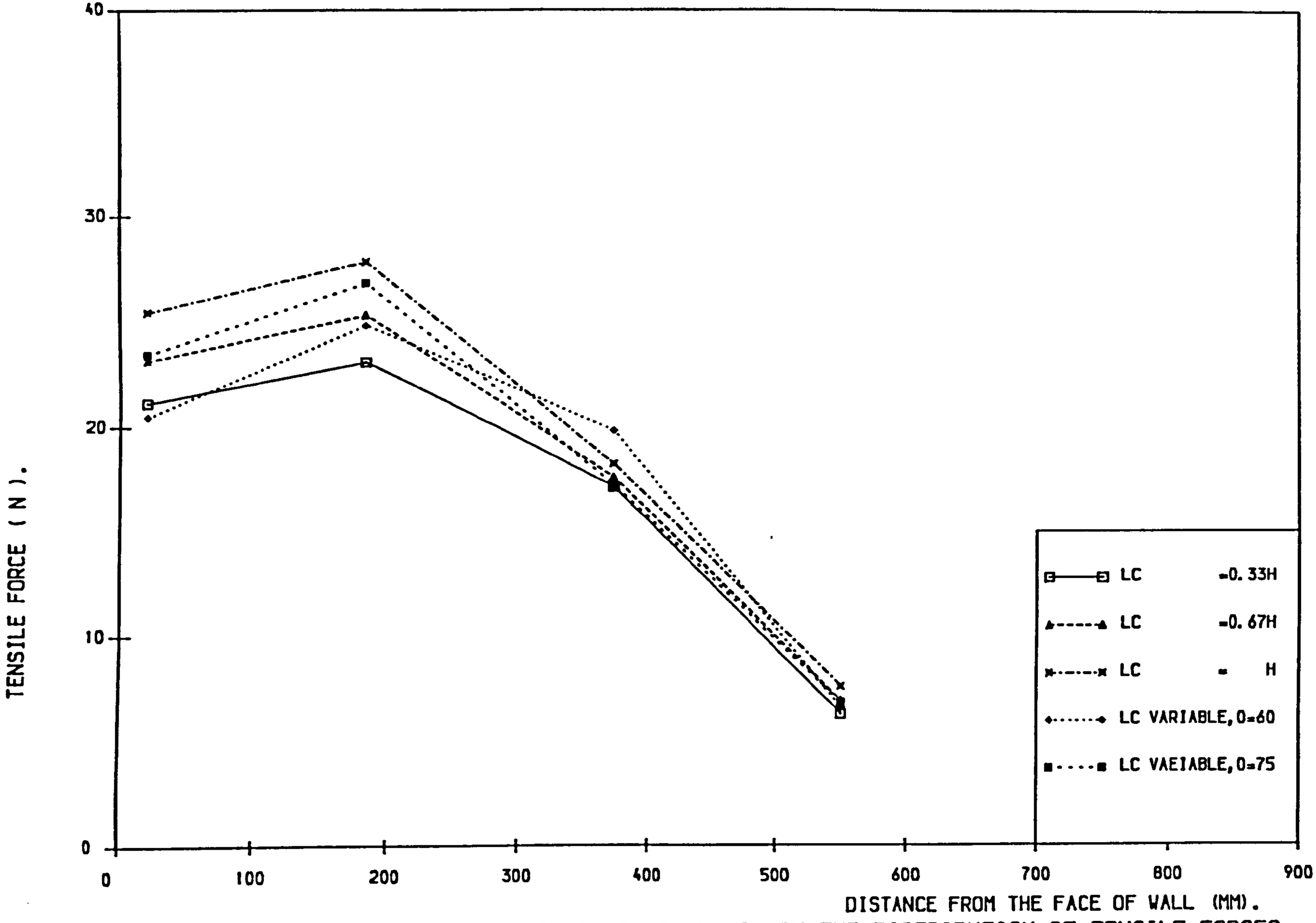

FIG. (5.24) THE EFFECT OF COMP. LENG. ON THE DISTRIBUTION OF TENSILE FORCES IN THE LOVER STRIP, CAT. III-1,2&3 AND CAT. IV-2&3.

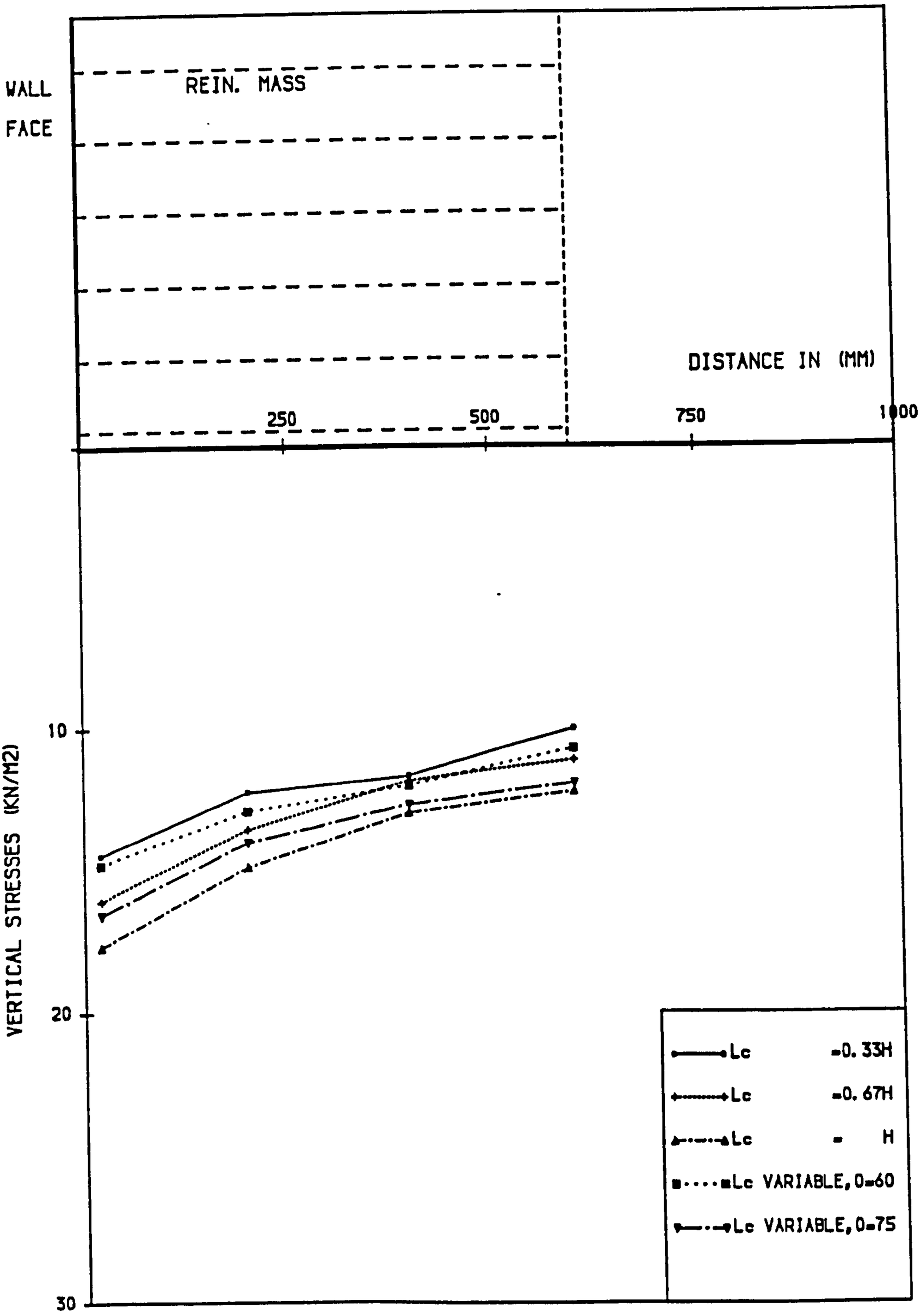

FIG. (5.25) THE EFFECT OF COMP. LENG. ON THE VERTICAL STRESSES UNDER REINF. MASS, CAT. III-1,2&3, CAT. IV-2&3.

compaction length have the same trend, i.e. the maximum value is near the toe and decreases towards the rear of the reinforced mass. An important point to note is that in the case of variable compaction length where $\theta = 75°$ and the relative density is near to the maximum relative density obtained during the tests, the vertical stress values are less than in the case of maximum compaction length used = H. This is because the compaction length at any layer is little less than H, and the compaction load is not adjacent to the wall face at any layer. Also there is some tilting near the toe, which increases when the compaction length = H.

5.4.3 The Distribution Of Earth Pressure

The distributions of horizontal stress or earth pressure on the wall face for three different uniform compaction lengths (0.33H, 0.67H, H) and for variable compaction length for $\theta = 60°$ & $75°$ are shown in Fig. (5.26). By increasing the compaction length the earth pressure distributions have been affected in both values and shape.

The maximum values are obtained when the compaction length = H, and the minimum when the compaction length = 0.33H. The values and the shape are close to each other in the case of compaction length = 0.67H & variable length for $\theta = 60°$. The important feature is that in the case of variable compaction length for $\theta = 75°$, the values are less than in the case of compaction length = H, where maximum relative density is obtained, but take almost the same shape .

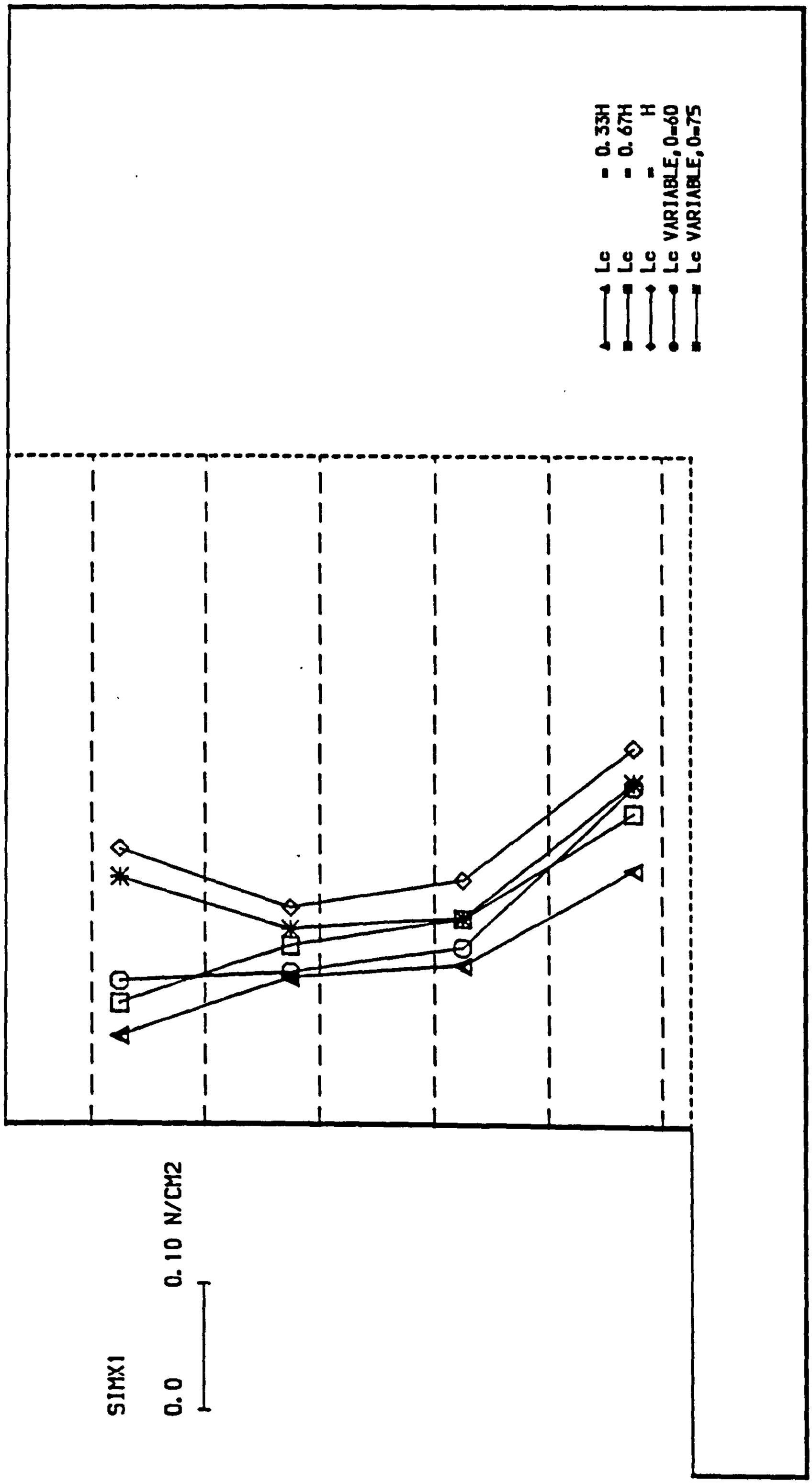

FIG. (5.26) THE EFFECT OF COMP. LENG. ON THE DISTRIBUTION OF HORIZONTAL STRESSES BEHIND THE WALL FACE CAT. III-1, 2&3 AND CAT. IV-2&3.

5.4.4 The Lateral Movement Of The Wall Face

Comparison between the lateral movement of the wall face due to different compaction lengths is shown in Fig. (5.27). In all cases of different compaction lengths (0.33H, 0.67H, H, variable length for θ = 60° & 75°) the lateral movements indicate that there is a translation and a rotational motion around the toe of the wall. By increasing the compaction length the lateral movements of the wall decrease. This is because the reinforced earth wall is a flexible system and take its stability from the stability and strength of the composite material (soil and reinforcement), and in the case of loose or weak soil (i.e. when compaction length = 0.33H) the lateral movements increase. On the other hand in the case of compaction length = H, at the maximum relative density and angle of internal friction obtained, the soil strength and its stability have improved, and there is less lateral movement because a large part of the horizontal stresses set up by the compaction plant are taken up by the reinforcing strip and do not result in high lateral movements at the wall face.

In the case of variable compaction length where θ = 75°, the lateral movement is close to case of compaction length = H and less at some points. This is because the compaction length at each layer is not adjacent to the wall face and covers most of the length of the reinforced mass.

5.4.5 State Of Stresses Behind The Wall Face

Fig. (5.28) shows the effect of different compaction lengths on the variation of earth pressure coefficient, i.e. the state of stresses behind the wall face, plotted as the ratio between the actual coefficient of earth pressure (K) and coefficient of earth pressure at rest (K_o) against depth/wall height ratio (Z/H).

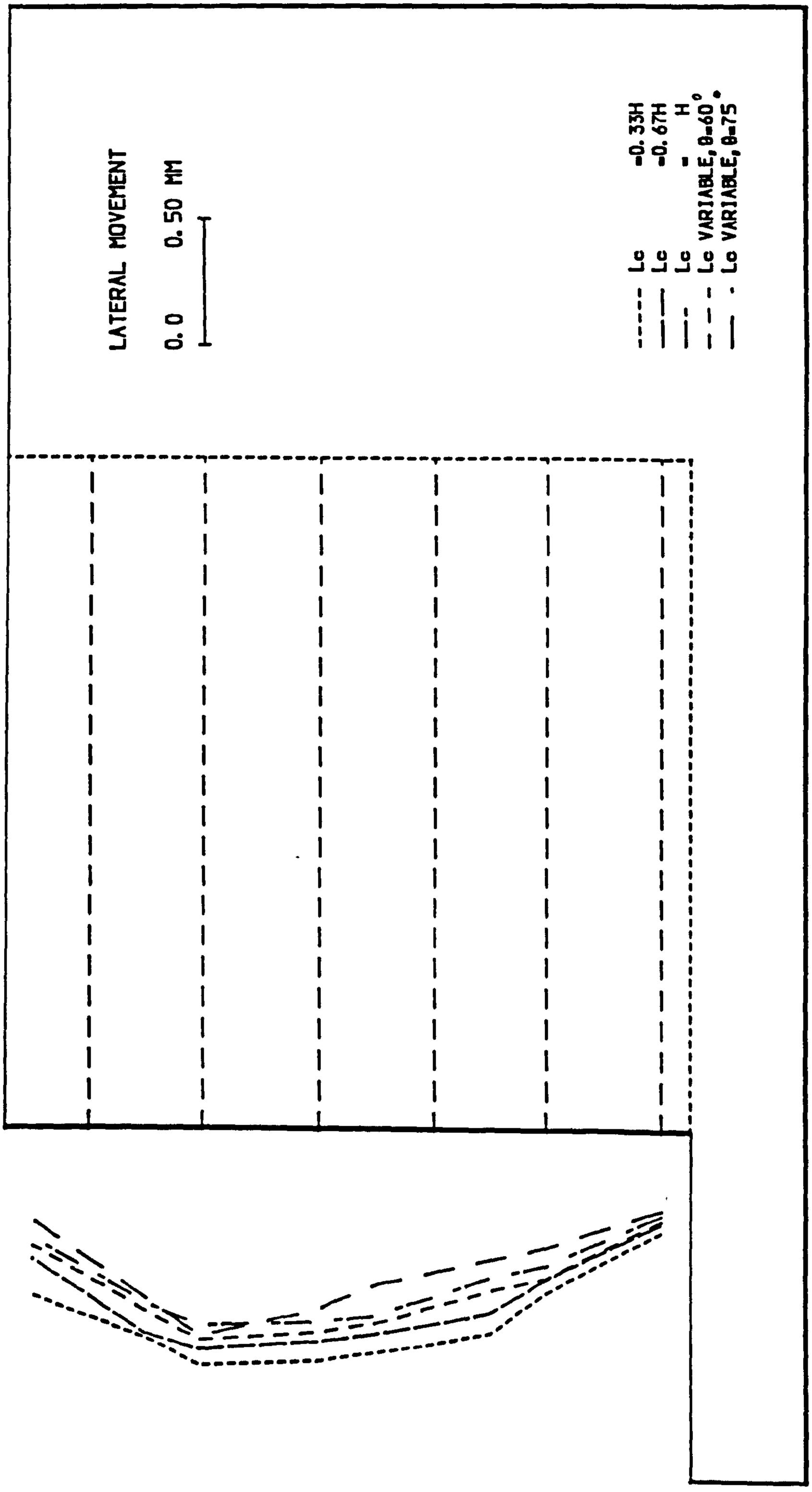

FIG. (5.27) THE EFFECT OF COMP. LENG. ON THE LATERAL MOVEMENT OF THE VALL FACE, CAT. III-1, 2&3 AND CAT. IV-2&3.

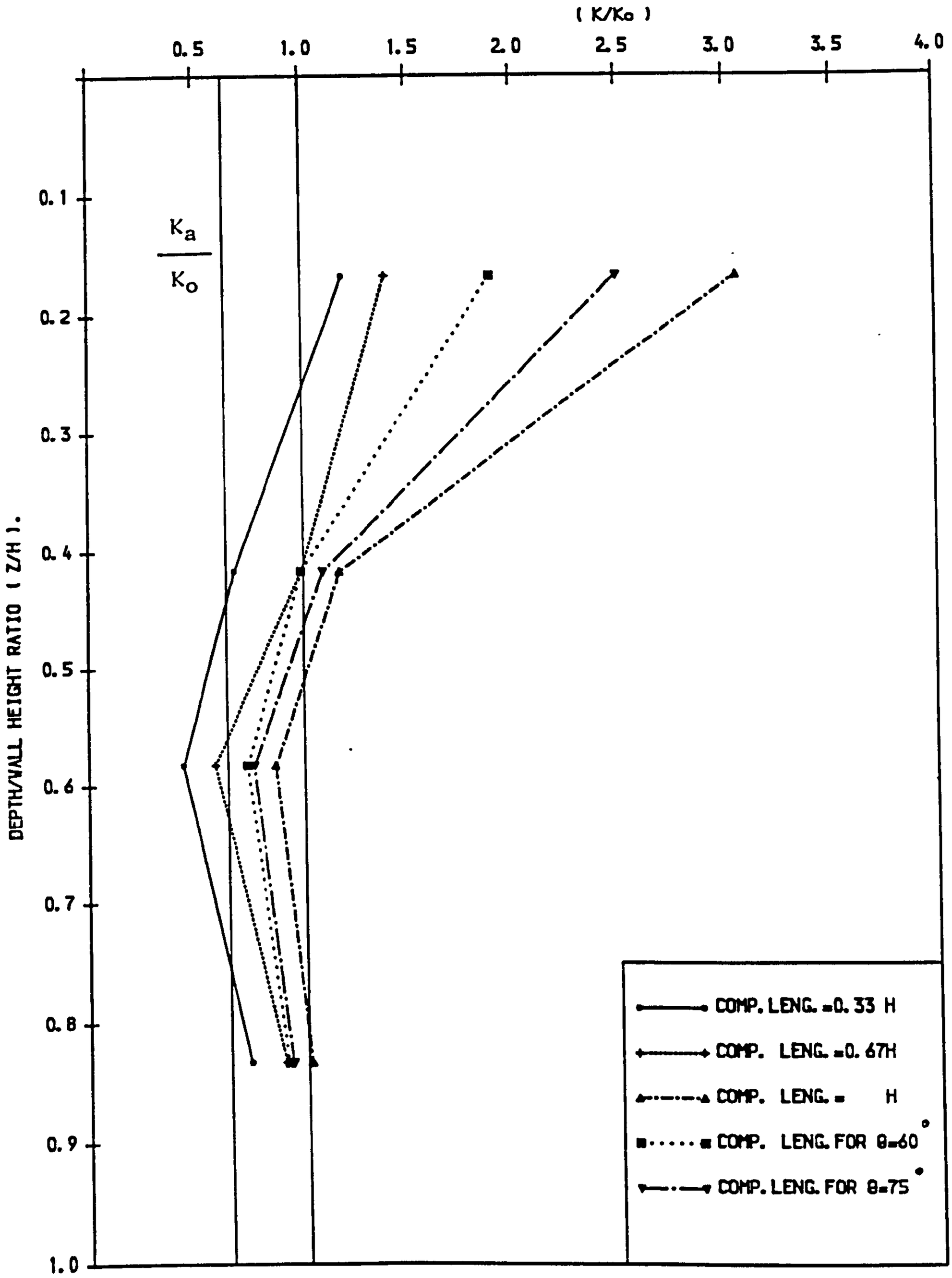

FIG. (5.28) THE EFFECT OF COMP. LENG. ON THE VARIATION OF EARTH PRESSURE COEFF., CAT. III-1, 2&3 AND CAT. IV-2&3.

From the Figure the state of stress in the upper third i.e. from the top to Z = 0.3H is greater than the at rest condition, ranging between 1.2 to 3 times the value for the at rest condition. This means that by increasing the compaction length the state of stresses increased to reach more than the at rest condition in the upper third of the wall height.

The values of coefficient of earth pressure decrease with an increase in the ratio (Z/H). They become less than the at rest condition, within the middle third and start to increase again to reach slightly more than the at rest condition near the bottom of the wall. As the compaction length increases, the depth at which the earth pressure falls below the at rest value increase and ranges from Z = 0.20 H to 0.55H for various compaction lengths.

It can be seen from the figure that by increasing the compaction length the value of (K/K_o) increases. The maximum values were obtained when the compaction length covered all the reinforced mass (i.e. the compaction length = H), on the other hand the minimum was obtained when the compaction length was 0.33H and reached less than the active state in the middle third of the wall height. Also it is interesting to note that the relation between (K/K_o) and (Z/H) takes almost the same shape for different compaction lengths.

5.5 EFFECT OF CONSTRUCTION METHOD ON THE BEHAVIOUR OF THE WALL

Comparisons were made from the results of the different model tests as follows:

1– CAT. III–3 represents the usual method of construction as in the

field. This will be referred to as method A.

2- CAT. IV-1 represents a different method of construction, where the wall face was prevented from movement during the construction process by using metal supports -as previously explained in Chapter 3- these supports being removed at the end of construction and readings taken before and after removing the wall supports. This will be refered to as method B.

It should be noted that the same compaction process and compaction length were used in both models. The comparisons will be shown in the different aspects of the reinforced earth model.

5.5.1 The Distribution Of Forces In The Strip

A comparison between the distribution of tensile forces in the lower strip is shown in Fig. (5.29). From the figure the following points can be noted:

(a) There is a significant difference between the values of tensile forces before and after wall movement in model test method B. The reason for this is that the tensile force mobilized in the strips is greatly affected by several factors. The most important is friction between the sand and the surfaces of the strip. As the friction increases the tensile forces increase. The tensile forces are mobilized when a relative movement between soil and strips takes place. Since this movement does not occur when wall movement is prevented, theoretically no tensile forces will be mobilized. But due to densification of soil as a result of compaction of the reinforced mass only and not all the backfill, a slight movement of sand grains will cause a small value of tensile force to mobilize. After wall movement large relative movement takes place, and the tensile forces

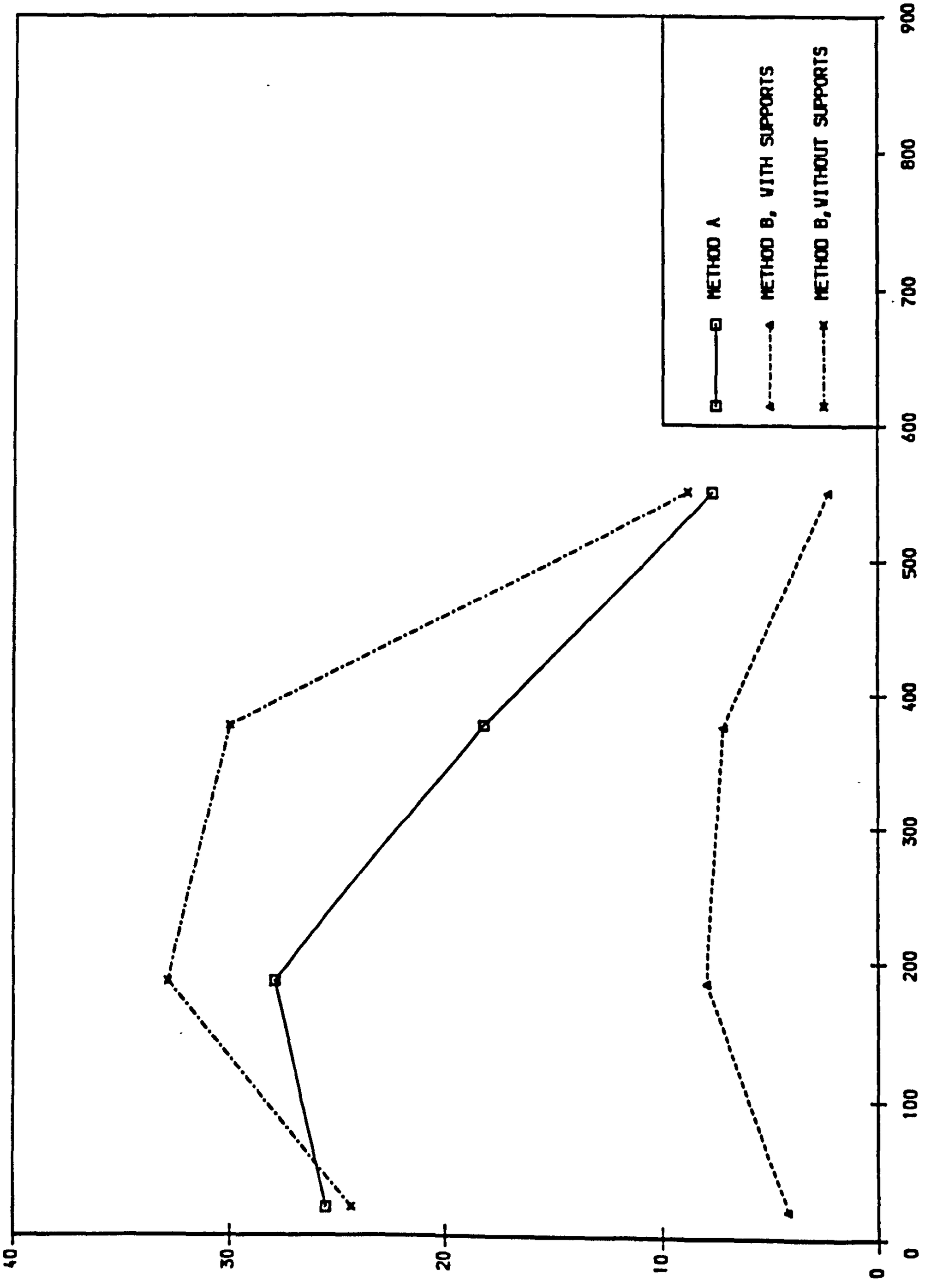

FIG. (5.29) THE EFFECT OF CONSTRUCTION ON THE TENSILE FORCES IN LOWER STRIP, CAT. III-3 AND CAT. IV-1.

are mobilized.

(b) The difference in the values and shape of the distribution of the tensile forces distribution in the strips between method (A) of and method (B), is due to the stresses which are locked in during construction as a result of the compaction load. These stresses locked in the soil were greater in method (B) than method (A) and a large portion of the horizontal stresses transmitted to the wall were resisted by the strip when the supports were removed.

5.5.2 The Vertical Stress Distribution Under The Reinforced Mass

This is given in Fig. (5.30). The distribution in all cases has the same trend, large at the toe and decreasing near the rear of the reinforced mass. The distribution has this shape in the case of method (A) because tilting of the wall at the toe takes place as a result of the compaction load. In method (B) the compaction load near the wall face does not dissipate in every direction because at the wall face movement was prevented, but near the rear of the reinforced mass a dissipation of compaction load could occur decreasing the value of stresses at the rear.

The values of stress before movement are bigger than after movement, because the soil cannot release some of stresses locked in during construction before movement. But after movement, the soil releases some of the stresses locked in during the construction process and hence the value of vertical stresses decreases, although the value is still larger than in method (A), where the soil loses a larger amount of locked in stress.

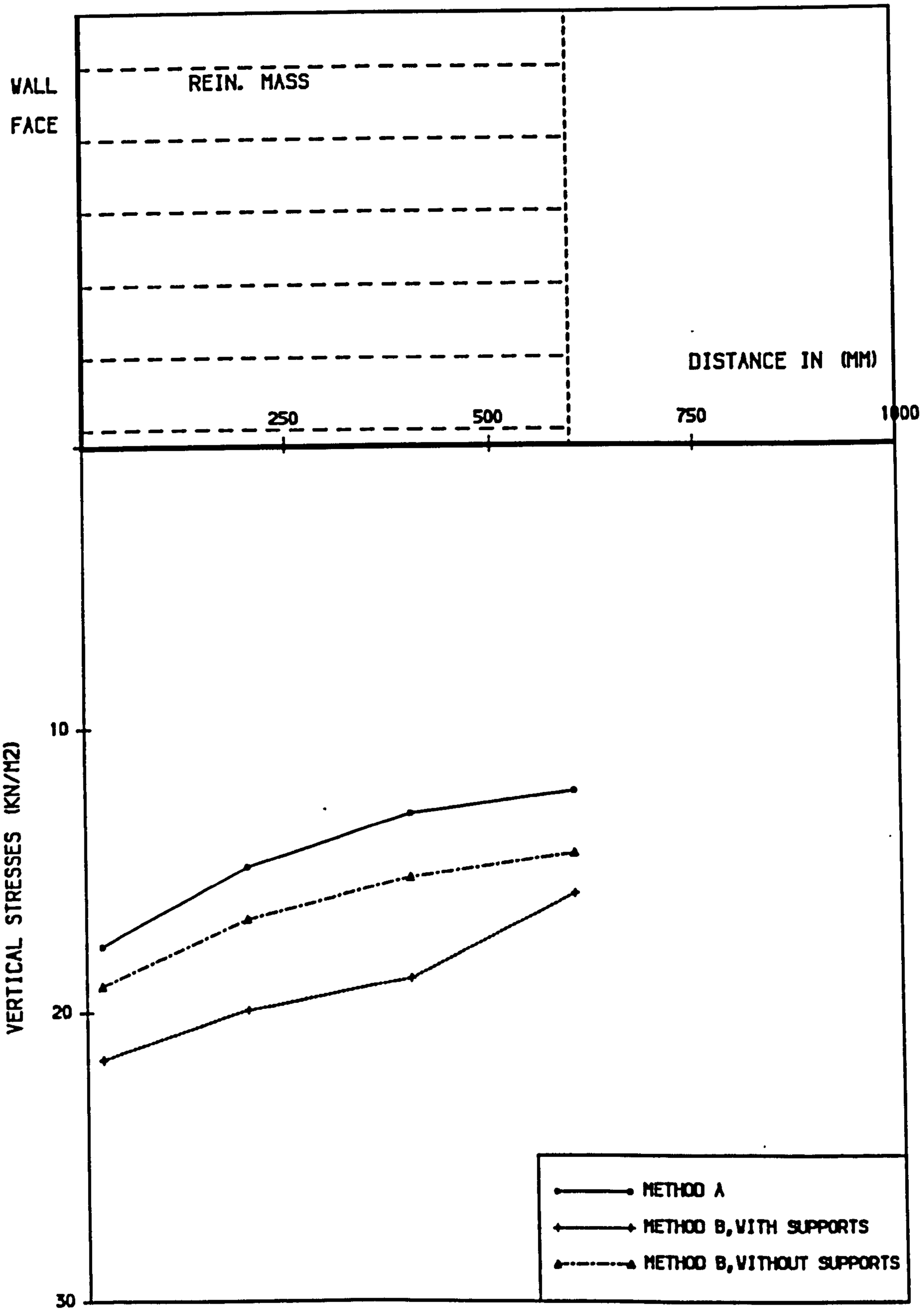

FIG. (5.30) THE EFFECT OF CONSTRUCTION METHOD ON THE VERTICAL STRESSES UNDER REIN. MASS., CAT. III-3&CAT. IV-1.

5.5.3 The Distribution Of Earth Pressure

Fig. (5.31) shows the effect of construction methods on the horizontal stresses or earth pressures behind the wall face. The comparison is between method (A) and method (B) (before and after removing the supports). The distribution of earth pressure before the wall supports are removed is a straight line and the value increases from the top to the bottom. The average pressure is 33% more than the value after the supports are removed. This is because the compaction plant was adjacent to wall face and most of the load caused by it was transmitted directly to wall face.

After the supports were removed, the earth pressure decreased. This is due to the movement of the wall which caused some release in soil densification and reduction in the horizontal stresses. It is noted that the earth pressure after the supports were removed is still about 13% more than the earth pressure from the method (A). The reason is that the soil rebounds during construction and retains less residual stresses than in the other case.

5.5.4 Lateral movement of the wall face

The distribution of lateral movement of the wall face due to the different methods of construction is shown in Fig. (5.32).

It was noted that during model test method B, and just after removing the wall supports, a sudden movement occurred. The movement stopped after several minutes and the final lateral movement is shown in the figure. In the case of method (A) the movement occurred gradually during the construction and the final shape is shown in the figure.

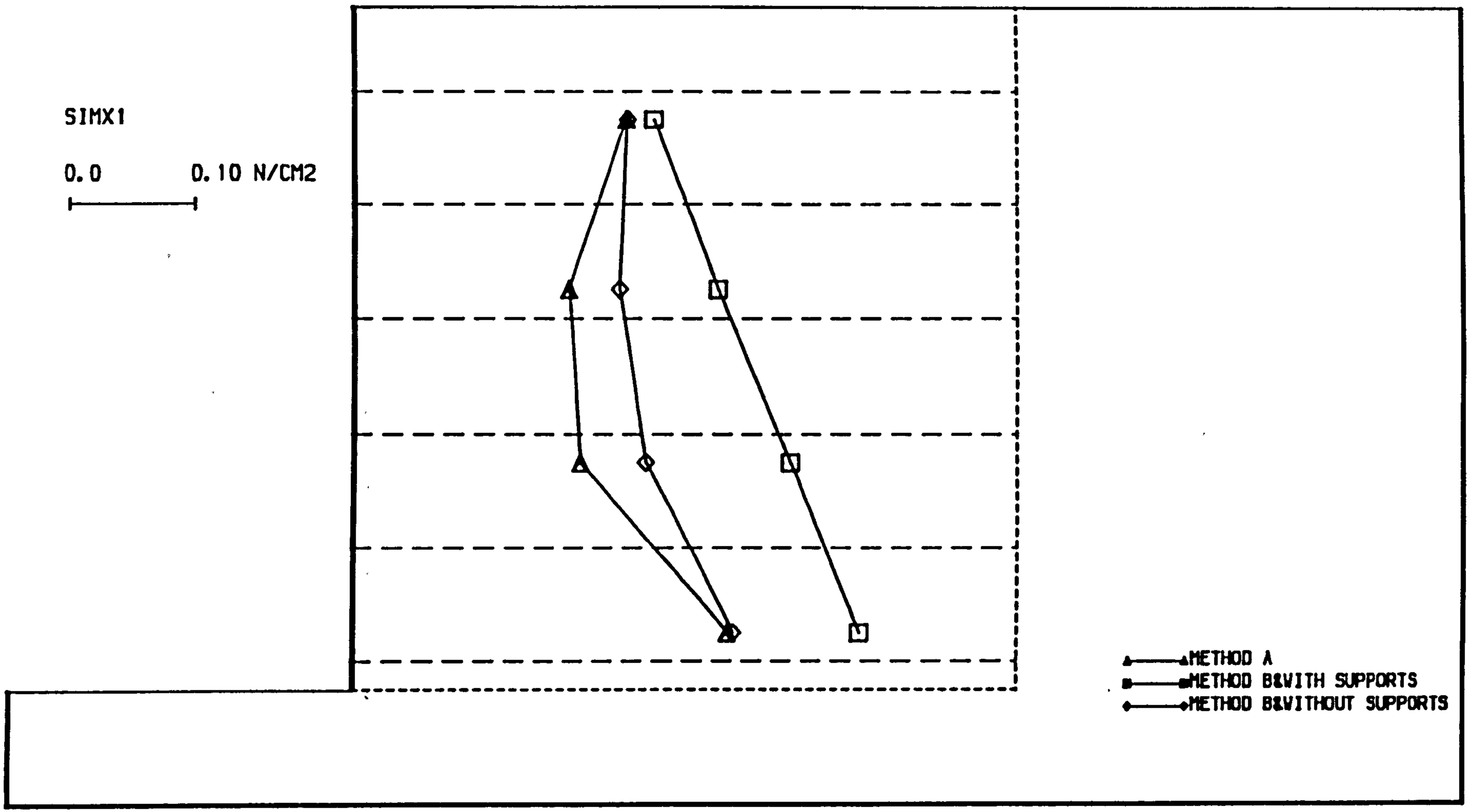

FIG. (5.31) THE EFFECT OF CONSTRUCTION ON THE MAX. HORIZ. STRESSES ON THE WALL FACE, CAT. III-3 AND CAT. IV-1.

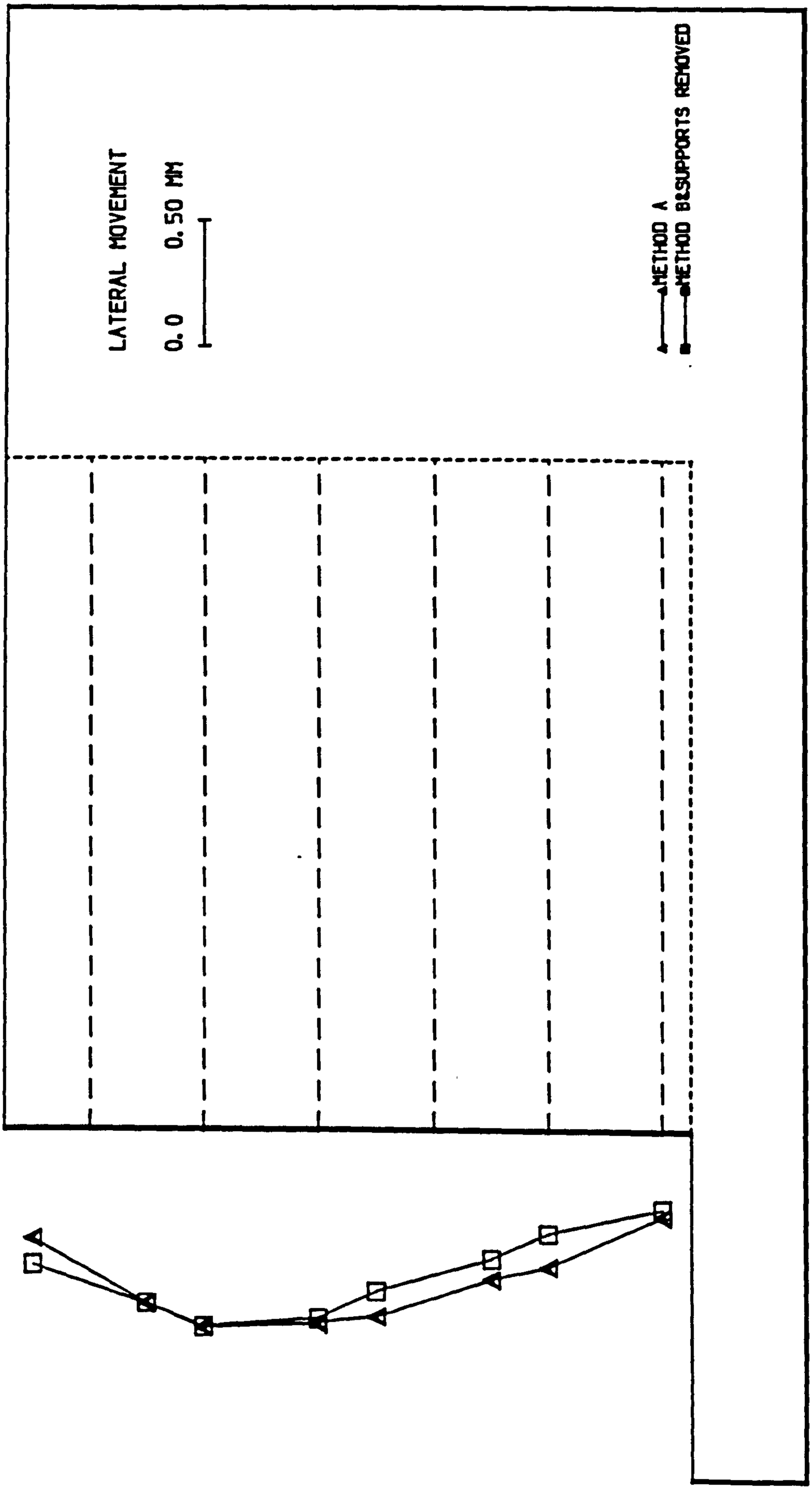

FIG. (5.32) THE EFFECT OF CONSTRUCTION ON THE LATERAL MOVEMENT OF THE WALL FACE, CAT. III-3 AND CAT. IV-1.

The movements in both cases are similar in shape, and the values of lateral movement are the same at the maximum point in the upper third of the wall. But in general the values of lateral movement after removing the supports is about 8% less than in method (A). This is due to an increase of forces in the strips which resist the earth pressure and the wall movement.

5.6 CONCLUSION

The results from preliminary model walls have been presented to check the performance of the instruments used in the models, and also to ensure the reproducibility and repeatability of the results. The results implied that the differences in readings in general are reasonable.

The behaviour of the different elements of a model reinforced earth retaining wall have been studied before, during and after compaction as the behaviour of the wall as one unit.

The effect of compaction length as well as different construction methods on the behaviour of the model has been presented.

All the results showed that the values of tensile forces in the strips, horizontal pressure on wall face and the distribution of vertical stress under the reinforced mass increased during compaction and were larger than before or after compaction. The values after compaction were greater than before compaction, ranging between 10 to 15% more.

This was because during the compaction process vertical stresses became

locked in due to densification of the soil, and this affected all the elements of the reinforced earth wall. After compaction the soil started to rebound and lost some of its densification and hence some – but not all– of the locked in vertical stresses, leading to the residual stresses which remained after compaction affecting all the elements of the wall.

The compaction length which covered most of the reinforced mass and at the same time was not too close to the wall face reduced this effect.

The method of construction which permitted movement to occur gradually helped to reduce and release the residual stresses, and hence reduced the effect.

The state of stresses behind the wall face was greater than the at rest condition especially in the upper third. In the middle third it was between active and at rest condition, at the lower third it was near the at rest condition.

From previous discussion it is obvious that the compaction process has a great effect on the behaviour of the wall. More theoretical study is needed to simulate and calculate the effect of compaction plant on the wall, and this will be shown in the next chapter.

CHAPTER 6

THEORETICAL STUDY OF COMPACTION

6.1 INTRODUCTION

The factors affecting modelling of reinforced earth compaction are described in this chapter, and a review and comments on existing theories of compaction are presented. New proposed models of compaction plant and a computer program to calculate horizontal stresses in a free field and on a vertical wall are explained. Comparisons between horizontal stresses in a free field or on a vertical wall resulting from the new models and from classical theories, experimental work and a full scale field test are illustrated to verify the workability of the models . A conclusion is given for this theoretical study on compaction.

6.2 FACTORS AFFECT MODELLING OF COMPACTION

Prediction of the behaviour of granular soils under applied loading such as compaction is a common problem in Geotechnics. Researchers such as: Terzaghi (1934), Spangler (1938), Broms (1971), Aggour and Brown (1974), Sherif and Mechey (1977), Ingold (1979), and Carder et al. (1980) have pointed out that compacting backfill behind a retaining wall can develop high lateral earth pressures which are greater than the normally assumed design pressure and cause unexpected deflections of the structure.

Prediction of the magnitude and distribution of the pressure during the period of compaction and the pressure remaining in the soil after compaction is very important for the correct design of earth structures such as reinforced earth retaining walls. Two main factors affect the prediction of the magnitude and distribution of lateral pressure, the first is related to the soil and the second to the compaction.

Since the compaction process involves compacting the backfill by means of compaction plant, both the previous factors affect each other and it can be said that the factors which influence the modelling of compaction are:

(1) Modelling of soil behaviour before and after compaction, including the following:

(a) Representing the nonlinear stress–strain characterstics of the soil in the analyses in a reasonable way before and after compaction. A large number of laboratory and theoretical studies have been performed for this reason, by Kondner (1963), Lade (1971), Khosla and Wu (1976), Duncan et al. (1980).

(b) Past loading / unloading history (stress path) is significant in terms of its potential for altering the performance and affecting the soil deformation as demonstrated in work by Lade and Duncan (1976), Lambrechts and Leonards (1978).

(2) Modelling of construction sequence:

The construction sequence in the field is as follows:

(a) Placement of layer of fill (lift).

(b) Compaction of layer of fill.

(c) Placement of structure (facing panels and reinforcement in the case of a reinforced earth retaining wall).

(d) Application of loads to completed structure.

Simulation of this real sequence of construction has a great effect on the compaction modelling. Theoretically it is not easy to idealize the problem and a special technique such as the finite element technique is required. Experimentally the simulation has been carried out as shown in the laboratory work (Chapter 2&3).

(3) Modelling of compaction plant:

One of the keys to the success of modelling compaction is the correct modelling of compaction plant, taking into account the nature of the problem as a three dimensional problem which allows for the three dimensional nature of stresses arising as a result of compaction loading. These include:

(a) The actual weight of compaction plant.

(b) The actual dimensions of compaction plant.

(c) Number of passes.

Most of the work done on modelling compaction, simulates the compaction plant as a point load or a line load or a load of finite extent, as will be obvious in the next section.

6.3 REVIEW OF PREVIOUS STUDIES ON COMPACTION

Several theories and analytical methods have been proposed to explain and/or analyze the lateral and residual earth pressures induced by soil compaction.

Attempts were made by Terzaghi (1920) to evaluate the lateral earth pressure coefficient (K_o) by loading and unloading samples of sand in a rigid steel frame which prevented the lateral expansion and contraction of the soil. The earth pressures in the horizontal and vertical direction were measured by thin steel strips which were placed horizontally and vertically in the soil. The coefficient of lateral earth pressure at rest (K_o) was assumed to correspond to the ratio of the forces required to pull the vertical and horizontal steel strips out of the soil.

Similar compressibility tests, where the lateral expansion of the samples was prevented, were carried out by Tschebotarioff and Welsh (1948). However these conditions are only indirectly related to the lateral pressures produced by compaction.

Rowe (1954) proposed a theory for the calculation of horizontal pressures mobilized on an earth structure. His work did not examine the effect of compaction on lateral earth pressures, but calculated earth pressures for conditions of wall deflection intermediate between the at-rest and fully active or fully passive conditions. His theory for the calculation of lateral pressures exerted on structures by cohesionless soil was based on the following assumptions:

(1) The degree of mobilization of the soil friction angle (φ) and the wall friction angle (δ) depends on the degree of interlocking of the soil grains, which depends on the frictional movement of the shear planes or slip strain defined as relative shear displacement/total slip plane length. The friction angle developed

increases from some relatively low value to a higher limiting or ultimate value as slip strain increases.

(2) Earth pressures acting on a retaining wall or structure may be calculated by a conventional limiting equilibrium method (gravity analysis of sliding wedges) using the frictional angles φ & δ developed.

The basic mechanics of Rowe's theory are illustrated schematically in Fig. (6.1.A&B). By considering all possible wedges from the smallest (at the top of the wall) to the largest (full wall height), distributions of lateral earth pressures acting can be determined. Rowe supported his theory by performing a series of direct shear tests on several different sands in order to obtain the friction angles developed at various levels of slip strain, using these values to calculate lateral earth pressures for sample problems.

He reported that after tamping a fill behind a wall, the lateral pressure will be almost as great as the value which acted under the preconsolidation pressure and he suggested that the final coefficient of earth pressure could be expressed as:

$$K_o' = K_o \ (1 + h_o/h) \qquad (6.1)$$

Where:

K_o' is final coefficient of earth pressure.

K_o is coefficient of earth pressure at rest.

h_o is equivalent soil height of surcharge load.

h is overburden height.

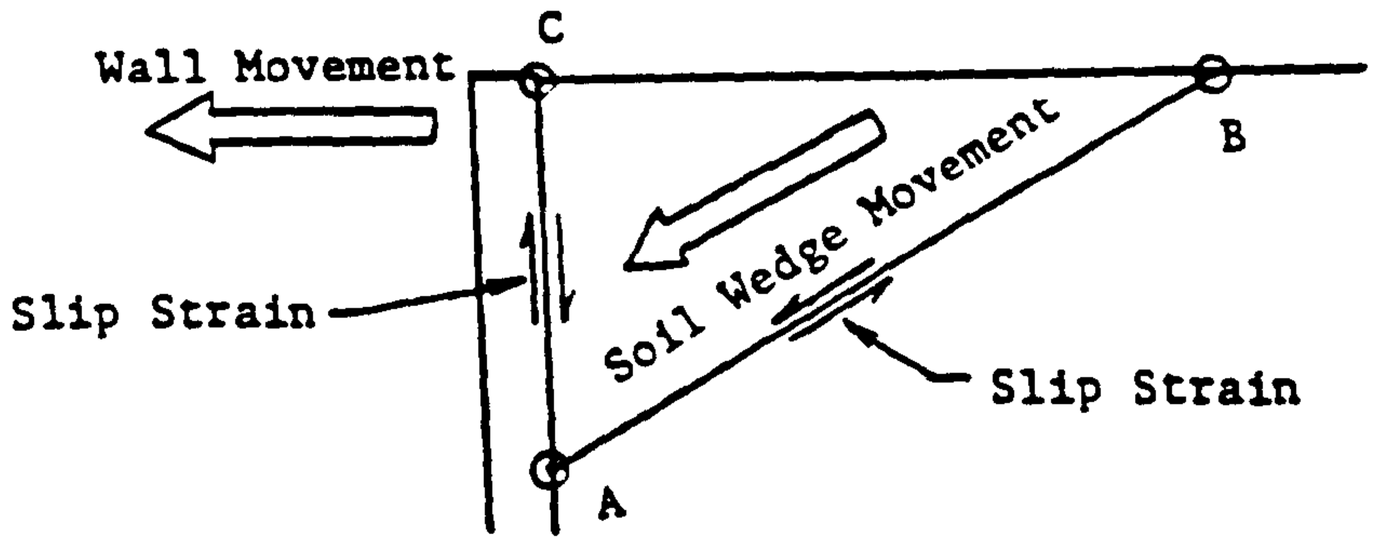

(A) SLIP STRAINS OF A TYPICAL SLIDING WEDGE.

(B) EXAMPLE OF FORCE EQUILIBRIUM ANALYSIS FOR A TYPICAL SLIDING WEDGE.

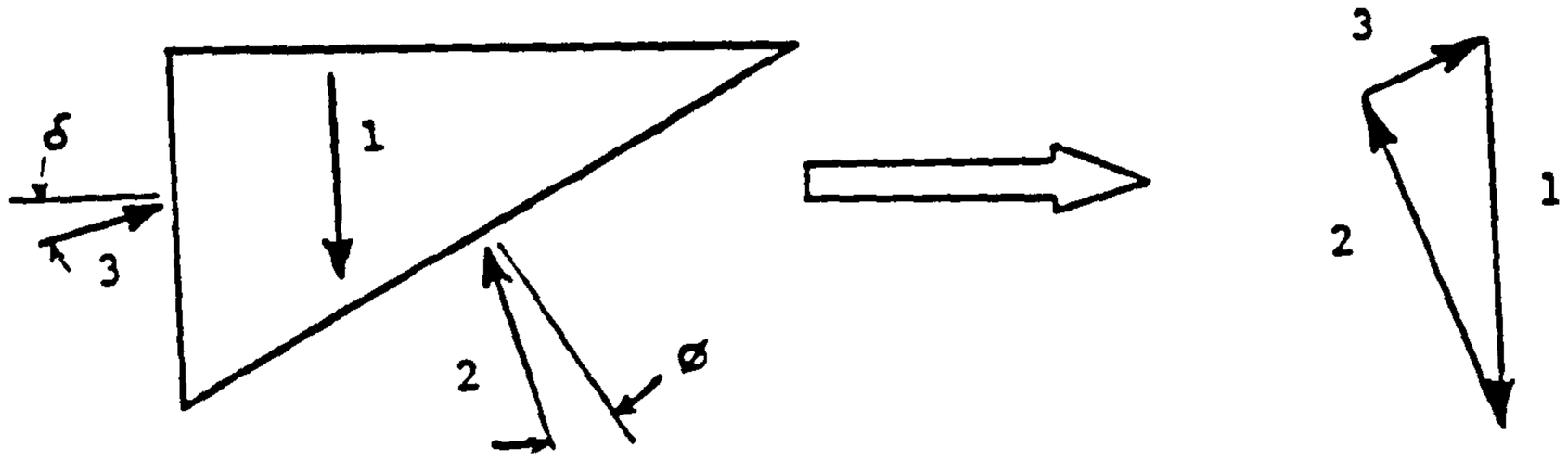

1 = Weight of soil.
2 = Force exerted on sliding wedge by underlying soil.
3 = Force exerted on sliding wedge by wall.
δ,Ø = Friction angles developed as a result of slipstrains.

FIG. (6. 1) MECHANICS OF ROWE'S THEORY (AFTER ROWE, 1954).

Rowe further suggested that the maximum residual lateral earth pressure would be limited by the remaining vertical pressure such that $K'_o < K_p$ (coefficient of passive earth pressure).

Sowers et al. (1957) introduced a theory to explain the residual lateral earth pressures induced by compaction which also considered sliding with strain reversal. They assumed that the soil mass consisted of individual incompressible particles and compaction took place by a movement making an angle of (β) with the direction of vertical pressure due to compaction (σ_{vc}). If the angle of friction between the particles is ψ as shown in Fig. (6.2.A) and horizontal pressure due to compaction is σ_{hc}, then the coefficient of earth pressure at rest (K_o) could be calculated as follows:

$$K_o = \frac{\sigma_{hc}}{\sigma_{vc}} = \frac{\tan (\beta - \psi)}{\tan \beta} \qquad (6.2)$$

If the vertical compacting pressure is reduced to σ_{vr} then the soil tries to recover to its original volume i.e. reversing the direction of the strain. In this case the friction force (R) on the plane of movement reverses as shown in Fig. (6.2.B) and the coefficient of residual pressure (K_r) can be expressed as follow:

$$K_r = \frac{\sigma_{vr}}{\sigma_{hr}} = \frac{\tan (\beta + \psi)}{\tan \beta} \qquad (6.3)$$

Sowers et al. performed a series of field and laboratory tests to examine the residual lateral earth pressures induced by compaction. Their analysis led to the following conclusions:

(i) Residual lateral pressures are of importance primarily when the structure

does not deform sufficiently to release earth pressure.

(ii) The residual pressure is a function of the vertical pressure remaining in the soil after compaction and is related to Poisson's ratio.

Schmidt (1967) carried out uniaxial strain tests (primary and rebound tests) under K_o conditions in order to measure the lateral and residual pressures. He used many soils of sand and clay and some of his results are shown in Fig. (6.3.A&B). He postulated an empirical expression to calculate the residual coefficient of earth pressure as follows:

$$K_r = K_o \left(\frac{\sigma_{vmax.}}{\sigma_v}\right)^{\alpha} \qquad (6.4)$$

Where:

K_r is Residual coefficient of earth pressure.

K_o is coefficient of earth pressure at rest.

σ_{vmax} is vertical pressure (σ_v) + vertical pressure due to compaction (σ_{vc}).

α is 0.3 – 0.5 for sand & (1.2 sin φ) for clay.

φ is angle of internal friction.

The equation can be written as follows:

$$K_o' = K_o \left(1 + \frac{h_o}{h}\right)^{\alpha} \qquad (6.5)$$

It is interesting to note the similarity between Rowe's early equation (1954) for residual compaction induced lateral earth pressure Equ. (6.1) and the above

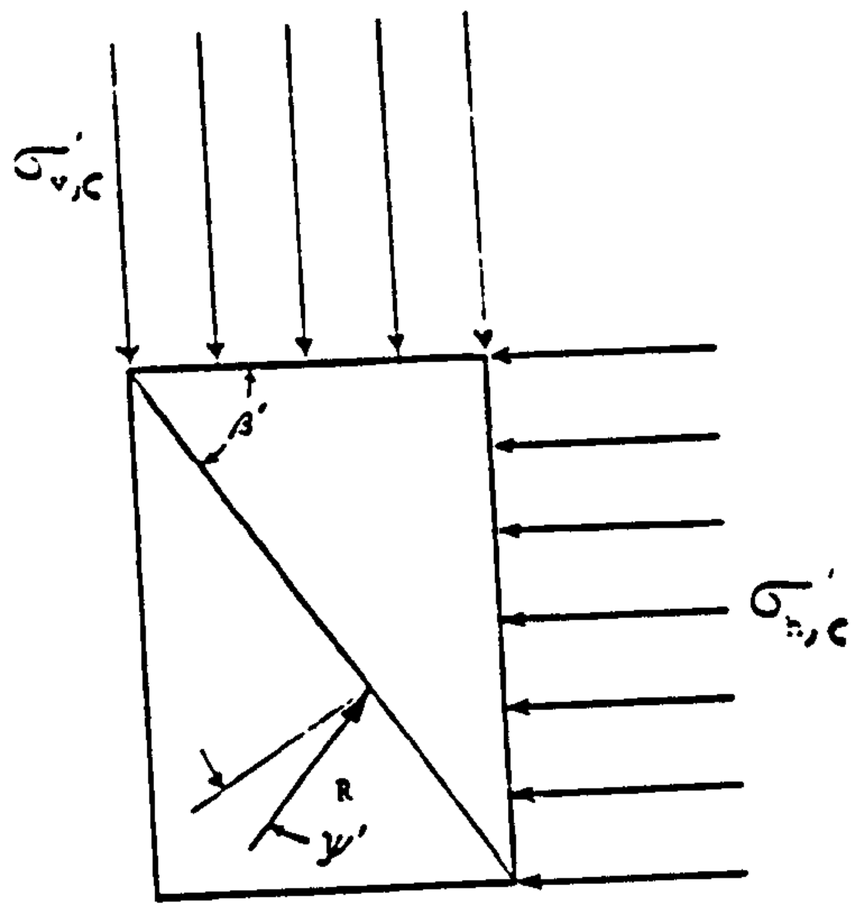

(a)

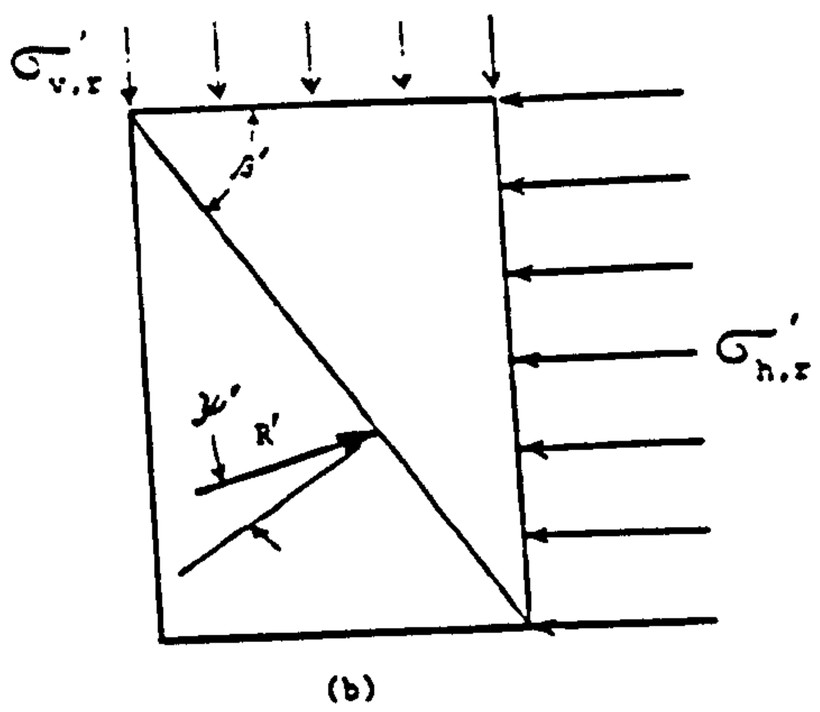

(b)

FIG. (6.2) MECHANICS OF RESIDUAL LATERAL PRESSURE (AFTER SOWERS ET AL., 1957).

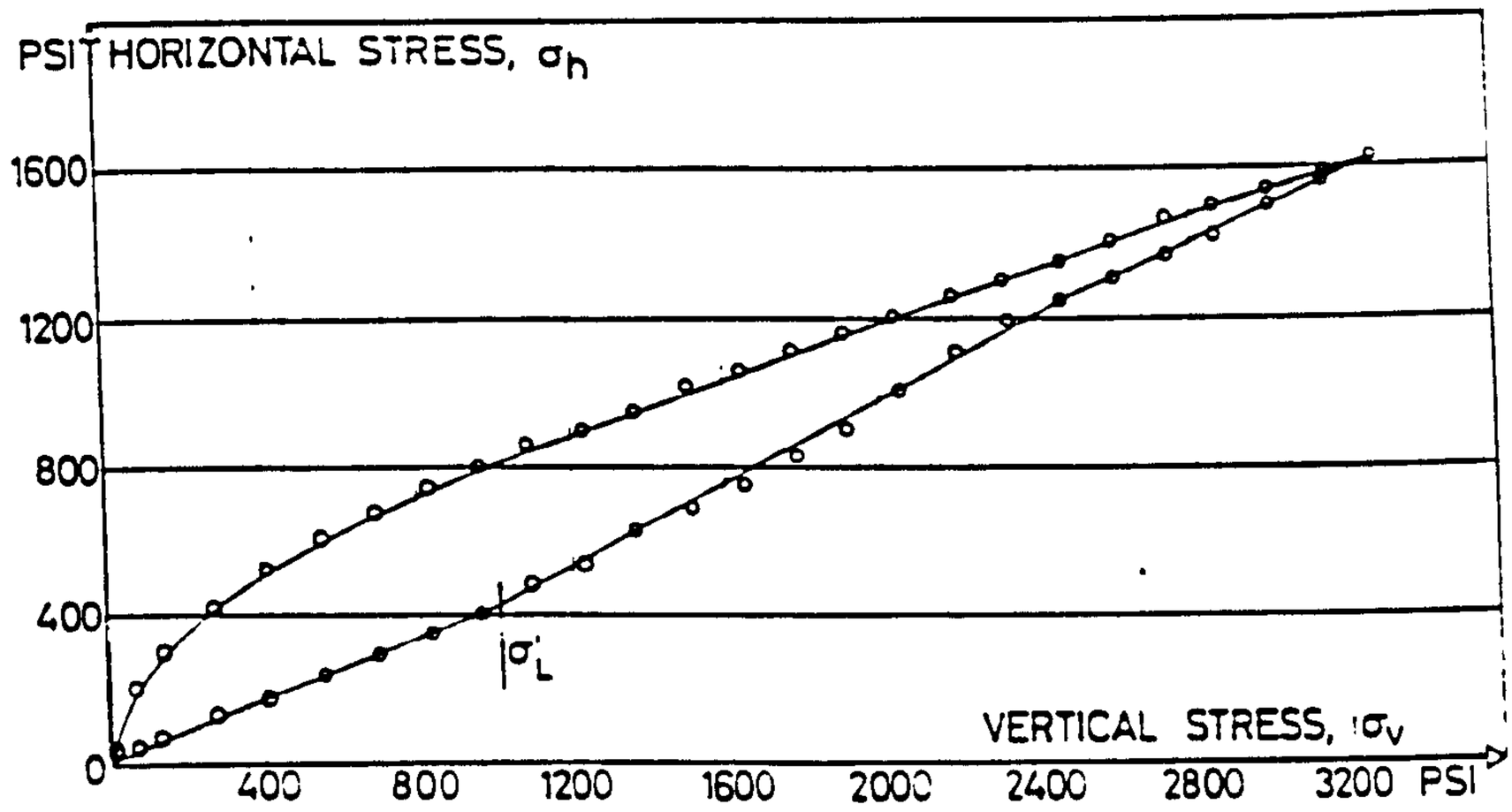

(A) PENNSYLVANIA SAND. VOID RATIO 0.68, RELATIVE DENSITY 0.70.

FIG. (6.3) UNIAXIAL STRAIN RESULT (AFTER SCHMIDT 1967).

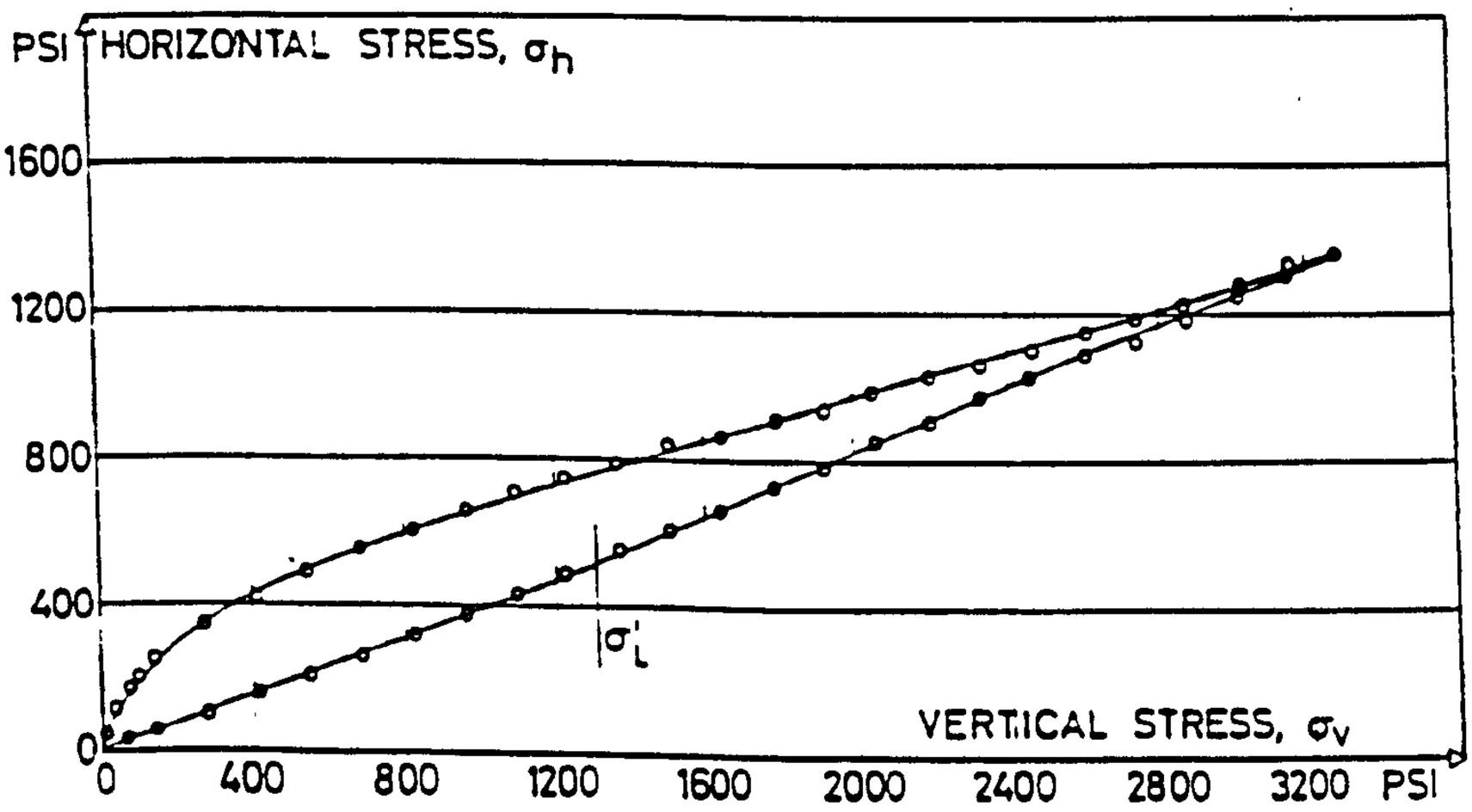

(B) WABASH RIVER SAND. VOID RATIO 0.55, RELATIVE DENSITY 0.55.

equation proposed by Schmidt (1967).

Broms (1971) presented a stress path theory to explain residual lateral earth pressures on rigid vertical non–yielding structures resulting either from compaction or other surcharge loading which is subsequently removed.

The theoretical basis for Broms' theory is illustrated in Fig. (6.4.A). An element of soil at depth is considered to exist at some initial stress state represented by point (A) with horizontal and vertical effective stresses of σ'_{ho} and σ'_{vo} respectively. Compaction of the soil is considered as a process of loading and unloading. When the overburden pressure is increased (loading) there is little change in lateral pressure until the ratio of lateral/vertical effective stresses is equal to K_o (point B), where K_o is the coefficient of earth pressure at rest. Thereafter, increased vertical stress is accompanied by increased lateral stress according to ($\sigma'_h = K_o \sigma'_v$), corresponding to primary or virgin loading until point C. The soil is therefore regarded as preloaded between A and B and as normally loaded between B and C with respect to the initial lateral earth pressure.

When the soil is unloaded (C to D) as shown in Fig. (6.4.A) the corresponding decrease of the lateral earth pressure will be small as has been pointed out by Rowe (1954). It will be assumed that this decrease is negligible until point D has been reached. With further decrease of overburden pressure the lateral earth pressure will decrease approximately in proportion to the overburden pressure ($\sigma'_h = K'_o \sigma'_v$) where K'_o is the earth pressure coefficient during unloading.

By following this type of stress path an element of soil can be brought to a final state represented by an effective coefficient of lateral earth pressure varying

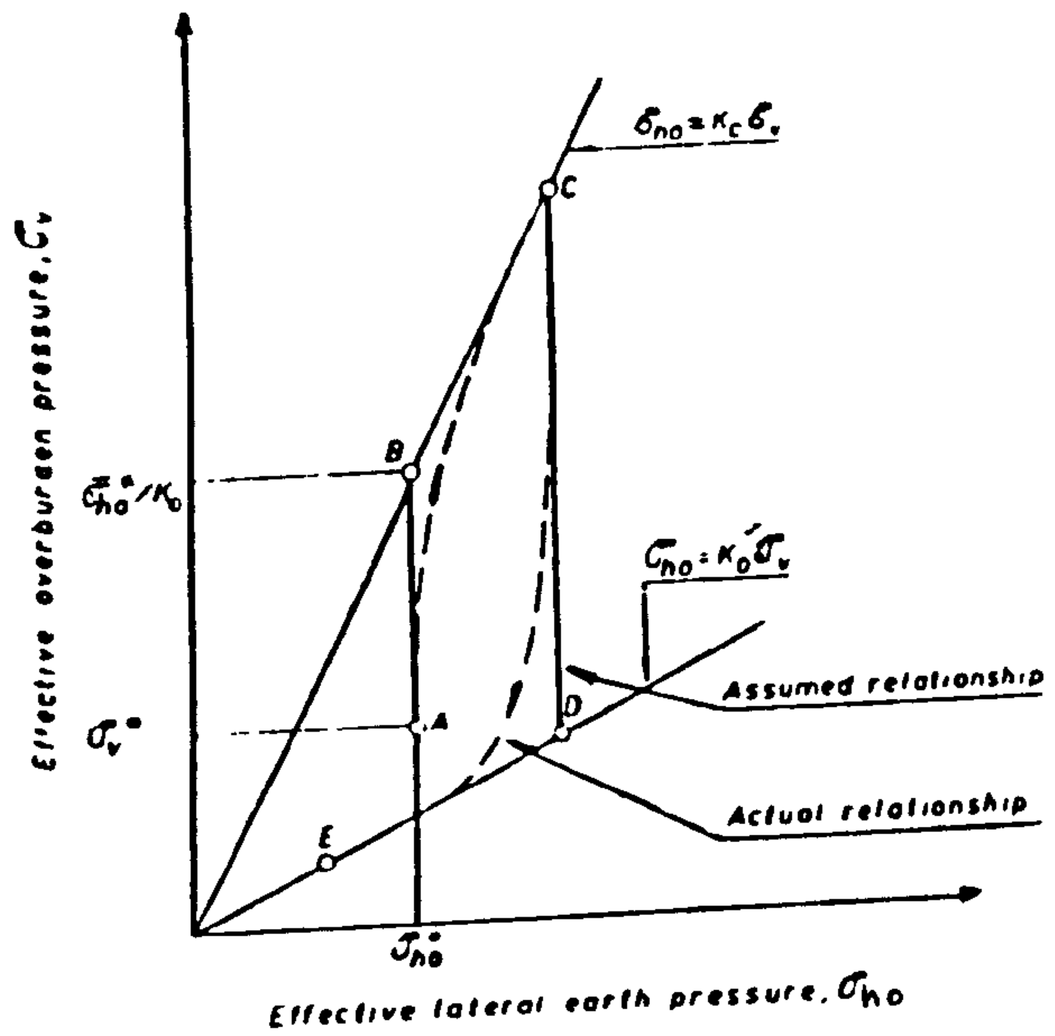

(A) GENERALIZED SOIL ELEMENT.

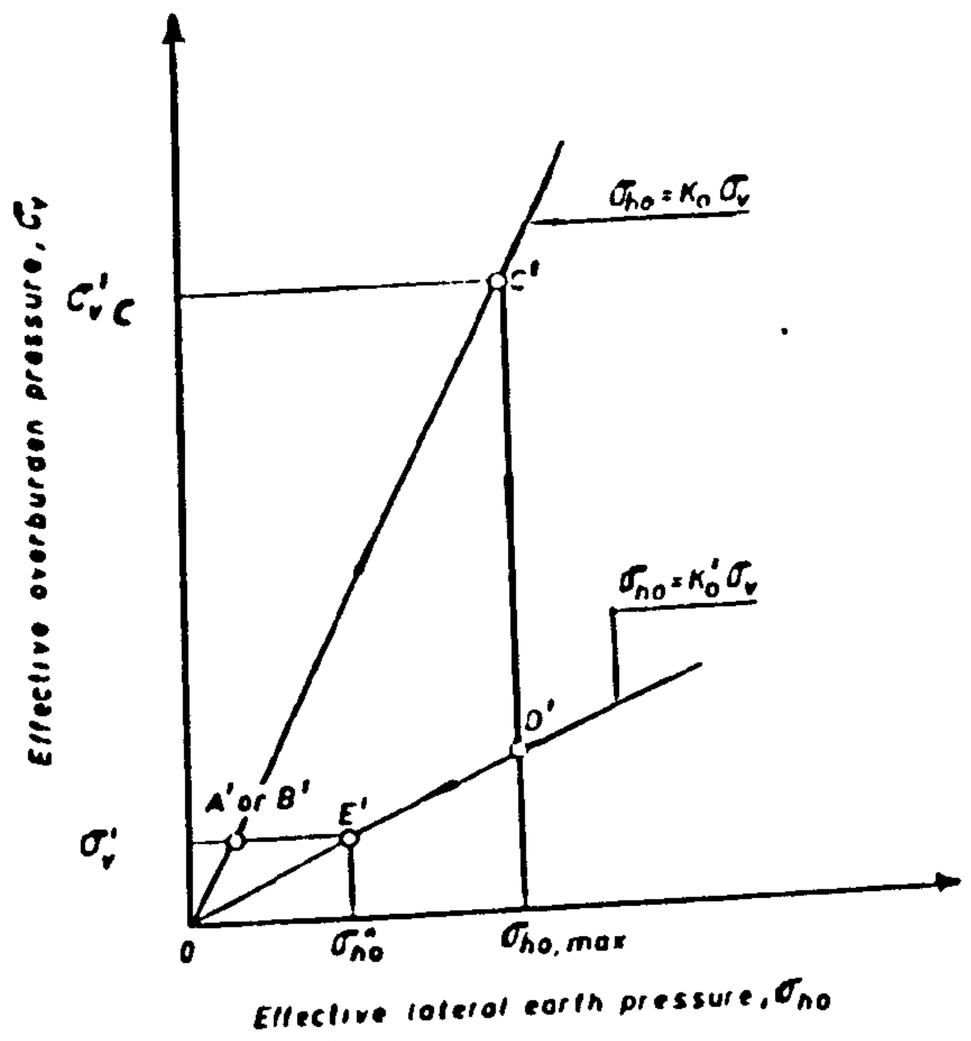

(B) SHALLOW SOIL ELEMENT ,
$Z < Z_{cr}$

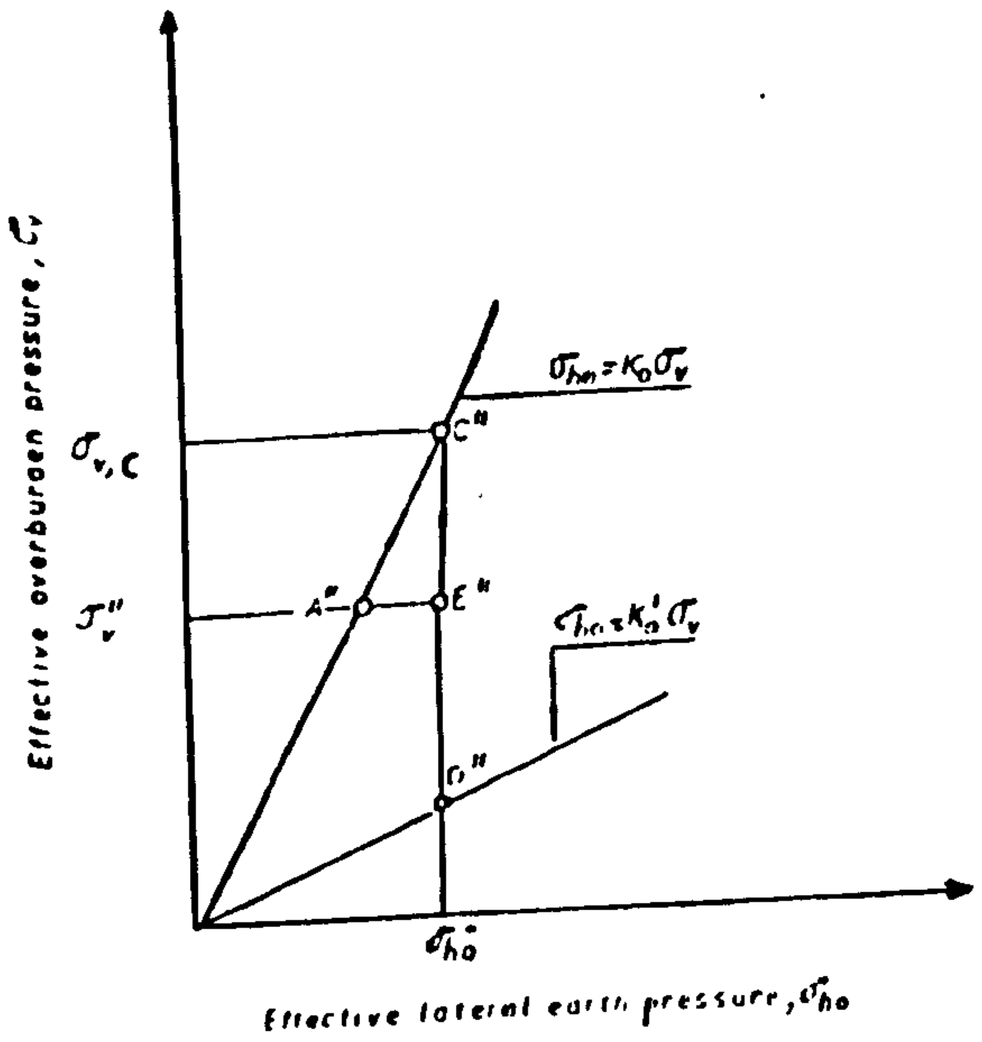

(C) DEEP SOIL ELEMENT ,
$Z > Z_{cr}$

FIG. (6.4) STRESS PATH DURING COMPACTION (AFTER BROMS, 1971).

as $K_o < K_{eff} < K'_o$ and the actual stress path followed by a real soil element might be as represented by the dashed line in Fig. (6.4.A).

Fig. (6.4.B) shows the loading path for a shallow soil element at depth $Z < Z_{cr}$ where Z_{cr} is a critical depth defined later. The soil is loaded from A ' to C ', then unloaded to E ', the later stages of unloading following the path ($\sigma'_h = K'_o \sigma'_v$) resulting in a final condition ($K_{eff} = K'_o$).

Fig. (6.4.C) shows the loading path for a deeper soil element at a depth $Z > Z_{cr}$. After loading from A " to C ", the unloading to E " is not sufficient to bring the soil element to the limiting condition (i.e. $\sigma'_h = K'_o \sigma'_{vmax}$), which would not be reached until the element was unloaded to D " .

In employing this theory to estimate the lateral pressures exerted on a vertical, rigid, nonyielding structure by compaction Broms considered the compaction plant to be represented by a load applied to the fill surface inducing vertical stresses which may be approximated as twice those calculated by the Boussinesq stress equation for an infinite half space (Terzaghi, 1942).

Following the previous process and knowing (or assuming) values of K_o and K'_o, a residual lateral pressure can be calculated. An example, for a 10.2 ton smooth wheel roller is shown by the shaded area in Fig. (6.5.A), where line 23 represents the residual lateral stresses for elements below Z_{cr} and line 02 represents the limiting stresses as controlled by the available overburden pressure and the limiting condition $\sigma_h = K'_o \sigma_v$, and point 2 where these two lines intersect, occurs at a depth Z_{cr} called the critical depth.

By considering the backfill process as the placement of a series of soil layers each deposited and then compacted in turn so that this stress distribution results

for each new layer, and by considering that the minimum lateral pressure possible at any depth (as a function of overburden) will be $\sigma_h = K_o \sigma_v$ and that at some depth of burial the compaction–induced lateral pressures will be surpassed in magnitude by at rest earth pressures due to the static overburden, a stress distribution as shown in Fig. (6.5.B) can be calculated. This type of lateral pressure distribution can be generalized as in Fig. (6.5.C).

Ingold (1979) proposed an analytical method to find the effect of compaction on the lateral and residual earth pressures. The method is based on:

(i) Broms' theory but extended to cases where wall deflections during backfilling were sufficient to induce an active condition in the lower layers of a backfill being deposited and compacted in lifts by assuming the virgin loading path to be ($\sigma_h = K_a \sigma_v$) instead of Broms' ($\sigma_h = K_o \sigma_v$). In addition, he suggested that passive failure controlled the other limiting condition and that therefore $K_o = K_p$. A stress path of a typical soil element is shown in Fig. (6.6.A).

(ii) The compaction plant was simulated as a line load and the expression ($\Delta\sigma_v = 2p/_{\pi}\ z$) derived by Holl (1941) was used for the distribution of vertical stress ($\Delta\sigma_v$) vertically below a line load (p) at the ground surface.

Closed form solutions were generated for critical depth (Z_{cr}) and critical height (h_c)where $K = K_a$, as well as for the residual lateral pressure at depths between Z_{cr} and h_{cr} as illustrated in Fig. (6.6.B,C&D). Ingold (1980 & 1983) extended his work to apply his theory to reinforced earth retaining walls.

Seed and Duncan (1983) introduced models to explain and calculate peak and residual compaction induced stresses either in free field or acting against vertical nondeflecting structures. They explained that compaction, accomplished by cyclic

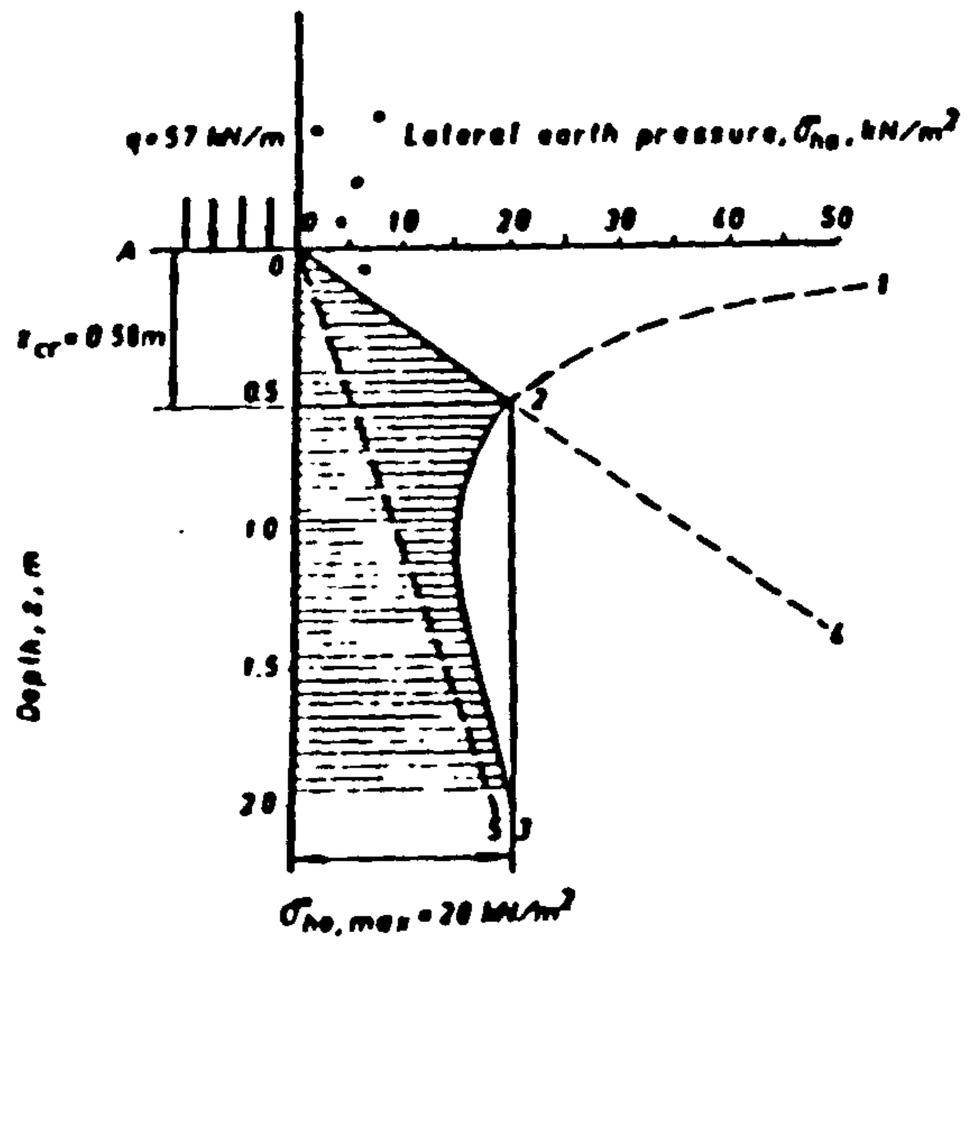

(A) SINGLE LAYER COMPACTED WITH 10.2 TON ROLLER.

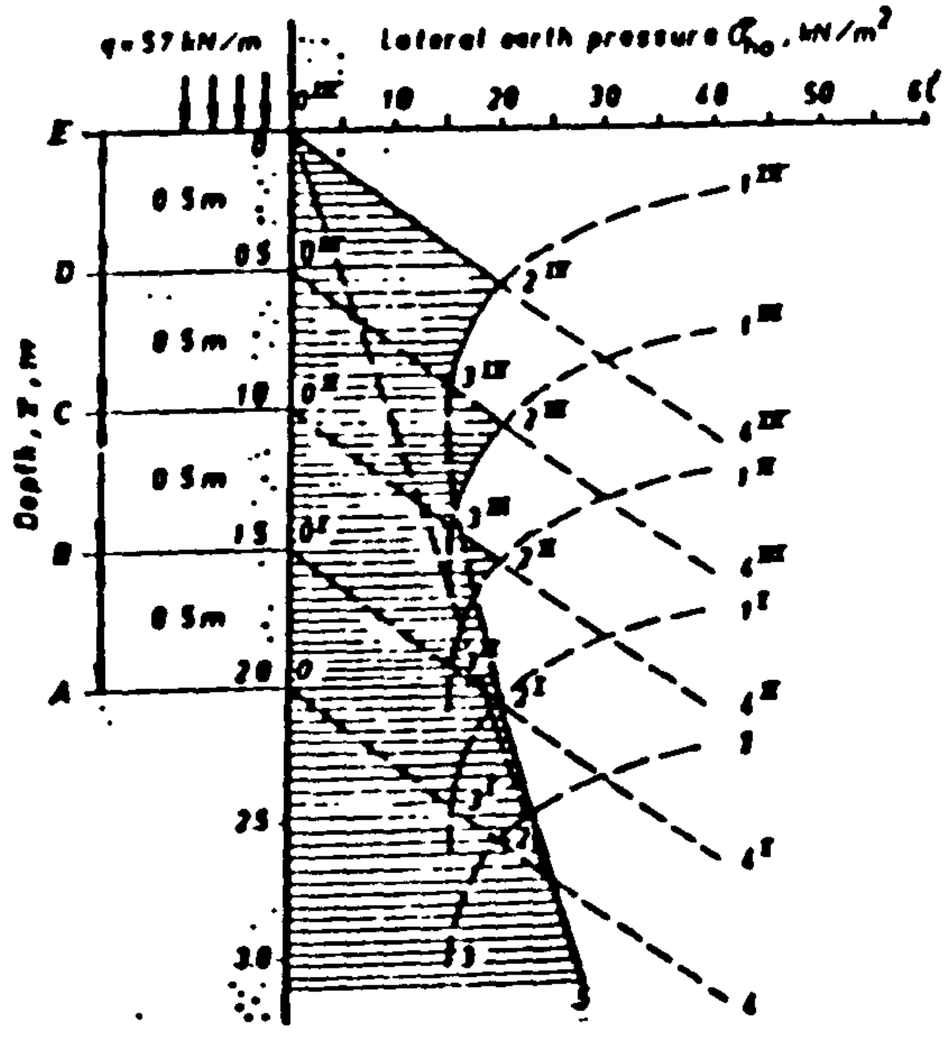

(B) FILL COMPACTED IN 0.50M LIFTS WITH 10.2 TON ROLLER

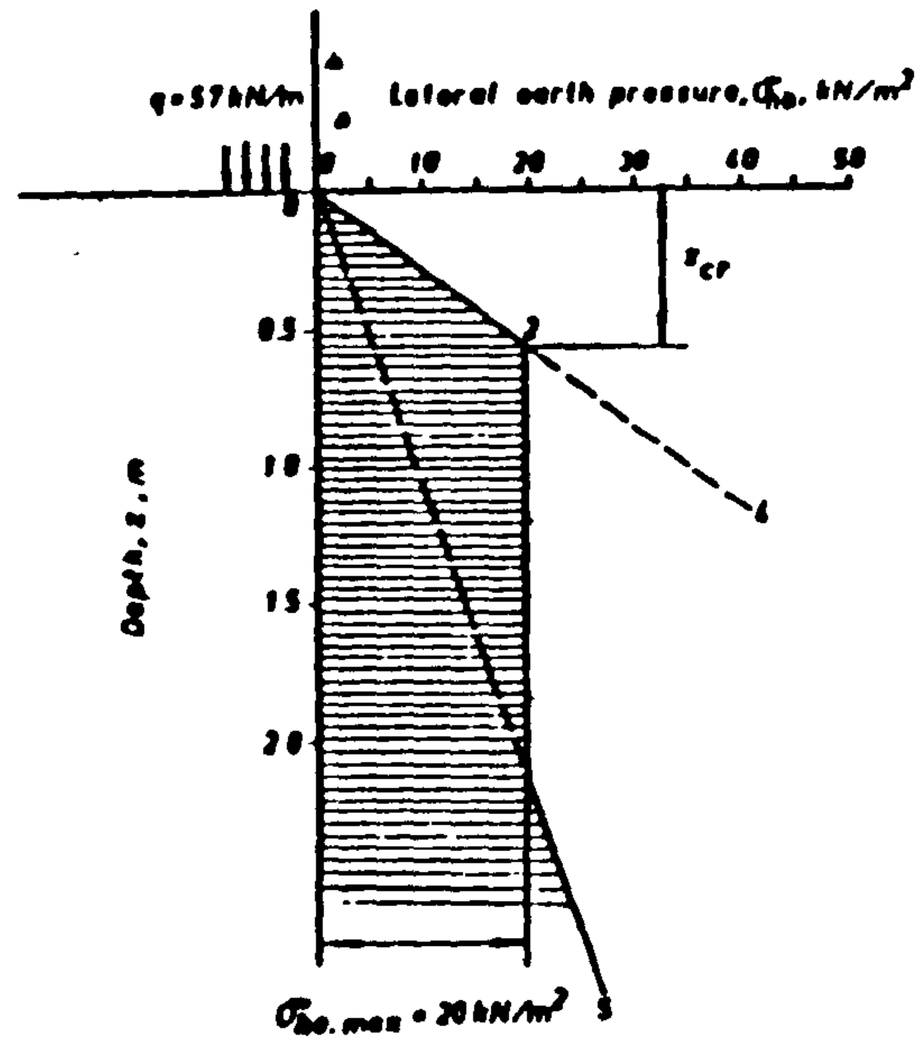

(C) GENERALIZED RESIDUAL LATERAL EARTH PRESSURE DISTRIBUTION.

FIG. (6.5) RESIDUAL LATERAL EARTH PRESSURE DISTRIBUTIONS (AFTER BROMS, 1971).

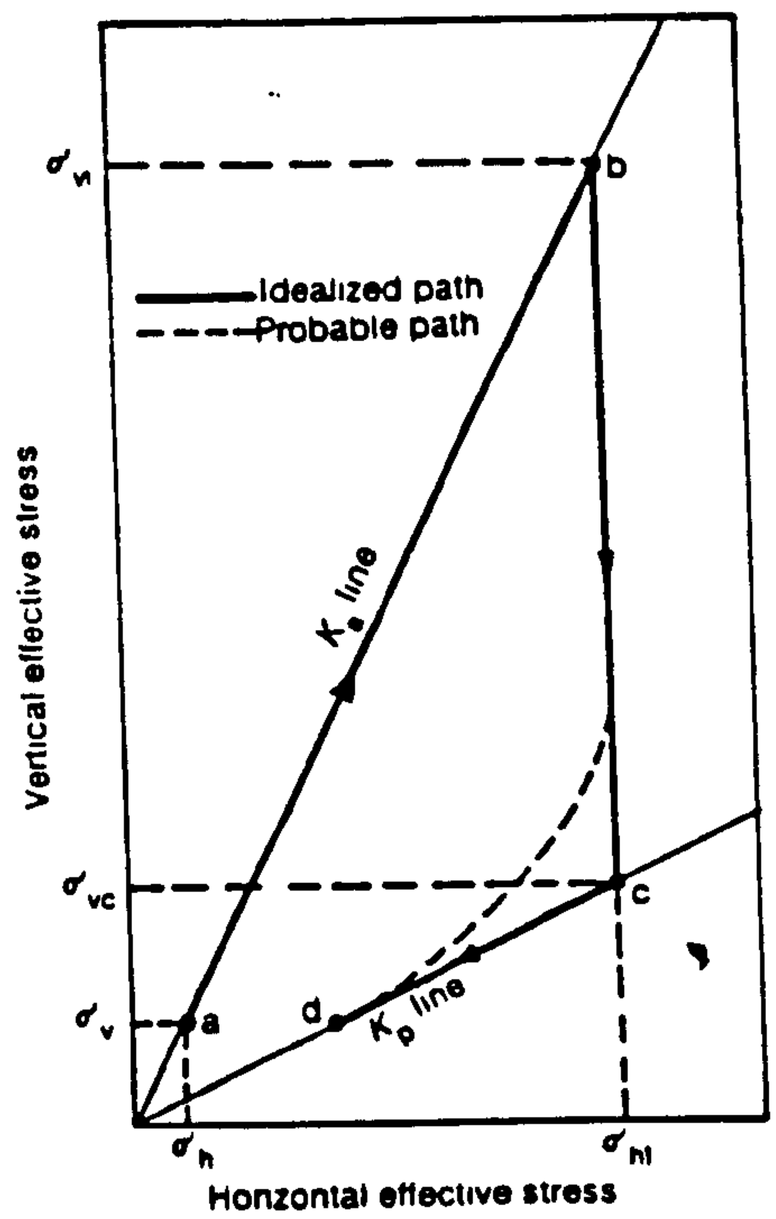

(A) IDEALIZED STRESS PATH.

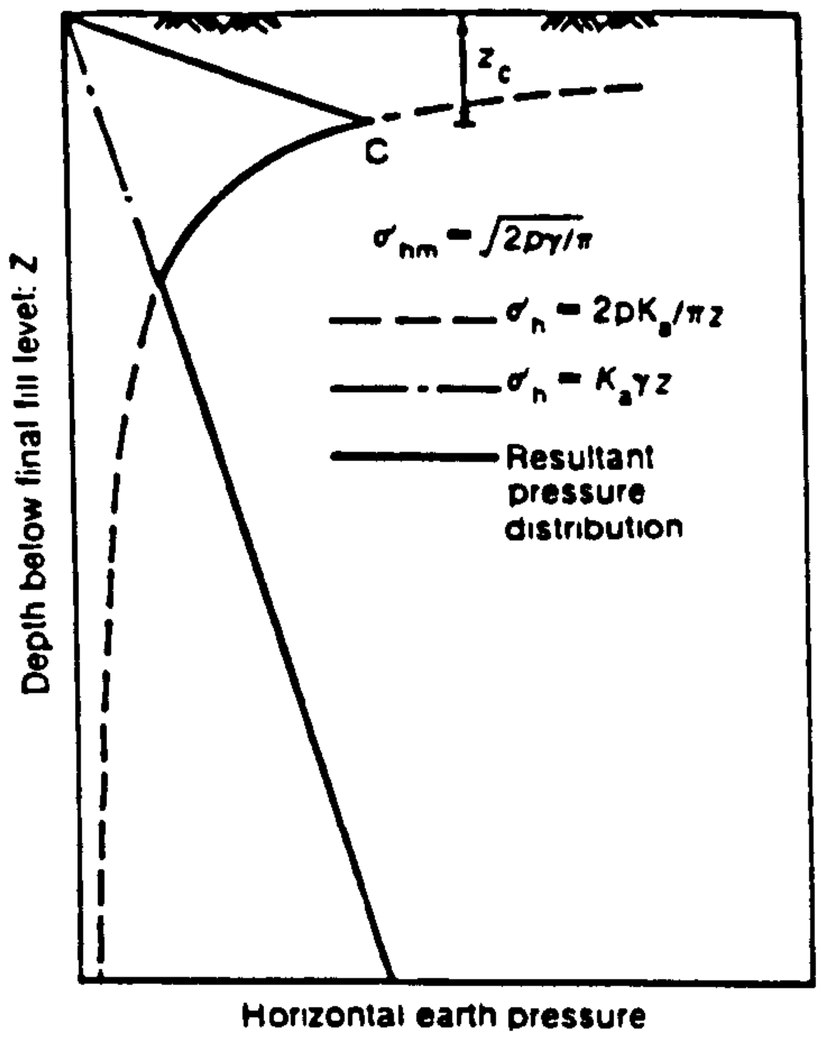

(B) HORIZONTAL PRESSURE DISTRIBUTION.

FIG. (6.6) STRESS PATH AND HORIZONTAL PRESSURE DISTRIBUTION (AFTER INGOLD, 1979).

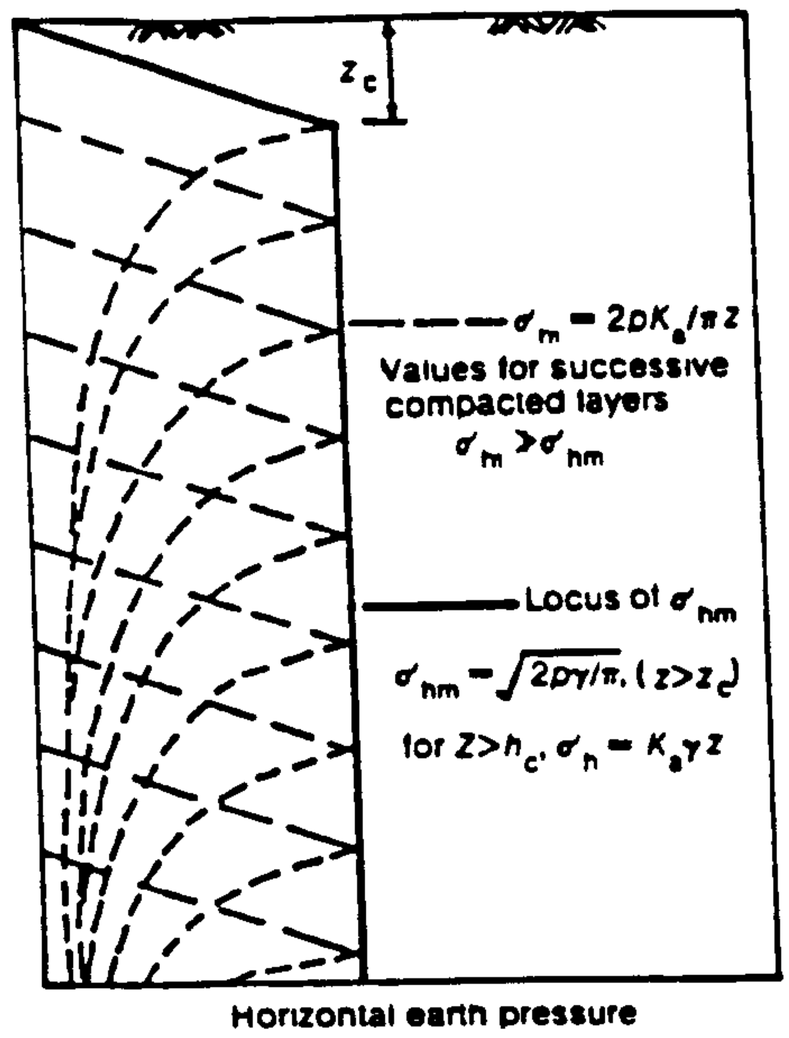

(C) HORIZONTAL PRESSURE DISTRIBUTION.

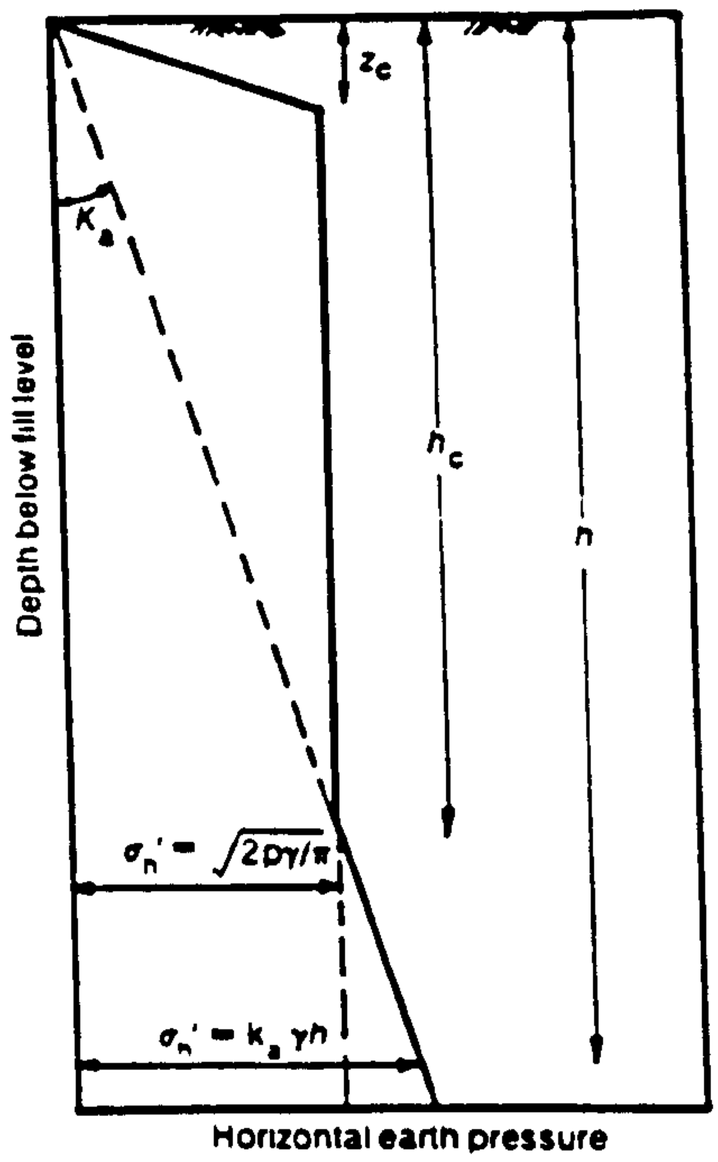

(D) HORIZONTAL PRESSURE DISTRIBUTION.

FIG. (6.6) CONT.

application and removal of a uniform, vertical surcharge loading of infinite lateral extent, is analogous to one dimensional cyclic over– consolidation loading/unloading, because principal effective stresses remain horizontal and vertical and no lateral displacements occur.

Seed and Duncan (1984 & 1986) extended their work to include deflected structures and compaction loading considered as a moving surface load of finite lateral extent.

6.4 COMMENT ON THE EXISTING THEORIES

In the foregoing section theories for calculation of compaction induced residual lateral earth pressures have been presented. The theory proposed by Sowers et al. (1957) did not provide good quantitative agreement with available field and laboratory data regarding residual compaction induced lateral earth pressures and for this reason it has not been widely used.

Rowe's work (1954) was early work to find the relationship between compaction and lateral earth pressures and contributed to later work by Broms (1971).

Broms (1971) provided a comprehensive theory of compaction induced earth pressures which has the following shortcomings:

(i) The calculation of peak lateral earth pressure against a wall as a result of surface loading by $\sigma_h = K_o \sigma_v$ is correct only when the surface loading is of infinite lateral extent. Calculation of pressure distribution against a wall based on vertical stresses and constant (K_o) does not generate correct results and moreover

the results are neither consistently conservative nor unconservative.

(ii) The assumption that reloading causes a negligible increase in lateral pressures until the K_o— line is reached, is unconservative both with respect to compaction loading as well as overburden loading resulting from placement of overlying layers of fill.

(iii) The assumption that unloading causes a negligible decrease in lateral pressures until the limiting (K_o') condition is reached, is over conservative.

For the above reasons Broms suggested the stress path illustrated by the dashed line in Fig. (6.4.A) but did not attempt to quantify this type of stress path. Broms' original theory is applicable only to rigid, non— deflecting walls.

Ingold's (1979) attempt to extend the theory to deflecting walls might have provided a reliable lower— bound solution if Broms' calculation of lateral stresses by $\sigma_h = K_o\ \sigma_v$ had been corrected. As it is not, Ingold's extension does not provide a reliable means of estimating residual compaction induced pressures acting against deflecting structures (Seed and Duncan, 1983).

The model suggested by Seed and Duncan (1983 & 1986) provided a good agreement with some field tests results (Seed et al., 1986), but the model is complex and includes many parameters which must be determined. They simulated the compaction load as a surface load of finite lateral extent which is not reproduced in the field. Such analyses are somewhat involved for use as a day to day design method.

In all the above theories the compaction plant was considered to be a point load or line load or moving load of lateral extent. The shortcoming of all the

above theories was that they did not consider the compaction plant as a three dimensional problem, i.e. no realistic simulation of compaction plant has been made, and this can have a great effect on the lateral earth pressure. It is therefore necessary to derive formulae to simulate the compaction plant taking into account the three dimensional nature of the problem. The assumptions and derivations of these formulae will be presented in the next section.

6.5 PROPOSED MODELS OF COMPACTION PLANT

As seen in previous sections many factors can affect the compaction model, one of the most important being modelling of the compaction plant. The models developed to simulate compaction have been point load, line load, moving line load, and line load of lateral extent. This meant that the problem was converted from three dimensions to two dimensions.

The models proposed here overcome this problem. A formula for horizontal stress arising from the compaction load has been developed for each model, taking into account the three dimensional effect of the compaction plant.

Most compaction processes for earth work can be accomplished by common equipment such as:

(a) Static or vibratory roller (unit or double drums).

(b) Static or vibratory pneumatic tired rollers.

(c) Vibratory compactors.

(d) Combination of (a) & (b).

These equipments differ to give heavy or light compaction, depending on the type of soil and project.

The three proposed models cover the above types of compaction plant and the choice of model depends on:

(i) Type of compaction plant used in the project which depends on the kind of soil.

(ii) The dimensions of the compaction plant.

6.5.1 First Proposed Model (Uniform Loaded Area)

The compaction load has been simulated as a moving uniform load over a finite area and can take any position as shown in Fig. (6.7.A) or the position which gives maximum horizontal stress at a certain point as shown in Fig. (6.7.B), where in the case of a reinforced earth retaining wall, plane XZ passes through the reinforcement in a vertical direction and also through the middle line of the area. The area is 2a x b and has a uniform load/unit area q, where:

2a is the long length of the compaction plant calculated between the axles of the wheels/drums in the case of a roller.

b is the width of drum or wheels.

X_o is the distance from the origin to the area.

q is the total static load of the plant/ 2axb (load/unit area).

P is the point (0,0,Z) at which the horizontal stress is required.

6.5.2 Assumptions

The following assumptions are considered in developing a formula for maximum horizontal stress due to compaction plant ($\Delta\sigma_{hm,c}$):

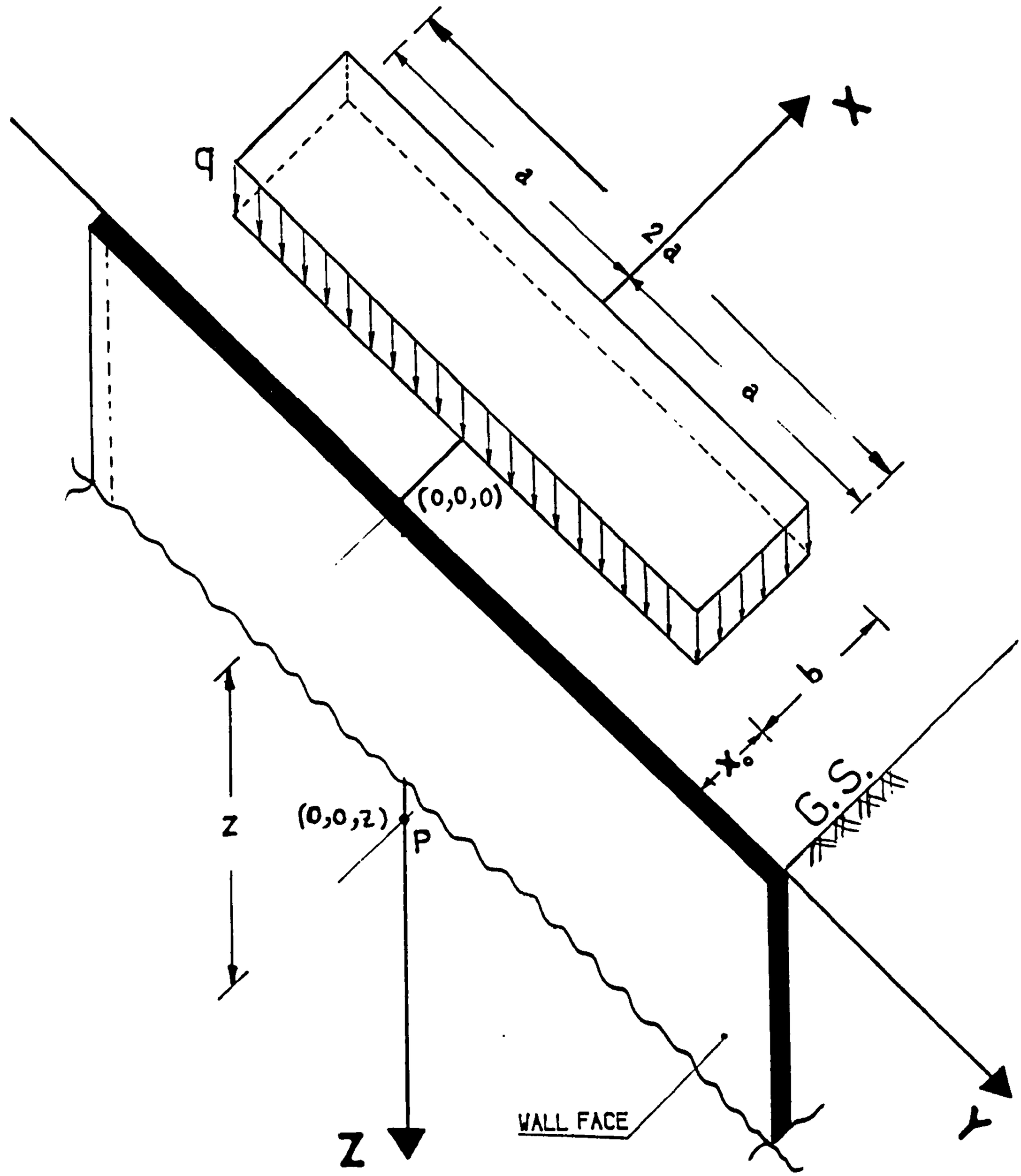

FIG. (6. 7. A) FIRST PROPOSED MODEL OF COMPACTION PLANT AS UNIFORM LOADED AREA.

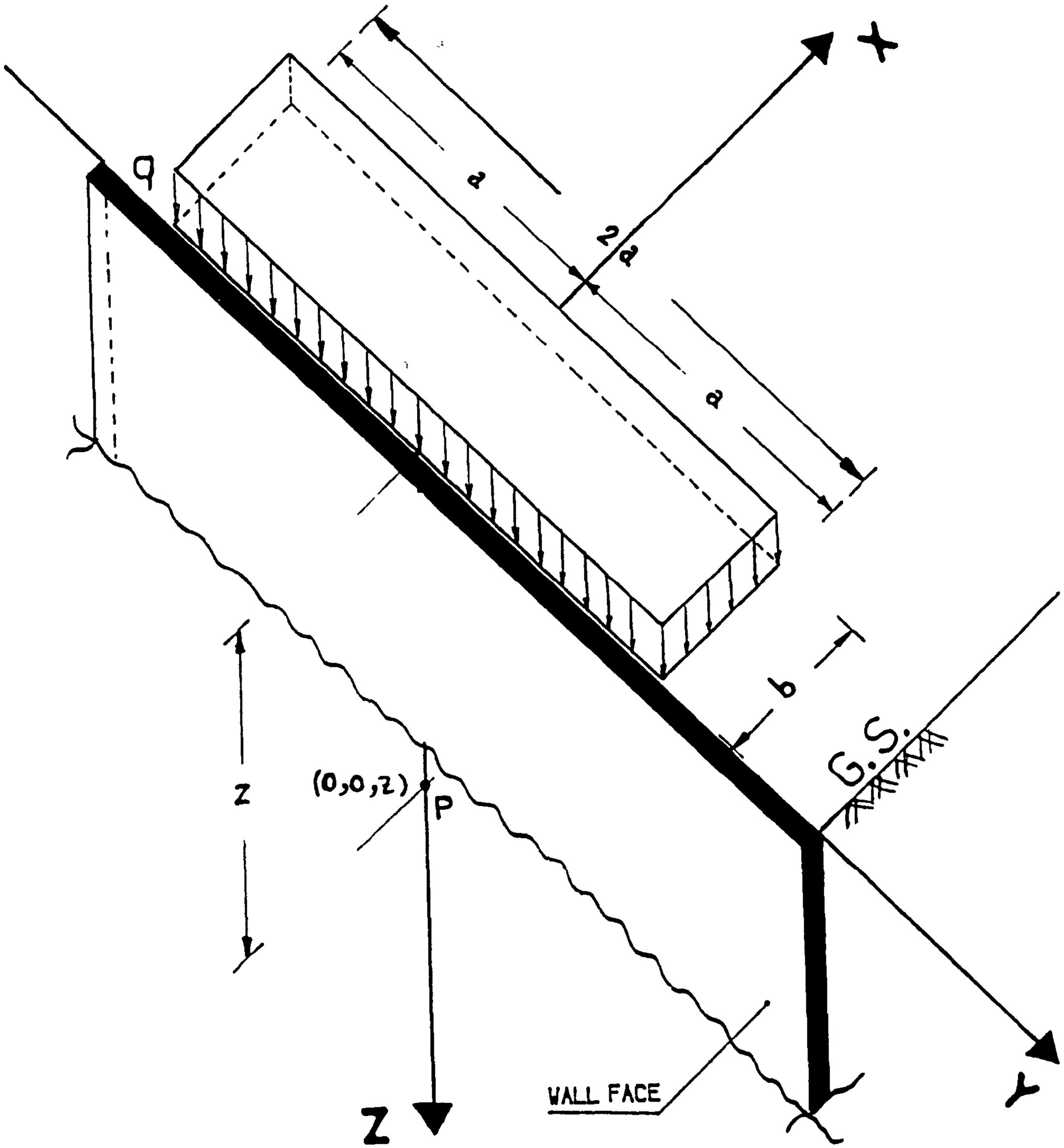

FIG. (6.7.B) POSITION OF LOAD WHICH GIVES MAXIMUM HORIZONTAL STRESS AT POINT P.

(a) Compaction load is a surface moving load and the long length of the load is parallel to the wall (i.e. compaction equipment passes parallel to the length of the wall as happens in the field).

(b) The effect of cyclic loading on the horizontal stress due to compaction process is taken into consideration by representing K_o as a function of stress history.

The K_o– OCR relationship in the soil developed by Mayne et al. (1982) is employed. They considered that the predictions of horizontal stress depend on the prediction of approximate values of K_o which also depend on stress history (OCR and $OCR_{max.}$). They postulated the following equation:

$$K_o = (1-\sin \varphi) \left[\frac{OCR}{OCR_{max}^{(1-\sin \varphi)}} + \frac{3}{4} \left(1- \frac{OCR}{OCR_{max}}\right) \right] \qquad (6.6)$$

Where:

K_o is coefficient of earth pressure at rest.

OCR is overconsolidation ratio ($\sigma_{vmax\ past}/\sigma_{v\ current}$).

OCR_{max} is $\sigma_{vmax}/\sigma_{vmin}$.

φ is angle of internal friction.

By knowing K_o & vertical stresses, $\Delta\sigma_{hm,c}$ can be estimated. In the case of uncompacted soil (virgin soil) OCR = OCR_{max} = 1 and K_o becomes equals to $(1-\sin \varphi)$, but for previously compacted soils the stresses induced by compaction loading are a function of the very complicated previous stress history of the soil at any point, and these stresses in previously compacted soils are thus very difficult to estimate accurately.

The maximum horizontal stress due to compaction load ($\Delta\sigma_{hm,c}$) is therefore calculated at any point during compaction as a result of the most critical position of the compaction plant and assuming the soil is previously uncompacted.

(c) Either in the free field or near retaining walls, horizontal stresses due to compaction plant ($\Delta\sigma_{x,c}$) can be calculated based on a linear elastic analysis such as Boussinesq's solution (1885).

The maximum horizontal stress at any point in a free field due to a uniform loaded finite area is bsaed on an equation derived in Appendix B Sec. (B.1), Eq. (B.16), for horizontal stresses due to point load as follows:

$$\sigma_x = \frac{Q}{2\pi}\left\{\frac{3X^2 Z}{R^5} - (1-2\nu)\left[\frac{Z}{R^3} - \frac{1}{R(R+Z)} + \frac{X^2(2R+Z)}{R^3\,(R+Z)^2}\right]\right\} \qquad (6.7.a)$$

For the rectangular area (a.b), Fig. (6.7.c), is

$$\sigma_{x_{(a.b)}} = \frac{q}{2\pi}\int_0^{X-b}\int_0^{Y-a}\left\{\frac{3X^2Z}{R^5} - (1-2\nu)\left[\frac{Z}{R^3} - \frac{1}{R(R+Z)} + \frac{X^2(2R+Z)}{R^3\,(R+Z)^2}\right]\right\} dy\,dx \qquad (6.7.b)$$

The solution of the above equation is based on numerical integrtion using program (BCOMPP) which will be explained later. For the rectangular area (2a.b), Fig. (6.7.c), is:

$$\Delta\sigma_{x,c} = \Delta\sigma_{x_{(2a.b)}} - 2\sigma_{x_{(a.b)}} \qquad (6.7.c)$$

The notation of the above Eqs. is shown in Fig. (6.7.C).

(d) The effect of the wall on soil stresses is determined using the method of images, Mindlin (1936) and Terzaghi's suggestion (1954).

The stress in equation (6.7) is in the free field and $\Delta\sigma_{h,c}$ is needed on the retaining wall. Using the method of images, Mindlin (1936) and the suggestion by Terzaghi (1954), the effects of a rigid wall on soil stresses can be approximated by modelling a second "imaginary" load of equal magnitude to the real load on an infinite half space at equal location from the location of an imaginary wall as shown in Fig. (6.8), measured in the direction normal to the wall. The imaginary load results in no lateral deflection at the imaginary vertical wall and exactly doubles the value of $\Delta\sigma_{x,c}$ at the wall hence:

$$\Delta\sigma_{h,c} = 2\ \Delta\sigma_{x,c} \qquad (6.8)$$

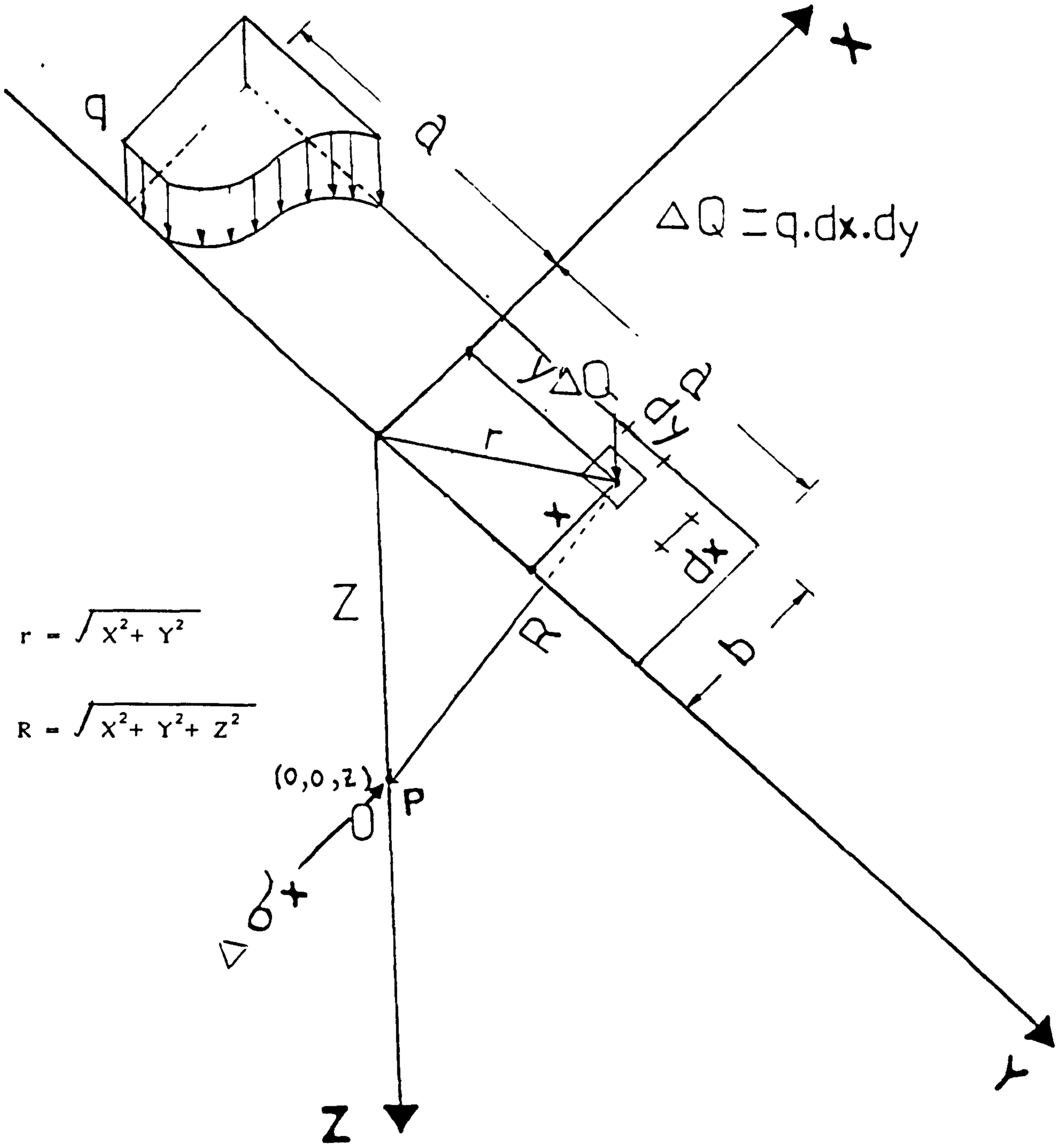

FIG. (6. 7. C) NOTATIONS OF EQUATION OF MAXIMUM HORIZONTAL STRESS DUE TO A RECTANGULAR LOADED AREA.

(e) Dynamic load of compaction load is taken as 2–3 times the static load in the case of vibratory rollers.

This assumption, based on a limited amount of field data, has been got by Whiffen (1954), D'Appolonia et al. (1969) and Toombs (1972) as shown in Fig. (6.9.A,B&C). It appears from these Figs. that the maximum dynamic loading induced by a vibratory roller may be modelled as approximately two to three times the static thrust of the roller or the maximum dynamic load indicated by the plant manufacturer should be taken.

Hence, the maximum horizontal stress is determined as follows:

$$\Delta\sigma_{hm,c} = 2\ \Delta\sigma_{h,c} \qquad (6.9)$$

(f) It has been suggested by many researchers such as Seed and Duncan (1983) that Poisson's ratio, ν for cohesionless soil can be calculated from:

$$\nu = \nu_m + \frac{1}{2}\ (0.5 - \nu_m) \qquad (6.10)$$

Where:

ν_m is K_o / $(1+K_o)$

K_o is $1-\ \sin\ \varphi$ for cohesionless soil.

φ is angle of internal friction of the soil.

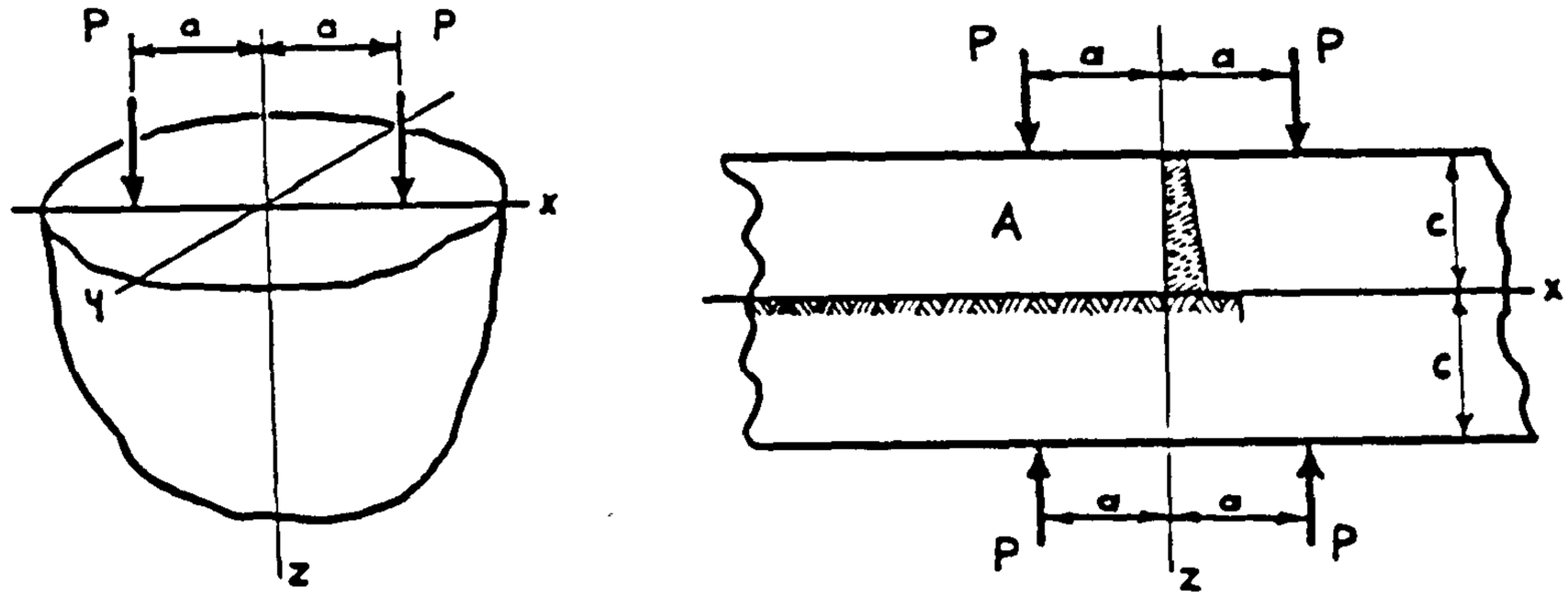

(A) WALL WITH INFINITE DEPTH. (B) WALL WITH FINITE DEPTH.

FIG. (6.8) METHOD OF IMAGES (AFTER MINDLIN, 1936).

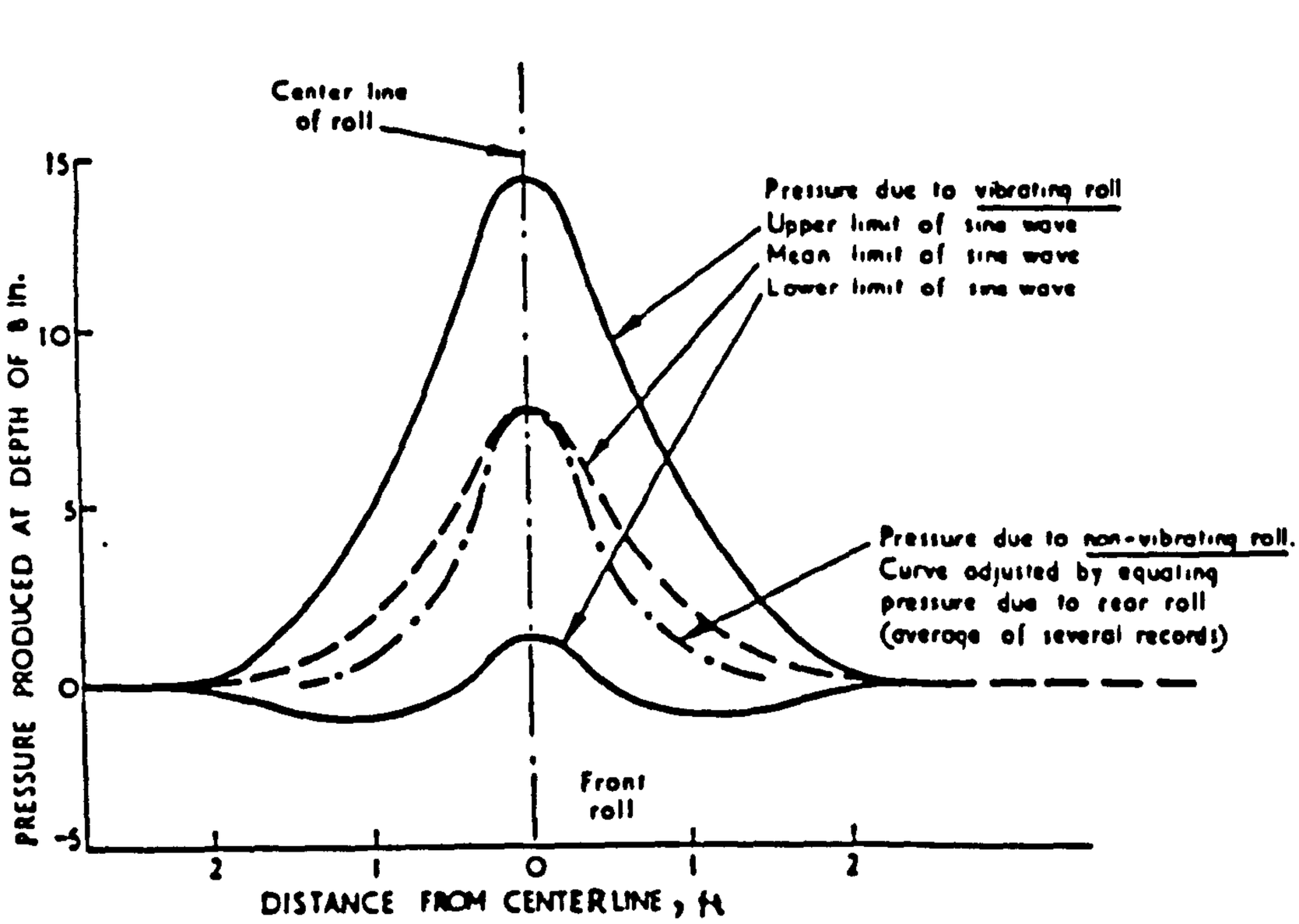

FIG. (6.9.A) MEASUREMENTS OF VERTICAL STRESSES INDUCED BY A 2.5 TON VIBRATORY ROLLER (AFTER WHIFFEN, 1954).

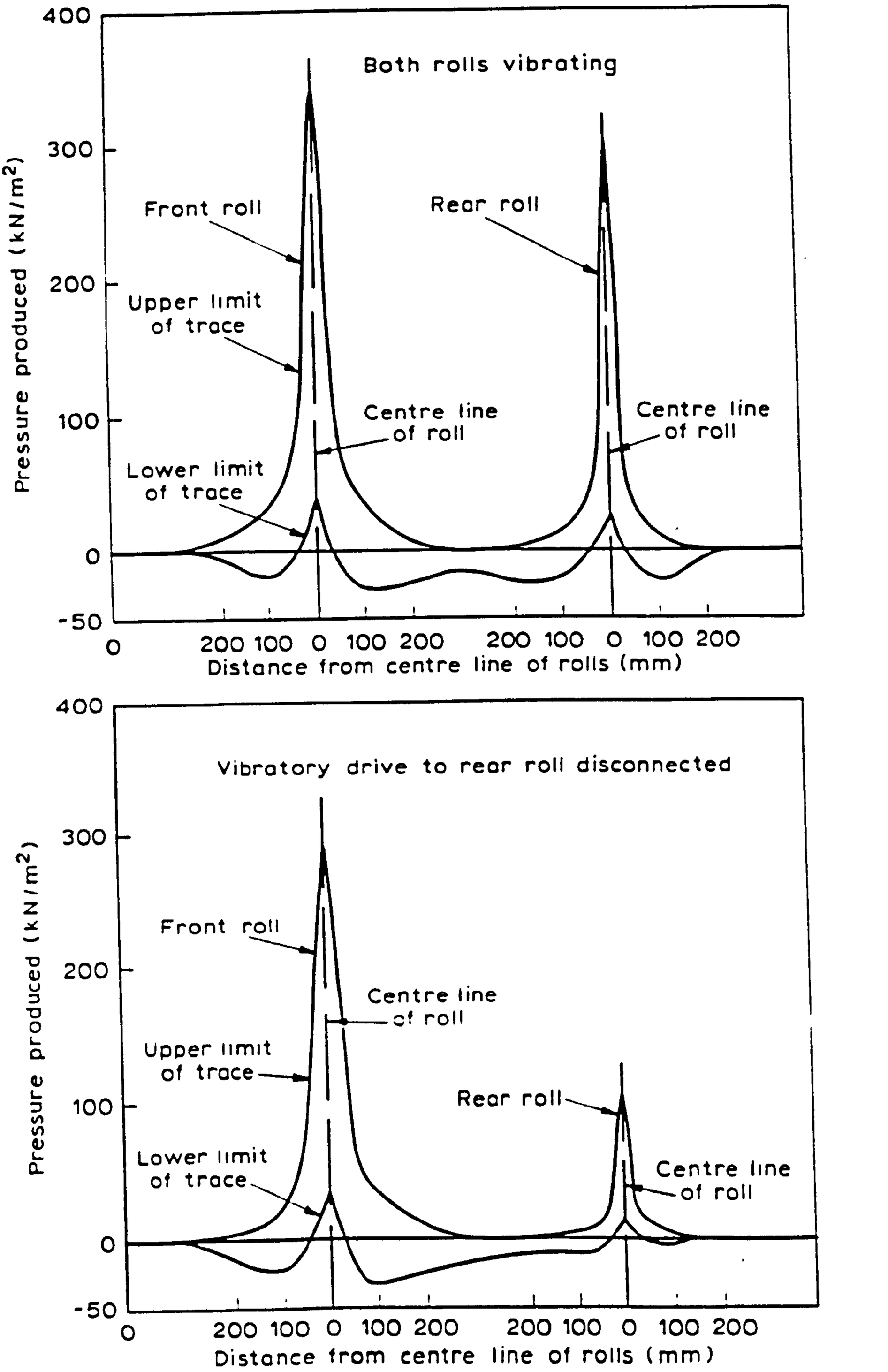

FIG. (6. 9. B) MEASUREMENTS OF VERTICAL PRESSURES IN WELL GRADED SAND AT A DEPTH OF 130 MM. WITH THE 7. 3 MG. DOUBLE VIBRATORY ROLLER (AFTER TOOMBS, 1972).

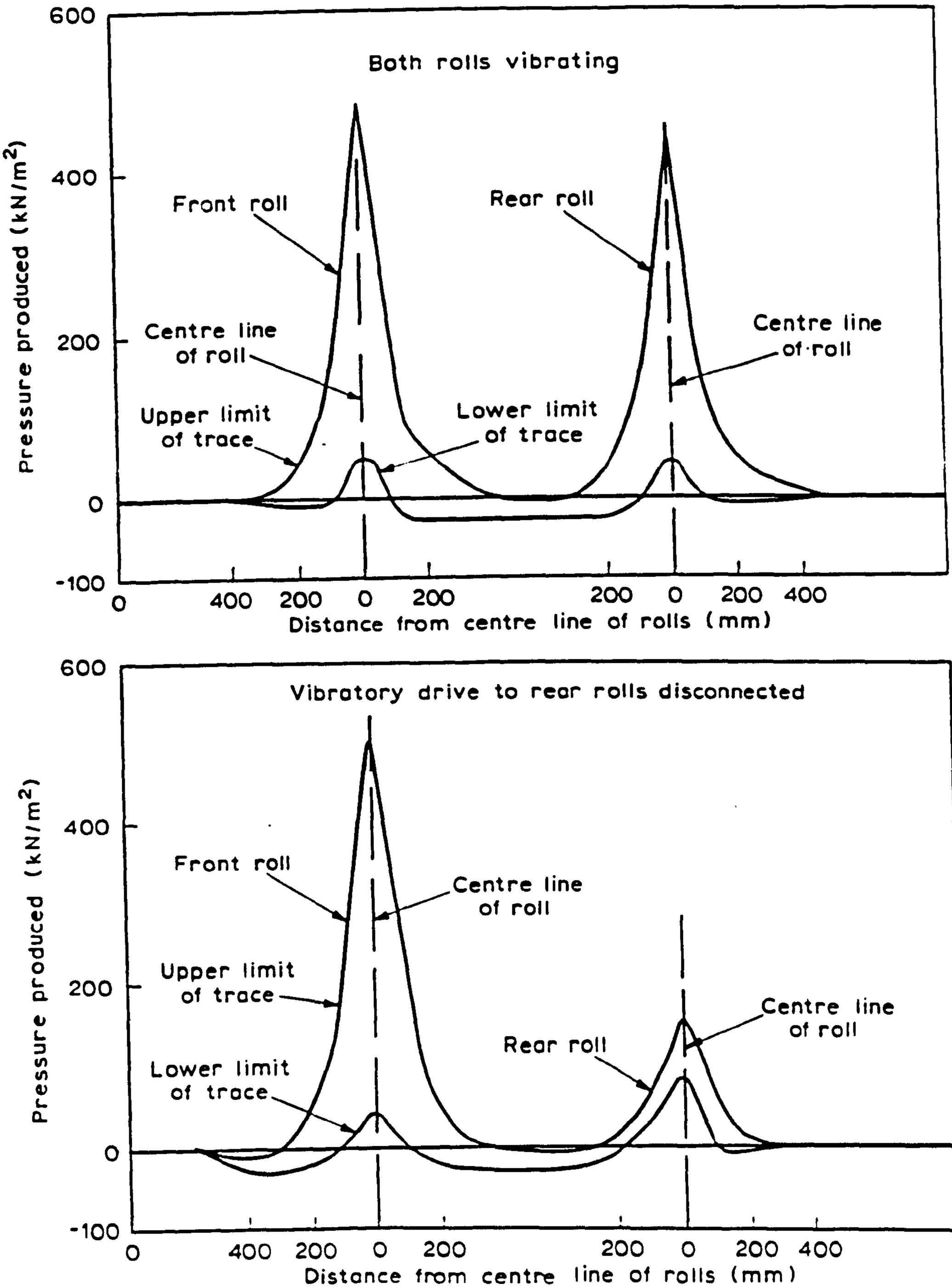

FIG. (6.9.C) MEASUREMENTS OF VERTICAL PRESSURES IN WELL GRADED SAND AT A DEPTH OF 130 MM. WITH THE 7.3 MG. DOUBLE VIBRATORY ROLLER (AFTER TOOMBS, 1972).

(g) The maximum horizontal stress $\Delta\sigma_{hm,c}$ calculated from equation (6.9) is valid for a reinforced earth retaining wall.

Since the author's research is concerned with a reinforced earth retaining wall with sand backfill and $\Delta\sigma_{hm,c}$ is calculated for the case of a rigid wall (nondeflecting structure), so $\Delta\sigma_{hm,c}$ is required for a deflecting structure such as a reinforced earth retaining wall.

However, $\Delta\sigma_{hm,c}$ in equation (6.9) still represents the best value for analysing the stresses against a deflected wall such as a reinforced earth retaining wall because:

(i) Only the maximum stress at any depth is required.

(ii) The effect of deflection on $\Delta\sigma_{hm,c}$ is reduced due to reapplication of the maximum compaction load after some wall deflection has occurred, because of the dynamic load effect and the number of passes of the compaction plant.

Hence the maximum horizontal stress on a reinforced earth retaining wall is

$$\Delta\sigma_{hm,c} = 2\ \Delta\sigma_{h,c} \qquad (6.11)$$

(h) Principal of superposition can be applied.

As shown in Fig. (6.10) to find the horizontal stress at point P for a uniformly loaded area A, the principal of superposition is applied as follows:

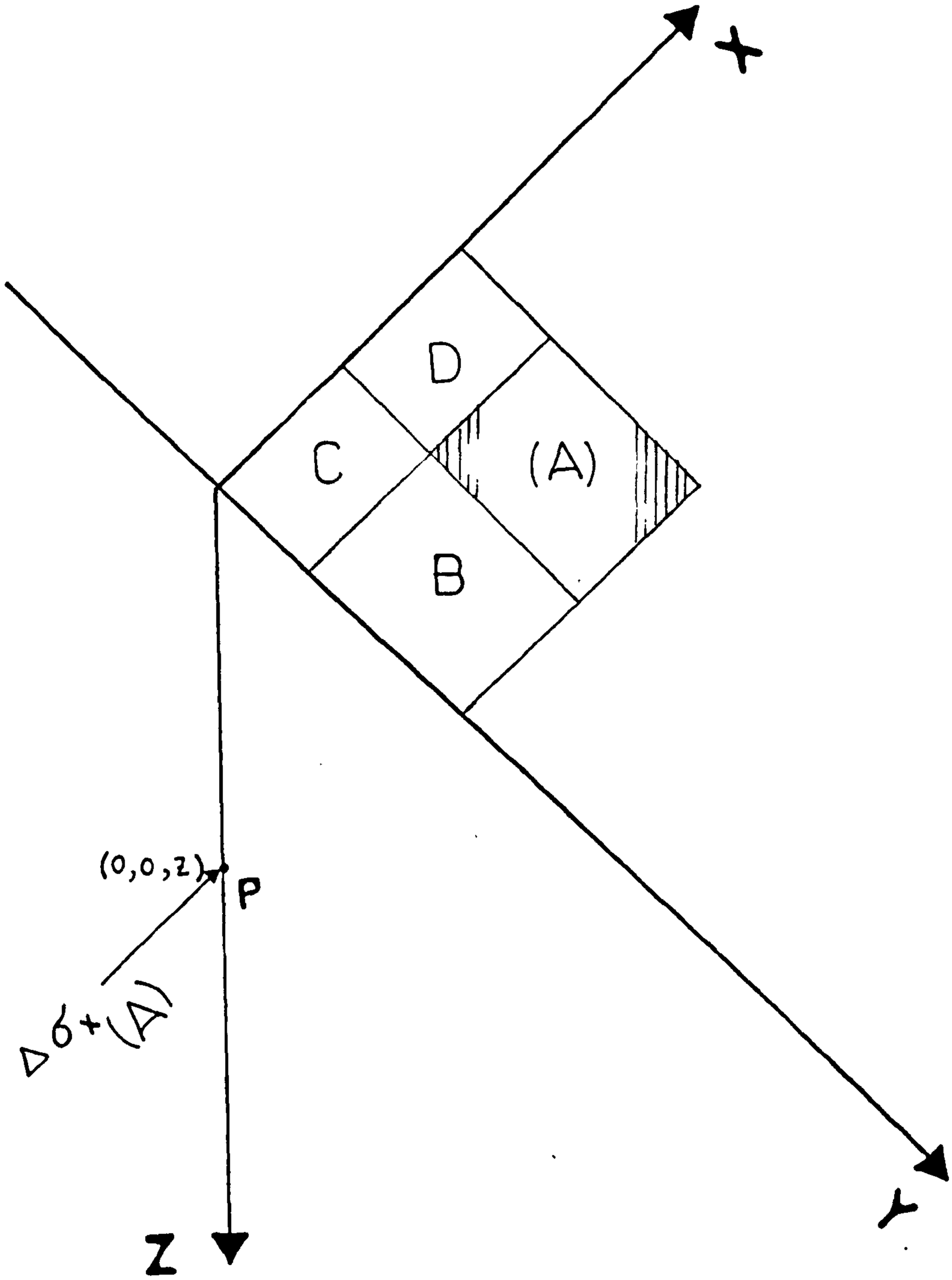

FIG. (6.10) PRINCIPLE OF SUPERPOSITION APPLIED TO CALCULATE HORIZONTAL STRESS AT POINT P DUE TO AREA (A).

$$\Delta\sigma_{(A)} = \Delta\sigma_{(A+B+C+D)} - \Delta\sigma_{(B+C)} - \Delta\sigma_{(D+C)} + \Delta\sigma_{C} \qquad (6.12)$$

6.5.3 Second Proposed Model (Two Line Loads Perpendicular To The Wall)

Assume the compaction plant consists of two moving line loads as shown in Fig. (6.11). The distance between the two loads is the distance between the axles of the front and rear wheels or drums of the compaction plant and equals 2a. The length of the line load is the width, b, of the wheels or drum of compaction plant. The load intensity ($\dot{q}_1$ & $\dot{q}_2$) is the load/unit length for rear/front drum or wheel. In the case of a unit roller compaction plant one line load only can be used.

6.5.4 Derivation Of An Expression For Horizontal Stress Due To Second Proposed Model

Several assumptions have been made in order to develop a formula for maximum horizontal stress $\Delta\sigma_{hm,c}$ due to two line loads with distance 2a between them. These assumptions are:

(a) Compaction load is simulated as two line loads of equal length perpendicular to the length of wall, and the distance between them is assumed to be as shown in Fig. (6.11) and as discussed in Sec. (6.5.3).

(b) The most critical position of the two loads which causes a maximum horizontal stress at point P (0,0,Z) is shown in Fig. (6.12) where $\dot{q}_1 > \dot{q}_2$.

(c) The maximum horizontal stress due to a compaction load in the free field or near the structure is based on a linear elastic analysis such as

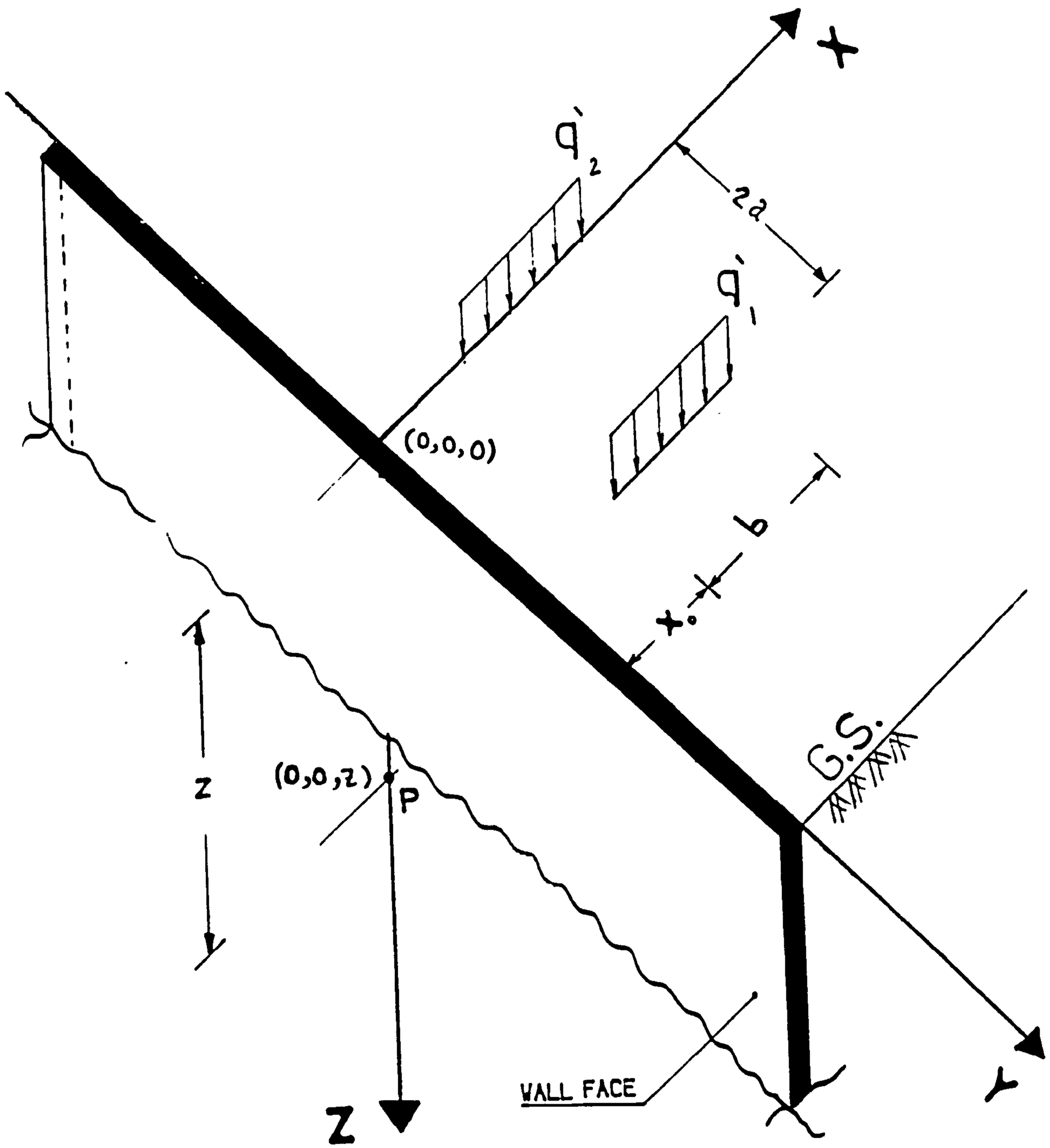

FIG. (6. 11) SECOND PROPOSED MODEL OF COMPACTION PLANT AS TWO UNIFORM LINE LOADS PERPENDICULAR TO THE WALL .

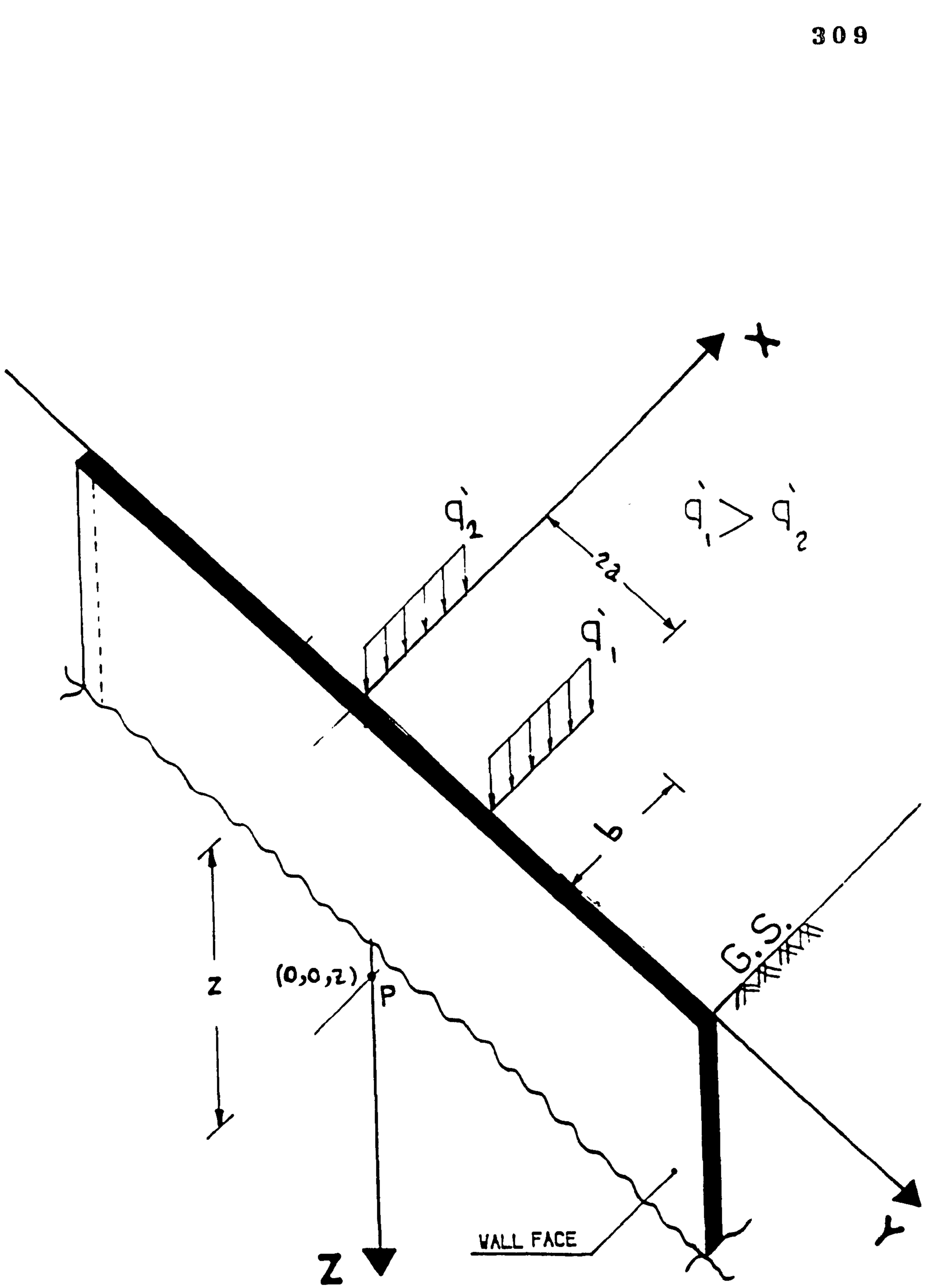

FIG. (6.12) POSITION OF LOADS WHICH GIVES MAXIMUM HORIZONTAL STRESS AT POINT P.

Boussinesq's solution (1885).

A formula for horizontal stress due to one line in a critical position at any point in a free field has been developed in Appendix B Sec. (B.2). The maximum horizontal stress $\Delta\sigma_{x,c}$ can be obtained from Eqs. (B.46.a&b), due to one line load in a position shown in Fig. (6.12):

$$\Delta\sigma_{x,c} = \frac{\dot{q}}{2\pi}\left[\frac{Zb^3(3Z^2+3Y^2+2B^2)}{5(Z^2+Y^2)B^5} - (1-2\nu)\left(\frac{bZ}{B\,(Z^2+Y^2)}\right)\right] \tag{6.13}$$

The notation of the above equation is shown in Fig. (6.13).

The maximum horizontal stress due to the critical position of the two line loads as shown in Fig. (6.12) can be obtained by applying equation (6.13) to both line loads and hence:

$$\Delta\sigma_{x,c} = \frac{\dot{q}_1}{2\pi}\left[\frac{Zb^3(3Z^2+3Y^2+2B^2)}{5(Z^2+Y^2)B^5} - (1-2\nu)\left(\frac{bZ}{B\,(Z^2+Y^2)}\right)\right] + \frac{\dot{q}_2}{2\pi}\left[\frac{b^3(3Z^2+2B^2)}{5ZB^5} - (1-2\nu)\left(\frac{b}{BZ}\right)\right] \tag{6.14}$$

Where:

Y is 2a (for load $\dot{q}_1$)

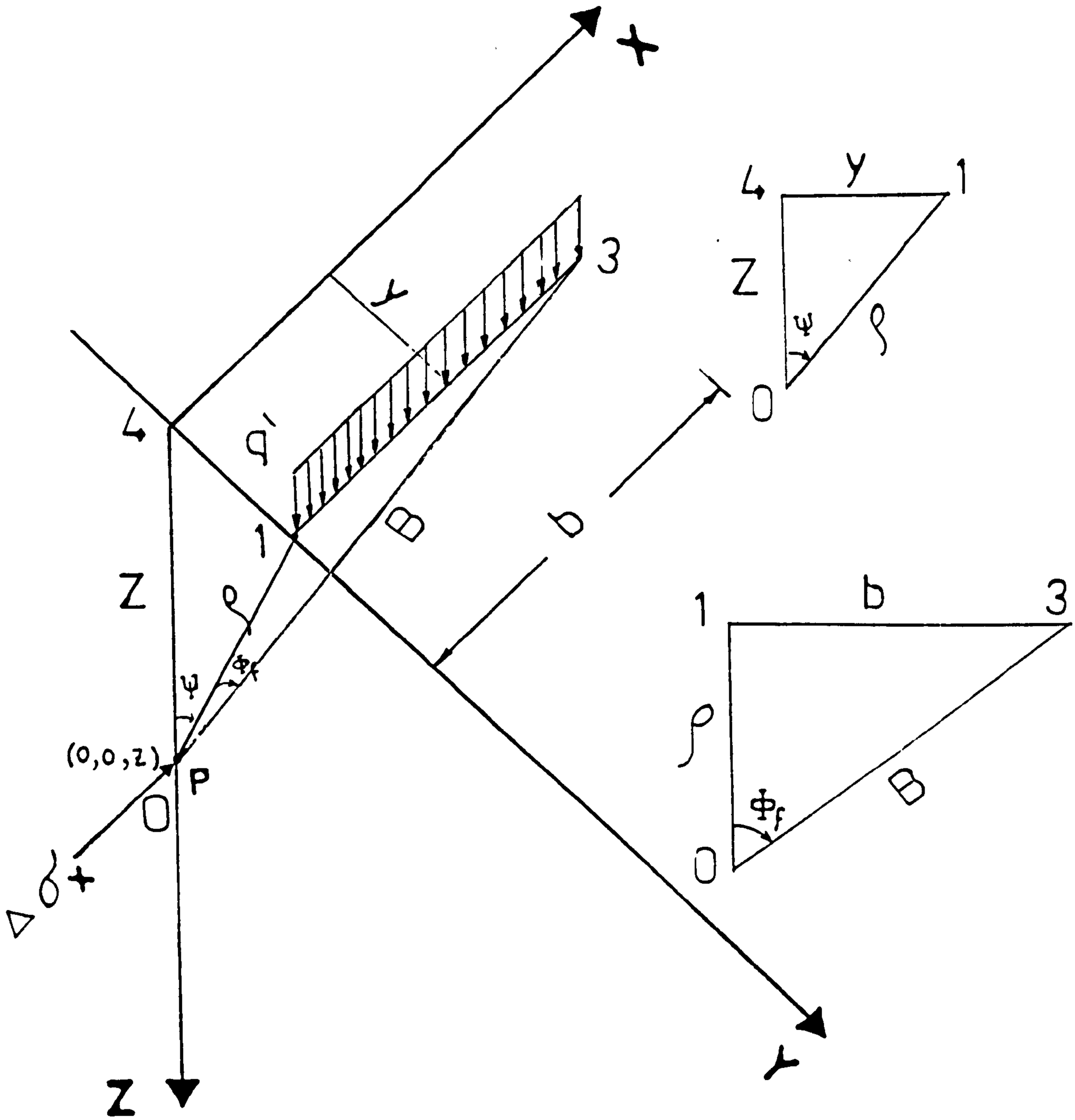

FIG. (6.13) NOTATIONS OF EQUATION OF MAXIMUM HORIZONTAL STRESS DUE TO LINE LOAD PERPENDICULAR TO THE WALL.

Y is zero (for load $\dot{q}_2$)

B is $\sqrt{b^2+ Z^2+ Y^2}$

Added to the above assumptions are those in Secs. (6.5.2.b,c,d,e,f&g) which have been used for the case of simulating the compaction load as a uniform loaded area.

From all the previous assumptions, the maximum horizontal stress due to compaction plant on a reinforced earth retaining wall, the main point of concern in this research, can be obtained as follows:

$$\Delta\sigma_{hm,c} = \frac{2\dot{q}_1}{\pi}\left[\frac{Z\,b^3}{(Z^2+Y^2)B^3} - (1-2\nu)\left(\frac{bZ}{B\,(Z^2+Y^2)}\right)\right]$$

$$+\frac{2\dot{q}_2}{\pi}\left[\frac{b^3}{Z\,B^3} - (1-2\nu)\left(\frac{b}{BZ}\right)\right] \qquad (6.15.a)$$

Or

$$\Delta\sigma_{hm,c} =$$

$$\frac{2\dot{q}_1\,\cos^2\psi}{Z\pi}\left[\sin\varphi_{1f}^3 - (1-2\nu)\sin\varphi_{1f}\right]$$

$$+\frac{2\dot{q}_2}{Z\pi}\left[\sin^3\varphi_{2f} - (1-2\nu)\sin\varphi_{2f}\right] \qquad (6.15.b)$$

Where,

In case of load q_2, Y & ψ are zero and ρ = Z.

6.5.5 Third Proposed Model (Two Line Loads Parallel To The Wall)

In this model the compaction plant has been simulated by two moving line loads of lateral extent and parallel to the wall as shown in Fig. (6.14). The length of the loads 2a is the distance between the axles of the front and rear wheels or drums of the compaction plant. The load intensity $\dot{q}$ is the load per unit length and equals the total load of compaction plant/length of compaction plant.

6.5.6 Derivation Of An Expression For Maximum Horizontal Stress Due To The Third Proposed Model

In order to develop a formula for maximum horizontal stress $\Delta\sigma_{hm,c}$ due to two line loads of length 2a separated by a distance b, the following assumptions are considered:

(a) Compaction load is simulated as two line loads of equal length and parallel to the wall. The most critical position of the two loads which causes a maximum horizontal stress at point P (0,0,Z) is shown in Fig. (6.15).

(b) The maximum horizontal stress due to a compaction load in the free field or near the retaining structure is based on a linear elastic solution by Boussinesq (1885).

The maximum horizontal stress at any point in a free field due to one line load of finite length and parallel to the wall is derived in Appendix B Sec. (B.3) and shown in the final equations (B.54.a&b) as follows:

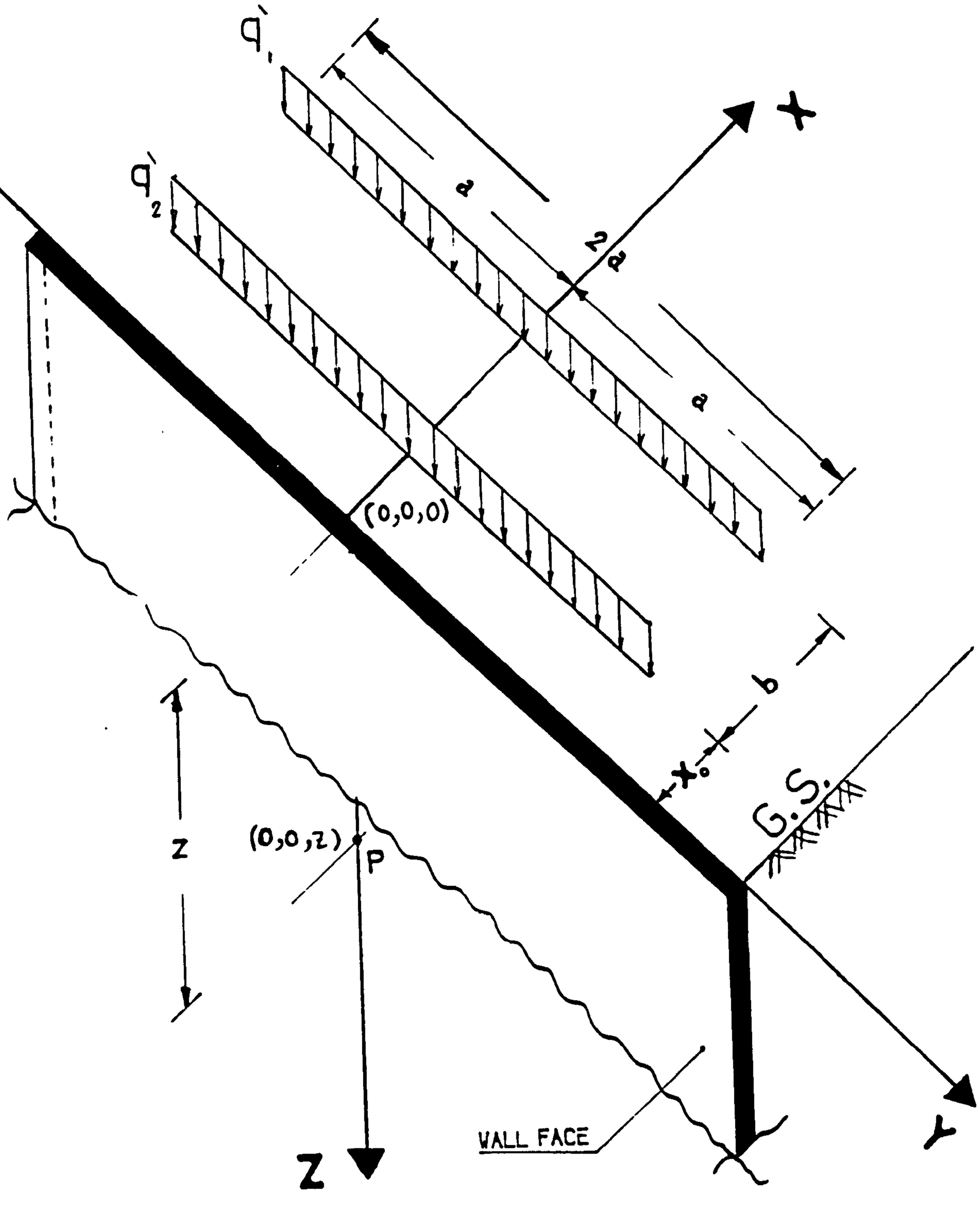

FIG. (6. 14) THIRD PROPOSED MODEL OF COMPACTION PLANT AS TWO UNIFORM LINE LOADS PARALLEL TO THE WALL.

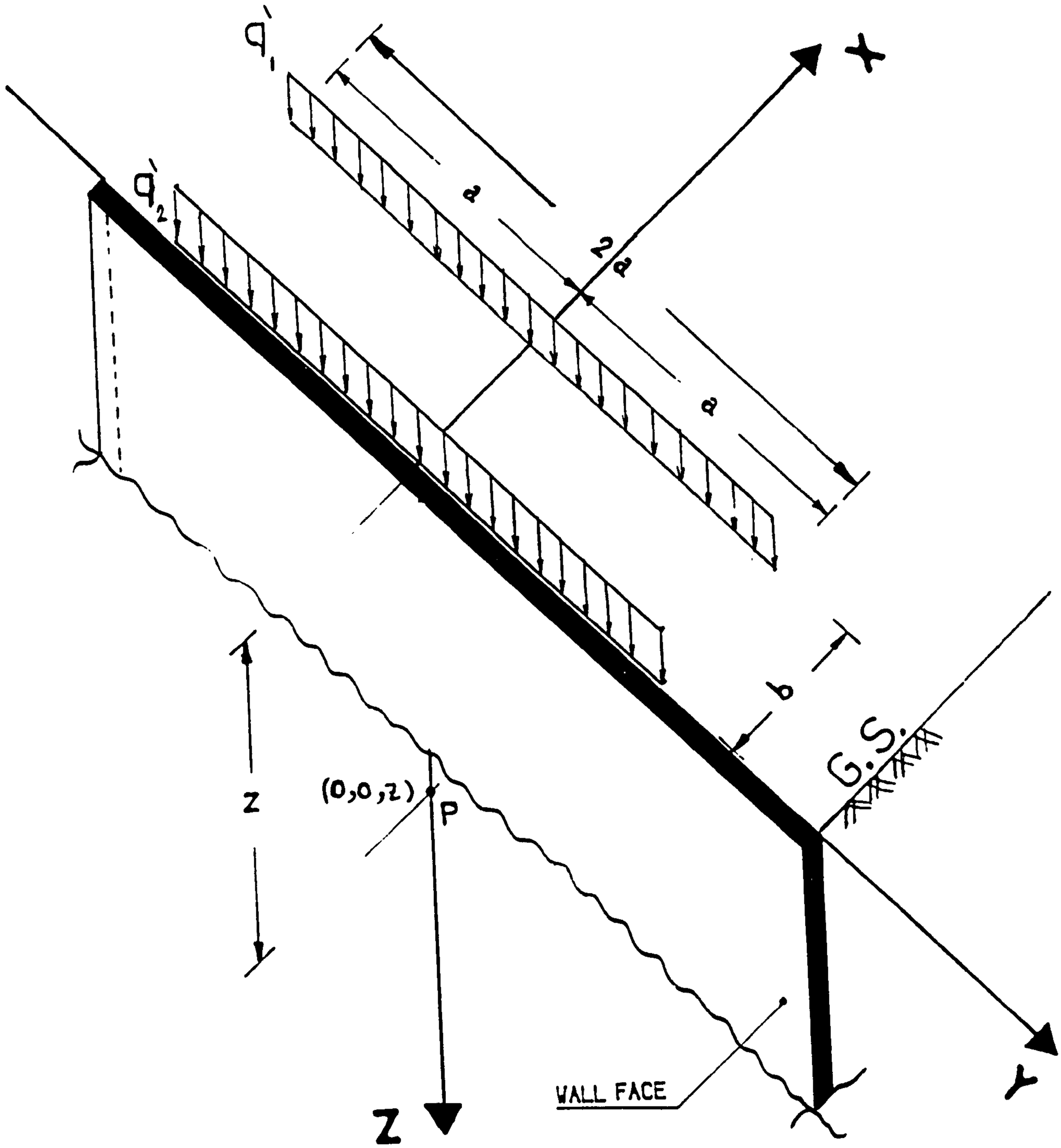

FIG. (6.15) POSITION OF LOADS WHICH GIVES MAXIMUM HORIZONTAL STRESS AT POINT P.

$$\Delta\sigma_{x,c} = \frac{\dot{q}}{2\pi}\left[\frac{3\,X^2Z}{(X^2+Z^2)^2}\left(\frac{a}{A}-\frac{1}{3}\frac{a^3}{A^3}\right)-(1-2\nu)\frac{aZ}{A(X^2+Z^2)}\right] \qquad (6.16.a)$$

Or

$$\Delta\sigma_{x,c} = +\frac{\dot{q}}{2\pi Z}\left[3\sin^2\psi\cos^2\psi\left(\sin\varphi_f-\frac{1}{3}\sin^3\varphi_f\right)\right.$$

$$\left.-(1-2\nu)\left(\cos^2\psi\sin\varphi_f\right)\right] \qquad (6.16.b)$$

The notations of the above equations are shown in Fig. (6.16).

The maximum horizontal stress due to the critical position of the two line loads representing the compaction loads as shown in Fig. (6.15) can be obtained by applying equations (6.16.a or b) and hence:

$$\Delta\sigma_{x,c} = \Delta\sigma_{x,c}{}_{(\text{first load})} + \Delta\sigma_{x,c}{}_{(\text{second load})} \qquad (6.17)$$

Using the above assumptions and those in Secs.(6.5.2.b,d,e,f,g and h) which have been used for the case of simulating the compaction load as a uniform loaded area, the maximum horizontal stress due to the compaction plant on a reinforced earth retaining wall can be obtained as follows:

$$\Delta\sigma_{hm,c} = \frac{4\dot{q}_1}{\pi}\left[\frac{3\,X^2Z}{(X^2+Z^2)^2}\left(\frac{a}{A}-\frac{1}{3}\frac{a^3}{A^3}\right)-(1-2\nu)\frac{aZ}{A(X^2+Z^2)}\right]$$

$$-\frac{4\dot{q}_2}{\pi}(1-2\nu)\left(\frac{a}{AZ}\right) \qquad (6.18.a)$$

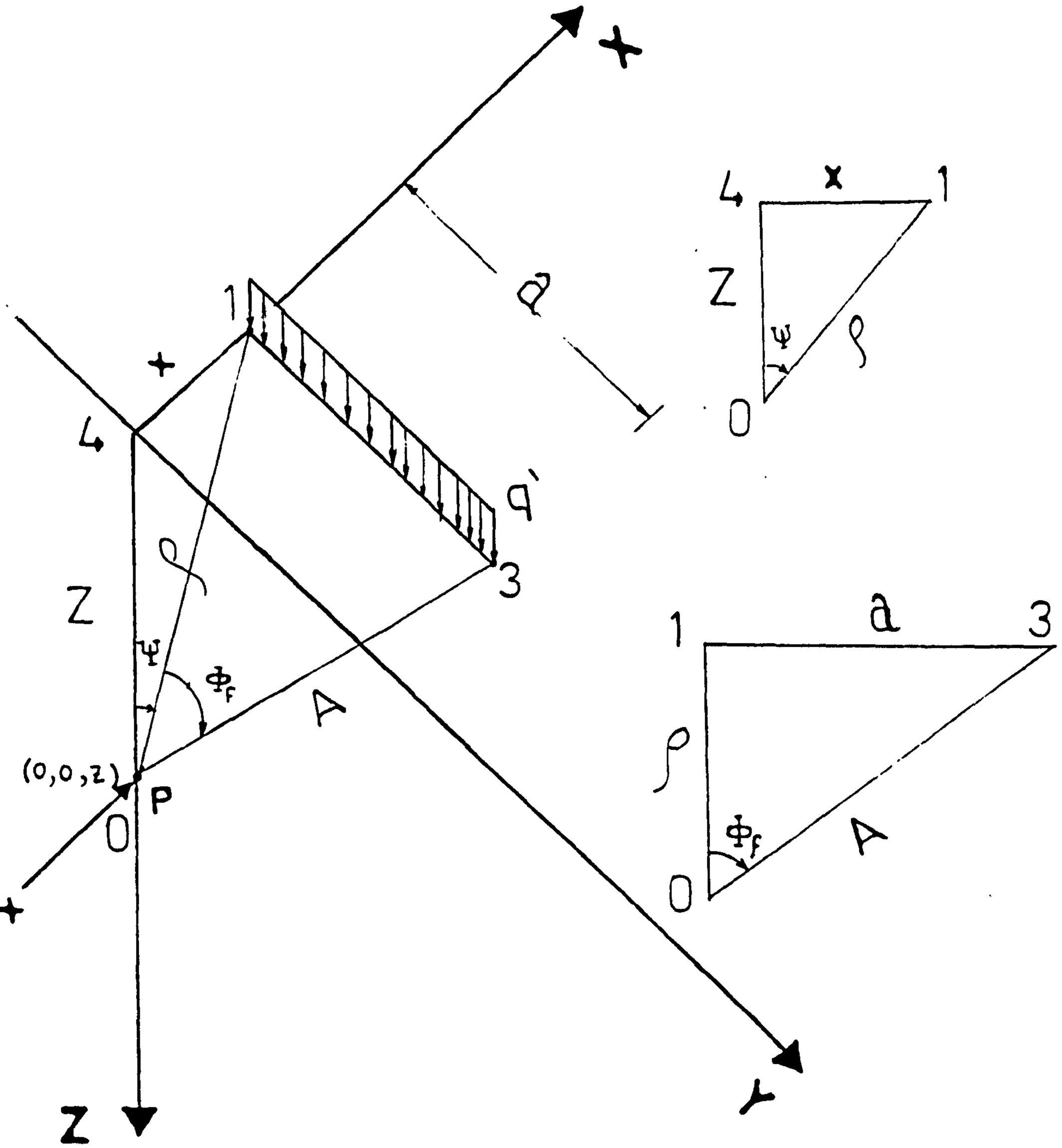

FIG. (6. 16) NOTATIONS OF EQUATION OF MAXIMUM HORIZONTAL STRESS DUE TO LINE LOAD PARALLEL TO THE WALL.

Or

$$\Delta\sigma_{hm,c} = \frac{4\dot{q}_1}{\pi Z}\left[3\sin^2\psi\cos^2\psi\left(\sin\varphi_f - \frac{1}{3}\sin^3\varphi_f\right) - (1-2\nu)\left(\cos^2\psi\sin\varphi_f\right)\right] - \frac{4\dot{q}_2}{\pi Z}(1-2\nu)\sin\varphi_f \quad (6.18.b)$$

Where in the case of a line load near the wall (second load) $X = 0.0$ & $\psi = 0.0$, and $\rho = Z$.

6.5.7 Fourth Proposed Model (Computer Program BCOMPP)

A computer program (BCOMPP) has been developed by the author in order to simulate the compaction plant loads and find the maximum horizontal stress in the free field or near the retaining structure. The program can find the horizontal stress due to any number and locations of loaded areas, Fig. (6.17), uniform line loads, Fig. (6.18&19)) respectively, and point loads, Fig. (6.20), static or dynamic at the same time.

The program has been written in Fortran 77 and run on an IBM – 3090 machine in Glasgow University. A Fortran 77 listing of the program is provided in Appendix C Sec (C.1). The assumptions considered in the program were:

(a) The method of analysis used in the program is a numerical integration method. The basic idea in this method , Green et al. (1986), is to evaluate an integral by evaluating the given function (f_x) at several points (a_n). The integral is taken to be the sum of these values, each of which has been weighted by

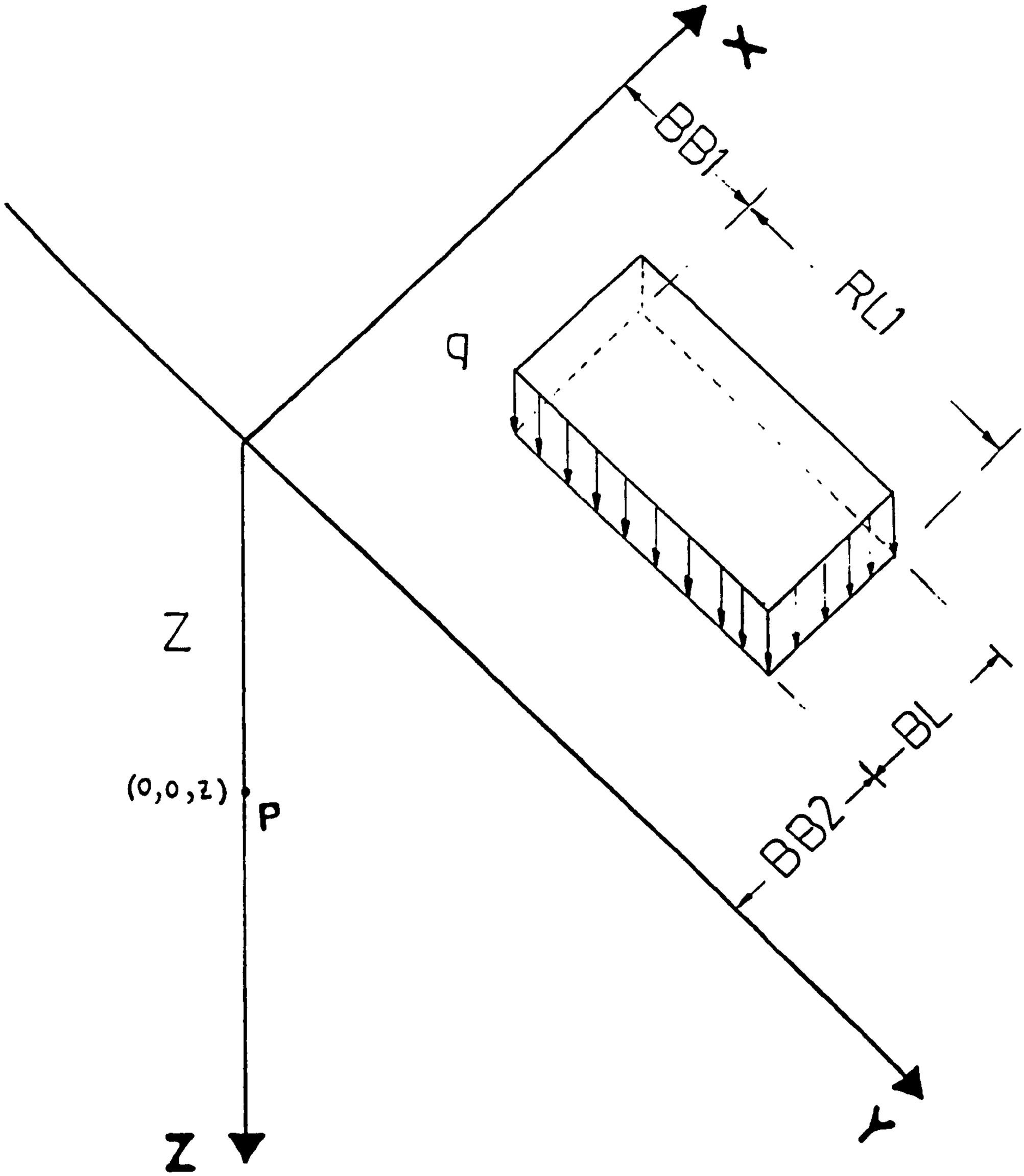

FIG. (6.17) INPUT DATA OF LOADED AREA FOR ROGRAM (BCOMPP).

FIG. (6.18) DATA OF LINE LOAD PARALLEL TO X– AXIS FOR PROGRAM (BCOMPP).

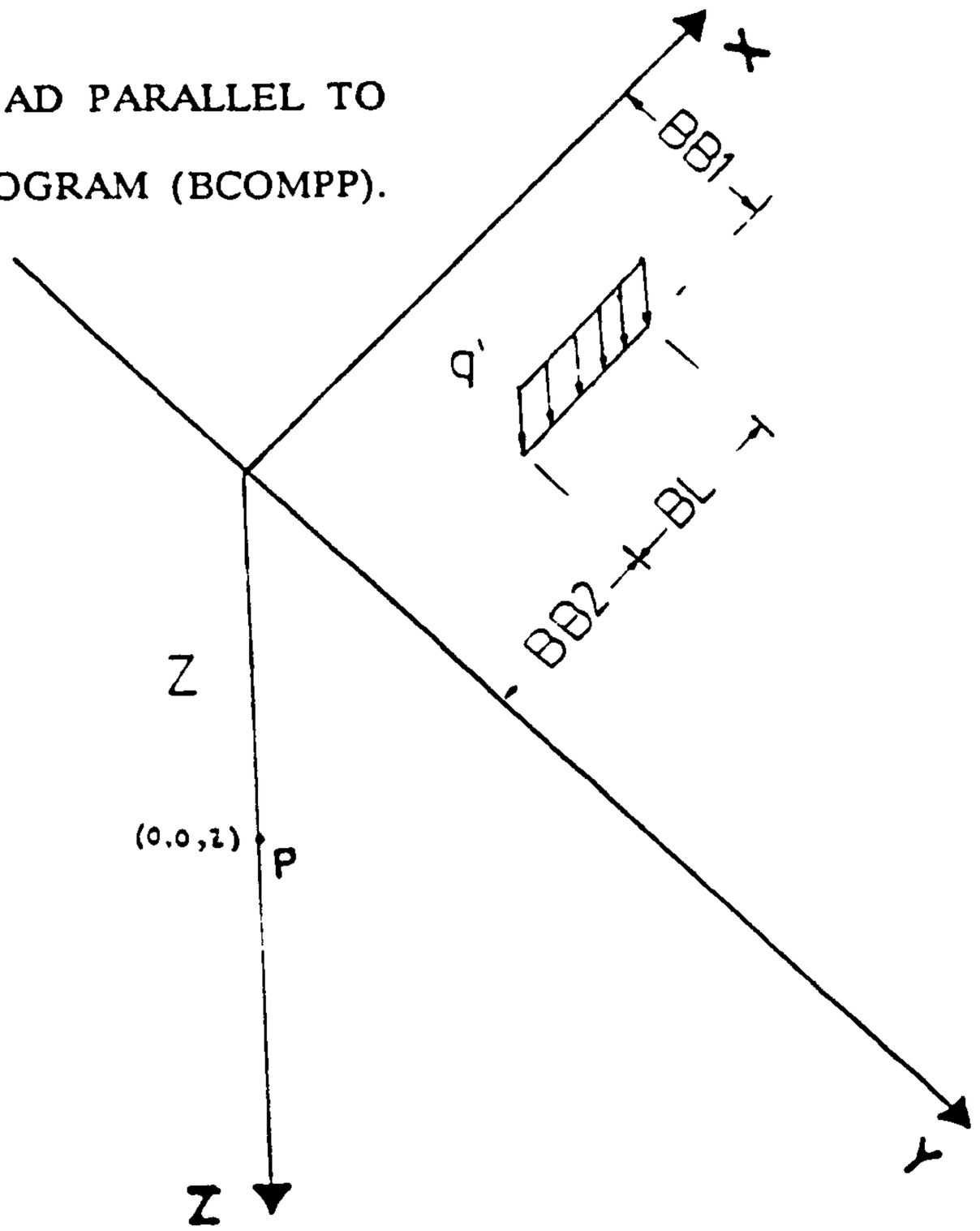

FIG. (6.19) DATA OF LINE LOAD PARALLEL TO Y– AXIS FOR PROGRAM (BCOMPP).

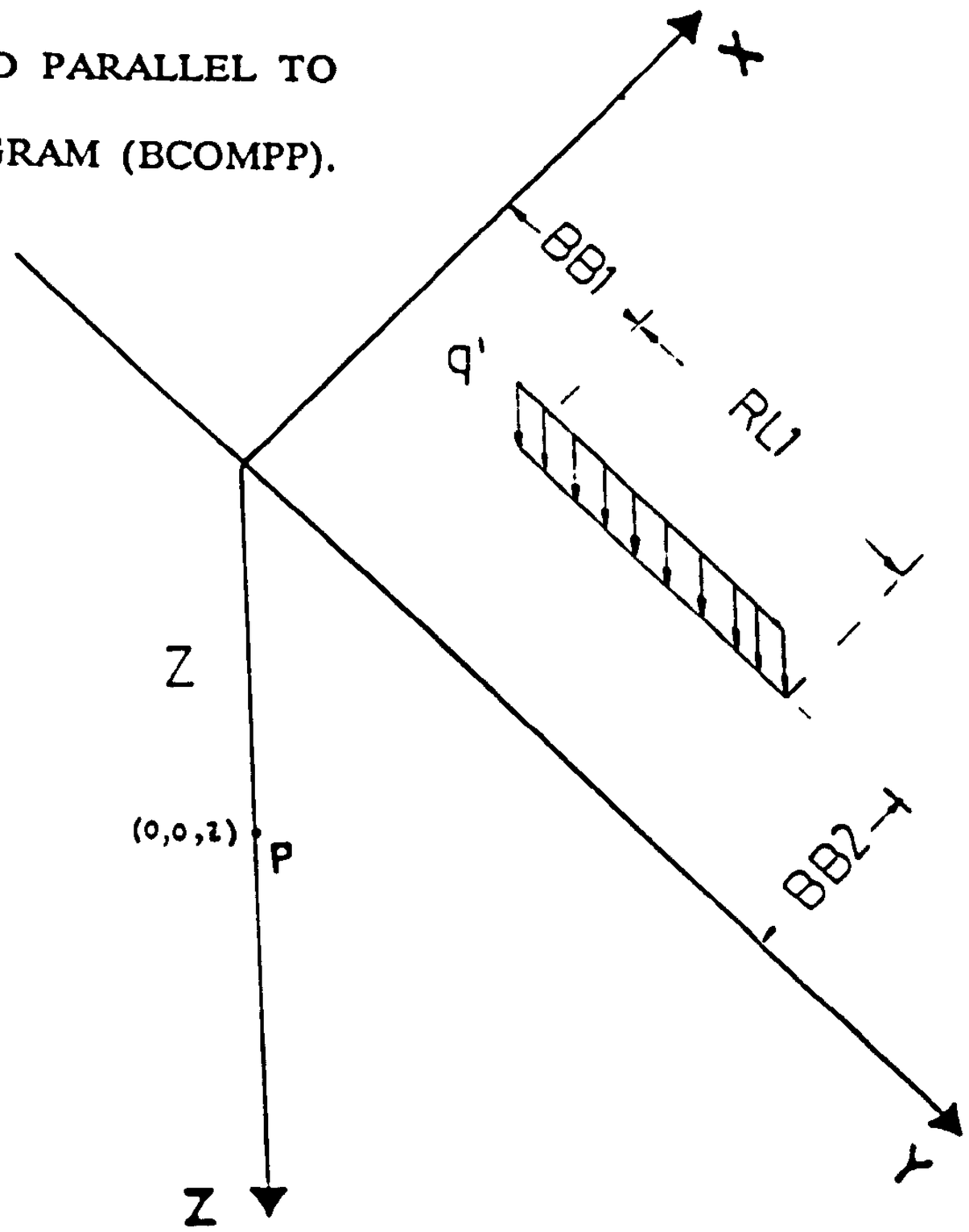

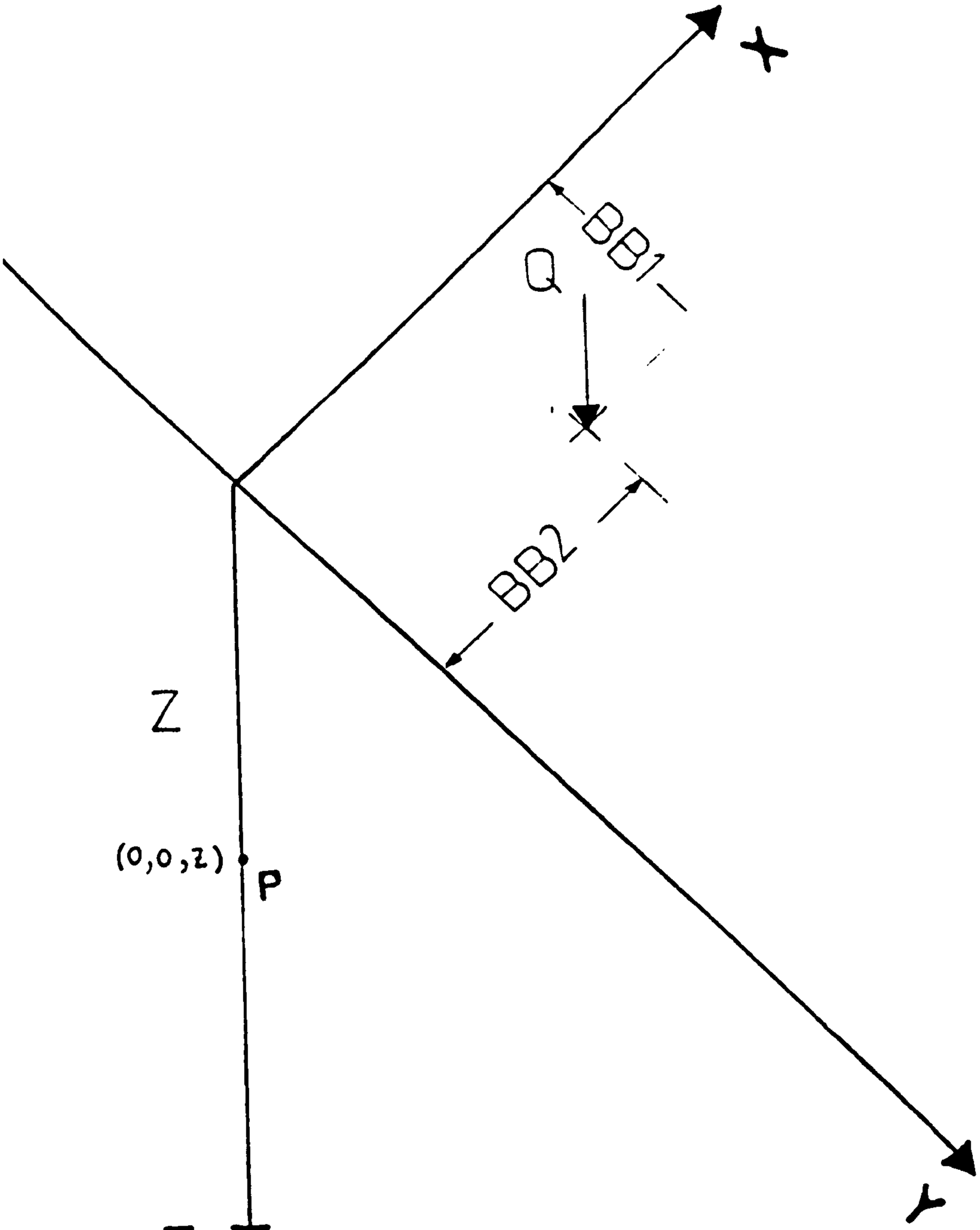

FIG. (6.20) *DATA OF POINT LOAD FOR PROGRAM (BCOMPP).*

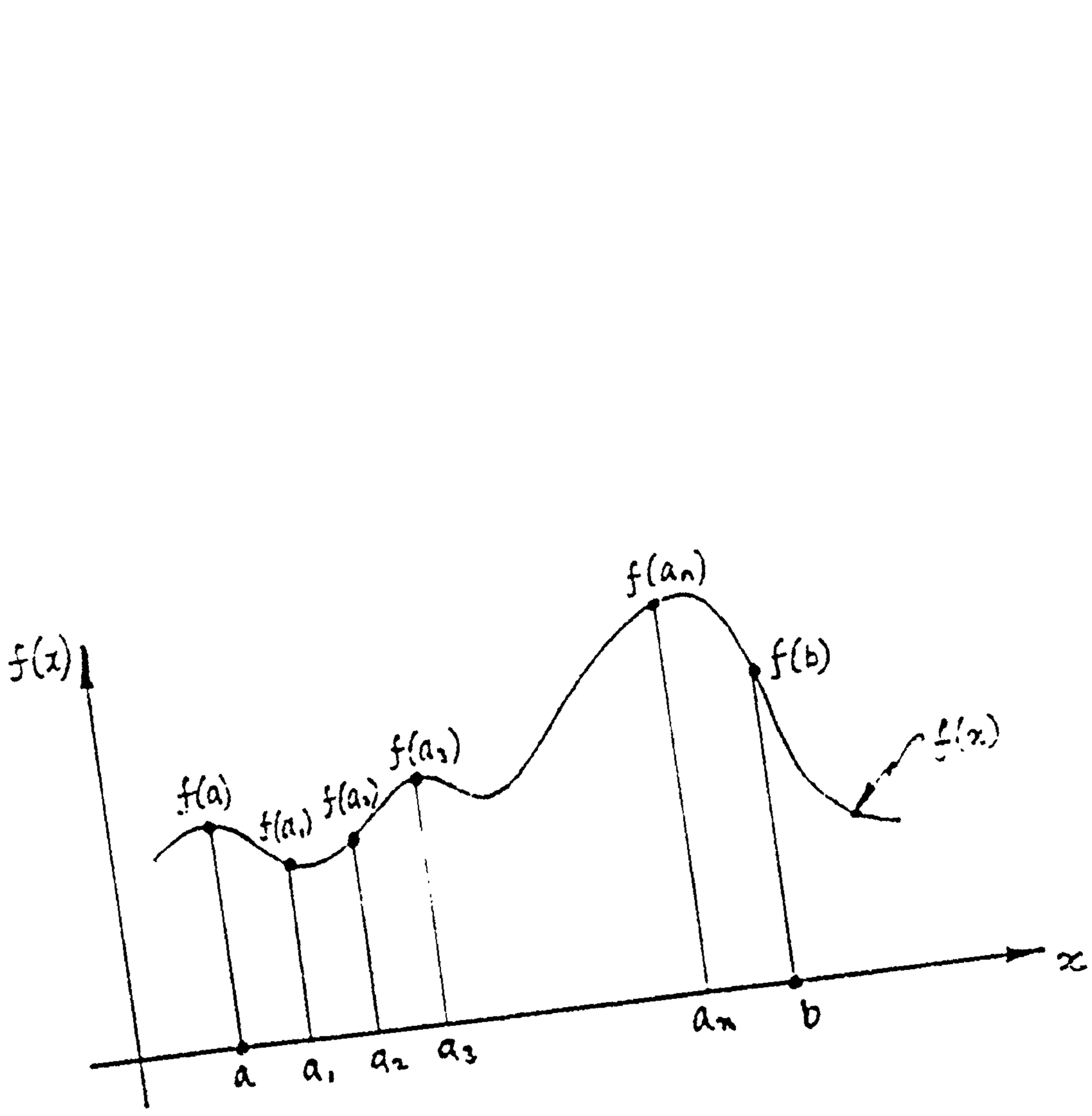

FIG. (6.21) THE VALUE OF FUNCTION F(X) AT SEVERAL POINTS (a_n).

some suitable factor (H_n), Fig. (6.21). Gaussian quadrature formulae were used and typical values of H & a are shown in Appendix C Sec (C.2).

(b) The horizontal stress in a free field or near retaining walls is based on a linear elastic solution by Boussinesq (1885).

(c) the principal of superposition of horizontal stresses due to different loads is applicable as discussed in Sec. (6.5.2.h).

A description of the input data of program BCOMPP is shown in Appendix C Sec (C.3). Typical data and results of one of the computer runs are shown in Appendix C Sec (C.4).

6.6 CHECK AND VERIFICATION OF THE PROPOSED MODELS OF COMPACTION PLANT

In order to check and verify the new models of compaction plant, comparisons were made with results from classical theories, the author's laboratory work, and other authors' experimental work using small or full scale retaining walls and finite element analyses.

6.6.1 General Examples

In order to get the general trend of the distribution of horizontal stresses in a dimensionless form in a free field and on a vertical retaining wall (assuming a friction less wall), three different loads are considered as follows:

(a) A unit loaded area of dimension 1.0 x 1.0 (unit area) and load density q (load/unit area) as shown in Fig. (6.22.A).

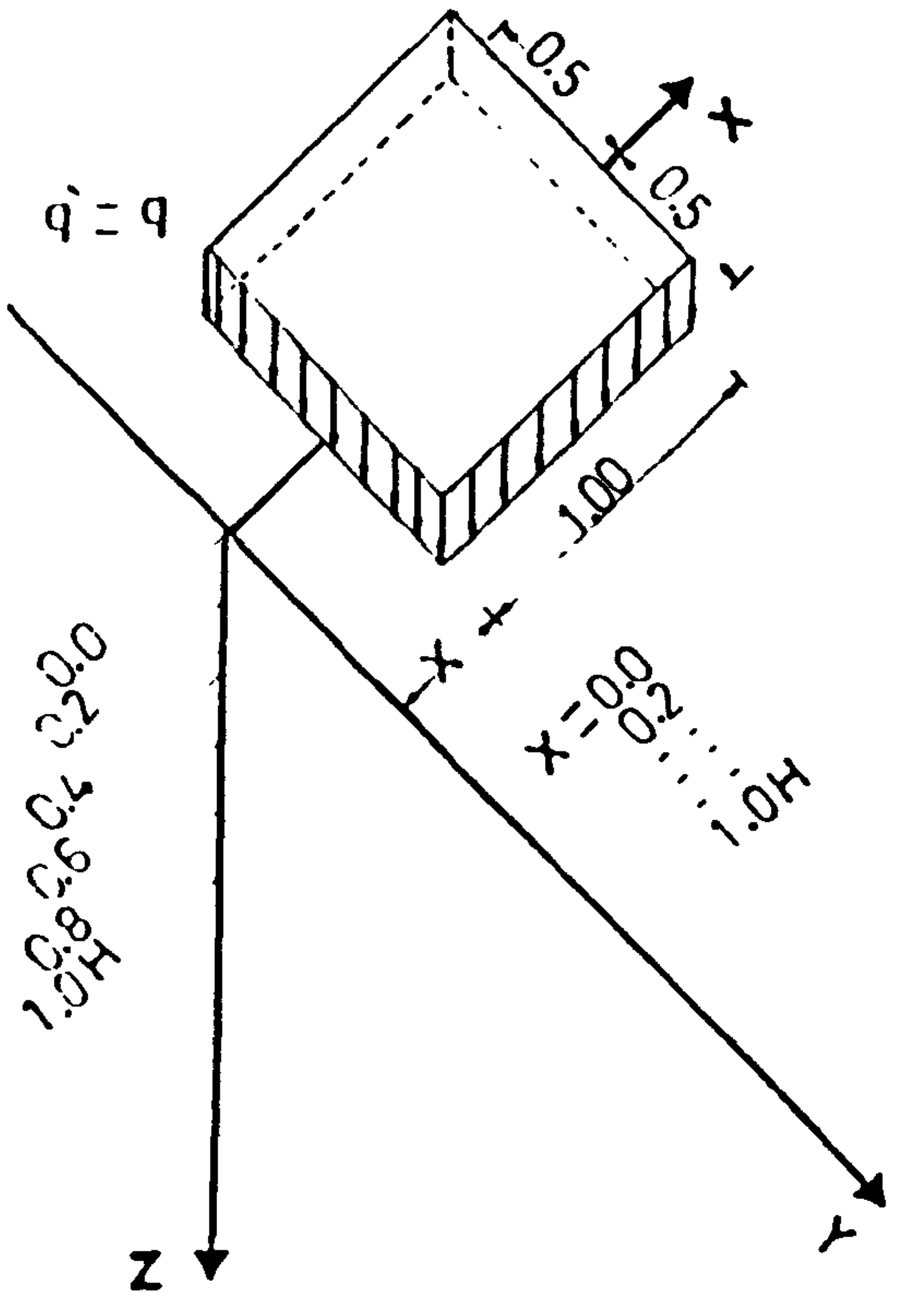

(A) LOADED AREA

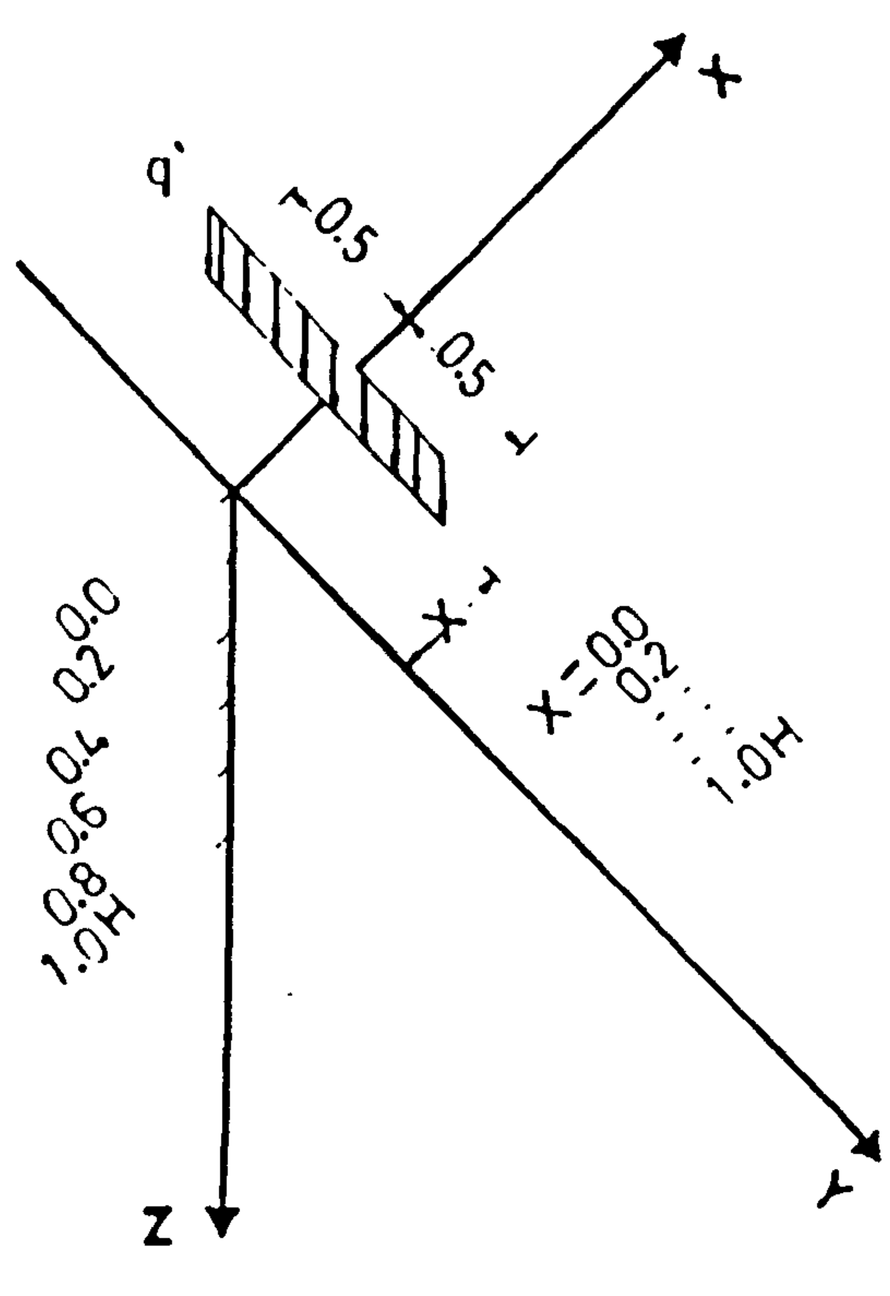

(B) LINE LOAD PARALLEL TO Y-AXIS

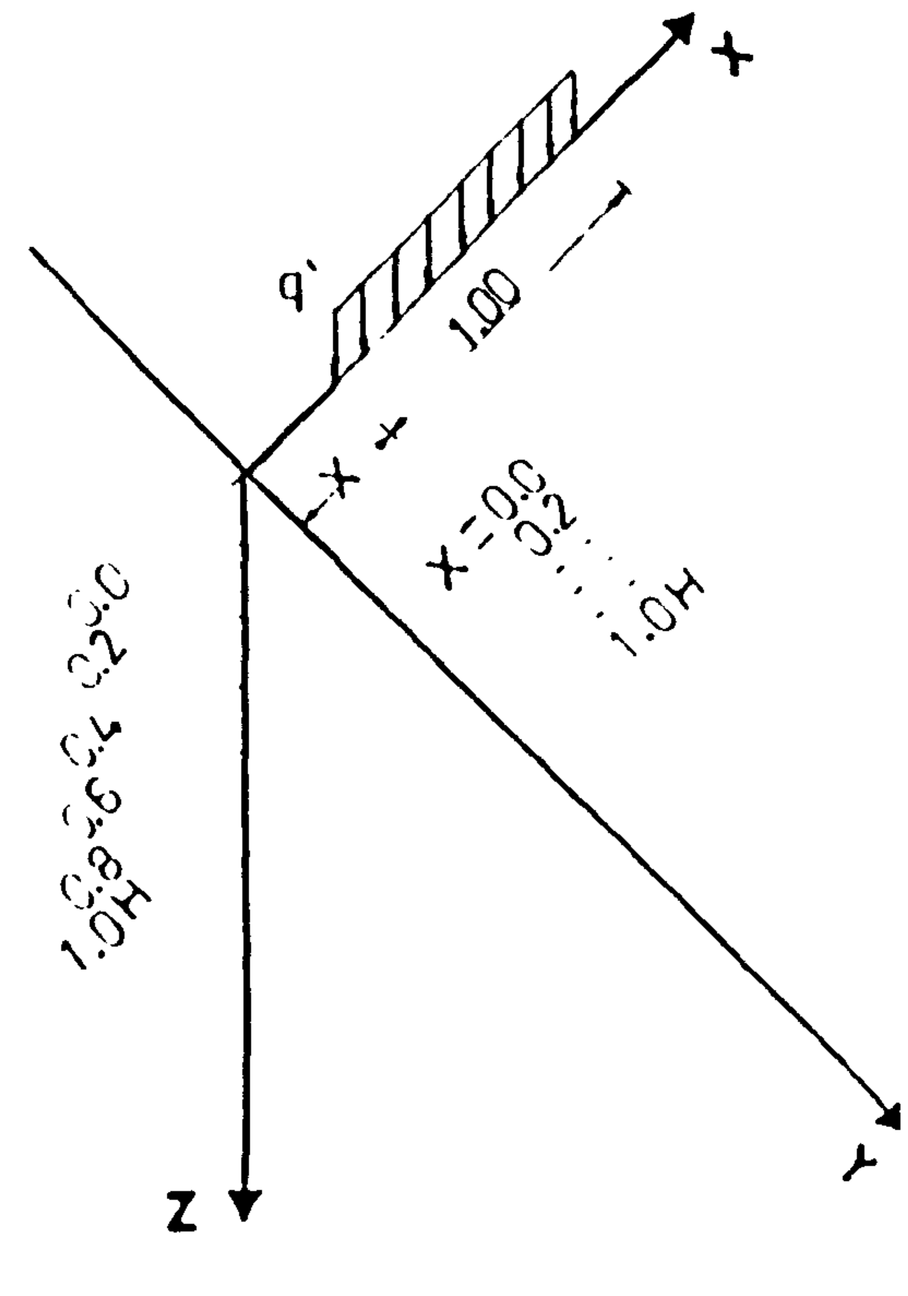

(C) LINE LOAD IN PLANE X-Z & PERPENDICULAR TO Y-AXIS.

FIG. (6.22) GENERAL EXAMPLES.

(b) A unit length of line load of intensity $\dot{q}$ (load/unit length), where $|\dot{q}| = |q|$ and the load is parallel to Y– axis as shown in Fig. (6.22.B).

(c) A unit length of line load of intensity $\dot{q}$ (load/unit length), where $|\dot{q}| = |q|$ and the load is perpendicular to the Y– axis, as shown in Fig. (6.22.C).

The maximum horizontal stresses at points on the Z– axis in a plane XZ which passes through the middle of the loads have been calculated . The depth of the points is a function of height (H) and the maximum horizontal stress is a function of load intensity q. The stresses have been obtained for different values of X, where X is the distance from plane ZY to the load. These are shown in Fig. (6.22). It should be noted that plane ZY represents the wall in the case of calculating stresses on vertical walls.

The distribution of maximum horizontal stresses due to a uniform loaded area in a free field and on a vertical wall using the author's computer program (BCOMPP) are shown in Figs. (6.23&24) respectively.

The general features of these distributions are:

(i) In both free field and vertical wall the stresses decrease as the depth increases.

(ii) The maximum values of stress occur at shallow depths within the upper third of the height.

(iii) Maximum values of stress are obtained when X = 0.0 i.e. the load is adjacent to plane YZ and the stress decreases as X increases.

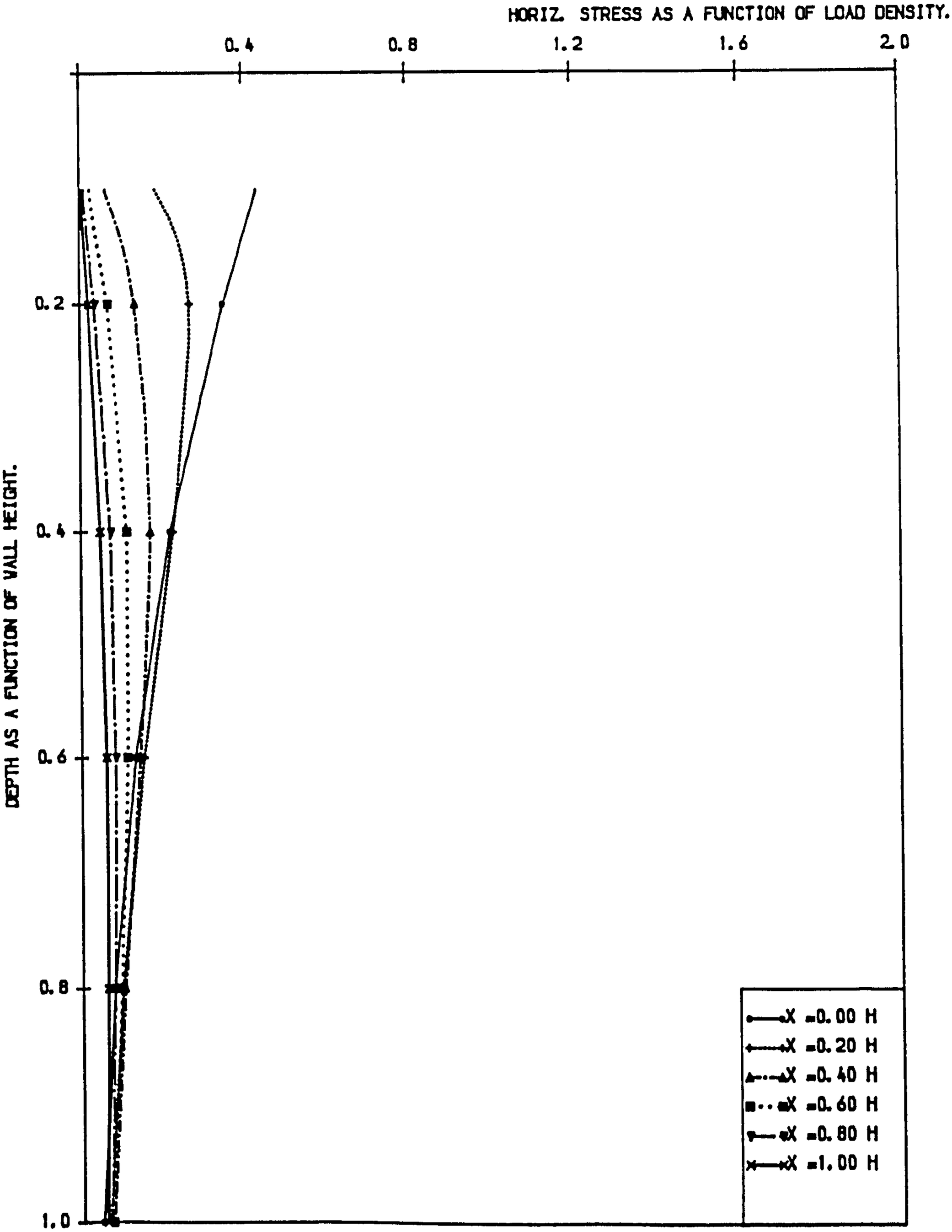

FIG. (6.23) DISTRIBUTION OF HORIZ. STRESSES IN FREE FIELD DUE TO UNIFORM LOADED AREA USING AUTHOR'S PROG. (BCOMPP).

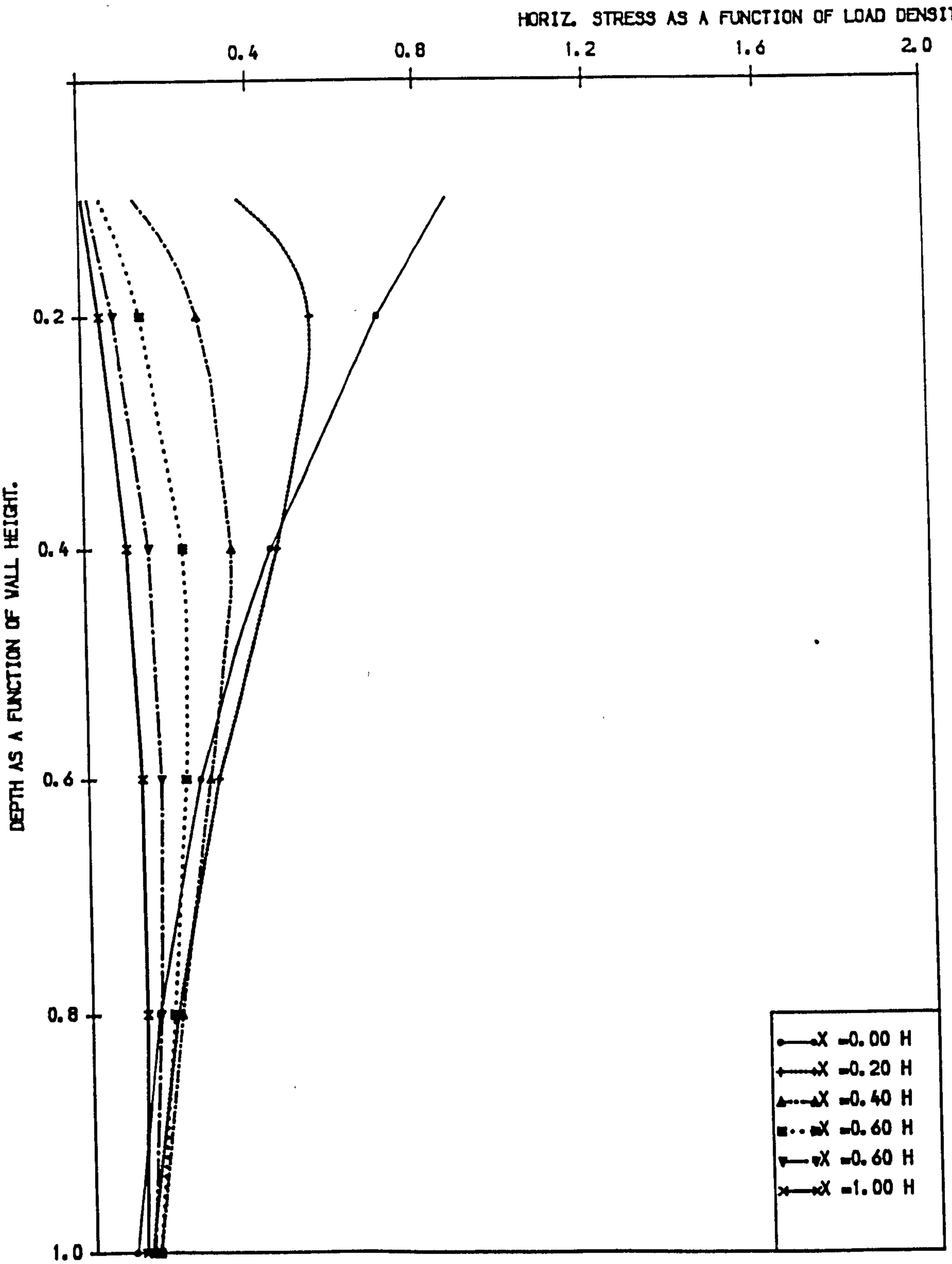

FIG. (6.24) DISTRIBUTION OF HORIZ. STRESSES ON VERTICAL WALL DUE TO UNIFORM LOADED AREA USING AUTHOR'S PROG. (BCOMPP).

(iv) The distribution of maximum horizontal stress on a vertical wall has almost the same shape as in a free field, but the values of the stresses are bigger. This is due to the presence of the wall which suddenly interrupts the lateral strain in the soil mass, causing an accumulation of stress.

Figs. (6.25 to 28) show the distribution of maximum horizontal stresses in a free field and on a vertical wall due to a line load parallel to the Y–axis. The general features of the curves are:

(i) The horizontal stresses decrease with increasing depth, and the maximum values occur at shallow depths. This agrees with the results of experimental work carried out by Spangler (1938) and by Terzaghi (1954).

(ii) The stresses at shallow depths increase with decreasing distance X and decrease with depth.

A comparison between the horizontal stresses calculated using the author's equations and the computer program (BCOMPP) is shown in Figs. (6.29&30). Good agreement is seen in the free field case as well as for the vertical wall.

The distribution of horizontal stresses due to a line load perpendicular to the Y–axis in a free field as well as on a vertical wall using the author's equations and computer program (BCOMPP) are shown in Figs. (6.31 to 34). The general features of the distributions are the same as in case of a uniform loaded area Sec. (6.6.1), and in addition, the horizontal stress near the surface i.e. when depth = 0.0 and X = 0.0 is infinite.

Comparisons between the stresses from the author's equation and the computer program (BCOMPP) are shown in Figs (6.35&36), and reasonable

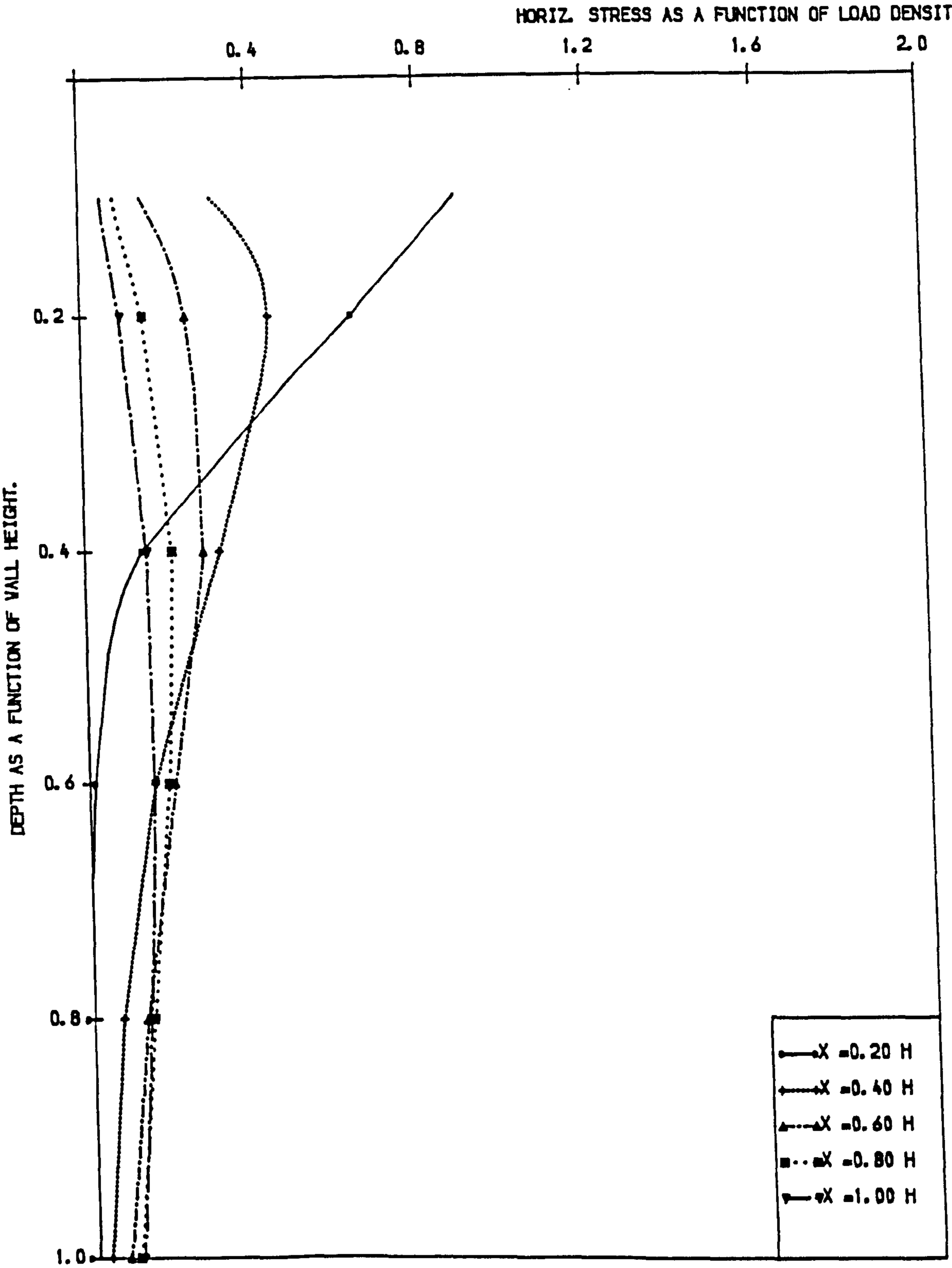

FIG. (6.25) DISTRIBUTION OF HORIZ. STRESSES IN FREE FIELD DUE TO LINE LOAD PARALLEL TO Y-AXIS USING AUTHOR'S EQUATION.

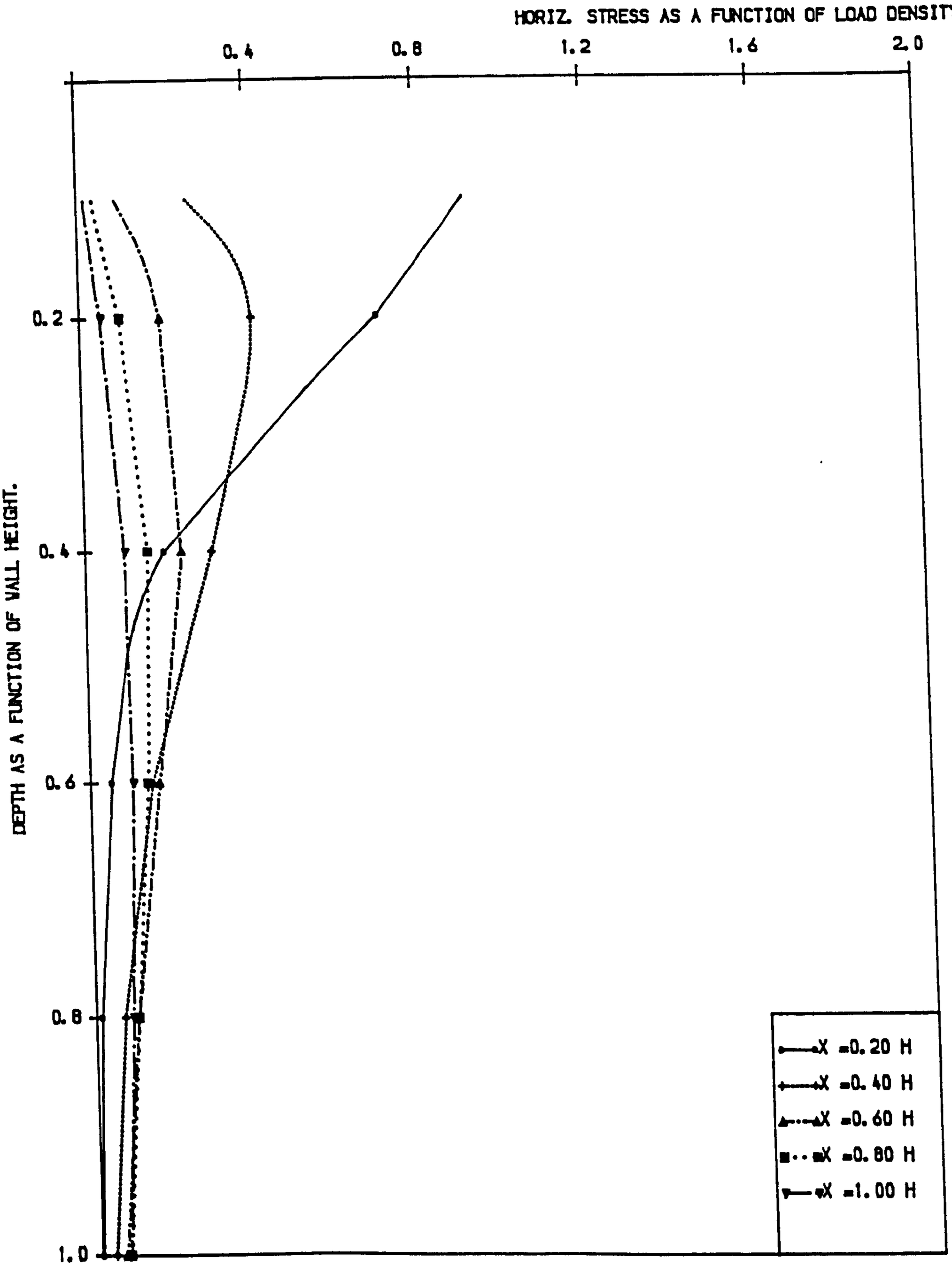

FIG. (6.26) DISTRIBUTION OF HORIZ. STRESSES IN FREE FIELD DUE TO LINE LOAD PARALLEL TO Y-AXIS USING PROG. (BCOMPP).

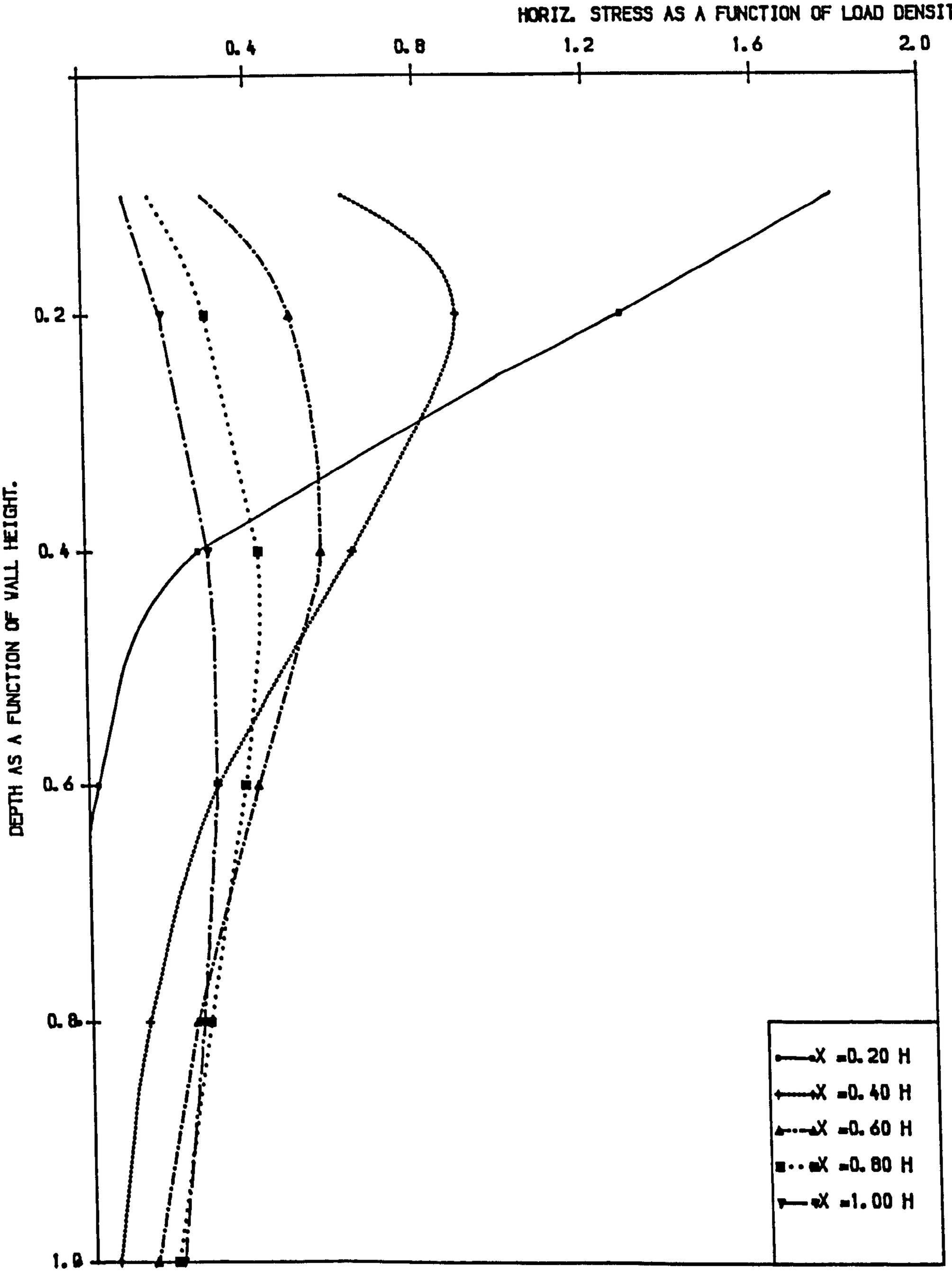

FIG. (6.27) DISTRIBUTION OF HORIZ. STRESSES ON VERTICAL WALL DUE TO LINE LOAD PARALLEL TO THE WALL USING AUTHOR'S EQUATION.

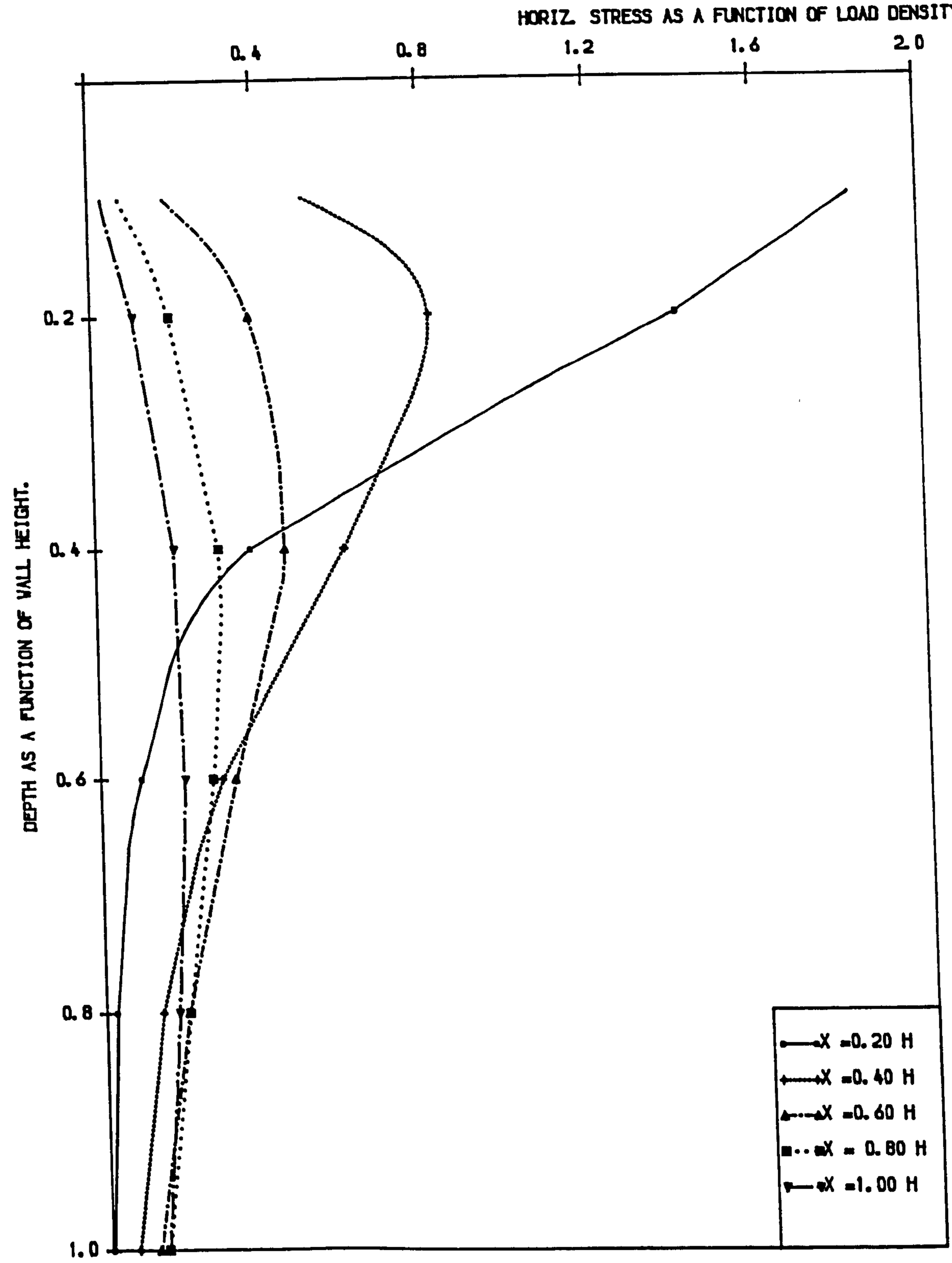

FIG. (6.28) DISTRIBUTION OF HORIZ. STRESSES ON VERTICAL WALL DUE TO LINE LOAD PARALLEL TO THE WALL USING PROG. (BCOMPP).

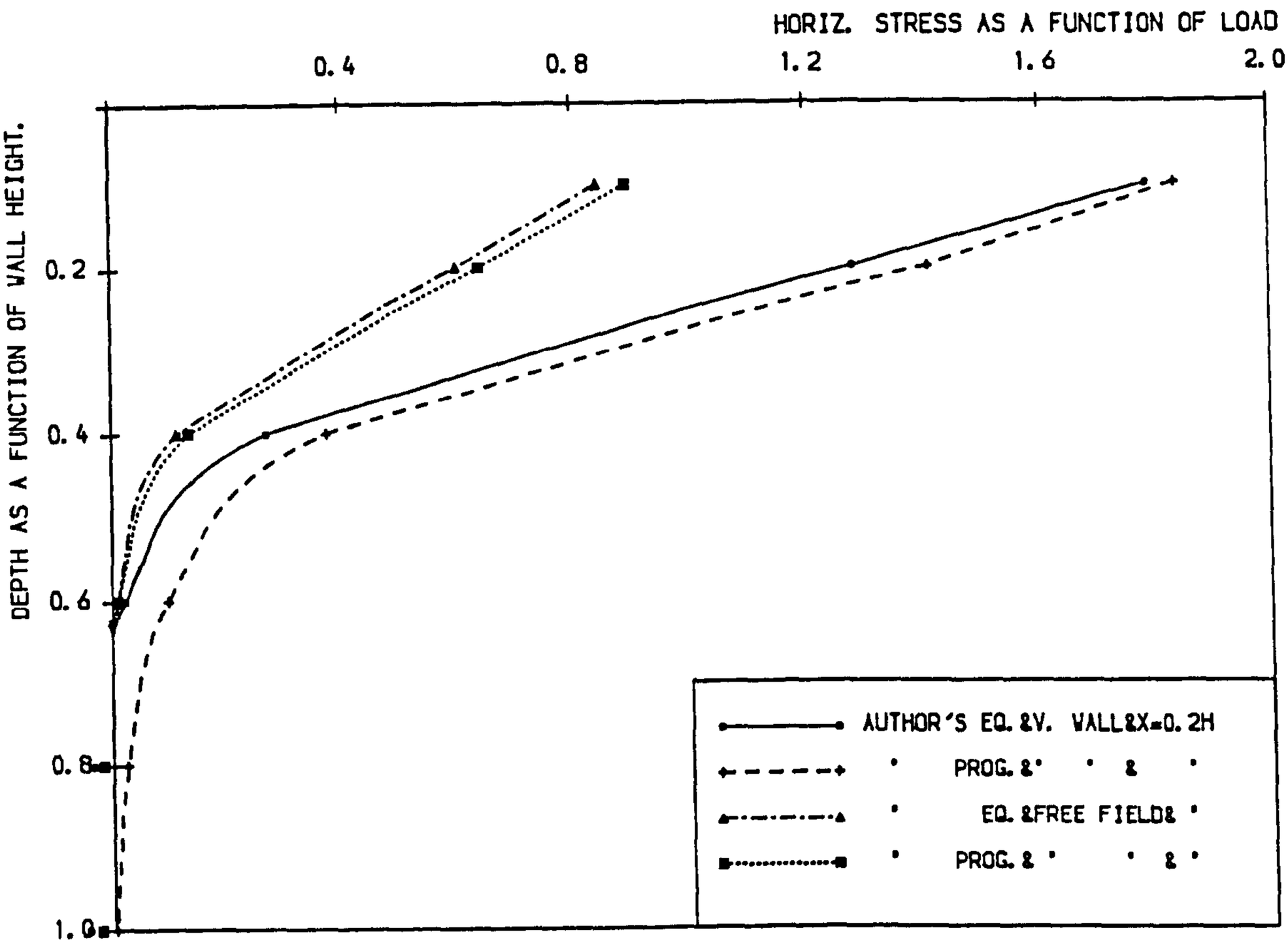

FIG. (6.29) COMPARISON BETWEEN HORIZ. STRESSES CALCULATED FROM LINE LOAD ON V. WALL&IN FREE FIELD, USING AUTHOR'S EQ. & PROG. (BCOMPP).

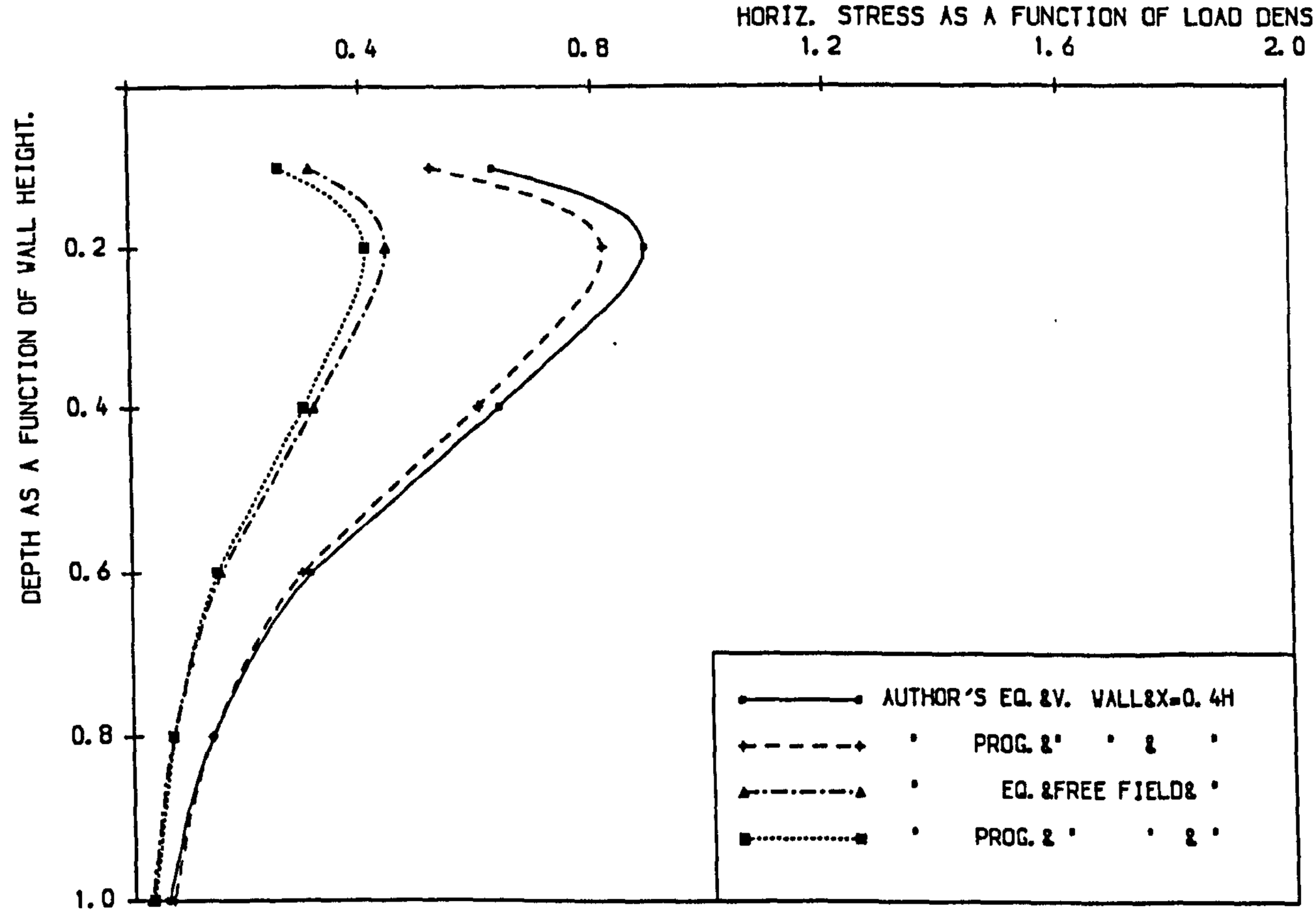

FIG. (6.30) COMPARISON BETWEEN HORIZ. STRESSES CALCULATED FROM LINE LOAD ON V. WALL&IN FREE FIELD, USING AUTHOR'S EQ. & PROG. (BCOMPP).

agreement can be seen.

6.6.2 Comparison With The Classical Theories

To ensure that proposed models give reasonable limits, a comparison between classical theories i.e. linear elastic solution by Boussinesq (1885) and Terzaghi (1942) and the proposed models has been made.

The distribution of maximum horizontal stresses with depth in a free field due to the loads shown in Fig.(6.37.A,B&C) using classical theories and due to the load in Fig. (6.37.D) using the first proposed model for a rectangular loaded area Sec. (6.5.1) are shown in Fig. (6.38). It is clear that the horizontal stresses due to rectangular area with dimensions 0.8 x 2.0 m and intensity (q), Fig. (6.37.D), must fall between the values of horizontal stresses from a concentrated load Q = 0.8x1.0xq, Fig. (6.37.B), and a very long strip with the same width and intensity, Fig. (6.37.A). Also it must be less than a very long line load parallel to Y− axis with the same intensity $|\dot{q}| = |q|$ Fig. (6.37.C).

The comparison shown in Fig. (6.38) verifies the above, so the results from the author's computer program (BCOMPP) fall within reasonable limits.

6.6.3 Comparison With Author's Laboratory Results

Comparison has been made between the measured horizontal stresses on the laboratory model of a reinforced earth retaining wall carried out by the author with the compaction apparatus used in the laboratory tests, Chapter 3, and the

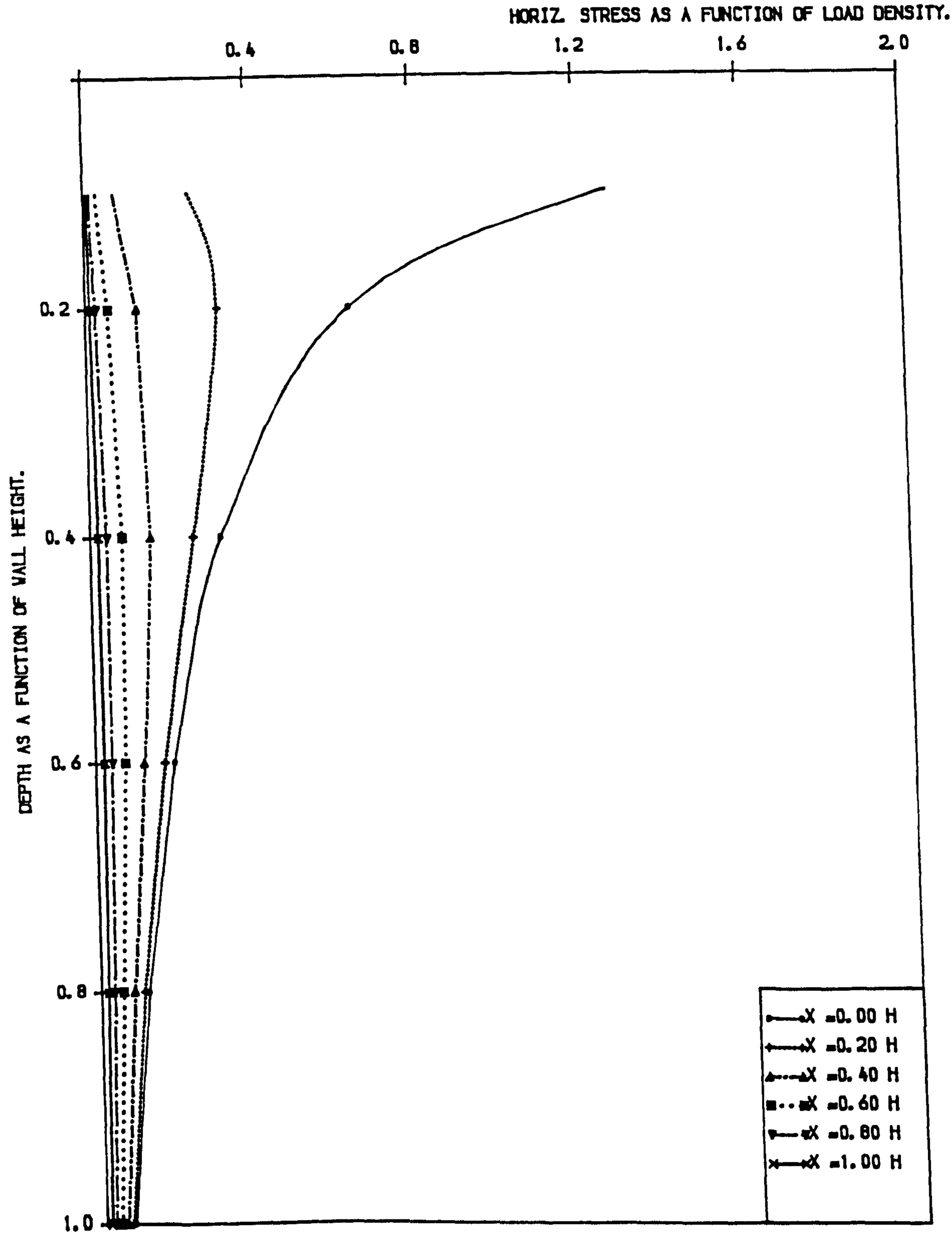

FIG. (6.31) DISTRIBUTION OF HORIZ. STRESSES IN FREE FIELD DUE TO LINE LOAD PERPENDICULAR TO Y-AXIS USING AUTHOR'S EQ.

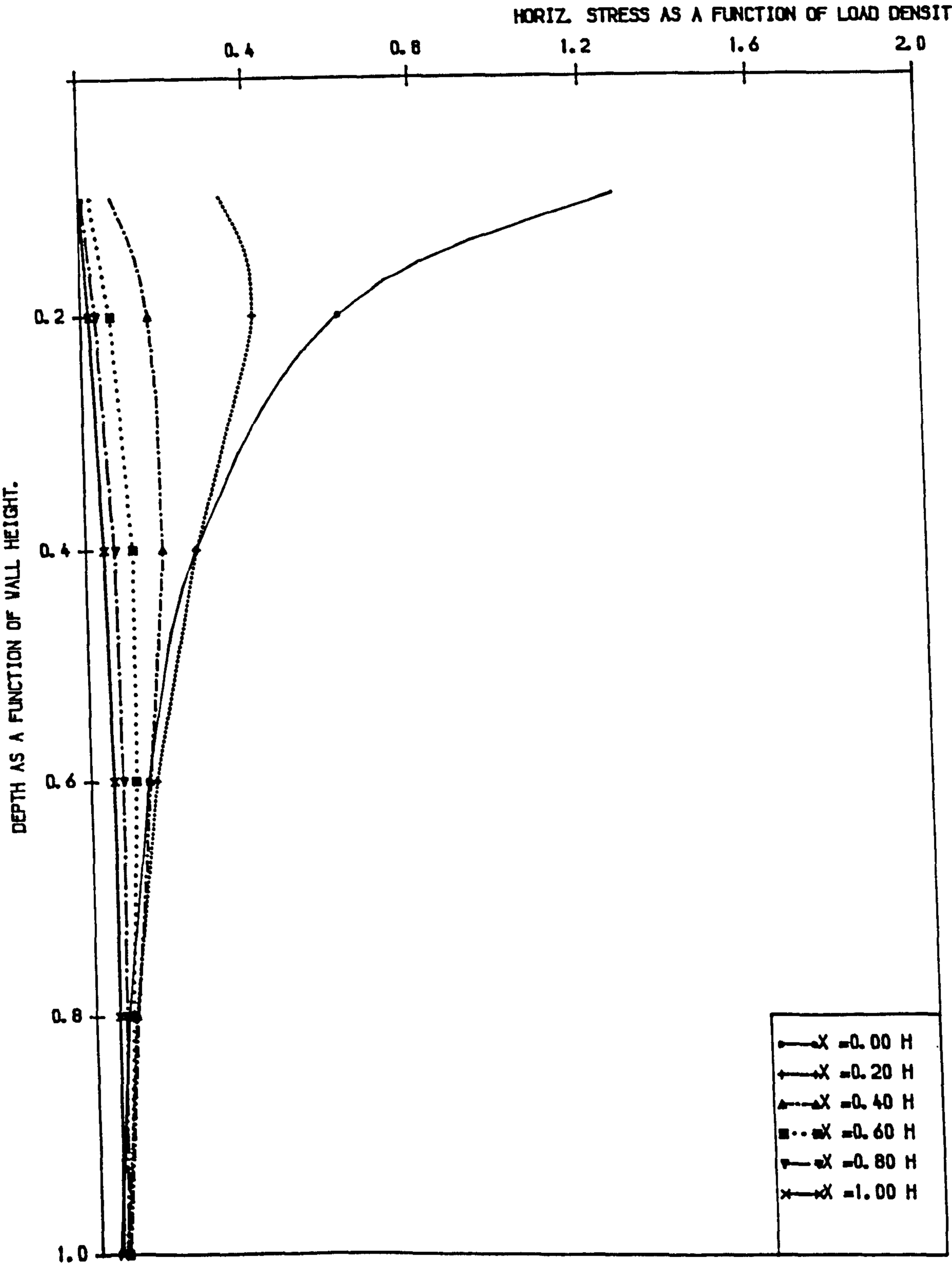

FIG. (6.32) DISTRIBUTION OF HORIZ. STRESSES IN FREE FIELD DUE TO LINE LOAD PERPENDICULAR TO Y-AXIS USING PROG. (BCOMPP).

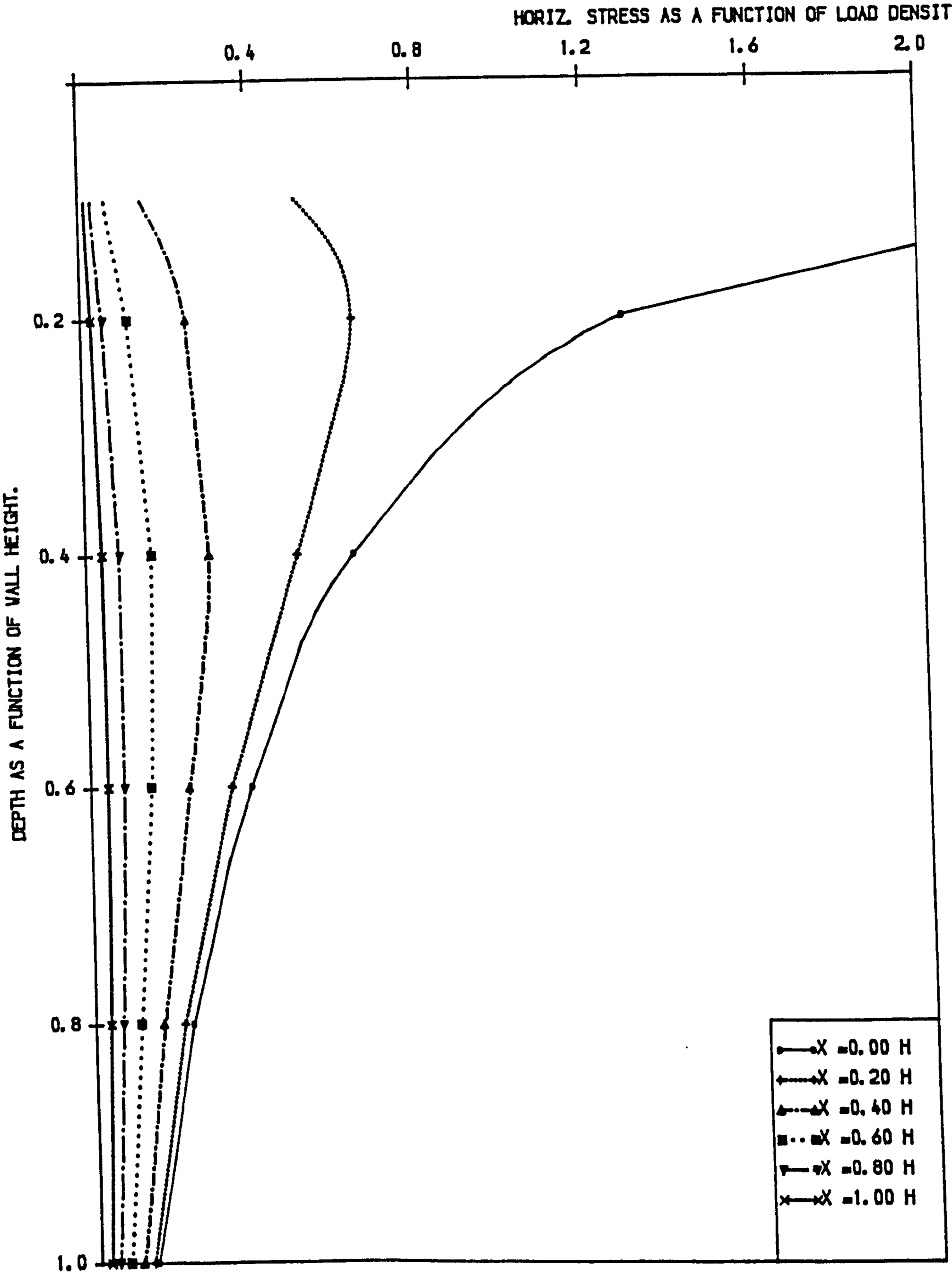

FIG. (6.33) DISTRIBUTION OF HORIZ. STRESSES ON VERTICAL WALL DUE TO LINE LOAD PERPENDICULAR TO THE WALL USING AUTHOR'S EQ..

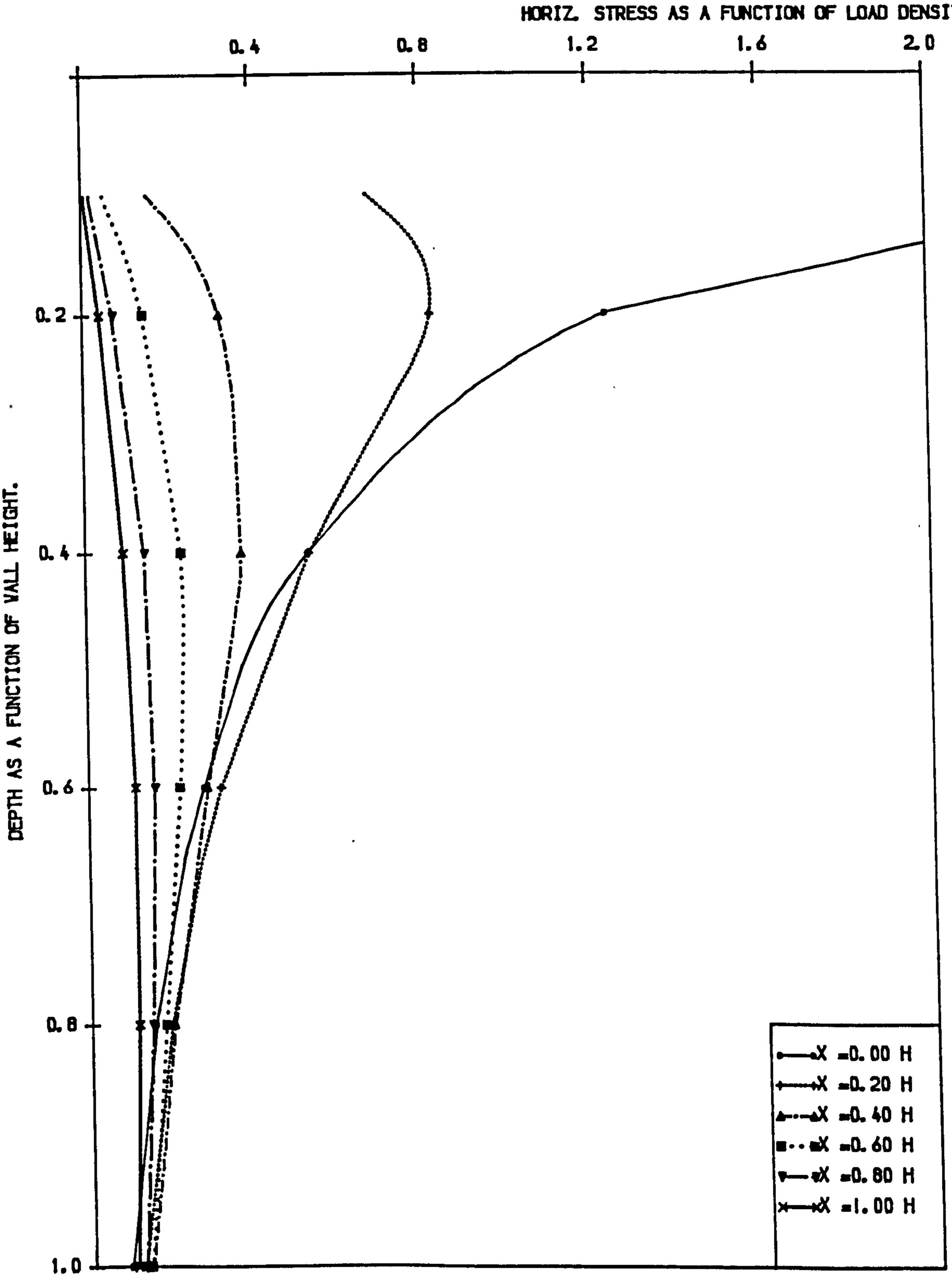

FIG. (6.34) DISTRIBUTION OF HORIZ. STRESSES ON VERTICAL VALL DUE TO LINE LOAD PERPENDICULAR TO THE VALL USING PROG. (BCOMPP).

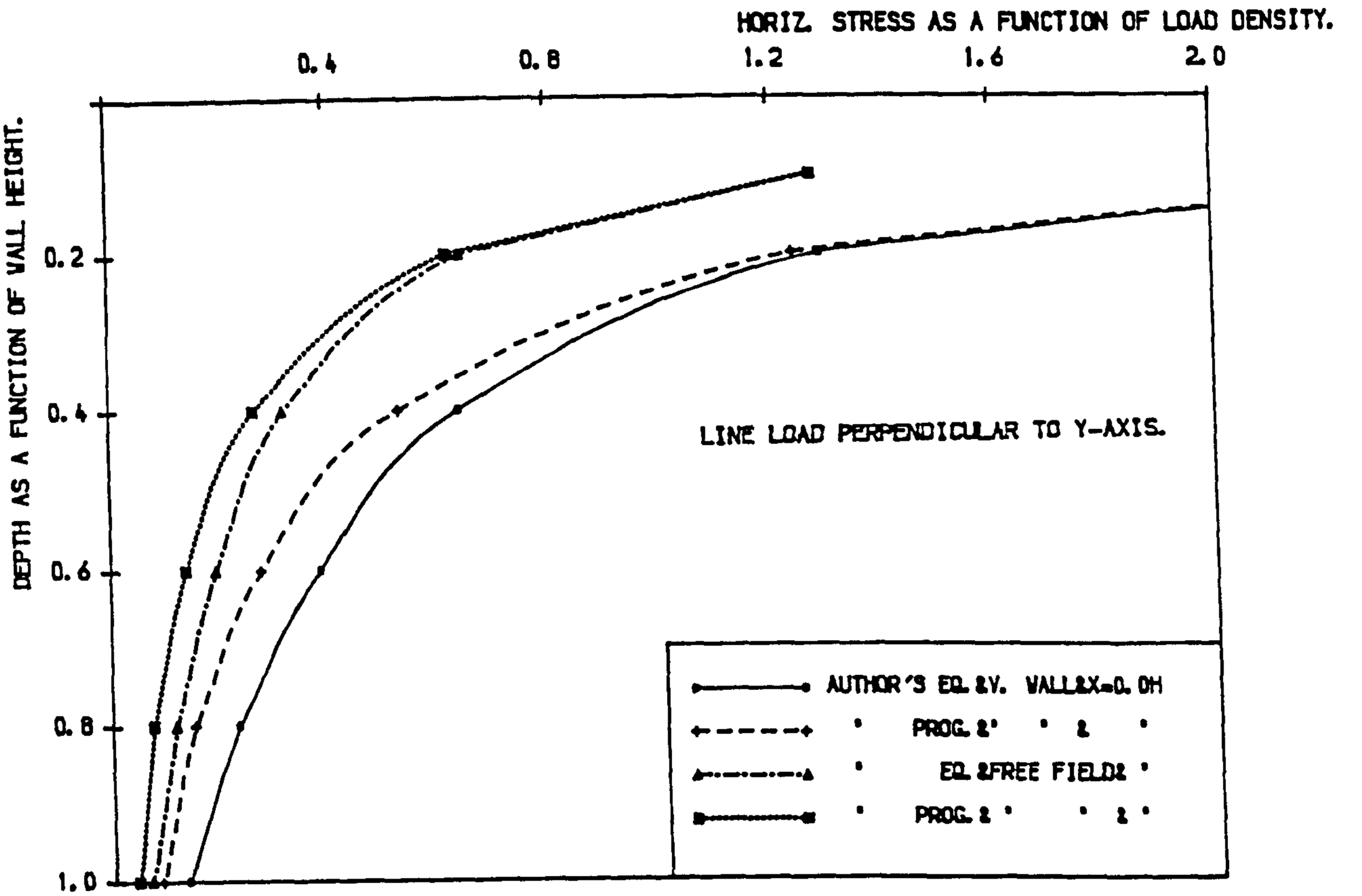

FIG. (6.35) COMPARISON BETWEEN HORIZ. STRESSES CALCULATED FROM LINE LOAD ON V. WALL&IN FREE FIELD, USING AUTHOR'S EQ. & PROG. (BCOMPP).

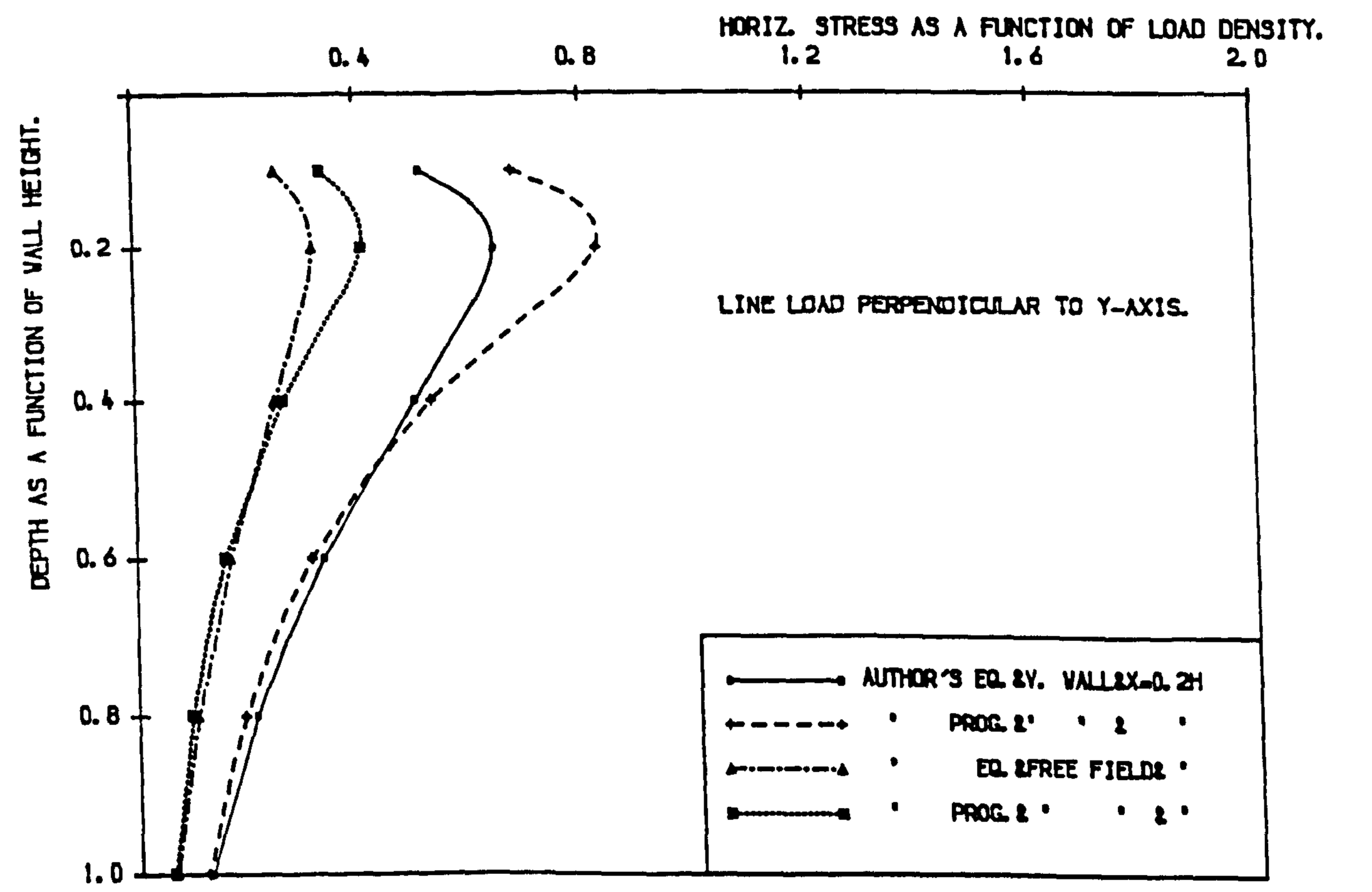

FIG. (6.36) COMPARISON BETWEEN HORIZ. STRESSES CALCULATED FROM LINE LOAD ON V. WALL&IN FREE FIELD, USING AUTHOR'S EQ. & PROG. (BCOMPP).

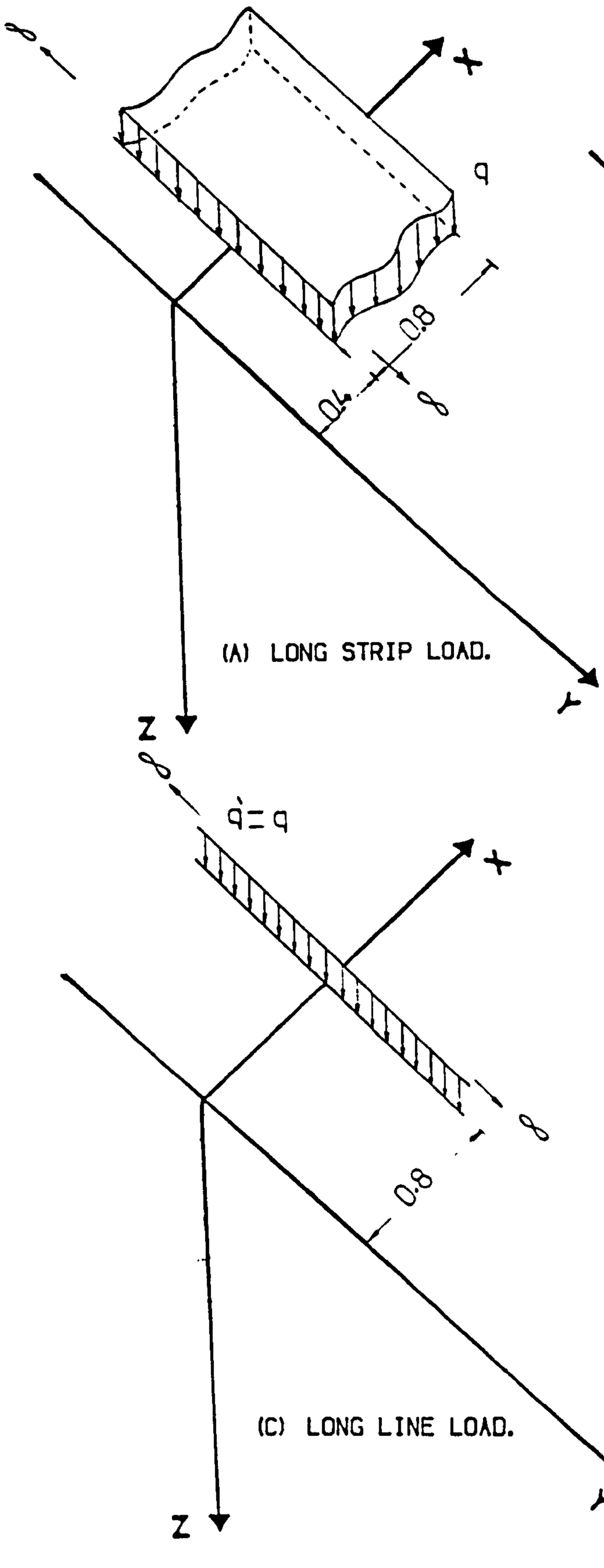

(A) LONG STRIP LOAD.

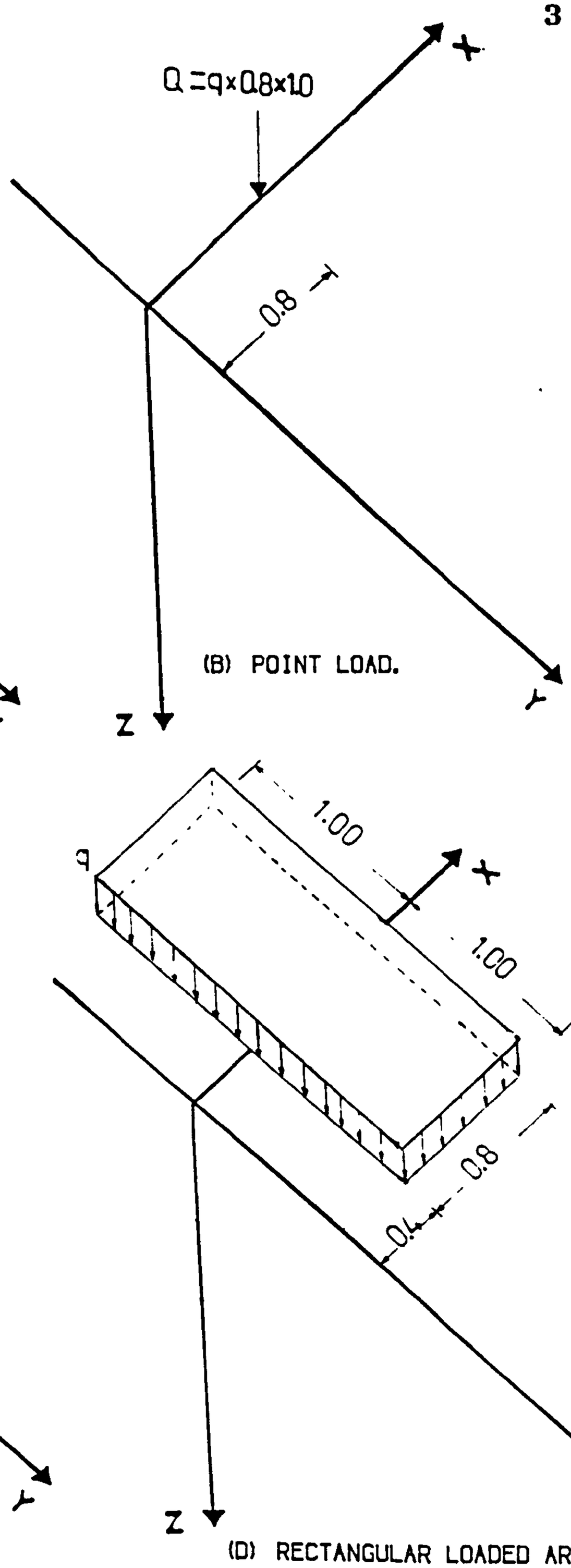

(B) POINT LOAD.

(C) LONG LINE LOAD.

(D) RECTANGULAR LOADED AREA.

FIG. (6.37) DATA USED FOR CLASSICAL THEORIES AND AUTHOR'S MODELS.

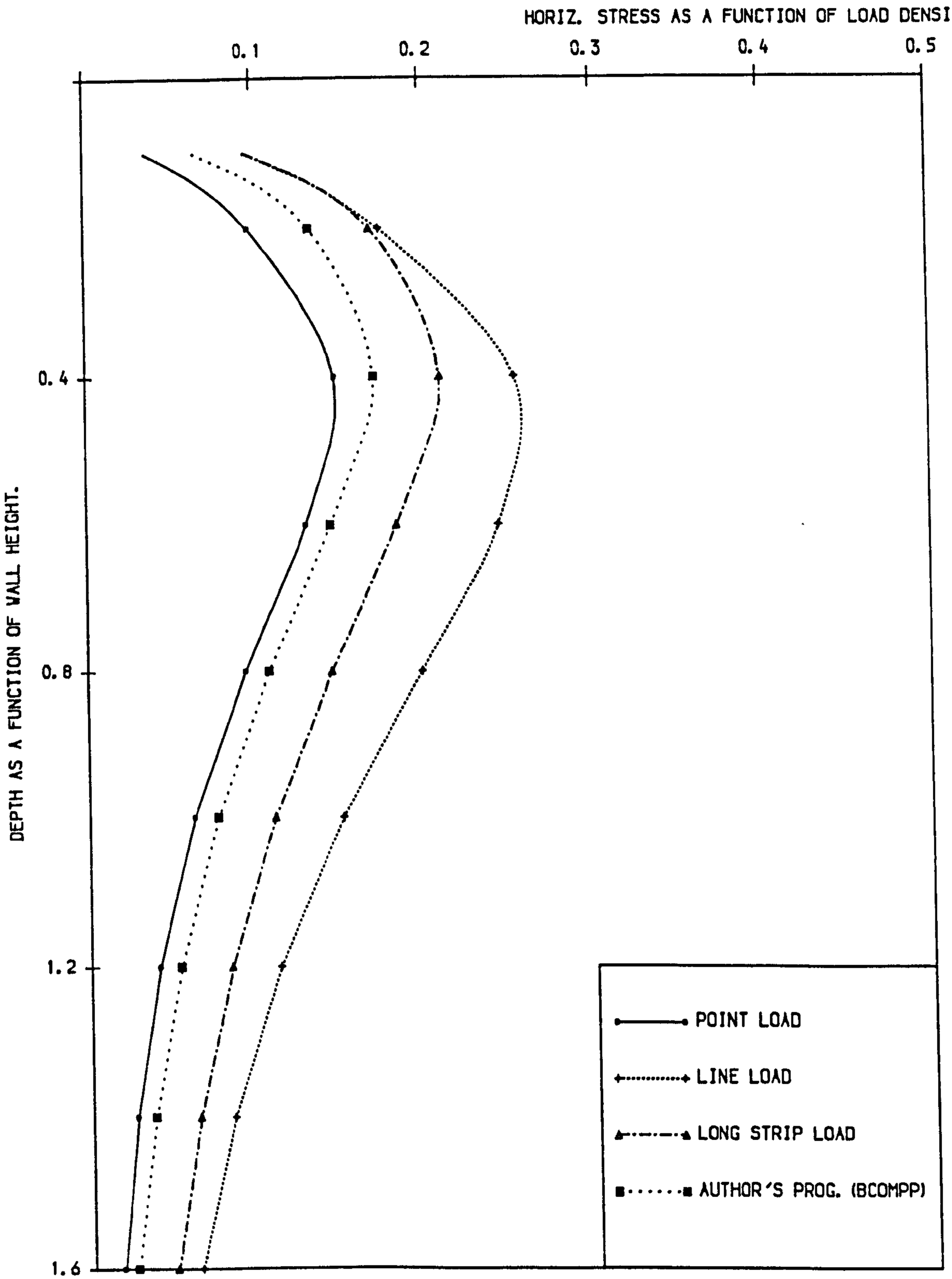

FIG. (6.38) COMPARISON BETWEEN HORIZ. STRESSES CALCULATED FROM AUTHOR'S PROG. (BCOMPP) &CLASSICAL SOLUTIONS.

results from the proposed models using the same laboratory data for different lengths of compaction (200, 400 & 600 mm). The comparisons are shown in Fig. (6.39 to 41). Good agreement is obtained especially when the compaction lengths are 200 mm and 600mm.

6.6.4 Comparison With Other Research's Laboratory Work

Sheriff and Mackey (1977) carried out tests in a model tank of inside dimensions (1200x1200x470 mm) made of steel plates and angles as shown in Fig. (6.42) one side of the tank being the model of a retaining wall. Horizontal stresses on the wall due to a cyclic line load of intensity 1.37 KN/ṁ, had been measured using eight small pressure cells, Fig. (6.42).

A comparison between the measured stresses and those calculated by the author's models using the same data are shown in Fig. (6.43.A&B). A better agreement is found at lower elevations than at upper elevations. This is probably due to the simulation of line load in their tests being not exactly the line load simulated in the model.

6.6.5 Comparison With Field Tests

There is only limited useful field data regarding horizontal stresses due to compaction. This may be because:

(a) It is difficult to obtain accurate and reliable measurements of horizontal or lateral earth pressure.

(b) Most of the results coming from concentrated loads involve previously compacted fills.

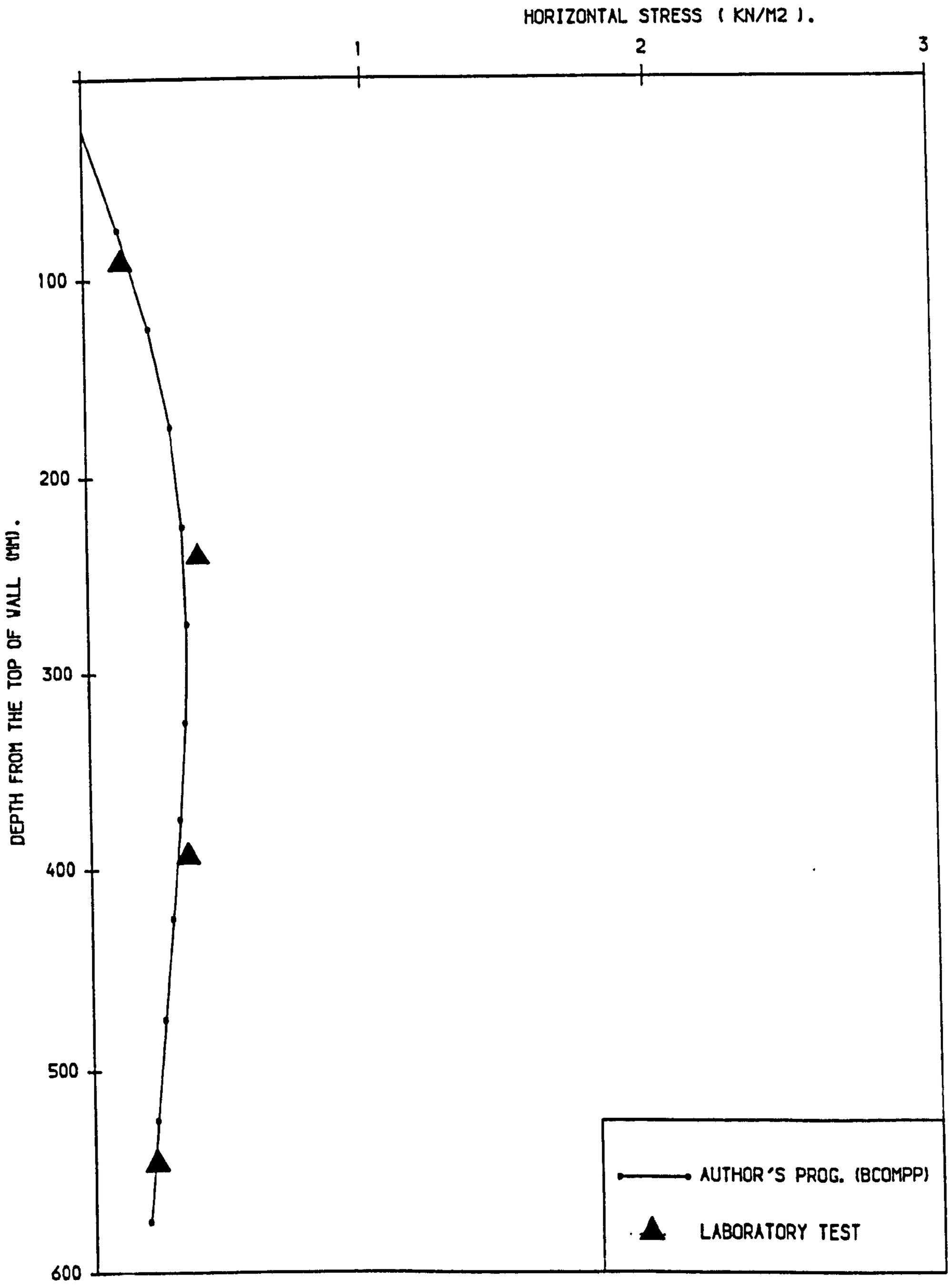

FIG (6. 39) COMPARISON OF HORIZ. STRESSES MEASURED FROM LAB. TEST& AUTHOR'S PROG. (BCOMPP) &COMP. LENG. =200. 0MM.

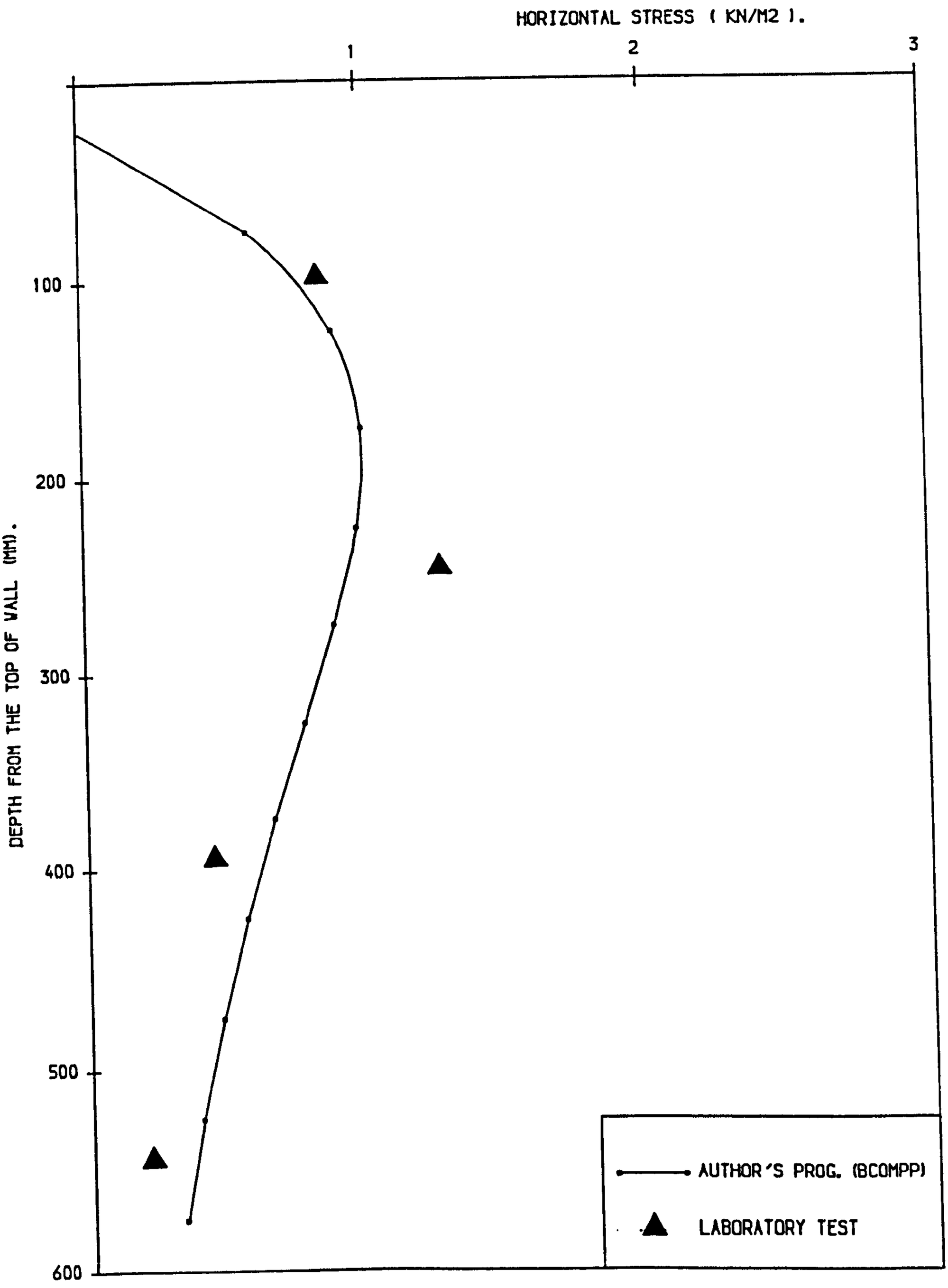

FIG. (6.40) COMPARISON OF HORIZ. STRESSES MEASURED FROM LAB. TEST &AUTHOR'S PROG. (BCOMPP) &COMP. LENG. =400.0MM.

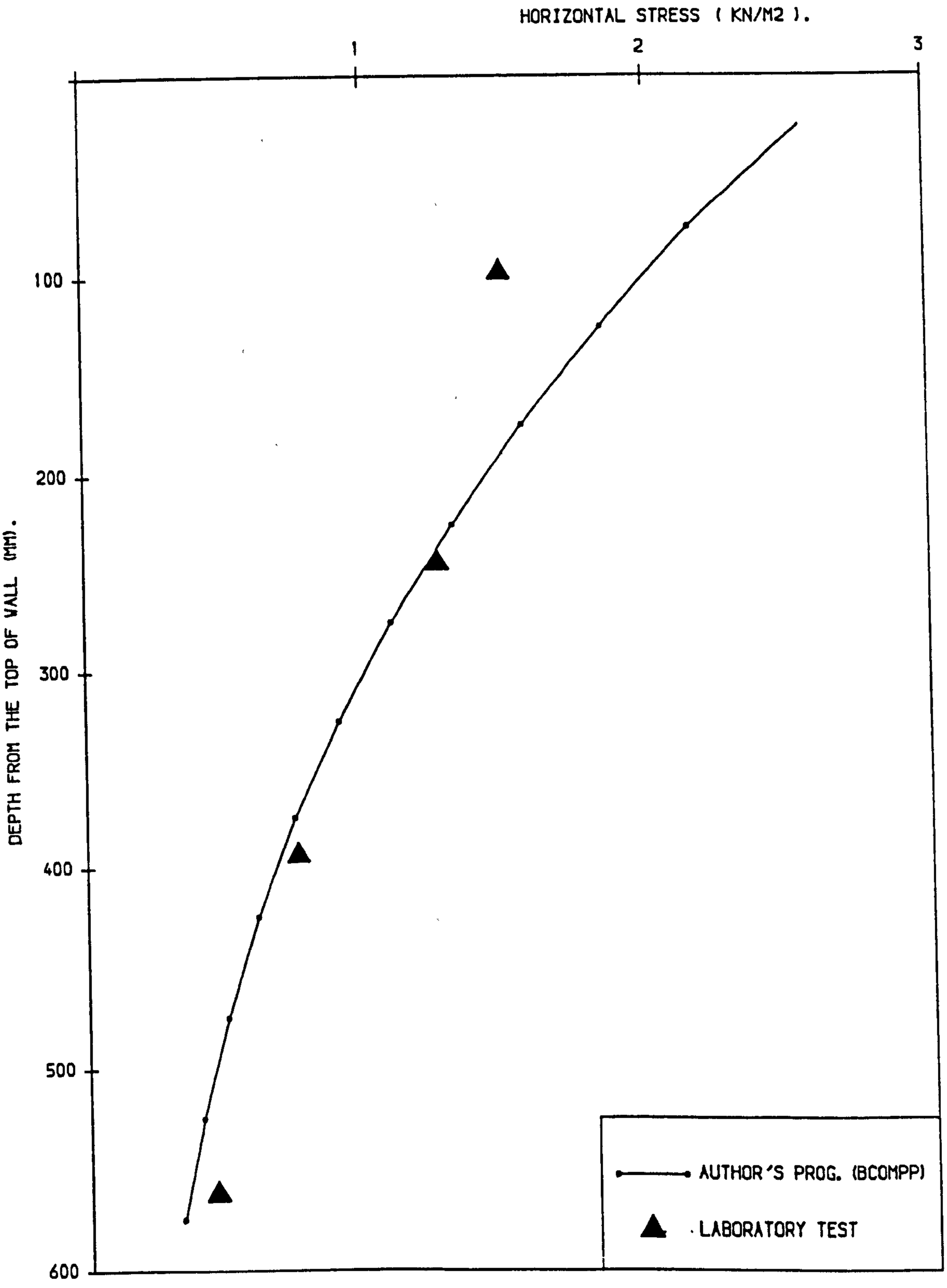

FIG. (6. 41) COMPARISON OF HORIZ. STRESSES MEASURED FROM LAB. TEST &AUTHOR'S PROG. (BCOMPP) &COMP. LENG. =600. 0MM.

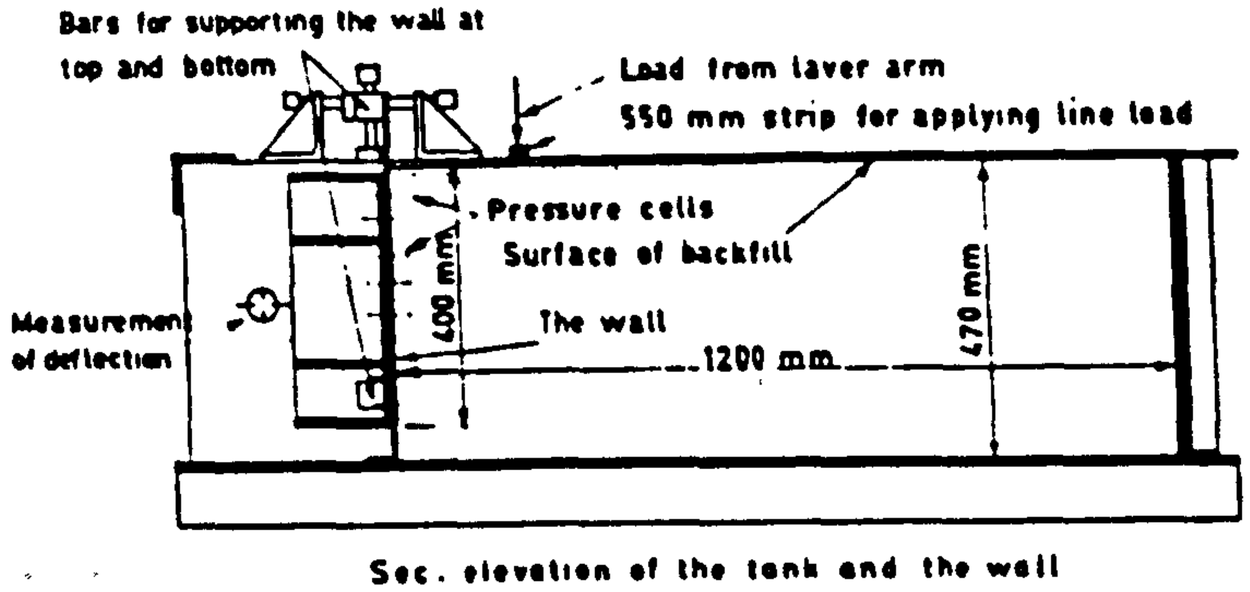

Sec. elevation of the tank and the wall

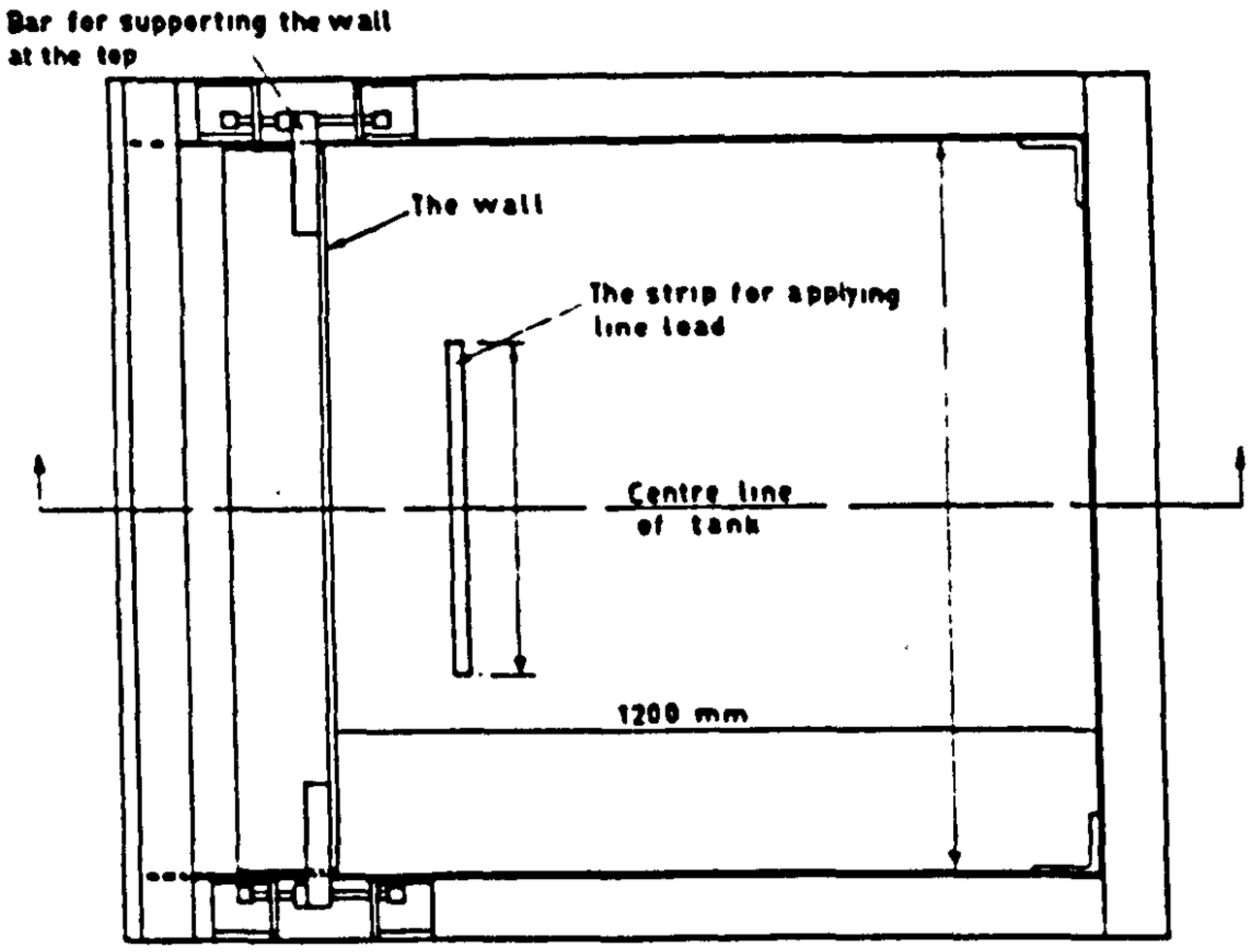

Plan of the tank

FIG. (6.42) DETAILS OF WALL MODEL AND LINE LOAD (AFTER SHERIF AND MACKEY, 1976).

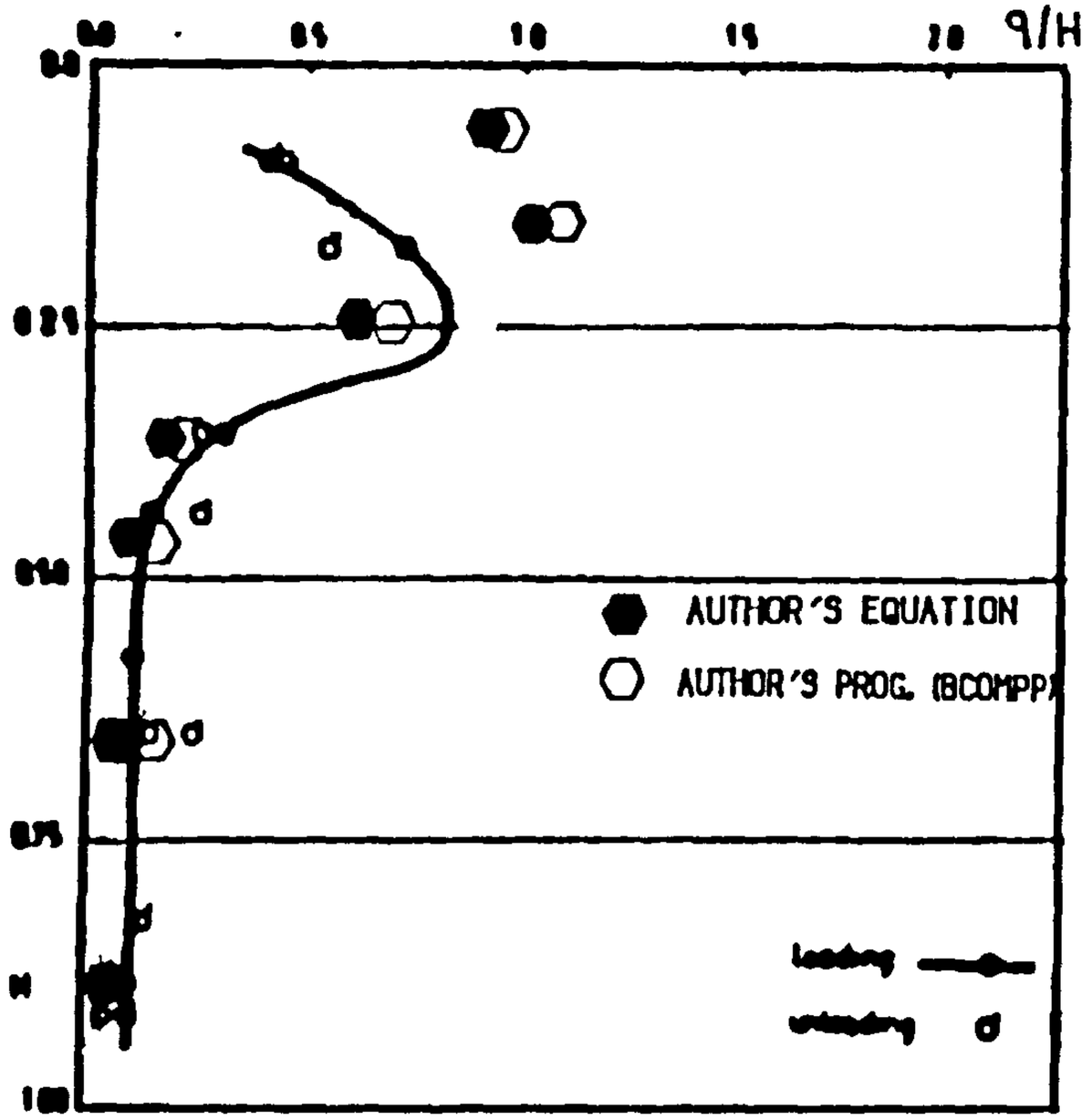

(A) LINE LOAD AT 0.188H FROM WALL.

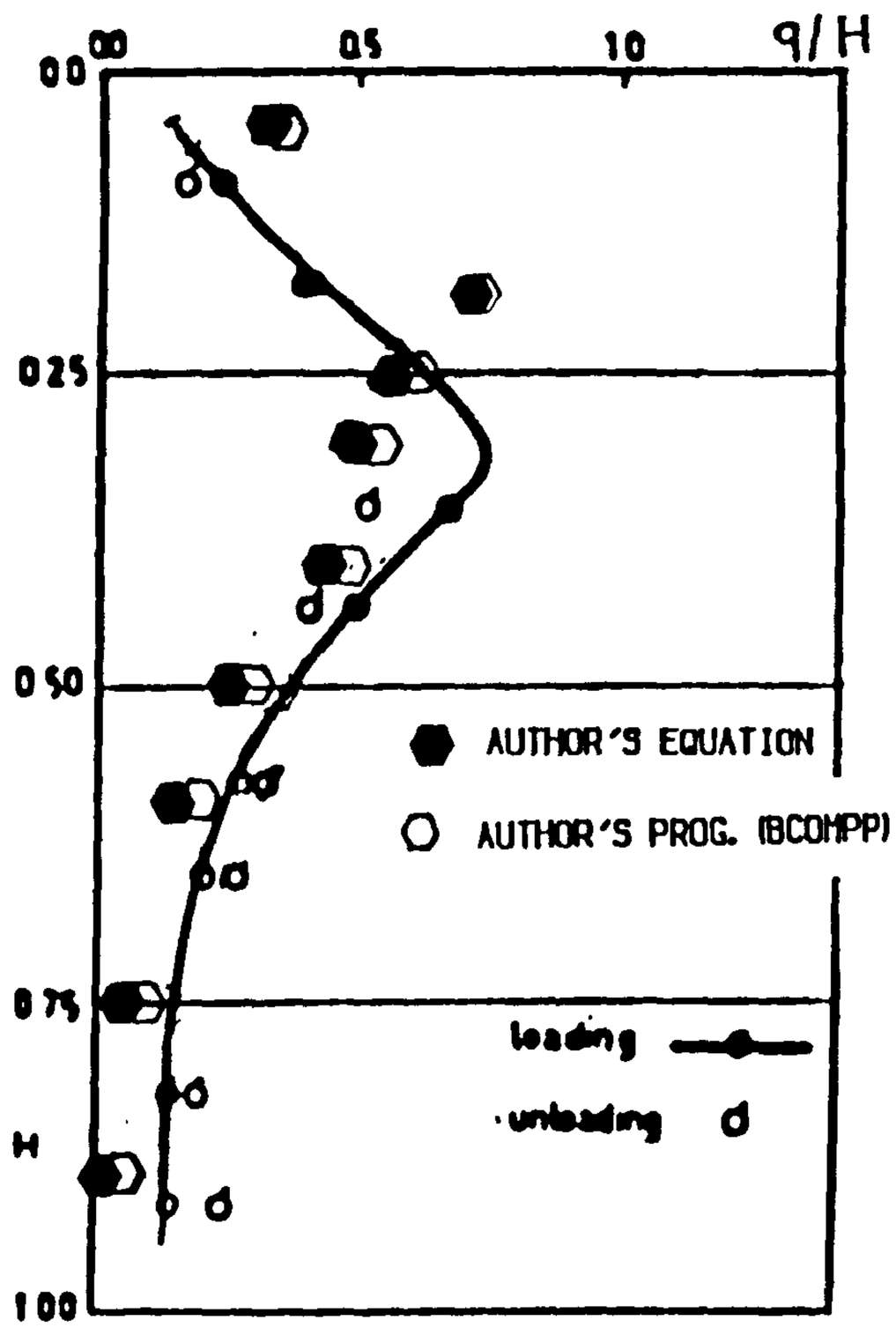

(B) LINE LOAD AT 0.313H FROM WALL.

FIG. (6.43) COMPARISON BETWEEN MEASURED HORIZONTAL STRESSES BY (SHERIF &MACKEY, 1976) AND CALCULATED BY THE AUTHOR'S MODELLS.

The first comparison has been made with a field test wall carried out by Spangler (1938), The recommendation in the Code of Practice No. 2 (1951) is based upon his work, and the code is for lateral pressure produced by superimposed load, Sims & Jones (1974).

Details of the wall and loads are shown in Figs. (6.44.A&B). A loosely dumped gravel backfill was placed behind the wall. Comparison between measured and calculated horizontal stresses due to concentrated and line loads are shown in Fig. (6.45 to 47) and good agreement can be seen. It should be noted that measurements from Gerber (1929) are also plotted in the Figures.

The second case was performed by Rehnman and Broms (1972). It included measurements of horizontal stresses acting against a vertical wall due to point loads as shown in Fig. (6.48.A). Two types of backfill of height 2.0 m behind the wall were used, a loosely dumped gravelly sand and a silty fine sand. The measurements were taken at three sections by means of twelve pressure cells as shown in Fig. (6.48.A). Two concentrated loads were developed from a 15t loader (Michigan 175 A).

When using the author's models to calculate horizontal stresses on the wall the concentrated loads have been changed to line loads of length assumed as the tyre width of the loader used in the tests and this is near reality, as shown in Fig. (6.48.B).

Comparisons between measured and calculated horizontal stresses in the case of loosely dumped gravelly sand are shown in Figs. (6.49 & 50). There is good agreement between measured and calculated stresses at sections 1 & 2 but at section 3 no good agreement is obtained.

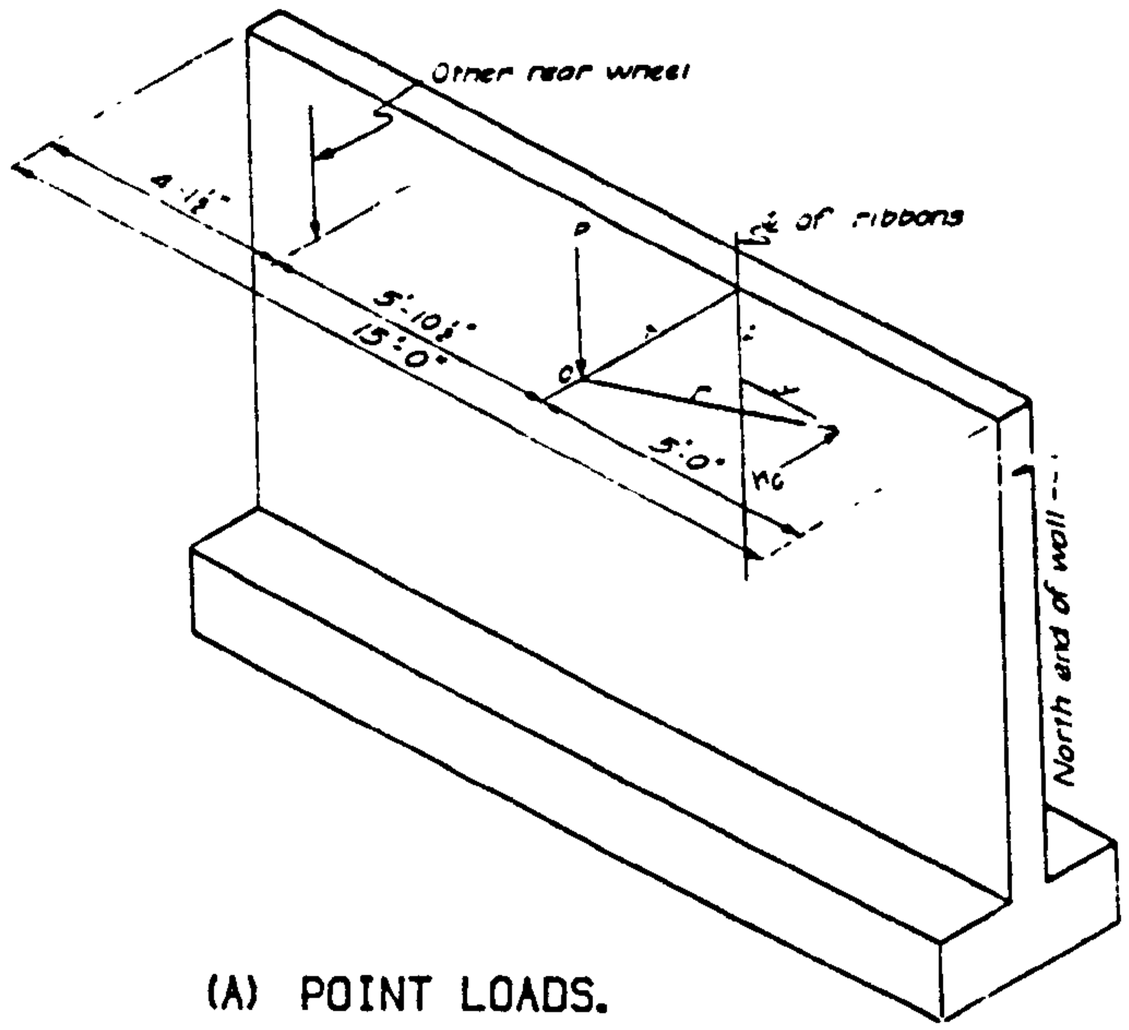

(A) POINT LOADS.

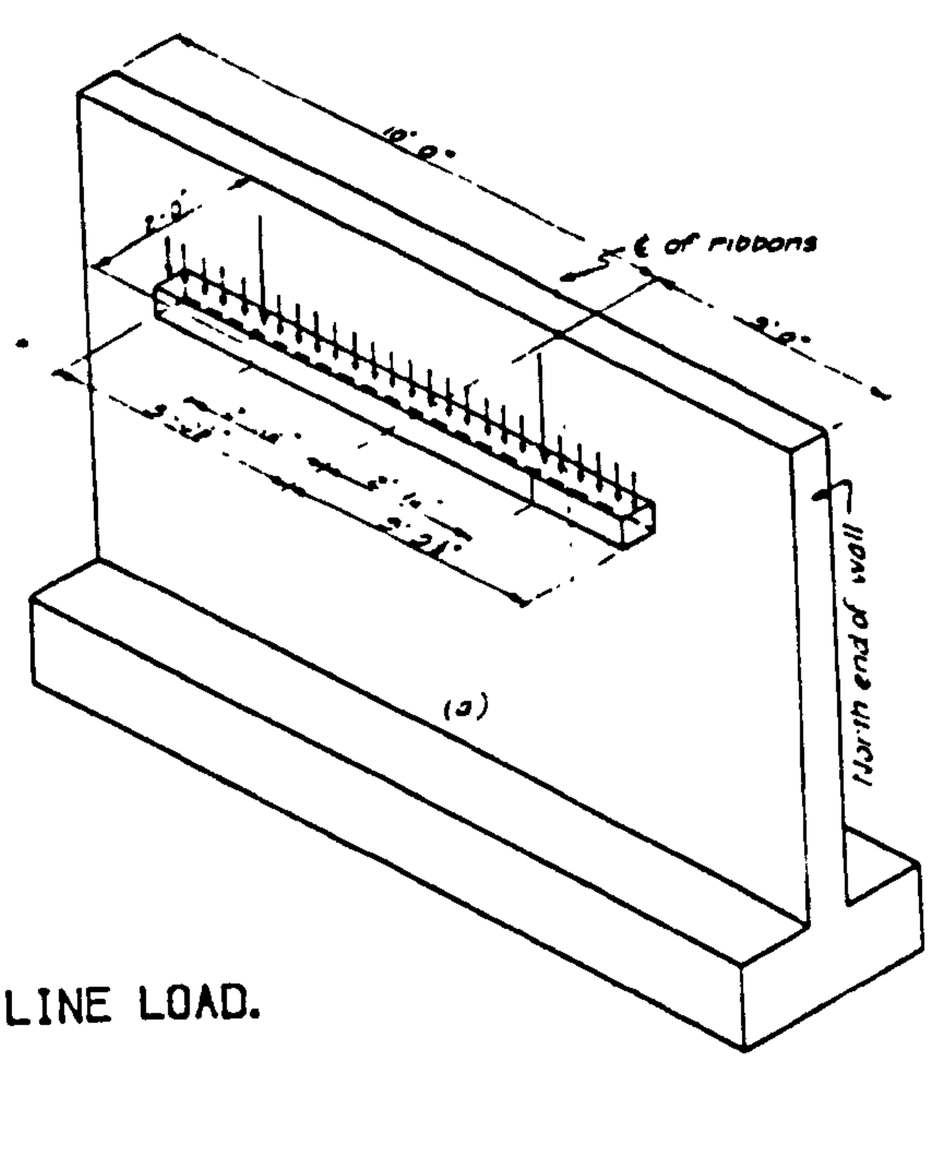

(B) LINE LOAD.

FIG. (6.44) DETAILS OF FIELD TEST WALL (SPANGLER, 1936&1938).

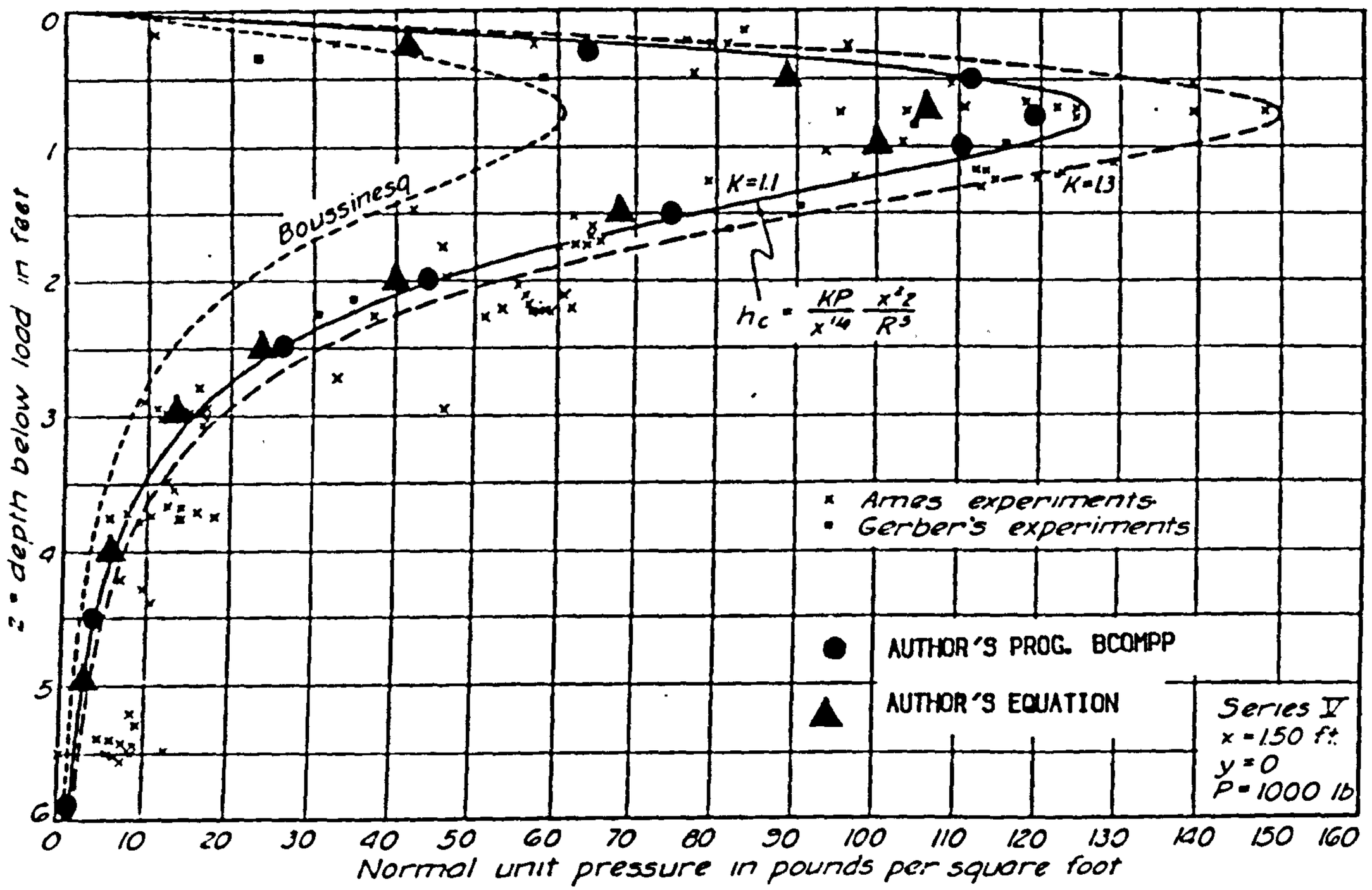

FIG. (6.45) COMPARISON BETWEEN MEASURED HORIZONTAL STRESSES DUE TO POINT LOAD BY SPANGLER, (1938) AND CALCULATED BY THE AUTHOR'S MODELS.

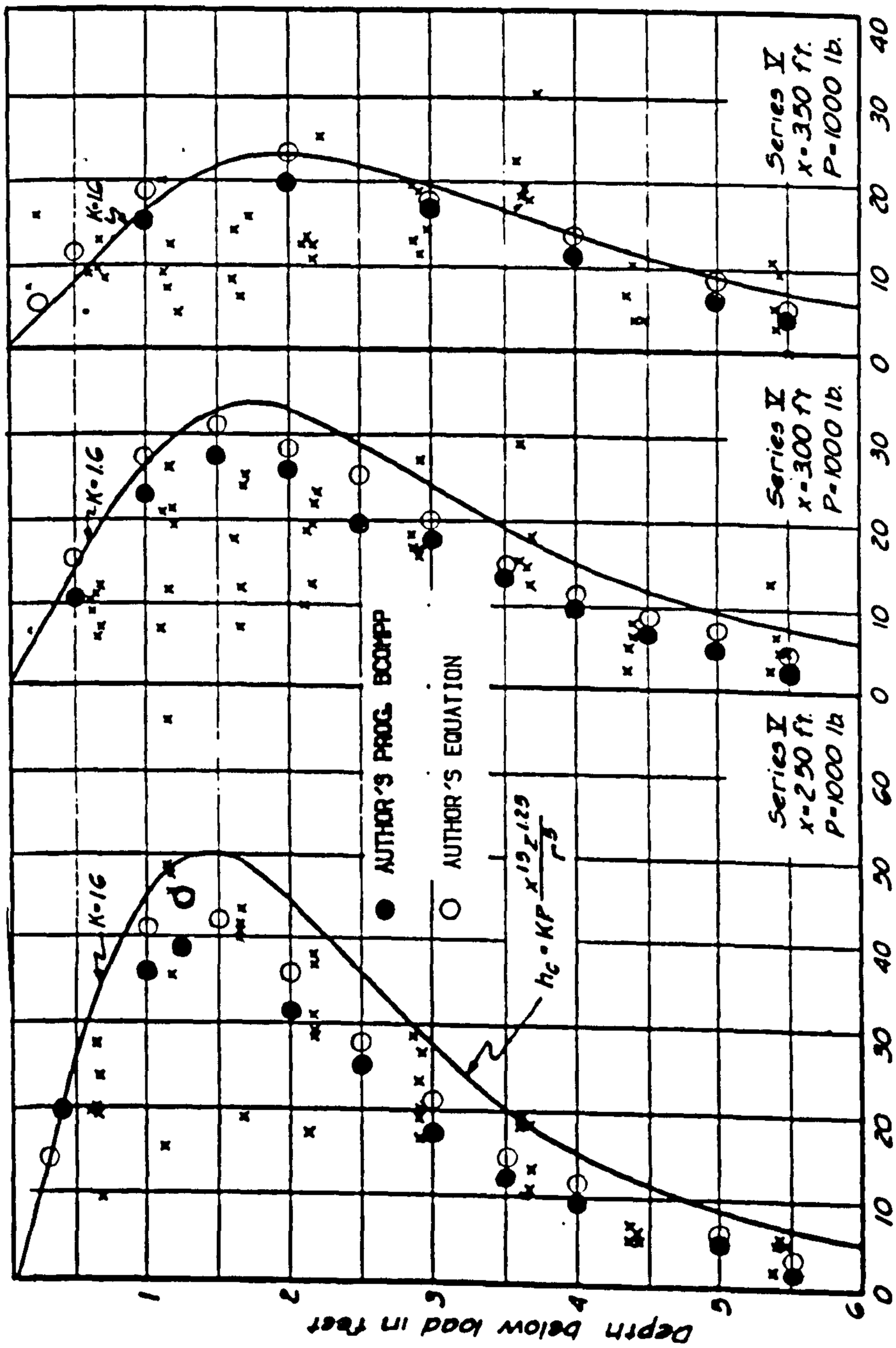

FIG. 16. 46) COMPARISON BETWEEN HORIZONTAL STRESSES DUE TO POINT LOAD MEASURED BY SPANGLER, (1938) AND CALCULATED BY THE AUTHOR'S MODELS.

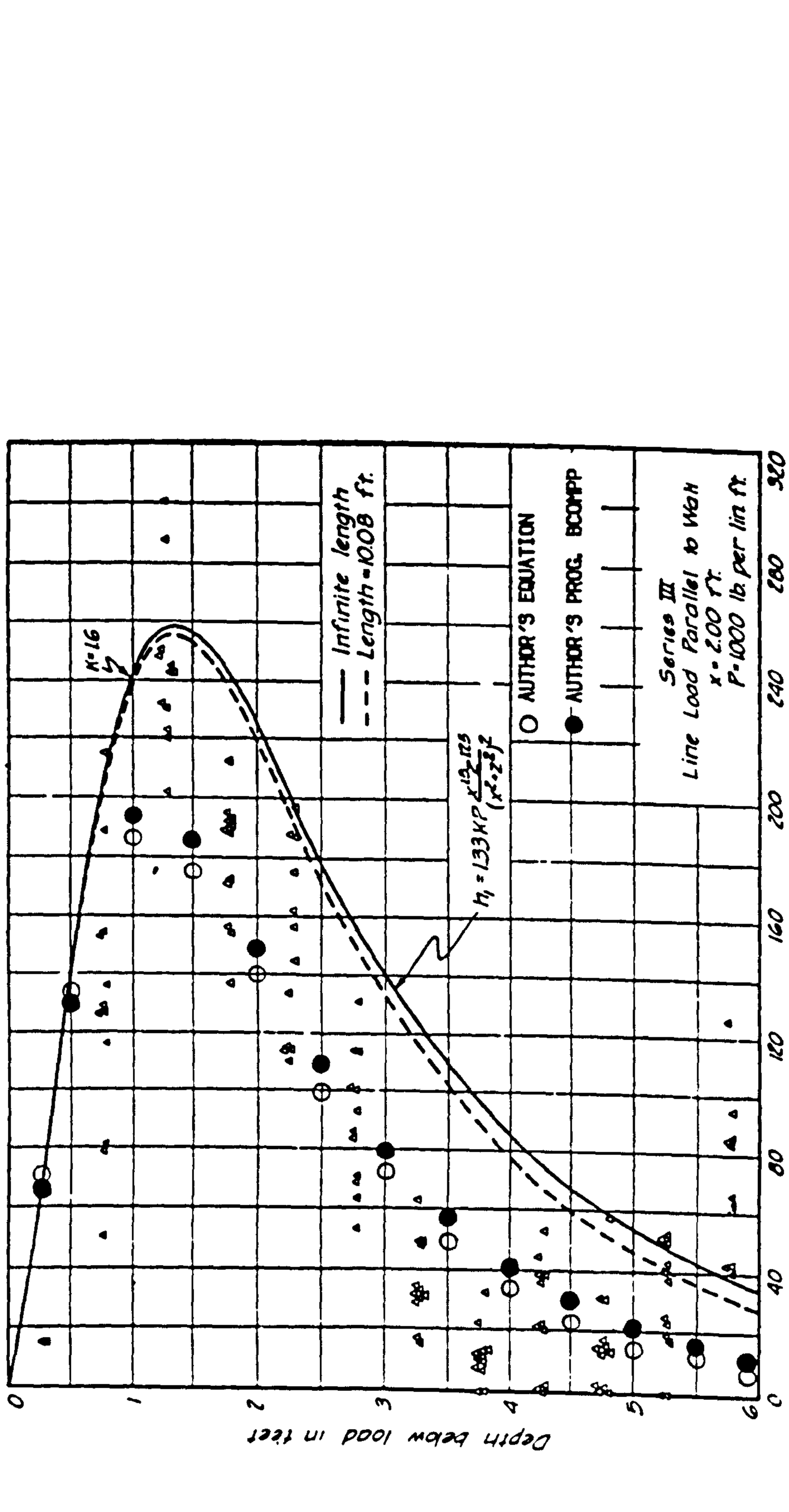

FIG. (6.47) COMPARISON BETWEEN HORIZONTAL STRESSES DUE TO LINE LOAD MEASURED BY SPANGLER, (1938) AND CALCULATED BY THE AUTHOR'S MODEL.

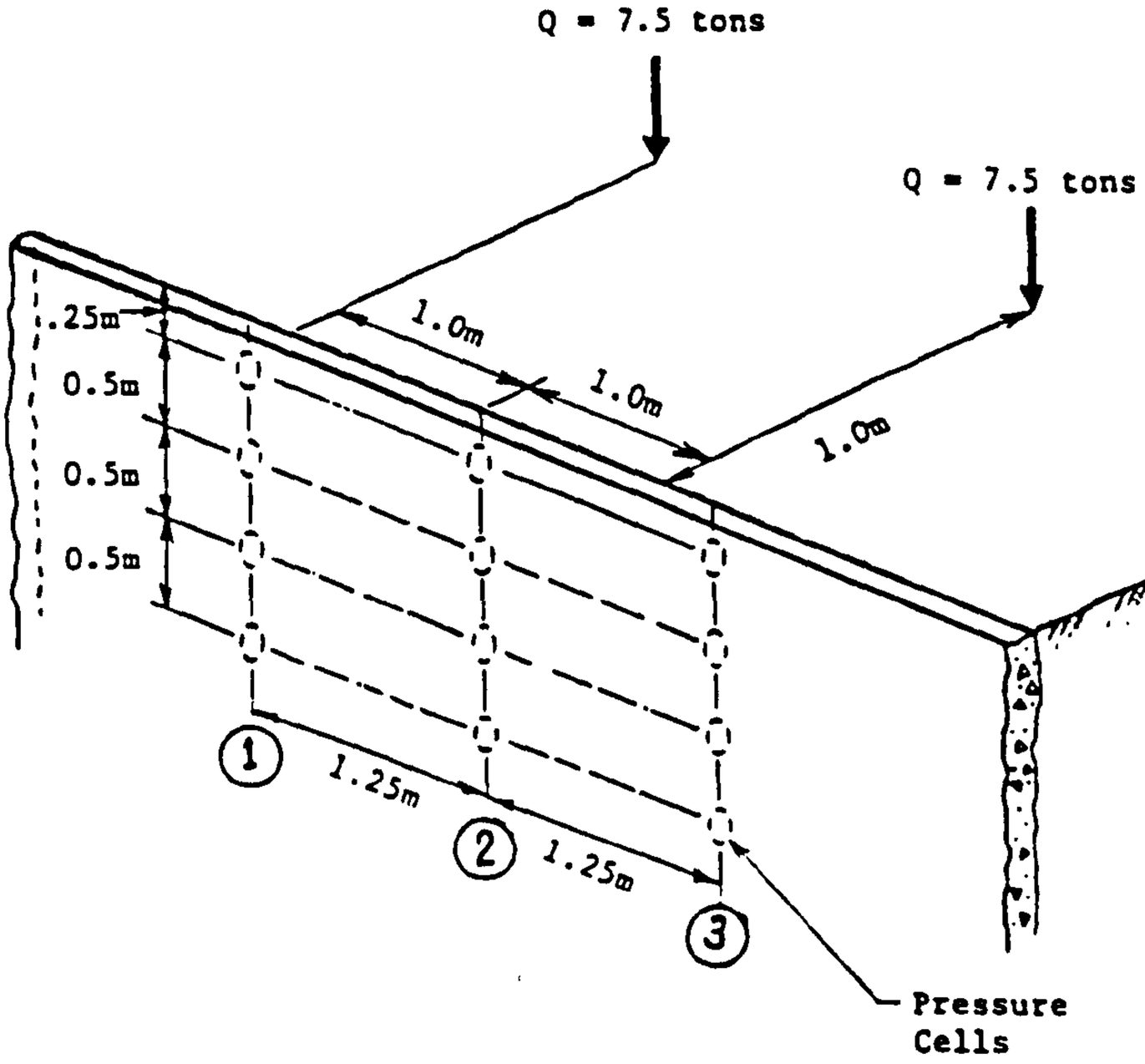

(A) POINT LOADS (AFTER REHNMAN&BROMS 1972).

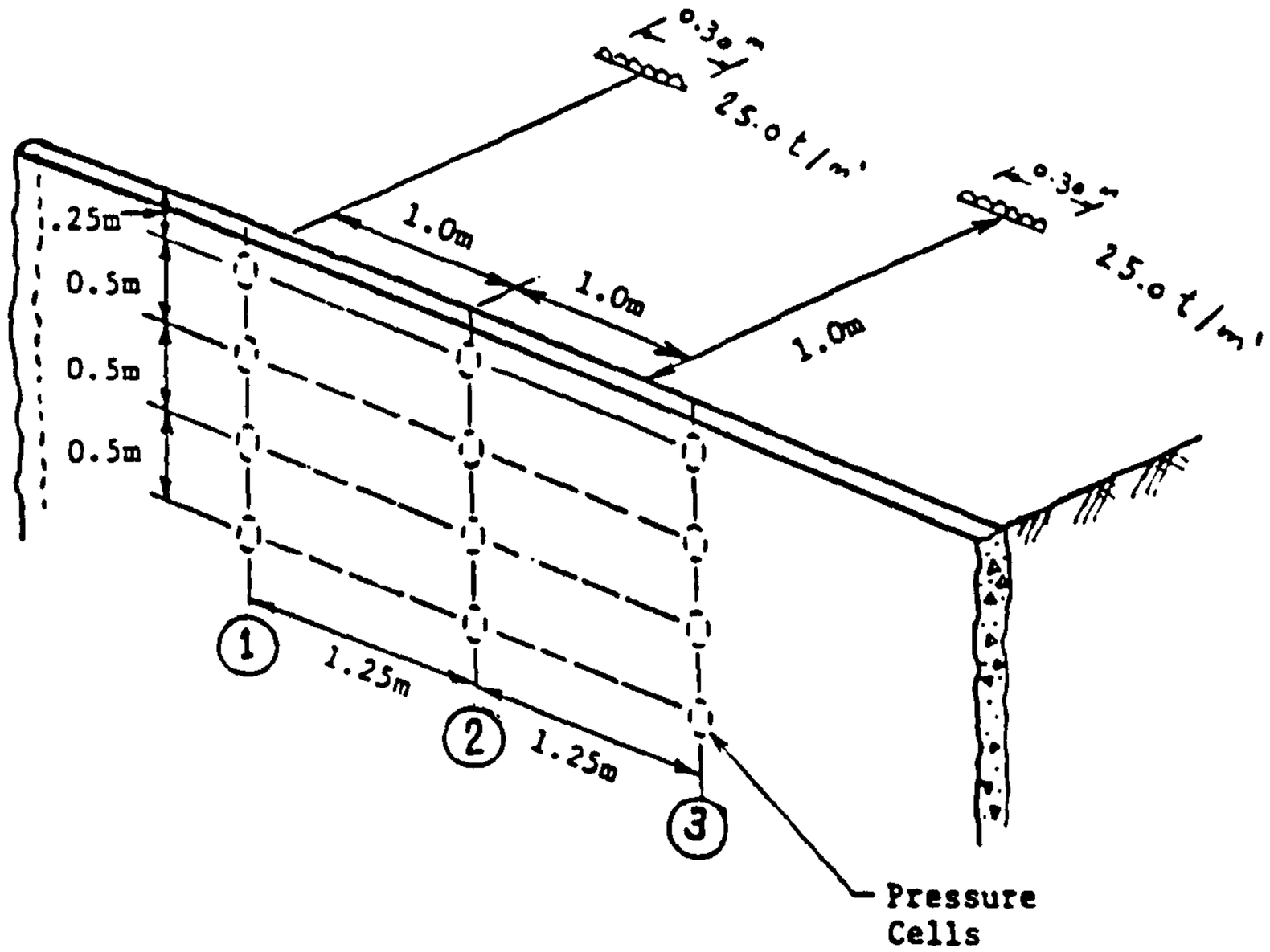

(B) LINE LOADS BY THE AUTHOR.

FIG. (6.48) REHNMAN AND BROMS TEST WALL (1972).

6.6.6 Comparison With Finite Element Analysis

Plane strain finite element analyses were performed by TRRL (1976) in order to explain the results of a series of large field tests as reported by Carder et al. (1977). These analyses were used to calculate the maximum horizontal stress distribution resulting from the operation of a 1.3 Mg twin vibratory roller at various distances from a stiff but deformed wall of height 2.0 m and using sand backfill.

A comparison between the horizontal stresses resulting from the TRRL analyses and the author's models is illustrated in Fig. (6.51). The two methods yielded good agreement at shallow depth and significantly different results at greater depths, which reflects the difficulty in modelling a 3 dimensional problem in 2 dimensions (plane strain). It should be noted that in the TRRL analyses a correction factor was applied to take into account the spreading of stress with depth.

6.7 CONCLUSION

An important factor which affects the development of a compaction model to estimate horizontal stresses in a free field and on a vertical wall is modelling of the compaction plant. There is a lack of information dealing with this due to the difficulty in simulating the problem and taking into account its three dimensional nature.

The three proposed models of compaction plant overcome this deficiency and cover any type of plant. The problem is considered as a three dimensional problem, i.e. the real dimensions, weight, and dynamic effect are considered.

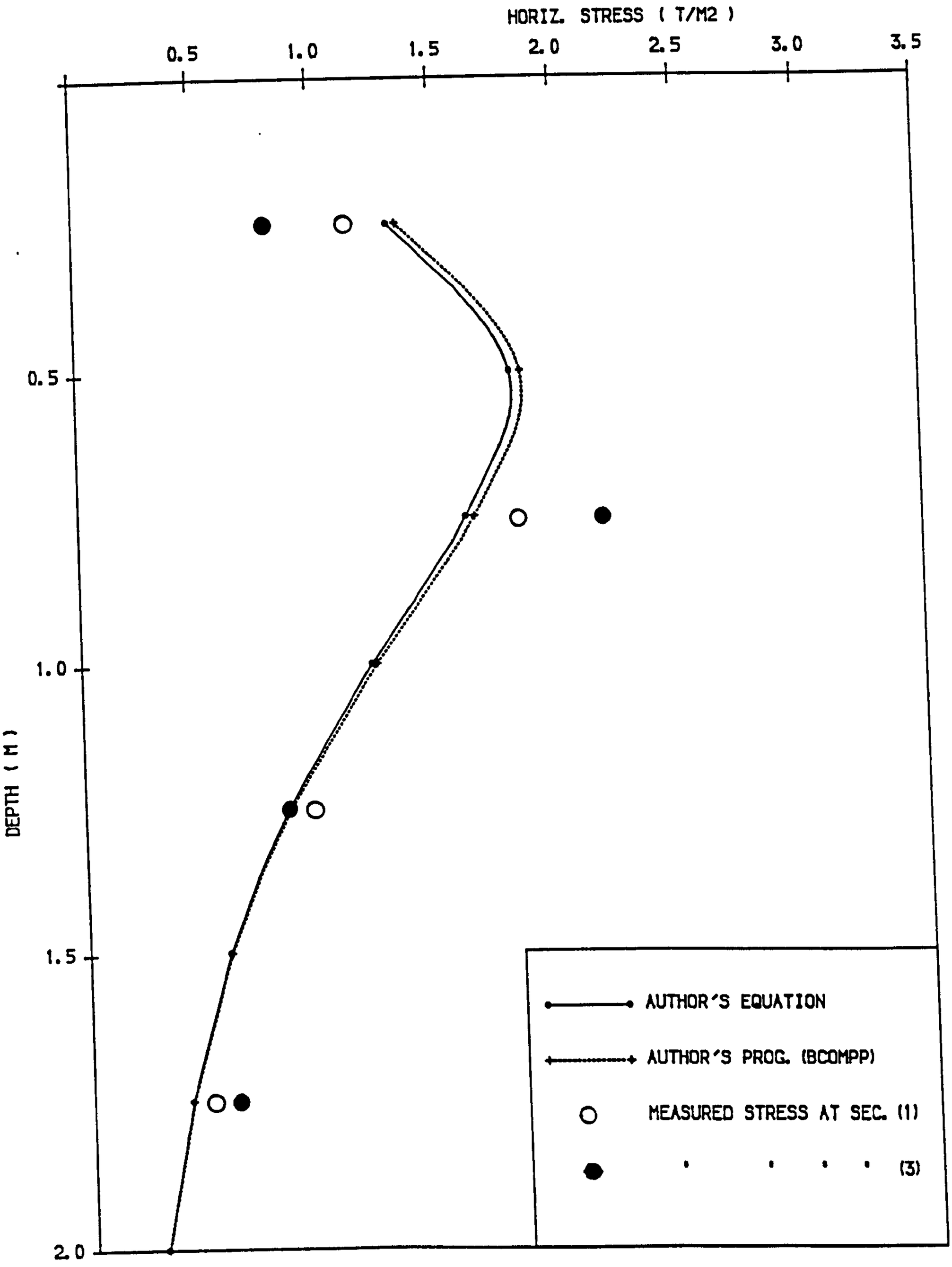

FIG. (6.49) COMPARISON BETWEEN MEASURED HORIZONTAL STRESSES BY REHNMAN &BROMS,(1972) AND CALCULATED BY THE AUTHOR'S MODELS.

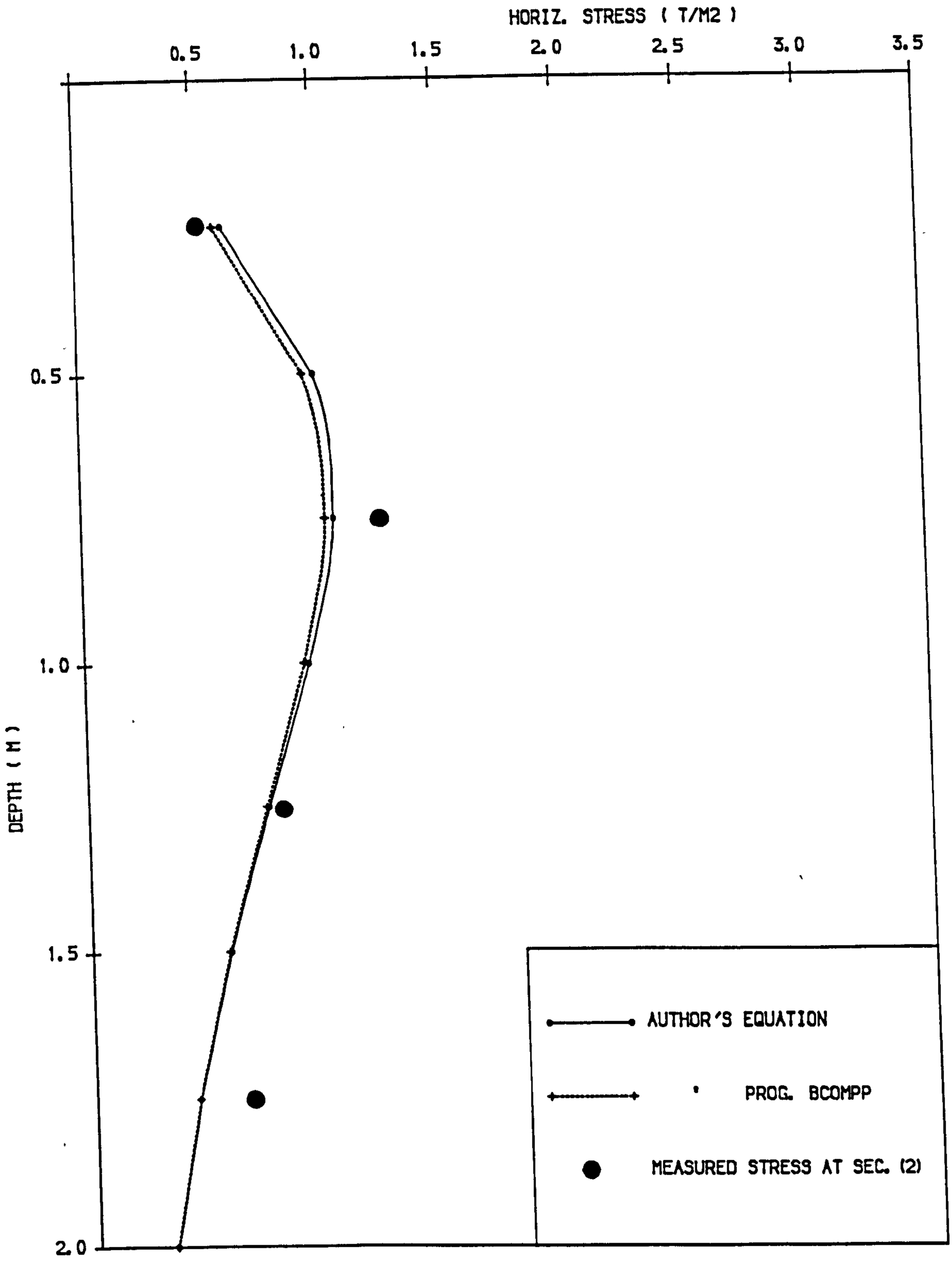

FIG. (6.50) COMPARISON BETWEEN MEASURED HORIZONTAL STRESSES BY (REHNMAN &BROMS, (1972) AND CALCULATED BY THE AUTHOR'S MODELS.

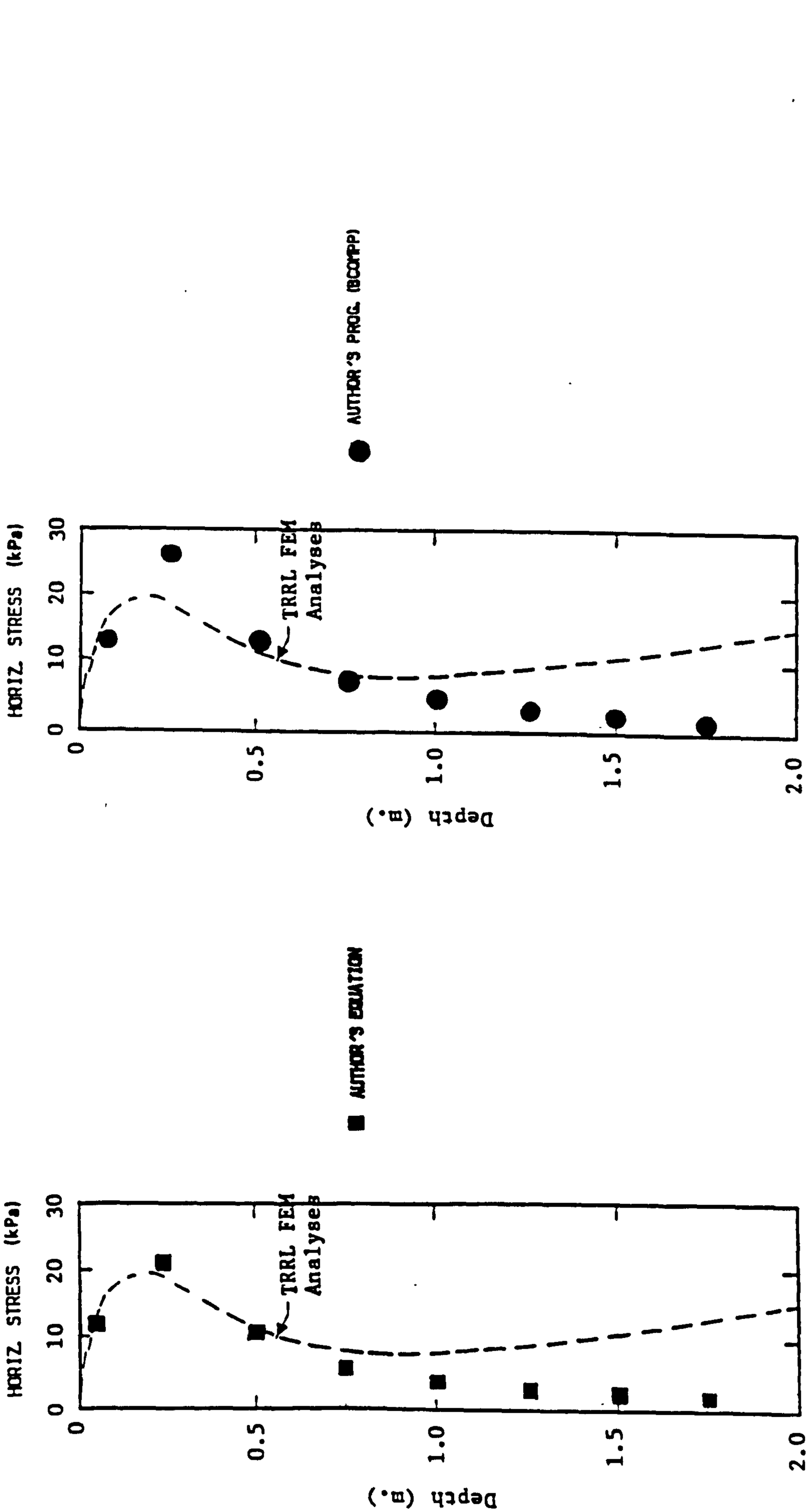

FIG. (6.51) COMPARISON BETWEEN HORIZONTAL STRESSES FROM PLANE STRAIN FINITE ELEMENT ANALYSES BY TRRL (1976) AND CALCULATED BY THE AUTHOR'S MODELS

The fourth proposed model is the computer program (BCOMPP). It overcomes this lack and is very convenient to use with a finite element simulation of a reinforced earth retaining wall and compaction. Comparisons with laboratory and field studies prove the usefulness of these models.

CHAPTER (7)

IDEALIZATION OF REINFORCED EARTH RETAINING WALLS USING THE FINITE ELEMENT METHOD

7.1 INTRODUCTION

The finite element method has a very wide range of application in various fields and this chapter sets out a brief history, basic mathematical relations and procedures employed in the method. It demonstrates the use of the finite element method in soil mechanics problems, emphasizing the reinforced earth retaining wall and explains the main concepts and how to tackle the problem. The different ways of modelling the compaction effects in the finite element method are discussed.

7.1.1 A Brief History Of The Finite Element Method

The finite element method is a numerical analysis technique established as an engineering tool of wide applicability. Its fields of application include not only structural engineering but also fluid flow, geotechnics, electricity and magnetism . It is now employed for design purposes in many branches of technology which require great accuracy and speed in the analysis.

Hinton and Owen (1977) pointed out that one of the principal advantages of the finite element method is the unifying approach it offers to the solution of

diverse engineering problem. Huebner and Thornton (1982) reported that the method was originally developed to study the stresses in complex air–frame structures and the label " Finite Element Method " first appeared in 1960, when it was used by Clough (1960) in a paper on plane elasticity problems. Since the late 1960's, researchers have done extensive work with the finite element method. By 1972 the finite element method had become the most active field of interest in the numerical solution of continuum problems and its range of application had been extended.

The range of application can be divided into three categories depending on the nature of the problem to be solved. These categories are:

(a) Equilibrium problems or time–independent problems. In these problems there is a need to find displacement or stresses and sometimes pressure, velocity and temperature distribution as in the area of solid and fluid mechanics.

(b) Eigen– value problems of solid and fluid mechanics. These are steady–state problems whose solution often requires the determination of the natural frequencies and modes of vibration of solids and fluids, as in the problem of interaction of lakes and dams.

(c) Time–dependent or propagation problems of continuum mechanics. These problems are the result of adding the time dimension to the problems of the first two categories.

The development of the method had beea summarized in a survey paper by (Oden, 1972). The method nowadays can deal with two and three dimensional, linear or nonlinear problems. A lot of work has still to be done and many

extensions of the finite element method will continue to appear.

7.1.2 Basic Operations Of The Finite Element Method:

The basic steps of the finite element method [Hinton and Owen (1977); Zienkiewicz (1977); Naylor and Pande (1981); Huebner and Thornton (1982); and Green et al. (1986)] can be summarized as:

(a) The continuum is discretised into a number of finite elements interconnected at a finite number of nodal points and the displacements at the nodes are taken as the basic unknowns of the problem. This involves defining the elements, nodes, boundary conditions, loading conditions and the material properties. Eight basic element types are illustrated in Fig. (7.1). An example of meshes which have been produced by discretising are shown in Fig. (7.2).

(b) The stiffness matrix [K^e] and other characteristics of each element are developed with respect to a convenient local coordinate system. [K^e] is calculated using a convenient method such as: unit– displacement, solution of differential equations or Castigliano theorem (I) (principal of minimum total potential energy).

(c) Development of transformation matrix (Jacobian matrix) to transform the stiffness matrix [K^e] from a local coordinate system to a generalized (global) coordinate system.

(d) The overall (global) stiffness matrix [K] is assembled from the stiffness of each element. This process satisfies the compatibility and equilibrium conditions of the problem and corresponds to summing the energy contributions

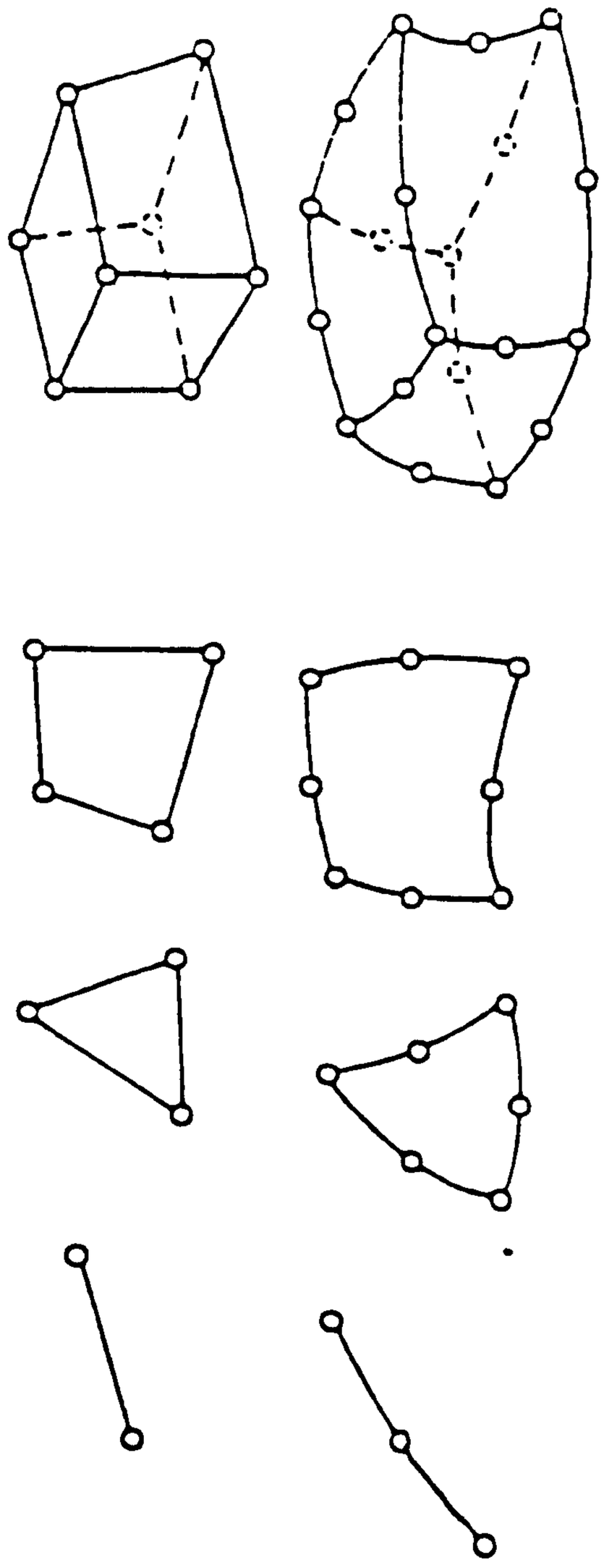

FIG. (7.1) SOME BASIC FINITE ELEMENTS.

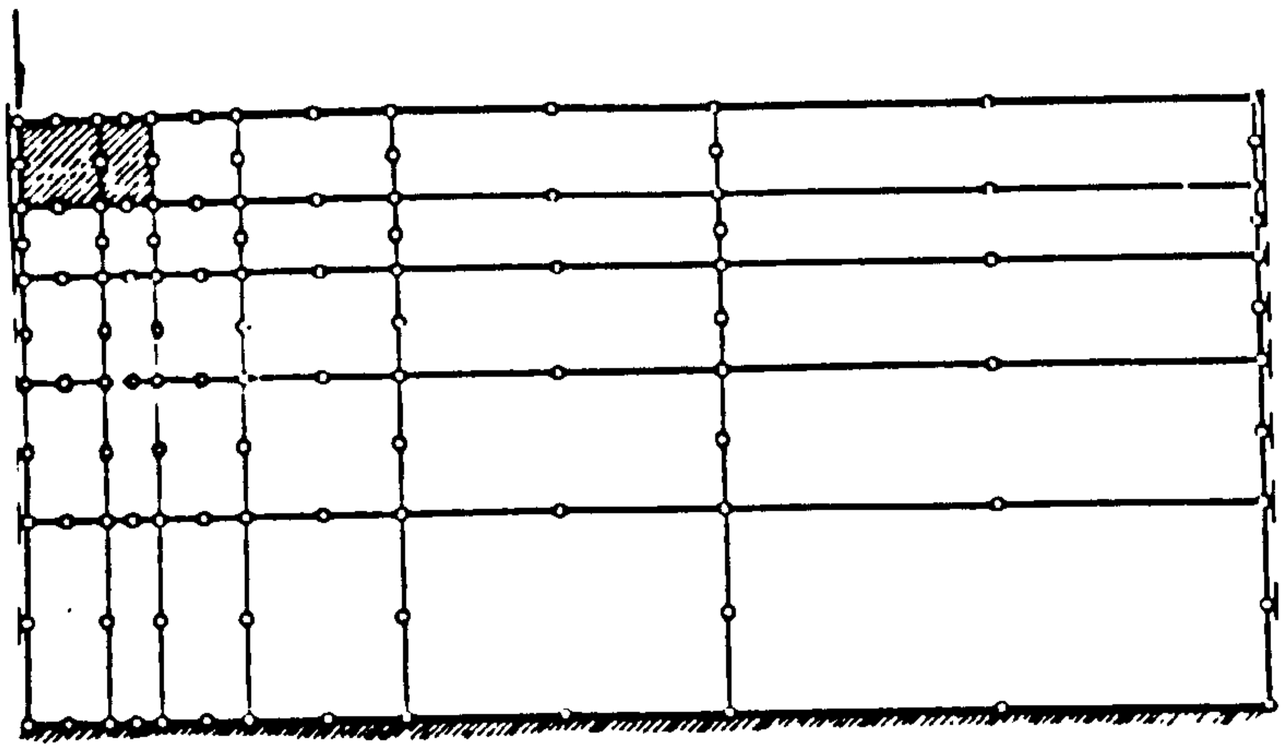

(A) FOOTING

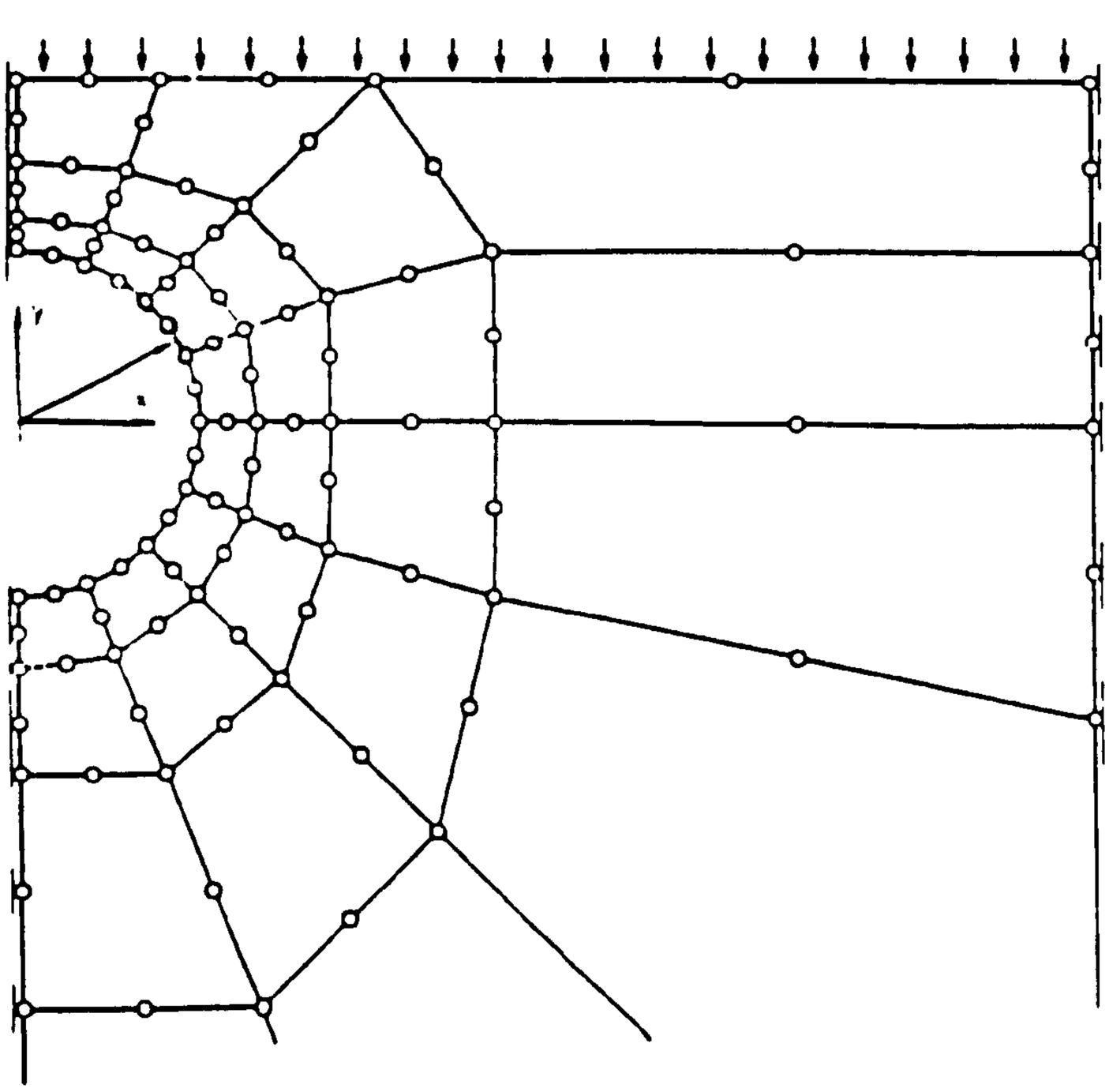

(B) MODEL TUNNEL

FIG. (7.2) EXAMPLES OF FINITE ELEMENT MESHES.

from each element to form the total potential energy of the continuum.

(e) Load vectors are also assembled from the consistent equivalent nodal force vectors of each element.

(f) The above two steps, together form the set of simultaneous equations which govern the problem. These equations are modified to incorporate the prescribed boundary conditions.

(g) A convenient method has been employed to solve the simultaneous equations. The most common procedures are usually based on Gaussian elimination and take into account the symmetry and banded properties of the global stiffness matrix [K].

(h) Transform the displacements matrix to local coordinates (i.e. the nodal displacements are then used with the appropriate element matrices to determine strains, stresses and any other secondary quantities).

7.1.3 Finite Element Method In Soil Mechanics Problems:

Girijavallabham and Reese (1968), showed that most soil mechanics problems are concerned with stresses and deformations in the soil due to boundary and body forces and problems can be tackled as axisymmetric or as plane strain problems.

(a) Elements:

The starting point of an analysis is the division of the soil mass into elements interconnected at a finite number of nodal points. The properties of

the elements are adjusted so that the assemblage of elements behaves in the same manner as the original continuum. In plane strain problems the element is represented by cartesian coordinates and in axi–symmetric cases by cylindrical coordinates as shown in Fig. (7.3 A,B,C&D) respectively.

(b) Determination of element stiffness matrix:

According to the principal of minimum total potential energy [Hinton and Owen. (1977); Zienkiewicz (1977); Naylor and Pande(1981); Huebner and Thornton (1982); and Green et al. (1986)] the total energy is defined as the sum of two different energies as follows:

$$\Pi = U + W \tag{7.1}$$

Where:

U is strain energy of the continuum (i.e. internal energy).

W is external energy due to external load.

For conservative force systems, the external energy is lost during loading and therefore (W) is a negative quantity.

$$U = \frac{1}{2} \int_{V} [\sigma]^{T} \epsilon \, dv \tag{7.2}$$

$$W = -\int_{V} [\delta]^{T} p \, dv + \int_{S} [\delta]^{T} q \, ds + \sum_{i=1}^{n} [\delta]^{T} r_i \tag{7.3}$$

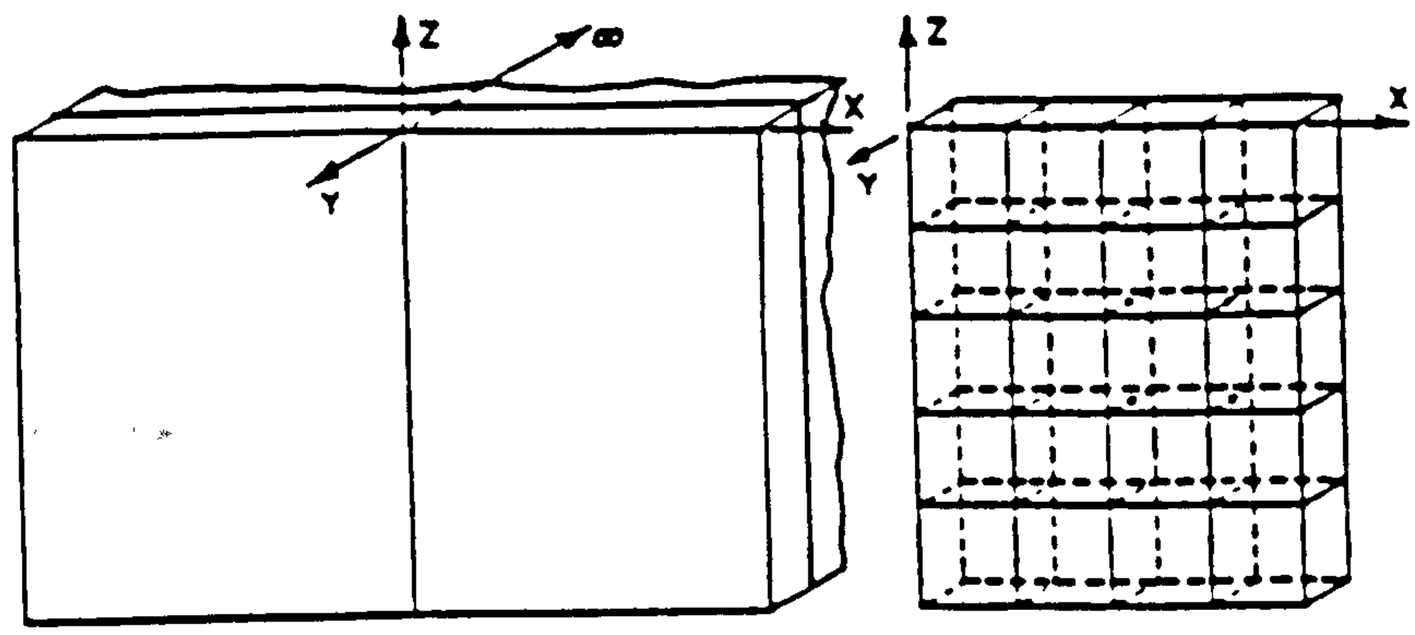

CONTINUUM

ASSEMBLAGE OF DISCRETE PLATE ELEMENTS

(A) PLANE STRAIN PROBLEM (IN X, Y, Z CARTESIAN COORDINATES).

x, y, z • LOCAL CYLINDRICAL COORDINATES

$u_{i,j}$ • DISPLACEMENT IN X DIRECTION AT NODAL POINT (i, j)

$w_{i,j}$ • DISPLACEMENT IN Z DIRECTION AT NODAL POINT (i, j)

a, b, b • DIMENSIONS OF THE ELEMENT IN X, Y, Z DIRECTIONS

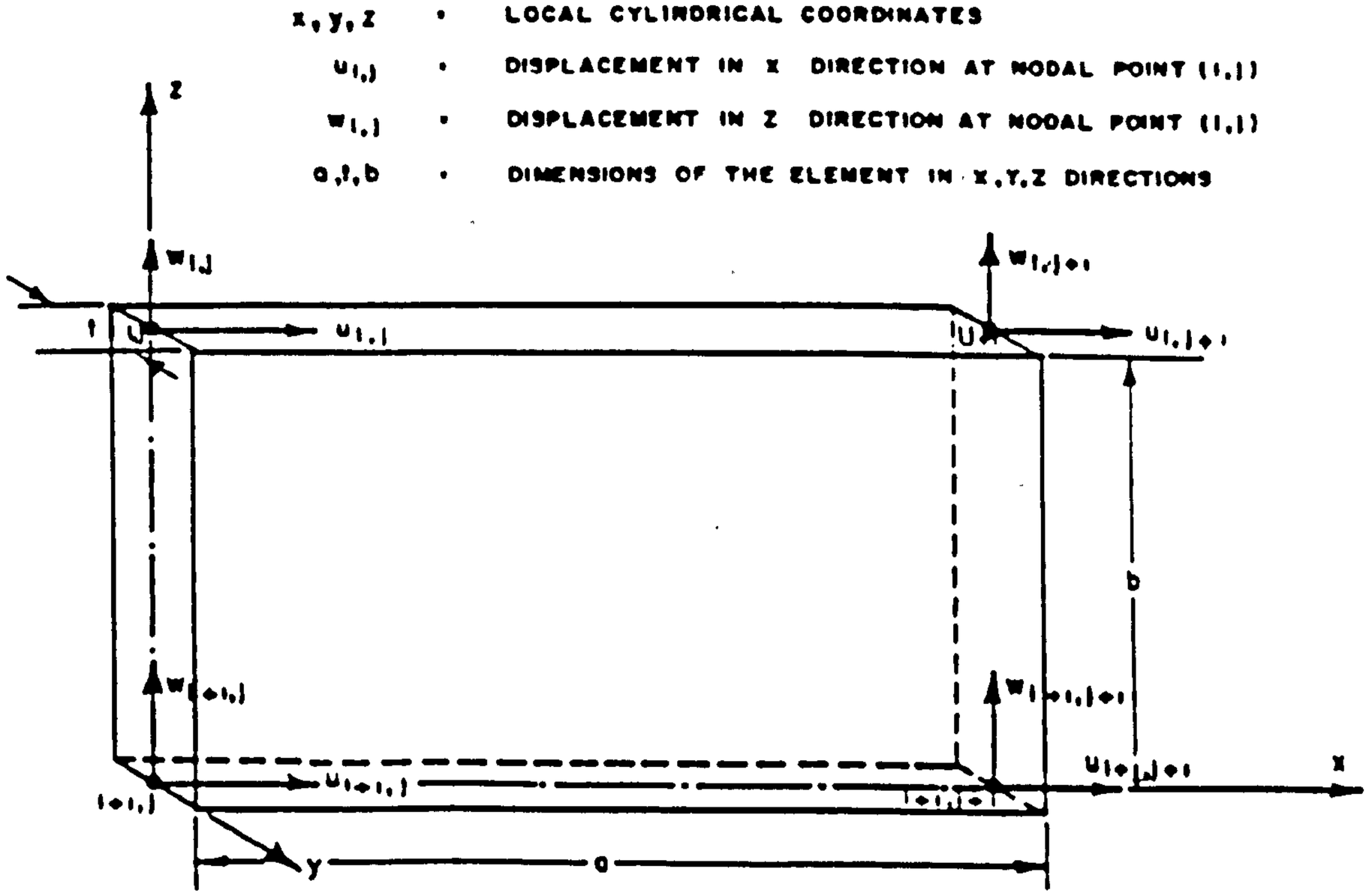

(B) A DISCRETE ELEMENT IN PLANE STRAIN.

FIG. (7.3) FINITE ELEMENT REPRESENTATION IN SOIL PROBLEMS (AFTER GIRIJAVALLABHAM AND REESE, 1968).

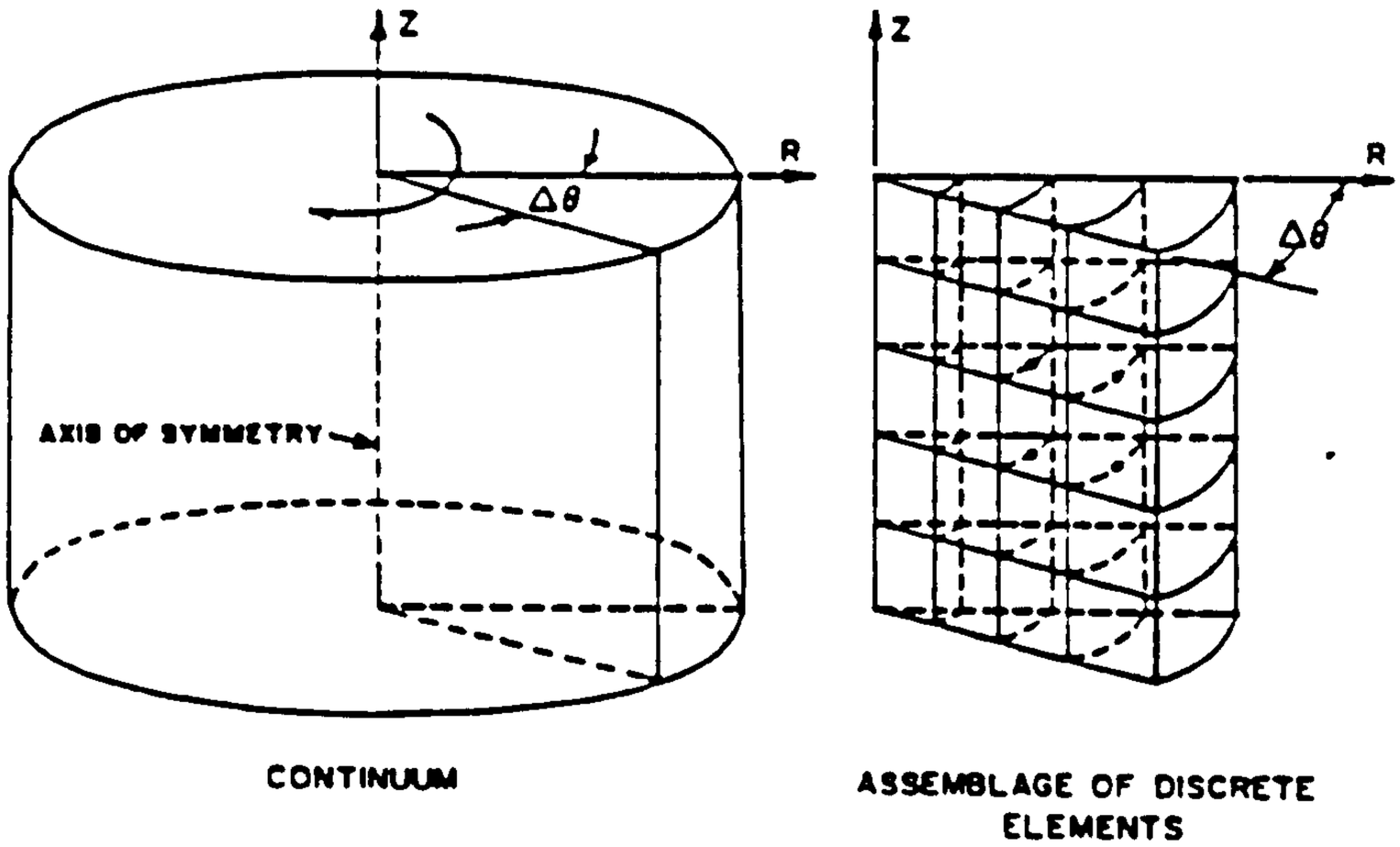

CONTINUUM

ASSEMBLAGE OF DISCRETE ELEMENTS

(C) AXISYMMETRIC PROBLEM (IN R, Z, O CYLINDRICAL COORDINATES) .

b • HEIGHT OF THE ELEMENT

r, z, θ • LOCAL CYLINDRICAL COORDINATES

u_{ij} • NODAL DISPLACEMENT IN r DIRECTION AT NODAL POINT (i, j)

w_{ij} • NODAL DISPLACEMENT IN Z DIRECTION AT NODAL POINT (i, j)

a_i, a_{i+1} • COORDINATES OF THE NODAL POINTS IN r DIRECTION

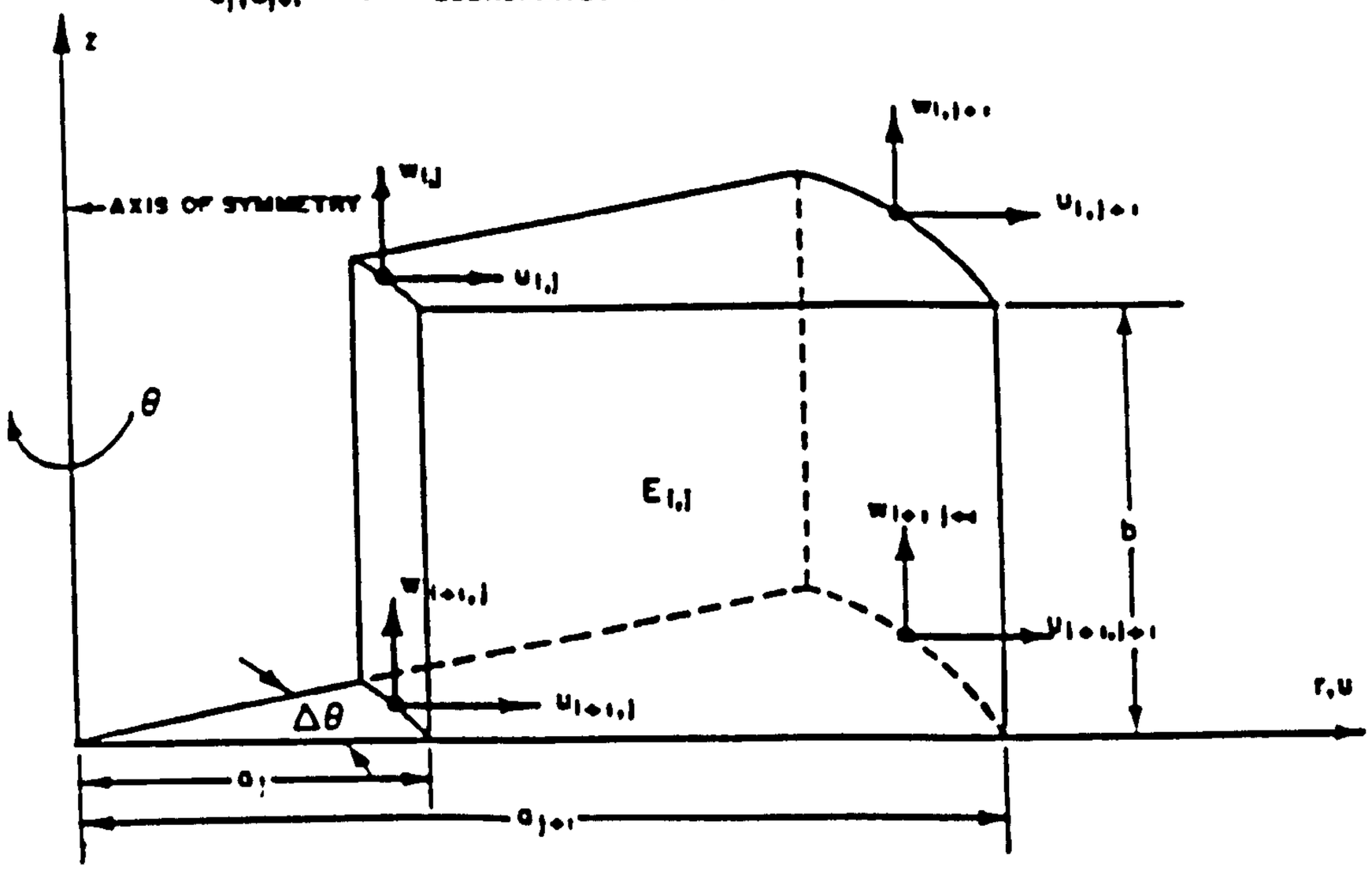

(D) A DISCRETE ELEMENT IN AXISYMMETRY.

FIG. (7.3) CONT.

where:

σ and δ are the stress and strain vectors respectively.

p is body forces per unit volume.

q is the applied surface forces per unit area.

r_i is up to n applied concentrated load.

δ is the displacement of any body.

v is the volume change of the continuum.

s is the load surface area.

In the finite element displacement method, the displacements have unknown values only at the nodal points so that the variation within any element is described in terms of the nodal values by means of an interpolation function.

$$\delta = N\ \delta^e \qquad (7.4)$$

where N is the set of interpolation functions, termed the shape functions, and δ^e is the vector of nodal displacements of the element. The element shape functions are chosen to fulfill two conditions to prevent singularities in the functions (i.e. no internal element energies are created):

(i) continuity condition, to guarantee continuity of the function between and within elements.

(ii)constant strain criteria, to be able to produce a constant value of strain throughout the element.

The strain within the element can be expressed in terms of the element

nodal displacement as:

$$\epsilon = B\ \delta^{e} \tag{7.5}$$

Where B is the strain matrix generally composed of derivatives of the shape functions. Finally the stresses may be related to the strains by use of an elasticity matrix D as follows:

$$\sigma = D\ \epsilon \tag{7.6}$$

From equations (7.1 to 6)

The total potential energy of the element (e) is:

$$II^{e} = \frac{1}{2}\int_{V_e} \left[\ \delta^{e}\ \right]^{T} \left[\ B\ \right]^{T} D\ B\ \delta^{e}\ dv - \int_{Ve} \left[\ \delta^{e}\ \right]^{T} \left[\ N\ \right]^{T} p\ dv$$

$$- \int_{Se} \left[\ \delta^{e}\ \right]^{T} \left[\ N\ \right]^{T} q\ ds - \sum_{i=1}^{n} \left[\ \delta^{e}\ \right]^{T} r_i \tag{7.7}$$

Where:

$[\ ]^{T}$ is the transpose of any matrix.

V_e is the element volume.

S_e is the element surface area.

Performance of the minimisation for the element (e) with respect to the nodal displacements δ^e for the element:

$$\frac{\partial I I^e}{\partial \delta^e} = \int_{V_e} [\ B\ ]^T\ D\ B\ \delta^e\ dv - \int_{Ve} [\ N\ ]^T\ p\ dv$$

$$- \int_{Se} [\ N\ ]^T q\ ds - \sum_{i=1}^{n} r_i = 0 \qquad (7.8)$$

i.e.

$$K^e\ \delta^e = F^e \qquad (7.9)$$

Where:

i.e. F^e is the equivalent nodal force for the element

$$F^e = \int_{V_e} [\ N\ ]^T\ p\ dv + \int_{Se} [\ N\ ]^T\ q\ ds + \sum_{i=1}^{n} r_i \qquad (7.10)$$

K^e is the element stiffness matrix.

i.e.

$$K^e = \int_{V_e} [\ B\ ]^T\ D\ B\ dv \qquad (7.11)$$

(c) Determination of overall stiffness matrix:

A transformation from local to global axes is done (using Jacobian matrix) and also summation of equation (7.8) over all the elements i.e.

$$\frac{\partial I I}{\partial \delta} - \frac{\partial}{\partial \delta} \sum I I^{e} - \sum \frac{\partial I I^{e}}{\partial \delta^{e}} = 0 \qquad (7.12)$$

and the overall stiffness matrix can be obtained, together with a system of equilibrium equations for the complete continuum. After inserting the approbriate boundary conditions and neglecting initial stresses and strains, these equations can be solved by any simultaneous equation solving technique to yield the unknown nodal displacements.

(d) As an example of above matrices, in two dimensional plane strain problems, assume u and v to be the x and y displacements which cause strains ϵ_x, ϵ_y and γ_{xy}. It is also assumed that each element in the continuum has n nodal points. The generalised displacements and forces for each element are:

$$\delta^{e} = \begin{bmatrix} \delta_1 \\ \delta_2 \\ \cdot \\ \delta_n \end{bmatrix} \qquad (7.13)$$

$$F^{e} = \begin{bmatrix} F_1 \\ F_2 \\ \cdot \\ F_n \end{bmatrix} \qquad (7.14)$$

The displacements at any point inside the element are expressed in terms of algebraic functions (N) which are the so–called shape functions. The functions have special coordinates or local coordinates as shown in Fig. (7.4.A). The shape function of the element equals the sum of the shape functions of each node:

$$N = \sum_{i=1}^{n} N_i \qquad (7.15)$$

Any function N_i must clearly supply a unit value when the coordinate values of node i are substituted and zero when the coordinates of any other nodes are inserted as shown in Fig. (7.4.B). An example of shape functions for an 8 noded quadrilateral is shown in Fig. (7.4.C).

The strains within the element are expressed directly in terms of the nodal displacement, by means of the [B] matrix (strain matrix) as shown in equation (7.5).

where:

$$\text{Strains} \quad \epsilon = \begin{bmatrix} \epsilon_x \\ \epsilon_y \\ \gamma_{xy} \end{bmatrix} = \begin{bmatrix} \partial u/\partial x \\ \partial v/\partial y \\ \partial u/\partial y + \partial v/\partial x \end{bmatrix} \qquad (7.16)$$

$$B = \sum_{i=1}^{n} B_i \qquad (7.17)$$

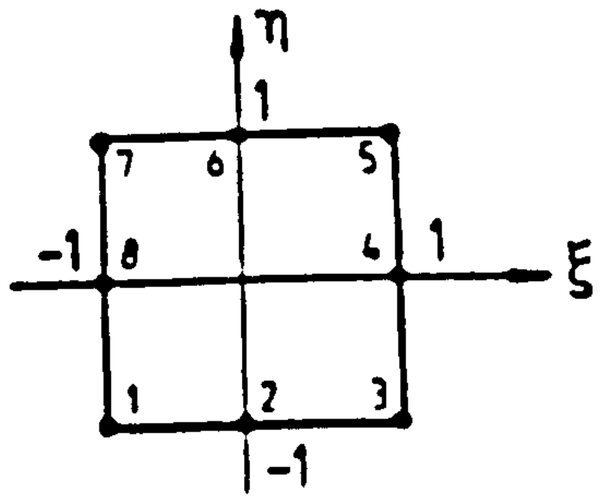

MAPPED ELEMENT

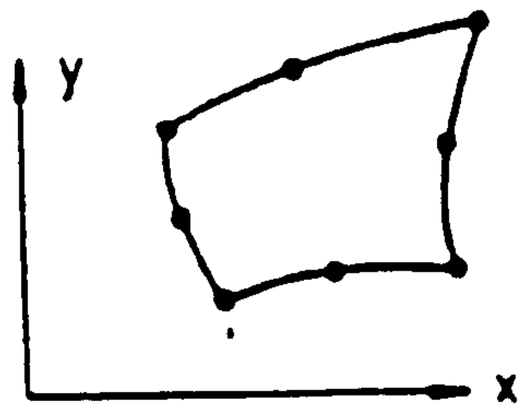

PARENT ELEMENT

FIG. (7.4.A) LOCAL AND GLOBAL COORDINATES OF AN ELEMENT (AFTER NAYLOR AND PANDE, 1981).

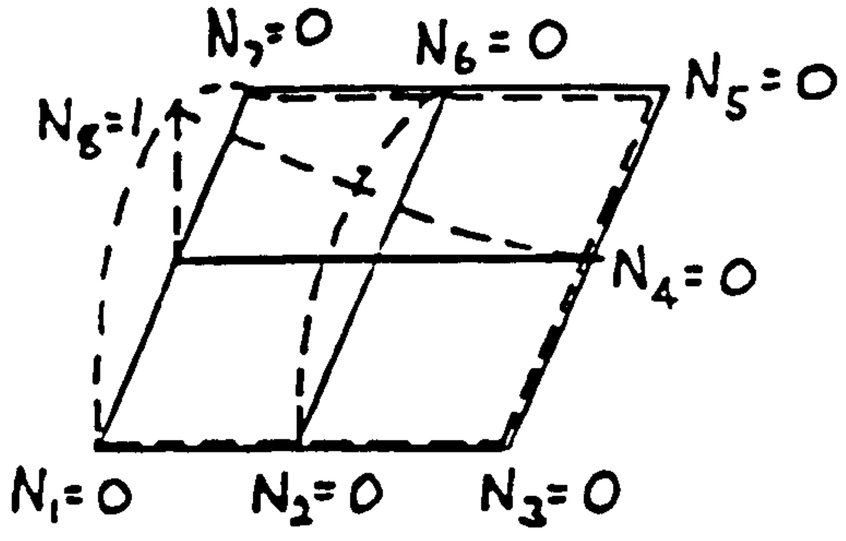

MIDSIDE SHAPE FUNCTION

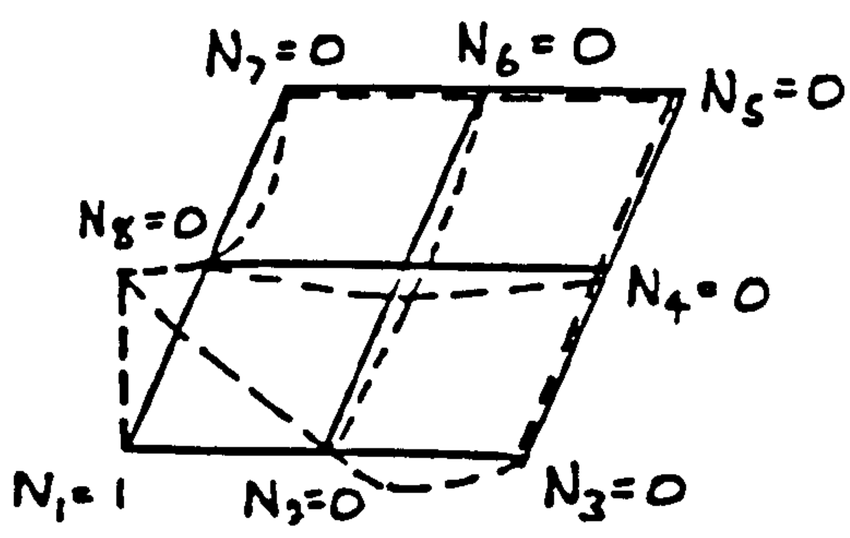

CORNER SHAPE FUNCTION

FIG. (7.4.B) SHAPE FUNCTION EQUAL UNITY AT NODES (AFTER GREEN ET AL., 1986).

NODE	N	ξ	η
1	$N_1 = (1-\xi)(1-\eta)(-1-\xi-\eta)/4$	-1	-1
2	$N_2 = (1-\xi^2)(1-\eta)/2$	0	-1
3	$N = (1+\xi)(1-\eta)(-1+\xi-\eta)/4$	+1	-1
4	$N = (1+\xi)(1-\eta^2)/2$	+1	0
5	$N = (1+\xi)(1+\eta)(-1+\xi+\eta)/4$	+1	+1
6	$N = (1-\xi^2)(1+\eta)/2$	0	+1
7	$N = (1-\xi)(1+\eta)(-1-\xi+\eta)/4$	-1	+1
8	$N = (1-\xi)(1-\eta^2)/2$	-1	0

FIG. (7.4.C) SHAPE FUNCTION FOR 8 NODED QUADILATERAL ELEMENT (AFTER GREEN ET AL., 1986).

$$B_i = \begin{bmatrix} \frac{\partial N_i}{\partial x} & 0 \\ 0 & \frac{\partial N_i}{\partial y} \\ \frac{\partial N_i}{\partial y} & \frac{\partial N_i}{\partial x} \end{bmatrix} \qquad (7.18)$$

This means that [B] contains cartesian derivatives of the shape functions N. The shape functions cannot be differentiated directly with respect to x and y because they are defined with respect to the local coordinate system ξ and η . The transformation from (ξ,η) coordinates to (x,y) coordinates can be achieved by Jacobian matrix as follows:

$$J = \begin{bmatrix} \frac{\partial x}{\partial \zeta} & \frac{\partial y}{\partial \zeta} \\ \frac{\partial x}{\partial \eta} & \frac{\partial y}{\partial \eta} \end{bmatrix} \qquad (7.19)$$

$$J = \begin{bmatrix} \frac{\partial N_1}{\partial \zeta} & \cdots & \frac{\partial N_n}{\partial \zeta} \\ \frac{\partial N_1}{\partial \eta} & \cdots & \frac{\partial N_n}{\partial \eta} \end{bmatrix} \begin{bmatrix} X_1 & Y^1 \\ X_2 & Y_2 \\ \vdots & \vdots \\ X_n & Y_n \end{bmatrix} \qquad (7.20)$$

Where:

$\partial N_i/\partial \zeta$ is the derivative of shape function (N_i) at node (i) with respect to ζ.

$\partial N_i/\partial \eta$ is the derivative of shape function (N_i) at node (i) with respect to η.

(x_i,y_i) are the cartesian coordinates of node (i).

Hence:

$$\begin{bmatrix} \frac{\partial N}{\partial x} \\ \frac{\partial N}{\partial y} \end{bmatrix} = \left[J^{-1} \right] \begin{bmatrix} \frac{\partial N}{\partial \xi} \\ \frac{\partial N}{\partial \eta} \end{bmatrix} \qquad (7.21)$$

$[\ J^{-1}\ ]$ is inverse of Jacobian matrix.

and an area $dA = dx.dy$ in the actual element can be expressed in terms of $d\xi\ d\eta$ as follows :

$$dA = dx\ dy = |\ J\ |\ d\xi\ d\eta \qquad (7.22)$$

Where:

$|J|$ is the determinate of the Jacobian matrix.

The relationship between stresses and strains can be achieved by [D] matrix as in equation (7.6)

Where:

$$\text{Stress} \quad \sigma = \begin{bmatrix} \sigma_x \\ \sigma_y \\ \sigma^{xy} \end{bmatrix} \qquad (7.23)$$

$$D = \frac{E(1-\nu)}{(1+\nu)\ (1-2\nu)} \begin{bmatrix} 1 & \frac{\nu}{1-\nu} & 0 \\ \frac{\nu}{1-\nu} & 1 & 0 \\ 0 & 0 & \frac{1-2\nu}{2(1-\nu)} \end{bmatrix} \qquad (7.24)$$

Where:

E is the modulus of elasticity and ν is Poisson's ratio.

7.2 DEFINITION OF THE PROBLEM:

The use of the finite element method for the analysis of a reinforced earth retaining wall needs more care, since the problem is three dimensional and includes soil structure interaction. The key to the success of any analysis involving soil is the use of an appropriate model for its constitutive behaviour.

Proper modelling for the finite element analysis of a reinforced earth wall is the key to success, and involves a reasonable simulation of:

(a) The mechanical behaviour of the backfill.

(b) Reinforced elements.

(c) Face elements.

(d) The interaction between these components of the wall.

(e) The sequence of the construction operation in the field as follows:

(i) Placement of new layers of backfill.

(ii) Compaction operations at the current fill surface.

(iii) Placement of new soil element.

(iv) Application of various types of loads to the compacted fill and / or structure.

7.2.1 General Approaches:

There are two general approaches to the finite element analysis of reinforced soil systems involving respectively:

(a) composite model

(b) discrete model

(a) composite model:

The use of composite materials for civil engineering applications is ages old, e.g., plain concrete and reinforced concrete. In a composite model of a reinforced earth retaining wall, it is assumed that if the reinforcing pattern is repeated a sufficiently large number of times the material can be considered homogeneous, or as a homogeneous material in which the varying properties are due to changes in the reinforcing spacing and / or properties. The reinforced material in such a case exhibits orthotropic behaviour. The composite properties of soil, reinforcing member, and their composite interaction must be determined, and once determined, standard finite element procedures are used to analyse complicated structures of the reinforced material (Hermann and Al– Yassin, 1978).

Popescu (1979) explained that the advantage of a composite representation is the economy of analysis achieved by not having to discretely represent each reinforcing member. The disadvantage is that the analysis does not directly yield detailed information about the stress and strain states at the interfaces of soil and reinforcing members, or about localized deformations near the edges of the reinforced mass.

(b) Discrete model:

The reinforced system is treated as a heterogeneous body. The soil and each element is considered in detail (Al– Hussaini and Johnson, 1978). Popescu (1979) added that the advantage of a discrete representation is that detailed information is directly obtained about the interaction of the soil and reinforcing member (e.g. bond stresses concentration, edge effects, etc). The chief disadvantage is excessive computation and cost for real structures containing a large number of reinforcing elements. A comparative study performed by Herrmann and Al– Yassin (1978) demonstrated that the two approaches yield very similar results and consequently they can be applied with equal accuracy to the analysis of reinforced soil systems. However in general for large two dimensional and three dimensional configurations, only the composite approach is economically feasible.

7.3 DIFFERENT CONCEPTS TO IDEALIZE THE PROBLEM

Different concepts have been used by researchers to idealize and model a reinforced earth retaining wall and apply the finite element method to solve the problem. These concepts are :

7.3.1 Unit Cell Concept: (Romstad et al., 1976)

Romstad et al. developed a composite model of a reinforced earth wall. In the concept, a small unit (unit cell) of the reinforced material is isolated as shown in Fig. (7.5). It simulates the composite characteristics of the material. Assumptions were employed to idealize the problem from three dimensions to two

dimensions and to determine the characteristics of the composite material as follows:

(a) The average value of strains for the cell are the same as the composite material. This is because the percentage of reinforcement is extremely small (less than 1% by volume).

(b) The displacements of all the points in the unit cell in plane 2−3, Fig. (7.5), are equal for both soil and strips, i.e. no slippage occurs between the soil and the strip, especially in the interior regions of the reinforced earth mass.

i.e.

$$\epsilon_1^{so} = \epsilon_1^{st} \tag{7.25}$$

$$\frac{\sigma_1^{so}}{E^{so}} = \frac{\sigma_1^{st}}{E^{st}} \tag{7.26}$$

(c) The problem is considered as a plane strain problem and the constitutive relationship for the composite material is:

$$\begin{bmatrix} \epsilon_1 \\ \epsilon_2 \\ \gamma_{12} \end{bmatrix} = \begin{bmatrix} c11 & c12 & c13 \\ c21 & c22 & c23 \\ c31 & c32 & c33 \end{bmatrix} \begin{bmatrix} \sigma_1 \\ \sigma_2 \\ \tau_{12} \end{bmatrix} \tag{7.27}$$

and the composite properties of the reinforced earth c_{11}, c_{12} and c_{13} (for

example) can be determined as follows:

Assume:

$$\sigma_1 = \sigma \tag{7.28}$$

$$\sigma_2 = \sigma_3 = 0 \tag{7.29}$$

$$c11 = \frac{\epsilon 1}{\sigma} = \frac{\epsilon_1^{so}}{\sigma} = \frac{\sigma_1^{so}}{\sigma\ E^{so}} \tag{7.30}$$

$$c12 = \frac{\epsilon 2}{\sigma} = \frac{\epsilon_2^{so}}{\sigma} = \frac{-\ \nu\ \sigma_2^{sc}}{\sigma\ E^{so}} \tag{7.31}$$

$$c1_3 = \frac{\epsilon_3}{\sigma} = \frac{\epsilon_3^{so}}{\sigma} = \frac{\sigma_3^{so}}{\sigma\ E^{so}} \tag{7.32}$$

The average value of the stress distribution (σ) over the cell faces is equal to the stresses in the equivalent composite material, i.e.

$$\sigma\ A^c = \sigma_1^{so}\ A^c + \sigma_1^{st}\ A^{st} \tag{7.33}$$

From Eqs. (7.26&33)

$$\sigma_1^{st} = \frac{\sigma\ A^c\ E^{st}}{A^c\ E^{so} + A^{st}\ E^{st}} \tag{7.34}$$

$$\sigma_1^{so} = \frac{\sigma\ A^c\ E^{so}}{A^c\ E^{so} + A^{st}\ E^{st}} \tag{7.35}$$

Substituting from equations (7.34 & 35) the composite material properties may be determined as follows:

$$c_{11} = \frac{A^c}{A^c E^{so} + A^{st} E^{st}} \tag{7.36}$$

$$c_{12} = \frac{-\nu A^c}{A^c E^{so} + A^{st} E^{st}} \tag{7.37}$$

$$c_{13} = \frac{-\nu A^c}{A^c E^{so} + A^{st} E^{st}} \tag{7.38}$$

The other properties (c_{21}, c_{22}, ...) are obtained in a similar way and the final constitutive relationship for the composite can be determined. They can be easily incorporated into existing finite element programs.

(d) The facing element is treated as a one dimensional axial strain element and its stiffness is incorporated directly into the composite element stiffness matrix. More rigid facing elements can be handled by utilizing a beam element.

(e) The edge effect arises because of the disturbances on the edges of the structures due to self equilibrating stress distribution. Therefore, at the edges the strains and forces in the reinforcements are predicted to be larger than the actual measured values.

(f) Once the equivalent composite stress and strain state is determined, the stresses and strains in the soil and the strip forces are calculated through back

calculations and by making assumptions about the actual strain in the reinforcement.

Where:

ϵ^{so} is strain in soil.

ϵ^{st} is strain in reinforcement.

σ^{so} is stress in soil.

σ^{st} is strain in reinforcement.

σ is stress in composite material.

A^{so} is soil area.

A^{st} is cross–section area of the reinforcement

A^{c} is composite area.

τ is shear stress.

Υ is shear strain.

ν is Poisson's ratio of the soil·

E is Modulus of elasticity [soil (E^{so}) & reinforcement (E^{st})].

Al–Yassin and Herrmann (1979) modified the composite finite element model developed by Romstad et al. (1978), to take into consideration reinforcement slippage and edge effect. Slippage between the reinforcement and the soil was allowed to occur by adding interface elements between the two surfaces. The composite material properties were, therefore, determined allowing for slippage. Fig. (7.6) shows a finite element grid frame reinforced earth wall model test by Al–Yassin and Herrmann (1979).

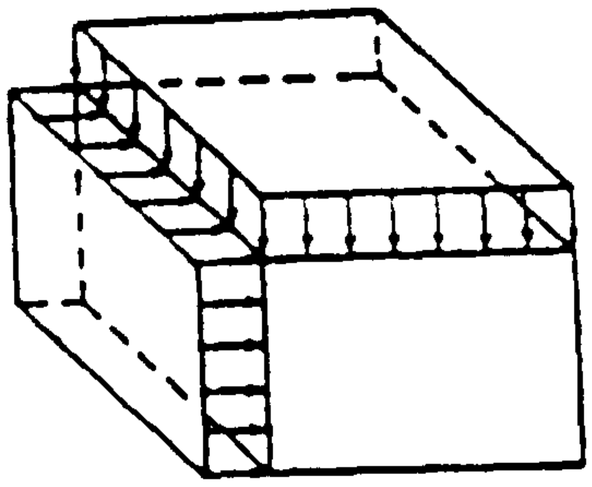

COMPOSITE STRESS STATE (σ_x = 0)

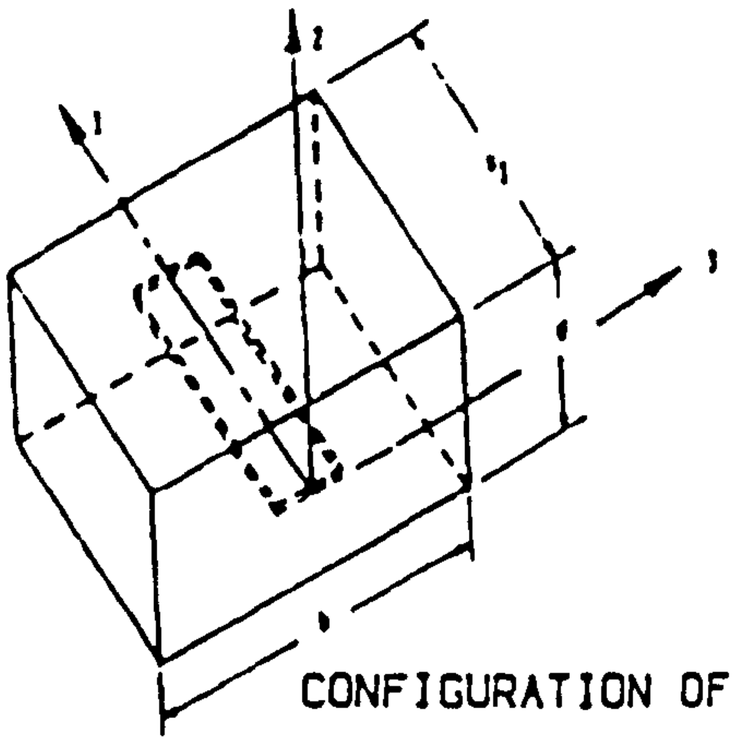

CONFIGURATION OF UNIT CELL

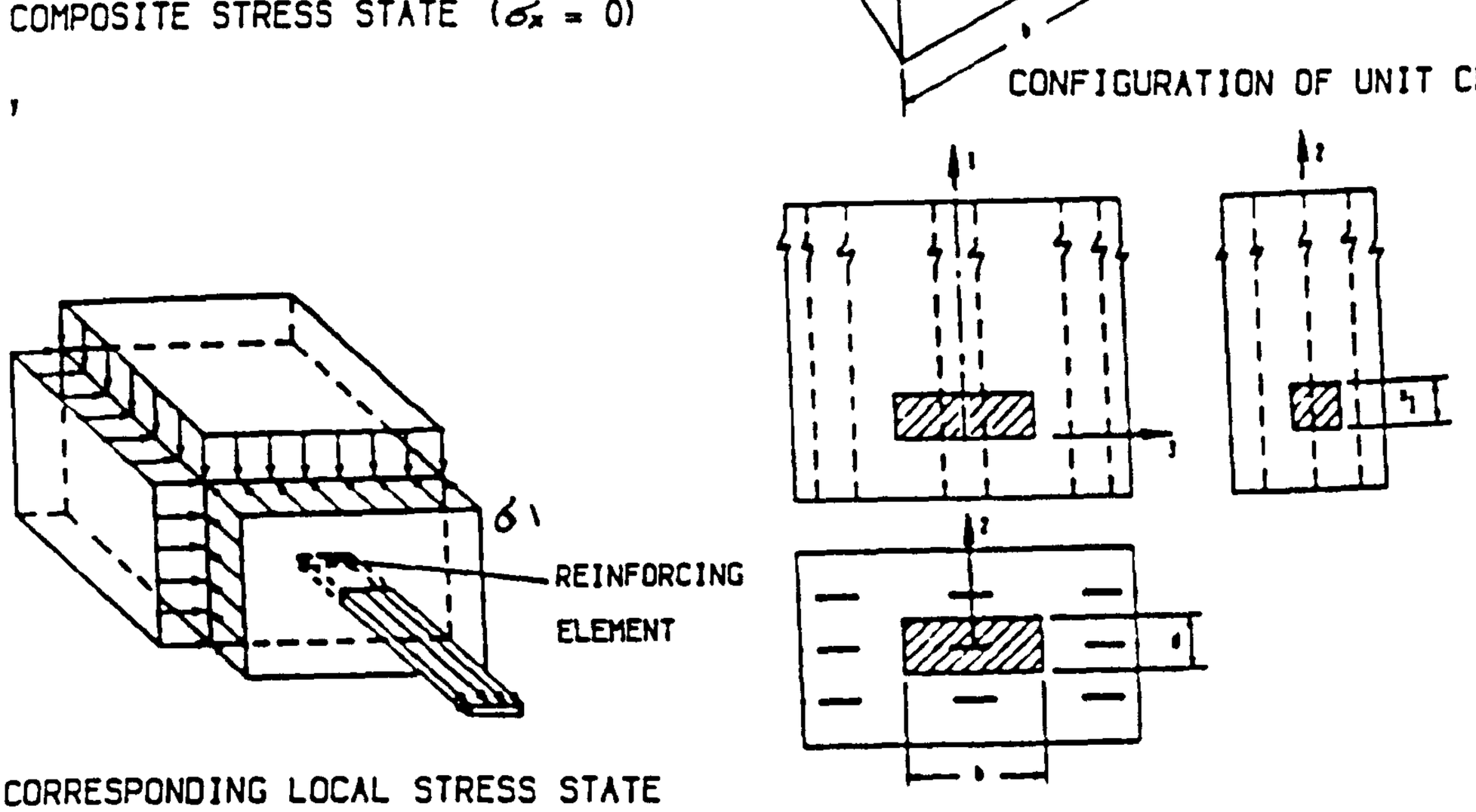

CORRESPONDING LOCAL STRESS STATE

FIG. (7.5) UNIT CELL REPRESENTATION OF REINFORCED EARTH AND COMPOSITE STRESSES (AFTER ROMSTAD ET AL., 1976).

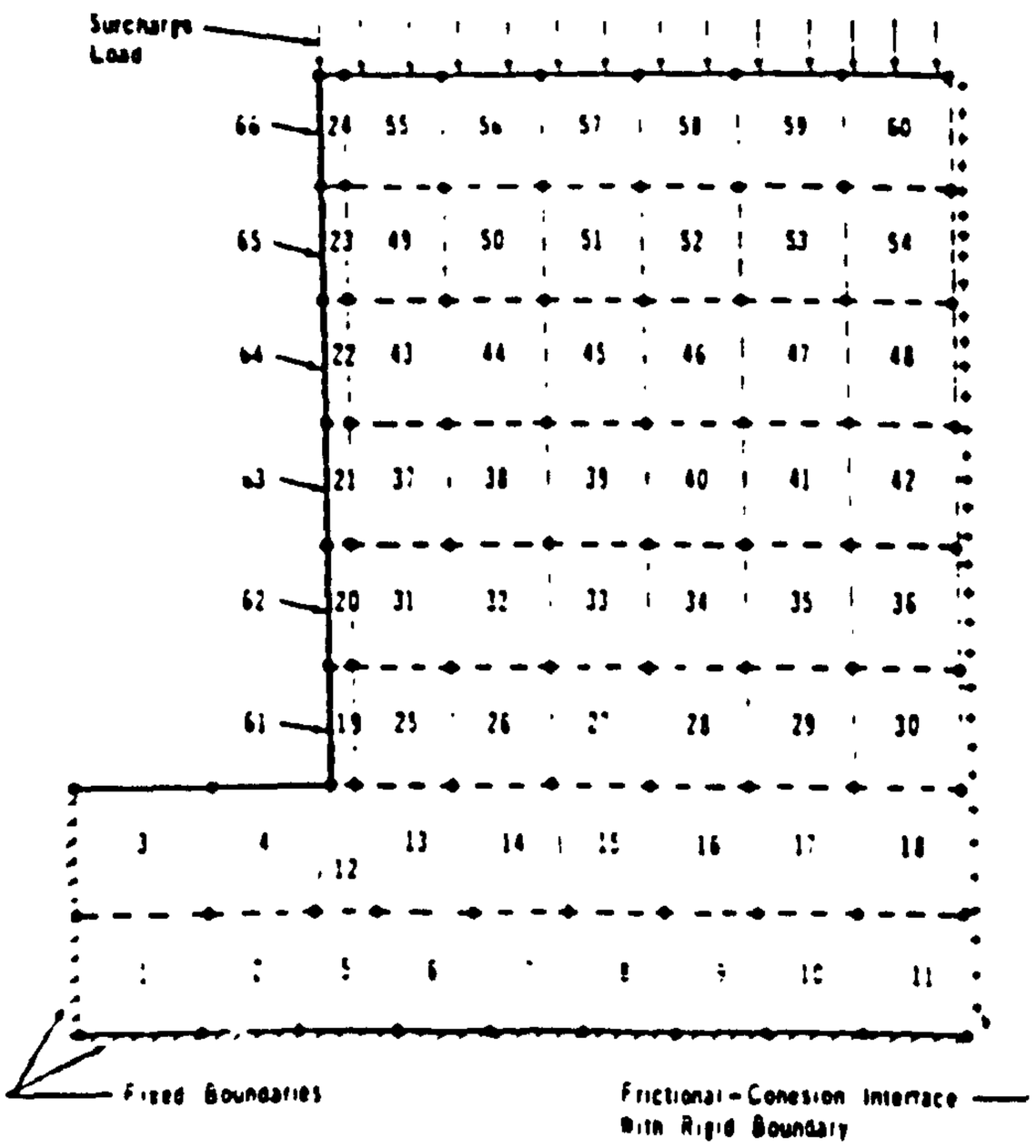

FIG. (7.6) FINITE ELEMENT MESH USING COMPOSITE APPROACH (AFTER AL YASSIN AND HERMANN, 1977).

7.3.2 Slipping Strip Concept: (Naylor and Richards, 1978)

A model of reinforced earth has been presented which allows slip to occur between the strips (reinforcement) and the soil when the yield stress is reached. The main features of the model are:

(a) The equivalent material:

The actual material as shown in Fig. (7.7.A) can be replaced by the material of Fig. (7.7.B) in which the strip is taken outside the soil and connected to it by a conceptual shear zone.

(b) The longitudinal stiffness of the strips:

This is incorporated in the areas ratio parameter, a, defined in terms of the strip cross–sectional area, a_s, the horizontal spacing, B, and the vertical spacing, T, of the strips, i.e

$$a = \frac{a_s}{BT} = \frac{bt}{BT} \qquad (7.39)$$

(c) The transfer of shear stress by bond between the strips and the soil:

This is idealized by making the surface area of the equivalent sheet of strips, which is connected to the soil by the conceptual shear zone, the same as the surface area of the actual strips, i.e

$$C = 2(b+t) \qquad (7.40)$$

Since, $t \ll b$ so:

$$C \simeq 2b \qquad (7.41)$$

The dimensionless bond area parameter

$$P = \frac{C}{T} \qquad (7.42)$$

(d) The transfer of shear through the soil in the vertical plane:

This is clearly shown in Fig. (7.8) and is achieved when $b << B$, which it usually is in practice.

(e) The conceptual shear zone is assigned an arbitrary thickness, e (usually e = unity).

(f) The model only allows the strips to move relative to the soil in the strip direction, i.e. an extra degree of freedom allows this movement (δ) Fig. (7.9).

(g) A Mohr—Coulomb criterion is used in the slip analysis to limit the shear stress on the strips (i.e. in the conceptual shear zone).

$$| \tau_s | < C_s + \sigma_n \tan \varphi_s \qquad (7.43)$$

Where C_s and φ_s define the strip/soil bond strength, and σn, the normal stress across the strips is assumed to be the same as the average stress transmitted through the soil across the plane containing the strips .

(h) A tangential technique is used to relax the shear modulus (G_s) to allow

relative displacement which will relax the bond shear stress (τ_s) to satisfy a bond criterion as shown in Fig. (7.10).

(i) The element stiffness matrices are obtained by superimposing a contribution to the longitidunal stiffness of the strips (measured by $a.E_s$ where E_s is the modulus of elasticity of the strip material) and the shear stiffness of the conceptual shear zone (measured by $P.e.G_s/B$).

(j) Construction of the wall was modelled by a single lift analysis.

A two dimensional finite element program has been used and the previous features have been incorporated. An example of the idealization of a reinforced earth wall using the above concept is shown in Fig. (7.11).

7.3.3 Equivalent plate concept: (Al–Hussaini and Johnson, 1978)

The reinforced earth wall was idealized as a two dimensional plane strain problem, assuming:

(a) The reinforcing strips (reinforcement) are replaced by a plate extending to the full width and breadth of the wall.

(b) The major response of the strips is provided by an axial stiffness. The total axial stiffness of the reinforcement (S) in the wall is:

$$S = \sum_{j-1}^{N} \frac{A_j E_j}{L_j} = N \frac{A_s E_s}{L_s} \qquad (7.44)$$

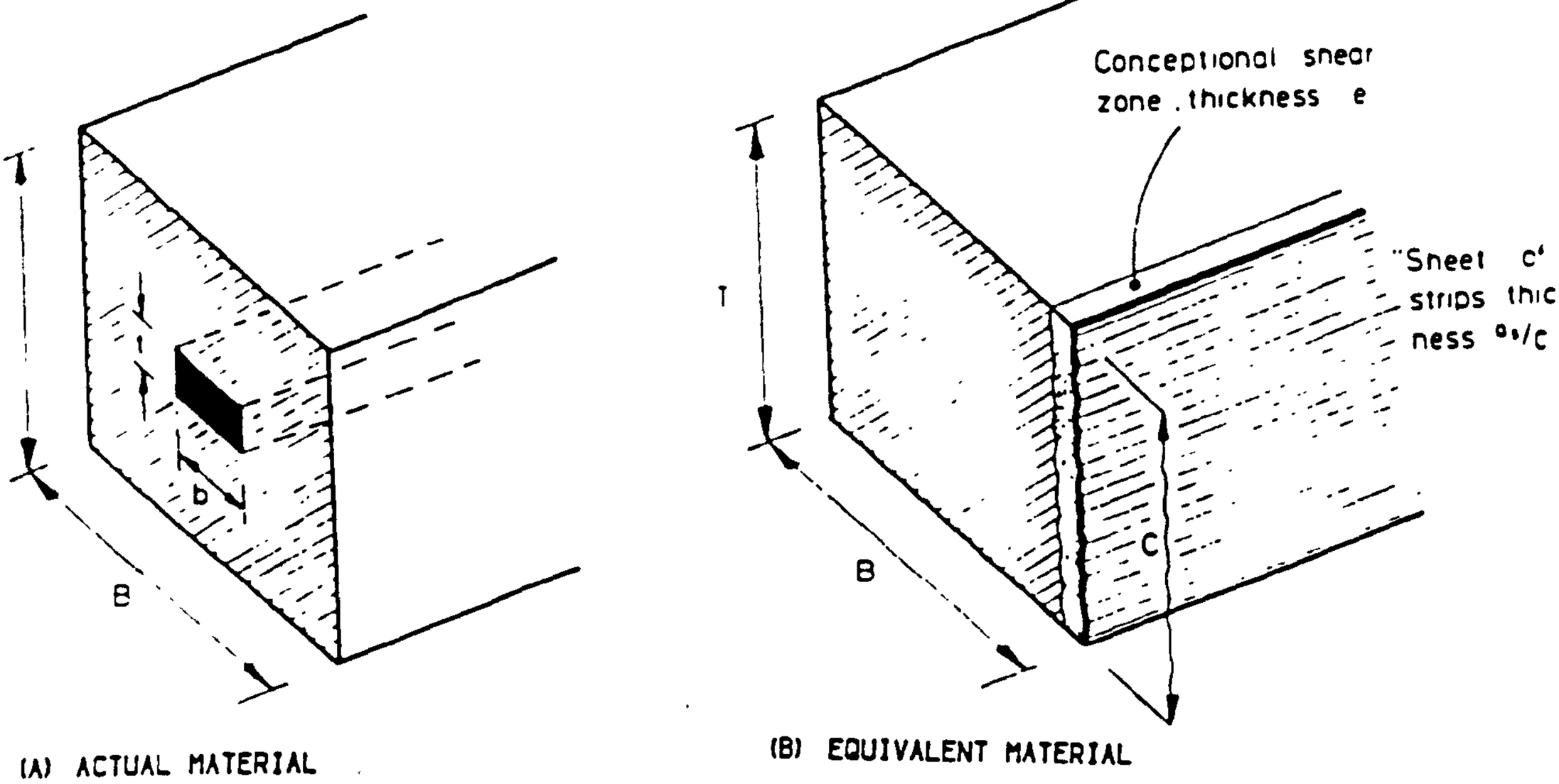

(A) ACTUAL MATERIAL

(B) EQUIVALENT MATERIAL

SOIL MATERIAL HALF WAY BETWEEN STRIPS

FIG. (7.7) TRANSFORMATION FROM ACTUAL TO EQUIVALENT MATERIAL (AFTER NAYLOR AND RICHARDS, 1978).

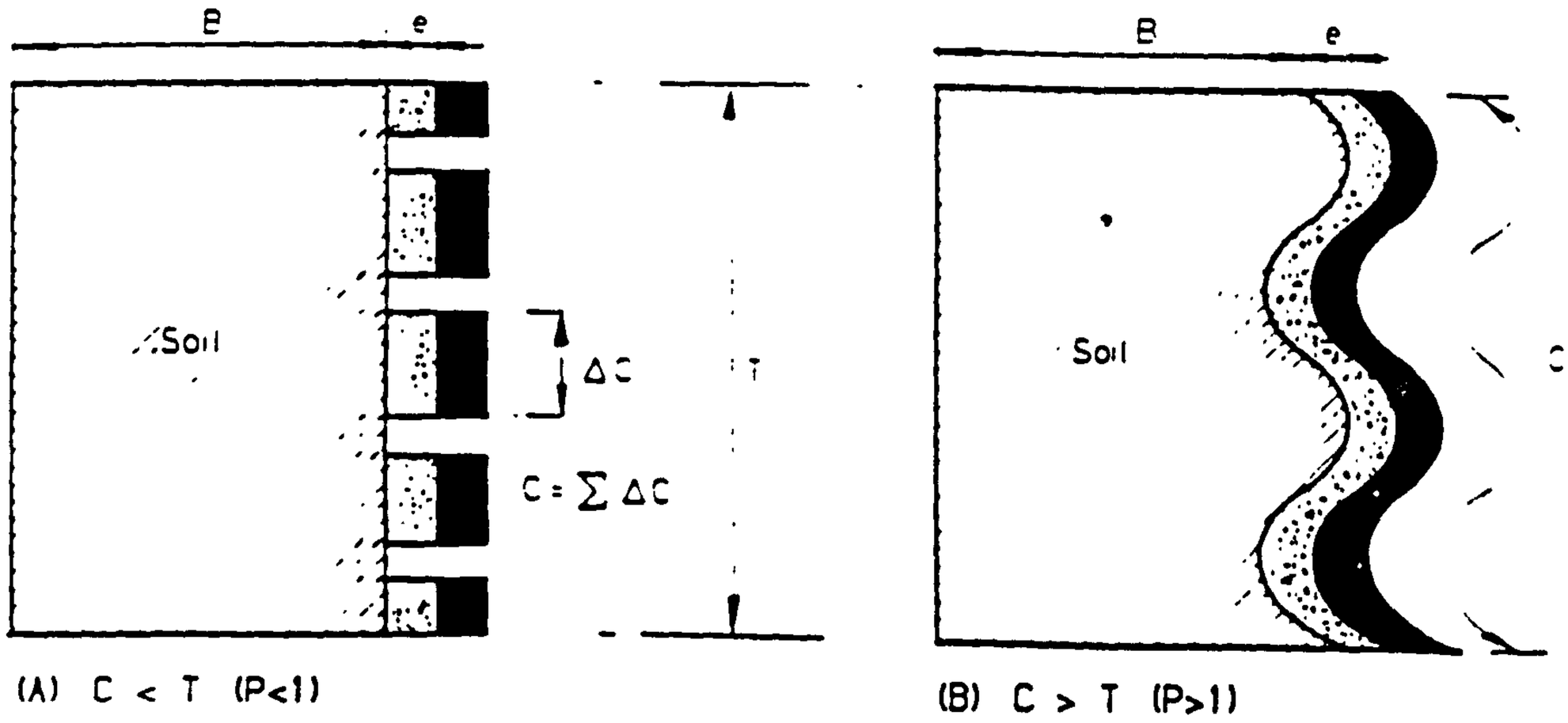

(A) C < T (P<1)

(B) C > T (P>1)

FIG. (7.8) MODELLING OF CONCEPTUAL SHEAR ZONE (AFTER NAYLOR AND RICHARDS, 1978).

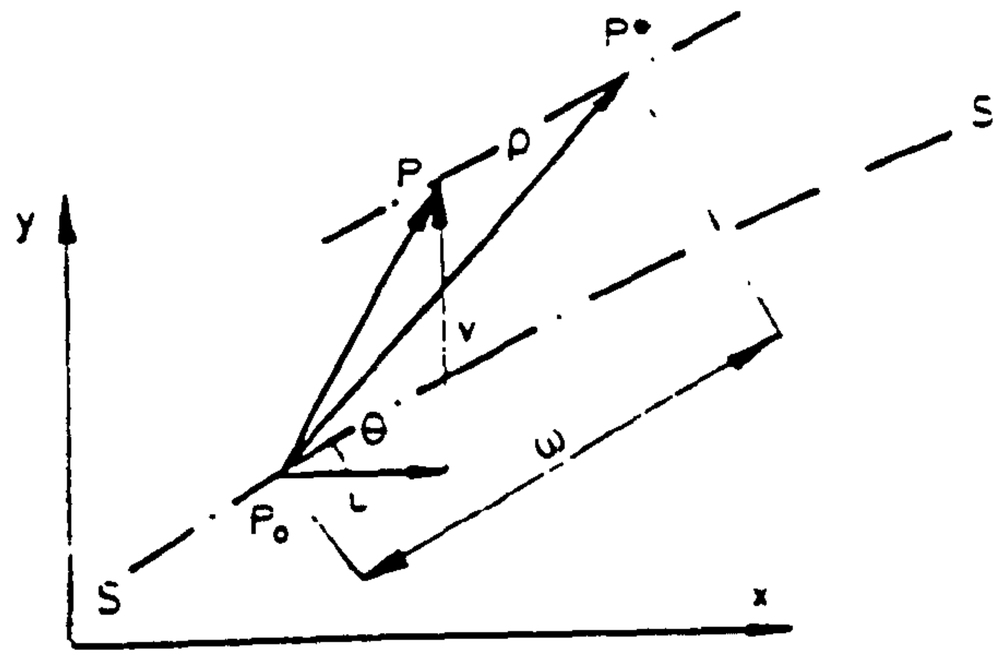

FIG. (7. 9) EXTRA DEGREE OF FREEDOM (ρ) TO ALLOW RELATIVE MOVEMENT OF THE STRIP TO THE SOIL (AFTER NAYLOR AND RICHARDS, 1978).

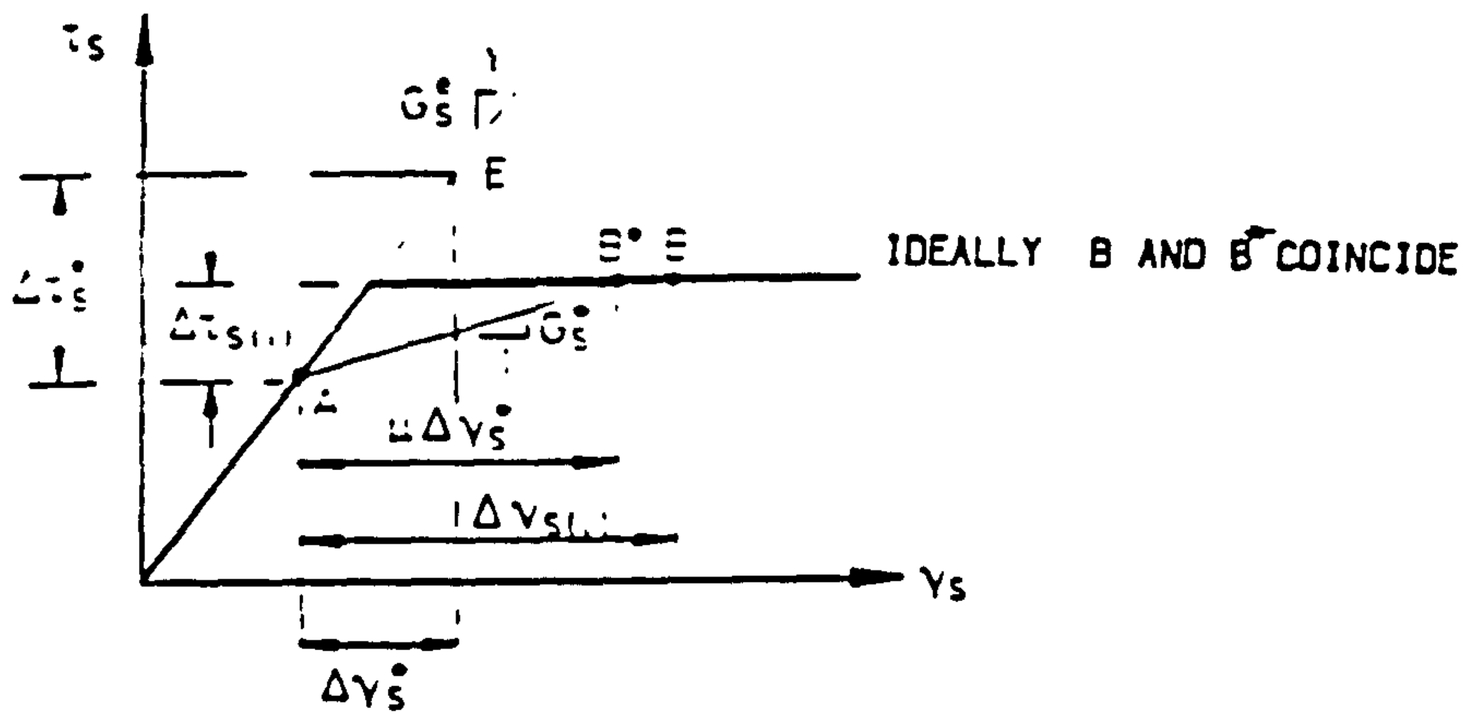

FIG. (7. 10) SHEAR ZONE STRESS STRAIN CURVE (AFTER NAYLOR AND RICHARDS, 1978).

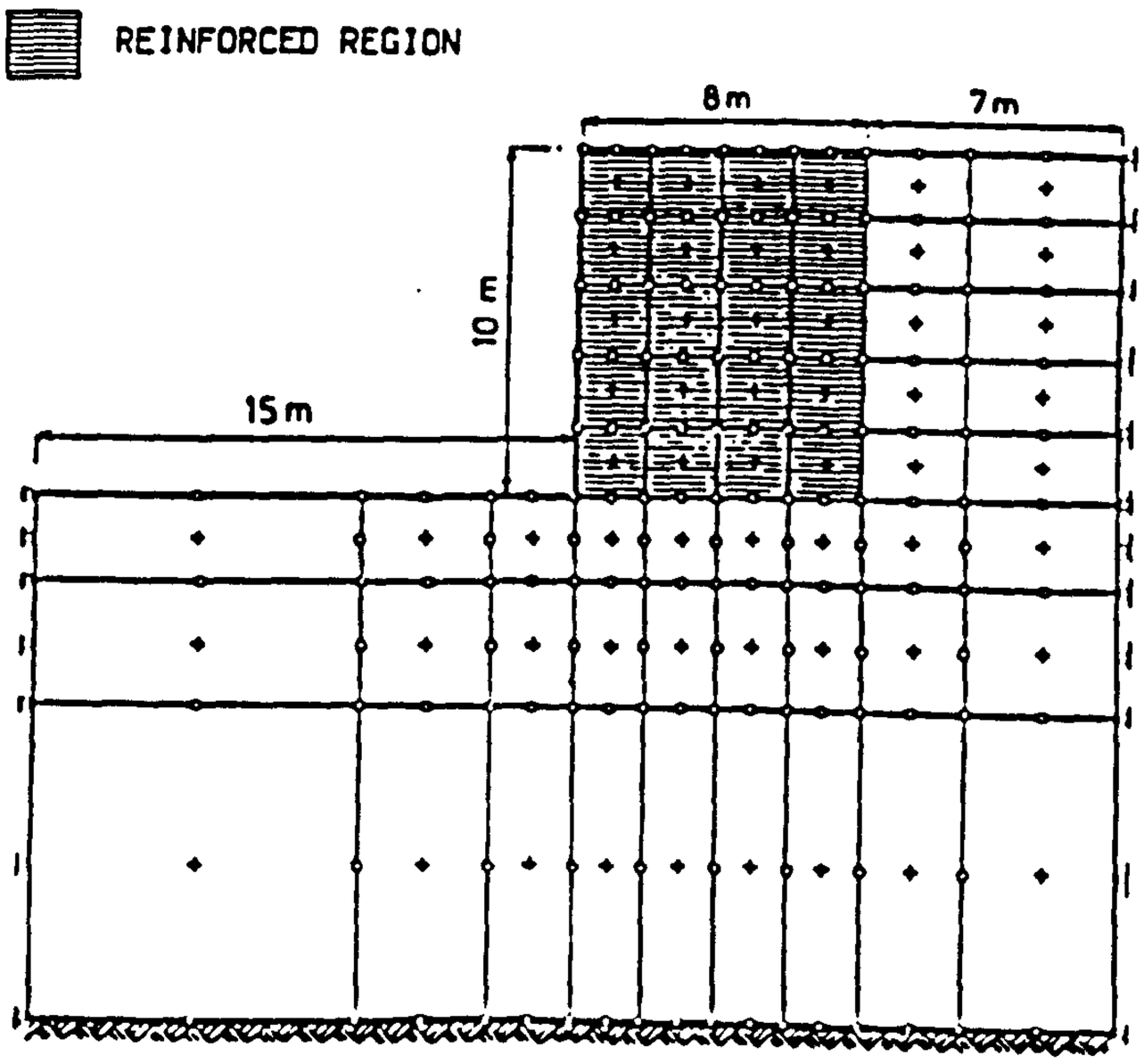

FIG. (7. 11) IDEALIZATION OF REINFORCED EARTH RETAINING WALL (AFTER NAYLOR AND RICHARDS, 1978).

Where:

N is the total number of strips in each row.

A_S is the cross sectional area of the reinforcing strip.

E_S is the modulus of elasticity of reinforcing strip.

L_S is the length of reinforcing strip.

The equivalent stiffness of the plate that substitutes for each row of strips (S_e) may be defined as:

$$S_e = \frac{A_e E_e}{L_e} \tag{7.45}$$

Where:

A_e is the equivalent cross sectional area of the strips.

L_e is the equivalent length of the strips.

E_e is the equivalent modulus of the strips.

S & S_e should be the same, and Ls & Le remain the same. The equivalent modulus E_e can be determined from:

$$E_e = \frac{N A_S E_S}{A_e} \tag{7.46}$$

(c) The facing element is replaced by ar. equivalent beam element of similar deflection response. The equation used to satisfy equal bending deformation response between the prototype and the model was:

$$\frac{E_a I_a}{L_a} = \frac{E_e I_e}{L_e} \tag{7.47}$$

$$L_a = L_e \tag{7.48}$$

$$E_e = E_a \frac{I_a}{I_e} \tag{7.49}$$

Where:

E_a is the modulus of elasticity of the facing panel.

I_a is the moment of inertia of the facing panel per unit width.

L_a is the length of the beam between two rows of reinforcing strips see S_z in Fig. (7.12).

I_e is the equivalenet moment of inertia per unit width.

(d) An interface element introduced by Goodman et al. (1968) was incorporated in a plane strain finite element program. A finite element mesh for a test reinforced earth wall which has been carried out by Al-Hussaini and Perry (1976) is shown in Fig. (7.12).

7.4 MODELLING OF COMPACTION IN FINITE ELEMENT METHOD

Only a few attempts have been made to model the compaction induced lateral earth pressure in finite element analysis techniques. The attempts have aimed at predicting the deflection of the structure produced during the period of compaction and the pressure remaining in the soil after compaction, together with the peak magnitude of the lateral earth pressure.

7.4.1 Finite Element Compaction Model: (Aggour and Brown, 1974)

Aggour and Brown were the first to attempt to model compaction by means of a two dimensional plane strain finite element analysis. They developed a finite element process to simulate compaction and residual lateral pressure on a wall which could deflect during incremental placement. The finite element iteration process developed by Aggour (1972) was employed.

The procedures of the model are as follow:

(a) Stress–strain relationship is shown in Fig. (7.13)

(b) The initial soil modulus is E_1 before compaction.

(c) Compaction is modelled as a uniform vertical load distributed over the full surface of the soil. After compaction the soil modulus is increased to a value E_2 due to density increase. Some deflection occurs.

(d) The strains, deflections, and stress distributions are modelled using an unloading modulus E^u_2 due to the removal of compaction load.

(e) A new fill layer with modulus E_1 is added to the top of the preceding layer. The increased stresses in the underlying layers are modelled using the soil modulus E_2.

(f) The stresses in both layers increase, and further deflections of the wall occur after applying a surface load to model compaction of the new layer. During this stage the upper soil layer modulus is increased to E_2.

(g) The compacting load is removed and the resulting wall deflections, strains

, and stress distributions are modelled using the modulus E^u_2 for both soil layers.

(h) The entire process is then incrementally repeated for all soil layers. Fig. (7.14) illustrates the method used to model the compaction and construction sequence.

(i) The effect of increasing the number of passes of the compaction plant was modelled by increasing the soil modulus E_2. The soil modulus was greater for unloading than for reloading.

Two examples were carried out using the above procedure. The first, was on a concrete wall and soil properties shown in Fig. (7.15). The fill was placed in five 4 inch lifts. A frictionless soil/wall interface was assumed. The results of this analysis are shown in Fig. (7.16.A).

The second example, used the same soil/wall geometry, but only the last soil lift placed was compacted. The results are shown in Fig. (7.16.B). The results of the example indicate increasing wall deflections, and residual lateral pressures near the top of the wall with increased compaction, and a decrease of the residual lateral pressures near the base of the wall with increased compaction due to increased wall deflections. The method needs further refinement to include:

(i) Consideration of the stresses induced by a realistic compaction plant of finite dimensions.

(ii) The use of non–linear soil properties.

(iii) More realistic representation of soil/wall interface conditions.

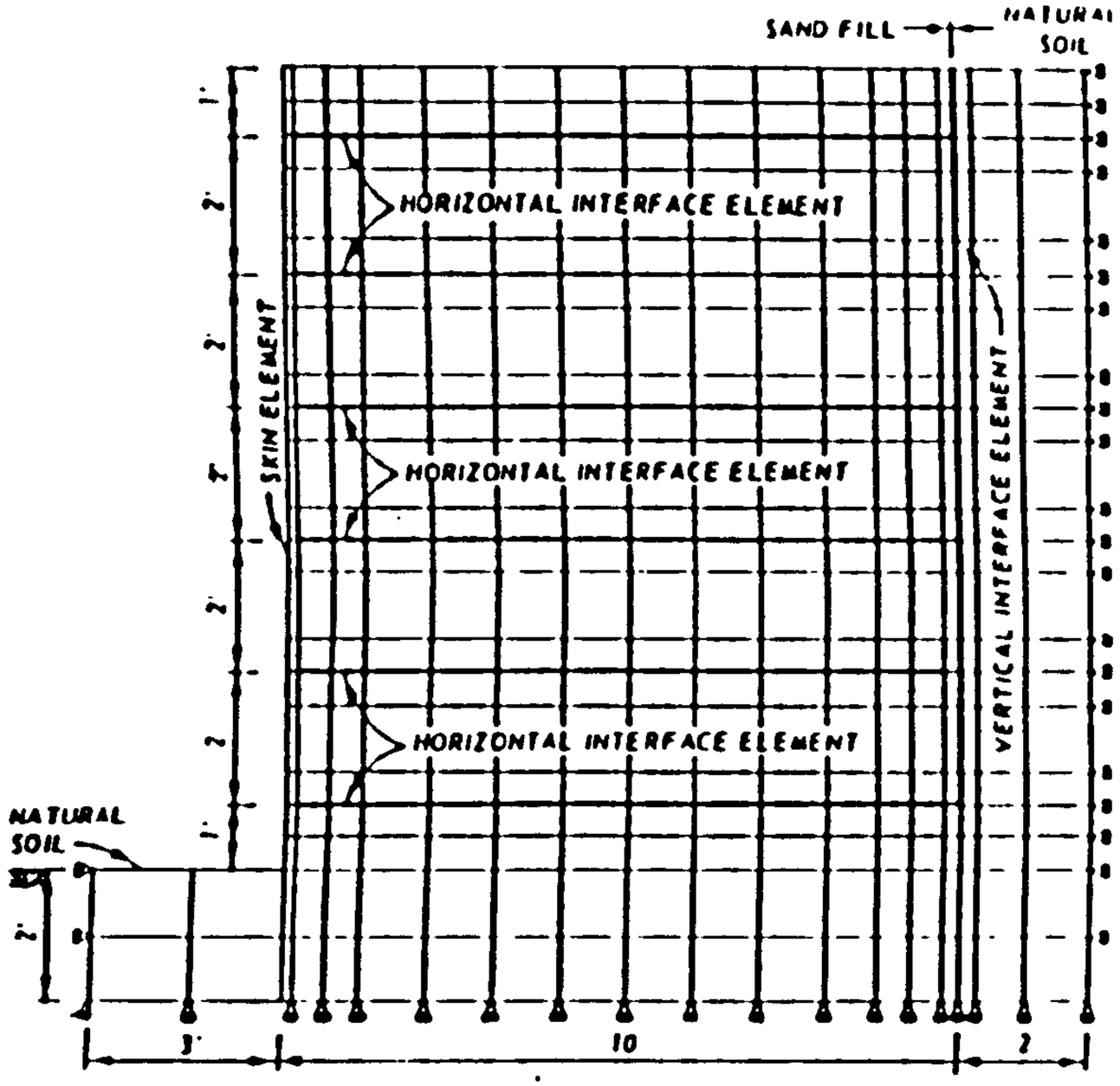

FIG. (7. 12) A FINITE ELEMENT MESH FOR V. E. S TEST REINFORCED EARTH VALL (AFTER AL-HUSSAINI AND JOHNSON, 1978).

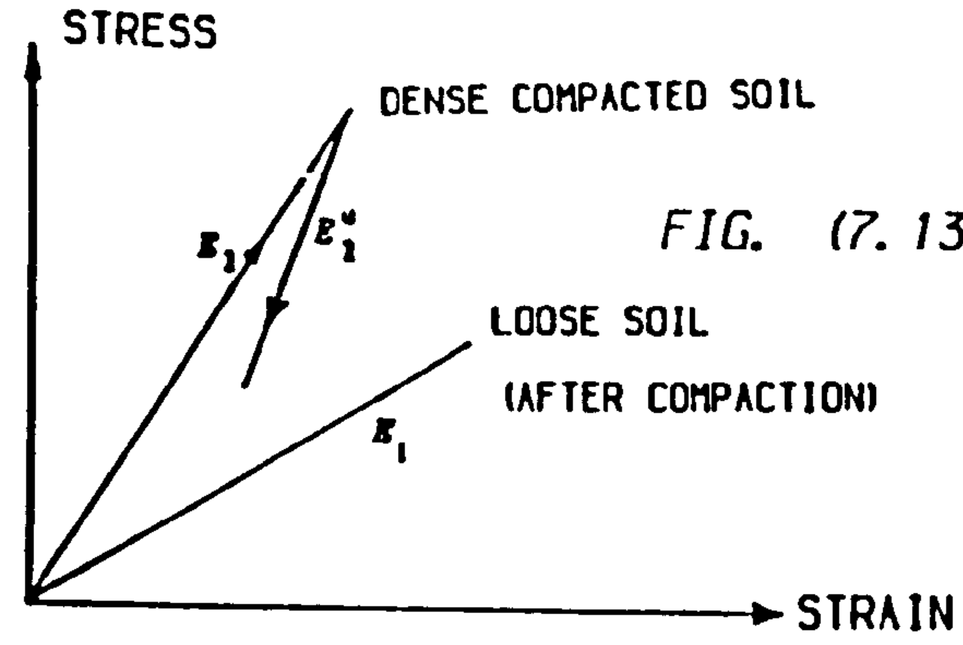

FIG. (7. 13) STRESS-STRAIN RELATIONSHIP (AFTER AGGOUR AND BROVN , 1974).

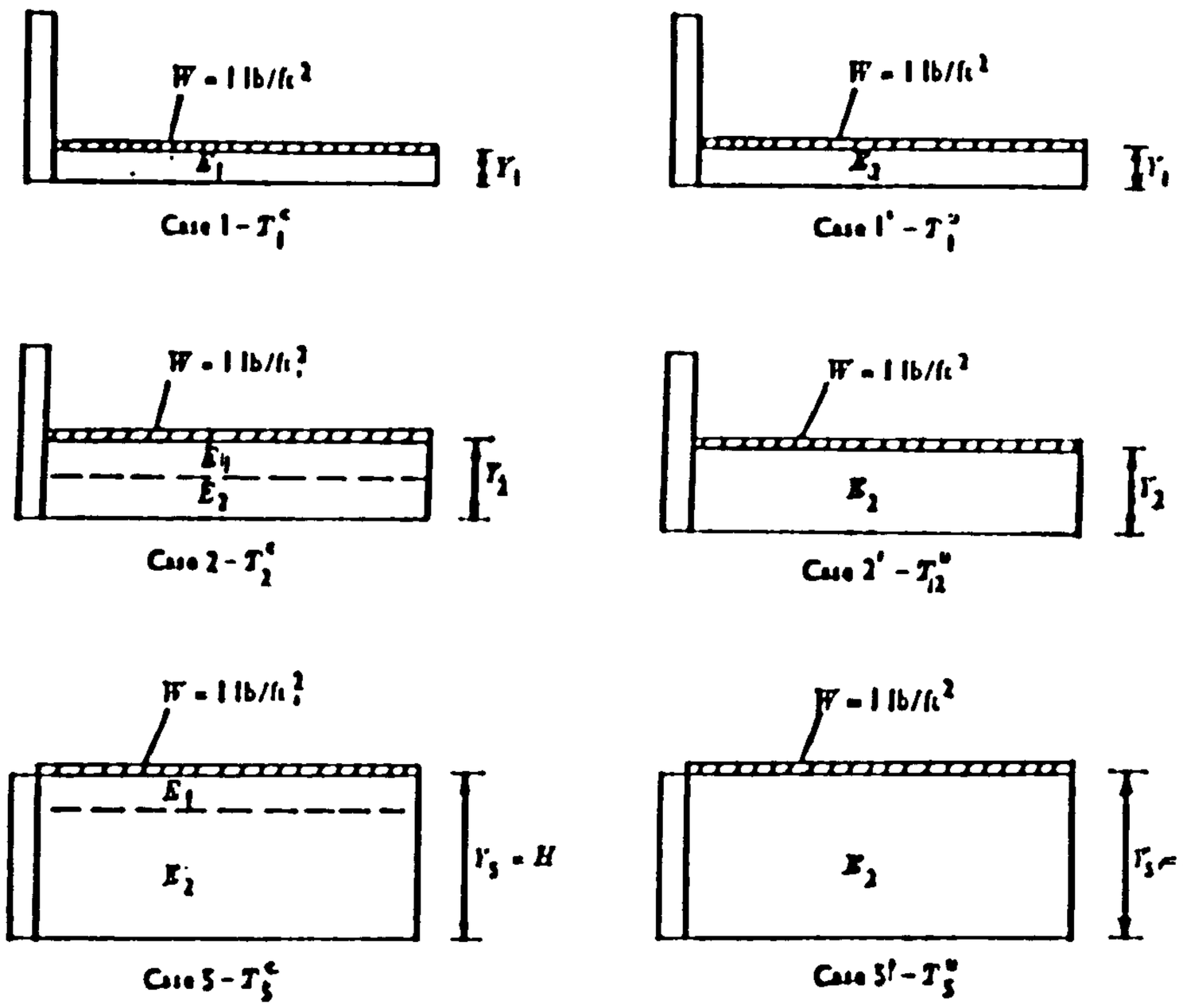

FIG. (7. 14) MODELLING OF COMPACTION AND CONSTRUCTION SEQUENCE (AFTER AGGOUR AND BROVN , 1974).

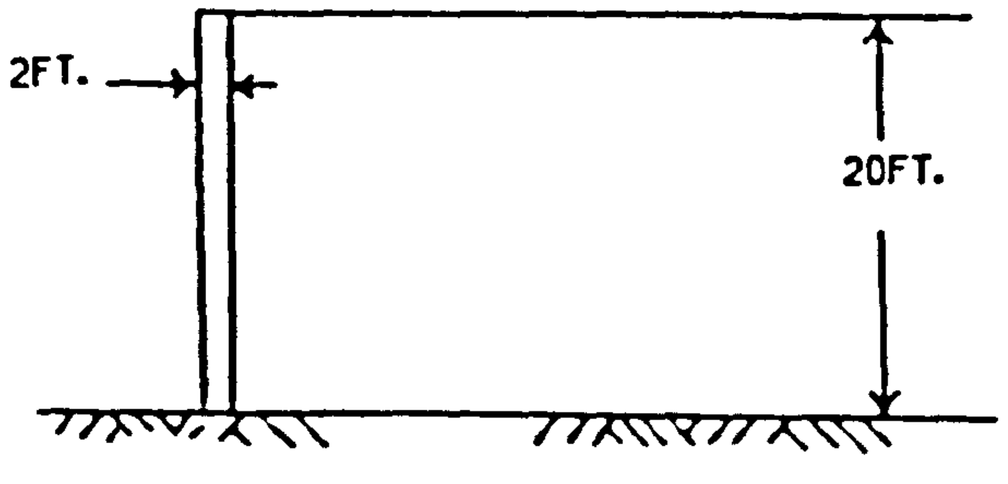

SOIL

γ_s =125 LB/FT2

ν_s =0.30

E_1 =36X10 LB/FT2

E_2 =144X10 LB/FT2

CONCRETE

E_c =432X10 LB/FT2

γ_c =150 LB/FT2

ν_c =0.2

NUMBER OF LAYERS=5

FIG. (7.15) CASE STUDIED (AFTER AGGOUR AND BROWN, 1974).

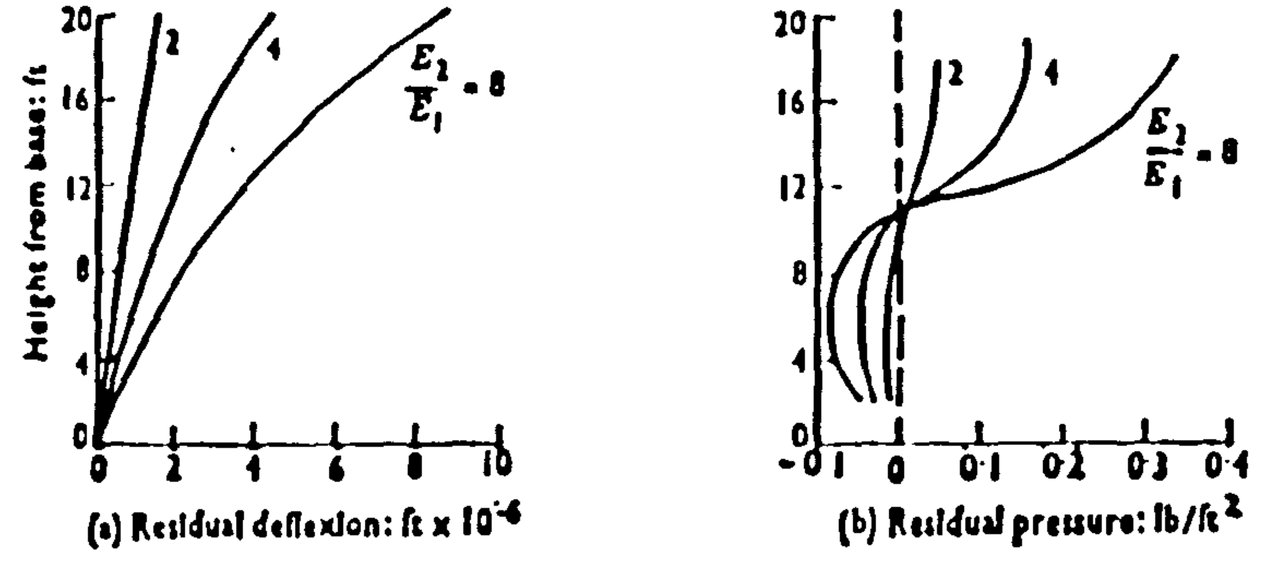

(A) RESIDUAL EFFECT OF NUMBER OF PASSES (W=1 LB/FT2)

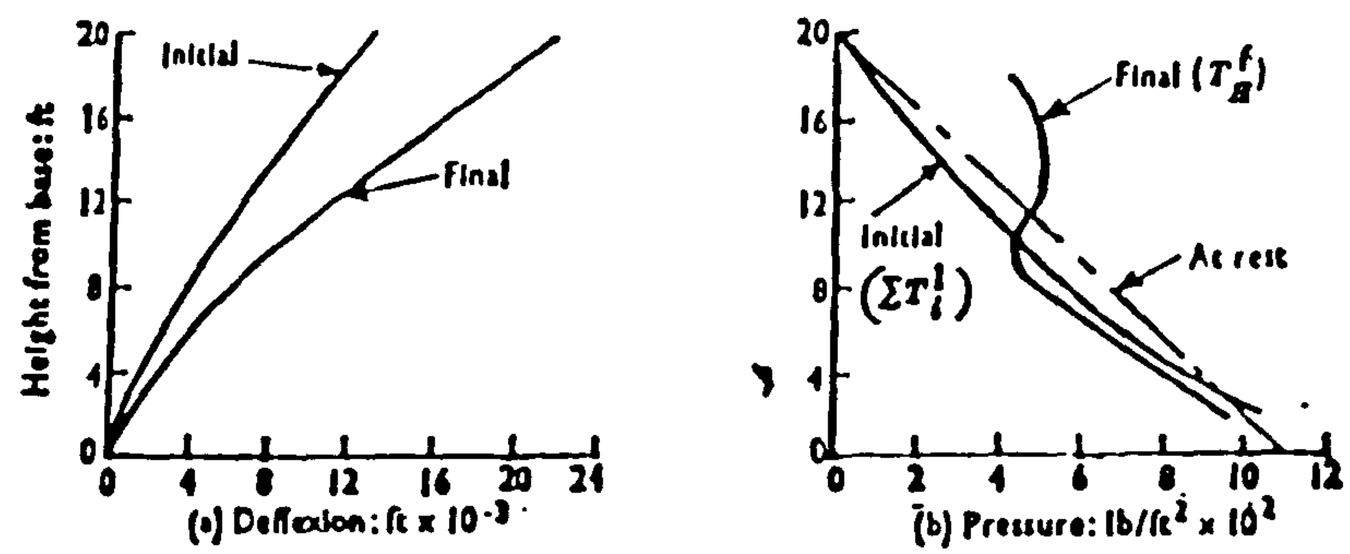

(B) FINAL CONDITIONS FOR E =8E (W=1000 LB/FT2)

FIG. (7.16) RESULT OF THE CASE STUDIES (AFTER AGGOUR AND BROWN, 1974).

7.4.2 Finite Element Compaction model: (TRRL, 1976)

Finite element analyses were performed at the Transport and Road Research Laboratory (TRRL) in England in order to explain the result of a series of large scale field tests as reported by Carder et al. (1977). These analyses were used to calculate the peak lateral stress distribution resulting from the operation of a vibratory compaction roller at various distances from a stiff but deformable wall Fig. (7.17).

The plane strain finite element analysis performed considered a roller of infinite length, although the finite length of the actual roller was taken into account by reducing the stresses acting on the wall at any given distance from the roller by a factor representing a "spreading" of stresses with distance through an area increasing by a spread angle of about 60 degrees. The soil/wall interface was modelled as completely frictionless. The vibrating compactor was modelled as a static line load of twice the magnitude of the static weight of the compactor divided by the length of the compaction roller.

The stresses generated by operation of the roller at a minimum distance of 0.15 m. from the wall (as in the actual test), for various fill heights, were calculated as shown in Fig. (7.18.A). The maximum lateral stresses induced by compaction were compared with the residual stresses measured during the actual tests and are shown in Fig. (7.18.B).

It should be noted that for the vibratory rollers investigated in the field studies, the measured dynamic loads were typically between 2−3 times the static roller weight D'Appolonia et al.,(1969), and that the assumed doubling of the static load in this case may have slightly under estimated the actual load imposed.

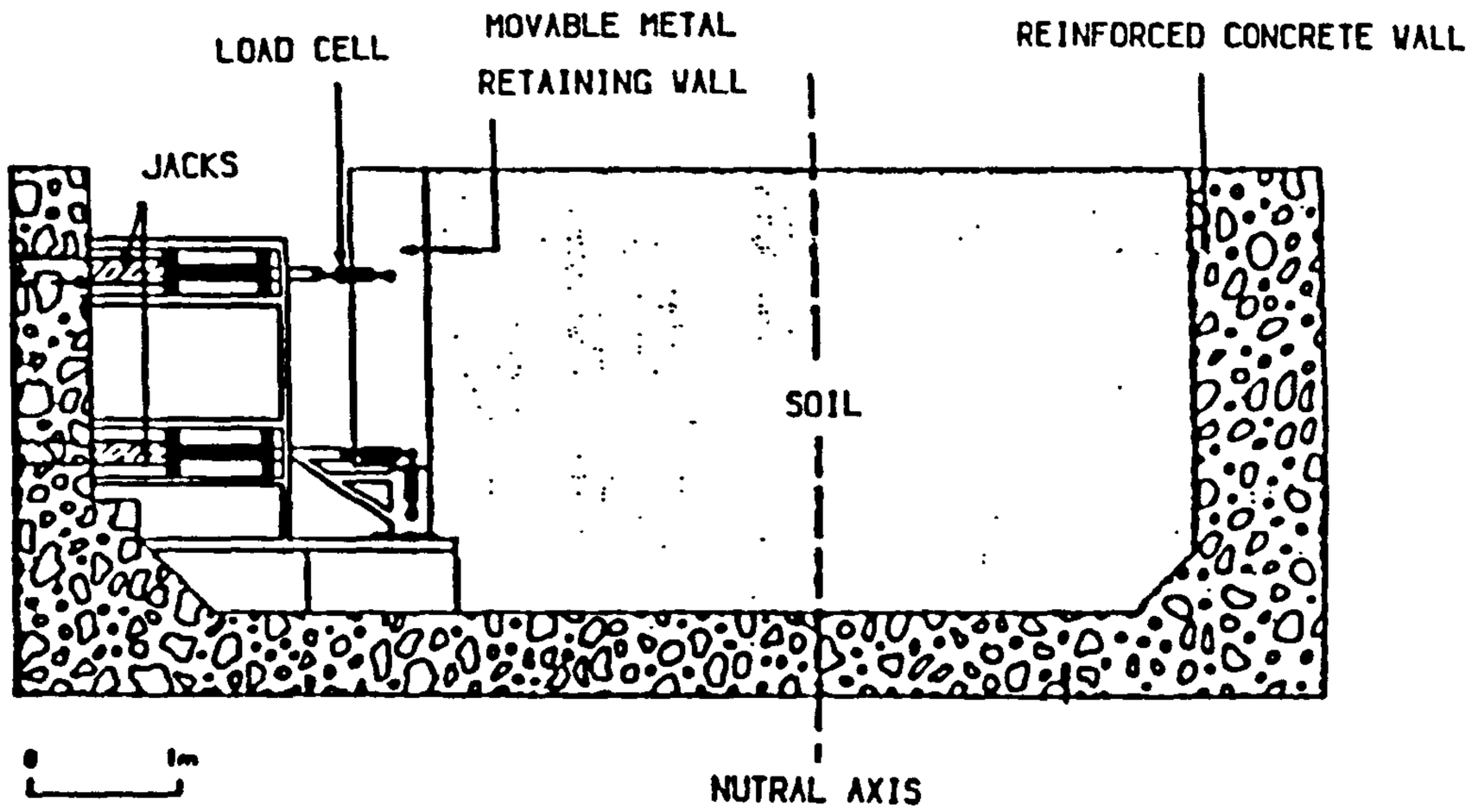

FIG. (7.17) TRRL EXPERIMENTAL WALL (AFTER CARDER ET AL., 1977).

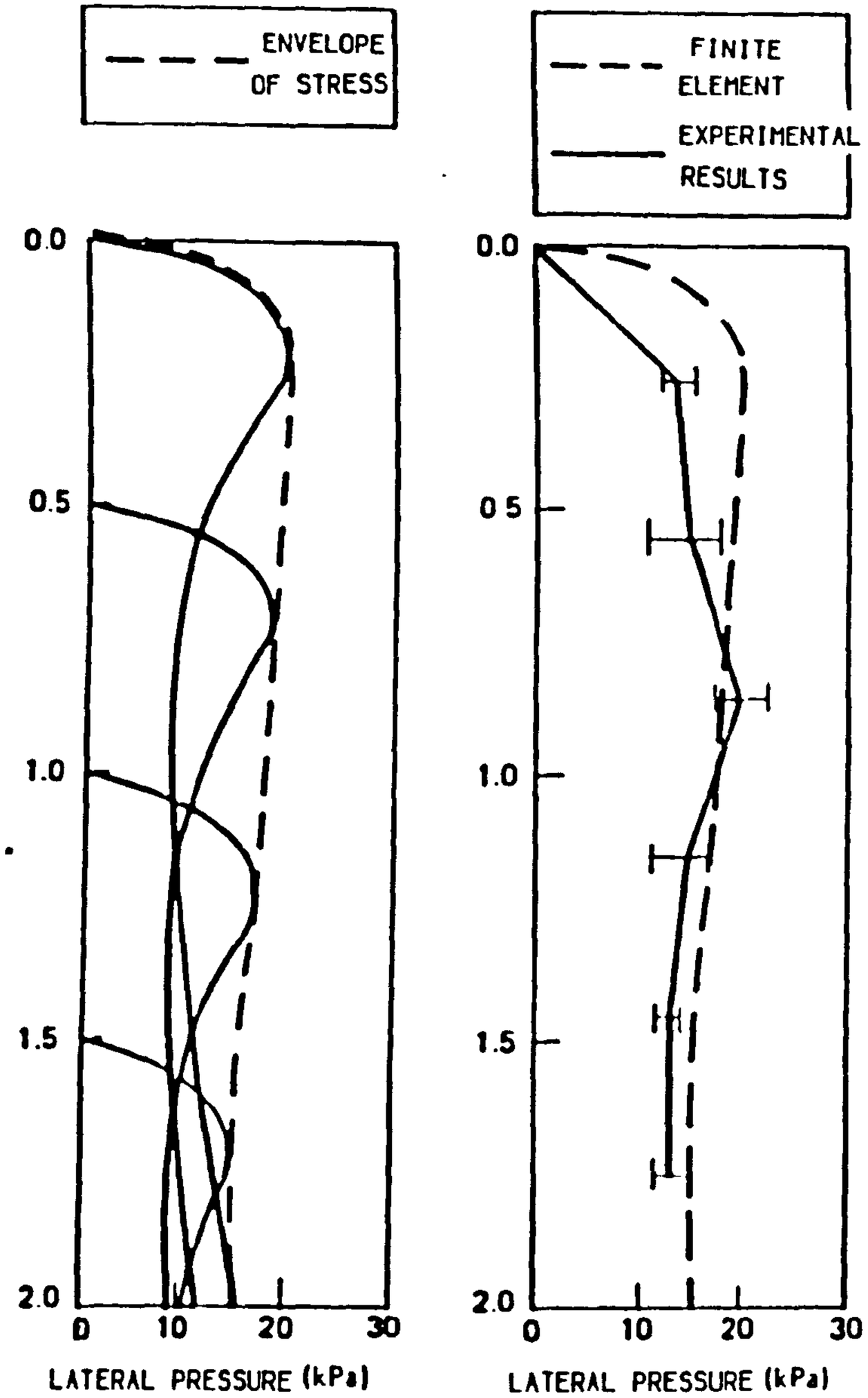

(A) EFFECT OF LAYER TYPE CONSTRUCTION

(B) COMPARISON WITH EXPERIMENTAL RESULTS

FIG. (7.18) TRRL FINITE ELEMENT ANALYSIS (AFTER TRRL, 1976).

7.4.3 Finite Element Compaction Model: (Katona, 1978)

Katona developed a finite element model to simulate the effects of compaction on the deflection of a culvert. The procedures used were as follows:

(a) The first layer was placed and compaction load was applied.

(b) As the second layer of fill was placed, the compaction surcharge pressure was applied to the surface of the new fill and simultanously applied as an equal uplift force acting at the base of the new layer of fill.

(c) Lateral pressures are generated in the new fill through a Poisson effect.

(d) The process was then repeated until the final fill layer was placed, at which point the compaction surcharge was first applied to the fill surface and then removed.

(e) All material properties were linear elastic and all soil/structure interfaces were modelled as totally adhesive boundaries. Examples of the results are shown in Fig. (7.19.A&B).

It should be noted, that there is no rational basis for determination of the magnitude of surcharge pressure to be used for modelling of compaction forces. In addition, no evidence is provided to indicate that either the magnitude or the pattern of calculated deflections provide a reasonable approximation of field performance for specific cases.

7.4.4 Finite Element Compaction Model: (Duncan and Jeyapalan, 1981)

Three different finite element analysis procedures were employed by Duncan

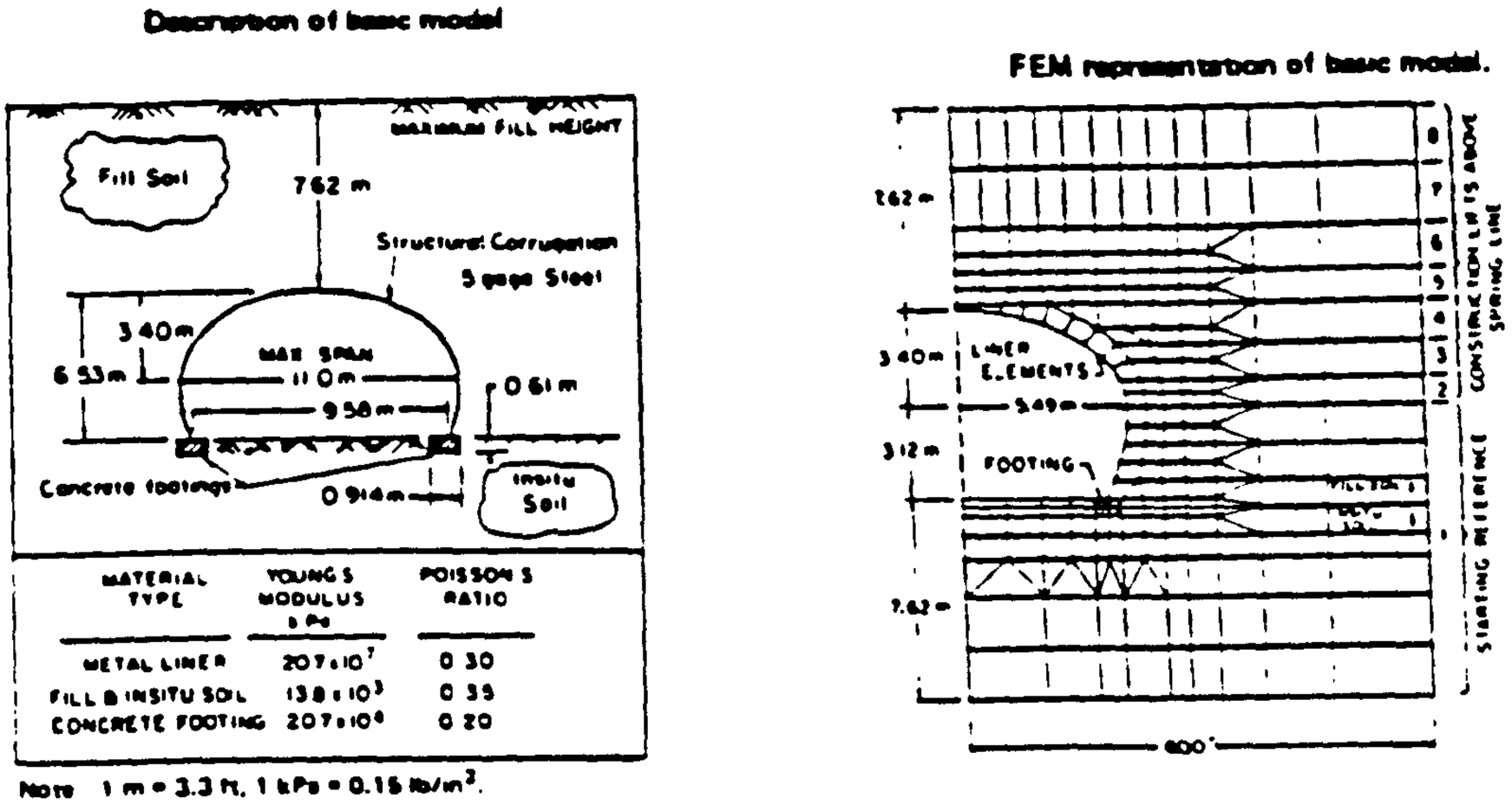

(A) EXAMPLE ANALYZED

(B) INFLUENCE OF LOADING CONDITIONS ON CROWN DEFLECTION.

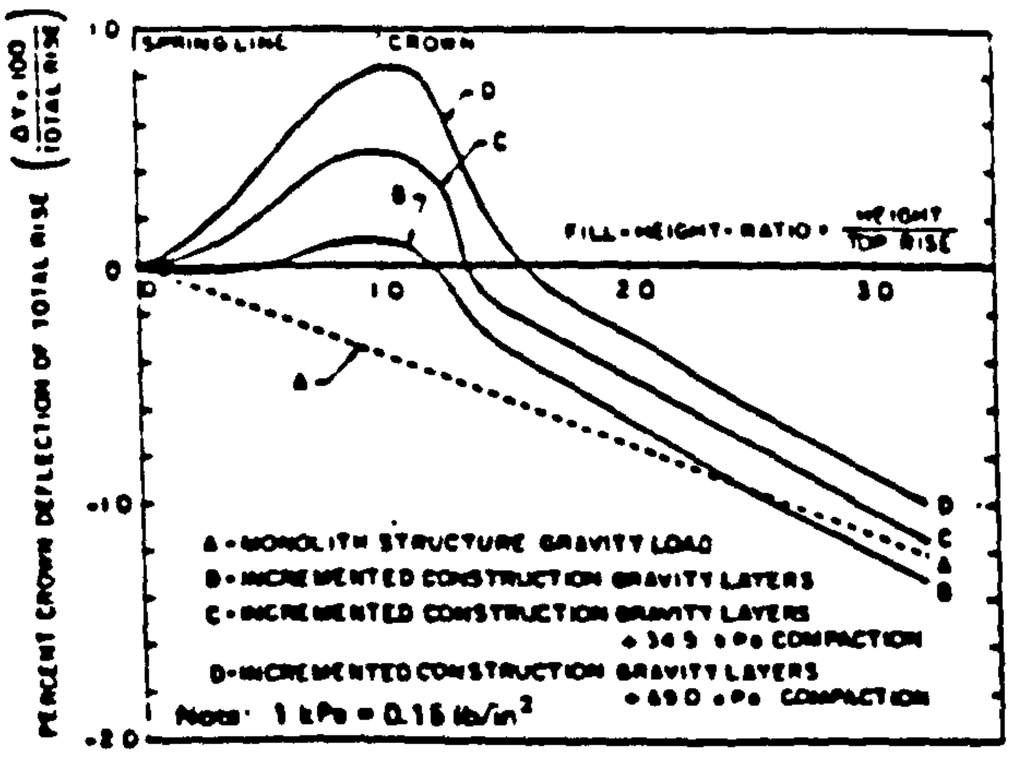

FIG. (7.19) FINITE ELEMENT ANALYSIS OF LONG SPAN CULVERT (AFTER KATONA, 1978).

& Jeyapalan (1981) to calculate the crown deflections and haunch movements observed during placement and compaction of backfill around and over a long–span aluminium culvert structure in Tice Valley, California.

All the analyses were performed used hyperbolic strength, stress–strain and bulk modulus parameters developed by Duncan et al. (1980) to model the non–linear soil behaviour, incrementally varing soil properties as a function of the existing stress states of each soil element at every stage of the analysis. Soil/structure interaction was simulated by interface elements. The first procedure was very similar to Aggour and Katona's. The second procedure was very similar to the first except that applied compaction surcharge pressures were not subsequently removed. This led to excessively large deflections and did not agree with field observation.

The third procedure was performed in several stages:

(a) A complete analysis was performed modelling all fill layers without any effect of compaction.

(b) The stresses and deflections calculated immediately after placement of the first layer were used as initial conditions for calculating the deflections resulting from compaction of this first layer.

(c) Compaction was again modelled as the application of a uniform surcharge pressure but not removed.

(d) This previous process was then repeated incrementally until the fill reached the crown of the culvert. After the fill had reached the crown , the

subsequent placement of additional layers of fill was modelled without further consideration of the effects of compaction. The results are shown in Fig. (7.20.A&B).

No attempt was made to model the actual compaction process with respect to the actual dimensions, weight of the compaction plant and number of passes.

7.5 CONCLUSION

The finite element method provides a good tool to tackle soil mechanics problems. Reinforced earth wall problems have been successfully approximated from three dimensions to two dimensions and represented by both composite and discrete finite element approaches. Both approaches seem to give good results when reinforcement slippage and edge effects are taken into account. The biggest advantage of the discrete model is that it gives direct knowledge of the individual components of the reinforced earth wall.

The models developed are unable to model the compaction stresses that may be realized when actually constructing an earth wall because the following are lacking:

(a) Modelling of nonlinear soil properties.

(b) Realistic modelling of soil/structure interaction.

(c) Consideration of the actual dimensions and weight of compaction plant.

(d) Consideration of the factors affecting the loading/unloading characteristics of the soil (K_o).

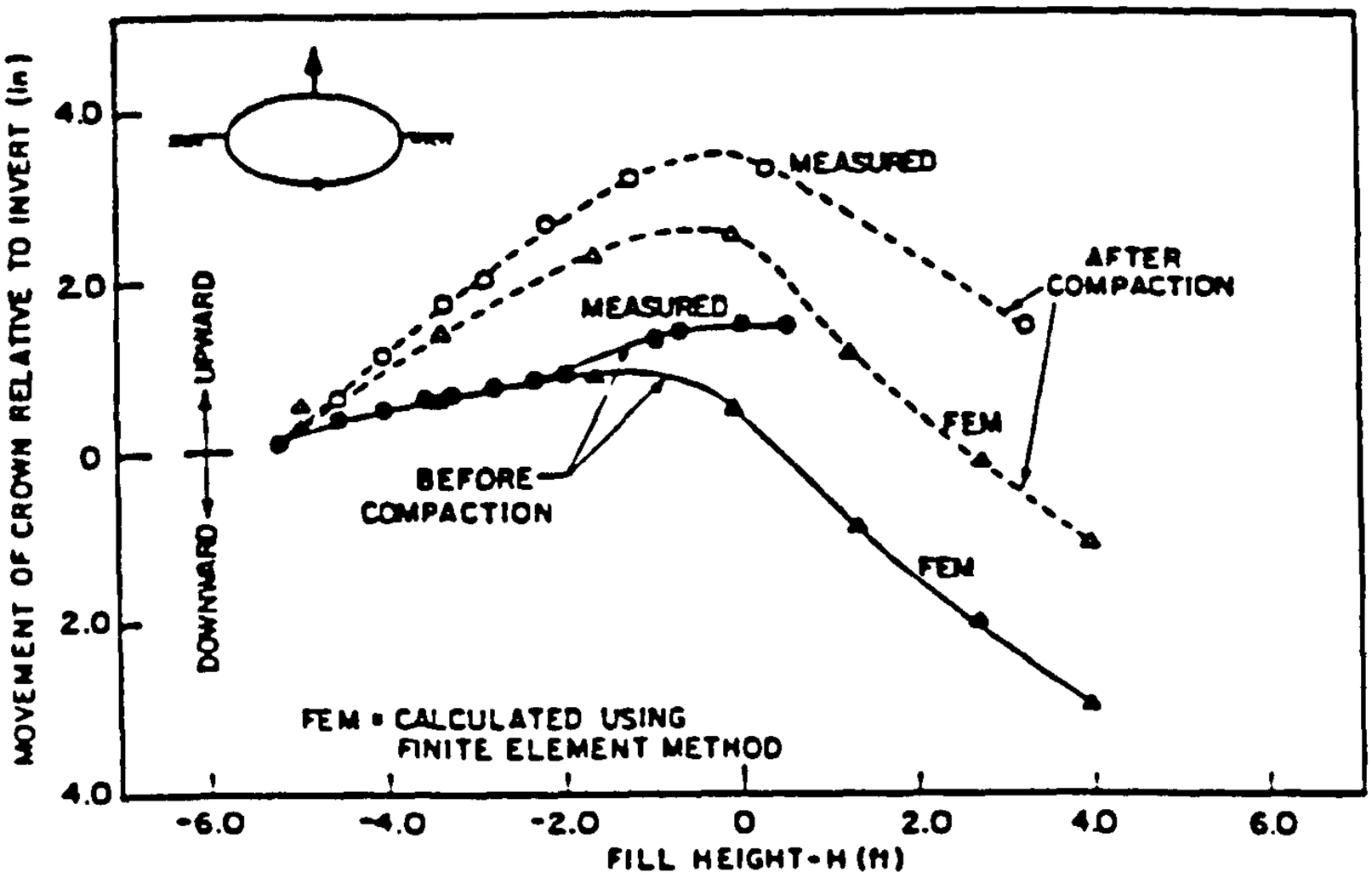

(A) COMPARISON OF MEASURED AND CALCULATED CROWN MOVEMENTS.

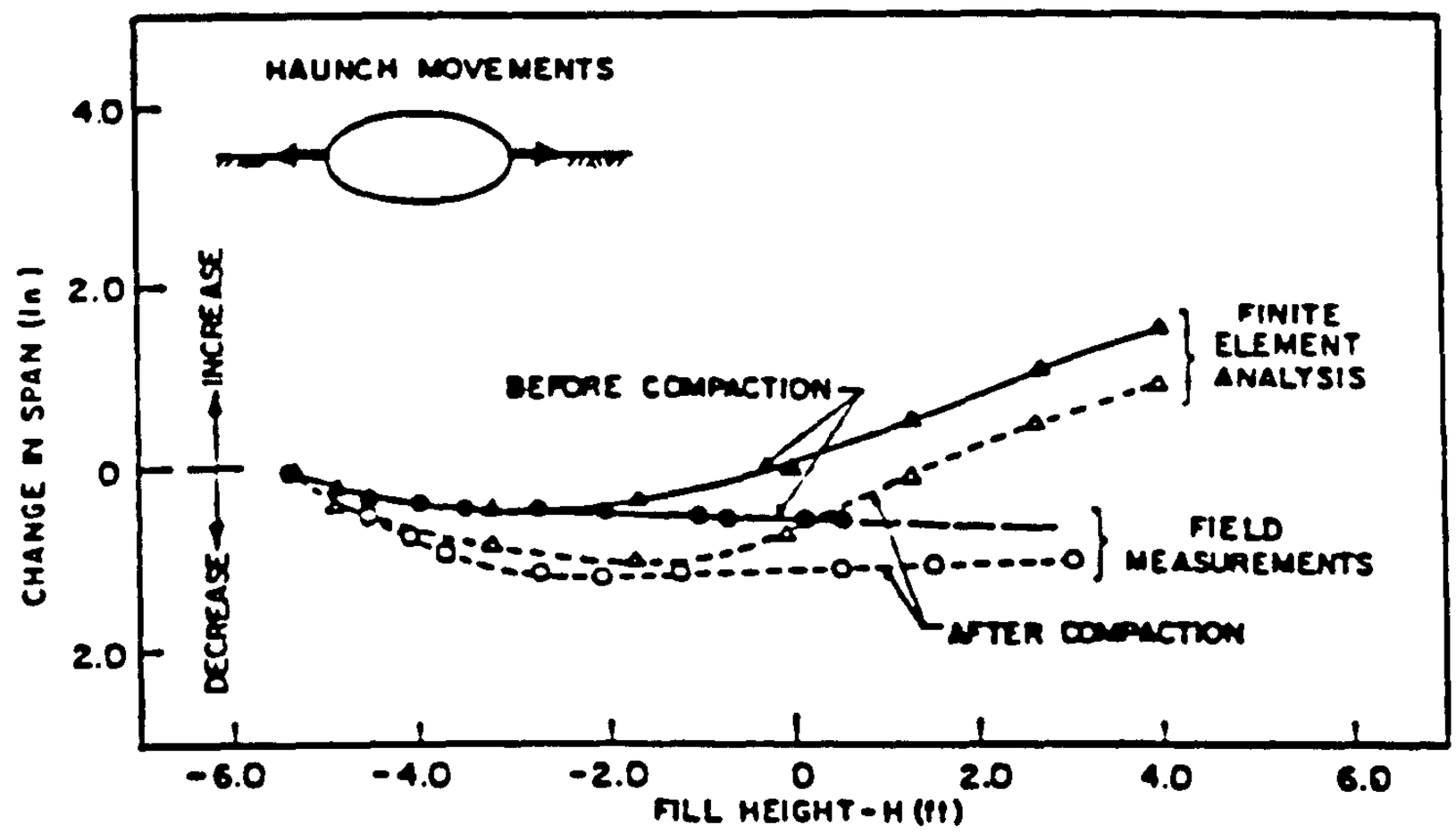

(B) COMPARISON OF MEASURED AND CALCULATED HAUNCH MOVEMENTS.

FIG. (7.20) FINITE ELEMENT ANALYSIS OF TICE VALLEY CULVERT (AFTER DUNCAN AND JEYAPLON, 1981).

In view of the foregoing statements it is obvious that existing techniques, although capable of providing results relating to reinforced earth walls, still suffer from being unable to fully take into account the effects of compaction and construction procedures. The following chapter will take these into account.

CHAPTER 8

COMPUTER ANALYSIS

BY FINITE ELEMENT METHOD

8.1 INTRODUCTION

This chapter presents finite element analysis techniques which provide a means of evaluating the effect of compaction on the behaviour of a reinforced earth retaining wall. The objectives of the study and the method of analysis are given. The main features and descriptions of the finite element program employed in the analysis are illustrated as well as a new method of modelling compaction plant. A detailed example of an idealization of one of the laboratory model tests, with the testing programme and data used are presented in this chapter, and a conclusion is given at the end.

8.2 OBJECTIVES OF THE PRESENT STUDY

Studying the effect of compaction on the behaviour of a reinforced earth retaining wall needs several variables and parameters to obtain a clearer understanding of the stresses and strains in the reinforced earth wall and the compaction effects on it.

The following parameters were measured in the model tests presented in

Chapter (2):

(i) The forces in the strips.

(ii) The horizontal and vertical pressure at the wall face.

(iii) The horizontal and vertical pressure just behind the reinforced mass.

(iv) The vertical and horizontal pressure at the bottom of reinforced mass.

(v) the horizontal deflection of the wall face.

These measurements were taken before, during and after compaction of each layer, and variable compaction lengths were also considered. Although these constitute most of the important parameters needed to study the performance of a reinforced earth wall under compaction effect, there are some variables which were either not observed nor could be calculated from the observed data. These are:

(i) The shear stress in the soil.

(ii) The principal stresses.

(iii) The angle of orientation of the major principal stresses with the horizontal.

(iv) Horizontal, vertical and total deflections in the soil.

(v) The shear strain in the soil.

(vi) The principal strains in the soil and their orientation.

(vii) The total movement of the wall face.

(viii) Bending moment, shearing force, and normal force in the wall face.

The present finite element analysis was carried out using a program SSCOMP (Seed & Duncan, 1988). The program was supplied by Professor Seed with the warning that it had not been fully tested and might require some development.

The program was adapted to simulate a small scale as well as a full scale model and increase its accuracy. The program, as developed, was used :

(i) To calculate all the variables previously outlined before and after compaction of each layer of soil, modelling the construction sequence as in the field.

(ii) To compare the theoretical values with the experimentally observed results from the model tests and obtain a more complete picture of the compaction effect on reinforced wall behaviour.

8.3 METHOD OF ANALYSIS

The analysis made by the program (SSCOMP) considers the soil, the reinforcing strips, the wall face, and their interaction. It is therefore based on the discrete analysis approach, which considers the characteristics of the individual components of the reinforced earth wall and their interaction as explained in Chapter (7). The analysis is also based on a consideration of:

(i) Non– linear soil behaviour.

(ii) Linear structural behaviour.

(iii) Modelling the sequence of construction as it happens in the field.

(iv) Modelling of compaction which produces horizontal stresses and deflections of the wall.

(v) The profile of effective horizontal stresses from compaction vs. depth which may be assigned at various locations (in X– direction). This profile is determined, using program (BCOMPP) devised by the author which takes into consideration the actual weight and dimensions of the compaction plant i.e. the nature of the three dimensional problem. Details of the program have been explained in Sec. (6.5.7). A Fortran list is provided in Appendix C Sec. (C.1).

8.4 DESCRIPTION AND FEATURES OF PROGRAM (SSCOMP)

The program is a general, plane strain, soil structure interaction program for static analysis of geotechnical problems including consideration of the compaction effects.

The original soil analysis technique was coded by Ozawa (program ISBILD, 1973), using the nonlinear finite element analysis procedures developed by Kulhway et al. (1969), and the soil structure interaction capability was programmed by Dickens (program SSTIP, 1973). Kais– way (1979) incorporated a new non– linear model of the soil developed by Duncan et al. (1980), in a program (SSTINP, 1979). The organization of program SSCOMP follows the general programming concepts and solution technique of the program SAP developed by Wilson (1970), (Seed and Duncan, 1984).

SSCOMP has been developed by Seed and Duncan (1983). They incorporated a new general bilinear model for analysis of the compaction effect and modified the nonlinear soil model. Program SSCOMP consists of the main program SSCOMP and twenty three subroutines.

8.4.1 Types Of Elements

There are five types of element to model the soil and soil structure interaction. They are as follows:

(a) Soil elements– four node, two dimensional isoparametric elements with compatible modes of displacement as shown in Fig. (8.1.A).

(b) Bar element– two node elements with axial stiffness only (no moment or shear resistance).

(c) Beam elements– also two node elements which can resist axial forces, shear forces and bending moments.

(d) Nodal links– made up of two springs which control the relative displacements between two nodal points , Fig. (8.1.B). This type was proposed by Goodman et al. (1968).

(e) Interface elements– the interface elements consist of two nodal links. Each link is made up of a normal and shear spring. The element thickness is zero and capable of modelling soil–structure interface conditions. The normal spring coefficient is nonlinear, stress dependent and inelastic. The interface element is a type proposed by Goodman et al. (1968) and shown in Fig. (8.1.C).

8.4.2 Models Employed In The Program

(a) Soil model

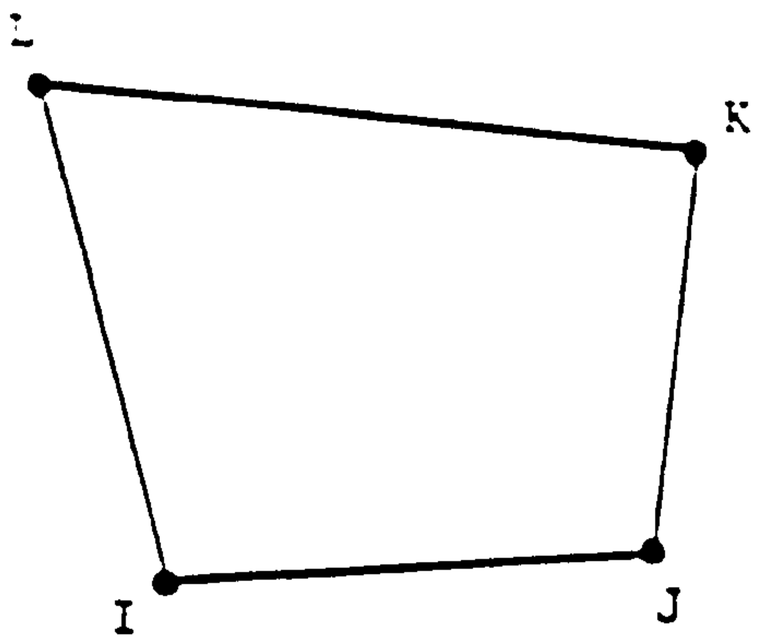

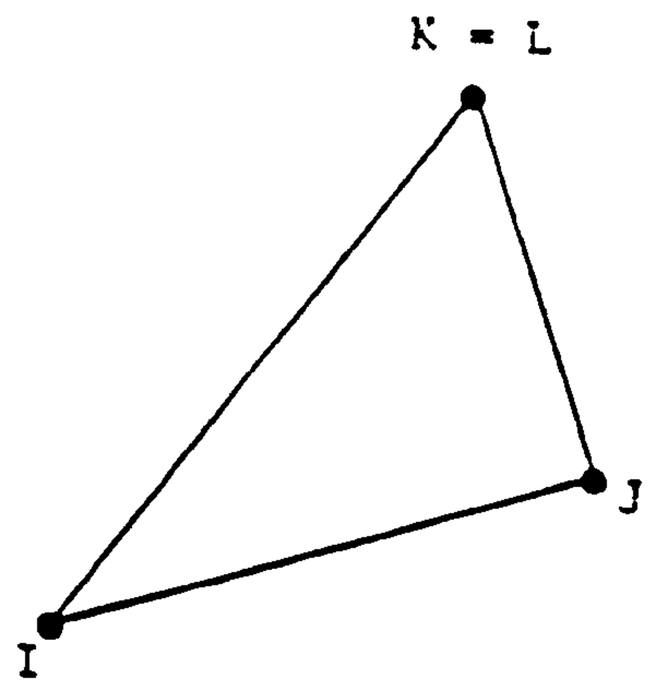

(A) SOIL ELEMENT.

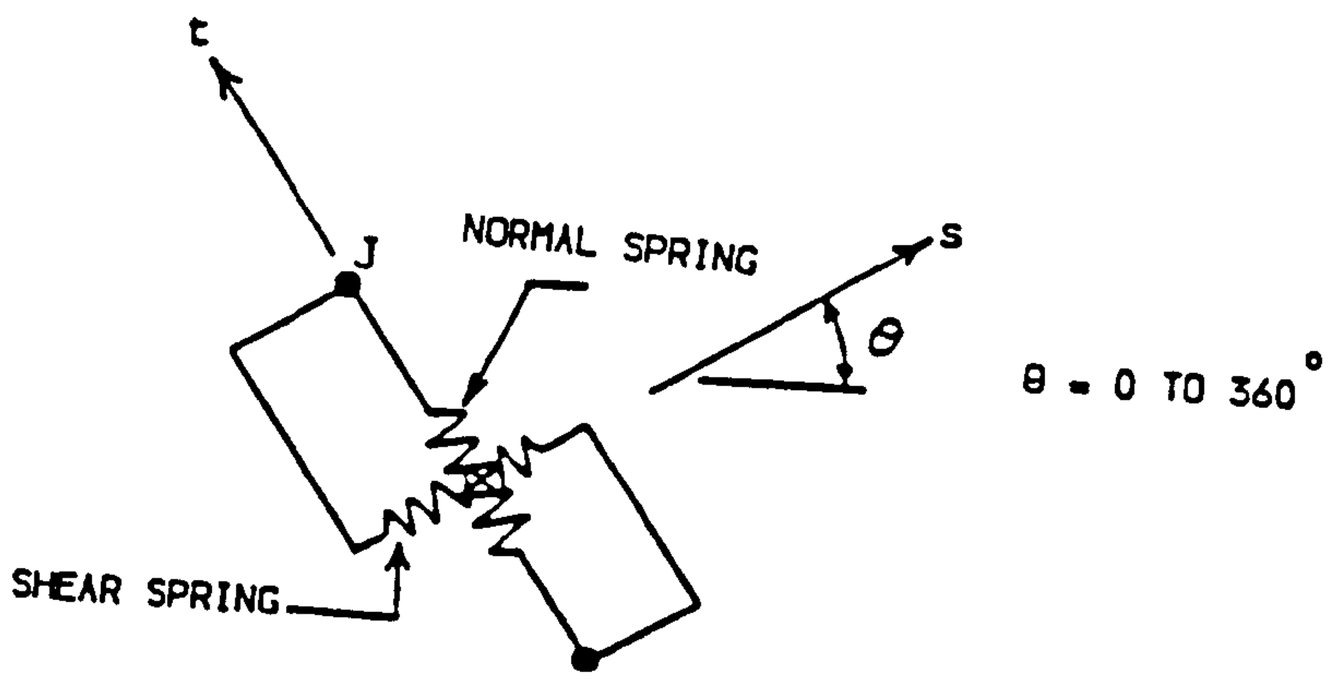

I

(B) NODAL LINK.

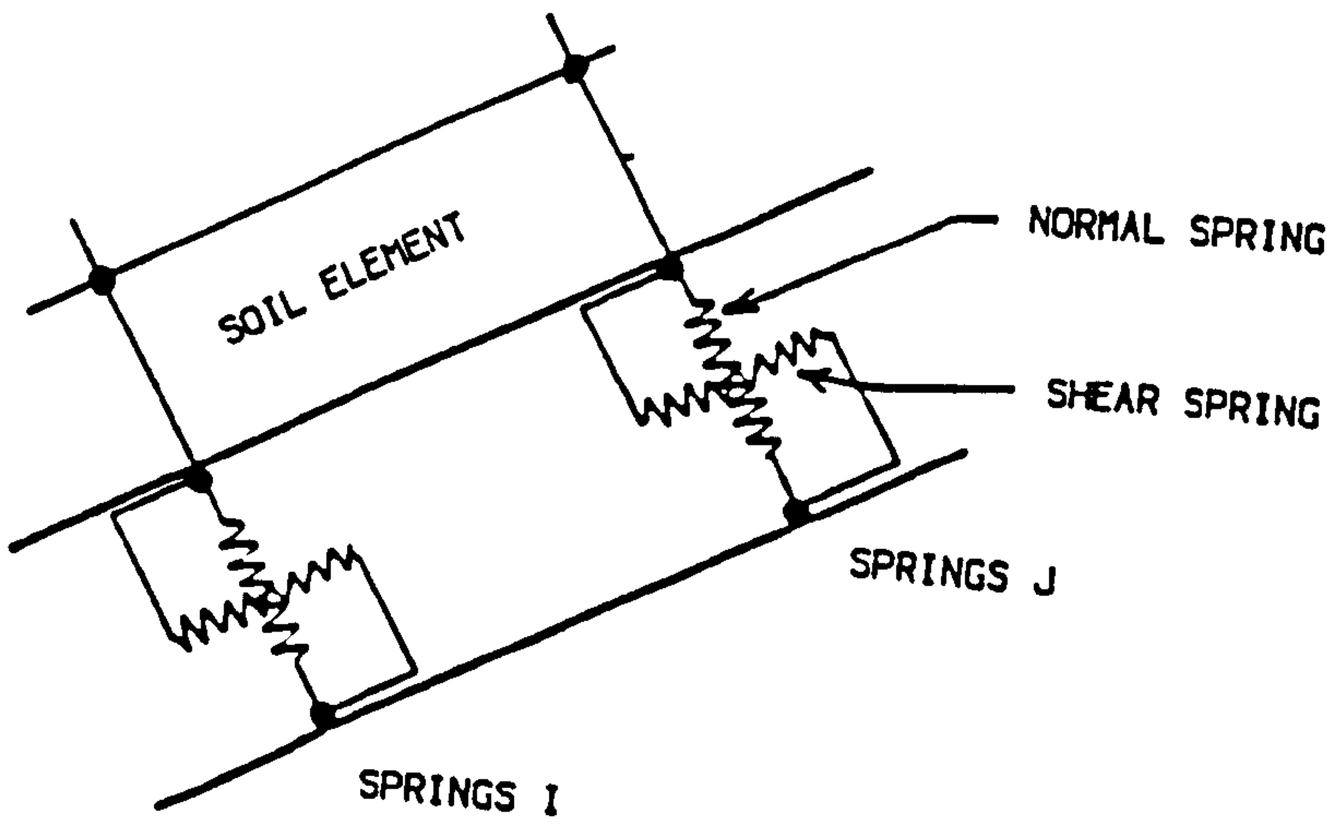

(C) INTERFACE ELEMENT.

FIG. (8. 1) TYPES OF ELEMENTS EMPLOYED IN PROGRAM (SSCOMP).

The non–linear stress–strain and volumetric strain behaviour of the soil is modelled using the hyperbolic formulation proposed by Duncan et al. (1980) and then modified by Seed and Duncan (1983). The original model by Duncan et al. (1980) employed a hyperbolic representation of the stress–strain relation Fig. (8.2.A&B). The model determines the soil moduli from the following relationships:

Tangent modulus,

$$E_t = (1 - R_f\ SL)^2\ K\ P_a\ \left(\frac{\sigma_3}{P_a}\right)^n \qquad (8.1)$$

Initial modulus.

$$E_i = K\ P_a\ \left(\frac{\sigma_3}{P_a}\right)^n \qquad (8.2)$$

Unloading–reloading modulus,

$$E_{ur} = K_{ur}\ P_a\ \left(\frac{\sigma_3}{P_a}\right)^n \qquad (8.3)$$

The bulk modulus,

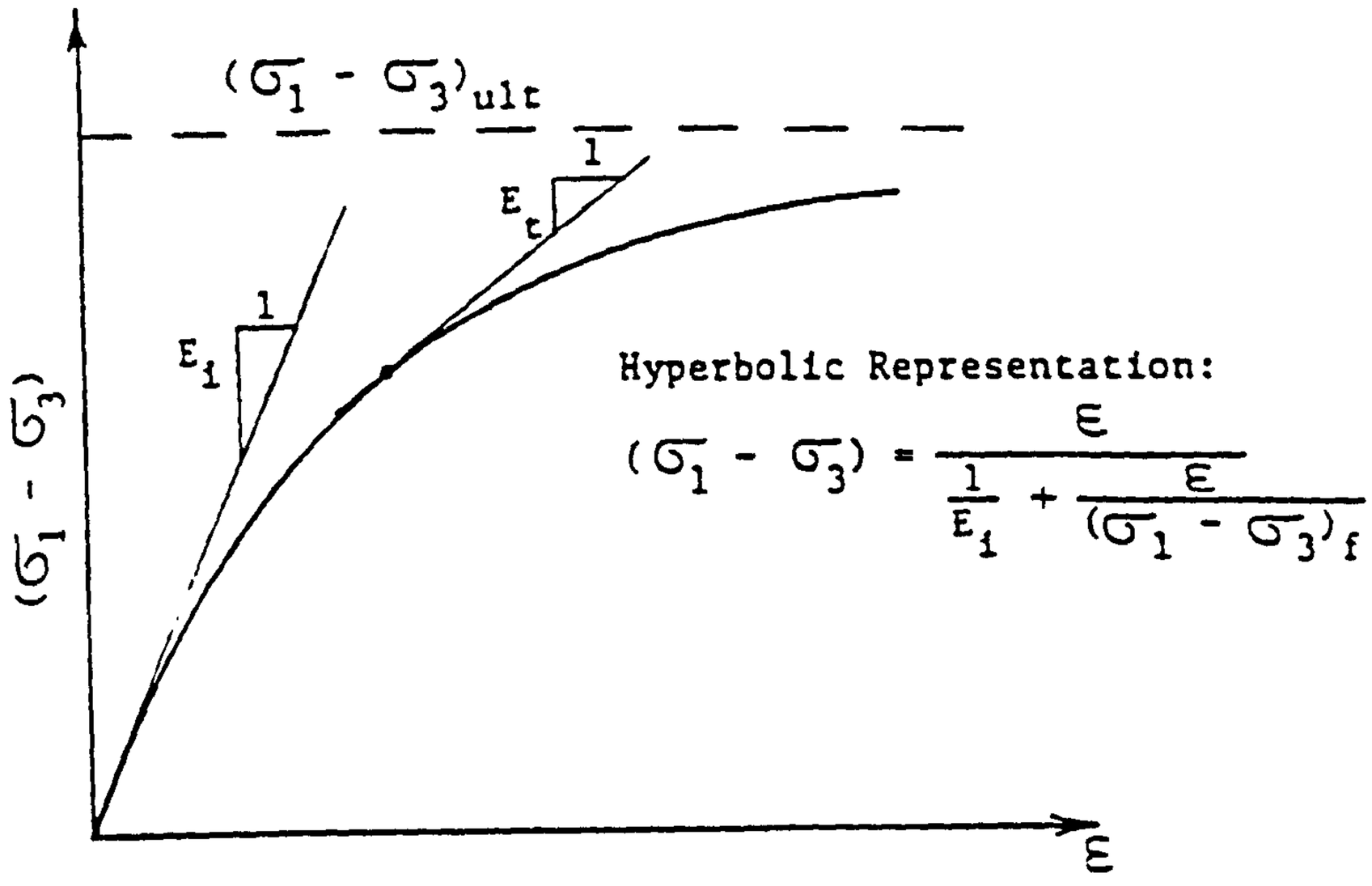

Hyperbolic Representation:

$$(\sigma_1 - \sigma_3) = \frac{\varepsilon}{\frac{1}{E_i} + \frac{\varepsilon}{(\sigma_1 - \sigma_3)_f}}$$

(A) HYPERBOLIC REPRESENTATION OF STRESS-STRAIN CURVE FOR PRIMARY LOADING.

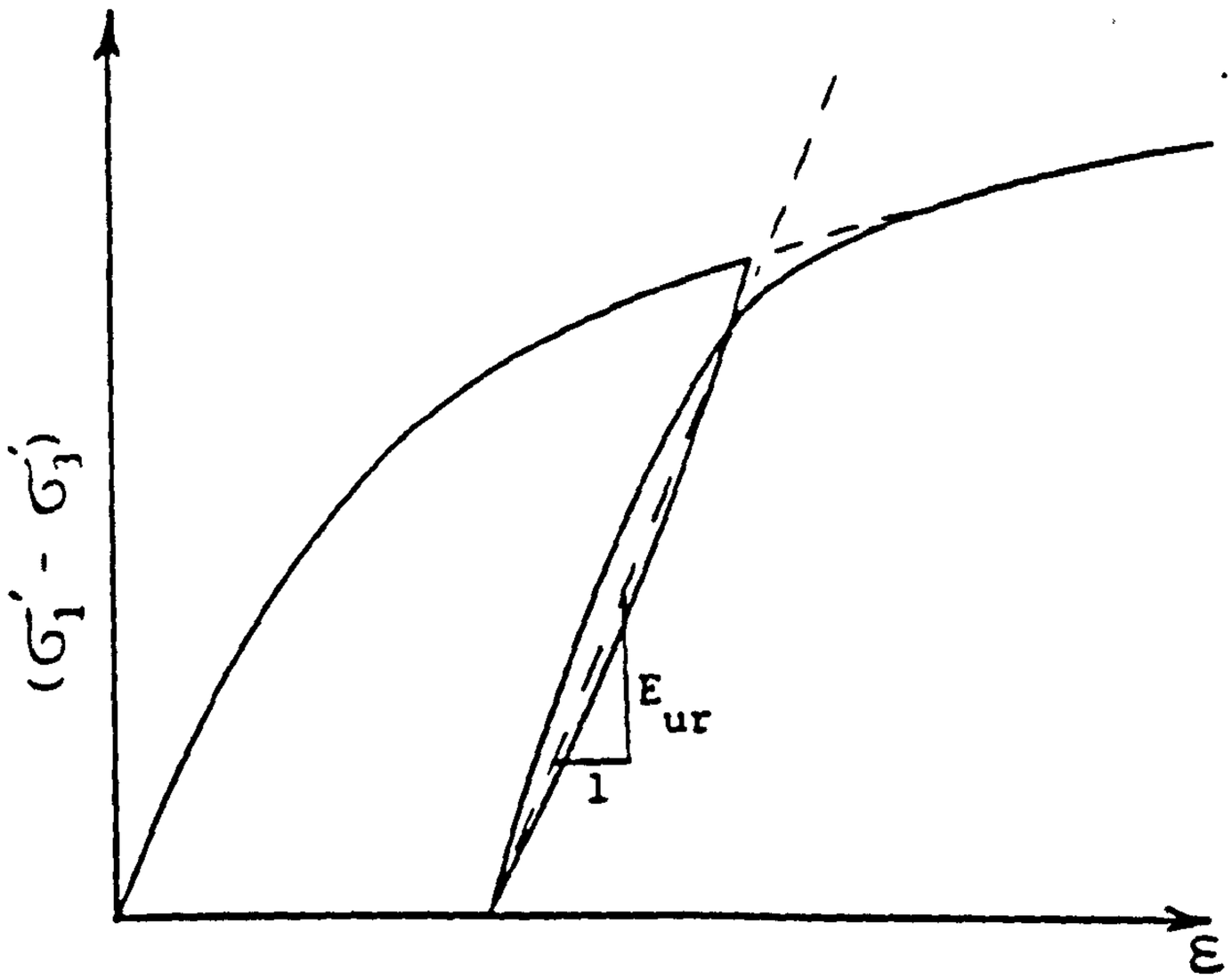

(B) LINEAR UNLOADING-RELOADING STRESS-STRAIN RELATIONSHIP.

FIG. (8.2) HYPERBOLIC SOIL MODEL (AFTER DUNCAN ET. AL., 1980).

$$B = K_B P_a \left(\frac{\sigma_3}{P_a} \right)^m \qquad (8.4)$$

The above model has been modified by Seed and Duncan (1983) to prevent underestimation of lateral stresses in soil elements with small confining stresses and low stress level, adopt the stress state criteria and eliminate the sudden discontinuity at the point of transition from a primary loading modulus (E_t) to the unloading– reloading modulus(E_{ur}) as shown in Fig. (8.3.A&B).

Where:

SL is stress level defined as $(\sigma_1 - \sigma_3)/(\sigma_1 - \sigma_3)_f$.

$(\sigma_1 - \sigma_3)_f$ is the deviator stress to cause failure.

K & n are dimensionless model parameter constants relating to E_i.

R_f is 0.60 to 0.90 for most soil.

P_a is atmospheric pressure.

K_{ur} is (1.2 to 3) K.

K_B & m are dimensionless model parameters

The soil layer being placed is assigned very small modulus values to simulate the fact that a newly added layer of fill has very low stiffness. For each soil element in the newly placed layer the program calculates initial stresses consistent with the overburden pressure at its centre and the slope of the soil surface.

(b) Structural model

The models of structural elements (bar & beam elements) were assumed to be linear i.e. in elastic stage.

(c) Compaction model

A general bilinear model has been used to represent compaction induced stresses within the reinforced soil mass. A brief description is given below and for more detail see Seed and Duncan (1983 & 1986). The model is a hysteretic

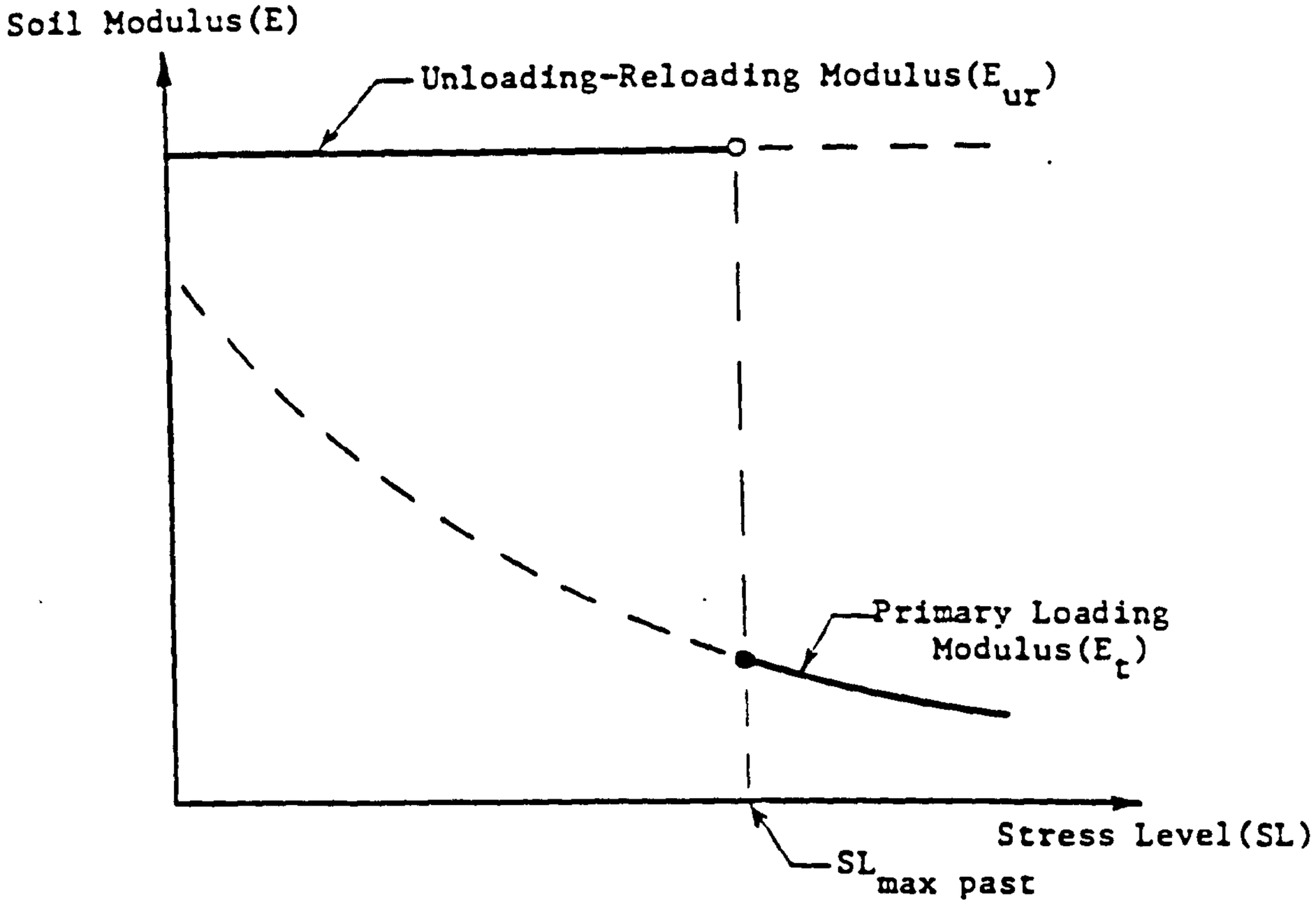

(A) PREVIOUS MODEL FOR UNLOADING-RELOADING MODULI.

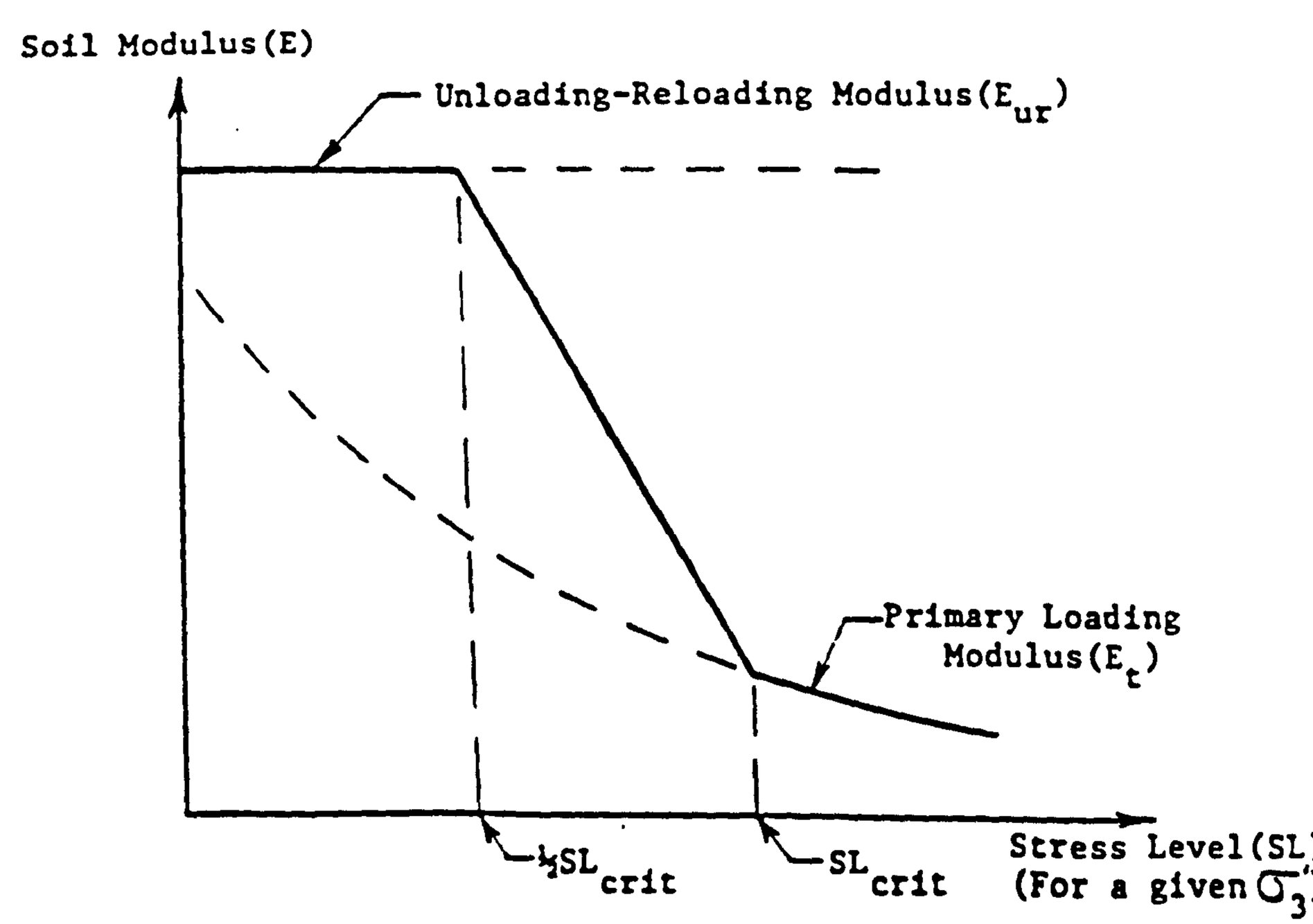

(B) PROPOSED MODEL FOR UNLOADING-RELOADING MODULI.

FIG. (8.3) MODIFIED HYPERBOLIC SOIL MODEL (AFTER SEED&DUNCAN, 1983).

soil model and was used to model the loading– unloading of the soil due to the compaction process. Fig. (8.4) shows the stress path for a single cycle of K_o loading– unloading– reloading.

Compaction induced stresses in previously uncompacted soils have been found to follow this type of stress path. During compaction, the stresses reach point A along the K_o line. After removal of compaction plant, the soil relaxes to point B. In the next loading increment the stress path moves along line BR. If the increment of loading is sufficiently large, the stress path will intercept the K_o loading line and continue up this line to a new maximum stress level. The model used in the program is based on a linear representation of the K_o loading– unloading stress path as shown in Fig. (8.5), and the parameters required for the model are shown in Table (8.1) and Fig. (8.5).

The analysis uses the maximum lateral compaction stresses ($\Delta\sigma_{hm,c}$) induced during compaction as a result of the most critical position of the compaction plant. Once the maximum lateral compaction stress profile for the whole wall is entered into SSCOMP, the compaction induced stresses are determined in two steps:

(i) The equivalent maximum increase in vertical stress $\Delta\sigma_{vm,e}$ is calculated:

$$\Delta\sigma_{vm,e} = \frac{\Delta\sigma_{hm,c}}{K_o} \qquad (8.5)$$

Where $\Delta\sigma_{hm,c}$ is the maximum increase in lateral stress.

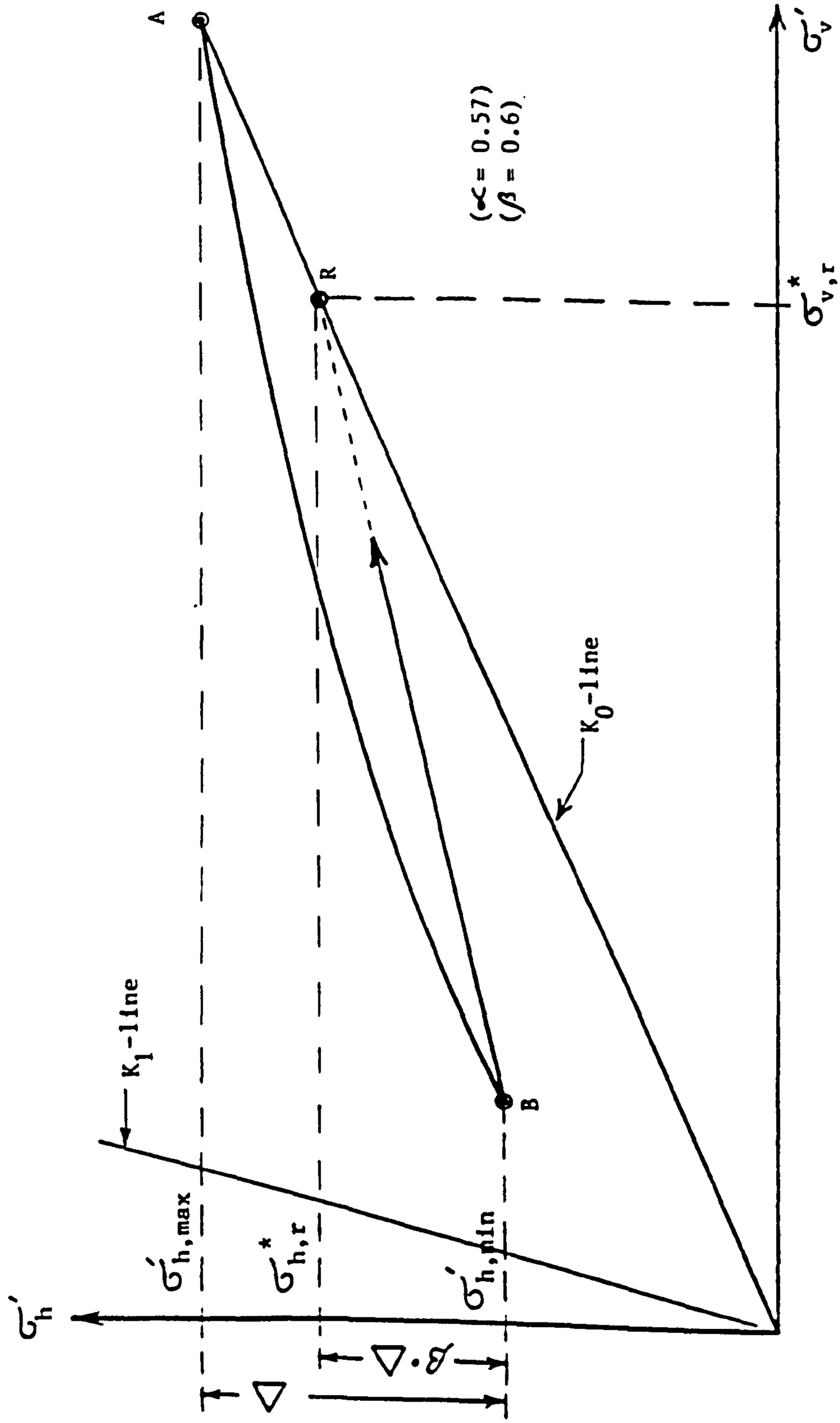

FIG. (18. 4) STRESS PATH FOR FIRST CYCLE-K_o LOADING/UNLOADING (AFTER SEED & DUNCAN, 1983).

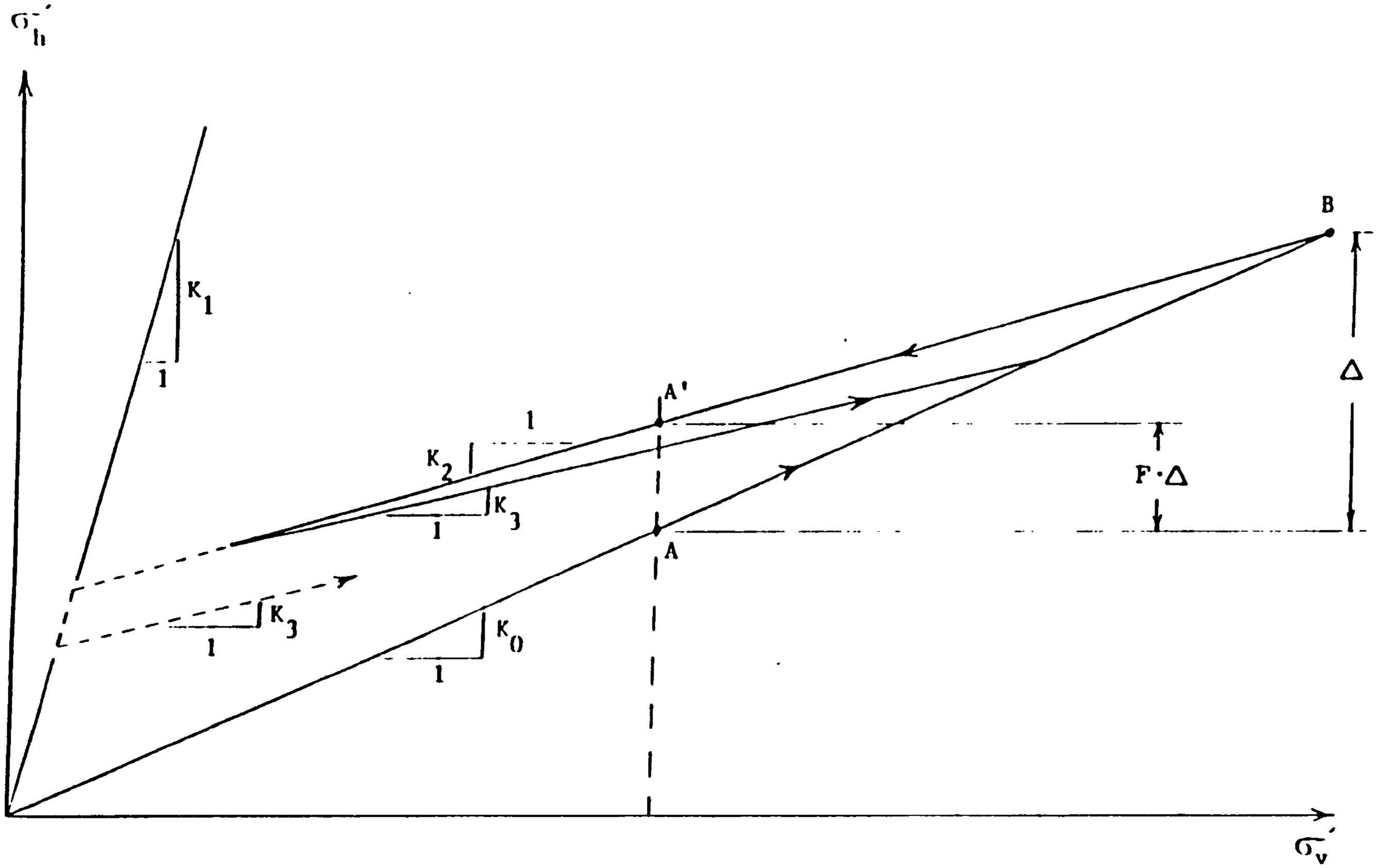

FIG. (8.5) LINEAR REPRESENTATION OF STRESS PATH FOR K_o LOADING/UNLOADING AND BASIC PARAMETERS OF BILINEAR MODEL (AFTER SEED&DUNCAN, 1983)

TABLE (8.1) BI-LINEAR K_o-LOADING/UNLOADING MODEL PARAMETERS (AFTER SEED&DUNCAN, 1983).

Parameter	Name or Description	Recommended Limits	Recommended Method of Estimation Based on Non-Linear Model Parameters
K_0	Coefficient of At-Rest Lateral Earth Pressure for Virgin Loading	$0 \leq K_0 \leq 1$	Same as Non-Linear Model (Recommended: $K_0 \approx 1 - \sin\phi'$)
$K_{1,\phi',B}$	Frictional Component of Limiting Coefficient of At-Rest Lateral Earth Pressure for Unloading	$K_0 \leq K_1 \leq K_p$	$K_1 \approx 2/3\ K_{1,\phi'} = (2/3)\ \tan^2(45 + \phi'/2)$
c_B'	Effective Stress Strength Envelope Cohesion Intercept	$c_B' \geq 0$	$c_B' \approx 0.8\ c'$
F or K_2 $K_2 = K_0(1-F)$	Fraction of Peak Lateral Compaction Stress Retained as Residual Stress for Virgin Soil Incremental Coefficient of At-Rest Lateral Earth Pressure for Unloading	$0 \leq F \leq 1$ $K_0 \geq K_2 \geq 0$	F (or K_2) should be chosen such that the bi-linear unloading stress path intersects the α-type non-linear unloading stress path at a suitable OCR. Recommended: $F = 1 - \frac{(OCR - OCR^{\alpha})}{(OCR - 1)}$ where a suitable OCR for "matching" the bi-linear and non-linear unloading curves is typically OCR $\approx$ 5.
K_3	Incremental Coefficient of At-Rest Lateral Earth Pressure for Reloading	$0 \leq K_3 \leq K_0$	K_3 K_2 ($= K_0 \times (1 - F)$)

Note: $\sigma_{h,lim}' = K_1\sigma_v'$ and $K_1 = K_{1,\phi',B} + \frac{2c_B'}{\sigma_3'}\sqrt{K_{1,\phi',B}}$

(ii) The bilinear model then generates a loading path based on the stress change $\Delta\sigma_{vm,e}$. Compaction loading– unloading is considered to result in no net change in vertical stress. After loading to the peak point, the bilinear model is used to simulate the unloading stress path to the original vertical effective stress prior to compaction.

(d) Model of the compaction loading– unloading

The result of the compaction process is that there is no change in the effective vertical stress, so the effects of multiple cycles of loading from a given compaction plant can be effectively modelled by considering loading cycles to the peak loading condition, followed by a single unloading cycle to the original effective stress.

(e) Modelling construction sequence

The actual construction sequence has been modelled by simulating the construction operations in a number of steps in an incremental analysis. These consist of:

(i) Placement of a layer of fill.

(ii) Compaction of layer of fill.

(iii) Placement of a structure.

(v) Application of loads to a complete structure and/or a partially or wholly completed soil mass.

Each increment is analyzed twice. The results of the second iteration of each increment are retained, and the changes in stress and strain in soil,

interface elements, the changes in force and moment in bar and beam elements, and the changes in nodal point displacement during each increment are added to the value at the begining of the new increment.

8.4.3 Flow Chart

The flow chart of the (SSCOMP) program and all subroutines employed in the program have been given as follows:

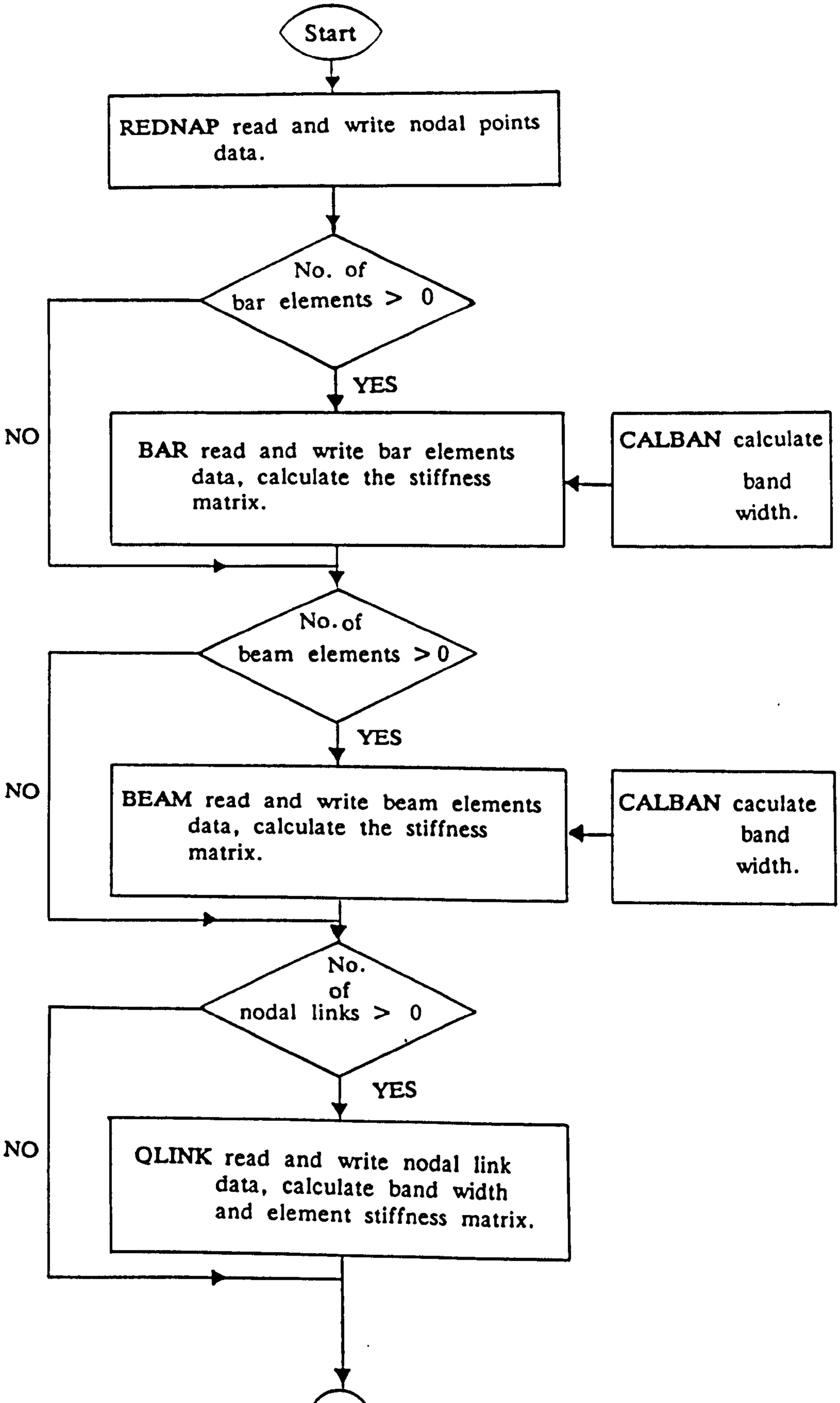
Start
REDNAP read and write nodal points data.
No. of bar elements > 0
YES
NO
BAR read and write bar elements data, calculate the stiffness matrix.
CALBAN calculate band width.
No. of beam elements > 0
YES
NO
BEAM read and write beam elements data, calculate the stiffness matrix.
CALBAN caculate band width.
No. of nodal links > 0
YES
NO
QLINK read and write nodal link data, calculate band width and element stiffness matrix.
1

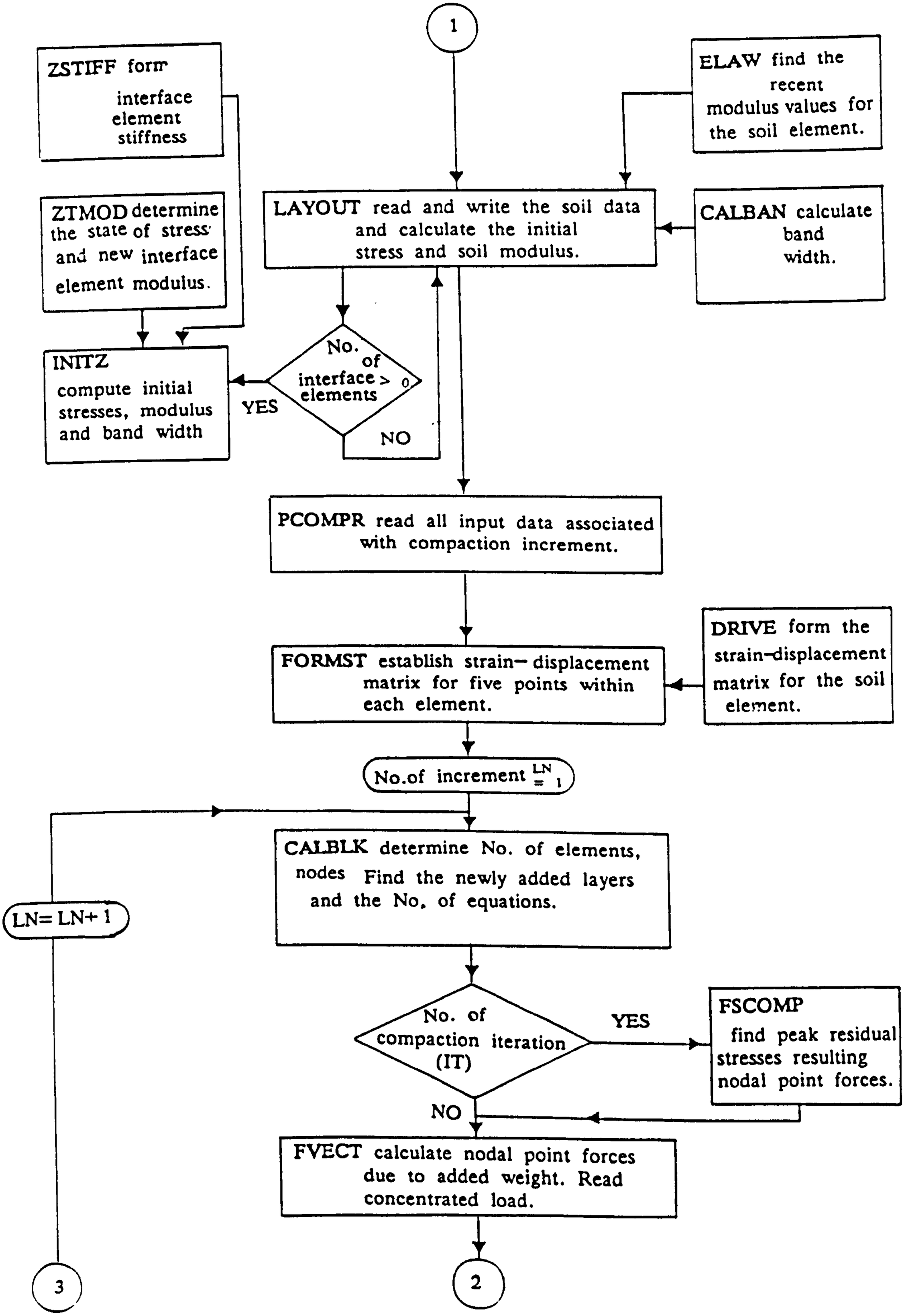
1
ZSTIFF form interface element stiffness
ELAW find the recent modulus values for the soil element.
ZTMOD determine the state of stress and new interface element modulus.
LAYOUT read and write the soil data and calculate the initial stress and soil modulus.
CALBAN calculate band width.
INITZ compute initial stresses, modulus and band width
No. of interface elements > 0
YES
NO
PCOMPR read all input data associated with compaction increment.
FORMST establish strain–displacement matrix for five points within each element.
DRIVE form the strain–displacement matrix for the soil element.
No.of increment LN = 1
CALBLK determine No. of elements, nodes Find the newly added layers and the No. of equations.
LN= LN+ 1
No. of compaction iteration (IT)
YES
NO
FSCOMP find peak residual stresses resulting nodal point forces.
FVECT calculate nodal point forces due to added weight. Read concentrated load.
3
2

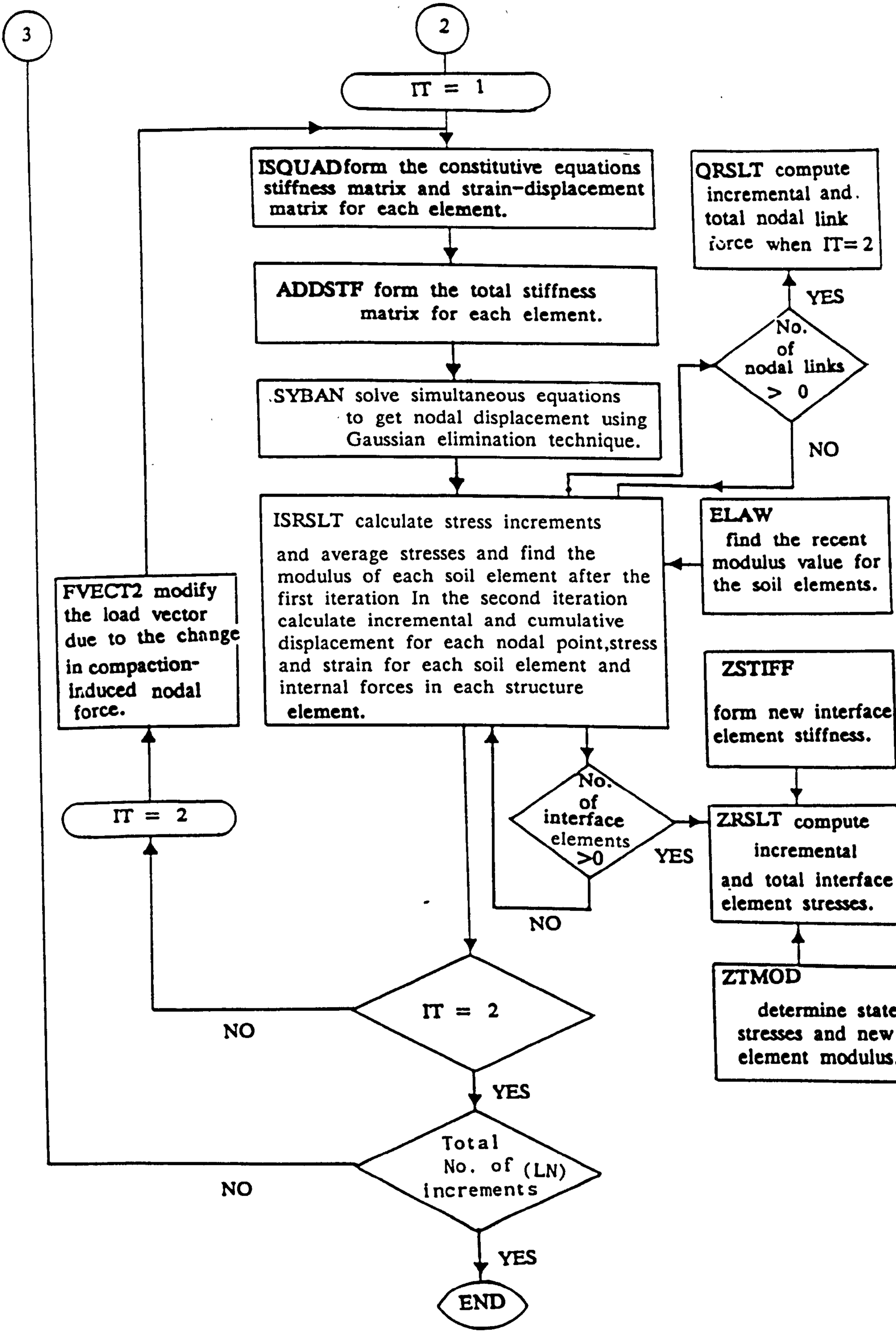
3
2
IT = 1
ISQUADform the constitutive equations stiffness matrix and strain-displacement matrix for each element.
ADDSTF form the total stiffness matrix for each element.
SYBAN solve simultaneous equations to get nodal displacement using Gaussian elimination technique.
ISRSLT calculate stress increments and average stresses and find the modulus of each soil element after the first iteration In the second iteration calculate incremental and cumulative displacement for each nodal point,stress and strain for each soil element and internal forces in each structure element.
QRSLT compute incremental and. total nodal link force when IT=2
YES
No. of nodal links > 0
NO
ELAW find the recent modulus value for the soil elements.
FVECT2 modify the load vector due to the change in compaction-induced nodal force.
IT = 2
NO
No. of interface elements >0
YES
NO
ZSTIFF form new interface element stiffness.
ZRSLT compute incremental and total interface element stresses.
ZTMOD determine state stresses and new element modulus.
IT = 2
NO
YES
Total No. of (LN) increments
NO
YES
END

8.5 A NEW MODELLING OF THE COMPACTION PLANT

As seen before the compaction induced lateral stresses are modelled on the basis of the maximum horizontal stress and once the maximum compaction lateral stress profile is entered into the program as input data, the compaction induced stresses can be determined. One of the key factors of success in modelling compaction is the best simulation of the compaction plant to produce this profile.

A computer program (BCOMPP) has been written by the author [Sec. (6.5.7)] to calculate the maximum compaction lateral stress profile. The main advantages of the program are:

(a) It takes into account the nature of the problem as a three dimensional problem.

(b) It allows for the simulation of the actual dimensions and weights of any compaction plant, i.e. as a moving load over finite dimensions in every direction, or two or one line load parallel or perpendicular to the wall.

(c) It allows for appropriate consideration of the three dimensional nature of the stresses arising as a result of such compaction loading within the framework of the incremental plane strain finite element analysis as in the SSCOMP program.

The explanation of the above program has been shown in [Sec. (6.5.7)] and a list of the program is shown in Appendix C– Sec. (C.1).

8.6 IDEALIZATION OF THE MODEL WALLS

Idealization was made to simulate the model used in the laboratory tests (Chapter 3) i.e. to simulate sand back fill, facing elements (perspex panels), reinforcement (aluminium foil strips), compaction apparatus used in laboratory tests (details of the equipment have been shown in Chapter 4), foundation under the reinforced mass (dense sand), and the boundary conditions (wooden box).

The idealization has been carried out using a finite element discrete approach idealization. Program BCOMPP (author's program) has been employed to simulate the actual compaction apparatus used in the laboratory tests and to calculate the maximum compaction lateral stress profile on the wall. The SSCOMP plane strain program has been employed to calculate soil stresses and deformations, forces in reinforcement, forces and moment in the facing units and wall deflection.

8.6.1 Finite Element Idealization

One of the laboratory tests models – as an example– is shown in Fig. (8.6). The wall consists of:

(a) Back fill

Sand back fill (600 mm height)

Dense sand foundation (100 mm height)

Length of sand back fill (1000 mm)

Length of sand foundation in front of the wall (300 mm)

The boundary is a smooth plywood box.

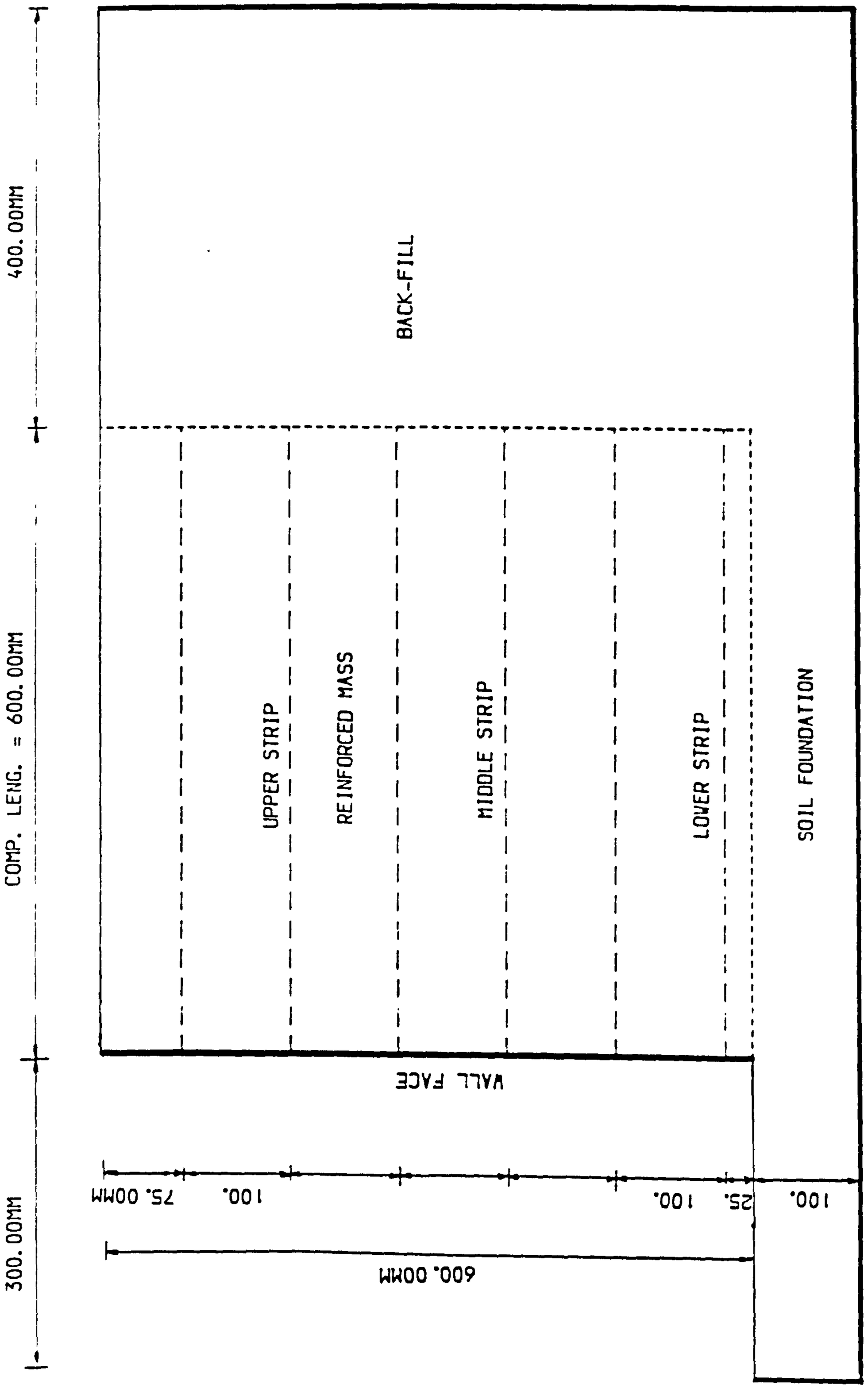

FIG. (8.6) THE MODEL REINFORCED EARTH WALL.

(b) Reinforcement

Aluminium foil strips 600 mm long by 12 mm by 0.1 mm thick, at equal horizontal and vertical spacing of 100 mm.

(c) Wall facing

This consists of perspex panels 150x150x18 mm thick, the length of the wall is 900 mm, and the connections between panels permit rotation i.e. act as hinges. Each panel has nine slots.

(d) Compaction length

compaction length is 600 mm i.e. covering the whole reinforced mass.

The wall–model was modelled as a two dimensional plane strain problem for the finite element analysis. Fig. (8.7) shows the finite element mesh which consists of:

(i) 388 nodes as the total number of nodes.

(ii) 194 four node isoparametric elements which represent soil back fill and soil foundation.

(iii) 18 beam elements to simulate the wall face and three hinges as the connection between the wall face panels.

(iv) 42 bar elements to idealize the reinforcement strips.

(v) 102 interface elements which represent the soil structure interaction between soil–wall face (beam elements) and soil–reinforcement(bar elements).

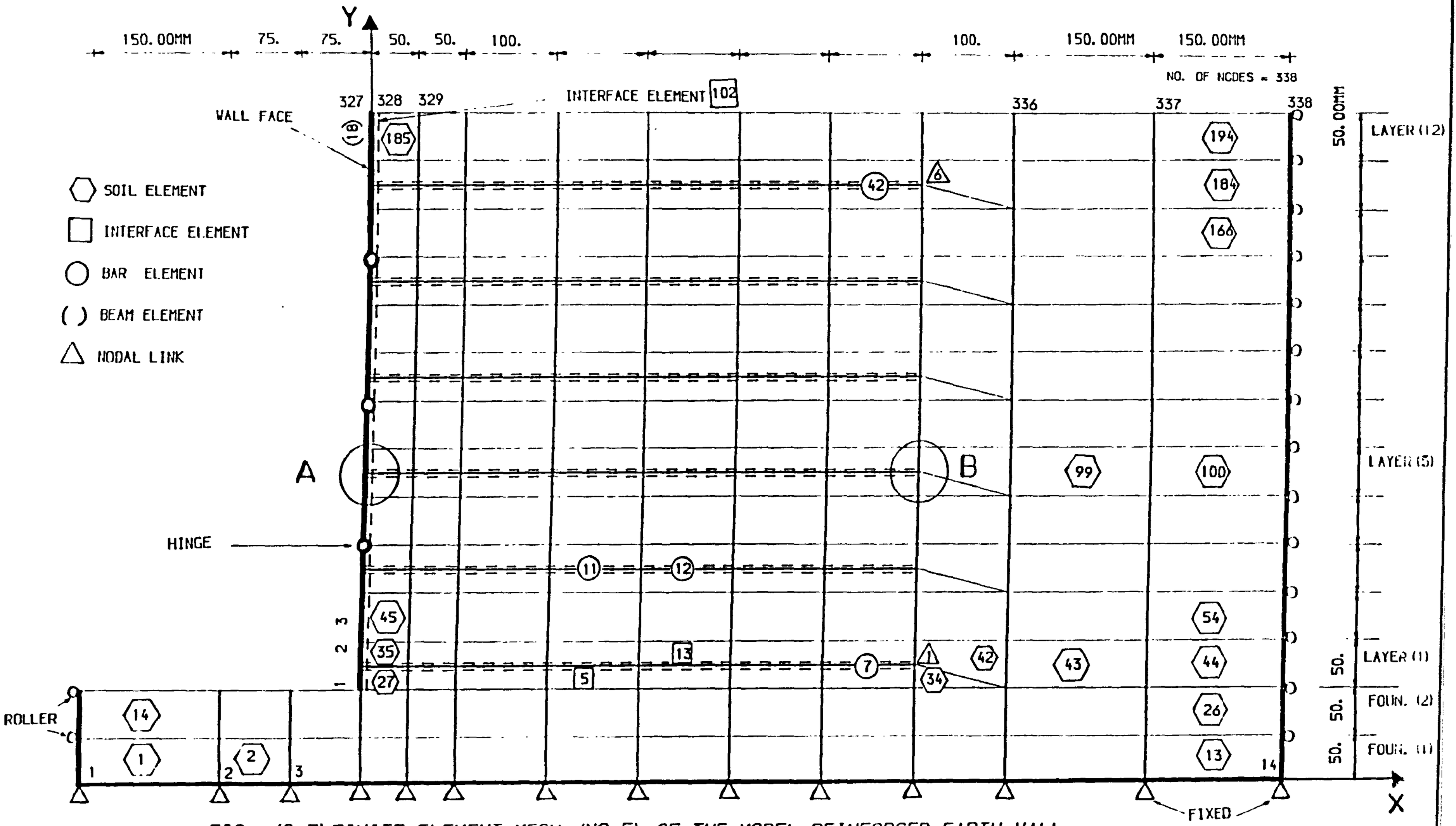

FIG. (8.7) FINITE ELEMENT MESH (NO. 5) OF THE MODEL REINFORCED EARTH WALL.

(vi) 6 nodal links at the ends of the strips to overcome the accumulation of stresses contributed from adjacent soil elements and to control the movement of the ends.

(vii) The boundary conditions at the left and right hand sides were set to allow no lateral movement and the sequence of construction as in laboratory tests was modelled using:

- Pre–existing foundation (two soil layers 1F & 2F).
- 12 soil placements (1S to 12S) i.e. 12 soil layers each 50 mm.
- 12 compaction increments, the length of each being 600 mm.
- The reinforcement was put in layers 1,3,5,7,9 & 11S.
- The panels of the wall face were put in four rows.

8.6.2 Interaction between soil and structural elements

One of the factors which leads to the success of the idealization of reinforced earth using the finite element technique is the slippage between soil and reinforcement or wall face. The correct modelling of the soil structure interaction must take into account an allowance for relative movement between the soil and the inclusion.

The problem can be overcome by putting interface elements between the soil and the wall face, and placing each reinforcement between the interface elements as shown in Figs. (8.7&8). These interface elements have been used in the finite element analysis to represent this relative movement.

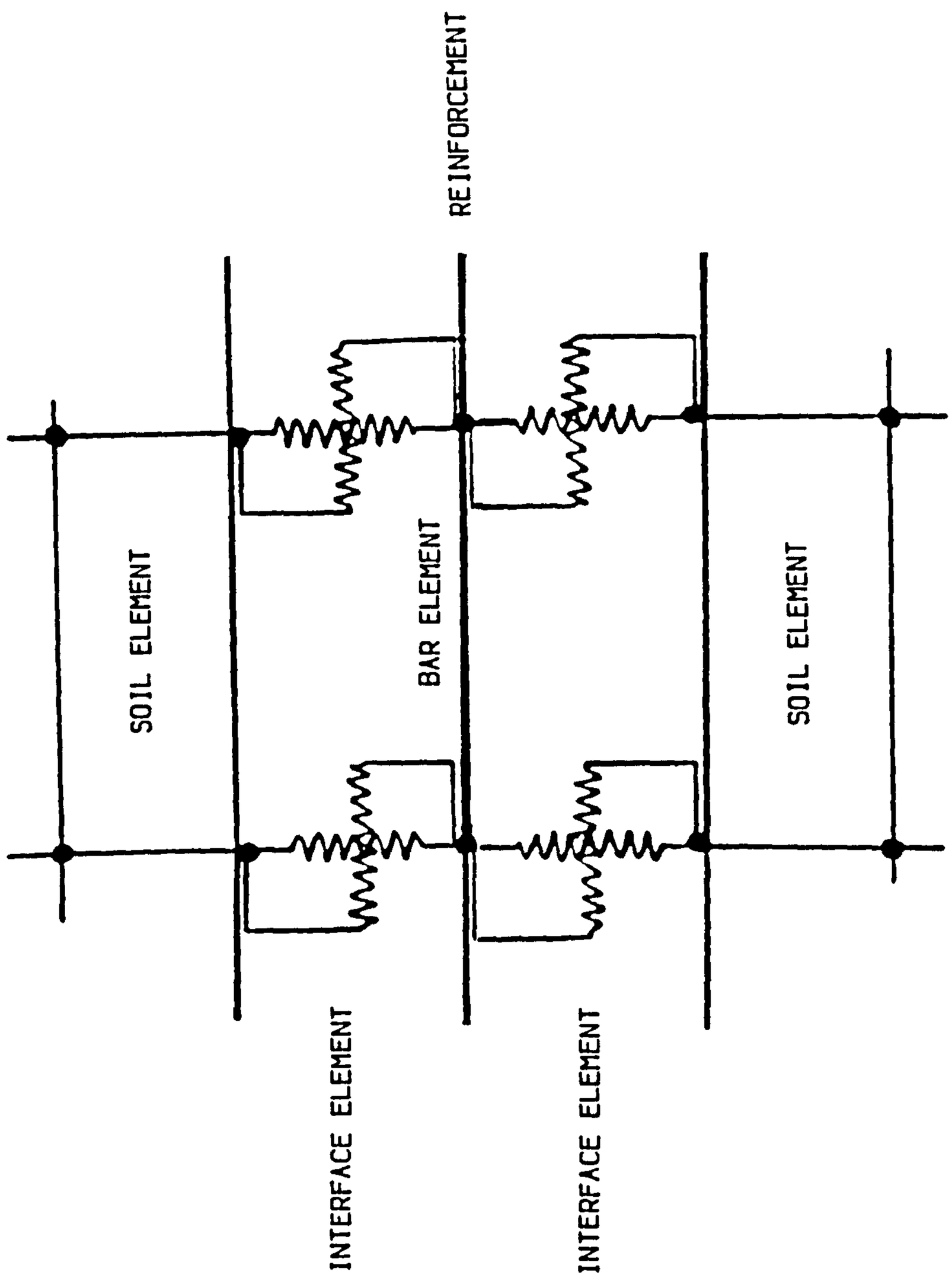

(8. 8) EACH REINFORCEMENT BETWEEN TWO INTERFACE ELEMENTS.

FIG.

8.6.3 Reinforcement– Wall Connection Model

Fig. (8.9) shows the representation used in the finite element model of the reinforcement– wall face connection as shown in Fig. (8.7) detail (A) of nodal point 152, four interface elements meet as follows:

Interface elements No. 35 & 50, which model the soil wall interaction, and elements No. 36 & 43, which model the soil reinforcement interaction. Nodes No, 143, 151, 152 & 160 all have the same initial geometric location. The interface elements are defined by the following nodal points,

Interface Element	Node			
	I	J	K	L
35	132	143	151	131
36	143	144	153	152
43	152	153	161	160
50	160	169	168	151

The bar element representing the reinforcement is connected to nodes 151 and 153. With this configuration, the bar (reinforcement) is rigidly connected to the wall (no relative movement) at node 151. However, at node 153 the bar is allowed to move relative to the soil.

Node 152 is essentially a dummy node, used to define interface elements 36 & 43 without connecting these elements to the reinforcement at the wall face.

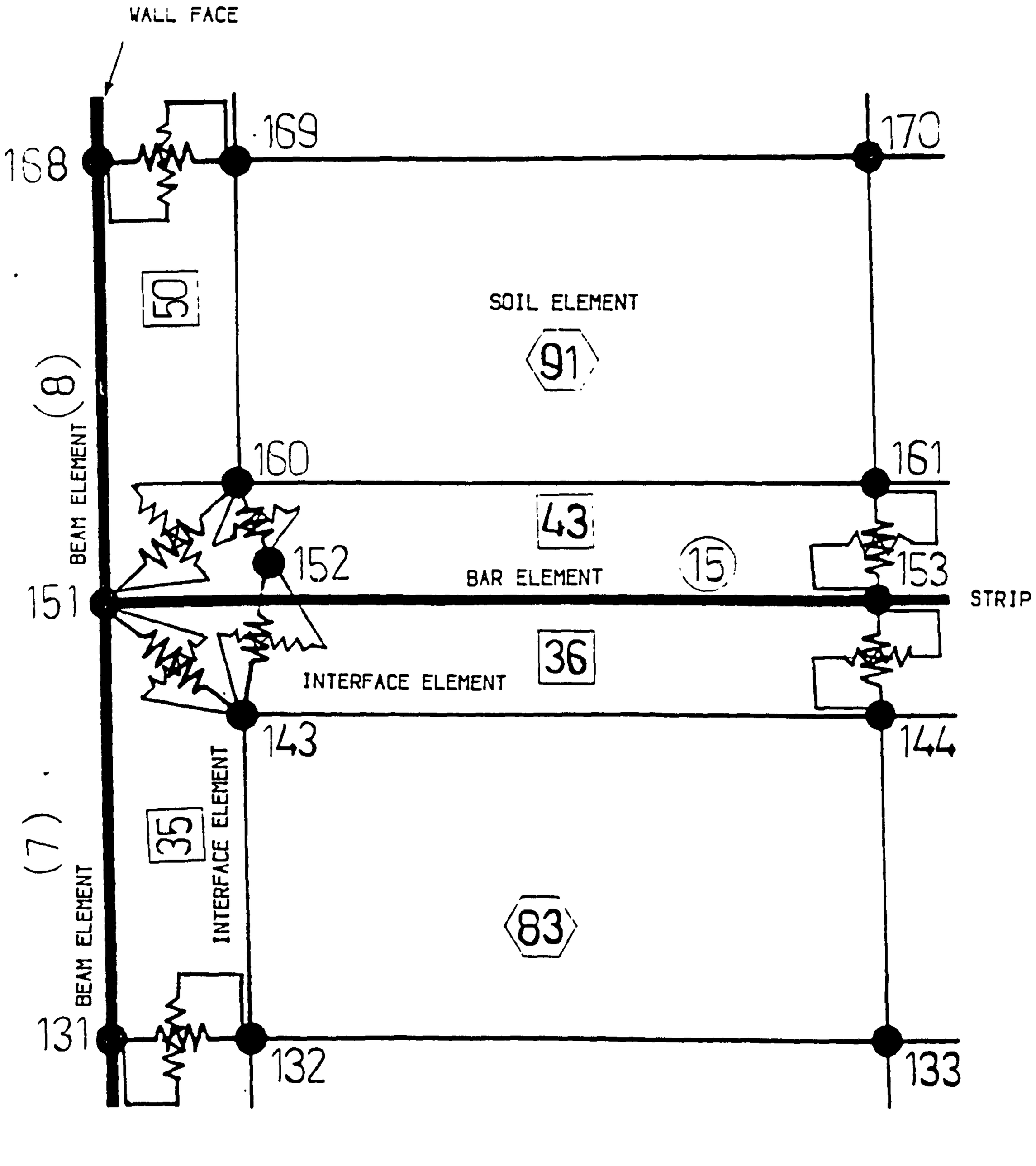

FIG. (8.9)' DETAIL (A) REINFORCEMENT / WALL CONNECTION.

8.6.4 Model Of The End Of Reinforcement

At the free end of the reinforcement, the proper modelling of the soil reinforcement interaction has an important effect on the analysis. The representation of the model is shown in Fig. (8.10)– detail of (B) in Fig.(8.7)–, where it is seen that nodes 150, 159 & 167 have the same initial geometric location. There are two adjacent soil elements, immediately to the right of the end of the reinforcement. The reinforcement is completely separated from these elements (90 & 98). These soil elements are connected to the interface elements and are defined by the following nodal points,

Soil Element	Node			
	I	J	K	L
90	139	140	150	150
98	167	140	177	176

This means that the end of the reinforcement is free to move without being connected to the non– reinforced soil mass, i.e. the soil behind the reinforced soil mass does not restrain the reinforcement from slipping. Thus the tensile force is equal to zero at the end of the reinforcement.

In order to reduce the nodal point forces on the soil nodes at the end of the reinforcement, i.e. nodes 150 & 167 as shown in Fig. (8.10), a nodal link is provided (No. 3). The vertical nodal point force on node 150 is taken as one quarter of the weight of the element 89 & 90. Similarly, the vertical nodal point force at node 167 is one quarter of the weight of the elements 97 & 98. The nodal link was added between those nodes to reduce the "squeezing effect"

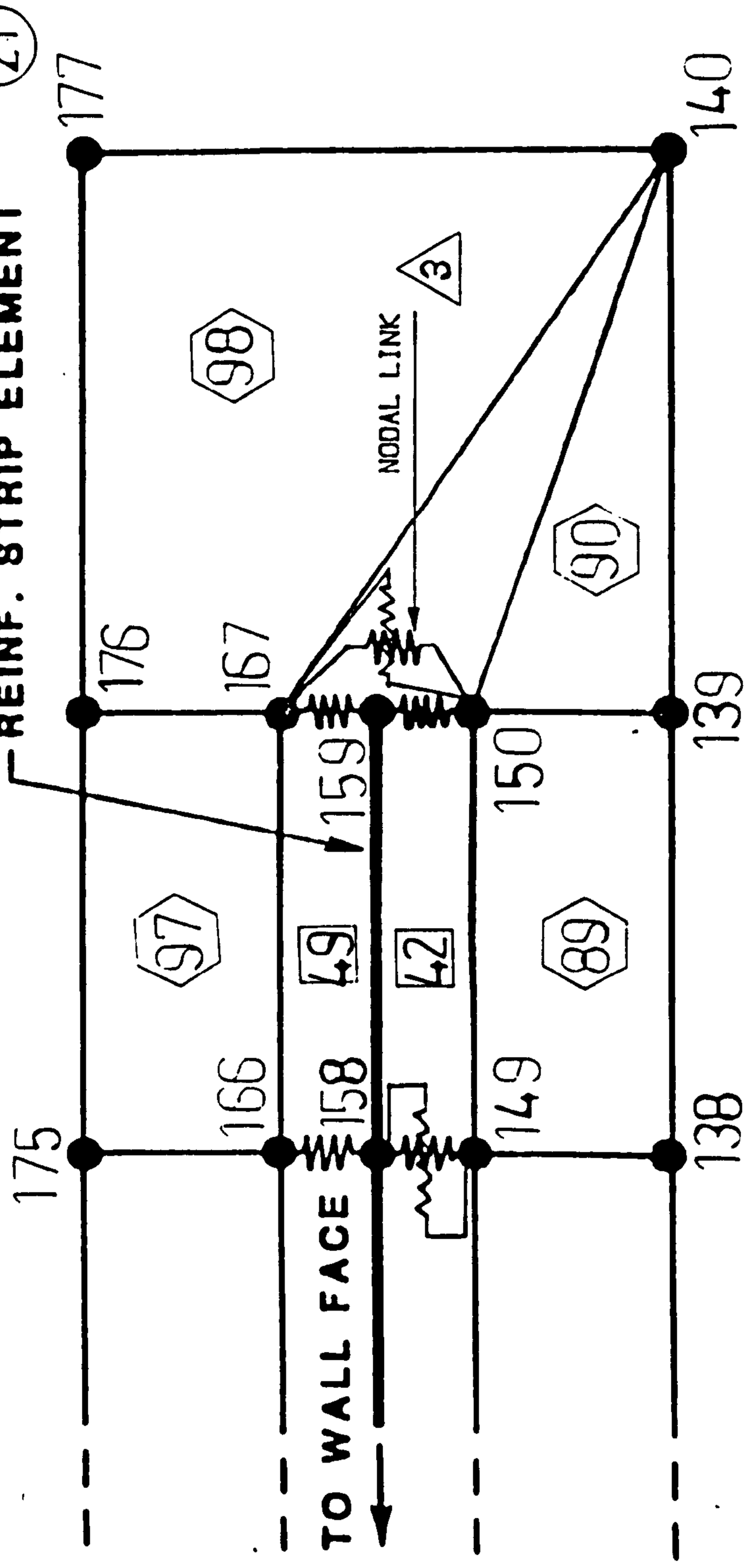

FIG. (8.10) DETAIL (B) FREE END OF THE REINFORCED STRIP.

on the end of the reinforcement.

The nodal link properties were set so that the normal force applied to the interface elements at node 150 & 167 was equal to that portion of the vertical force coming from soil elements 89 & 97 respectively. The nodal link therefore allowed the finite element model to correctly represent the vertical stresses applied along the length of the reinforcement.

8.6.5 Structural Elements

(a) Reinforcement

The reinforced strip was modelled using bar elements, which transmit axial force only . The bar elements are assumed to behave linear elastically. The finite element analysis is two dimensional, so the assumption of considering the reinforcement to be continuous for the length of the wall was employed.

In practice the reinforcement is not continuous and the strips were located every 10 cm along the length of wall. The cross– sectional area of reinforcement per unit length of the wall face in the finite element model must be adjusted to give the wall in the finite element analysis the same stiffness as the actual wall, i.e.

$$A_{s.f.e} = \frac{A_s}{S_h} \qquad (8.6)$$

Where:

$A_{s.f.e}$ is the cross sectional area of strip/unit length in finite element

analysis.

A_s is the actual cross sectional area of the strip.

S_h is the horizontal distance between the strips.

(b) Wall face

The wall face consists of 24 panels (4 rows in the vertical direction with 6 panels in each row). The perspex panels were represented in the finite element analysis as beam elements. The connections between the rows were represented as hinges which are similar to the actual wall where the joints are continuous. These hinges and beam elements are seen in Fig.(8.7).

(c) Soil representation

Sand back fill and foundation was represented by four node isoparametric elements. 194 soil elements simulate the soil mass as follows:

The foundation under the reinforced mass consists of two layers of very dense sand (50 mm each) which contains 26 elements (from 1 to 26).

12 construction layers (50 mm each) consist of 178 elements (from 27 to 194) which include the reinforced soil mass and the soil behind it. An example of the way in which the soil elements are defined in the program is shown in Fig. (8.7),

Soil Element	Node			
	I	J	K	L
193	324	325	337	336
194	325	326	338	337

8.6.6 Boundary Conditions

Two boundary conditions were employed, the first at the bottom of the model, the second at the left and right hand sides of the model. At the bottom the nodes were treated as fixed i.e. with no horizontal or vertical movement or rotation. The nodes at the sides were free to move in the vertical direction and rotate , but were restrained in the horizontal direction. The rest of the nodes were allowed to move in a horizontal and vertical direction and to rotate.

8.6.7 Profile Of The Lateral Compaction Stresses

The lateral earth pressure profile used to simulate the effects of compacting the back fill behind the wall was determined using the computer program BCOMPP. This program is capable of simulating the actual weight and dimensions of the apparatus used in the laboratory tests to provide the compaction pressure. It also can be used for small scale models or prototypes.

The program calculates the horizontal effective stresses produced by compaction equipment at any point in a free field or on a vertical wall. The compaction equipment may be simulated as point loads, line loads (parallel or perpendicular to the wall) or a uniform loaded area.

Compaction profiles are shown in Fig. (8.11), The three profiles are for distances 0.0, 200.0 & 400.0 mm from the wall face and for compaction lengths 600.0, 400.0 & 200.0 mm respectively. These curves were developed by representing the compaction plant as a moving rectangular loaded area and varying the location of these loads on the ground surface to induce the maximum lateral stress at the wall face and to simulate the actual model test procedures.

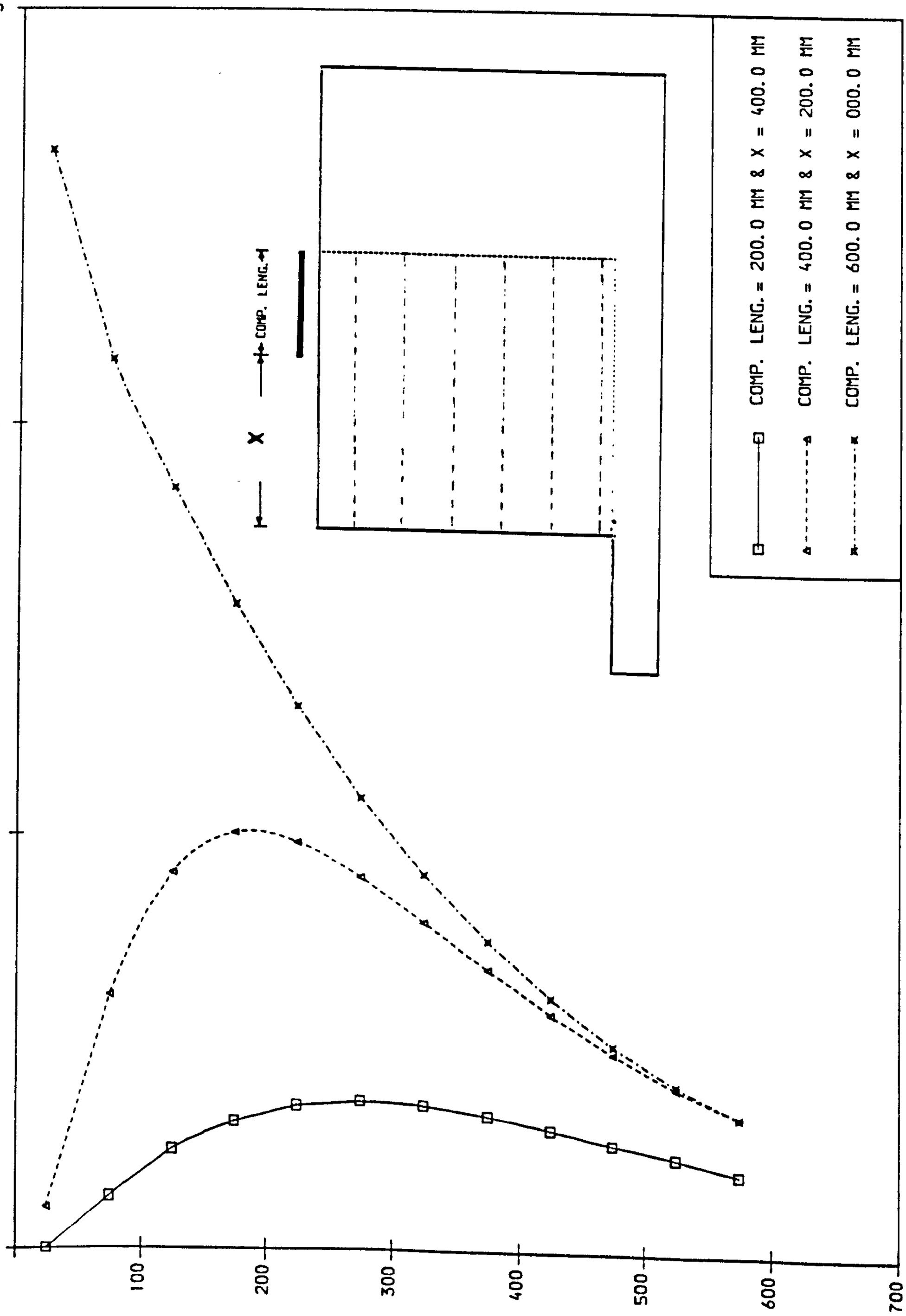

FIG. (8.11) HORIZONTAL PRESSURE DUE TO COMPACTION APPARATUS.

8.7 TESTING PROGRAMME

13 Computer– runs were carried out to simulate three CATS. of the model tests (CAT. II, III, IV – Chapter 3), and adding some tests which could not be carried out experimentally. All material properties were similar to those in the laboratory tests. The finite element program SSCOMP was employed for the finite element analysis and program BCOMPP produced a profile of compaction lateral stresses. Table (8.2) shows the testing program with the parameters for each test, and also illustrates the configurations of the tests as follows:

– computer runs 1 & 2 for CAT. II.

– computer runs 3, 4 & 5 for CAT. III.

– computer runs 9 to 13 for CAT. IV.

– computer runs 6, 7 & 8 for additional tests.

8.8 DATA USED

8.8.1 Properties Of The Materials

(a) Soil properties

A non– linear soil model (hyperbolic stress strain model) developed by Duncan et al. (1980) and modified by Seed and Duncan has been used. The strength characteristics and hyperbolic parameters were determined using dry

TABLE (8.2) TESTING PROGRAMME.

Run No.	Reinforcement Aluminium foil strips S_h mm	S_v mm	L mm	t_1 mm	b mm	wall face	wall height	soil found.	sand back fill (Rd)%	Remarks
1	100	100	600	0.10	12	It consists of 24 perspex panels. Each one 150 × 18 mm	In all runs, the height is 600 mm	Two sand layers 50 mm each of relative density R_d = 75%	7.62	without compaction (using raining device)
2	100	100	600	0.10	12				45.21	without compaction (using raining device)
3	100	100	600	0.10	12				15.91	compaction length = 200 mm & 400 mm from the wall face
4	100	100	600	0.10	12				51.00	compaction length = 400 mm & 200 mm from the wall face
5	100	100	600	0.10	12				75.67	compaction length = 600 mm & 0 mm from the wall face
6	100	100	600	0.10	12				15.91	without compaction but the same density as in (3)
7	100	100	600	0.10	12				51.00	without compaction but the same density as in (4)
8	100	100	600	0.10	12				75.67	without compaction but the same density as in (5)
9	100	100	600	0.10	12				77.45	compaction length = 600 mm and preventing wall from movement
10	100	100	600	0.10	12				62.60	variable compaction length (θ = 75°)
11	100	100	600	0.10	12				52.77	variable compaction length (θ = 60°)
12	150	150	600	0.10	12				75.30	compaction length = 600 mm
13	100	100	300	0.10	12				56.45	compaction length = 300 mm

triaxial tests as in Chapter (3) and some of them were estimated from tables prepared by Duncan et al. (1980), which lists the hyperbolic parameters for 80 different soils, as determined from triaxial test data.

(b) Soil– structure interaction properties

The properties of soil reinforcement and soil– wall face were determined by pull– out and shear box tests as described in Chapter (3). These properties were employed as interface element properties which simulate soil structure interaction.

(c) Structural element properties

A linear elastic model was used to represent both wall face (beam element) and reinforcement (bar element). The properties of the bar element were determined using the tensile tests on aluminium foil strips previously described in Chapter (3). The beam element properties (of perspex material) were based on work by I.C.I. (1973). A brief summary of the different soil model parameters as well as the structural element properties for all the computer runs are given in Table (8.3)

8.8.2 Data Used

Methods of entering data are summarized in Table (8.4). Details of finite element meshes used for all runs are shown in Fig. (8.12.A,B,C,D,E&F)and Table(8.5). Typical data for one of the computer runs (No. 12) is shown in Appendix C– Sec. (C.5).

TABLE (8.3) DATA USED IN THE RUNS.

Run No.	Soil material properties, for hyperbolic model										Bilinear model					reinf.		wall face	
	γ	K	n	R_f	K_B	m	C	φ	$\Delta\varphi$	$\dot{\varphi}$	K_o	$K_{ii\ B}$	$\dot{C}_B$	K_2	K_3	A	I	A	I
1	14.7	150	0.4	0.7	50	0.2	0.0	33	3	30	0.46	2	0.0	0.32	0.32	0012	0.0	1.8	.486
2	16.3	380	0.4	0.7	370	0.2	0.0	44.3	6.2	38.1	0.38	2.8	0.0	0.26	0.26	0012	0.0	1.8	.486
3	15.0	200	0.4	0.7	100	0.2	0.0	36.5	3	33.5	0.45	2.31	0.0	0.31	0.31	0012	0.0	1.8	.486
4	16.0	420	0.4	0.7	430	0.2	0.0	45.6	6.6	39.0	0.37	2.93	0.0	0.26	0.26	0012	0.0	1.8	.486
5	17.6	560	0.4	0.7	640	0.2	0.0	53.0	8.7	44.3	0.31	3.75	0.0	0.21	0.21	0012	0.0	1.8	.486
6	15.0	200	0.4	0.7	100	0.2	0.0	36.5	3	33.5	0.45	2.31	0.0	0.31	0.31	0012	0.0	1.8	.486
7	16.6	420	0.4	0.7	430	0.2	0.0	45.6	6.6	39.0	0.37	2.93	0.0	0.26	0.26	0012	0.0	1.8	.486
8	17.6	560	0.4	0.7	640	0.2	0.0	53.0	8.7	44.3	0.31	3.75	0.0	0.21	0.21	0012	0.0	1.8	.486
9	17.7	570	0.4	0.7	650	0.2	0.0	53.4	8.92	44.5	0.30	3.79	0.0	0.21	0.21	0012	0.0	1.8	.486
10	16.7	435	0.4	0.7	450	0.2	0.0	47	7	40	0.36	3.07	0.0	0.25	0.25	0012	0.0	1.8	.486
11	15.8	310	0.4	0.7	270	0.2	0.0	41.7	5.4	36.3	0.41	2.59	0.0	0.28	0.28	0012	0.0	1.8	.486
12	17.6	560	0.4	0.7	640	0.2	0.0	52.9	8.70	44.2	0.31	3.75	0.0	0.21	0.21	0012	0.0	1.8	.486
13	16.8	450	0.4	0.7	470	0.2	0.0	47.3	7.08	40.2	.36	3.09	0.0	0.25	0.25	0012	0.0	1.8	.486

E for reinforcement and perspex are 918000 & 29539 Kg/cm² respectively.

TABLE (8.4) SUMMARY OF INPUT DATA.

INFORMATION	DETAILS
1- Title	General title of the problem to be analysed.
2- Control data	These provide the necessary information to control the analyses, such as No. of nodes, soil elements, different types of elements and materials. Also number of soil layers, compaction increment and load increment and codes for print or not print the data and initial stresses.
3- Construction sequence	Each solution increment of one of the three types of (soil placement,compaction or loading increment) has a sequence number defining its order of occurrence in the overall solution sequence.
4- Nodal points and boundary conditions	Nodal points have to be read in sequence within their coordinates and specifying the degrees of freedom.
5- Element material properties and connection data	The material of the structure elements has linear properties. The soil elements material has non-linear properties. Connection data must be given for structural elements but in the soil elements a self generation technique is used.

TABLE (8.4) CONT.

6- Position of the new fill surface	The shape of the surface of the newly placed layer is define by specified nodal points to calculate the stresses to be assigned to newly placed soil elements and also in assigning compaction induced stresses specified by means of peak compaction pressure profile.
7- Foundation layer	Information about foundation layers has been provided such as: number of layers, materials, different types of elements and the levels.
8- Compaction	All information about compaction such as: compaction pressure profiles, nodal points defining depth of compaction forces and stresses are given.
9- Codes	Codes to indicate whether the output is to be printed or punched are as follows: 0 no print 1 print 2 print and punch

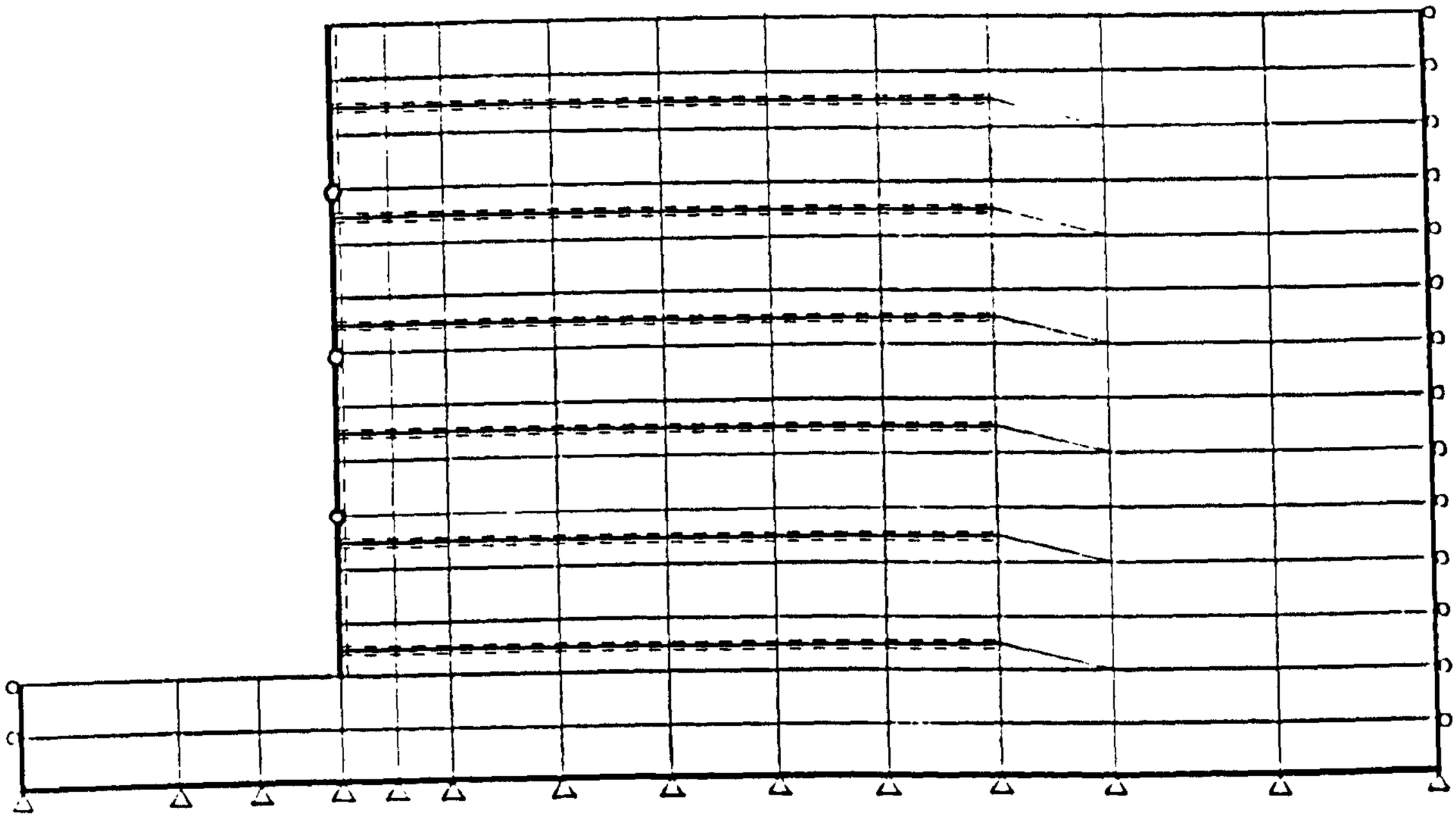

(A) MESH NO. 1 (MODEL TESTS CAT. II & III)

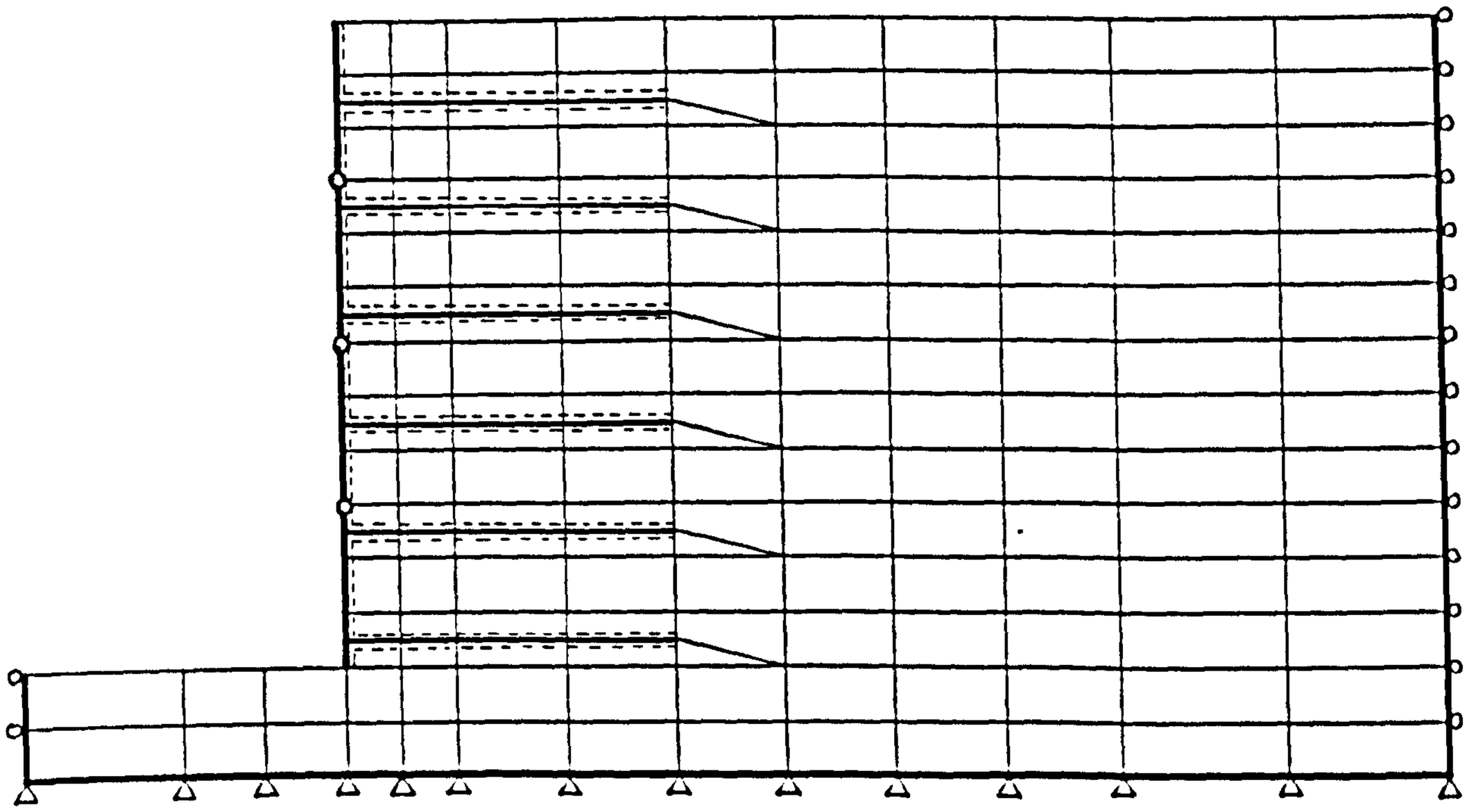

(B) MESH NO. 2 (MODEL TEST CAT. IV-5)

FIG. (8.12) FINITE ELEMENT MESH FOR DIFFERENT MODEL REINFORCED EARTH WALLS.

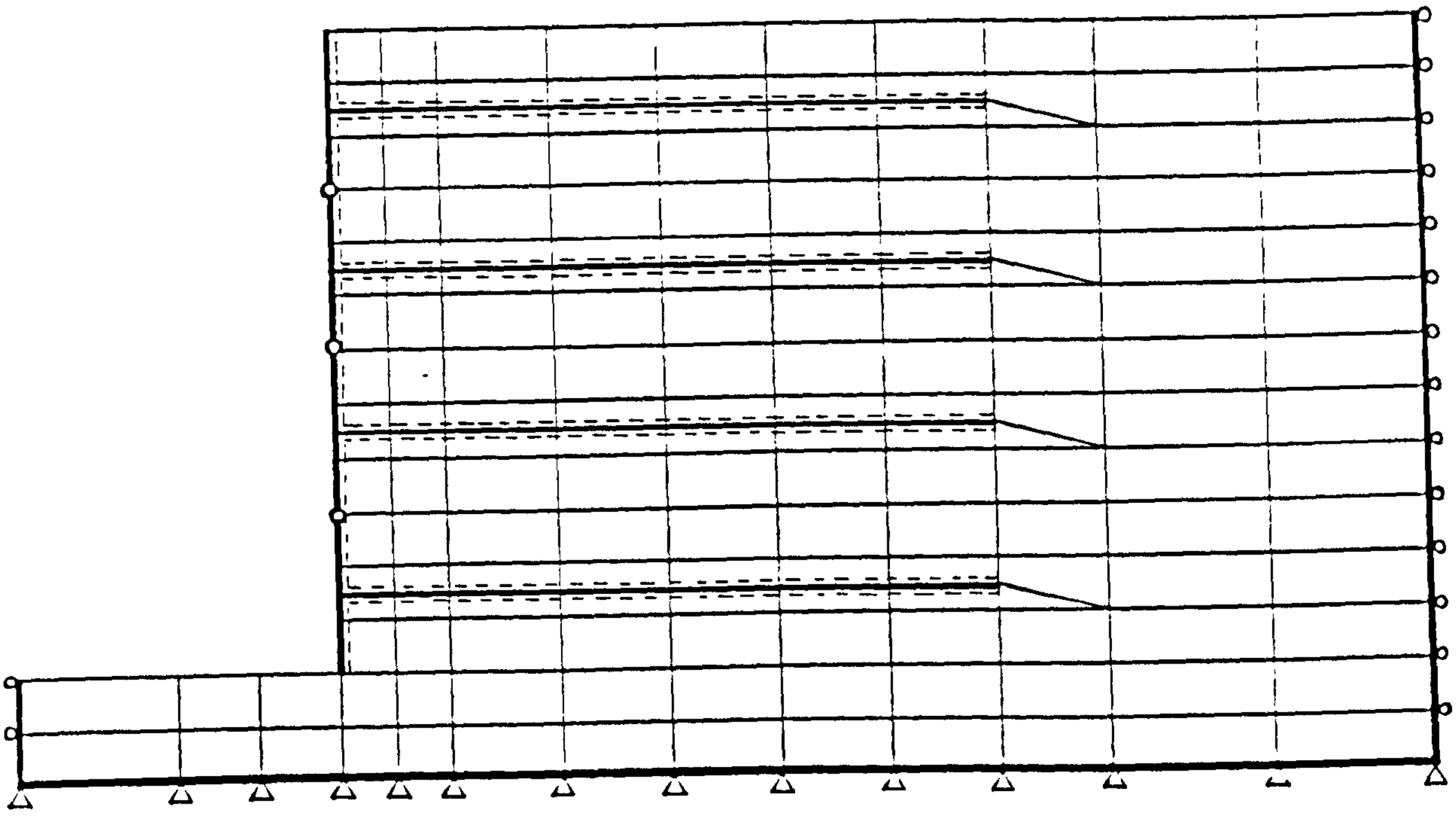

(C) MESH NO. 3 (MODEL TEST CAT. IV-4)

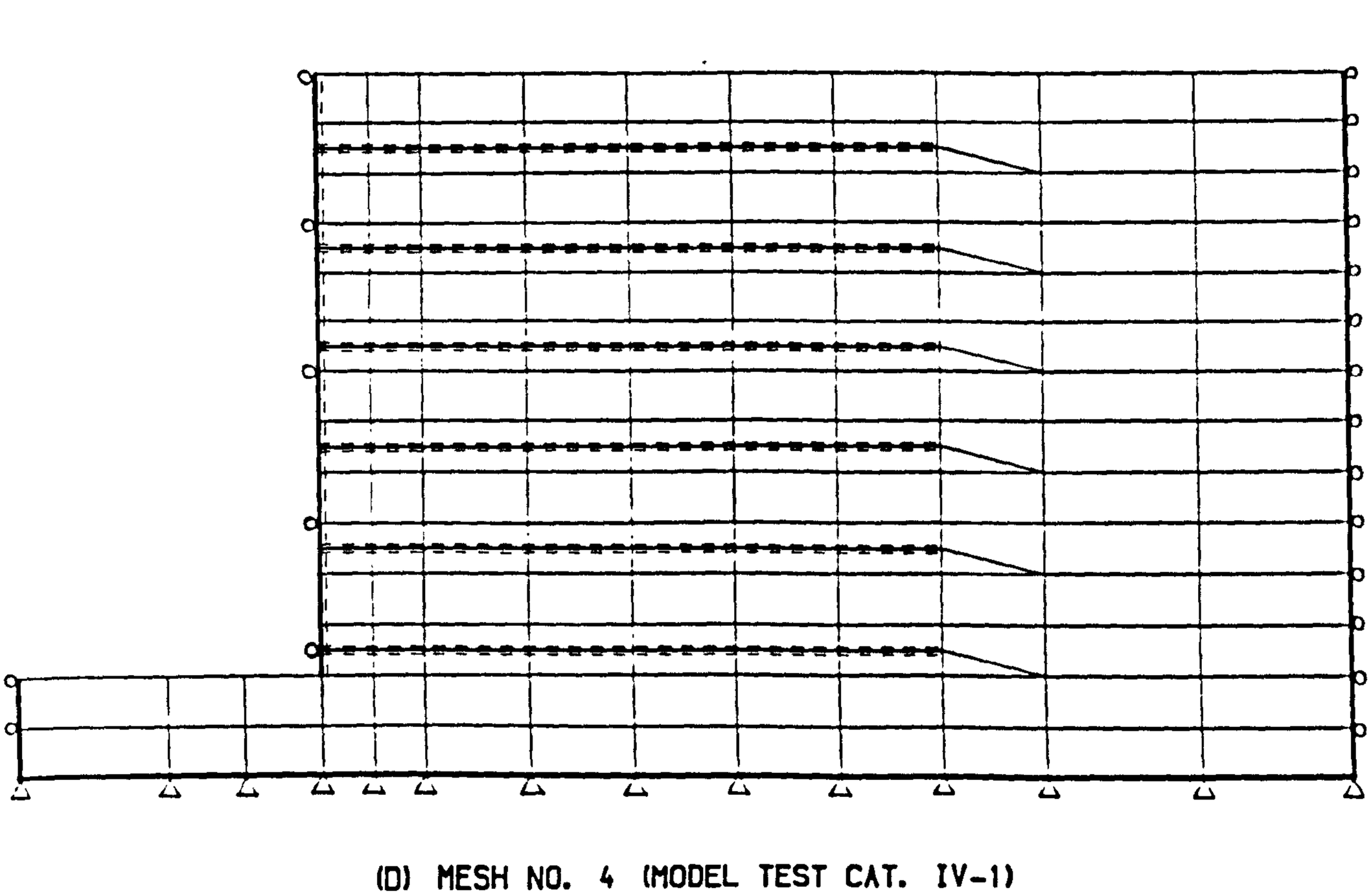

(D) MESH NO. 4 (MODEL TEST CAT. IV-1)

FIG. (8.12) CONT.

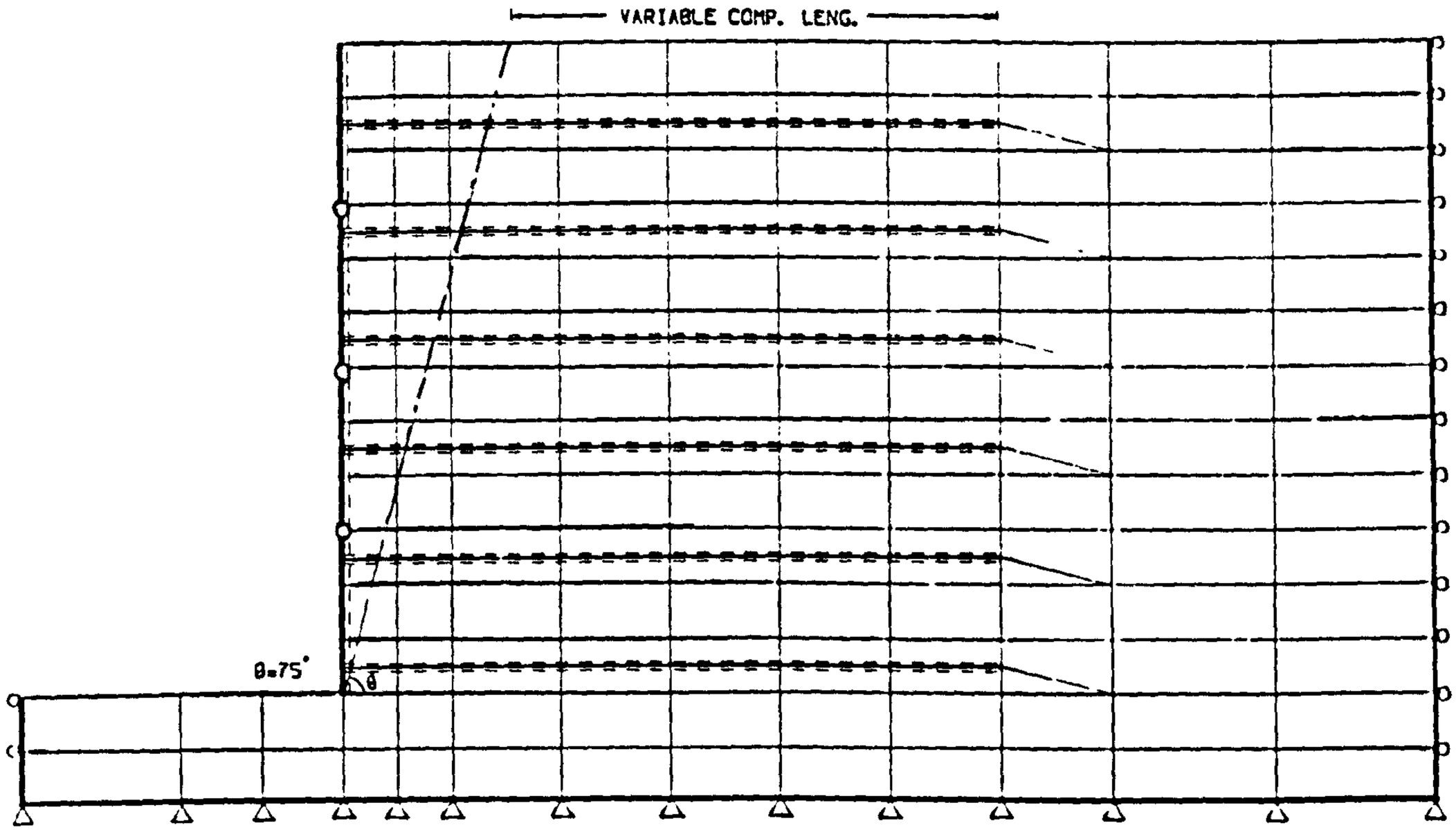

(E) MESH NO. 5 (MODEL TEST CAT. IV-2)

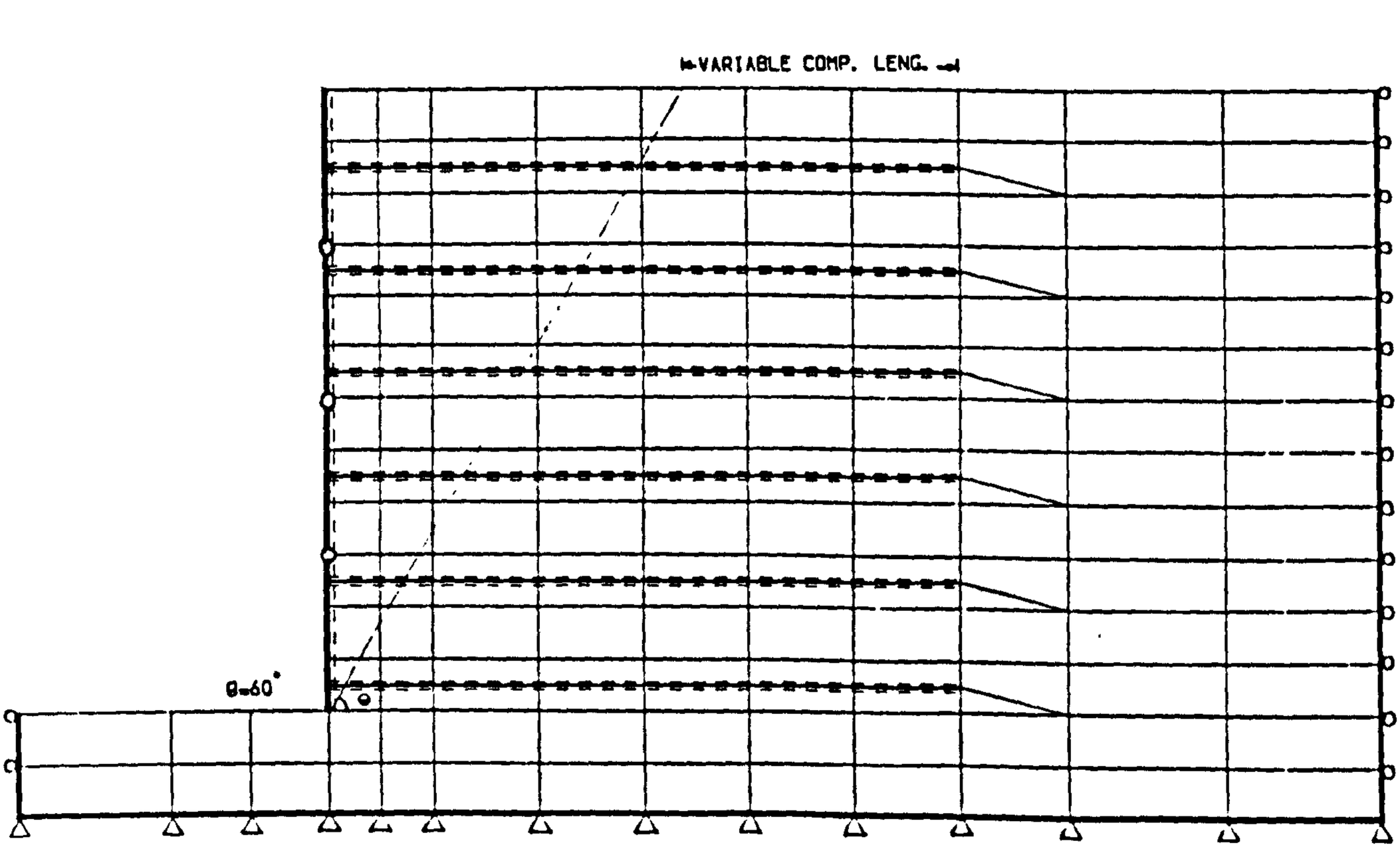

(F) MESH NO. 6 (MODEL TEST CAT. IV-3)

FIG. (8.12) CONT.

TABLE (8.5) DETAILS OF F.E. MESHES USED IN THE RUNS ON THE MODELS.

Run No.	Mesh No.	No. of found. layer	No. of soil layer	No. of nodes	No. of soil elem.	No. of bar elem.	No. of beam elem.	No. of inter. elem.	No. of links	construction increment		
										soil	comp.	loads
1	1	2	12	338	194	42	18	102	6	12	12	–
2	1	2	12	338	194	42	18	102	6	12	12	–
3	1	2	12	338	194	42	18	102	6	12	12	–
4	1	2	12	338	194	42	18	102	6	12	12	–
5	1	2	12	338	194	42	18	102	6	12	12	–
6	1	2	12	338	194	42	18	102	6	12	12	–
7	1	2	12	338	194	42	18	102	6	12	12	–
8	1	2	12	338	194	42	18	102	6	12	12	–
9	4	2	12	338	194	42	18	102	6	12	12	–
10	5	2	12	338	194	42	18	102	6	12	12	–
11	6	2	12	338	194	42	18	102	6	12	12	–
12	3	2	12	288	178	28	16	72	4	12	12	–
13	2	2	12	284	176	24	18	66	6	12	12	–

8.9 CONCLUSION

Program BCOMPP has been used to find the profile of horizontal stresses on the laboratory reinforced earth wall using the actual dimensions and weight of the compaction equipment employed in the model tests.

Idealization of the model for different model tests has been presented. Employing program SSCOMP which includes a compaction model, the result of model tests can be obtained and will be presented in the next chapter.

CHAPTER 9

RESULTS AND DISCUSSION

OF

FINITE ELEMENT ANALYSIS

9.1 INTRODUCTION

This chapter presents the results obtained by idealizing the various models of reinforced earth walls carried out in the laboratory by the author as explained in chapter (3) and (8). The results are presented in two sections as follows:

(1) The compaction effect on the behaviour of the reinforced earth wall as fields of deformation and stresses within, behind and under the reinforced mass. The total displacement in the reinforced mass and lateral movement of the wall face. The distribution of tensile forces in the reinforcement as well as the internal forces in the wall face.

(2) The effect of the variation in compaction length on the behaviour of the reinforced earth wall.

The above results were obtained using the idealisation of model tests carried out in the laboratory, and programs (BCOMPP) and (SSCOMP) have been employed. The conclusion of this study is presented at the end of this chapter.

9.2 EFFECT OF COMPACTION ON THE BEHAVIOUR OF THE REINFORCED EARTH WALL

The effect of compaction on the behaviour of reinforced earth can be seen by comparing the results obtained from two computer runs. The first is run No. 5, which simulates the laboratory model test (CAT. III−3), with the highest relative density (R_d = 75.67%) which can be achieved using compaction. The second run is No. 8 which has the same parameters but is carried out without compaction.

It should be noted that this run does not simulate any model test carried out in the laboratory. This is because it is very difficult to reach this high relative density in a laboratory model without compaction. Also it should be noted that all results has been obtained per unit length of the wall except the distribution of forces in the strips which are obtained for individual strips.

9.2.1 Fields Of Deformations

Major and minor principal strains (ϵ_1 & ϵ_3) in the sand backfill in both the reinforced earth mass and the backfill behind and under it are shown in Figs. (9.1&2) with and without compaction respectively. The compaction length used is 600.0 mm at zero distance behind the wall i.e. adjacent to the wall back.

In Figs. (9.1&2), the values of major principal strain ϵ_1 (compression) and minor principal strain ϵ_3 (tension) increase behind the wall face , around the reinforcement and near the boundaries of the reinforced mass. Also, compaction causes the rotation of axes.

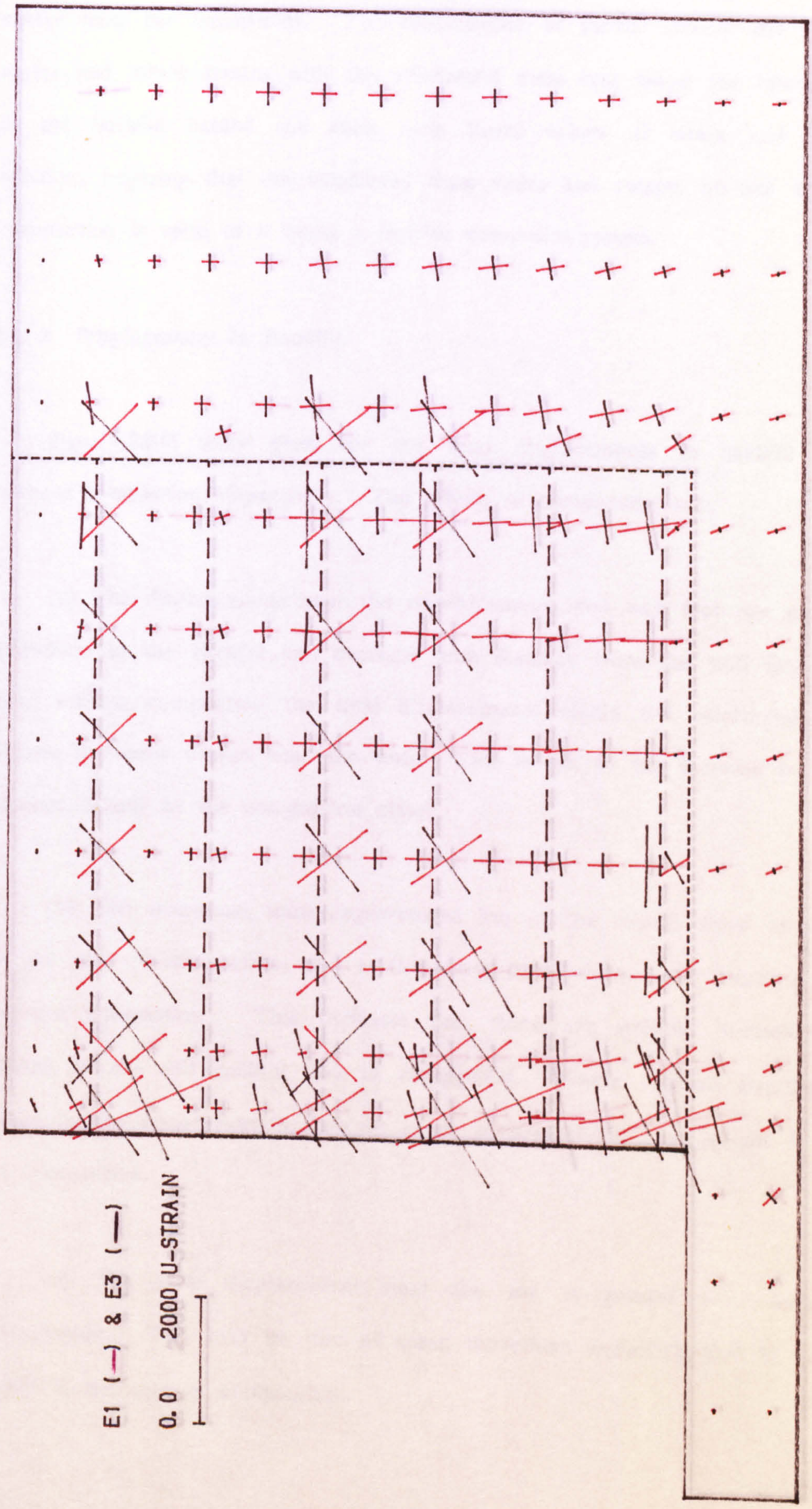

FIG. (9.1) FIELDS OF DEFORMATIONS (PRINCIPAL STRAINS E1&E3, COMP. LENG.

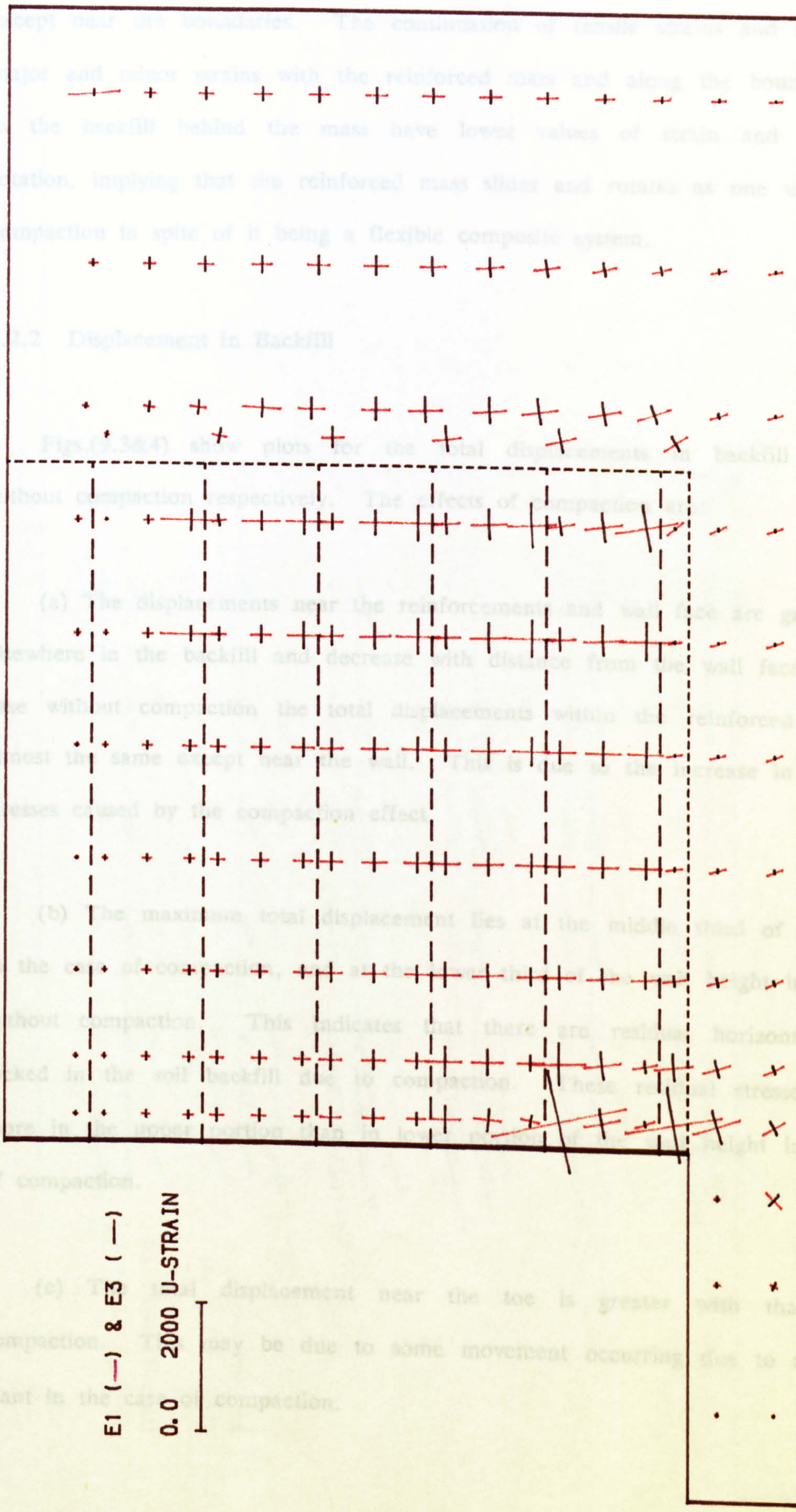

FIG. (9.2) FIELDS OF DEFORMATIONS (PRINCIPAL STRAINS E1&E3, WITHOUT COMP. USING THE SAME DENSITY AS COMP. LENG. = 600.0 MM).

The backfill behind the reinforced soil mass was not affected too much except near the boundaries. The continuation of tensile strains and rotation of major and minor strains with the reinforced mass and along the boundaries and in the backfill behind the mass have lower values of strain and almost no rotation, implying that the reinforced mass slides and rotates as one unit due to compaction in spite of it being a flexible composite system.

9.2.2 Displacement In Backfill

Figs.(9.3&4) show plots for the total displacements in backfill with and without compaction respectively. The effects of compaction are:

(a) The displacements near the reinforcements and wall face are greater than elsewhere in the backfill and decrease with distance from the wall face. In the case without compaction the total displacements within the reinforced mass are almost the same except near the wall. This is due to the increase in horizontal stresses caused by the compaction effect.

(b) The maximum total displacement lies at the middle third of the height in the case of compaction, and at the lower third of the wall height in the case without compaction. This indicates that there are residual horizontal stresses locked in the soil backfill due to compaction. These residual stresses increase more in the upper portion than in lower portion of the wall height in the case of compaction.

(c) The total displacement near the toe is greater with than without compaction. This may be due to some movement occurring due to compaction plant in the case of compaction.

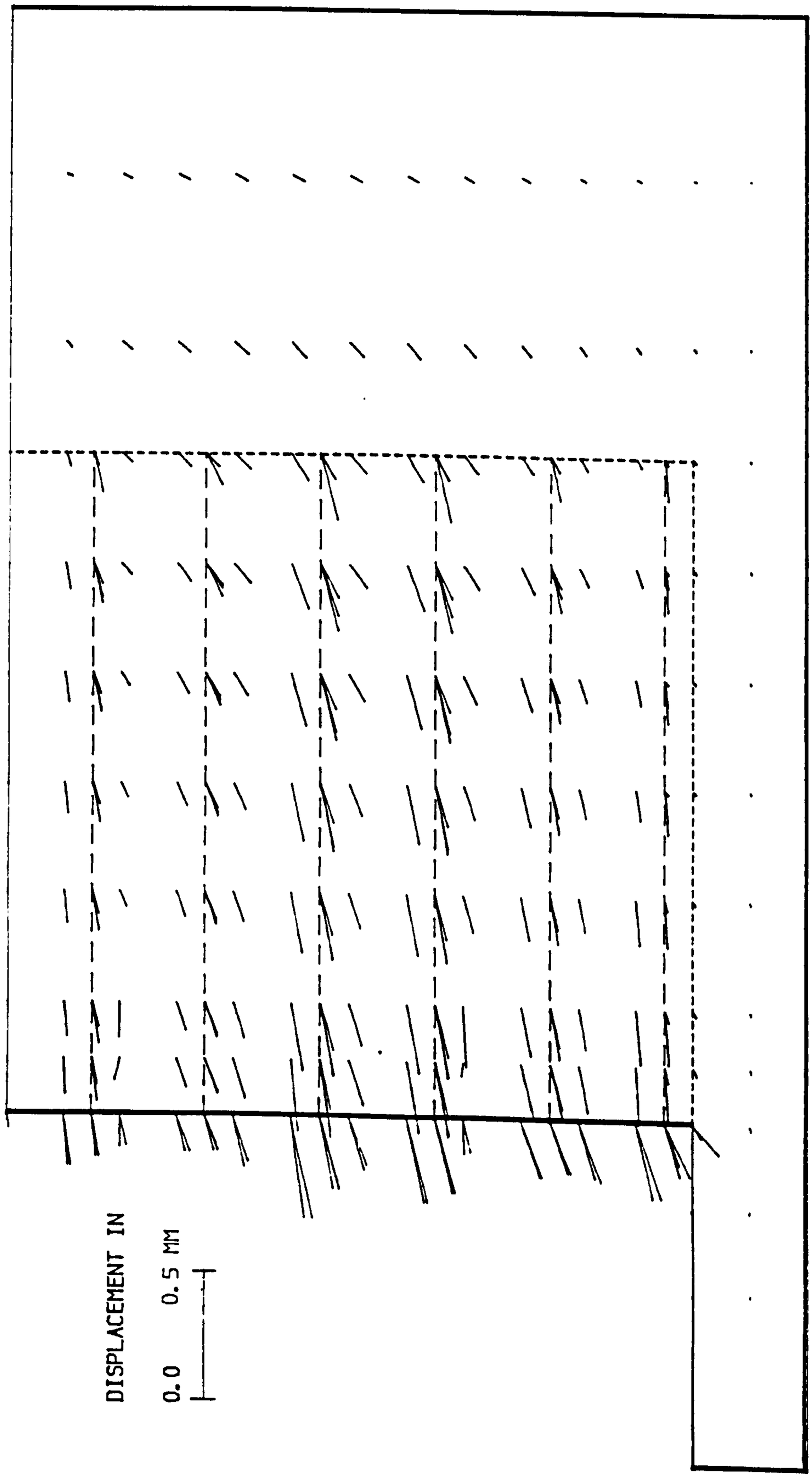

(9.3) DISPLACEMENTS IN BACKFILL SOIL (COMP. LENG.=600.0 MM)

FIG.

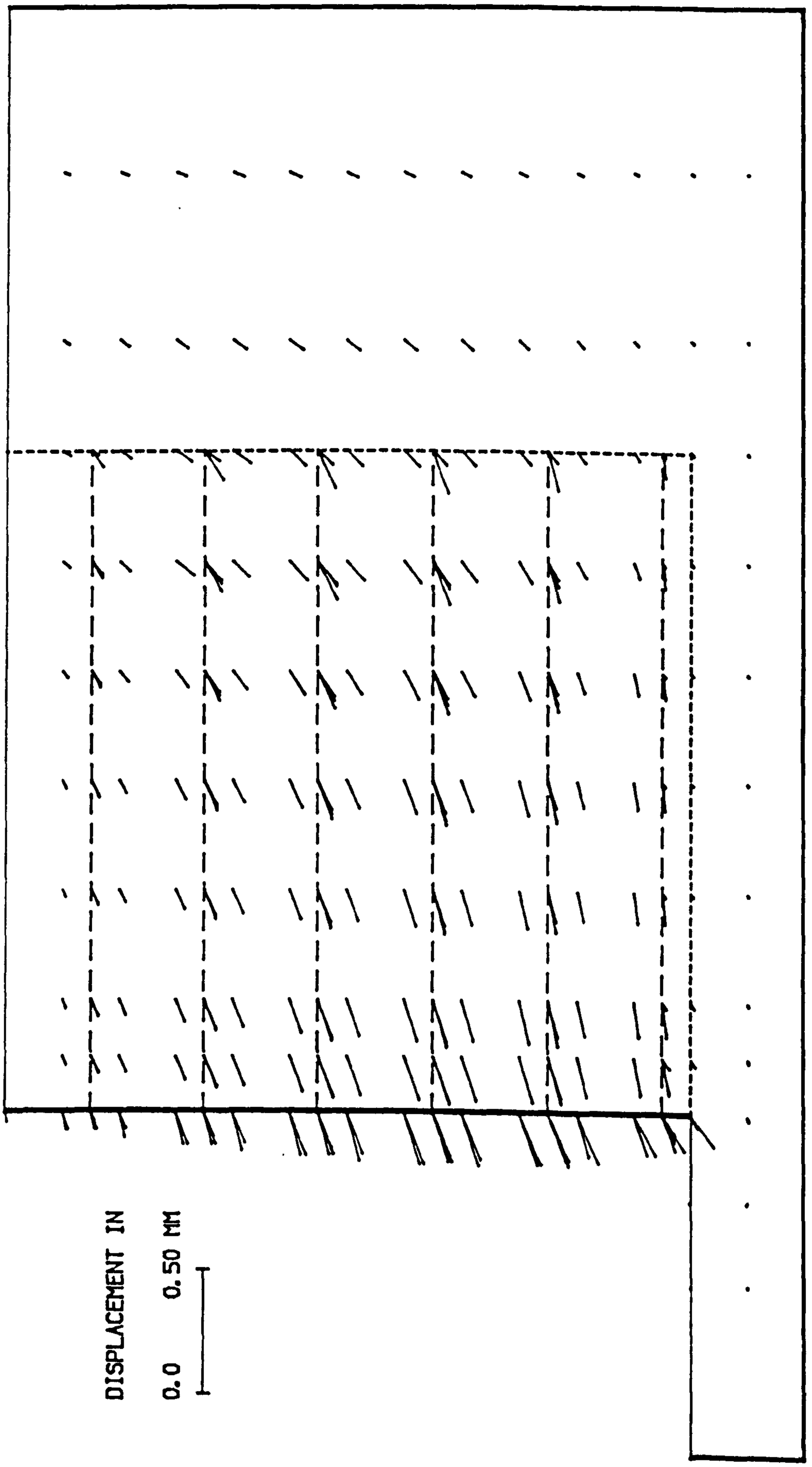

FIG. (9.4) DISPLACEMENTS IN BACKFILL SOIL (WITHOUT COMP. & USING THE SAME DENSITY AS COMP. LENG. = 600.0 MM).

(d) The compaction has almost no effect either on the backfill behind the reinforced mass or in the foundation. This may be due to the high stiffness in the foundation and the boundary condition assumed in the idealization.

9.2.3 Lateral Movement Of The Wall Face

Lateral movements of the wall face of the reinforced earth wall are shown in Figs. (9.5&6) for the case of compaction and no compaction respectively. Generally the lateral movement in the case of compaction is 1.5 to 2 times that of the case without compaction.

The lateral movement in the upper half of the wall face is greater than in the lower half when using compaction and vice versa in the case of no compaction, due to the deflection which has occurred during compaction. In both cases the lateral movement of the toe is bigger than the top which implies that there is sliding and rotation of the reinforced mass.

9.2.4 Shear Strain Contours

The contours of maximum shear strain deformation due to compaction and without compaction of the reinforced earth wall model are shown in Figs. (9.7 & 8) respectively. The Figs. show the effect of compaction on maximum shear strain, indicating a concentration of contours near the wall face and around the reinforcement (strips) especially in the upper portions of the wall. Also near the toe, there is a concentration of contours. On the other hand in the case of no compaction, there are no large variations or concentrations in shear strain contours and most of the reinforced mass has a constant shear strain except in the upper part of the wall.

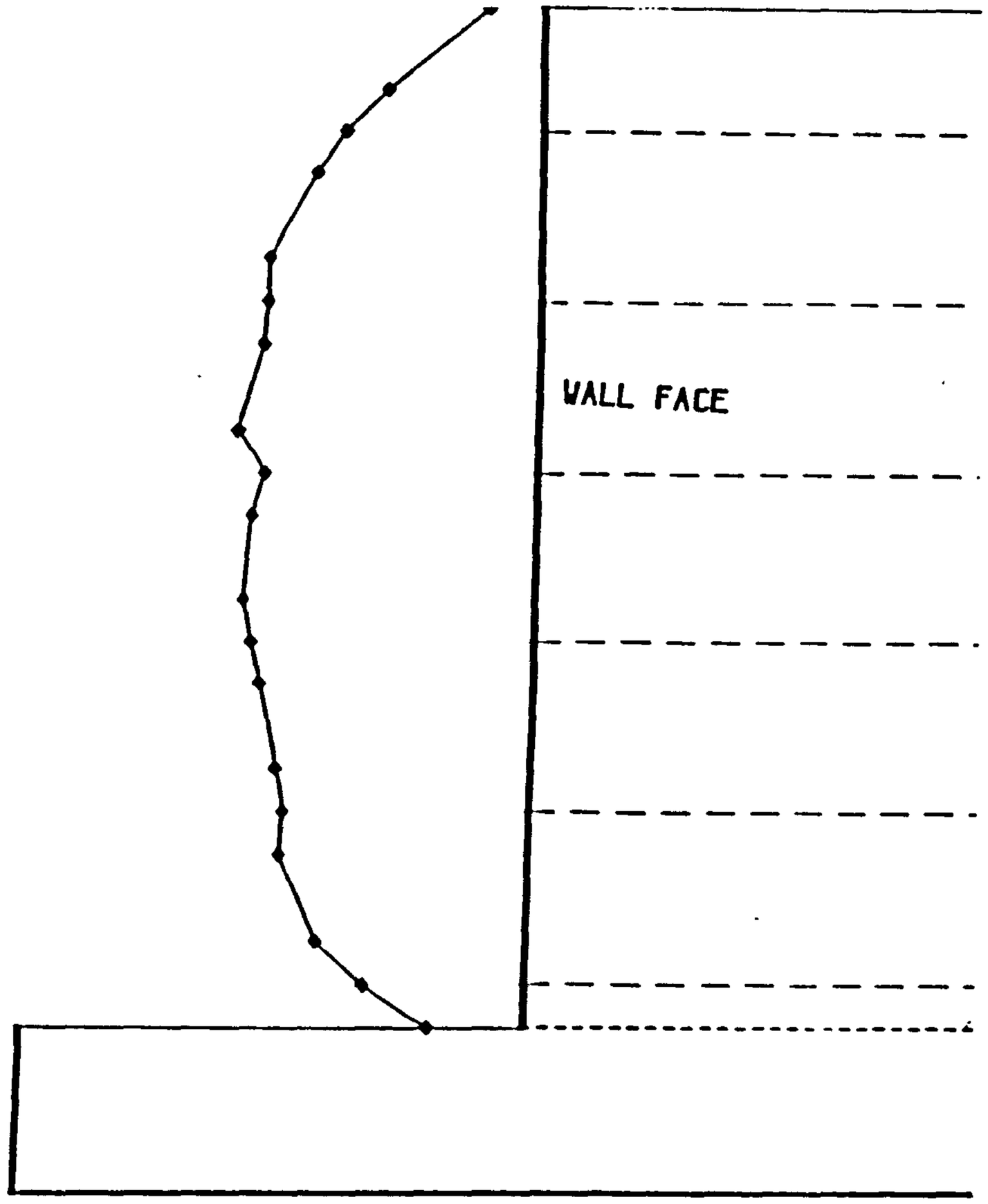

FIG. (9.5) THE CASE WITH COMP. LENG. = H

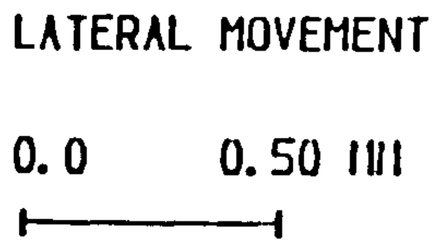

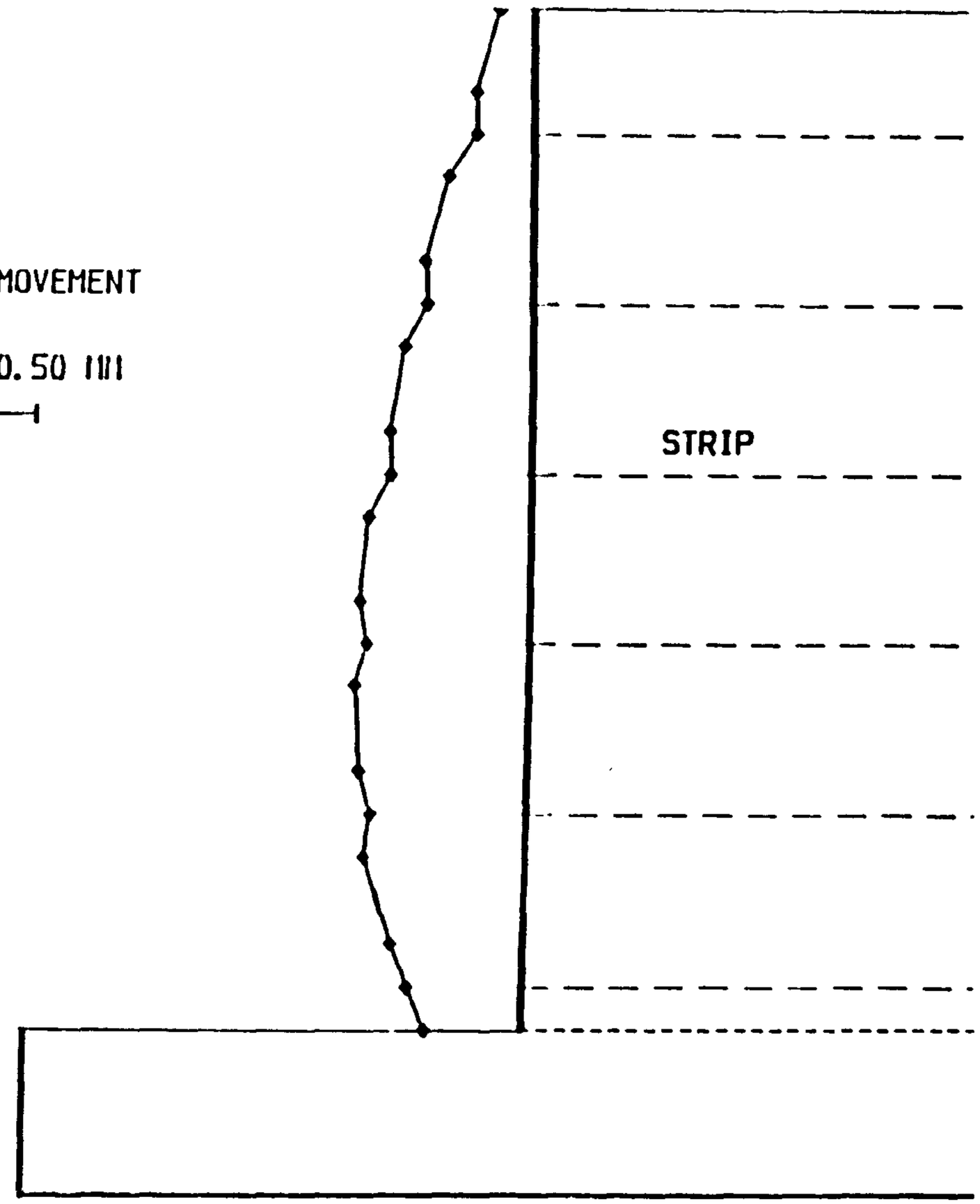

FIG. (9.6) THE CASE WITH NO COMP. & USING THE SAME DENSITY AS IN THE CASE OF COMP.

KEY	Z STRAIN
1	0.000
2	0.020
3	0.040
4	0.080
5	0.160
6	0.320
7	0.640

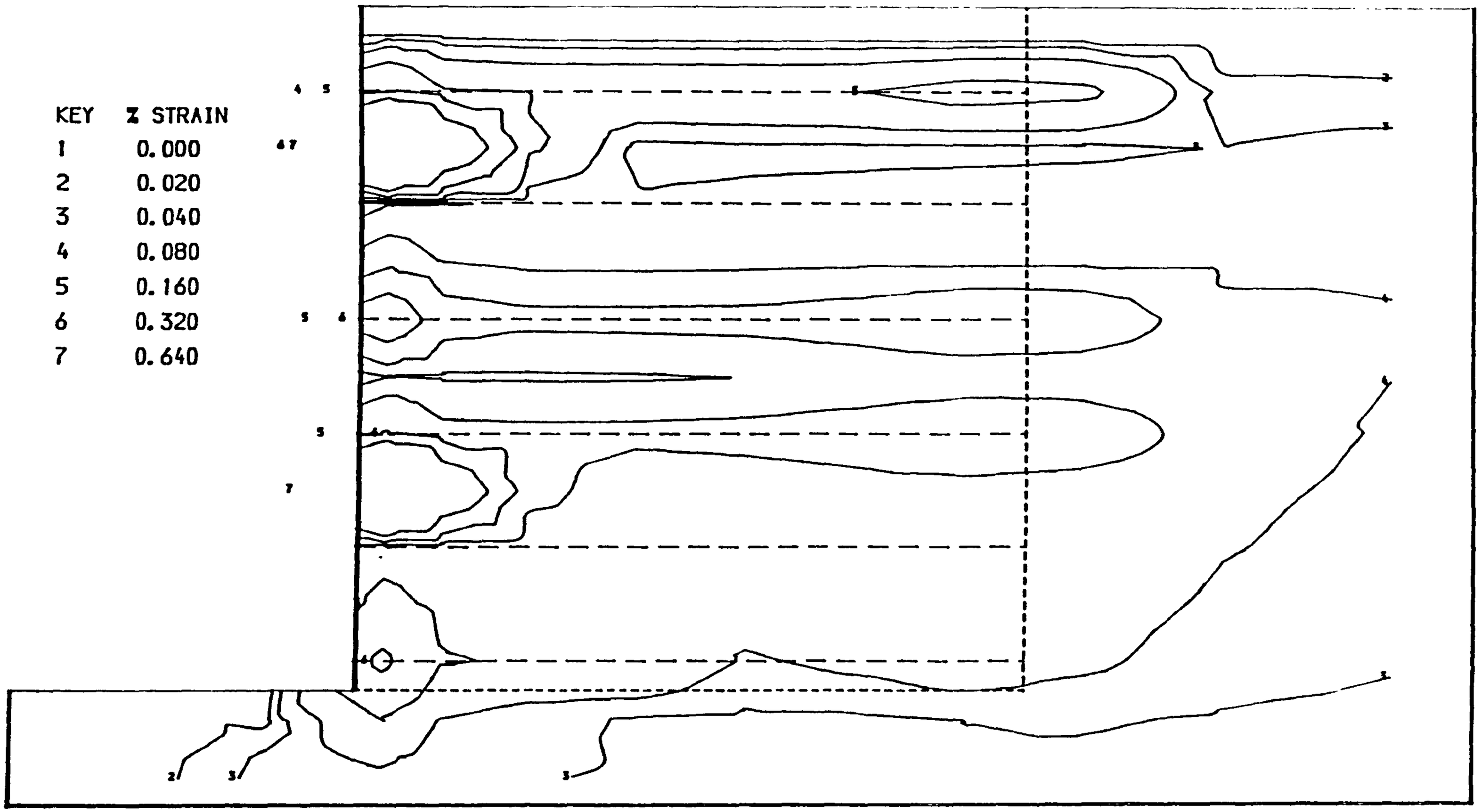

FIG. (9.7) MAX. SHEAR STRAIN CONTOURS, COMP. LENG. = 600.0 MM.

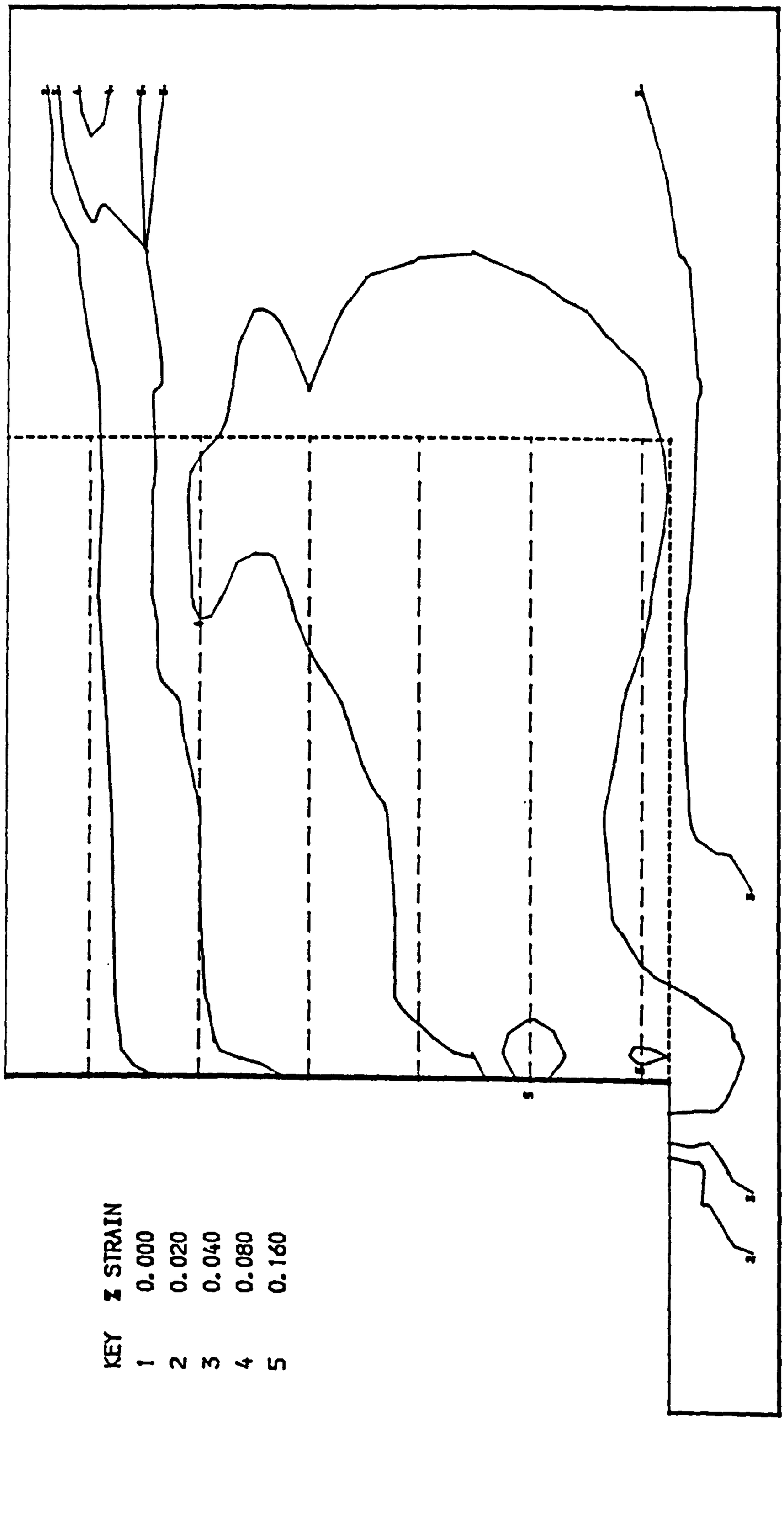

FIG. (9.8) MAX. SHEAR STRAIN CONTOURS (WITHOUT COMP. & USING THE SAME DENSITY AS COMP. LENG. = 600.0 MM).

Shear strain has occurred due to large deformations in the backfill due to compaction particularly behind the wall face and around the reinforced strips, where these deformations allow the friction forces between the soil and strips to mobilize to carry more tensile forces from the surrounding soil.

9.2.5 The Principal Stresses In Backfill

Soil element normal stresses are positive in compression. Figs. (9.9&10) show the major and minor principal stresses (SIG1 & SIG3) respectively and their orientation in the backfill of the reinforced earth retaining wall models with and without compaction respectively.

In both Figs. the major principal stress is compressive & the minor stress is compressive. The principal stresses increase with increasing depth of the backfill. This is obviously due to increase in the vertical stresses.

The minor principal stress in the case of compaction increases due to the additional and residual horizontal stress caused by the compaction load. The change of orientation of the principal stresses is slight within the reinforced mass, increasing clockwise just behind the wall face, and the reinforced mass and behind it.

The explanation is that the reinforced earth retaining wall models were not designed up to failure but under the normal working load which occurs in the field. Also this gives an impression that the presence of reinforcement in the soil gives it other properties which make the new composite material act as one unit.

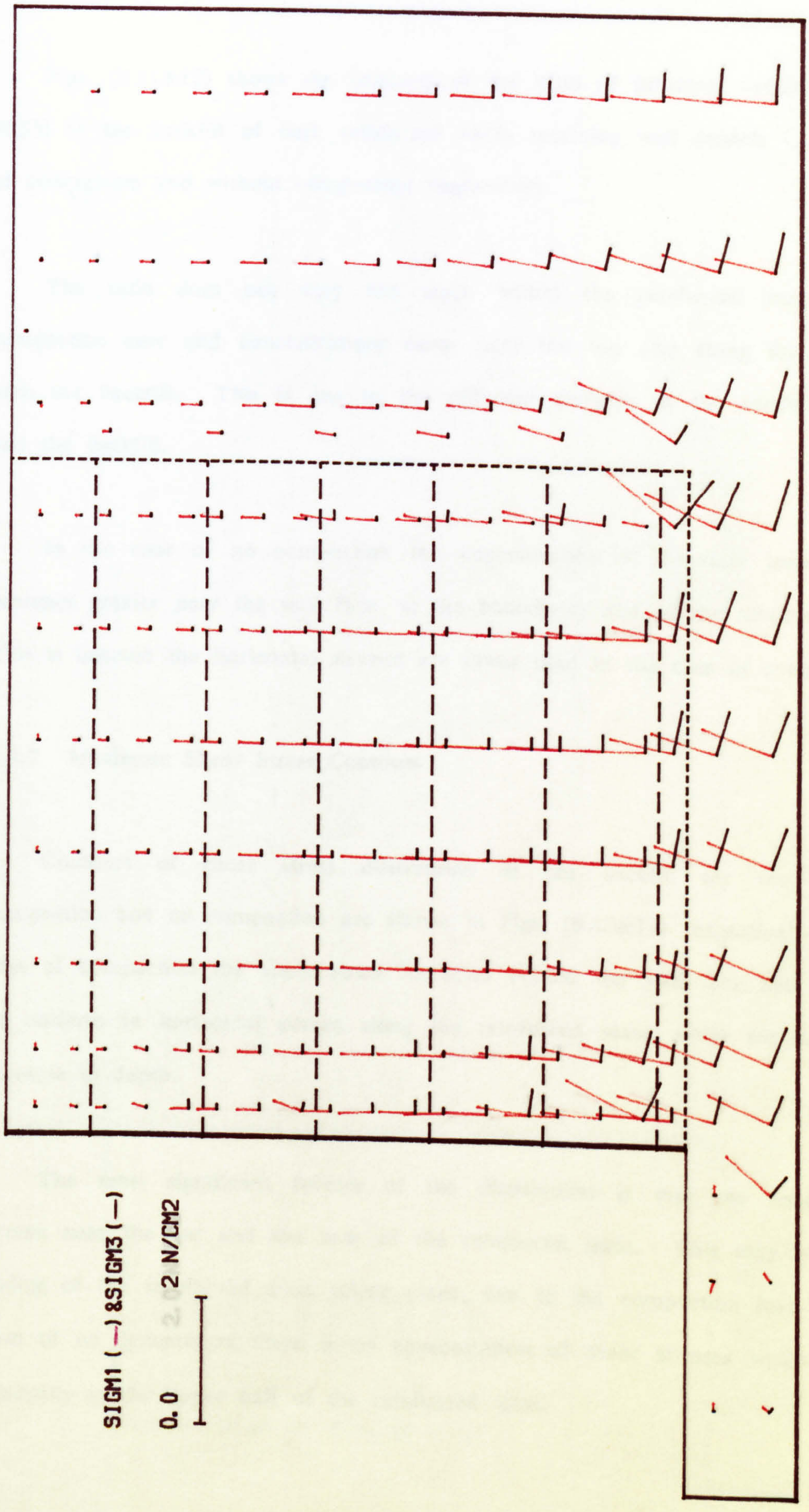

FIG. (9.9) THE PRINCIPAL STRESSES (SIGM1&SIGM3) IN BACKFILL SOIL, COMP. LENG. = 600. MM.

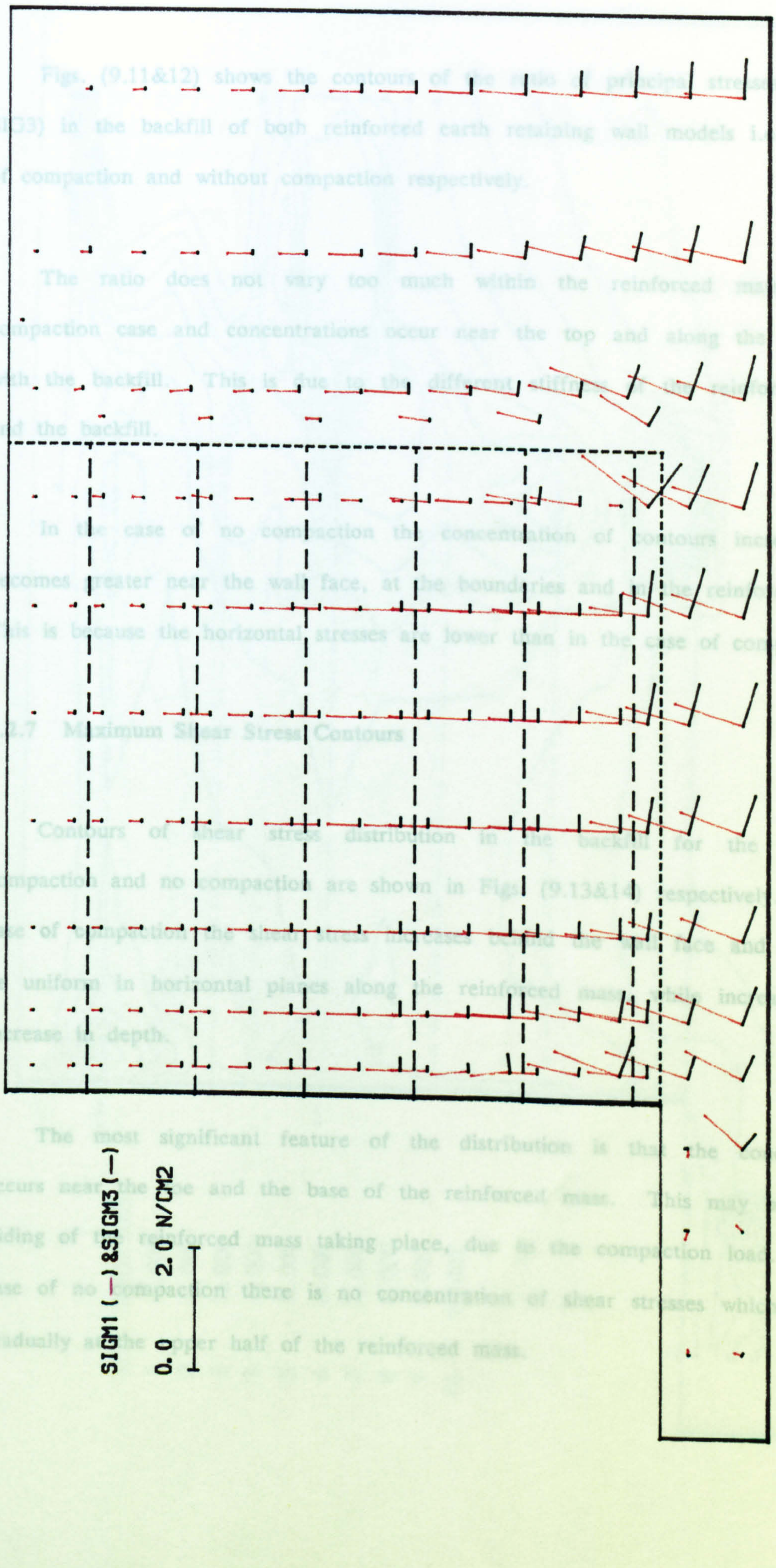

FIG. 19.10 THE PRINCIPAL STRESSES (SIGM1&SIGM3) IN BACKFILL SOIL (WITHOUT COMP. USING THE SAME DENSITY AS COMP. LENG. = 600.0 MM).

9.2.6 The Contours Of Ratio Of Principal Stresses

Figs. (9.11&12) shows the contours of the ratio of principal stresses (SIG1 / SIG3) in the backfill of both reinforced earth retaining wall models i.e. in case of compaction and without compaction respectively.

The ratio does not vary too much within the reinforced mass in the compaction case and concentrations occur near the top and along the boundary with the backfill. This is due to the different stiffness of the reinforced mass and the backfill.

In the case of no compaction the concentration of contours increases and becomes greater near the wall face, at the boundaries and in the reinforced mass. This is because the horizontal stresses are lower than in the case of compaction.

9.2.7 Maximum Shear Stress Contours

Contours of shear stress distribution in the backfill for the cases of compaction and no compaction are shown in Figs. (9.13&14) respectively. In the case of compaction the shear stress increases behind the wall face and seems to be uniform in horizontal planes along the reinforced mass, while increasing with increase in depth.

The most significant feature of the distribution is that the concentration occurs near the toe and the base of the reinforced mass. This may be due to sliding of the reinforced mass taking place, due to the compaction load. In the case of no compaction there is no concentration of shear stresses which increase gradually at the upper half of the reinforced mass.

KEY	SIG1/SIG3
1	1.000
2	2.000
3	3.000
4	4.000
5	5.000
6	6.000
7	7.000
8	8.000
9	9.000
10	10.000

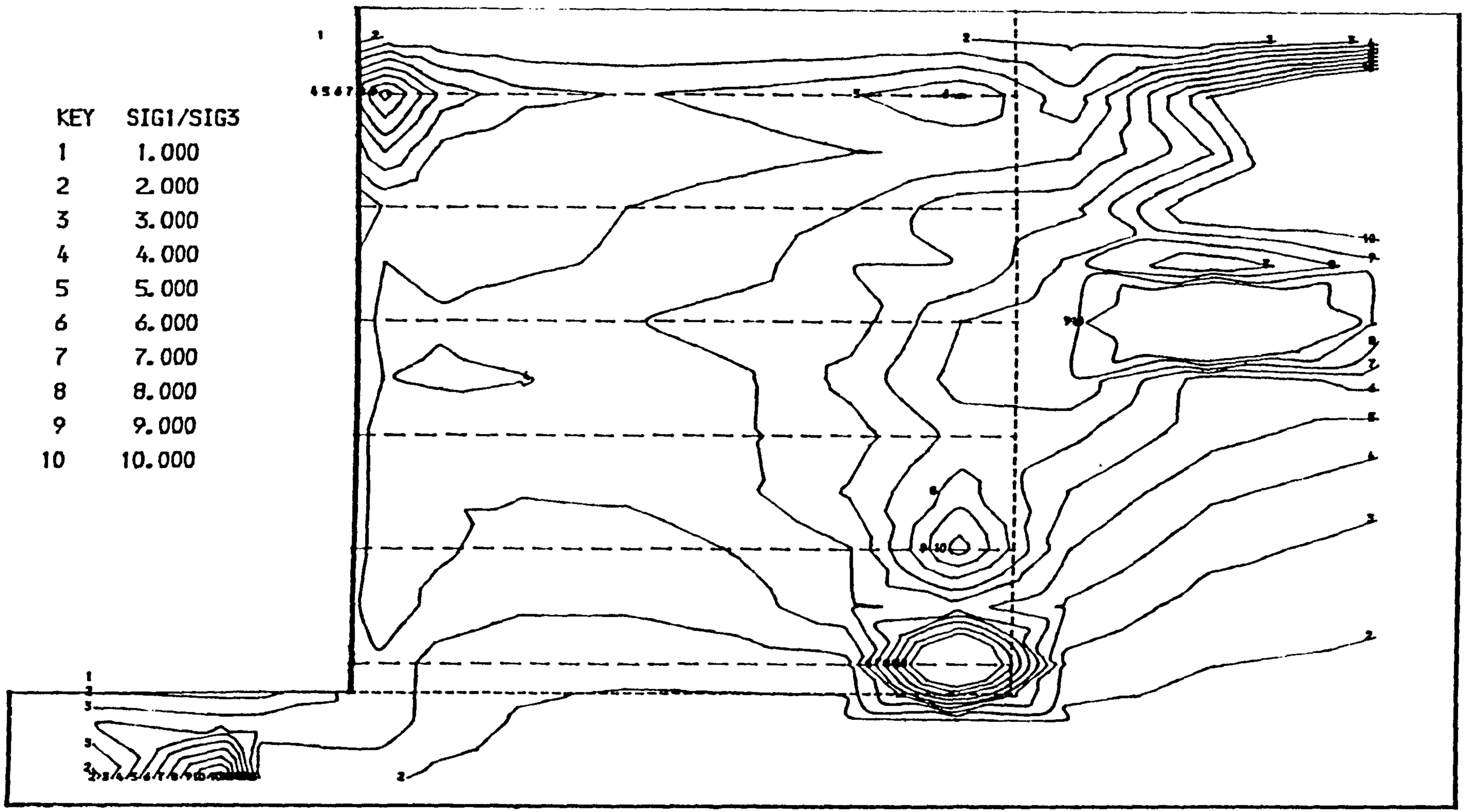

FIG. (9.11) THE CONTOURS OF RATIO OF PRINCIPAL STRESS (SIG1/SIG3), COMP. LENG. = 600.0 MM.

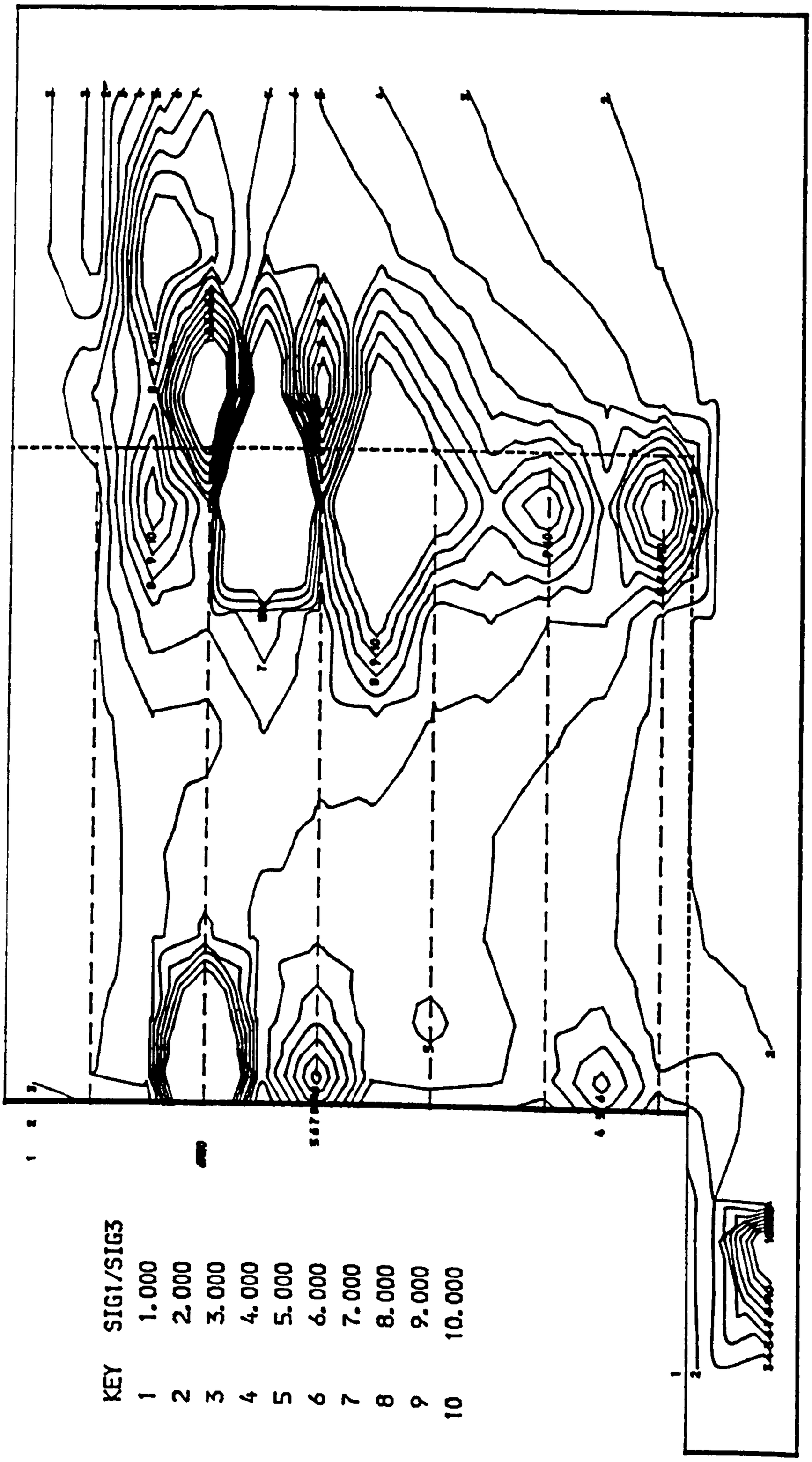

FIG. (9.12) THE CONTOURS OF RATIO OF PRINCIPAL STRESS (SIG1/SIG3), (WITHOUT COMP. & USING THE SAME DENSITY AS COMP. LENG. = 600.0 MM).

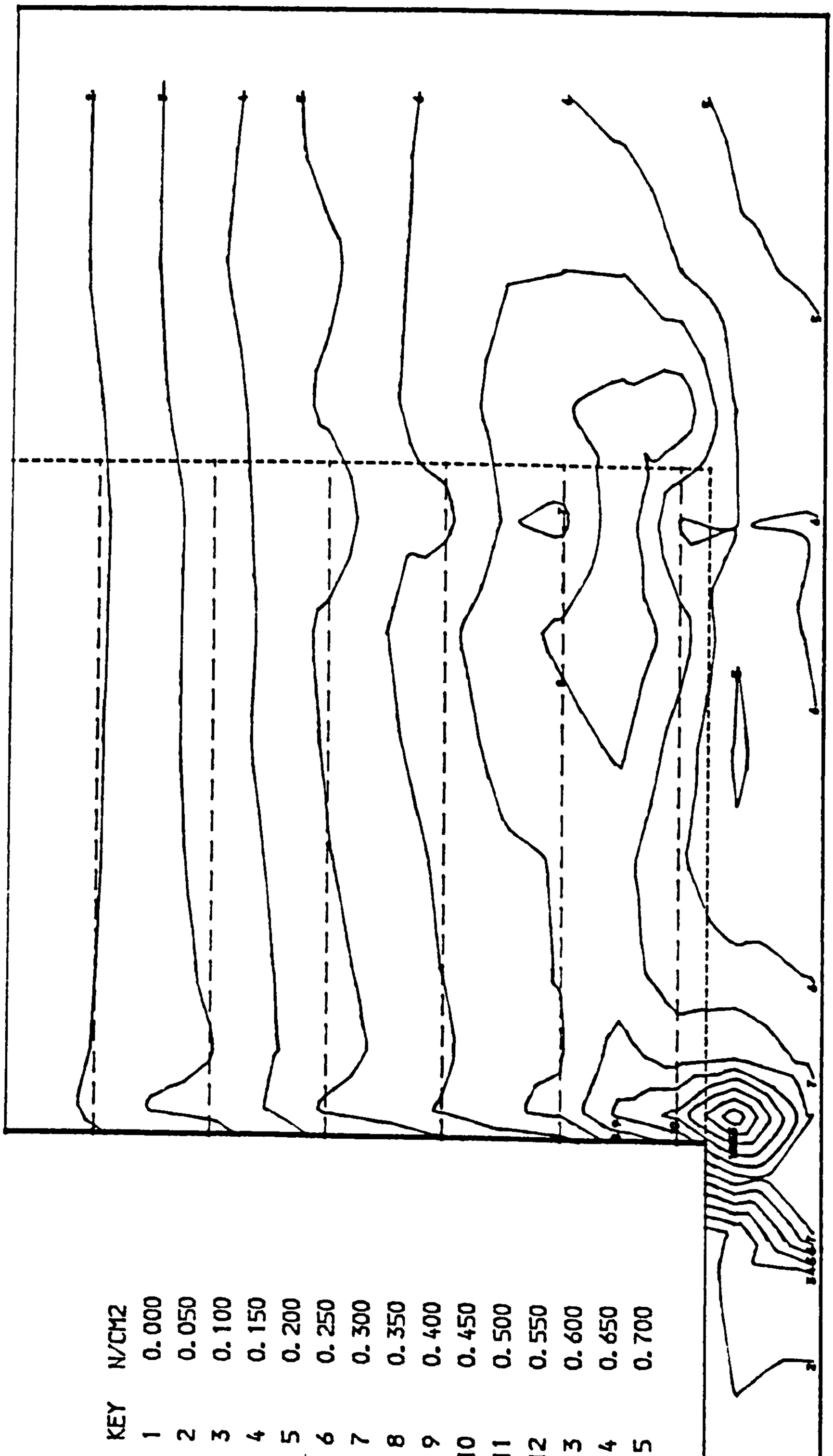

KEY	N/CM2
1	0.000
2	0.050
3	0.100
4	0.150
5	0.200
6	0.250
7	0.300
8	0.350
9	0.400
10	0.450
11	0.500
12	0.550
13	0.600
14	0.650
15	0.700

FIG. (9.13) MAX. SHEAR STRESS CONTOURS, COMP. LENG. = 600.0 MM.

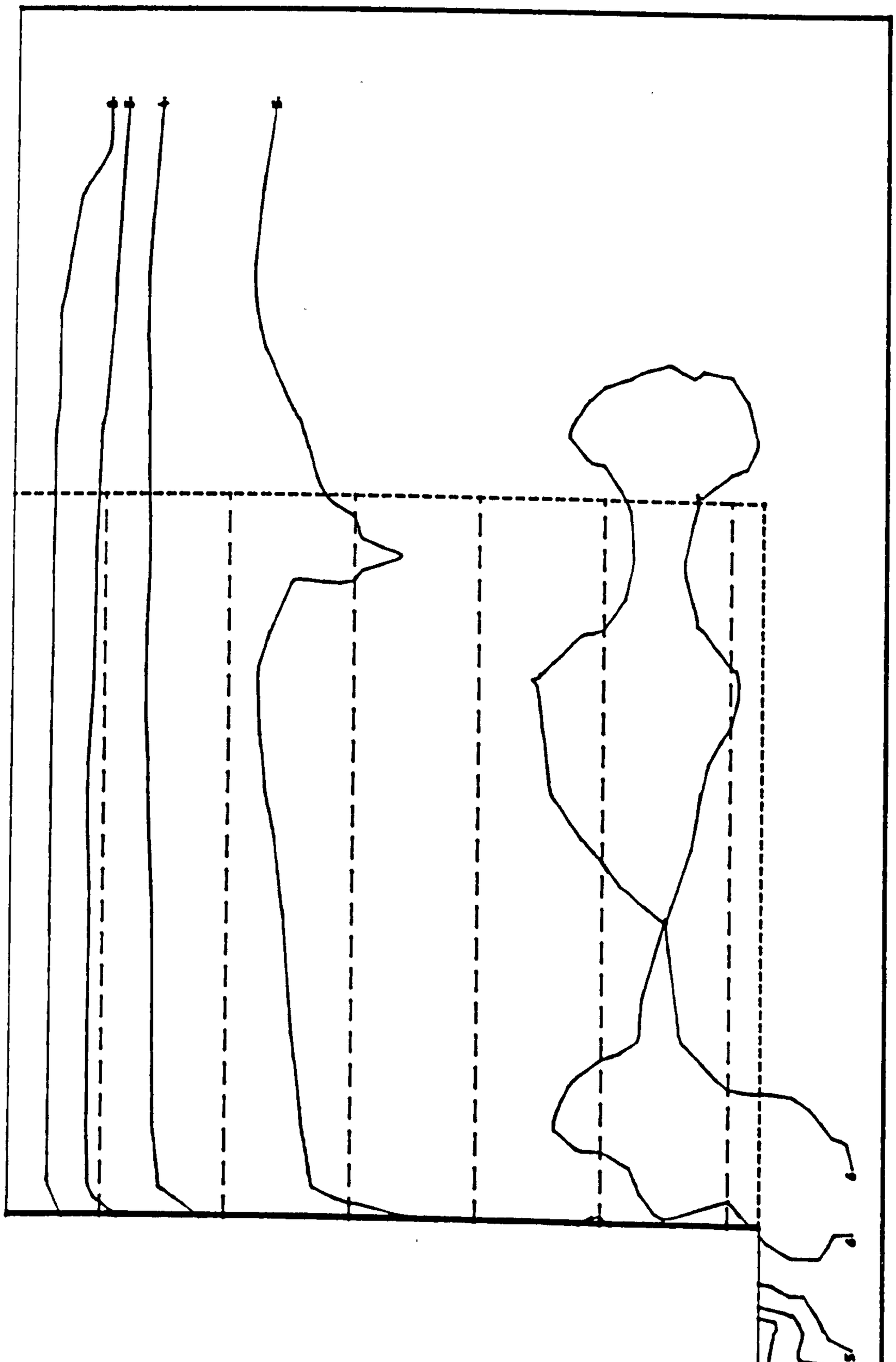

FIG. (9.14) MAX. SHEAR STRESS CONTOURS (WITHOUT COMP. & USING THE SAME DENSITY AS COMP. LENG. = 600.0 MM).

9.2.8 State Of Stresses in the Backfill

Contours of coefficient of earth pressure (K) calculated as the ratio between horizontal stress (σ_x) and vertical stress (σ_y) are shown in Figs. (9.15&16) for the cases of compaction and no compaction respectively.

In the case of compaction the value of coefficient of earth pressure (K) near the top varies from 0.1 to 0.4, behind the wall from 0.2 to 0.3, near the base from 0.3 to 0.4, and within the mass from 0.2 to 0.3 . The average value within the mass is 0.25. Comparing these values with the values of active and at rest condition, which are 0.18 & 0.31 respectively, it can be seen that the state of stress within the upper third of the wall is more than the at rest condition and decreases to near the at rest condition within the rest of the reinforced mass. This is due to the increase in horizontal stresses caused by the compaction load effect.

In the case of no compaction the average value within the mass is 0.2 which is between the active and at rest condition. This is due to the horizontal stresses being smaller than in the case of compaction, while there is no big difference in vertical stresses.

9.2.9 Distribution of Horizontal Stresses

Figs. (9.17 & 18) show the distribution of horizontal stresses at three sections (behind the wall face, at the middle and behind the reinforced mass), for all cases of using compaction and without compaction respectively.

It can be seen that the earth pressure in the case of compaction exceeds the

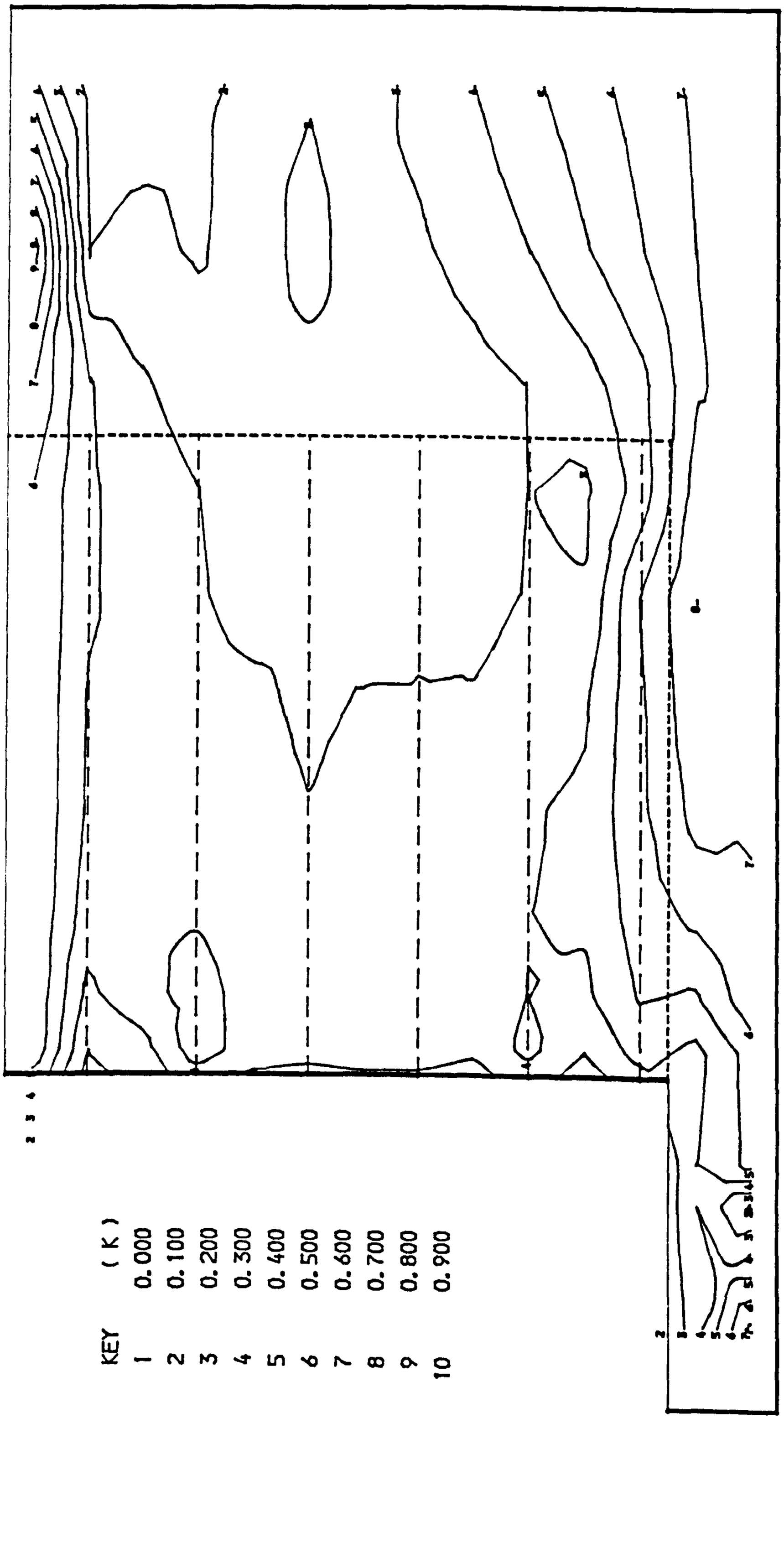

KEY (K)
1 0.000
2 0.100
3 0.200
4 0.300
5 0.400
6 0.500
7 0.600
8 0.700
9 0.800
10 0.900

FIG. (9.15) THE CONTOURS OF STATE OF STRESSES IN THE BACKFILL SOIL (COEFFICIENT OF EARTH PRESSURE VALUES), COMP. LENG. = 600.0 MM.

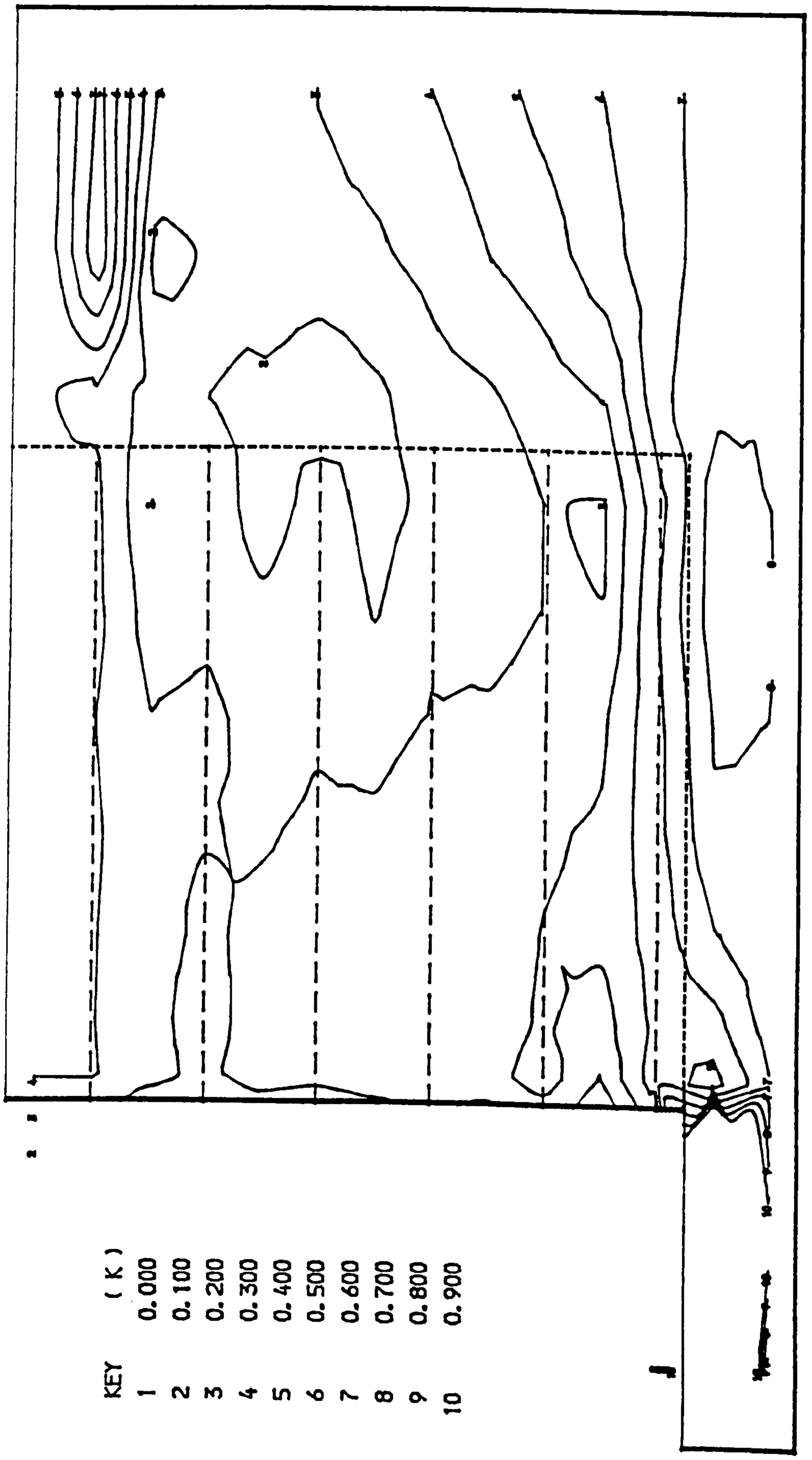

FIG. (9.16) THE CONTOURS OF STATE OF STRESSES IN THE BACKFILL SOIL (COEFF. OF EARTH PRESSURE VALUES), WITHOUT COMP. & USING THE SAME DENSITY AS COMP. LENG. = 600.0 MM

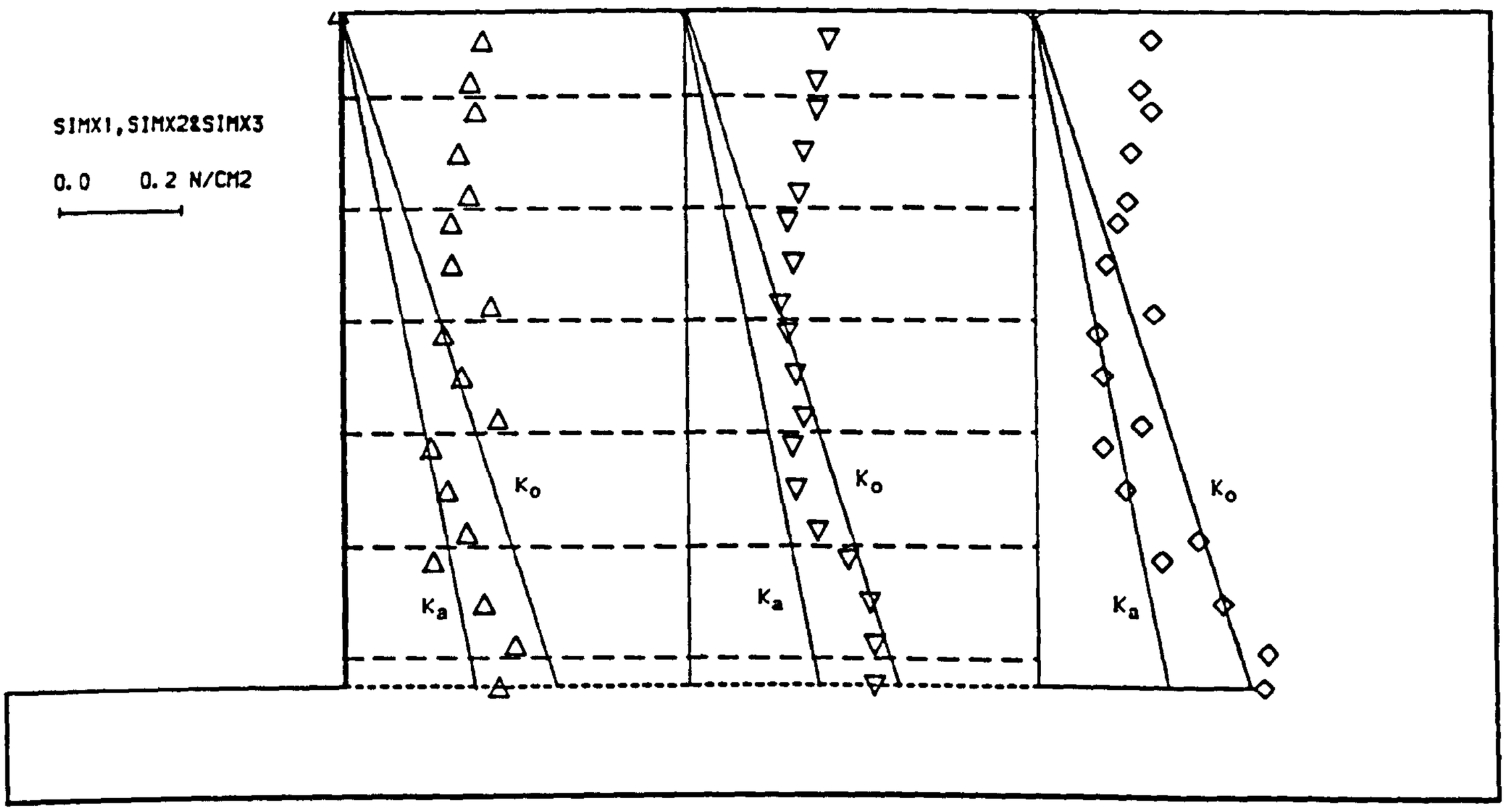

FIG. (9.17) MAX. HORIZ. STRESSES AT THE FACE OF VALL, MIDDLE&BEHIND REINF. MASS, COMP. LENG. =600.0 MM.

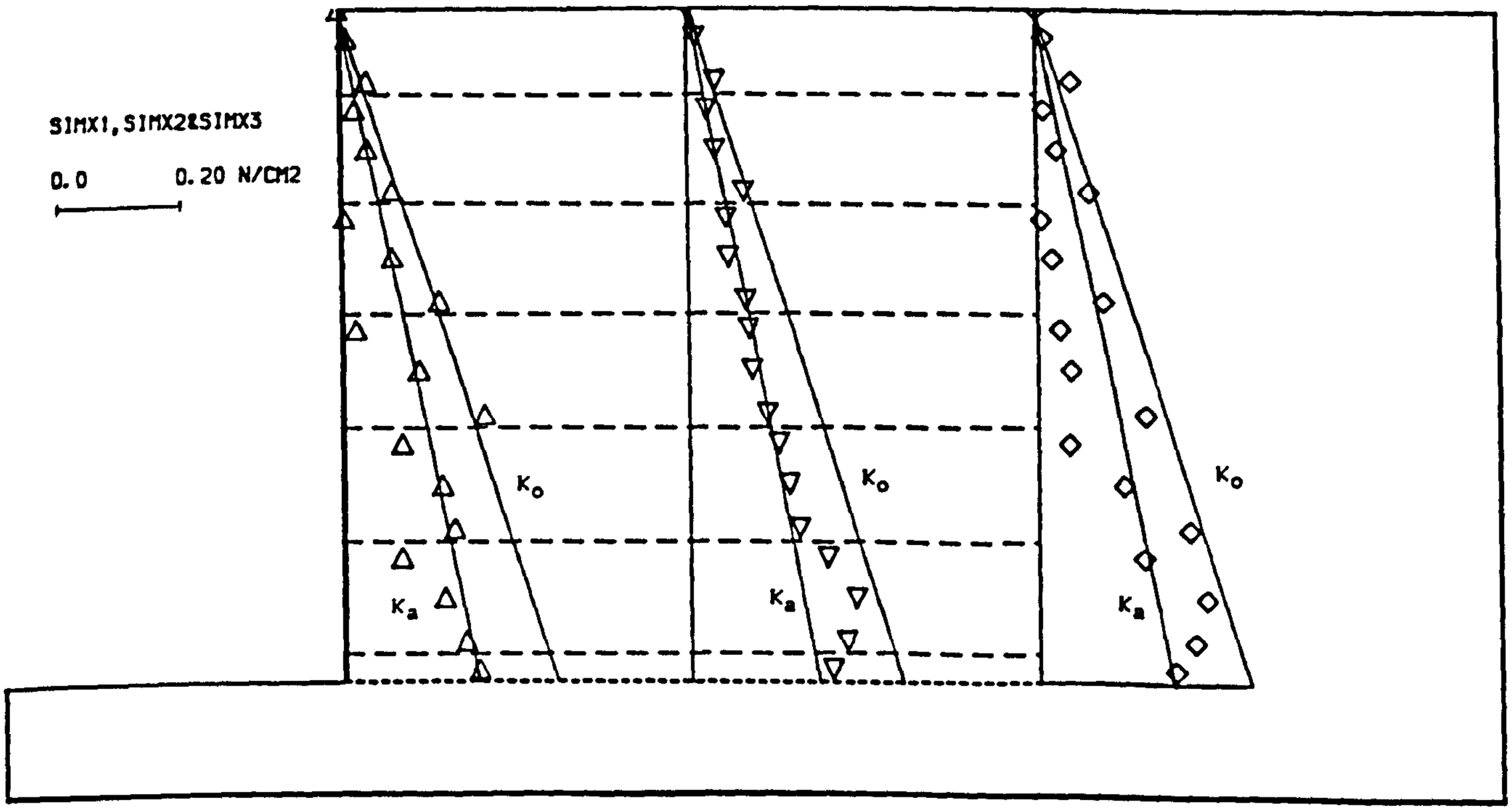

FIG. (9.18) MAX. HORIZ. STRESSES AT THE FACE OF VALL, MIDDLE&BEHIND REINF. MASS, VITHOUT COMP. & USING THE SAME DENSITY AS COMP. LENG. = 600.0 MM.

at rest condition in the upper third at the three vertical planes, at times reaching more than double the earth pressure at rest. It approaches the at rest condition within the middle third.

At the lower third in the plane behind the wall face it reaches the active state, in the middle plane in the reinforced mass it is between the active and at rest condition, and behind the reinforced mass it varies from active to greater than the at rest conditions.

In the case of no compaction, the distribution of earth pressure at the wall face and behind the reinforced mass varies from the active condition near the top to the at–rest condition near the base. The average distribution is near the active state. Values lower than the active state are due to the assumption employed in the program that the behaviour of the soil is isotropic. At the middle plane the earth pressure is fairly coincident with the active state, expect near the base where it lies between the active and at rest condition.

From the above description it can be seen that compaction has a great effect on the earth pressure by changing the state of stresses within the backfill to be greater than the at–rest condition in some places within the reinforced mass. This is due to the residual horizontal stresses locked in the soil by the compaction.

9.2.10 Distribution Of Vertical Stresses Under the Reinforced Mass

Vertical stresses under the reinforced mass with and without compaction are shown in Figs. (9.19&20) respectively. The general pattern of distribution is almost the same in each case, values near the toe being greatest because the

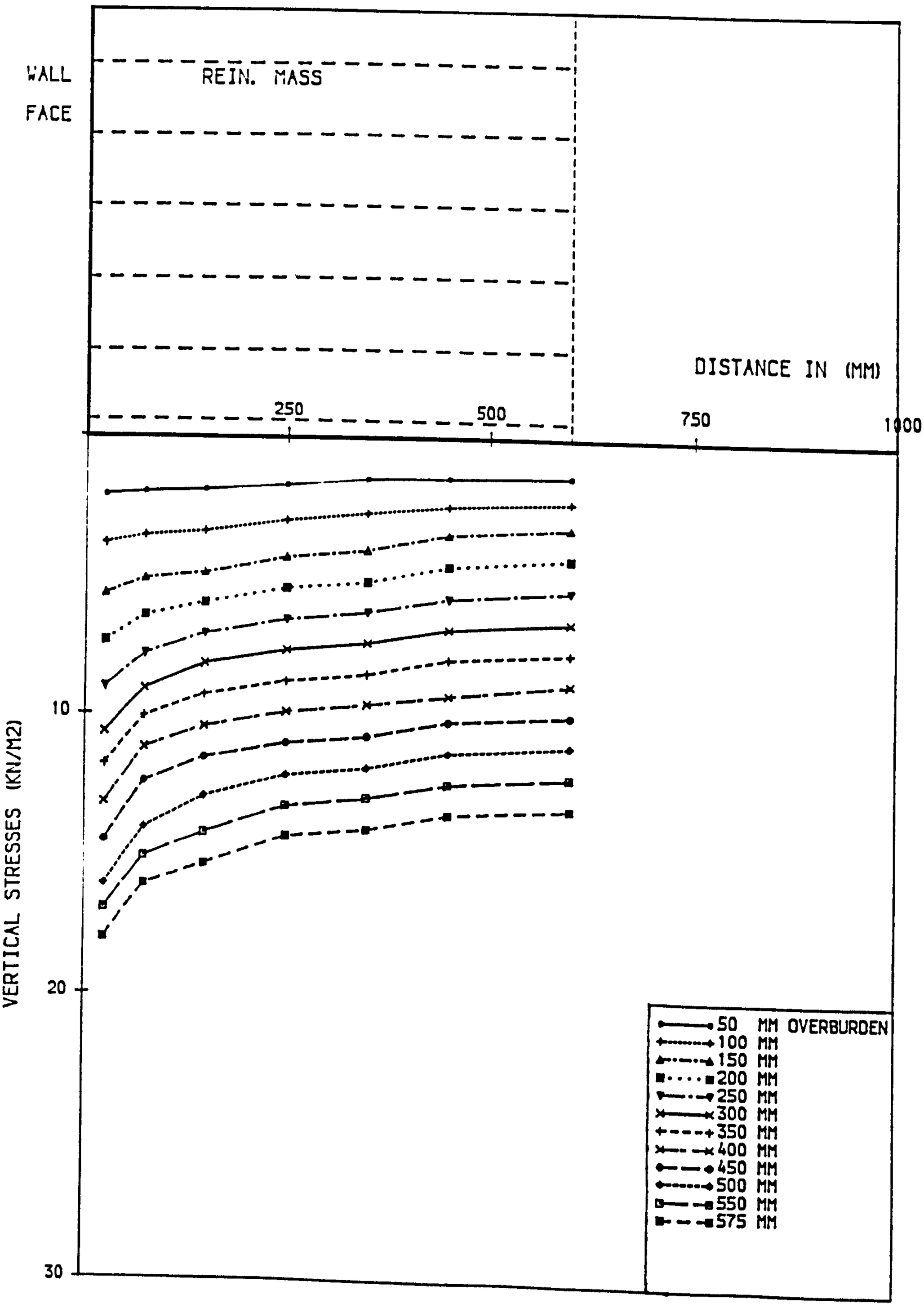

FIG. (9.19) DISTRIBUTION OF VERTICAL STRESSES UNDER THE REINF. MASS & COMP. LENG. = 600.00 MM.

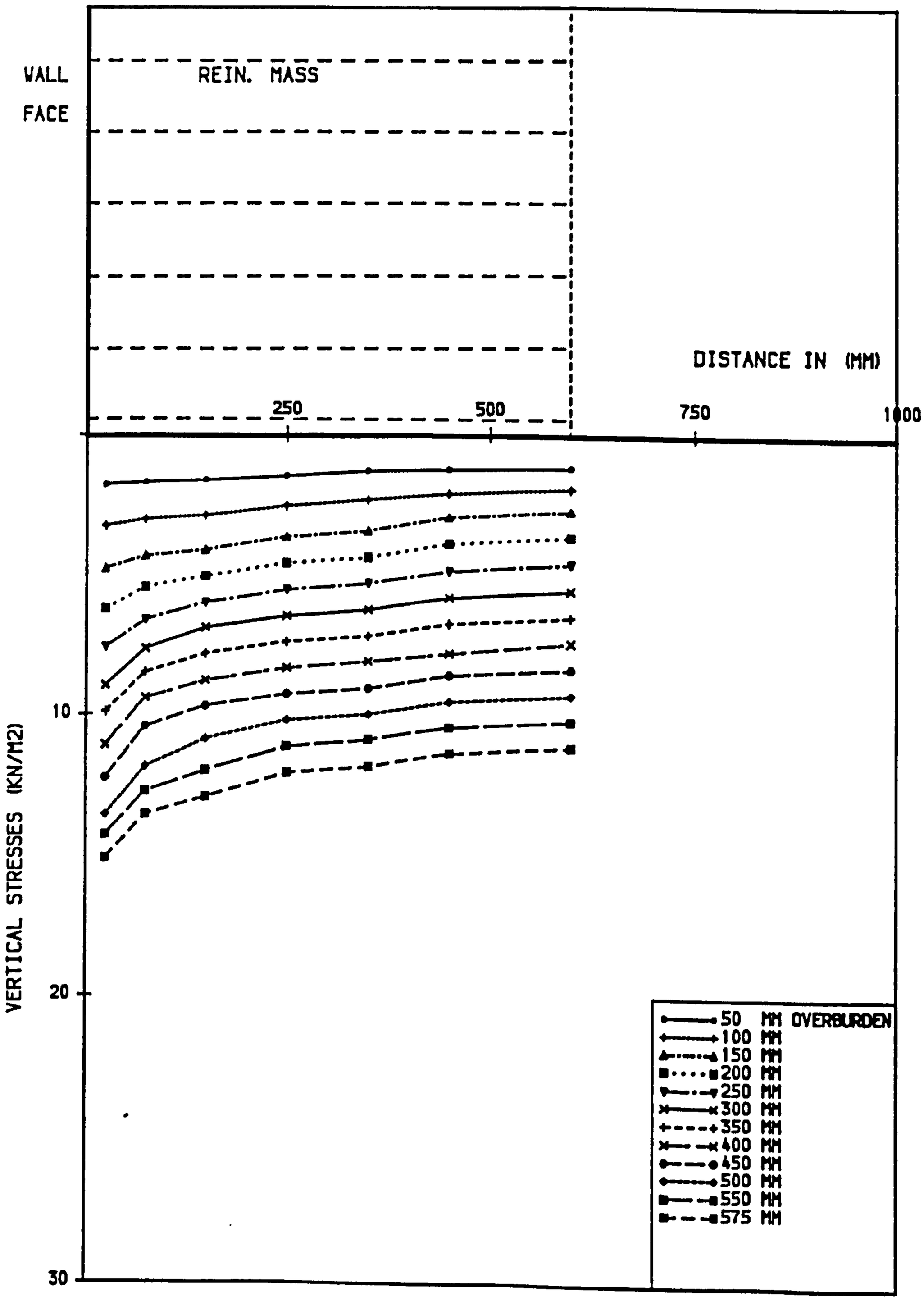

FIG. (9.20) VERTICAL STRESSES UNDER THE REINF. MASS, WITHOUT COMP. & USING THE SAME DENSITY AS COMP. LENG. = 600.0 MM.

reinforced earth wall acts as a flexible footing over the sand.

In the compaction case, the values near the toe are larger than for the case without compaction, and start to decrease rapidly to a point at about 10% of the base width, before increasing slightly towards the reinforced mass boundary. The reason for this is that tilting at the toe of the flexible system takes place due to the compaction load.

9.2.11 Distribution Of Forces In The Strips

These are given in Figs. (9.21,22&23) for the case of compaction and Figs. (9.24,25&26) for the case of no compaction. The distributions are given for three strips in each case as these represent the same strips which were mentioned in the model tests. They are as follows:

(a) Upper strip at 175 mm from the top.

(b) Middle strip at 375 mm from the top.

(c) Lower strip at 575 mm from the top.

In all Figs. the overburden indicates the height of the fill from the base of reinforced mass. In both cases the distributions are shown to be non uniform and all the forces are tensile. The largest tensile forces occur within the front half of the strips, and this may be due to the rigidity of wall face material. The forces decrease towards the free end and reach zero.

Also the forces decrease near the wall face but do not reach zero. The forces are greater in the lower strips than in the upper strips because of the increase in vertical stress with depth.

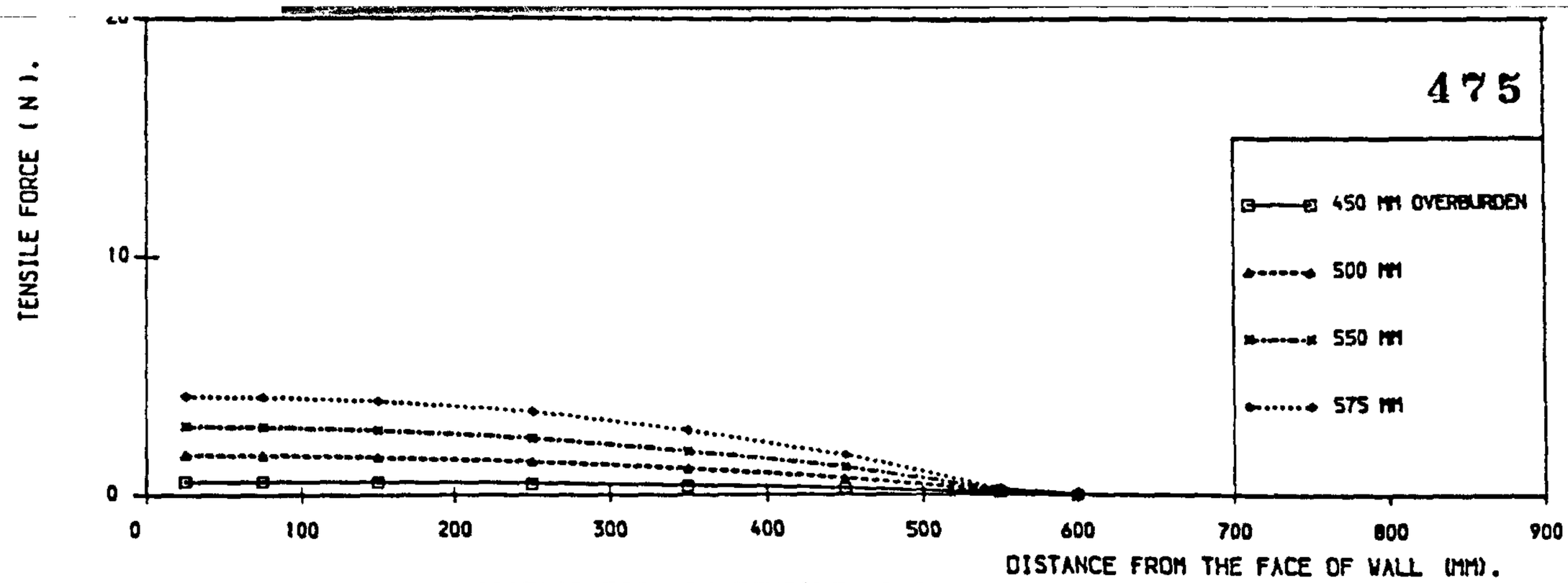

FIG. (9.21) DISTRIBUTION OF TENSILE FORCE IN UPPER STRIP (COMP. LENG. = 600.0 MM)

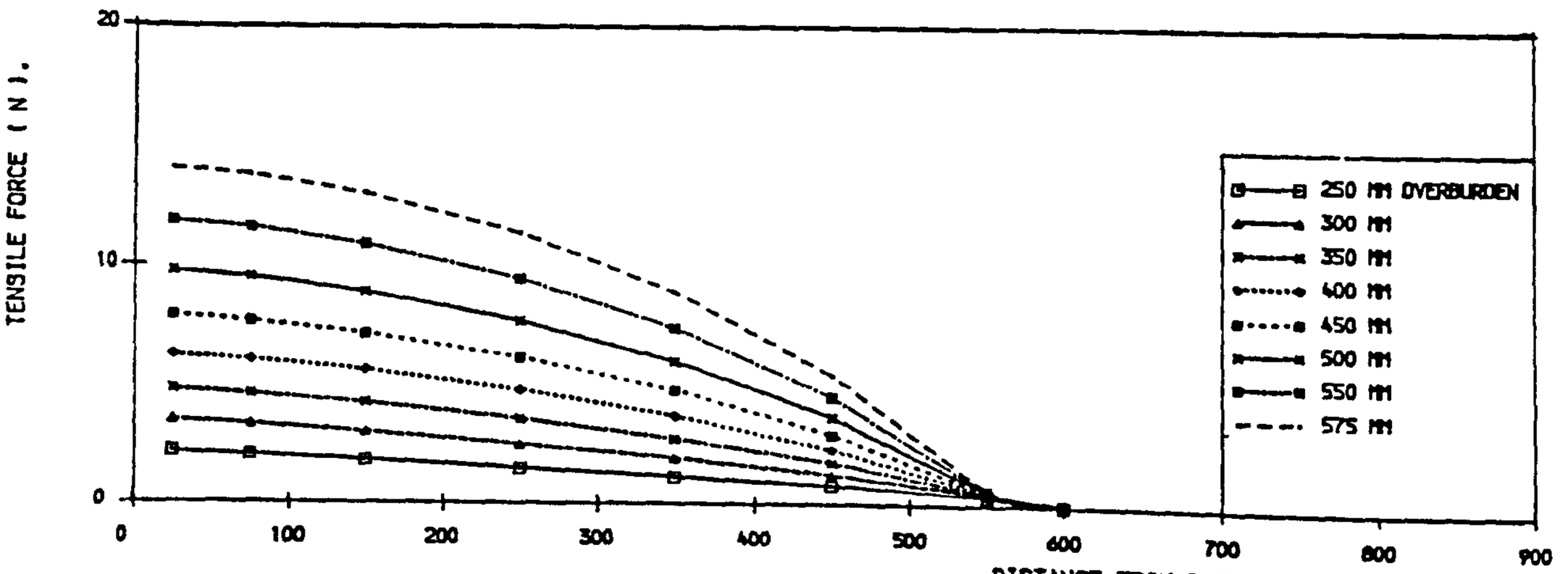

FIG. (9.22) DISTRIBUTION OF TENSILE FORCE IN MIDDLE STRIP (COMP. LENG. = 600.0 MM)

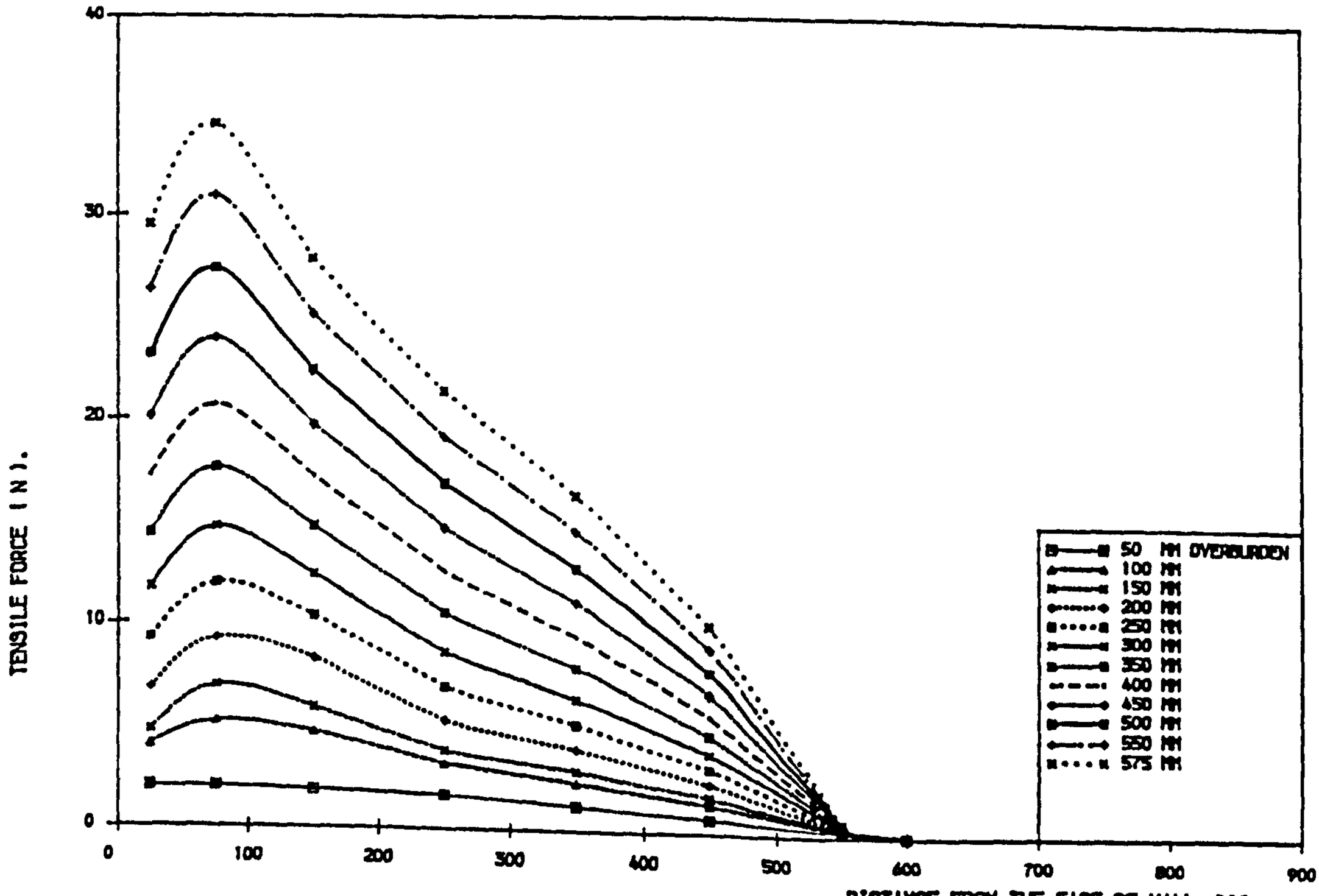

FIG. (9.23) DISTRIBUTION OF TENSILE FORCE IN LOWER STRIP (COMP. LENG. = 600.0 MM)

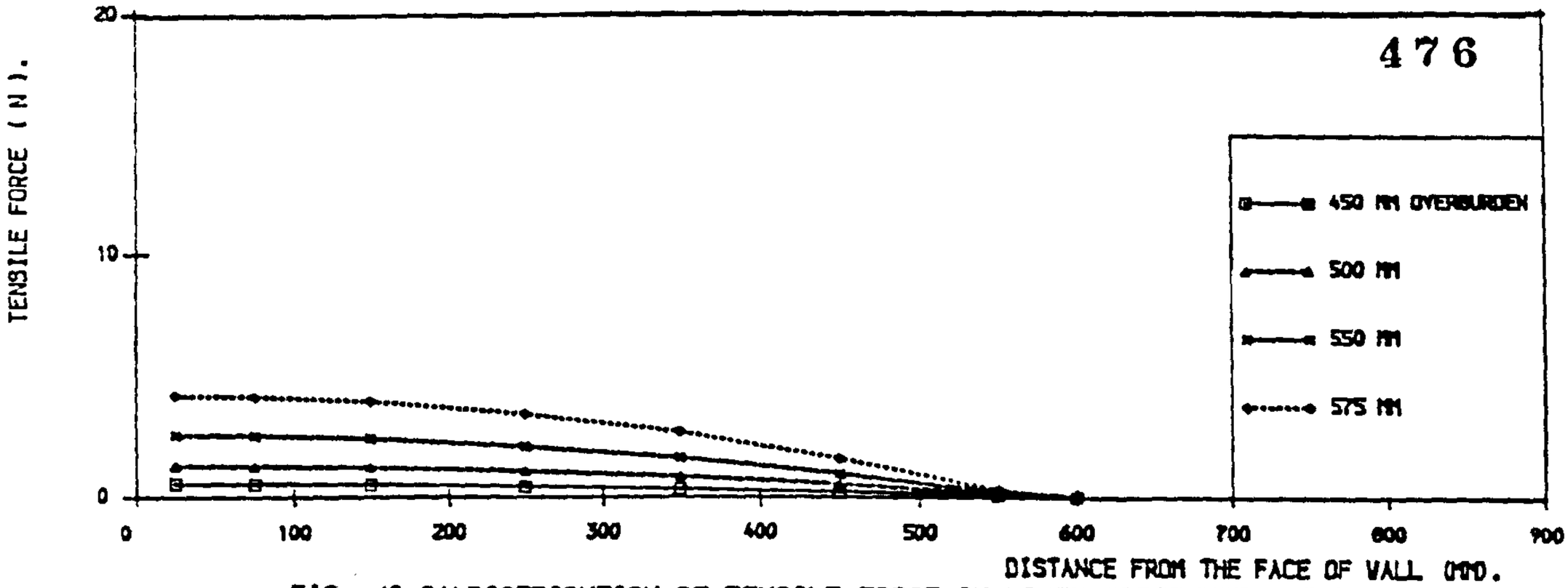

FIG. (9.24) DISTRIBUTION OF TENSILE FORCE IN UPPER STRIP (WITHOUT COMP. & USING THE SAME DENSITY AS COMP. LENG. =600.0 MM).

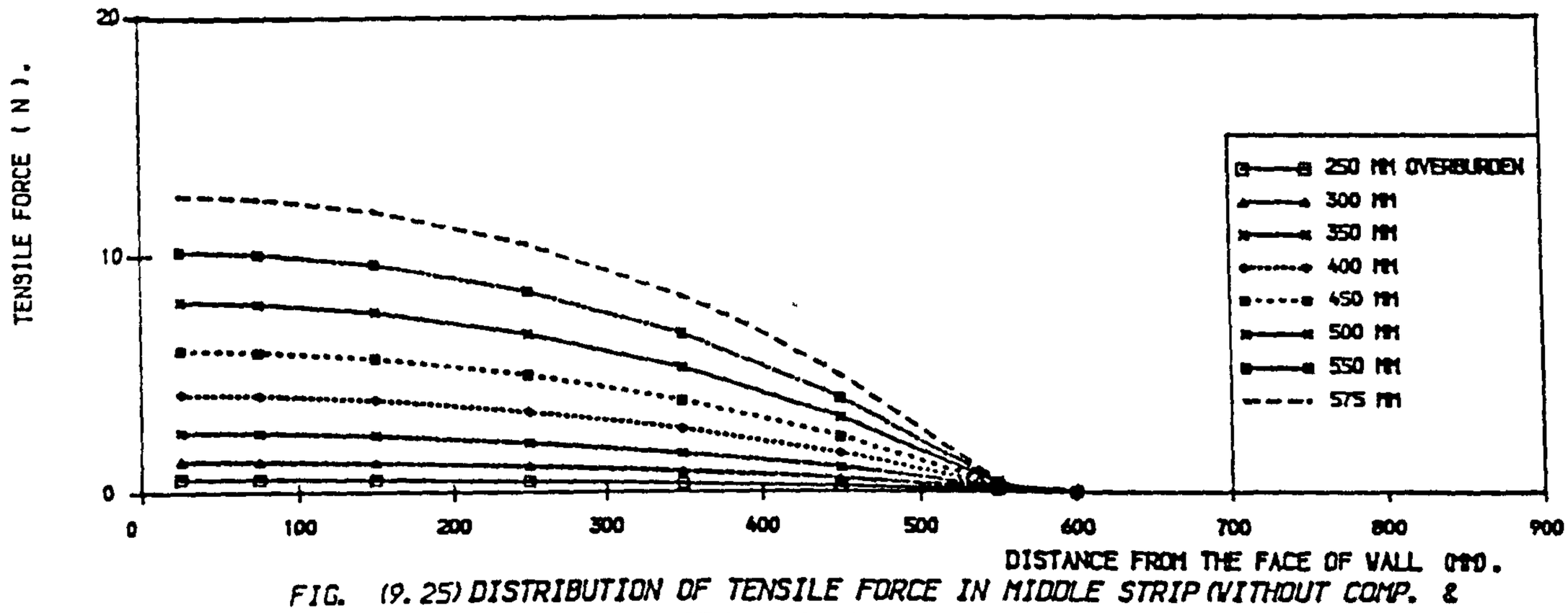

FIG. (9.25) DISTRIBUTION OF TENSILE FORCE IN MIDDLE STRIP (WITHOUT COMP. & USING THE SAME DENSITY AS COMP. LENG. = 600.0 MM).

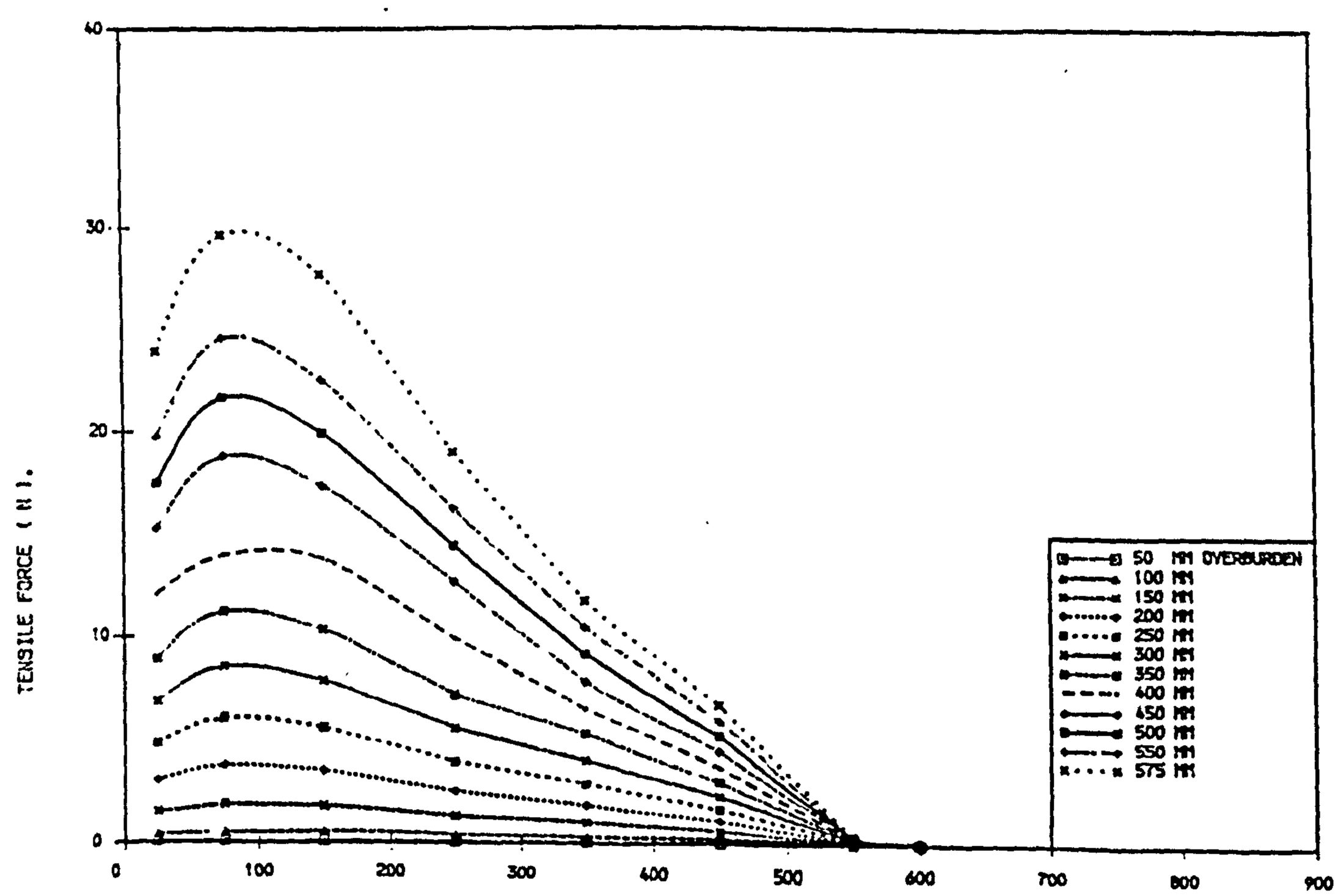

FIG. (9.26) DISTRIBUTION OF TENSILE FORCE IN LOWER STRIP (WITHOUT COMP. & USING THE SAME DENSITY AS COMP. LENG. = 600.0 MM).

The value of maximum tensile force in the lower strip in the case of compaction is 17% higher than in the case of no compaction. The position of maximum tensile force lies at 0.13 length of the wall face in the case of compaction and at 0.17 the length in no compaction. This is due to the increase in horizontal stresses and movement in the case of compaction, which helps to mobilize and increase the tensile force in the strip.

9.2.12 Distribution Of Internal Forces In The Wall Face

The distribution of normal forces, shear forces and bending moment in the wall face in both cases of compaction and no compaction are shown in Figs. (9.27&28); Figs. (9.29&30); and Figs. (9.31&32) respectively.

Since the results obtained from finite element methods are at the nodes of the mesh only, distributions of normal and shear forces and bending moment have been constructed by connecting the values at the nodes. This will affect the shape of distribution (i.e. the degree of the curves) but gives a reasonable idea of the value of the internal forces in the wall face, which should assist in design.

In both cases the normal forces, Figs. (9.27&28), are compressive and non−uniform and reach their maximum values at the lower third of the wall. It is interesting to note that the normal force occurs due to friction between the back surface of the wall face and the back fill as assumed in the finite element program. In the case of compaction the values are only slightly larger than with no compaction. This is due to the friction forces mobilized between the wall back and the soil due to displacements of the soil in vertical direction being slightly higher in the case of compaction.

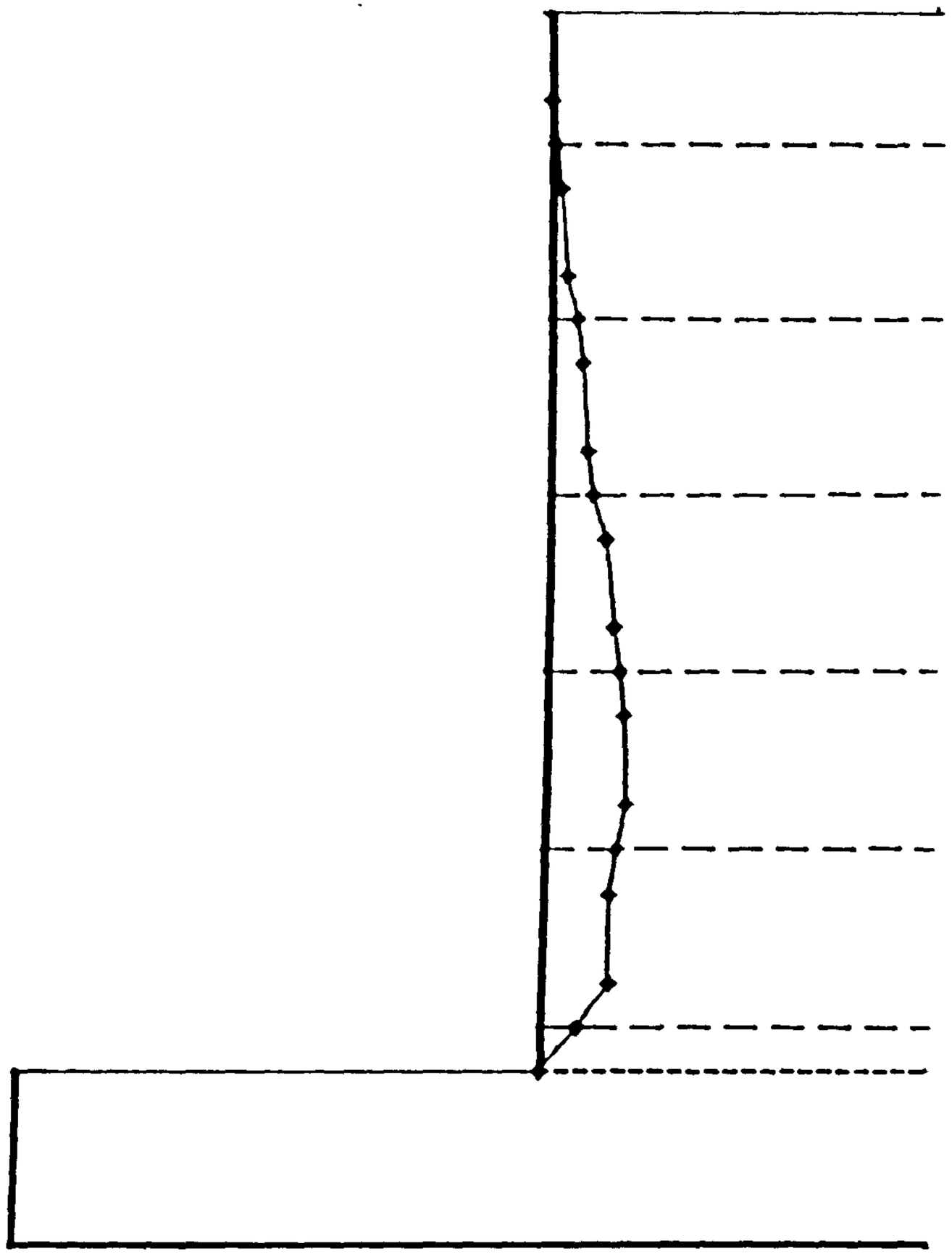

FIG. (9.27) COMP. LENG. = 600.0 MM.

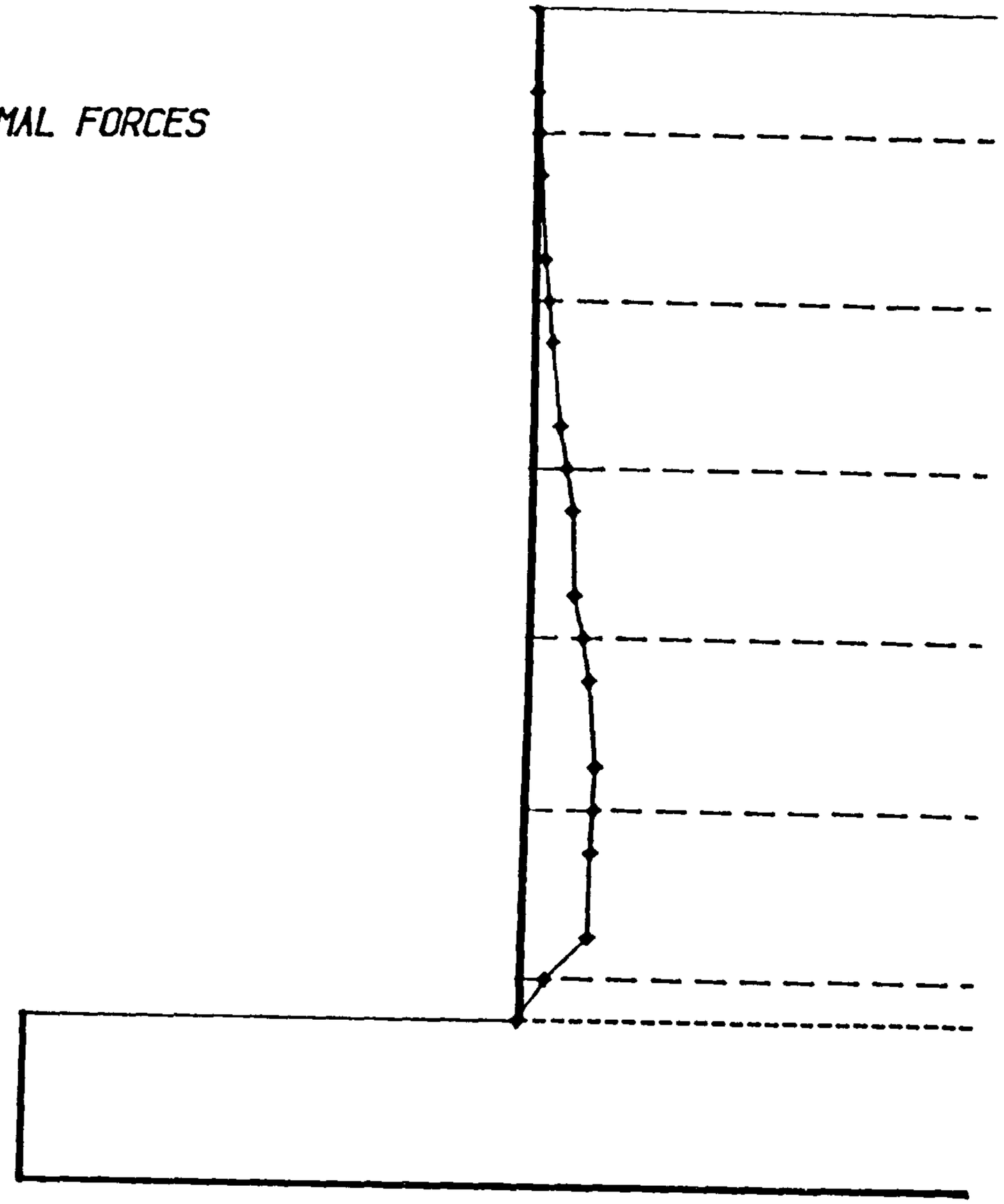

FIG. (9.28) WITHOUT COMP. & USING THE SAME DENSITY AS COMP. LENG. = 600.0 MM.

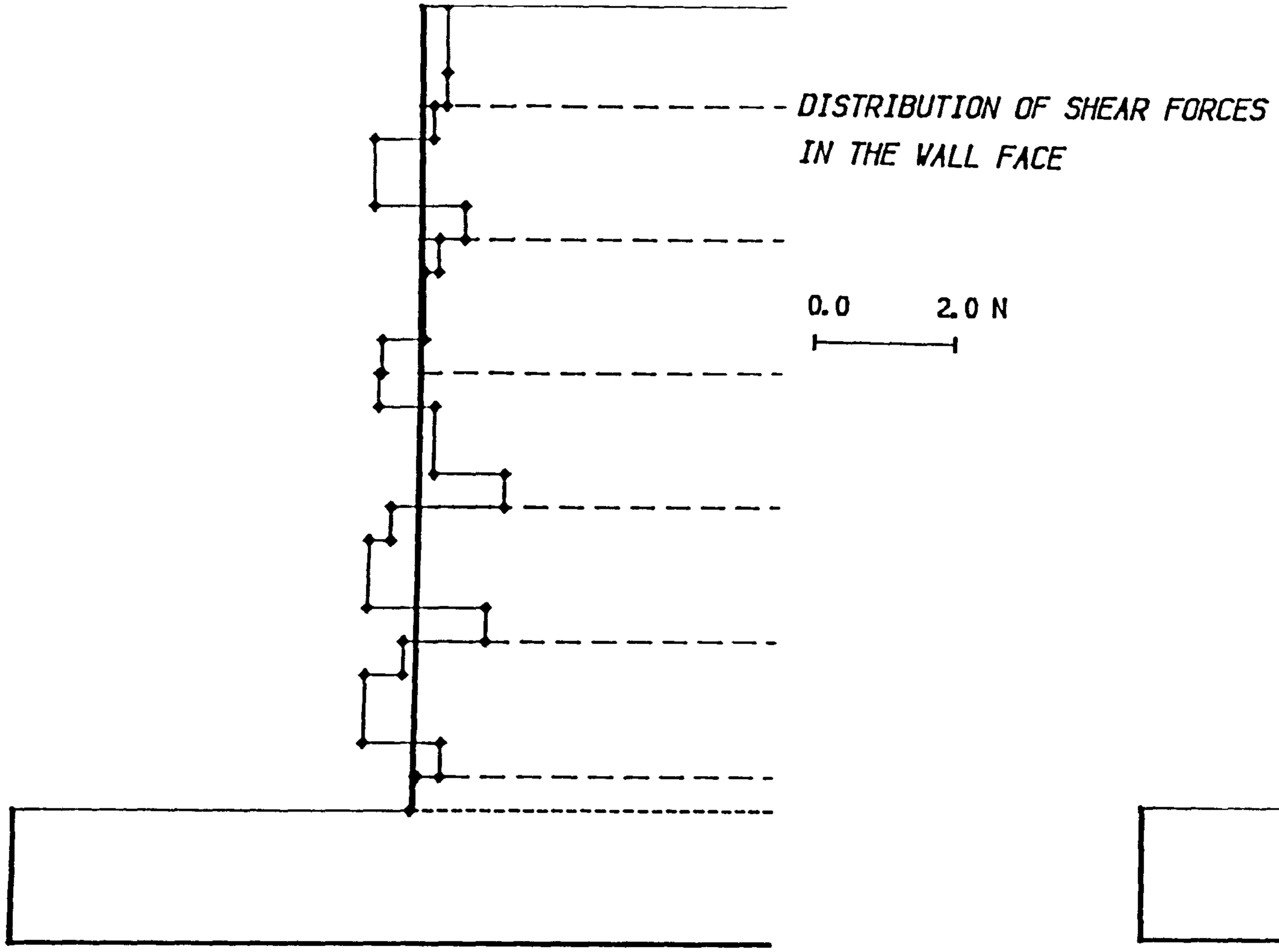

FIG. (9.29) COMP. LENG. = 600.0 MM.

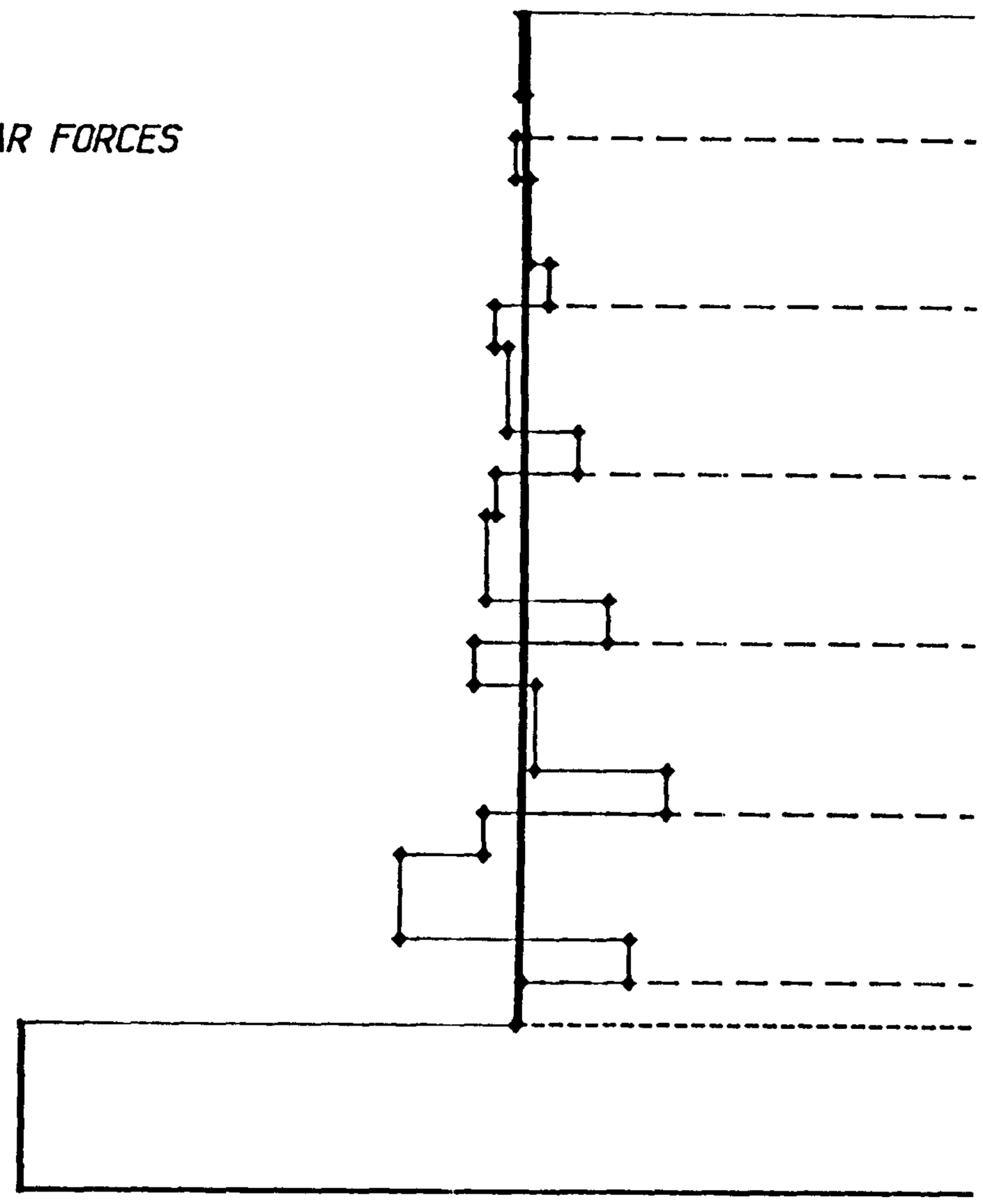

FIG. (9.30) WITHOUT COMP. & USING THE SAME DENSITY AS COMP. LENG. = 600.0 MM.

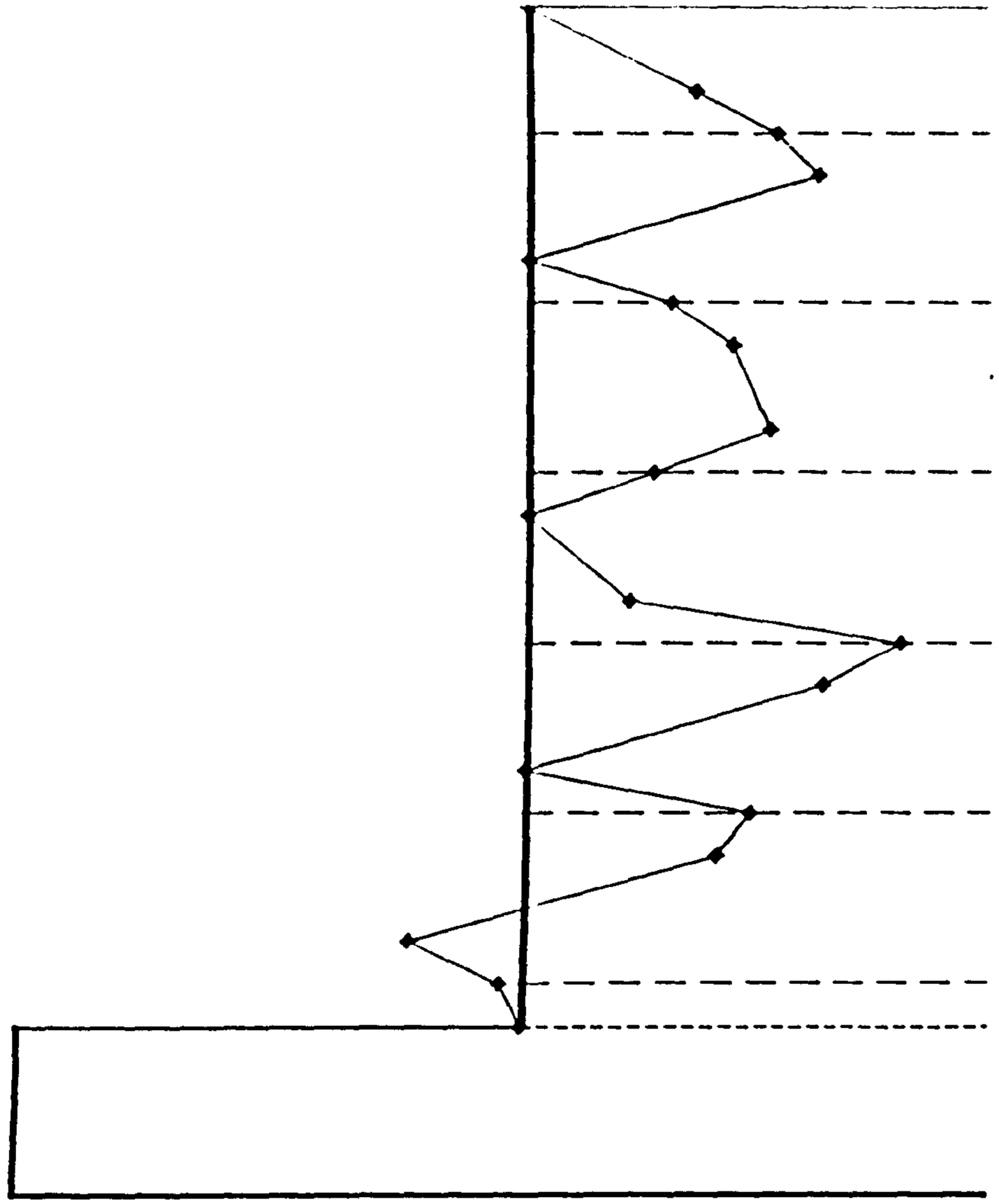

FIG. (9.31) COMP. LENG. = 600.0 MM.

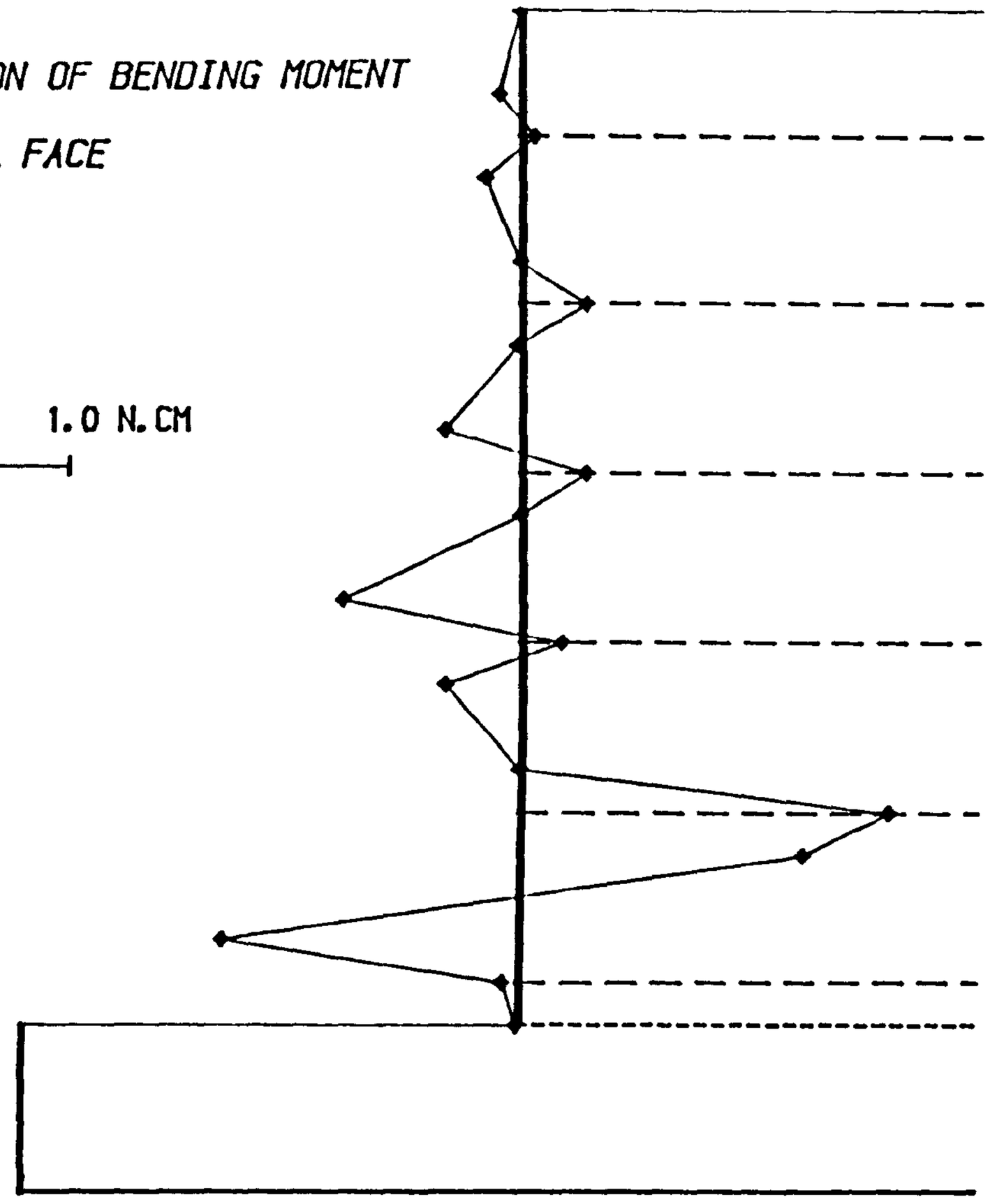

FIG. (9.32) WITHOUT COMP. & USING THE SAME DENSITY AS COMP. LENG. = 600.0 MM.

The shear force distribution is shown in Figs.(9.29&30), the values in the case of compaction being smaller than in the no compaction case. This is because a higher proportion of the horizontal stresses which cause shear forces in the wall face, have been taken by the strips.

The maximum shear force occurs in the lower third of the wall height in the case of no compaction and in the middle third in the compaction case. This agrees with the position of maximum lateral movement of the wall as discussed previously in Sec. (9.2.3).

The bending moment distributions are shown In Figs. (9.31&32). From these it can be seen that the effect of compaction is to cause the B.M. to become wholly of the same sign, compared to the no compaction case in which the B.M. changes sign up the height of the wall. The reason for this is the increase in the tensile forces in the strips due to compaction, which will increase the reaction at the connections of the panels and hence give the B.M. a unique sign.

Obviously, since three hinges were assumed at the face in the model idealization, Chapter 8, the B.M. at these points is zero as shown.

9.3 EFFECT OF COMPACTION LENGTH ON THE BEHAVIOUR OF REINFORCED EARTH RETAINING WALL

Comparisons have made between the results of five computer runs with different lengths of compaction, to determine the effect of various compaction lengths on the behaviour of reinforced earth retaining walls with sand backfill.

The five computer runs simulate five model tests carried out in the laboratory. The five runs are as follows:

(1) Run No. 3 represents model test CAT. III−1, where compaction length equals 200 mm i.e. 0.33H and distance 0.67H from wall face (H is height of the wall).

(2) Run NO. 4 represents model test CAT. III−2, where compaction length equals 400 mm i.e. 0.67H and distance 0.33H from wall face.

(3) Run NO. 5 represents model test CAT. III−3, where compaction length equals 600 mm i.e. H and distance zero from the wall face.

(4) Run No. 10 represents model test CAT. IV−2, with a variable compaction length behind a plane inclined at 75 degrees to the horizontal and at a variable distance from wall face.

(5) Run No. 11 represents model test CAT. IV−3, with a variable compaction length behind a plane inclined at 60 degrees to the horizontal and at a variable distance from wall face.

The effect of compaction length on the behaviour of the reinforced earth wall is shown in the following sections.

9.3.1 Lateral Movement Of The Wall Face

Fig. (9.33) compares the lateral movements of the wall face due to different compaction lengths. The most important feature shown is that there is a translation and rotation about the top and bottom of wall. The maximum movement occurs at the middle third of the wall height. The lateral movement

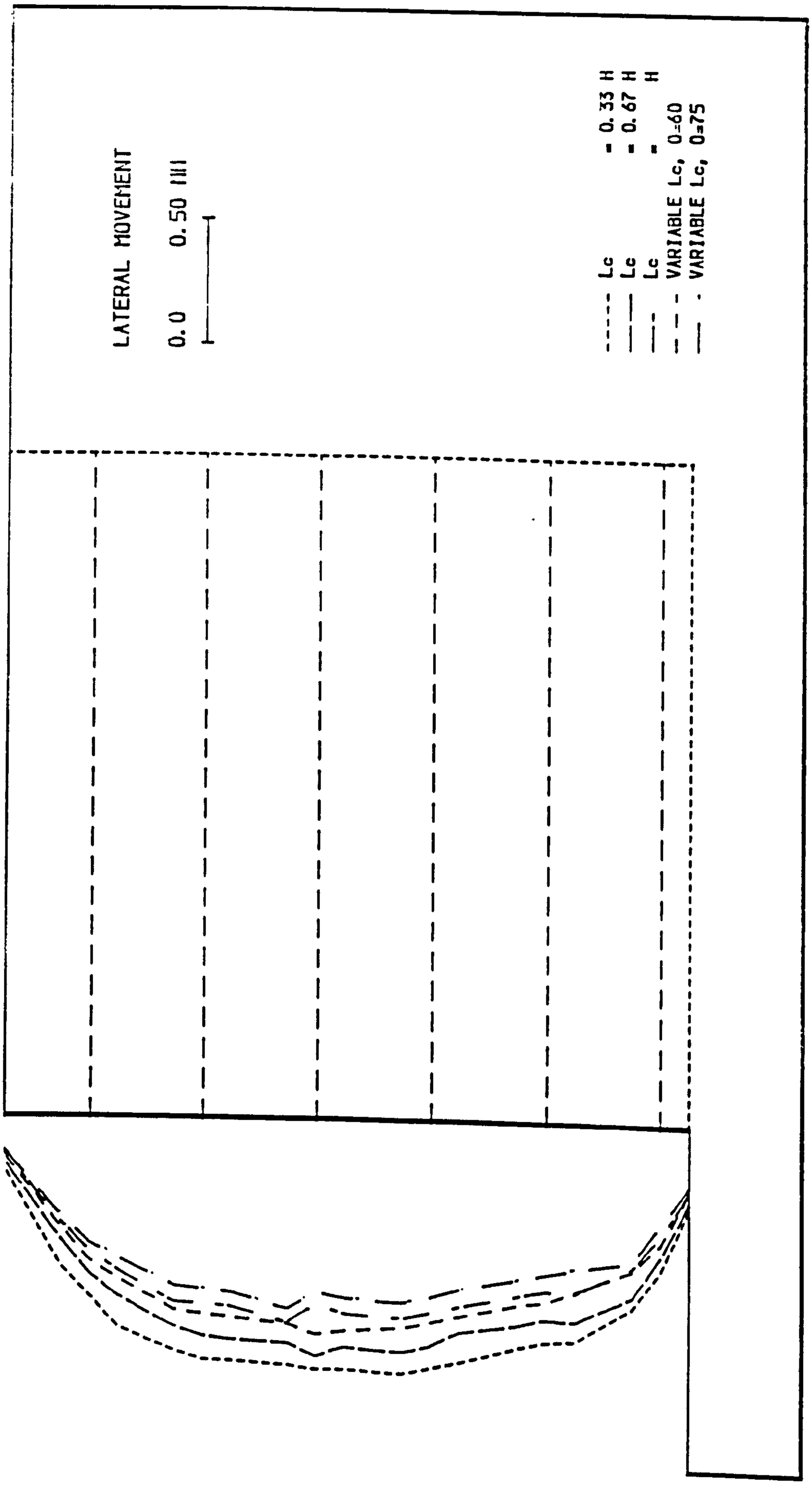

FIG. (9.33) EFFECT OF COMP. LENG. ON THE LATERAL MOVEMENT OF THE VALL FACE.

in the case of a compaction length 0.33H at distance 0.67H from the wall face has the largest value. This is due to the relative density and angle of internal friction in this run having the lowest values (Rd = 15.91% & φ = 35.5 degree). As the reinforced system is a flexible system and takes its stability from the stability and strength of the composite material (soil & reinforcement), then in the case of loose or weak soil the lateral movement increases. On the other hand in the case of compaction length equal to 1.0H, at the maximum relative density obtained (Rd = 75.67%) and maximum angle of internal friction (φ = 44.3 degree), the soil strength and its stability have improved. However due to the compaction load being adjacent to the wall face, a large part of the horizontal stresses due to compaction have been transmitted directly to the wall face causing lateral movement.

The case which gives high relative density (Rd = 62.60%) and least lateral movement is the variable compaction length case where θ = 75 degrees. The reason is the compaction length in each layer is not adjacent to the wall face but covers most of the length of the strips.

9.3.2 The Distribution Of Forces In The Strip

The distributions of tensile forces in the lower strips are shown in Fig. (9.34) as the results from five computer runs. It is obvious from the figure that increasing the compaction length increases the forces in the strips particularly in the front half of the strips where the maximum tensile force lies. This is due to the increase in horizontal stresses due to compaction plant which are locked in the soil.

In the case of compaction length = 1.0H which covers all the reinforced

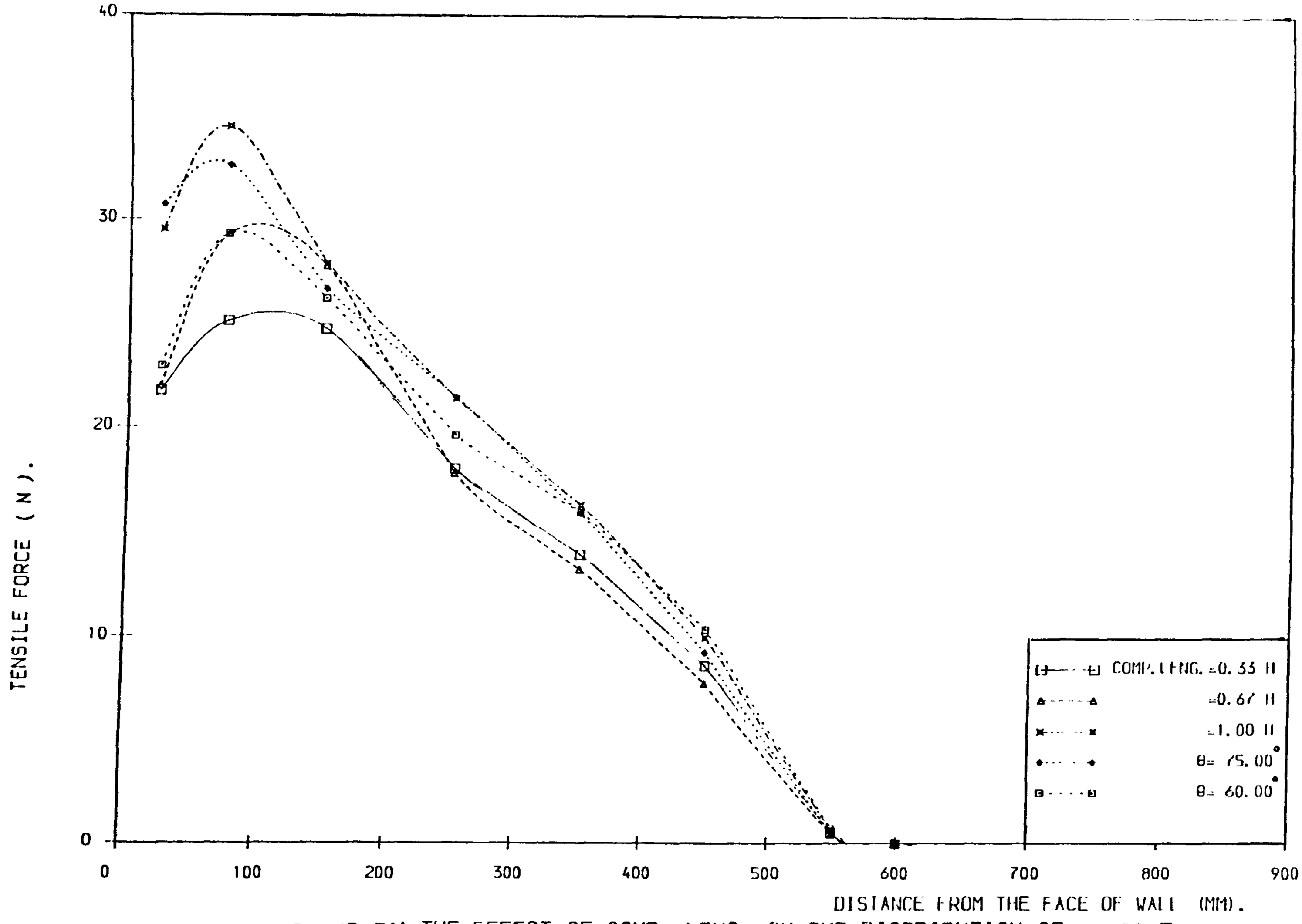

FIG. (9. 34) THE EFFECT OF COMP. LENG. ON THE DISTRIBUTION OF TENSILE FORCE IN LOWER STRIP.

mass, the maximum tensile force has been obtained, because a large proportion of the horizontal stresses transmitted to the wall is resisted by the strips. In the case of variable length where (θ) has different values, it is seen that by increasing θ the tensile force increases. This is due to a larger part of the reinforced mass having been compacted.

9.3.3 Position Of Maximum Tensile Forces In The Strips

The positions of the maximum tensile forces in the strips are shown in Fig. (9.35). By increasing the compaction length the position of the maximum tensile force moves towards the wall face. The nearest position is in the case of compaction length = 1.00H and farthest is in the case of compaction length = 0.33H.

In the case of variable compaction length where θ = 75 degrees, the position of the maximum tensile force is near to that from compaction length = 1.0H. When θ = 60 degrees, it is near compaction length = 0.67H. The reason for the position of the tensile force moving towards the wall face when the compaction length increases is the higher angle of internal friction (φ) associated with the compaction length near the wall. This makes a greater part of the reinforcement lie in more stable soil and this part decreases as the compaction length is reduced, causing the position of maximum tensile force to move farther from the wall face.

9.3.4 The Distribution Of Vertical Stresses Under The Wall

This is given in Fig. (9.36). The distribution in all cases of different compaction length has the same shape, i.e. nonuniform under most of the

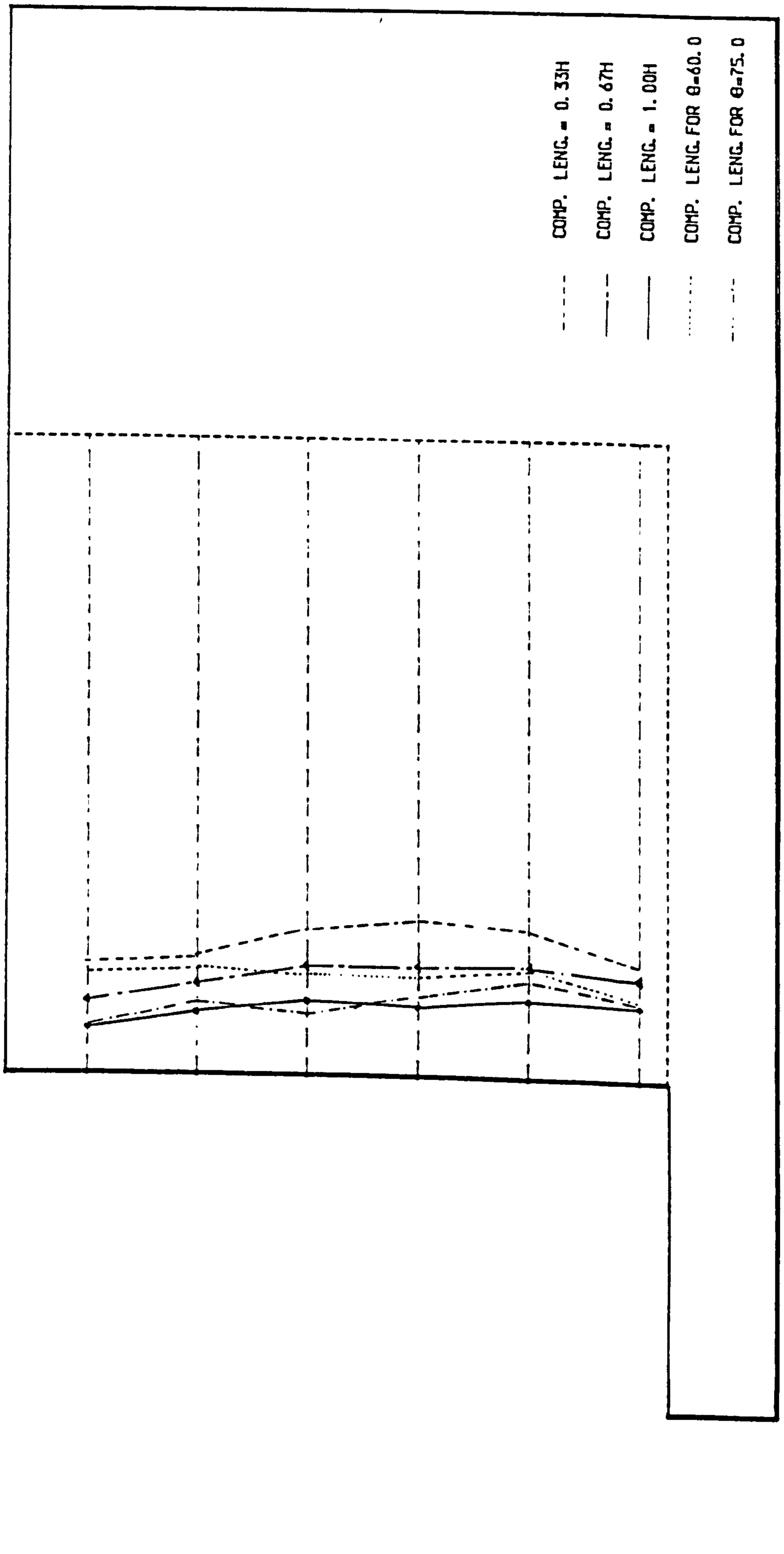

FIG. (9.35) EFFECT OF COMP. LENG. ON THE POSITION OF MAXIMUM TENSILE FORCE IN THE STRIPS.

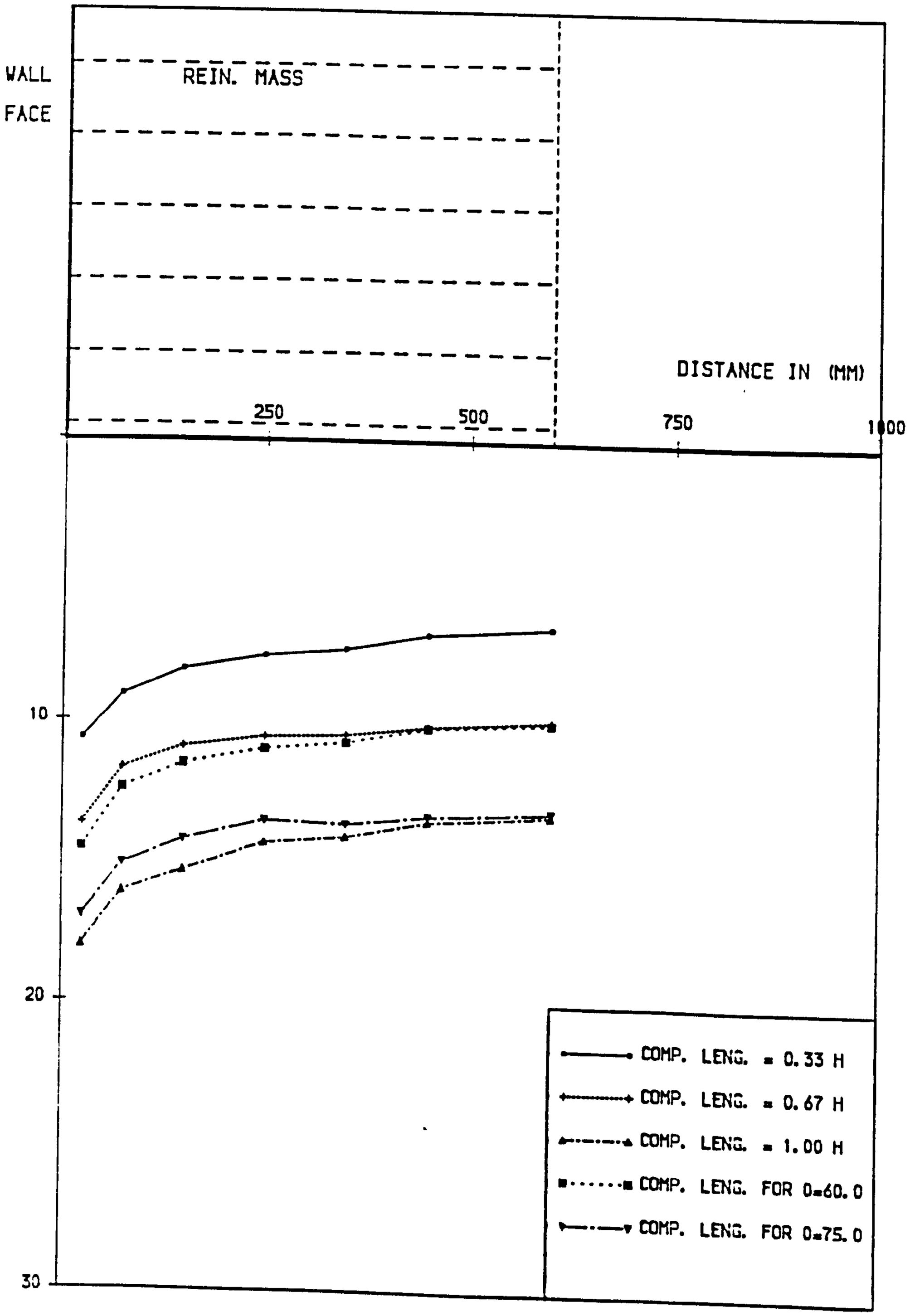

FIG. (9.36) EFFECT OF COMP. LENG. ON THE DISTRIBUTION OF VERTICAL STRESSES UNDER THE REINF. MASS.

reinforced mass with the maximum value near the toe. By increasing the compaction length the values of the vertical stresses increase. The important feature is in the case of variable compaction length where θ = 75 degrees and the relative density (62.60%) is near the maximum relative density which can be obtained in the laboratory. In this case the vertical stress values are less than in the case of maximum compaction length = 1.00H. This is because the compaction length at any layer is less than 1.00H, and the compaction load is not adjacent to the wall back at any layer. Also there is some tilting near the toe, which increases when the compaction length = 1.0H.

9.3.5 The Distribution Of Earth Pressure

The distribution of earth pressure or horizontal stress at three vertical planes (behind the wall face, at the middle and behind the reinforced mass) are shown in Figs. (9.37 to 41), for the five different compaction lengths of 0.33H, 0.67H, 1.0H, and variable length for θ = 75 & 60 degrees respectively.

By increasing the compaction length from 0.33 to 0.67 to 1.0H as in Figs. (9.37,38&39), the earth pressure has been affected in both value and distribution. It starts near the active to at rest condition in the case of compaction length = 0.33H and is sometimes more than the active condition as in case of 0.67 H. In the case of compaction length = 1.0H the values of the earth pressure are nearer the at rest condition over the lower two thirds and greater in the upper third of the wall height.

In the other two cases where the compaction length is variable, the distribution is near the at rest condition and greater than it in some places as θ increases, Figs. (9.40&41).

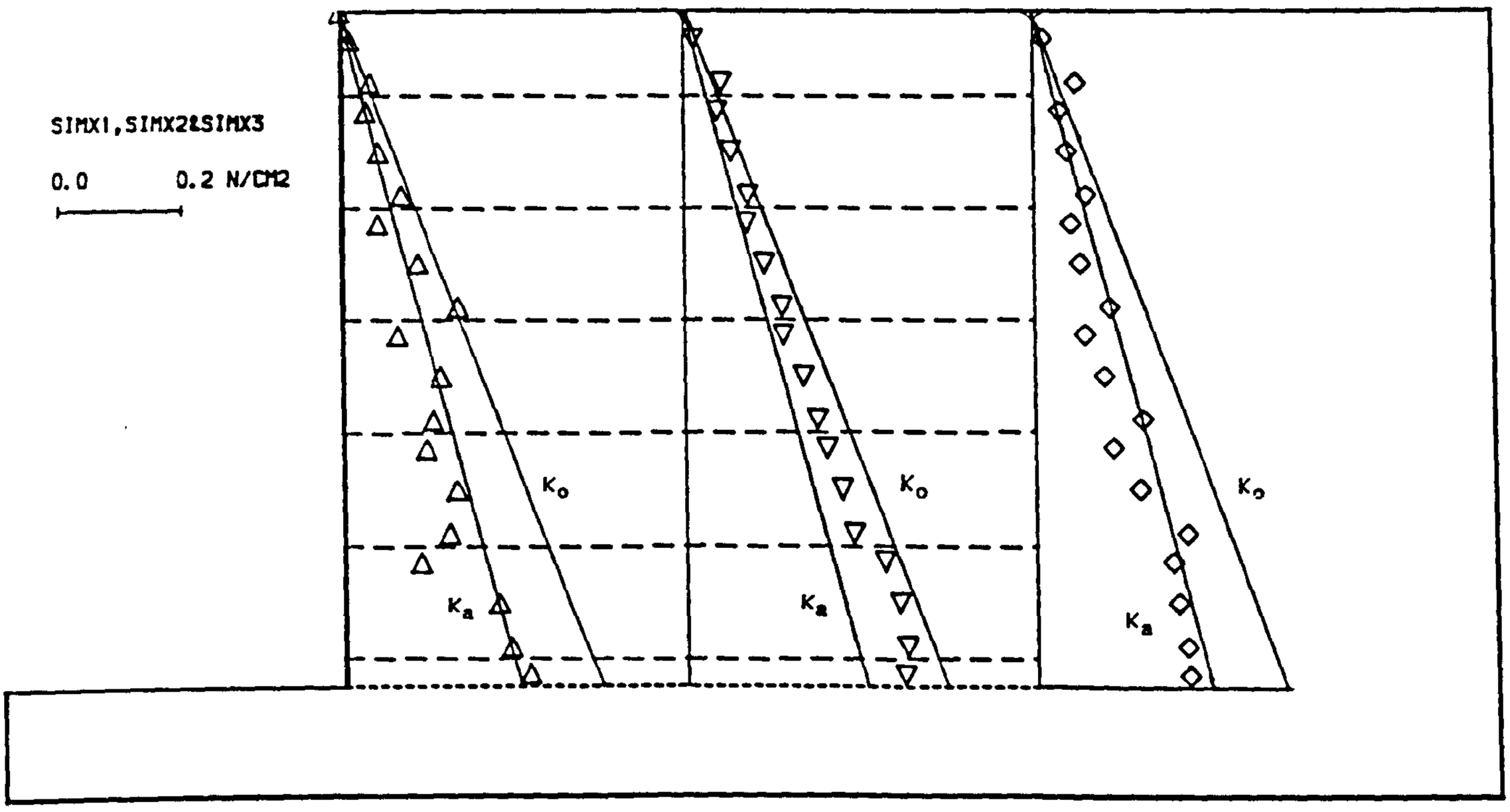

FIG. (9.37) MAX. HORIZ. STRESSES AT THE FACE OF WALL, MIDDLE&BEHIND REINF. MASS, COMP. LENG. = 200.0 MM.

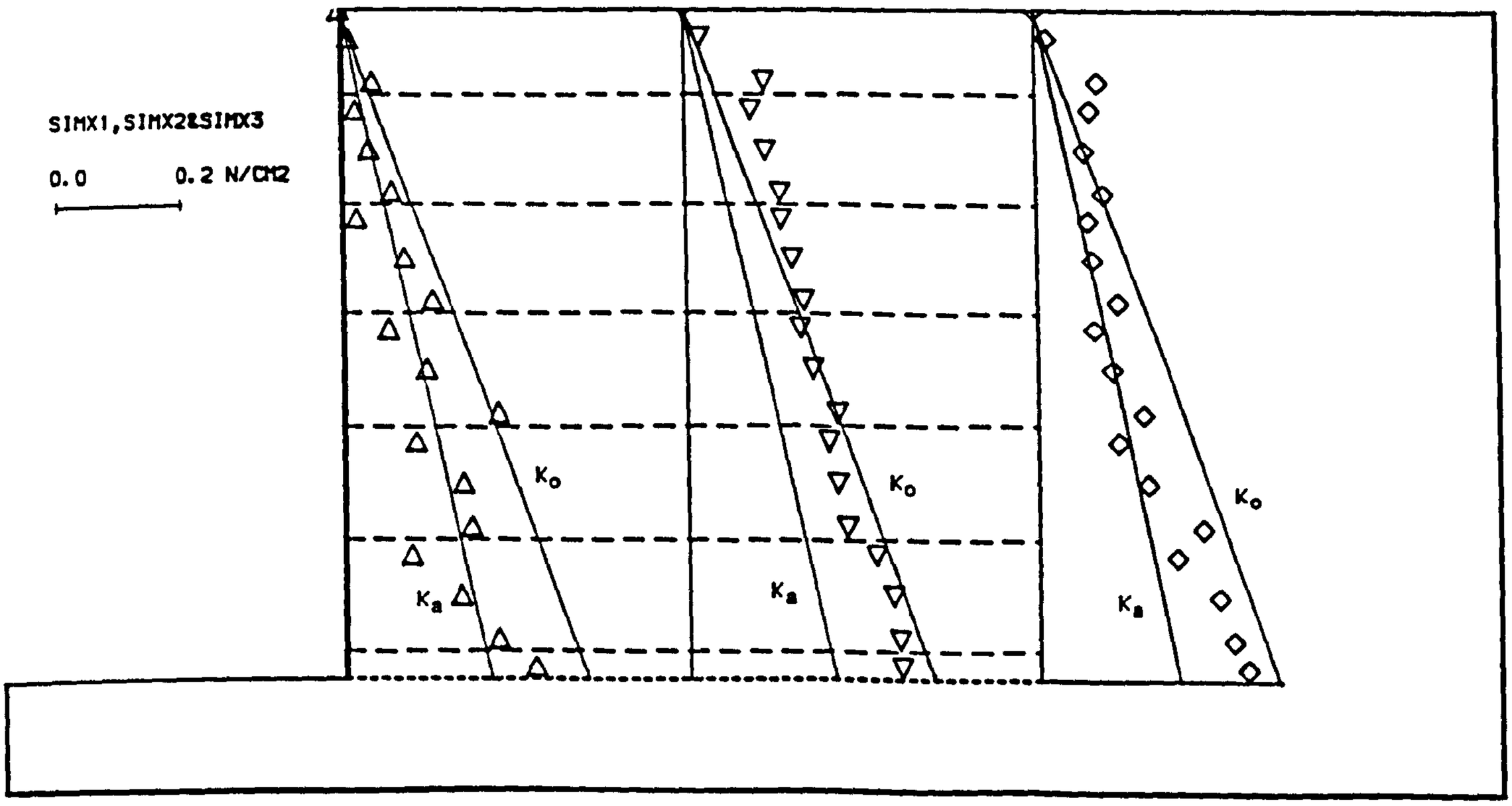

FIG. (9.38) MAX. HORIZ. STRESSES AT THE FACE OF WALL, MIDDLE&BEHIND REINF. MASS, COMP. LENG. = 400.0 MM.

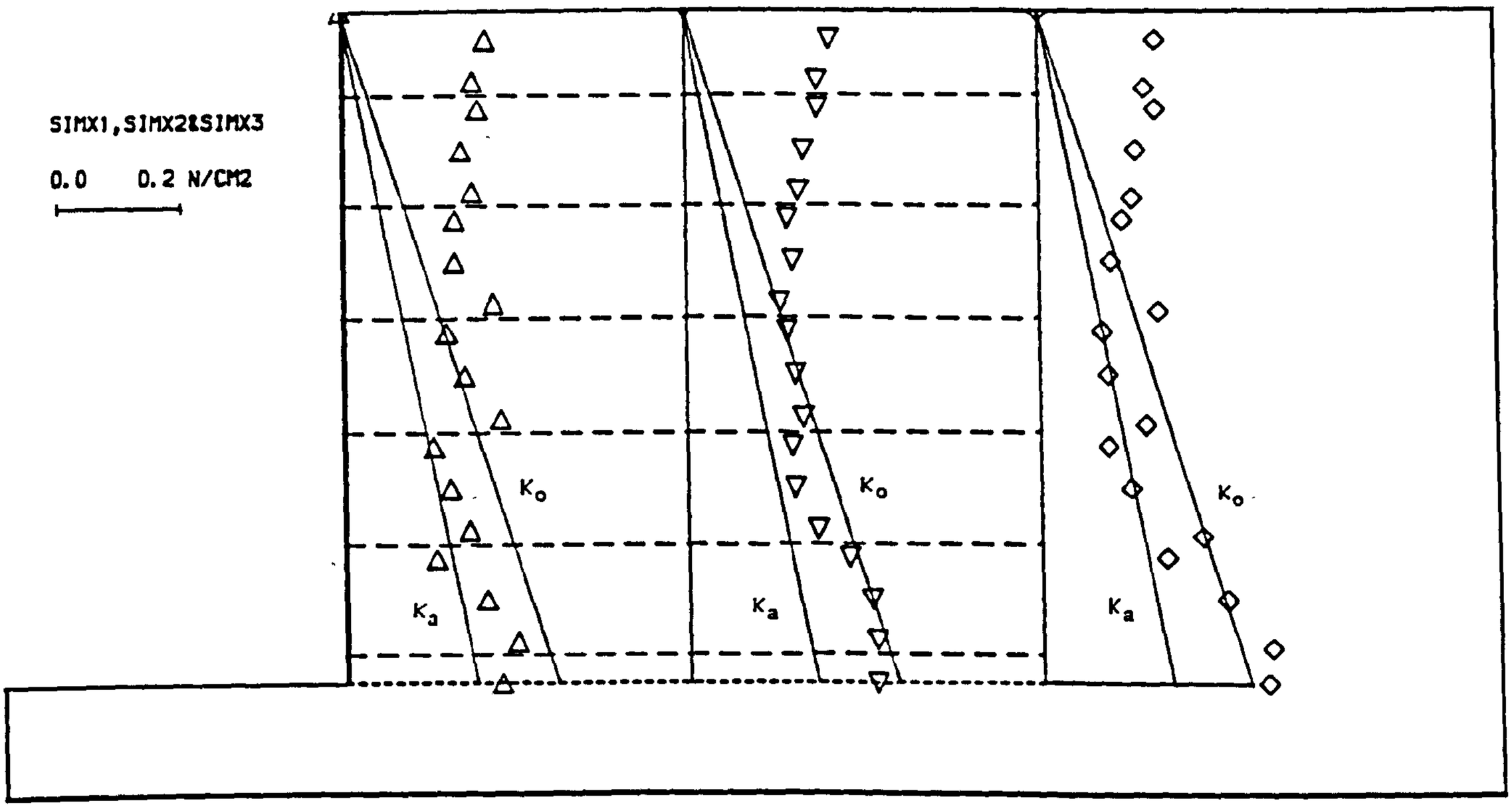

FIG. (9.39) MAX. HORIZ. STRESSES AT THE FACE OF WALL, MIDDLE&BEHIND REINF. MASS, COMP. LENG. =600.0 MM.

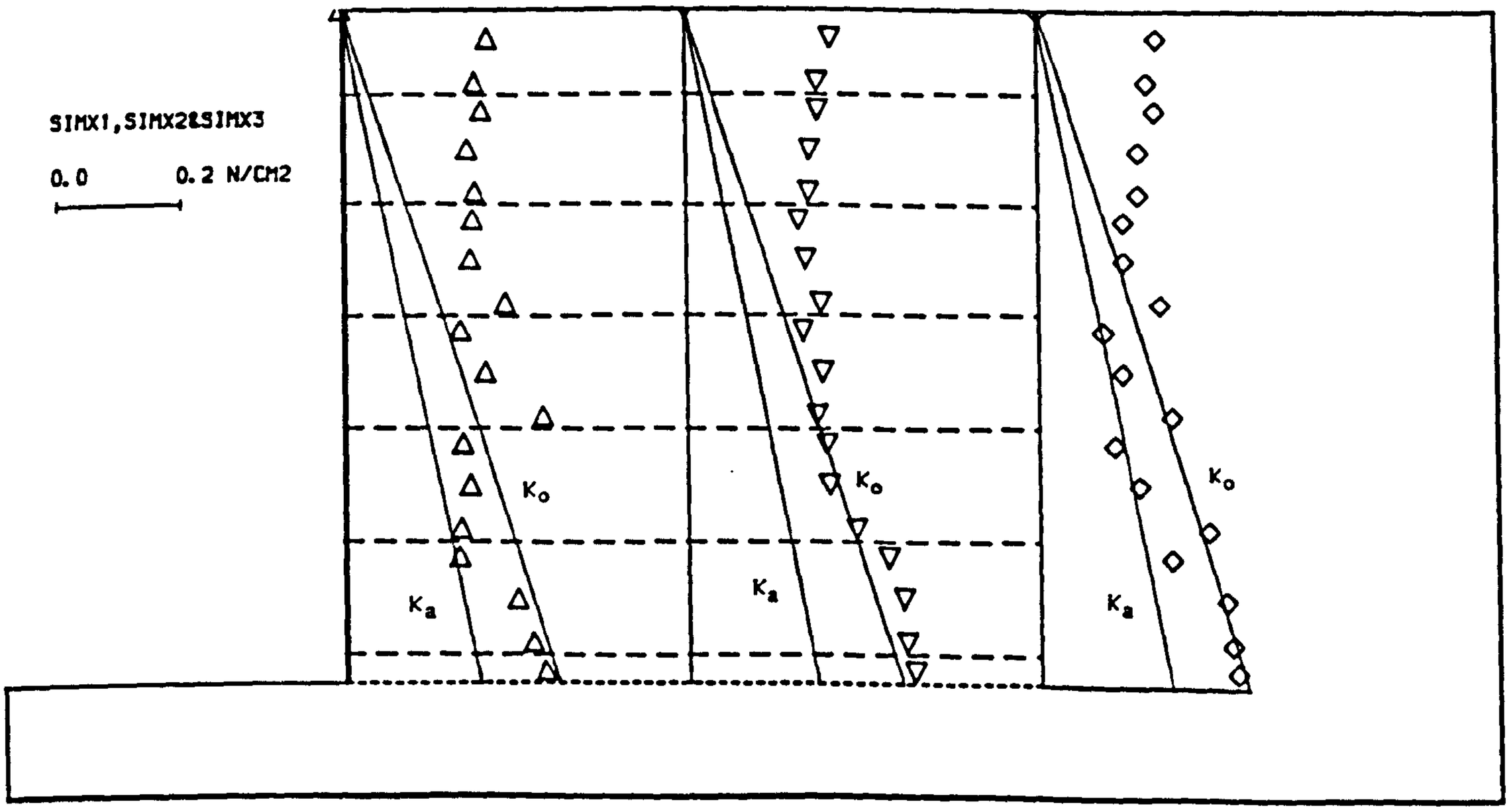

FIG. (9.40) MAX. HORIZ. STRESSES AT THE FACE OF WALL, MIDDLE&BEHIND REINF. MASS, VARIABLE COMP. LENG. AND THETA = 75.00 DEGREES.

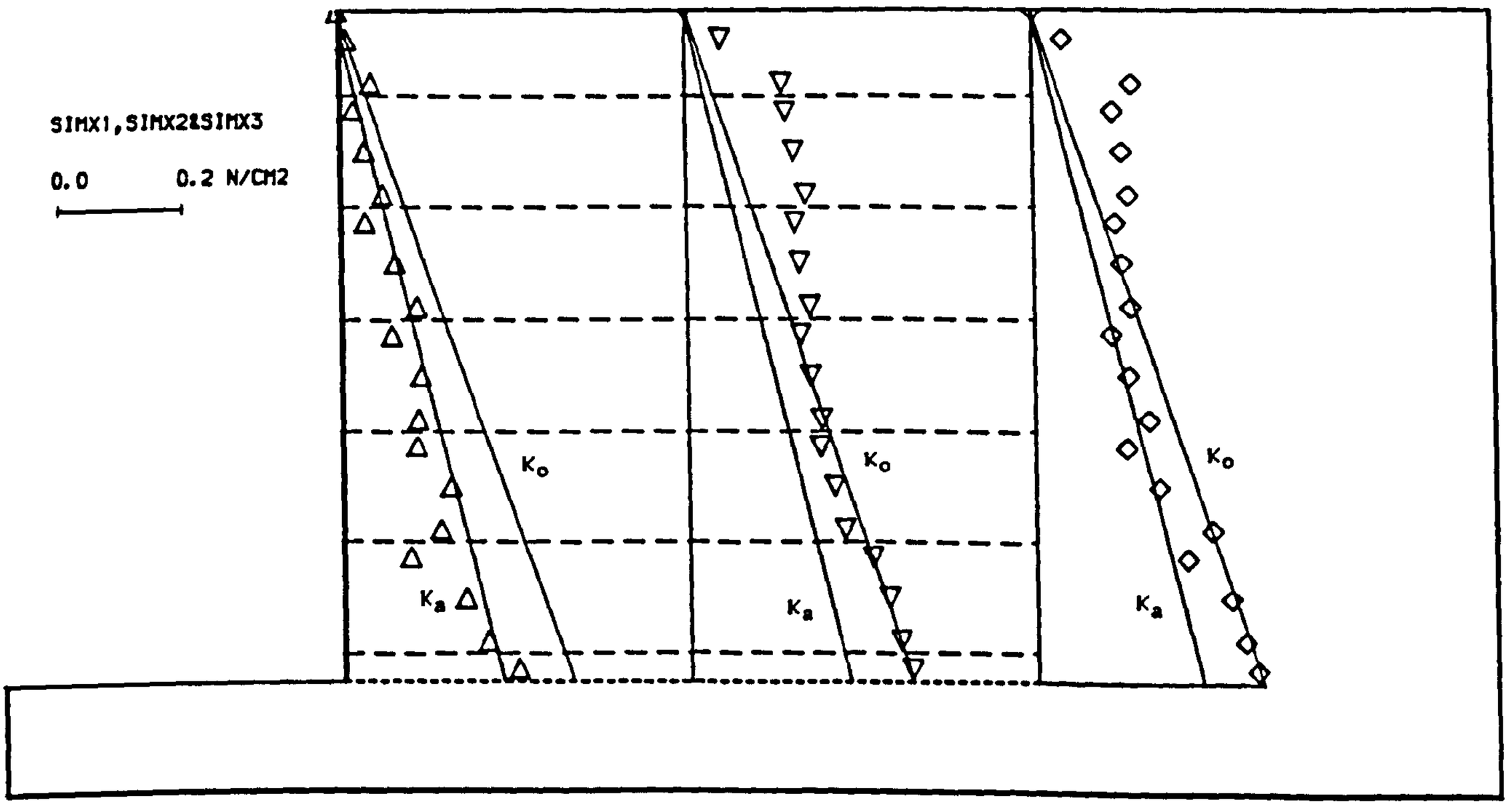

FIG. (9.41) MAX. HORIZ. STRESSES AT THE FACE OF WALL, MIDDLE&BEHIND REINF. MASS, VARIABLE COMP. LENG. AND THETA = 60.00 DEGREES.

Fig. (9.42) shows the effect of compaction length on the variation of earth pressure coefficient i.e. the state of stress within the reinforced mass, plotted as the ratio between the actual coefficient of earth pressure (K) at certain depth and coefficient of active earth pressure (K_a) against depth/wall height ratio (Z/H). From the Fig. the state of stress changes from more than the active state near the top of the wall (sometimes more than the at rest condition as shown in above discussion) and decreases with depth to reach the active state after a depth depending on the compaction length. As the compaction length increases, the depth at which the earth pressure falls below the active value increases and ranges from Z = 0.57H (at compaction length = 0.33H) to Z = 0.76H (at compaction length 1.00H & in the case of variable compaction length where θ = 75 degrees).

9.4 CONCLUSION

Since compaction is needed in any earthwork project especially in a flexible system such as a reinforced earth wall, an understanding of its behaviour under compaction load, assists in the design.

Program BCOMPP with program SSCOMP was used to study the behaviour of reinforced earth retaining wall model tests which were carried out in the laboratory. The programs serve as a versatile mathematical tool using numerical integration and finite element methods, which can be used not only to assess the effect of compaction on wall behaviour but also to help in designing the wall by providing the internal forces in the wall face, earth pressure distribution at any section, forces in the strips, and vertical stress, and in assessing the relative influence of various parameters on the reinforced earth wall.

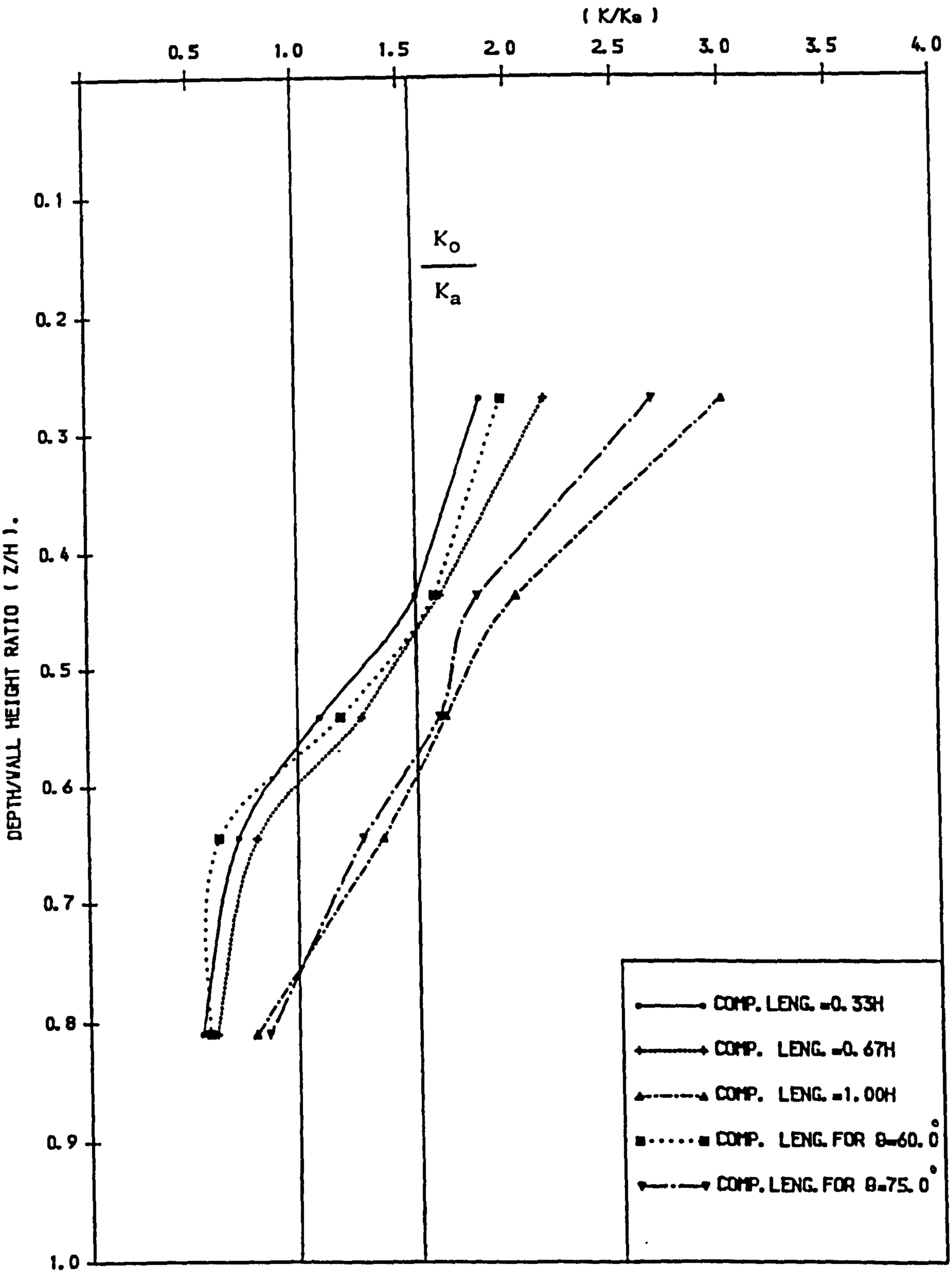

FIG. (9.42) EFFECT OF COMP. LENG. ON THE VARIATION OF EARTH PRESSURE.

The keys to the success of these programs are:

(1) Simulating the compaction plant as closely as possible to the field.

(2) Simulating or modelling the compaction process as it occurs in the field.

The compaction effect has been studied on the different elements of reinforced earth such as the wall face, soil backfill and reinforcing strips. Compaction increases the lateral movement of the wall and the deformation and stresses within the reinforced mass.

The state of stress within the reinforced mass is very near to the at rest condition and greater at the upper third of wall height. Sliding and tilting of the reinforced mass occurs due to compaction and these increase the vertical stress under the mass. Both the magnitude and position of tensile forces in the strip are affected by the compaction length. By increasing it the force increases and moves towards the wall face within the front half of the strip.

The main reasons for these influences are:

(a) The horizontal stresses within the reinforced mass reach their maximum values during the compaction process and residual horizontal stresses due to compaction are locked in the soil during backfilling.

(b) The presence of compaction load adjacent to the wall face.

Using variable compaction lengths which cover most of reinforced mass and at the same time are not adjacent to the wall back reduces the effect. Comparisons between results from model laboratory tests and finite element analysis will be presented in the next chapter in order to enhance and check the finite element results.

CHAPTER 10

COMPARISON BETWEEN EXPERIMENTAL AND THEORETICAL WORK

10.1 INTRODUCTION

The experimental results from the model reinforced earth retaining wall were presented in Chapter 5. The computer predictions using finite element analysis and compaction plant model for the same model walls used in the laboratory were discussed in Chapter 9. In this chapter a comparison is presented between the experimental and theoretical results to assess the success of the simulation of compaction plant using program (BCOMPP) and simulation of construction procedure and finite element analysis using program (SSCOMP).

The comparison is made between the results obtained from model test CAT. III−3 (Chapter 3) and computer run No. 5 (Chapter 9). This run simulates the model test CAT. III−3, i.e. the same dimensions of the model wall, compaction length and construction procedure used in the model. This model test was chosen because the compaction length covers all the reinforced mass as in the field as well as the construction procedure. The conclusion of the comparison is given at the end of the chapter.

10.2 COMPARISON BETWEEN EXPERIMENTAL AND COMPUTER RESULTS

The comparison between the experimental wall CAT. III−3 and computer run No. 5 is presented as follows:

10.2.1 Forces In The Strips

The distribution of observed tensile forces in the lower reinforcing strip after construction is completed in the model test and the computer predicted tensile forces in the same strip are shown in Fig. (10.1). This shows that both distributions are nonuniform, all the forces are tensile and the values are not zero near the wall face and approach the zero towards the free end.

The values obtained experimentally in the front third of the strip near the wall face are slightly smaller than the those from the computer and vice versa over the rest of strip length. This difference is due to the connection between the strip and the wall face. In the case of the finite element analysis the connection idealized ensures that relative movement between the wall face and the strip does not occur, while in the experimental model this movement might have happened.

10.2.2 Vertical Stresses

Comparison between the distributions of vertical stress under the reinforced mass from experimental and computer results are shown in Fig. (10.2). The distributions were obtained after the end of construction. In the front half under the reinforced mass, the predicted vertical soil stress by computer lies very near to the observed values obtained experimentally. In the rear half the values from

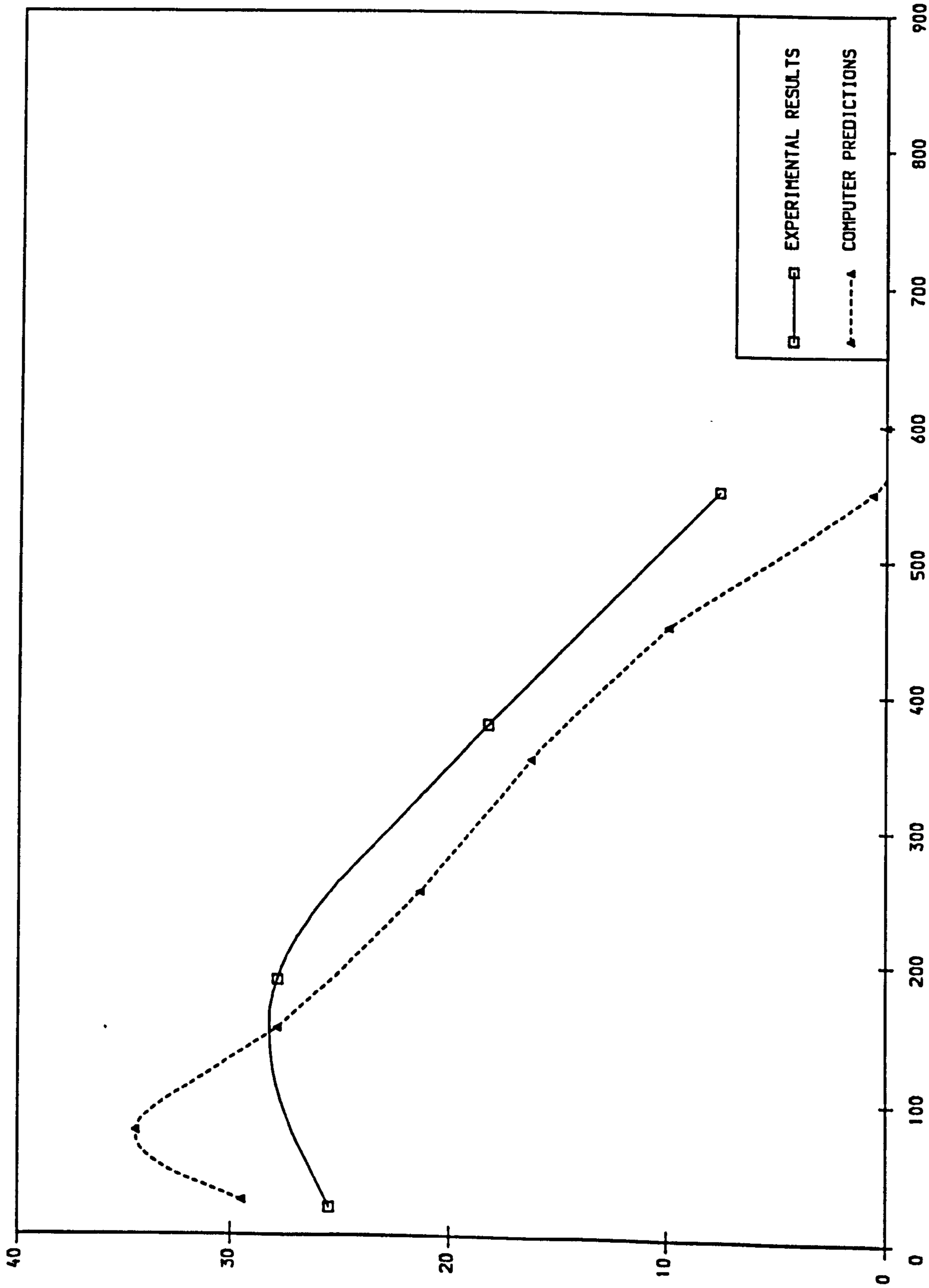

FIG. (10.1) DISTRIBUTION OF TENSILE FORCE IN LOWER STRIP, COMP. L

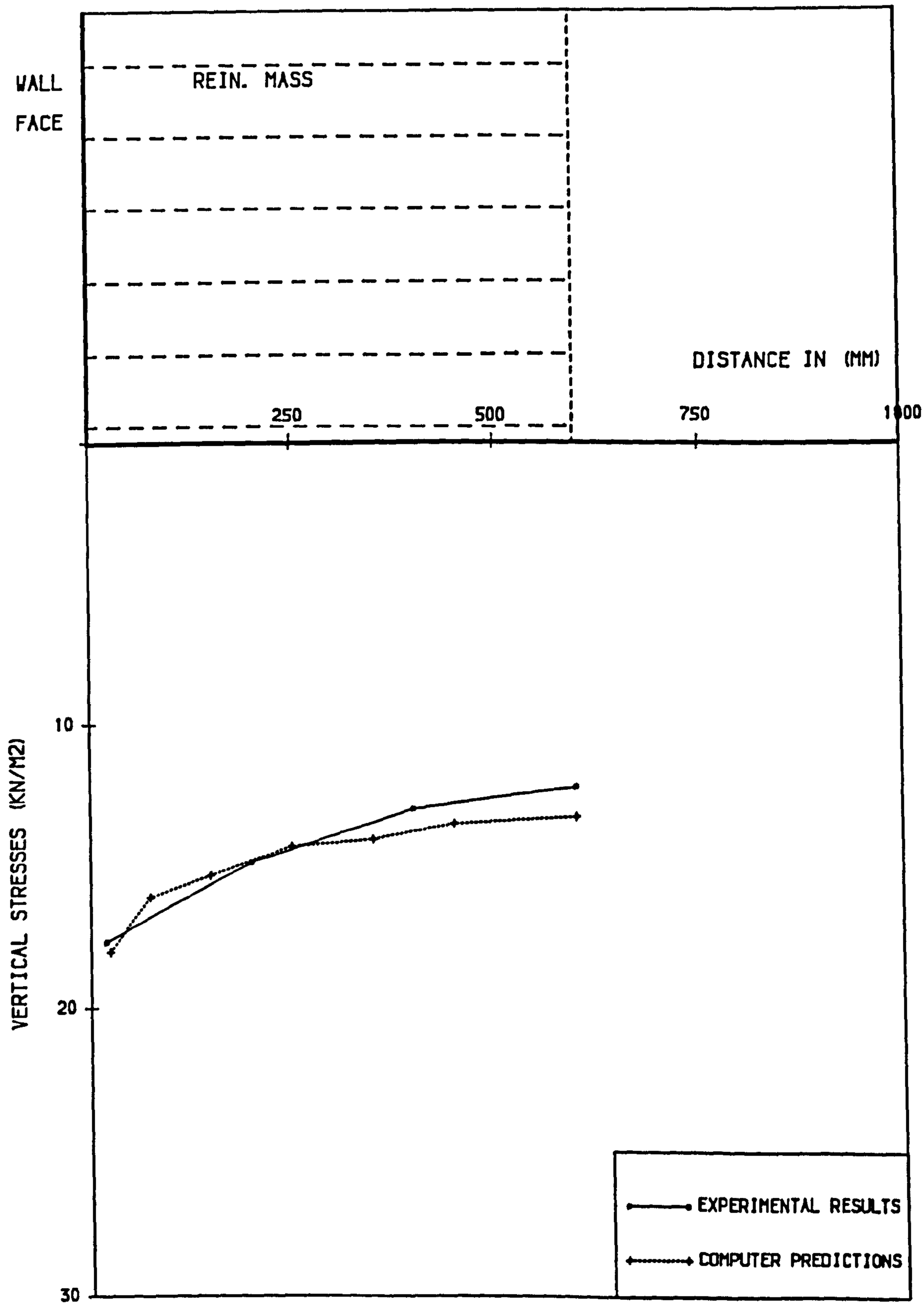

FIG. (10.2) DISTRIBUTION OF VERTICAL STRESSES UNDER THE REINF. MASS & COMP. LENG. = 600.00 MM.

computer are slightly greater than the experimental values. The reason is the density of the backfill behind the reinforced mass in the case of the computer analysis is the same as in the reinforced mass, but in the case of the experimental model the density in the reinforced mass is greater than behind it. It is very difficult to simulate this difference in the computer analysis.

10.2.3 Horizontal Stresses

The distribution of horizontal stress behind the wall face obtained from the experimental model and the computer predictions are shown in Fig. (10.3). The distribution was obtained after the end of construction. There is quite a good agreement in the upper half of the wall where both of the distributions are greater than the at rest condition. In the lower half of the wall height the values obtained experimentally are slightly greater than those obtained from the computer. This is due to the effect of boundary conditions in the case of the finite element analysis.

10.2.4 Lateral Movement

Comparison between lateral movements of the wall face from experimental results and computer predictions are shown in Fig. (10.4). The comparison indicates a good agreement especially at the upper half of the wall height. Both of the distributions show that there is a translation and rotational motion. The small difference in the values near the toe of the wall is due to the boundary condition near the toe which cannot simulate exactly the true condition in the model.

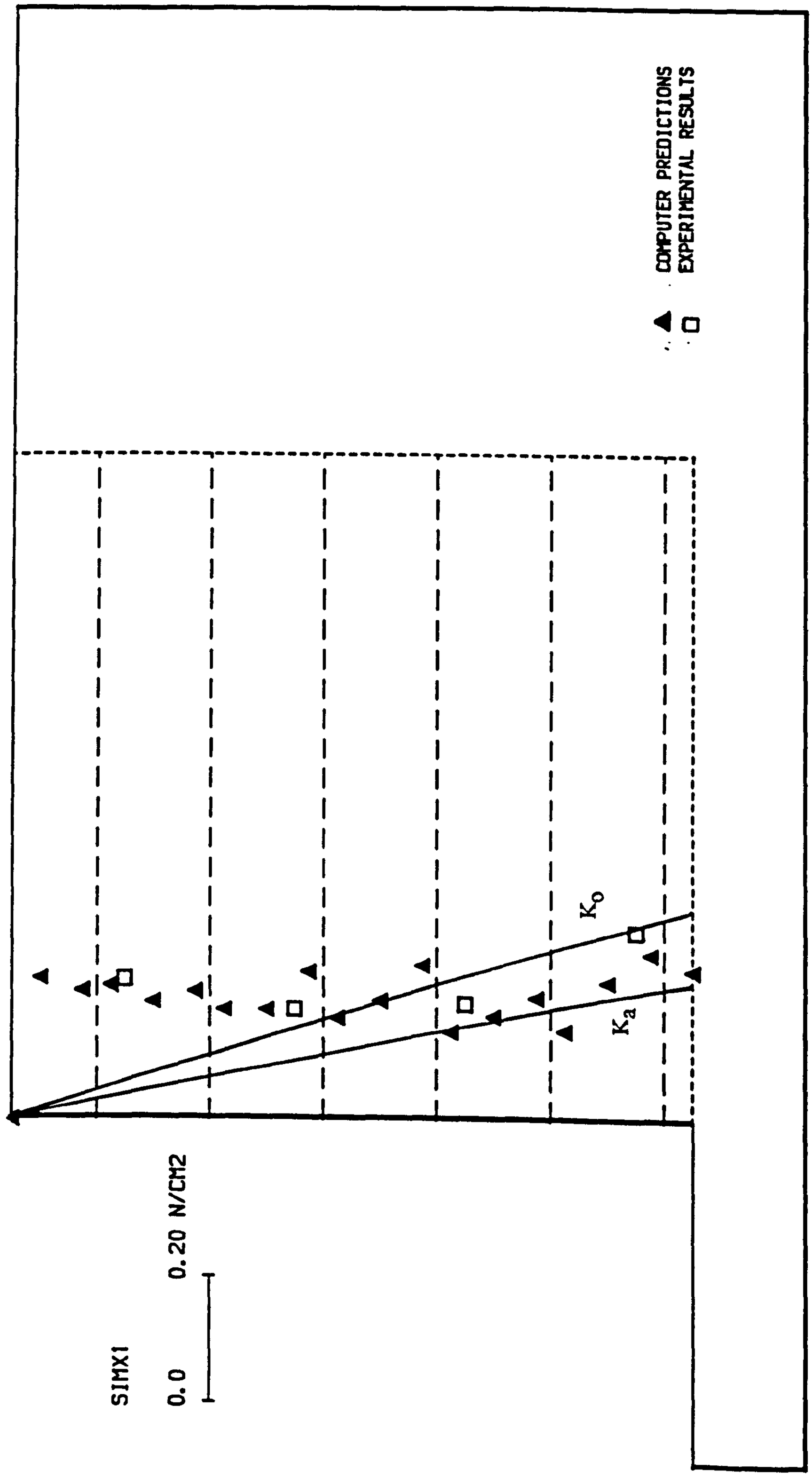

(10.3) THE DISTRIBUTION OF HORIZONTAL PRESSURE BEHIND THE WALL FACE, COMP. LENG. = 600.00 MM.

FIG.

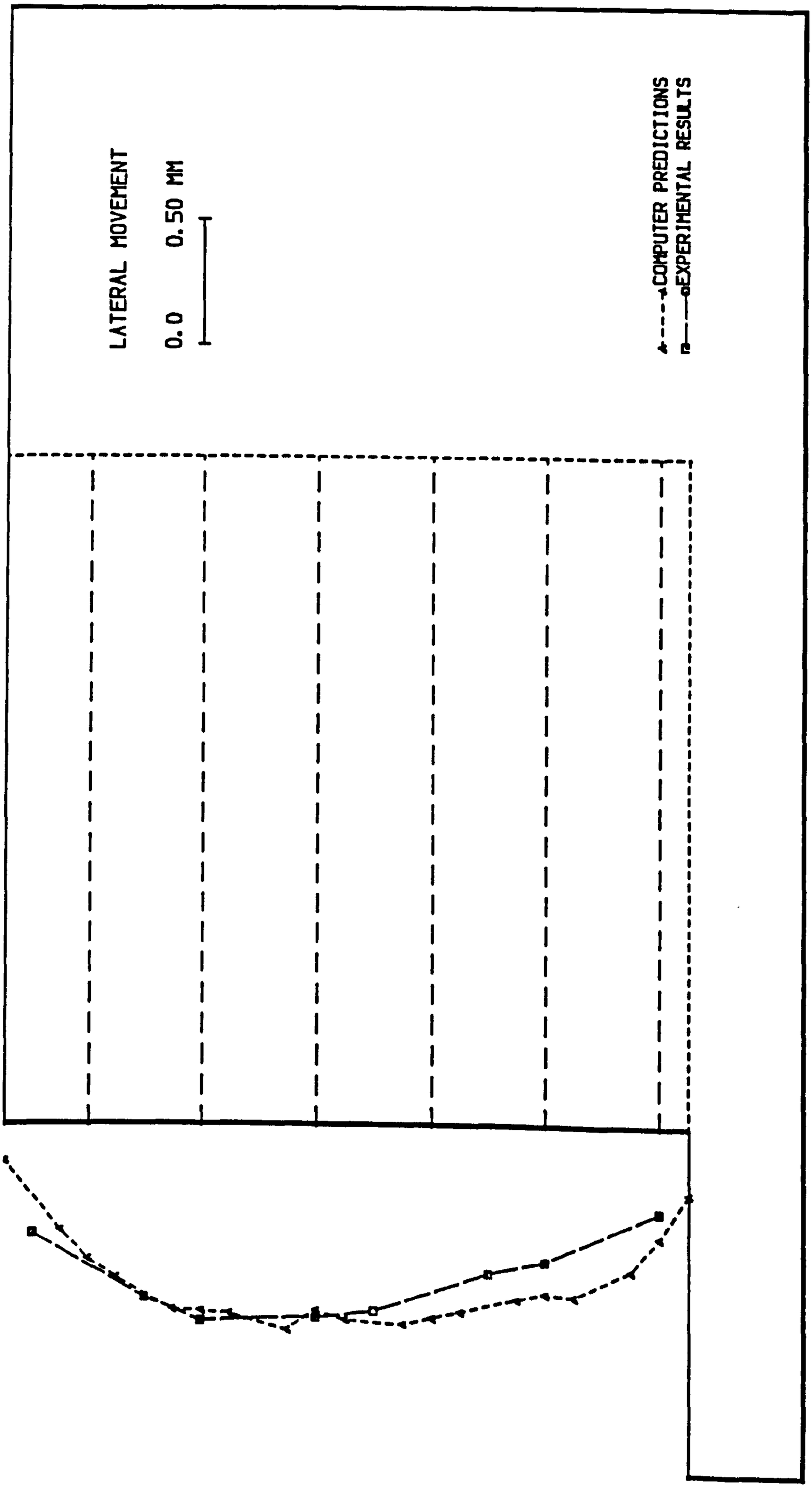

FIG. 110.4) LATERAL MOVEMENT OF THE WALL FACE, COMP. LENG. = 600.00 MM &

10.2.5 State Of Stress

Fig. (10.5) shows the comparison between the states of stress in the reinforced mass behind the wall face obtained from the experimental model and computer predictions. The results are plotted as the ratio between the actual coefficient of earth pressure (K) and the coefficient of earth pressure at rest (K_o) against depth/wall height ratio (Z/H).

In general there is fairly good agreement between the results especially in the upper half of the wall. It is noted that at depth 0.52H both the computer prediction and experimental results coincide at the at rest condition. In the lower half of the wall height there is some difference in the values, which at depth 0.59H is near the active state in the case of the computer analysis and near the at rest condition in the case of the experimental model.

10.3 CONCLUSION

Total agreement between experimental and computer results is difficult to achieve because of the complex interaction between the various components of the reinforced earth retaining wall. Also the boundary conditions and the geometry of the mesh have a siginificant effect on the finite element analysis.

However the comparison made between finite element predictions and experimental results demonstrates the capability of the computer program (SSCOMP) using the discrete finite element approach to predict the behaviour of a reinforced earth wall.

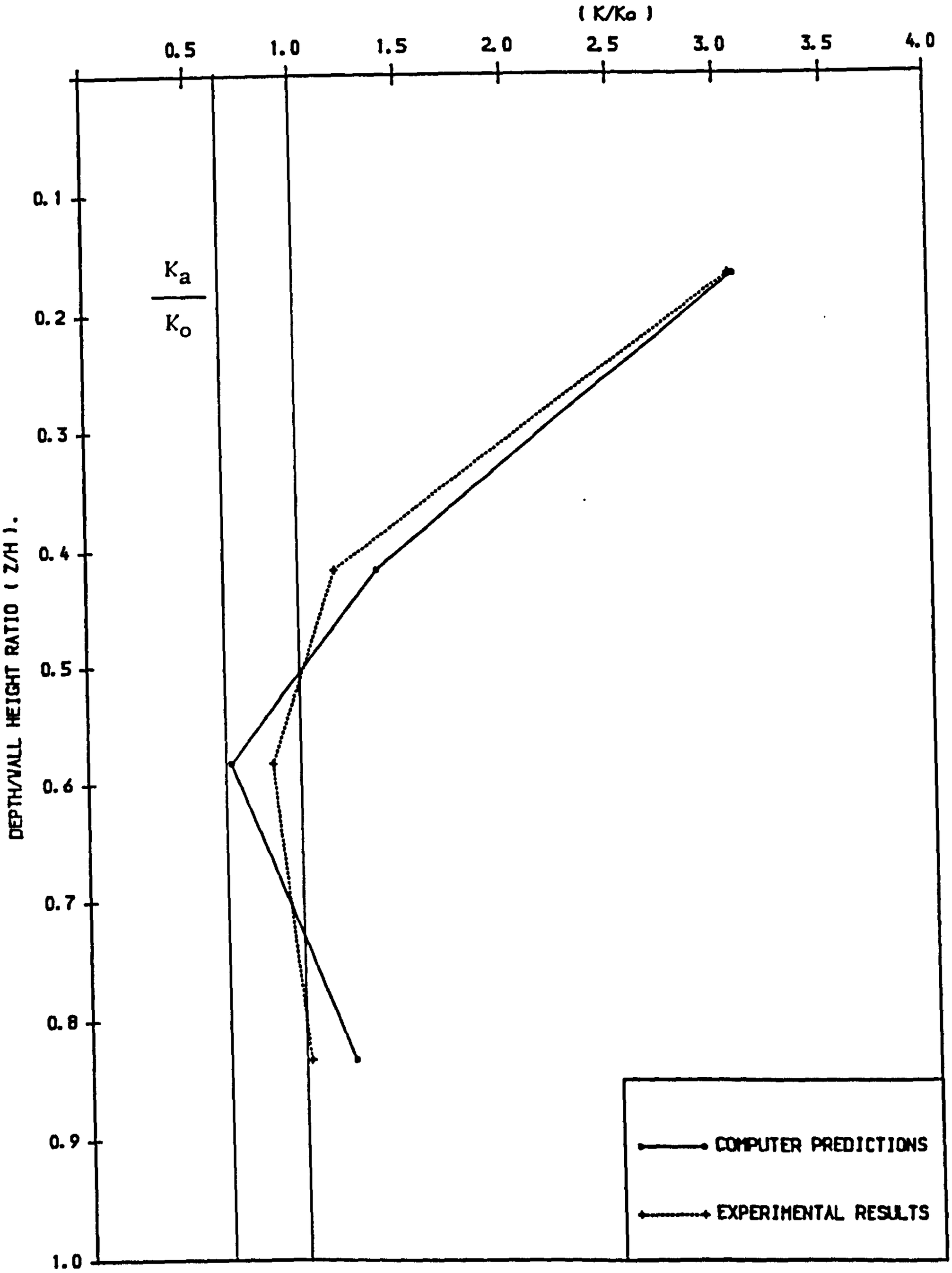

FIG. (10.5) THE VARIATION OF EARTH PRESSURE COEFFICIENT BEHIND THE WALL FACE, COMP. LENG. = 600.00 MM.

The success of comparison was due to several reasons such as:

– The soil was modelled in the finite element analysis as nonlinear, which is near reality.

– The stiffness of the wall face as well as the interface between the sand and the wall face were taken into account.

– The construction procedure as followed in the field was modelled in the program.

– The compaction plant was simulated using program (BCOMPP), with its actual load and dimensions.

CHAPTER 11

CONCLUSIONS

11.1 INTRODUCTION

In the present research a model of a reinforced earth wall (6 m high) has been designed and constructed using dry sand as a backfill. The construction sequence used in a full scale wall was followed such as sand layer spreading, application of vibratory compaction and the use of temporary supports. Instrumentation was developed and calibrated to monitor the model wall behaviour before , during and after compaction of each layer.

Conclusions based on the studies presented in the preceding chapters on the reinforced earth retaining wall and compaction, will be outlined. The detailed conclusions have been recorded at the end of each chapter of the research. The conclusions are presented in three sections as follows:

- Conclusions drawn from the laboratory investigation.
- Conclusions drawn from theoretical studies of compaction.
- Conclusions drawn from the computer analysis using the finite element method.

The recommendations for future work are given at the end of the chapter.

11.2 CONCLUSIONS FROM LABORATORY INVESTIGATION

The conclusions drawn from this investigation are:

(1) The construction procedure as well as the use of vibratory compaction plant could be simulated successfully in model scale tests, which are economic and give an insight into different aspects of reinforced earth retaining wall behaviour. The vibratory compaction plant was simulated by two identical vibrators mounted together on a metal plate and contra–rotating to give vertical vibrations. The techniques used in forming sand beds were sand raining using a sand spreader and compaction with a vibratory compaction device.

(2) Two methods of calibrating the uniformity of sand beds in the model were used. These methods were temporary metal cylinders (single cylinders) and permanent perspex cylinders (composite cylinders). The composite cylinders were thought to provide a more realistic answer than the single cylinder method.

(3) Vibratory compaction is recommended when maximum dry density is required for cohesionless soil such as dry sand. The density is influenced by the time of vibration, thickness of lift and number of lifts.

(4) The preliminary model wall tests were carried out to check the performance of the instrumentations used in the model tests such as strain gauges, pressure cells and LVDTs. The results implied that the reproducibility and repeatability were reasonable.

(5) The reinforced earth retaining wall is a flexible system consisting of a composite material (soil and reinforcement) which gets its strength from the

apparent cohesion between soil and reinforcement. This can be developed by increasing the density of the composite material. This density increase has never been reached without using compaction, therefore compaction is a very important item in the construction process. Without compaction the system has no strength and will fail due to its own weight.

(6) During the compaction process stresses are locked in the soil due to the compaction plant. These locked–in stresses affect all the elements of the reinforced earth retaining wall. After compaction the soil starts to rebound and loses some of its densification and hence loses some – but not all – of the stresses locked in. Residual stresses remain after compaction affecting all elements of the wall.

(7) The values of the residual stresses range approximately between 0.15 to 0.3 times the effective vertical stresses.

(8) The distribution of vertical stresses under the reinforced mass increase near the wall face and decrease rapidly in the first third of the length of reinforced mass and more gradually towards the end of the reinforced mass. This is due to tilting of the face of the wall due to compaction. The values increase during compaction and decrease after compaction but are still greater than before compaction.

(9) The distribution of tensile force in the reinforcing strips is non linear. It is zero at the free end of the strip and increases towards the wall face to reach its maximum value within the front third of the strip length and then decreases towards the wall but does not reach zero at the wall face. The maximum values are obtained during compaction, reaching up to 30% more than

before compaction. After compaction the vaiues decrease but are still about 17% more than before compaction. The values of the forces increase with increasing depth of the reinforcing strip.

(10) The distribution of earth pressure behind the reinforced mass is very near to the active state before and after compaction. During compaction it increases slightly especially in the top third of the wall height to reach the at rest condition.

(11) The distribution of earth pressure behind the wall face during compaction increases significantly due to horizontal pressure coming directly from the compaction plant. The values reached approximately three times the values before compaction near the top of the wall.

(12) After compaction the values of earth pressure behind the wall face decrease but are still larger than the at rest condition in the upper third and decrease with depth to become very close to the at rest condition near the bottom of the wall.

(13) The lateral movement of the wall face indicates that sliding and rotational movement about the toe of the wall takes place. The movement in the upper half of the wall is greater than the lower half.

(14) The lateral movement after compaction is larger than in cases of before and during compaction. Because some densification, which has been gained during compaction, is released after compaction, this causes excess movement which adds to the movement due to the compaction plant and the earth pressure.

(15) Increasing the compaction length affects the behaviour of the reinforced earth wall, and the values of horizontal pressure on the wall face, forces in the strips, vertical stresses and the state of stresses in the reinforced mass increase significantly.

(16) Using a uniform compaction length at all the layers of backfill is more practical than a variable compaction length along the layers.

(17) The state of stress behind the wall face is greater than the at rest condition especially in the upper third. In the middle third it is between the active and the at rest condition, and at the lower third it is near the at rest condition.

(18) The method of construction has a great effect on the behaviour of a reinforced earth retaining wall. It is recommended that a method of construction is used which permits the wall movement to occur gradually to reduce and release the residual stresses which result from the effect of compaction plant during compaction of the backfill layers.

11.3 CONCLUSIONS FROM THEORETICAL STUDIES OF COMPACTION

The conclusions drawn from the theoretical studies of compaction are:

(1) The factors affecting the modelling of compaction in any theoretical analysis are:

a– The correct modelling of the soil behaviour before and after compaction, i.e.

- Stress & strain characteristics of the soil.
- Stress path of the soil.

b- The modelling of construction sequence in the field is as follows:

- Placement of layer of fill (lift)
- Compaction of the layer of fill.
- Placement of structures (facing panels & reinforcement in the case of a reinforcing earth retaining wall).
- Application of external loads.

c- The true modelling of the compaction plant.

(2) Most of the existing theories dealing with theoretical models of compaction have concentrated on the soil behaviour and construction sequences. They have modelled the compaction plant as point or line loads, i.e. they consider the compaction plant as a two dimensional problem. Since the problem is a three dimensional problem, no realistic simulation has been made, and this can have a great effect on the lateral stresses.

(3) Three proposed theoretical compaction models have been developed by the author to overcome this difficulty and cover most types of compaction plant. The real dimensions, weight of compaction plant and dynamic effect have been considered.

(4) The fourth proposed model of the compaction plant suggested by the author, is the computer program (BCOMPP). The analysis employed in the program was numerical integration. The real dimensions, and weight of the

compaction plant as well as the dynamic effect can be simulated in the program. It is convenient to use with a finite element simulation of a reinforced earth retaining wall and compaction.

(5) Comparisons with laboratory and field studies prove the usefulness of these models to calculate the lateral pressure due to the compaction plant in either a free field or on the retaining walls.

11.4 CONCLUSIONS FROM THE FINITE ELEMENT ANALYSIS

Adding to the previous conclusions from laboratory results the following conclusions were drawn from the finite element analysis:

(1) The computer program (SSCOMP) includes a non–linear stress–strain model for cohesionless soil, a linear model for reinforcement and a model of compaction induced stresses.

(2) A static plane strain finite element analysis procedure calculates soil and structural stresses and deformations and their interaction resulting from placement and compaction of fill layers of arbitrary geometry either in a free field or adjacent to deflecting or nondeflecting structures such as retaining walls. Fill placement and compaction is modelled incrementally.

(3) The program takes into consideration the rigidity of the wall face, interaction between soil and structural elements (wall face & reinforcement) and construction sequence.

(4) The computer program (BCOMPP) was used to simulate the real weight and dimensions of the compaction plant and its dynamic effect.

(5) The process of compaction in program (SSCOMP) is considered directly to increase only the residual lateral soil stresses and the residual lateral earth pressures at the soil/structure interface.

(6) The two programs served together to predict the behaviour of the model tests carried out in the laboratory before and after compaction.

(7) The fields of deformations due to compaction provided by the programs indicate that the values of major principal strain are compressive i.e. downward, and the minor principal strain is tensile i.e. outward. These values increase behind the wall face and around the reinforcement. Also the compaction causes the rotation of axes anti– clockwise.

(8) The values of principal stresses in the backfill due to compaction indicate that the major principal stresses are compressive i.e. effect downward and the minor principal stresses are tensile i.e. effect outward.

(9) The change of orientation of principal stresses due to compaction is slight within the reinforced mass, increasing clockwise just behind the wall face and behind the reinforced mass. This proves that after adding reinforcement to the soil the composite material behaves as one unit.

(10) The state of stresses within the reinforced mass is very close to the at rest condition. Near the top it is slightly greater than the at rest condition.

(11) The position of the maximum tensile force is affected by the change of the compaction length. By increasing the compaction length the value increases and the position moves towards the wall face.

(12) Comparison between the experimental results and the computer predictions shows reasonable agreement between experimental and computer because total agreement is difficult to achieve. This is because many factors play a significant role in the finite element results, such as location and kind of boundary condition, idealization of the problem and geometry of mesh.

(13) The comparison demonstrated the capability of the programs (SSCOMP) & (BCOMPP) to predict the behaviour of a reinforced earth wall under the compaction effect.

11.5 RECOMMENDATIONS FOR FURTHER STUDIES

The following recommendations are made for further studies on reinforced earth retaining walls:

(1) Study of the behaviour of model walls under the effect of compaction using:

a– Different types of backfill material and reinforcement.

b– Different types of connections between the wall and reinforcement, which give different connection rigidities.

c– Different wall face rigidities.

(2) There is a need to develop a model study and an analytical model to simulate the effect of compaction induced pore pressures, as well as their

dissipation with time.

(3) More field studies with accurate and reliable measurements of compaction effect on reinforced earth retaining walls are needed to get a suitable basis for quantitative evaluation of this effect.

(4) Different parametric studies on aspects of reinforced earth retaining wall can be obtained using programs (BCOMPP) & (SSCOMP).

(5) The finite element program (SSCOMP) may be extended to assess the behaviour of reinforced earth retaining walls during compaction by incorporating dynamic finite element procedures instead of static finite element procedures.

(6) Study of a reinforced earth wall with reinforcement in three directions in the backfill as an idea to increase the rigidity of a reinforced mass and decrease the earth pressure on the wall face where no rigid connections are needed between the wall face and the reinforcement.

REFERENCES

- Aggour, M.S. (1972).
"Retaining Wall in Seismic Area"
Ph. D. Thesis Submitted to University of Washington, Seattle, Washington.

- Anon (1967).
"Large Dams in Australia".
General Report, The Proceeding of 9th Int. Cong., Large Dams, Vol. IV, Istanbul.

- Aggour, M.S. & Brown, C.B. (1974).
"The Predictions of Earth Pressure on Retaining walls due to compaction".
Geotechnique, London, Vol. 24, No. 4, PP. 489–502.

- Al–Hussaini, M. & Perry, E.B. (1976).
"Effect of Horizontal Reinforcement on Stability of Earth Masses".
Technical Report, No. S–76–11, U.S. Army Engineer Waterways Experimental Station, Vicksburg, Miss.

- Al–Hussaini, M. & Johnson, L.D. (1978).
"Numerical Analysis of A Reinforced Earth Wall".
The Proceeding of The Sym. on Earth Reinforcement, ASCE, Pittsburgh, PP. 98–126.

- Al–Hussaini, M. & Perry, E.B. (1978).
"Field Experiment of Reinforced Earth Wall".
The Proceeding of The Sym. on Earth Reinforcement, ASCE, Pittsburgh, PP. 127–156.

- Al–Yassine, Z. & Herrmann, L.K. (1977).
"Finite Element Analysis of Reinforced Earth Wall"
Int. Conf. on Soil Reinforcement, Vol. 1, Paris, PP. 3–9.

- Boussinesq, J. (1855).
"Application des potentails a l'etude de l'equelibre et de mouvement des solids elastique"
Paris, Gauthier–Villars.

- Bernhard, R.K. (1952).
  "State and Dynamic Soil Compaction"
  Highway Research Board, Vol. 31, PP. 261.

- Butterfield, R. & Andrawes, K.Z. (1970).
  "An Air Activated Sand Spreader for Forming Uniform Sand Beds"
  Geotechnique, London, Vol. 20, Technical Notes, PP. 26.

- Broms, B. (1971).
  "Lateral Earth Pressures Due To Compaction of Cohesionless Soils"
  Proceeding 4th Conf. on Soil Mechanics, Budapest, PP. 373–384.

- Banerjee, P.K., January (1975).
  "Principles of analysis and design of reinforced earth retaining walls"
  The Journal of Highway Engineering, PP. 13–18.

- Bolton, M.D., Choudhury, S.P. (1976).
  "Reinforced Earth"
  UMIST/TRRL Research Contact, First Report.

- Bolton, M.D., Choudhury, S.P. & Pang, P.L. (1977).
  "Modelling Reinforced Earth"
  TRRL, SR. 457 , PP. 22–31.

- Boden, J.B., Irwin, M.J. & Pocock, R.G. (1977).
  "Construction of Experimental Reinforced Earth Walls at The TRRL"
  TRRL, SR. 457 , PP. 162–194.

- Boden, J.B., Irwin, M.J. & Pocock, R.G. (1978).
  "Construction of Experimental Reinforced Earth Walls"
  Ground Engineering, Vol. 11, No.7.

- Bacot, J., Iltis, M., Larel, P., Paumier, T. & Sanglerat, G. (1978).
  "Study of The Soil Reinforcement Friction Coefficient"
  The Proceeding of The Sym. on Earth Reinforcement, ASCE, Pittsburg, PP. 157–185.
- Baguelin, F. (1978).
  "Construction and Instrumentation of Reinforced Earth Walls in France"

The Proceeding of The Sym. on Earth Reinforcement, ACSE, Pittsburgh, PP. 186–201.

– Bassett, R.H. & Last, N.C. (1978).
"Reinforcing Earth Below Footing and Embankements"
The Proceeding of The Sym. on Earth Reinforcement, ASCE, Pittsburgh, PP. 202–231.

– Binquet, J. (1978).
"Analysis of Failure of Reinforced Earth Walls"
The Proceeding of The Sym. on Earth Reinforcement, ASCE, Pittsburgh, PP. 232–251.

– Biarez, J. (1980).
"General Report"
Int. Conf. on Compaction, Paris, Vol. III.

– de Buhan P., Salencon, J. & Siad, L. (1986).
"Critere de Resistance pour le Nateriau (Terre Armee)"
C.R. Acad. Sci. Paris 302, Serie II, 377–381.

– de Buhan, P., Mangiavacchi, R., Nova, L., Pellegrini, G. & Salencon, J. (1989).
"Yield Design of Reinforced Earth Walls by a Homogenization Method"
Geotechnique, London, Vol. 39, No. 2, PP. 189–201.

– Boyd, M.S. October (1988).
"Reinforced Earth Bridge Abutments"
International Geotechnical Sym. On Theory and Practice of Earth Reinforcement, Fukuoka, Japan, PP. 499–503.

– Benltayef, M.A. & Subrahmanyam, M.S. September (1989).
"Stabilization of Sand with Fiber Reinforcement"
2th Int. Conf. on Foundation and Tunnels, London, Vol. 2, PP. 125–130.

– Coulomb, C.A. (1776).
"Essai sur une Application des Regles des Maximus et Minimus a Quelques Problemes de Statique Relatifs a L'Architecture"

Mem. Acad. R. Pres. Div. Sa V 7, Paris, PP. 343–382.

– Coyne, M.A. (1927).
"Murs de Soutenement et Murs de Quai a Echelle"
Le Genie Civil, Tome XC1, October.

– Converse, F.J. (1953).
"Compaction of Sand at Resonant Frequency"
ASTM Sym. on Dynamic Testing of Soil, STP 156, PP. 124.

– Civil Engineering Code of Practice CP2 (1951)
"Earth Retaining Structures"
Institution of Civil Engineers.

– Clough, R.W. (1960).
"The Finite Element Method in Plane Strain Analysis"
The Proceeding of 2nd ASCE Conf. on Electronics Computation, September, Pittsburgh.

– Clough, R.W. (1969).
"Comparison of Three–Dimensional Finite Elements"
Proceedings of the Sym. on Application of Finite Element Methods in Civil Engineering, Vanderbilt University, Nashville / Tenn., PP. 1–26.

– Coyle, H.M., Bartoskewitz, R.E., Milberger, L.J. & Butler, H.D. (1974).
"Field Measurements of Lateral Earth Pressures on a Cantilever Retaining Wall". LRR, S 17, PP. 16–29.

– Coyle, H.M. & Bartoskewitz, R.E. (1976).
"Earth Pressure on Precast Panel Retaining Wall"
Journal of Geotechnical Engineering Division, Vol. 102, No. GT5, May, ASCE, PP. 441–456.

– Carder, D.R. & Krawczyk, J.V. (1975).
"Performance of Cells Designed to Measure Soil Pressure on Earth Retaining Structures". TRRL, LR 689.

– Carder, D.R. & Pocock, R.G. (1977).
"Experimental Retaining Wall Facility– Lateral Stress Measurements with Sand

Backfill".
TRRL, LR 766.

– Carder, D.R., Murray, R.T. & Krawczyk, J.V. (1980).
"Earth Pressure Against an Experimental Retaining Wall Backfill With Silty Clay".
TRRL, LR 946.

– Carder, D.R. (1988).
"Earth Pressures on Retaining Walls and Abutments"
Ground Engineering, Vol. 12, No. 2, PP. 7–10.

– Christie, L.F. & El–Hadi, K.M. (1977).
"Some Aspects of The Design of Earth Dams Reinforced with Fabric"
Proceeding of Int. Conf. on the Use of Fabrics in Geotechnics, Paris, Vol. 1, PP. 99–103.

– Cassard, A., Kern, F. & Mathieu, G. (1979).
"Use of Reinforcement Techniques in Earth Dams"
Int. Conf. on Soil Reinforcement, Vol. I, Paris, PP. 229–233.

– D'Appolonia, D.J., Whitman, R.V. & D'Appolonia, E. (1969).
"Sand Compaction with Vibratory Rollers"
Journal of the Soil Mechanics and Foundation Division, ASCE, Vol. 95, No. SM1, January, PP. 263–284.

– Darbin, M., Jailloux, J.M. & Montuells, J. (1978).
"Performance and Research on the Durability of Reinforced Earth Reinforcing Strips"
The Proceeding of The Sym. on Earth Reinforcement, ASCE, Pittsburgh, PP. 305–333.

– Duncan, J.M., Byrne, P., Wang, K.S. & Mabry, P. (1980).
"Strength, Stress–Strain and Bulk Modulus Parameters for Finite Element Analysis of Stresses and Movement in Soil Masses"
Report No. UCB/GT/80–01, University of California, Civil Engineering Department, Berkeley.

– Duncan, J.M., Jeyapalan, J.K. (1981).

"Deflection of Flexible Culverts Due to Backfill Compaction"
A Paper prepared for The Transportation Research Board Sym. on Soil Structure Interaction of Subsurface Conduits.

- **Duncan, J.M. & Seed, R.B. (1986).**
"Compaction–Induced Earth Pressures Under K_o–Condition"
Journal of Geotechnical Engineering, Vol. 112, No. 1, PP. 1–23.

- **Delmas, P., Berche, J.c. & Gourc, J.P. (1986).**
"Le Dimensionnement des Ouvrages Reinforces par Geotextile: Programme CARTAGE"
Liaison des LPC, No. 142.

- **DuBois, D.D. (1981).**
"Laboratory and Field Studies of The Textile Reinforcement of Earthfills"
Ph. D. Thesis Submitted to The Queen's University, Belfast, U.K..

- **Department of Transport (1987).**
"Reinforced Earth Retaining Walls and Bridge Abutments for Embankment"
Technical Memorandum (Bridges) BE 3/78 (revised, 1987), U.K..

- **Feda, J. (1961).**
"Research on the Bearing Capacity of Loose Sand"
The Proceeding of 5th Int. Conf. on Soil Mechanics and Foundation Engineering, Paris, Vol. I, PP. 635–642.

- **Fraser, J.B. (1962).**
"A Steel Faced Rockfill Dam for Papua"
Transport Institute of Engineers, Australia, Vol. CE4, No. 2.

- **Forssblade, L. (1965).**
"Investigation of Soil Compaction by Vibration"
Acta Polytechnica Scandinavica, CI34, Stockholm.

- **Finlay, T.W. (1977).**
"Performance of a Reinforced Earth Structure at Granton"
TRRL, SR 457, PP. 210–212.

- **Finlay, T.W. & Sutherland, H.B. (1977).**
"Field Measurements on a Reinforced Earth Wall at Granton"
The Proceeding of 9th Int. Conf. on Soil Mechanics and Foundation

Engineering, Vol. I, Tokyo, PP. 511–516.

– Finlay, T.W. (1978).
"Performance of a Reinforced Earth Structure at Granton"
Ground Engineering, Vol. 11, No. 7, PP. 42–44.

– Finlay, T.W. (1989).
"Special Communication"

– Fannin, R.J. & Hermann, S. (1988).
"Field Behaviour of Two Instrumented Reinforced Soil Slopes"
The Proceeding of Int. Geot. Sym. on Theory and Practice of Earth Reinforcement, October, Japan, PP. 277–282.

– Fukuoka, M. (1988).
"Earth Reinforcement West and East"
The Proceeding of Int. Geot. Sym. on Theory and Practice of Earth Reinforcement, October, Japan, PP. 33–47.

– Gerber, E. (1929).
"Untersuchugen Uber die Duchuertulung in Ortlich Belasteten Sand"
Diss A.–G. Gerb. Leemann, Zurich, 1929: From Spangler, M.G. (1938).
"Lateral Pressures on Retaining Walls Caused by Superimposed Loads"
Proceeding of Highway Research Board, Part II, PP. 57–65.

– Girijavallabhan, C.V. & Reese, L.C. (1968).
"Finite Element Method for Problems in Soil Mechanics"
Journal of Soil Mechanics and Foundations Division, Vol. 94, No. SM2, March, ASCE, PP. 437–497.

– Goodman, R.E., Taylor, R.L. & Brekke,T.L (1968).
"A Model for The Mechanics of Jointed Rock"
Journal of Soil Mechanics and Foundation Division, Vol. 94, No. SM3, May, ASCE, PP. 637–659.

– Green, D., Brown, D.K., Phillips, D. & Thomson, R. (1986).
"Finite Element Modelling Techniques in the Design Process"
Course in Finite Element Technique, September, University of Glasgow.

- Gourc, J.P., Ratel, A. & Delmas, P. (1986).
  "Design of Fabric Retaining Walls: the Displacement Method"
  3rd Int. Conf. on Geotextile and Geomembrane, Vienna.

- Gourc J.P., Ratel, A. & Gotteland, P. (1987).
  "Design of Reinforced Soil Retaining Walls, Analysis and Comparison of Existing Methods and Proposal for A New Approach"
  Nato Grant, The Use of Polymers to Reinforced Soil, Kingston.

- Gourc, J.P., Gotteland, P. & Delmas, P. (1988).
  "Design of Geosynthetic Retaining Walls: Displacement Method and Two Block Method, Comparison and Charts"
  International Geotechnical Sym. On Theory and Practice of Earth Reinforcement, Fukuoka, Japan, PP. 517–522.

- Holl, D.L. (1941).
  "Plane Strain Distribution of Stress in Elastic Media"
  Iowa Engineering Experimental Station, The Iowa State College Bulletin, No. 148, PP. 1–55.

- Hansen, B. (1961).
  "The Bearing Capacity of Sand, Tested by Loading Circular Plates"
  The Proceeding of 5th Int. Conf. on Soil Mechanics and Foundation Engineering, Paris, Vol. I, PP. 659–664.

- Hadala, P.F. (1967)
  "The Effect of Placement Method on The Response of Soil Stress Gauges"
  The Proceeding of The Sym. on Wave Propagation and Dynamic Properties of Earth Materials, Albuquerque, PP. 255–263.

- Holden, J.c. (1967).
  "Stresses and Strains in A Sand Mass Subjected to A Uniform Circular Load"
  Ph. D. Thesis, University of Melbourne.

- Hinton, E. & Owen, D.R.J. (1977).
  "Finite Element Programming"
  Academic Press, New York.

- Hausmann, M.R. & Lee, K.L. (1978).
  "Rigid Model Wall with Soil Reinforcement"
  The Proceeding of The Sym. on Earth Reinforcement, ASCE, Pittsburgh, PP. 400–427.

- Herrmann, L.R. & Al Yassin, Z. (1978).
  "Numerical Analysis of Reinforced Soil Systems"
  The Proceeding of The Sym. on Earth Reinforcement, ASCE, Pittsburgh, PP. 428–457.

- Hoshiya, M. (1978).
  "Strength of Reinforced Earth Retaining Walls"
  The Proceeding of The Sym. on Earth Reinforcement, ASCE, Pittsburgh, PP. 458–472.

- Hutchison, N.J. (1982).
  "Groups of Flate Anchors in Sand"
  Report for SECR Marine Technology Programme Project CE1.

- Huebner, K.H. & Thornton, E.A. (1982).
  "The Finite Element Method for Engineers"
  Second Edition, John Wiley&Sons, New York.

- Hollinghurst, E. & Murray, R.T. (1986).
  "Reinforced Earth Retaining Wall at A3/A322 Interchange: Design, Construction and Cost"
  Proceeding of Institution of Civil Engineers, Part 1, No. 80, October, PP. 1327–1341.

- I.C.I. (1973).
  "Perspex Arcylic Sheets"
  Technical Service Note, PX122, Sheet Group ICI, Plastic Division, Welwyn Garden City, Herts.

- Ingold, T.S. (1979).
  "Retaining Wall Performance Backfilling"
  Journal of Geotechnical Engineering Division, Vol. 105, No. GT5, May, ASCE, PP. 613–626.

- Ingold, T.S. (1979).
"The Effects of Compaction on Retaining Walls"
Geotechnique, Vol. 29, No. 3, September, PP. 265–283.

- Ingold, T.S. (1980).
"Review Paper – Reinforced Earth"
The Int. Journal of Cement Composities, Vol. 2, No. 3, August, PP. 119–142.

- Ingold, T.S. (1980).
"Lateral Earth Pressures Induced by Compaction"
Int. Conf. On Compaction, Vol. I, April, Paris, PP. 142–150.

- Ingold T.S. (1980).
"Reinforced Clay"
Ph. D. Thesis Submitted to University of Surrey, May.

- Ingold, T.S. (1981).
"Reinforced Earth Theory and Design"
Highway Engineering, July, PP. 2–15.

- Ingold, T.S. (1982).
"Reinforced Earth"
Thomas Telford Ltd., London.

- Ingold, T.S. (1982).
"A Reconsideration of Retaining Wall Design"
Journal of Institution of Structural Engineers, Vol. 60B, No. 4, December, GB, PP. 83–92.

- Ingold, T.S. (1983).
"The Design of Reinforced Soil Walls by Compaction Theory"
Journal of Institution of Structural Engineers, Vol. 61A, No. 7, July, GB, PP. 205–211.

- Ingold, T.S. & Millar, K.S. (1983).
"Drained Axisymmetric Loading of Reinforced Clay"

The Journal of Geotechnical Engineering, Vol. 109, No. 7, July, ASCE, PP. 883–898.

– Ingold, T.S. (1988).
"Long Term Performance Requirements for Polymeric Soil Reinforcement in The U.K."
The Proceeding of Int. Geot. Sym. on Theory and Practice of Earth Reinforcement, October, Japan, PP. 523–528.

– Jones, C.J.F.P. (1973).
"Field Measurements of Earth Pressures Against Motorway Retaining Walls and Bridge Abutments"
Proceeding Sym. in Field Instrumentation in Geotechnical Engineering Part I, British Geotechnical Society.

– Jones, C.J.F.P. (1977).
"British Patert Specification No. 1485005"

– Jones, C.J.F.P. (1977).
"Practical Design Considerations"
TRRL, SR 457, PP. 39–46.

– Jones, C.J.F.P. (1978).
"The York Method of Reinforced Earth Construction"
The Proceeding of The Sym. on Earth Reinforcement, ASCE, Pittsburgh, PP. 501–527.

– Jones, C.J.F.P. (1979).
"Lateral Earth Pressures Acting on The Facing Units of Reinforced Earth"
Int. Conf. on Soil Reinforcement, Vol. I, Paris, PP. 445–449.

– Jones, C.J.F.P. (1985).
"Design and Construction Methods"
The Proceeding of The Sym. on Polymer Grid Reinforcement, London, Paper 6.1.

– Jones, C.J.F.P. (1985).
"Earth Reinforcement and Soil Structure"
Butterworths and Co. (Publishers) Ltd., London.

- Jones, C.J.F.P. (1988).
  "Predicting the Behaviour of Reinforced Soil Structures"
  International Geotechnical Sym. On Theory and Practice of Earth Reinforcement, Fukuoka, Japan, PP. 535–540.
- Juran, I., Schlosser, F., Long, T.N. & Legeay, G. (1978).
  "Full Scale Experiment on a Reinforced Earth Bridge Abutment in Lille"
  The Proceeding of The Sym. on Earth Reinforcement, ASCE, Pittsburgh, PP. 556–584.
- Juran, I. & Christopher, B. (1989).
  "Laboratory Model Study on Geosynthetic Reinforced Retaining Walls"
  Journal of Geotechnical Engineering, Vol. 115, No. 7, July, PP. 905–920.
- Jone, N.W.M. (1979).
  "Reinforced Soil"
  Chartered Municipal Engineer, Vol. 106, June, PP. 175–181.
- Kogler, F. & Scheiding, A. (1927).
  Die Bautchink, 31, July 15.
  From: Peattie, K.R. and Sparrow, R.W. (1954).
  "The Fundamental Action of Earth Pressure Cells"
  Journal of The Mechanics and Physics of Solids, Vol. 2, PP. 141–155.
- Kolbuszewski, J. (1948.a).
  "Study of The Maximum and Minimum Porosities of Sand"
  The Proceedings of 2th Int. Conf. on Soil Mechanics, Vol. I, PP. 158–165.
- Kolbuszewski, J. (1948.b).
  "Study of The Maximum and Minimum Porosities of Sand"
  The Proceedings of 2th Int. Conf. on Soil Mechanics, Vol. I, PP. 47–49.
- Kolbuszewski, J. & Jones, R.H. (1961).
  "The Preparation of Sand Samples For Laboratory Testing"
  Proceeding of The Midland Soil Mechanics and Foundation Engineering Society, Vol. 4, Paper A6.
- Kondner, R.L. (1963).
  "Hyperbolic Stress–Strain Response: Cohesive Soils"

Journal of the Soil Mechanics and Foundations Division, ASCE, Vol. 89, No. SM1, February, PP. 115–143.

– Khosla, V.K & Tien, H.Wu. (1976).
"Stress–Strain Behaviour of Sand"
Journal of Geotechnical Engineering Division, Vol. 102, No. GT4, April, ASCE, PP. 303–321.

– Katona, M.G. (1978).
"Analysis of Long Span Culverts by The Finite Element Method"
Transaction Research Record, No. 678, PP. 59–66.

– Koerner, R.M. & Welah, J. (1980).
"Construction and Geotechnical Engineering Using Synthetic Fabric"
John Wiley and Sons, New York.

– Lallemand, M.F. (1959).
"French Patent Specification No. 1173383"

– Lewis, W.A. (1961).
"Recent Research into The Compaction of Soil by Vibratory Compaction Equipment"
The Proceeding of 5th Int. Conf. on Soil Mechanics and Foundation Engineering, Vol. II, Paris, PP. 261–268.

– Lazebnik, G.E. & Chernysheva, E.I. (1968).
"Certain Errors in Experimental Determination of Earth Pressure on Models of Retaining Walls"
Hydrotechnical Construction, Vol. 4, PP. 333–339.

– Lade, P.V. (1971).
"The Stress–Strain and Strength Characteristics of Cohesionless Soils"
Ph. D. Thesis submitted to University of California, Berkeley, California.

– Lade, P.V. & Duncan,J.M. (1976).
"Stress Path Dependent Behaviour of Cohesionless Soil"
Journal of Geotechnical Engineering Division, Vol. 102, No. GT1, May, ASCE, PP. 51–68.

– Lee, K.L., Adams, B.D. & Vagneron, J.M. (1973).

"Reinforced Earth Retaining Walls"
Journal of the Soil Mechanics and Foundation Division, ASCE, Vol. 99, No. SM10, October, PP. 745–764.

– Lee, K.L. (1976).
"Reinforced Earth– An Old Idea in A New Setting"
New Horizons in Construction Material, Envo. Publ. Co. Inc. Pennsylvania, Vol. I, PP. 655–682.

– Lambrechts, J.R. & Leonards, G.A. (1978).
"Effects of Stress History on Deformation of Sand"
Journal of Geotechnical Engineering Division, ASCE, Vol. 104, No. GT11, PP. 1371–1387).

– Long, N.T., Guegan, y., & Legeay, G. (1972).
"Etude de la Terre Armee a L'appareil Triaxial"
Rapport de Recherche, No. 17, LCPC.

– Long, N.T. (1977)
"Written Contribution to Session II"
TRRL, SR 457.

– Lamb, T.W., Whitman, R.V. (1979).
"Soil Mechanics"
John Wiley & Sons, New York.

– Munster, A. (1930).
"United States Patent Specification No. 2145396"

– Mindlin, R. D. (1936).
"Pressure Distribution on Retaining Walls"
The Proceeding of 1st Int. Conf. On Soil Mechanics and Foundation Engineering, Vol. III, PP. 155–156.

– Monfore, G.E. (1950).
"An Analysis of the Stress Distribution in and Near Stress Gauges Embedded in Elastic Solids"
U.S. Department of Interior, Bureau of Reclamation , Research and Geology

Division, Structural Research Laboratory, Report No. SP–26.

– Macrae, J.C. & Gray, W.A. (1961).
"Significance of The Properties of Materials in The Packing of Real Spherical Particles"
British Journal of Applied Physics, Vol. 12, PP. 164–172.

– Mackey, R.D. (1963).
"An Investigation of The Factors Controlling The Shear Strength of Granular Materials"
Ph. D. Thesis Submitted to University of Leeds, Civil Engineering Department.

– Morgan, J.R. & Gerrard, C.M. (1968).
"Free Field Measurements of Stresses and Strains in Soils"
The Proceedings of 4th Conference of The Australian Road Research Board, Melbourne, Vol. 4, Part 2, PP. 1743–1760

– Milligan, G.W. (1974).
"The Behaviour of Rigid and Flexible Retaining Walls in Sand"
Ph. D. Thesis Submitted to University of Cambridge, Civil Engineering Department.

– McGown A , Andrawes K.Z. & Al–Hasani, M.M. (1978).
"Effect of Inclusion Properties on The Behaviour of Sand"
Geotechnique. London, Vol. 28, No. 3, PP. 327–346.

– McKittrick, D.P. (1978).
"Reinforced Earth: Application of Theory and Research to Practice"
Ground Engineering, January, Vol. 12, No. 1.

– McKittrick, D.P. (1978).
"Design, Construction,Technology and Performance of Reinforced Earth Structures"
The Proceeding of The Sym. on Earth Reinforcement, ASCE, Pittsburgh, PP. 596–617.

– McKittrick, D.P. (1978).
"Reinforced Earth: Application of Theory and Research to Practice"

Proceeding of Sym. on Soil Reinforcing and Stability Techniques, NSW Institute of Technology, Supplementary Volume, PP. 1–44.

– McKittrick, D.P. & Darbin, M. (1979).
"World–Wide Development and Use of Reinforced Earth Structures"
Ground Engineering, Vol. 12, No. 2, PP. 15–21.

– McKittrick, D.P. & Wojciechowski, L.J. (1979).
"Example of Design and Construction of Seismically Resistant Reinforced Earth Structure"
Int. Conf. on Soil Reinforcement, Vol. I, Paris, PP. 95–100.

– Mitchell, J.K. & Schlosser, F. (1979).
"General Report"
Int. Conf. on Soil Reinforcement, Vol. III, Paris, PP. 25–39.

– Mayne, P.W. & Kulhawy, F.H. (1982)
"K_o–OCR Relationships in Soil"
Journal of Geotechnical Engineering Division, Vol. 108, No. GT6, June, ASCE, PP. 851–872.

– Measurements Group Inc. (1982).
"Design Considerations for Diaphragm Pressure Transducers"
Technical Note, TN.–510.

– Murray, R.T (1977)
"Research at the TRRL to Develop Design Criteria"
TRRL, SR 457, PP. 55–73.

– Murray, R.T. & Boden, J.B. (1979).
"Reinforced Earth Wall Constructed with Cohesive Fill"
Int. Conf. on Soil Reinforcement, Vol. 1, Paris, PP. 569–577.

– Murray, R.T. (1980).
"Fabric Reinforced Earth Walls: Development of Design Equations"
Ground Engineering, October, Vol. 13, No. 7.

– Murray, R.T. (1981).
"Fabric Reinforced Earth Walls: Development of Design Equations"

TRRL, SR 496.

- Murray, R.T. (1982).
"An Analytical Study of Geotextile Reinforced Embankments and Cuttings"
Proceeding of 2nd Int. Conf. on Geotextiles, Las Vegas, Vol. 3, PP. 707–713.

- Murray, R.T. & Hollinghurst, E. (1986).
"Reinforced Earth Retaining Wall at A3/A322 Interchange: Instrumentation, Site Observation and Performance"
Proceeding of Institution of Civil Engineers, Part 1, No. 80, October, PP. 1343–1362.

- Michalski, P., Watson, R.W. & Finlay, T.W (1986).
"The Influence of Acceleration and Frequency on Effects of Vibratory Compaction of Coal Mining Wastes / Minestone"
Ground Engineering, Vol. 19, No. 3, PP. 17–20.

- New Civil Engineer (1975).
"The Battle Over Reinforced Earth"
New Civil Engineer, February.

- Naylor, D.J. & Richards, H. (1978).
"Slipping Strip Analysis of Reinforced Earth"
Int. Journal of Numerical and Analytical Method in Geomechanics, Vol. 2, Part 4, PP. 343–366.

- Naylor, D.J. & Pande, G.N. (1981).
"Finite Element in Geotechnical Engineering"
Pineridge Press, Swansea, U.K.

- Oden, J.T. (1972).
"Some Aspects of Recent Contributions to the Mathematical Theory of Finite Element"
Proceeding of 2nd U.S.– Japan Seminar on Advances in Computational Methods in Structural Mechanics and Design, University of Alabama.

- Osman, M.A. (1977)
"An Analytical and Experimental Study of Reinforced Earth Walls"
Ph. D. Thesis Submitted to University of Glasgow, Civil Engineering

Department.

– Osman, M.A., Finlay, T.W. & Sutherland, H.B. (1979).
"The Internal Stability of Reinforced Earth Walls"
Int. Conf. on Soil Reinforcement, Vol. I, Paris, PP. 107–112.

– Osman, E. (1980).
"Model Study and Finite Element Analysis of Reinforced Earth Retaining Wall"
M. Sc. Thesis Submitted to University of Assiut, Civil Engineering Department, Egypt.

– Peattie, K.R & Spparrow, R.W. (1954).
"The Fundamental Action of Earth Pressure Cells"
Journal of The Mechanics and Physics of Solids, Vol. 2, PP. 141–155.

– Parkin, A., Trollope, D.H. & Lawson, J.D. (1966).
"Rockfill Structures subject to Water Flow"
Journal of the Soil Mechanics and Foundation Division, ASCE, Vol. 92, No. SM6, PP. 135–151.

– Pells, H.N.F. (1969).
"Reinforcement of Rockfill Dams in South Africa"
The Proceeding of 7th Int. Conf. on Soil Mechanics and Foundation Engineering, Vol. II.

– Price, D.I. (1975).
"Reinforced Earth in The U.K."
Ground Engineering, Vol. 8, No. 2, PP 19–24.

– Price, D.I. (1977).
"Construction in Reinforced Earth"
TRRL, SR 457.

– Price, D.I. (1978).
"Aspects of reinforced earth in The U.K."
Ground Engineering, September, PP. 48-- 50.

– Popescu, E.M. (1979).
"Some Considerations on The Design Methods of Reinforced Earth Retaining

Walls"
Int. Conf. on Soil Reinforcement, Vol. I, Paris, PP. 131–137.

– Pople, J. (1980).
"BSSM Strain Measurement Reference Book"
British Society for Strain Measurement.

– Quyang Zhong Chun (1988).
"26 m Height Reinforced Soil Quay Wall: Design and Full Scale Test"
International Geotechnical Sym. On Theory and Practice of Earth Reinforcement, Fukuoka, Japan, PP. 599–604.

– Uezawa, H. and Kornine, T. (1975).
"Reinforcement of Embankments Using Net"
Telgudo–Doboka, Japan, Vol.17, No. 5, PP. 21–24.

– Rankine, W.J.M. (1857).
"On Stability of Loose Earth"
Transaction, Royal Society, London, Vol. 147.

– Redshaw S.C. (1954).
"A Sensitive Miniature Pressure Cell"
The Stress Analysis Group Conference of the Institute of Physics, March, Nottingham, Vol. 31, PP. 467–

– Rowe, P.W. (1954).
"A Stress–Strain Theory for Cohesionless Soil with Application to Earth Pressure at Rest and Moving Walls"
Geotechnique, London, Vol. 4, No. 2, PP. 70–88.

– Rowe, P. W. (1971).
"Large Scale Laboratory Model Retaining Wall Apparatus, Stress–Strain Behaviour of Soils"
Proceeding of the Roscoe Memorial Sym., Cambridge University, Edited by Parry, R.H.G., PP. 441–449.

– Rehnman, S.E. & Broms, B.B. (1972).
"Lateral Pressures on Basement Walls. Results from Full Scale Tests"
The Proceeding of 5th European Conference on Soil Mechanics, Madrid,

PP. 189–197.

– Romstad, K.M., Herrmann, L.R. & Shen, C.K. (1976)
"Integrated Study of Reinforced Earth: I. Theoretical Foundation"
Journal of Geotechnical Engineering Division, Vol. 102, No. GT5, May, ASCE.

– Romstad, K.M., Al–Yassin, Z., Hermann, L.R. & Shen, C.K. (1978).
The Proceeding of The Sym. on Earth Reinforcement, ASCE, Pittsburgh, PP. 685–713.

– Reddy, D.V., Bobby, W. & Mahrenholtz, O. (1979).
"Ultimate Load Behaviour of (cut–and–cover) Underground Nuclear Reactor Containments with Reinforced Earth Backfill"
Int. Conf. on Soil Reinforcement, Vol. I, Paris, PP. 347–353.

– Rugger, R. (1986).
"Geotextiles Reinforced Soil Structures on which Vegetation can be Established"
Proceeding of 3rd Int. Conf. on Geotextiles, Vienna, Austria,Vol. 2, PP. 453–458.

– Schroeter, A. (1933).
"British Patent Specification No. 397492"

– Spangler, M.G. (1938).
"Lateral Pressures on Retaining Walls Caused by Superimposed Loads"
Proceeding of Highway Research Board, Part II, PP. 57–65.

– Sowers, G.F., Robb, A.D., Mullis, C.H. & Glenn, A.J. (1957).
"The Residual Lateral Pressures Produced by Compacting Soils"
4th Int. Conf. on Soil Mechanics and Foundations Engineering, Vol. 2, London, PP. 243–247.

– Schmidt, B. (1967).
"Lateral Stresses in Uniaxial Strain"
Geoteknisk Institute, The Danish Geotechnical Institute Bulletin No. 23, Copenhagen, PP. 5–11.

– Sims, F.A. & Jones, C.J.F.P (1974).

"Comparison between Theoretical and Measured Earth Pressures Acting On a Large Motorway Retaining Wall"
The Journal of Institution of Highway Engineers, December, PP. 26–29.

– Steiner, R.S. (1975).
"Reinforced Earth Bridges Highway Sinkhole"
Civil Engineering, ASCE, July, PP. 54–56.

– Schlosser, F. & Long, N.T. (1972).
"Comportement de la Terre Armee Dans les Ouvrages de Soutenement"
The Proceeding of 5th European Conf. on Soil Mechanics and Foundations, Vol. 1, PP. 299–306.

– Schlosser, F. (1977).
"Experience on Reinforced Earth in France"
TRRL, SR 457.

– Schlosser, F. & Long, N.T. (1974).
"Recent Results in French Research on Reinforced Earth"
Journal of Construction Division, ASCE, Vol. 100, No. CO3, September, PP. 223–237.

– Schlosser, F. & Elias, V. (1978).
"Friction in Reinforced Earth"
The Proceeding of The Sym. on Earth Reinforcement, ASCE, Pittsburgh, PP. 735–763.

– Subbaroa, C. (1977).
"Vibratory Densification of Cohesionless Media"
Proceeding of Int. Symp. on Soil Structure Interaction, University of Roorkee, India, January, PP. 173–179.

– Smith, G.N. (1977).
"Summary of Session I, II, III, and Discussion"
TRRL, SR 457

– Smith, G.N. (1977).
"Principles of Reinforced Earth Design"

TRRL, SR 457, PP. 2–13.

– Sheriff, M.M. & Mackey, R.D. (1977).
"Pressures on Retaining Wall with Repeated Loading"
Journal of Geotechnical Engineering Division, ASCE, Vol. 103, No. GT11, November, PP. 1341–1345.

– Swiger, W.F. (1978).
"Summary Report"
The Proceeding of The Sym. on Earth Reinforcement, ASCE, Pittsburgh, PP. 880–885.

– Seed, R.B. & Duncan, J.M. (1983)
"Soil Structure Interaction Effects of Compaction Induced Stresses and Deflections"
Report No. UCB/GT/83–06, Department of Civil Engineering, University of California, Berkeley.

– Seed, R.B. & Duncan, J.M. (1984).
"A Finite Element Analysis Program for Evaluation of Soil Structure Interaction and Compaction Effects"
Report No. UCB/GT/84–02, February, Department of Civil Engineering, University of California, Berkeley.

– Seed, R.B. & Duncan, J.M. (1986).
"F.E. Analyses: Compaction–Induced Stresses and Deformations"
The Journal of Geotechnical Engineering, Vol. 112, No. 1, January, ASCE, PP. 23–43.

– Seed, R.B., Collin, J.G. & Mitchell, J.K. (1986).
"F.E.M. Analyses of Compacted Reinforced soil Walls"
The Proceeding of 2th Int. Conf. on Numerical Method in Geomechanics, April, Belgium.

– Salencon, J. (1984).
"Yield Strength of Anisotropic Soils"
Invited Lecture, Proceeding of 16th ICTAM LYNGBY, Denmark, North Holand Publishers, London PP. 369–386.

– Schneirder, H.p. & Holtze, R.D. (1986).

"Design of Slopes Reinforced with Geotextiles and Geogrids"
Geotextiles and Geomembranes, Elsevier Applied Science Publishers Ltd., England, PP. 29–51.

– Schmertmann, G.R. et al. (1987).
"Design Charts for Geogrid–Reinforced Soil Slopes"
Proceeding of Geosynthetics 87 Conf. New Orleans, Industrial Fabrics Association Int., Vol. 1, PP. 108–120.

– Terzaghi, K. (1920).
"Old Earth Pressure Theories and New Test Results"
Engineering News Record, Vol. 85, PP. 632–637.

– Terzaghi, K. (1934).
"Large Retaining Wall Tests"
Engineering News Record, Vol. 112, PP. 136–140.

– Terzaghi, K. (1942).
"Theoretical Soil Mechanics"
John Wiley and Sons, INC., 4th edition (1966).

– Terzaghi, K. & PecK, R.B. (1948).
"Soil Mechanics in Engineering Practice"
John Wiley and Sons, Inc., New York.

– Terzaghi, K. (1954).
"Theoretical and Real Pressures on Anchored Bulkheads"
Transaction of ASCE, Vol. 119, PP. 1244–1280.

– Taylor, D.W. (1947).
"Pressure Distribution Theories, Earth Pressure Cell Investigation and Pressure Distribution Data"
U.S. Waterways Experimental Station.

– Tschebotarioff, G.P. & Welch, J.K. (1948).
"Effect of Boundary Conditions on Lateral Earth Pressures"
2nd Int. Conf. On Soil Mechanics, PP. 308–313.

– Trollope, D.H. & Currie, D.T. (1960).
"Small Embedded Earth Pressure Cells– Their Design and Calibration"

The Proceeding of 3rd Australia– New Zealand Conf. On Soil Mechanics and Foundation Engineering.

– Toombs, A.F. (1972).
"The Performance of Bomag BW 75S and BW 200 Double Vibrating Rollers in The Compaction of Soil"
TRRL, LR 480.

– TRRL (1976).
"Finite Element Analysis of Stresses Against Retaining Walls"
TRRL, Leaflet, LF 631.

– U.S. Corps of Engineerings (1944).
"Soil Pressure Cell Investigation"
Technical Memorandum, No. 201–1, U.S. Waterways Experiment Station.

– Vidal, H. (1967).
"Patent Specification No. 1069361, Improvement in Construction Works"
The Patent Office, London, 16 PPS.

– Vidal, H. (1969).
"The Principle of Reinforced Earth"
Highway Research Record, No. 282, PP. 1–16.

– Vidal, H. (1970).
"Reinforced Earth Steel Retaining Wall"
Civil Engineering, February, ASCE, PP. 72–73.

– Vidal, H. (1978).
"The Development and Future of Reinforced Earth, Keynote Address"
The Proceeding of The Sym. on Earth Reinforcement, ASCE, Pittsburgh, PP. 1–61.

– Vidal, H. (1986).
"La Petite Histoire de la Terre Armee"
Revue Generale des Routes et des Aerodromes, No. 635, Novembre, PP. 65–72.

– Weiss, A. (1951).

"Construction Technique of Passing Floods over Earth Dams"
Transactions of ASCE, Vol. 116.

– Whiffen, A.C. (1954).
"The Pressure Generated in Soil by Compaction Equipment"
American Society for Testing and Materials Sym. on Dynamic Testing of Soils, PP. 186–210.

– Walker, B.P. & Whitaker, T. (1967).
"An Apparatus for Forming Uniform Beds of Sand for Model Foundation Tests"
Geotechnique, Vol. 17, PP. 101–107.

– Whinterkorn, H.F. & Fang, H.Y. (1975).
"Foundation Engineering Handbook"
Van Nostrand Reinhold Company, London.

– Window, A.L. & Holister, G.S. (1982).
"Strain Gauge Technology"
Applied Science Publishers"

– Whiteford, D.A. (1983).
"The Effect of Disturbance of The Sand Bed due to Installation"
Research Report, Department of Civil Engineering, University of Glasgow.

– Wang, T.C.W. (1986)
"The Behaviour of Plate Anchor Groups in Sand"
M. Sc. Thesis Submitted to University of Glasgow, Civil Engineering Department.

– Zienkiewcz, O.C. (1977).
"The Finite Element Method"
McGraw Hill, 3rd edition.

– Zakaria, I.B. (1986).
"The Effect on The Uplift Resistance of Anchors of Ground Disturbance During Placing"
M. Sc. Thesis Submitted to University of Glasgow, Civil Engineering Department.

APPENDIX A

A.1 CALIBRATION FACTORS FOR STRAIN GAUGES

The calibration factors for the strain gauges are shown in Table (A.1).

TABLE (A.1) CALIBRATION FACTORS.

STRAIN GAUGE No.	CALIB. FACTOR N/μ-strain	STRAIN GAUGE No.	CALIB. FACTOR N/μ-strain	STRAIN GAUGE No.	CALIB. FACTOR N/μ-strain
1	00.1393	12	00.1279	23	00.1350
2	00.1329	13	00.1288	24	00.1339
3	00.1340	14	00.1329	25	00.1381
4	00.1386	15	00.1358	26	00.1364
5	00.1403	16	00.1298	27	00.1340
6	00.1339	17	00.1392	28	00.1296
7	00.1431	18	00.1354	29	00.1367
8	00.1322	19	00.1286	30	00.1370
9	00.1299	20	00.1338	31	00.1385
10	00.1340	21	00.1410	32	00.1339
11	00.1262	22	00.1340	33	00.1391

TABLE (A.1) CONT.

34	00.1353	45	00.1299	56	00.1295
35	00.1369	46	00.1298	57	00.1339
36	00.1360	47	00.1359	58	00.1385
37	00.1357	48	00.1356	59	00.1376
38	00.1303	49	00.1288	60	00.1342
39	00.1403	50	00.1292	61	00.1342
40	00.1331	51	00.1374	62	00.1297
41	00.1278	52	00.1296	63	00.1359
42	00.1268	53	00.1308	64	00.1315
43	00.1304	54	00.1340	65	00.1319
44	00.1257	55	00.1334	66	00.1291

A.2 CALIBRATION FACTORS FOR PRESSURE CELLS

The calibration factors are shown in table (A.2)

TABLE (A.2) CALIBRATION FACTORS

PRESSURE CELL No.	CALIB. FACTOR ($\frac{kN/m^2}{\mu\text{-strain}}$)	PRESSURE CELL No.	CALIB. FACTOR ($\frac{kN/m^2}{\mu\text{-strain}}$)
1	00.0668	9	00.0729
2	00.0764	10	00.0844
3	00.0814	11	00.0778
4	00.0792	12	00.1391
5	00.0720	13	00.0823
6	00.0627	14	00.0813
7	00.0813	15	00.1199
8	00.0822	16	00.0925

A.3 DESIGN OF VIBRATORY COMPACTION APPARATUS

According to the previous factors affecting the compaction, Chapter 4, the following assumptions were considered in designing the compaction apparatus to obtain the best densification, i.e.

- Acceleration is 1.5g.
- Frequency f is 25 HZ, i.e. 25 cycle/sec.

According to Terzaghi (1942), the following equations were employed:
The angular velocity of eccentric weight of vibrator is,

$$\omega = 2 \pi f \tag{A.1}$$

The centrifugal force produced from two vibrators is

$$F_c = 2 \frac{\Delta W}{g} r \omega^2 \tag{A.2}$$

$$a = \frac{F_c}{C_s} \tag{A.3}$$

$$C_s = A d_s \tag{A.4}$$

$$d_s = \frac{4 \pi^2 f^2}{A} \quad \frac{W}{g} \tag{A.5}$$

Where:

f is the frequency .

g is the gravity acceleration.

r is the eccentricity.

ΔW is the eccentric weight.

a is the amplitude.

C_s is the spring coefficient.

d_s is the dynamic coefficient of subgrade reaction.

A is the area of base plate.

W is the weight of vibrators, base plate, and compacted soil.

The amplitude from peak to peak can be given from an equation suggested by the vibrator manufacturer as follows:

$$A_{mp} = \frac{1.786 \times 10^6 \times F_c}{f^2 \quad W} \qquad (A.6)$$

Where $A_{mp} = 2a$

From the available data for the vibrators such as, the weight, the frequency and the weight of base plate and the required soil density after compaction, F_c can be calculated to adjust the vibrators to give the required degree of compaction. The thickness of compacted soil can also be determined.

APPENDIX B

DERIVATION OF FORMULAE FOR HORIZONTAL STRESSES

B.1 DERIVATION OF THE FORMULA FOR HORIZONTAL STRESS DUE TO A POINT LOAD

According to Fig. (B.1), the following parameters are defined:

Q = Concentrated load.

Z = Depth of the point.

(X,Y,Z) = Coordinate of point at which the horizontal stress is required.

$R = \sqrt{X^2+ Y^2+ Z^2}$

$r = \sqrt{X^2+ Y^2}$

ψ = Angle between Z & R.

θ = Angle between r & X.

σ_θ = Tangential stress at point (X,Y,Z).

σ_r = Radial stress at point (X,Y,Z).

σ_X = horizontal stress at point (X,Y,Z).

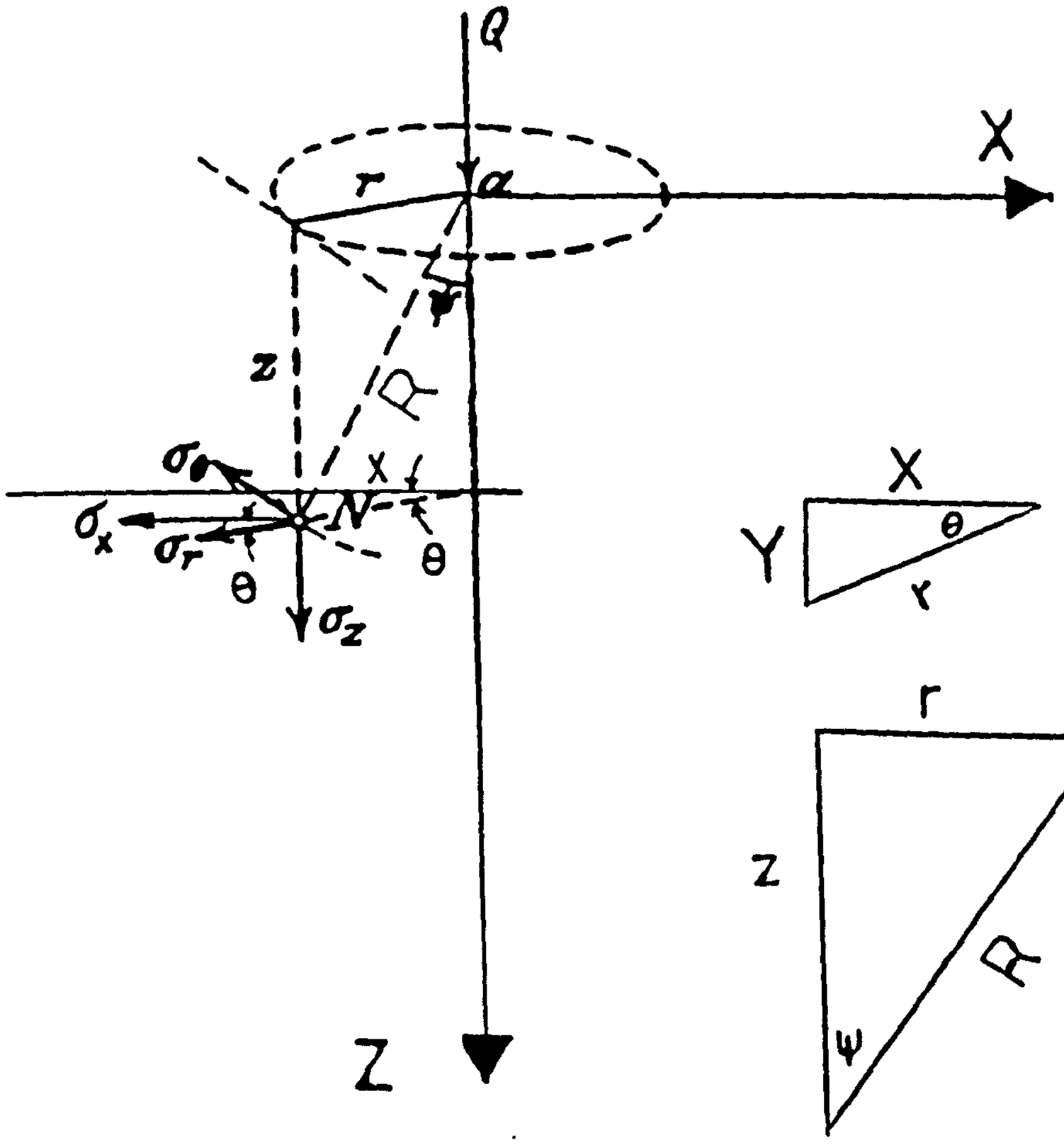

FIG. (B.1) RADIAL , TANGENTIAL AND HORIZONTAL STRESSES DUE TO POINT LOAD.

According to Boussinesq's equation (Terzaghi, 1942), the radial stress σ_r & the tangential stress σ_θ due to a concentrated load Q are shown in Fig. (B.1) and are calculated as follows:

$$\sigma_r = \frac{Q}{2\pi Z^2}\left[3\cos^3\psi \sin\psi - (1-2\nu)\frac{\cos^2\psi}{1+\cos\psi} \right] \qquad (B.1)$$

$$\sigma_\theta = -(1-2\nu)\frac{Q}{2\pi Z^2}\left[\cos^3\psi - \frac{\cos^2\psi}{1+\cos\psi} \right] \qquad (B.2)$$

Where:

ν = Poisson's ratio.

From the above two equations and the geometry, the horizontal stress σ_x which is independent of the location of Q can be determined as follows:

$$\sigma_x = \sigma_r \cos^2\theta + \sigma_\theta \sin^2\theta \qquad (B.3)$$

According to Fig. (B.1) the following relations can be determined as follows:

$$\tan \theta = \frac{Y}{X} \qquad \text{(B.4)}$$

$$\sin \theta = \frac{Y}{r} \qquad \text{(B.5)}$$

$$\cos \theta = \frac{X}{r} \qquad \text{(B.6)}$$

$$\tan \psi = \frac{r}{Z} \qquad \text{(B.7)}$$

$$\sin \psi = \frac{r}{R} \qquad \text{(B.8)}$$

$$\cos \psi = \frac{Z}{R} \qquad \text{(B.9)}$$

From the above geometric relations the radial and tangential stresses σ_r & σ_θ respectively can be written as follows:

$$\sigma_r = \frac{Q}{2\pi} \left\{ \frac{3\, r^2\, Z}{R^5} - (1-2\nu) \left[\frac{1}{R(R+Z)} \right] \right\} \qquad \text{(B.10)}$$

$$\sigma_\theta = -\frac{Q}{2\pi} \left[(1-2\nu) \left[\frac{Z}{R^3} - \frac{1}{R(R+Z)} \right] \right] \qquad \text{(B.11)}$$

The horizontal stress σ_x can be determined from Eqs.(B.3,10&11)

as follows:

$$\sigma_x = \frac{Q}{2\pi}\left\{\frac{3\,r^2\,Z}{R^5} - (1-2\nu)\left[\frac{1}{R(R+Z)}\right]\right\}\frac{X^2}{r^2} +$$

$$\frac{Q}{2\pi}\left\{-(1-2\nu)\left[\frac{Z}{R^3} - \frac{1}{R(R+Z)}\right]\right\}\frac{Y^2}{r^2} \qquad (B.12)$$

Hence,

$$\sigma_x = \frac{Q}{2\pi}\left\{\frac{3\,r^2 Z}{R^5} - (1-2\nu)\left[\frac{1}{R(R+Z)}\right]\right\}\frac{X^2}{r^2} +$$

$$\frac{Q}{2\pi}\left\{-(1-2\nu)\left[\frac{Z}{R^3} - \frac{1}{R(R+Z)}\right]\right\}\frac{(r^2 - X^2)}{r^2} \qquad (B.13)$$

$$\sigma_x = \frac{Q}{2\pi}\left\{\frac{3\,r^2Z}{R^5} - (1-2\nu)\left[\frac{1}{R(R+Z)}\right]\right\}\frac{X^2}{r^2} +$$

$$\frac{Q}{2\pi}\left\{-(1-2\nu)\left[\frac{Z}{R^3} - \frac{1}{R(R+Z)}\right]\right\}\left(1 - \frac{X^2}{r^2}\right) \qquad (B.14)$$

$$\sigma_x = \frac{Q}{2\pi}\left\{\frac{3\,X^2Z}{R^5} - (1-2\nu)\left[\frac{Z}{R^3} - \frac{1}{R(R+Z)}\right.\right.$$

$$\left.\left. + \frac{2\,X^2}{r^2R(R+Z)} - \frac{Z\,X^3}{r^2R^3}\right]\right\} \qquad (B.15)$$

The final expression for the horizontal stress σ_x dut to point load can be obtained in the following equation:

$$\sigma_x = \frac{Q}{2\pi}\left\{\frac{3X^2\,Z}{R^5} - (1-2\nu)\left[\frac{Z}{R^3} - \frac{1}{R(R+Z)}\right.\right.$$

$$\left.\left. + \frac{X^2(2R+Z)}{R^3\,(R+Z)^2}\right]\right\} \qquad (B.16)$$

– Horizontal stress in the free field due to a rectangular loaded area

For a rectangular loaded area (a.b) shown in Fig. (B.2) with a load intensity equal to q (load/unit area), the horizontal stress at point P (0,0,Z) i.e. under the corner of the loaded area is derived as follows:

$$\Delta Q = q\ dA = q\ dx\ dy \tag{B.17}$$

Where:

ΔQ is a finite concentrated load.

According to Eqs. (B.16&17), the horizontal stress due to ΔQ is

$$\Delta\sigma_x = \frac{q\ dx\ dy}{2\pi}\left\{\frac{3X^2Z}{R^5} - (1-2\nu)\left[\frac{Z}{R^3} - \frac{1}{R(R+Z)} + \frac{X^2(2R+Z)}{R^3\ (R+Z)^2}\right]\right\} \tag{B.18}$$

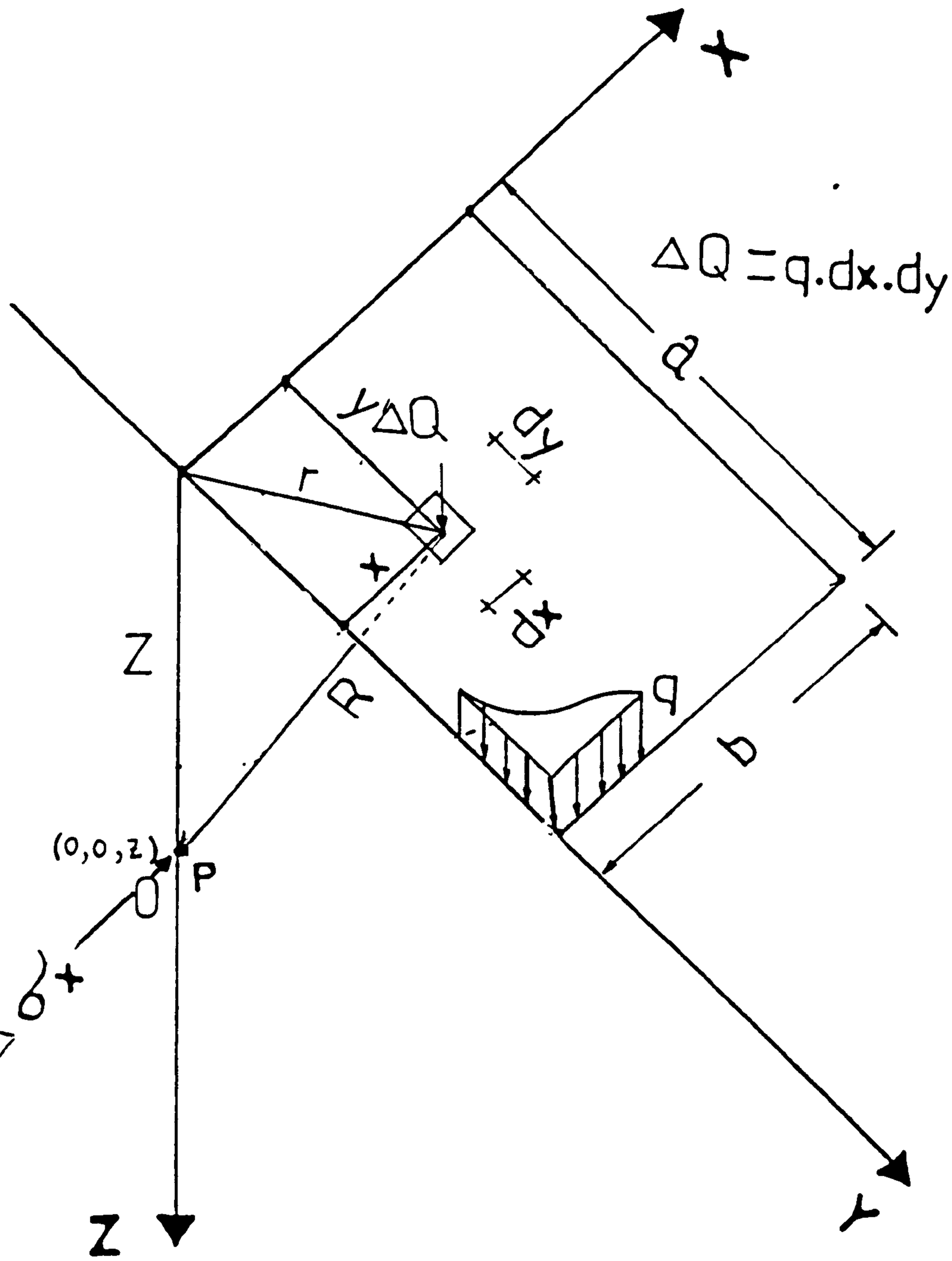

FIG. (B. 2) PARAMETER OF UNIFORM LOADED AREA (axb).

$$\sigma_x = \int_A \Delta\sigma_x \, dA \tag{B.19}$$

$$\sigma_x = \frac{q}{2\pi} \int_0^{X-b} \int_0^{Y-a} \left\{ \frac{3X^2Z}{R^5} - (1-2\nu) \left[\frac{Z}{R^3} - \frac{1}{R(R+Z)} + \frac{X^2(2R+Z)}{R^3\,(R+Z)^2} \right] \right\} dy\, dx \tag{B.20}$$

The solution of the above Eq. (B.20) has been obtained using author's computer program (BCOMPP), Appendix C.

B.2 DERIVATION OF THE FORMULA FOR HORIZONTAL STRESS DUE TO A LINE LOAD OF FINITE LENGTH PERPENDICULAR TO THE Y AXIS

Assume a line load of intensity $\dot{q}$ (load/unit length) lying in the position shown in Fig. (B.3), i.e. parallel to X-axis. σ_x is required at point P (0,0,Z). According to the Fig. these relations can be obtained:

$$\tan \psi = \frac{Y}{Z} \tag{B.21}$$

$$\sin \psi = \frac{Y}{\rho} \tag{B.22}$$

$$\cos \psi = \frac{Z}{\rho} \tag{B.23}$$

$$\tan \varphi = \frac{X}{\rho} \tag{B.24}$$

$$dx = \rho \sec^2 \varphi \, d\varphi \tag{B.25}$$

$$\sin \varphi = \frac{X}{R} \tag{B.26}$$

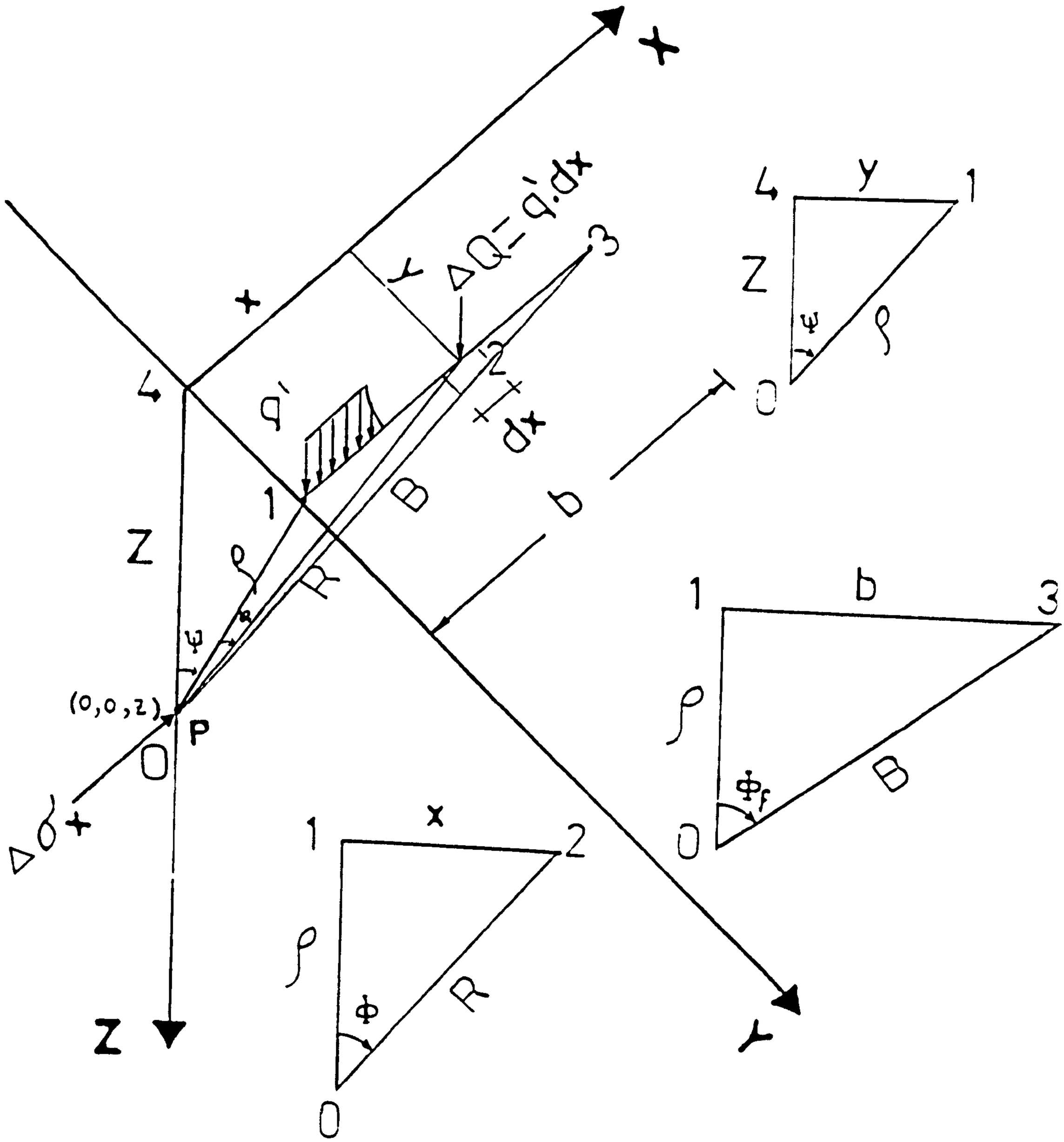

FIG. (B. 3) PARAMETERS OF UNIFORM LINE LOAD OF LENGTH b.

$$\cos \varphi = \frac{\rho}{R} \tag{B.27}$$

$$\tan \varphi_f = \frac{b}{\rho} \tag{B.28}$$

$$\sin \varphi_f = \frac{b}{B} \tag{B.29}$$

$$\cos \varphi_f = \frac{\rho}{R} \tag{B.30}$$

$\Delta\sigma_x$ due to a finite concentrated load ($\Delta Q = \dot{q}\, dx$) at a point of application (x,y,0), is determined from Eq. (B.16) Sec. (B.1) as:

$$\Delta\sigma_x = \frac{\dot{q}\, dx}{2\pi} \left\{ \frac{3X^2 Z}{R^5} - (1-2\nu) \left[\frac{Z}{R^3} - \frac{1}{R(R+Z)} + \frac{X^2(2R+Z)}{R^3\,(R+Z)^2} \right] \right\} \tag{B.31}$$

Due to line load:

$$\sigma_x = \frac{\dot{q}}{2\pi}\int_0^{X-b}\left\{\frac{3X^2Z}{R^5} - (1-2\nu)\left[\frac{Z}{R^3} - \frac{1}{R(R+Z)} + \frac{X^2(2R+Z)}{R^3\,(R+Z)^2}\right]\right\} dx \qquad \text{(B.32)}$$

The relations from Eqs. (B.21 to 30) can be used to transfer integration to cylindrical coordinates and the terms of the above Eq. becomes:

$$T_{1f} = \int_0^{X-b}\frac{3X^2Z}{R^5}\,dx = \int_0^{\varphi_f}\frac{3Z}{\rho^2}\sin^2\varphi\cos\varphi\,d\varphi \qquad \text{(B.33)}$$

$$T_{2f} = \int_0^{X-b}\frac{Z}{R^3}\,dx = \int_0^{\varphi_f}\frac{Z}{\rho^2}\cos\varphi\,d\varphi \qquad \text{(B.34)}$$

$$T_{3_f} = \int_0^{X-b} \frac{-1}{R(R+Z)}\, dx = \int_0^{\varphi_f} \frac{-1}{\rho + Z\cos\varphi}\, d\varphi \qquad (B.35)$$

$$T_{4_f} = \int_0^{X-b} \frac{X^2(2R+Z)}{R^3\,(R+Z)^2}\, dx = \int_0^{X-b} \frac{X^2}{R^2(R+Z)^2} + \frac{X^2}{R^3(R+Z)}\, dx$$

$$= \int_0^{\varphi_f} \left\{ \frac{\rho \sin^2\varphi}{(\rho + Z\cos\varphi)^2} + \frac{\sin^2\varphi}{(\rho + Z\cos\varphi)} \right\} d\varphi \qquad (B.36)$$

For one case $\dot{q}$, Z, ν, and ρ are constant and from the above Eqs. σ_X can be obtained:

$$\sigma_X = \frac{\dot{q}}{2\pi} \left\{ T_{1_f} - (1-2\nu)\,(T_{2_f} + T_{3_f} + T_{4_f}) \right\} \qquad (B.37)$$

$$\sigma_X = \frac{\dot{q}}{2\pi} \left[\frac{Z\, b^3}{(Z^2+Y^2)B^3} - (1-2\nu)\left(\frac{bZ}{B\,(Z^2+Y^2)}\right) \right]$$

(B.38.a)

Or

$$\sigma_x = \frac{\dot{q}\cos^2\psi}{2\pi Z}\left\{ \left(\sin\varphi_f^3 - (1 - 2\nu)\left(\sin\varphi_f \right) \right\} \right.$$

(B.38.b)

B.3 DERIVATION OF THE FORMULA FOR HORIZONTAL STRESS DUE TO A LINE LOAD OF FINITE LENGTH PARALLEL TO THE Y-AXIS

Assume a line load of intensity $\dot{q}$ (load/unit length) Fig. (B.4) parallel to the Y-axis. σ_x is required at point (0,0,Z). The following geometrical relations can be determined:

$$\tan \psi = \frac{X}{Z} \tag{B.39}$$

$$\sin \psi = \frac{X}{\rho} \tag{B.40}$$

$$\cos \psi = \frac{Z}{\rho} \tag{B.41}$$

$$\tan \varphi = \frac{Y}{\rho} \tag{B.42}$$

$$dy = \rho \sec^2 \varphi \, d\varphi \tag{B.43}$$

$$\sin \varphi = \frac{Y}{R} \tag{B.44}$$

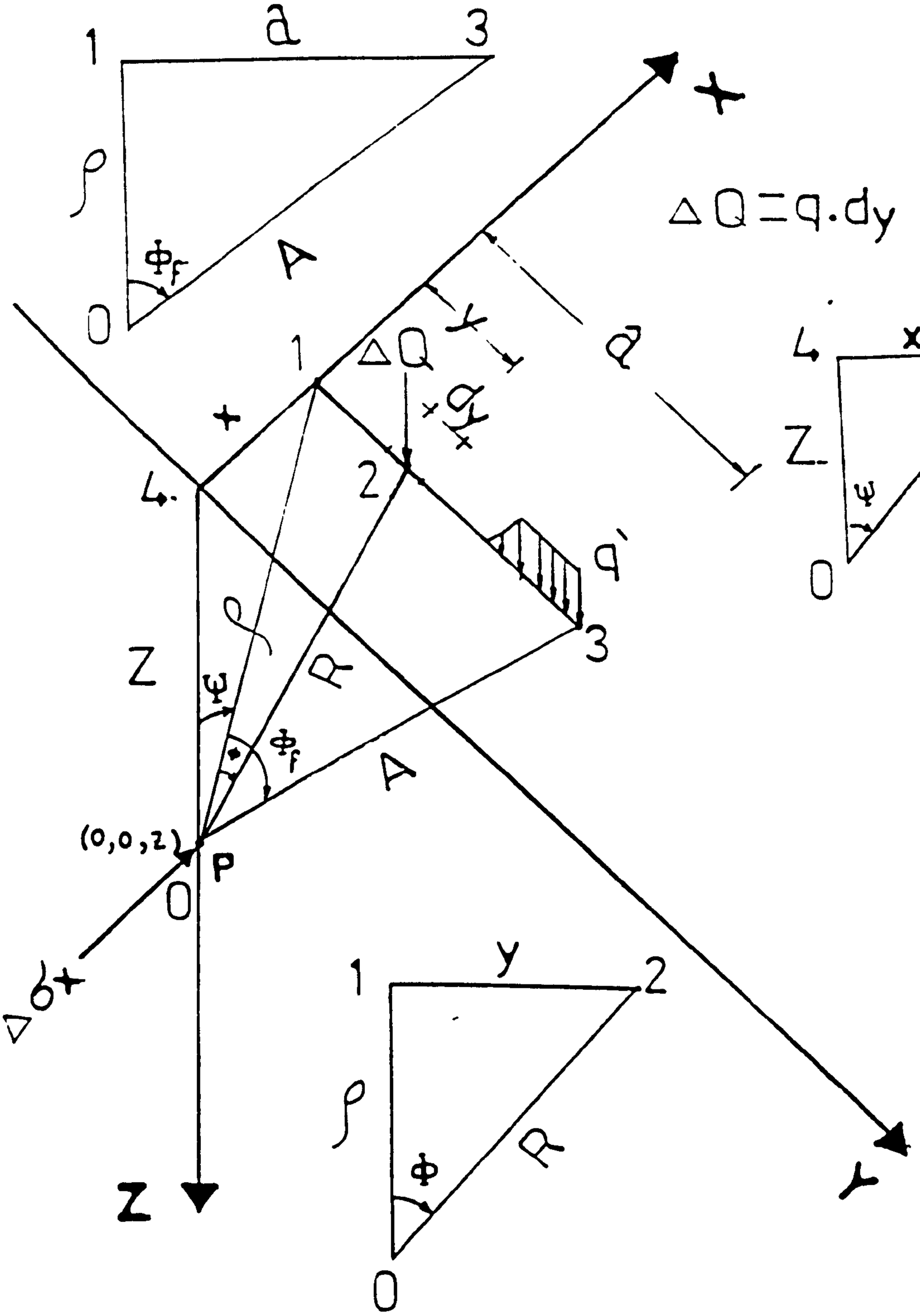

FIG. (B. 4) PARAMETER OF UNIFORM LINE LOAD OF LENGTH, a.

$$\cos \varphi = \frac{\rho}{R} \tag{B.45}$$

$$\tan \varphi_f = \frac{a}{\rho} \tag{B.46}$$

$$\sin \varphi_f = \frac{a}{A} \tag{B.47}$$

$$\cos \varphi_f = \frac{\rho}{R} \tag{B.48}$$

$\Delta\sigma$ due to a finite concentrated load ($\Delta Q = \dot{q}\, dy$) at a point of application (x,y,0) is determined from Eq.(B.16) in Sec. B.1, hence

$$\sigma_x = \frac{\dot{q}}{2\pi} \int_0^{Y-a} \left\{ \frac{3X^2 Z}{R^5} - (1-2\nu) \left[\frac{Z}{R^3} - \frac{1}{R(R+Z)} + \frac{X^2(2R+Z)}{R^3\,(R+Z)^2} \right] \right\} dy \tag{B.49}$$

The relations from Eqs.(B.39 to 48) can be used to transfer integration to cylindrical coordinates and the terms of the above Eq become:

$$T_{1f} = \int_0^{Y=a} \frac{3X^2Z}{R^5}\,dy = \int_0^{\varphi_f} \frac{3X^2Z}{\rho^4}\cos^3\varphi\,d\varphi \qquad (B.50)$$

$$T_{2f} = \int_0^{Y=a} \frac{Z}{R^3}\,dy = \int_0^{\varphi_f} \frac{Z}{\rho^2}\cos\varphi\,d\varphi \qquad (B.51)$$

$$T_{3f} = \int_0^{Y=a} \frac{-1}{R(R+Z)}\,dy = \int_0^{\varphi_f} \frac{-1}{\rho + Z\cos\varphi}\,d\varphi \qquad (B.52)$$

$$T_{4f} = \int_0^{Y=a} \frac{X^2(2R+Z)}{R^3\,(R+Z)^2}\,dy = \int_0^{Y=a} \frac{X^2}{R^2(R+Z)^2} + \frac{X^2}{R^3(R+Z)}\,dy$$

$$-\int_0^{\varphi_f} \left\{ \frac{X^2 \cos^2\varphi}{\rho\ (\rho + Z\cos\varphi)^2} + \frac{X^2\cos^2\varphi}{\rho^2\ (\rho + Z\cos\varphi)} \right\} d\varphi \qquad \text{(B.53)}$$

For one case $\dot{q}$, Z, ν, and x are constant and from the above Eqs. σ_x can be obtained:

$$\sigma_x = \frac{\dot{q}}{2\pi} \left[\frac{3\,X^2 Z}{(Z^2+X^2)^2} \left(\frac{a}{A} - \frac{a^3}{3A^3} \right) - (1-2\nu)\, \frac{a\,Z}{A\,(Z^2+X^2)} \right]$$

. (B.54.a)

Or

$$\sigma_x = \frac{\dot{q}\cos^2\psi}{2\pi Z} \left\{ 3\sin^2\psi \left(\sin\varphi_f - \frac{1}{3}\sin^3\varphi_f \right) - (1-2\nu)\,(\sin\varphi_f) \right\} \qquad \text{(B.54.b)}$$

In the case of a very long line load which extends from :

$Y = +\infty$ to $Y = -\infty$ and $\nu = 0.5$ & $\varphi_f = \frac{\pi}{2}$

Eq. (B.54.b) becomes the same Eq. as in Terzaghi (1942), i.e.

$$\sigma_x = \frac{\dot{q}}{\pi Z} (2 \sin^2\psi \cos^2\psi) \qquad (B.55)$$

APPENDIX C

C.1 FORTRAN 77 LIST OF PROGRAM BCOMPP

```
C   ***********************************************
C   *                                             *
                    PROGRAM BCOMPP
C   *                                             *
C   *                      BY                     *
C   *                  EMAD OSMAN                 *
C   *              CIVIL ENGING. DEPT.            *
C   *              GLASGOW  UNIVERSITY            *
C   *                                             *
C   ***********************************************
C
C  ***************************************************
C  * PROG. BCOMPP CALCULATES THE HORIZONTAL STRESS AT *
C  * SPECIFIED POINTS IN FREE FIELD OR ON RETAINING WALLS *
C  * DUE TO POINT LOAD,LINE LOAD PARALLEL OR PERPENDICULAR *
C  * TO WALL  AND LOADED AREA WITH UNIFORM LOAD. THE LOAD *
C  * MAY BE STATIC OR DYNAMIC. ANY NUMBER OF LOADS CAN BE *
C  * USED AT THE SAME TIME.
C  * THE PROGRAM CONSIDERS THE THREE DIMENSIONAL NATURE OF *
C  * THE PROBLEM.
C  * THE SOLUTION IS BASED ON A LINEAR ELASTIC SOLUTION BY *
C  * BOUSSINESQ'S SOLUTION.                          *
C  * THE METHOD OF ANALYSIS USED IS NUMERICAL INTEGRATION. *
C  ***************************************************
C
C    SYMBOLS USED :
C    -------------
C     N  -NO. OF GAUSS POINTS
C     K  -NO. OF DIVISIONS (STRIPS) OF LOADED AREA
C     L  -NO. OF VARIATIONS OF Z
C     NL -NUMBER OF LOADED AREAS OR LINE LOAD OR POINT LOAD
C     U  -POISSON'S RATIO
C     Q  -DENSITY OF LOADED AREA "  "     "    "   "   "
C     RL1-LENGTH OF LOADED AREA OR HALF LENGTH IN CASE OF
C         SYMMETRY.
C     BL -WIDTH OF LOADED AREA OR LINE LOAD
C     BB1-DISTANCE OF LOADED AREA OR LINE OR POINT LOAD FROM X AXIS
C     BB2-DISTANCE OF LOADED AREA "   "   "   "   "   "   Y "
C     THE COORDINATES OF THE POINT WHERE STRESS IS REQUIRED,
C     ARE XP,YP & Z.
C     IF (XP,YP,Z)=(0.0,0.0,Z)THIS MEANS THAT THE POINT LIES
C     ON Z AXIS.
C     D,W &SY CODES TO TAKE THE DYNAMIC EFFECT INTO
C     CONSIDERATION.
C     D  -0.0 NO DYNAMIC EFFECT & 1.0 FOR EFFECT.
C     W  -0.0 NO WALL EFFECT&1.0 FOR SYMMETRY.
C     SY -0.0 NO SYMMETRY&1.0 FOR SYMMETRY.
C
C     UNITS IN METRE &TONNE OR FOOT & POUND.
C
C     IN CASE OF VERY LONG STRIP LOAD,PUT RL1= 2000.0 M OR FT.
C     "   "   "   "    "    LINE LOAD PARALLEL TO THE WALL,PUT
C     RL1=2000.0 M OR FT.
C     IN CASE OF VERY LONG LINE LOAD PARALLEL TO THE WALL,PUT
C     BL =2000.0 M OR FT.
C
C ***************************************************************
```

```
C
C     UNITS IN METRE &TONNE OR FOOT & POUND.
C     IN CASE OF VERY LONG STRIP LOAD,PUT RL1= 2000.0 M OR FT.
C     "   "   "   "    "    LINE LOAD PARALLEL TO THE WALL,PUT
C     RL1=2000.0 M OR FT.
C     IN CASE OF VERY LONG LINE LOAD PARALLEL TO THE WALL,PUT
C     BL =2000.0 M OR FT.
C     +VE. HORIZ. STRESS MEANS TENSION IN THE SOIL.
C     -VE.   "      "      "   COMPRESION IN THE SOIL.
C ***************************************************************
      DIMENSION A(100),H(100),RL1(100),BL(100), Z(100)
     *,SUMT(100),TSIG(100),Q(100),BB1(100),BB2(100)
      CHARACTER TITLE*72
C
C     GAUSS COEFFICIENTS A & H
C
      A(1)=  0.9602898565
      A(2)=  0.7966664774
      A(3)=  0.5255324099
      A(4)=  0.1834346424
      A(5)= -0.9602898565
      A(6)= -0.7966664774
      A(7)= -0.5255324099
      A(8)= -0.1834346424
      H(1)= 0.1012285363
      H(2)= 0.2223810345
      H(3)= 0.3137066459
      H(4)= 0.3626837834
      H(5)= 0.1012285363
      H(6)= 0.2223810345
      H(7)= 0.3137066459
      H(8)= 0.3626837834
C
      PI  =3.14159
C
C     READ AND WRITE TITLE
C
      READ(5,180) TITLE
  180 FORMAT(A72)
      WRITE(6,181) TITLE
  181 FORMAT(5X,A67,//)
C
C    READ MODE TO SORT OUT THE TYPE OF LOAD
      READ(5,*) MODE
      IF(MODE.EQ.1) GO TO 1000
      IF(MODE.EQ.2) GO TO 1001
      IF(MODE.EQ.3) GO TO 1002
      IF(MODE.EQ.4) GO TO 1003
C
C    ****************************************
C    * HORIZONTAL STRESS DUE TO :           *
C    * UNIFORMLY LOADED RECTANGULAR AREA.   *
C    *                                      *
C    ****************************************
C
 1000 READ(5,*) N,K,L,NL,U,XP,YP,D,W,SY
```

```
      READ(5,*) (RL1(JJ),JJ=1,NL)
      READ(5,*) (BL(JJ) ,JJ=1,NL)
      READ(5,*) (BB1(JJ),JJ=1,NL)
      READ(5,*) (BB2(JJ),JJ=1,NL)
      READ(5,*) (Q(JJ)  ,JJ=1,NL)
      WRITE(6,100)
  100 FORMAT(13X,'LOADED  AREA',18X,'COORDINATES ',25X,'HORIZONTAL'
     *,//,12X,'AND DIMENSIONS',22X,'OF',30X,'STRESSES',//,
     *       'LENGTH',2X,'WIDTH',3X,'X-DISTANCE',2X,'Y-DISTANCE',6X,
     *        'THE POINT',//,
     * 2X,'RL1',5X,'BL',6X,'BB1',8X,'BB2',8X,'XP',6X,'YP',6X,'Z',14X
     *,'SUMT',/)
      WRITE(6,200)XP,YP
  200 FORMAT(37X,F6.3,2X,F6.3)
      C1=1-2*U
      DO 40 JJ=1,NL
      WRITE(6,201) RL1(JJ),BL(JJ),BB1(JJ),BB2(JJ)
  201 FORMAT(1X,4(F7.3,2X))
      CK=K
      RL=RL1(JJ)/CK
      B =BL(JJ)
      DO 30 II=1,L
      SUMT(II)=0.0
      B1=BB1(JJ)
      B2=BB2(JJ)
      DO 20 M=1,K
      XR=XP-(.5*B)-B2
      YR=YP-(.5*RL)-B1
      SUM=0.0
      DO 10 I=1,N
      DO 10 J=1,N
      X=XR-0.5*B*A(I)
      Y=YR-0.50*RL*A(J)
      R=SQRT(X**2+Y**2)
      P=ATAN(R/Z(II))
      T=ATAN(Y/X)
      CP=COS(P)
      SP=SIN(P)
      CT=COS(T)
      ST=SIN(T)
      C2=SP**2
      C3=CP**3
      C4=CP**2
      C5=CT**2
      C6=ST**2
      C7=Z(II)**2
      SIGX= ((3.*C2*C3-C1*C4/(1.+CP))*C5-(C1*(C3-C4/(1.+CP))
     .*C6))/(2.*PI*C7)*H(I)*H(J)
      SUM =SUM+SIGX
   10 CONTINUE
      SUM1=SUM*0.25*RL*B*Q(JJ)
C     EFFECT OF SYMMETRY
      IF(SY.EQ.0.0) GO TO 224
      SUM1=SUM1*2.0
C
C     FOR WALL EFFECT ONLY
```

```
C
  224 IF(W.EQ.0.0) GO TO 223
      SUM1=SUM1*2.0
C
C     FOR DYNAMIC EFFECT ONLY
C
 223  IF(D.EQ.0.0) GO TO 222
      SUM1=SUM1*2.0
      SUMT(II)=SUM1+SUMT(II)
      B1=RL+B1
   20 CONTINUE
      WRITE(6,300) Z(II),SUMT(II)
 300  FORMAT(52X,F7.3,9X,1PE20.10)
      IF(NL.NE.1) GO TO 303
      TSIG(II)=0.0
303   TSIG(II)=TSIG(II)+SUMT(II)
  30 CONTINUE
  40 CONTINUE
      IF(NL.EQ.1) GO TO 328
      WRITE(6,305)
305   FORMAT(1X,/,72X,'TOTAL STRESSES',/)
      DO 327 I=1,L
      WRITE(6,306)  Z(I),TSIG(I)
306   FORMAT(52X,F7.3,9X,1PE20.10)
327   CONTINUE
328   GO TO 1004
C   ***************************************
C   *HORIZONTAL STRESS DUE TO :           *
C   *UNIFORM LINE LOAD WITH FINITE        *
C   *LENGTH PERPENDICULAR TO THE WALL.    *
C   ***************************************
C
 1001 READ(5,*) N,L,NL,U,XP,YP,D,W,SY
      READ(5,*) (Z(II)  ,II=1,L )
      READ(5,*) (BL(JJ) ,JJ=1,NL)
      READ(5,*) (BB1(JJ),JJ=1,NL)
      READ(5,*) (BB2(JJ),JJ=1,NL)
      READ(5,*) (Q(JJ)  ,JJ=1,NL)
      WRITE(6,101)
  101 FORMAT(6X,'LINE LOAD  ',18X,'COORDINATES OF',24X,'HORIZONTAL'
     *,//,   4X,'LENGTH',8X,'INTEN',17X,'THE POINT',24X,'PRESSURE',
     *//,6X,'B  ',10X,'Q',10X,'XP',10X,'YP',10X,'Z',17X,'SUMT',/)
      WRITE(6,200)XP,YP
      C1=1-2*U
      DO 70 JJ=1,NL
      WRITE(6,400) BL(JJ),Q(JJ)
400 FORMAT(5X,F7.3,6X,F7.3)
      B=BL(JJ)
      DO 60 II=1,L
      SUM =0.0
      B1=BB1(JJ)
      B2=BB2(JJ)
```

```
      XR=XP-(.5*B)-B2
      YR=YP-B1
      DO 50 I=1,N
      X=XR-0.5*B*A(I)
      Y=YR
      R=SQRT(X**2+Y**2)
      P=ATAN(R/Z(II))
      IF(X.EQ.0.0) GO TO 3
      T=ATAN(Y/X)
      GO TO 4
    3 T=0.50*PI
    4 CP=COS(P)
      SP=SIN(P)
      CT=COS(T)
      ST=SIN(T)
      C2=SP**2
      C3=CP**3
      C4=CP**2
      C5=CT**2
      C6=ST**2
      C7=Z(II)**2
      SIGX= ((3.*C2*C3-C1*C4/(1.+CP))*C5-(C1*(C3-C4/(1.+CP))
     .*C6))/(2.*PI*C7)*H(I)
      SUM =SUM+SIGX
   50 CONTINUE
      SUM =SUM*0.50*B*Q(JJ)
C     EFFECT OF SYMMETRY
C
      IF(SY.EQ.0.0) GO TO 114
      SUM=SUM*2.0
C
C     FOR WALL EFFECT ONLY
C
  114 IF(W.EQ.0.0) GO TO 113
      SUM =SUM*2.
C
C     FOR DYNAMIC EFFECT ONLY
C
  113 IF(D.EQ.0.0) GO TO 111
      SUM =SUM*2.0
  111 CONTINUE
      SUMT(II)=SUM
      WRITE(6,410) Z(II),SUMT(II)
  410 FORMAT(52X,F7.3,9X,1PE20.10)
      IF(NL.NE.1) GO TO 411
      TSIG(II)=0.0
  411 TSIG(II)=TSIG(II)+SUMT(II)
   60 CONTINUE
   70 CONTINUE
      IF(NL.EQ.1) GO TO 428
      WRITE(6,405)
  405 FORMAT(1X,/,72X,'TOTAL STRESSES',/)
      DO 427 I=1,L
      WRITE(6,406)  Z(I),TSIG(I)
  406 FORMAT(52X,F7.3,9X,1PE20.10)
  427 CONTINUE
```

```
 428  GO TO 1004
C
C   ***********************************************
C   *HORIZONTAL STRESS DUE TO :                   *
C   *UNIFORM LINE LOAD WITH FINITE LENGTH         *
C   *PARALLEL TO THE WALL.                        *
C   ***********************************************
C
 1002 READ(5,*) N,L,NL,U,XP,YP,D,W,SY
      READ(5,*) (Z(II)   ,II-1,L )
      READ(5,*) (RL1(JJ),JJ-1,NL)
      READ(5,*) (BB1(JJ),JJ-1,NL)
      READ(5,*) (BB2(JJ),JJ-1,NL)
      READ(5,*) (Q(JJ)   ,JJ-1,NL)
      WRITE(6,701)
701 FORMAT(6X,'LINE LOAD  ',18X,'COORDINATES OF',24X,'HORIZONTAL'
    *,//,   4X,'LENGTH',8X,'INTEN',17X,'THE POINT',24X,'PRESSURE',
    *//,6X,'B  ',10X,'Q',10X,'XP',10X,'YP',10X,'Z',17X,'SUMT',/)
      WRITE(6,200)XP,YP
      C1-1-2*U
      DO 770 JJ-1,NL
      WRITE(6,700) RL1(JJ),Q(JJ)
700 FORMAT(5X,F7.3,6X,F7.3)
      B-RL1(JJ)
      DO 760 II-1,L
      SUM -0.0
      B1-BB1(JJ)
      B2-BB2(JJ)
      XR-XP-B2
      YR-YP-(0.50*B)-B1
      DO 750 I-1,N
      X-XR
      Y-YR-0.50*B*A(I)
      R-SQRT(X**2+Y**2)
      P-ATAN(R/Z(II))
      IF(X.EQ.0.0) GO TO 1
      T-ATAN(Y/X)
      GO TO 2
 1    T-0.50*PI
 2    CP-COS(P)
      SP-SIN(P)
      CT-COS(T)
      ST-SIN(T)
      C2-SP**2
      C3-CP**3
      C4-CP**2
      C5-CT**2
      C6-ST**2
      C7-Z(II)**2
      SIGX- ((3.*C2*C3-C1*C4/(1.+CP))*C5-(C1*(C3-C4/(1.+CP))
     .*C6))/(2.*PI*C7)*H(I)
      SUM -SUM+SIGX
  750 CONTINUE
      SUM -SUM*0.50*B*Q(JJ)
C     EFFECT OF SYMMETRY
      IF(SY.EQ.0.0) GO TO 714
```

```
      SUM=SUM*2.0
C
C     FOR WALL EFFECT ONLY
C
  714 IF(W.EQ.0.0) GO TO 713
      SUM =SUM*2.
C
C     FOR DYNAMIC EFFECT ONLY
C
 713  IF(D.EQ.0.0) GO TO 711
      SUM =SUM*2.0
 711  CONTINUE
      SUMT(II)=SUM
      WRITE(6,710) Z(II),SUMT(II)
 710  FORMAT(52X,F7.3,9X,1PE20.10).
      IF(NL.NE.1) GO TO 811
      TSIG(II)=0.0
 811  TSIG(II)=TSIG(II)+SUMT(II)
  760 CONTINUE
  770 CONTINUE
      IF(NL.EQ.1) GO TO 728
      WRITE(6,705)
 705  FORMAT(1X,/,72X,'TOTAL STRESSES',/)
      DO 727 I=1,L
      WRITE(6,706)  Z(I),TSIG(I)
      FORMAT (52X,F7.3,9X,1PE20.10)
 728  GO TO 1004
C    ***************************************
C    *HORIZONTAL STRESS DUE TO :           *
C    *CONCENTRATED LOAD.                   *
C    *                                     *
C    ***************************************
 1003 READ(5,*) NL,L,U,XP,YP,D,W,SY
      READ(5,*) (Z(II)  ,II-1,L )
      READ(5,*) (BB1(JJ),JJ-1,NL)
      READ(5,*) (BB2(JJ),JJ-1,NL)
      READ(5,*) (Q(JJ)  ,JJ-1,NL)
      WRITE(6,102)
  102 FORMAT(6X,' LOAD DATA ',18X,'COORDINATES OF',24X,'HORIZONTAL'
     *,//,   4X,'COORD',8X,'VALUE',17X,'THE POINT',24X,'PRESSURE',//
,
     *4X,'XL', 6X,'YL',6X,'Q',10X,'XP',10X,'YP',10X,'Z',17X,'SUMT',/
)
      WRITE(6,202)XP,YP
  202 FORMAT(29X,F7.3,5X,F7.3)
      C1=1-2*U
      DO 90 JJ=1,NL
      WRITE(6,401)  BB2(JJ),BB1(JJ),Q(JJ)
401 FORMAT(4X,F7.3,1X,F7.3,1X,F7.3)
      DO 80 II=1,L
      SUM =0
      B1=BB1(JJ)
      B2=BB2(JJ
      XR=XP-B2
      YR=YP-B1
      X=XR
```

```
      Y=YR
      R=SQRT(X**2+Y**2)
      P=ATAN(R/Z(II))
      T=ATAN(Y/X)
      CP=COS(P)
      SP=SIN(P)
      CT=COS(T)
      ST=SIN(T)
      C2=SP**2
      C3=CP**3
      C4=CP**2
      C5=CT**2
      C6=ST**2
      C7=Z(II)**2
      SIGX= ((3.*C2*C3-C1*C4/(1.+CP))*C5-(C1*(C3-C4/(1.+CP))
     .*C6))/(2.*PI*C7)
      SUM =SUM+SIGX
      SUM =SUM*Q(JJ)
C     EFFECT OF SYMMETRY
      IF(SY.EQ.0.0) GO TO 334
      SUM=SUM*2.0
C     FOR WALL EFFECT ONLY
  334 IF(W.EQ.0.0) GO TO 333
      SUM =SUM*2.
C     FOR DYNAMIC EFFECT ONLY
  333 IF(D.EQ.0.0) GO TO 335
      SUM =SUM*2.0
  335 CONTINUE
      SUMT(II)=SUM
      WRITE(6,500) Z(II),SUMT(II)
  500 FORMAT(52X,F7.3,9X,1PE20.10)
      IF(NL.NE.1) GO TO 503
      TSIG(II)=0.0
  503 TSIG(II)=TSIG(II)+SUMT(II)
   80 CONTINUE
   90 CONTINUE
      IF(NL.EQ.1) GO TO 1004
      WRITE(6,305)
  505 FORMAT(1X,/,72X,'TOTAL STRESSES',/)
      DO 527 I=1,L
      WRITE(6,506)  Z(I),TSIG(I)
  506 FORMAT(52X,F7.3,9X,1PE20.10)
  527 CONTINUE
 1004 STOP
      END
```

****

C.2 GAUSSIAN QUADRATURE FORMULA COEFFICIENTS

$$\int_{-1}^{1} f(x)dx = \sum_{j=1}^{n} H_j f(a_j),$$

$\pm a$	H
$n = 2$	
0·57735 02691 89626	1·00000 00000 00000
$n = 3$	
0·77459 66692 41483	0·55555 55555 55556
0·00000 00000 00000	0·88888 88888 88889
$n = 4$	
0·86113 63115 94053	0·34785 48451 37454
0·33998 10435 84856	0·65214 51548 62546
$n = 5$	
0·90617 98459 38664	0·23692 68850 56189
0·53846 93101 05683	0·47862 86704 99366
0·00000 00000 00000	0·56888 88888 88889
$n = 6$	
0·93246 95142 03152	0·17132 44923 79170
0·66120 93864 66265	0·36076 15730 48139
0·23861 91860 83197	0·46791 39345 72691
$n = 7$	
0·94910 79123 42759	0·12948 49661 68870
0·74153 11855 99394	0·27970 53914 89277
0·40584 51513 77397	0·38183 00505 05119
0·00000 00000 00000	0·41795 91836 73469
$n = 8$	
0·96028 98564 97536	0·10122 85362 90376
0·79666 64774 13627	0·22238 10344 53374
0·52553 24099 16329	0·31370 66458 77887
0·18343 46424 95650	0·36268 37833 78362

C.3 DESCRIPTION OF INPUT DATA OF PROGRAM BCOMPP

The free format reads are used in entering the data of the program as follows:

The units used are meter and tonne or foot and pound.

Card 1

Title card for program identification.

Card 2

Mode card to sort out the type of load.

Mode : 1 for loaded areas.

2 for line loads perpendicular to the wall.

3 for line loads parallel to the wall.

4 for concentrated loads.

(a) Loaded areas: Fig. (C.1)

Card 3

N, K, L, NL, ν, X_p, Yp, D, W, S

Where:

N = Number of Gaussian Quadrature points (2 to 8).

K = Number of strips in one loaded area. This to increase the accuracy of calculation. It can taken as any value from 1 to 10 (more accuracy).

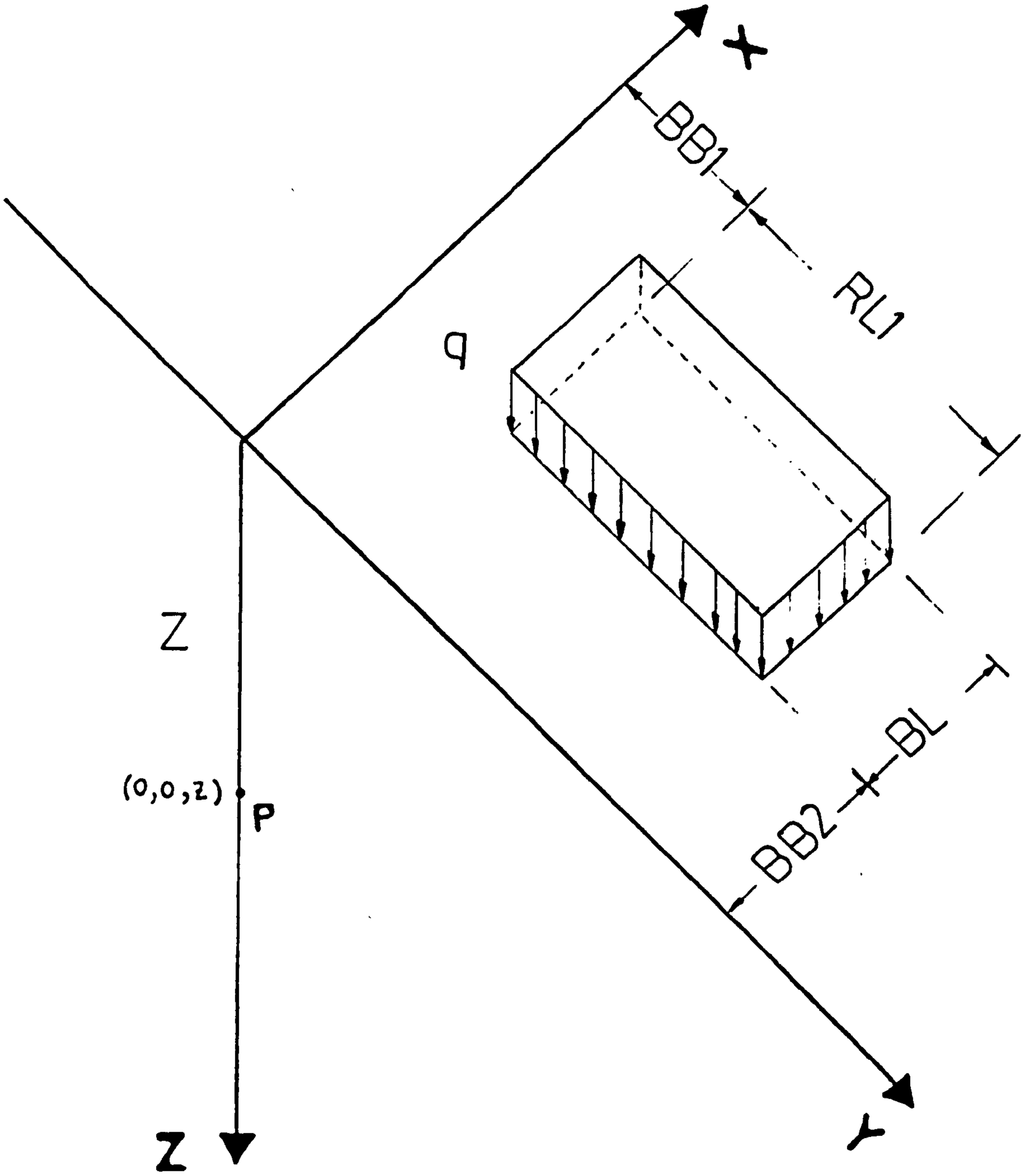

FIG. (C. 1) INPUT DATA OF LOADED AREA FOR ROGRAM (BCOMPP).

L = Number of points in Z direction where horizontal stresses are needed.

NL = Number of loaded areas.

ν = Poisson's ratio

X_p = X− coordinate of the point where stress is required and equals zero for all points.

Yp = Y− coordinate of the point where stress is required and equals zero for all points.

D = Code to take into account the effect of dynamic load.

If D = 0.0 the effect is not taken.

If D = 1.0 the effect is taken.

W = Code to take into account the effect of the retaining wall.

If W = 0.0, i.e. the horizontal stress in the free field.

If W = 1.0, i.e. the horizontal stress on the retaining wall and the effect of the wall must be considered.

S = Code to take load symmetry into consideration.

If S = 0.0 means no symmetry.

If S = 1.0 there is symmetry.

Card 4

Z(II) depths of points of interests.

II = 1 to L

Card 5

RL1(JJ), BL(JJ)

RL1(JJ) the length of the loaded area parallel to Y− axis as shown in Fig. (C.1).

JJ number of each area where there are several areas, its value equals 1 to NL.

RL1 is 2000.0 m or f in case of strip load.

BL(JJ) the length of the loaded area parallel to X– axis as shown in Fig. (C.1).

JJ 1 to NL.

Card 6

BB1(IN) the length of the loaded area parallel to the X– axis as shown in Fig. (C.1).

IN 1 to NL

Card 7

BB2(IN) the distance between the loaded area and the Y– axis.

IN 1 to NL

Card 8

Q(JJ) load/unit area for each area.

JJ 1 to NL

In the case of loads symmetrical about the X– axis, the data of half the loads are considered.

(b) For line loads parallel to the X– axis: Fig. (C.2)

Card 3

N, L, NL, r, X_p, Yp, D, W, S

The same description as parameters in Sec. (C.3.a).

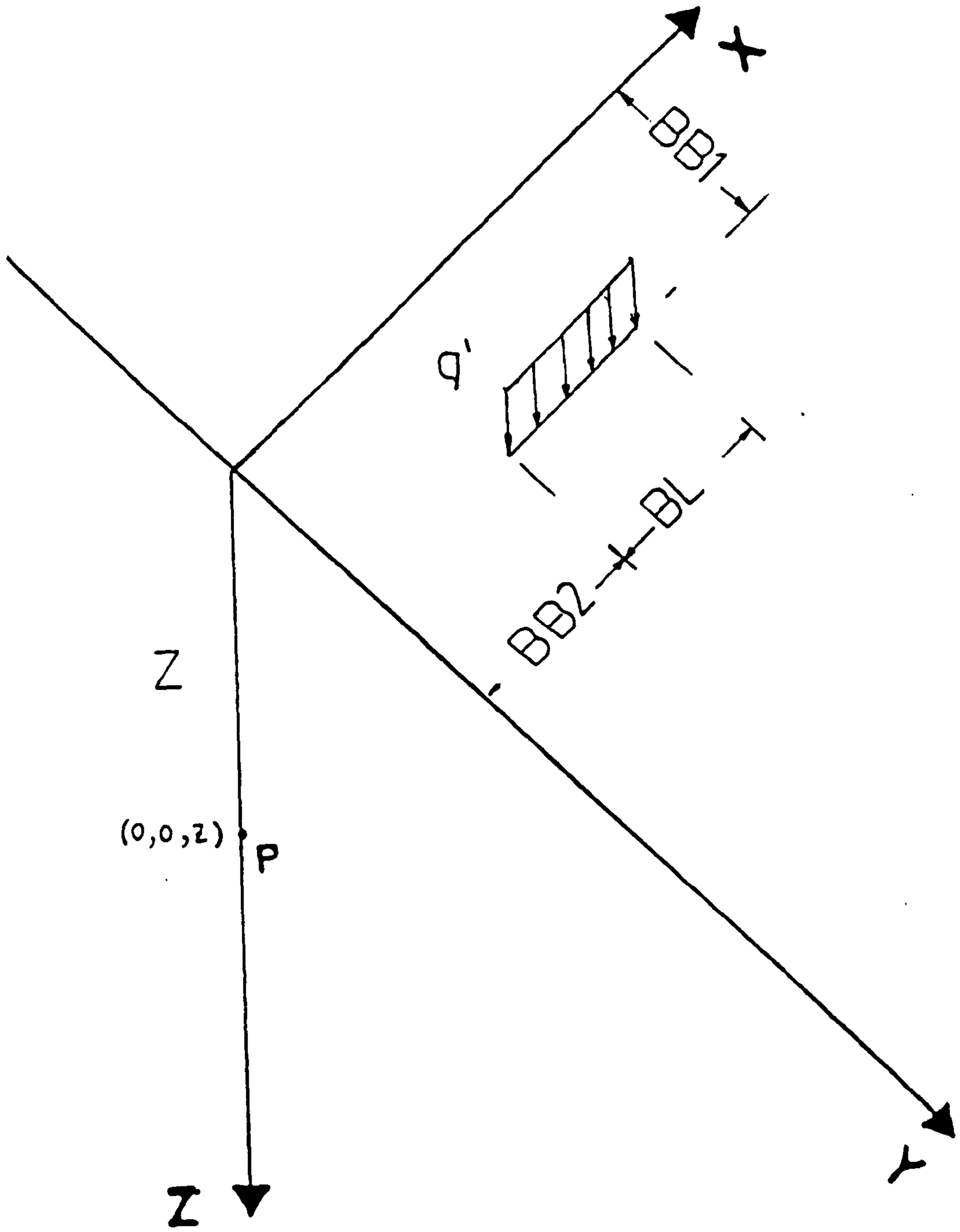

FIG. (C.2) INPUT DATA FOR LINE LOAD PARALLEL TO X-AXIS FOR PROGRAM (BCOMPP).

Card 4

Z(II) depths of points of interest.

II 1 to L

Card 5

BL(JJ) length of line load as shown in Fig. (C.2).

JJ 1 to NL

Card 6

BB1(JJ) distance from X–axis to the load.

JJ 1 to NL

Card 7

BB2(JJ) distance from Y–axis to the load.

JJ 1 to NL

Card 8

Q(JJ) load/unit length for each line load.

JJ 1 to NL

In the case of symmetry about the X–axis, the data of half loads are considered.

(c) For line loads parallel to the Y–axis: Fig. (C.3)

Card 3

N, L, NL, r, X_p, Y_p, D, W, S

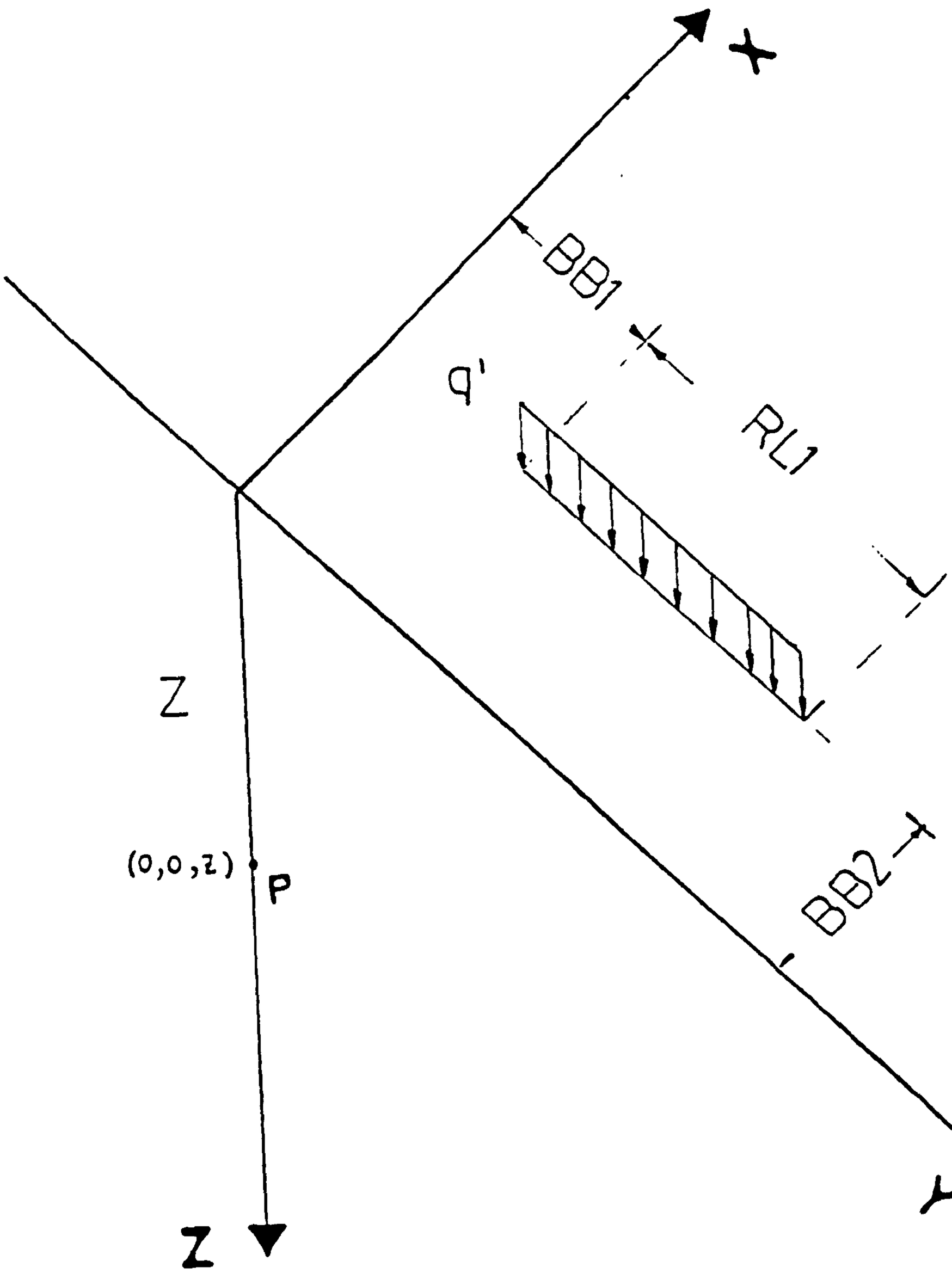

FIG. (C.3) INPUT DATA FOR LINE LOAD PARALLEL TO Y-AXIS FOR PROGRAM (BCOMPP).

The same description as parameters in Sec. (c.3.a).

Card 4

Z(II) depths of points of interest.

II 1 to L

Card 5

RL1(JJ) the length of the line load Fig. (C.3).

JJ 1 to NL

In the case of a very long line load put RL1 = 2000.0 m or f.

Card 6

BB1(JJ), BB2(JJ), Q(JJ)

BB1(JJ) the distance from the X−axis to the load Fig. (C.3.c).

JJ 1 to NL

BB2(JJ) the distance from the Y−axis to the load, Fig. (C.3.c)

JJ 1 to NL

Q(JJ) load/unit length for each area.

JJ 1 to NL

In the case of load symmetry about the X−axis the data of half of the load only is considered.

(d) For concentrated loads: Fig. (C.4)

Card 3

NL, L, ν, Xp, Y_p, D, W, S

The same description as in Sec. (C.3.a).

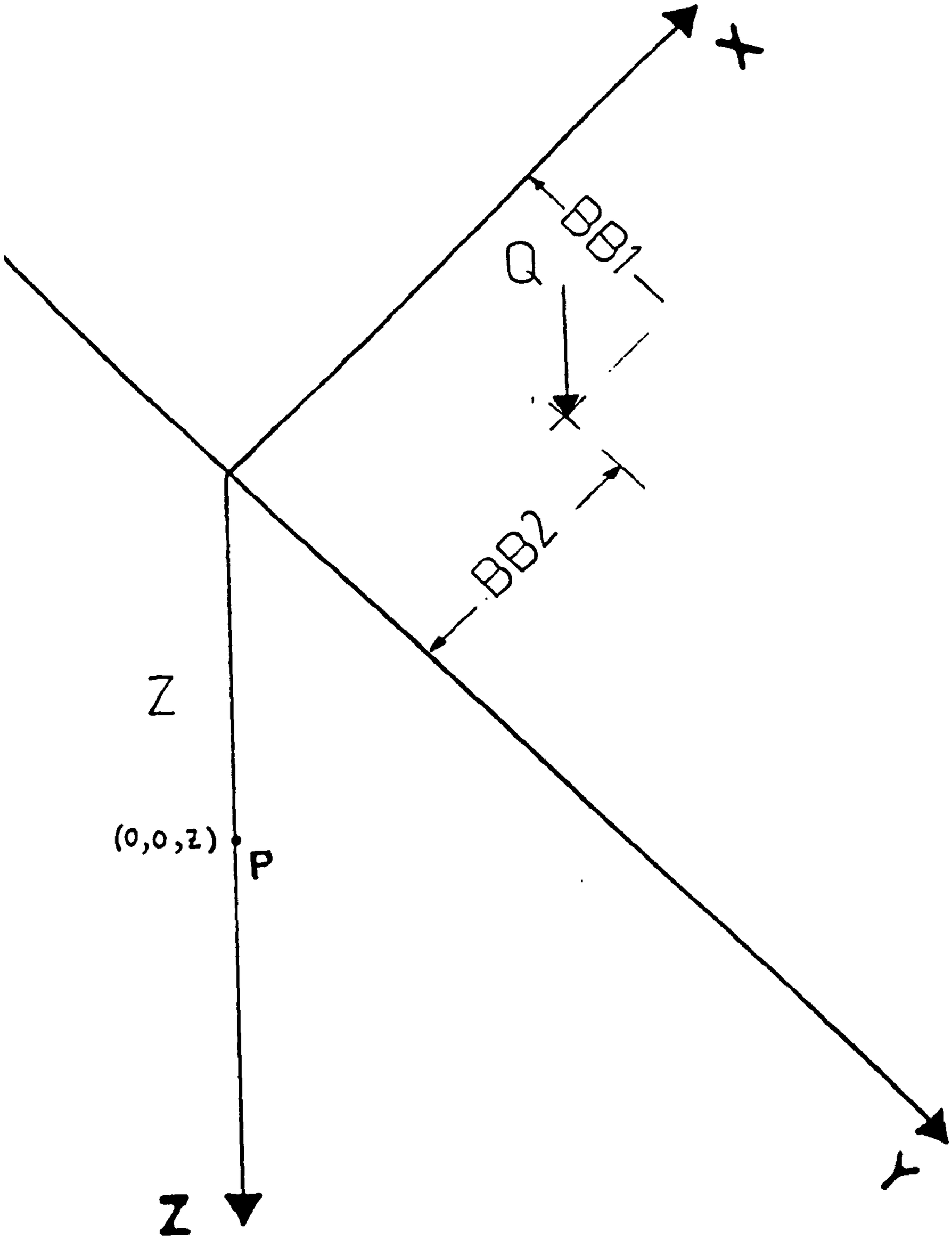

FIG. (C. 4) INPUT DATA OF POINT LOAD FOR PROGRAM (BCOMPP).

Card 4

Z(JJ)

Card 5

BB1(JJ)

Card 6

BB2(JJ)

The same description as in Sec. (C.3.c)

Card 7

Q(JJ) point load

JJ 1 to NL

C.4 TYPICAL INPUT DATA AND RESULT FOR PROGRAM (BCOMPP)

INPUT DATA:

HORIZONTAL STRESS DUE TO LOADED AREA (1.0X1.0) ON VERTICAL WALL

```
          1
          8     1     6     6     0.40  0.00  0.00  1.00  1.00  1.00
          0.10  0.20  0.40  0.60  0.80  1.00
          0.50  0.50  0.50  0.50  0.50  0.50
          1.00  1.00  1.00  1.00  1.00  1.00
          0.00  0.00  0.00  0.00  0.00  0.00
          0.00  0.20  0.40  0.60  0.80  1.00
          1.00  1.00  1.00  1.00  1.00  1.00
```

RESULT:

LOADED AREA		COORDINATES OF			HORIZONTAL
LENGTH	WIDTH	THE POINT			PRESSURE
RL1	B	XP	YP	Z	SUMT
		0.000	0.000		
0.50	1.00				
				0.100	1.4299459500E+00
				0.200	1.1534299900E+00
				0.400	7.1684753900E-01
				0.600	4.2950904400E-01
				0.800	2.5469768000E-01
				1.000	1.5165811800E-01
0.50	1.00				
				0.100	6.1529982100E-01
				0.200	8.8890725400E-01
				0.400	7.4150532500E-01
				0.600	5.0021702100E-01
				0.800	3.2499378900E-01

0.50	1.00		
		0.100	2.0792496200E-01
		0.200	4.4752240200E-01
		0.400	5.6621557500E-01
		0.600	4.6750718400E-01
		0.800	3.4276461600E-01
		1.000	2.4183720400E-01
0.50	1.00		
		0.100	8.0531120300E-02
		0.200	2.2873789100E-01
		0.400	3.7731879900E-01
		0.600	3.7499100000E-01
		0.800	3.1270963000E-01
		1.000	2.4224907200E-01
0.50	1.00		
		0.100	3.1902402600E-02
		0.200	1.2496054200E-01
		0.400	2.4619758100E-01
		0.600	2.8071421400E-01
		0.800	2.6161044800E-01
		1.000	2.2126591200E-01
0.50	1.00		
		0.100	1.0956939300E-02
		0.200	7.2225987900E-02
		0.400	1.6347515600E-01
		0.600	2.0586222400E-01
		0.800	2.0949810700E-01
		1.000	1.9107765000E-01
			TOTAL STRESSES
		0.100	2.3765602100E+00
		0.200	2.9157819700E+00
		0.400	2.8115577700E+00
		0.600	2.2587995500E+00
		0.800	1.7062730800E+00
		1.000	1.2582387900E+00

C.5 FINITE ELEMENT COMPUTER PROGRAM SSCOMP

```
      PROGRAM SSCOMP                                                    S1 00010
C     PROGRAM SSCOMP(UNIT1,UNIT2,UNIT3,UNIT4,UNIT5,UNIT6,UNIT7,UNIT8,   S1 00020
C    1 UNIT9,UNIT10,UNIT11,UNIT12,UNIT13,UNIT14,UNIT15,UNIT16,UNIT17,   S1 00030
C    1 UNIT18,UNIT19,UNIT20)                                            S1 00040
C                                                                       S1 00050
C                                                                       S1 00060
C     ...........FREE FORMAT VERSION...........                         S1 00070
C                                                                       S1 00080
C     UNIT 5 IS FOR READING DATA IN.                                    S1 00090
C     UNIT 6 IS FOR WRITING RESULTS OUT.                                S1 00100
C     RESULTS WRITTEN ON UNIT 7 ARE USED AS PRE-EXISTING PARTS. HOWEVER, S1 00110
C     UNIT 20(BEFORE WAS 7) IS ALSO USED AS TEMPORARY STORAGE IN THIS VAS1 00120
C     THEREFORE, UNIT 7 USED AS PRE-EXISTING DATA STORAGE DOESN'T WORK  S1 00130
C     ANY MORE,SO FIXED FORMAT HAS BEEN USED IN WRITING ON UNIT 7.      S1 00140
C                                                                       S1 00150
C                                                                       S1 00160
C                                                                       S1 00170
C     PROGRAM SSCOMP IS A FINITE ELEMENT PROGRAM FOR ANALYSIS OF SOIL-  S1 00180
C     STRUCTURE INTERACTION, INCLUDING CONSIDERATION OF COMPACTION-     S1 00190
C     INDUCED LATERAL STRESSES.                                         S1 00200
C                                                                       S1 00210
C     LATEST REVISION - AUGUST 27, 1983                                 S1 00220
C     BY SEED & DUNCAN                                                  S1 00230
C     CIVIL ENG. DEPT.                                                  S1 00240
C     BERKELEY UNIVERSITY                                               S1 00250
C     U.S.A                                                             S1 00260
C                                                                       S1 00270
C                                                                       S1 00280
C     CORRECTED  BY MAKRAM JABER , MAY 1987                             S1 00290
C     CIVIL ENG. DEPT.                                                  S1 00300
C     BERKELEY UNIVERSITY                                               S1 00310
C     U.S.A                                                             S1 00320
```

```
C
C     TWO CONTROL VARIABLES, NREDUC AND NSEGM, HAVE BEEN ADDED.                S1 00330
C     THEY ARE INPUT IN THAT ORDER ON A NEW CONTROL CARD LOCATED               S1 00340
C     IN THE SECOND POSITION AFTER THE HEADING CARD.                           S1 00350
C     NREDUC - 1 : THE STIFFNESS OF NEWLY PLACED SOIL ELEMENTS IS              S1 00360
C                  REDUCED BY A FACTOR OF 0.5                                  S1 00370
C            - 0 : FULL STIFFNESS IS USED                                      S1 00380
C     NSEGM  - 1 : USE FOR A SEGMENTED FACING REINFORCED EARTH                 S1 00390
C                  STRUCTURE                                                   S1 00400
C            - 0 : USE FOR ALL OTHER CASES                                     S1 00410
C                                                                              S1 00420
C                                                                              S1 00430
C     MODIFIED BY:                                                             S1 00440
C                 EMAD OSMAN , MAY 1989                                        S1 00450
C                 CIVIL ENG. DEPT.                                             S1 00460
C                 GLASGOW UNIVERSITY.                                          S1 00470
C                 U.K.                                                         S1 00480
C                                                                              S1 00490
C     TO EMPLOY FOR SMALL SCALE MODELS AS                                      S1 00500
C     WELL AS LARGE SCALE MODELS.                                              S1 00510
C                                                                              S1 00520
C                                                                              S1 00530
C                                                                              S1 00540
C                                                                              S1 00550
      COMMON/COMPAC/PDEPTH(20,17),PCOMP(20,17),IPROF(20),XPROF(20),            S1 00560
     1 INTCOM(50,3),N1HUMP(10),NPSOFT(10),EMPRC(20,4),IFXC(100),               S1 00570
     2 FXC(100),NNPFC,NOCOMP                                                  S1 00580
      COMMON/STRUCT/KEYSTR,NMNPST,LNSTRL,LNSTRU,NBREMT,NBMEMT,NSTRET,          S1 00590
     1 NBRF,NBMF,NINTF,NSTIFF,NFDISP,NGRVLD                                   S1 00600
      COMMON /ISOP/ E1,E2,RR(4),ZZ(4),LM(8),P(8),S(8,8),STR(3,8),              S1 00610
     1 STS(3,8),VJAC                                                          S1 00620
      COMMON/STPROP/PROP(20,8),MAT(100,3)                                      S1 00630
      COMMON/UNLOAD/IFXU(100),FXU(100),INTUNL(50,3),DELXC(400),                S1 00640
     1 NINCRU(60),NNPFXU,NUMFXU                                               S1 00650
      DIMENSION HED(18),T(10),NNLAY(20),NNFORC(20),NNCOMP(20)                  S1 00660
```

```
      CHARACTER*15 FINAME,FONAME                                          S1 00670
C                                                                         S1 00680
C     PROGRAM CAPACITY CONTROLLED BY THE FOLLOWING FOUR STATEMENTS        S1 00690
C                                                                         S1 00700
      COMMON A(15500)                                                     S1 00710
      COMMON B(3000)                                                      S1 00720
      COMMON C(1500)                                                      S1 00730
      MTOTAL=15500                                                        S1 00740
      MBTOTL=3000                                                         S1 00750
      MCTOTL=1500                                                         S1 00760
C                                                                         S1 00770
C     PROGRAM CONTROL DATA                                                S1 00780
C                                                                         S1 00790
C                                                                         S1 00800
C                                                                         S1 00810
      NUMFXU=0                                                            S1 00820
  100 READ(5,1001) HED                                                    S1 00830
      READ(5,*) NUMELT,NUMNPT,NFEL,NFNP,NUMCEL,NUMCNP,NUMMAT,             S1 00840
     1 NLAY,NCOMP,NFORCE,NPRINT,NSTOP                                     S1 00850
      READ(5,*)NREDUC,NSEGM                                               S1 00860
      NOCOMP=NCOMP                                                        S1 00870
      IF( NUMNPT.EQ. 0) STOP                                              S1 00880
      READ(5,*) NMNPST,NBREMT,NBRMAT,NBMEMT,NBMMAT,NBRF,NBMF              S1 00890
      READ(5,*) NUMQ                                                      S1 00900
      NUMLD=NLAY+NFORCE+NCOMP                                             S1 00910
      READ(5,*) NUMZ,NUMZC,NUMZF,NZMAT,NZCODE                             S1 00920
C                                                                         S1 00930
      DO 102 I=1,20                                                       S1 00940
      NNCOMP(I)=0                                                         S1 00950
      NNLAY(I) = 0                                                        S1 00960
  102 NNFORC(I) = 0                                                       S1 00970
      IF(NLAY.EQ.0) GO TO 116                                             S1 00980
      READ(5,*) (NNLAY(I),I=1,NLAY)                                       S1 00990
  116 IF(NCOMP.EQ.0) GO TO 117                                            S1 01000
```

```
      READ(5,*) (NNCOMP(I),I=1,NCOMP)                                    S1 01010
  117 IF(NFORCE.EQ.0) GO TO 118                                           S1 01020
      READ(5,*) (NNFORC(I),I=1,NFORCE)                                    S1 01030
  118 CONTINUE                                                            S1 01040
      READ(5,*) SCFAC                                                     S1 01050
        READ(5,*) PATM,GAMW                                               S1 01060
      NBMBR  = NBREMT+ NBMEMT                                             S1 01070
      WRITE(6,2000) HED                                                   S1 01080
      WRITE(6,2010)NUMNPT,NBREMT,NBRMAT,NBMEMT,NBMMAT,NUMQ,NUMZ,NUMZC,   S1 01090
     1 NUMZF,NZMAT,NUMELT,NUMMAT,NFEL,NFNP,NUMCEL,NUMCNP,NLAY,NCOMP,      S1 01100
     2 NFORCE                                                             S1 01110
      WRITE(6,2035)SCFAC,PATM,GAMW                                        S1 01120
C                                                                         S1 01130
      WRITE(6,2014)NUMLD                                                  S1 01140
      IF(NUMLD.LE.0) GO TO 111                                            S1 01150
      DO 109 I=1,NUMLD                                                    S1 01160
      IF(NLAY.EQ.0) GO TO 105                                             S1 01170
      DO 104 J=1,NLAY                                                     S1 01180
      IF(NNLAY(J).EQ.I) GO TO 107                                         S1 01190
  104 CONTINUE                                                            S1 01200
  105 CONTINUE                                                            S1 01210
      IF(NCOMP.EQ.0) GO TO 113                                            S1 01220
      DO 112 L=1,NCOMP                                                    S1 01230
      IF(NNCOMP(L).EQ.I) GO TO 114                                        S1 01240
  112 CONTINUE                                                            S1 01250
  113 IF(NFORCE.EQ.0) GO TO 109                                           S1 01260
      DO 106 K=1,NFORCE                                                   S1 01270
      IF(NNFORC(K).EQ.I) GO TO 108                                        S1 01280
  106 CONTINUE                                                            S1 01290
      GO TO 109                                                           S1 01300
  107 WRITE(6,2015)I,J                                                    S1 01310
      GO TO 109                                                           S1 01320
  114 WRITE(6,2017)I,L                                                    S1 01330
      GO TO 109                                                           S1 01340
```

```
  108 WRITE(6,2016)I,K                                                  S1 01350
  109 CONTINUE                                                          S1 01360
      IF (NLAY.GT.0.AND.NREDUC.EQ.1) WRITE (6,9900)                     S1 01370
C     BLOCK OUT VARIABLES IN C-VECTOR                                   S1 01380
      NC1=1                                                             S1 01390
      NC2=NC1+NUMNPT                                                    S1 01400
      NC3=NC2+NUMNPT                                                    S1 01410
C                                                                       S1 01420
C     BLOCK OUT VARIABLES IN B-VECTOR                                   S1 01430
C                                                                       S1 01440
  111 NB1=1                                                             S1 01450
      NB2=NB1+NUMELT                                                    S1 01460
      NB3=NB2+NUMELT                                                    S1 01470
      NB4=NB3+NUMELT                                                    S1 01480
      NB5=NB4+NUMELT                                                    S1 01490
      NB6=NB5+NUMELT                                                    S1 01500
      NB7=NB6+NUMELT                                                    S1 01510
      NB8=NB7+NUMELT                                                    S1 01520
      IF(NB8.GT.MBTOTL) GO TO 125                                       S1 01530
C                                                                       S1 01540
C     BLOCK OUT VARIABLES IN A-VECTOR                                   S1 01550
C                                                                       S1 01560
      N1 = 1                                                            S1 01570
      N2= N1+ 3*NUMNPT                                                  S1 01580
      N3 = N2+ NUMNPT                                                   S1 01590
      N4 = N3+ NUMNPT                                                   S1 01600
      N5 = 12*(NUMMAT+NZMAT)                                            S1 01610
      IF( 3* NBRMAT.GT. N5) N5= 3*NBRMAT                                S1 01620
      IF( 6* NBMMAT.GT. N5) N5 = 6*NBMMAT                               S1 01630
       N5 = N4 + N5                                                     S1 01640
      N6 = 5*NUMELT                                                     S1 01650
      IF( 3*NBREMT.GT. N6) N6= 3*NBREMT                                 S1 01660
      IF( 3*NBMEMT.GT. N6) N6 = 3*NBMEMT                                S1 01670
      N6 = N5 + N6                                                      S1 01680
```

```
N7=N6+NUMELT                                                    S1 01690
N8=N7+NUMELT                                                    S1 01700
N9=N8+NUMELT                                                    S1 01710
N10=N9+NUMCEL+1                                                 S1 01720
N11=N10+NUMCNP+NMNPST+1                                         S1 01730
N12=N11+2*NUMLD                                                 S1 01740
N13=N12+2*NUMLD                                                 S1 01750
N14=N13+  NUMLD*20                                              S1 01760
N15=N14+NUMLD                                                   S1 01770
N16 = N15 + NUMQ*2                                              S1 01780
N17 = N16+ NUMLD                                                S1 01790
N18 = N17+NUMQ*5                                                S1 01800
N19 = N18 + NUMZ*6                                              S1 01810
N20 = N19 + NUMZ*4                                              S1 01820
N21 = N20 + NUMZ*4                                              S1 01830
N22 = N21 + NUMZ*2                                              S1 01840
N23 = N22 + NUMZ*4                                              S1 01850
N24 = N23 + NUMZ*4                                              S1 01860
N25 = N24 + NLAY*2                                              S1 01870
N26=N25+NUMNPT                                                  S1 01880
N26A=N26+NUMNPT                                                 S1 01890
N27=N26A+NUMNPT                                                 S1 01900
N28=N27+3*NUMELT                                                S1 01910
N29=N28+3*NUMELT                                                S1 01920
N28A=N28+NUMELT                                                 S1 01930
N28B=N28A+NUMELT                                                S1 01940
ICHECK=NBREMT+5*NBMEMT                                          S1 01950
N27A=N27+ICHECK                                                 S1 01960
IF(3*NUMELT.LT.ICHECK)N29=N27A+ICHECK                           S1 01970
N30=N29+3*MAX0(NUMELT,NUMNPT)                                   S1 01980
NN1=N29+NUMELT                                                  S1 01990
NN2=NN1+NUMELT                                                  S1 02000
MTMN15=MTOTAL-N25                                               S1 02010
NN3=N29+2*NUMNPT                                                S1 02020
```

```
      IF (NN3 .GT. N30) N30=NN3                                          S1 02030
      IF (N30 .LT. MTOTAL) GO TO 130                                     S1 02040
  125 WRITE(6,5000)                                                      S1 02050
      CALL EXIT                                                          S1 02060
C                                                                        S1 02070
C      INPUT NODAL POINTS AND NUMBER EQUATIONS                           S1 02080
C                                                                        S1 02090
  130 CALL READNP( A(N1), A(N2), A(N3), NUMNPT, NEQ,SCFAC,NPRINT)        S1 02100
      MBAND =0                                                           S1 02110
C                                                                        S1 02120
C      INPUT AND CALCULATE ALL STRUCTURAL DATA                           S1 02130
C                                                                        S1 02140
C     STRUCTURAL TAPE FILES                                              S1 02150
C                                                                        S1 02160
      NSTIFF = 12                                                        S1 02170
      NFDISP = 13                                                        S1 02180
      NGRVLD = 14                                                        S1 02190
      NINTF=15                                                           S1 02200
      REWIND NSTIFF                                                      S1 02210
      REWIND NFDISP                                                      S1 02220
      REWIND NGRVLD                                                      S1 02230
      IF( NBMBR.LT. 1) GO TO 60                                          S1 02240
      IF(NPRINT.EQ.1)WRITE(6,2200)                                       S1 02250
      IF( NBREMT .LT. 1) GO TO 40                                        S1 02260
      CALL BAR(A(N1), A(N2), A(N3), A(N4), A(N5), NUMNPT, NBREMT,        S1 02270
     1    NBRMAT, MBAND,NPRINT)                                          S1 02280
   40 IF( NBMEMT .LT. 1) GO TO 60                                        S1 02290
      CALL BEAM( A(N1), A(N2), A(N3), A(N4), A(N5),                      S1 02300
     1  NUMNPT, NBMEMT, NBMMAT, MBAND,NPRINT)                           S1 02310
   60 CONTINUE                                                           S1 02320
      ISTOP = 0                                                          S1 02330
      WRITE(NGRVLD)(ISTOP,I=1,11)                                        S1 02340
      IF(NUMQ.LE.0) GO TO 70                                             S1 02350
      CALL QLINKS(A(N1),A(N15),A(N16),A(N17),NUMQ,NUMNPT,NUMLD,MBAND,    S1 02360
```

```
     1NPRINT)                                                                  S1 02370
   70 CONTINUE                                                                 S1 02380
C                                                                              S1 02390
C     READ AND WRITE INPUT DATA AND SET UP INITIAL CONDITIONS                  S1 02400
C                                                                              S1 02410
      NUMMZT = NUMMAT + NZMAT                                                  S1 02420
      CALL LAYOUT (A(N4),A(N1),A(N2),A(N3),A(N5),A(N6),A(N7),A(N8),            S1 02430
     1 A(N9),A(N10),A(N11),A(N12),A(N13),A(N14),A(N25),A(N27),                 S1 02440
     2 A(N27),A(N28),A(N29),A(NN1),A(NN2),A(N18),A(N19),A(N20),A(N21),         S1 02450
     3A(N22),A(N23),A(N24),NUMZ,NUMZF,NUMZC,NZMAT,NZEL,NUMELT,NUMNPT,          S1 02460
     4 NUMCEL,NUMCNP, NFEL,NUMMZT,NUMLD,NLAY,NEQ,NEQB,MBAND,PATM,MTMN15,       S1 02470
     5NMXEQB,NPRINT,SCFAC,GAMW,NZCODE,B(NB1),B(NB2),B(NB3),B(NB4),             S1 02480
     6 B(NB6),B(NB7),NREDUC)                                                   S1 02490
      IF(NCOMP.EQ.0) GO TO 80                                                  S1 02500
      INC1P=NNLAY(1)                                                           S1 02510
      INC1C=NNCOMP(1)                                                          S1 02520
      CALL PCOMPR(ISTOP,A(N27),A(N28),INC1P,INC1C,NCOMP,NUMLD,NPRINT)          S1 02530
      IF(ISTOP.EQ.1) GO TO 9999                                                S1 02540
   80 IF(NUMLD.LE.0) STOP                                                      S1 02550
      N31=N30+NEQ                                                              S1 02560
      N32=N31+NEQB                                                             S1 02570
      IF (N32 .LT. MTOTAL) GO TO 140                                           S1 02580
      WRITE(6,5000)                                                            S1 02590
      CALL EXIT                                                                S1 02600
C                                                                              S1 02610
C     FORM STRAIN-DISPLACEMENT MATRIX FOR ALL ELEMENTS ,STORE ON TAPE 20       S1 02620
C                                                                              S1 02630
  140 CALL FORMST (A(N2),A(N3),A(N5),NUMELT)                                   S1 02640
      KEYSTR = 0                                                               S1 02650
      NSTRET=0                                                                 S1 02660
      LASTNL=0                                                                 S1 02670
      DO 400 LN=1,NUMLD                                                        S1 02680
      NUMMCF=0                                                                 S1 02690
      IF(NSTOP.NE.0.AND.LN.GT.NSTOP) STOP                                      S1 02700
```

```
      LNST = 0                                                                  S1 02710
      IF(LNSTRL.GT.0) LNST = NNLAY(LNSTRL)                                      S1 02720
      IF(LN .NE. LNST)   GO TO 150                                              S1 02730
      KEYSTR = 1                                                                S1 02740
  150 WRITE(6,2000) HED                                                         S1 02750
C                                                                               S1 02760
C     DETERMINE CONTROL DATA FOR EACH LAYER                                     S1 02770
C                                                                               S1 02780
      CALL CALBLK (A(N1),A(N9),A(N10),A(N11),A(N12),A(N13),NUMELT,              S1 02790
     1 NUMNPT,NUMCEL,NUMCNP,NFEL,NFNP,NUMLD,NLAY,LN,MBAND,NUMEL,NUMNP,          S1 02800
     2 NELCAL,NNPCAL,NELRED,NNPRED,NEQ,NEQB,NBLOCK,NMXEQB,NNLAY,NNFORC,         S1 02810
     3 NNCOMP,NREDUC,ITCOMP,ITFORC,LASTNL,B(NB7))                               S1 02820
      NOUT=NUMNP                                                                S1 02830
      IF(NSEGM.EQ.1)NOUT=NNPCAL                                                 S1 02840
      NN1=N27+NEQ                                                               S1 02850
      IF(ITCOMP.NE.1) GO TO 155                                                 S1 02860
      CALL FSCOMP(A(N13),B(NB1),B(NB2),A(N12),A(N2),A(N3),A(N27),               S1 02870
     2 B(NB3),B(NB4),NUMLD,LASTNL,IQUIT,NUMELT,NUMEL,NUMMZT,A(N4),              S1 02880
     3 A(N5),PATM,NUMMCF,A(N6),A(N7),A(N8),B(NB5),A(N28),A(N28A),B(NB6),        S1 02890
     4 B(NB7))                                                                  S1 02900
      IF(IQUIT.EQ.1) GO TO 9999                                                 S1 02910
  155 CONTINUE                                                                  S1 02920
C                                                                               S1 02930
C     SET UP LOAD VECTOR                                                        S1 02940
C                                                                               S1 02950
      CALL FVECT (A(N4),A(N1),A(N2),A(N3),A(N5),A(N9),A(N11),A(N25),            S1 02960
     1 A(N26),A(N26A),NUMELT,NUMNPT,NUMCEL,NUMMZT,NUMLD,                        S1 02970
     2 NLAY,LN,NUMNP,NNLAY,NNFORC,ITCOMP,NUMMCF,C(NC1),C(NC2),                  S1 02980
     3 C(NC3))                                                                  S1 02990
      IF(NSTOP.EQ.0) GO TO 350                                                  S1 03000
      DO 300 ITER=1,2                                                           S1 03010
      IT = ITER                                                                 S1 03020
      CALL FVECT2 (A(N1),C(NC1),C(NC2),C(NC3),A(N25),A(N26),                    S1 03030
     1A(N26A),A(N27),A(NN1),NEQ,NEQB,NUMNPT,NUMNP,ITCOMP,ITFORC                 S1 03040
```

```
     2 ,NUMMCF,IT,NOUT,IPRINT)                                                  S1 03050
       IF(NUMEL.NE.0) GO TO 160                                                 S1 03060
       IT=2                                                                     S1 03070
       GO TO 170                                                                S1 03080
  160 CONTINUE                                                                  S1 03090
C                                                                               S1 03100
C      CALCULATE ELEMENT STIFFNESS MATRIX FOR ALL ELEMENTS ,STORE               S1 03110
C                                                                 ON TAPE 3     S1 03120
C      CALCULATE STRESS-DISPLACEMENT MATRIX FOR ALL ELEMENTS ,STORE             S1 03130
C                                                                 ON TAPE 11    S1 03140
C                                                                               S1 03150
       CALL ISQUAD (A(N5),A(N6),A(N7),A(N8),A(N9),NUMELT,NUMCEL,NUMEL,          S1 03160
     1 NELCAL,NELRED,NREDUC)                                                    S1 03170
  170 CONTINUE                                                                  S1 03180
       NE2B=2*NEQB                                                              S1 03190
       NN1=N25+NE2B*MBAND                                                       S1 03200
       NN2=NN1+NE2B                                                             S1 03210
C                                                                               S1 03220
C      FORM TOTAL STIFFNESS MATRIX ,STORE ON TAPE 3                             S1 03230
C                                                                               S1 03240
       CALL ADDSTF (A(N25),A(NN1),A(N16),A(N24),NUMQ,NUMZ,NZEL,NUMEL,           S1 03250
     1 NEQB,NE2B,NBLOCK,MBAND,LN,NLAY,NNLAY)                                    S1 03260
       NSB=(MBAND+1)*NEQB                                                       S1 03270
       NNN1=N25+NSB                                                             S1 03280
       NNN2=NNN1+NSB                                                            S1 03290
C                                                                               S1 03300
C      SOLVE FOR DISPLACEMENT UNKNOWNS                                          S1 03310
C                                                                               S1 03320
       CALL SYMBAN (A(N25),A(NNN1),A(NNN2),NEQB,MBAND,NBLOCK,NSB,               S1 03330
     1 4,3,1,2,2)                                                               S1 03340
C      CALL SECOND (T(8))                                                       S1 03350
C                                                                               S1 03360
C      EVALUATE RESULTS                                                         S1 03370
C                                                                               S1 03380
```

```
      CALL ISRSLT (A(N4),A(N1),A(N5),A(N6),A(N7),A(N8),A(N9),A(N10),     S1 03390
     1 A(N14),A(N25),A(N27),A(N27A),A(N27), A(N28),A(N29),A(N29),       S1 03400
     2A(N30),A(N31),A(N15),A(N16),A(N17),A(N18),A(N19),A(N20),A(N21),   S1 03410
     2 A(N22),A(N23),A(N24), NUMQ,NUMZ,NUMZF,NUMZC,NZMAT,NZEL,          S1 03420
     2         PATM,NUMELT,NUMNPT,NUMCEL,NUMCNP,NUMMZT,NUMLD,NLAY,LN,   S1 03430
     3 IT,NPRINT, NUMEL,NUMNP,NELCAL,NNPCAL,NELRED,NNPRED,NEQ,NEQB,     S1 03440
     4 NBLOCK,NNLAY,NNFORC,B(NB3),NREDUC,ITCOMP,NNCOMP,B(NB4),B(NB5),   S1 03450
     5 B(NB6),A(N3),NOUT,IPRINT)                                       S1 03460
  300 CONTINUE                                                         S1 03470
  350 CONTINUE                                                         S1 03480
      IF( KEYSTR.EQ. 0) GO TO 400                                      S1 03490
      KEYSTR = 0                                                       S1 03500
      GO TO 150                                                        S1 03510
  400 CONTINUE                                                         S1 03520
      GO TO 9999                                                       S1 03530
 1000 FORMAT (12A6/16I5)                                               S1 03540
 1001 FORMAT(18A4)                                                     S1 03550
 1500 FORMAT (16I5)                                                    S1 03560
 1600 FORMAT(2G10.3)                                                   S1 03570
 2000 FORMAT ('\f',18A4)                                               S1 03580
 2010 FORMAT (/,                                                       S1 03590
     1 40H TOTAL NUMBER OF NODES****************** ,I3//               S1 03600
     2 40H NUMBER OF BAR ELEMENTS***************** ,I3//               S1 03610
     3 40H NUMBER OF DIFF. BAR MATERIALS********** ,I3//               S1 03620
     4 40H NUMBER OF BEAM ELEMENTS**************** ,I3//               S1 03630
     5 40H NUMBER OF DIFF. BEAM MATERIALS********* ,I3//               S1 03640
     5 40H NUMBER OF NODAL LINKS ****************** ,I3//              S1 03650
     5 40H NUMBER OF INTERFACE ELEMENTS*********** ,I3//               S1 03660
     5 40H NO. OF INTERFACE ELE. IN PREEXIST. PART ,I3//               S1 03670
     5 40H NUMBER OF INTERFACE ELE. IN FOUNDATION* ,I3//               S1 03680
     5 40H NUMBER OF INTERFACE MATERIALS********** ,I3//               S1 03690
     6 40H TOTAL NUMBER OF SOIL ELEMENTS********** ,I3//               S1 03700
     7 40H NUMBER OF DIFF. SOIL MATERIALS********* ,I3//               S1 03710
     8 40H NUMBER OF ELEMENTS IN FOUNDATION******* ,I3//               S1 03720
```

```
     9 40H NUMBER OF NODES IN FOUNDATION********** ,I3//                  S1 03730
     1 40H NUMBER OF PREEXISTING ELEMENTS********* ,I3//                  S1 03740
     2 40H NUMBER OF PREEXISTING NODES************ ,I3//                  S1 03750
     3 40H NUMBER OF CONSTRUCTION LAYERS********** ,I3//                  S1 03760
     4 40H NUMBER OF COMPACTION INCREMENTS******** ,I3//                  S1 03770
     4 40H NUMBER OF LOAD CASES****************** ,I3)                    S1 03780
2014 FORMAT('\f',35HCOMPUTATION SEQUENCE FOR A TOTAL OF,I5,12H INCREMENS1 03790
    1TS /     ,52H************************************************** S1 03800
    2/)                                                                  S1 03810
2015 FORMAT(/,14H INCREMENT NO.,I3,5X,16HPUT ON LAYER NO.,I3)            S1 03820
2016 FORMAT(/,14H INCREMENT NO.,I3,5X,16HAPPLY LOAD CASE ,I3)            S1 03830
2017 FORMAT(/,14H INCREMENT NO.,I3,5X,15HCOMPACTION STEP,I3)             S1 03840
2035 FORMAT(/,24HSCALING FACTOR *********,F12.5//,                       S1 03850
    1           24HATMOSPHERIC PRESSURE ***,F12.5//,                     S1 03860
    2           24HUNIT WEIGHT OF WATER ***,F12.5/)                      S1 03870
5000 FORMAT (// 17H STORAGE EXCEEDED)                                    S1 03880
2200 FORMAT('\f',37H STRUCTURAL ELEMENTS - LINEAR ELASTIC,//)            S1 03890
9900 FORMAT(///,' STIFFNESS OF NEWLY PLACED SOIL ELEMENTS WILL BE REDUCS1 03900
    1ED BY A FACTOR OF 0.5 ')                                            S1 03910
9999 STOP                                                                S1 03920
     END                                                                 S1 03930
```

TYPICAL INPUT DATA:

```
OSMAN12 TEST R.E.W(COMP. LENG.-60.0 CM & Sh -Sv - 15.0 CM)
178   288    26    44  0  0  2  12  12  0  1  24
1    1
45  28   1    16    1    0    0
4
72    0    0   2   0
1    3    5   7   9  11  13  15  17  19  21  23
2    4    6   8  10  12  14  16  18  20  22  24
1.0
1.033  0.001
```

```
1     -30.0     0.0      1      1      1
2     -15.0     0.0      1      1      1
3      -7.5     0.0      1      1      1
4       0.0     0.0      1      1      1
5       5.0     0.0      1      1      1
6      10.0     0.0      1      1      1
7      20.0     0.0      1      1      1
8      30.0     0.0      1      1      1
9      40.0     0.0      1      1      1
10      50.0     0.0      1      1      1
11      60.0     0.0      1      1      1
12     70.0     0.0      1      1      1
13     85.0     0.0      1      1      1
14    100.0     0.0      1      1      1
15    -30.0     5.0      1      0      0
16    -15.0     5.0      0      0      0
17     -7.5     5.0      0      0      0
18      0.0     5.0      0      0      0
19      5.0     5.0      0      0      0
20     10.0     5.0      0      0      0
21     20.0     5.0      0      0      0
22     30.0     5.0      0      0      0
23     40.0     5.0      0      0      0
24     50.0     5.0      0      0      0
25     60.0     5.0      0      0      0
26     70.0     5.0      0      0      0
27     85.0     5.0      0      0      0
28    100.0     5.0      1      0      0
29    -30.0    10.0      1      0      0
30    -15.0    10.0      0      0      0
31     -7.5    10.0      0      0      0
32      0.0    10.0      0      0      0
33      0.0    10.0      0      0      0
34      0.0    10.0      0      0      0
35      5.0    10.0      0      0      0
36     10.0    10.0      0      0      0
37     20.0    10.0      0      0      0
38     30.0    10.0      0      0      0
39     40.0    10.0      0      0      0
40     50.0    10.0      0      0      0
41     60.0    10.0      0      0      0
42     70.0    10.0      0      0      0
43     85.0    10.0      0      0      0
44    100.0    10.0      1      0      0
```

45	0.0	15.0	0	0	0
46	0.0	15.0	0	0	0
47	5.0	15.0	0	0	0
48	10.0	15.0	0	0	0
49	20.0	15.0	0	0	0
50	30.0	15.0	0	0	0
51	40.0	15.0	0	0	0
52	50.0	15.0	0	0	0
53	60.0	15.0	0	0	0
54	70.0	15.0	0	0	0
55	85.0	15.0	0	0	0
56	100.0	15.0	1	0	0
57	0.0	17.5	0	0	0
58	5.0	17.5	0	0	0
59	10.0	17.5	0	0	0
60	20.0	17.5	0	0	0
61	30.0	17.5	0	0	0
62	40.0	17.5	0	0	0
63	50.0	17.5	0	0	0
64	60.0	17.5	0	0	0
65	00.0	17.5	0	0	0
66	00.0	17.5	0	0	0
67	5.0	17.5	0	0	0
68	10.0	17.5	0	0	0
69	20.0	17.5	0	0	0
70	30.0	17.5	0	0	0
71	40.0	17.5	0	0	0
72	50.0	17.5	0	0	0
73	60.0	17.5	0	0	0
74	00.0	17.5	0	0	0
75	5.0	17.5	0	0	0
76	10.0	17.5	0	0	0
77	20.0	17.5	0	0	0
78	30.0	17.5	0	0	0
79	40.0	17.5	0	0	0
80	50.0	17.5	0	0	0
81	60.0	17.5	1064	0	0
82	0.0	20.0	0	0	0
83	0.0	20.0	0	0	0
84	5.0	20.0	0	0	0
85	10.0	20.0	0	0	0
86	20.0	20.0	0	0	0
87	30.0	20.0	0	0	0
88	40.0	20.0	0	0	0
89	50.0	20.0	0	0	0
90	60.0	20.0	0	0	0
91	70.0	20.0	0	0	0
92	85.0	20.0	0	0	0
93	100.0	20.0	1	0	0
94	0.0	25.0	0	0	0
95	0.0	25.0	0	0	0
96	5.0	25.0	0	0	0
97	10.0	25.0	0	0	0
98	20.0	25.0	0	0	0
99	30.0	25.0	0	0	0
100	40.0	25.0	0	0	0

101	50.0	25.0	0	0	0
102	60.0	25.0	0	0	0
103	70.0	25.0	0	0	0
104	85.0	25.0	0	0	0
105	100.0	25.0	1	0	0
106	00.0	30.0	0	0	0
107	00.0	30.0	0	0	0
108	5.0	30.0	0	0	0
109	10.0	30.0	0	0	0
110	20.0	30.0	0	0	0
111	30.0	30.0	0	0	0
112	40.0	30.0	0	0	0
113	50.0	30.0	0	0	0
114	60.0	30.0	0	0	0
115	70.0	30.0	0	0	0
116	85.0	30.0	0	0	0
117	100.0	30.0	1	0	0
118	00.0	32.5	0	0	0
119	5.0	32.5	0	0	0
120	10.0	32.5	0	0	0
121	20.0	32.5	0	0	0
122	30.0	32.5	0	0	0
123	40.0	32.5	0	0	0
124	50.0	32.5	0	0	0
125	60.0	32.5	0	0	0
126	00.0	32.5	0	0	0
127	00.0	32.5	0	0	0
128	5.0	32.5	0	0	0
129	10.0	32.5	0	0	0
130	20.0	32.5	0	0	0
131	30.0	32.5	0	0	0
132	40.0	32.5	0	0	0
133	50.0	32.5	0	0	0
134	60.0	32.5	0	0	0
135	0.0	32.5	0	0	0
136	5.5	32.5	0	0	0
137	10.0	32.5	0	0	0
138	20.0	32.5	0	0	0
139	30.0	32.5	0	0	0
140	40.0	32.5	0	0	0
141	50.0	32.5	0	0	0
142	60.0	32.5	1125	0	0
143	0.0	35.0	0	0	0
144	0.0	35.0	0	0	0
145	5.0	35.0	0	0	0
146	10.0	35.0	0	0	0
147	20.0	35.0	0	0	0
148	30.0	35.0	0	0	0
149	40.0	35.0	0	0	0
150	50.0	35.0	0	0	0
151	60.0	35.0	0	0	0
152	70.0	35.0	0	0	0
153	85.0	35.0	0	0	0
154	100.0	35.0	1	0	0
155	0.0	40.0	0	0	0
156	0.0	40.0	0	0	0

157	5.0	40.0	0	0	0
158	10.0	40.0	0	0	0
159	20.0	40.0	0	0	0
160	30.0	40.0	0	0	0
161	40.0	40.0	0	0	0
162	50.0	40.0	0	0	0
163	60.0	40.0	0	0	0
164	70.0	40.0	0	0	0
165	85.0	40.0	0	0	0
166	100.0	40.0	1	0	0
167	0.0	45.0	0	0	0
168	0.0	45.0	0	0	0
169	5.0	45.0	0	0	0
170	10.0	45.0	0	0	0
171	20.0	45.0	0	0	0
172	30.0	45.0	0	0	0
173	40.0	45.0	0	0	0
174	50.0	45.0	0	0	0
175	60.0	45.0	0	0	0
176	70.0	45.0	0	0	0
177	85.0	45.0	0	0	0
178	100.0	45.0	1	0	0
179	0.0	47.5	0	0	0
180	5.0	47.5	0	0	0
181	10.0	47.5	0	0	0
182	20.0	47.5	0	0	0
183	30.0	47.5	0	0	0
184	47.5	40.0	0	0	0
185	50.0	47.5	0	0	0
186	60.0	47.5	0	0	0
187	00.0	47.5	0	0	0
188	00.0	47.5	0	0	0
189	5.0	47.5	0	0	0
190	10.0	47.5	0	0	0
191	20.0	47.5	0	0	0
192	30.0	47.5	0	0	0
193	47.5	47.5	0	0	0
194	50.0	47.5	0	0	0
195	60.0	47.5	0	0	0
196	0.0	47.5	0	0	0
197	5.0	47.5	0	0	0
198	10.0	47.5	0	0	0
199	20.0	47.5	0	0	0
200	30.0	47.5	0	0	0
201	40.0	47.5	0	0	0
202	50.0	47.5	0	0	0
203	60.0	47.5	1186	0	0
204	0.0	50.	0	0	0
205	0.0	50.	0	0	0
206	5.0	50.	0	0	0
207	10.0	50.	0	0	0
208	20.0	50.	0	0	0
209	30.0	50.	0	0	0
210	40.0	50.	0	0	0
211	50.0	50.	0	0	0
212	60.0	50.	0	0	0

213	70.0	50.	0	0	0
214	85.0	50.	0	0	0
215	100.0	50.	1	0	0
216	0.0	55.	0	0	0
217	0.0	55.	0	0	0
218	5.0	55.	0	0	0
219	10.0	55.	0	0	0
220	20.0	55.	0	0	0
221	30.0	55.	0	0	0
222	40.0	55.	0	0	0
223	50.0	55.	0	0	0
224	60.0	55.	0	0	0
225	70.0	55.	0	0	0
226	85.0	55.	0	0	0
227	100.0	55.	1	0	0
228	0.0	60.	0	0	0
229	0.0	60.	0	0	0
230	5.0	60.	0	0	0
231	10.0	60.	0	0	0
232	20.0	60.	0	0	0
233	30.0	60.	0	0	0
234	40.0	60.	0	0	0
235	50.0	60.	0	0	0
236	60.0	60.	0	0	0
237	70.0	60.	0	0	0
238	85.0	60.	0	0	0
239	100.0	60.	1	0	0
240	0.0	62.5	0	0	0
241	5.0	62.5	0	0	0
242	10.0	62.5	0	0	0
243	20.0	62.5	0	0	0
244	30.0	62.5	0	0	0
245	40.0	62.5	0	0	0
246	50.0	62.5	0	0	0
247	60.0	62.5	0	0	0
248	0.0	62.5	0	0	0
249	0.0	62.5	0	0	0
250	5.0	62.5	0	0	0
251	10.0	62.5	0	0	0
252	20.0	62.5	0	0	0
253	30.0	62.5	0	0	0
254	40.0	62.5	0	0	0
255	50.0	62.5	0	0	0
256	60.0	62.5	0	0	0
257	0.0	62.5	0	0	0
258	5.0	62.5	0	0	0
259	10.0	62.5	0	0	0
260	20.0	62.5	0	0	0
261	30.0	62.5	0	0	0
262	40.0	62.5	0	0	0
263	50.0	62.5	0	0	0
264	60.0	62.5	1247	0	0
265	0.0	65.0	0	0	0
266	0.0	65.0	0	0	0
267	5.0	65.0	0	0	0
268	10.0	65.0	0	0	0

269	20.0	65.	0	0	0
270	30.0	65.	0	0	0
271	40.0	65.	0	0	0
272	50.0	65.	0	0	0
273	60.0	65.	0	0	0
274	70.0	65.	0	0	0
275	85.0	65.	0	0	0
276	100.0	65.	1	0	0
277	0.0	70.	0	0	0
278	0.0	70.	0	0	0
279	5.0	70.	0	0	0
280	10.0	70.	0	0	0
281	20.0	70.	0	0	0
282	30.0	70.	0	0	0
283	40.0	70.	0	0	0
284	50.0	70.	0	0	0
285	60.0	70.	0	0	0
286	70.0	70.	0	0	0
287	85.0	70.	0	0	0
288	100.0	70.	1	0	0

1	918000.0	0.0008	0.00

1	65	67	1
2	67	68	1
3	68	69	1
4	69	70	1
5	70	71	1
6	71	72	1
7	72	73	1
8	126	128	1
9	128	129	1
10	129	130	1
11	130	131	1
12	131	132	1
13	132	133	1
14	133	134	1
15	187	189	1
16	189	190	1
17	190	191	1
18	191	192	1
19	192	193	1
20	193	194	1
21	194	195	1
22	248	250	1
23	250	251	1
24	251	252	1
25	252	253	1
26	253	254	1
27	254	255	1
28	255	256	1

1	29539.0	0.486	1.8	0.0	0.0	0.0	0.9	0.9

1	33	45	1	0	1
2	45	65	1	1	1

3	65	82	1	1	1
4	82	94	1	1	0
5	94	106	1	0	1
6	106	126	1	1	1
7	126	143	1	1	1
8	143	155	1	1	0
9	155	167	1	0	1
10	167	187	1	1	1
11	187	204	1	1	1
12	204	216	1	1	0
13	216	228	1	0	1
14	228	248	1	1	1
15	248	265	1	1	1
16	265	277	1	1	0

1	64	81	0.0	10000.0	100000000.0	0.0	0.0
2	125	142	0.0	10000.0	100000000.0	0.0	0.0
3	186	203	0.0	10000.0	100000000.0	0.0	0.0
4	247	264	0.0	10000.0	100000000.0	0.0	0.0

0 0 1 1 1 1 1 1 2 2 2 2 2 2 3 3
3 3 3 3 4 4 4 4

1	34	46	45	33	1	27
2	46	57	65	45	1	37
3	57	58	67	66	2	37
4	58	59	68	67	2	38
5	59	60	69	68	2	39
6	60	61	70	69	2	40
7	61	62	71	70	2	41
8	62	63	72	71	2	42
9	63	64	73	72	2	43
10	66	67	75	74	2	45
11	67	68	76	75	2	46
12	68	69	77	76	2	47
13	69	70	78	77	2	48
14	70	71	79	78	2	49
15	71	72	80	79	2	50
16	72	73	81	80	2	51
17	74	83	82	65	1	45
18	83	95	94	82	1	55
19	95	107	106	94	1	65
20	107	118	126	106	1	75
21	118	119	128	127	2	75
22	119	120	129	128	2	76
23	120	121	130	129	2	77
24	121	122	131	130	2	78
25	122	123	132	131	2	79
26	123	124	133	132	2	80
27	124	125	134	133	2	81
28	127	128	136	135	2	83
29	128	129	137	136	2	84
30	129	130	138	137	2	85
31	130	131	139	138	2	86
32	131	132	140	139	2	87
33	132	133	141	140	2	88

```
34    133     134     142     141     2       89
35    135     144     143     126     1       83
36    144     156     155     143     1       93
37    156     168     167     155     1       103
38    168     179     187     167     1       113
39    179     180     189     188     2       113
40    180     181     190     189     2       114
41    181     182     191     190     2       115
42    182     183     192     191     2       116
43    183     184     193     192     2       117
44    184     185     194     193     2       118
45    185     186     195     194     2       119
46    188     189     197     196     2       121
47    189     190     198     197     2       122
48    190     191     199     198     2       123
49    191     192     200     199     2       124
50    192     193     201     200     2       125
51    193     194     202     201     2       126
52    194     195     203     204     2       127
53    196     205     204     187     1       121
54    205     217     216     204     1       131
55    217     229     228     216     1       141
56    229     240     248     228     1       151
57    240     241     250     249     2       151
58    241     242     251     250     2       152
59    242     243     252     251     2       153
60    243     244     253     252     2       154
61    244     245     254     253     2       155
62    245     246     255     254     2       156
63    246     247     256     255     2       157
64    249     250     258     257     2       159
65    250     251     259     258     2       160
66    251     252     260     259     2       161
67    252     253     261     260     2       162
68    253     254     262     261     2       163
69    254     255     263     262     2       164
70    255     256     264     263     2       165
71    257     266     265     248     1       159
72    266     278     277     265     1       169

1  0.0    20.0    0.0  100000000.0    5500   7500   0.50    0.70
2  0.0    30.0    0.0  100000000.0    5000   6000   1.0     0.9

1  0.00179    600.0    0.40    0.70    700    0.20    0.0    49.   9.   0.3    0
3.85    0.0          0.21    0.0     0.21

2  0.00176   560.0     0.4     0.7    640.0  0.20    0.0    47.3   8.72  .31   0
3.75    0.0    0.21    0.0    0.21

1       1       2       16      15      1
14      15      16      30      29      1
16      17      18      32      31      1
17      18      19      35      34      1
18      19      20      36      35      1
27      34      35      47      46      2
37      46      47      58      57      2
```

```
44      53      54      64      64      2
45      74      75      84      83      2
52      81      54      91      90      2
53      54      55      92      91      2
55      83      84      96      95      2
65      95      96      108     107     2
75      107     108     119     118     2
82      114     115     125     125     2
83      135     136     145     144     2
90      142     115     152     151     2
91      115     116     153     152     2
93      144     145     157     156     2
103     156     157     169     168     2
113     168     169     180     179     2
120     175     176     186     186     2
121     196     197     206     205     2
128     203     176     213     212     2
129     176     177     214     213     2
131     205     206     218     217     2
141     217     218     230     229     2
151     229     230     241     240     2
158     236     237     247     247     2
159     257     258     267     266     2
166     264     237     274     273     2
167     237     238     275     274     2
169     266     267     279     278     2
178     275     276     288     287     2

1   27  36  45  56  45  56  0 0 0 0 0 0 0 0
2   37  54  57  93  82  93  0 0 0 0 0 0 0 0
3   55  64  94  105 94  105 0 0 0 0 0 0 0 0
4   65  74  106 117 106 117 0 0 0 0 0 0 0 0
5   75  92  118 154 143 154 0 0 0 0 0 0 0 0
6   93  102 155 166 155 166 0 0 0 0 0 0 0 0
7   103 112 167 178 167 178 0 0 0 0 0 0 0 0
8   113 130 179 215 204 215 0 0 0 0 0 0 0 0
9   131 140 216 227 216 227 0 0 0 0 0 0 0 0
10  141 150 228 239 228 239 0 0 0 0 0 0 0 0
11  151 168 265 276 265 276 0 0 0 0 0 0 0 0
12  169 178 277 288 277 288 0 0 0 0 0 0 0 0

1       1       1
2       2       17
3       18      18
4       19      19
5       20      35
6       36      36
7       37      37
8       38      53
9       54      54
10      55      55
11      56      71
12      72      72

1   1   1   1   1   1   1   1   1   1   1   1   1   1   1
1   1   1   1   1   1   1   1   1
```

```
0  12

33  45   65   67   68   69   70   71   72   73  82   94   106
126 128  129  130  131  132  133  134  143  155 167  187  189
190 191  192  193  194  195  204  216  228  248 250  251  252
253 254  255  256  265  277

2   0.0

1   1   1   13   5.0
2   1   14  26  10.0
2
1    13

0.0   0.0    2.50      0.0   7.50    0.0      12.5   0.0
17.50  0.0   22.50    0.0   27.50      0.0     32.50   0.0
37.50   0.0    42.5     0.0     47.50    0.0    52.50  0.0
57.50   0.0

2     13

0.0   0.0    2.50   0.02356  7.50   0.02156   12.50    0.01842
17.50   .01562  22.50    .01310   27.50   0.01089  32.50  0.00899
37.50   0.00738    42.50    0.00260     47.50    0.00493     52.50    0.00
57.50   0.00328

1    2    0    1    6    0

2     60.     1     85.
27   46   34
29  33   45   55   43   44

2       2       0       2       4       0
2      60.      1      85.
37   57   46
45   83   74
82   92   55   56

3    2    0    1    4    0
2    60.  1    85.
55     95      83
94   104   92     93

4       2       0       1       4       0
2    60.  1    85.
65     107     95
106    116    104    105

5       2       0       2       4       0
2     60.  1     85.
75      118     107
83      144     135
143   153   116   117

6       2       0       1       4       0
2     60.  1     85.
```

```
93      156     144
155     165     153     154

7       2       0       1       4       0
2     60.   1     85.
103     168     156
167    177    165    166

8       2       0       2       4       0
2     60.   1     85.
113     179     168
121     205     196
204     214     177     178

9       2       0       1       4       0
2     60.   1     85.
131     217     205
216     226     214     215

10      2       0       1       4       0
2     60.   1     85.
141     229     217
228     238     226      227

11      2       0       2       4       0
2     60.   1     85.
151     240     229
159     266     257
265    275      238    239

12      2       0       1       4       0
2     60.   1     85.
169     278     266
277     287     275     276

1    0
2    -1
3    -1
4    -1
5    -1
6    -1
7    -1
8    -1
9    -1
10   -1
11   -1
12   -1
13   -1
14   -1
15   -1
16   -1
17   -1
18   -1
19   -1
20   -1
21   -1
```